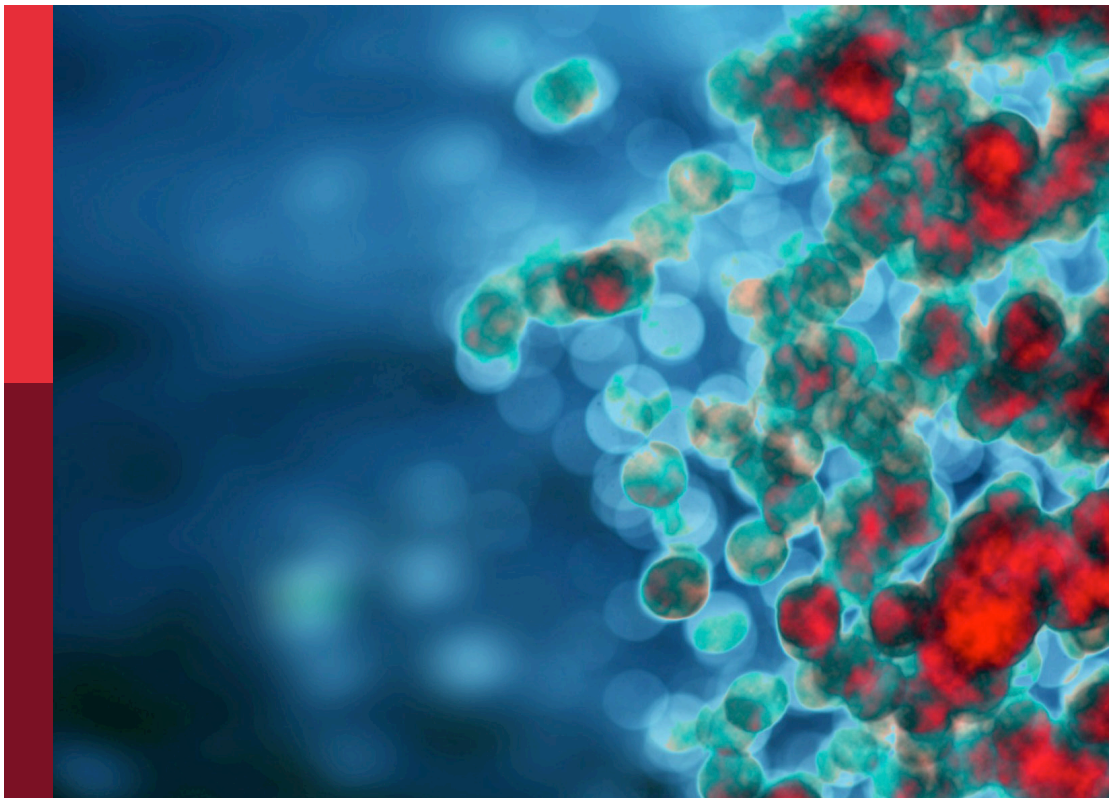
frontiers | Research Topics

Deciphering the T cell response in SARS-CoV-2 infection

Edited by
Alessio Mazzoni, Sara De Biasi, Pia Kvistborg and Laura Maggi

Published in
Frontiers in Immunology



FRONTIERS EBOOK COPYRIGHT STATEMENT

The copyright in the text of individual articles in this ebook is the property of their respective authors or their respective institutions or funders. The copyright in graphics and images within each article may be subject to copyright of other parties. In both cases this is subject to a license granted to Frontiers.

The compilation of articles constituting this ebook is the property of Frontiers.

Each article within this ebook, and the ebook itself, are published under the most recent version of the Creative Commons CC-BY licence. The version current at the date of publication of this ebook is CC-BY 4.0. If the CC-BY licence is updated, the licence granted by Frontiers is automatically updated to the new version.

When exercising any right under the CC-BY licence, Frontiers must be attributed as the original publisher of the article or ebook, as applicable.

Authors have the responsibility of ensuring that any graphics or other materials which are the property of others may be included in the CC-BY licence, but this should be checked before relying on the CC-BY licence to reproduce those materials. Any copyright notices relating to those materials must be complied with.

Copyright and source acknowledgement notices may not be removed and must be displayed in any copy, derivative work or partial copy which includes the elements in question.

All copyright, and all rights therein, are protected by national and international copyright laws. The above represents a summary only. For further information please read Frontiers' Conditions for Website Use and Copyright Statement, and the applicable CC-BY licence.

ISSN 1664-8714
ISBN 978-2-8325-5195-0
DOI 10.3389/978-2-8325-5195-0

About Frontiers

Frontiers is more than just an open access publisher of scholarly articles: it is a pioneering approach to the world of academia, radically improving the way scholarly research is managed. The grand vision of Frontiers is a world where all people have an equal opportunity to seek, share and generate knowledge. Frontiers provides immediate and permanent online open access to all its publications, but this alone is not enough to realize our grand goals.

Frontiers journal series

The Frontiers journal series is a multi-tier and interdisciplinary set of open-access, online journals, promising a paradigm shift from the current review, selection and dissemination processes in academic publishing. All Frontiers journals are driven by researchers for researchers; therefore, they constitute a service to the scholarly community. At the same time, the *Frontiers journal series* operates on a revolutionary invention, the tiered publishing system, initially addressing specific communities of scholars, and gradually climbing up to broader public understanding, thus serving the interests of the lay society, too.

Dedication to quality

Each Frontiers article is a landmark of the highest quality, thanks to genuinely collaborative interactions between authors and review editors, who include some of the world's best academicians. Research must be certified by peers before entering a stream of knowledge that may eventually reach the public - and shape society; therefore, Frontiers only applies the most rigorous and unbiased reviews. Frontiers revolutionizes research publishing by freely delivering the most outstanding research, evaluated with no bias from both the academic and social point of view. By applying the most advanced information technologies, Frontiers is catapulting scholarly publishing into a new generation.

What are Frontiers Research Topics?

Frontiers Research Topics are very popular trademarks of the *Frontiers journals series*: they are collections of at least ten articles, all centered on a particular subject. With their unique mix of varied contributions from Original Research to Review Articles, Frontiers Research Topics unify the most influential researchers, the latest key findings and historical advances in a hot research area.

Find out more on how to host your own Frontiers Research Topic or contribute to one as an author by contacting the Frontiers editorial office: frontiersin.org/about/contact

Deciphering the T cell response in SARS-CoV-2 infection

Topic editors

Alessio Mazzoni — University of Florence, Italy
Sara De Biasi — University of Modena and Reggio Emilia, Italy
Pia Kvistborg — The Netherlands Cancer Institute (NKI), Netherlands
Laura Maggi — University of Florence, Italy

Citation

Mazzoni, A., De Biasi, S., Kvistborg, P., Maggi, L., eds. (2024). *Deciphering the T cell response in SARS-CoV-2 infection*. Lausanne: Frontiers Media SA.
doi: 10.3389/978-2-8325-5195-0

Table of contents

06 Editorial: Deciphering the T cell response in SARS-CoV-2 infection
Laura Maggi, Alessio Mazzoni and Sara De Biasi

08 Chronic Immune Activation and CD4+ T Cell Lymphopenia in Healthy African Individuals: Perspectives for SARS-CoV-2 Vaccine Efficacy
Dawit Wolday, Francis M. Ndungu, Gloria P. Gómez-Pérez and Tobias F. Rinke de Wit

17 BCG Vaccine Derived Peptides Induce SARS-CoV-2 T Cell Cross-Reactivity
Peter J. Eggenhuizen, Boaz H. Ng, Janet Chang, Ashleigh L. Fell, Rachel M. Y. Cheong, Wey Y. Wong, Poh-Yi Gan, Stephen R. Holdsworth and Joshua D. Ooi

29 Degenerate CD8 Epitopes Mapping to Structurally Constrained Regions of the Spike Protein: A T Cell-Based Way-Out From the SARS-CoV-2 Variants Storm
Carolina Boni, Davide Cavazzini, Angelo Bolchi, Marzia Rossi, Andrea Vecchi, Camilla Tiezzi, Valeria Barili, Paola Fisicaro, Carlo Ferrari and Simone Ottonello

42 Regulatory T Cells as Predictors of Clinical Course in Hospitalised COVID-19 Patients
Sara Caldrer, Cristina Mazzi, Milena Bernardi, Marco Prato, Niccolò Ronzoni, Paola Rodari, Andrea Angheben, Chiara Piubelli and Natalia Tiberti

53 Comprehensive Analysis of CD4+ T Cell Response Cross-Reactive to SARS-CoV-2 Antigens at the Single Allele Level of HLA Class II
You-Seok Hyun, Yong-Hun Lee, Hyeong-A Jo, In-Cheol Baek, Sun-Mi Kim, Hyun-Jung Sohn and Tai-Gyu Kim

65 SARS-CoV-2 Spike-Specific CD4+ T Cell Response Is Conserved Against Variants of Concern, Including Omicron
Alessio Mazzoni, Anna Vanni, Michele Spinicci, Manuela Capone, Giulia Lamacchia, Lorenzo Salvati, Marco Coppi, Alberto Antonelli, Alberto Carnasciali, Parham Farahvachi, Nicla Giovacchini, Noemi Aiezza, Francesca Malentacchi, Lorenzo Zammarchi, Francesco Liotta, Gian Maria Rossolini, Alessandro Bartoloni, Lorenzo Cosmi, Laura Maggi and Francesco Annunziato

73 Heterologous Immunity Between SARS-CoV-2 and Pathogenic Bacteria
Peter J. Eggenhuizen, Boaz H. Ng, Janet Chang, Rachel M.Y. Cheong, Anusha Yellapragada, Wey Y. Wong, Yi Tian Ting, Julie A. Monk, Poh-Yi Gan, Stephen R. Holdsworth and Joshua D. Ooi

91 T-Cell Repertoire Characteristics of Asymptomatic and Re-Detectable Positive COVID-19 Patients
Yizhe Li, Jian Hu, Yongsi Wang, Dongdong Liu, Yaling Shi, Jiaqi Zhang, Yuntao Liu, Dongzi Lin, Jing Lin, Wei Hu, Haolan He, Wei Wang, Wentao Fan, Linlin Li, Dawei Wang, Kejian Wang and Jianhua Xu

100 Children and Adults With Mild COVID-19: Dynamics of the Memory T Cell Response up to 10 Months
Patricia Kaaijk, Verónica Olivo Pimentel, Maarten E. Emmelot, Martien C. M. Poelen, Alper Cevirgel, Rutger M. Schepp, Gerco den Hartog, Daphne F.M. Reukers, Lisa Beckers, Josine van Beek, Cécile A. C. M. van Els, Adam Meijer, Nynke Y. Rots and Jelle de Wit

115 Corrigendum: Children and Adults With Mild COVID-19: Dynamics of the Memory T Cell Response Up to 10 Months
Patricia Kaaijk, Verónica Olivo Pimentel, Maarten E. Emmelot, Martien C. M. Poelen, Alper Cevirgel, Rutger M. Schepp, Gerco den Hartog, Daphne F. M. Reukers, Lisa Beckers, Josine van Beek, Cécile A. C. M. van Els, Adam Meijer, Nynke Y. Rots and Jelle de Wit

128 Long Lasting Cellular Immune Response Induced by mRNA Vaccination: Implication for Prevention Strategies
Laura Vitiello, Lucia Gatta, Sara Ilari, Stefano Bonassi, Mario Cristina, Filippo Ciatti, Massimo Fini, Stefania Proietti, Patrizia Russo, Carlo Tomino and Dolores Limongi

137 Humoral and Cellular Immunogenicity and Safety of Five Different SARS-CoV-2 Vaccines in Patients With Autoimmune Rheumatic and Musculoskeletal Diseases in Remission or With Low Disease Activity and in Healthy Controls: A Single Center Study
Gábor J. Szebeni, Nikolett Gémes, Dániel Honfi, Enikő Szabó, Patrícia Neuperger, József Á. Balog, Lajos I. Nagy, Zoltán Szekanecz, László G. Puskás, Gergely Toldi and Attila Balog

148 CD8⁺ T Cells in SARS-CoV-2 Induced Disease and Cancer—Clinical Perspectives
Keywan Mortezaee and Jamal Majidpoor

168 *In Silico* Analysis Predicts a Limited Impact of SARS-CoV-2 Variants on CD8 T Cell Recognition
Olga I. Isaeva, Steven L. C. Ketelaars and Pia Kvistborg

179 Remodeling of T Cell Dynamics During Long COVID Is Dependent on Severity of SARS-CoV-2 Infection
Milena Wiech, Piotr Chroscicki, Julian Swatler, Dawid Stepnik, Sara De Biasi, Michal Hampel, Marta Brewinska-Olchowik, Anna Maliszewska, Katarzyna Sklinda, Marek Durlik, Waldemar Wierzba, Andrea Cossarizza and Katarzyna Piwocka

197 A ubiquitous bone marrow reservoir of preexisting SARS-CoV-2-reactive memory CD4⁺ T lymphocytes in unexposed individuals
Jinchan Li, Simon Reinke, Yu Shen, Lena Schollmeyer, Yuk-Chien Liu, Zixu Wang, Sebastian Hardt, Christian Hipfl, Ute Hoffmann, Stefan Frischbutter, Hyun-Dong Chang, Tobias Alexander, Carsten Perka, Helena Radbruch, Zhihai Qin, Andreas Radbruch and Jun Dong

209 Booster dose of mRNA vaccine augments waning T cell and antibody responses against SARS-CoV-2
Feyza Gül Özbay Kurt, Alisa Lepper, Catharina Gerhards, Mathis Roemer, Samantha Lasser, Ihor Arkhypov, Rebekka Bitsch, Peter Bugert, Peter Altevogt, Cécile Gouttefangeas, Michael Neumaier, Jochen Utikal and Viktor Umansky

222 Dissecting CD8+ T cell pathology of severe SARS-CoV-2 infection by single-cell immunoprofiling
Felix Schreibing, Monica T. Hannani, Hyojin Kim, James S. Nagai, Fabio Ticconi, Eleanor Fewings, Tore Bleckwehl, Matthias Begemann, Natalia Torow, Christoph Kuppe, Ingo Kurth, Jennifer Kranz, Dario Frank, Teresa M. Anslinger, Patrick Ziegler, Thomas Kraus, Jürgen Enczmann, Vera Balz, Frank Windhofer, Paul Balfanz, Christian Kurts, Gernot Marx, Nikolaus Marx, Michael Dreher, Rebekka K. Schneider, Julio Saez-Rodriguez, Ivan Costa, Sikander Hayat and Rafael Kramann

245 Immunoinformatics design of B and T-cell epitope-based SARS-CoV-2 peptide vaccination
Muhammad Shehzad Khan, Ibrar Muhammad Khan, Syed Umair Ahmad, Ishrat Rahman, Muhammad Zahoor Khan, Muhammad Shah Zeb Khan, Zain Abbas, Shumaila Noreen and Yong Liu

262 Detailed characterization of SARS-CoV-2-specific T and B cells after infection or heterologous vaccination
Domenico Lo Tartaro, Annamaria Paolini, Marco Mattioli, Julian Swatler, Anita Neroni, Rebecca Borella, Elena Santacroce, Alessia Di Nella, Licia Gozzi, Stefano Busani, Michela Cuccorese, Tommaso Trenti, Marianna Meschiari, Giovanni Guaraldi, Massimo Girardis, Cristina Mussini, Katarzyna Piwocka, Lara Gibellini, Andrea Cossarizza and Sara De Biasi

276 Prognostic immune markers identifying patients with severe COVID-19 who respond to tocilizumab
Sara De Biasi, Marco Mattioli, Marianna Meschiari, Domenico Lo Tartaro, Annamaria Paolini, Rebecca Borella, Anita Neroni, Lucia Fidanza, Stefano Busani, Massimo Girardis, Francesca Coppi, Anna Vittoria Mattioli, Giovanni Guaraldi, Cristina Mussini, Andrea Cossarizza and Lara Gibellini

290 Effect of antiviral and immunomodulatory treatment on a cytokine profile in patients with COVID-19
Diana Martonik, Anna Parfieniuk-Kowerda, Aleksandra Starosz, Kamil Grubczak, Marcin Moniuszko and Robert Flisiak

307 Identification of mouse CD4$^+$ T cell epitopes in SARS-CoV-2 BA.1 spike and nucleocapsid for use in peptide:MHCII tetramers
Laura Bricio-Moreno, Juliana Barreto de Albuquerque, Jake M. Neary, Thao Nguyen, Lucy F. Kuhn, YeePui Yeung, Kathryn M. Hastie, Sara Landeras-Bueno, Eduardo Olmedillas, Chitra Hariharan, Anusha Nathan, Matthew A. Getz, Alton C. Gayton, Ashok Khatri, Gaurav D. Gaiha, Erica Ollmann Saphire, Andrew D. Luster and James J. Moon

frontiers | Frontiers in Immunology

TYPE Editorial
PUBLISHED 10 July 2024
DOI 10.3389/fimmu.2024.1419167

Check for updates

OPEN ACCESS

EDITED AND REVIEWED BY
Mariolina Salio,
Immunocore, United Kingdom

*CORRESPONDENCE
Laura Maggi
laura.maggi@unifi.it

RECEIVED 17 April 2024
ACCEPTED 02 July 2024
PUBLISHED 10 July 2024

CITATION
Maggi L, Mazzoni A and De Biasi S (2024) Editorial: Deciphering the T cell response in SARS-CoV-2 infection.
Front. Immunol. 15:1419167.
doi: 10.3389/fimmu.2024.1419167

COPYRIGHT
© 2024 Maggi, Mazzoni and De Biasi. This is an open-access article distributed under the terms of the Creative Commons Attribution License (CC BY). The use, distribution or reproduction in other forums is permitted, provided the original author(s) and the copyright owner(s) are credited and that the original publication in this journal is cited, in accordance with accepted academic practice. No use, distribution or reproduction is permitted which does not comply with these terms.

Editorial: Deciphering the T cell response in SARS-CoV-2 infection

Laura Maggi[1]*, Alessio Mazzoni[1] and Sara De Biasi[2]

[1]Department of Clinical and Experimental Medicine, School of Human Health Sciences, University of Florence, Firenze, Italy, [2]Department of Medical and Surgical, Maternal-Infantile and Adult Sciences, University of Modena and Reggio Emilia, Modena, Italy

KEYWORDS

T cells, immunological memory, SARS-CoV-2, vaccine, COVID-19

Editorial on the Research Topic
Deciphering the T cell response in SARS-CoV-2 infection

COVID-19 is an infectious disease emerged in 2020, caused by the novel coronavirus SARS-CoV-2. The immune system has a primary role in pathogen elimination and a rapid and effective response can limit disease severity. In this context, T cells play the major role in cell mediated adaptive immune response.

The aim of this Research Topic was to collect and build a comprehensive and specific consensus signature of T cell immunity in SARS-CoV-2 infection as well as following vaccination. In particular, twenty-three articles have been published under this Research Topic including Brief Research Reports, Original Researches and Reviews, covering the topic of the issue.

The characterization of T cell response, including both the polyclonal and the SARS-CoV-2 specific response, is crucial to define the status of the immune response at different stages of COVID-19, it can be important for improving disease diagnosis and it may represent a possible parameter for monitoring the efficacy of therapeutical treatments. Severe COVID-19 patients were characterized by an increase of exhausted and terminal differentiated CD8+ T cells (Mortezaee and Majidpoor; Schreibing et al.) and by a reduction of circulating Th1 and Treg cells: the impaired frequency of the latter at baseline may predict a clinical worsening during hospitalization (Caldrer et al.). In the case of mild-moderate COVID-19, SARS-CoV-2 specific T cells were reduced but detectable up to 10 months after symptoms onset in both adults and children, even if lower in the latter cohort (Kaaijk et al.), whereas a specific set of V-J gene combination has been associated to asymptomatic and re-detectable positive cases, different from symptomatic ones (Li et al.). Cytokine storm plays a major role in the immunopathogenesis of severe COVID-19 suggesting the use of immunomodulatory drugs in association with antivirals as treatments for COVID-19 and leading to a downregulation of pro-inflammatory cytokines (Martonik et al.). Interestingly, the levels of pro-inflammatory cytokines during the infection phase could predict the response to Tocilizumab (anti-IL6R) treatment (De Biasi et al.). Instead, the entity of CD4+ and CD8+ T cells immune disfunction described at 6 months from severe COVID-19 correlated with the development/persistence of long COVID symptoms (Wiech et al.), even if these clinical manifestations are not strictly related to severe COVID-19

group and all infected patients could develop long COVID-19 despite initial T cells dysfunction.

In the first wave of COVID-19 pandemic, the different grade of disease may have been partially influenced by pre-existing memory T cells directed against other coronaviruses and cross reactive to SARS-CoV-2, found mainly in bone marrow but also in blood of unexposed subjects, derived by cross-reaction with other antigens (Eggenhuizen et al.; Eggenhuizen et al.; Li et al.) and potentially restricted to specific HLA class II allotypes (Hyun et al.). In the subsequent waves of COVID-19 the clinical course of the disease was mainly impacted by emerged viral variants and by vaccination campaign. Mutations occurring on the different SARS-CoV-2 variants evolved after Wuhan strain, affected mainly the neutralizing activity of specific antibodies, whereas immunological memory mediated by specific CD4+ and CD8+ T cells was highly conserved (Boni et al.; Isaeva et al.; Mazzoni et al.). The characterization of the T cell response can be very informative to decipher SARS-CoV-2-specific T cells associated with viral clearance but also useful for vaccine development and for planning vaccination strategies. Many studies supported the concept that anti-SARS-CoV-2 vaccine is able to induce anti-Spike adaptive immune response in healthy subjects with a persistence of Spike specific IgG serum levels and circulating CD4+ and CD8+ T cells up 7 months after two-dose mRNA vaccine (Vitiello et al.) and that the booster dose efficiently increased them (Kurt et al.). Similar data were obtained also in cohort of patients with autoimmune rheumatic and musculoskeletal disease, even if the entity of immunogenicity was reduced in case of B-cell depleting therapy; however, these data demonstrated the safety of vaccination and the importance to promote it also in these subjects to prevent severe COVID-19 (Szebeni et al.). Interestingly, SARS-CoV- 2-specific adaptive immune response induced by vaccine was described to be in part different form that induced by natural infection mainly in terms of Th1 polarization and highly polyfunctional T cells population in the former ones (Lo Tartaro et al.). Improving vaccines design and vaccination strategy could derive from: 1) studies based on vaccinome approach leading to identification of antigenic epitopes selected from in-silico models of immune response prediction and to design a multi-epitope subunit vaccine (Khan et al.); 2) investigation of hypo-responsiveness to infections and vaccination in patients characterized by chronic immune activation leading to CD4+ T cells lymphopenia (Wolday et al.).

Even if the enormous number of subjects infected with SAR-CoV-2 and/or vaccinated allowed to conduct most of SARS-CoV-2 related immunological studies on human samples, COVID-19 mouse models lead to identification of immunogenic peptides of Spike and nucleocapsid protein for CD4+ T cells by MHC II tetramers (Bricio-Moreno et al.). Moreover, these results paved the way to use COVID-19 mouse models to further investigate the features of adaptive T cells immune response for human translational applications.

In conclusion, this Research Topic, with a variety of articles, has provided novel insight on different aspects of the role T cells mediated immune response in case of COVID19 or SARS-CoV-2 vaccination, with promising outcomes and future perspectives. As Editors, we would like to thank all the contributing authors and the people in Frontiers in Immunology for their support and to give us the opportunity to manage this Research Topic.

Author contributions

LM: Writing – original draft. AM: Writing – original draft. SB: Writing – original draft.

Conflict of interest

The authors declare that the research was conducted in the absence of any commercial or financial relationships that could be construed as a potential conflict of interest.

The author(s) declared that they were an editorial board member of Frontiers, at the time of submission. This had no impact on the peer review process and the final decision.

Publisher's note

All claims expressed in this article are solely those of the authors and do not necessarily represent those of their affiliated organizations, or those of the publisher, the editors and the reviewers. Any product that may be evaluated in this article, or claim that may be made by its manufacturer, is not guaranteed or endorsed by the publisher.

frontiers in Immunology

MINI REVIEW
published: 17 June 2021
doi: 10.3389/fimmu.2021.693269

Chronic Immune Activation and CD4$^+$ T Cell Lymphopenia in Healthy African Individuals: Perspectives for SARS-CoV-2 Vaccine Efficacy

Dawit Wolday[1*], *Francis M. Ndungu*[2], *Gloria P. Gómez-Pérez*[3] *and Tobias F. Rinke de Wit*[3,4]

[1] Department of Medicine, Mekelle University College of Health Sciences, Mekelle, Ethiopia, [2] Department of Global Health, Kenyan Medical Research Institute (KEMRI) – Wellcome Research Programme, Nairobi, Kenya, [3] Amsterdam Institute of Global Health and Development, Department of Global Health, Amsterdam University, Amsterdam, Netherlands, [4] Joep-Lange Institute, Amsterdam, Netherlands

OPEN ACCESS

Edited by:
Sara De Biasi,
University of Modena and Reggio Emilia, Italy

Reviewed by:
Henrique Borges da Silva,
Mayo Clinic Arizona, United States
Francesco Nicoli,
University of Ferrara, Italy

***Correspondence:**
Dawit Wolday
dawwol@gmail.com;
dawit.wolday@mu.edu.et

Specialty section:
This article was submitted to T Cell Biology, a section of the journal Frontiers in Immunology

Received: 10 April 2021
Accepted: 04 June 2021
Published: 17 June 2021

Citation:
Wolday D, Ndungu FM, Gómez-Pérez GP and de Wit TFR (2021) Chronic Immune Activation and CD4$^+$ T Cell Lymphopenia in Healthy African Individuals: Perspectives for SARS-CoV-2 Vaccine Efficacy. Front. Immunol. 12:693269. doi: 10.3389/fimmu.2021.693269

Chronic immune activation has been considered as the driving force for CD4$^+$ T cell depletion in people infected with HIV-1. Interestingly, the normal immune profile of adult HIV-negative individuals living in Africa also exhibit chronic immune activation, reminiscent of that observed in HIV-1 infected individuals. It is characterized by increased levels of soluble immune activation markers, such as the cytokines interleukin (IL)-4, IL-10, TNF-α, and cellular activation markers including HLA-DR, CD-38, CCR5, coupled with reduced naïve and increased memory cells in CD4$^+$ and CD8$^+$ subsets. In addition, it is accompanied by low CD4$^+$ T cell counts when compared to Europeans. There is also evidence that mononuclear cells from African infants secrete less innate cytokines than South and North Americans and Europeans *in vitro*. Chronic immune activation in Africans is linked to environmental factors such as parasitic infections and could be responsible for previously observed immune hypo-responsiveness to infections and vaccines. It is unclear whether the immunogenicity and effectiveness of anti-SARS-CoV-2 vaccines will also be reduced by similar mechanisms. A review of studies investigating this phenomenon is urgently required as they should inform the design and delivery for vaccines to be used in African populations.

Keywords: Africa, chronic immune activation, SARS-CoV-2, vaccine, hyporesponsiveness, COVID-19, helminths

INTRODUCTION

CD4$^+$ T cells play a pivotal role in the regulation of the immune system, protecting the host against various pathogens and autoimmunity (1). CD4$^+$ T cells modulate the immune response by orchestrating responses of B-cells, CD8$^+$ T cells and other components of the immune system. To do so, CD4$^+$ T cells, also designated as T-helper (TH) cells, branch into five major subsets: TH1, TH2, TH17, follicular T helper (TFH) and regulatory T cells (Treg) CD4$^+$ T cells (1). These different subsets of TH cells are differentiated by the expression of different lineage markers and transcription factors as well as the production of different cytokines. TH1 subsets express transcription factor T-

bet, produce interferon (IFN)-γ, and they exert effector function against intracellular microorganisms, such as mycobacteria and viruses; TH2 subsets express transcription factor GATA-3, produce the cytokines interleukin (IL)-4, IL-5, IL-6, IL-13, and they exert effector function against extracellular organisms, such as helminths; TH17 subsets express transcription factor RORγT, produce IL-17, as well as IL-22, and they exert effector function against intracellular organisms, such as bacteria and fungi; TFH $CD4^+$ T cells express transcription factor Bcl6, produce IL-21 and their effector function is to help B-cells produce immunoglobulins; Tregs express FoxP3 transcription factor, produce the cytokines IL-10 and transformation growth factor (TGF)-β, and their effector functions include immune homeostasis (1). Tregs propitiate an adequate immune response by helping in the recruitment of T cells, facilitating the removal of pathogens and preventing excessive tissue damage; hence they are critical in the prevention of autoimmunity and other forms of immune dysregulation (2). The differentiation of $CD4^+$ T cells into the various subsets described above is highly dependent on the prevailing cytokine environment (1). Notably, dysregulation in $CD4^+$ T cell immune responses may result in failure to protect the host from an infection or can lead to autoimmunity.

Previous reports showed that chronic immune activation is linked to the pathogenesis of $CD4^+$ T cell lymphopenia in patients with HIV-1 infection (3). Moreover, the background immune profile of adult HIV-negative individuals living in Africa demonstrate a phenomenon of chronic immune activation, reminiscent of that observed in HIV-1 infected individuals. Here, we reviewed the potential influence of chronic immune activation or immune dysregulation and low $CD4^+$ T cell count background against pathogens and vaccines on individuals residing in Africa. In addition, we discuss the potential role of altered immune responses that may impact on SARS-CoV-2 vaccine efficacy.

CHRONIC IMMUNE DYSREGULATION IN AFRICANS

Systemic persistent immune activation has been considered as the driving force of $CD4^+$ T cell depletion in people infected with HIV-1 (3). More importantly, effective antiretroviral therapy (ART) and suppressed HIV-1 viremia, appears not to reduce the accompanying chronic immune activation in these patients (3). One of the mechanisms leading to systemic chronic immune activation in HIV-1 infected patients has been ascribed to HIV-driven dysbiosis of the gut microbiota and microbial translocation into the blood stream (4–7). Interestingly, the immune profile of adult HIV-negative individuals living in Africa exhibit chronic immune activation, reminiscent of that observed in HIV-1 infected individuals (8–17). In addition, chronic immune activation in these apparently healthy individuals of African origin is accompanied by significantly lower $CD4^+$ T cell counts and CD4/CD8 ratio when compared to Europeans (8–23).

Such a skewed immune background profile of the African population may have a "double-edged sword" outcomes when the host encounters another pathogen or when administered a vaccine. Whereas chronic immune activation with skewed TH2 and Treg background may increase risk of infections, in particular for responses that depend on TH1 immune responses, it may provide protection against chronic inflammatory conditions, such as allergy or autoimmunity. In the same token, chronic immune activation may reduce the potential efficacy of vaccines, including those targeted against SARS-CoV-2 infection. The immune profile of apparently healthy and HIV-negative Africans is characterized by increased levels of soluble and cellular markers for chronic immune activation. Soluble immune activation markers consisted of elevated levels of IgE, IgG, placental isoferritin and p75 soluble tumor necrosis factor (TNF) receptor (8). In addition to increased eosinophilia, the expressions of HLA-DR, CD38, CD28, CCR5, Ki67 in $CD4^+$ as well as $CD8^+$ T cell subsets among Africans is significantly higher when compared to Europeans (8–17). Reduction in $CD4^+$ and $CD8^+$ naïve T cells, whereas increase in $CD4^+$ and $CD8^+$ memory T cells, as well as increase in CCR5 expression were observed in these population. The background profile is also characterized by predominant TH2 and Treg immune response (9), and marked increase in lymphocyte apoptosis (10). In addition, chronic immune activation in apparently healthy individuals residing in Africa is accompanied by $CD4^+$ T cell counts that are significantly lower when compared to Europeans (8–23). For example, absolute $CD4^+$ T cell count among adult healthy Ethiopians is around 700 cells/μL on average as compared to around 1,100 cells/μL among the Dutch population or Israelis (9–17).

UNDERLYING CAUSES OF IMMUNE DYSREGULATION IN AFRICANS

The reason for observed chronic immune activation, low $CD4^+$ T cell count and inverted CD4/CD8 ratio in the African population remains poorly understood. Nonetheless, we noted that it is not genetic in origin, but something that is acquired during life (9, 15, 17). Earlier, we studied changes in T-cell receptor excision circles (TRECs), HLA-DR and CD31 expression on $CD4^+$ T cells and T-cell telomere lengths with age in healthy Ethiopian and Dutch individuals. At birth, $CD4^+$ naïve T cell numbers and TREC contents in Ethiopians were found to be comparable to those in Dutch neonates (17). At very young age, however, both $CD4^+$ naïve T cell numbers and TREC contents fell dramatically in Ethiopians, but not in Dutch children. These differences between Ethiopian and Dutch individuals remained persistently into adulthood, because $CD4^+$ naïve T cell numbers and TREC contents decreased at similar rates with age in Ethiopian and Dutch individuals (13, 17). In addition, telomere lengths in Ethiopian individuals tended to be shorter than the Dutch counterparts (17). Though the changes we observed in $CD4^+$ T cell counts and their activation status occurred at earlier ages in life, as early as five years,

TABLE 1 | Summary of the helminth-induced hyporesponsive immune responses to heterologous infections and vaccines.

Impact on target disease	Co-infection	Effects on immune system	Outcomes	References
Infectious diseases:				
TB	Helminths	↓ $CD3^+$, $CD4^+$, $CD8^+$, NK, $CD4^+CD25^{high}$ T cell subsets ↑ Tregs ↓ IFN-γ ↑ IL-10 ↑ IL-5 ↑ eosinophilia ↓ mycobacteria-specific B-cell responses ↑ arginase-1-expressing macrophages in the lung, type 2 granulomas	↑ susceptibility/ progression Persistent MTB infection Protracted TB clinical course ↓ sputum smear positivity for acid fast bacilli ↑ lung inflammation	(40–45)
Hepatitis C virus	*S. mansoni*	↑ $GrzB^+$ Tregs ↓ hepatitis C virus-induced antiviral immunity	↑ hepatitis C viral load, transaminases ↑ circulating levels of hepatitis C virus NS4 protein and extracellular-matrix deposition ↑ aggravated liver disease	(46, 47)
HIV-1	Helminths	↓ $CD4^+$ T cell counts ↑ CCR5 and CXCR4 expression in $CD4^+$ T cells	↑ disease progression ↑ HIV-1 viral load ↑ HIV-1 acquisition	(48–51)
Vaccines:				
Tetanus toxoid	*S. mansoni*	↓ tetanus toxoid-specific TH1 responses (IFN-γ) ↑TH2 responses (IL-4)	↓ vaccine efficacy	(52)
Malaria	Helminths	↓ lymphoproliferation ↓ IFN-γ responses	↓ vaccine efficacy	(53)
BCG	Helminths	↓ lymphoproliferation ↓ IFN-γ responses ↓ IFN-γ response among children sensitized *in utero*	↓ vaccine efficacy ↓ vaccine efficacy in prenatally sensitized children	(53, 54)
Hepatitis B	*S. mansoni*	↓ anti-hepatitis-B surface antibody titers	↓ vaccine efficacy	(55)
Cholera	Helminths	↓fecal and serum IgA immune responses to the B subunit of cholera toxin	↓vaccine efficacy	(56)
Pneumococcal	Helminth	↓ opsonization *S. pneumoniae*	↓ vaccine efficacy	(57)
H1N1 influenza A	Helminth	↓ anti-H1N1 antobody titers ↑ IL-10-dependent type 1 Tregs	↓ vaccine efficacy	(58)
Malaria vaccine candidate	*T. trichiura*	↓ antibody response to GMZ2 malaria vaccine candidate	↓ vaccine efficacy	(59)
HIV vaccine candidate	*S. mansoni*	↓ HIV-specific cellular responses ↓ Env-specific antibody responses	↓ vaccine efficacy	(60)
Antihelminthic therapy:				
BCG or TB disease + HIV	Helminth	↓ $CD4^+$ $FoxP3^+$ T cells (Tregs) ↑ MTB-specific TH1 immunity ↓ eosinophilia ↓ IL-10	↓ disease severity ↑ vaccine efficacy ↑ clinical improvement	(43, 61–63)
pRBC	Helminth	↑ proinflamatory cytokines ↓ expression of CTLA-4 on $CD4^+$ T cells	↑ vaccine efficacy	(61)
Cholera vaccine	*A.lumbricoides*	↑ serum vibriocidal antibody titers	↑ vaccine efficacy	(63)
HIV-1	Helminths	↑ in $CD4^+$ T cell counts	↓ HIV-1 viral load ↓ HIV disease progression	(48, 49, 64, 65)
HIV vaccine Candidate	*S. mansoni*	↑ HIV-specific cellular response	↑ vaccine efficacy	(60)

CTLA, cytotoxic T lymphocyte-associated antigen 4; IFN, interferon; IL, interleukin; pRBC, Plasmodium falciparum-infected red blood cells; TB, tuberculosis; MTB, Mycobacterium tuberculosis; TH, T helper cells; Tregs, regulatory T cells.

adolescence and middle-aged adults, these changes appear to be reminiscent of immunosenescence (24). This state of dysregulated immune response associated with older age later during life is characterized by a chronic low-level inflammation (also known as "inflammaging") and a decline of the immune system function (24).

These findings showing that immune activation increased with increasing age strengthen the notion that that external/ environmental factors play significant role in inducing chronic immune activation (9). In addition, Ethiopian migrants to Israel who stayed longer period of time (> 5 years) indeed exhibited reversal in terms of increased $CD4^+$ T cell counts and CD4/CD8 ratio as well as reduction in chronic immune activation (8, 10). Increased activation-induced lymphocyte apoptosis could be also one of the underlying mechanisms leading to the observed low $CD4^+$ T cell among the Ethiopian population (10). In addition, tuberculosis (TB) patients have been shown to exhibit T cell immune activation (25), and hence latent TB, highly prevalent in

Africa (26), may drive immune activation in this population. The role of viral infections, such as hepatitis C virus (HCV), cytomegalovirus and Epstein-Barr virus, in inducing immune activation in Africans remains unknown.

Among the environmental factors that drive immune activation in Africa is infection by parasites, in particular helminths. An estimated 2 billion of the world's population is infected with helminth parasites (27). Chronic helminthic infections are often associated with the development of TH2-biased and alternatively activated macrophages (M2) and type 2 innate lymphoid cells (2, 28). These responses are accompanied with the induction of cytokines such as IL-4, IL-5, IL-13, and increased eosinophilia, IgE as well as goblet cell hyperplasia. Whereas the TH2-skewed immune responses are important in controlling helminthic infections, they are also considered to play an important role in the repair of tissue damage as a result of helminth infections (2, 28). Besides inducing TH2 immune responses, helminths also induce a strong regulatory networks, characterized by the induction of Tregs (2, 28). The induction of Tregs enhances survival and persistence of helminths within their host, and concomitantly may affect responses to heterologous infection, antigen, or vaccine. Indeed, several reports have demonstrated that infection by intestinal helminth is associated with chronic immune activation (8, 10, 12, 16, 29, 30). Interestingly, deworming resulted in reversal of immune activation, characterized by decreased eosinophilia, reduced expressions of HLA-DR, increased naïve cells and reduced memory cells (8, 10, 12, 16). Similar to infection with HIV-1, helminths also can cause microbial translocation (31–33), that may eventually lead to systemic chronic immune activation. Furthermore, profound $CD4^+$ T lymphopenia and immune activation in the absence of HIV-1 infection among patients with malaria has been demonstrated (34, 35). The more severe form of *P. falciparum* resulted in significantly higher $CD4^+$ T cell reduction or immune activation than the milder form of *P. vivax* (34, 35). Given the fact that $CD4^+$ T cell count was determined from the peripheral blood, however, we assume that this was due to lymphocyte redistribution rather than direct $CD4^+$ T cell death. We assume that macrophages engulf red blood cells laden with malarial parasites and migrate to the spleen or liver and TH1 cells are then redistributed from the periphery to these organs to activate the intracellular killing mechanism of the macrophage.

In addition to helminths, socio-demographic factors may influence $CD4^+$ T cell counts. $CD4^+$ T cell counts were independently and positively associated with female gender, cigarette smoking and khat (*Catha Edulis*) chewing (21). However, there is paucity of data with regard to the effect of diet on $CD4^+$ T cell count differences among populations. We and others reported previously that body mass index was positively correlated with $CD4^+$ T cell counts (21, 36). In addition, HIV-negative children with malnutrition from Uganda exhibited lower CD4% when compared to non-malnourished children (37). Increased exposure to ultraviolet light during summer has been reported to decrease $CD4^+$ T cell counts among Europeans (38, 39). Overall, differences in $CD4^+$ T cell counts between populations may be attributed to differences in diet, genetic, ethnicity, gender, residence, altitude, methods used to enumerate the cells and other yet unidentified factors.

EFFECTS OF CHRONIC IMMUNE ACTIVATION ON IMMUNE RESPONSE TO OTHER INFECTIONS OR VACCINES

Systemic chronic immune activation may potentially be detrimental to the host. Notably, T cell hyporesponsiveness induced by helminths may result in increased susceptibility to infections, or reduced responses to vaccines (**Table 1**). Several studies have demonstrated that co-infection with helminths is associated with increased susceptibility to heterologous infections. For example, concomitant infection with helminths in patients with TB results in a plethora of immune responses with unfavorable clinical outcomes (40–42). Helminths-driven immune modulation in these conditions included reduced $CD3^+$, $CD4^+$, $CD8^+$, natural killer (NK), $CD4^+CD25^{high}$ and IFN-γ responses, but increased eosinophilia, Tregs, IL-4, IL-5 and IL-10 responses. Notably, individuals with latent TB infection co-infected with helminths had lower frequency of $CD4^+IFN\text{-}\gamma^+$ T cells and increased in $CD4^+FoxP3^+$ T cells (Tregs) compared to those without helminth co-infection (43). Although protective immunity against TB is considered to be dependent on cellular immune responses, mycobacteria-specific humoral immune responses have been proposed to play an important role in protection. However, co-infection with *Strongloides stercoralis* has been shown to reduce mycobacteria-specific B-cell responses (44). Unfavorable consequences include increased susceptibility to TB, persistence in *Mycobacterium tuberculosis* as well as more protracted TB disease course. In addition, studies conducting in experimental animal models demonstrated that helminth co-infection induced expression of arginase-1 by macrophages within the lung tissue resulting in enhanced inflammation and disease severity (45).

Several reports have also showed that co-infection with helminths can attenuate immune response to important viruses with negative outcomes. For example, HCV patients co-infected with the helminth *Schistosoma mansoni* showed significantly increased $GrzB^+$ Treg response, indicating reduced HCV-induced TH1 and attenuated antiviral immunity (46, 47). In these patients, helminth co-infection led to aggravated HCV-related liver disease characterized by significantly elevated HCV load and transaminases when compared to patients infected with HCV only. Previous studies undertaken by us and others demonstrated that co-infection with helminths correlated with much lower $CD4^+$ T cell counts and significantly higher HIV-1 viral load compared to those without helminth coinfection (48–50), and plasma HIV-1 viral load strongly correlated to the intensity of helminth infection (48). In addition, a recent systemic review reported that co-infection with schistosomes increased the risk of HIV-1 acquisition by 4-fold, through

mechanisms involving increased expression of CCR5 and CXCR4 HIV-1 co-receptors on $CD4^+$ T cells and cervical mucosa lesions (51).

Likewise, several earlier reports showed that helminth-induced chronic immune activation leads to a significant negative effect on vaccine efficacy. Whereas tetanus toxoid-specific TH1 (IFN-γ) immune responses were significantly attenuated in individuals with *S. mansoni* infection, TH2 (IL-2) responses were significantly increased (52). Children infected with helminths showed significant reduction in lymphoproliferative responses to *Plasmodium falciparum*-infected red blood cells (pRBC) and BCG compared to those without helminths (53). Notably, both lymphoproliferative and IFN-γ responses were significantly increased upon $CD4^+CD425^{high}$ T cell depletion, indicating that Tregs modulate helminth-driven immune responses to mycobacterial and malarial antigens. Children infected with the helminth *S. mansoni* when given hepatitis B vaccine showed significantly reduced hepatitis B virus surface antibody (anti-HBs) titers compared to helminth uninfected children (55). Similarly, patients with cholera co-infected with helminths had reduced fecal and serum IgA immune responses to the B subunit of cholera toxin (CTB) when compared to those without helminth co-infection (56). Interestingly, prenatal sensitization *in utero* has also been reported to reduce vaccine efficacy. Children of helminth-infected mothers showed significantly lower IFN-γ responses to the mycobacterial antigen – purified protein derivative (PPD) following vaccination with BCG compared to children of helminth uninfected mothers (54). Similarly, other investigators also demonstrated using animal experiments that helminths attenuated vaccine efficacy. Administration of pneumococcal vaccine to mice chronically infected with helminths was impaired due to failure to opsonize effectively *S. pneumonia* for killing by alveolar macrophages (57). In another recent study, helminth infection was reported to suppress the efficacy of vaccination against seasonal influenza (58). Helminth-infected mice had reduced quantity and neutralizing quality of antibody responses following vaccination with H1N1 influenza A virus, and attenuated vaccine efficacy was accompanied with increased levels of IL-10-dependent type 1 Tregs. Other investigators have reported similar reduced responses to vaccine candidates among individuals infected with helminths. A study (59) demonstrated that antibody responses to a blood stage malaria vaccine candidate GMZ2 was significantly lower in *Trichuris trichiura* infected children when compared to the antibody responses among parasite negative controls. Using an animal experimental model (60), it was shown that *S. mansoni* infected mice had significantly lower HIV-1-specific immune responses after prime-boost vaccination with DNA+MVA, or MVA+gp120 compared to uninfected control mice. In addition, gp140 Env-specific antibody responses were significantly in *S. mansoni* infected mice compared to controls.

Notably, anthelminthic treatment led to improved immune responses. For example, there was a decrease in the frequency of Treg cells accompanied with increased $CD4^+$IFN-γ^+ T cells after anthelmintic treatment of individuals with latent TB infection (43). In addition, cell-mediated immune responses to mycobacterial antigens following BCG immunization improved significantly among those who received anthelminthic therapy before vaccination when compared to controls (61–63). Deworming also can lead to improved antimalarial immune responses (61). Similarly, albendazole treatment of children infected with ascariasis enhanced the vibriocidal antibody response to live attenuated oral cholera vaccine (66). In addition, deworming resulted in increased $CD4^+$ T cell counts, or reduced viral load in HIV-infected patients (48, 49, 64, 65), and increased HIV-1-specific cellular immune responses to HIV-1 vaccine candidate (60).

Exposure to specific microbial antigens has been shown to induce a sustained epigenetic alteration in innate immunity [reviewed in (67)]. Such alterations result in an enhanced immune response to a repeat challenge by the same antigen, or to heterologous one. This phenomenon is termed as "trained immunity". The concept of trained immunity was originally discovered in studies involving BCG vaccine (67). The studies have provided evidence that BCG-induced trained immunity can protect against multitude of diseases, including respiratory infections and cancer. The concept of trained immunity is, however, in contrast to helminth-induced hyporesponsiveness described in the earlier sections of this review.

CHRONIC IMMUNE ACTIVATION IN AFRICANS AND COVID-19

COVID-19 patients, like those infected with HIV-1, exhibit also lymphopenia (68). Will low baseline $CD4^+$ T cell counts among African individuals increase risk of COVID-19 severity? Though this remains to be elucidated, we hypothesize that this is not the case. We base this on the observations we made showing that 74% of all SARS-CoV-2 infections are asymptomatic and only 4.4% present with severe COVID-19 (69). Furthermore, parasites indeed appear to protect against severe COVID-19 (70), by counteracting against excessive TH1-induced hyperinflammation (71).

Similarly, despite low baseline $CD4^+$ T cell counts and background chronic immune activation, earlier studies we conducted in Ethiopia showed that disease progression among HIV-1 infected patients was not accelerated (72). Indeed, it was similar when compared to their counterparts from Dutch who had relatively higher baseline $CD4^+$ T cell count and very little immune activation. The rate of average $CD4^+$ T cell count decline, in the absence of antiretroviral therapy, was around 36 and 66 cells/year in the Ethiopians and the Dutch, respectively (72). The findings suggested that the rate of $CD4^+$ T cell decline was the most important factor associated with disease progression rather than baseline $CD4^+$ T cell count. The proportion of proliferating Ki67+ cells within the naïve and memory $CD4^+$ T cell subsets were lower in HIV-infected Ethiopians compared to Dutch HIV-infected patients matched for $CD4^+$ T-cell count (17). Thus, the slower $CD4^+$ T cell decline

in HIV-infected Ethiopians might be explained by lower levels of proliferation.

Taken these observations, the important question is whether underlying chronic immune activation among Africans will impact on vaccine efficacies for SARS-CoV-2. Response to existing vaccines, such as BCG, yellow fever, rotavirus, polio, tetanus, influenza (73–76), as well as to candidate vaccines, such as for TB, malaria, Ebola and HIV-1, are lower when compared to responses in individuals in the northern hemisphere (77–80). Though the lower responses exhibited to the vaccines in the LMICs was observed irrespective of helminth status in the countries investigated, it is considered that co-infection with helminths is highly significant (81–83). Therefore, it is tempting to speculate that we might see similar reduced vaccine efficacies for SARS-COV-2 in LMICs (**Figure 1**). This notion is supported by a study that revealed Gabonese children living in rural areas with high incidence of helminth infection exhibited reduced anti-H1N1 and anti-B responses to a seasonal influenza vaccine compared to children living in semi-urban areas with lower incidence for helminth infection (83). Moreover, reduced vaccine efficacy has already been reported for various SARS-CoV-2 vaccines against the 'South African variant', B.1.351 (84). This reduction in efficacy was attributed to the specific B.1.351 mutations, particularly in the Spike-protein. However, the alternative explanation could be that the immune system of South African vaccine trial participants is skewed towards TH2, hyperactivated with low $CD4^+$ T cells and therefore show less stimulation by SARS-CoV-2 vaccines.

In conclusion, studies are needed to evaluate the various factors that could potentially determine a reduced SARS-CoV-2 vaccine efficacy in Africa (85). These include both the effects of underlying immune activation status as described above as well as the influence of certain SARS-CoV-2 mutations. The current COVAX efforts in Africa will provide ample opportunities to evaluate these factors and findings should feed into COVAX vaccine distribution policies. Despite growing vaccine hesitancy in Africa, the roll-out of COVAX remains decisively important to avoid a situation of many years of persistence of significant SARS-CoV-2 outbreaks on the continent. Such events, particularly in immunocompromised individuals can lead to the emergence of new variants that could spread elsewhere in the world. The first evidence of such events is accumulating with a variant from Central Africa transmitting into Europe (86).

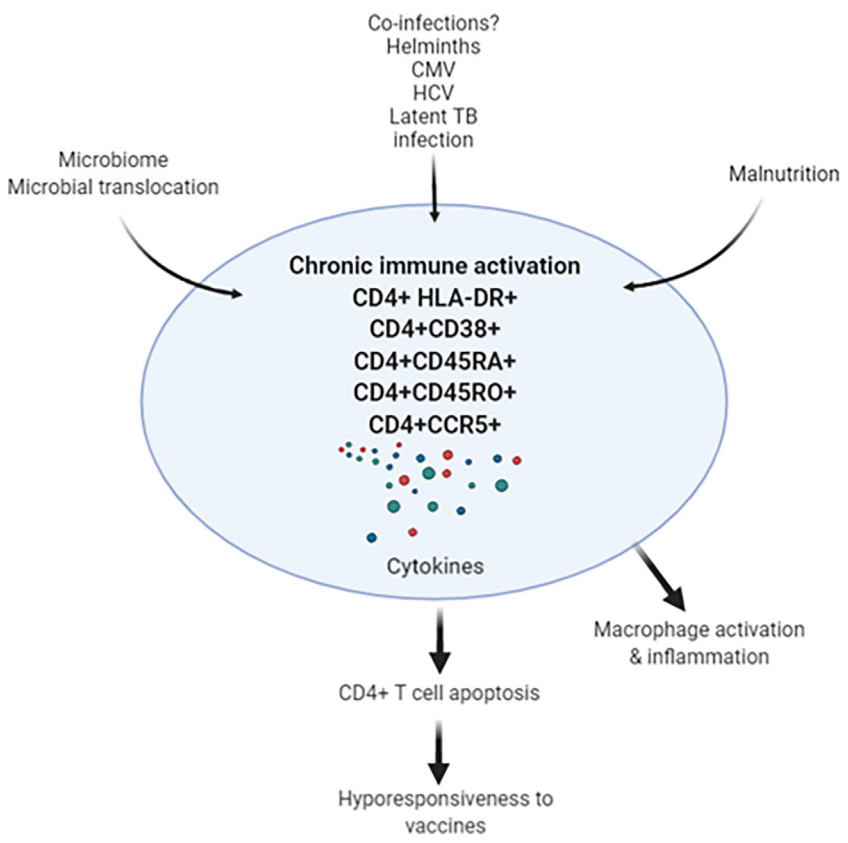


FIGURE 1 | Chronic immune activation in apparently health Africans may be related to leaky gut, co-infections (such as helminths, CMV, HCV and latent TB infection) results in activation-induced $CD4^+$ T cell apoptosis. In turn, depletion of $CD4^+$ T cells may result in decreased response to SARS-CoV-2 vaccine in the African population. CMV, cytomegalovirus; HCV, hepatitis C virus; TB, tuberculosis.

For all of the above reasons, we recommend that roll-out of COVAX and its potential reduced effectiveness due to different immune system backgrounds is proactively accompanied thorough information campaigns that involve African communities (87). Such campaigns should put into perspective the negative connotations that could be associated with the potential finding of generally reduced SARS-CoV-2 vaccine efficacy in African populations. Finally, we strongly recommend that highly prevalent infections, as the ones discussed in this manuscript, should be controlled for in future vaccine trials, not only for SARS-CoV-2 infection, to assess the real magnitude of the impact of these conditions on vaccine efficacy, to guide the design of African-tailored vaccines if needed. Eventually, an approach could emerge that involves the message: first deworm, then vaccinate.

AUTHOR CONTRIBUTIONS

DW and TR conceived the idea and drafted the review. All authors contributed to the article and approved the submitted version.

FUNDING

This work was supported by the European and Developing Countries Clinical Trials Partnership (EDCTP) - European Commission (Project ID: RIA2020EF-2905), The Hague, The Netherlands and the Joep Lange Institute for Global Health and Development, Amsterdam, The Netherlands.

REFERENCES

1. Zhu X, Zhu J. Cd4 T Helper Cell Subsets and Related Human Immunological Disorders. *Int J Mol Sci* (2020) 21:8011–37. doi: 10.3390/ijms21218011
2. White MPJ, McManus CM, Maizels RM. Regulatory T-cells in Helminth Infection: Induction, Function and Therapeutic Potential. *Immunol* (2020) 160:248–60. doi: 10.1111/imm.13190
3. Paiardini M, Müller-Trutwin M. HIV-Associated Chronic Immune Activation. *Immunol Rev* (2014) 254:78–101. doi: 10.1111/imr.12079
4. Kroeze S, Ondoa P, Kityo CM, Siwale M, Akanmu S, Wellington M, et al. Suboptimal Immune Recovery During Antiretroviral Therapy With Sustained HIV Suppression in sub-Saharan Africa. *AIDS* (2018) 32):1043–51. doi: 10.1097/QAD.0000000000001801
5. Dillon SM, Lee EJ, Kotter CV, Austin GL, Dong Z, Hecht DK, et al. An Altered Intestinal Mucosal Microbiome in HIV-1 Infection is Associated With Mucosal and Systemic Immune Activation and Endotoxemia. *Mucosal Immunol* (2014) 7:983–94. doi: 10.1038/mi.2013.116
6. Gootenberg DB, Paer JM, Luevano JM, Kwon DS. HIV-Associated Changes in the Enteric Microbial Community: Potential Role in Loss of Homeostasis and Development of Systemic Inflammation. *Cur Opin Infect Dis* (2017) 30:31–43. doi: 10.1097/QCO.0000000000000341
7. Brenchley JM, Price DA, Schacker TW, Asher TE, Silvestri G, Rao S, et al. Microbial Translocation is a Cause of Systemic Immune Activation in Chronic HIV Infection. *Nat Med* (2006) 12:1365–71. doi: 10.1038/nm1511
8. Bentwich Z, weisman Z, Moroz C, Bar-Yehuda S, Kalinkovich A. Immune Dysregulation to Ethiopian Immigrants in Israel: Relevance to Helminth Infections? *Clin Exp Immunol* (1996) 103:239–43. doi: 10.1046/j.1365-2249.1996.d01-612.x
9. Clerici M, Butto S, Lukwiya M, Sarasella M. Immune Activation in Africa is Environmentally-Driven and is Associated With Upregulation of CCR5. *AIDS* (2000) 14:2083–92. doi: 10.1097/00002030-200009290-00003
10. Kalinkovich A, Weisman Z, Greenberg Z, Nahmias J, Eitan S, Stein M, et al. Decreased CD4 and Increased CD8 Counts With T Cell Activation is Associated With Chronic Helminth Infection. *Clin Exp Immunol* (1998) 114:414–21. doi: 10.1046/j.1365-2249.1998.00736.x
11. Messele T, Abdulkadir M, Fontanet A, Petros B, Hamann D, Koot M, et al. Reduced Naive and Increased Activated CD4 and CD8 Cells in Healthy Adult Ethiopians Compared With Their Dutch Counterparts. *Clin Exp Immunol* (1999) 115:443–50. doi: 10.1046/j.1365-2249.1999.00815.x
12. Borkow G, Leng Q, Weisman Z, Stein M, Galai N, Kalinkovich A, et al. Chronic Immune Activation Associated With Intestinal Helminth Infections Results in Impaired Signal Transduction and Anergy. *J Clin Invest* (2000) 106:1053–60. doi: 10.1172/JCI10182
13. Hazenberg MD, Otto SA, Cohen Stuart JW, Verschuren MC, Borleffs JC, Boucher CA, et al. Increased Cell Division But Not Thymic Dysfunction Rapidly Affects the T-cell Receptor Excision Circle Content of the Naive T Cell Population in HIV-1 Infection. *Nat Med* (2000) 6:1036–42. doi: 10.1038/79549
14. Kassu A, Tsegaye A, Petros B, Wolday D, Roos MTL, Hamann D, et al. Distribution of Lymphocyte Subsets in Healthy HIV-negative Adult Ethiopians From Different Geographical Locales. *Clin Diagn Lab Immunol* (2001) 8:1171–6. doi: 10.1128/CDLI.8.6.1171-1176.2001
15. Tsegaye A, Wolday D, Otto S, Petros B, Assefa T, Alebachew T, et al. Immunophenotyping of Blood Lymphocytes at Birth, During Childhood, and During Adulthood in HIV-1-uninfected Ethiopians. *Clin Immunol* (2003) 109:338–46. doi: 10.1016/j.clim.2003.08.008
16. Kassu A, Tsegaye A, Wolday D, Petros B, Aklilu M, Sanders EJ, et al. Role of Incident and/or Cured Intestinal Parasitic Infections on Profile of CD4+ and CD8+ T Cell Subsets and Activation Status in HIV-infected and Uninfected Adult Ethiopians. *Clin Exp Immunol* (2003) 132:113–9. doi: 10.1046/j.1365-2249.2003.02106.x
17. Vrisekoop N. Immune Abnormalities in Healthy Ethiopians are Induced by Chronic Immune Activation and Start at Early Age. PhD Thesis. The Netherlands: Utrecht University (2007) p. 48–73.
18. Pollack S, Fuad B, Etzioni A. Cd4 T-lymphopenia Without Opportunistic Infections in HIV-seronegative Ethiopian Immigrants to Israel. *Lancet* (1993) 342:50–1. doi: 10.1016/0140-6736(93)91912-6
19. Tsegaye A, Messele T, Tilahun T, Hailu E, Sahlu T, Doorly R, et al. Immunohematological Reference Ranges for Adult Ethiopians. *Clin Diag Lab Immunol* (1999) 6:410–4. doi: 10.1128/CDLI.6.3.410-414.1999
20. Kassa E, Rinke de Wit TF, Hailu E, Girma M, Messele T, Mariam HG, et al. Evaluation of the World Health Organization Staging System for HIV Infection and Disease in Ethiopia: Association Between Clinical Stages and Laboratory Markers. *AIDS* (1999) 13:381–9. doi: 10.1097/00002030-199902250-00011
21. Abuye C, Tsegaye A, West CE, Versloot P, Sanders EJ, Wolday D, et al. Determinants of CD4 Counts Among HIV-negative Ethiopians: Role of Body Mass Index, Gender, Cigarette Smoking, Khat (*Catha Edulis*) Chewing, and Possibly Altitude? *J Clin Immunol* (2005) 25:127–33. doi: 10.1007/s10875-005-2818-y
22. Karita E, Ketter N, Price MA, Kayitenkore K, kaleebu P, Nanvubya A, et al. CLSI-Derived Hematology and Biochemistry Reference Intervals for Healthy Adults in Eastern and Southern Africa. *PLoS One* (2009) 4:e4401. doi: 10.1371/journal.pone.0004401
23. Gize A, Mathewos B, Moges B, Workineh M, Gedefaw L. Establishment Normal Reference Intervals for CD3+, Cd4+, CD8+ and CD4/CD8 Ratio of T Lymphocytes in HIV-negative Adults From University of Gondar Hospital, North-west Ethiopia. *AIDS Res Treat* (2014) 2014:267450. doi: 10.1155/2014/267450
24. Herranz N, Gil J. Mechanisms and Functions of Cellular Senescence. *J Clin Invest* (2018) 128:1238–46. doi: 10.1172/JCI95148
25. Vanham G, Edmonds K, Qing L, Hom D, Toossi Z, Jones B, et al. Generalized Immune Activation in Pulmonary TB: Co-Activation With HIV Infection. *Clin Exp Immunol* (1996) 103:30–4. doi: 10.1046/j.1365-2249.1996.907600.x
26. Tegbaru B, Wolday D, Messele T, Legesse M, Mekonnen Y, Miedema F, et al. Tuberculin Skin Test Conversion and Reactivity Rates Among Adults With and Without Human Immunodeficiency Virus in Urban Settings in Ethiopia. *Clin Vaccine Immunol* (2006) 13:784–9. doi: 10.1128/CVI.00098-06

27. Herricks JR, Hotez PJ, Wanga V, Coffeng LE, Haagsma JA, Basáñez M-G, et al. The Global Burden of Disease Study 2013: What Does it Mean for the Ntds? *PloS Negl Trop Dis* (2017) 11:e0005424. doi: 10.1371/journal.pntd.0005424
28. Allen JE, Sutherland TE. Host Protective Roles of Type 2 Immunity: Parasite Killing and Tissue Repair, Flip Sides of the Same Coin. *Semin Immunol* (2014) 26:329–40. doi: 10.1016/j.smim.2014.06.003
29. Chachage M, Podola L, Clowes P, Nsojo A, bauer A, Mgaya O. Helminth-Associated Immune Activation and HIV Co-Receptor Expression. *PLoS Negl Trop Med* (2014) 8:e2755. doi: 10.1371/journal.pntd.0002755
30. Mkhize-Kwitshana ZL, Taylor MI, Jooste P, Walzl G. The Influence of Different Helminth Infection Phenotypes on Immune Responses Against HIV in Co-Infected Adults in South Africa. *BMC Infect Dis* (2011) 11:273–84. doi: 10.1186/1471-2334-11-273
31. Onguru D, Liang Y, Griffith Q, Nikolajczyk B, Mwinzi P, Ganley-Leal L. Human Schistosomiasis is Associated With Endotoxemia and Toll-like Receptor 2- and 4-Bearing B Cells. *Am J Trop Med Hyg* (2011) 84:321–4. doi: 10.4269/ajtmh.2011.10-0397
32. George PJ, Anuradha R, Kumar NP, Kumaraswani V, Nutman TB, Babu S. Evidence of Microbial Translocation Associated With Perturbations in T Cell and Antigen Presenting Cell Homeostasis in Hookworm Infections. *PLoS Negl Trop Dis* (2012) 6:e1830. doi: 10.1371/journal.pntd.0001830
33. Rajamanickam A, Munisankar S, Bhootra Y, Dolla C, Nutman TB, Babu S. Microbial Translocation Associated With an Acute-Phase Response and Elevations in MMP-1, Ho-1, and Proinflammatory Cytokines in *Strongyloides Stercoralis* Infection. *Infect Immun* (2017) 85:e00772–16. doi: 10.1128/IAI.00772-16
34. Kassa D, Petros B, Mesele T, Hailu E, Wolday D. Characterization of Peripheral Blood Lymphocyte Subsets in Patients With Acute Plasmodium Falciparum and P. Vivax Malaria Infections at Wonji Sugar Estate, Ethiopia. *Clin Vaccine Immunol* (2006) 13:376–9. doi: 10.1128/CVI.13.3.376-379.2006
35. Worku S, Bjorman A, Troye-Blomberg M, Jemaneh L, Farnert A, Christensson B. Lymphocyte Activation and Subset Redistribution in the Peripheral Blood in Acute Malaria Illness: Distinct γδ T Cell Patterns in *Plasmodium Falciparum* and *P. Vivax* Infections. *Clin Exp Immunol* (1997) 108:34–41. doi: 10.1046/j.1365-2249.1997.d01-981.x
36. Kam KM, Leung WL, Kwok MY, Hung MY, Lee SS, Mak WP. Lymphocyte Subpopulation Reference Ranges for Monitoring Human Immunodeficiency Virus-Infected Chinese Adults. *Clin Diagn Lab Immunol* (1996) 3:326–30. doi: 10.1128/cdli.3.3.326-330:1996
37. Bachou H, Tylleskär T, Downing R, Tumwine JK. Severe Malnutrition With and Without HIV-1 Infection in Hospitalised Children in Kampala, Uganda: Differences in Clinical Features, Haematological Findings and CD4+ Cell Counts. *Nutr J* (2006) 5:27–34. doi: 10.1186/1475-2891-5-27
38. Paglieroni TG, Holland PV. Circannual Variation in Lymphocyte Subsets, Revisited. *Transfusion* (1994) 34:512–624. doi: 10.1046/j.1537-2995.1994.34694295067.x
39. Falkenbach A, Sedlmeyer A. Travel to Sunny Countries is Associated With Changes in Immunological Parameters. *Photodermatol Photoimmunol Photomed* (1997) 13:139–42. doi: 10.1111/j.1600-0781.1997.tb00217.x
40. Resende Co T, Hirsch CS, Toossi Z, Dietze R, Ribeiro-Rodrigues R. Intestinal Helminth Co-Infection has a Negative Impact on Both Anti-*Mycobacterium TB* Immunity and Clinical Response to TB Therapy. *Clin Exp Immunol* (2007) 147:45–52. doi: 10.1111/j.1365-2249.2006.03247.x
41. Abate E, Belayneh M, Idh J, Diro E, Elias D, Britton S, et al. Asymptomatic Helminth Infection in Active TB is Associated With Increased Regulatory and Th-2 Responses and a Lower Sputum Smear Positivity. *PLoS Negl Trop Dis* (2015) 9:e0003994. doi: 10.1371/journal.pntd.0003994
42. Tristao-Sa R, Ribeiro-Rodrigues R, Johnson LT, Pereira FE, Dietze R. Intestinal Nematodes and Pulmonary TB. *Rev Soc Bras Med Trop* (2002) 35:533–5. doi: 10.1590/S0037-86822002000500020
43. Toulza F, Tsang L, Ottenhoff TH, Brown M, Dockrell HM. Mycobacterium Tuberculosis-Specific CD4+ T-Cell Response is Increased, and Treg Cells Decreased, in Anthelmintic-Treated Patients With Latent TB. *Eur J Immunol* (2016) 46:752–61. doi: 10.1002/eji.201545843
44. Anuradha R, Munisankar S, Bhootra Y, Dolla C, Kumaran P, Nutman TB, et al. Modulation of *Mycobacterium Tuberculosis*-Specific Humoral Immune Responses is Associated With *Strongyloides Stercoralis* Coinfection. *PLoS Negl Trop Dis* (2017) 11:e0005569. doi: 10.1371/journal.pntd.0005569
45. Monin L, Griffiths KL, Lam WY, Gopal R, Kang DD, Ahmed M, et al. Helminth-Induced Arginase-1 Exacerbates Lung Inflammation and Disease Severity in TB. *J Clin Invest* (2015) 125:4699–713. doi: 10.1172/JCI77378
46. Loffredo-Verde E, Abdel-Aziz I, Albrecht J, El-Guindy N, Yacob M, Solieman A, et al. Schistosome Infection Aggravates HCV-related Liver Disease and Induces Changes in the Regulatory T-cell Phenotype. *Parasit Immunol* (2015) 37:97–104. doi: 10.1111/pim.12171
47. Attallah AM, Abdallah SO, Albannan MS, Omran MM, Attallah AA, Farid K. Impact of Hepatitis C Virus/Schistosoma Mansoni Coinfection on the Circulating Levels of HCV-NS4 Protein and Extracellular-Matrix Deposition in Patients With Different Hepatic Fibrosis Stages. *Am J Trop Med Hyg* (2016) 95:1044–50. doi: 10.4269/ajtmh.16-0129
48. Wolday D, Gebremariam Z, Britton S, Galai N, Landay A, Bentwich Z. Treatment of Intestinal Worms is Associated With Decresed HIV Plasma Viral Load. *J Acquir Immune Defic Syndr* (2002) 31:56–62. doi: 10.1097/00126334-200209010-00008
49. Mulu A, Maier M, Liebert UG. Deworming of Intestinal Helminths Reduces HIV-1 Subtype C Viremia in Chronically Co-Infected Individuals. *Int J Infect Dis* (2013) 17:e897–901. doi: 10.1016/j/ijid.2013.03.022
50. Morawski BM, Yunus M, Kerukadho E, Turyasingura G, Barbra L, Ojok AM, et al. Hookworm Infection is Associated With Decreased CD4+ T Cell Counts in HIV-infected Adult Ugandans. *PLoS Negl Trop Dis* (2017) 11:e0005634. doi: 10.1371/journal.pntd.0005634
51. Furch BD, Koethe JR, Kayamba V, Heimburger DC, Kelly P. Interactions of *Schistosoma* and HIV in Sub-Saharan Africa: A Systematic Review. *Am J Trop Med Hyg* (2020) 102:711–8. doi: 10.4269/ajtmh.19-0494
52. Sabin EA, Araujo M, Carvalho EM, Pearce EJ. Impairment of Tetanus Toxoid-Specific Th1-like Immune Responses in Humans Infected With Schistosoma Mansoni. *J Infect Dis* (1996) 173:269–72. doi: 10.1093/infdis/173.1.269
53. Wammes LJ, Hamid F, Wiria AE, de Gier B, Sartono E, Maizels RM, et al. Regulatory T Cells in Human Geohelminth Infection Suppress Immune Responses to BCG and *Plasmodium Falciparum*. *Eur J Immunol* (2010) 40:437–42. doi: 10.1002/eji.200939699
54. Malhotra I, Mungai P, Wamachi A, Kioko J, Ouma JH, Kazura JW, et al. Helminth- and Bacillus Calmette-Guerin-induced Immunity in Children Sensitized In Utero to Filariasis and Schistosomiasis. *J Immunol* (1999) 162:6843–8.
55. Ghaffar YA, Kamel M, Abdel Wahab MF, Dorgham LS, Saleh MS, El Deeb AS. Hepatitis B Vaccination in Children Infected With *Schistosoma Mansoni*: Correlation With Ultrasonographic Data. *Am J Trop Med Hyg* (1990) 43:516–9. doi: 10.4269/ajtmh.1990.43.516
56. Harris JB, Podolsky MJ, Bhuiyan TR, Chowdhury F, Khan AI, Larocque RC, et al. Immunologic Responses to *Vibrio Cholerae* in Patients Co-Infected With Intestinal Parasites in Bangladesh. *PLoS Negl Trop Dis* (2009) 3:e403. doi: 10.1371/journal.pntd.0000403
57. Apiwattanakul N, Thomas PG, Iverson AR, McCullers JA. Chronic Helminth Infections Impair Pneumococcal Vaccine Responses. *Vaccine* (2014) 32:5405–10. doi: 10.1016/j.vaccine.2014.07.107
58. Hartmann W, Brunn ML, Stetter N, Gagliani N, Muscate F, Stanelle-Bertram S, et al. Helminth Infections Suppress the Efficacy of Vaccination Against Seasonal Influenza. *Cell Rep* (2019) 29:2243–56. doi: 10.1016/j.celrep.2019.10.051
59. Esen M, Mordmüller B, de Salazar PM, Adegnika AA, Agnandji ST, Schaumburg F, et al. Reduced Antibody Responses Against *Plasmodium Falciparum* Vaccine Candidate Antigens in the Presence of *Trichuris Trichiura*. *Vaccine* (2012) 30:7621–4. doi: 10.1016/j.vaccine.2012.10.026
60. Dzhivhuho GA, Rehrl SA, Ndlovu H, Horsnell WGC, Brombacher F, Williamson AL, et al. Chronic Schistosomiasis Suppresses HIV-specific Responses to DNA-MVA and MVA-gp140 Env Vaccine Regimens Despite Anti-Helminthic Treatment and Increases Helminth-Associated Pathology in a Mouse Model. *PLoS Pathog* (2018) 14:e1007182. doi: 10.1371/journal.ppat.1007182
61. Wammes LJ, Hamid F, Wiria AE, May L, Kaisar MMM, Prasetyani-Gieseler MA, et al. Community Deworming Alleviates Geohelminth-Induced Immune Hyporesponsiveness. *Proc Natl Acad Sci U S A* (2016) 113:12526–31. doi: 10.1073/pnas.1604570113
62. Abate E, Elias D, Getachew A, Alemu S, Diro E, Britton S, et al. Effects of Albendazole on the Clinical Outcome and Immunological Responses in

Helminth Co-Infected TB Patients: A Double Blind Randomised Clinical Trial. *Int J Parasitol* (2015) 45:133–40. doi: 10.1016/j.ijpara.2014.09.006
63. Elias D, Wolday D, Akuffo H, Petros B, Britton S. Effect of Deworming on Human T Cell Responses to Mycobacterial Antigens in Helminth-Exposed Individuals Before and After *Bacilli Calmette-Guérin* (BCG) Vaccination. *Clin Exp Immunol* (2001) 123:219–25. doi: 10.1046/j.1365-2249.2001.01446.x
64. Ivan E, Crowther NJ, Mutimura E, Rucogoza A, Janssen S, Njunwa KK, et al. Effect of Deworming on Disease Progression Markers in HIV-1–infected Pregnant Women on Antiretroviral Therapy: A Longitudinal Observational Study From Rwanda. *Clin Infect Dis* (2015) 60:135–42. doi: 10.1093/cid/ciu715
65. Walson JL, Otieno PA, Mbuchi M, Richardson BA, Lohman-Payne B, Macharia SW, et al. Albendazole Treatment of HIV-1 and Helminth Co-Infection: A Randomized, Double-Blind, Placebo-Controlled Trial. *AIDS* (2008) 22:1601–9. doi: 10.1097/QAD.0b013e32830a502e
66. Cooper PJ, Chico ME, Losonsky G, Sandoval C, Espinel I, Sridhara R, et al. Albendazole Treatment of Children With Ascariasis Enhances the Vibriocidal Antibody Response to the Live-Attenuated Oral Cholera Vaccine CVD 103-Hgr. *J Infect Dis* (2000) 182:1199–206. doi: 10.1086/315837
67. Netea MG, Dominguez-Andres J, Barreiro LB, Chavakis T, Divangahi M, Fuchs E, et al. Defining Trained Immunity and its Role in Health and Disease. *Nat Rev Immunol* (2020) 20:375–88. doi: 10.1038/s41577-020-0285-6
68. Peng X, Ouyang J, Isnard S, Lin J, Fombuena B, Zhu B, et al. Sharing CD4+ T Cell Loss: When Covid-19 and HIV Collide on Immune System. *Front Immunol* (2021) 11:596631. doi: 10.3389/fimmunol.2020.596631
69. Abraha HE, Gessesse Z, Gebrecherkos T, Kebede Y, Weldegiorghis AW, Tequare MH, et al. Clinical Features and Risk Factors Associated With Morbidity and Mortality Among COVID-19 Patients in Northern Ethiopia. *Int J Infect Dis* (2021) 105:776–83. doi: 10.1016/j.ijid.2021.03.037
70. Gebrecherkos T, Gessesse Z, Kebede Y, Gebreegzabheer A, Tasew G, Abdulkader M, et al. Effect of Co-Infection With Parasites on Severity of COVID-19. *medRxiv* (2021). doi: 10.1101/2021.02.02.212.50995
71. Wolday D, Tasew G, Amogne W, Urban B, Schallig HD, Harris V, et al. Interogating the Impact of Intestinal-Microbiome on Pathogenesis of COVID-19 in Sub-Saharan Africa. *Front Microbiol* (2021) 12:614522. doi: 10.3389/fmicb.2021.614522
72. Mekonnen Y, Geskus RB, Hendriks JCM, Messele T, Borghans J, Miedema F, et al. Low CD4 T Cell Counts Before HIV-1 Seroconversion do Not Affect Disease Progression in Ethiopian Factory Workers. *J Infect Dis* (2005) 192:739–48. doi: 10.1086/432545
73. Muyanja E, Ssemaganda A, Ngauv P, Cubas R, Perrin H, Srinivasan D, et al. Immune Activation Alters Cellular and Humoral Responses to Yellow Fever 17D Vaccine. *J Clin Invest* (2014) 124:3147–58. doi: 10.1172/JCI75429
74. Black GF, Weir RE, Floyd S, Bliss L, Warndorff DK, Crampin AC, et al. BCG-induced Increase in Interferon-Gamma Response to Mycobacterial Antigens and Efficacy of BCG Vaccination in Malawi and the UK: Two Randomized Controlled Studies. *Lancet* (2002) 359:1393–401. doi: 10.1016/S01400-6736(02)08353-8
75. Kirkpatrick BD, Colgate ER, Mychaleckyj JC, Haque R, Dickson DM, Carmolli MP, et al. The "Performance of Rotavirus and Oral Polio Vaccines in Developing Countries" (PROVIDE) Study: Description of Methods of an Interventional Study Designed to Explore Complex Biologic Problems. *Am J Trop Med Hyg* (2015) 92:744–51. doi: 10.4269/ajtmh.14-0518
76. Kabagenyi J, Natukunda A, Nassuuna J, Sanya RE, Nampijja M, Webb EL, et al. Urban-Rural Differences in Immune Responses to Mycobacterial and Tetanus Vaccine Antigens in a Tropical Setting: A Role for Helminths? *Parasitol Int* (2020) 78:102132. doi: 10.1016/j.parint.2020.102132
77. Tanner R, Kakalacheva K, Miller E, Pathan AA, Chalk R, Sander CR, et al. Serum Indoleamine 2,3-Dioxygenase Activity is Associated With Reduced Immunogenicity Following Vaccination With MVA85A. *BMC Infect Dis* (2014) 14:660–72. doi: 10.1186/s12879-014-0660-7
78. Agnandji ST, Lell B, Fernandes JF, Abossolo BP, Methogo BG, Kabwende AL, et al. A Phase 3 Trial of RTS,S/AS01 Malaria Vaccine in African Infants. *N Engl J Med* (2012) 367:2284–95. doi: 10.1056/NEJMoa1208394
79. Jongo SA, Urbano V, Church LWP, Olotu A, Manock SR, Schindler T, et al. Immunogenicity and Protective Efficacy of Radiation-Attenuated and Chemo-Attenuated PfSPZ Vaccines in Equatoguinean Adults. *Am J Trop Med Hyg* (2021) 104:283–93. doi: 10.4269/ajtmh.20-0435
80. Venkatraman N, Ndiaye BP, Bowyer G, Wade D, Sridhar S, Wright D. Et al. Safety and Immunogenicity of a Heterologous Prime-Boost Ebola Virus Vaccine Regimen in Healthy Adults in the United Kingdom and Senegal. *J Infect Dis* (2019) 219:1187–97. doi: 10.1093/infdis/jiy639
81. de Ruiter K, Jochems SP, Tahapary DL, Stam KA, König M, van Unen V, et al. Helminth Infections Drive Heterogeneity in Human Type 2 and Regulatory Cells. *Sci Transl Med* (2020) 12:eaaw3703. doi: 10.1126/scitranslmed.aaw3703
82. Nkurunungi G, Zirimenya L, Natukunda A, Nassuuna J, Oduru G, Ninsiima C, et al. Population Differences in Vaccine Responses (POPVAC): Scientific Rationale and Cross-Cutting Analyses for Three Linked, Randomized Controlled Trials Assessing the Role, Reversibility and Mediators of Immunomodulation by Chronic Infections in the Tropics. *BMJ Open* (2021) 11:e040425. doi: 10.1136/bmjopen-2020-040425
83. van Riet E, Adegnika AA, Retra K, Vieira R, Tielens AG, Lell B, et al. Cellular and Humoral Responses to Influenza in Gabonese Children Living in Rural and Semi-Urban Areas. *J Infect Dis* (2007) 196:1671–8. doi: 10.1086/522010
84. Voysey M, Clemens SAC, Madhi SA, Weckx LY, Folegatti PM, Aley PK, et al. Single-Dose Administration and the Influence of the Timing of the Booster Dose on Immunogenicity and Efficacy of ChAdOx1 nCoV-19 (AZD1222) Vaccine: A Pooled Analysis of Four Randomized Trials. *Lancet* (2021) 397:881–91. doi: 10.1016/50140-6736(21)00432-3
85. Koff WC, Schenkelberg T, Williams T, Baric RS, McDermott A, Cameron CM, et al. Development and Deployment of COVID-19 Vaccines for Those Most Vulnerable. *Sci Transl Med* (2021) eabd1525. doi: 10.1126/scitranslmed.abd1525
86. Hong SL, Potter B, Calvignac-Spencer S, Niatou-Singa FS, Tombolomako TB, Fuh-Neba T, et al. Travel-Driven Emergence and Spread of SARS-CoV-2 Lineage B.1.620 With Multiple VOC-like Mutations and Deletions in Europe. *medRxiv* (2021). doi: 10.1101/2021.05.04.21256637. Available as preprint.
87. Afolabi AA, Ilesanmi OS. Dealing With Vaccine Hesitancy in Africa: The Prospective COVID- 19 Vaccine Context. *Pan Afr Med J* (2021) 38:3. doi: 10.11604/pamj.2021.38.3.27401

Conflict of Interest: The authors declare that the research was conducted in the absence of any commercial or financial relationships that could be construed as a potential conflict of interest.

Copyright © 2021 Wolday, Ndungu, Gómez-Pérez and de Wit. This is an open-access article distributed under the terms of the Creative Commons Attribution License (CC BY). The use, distribution or reproduction in other forums is permitted, provided the original author(s) and the copyright owner(s) are credited and that the original publication in this journal is cited, in accordance with accepted academic practice. No use, distribution or reproduction is permitted which does not comply with these terms.

frontiers in Immunology

ORIGINAL RESEARCH
published: 05 August 2021
doi: 10.3389/fimmu.2021.692729

BCG Vaccine Derived Peptides Induce SARS-CoV-2 T Cell Cross-Reactivity

*Peter J. Eggenhuizen[1], Boaz H. Ng[1], Janet Chang[1], Ashleigh L. Fell[1], Rachel M. Y. Cheong[1], Wey Y. Wong[1], Poh-Yi Gan[1,2], Stephen R. Holdsworth[1,2] and Joshua D. Ooi[1]**

[1] Centre for Inflammatory Diseases, Department of Medicine, Monash Medical Centre, School of Clinical Sciences, Monash University, Clayton, VIC, Australia, [2] Department of Immunology, Monash Health, Monash Medical Centre, Clayton, VIC, Australia

Epidemiological studies and clinical trials suggest Bacillus Calmette-Guérin (BCG) vaccine has protective effects against coronavirus disease 2019 (COVID-19). There are now over 30 clinical trials evaluating if BCG vaccination can prevent or reduce the severity of COVID-19. However, the mechanism by which BCG vaccination can induce severe acute respiratory syndrome coronavirus 2 (SARS-CoV-2)-specific T cell responses is unknown. Here, we identify 8 novel BCG-derived peptides with significant sequence homology to either SARS-CoV-2 NSP3 or NSP13-derived peptides. Using an *in vitro* co-culture system, we show that human CD4+ and CD8+ T cells primed with a BCG-derived peptide developed enhanced reactivity to its corresponding homologous SARS-CoV-2-derived peptide. As expected, HLA differences between individuals meant that not all persons developed immunogenic responses to all 8 BCG-derived peptides. Nevertheless, all of the 20 individuals that were primed with BCG-derived peptides developed enhanced T cell reactivity to at least 7 of 8 SARS-CoV-2-derived peptides. These findings provide an *in vitro* mechanism that may account, in part, for the epidemiologic observation that BCG vaccination confers some protection from COVID-19.

Keywords: COVID-19, BCG, heterologous immunity, cross-protection, T cell, vaccine

OPEN ACCESS

Edited by:
Pia Kvistborg, The Netherlands Cancer Institute (NKI), Netherlands

Reviewed by:
Carmen Fernández, Stockholm University, Sweden
Harlan Pierre Jones, University of North Texas Health Science Center, United States

***Correspondence:**
Joshua D. Ooi
joshua.ooi@monash.edu

Specialty section:
This article was submitted to T Cell Biology, a section of the journal Frontiers in Immunology

Received: *09 April 2021*
Accepted: *13 July 2021*
Published: *05 August 2021*

Citation:
Eggenhuizen PJ, Ng BH, Chang J, Fell AL, Cheong RMY, Wong WY, Gan P-Y, Holdsworth SR and Ooi JD (2021) BCG Vaccine Derived Peptides Induce SARS-CoV-2 T Cell Cross-Reactivity. Front. Immunol. 12:692729. doi: 10.3389/fimmu.2021.692729

INTRODUCTION

Severe acute respiratory syndrome coronavirus 2 (SARS-CoV-2) causes coronavirus disease 2019 (COVID-19) (1, 2). Alongside other immune cells, T cells are pivotal in mounting a successful immune response against COVID-19 as recovered individuals exhibit SARS-CoV-2 specific T cell memory, while T cell dysfunction and imbalance has been reported as a hallmark of severe COVID-19 (3, 4). Both CD4+ and CD8+ T cells have been implicated in COVID-19 with CD4+ T cells being broadly Th1-like by the secretion of cytokines interleukin-2 (IL-2), interferon gamma (IFN-γ) and tumor necrosis factor (TNF), and CD8+ T cells also secreting TNF and IFN-γas well as effecting direct target cell lysis through the secretion of perforin and granzymes (5). Cross-reactive T cells between other human coronaviruses and SARS-CoV-2 have been identified, suggesting the potential role for T cell cross-protection in COVID-19 (6, 7). Here we investigated whether cross-reactive SARS-CoV-2-specific T cells can arise from Bacillus Calmette-Guérin (BCG)-derived peptide sensitization *in vitro*.

BCG vaccine containing live attenuated *Mycobacterium bovis*, hereafter referred to as BCG, typically vaccinates against tuberculosis (TB). BCG can also induce cross-protection against pathogens unrelated to TB through heterologous immunity, which although is generally not as effective as homologous immunity, may result in reduced disease severity or protective immunity (8). The cross-protective effects have shown to reduce all-cause mortality in children and respiratory tract infections in adults (9–12). One established mechanism of cross-protection is through BCG epigenetically modifying innate immune cells in the form of trained innate immunity lasting up to one year (13, 14). The heterologous effect of BCG vaccination on T cells has been demonstrated in other viral infections such as murine vaccinia virus and HPV papillomatosis (15–18).

Given the heterologous effects of BCG vaccination, there are over 30 clinical trials globally to test the cross-protective effect of BCG in COVID-19, notably the BRACE study involving 10,000 healthcare workers in Australia and the Netherlands (19). The majority of clinical trials addressing this are currently recruiting or ongoing. To date, at least 4 have concluded and shown BCG can provide some benefit in COVID-19 (20–23). Additionally, large country-level epidemiological analyses, as well as a study of > 6000 health care workers, have shown a negative correlation between BCG vaccination status, COVID-19 disease severity and SARS-CoV-2 IgG seroprevalence (24–27).

Here we show an *in vitro* mechanism whereby BCG-peptide-primed T cells have the capacity to cross-react with SARS-CoV-2-peptide homologues.

METHODS

Patient Samples

Whole blood was collected from healthy donors with no prior known infection with TB or COVID-19 and who tested negative for serum IgG/IgM SARS-CoV-2 antibodies by SARS-CoV-2 Colloidal Gold Immunochromatography Assay Kit (MyBioSource). Donor characteristics are summarized in **Tables S2A, B**.

Statistics

Data was analyzed using R Studio ver.1.3.959 and GraphPadPrism 7 (Graphpad Software Inc.). A Shapiro-Wilk test was used to determine normality followed by two-tailed, Wilcoxon-matched-pairs-signed-rank test to compare responses of BCG-primed with control-primed samples from responders. A two-tailed, Mann-Whitney test was used to compare responses of BCG vaccinated and BCG unvaccinated individuals.

Study Approval

The study was conducted according to the Declaration of Helsinki; approved by Monash University HREC project ID 25834. Donors provided written informed consent.

Data Reporting

No statistical methods were used to pre-determine sample size. The experiments were not randomized. The investigators were not blinded to allocation during experiments and assessment of outcomes.

HLA Typing

Seven donors underwent high resolution class I and II molecular sequence-based typing performed by the Australian Red Cross Victorian Transplantation and Immunogenetics Service by next-generation sequencing. Three donors underwent low-resolution HLA-DR typing at the same provider. HLA typing results are contained within **Table S2B**.

HLA Binding Prediction and Allele Coverage

Global allele coverage of HLA-typed donors was assessed at IEDB Analysis Resource – Population Coverage (28). NetMHCpan-4.1 and NetMHCIIpan-4.0 were used to predict binding affinity of homologous peptides to a globally representative collection of MHCI or MHCII alleles plus the alleles of our HLA-typed donors using artificial neural networks (29–31). For each region of homology, 9mers for MHCI and 15mers for MHCII overlapping by 1 amino acid underwent affinity analysis. Affinity rank was generated that normalizes prediction score by comparing to prediction of a set of random peptides. An affinity rank score of < 2 was called a strong binder. An affinity rank score of ≥ 2 and ≤ 10 was called a binder. An affinity score of > 10 was called a non-binder.

Sequence Alignment

Protein BLAST search of the SARS-CoV-2 proteome (sequence ID NC_045512.2) restricted to *Mycobacterium bovis* (BCG) was performed using the NCBI blastp suite (https://blast.ncbi.nlm.nih.gov/Blast.cgi). Protein sequences from SARS-CoV-2 NSP3 (YP_009725299.1), SARS CoV-2 NSP13 (YP_009725308.1), BCG RecB nuclease (KAF3412556.1), BCG UPF0189 protein (AHM07651.1), BCG Macro domain containing protein (WP_003909539.1), BCG zinc metalloprotease FtsH (AMC52863.1) and human CLIP (NP_001020330.1) were obtained from the NCBI Database (https://www.ncbi.nlm.nih.gov/protein/). Sequence alignment of SARS-CoV-2 and BCG homologues was performed using EMBOSS Needle Pairwise Sequence Alignment (32).

Peptides

15mer peptides were synthesized with an N-terminal free amine (H-) and a free acid group at the C-terminus (-OH). Peptides were ≥ 90% pure as assessed by reversed-phase high-performance liquid chromatography (RP-HPLC) (Mimotopes). Peptide sequences used in this study can be found in **Table S1** and control peptide $CLIP_{103\text{-}117}$ (PVSKMRMATPLLMQA). Lyophilized peptide was reconstituted in sterile MilliQ water with 5% (v/v) DMSO (Sigma). Final concentration of peptides used in culture was 10μg/mL and final concentration of DMSO in the cultures was 0.005% (v/v).

Monocyte Derived DC Production

Human PBMCs were freshly isolated from whole donor blood in K2EDTA anticoagulant Vacutainers (BD) using Lymphoprep density gradient medium (Stemcell) and SepMate tubes (Stemcell). PBMCs were enumerated in a haemocytometer with trypan blue 0.4% (Sigma) and the CD14+ CD16- monocytes were then magnetically separated using EasySep

Human Monocyte Isolation Kit and EasySep Magnet following manufacturer's instructions (Stemcell). Freshly isolated monocytes were then enumerated in a haemocytometer with 0.4% trypan blue and if viability was ≥90%, differentiation culture was established to differentiate the monocytes into dendritic cells using ImmunoCult Dendritic Cell Culture Kit following instructions of the manufacturer (Stemcell). According to the protocol (Stemcell), immature DCs used in the intracellular cytokine staining (ICS) co-culture did not receive maturation supplement on day 5 of culture and mature DCs used in the proliferation and memory co-culture received maturation supplement on day 5 of culture. After 7 days culture, immature DCs were used for the ICS co-culture and mature DCs were used for the proliferation co-culture.

T Cell Isolation

Human CD3+ T cells were isolated from fresh whole donor blood in K2EDTA tubes using RosetteSep HLA T Cell Enrichment Cocktail according to instructions of the manufacturer (Stemcell). Isolated CD3+ T cells were enumerated in a haemocytometer with 0.4% trypan blue (Sigma) and only used when viability was ≥90%. CD3+ T cells were then used in the ICS and proliferation co-cultures.

ICS Co-Culture Setup

An ICS co-culture assay to assess T cell cross-reactivity was adapted from previously published methods for the measurement of T cell cross-reactivity (33). Specifically, ICS co-culture was initiated with 100,000 freshly isolated human CD3+ T cells, 10,000 human immature monocyte-derived DCs and 10μg/mL of BCG peptide from PP1-8 (**Figure 1**) or control peptide (PVSKMRMATPLLMQA) in a 96 well round-bottom plate (Corning) at 100μL per well of complete RPMI (Gibco) supplemented with 10% autologous human serum, 100 U/mL penicillin and 0.1 mg/mL streptomycin (Gibco), 2mM L-glutamine (Gibco) and 50μM 2-mercaptoethanol (Sigma). Positive assay control received anti-human CD2, anti-human CD3, and anti-human CD28 coated MACS iBeads at a ratio of 1 bead:2cells prepared from the human T cell activation/expansion kit as per the manufacturer's instructions (Miltenyi). Negative assay control received no peptides. Co-culture was incubated at 37°C in a CO_2 incubator (Binder). Five days later, the co-culture was supplemented with 40IU/mL recombinant human IL-2 (Stemcell) and reincubated. On day 7 of co-culture, cells were rested by washing twice in 250μL PBS to remove peptides and resuspended in 100μL fresh complete RPMI formulated as above with no peptides and reincubated. On day 9 of co-culture, cells were restimulated by washing twice with 250μL PBS then 10,000 freshly-cultured, immature DCs were added per well with 10μg/mL of SARS-CoV-2 peptide from PP1-8 (**Figure 1**) or control peptide (PVSKMRMATPLLMQA) and 1μg/mL anti-human CD28 monoclonal antibody (clone CD28.2, eBioscience) in serum-free RPMI. Positive assay control received anti-human CD2, anti-human CD3, and anti-human CD28 coated MACS iBeads at a ratio of 1 bead:2cells. Negative assay control received no peptides. To pulse the DCs with peptide, co-culture was incubated for 2 hours at 37°C in a CO_2 incubator (Binder). After 2 hours, media was adjusted to contain 10% autologous serum and 1X protein transport inhibitor cocktail containing brefeldin A and monensin (eBioscience) was added and reincubated. After 6 hours at 37°C in a CO_2 incubator, cells were harvested for flow cytometric analysis by ICS. The entire culture system was setup to be autologous.

HLA blocking was performed on selected HLA-typed donor samples as per the aforementioned ICS co-culture setup with the additional step of adding the respective blocking antibody on day 9. Blocking antibodies mouse anti-human HLA-DR (clone L243, Abcam), mouse anti-human HLA-DQ (clone SPV-L3, Novus Biologicals), mouse anti-human HLA-A/B/C (clone W6/32, eBioscience) and isotype control mouse IgG2a kappa (clone eBM2a, eBioscience) were incubated at 10μg/mL with immature DCs for 1hr at 37°C in a CO_2 incubator prior to addition of peptide and T cells.

Comparison of BCG vaccinated and unvaccinated individuals was performed as per the aforementioned ICS co-culture setup and instead performing only one stimulation using the SARS-CoV-2 peptide.

Proliferation Co-Culture Setup

Proliferation co-culture was initiated with 100,000 freshly isolated CD3+ T cells stained with cell proliferation dye Cell Trace Yellow (CTY) according to the manufacturer (Invitrogen), 10,000 human mature DCs and 10μg/mL of BCG peptide from PP1-8 (**Figure 1**) or control peptide (PVSKMRMATPLLMQA) in a 96 well round-bottom plate (Corning) at 100μL per well of complete RPMI (Gibco) supplemented with 10% autologous human serum, 100 U/mL penicillin and 0.1 mg/mL streptomycin (Gibco), 2mM L-glutamine (Gibco) and 50μM 2-mercaptoethanol (Sigma). Positive assay control received anti-human CD2, anti-human CD3, and anti-human CD28 coated MACS iBeads at a ratio of 1 bead:2cells prepared from the human T cell activation/expansion kit as per the manufacturer's instructions (Miltenyi). Negative assay control received no peptides. Co-culture was incubated at 37°C in a CO_2 incubator (Binder). Seven days later, cells were washed twice in 250uL PBS to remove peptides and resuspended in 100μL complete RPMI formulated as above with no peptides and reincubated. On day 9 of co-culture, cells were washed twice in 250μL PBS and stained with Cell Trace Violet (CTV) cell proliferation dye according to the manufacturer's instructions (Invitrogen). Then 10,000 freshly-cultured, human mature DCs were added per well with 10μg/mL of SARS-CoV-2 peptide from PP1-8 (**Figure 1**) or control peptide (PVSKMRMATPLLMQA). Positive assay control received anti-human CD2, anti-human CD3, and anti-human CD28 coated MACS iBeads at a ratio of 1 bead:2cells. Negative assay control received no peptides. Co-culture was incubated at 37°C in a CO_2 incubator for 7 days then harvested for flow cytometric analysis. The entire culture system was setup to be autologous.

ICS Flow Cytometry Staining and Analysis

After culturing, cells were stained with Live/Dead Fixable Near Infra-Red Dead Cell Stain Kit according to the manufacturer's instructions (Invitrogen). Cells were then stained with surface markers anti-human CD3 Brilliant Violet 510 (clone OKT3, Biolegend), anti-human CD4 APC (clone OKT4, eBioscience),

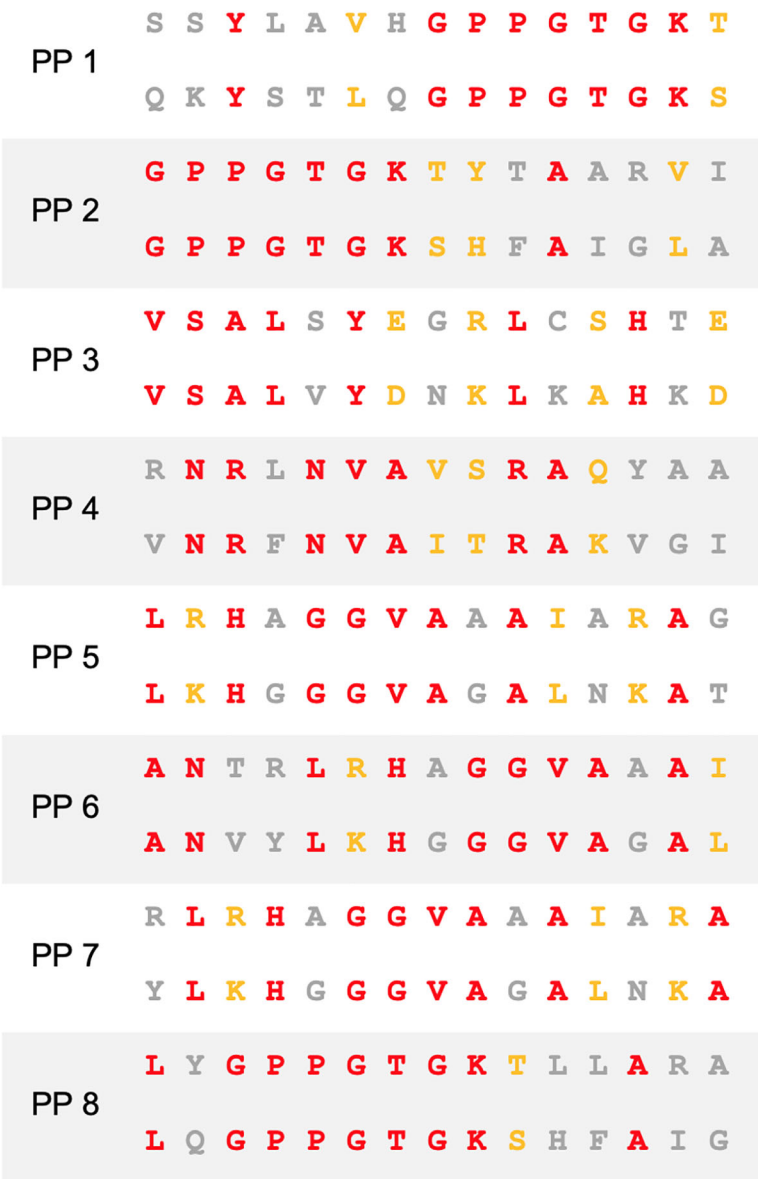


FIGURE 1 | Sequence homology between BCG and SARS-CoV-2. Amino acid sequence alignment of peptide pairs (PP) of BCG (top) and SARS-CoV-2 (bottom) used in this study. Red–identity. Yellow–similarity. Grey–no identity/similarity.

anti-human CD8 Alexa Fluor 488 (clone HIT8a, Biolegend) and anti-human CD69 Brilliant UV 395 (clone FN50, BD). After surface staining, cells were fixed and permeabilized with Transcription Factor Staining Buffer Set according to the manufacturer's instructions (eBioscience). Cells were subsequently stained for intracellular markers with anti-human IFN-γ PE Cy7 (clone 4S.B3, eBioscience), anti-human TNF Brilliant Violet 421 (clone Mab11, Biolegend), anti-human IL-2 Brilliant Blue 700 (clone MQ1-17H12, BD) and anti-human perforin PE (clone B-D48, Biolegend). Single color controls were prepared using UltraComp eBeads (Invitrogen) for single color control antibodies and ArC amine reactive compensation bead kit (Invitrogen) for Live/Dead single color control. After staining, cells were resuspended in PBS and acquired on an LSR-Fortessa X20 flow cytometer (BD) using BD FACSDiva software version 8.0.1. Samples were analyzed in FlowJo 10.6.2. FMO controls were used to determine positive gating (**Figure S3**). Individuals that responded in the given parameters to SARS-CoV-2 after BCG priming (**Figure 2**) were defined as showing positive staining after subtraction of the primary SARS-CoV-2 response control (control peptide-primed, SARS-CoV-2 peptide stimulated). A non-responder was defined as showing no positive staining after

subtraction of the primary SARS-CoV-2 response control. For statistical analysis (**Figure 3** and **Figures S5, S6**), the responders were selected as those with positive staining after subtraction of the primary SARS-CoV-2 response control or restimulation background control (BCG primed, irrelevant peptide restimulated). The responders then had the restimulation background control (BCG primed and irrelevant peptide restimulated) subtracted from the corresponding BCG primed, SARS-CoV-2 test sample and the primary SARS-CoV-2 response control to remove any assay related background stimulation.

Proliferation Flow Cytometry Staining and Analysis

After culturing, cells were stained with Live/Dead Fixable Near Infra-Red Dead Cell Stain Kit according to the manufacturer's instructions. Cells were then stained with surface markers anti-human CD3 PerCP (clone SK7, Biolegend), anti-human CD4 APC (clone OKT4, eBioscience), and anti-human CD8 Alexa Fluor 488 (clone HIT8a, Biolegend). Single color controls were prepared using UltraComp eBeads (Invitrogen) for single color control antibodies, ArC amine reactive compensation bead kit (Invitrogen) for Live/Dead single color control and Cell Trace Violet and Cell Trace Yellow single stained co-cultured cells along with unstained co-cultured cells. After staining, cells were resuspended in 0.5% BSA, 2mM EDTA/PBS and acquired on an LSR-Fortessa X20 flow cytometer (BD) using BD FACSDiva software version 8.0.1.fcs files were analyzed in FlowJo 10.6.2. All fluorescence based gating except CTY, and CTV is determined based on fluorescence minus one (FMO) controls (**Figure S4**). CTV and CTY gating are based on the point at which the first cell division took place visible by fluorescence dye dilution. Individuals that showed a proliferation response when BCG primed, SARS-CoV-2 restimulated (**Figure 2**) were defined as showing positive staining after subtraction of the primary SARS-CoV-2 response control (irrelevant peptide primed, SARS-CoV-2 peptide stimulated). A non-responder was defined as showing no positive staining after subtraction of the primary SARS-CoV-2 response control. For statistical analysis (**Figure 4**), the responders were selected as those with positive staining after subtraction of the primary SARS-CoV-2 response control or restimulation background control (BCG primed, irrelevant peptide restimulated). Proliferation in response to BCG priming and SARS-CoV-2 restimulation was calculated as the proportion of CD4+ or CD8+ cells that underwent proliferation post-priming and post-restimulation ($CTY^{lo}CTV^{lo}$) of total proliferated cells ($CTY^{lo}CTV^{lo}$ and CTY^{lo} CTV^{high}).

RESULTS

SARS-CoV-2 Amino Acid Homology With BCG

T cells specific for SARS-CoV-2 are well recognized as pivotal in mounting a successful immune response to COVID-19 (5). To determine whether homology exists between BCG and SARS-CoV-2, we first performed NCBI Protein Blast searches against the SARS-CoV-2 proteome, restricting results to BCG proteins.

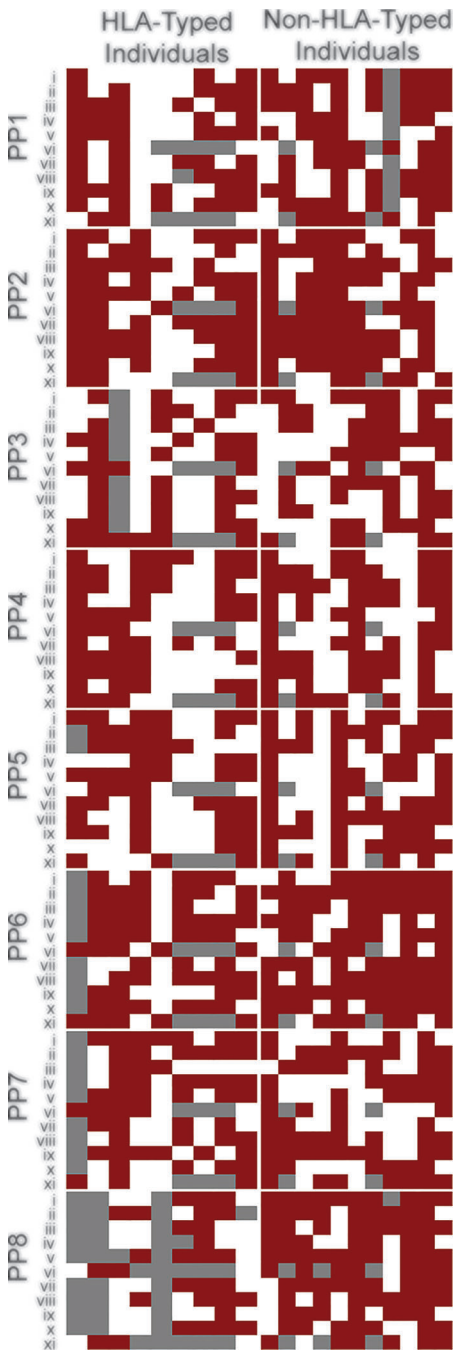


FIGURE 2 | BCG induces broad cross-reactive T cell responses across individuals. Heat map of individuals representing global HLA coverage shows improved SARS-CoV-2 T cell responses when pre-stimulated with BCG peptide. Individual donor T cell responses to the 8 peptide pairs (PP1-PP8) across 11 parameters (i-xi) determined by flow cytometry. i–CD8+IFN-γ, ii–CD8+TNF, iii–CD8+IL-2, iv–CD8+CD69, v–CD8+Perforin, vi–CD8 +proliferation, vii–CD4+IFN-γ, viii–CD4+TNF, ix–CD4+IL-2, x–CD4+CD69, xi–CD4+proliferation. A responder (red) is defined as showing a positive response after subtraction of the control-primed response to SARS-CoV-2. A non-responder (white) is defined as showing no positive staining after subtraction of the control response. Grey –no data. Individuals were grouped by known or unknown HLA-type highlighting similar patterns between them.

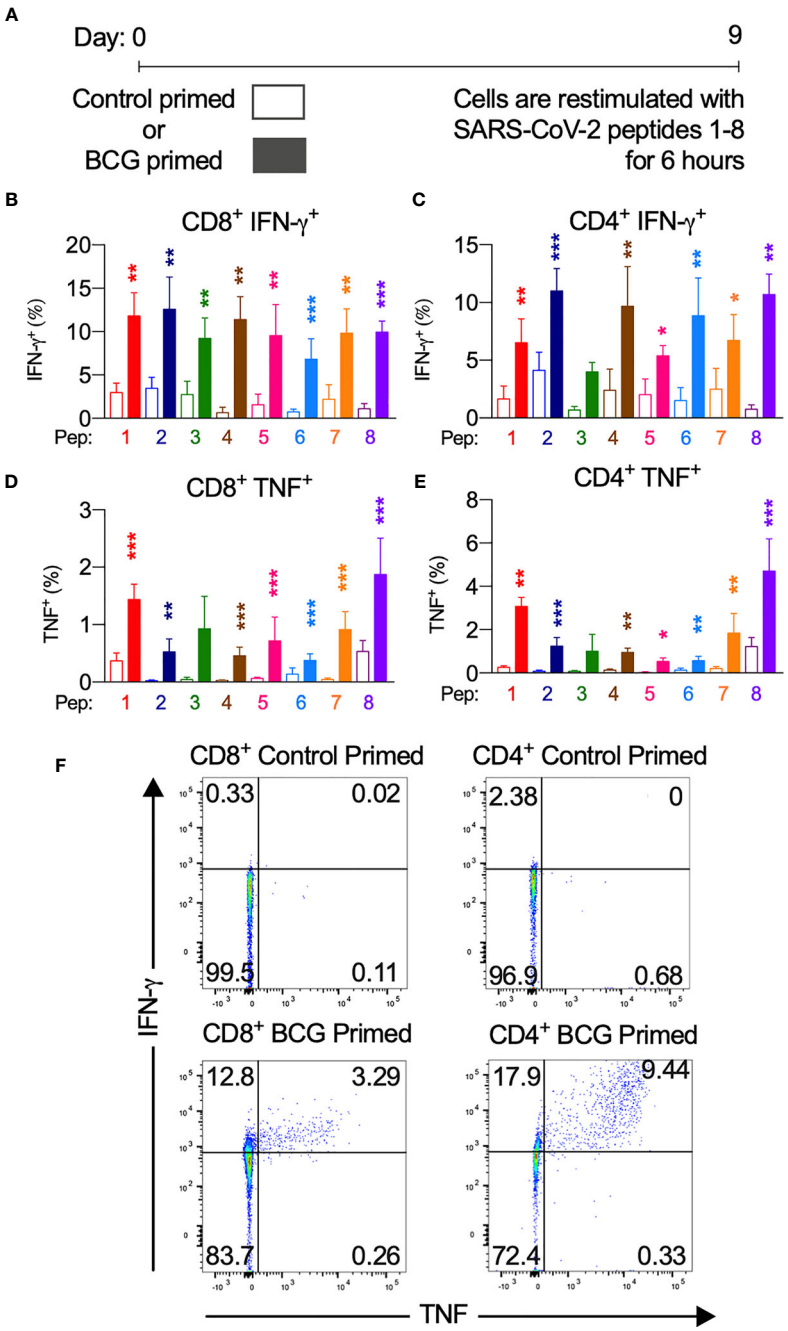


FIGURE 3 | BCG priming enhances SARS-CoV-2 T cell responses. BCG-peptide-primed T cells restimulated with SARS-CoV-2-peptide-pulsed DCs analysed by flow cytometry. Unshaded bars- Control primed (irrelevant peptide, PVSKMRMATPLLMQA), then SARS-CoV-2-peptide1-8 restimulated. Shaded bars– BCG peptide 1-8 primed then SARS-CoV-2-peptide homologue restimulated. **(A)** Brief culture timeline, **(B)** CD8+IFN-γ+ responses (n = 9-12), **(C)** CD4+IFN-γ+ responses (n = 5-13), **(D)** CD8+TNF+ responses (n = 4-14), **(E)** CD4+TNF+ responses (n = 6-16), **(F)** Representative TNF (x-axis) and IFN-γ (y-axis) dot plots of a responder donor with their corresponding SARS-CoV-2 primary response control. $^{*}P < 0.05$, $^{**}P < 0.01$,$^{***}P < 0.001$ by Wilcoxon-matched-pairs-signed-rank test, comparing magnitude of response to SARS-CoV-2 peptides with or without BCG priming.

Regions of protein sequence homology were identified between BCG sequences and the non-structural proteins NSP3 and NSP13 located in ORF1ab of SARS-CoV-2 (**Figure 1** and **Table S1**). When processed as 15mers for MHCII presentation, these regions exhibit up to 60% identity and 73.3% similarity between BCG and SARS-CoV-2 (**Table S1A**). Percent identity and similarity of constituent 9mers for MHCI presentation are up to 88.8% and 100%, respectively (**Table S1B**).

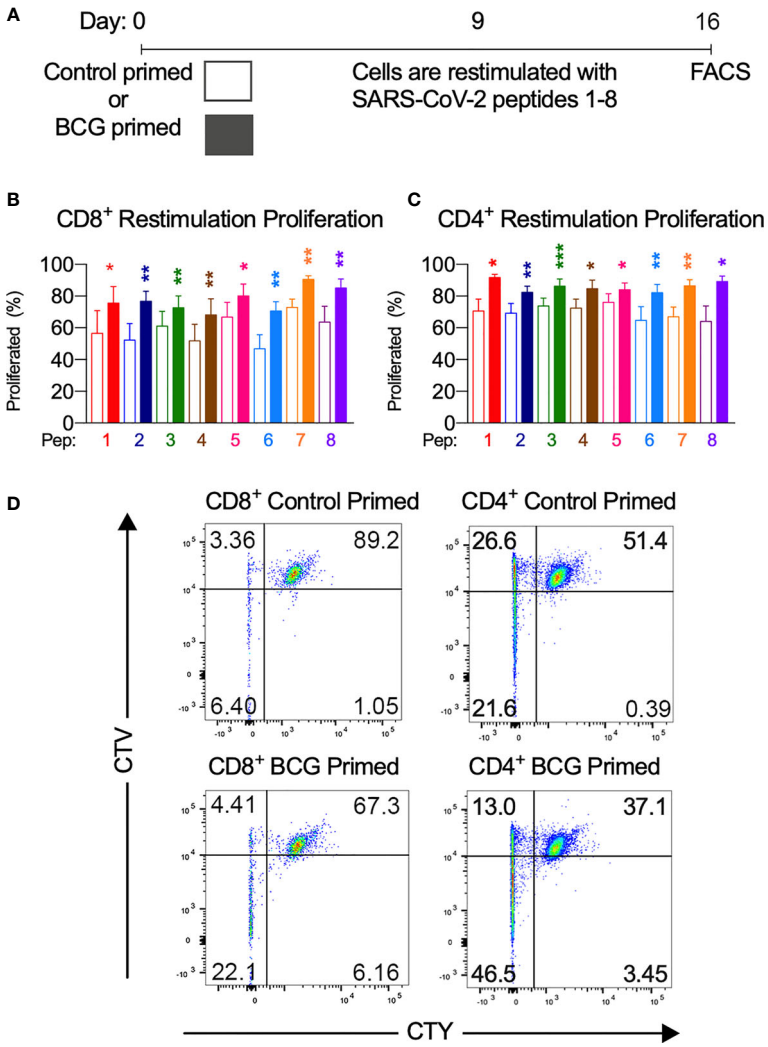


FIGURE 4 | BCG priming enhances T cell proliferation. **(A)** Brief culture timeline. **(B)** CD8+ restimulation proliferation is enhanced by BCG priming (*n*=9-12). **(C)** CD4+ restimulation proliferation is enhanced by BCG priming (*n*=6-11). Unshaded bars– Control-primed (irrelevant peptide, PVSKMRMATPLLMQA), then SARS-CoV-2-peptide restimulated. Shaded bars– BCG peptide primed then SARS-CoV-2-peptide homologue restimulated. **(D)** Representative CTV *vs.* CTY dot plots of CD4+ and CD8+ cultured cells indicating proliferation. Top right quadrant gate ($CTY^{hi}CTV^{hi}$ cells) did not proliferate upon priming or restimulation. Top left quadrant gate ($CTY^{lo}CTV^{hi}$ cells) proliferated upon priming but not with restimulation. Bottom left quadrant gate ($CTY^{lo}CTV^{lo}$ cells) proliferated upon both priming and restimulation. $^{*}P < 0.05$, $^{**}P < 0.01$, $^{***}P < 0.001$ by Wilcoxon-matched-pairs-signed rank test, comparing the magnitude of response to SARS-CoV-2 peptides with or without BCG priming.

To assess the capacity of BCG epitopes to bind HLA alleles that broadly cover the global population, we performed *in silico* prediction analyses of peptide-MHC binding affinity using NetMHCIIpan 4.0 and NetMHCpan 4.1 across each region of homology as 9mers or 15mers overlapping by 1 amino acid residue in MHCI and MHCII binding, respectively (29). HLA alleles in the analysis were selected based on previously reported reference sets giving maximal global population coverage (28, 30). We found that the BCG derived peptides with homologous sequences to SARS-CoV-2 peptides exhibited broad MHC class II and MHC I binding capacity (**Figures S1, S2**).

To determine the cross-reactive immunogenicity of these BCG derived peptides across diverse HLA-types, we selected 10 healthy HLA-typed blood donors with different HLA types (**Table S2B**). Based on IEDB population coverage, our collection of HLA-typed individuals gave a global MHC class I and II coverage of 97.21% and 99.97%, respectively (34). In addition, binding affinity predictions of the homologous peptides to HLA alleles from the 10 HLA-typed donors used in this study were analyzed (**Figures S1, S2**). To determine if HLA-typing was necessary, we also tested the cross-reactive immunogenicity of the BCG derived peptides on 10 non-HLA-typed persons. Based

on high homology and strong binding, a selection of eight different 15mer peptide pairs (PP1-8) were chosen for subsequent experimentation on human donors (**Figure 1**). The 15mers are of an appropriate length to be presented by MHC class II to CD4+ T cells. Each 15mer contained within it 7 different 9mers (**Table S1B**), which, after antigen processing in immature dendritic cells (DCs), can be presented to CD8+ T cells *via* MHC class I.

T Cell Cross-Reactivity

To determine if priming with BCG peptide enhances T cell responses to SARS-CoV-2 peptides, we compared CD4+ and CD8+ T cell responses to SARS-CoV2 peptides using cells that were either primed with irrelevant control peptide (PVSKMRMATPLLMQA) or BCG peptide. CD3+ T cells were isolated from donors (n=20, **Table S2A**) and co-cultured with DCs *in vitro*. Individual BCG peptides were first used to sensitize and expand the BCG-specific T cells, simulating a BCG vaccination. T cells were then rested for two days without antigen stimulation then re-stimulated with corresponding homologous SARS-CoV-2 peptides. To measure T cell responses, we performed intracellular cytokine staining (ICS) for IFN-γ, TNF, IL-2, perforin; surface staining for the early T cell activation marker CD69, and a two-color proliferation assay to differentiate between a primary proliferative and secondary proliferative response. A positive response was defined as an increase compared to control. All individuals (n=20) exhibited a positive response to at least 7 out of 8 SARS-CoV-2 peptides (**Figure 2**).

Next, we assessed the degree of SARS-CoV-2 T cell reactivity enhancement conferred by BCG priming compared to control primed T cells (**Figure 3**, and **Figures S5, S6**). In CD8+ cytotoxic T cells, IFN-γ, TNF and IL-2 cytokine production across at least 7 of the 8 peptide pairs significantly increased (**Figure 3** and **Figure S5A**). IFN-γ mean fold increase in expression ranged from 2.3-fold (PP3) to 16.3-fold (PP4). Mean fold increase in TNF expression from CD8+ cells ranged from 1.7-fold (PP6) to 23.9-fold (PP2). IL-2 production from CD8+ cells showed a mean fold increase from 3.1-fold (PP2) to 33.1-fold (PP5).

CD4+ T helper cells exhibited similarly significantly increased IFN-γ, TNF and IL-2 production across at least 7 of the 8 peptide pairs (**Figure 3** and **Figure S6A**). In CD4+ cells from responder individuals, IFN-γ mean fold increase in expression ranged from 1.7-fold (PP2, PP5 & PP7) to 12.9-fold (PP8). Mean fold increase in TNF from CD4+ cells ranged from 2.9-fold (PP8) to 14.1-fold (PP2 & PP5). IL-2 production from CD4+ cells showed a mean fold increase from 2.1-fold (PP5) to 12.3-fold (PP8).

To confirm that the observed cross-reactive T cell responses arise from peptide-MHC interaction with the T cell, we blocked HLA and measured T cell cytokine responses, as above. We identified 15mers and 9mers for CD4+ and CD8+ responses, respectively that were *in silico* predicted to bind to one HLA allele only out of all HLA alleles of a HLA-typed individual. We then selectively blocked this response using a blocking antibody against that particular HLA (either anti-HLA-DR or anti-HLA-DQ for MHC class II blocking of CD4+ T cell responses and anti-HLA-A/B/C for MHC class I blocking of CD8+ T cell responses). Without HLA blocking or blocking with isotype control antibody, T cell IFN-γ and TNF were predictably high. Upon HLA-specific blocking, there was a near complete abrogation of cytokine responses indicating that the T cell restimulation responses arise from cross-reactive T cell receptor binding to peptide-MHC on the DCs (**Figure S8**).

Since the COVID-19 CD8+ response involves the secretion of perforin and granzymes for an effective antiviral response, we measured perforin expression by ICS. We found that CD8+ T cells primed with BCG-derived peptides had an enhanced perforin expression upon SARS-CoV-2 restimulation when compared to control primed cells (**Figure S5B**). Cross-reactive perforin expression in responders was significantly increased across all 8 peptide pairs with a mean fold-increase ranging from 1.9-fold (PP1) to 47.2-fold (PP4).

In order to mount an effective T cell response to COVID-19, antigen-specific T cells must become activated and undergo clonal expansion. To assess whether T cells pre-stimulated with BCG-derived peptides exhibit enhanced T cell activation when restimulated with SARS-CoV-2 homologues, expression of early T cell activation marker CD69 was assessed by flow cytometry. We show that when compared to a SARS-CoV-2 primary response, the BCG primed T cells increased CD69 expression across 7 of the 8 peptide pairs in CD4+ and CD8+ T cells (**Figures S5C, S6B**). CD69 expression in responders showed a mean fold-increase ranging from 3.2-fold (PP1) to 29.6-fold (PP5) for CD4+ cells and from 1.7-fold (PP1) to 10.5-fold (PP2) for CD8+ cells.

To assess whether T cells primed with BCG derived peptides show enhanced T cell proliferation upon SARS-CoV-2 peptide restimulation, cell proliferation dye cell trace yellow (CTY) was used to assess the proliferation after BCG priming followed by cell trace violet (CTV) to assess the proliferation after SARS-CoV-2 restimulation. All donor samples primed with BCG peptide developed enhanced T cell proliferation to at least 3 out of the 8 SARS-CoV-2 peptides tested (**Figure 2**). The magnitude of the enhanced proliferative response was also assessed in BCG-primed individuals who responded SARS-CoV-2 restimulation. Specifically, we compared the SARS-CoV-2 peptide induced proliferation in cells that were first sensitized with BCG peptide or with control peptide. In all of the tested peptide pairs (PP1-PP8) and across both CD4+ and CD8+ T cells, BCG peptide sensitized cells developed significantly enhanced proliferation to its SARS-CoV-2 homologous peptide (**Figure 4**). In the responders, T cell proliferation was enhanced in CD8+ T cells between 19% (PP3 and PP5) to 51% (PP6) and in CD4+ T cells by 11% (PP5) to 39% (PP8).

We analyzed an equal number of males and females in this study (n=10 each) and no significant sex-specific differences were found in the parameters measured.

To compare SARS-CoV-2 peptide T cell responses between BCG-vaccinated and BCG-unvaccinated individuals, CD3+ T cell and immature DC co-cultures were pulsed with one of the 8 SARS-CoV-2 peptides (**Figure 1**) for 6hr and IFN-γ and TNF

responses were measured by ICS (**Figure S9**). Across all 8 SARS-CoV-2 peptides and across the four tested parameters ($CD8^+$ IFN-γ, CD8 TNF^+, CD4 IFN-γ and $CD4^+$ TNF), a trend was observed for increased SARS-CoV-2 peptide-induced $CD4^+$ and $CD8^+$ T cell responses in BCG vaccinated individuals compared to unvaccinated. However, this trend only reached significance in 3 parameters, namely peptide 5 on TNF production in CD8+ cell, peptide 3 on TNF production in CD4+ cells and peptide 8 on IFN-γ production in CD4+ cells.

DISCUSSION

T cell-dependent heterologous immunity can occur in a number of different ways, which can be broadly summarized as either TCR-dependent or TCR-independent. TCR-independent heterologous immunity can arise through nonspecific activation by virus-induced cytokines such as IL-12 and IL-18 without TCR involvement whereby the second infection stimulates memory T cells from the first infection (35, 36). TCR-dependent heterologous immunity can arise from direct cross-reactivity between unrelated pathogens, whereby memory T cells generated by the first infection/immunization cross-react with antigens from the second infection (37). It is this instance of TCR-dependent heterologous immunity which we propose as a potential mechanism for cross-reactivity between BCG vaccination and SARS-CoV-2 infection.

Similar epitopes shared between BCG and SARS-CoV-2 have recently been identified as having the potential for cross-reactive adaptive immunity (38). We identified 8 novel protein sequences with significant homology between BCG and NSP3 and NSP13 of SARS-CoV-2. NSP3 is a papain-like proteinase that shares a macro-domain with BCG proteins: macro-domain-containing protein and UPF0189 protein. This macro-domain-containing protein is conserved among the *Mycobacterium tuberculosis* complex including BCG (accession number WP_003909539.1), which encompasses strains used in BCG vaccine worldwide such as Pasteur and Connaught. NSP13 is a helicase that shares homology with BCG proteins RecB nuclease and zinc-metalloprotease-FtsH. Both RecB nuclease and zinc-metalloprotease-FtsH contain a walker-A-motif sequence that is identical in NSP13 of SARS-CoV-2. Additionally, RecB nuclease contains two other regions of homology with NSP13 around amino acid residues 952-966 and 1093-1107. As previously reported, NSP13 is highly conserved between other human coronaviruses. Thus, the T cell cross-protective potential of BCG may exist not only for SARS-CoV-2 but potentially with other human coronaviruses that cause the common cold (229E, NL63, OC43 and HKU1) and the more serious human coronaviruses SARS-CoV and Middle East respiratory syndrome coronavirus (MERS-CoV). NSP3 is, however, not as widely conserved among coronaviruses (6, 39).

For T cells to respond to antigen homologues, a significant degree of homology must also be paired with the capacity of an immunogenic peptide to bind cognate MHC class I or II. In the context of COVID-19, HLA binding has been reported as important in COVID-19 severity. Patients with mild COVID-19 presented MHCI molecules with a higher theoretical affinity than those with moderate to severe COVID-19 (31). We showed through *in silico* binding prediction assays that the BCG derived peptides with homologous sequences to SARS-CoV-2 peptides exhibited broad MHC class I and II binding capacity permitting antigen presentation across a globally representative HLA pool (**Figures S1, S2**). From these peptides, a selection of 8 homologue pairs were selected for *in vitro* co-culture analysis based on both high homology and high and broad peptide-HLA affinity (**Figure 1**).

The T cell responses measured were IFN-γ, TNF, IL-2, perforin and surface staining for the early T cell activation marker CD69, as well as a two-color proliferation assay to differentiate between a primary proliferative and secondary proliferative response. The enhanced cross-reactive response in BCG-primed, SARS-CoV-2 restimulated compared to not BCG-primed (**Figure 2**) confirms the high and broad HLA binding affinity prediction. We also show these cross-reactive peptides are immunogenic as they can elicit CD4+ Th1-like responses and robust CD8+ responses upon SARS-CoV-2 restimulation.

IFN-γ, TNF and IL-2 cytokine responses were significantly increased across at least 7 of the 8 peptide pairs tested in both CD4+ and CD8+ T cells. Patterns of cytokine production were varied between individuals and peptide pairs, which is reflected in the complex pattern of T cell cytokine expression and phenotypes that BCG vaccination is known to produce (40). Indeed, the IFN-γ and TNF response was mixed with some individuals making only IFN-γ or TNF in response to a particular peptide pair and some being positive for both (**Figure S7**). This observation is concordant with previously reported responses in COVID-19 (5, 6).

In CD8+ T cells, the target cell lysis protein, perforin, was significantly increased in the BCG-primed group compared to control-primed across all 8 peptide pairs (**Figure S5B**). The heightened perforin response suggests cross-reactive CD8+ T cells have the capacity to affect a superior antiviral response by target cell lysis. CD4+ and CD8+ T cell activation and proliferation were measured by activation marker CD69 expression and cell proliferation dye dilution. In at least 7 of the 8 tested peptide pairs across CD4+ and CD8+ T cells, BCG peptide sensitized cells developed significantly enhanced activation and proliferation to its SARS-CoV-2 homologous peptide (**Figures S5C**, **S6B**). The increase in T cell activation permits clonal expansion of the cross-reactive T cells and the development of their effector functions, which is necessary in mounting an effective immune response against SARS-CoV-2.

HLA-blocking experiments showed the T cell cytokine responses were abrogated when the HLA was blocked (**Figure S8**). This indicates the mechanism is the result of TCR-dependent heterologous immunity whereby BCG-primed, SARS-CoV-2 restimulation responses arise from peptide-MHC on the DCs binding to a cross-reactive T cell receptor on CD4+ or CD8+ T cells.

Assessing the 11 tested parameters in this study across both $CD4^+$ and $CD8^+$ T cells, it can be seen that all 8 identified

peptides are capable of eliciting significant T cell cross-reactivity across a broad range of HLA-typed individuals. Therefore, instead of identifying one dominant epitope, a set of 8 epitopes were identified. Further characterization and delineation of these cross-reactive epitopes will assist in deeper understanding of this mechanism such as by using alanine substitution assays to determine the dominant amino acids at play here and antigen-specific tetramers to quantify the natural frequency of cross-reactive T cells. The 8 epitopes capable of T cell cross-reactivity would likely have an additive effect when administered altogether such as in a BCG vaccine.

A comparison of the SARS-CoV-2 peptide immune response in COVID-19 unaffected individuals either vaccinated with BCG or never vaccinated with BCG showed the BCG vaccinated individuals exhibited across all peptides a trend to increased TNF and IFN-γ responses in $CD4^+$ and $CD8^+$ T cells and three of these parameters were statistically significant (**Figure S9**). Despite the lack of statistical significance, this is still a noteworthy result since the BCG vaccinated group were all adults who received their BCG vaccination decades earlier during childhood. Further studies are needed to assess whether a recent BCG vaccination or booster, such as those being administered in the clinical trials, would enhance cross-reactive T cells. Another case for consideration is the low frequency of memory T cells present in peripheral blood compared to other sites such as the spleen and lymph nodes, which may restrict the ability to properly identify and characterize the cross-reactive memory T cells. The low number of cells assayed also further restricted the ability to assess the presence of these antigen-specific T cells.

Further research into the clinical significance of such cross-reactive T cells is critical to characterize any protective benefits observed in COVID-19. Samples and data from the clinical trials and further observational or epidemiological studies will be valuable in determining the extent of any clinical significance in protection from COVID-19.

Collectively, the tested parameters indicate that BCG-primed T cells are able to produce superior effector functions upon SARS-CoV-2-peptide restimulation compared to those not presensitized with BCG peptides. The observed cross-reactive effects of CD4+ and CD8+ T cells may be of importance in swift and effective viral clearance of SARS-CoV-2, reducing the severity of symptoms in COVID-19 patients pre-vaccinated with BCG. However, the *in vivo* effect of these cross-reactive T cells in BCG vaccinated individuals, especially memory T cell subsets remains to be determined.

The continuation of the more than 30 clinical trials assessing the role of BCG in COVID-19 is necessary to further gain insights into the extent of the protective effect. Once enough data is available about the extent of the protective effect BCG could have in COVID-19, a decision about its adoption as a vaccination in lieu of a specific COVID-19 vaccine could lead to improved patient outcomes. This is particularly important in settings where COVID-19 vaccine availability remains scarce or non-existent and in high-risk groups such as health care workers and the elderly.

CONCLUSIONS

Collectively, our results demonstrate CD4+ and CD8+ T cells specific for BCG peptides cross-react with SARS-CoV-2 peptides. These data provide a possible mechanistic explanation for the observed negative epidemiological associations between BCG vaccinations and COVID-19 severity and mortality and support the continuation of clinical trials around the world, particularly in people at high-risk of contracting SARS-CoV-2 or with a heightened risk of COVID-19 mortality.

DATA AVAILABILITY STATEMENT

The original contributions presented in the study are included in the article/**Supplementary Material**. Further inquiries can be directed to the corresponding author.

ETHICS STATEMENT

The studies involving human participants were reviewed and approved by Monash University Human Research Ethics Committee. The patients/participants provided their written informed consent to participate in this study.

AUTHOR CONTRIBUTIONS

PE designed and performed research, analyzed data, and wrote the manuscript. BN performed experiments and analyzed data. JC and AF performed experiments. WW analyzed data. RC, P-YG, and SH analyzed data and provided intellectual input. JO designed research, analyzed data, and wrote the manuscript. All authors contributed to the article and approved the submitted version.

FUNDING

This work was supported by Monash Health Foundation COVID-19 Research Fund Grant. The funders had no role in study design, data collection and analysis, decision to publish, or preparation of the manuscript.

ACKNOWLEDGMENTS

We thank donors for their blood donations. Authors would like to thank Anita Cummins, Kathleen Elford, Susan Morton, and Ai-Li Yeo for phlebotomy and Seiya Fukada for technical assistance.

SUPPLEMENTARY MATERIAL

The Supplementary Material for this article can be found online at: https://www.frontiersin.org/articles/10.3389/fimmu.2021.692729/full#supplementary-material

REFERENCES

1. Zhou P, Yang XL, Wang XG, Hu B, Zhang L, Zhang W, et al. A Pneumonia Outbreak Associated With a New Coronavirus of Probable Bat Origin. *Nature* (2020) 579(7798):270–3. doi: 10.1038/s41586-020-2012-7
2. Le TT, Cramer JP, Chen R, Mayhew S. Evolution of the COVID-19 Vaccine Development Landscape. *Nat Rev Drug Discov* (2020) 19(10):667–8. doi: 10.1038/d41573-020-00151-8
3. Laing AG, Lorenc A, Del Molino Del Barrio I, Das A, Fish M, Monin L, et al. A Dynamic COVID-19 Immune Signature Includes Associations With Poor Prognosis. *Nat Med* (2020) 26(10):1623–35. doi: 10.1038/s41591-020-1038-6
4. Peng Y, Mentzer AJ, Liu G, Yao X, Yin Z, Dong D, et al. Broad and Strong Memory CD4(+) and CD8(+) T Cells Induced by SARS-CoV-2 in UK Convalescent Individuals Following COVID-19. *Nat Immunol* (2020) 21 (11):1336–45. doi: 10.1038/s41590-020-0782-6
5. Altmann DM, Boyton RJ. SARS-CoV-2 T Cell Immunity: Specificity, Function, Durability, and Role in Protection. *Sci Immunol* (2020) 5(49): eabd6160. doi: 10.1126/sciimmunol.abd6160
6. Le Bert N, Tan AT, Kunasegaran K, Tham CYL, Hafezi M, Chia A, et al. SARS-CoV-2-Specific T Cell Immunity in Cases of COVID-19 and SARS, and Uninfected Controls. *Nature* (2020) 584(7821):457–62. doi: 10.1038/s41586-020-2550-z
7. Grifoni A, Weiskopf D, Ramirez SI, Mateus J, Dan JM, Moderbacher CR, et al. Targets of T Cell Responses to SARS-CoV-2 Coronavirus in Humans With COVID-19 Disease and Unexposed Individuals. *Cell* (2020) 181(7):1489–501 e15. doi: 10.1016/j.cell.2020.05.015
8. Welsh RM, Che JW, Brehm MA, Selin LK. Heterologous Immunity Between Viruses. *Immunol Rev* (2010) 235(1):244–66. doi: 10.1111/j.0105-2896.2010.00897.x
9. Higgins JP, Soares-Weiser K, Lopez-Lopez JA, Kakourou A, Chaplin K, Christensen H, et al. Association of BCG, DTP, and Measles Containing Vaccines With Childhood Mortality: Systematic Review. *BMJ* (2016) 355: i5170. doi: 10.1136/bmj.i5170
10. Nemes E, Geldenhuys H, Rozot V, Rutkowski KT, Ratangee F, Bilek N, et al. Prevention of M. Tuberculosis Infection With H4:IC31 Vaccine or BCG Revaccination. *N Engl J Med* (2018) 379(2):138–49. doi: 10.1056/NEJMoa1714021
11. Wardhana, Datau EA, Sultana A, Mandang VV, Jim E. The Efficacy of Bacillus Calmette-Guerin Vaccinations for the Prevention of Acute Upper Respiratory Tract Infection in the Elderly. *Acta Med Indones* (2011) 43(3):185–90.
12. Ohrui T, Nakayama K, Fukushima T, Chiba H, Sasaki H. [Prevention of Elderly Pneumonia by Pneumococcal, Influenza and BCG Vaccinations]. *Nihon Ronen Igakkai Zasshi* (2005) 42(1):34–6. doi: 10.3143/geriatrics.42.34
13. Kleinnijenhuis J, Quintin J, Preijers F, Benn CS, Joosten LA, Jacobs C, et al. Long-Lasting Effects of BCG Vaccination on Both Heterologous Th1/Th17 Responses and Innate Trained Immunity. *J Innate Immun* (2014) 6(2):152–8. doi: 10.1159/000355628
14. O'Neill LAJ, Netea MG. BCG-Induced Trained Immunity: Can it Offer Protection Against COVID-19? *Nat Rev Immunol* (2020) 20(6):335–7. doi: 10.1038/s41577-020-0337-y
15. Goodridge HS, Ahmed SS, Curtis N, Kollmann TR, Levy O, Netea MG, et al. Harnessing the Beneficial Heterologous Effects of Vaccination. *Nat Rev Immunol* (2016) 16(6):392–400. doi: 10.1038/nri.2016.43
16. de Castro MJ, Pardo-Seco J, Martinon-Torres F. Nonspecific (Heterologous) Protection of Neonatal BCG Vaccination Against Hospitalization Due to Respiratory Infection and Sepsis. *Clin Infect Dis* (2015) 60(11):1611–9. doi: 10.1093/cid/civ144
17. Mathurin KS, Martens GW, Kornfeld H, Welsh RM. CD4 T-Cell-Mediated Heterologous Immunity Between Mycobacteria and Poxviruses. *J Virol* (2009) 83(8):3528–39. doi: 10.1128/JVI.02393-08
18. Vetskova EK, Muhtarova MN, Avramov TI, Stefanova TR, Chalakov IJ, Nikolova MH. Immunomodulatory Effects of BCG in Patients With Recurrent Respiratory Papillomatosis. *Folia Med (Plovdiv)* (2013) 55(1):49–54. doi: 10.2478/folmed-2013-0005
19. Curtis N, Sparrow A, Ghebreyesus TA, Netea MG. Considering BCG Vaccination to Reduce the Impact of COVID-19. *Lancet* (2020) 395 (10236):1545–6. doi: 10.1016/S0140-6736(20)31025-4
20. Amirlak l, Haddad R, Hardy JD, Khaled NS, Chung MH, Amirlak B. Effectiveness of Booster BCG Vaccination in Preventing Covid-19 Infection. *medRxiv* (2020) 2020.08.10.20172288. doi: 10.1101/2020.08.10.20172288
21. Kumar NP, Padmapriyadarsini C, Rajamanickam A, Bhavani PK, Nancy A, Jayadeepa B, et al. BCG Vaccination Induces Enhanced Frequencies of Memory T and B Cells and Dendritic Cell Subsets in Elderly Individuals. *medRxiv* (2020) 2020.10.22.20217471. doi: 10.1101/2020.10.22.20217471
22. Padmanabhan U, Mukherjee S, Borse R, Joshi S, Deshmukh R. Phase II Clinical Trial for Evaluation of BCG as Potential Therapy for COVID-19. *medRxiv* (2020) 2020.10.28.20221630. doi: 10.1101/2020.10.28.20221630
23. Tsilika M, Taks E, Dolianitis K, Kotsaki A, Leventogiannis K, Damoulari C, et al. Activate-2: A Double-Blind Randomized Trial of BCG Vaccination Against Covid19 In Individuals at Risk. *medRxiv* (2021) 2021.05.20.21257520. doi: 10.1101/2021.05.20.21257520
24. Escobar LE, Molina-Cruz A, Barillas-Mury C. BCG Vaccine Protection From Severe Coronavirus Disease 2019 (COVID-19). *Proc Natl Acad Sci USA* (2020) 117(30):17720–6. doi: 10.1073/pnas.2008410117
25. Berg MK, Yu Q, Salvador CE, Melani I, Kitayama S. Mandated Bacillus Calmette-Guerin (BCG) Vaccination Predicts Flattened Curves for the Spread of COVID-19. *Sci Adv* (2020) 6(32):eabc1463. doi: 10.1126/sciadv.abc1463
26. Hauer J, Fischer U, Auer F, Borkhardt A. Regional BCG Vaccination Policy in Former East- and West Germany may Impact on Both Severity of SARS-CoV-2 and Incidence of Childhood Leukemia. *Leukemia* (2020) 34(8):2217–9. doi: 10.1038/s41375-020-0871-4
27. Rivas MN, Ebinger JE, Wu M, Sun N, Braun J, Sobhani K, et al. BCG Vaccination History Associates With Decreased SARS-CoV-2 Seroprevalence Across a Diverse Cohort of Health Care Workers. *J Clin Invest* (2021) 131(2): e145157. doi: 10.1172/JCI145157
28. Weiskopf D, Angelo MA, de Azeredo EL, Sidney J, Greenbaum JA, Fernando AN, et al. Comprehensive Analysis of Dengue Virus-Specific Responses Supports an HLA-Linked Protective Role for CD8+ T Cells. *Proc Natl Acad Sci USA* (2013) 110(22):E2046–53. doi: 10.1073/pnas.1305227110
29. Reynisson B, Alvarez B, Paul S, Peters B, Nielsen M. NetMHCpan-4.1 and NetMHCIIpan-4.0: Improved Predictions of MHC Antigen Presentation by Concurrent Motif Deconvolution and Integration of MS MHC Eluted Ligand Data. *Nucleic Acids Res* (2020) 48(W1):W449–54. doi: 10.1093/nar/gkaa379
30. Greenbaum J, Sidney J, Chung J, Brander C, Peters B, Sette A. Functional Classification of Class II Human Leukocyte Antigen (HLA) Molecules Reveals Seven Different Supertypes and a Surprising Degree of Repertoire Sharing Across Supertypes. *Immunogenetics* (2011) 63(6):325–35. doi: 10.1007/s00251-011-0513-0
31. Iturrieta-Zuazo I, Rita CG, Garcia-Soidan A, de Malet Pintos-Fonseca A, Alonso-Alarcon N, Pariente-Rodriguez R, et al. Possible Role of HLA Class-I Genotype in SARS-CoV-2 Infection and Progression: A Pilot Study in a Cohort of Covid-19 Spanish Patients. *Clin Immunol* (2020) 219:108572. doi: 10.1016/j.clim.2020.108572
32. Madeira F, Park YM, Lee J, Buso N, Gur T, Madhusoodanan N, et al. The EMBL-EBI Search and Sequence Analysis Tools APIs in 2019. *Nucleic Acids Res* (2019) 47(W1):W636–41. doi: 10.1093/nar/gkz268
33. Balz K, Trassl L, Hartel V, Nelson PP, Skevaki C. Virus-Induced T Cell-Mediated Heterologous Immunity and Vaccine Development. *Front Immunol* (2020) 11:513. doi: 10.3389/fimmu.2020.00513
34. Bui HH, Sidney J, Dinh K, Southwood S, Newman MJ, Sette A. Predicting Population Coverage of T-Cell Epitope-Based Diagnostics and Vaccines. *BMC Bioinf* (2006) 7:153. doi: 10.1186/1471-2105-7-153
35. Raue HP, Brien JD, Hammarlund E, Slifka MK. Activation of Virus-Specific CD8+ T Cells by Lipopolysaccharide-Induced IL-12 and IL-18. *J Immunol* (2004) 173(11):6873–81. doi: 10.4049/jimmunol.173.11.6873
36. Gilbertson B, Germano S, Steele P, Turner S, Fazekas de St Groth B, Cheers C. Bystander Activation of CD8+ T Lymphocytes During Experimental Mycobacterial Infection. *Infect Immun* (2004) 72(12):6884–91. doi: 10.1128/IAI.72.12.6884-6891.2004
37. Kim SK, Cornberg M, Wang XZ, Chen HD, Selin LK, Welsh RM. Private Specificities of CD8 T Cell Responses Control Patterns of Heterologous Immunity. *J Exp Med* (2005) 201(4):523–33. doi: 10.1084/jem.20041337
38. Urbán S, Paragi G, Burián K, McLean GR, Virok DP. Identification of Similar Epitopes Between Severe Acute Respiratory Syndrome Coronavirus-2 and

Bacillus Calmette–Guérin: Potential for Cross-Reactive Adaptive Immunity. *Clin Trans Immunol* (2020) 9(12):e1227. doi: 10.1002/cti2.1227

39. Wu A, Peng Y, Huang B, Ding X, Wang X, Niu P, et al. Genome Composition and Divergence of the Novel Coronavirus (2019-Ncov) Originating in China. *Cell Host Microbe* (2020) 27(3):325–8. doi: 10.1016/j.chom.2020.02.001
40. Soares AP, Scriba TJ, Joseph S, Harbacheuski R, Murray RA, Gelderbloem SJ, et al. Bacillus Calmette-Guerin Vaccination of Human Newborns Induces T Cells With Complex Cytokine and Phenotypic Profiles. *J Immunol* (2008) 180 (5):3569–77. doi: 10.4049/jimmunol.180.5.3569

Conflict of Interest: The authors declare that the research was conducted in the absence of any commercial or financial relationships that could be construed as a potential conflict of interest.

Publisher's Note: All claims expressed in this article are solely those of the authors and do not necessarily represent those of their affiliated organizations, or those of the publisher, the editors and the reviewers. Any product that may be evaluated in this article, or claim that may be made by its manufacturer, is not guaranteed or endorsed by the publisher.

Copyright © 2021 Eggenhuizen, Ng, Chang, Fell, Cheong, Wong, Gan, Holdsworth and Ooi. This is an open-access article distributed under the terms of the Creative Commons Attribution License (CC BY). The use, distribution or reproduction in other forums is permitted, provided the original author(s) and the copyright owner(s) are credited and that the original publication in this journal is cited, in accordance with accepted academic practice. No use, distribution or reproduction is permitted which does not comply with these terms.

frontiers in Immunology

REVIEW
published: 08 September 2021
doi: 10.3389/fimmu.2021.730051

Degenerate CD8 Epitopes Mapping to Structurally Constrained Regions of the Spike Protein: A T Cell-Based Way-Out From the SARS-CoV-2 Variants Storm

Carolina Boni[1†], Davide Cavazzini[2†], Angelo Bolchi[2,3†], Marzia Rossi[1,4], Andrea Vecchi[1], Camilla Tiezzi[1], Valeria Barili[1,4], Paola Fisicaro[1,4], Carlo Ferrari[1,4‡] and Simone Ottonello[2,3‡]*

[1] Laboratory of Viral Immunopathology, Unit of Infectious Diseases and Hepatology, Azienda-Ospedaliero-Universitaria di Parma, Parma, Italy, [2] Department of Chemistry, Life Sciences and Environmental Sustainability, University of Parma, Parma, Italy, [3] Interdepartmental Center Biopharmanet-Tec, University of Parma, Parma, Italy, [4] Department of Medicine and Surgery, University of Parma, Parma, Italy

OPEN ACCESS

Edited by:
Sara De Biasi,
University of Modena and Reggio Emilia, Italy

Reviewed by:
Eun Young Choi,
Seoul National University, South Korea
Jonathan Soboloff,
Temple University, United States

***Correspondence:**
Carlo Ferrari
carlo.ferrari@unipr.it

[†]These authors have contributed equally to this work

[‡]These authors jointly supervised this work

Specialty section:
This article was submitted to T Cell Biology, a section of the journal Frontiers in Immunology

Received: 24 June 2021
Accepted: 11 August 2021
Published: 08 September 2021

Citation:
Boni C, Cavazzini D, Bolchi A, Rossi M, Vecchi A, Tiezzi C, Barili V, Fisicaro P, Ferrari C and Ottonello S (2021) Degenerate CD8 Epitopes Mapping to Structurally Constrained Regions of the Spike Protein: A T Cell-Based Way-Out From the SARS-CoV-2 Variants Storm. Front. Immunol. 12:730051. doi: 10.3389/fimmu.2021.730051

There is an urgent need for new generation anti-SARS-Cov-2 vaccines in order to increase the efficacy of immunization and its broadness of protection against viral variants that are continuously arising and spreading. The effect of variants on protective immunity afforded by vaccination has been mostly analyzed with regard to B cell responses. This analysis revealed variable levels of cross-neutralization capacity for presently available SARS-Cov-2 vaccines. Despite the dampened immune responses documented for some SARS-Cov-2 mutations, available vaccines appear to maintain an overall satisfactory protective activity against most variants of concern (VoC). This may be attributed, at least in part, to cell-mediated immunity. Indeed, the widely multi-specific nature of CD8 T cell responses should allow to avoid VoC-mediated viral escape, because mutational inactivation of a given CD8 T cell epitope is expected to be compensated by the persistent responses directed against unchanged co-existing CD8 epitopes. This is particularly relevant because some immunodominant CD8 T cell epitopes are located within highly conserved SARS-Cov-2 regions that cannot mutate without impairing SARS-Cov-2 functionality. Importantly, some of these conserved epitopes are degenerate, meaning that they are able to associate with different HLA class I molecules and to be simultaneously presented to CD8 T cell populations of different HLA restriction. Based on these concepts, vaccination strategies aimed at potentiating the stimulatory effect on SARS-Cov-2-specific CD8 T cells should greatly enhance the efficacy of immunization against SARS-Cov-2 variants. Our review recollects, discusses and puts into a translational perspective all available experimental data supporting these "hot" concepts, with special emphasis on the structural constraints that limit SARS-CoV-2 S-protein evolution and on potentially invariant and degenerate

CD8 epitopes that lend themselves as excellent candidates for the rational development of next-generation, CD8 T-cell response-reinforced, COVID-19 vaccines.

Keywords: SARS-Cov-2, CD8 T cells, CD8 T cell epitopes, neutralizing antibodies, SARS-Cov-2 variants, spike region

INTRODUCTION

SARS-Cov-2 is a single-stranded RNA virus composed of four main structural and 16 non-structural proteins encoded by at least 6 open reading frames contained within genomic and subgenomic RNA regions (1–3). Among the spike (S), membrane (M), envelope (E), and nucleocapsid (N) structural proteins, a key biological and pathogenetic role is played by the trimeric spike glycoprotein (the main component of the available vaccines), which is responsible for the attachment of the virus to host receptors and is the main target of neutralizing antibodies that can block virus entry into target cells (4–6). The spike protein protrudes as a homotrimer from the viral surface in a metastable 'prefusion' state (7–9). Each monomer is composed of two subunits: S1, which is primarily involved in host cell recognition *via* the RBD with structural support by the N-terminal domain (NTD), and the S2 subunit, which is mainly comprised of α-helixes, such as the heptad repeat 1 and 2 helixes (HR1 and HR2) and the central helix (CH) (see below for further details) (7). Additional S1 subunit modules are the C-terminal (CTD-1 and CTD-2) domains, which are involved in key intermolecular contacts with the S2 subunit within the trimeric S structure. In fact, upon interaction with the host cell surface, the primed S1 subunit is shed and the S2 subunit undergoes a dramatic conformational change that promotes the transition to the 'postfusion' state, ultimately leading to viral fusion and cell entry, mediated by the S2 fusion peptide (10).

As all RNA viruses, SARS-Cov-2 is prone to mutations, but its mutation rate is restrained by the proof-reading activity of an exoribonuclease (non-structural protein 14) that substantially reduces mistaken nucleotide incorporation into nascent RNA molecules (11, 12). Despite this proof-reading activity, SARS-Cov-2 remains capable of accumulating mutations, that upon selection and subsequent fixation can interfere with virus recognition by the immune system, thus compromising immune-protection. New mutations tend to be fixed either because of the enhanced infection and transmission capacity they confer and/or because they allow variant viruses to evade control by neutralizing antibodies and cytotoxic CD8 T cells, with preferential elimination of the parental virus and selection of the mutated strain. Both mechanisms are thought to be causally involved in the selection of SARS-Cov-2 variants (the so-called Variants of Concern – VoC - and Variants of Interest - VoI). Indeed, some of these variants become more infectious and can spread more quickly due to a mutationally acquired enhancement of the binding affinity between the spike protein Receptor Binding Domain (RBD) and Angiotensin-Converting Enzyme 2 (ACE2), the main virus receptor exposed on the surface of target host cells. The same mutations can also allow the virus to escape neutralization by circulating anti-spike antibodies, produced in the context of a humoral immune response.

The possibility of a complete virus escape, however, is theoretically limited by the polyclonality and multispecificity of the antibody response (13). This would obviously imply that different spike regions are simultaneously recognized by polyclonal anti-spike antibodies of different specificity, elicited by the virus (or by a vaccine) in each patient. Moreover, a variable proportion of the elicited antibodies may be directed against largely invariable spike regions, i.e., protein regions whose mutational change would severely impair the fitness of the virus (14–18). Thus, loss of immune-recognition of a certain spike region caused by a mutational event, should, in principle, be compensated by the persistent recognition of the virus by antibody molecules directed against spike regions that have not changed or that are intrinsically not permissive to amino acid substitutions because of structural or functional constraints. This concept is only partially confirmed by recent evidence suggesting that wild type spike-induced antibodies in vaccinees and convalescent patients have a diminished neutralizing capacity *in vitro* against some of the most recent spike variants (19–21), an immune-reactivity reduction that, however, does not appear to be strong enough to cause a complete loss of anti-viral protection *in vivo* (22–25). To this persistence of protection *in vivo* may also contribute a process of antibody maturation, which has been reported to increase the neutralizing potency and breadth of protection of the antibody response (26–29). As we will discuss in detail in this review, a persisting, vaccine-stimulated CD8 T cell effector function is also potentially capable of compensating the negative effect of escape spike mutations on antibody responses.

CD8 T CELLS IN ANTI-SARS-COV-2 PROTECTION

In addition to circulating antibodies, an important role in antiviral protection is played by cytotoxic CD8 T cells. Although not capable of preventing infection by neutralizing free viral particles and blocking their entry into host cells, CD8 T cells can avoid the spread of infection by eliminating infected cells through their cytotoxic activity and by purging intracellular virus through non-cytolytic mechanisms mediated by antiviral cytokine secretion at the site of infection (30–32). The importance of CD8 T cells is further indicated by the recent observation that SARS-Cov-2 spike protein can induce cell fusion and can exploit this mechanism for cell to cell spread, escaping antibody neutralization (33, 34). Data derived from

infected patients indicate that CD8-mediated control of infection should be considerably less affected by mutational loss of immune reactivity, because CD8 T cell responses are broadly multi-specific (35–38). This makes mutation-mediated virus escape from CD8 T cell control much more unlikely than virus escape from neutralizing antibodies, meaning that even in case of a decline or loss of antibody neutralizing activity against SARS-Cov-2 variants, the persisting activity of cytotoxic CD8 T cells can likely limit or prevent a severe evolution of infection. Such a role of CD8 T cells in SARS-Cov-2 control is further corroborated by evidence indicating that T cell memory responses have an intrinsic capacity to persist for a very long time (up to 17 years after SARS-Cov-1 infection) (36), remaining detectable well after antibody waning. Additional support to a prominent CD8 T cell-mediated protective activity is provided by available sequencing and immunological data (39–43).

Thirty-one amino acid substitutions and three amino acid deletions arising from multiple selected mutations have been identified by comparing the *in silico* translated spike polypeptide sequences derived from the UK (Alpha), South-African (Beta), Brazilian (Gamma), Californian (Epsilon), Indian (Delta) VoCs, as well as Nigerian (Eta) and New Yorker (Iota) VoIs with the sequence of the original Wuhan SARS-Cov-2 strain (GISAID data base - https://cov.lanl.gov/content/index) (44–55). Twenty-three of these amino acid changes are located in spike regions that encompass recently described CD8 epitopes and account for a total of 35 CD8 T cell epitopes with mutated sequences (56–62). The remaining 11 variant mutations, instead, do not affect any known CD8 epitope. The linear distribution of CD8 epitopes-containing variant mutations along the spike polypeptide sequence and the spatial location of each mutation within the 3D structure of a spike monomer are shown in **Figure 1** in the context of a single spike monomer.

A number of CD8 T cell epitopes (n=133), presented to CD8 T cells by different HLA class I alleles, has been reported to be located within unmutated spike regions (56–74). They are characterized by different levels of immunodominance and endowed with different CD8 T cell stimulatory capacities, as deduced from the intensity of CD8 responses measured by functional assays [e.g., TCR-dependent Activation Induced

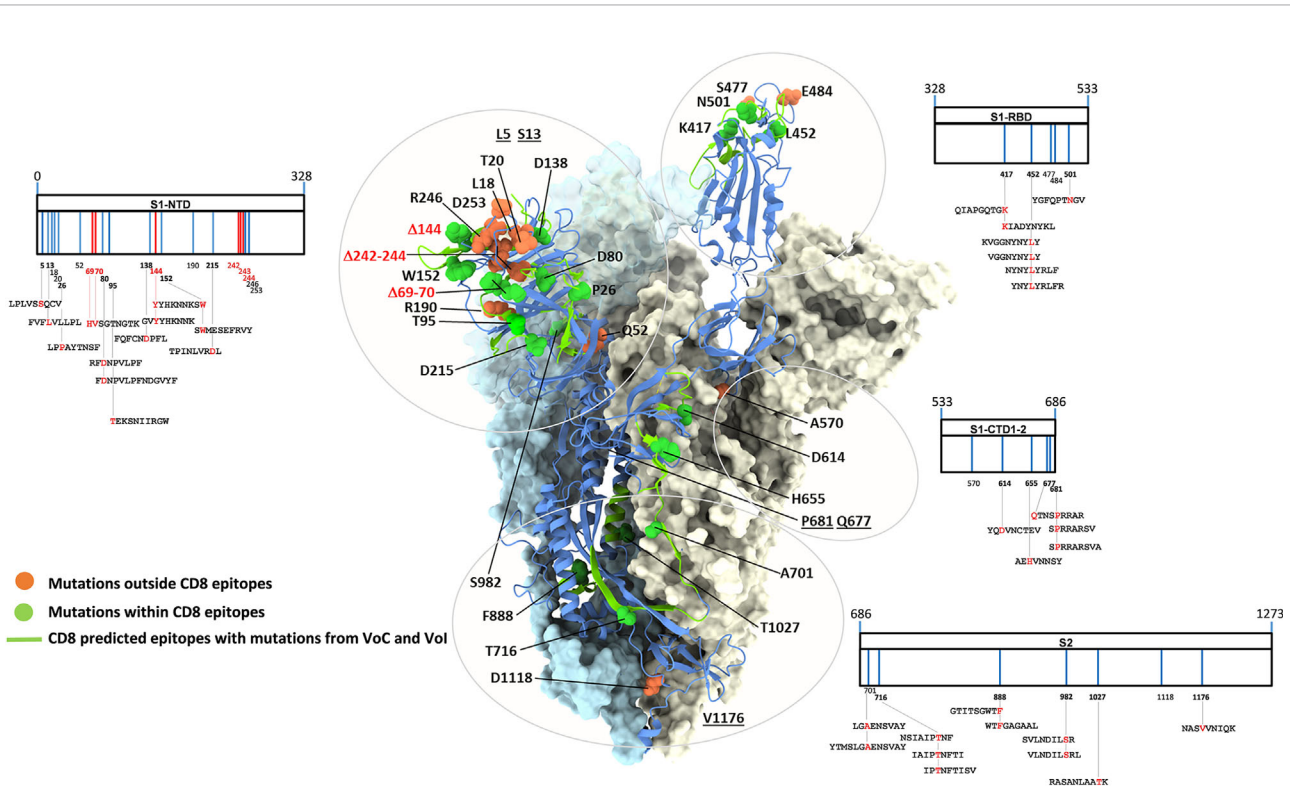


FIGURE 1 | SARS-CoV-2 spike mutation and deletion map of the prominent circulating VoC/VoI and SARS-Cov-2-specific CD8 T cell epitopes containing mutations. SARS-CoV-2 spike organization: each vertical line within the external charts indicates individual amino acid mutations or deletions of the UK, South Africa, Brazil, Nigeria, California, New Yorker and India variants (in blue and red, respectively) among the S1 and S2 subunits and the Receptor Binding Domain (RBD). SARS-CoV-2-specific CD8 T cell epitopes within the spike protein described in the literature and containing variant mutations are depicted at the bottom of each chart. All amino acid sequences of the 35 CD8 T cell epitopes are reported; mutation and deletion sites are indicated by their position number (numbers in bold indicate mutations contained in described epitopes) and are depicted in red within the epitope sequences. The trimer structure of a spike ectodomain (PDB 6ZXN), with one protomer in *blue cartoon* (RBD-up) and the two other protomers (both RBD-down) represented as *light blue* and *ice* surfaces, is shown as a reference in the *central part* of the figure. Mutation-affected residues outside or within CD8 epitopes are represented as *orange* and *green* spheres, respectively. Spike secondary structure elements containing CD8 epitopes affected by variant mutations are shown as *green* ribbons. Specific amino acids located within unresolved regions or targeted by deletions are *underlined* or shown in *red*, respectively. Glycan-modified regions as well as the NTD surface of one spike protomer were omitted for clarity.

Marker (AIM) and Elispot assays] and through the assessment of the frequency of circulating, multimer-positive SARS-Cov-2 specific CD8 T cells (56–74). In particular, 85 of these epitopes are recognized by CD8 T cells in association with the most highly represented HLA-class I alleles (frequency > 5%, as calculated by their median expression value in the world population), namely HLA A*01, A*02, A*03, A*11, A*24, A*26, A*31, A*68, B*07, B*08, B*15, B*35, B*40, B*44, B*51, whereas 13 additional epitopes are presented to CD8 T cells by less represented HLA-class I alleles, such as HLA A*23, A*29, A*30, A*32, B*53, B*57 (**Figure 2A**). Importantly, the remaining 35 epitopes described so far share a degenerate HLA class I presentation, and can be recognized by CD8 T cells in the context of different HLA-class I alleles (**Figure 2B**). Finally, available data indicate that different epitopes can be simultaneously recognized by individual patients confirming the multi-specificity of CD8 T cell responses (56).

To gain a deeper insight into the effect of SARS-Cov-2 mutations on CD8 T cells responses, we analyzed 1,400,000 million spike protein sequences retrieved (as of June 1st 2021) from the daily updated GISAID database. Considering the Shannon entropy (SE; a measure of variability of genetic mutations (75) for each amino acid position, calculated on a multiple alignment of spike protein sequences), we identified eight additional and potentially significant amino acid changes

A

Epitopes within non mutated sequences

HLA class I alleles with > 5% frequency

	A*01	A*02	A*03	A*11	A*24	A*26	A*31	A*68	B*07	B*08	B*15	B*35	B*40	B*44	B*51	TOT
N. of epitopes	0	11	5	0	14	6	3	6	5	4	1	5	8	11	6	85

HLA class I alleles with < 5% frequency

	A*23	A*29	A*30	A*32	B*53	B*57	TOT
N. of epitopes	0	5	2	1	2	3	13

B

Degenerate CD8 T cell epitopes in relation to their HLA class I restriction (n = 35)

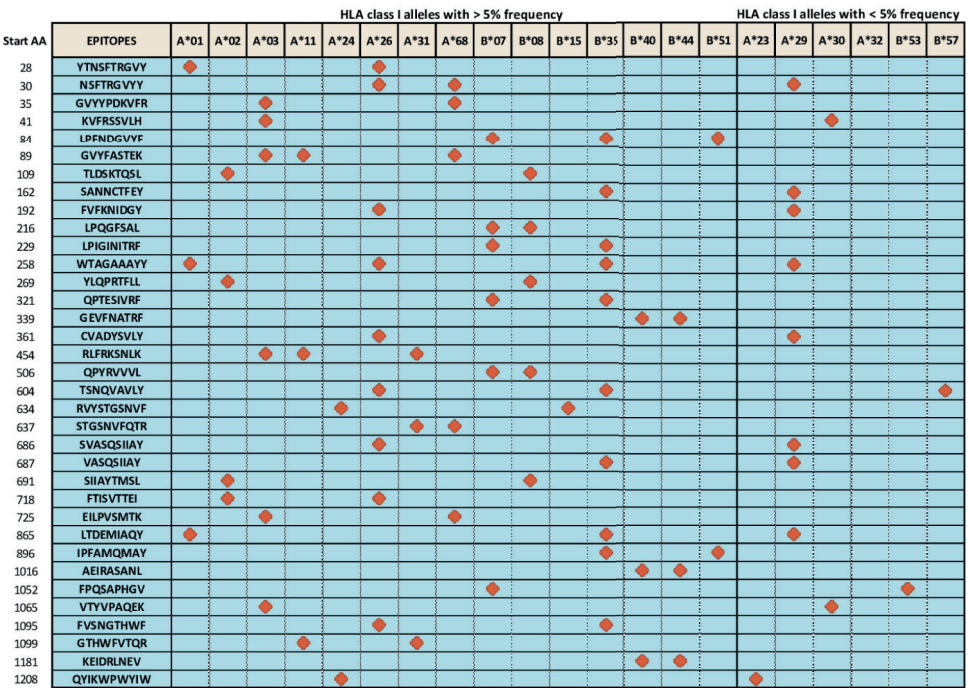


FIGURE 2 | Distribution of SARS-Cov-2 CD8 T epitopes located within non mutated sequences of the spike region in relation to their HLA restriction. **(A)** CD8 T cell epitopes located within non mutated sequences of the spike region recognized by CD8 T cells in association with individual HLA-class I alleles with frequencies > 5% (top) and < 5% (bottom). **(B)** Thirty-five CD8 T cell epitopes characterized experimentally as degenerate because capable of recognizing individual viral epitopes in the context of different HLA-class I alleles simultaneously are represented according to the HLA class I allele frequency (> or < 5%). All amino acid sequences are reported on the left. Red symbols indicate the HLA class I molecule able to present a given epitope to CD8 T cells.

(SE values > 0.05, corresponding to a frequency of variation of more than 1% with respect to the Wuhan spike sequence). Four of these changes are located in regions spanning previously described CD8 T cell epitopes (S98F, A222V, A262S, T732A), while the other four (N439K, T478K, Q675I/R, K1191N) map to spike regions where no CD8 T cell epitopes have been described so far.

We then assessed if some of the epitopes that span spike sequences which have thus far been spared from mutation are actually located within spike regions unable to tolerate any sequence variation because of their essential role for proper structure/function of the virus. By referring to the two subunits of the spike protein, a significantly lower sequence variation was found to be associated to the S2 fusion subunit (Avg SE= 6.2x10e-3) compared to the S1-RBD-containing subunit (Avg SE=1.3x10e-2). This fits with the key role played by the latter subunit in the recognition of host cell receptors (ACE2, but also neuropilin and some newly identified membrane lectins) (76, 77) through the RBD and the NTD domains as well as with its role as the main target of neutralizing antibodies. Mutations that increase the binding affinity of the S1 subunit for its receptors and/or enable escape from neutralizing antibodies are, in fact, instrumental to virus propagation and highly prone to selection and fixation. Conversely, the less exposed S2 subunit, which upon S1 dissociation undergoes a large conformational change ultimately leading to viral-host cell membrane fusion, is a less likely candidate for viral evolution. This differential sequence conservation is also in keeping with the amino acid sequence identity (S2>S1) shared by the spike subunits of different SARS-CoV-2 variants and of more distantly related SARS-CoV viruses. Also in the case of this broader-range comparison, the S2 subunit appears to be considerably less variable (89% identity) than the S1 subunit (65% identity).

Using SE values of 0.0025, 0.001 and 0.0005 as decreasing entropy thresholds, we then arbitrarily defined three levels of amino acid (AA) residue conservation, which allowed us to tag different spike regions as 'conserved', 'highly conserved' and 'hyper conserved', respectively (see **Figures 3**, **4A**, where epitopes classified as above are color-coded in yellow, red and purple, respectively).

Interestingly, 37 previously reported CD8 epitopes, varying in length from 8 to 12 AA, plus four additional putative epitopes identified with NetMHC-4.0 (79) and characterized by probability scores comparable to or higher than those of experimentally validated epitopes, all map to structurally constrained regions of the spike protein (**Figure 4B**). Although some of the 37 immunogenic sequences are extensively overlapping (e.g., the FERDISTEI and FERDISTEIY sequences both starting at AA 464; **Figure 3**), and thus likely correspond to the same core epitope, a sizeable number of non-redundant CD8 epitopes appears to be located within conserved spike structural elements, whose mutation would compromise SARS-CoV-2 functionality (**Figures 3**, **4**). The distribution of CD8 T cell epitopes within spike regions of different sequence conservation with indication of their main features is reported in **Table 1**.

Although the CD8 epitopes discussed in this section have originally been identified in infected and convalescent patients, available studies in vaccinees (43, 80–83) confirm a substantial enrichment of CD8 T cell epitopes within the S2 domain, which contrasts with the lower CD8 epitope representation found in the S1 N-terminal domain (83).

PREDICTED INVARIANCE OF A SUBSET OF CD8 T CELL EPITOPES RESULTING FROM SPECIFIC STRUCTURAL AND FUNCTIONAL CONSTRAINTS THAT LIMIT SPIKE PROTEIN EVOLVABILITY

We then took advantage of multiple spike structures (6, 10, 84, 85) to precisely map specific CD8 T cell epitopes within functionally and structurally distinct regions of the spike protein. In fact, a number of predictably invariant CD8 T cell epitopes map to specific spike regions with different degrees of sequence and structural conservation such as the RBD core, the carboxy-terminal 1 (CTD1) and 2 (CTD2) domains within the S1 subunit and throughout the S2 subunit (**Figure 4B**).

Even the S1 subunit N-terminal domain (NTD), which holds approximately 50% of all spike VoC mutations and represents the only site of amino acid deletions so far (**Figure 1**), contains a few peptide segments that are significantly conserved (e.g., AA 34-48 and AA 119-137) (**Figures 3**, **5A**). The conserved AA 34-48 sequence, in particular, is close to the CTD1 of the adjacent protomer. This proximity region, which modulates spike conformational dynamics and is positionally shifted upon RBD binding to the ACE2 receptor, contains three epitopes (starting AA positions: 35, 36 and 41), two of which can be presented to CD8 T cells by more than one allele (AA 35-44 and 41-49).

A region of more marked structural/functional constraining within the S1 subunit, is the RBD (AA 328-533), a key domain for ACE2 receptor engagement, which is specifically mediated by the receptor-binding motif (RBM; AA 437-508) and only takes place when the spike protein is in the 'up conformation'. Despite the sustained average mutation rate of this domain, there is a subset of conserved peptides located within the RBD core β-structure, part of the flanking regions, and the hinge loops that connect the RBD to the CTD1 (**Figure 5B**). These regions are key to the 'up' to 'down' transition. In fact, they control the dynamic interaction between the RBD and the NTD domains of adjacent protomers and are involved in the sensing and transduction of specific conformational inputs from the S2 subunit (see **Figure 5B**, where the RBD is shown in the most interaction-competent, 'down' conformation). Eleven CD8 epitopes map to these conserved RBD regions and some of them can be presented to CD8 T cells by the most highly represented HLA-class I alleles (see **Figures 2**, **3** for specific epitope ranking). Interestingly, the AA 456-474 RBM sub-segment that interacts with the NTD of the adjacent protomer is characterized by a very low mutation rate and harbors at least three CD8 epitopes (one of which degenerate and with high predicted MHC-I binding affinities) comprised between amino acid residues R454 and Y473 (**Figure 5B**). In contrast to the high mutability of the upper

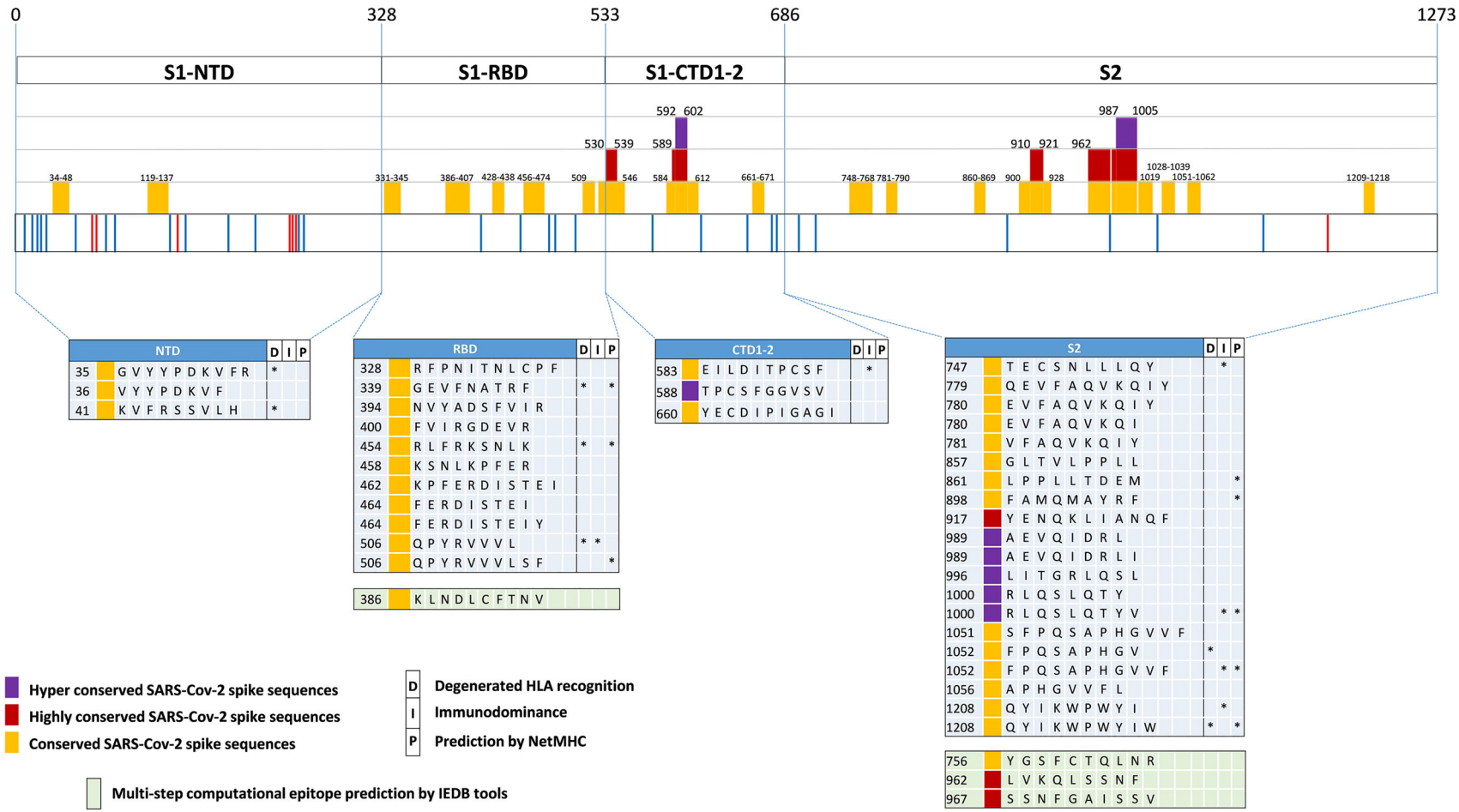


FIGURE 3 | SARS-Cov-2-specific CD8 T cell epitopes contained within conserved SARS-CoV-2 spike sequences. Violet, red and yellow areas within the SARS-CoV-2 spike region indicate the conserved SARS-Cov-2 spike sequences according to their preservation levels from mutations (the AA extension of each conserved region is indicated above the violet, red and yellow rectangles). SARS-CoV-2 spike mutation and deletion map of the prominent circulating VoC and VoI are represented below. Thirty-seven CD8 T cell epitope containing sequences reported in the literature and contained within these conserved regions are shown at the bottom according to their location within the S1/S2 subunits and the RBD region. Epitopes located within conserved, highly conserved and hyper-conserved sequences are marked by yellow, red and violet squares, respectively, on the left of the epitope sequences. The asterisks on the right of the sequence (*) indicate: *column marked by D*, epitopes characterized experimentally as degenerate because capable of recognizing individual viral epitopes in the context of different HLA-class I alleles simultaneously; *column marked by I*, immunodominant epitopes, defined as capable of eliciting positive responses in three or more donors/studies, derived from (78) and references therein*; column marked by P*, epitopes with a high prediction score by means of *NetMHC 4.0 Server* (all predicted to be recognized by multiple HLA-class I alleles with overall worldwide frequency higher than 20% and with high binding affinity for 30% of peptide/HLA interactions; http://www.cbs.dtu.dk/services/NetMHC/). Additional four CD8 T cell epitopes, selected through multi-step computational prediction IEDB tools (https://www.iedb.org/), are indicated in the green area. These latter epitopes are calculated based on the 27 most frequent worldwide HLA through the *Proteasomal cleavage/TAP transport/MHC class I combined predictor*. This tool allows to calculate a total score that combines the proteasomal cleavage, transport by the transporter associated with antigen processing (TAP) and MHC binding predictions. The identified epitopes are selected according to IC50 (*half maximal inhibitory concentration*) values <50 nM (considered high affinity); total score value > 75° percentile and further confirmed with *NetMHC 4.0 Server* by using artificial neural networks (ANNs).

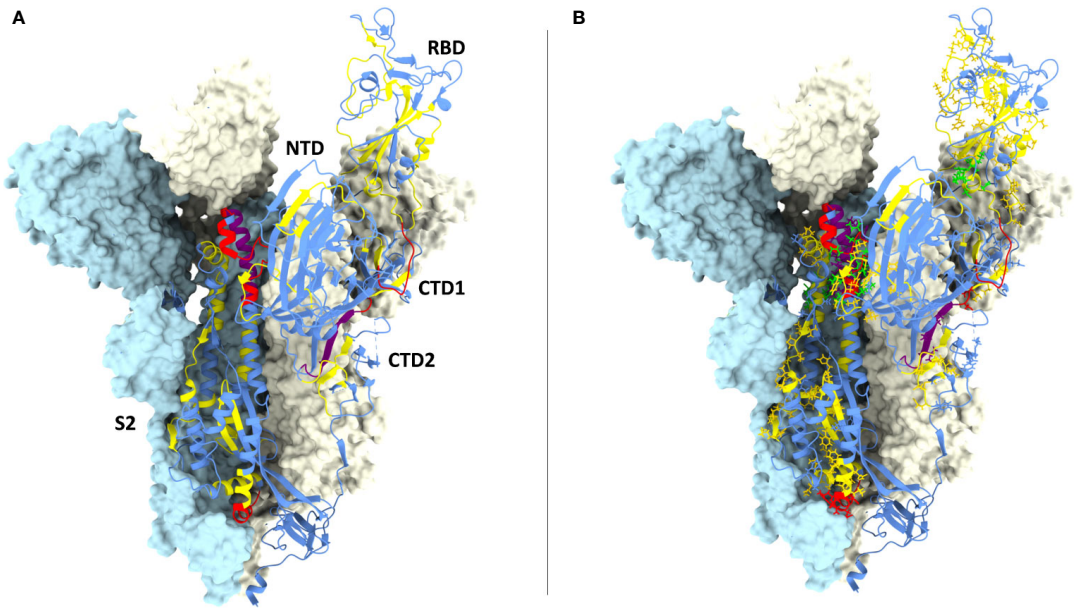


FIGURE 4 | CD8 epitopes mapping to spike conserved regions. **(A)** Structure of one spike S1 ectodomain (PDB 6ZXN) shown in ribbon representation, with the receptor-binding domain (RBD) in the 'up' conformation; the N-terminal domain (NTD), the two carboxy-terminal domains (CTD1 and CTD2) and the S2 subunit are indicated. The other two protomers of the spike trimer are shown as *opaque azur* and *pale-yellow* molecular surfaces (the RBD and the CTD1 domains of the *azur* protomer are omitted for clarity). The spike ribbon is colored to indicate regions of different amino acid residue entropy (*i.e.*, degree of conservation): *blue* (no conservation), *yellow* ('conserved'), *red* ('highly conserved'), *purple* ('hyper conserved'); see the text for a definition of the entropy value thresholds associated to each class of conservation. **(B)** Same as **(A)** but with the amino acid residues of previously reported CD8 epitopes shown in a stick representation, colored-coded in *yellow*, *red* and *purple* according to their level of conservation; the four top-scoring CD8 epitopes identified by bioinformatic analysis (see legend to **Figure 3**) are shown in *green*.

portion of the RBM, this RBM sub-segment, which is laterally positioned with respect to the main body of the RBD, as well as other RBD flanking regions are highly conserved and are specifically targeted by some class 3 and 4 neutralizing antibodies (86). Of note, S309, a class 3 cross-neutralizing antibody initially isolated from a SARS-CoV patient, is directed against an N343 glycan that maps to a conserved RBD flanking region (AA 331-345) and its RBD footprint partially overlaps two CD8 epitopes (AA 328-338 and 339-347) (87). Likely due to the structural/functional constraints (and presumed sequence invariance) of its RBD target, the neutralizing activity of S309 has proven to be resilient to a number of SARS-Cov-2 mutations, so far, and is considered a very promising candidate for a broadly protective monoclonal antibody therapy (88). Because of the co-existence of the B-cell epitopes targeted by the most potent neutralizing antibodies and of multiple CD8 epitopes within a conserved region, the RBD lends itself as a key site for the development of artificially multimerized, multi-functional (humoral and cellular immunity) pan-coronavirus vaccines.

A subset of conserved CD8 epitopes are located within the CTD2 domain, which includes the hyper conserved AA 592-602 sequence (Avg SE=1.5 x10e-4) and the slightly more variable AA 589-591 sequence (Avg SE=8.8x10e-4). A CD8 T cell epitope (AA 588-597) is close to and partially overlaps these highly conserved sequences, while another one (AA 660-670) is located in the smaller β-sheet of CTD2 (**Figure 5C**). The structurally dynamic and highly flexible 630-loop (AA 610-630), which is also located in this region, is crucial for the crosstalk between the S1 and the S2 subunits. When conformationally ordered, this loop interacts with the above mentioned highly conserved sequences through hydrophobic interactions and stabilizes the CTD2. This interaction, which enhances spike stability, thus preventing premature dissociation of the S1 subunit and the concomitant loss of spike functionality, plays a key role in the fine-tuning of the RBD up to down transition (84, 89). Indeed, the D614G mutation increases S1 stability and by stiffening the 630-loop, it strongly stabilizes the whole spike protein (84). Another CD8 epitope (AA 583-592) maps to the C-terminal portion of CTD1 (**Figure 5C**). This domain acts as a structural relay connecting the RBD to the S2 subunit through the so-called Fusion Peptide Proximal Region (FPPR), which, when conformationally ordered, can clamp down the entire RBD (10) (see **Figure 5C**).

By far the strongest sequence conservation entails the S2 subunit, where the central helix (CH) region and the helixes located at the N- and the C-terminal ends of heptad repeat 1 (HR1) appear to be the most conserved (**Figure 5D**). In keeping with its extremely low sequence variation, the S2 subunit holds the highest number (a total of 20) of putatively conserved CD8 epitopes, many of which belong to the top-scoring classes of predicted MHC-1 affinities (**Figures 3**, **5D**). In particular, starting from the AA 989-1000 region, at least three CD8 T cell epitopes map to the nearly invariant AA 987-1005 sequence of

TABLE 1 | Distribution of CD8 T cell epitopes within spike regions of different sequence conservation.

			Spike Regions			
			S1-NTD (328 aa)	S1-RBD (205 aa)	S1 CTD1-2 (153 aa)	S2 (587 aa)
Hyper-Conserved sequences	**Hyper-conserved over total sequence length (% overall spike region)**		**0%**	**0%**	**7%**	**3%**
	Epitopes (n.)	Total	0	0	1	5
		Degenerate*	0	0	0	0
		Immunodominant**	0	0	0	1
		Immunodominant and degenerate	0	0	0	0
Higly Conserved sequences	**Highly conserved over total sequence length (% overall spike region)**		**0%**	**2%**	**1%**	**9%**
	Epitopes (n.)	Total	0	0	0	1
		Degenerate*	0	0	0	0
		Immunodominant**	0	0	0	0
		Immunodominant and degenerate	0	0	0	0
Conserved sequences	**Conserved over total sequence length (% overall spike region)**		**10%**	**43%**	**35%**	**25%**
	Epitopes (n.)	Total	3	11	2	14
		Degenerate*	2	3	0	2
		Immunodominant**	0	1	1	3
		Immunodominant and degenerate	0	1	0	0
Other less conserved sequences	**Less conserved over total sequence length (% overall spike region)**		**90%**	**55%**	**57%**	**63%**
	Epitopes (n.)	Total (n. containing variant mutations)	42 (12)	18 (7)	16 (5)	55 (11)
		Degenerate*	12	1	3	12
		Immunodominant**	8	3	0	18
		Immunodominant and degenerate	7	1	0	6

Degenerated HLA recognition.

***Derived from (78) and references therein.*

the CH region (Avg SE=1.1x10e-4). This region is located in the innermost portion of the trimeric spike protein and serves as a pivot point during S2 transition from a prefusion to a postfusion conformation (**Figure 5D**). Critical for this transition is the flexibility of the hinge-loop located on the top of the HR1 and the CH helices. In fact, stiffening of this loop by Pro substitution of K986 and V987 (a modification introduced in many of the present spike-based vaccines) strongly reduces S2 flexibility and prevents the conformational changes associated with receptor interaction (7, 90, 91). Proline substitution of four additional S2 subunit residues (F817P, A892P, A899P, A942P), as in the HexaPro spike derivative (92), has similarly been shown to further impair the postfusion transition, thus significantly increasing spike protein stability and immunogenicity. One of these residues (A899) is part of the best-scoring CD8 epitope (AA 898-906) retrieved by NetMHC-4.0 prediction (**Figure 5D**) (92). On the other hand, the extremely low mutation rate (Avg SE=2.5x10e-4) of the AA 910-921 HR1 region, which contains one CD8 epitope (AA 917-927), likely reflects its interaction, after the postfusion structural rearrangement, with helix HR2. This interaction is involved in the formation of a six-helix bundle structure in the apical postfusion region 6HB-2 (close to the transmembrane fusion peptide), which, in turn, is critical for viral-host cell membrane fusion and virus internalization (10) (see **Figure 5D**).

Upon conversion to the postfusion form, some of the remaining CD8 epitopes located in the S2 subunit, either become part of another six-helix bundle (6HB-1; CD8 epitope comprised between AA 747-756), or of the connector β-sheet (four conserved epitopes comprised between AA 1051 and 1063) (**Figure 5D**) (10). A summary of the CD8 T cell epitopes that are located within conserved spike sequences which cannot tolerate the emergence of mutations because of their critical functional or structural roles is reported in **Table 2**.

FINAL REMARKS

Our literature search and *in silico* prediction analysis confirms, and actually underlines, the fact that the cytotoxic CD8 T cell activity induced by SARS-CoV-2 infection is widely multispecific in the context of individual HLA class I alleles and that some of the relevant degenerate and immunodominant epitopes are located within conserved spike regions that cannot tolerate mutational changes (**Tables 1**, **2**). Thus, even in the event of abrogation of specific CD8 T cell responses directed against epitopes that have been inactivated as a result of SARS-CoV-2 variant mutations, the evidence that CD8-mediated responses are not only widely multispecific but can also target highly conserved (and potentially invariable) spike sequences makes mutation-mediated evasion from the overall protection afforded by CD8 T cells most unlikely. The ability of genetic vaccines to stimulate the endogenous synthesis of the spike protein should

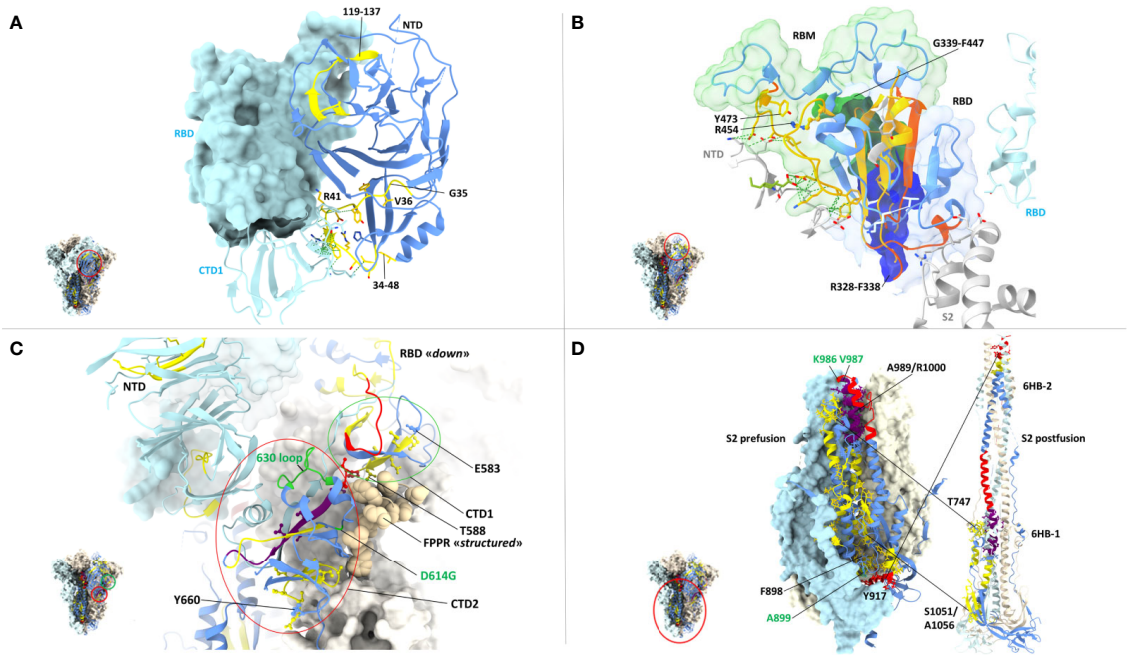


FIGURE 5 | Close-up view of specific CD8 epitope-containing regions of the spike protein. **(A)** CD8 T cell epitopes mapping to the N-terminal domain (NTD) of one spike protomer (shown as a ribbon representation in the *right-side*) and to the interface region with an adjacent protomer (shown in *azur* in the *left-side*), whose RBD (shown in the 'closed' conformation) and CTD1 domains are indicated. The specific spike region under examination is circled in *red* in the trimer structure shown in the *left-side lower* part. The color-code for NTD sequence conservation is the same as in **Figure 4**, with non-conserved regions in *blue* and conserved regions (34-48 and 119-137) *in yellow*; part of the non-conserved NTD ribbon strand close to the 34-48 segment has been omitted for clarity. The side-chains of CD8 epitope amino acids mapping to the conserved NTD region comprised between AA positions 34-48 are shown as *yellow* sticks, and their contacts with the adjacent CTD1 protomer as dotted *green* lines. The corresponding epitope starting residue is shown in *black*. PDB code (spike D614G): 7KRQ. **(B)** CD8 epitopes mapping to receptor-binding domain (RBD) conserved regions and to intermolecular contacts with adjacent spike protomers. The specific spike region under examination is circled in *red* in the trimer structure shown in the *left-side lower* part. The RBD is shown in the 'closed conformation' as a ribbon representation, with conserved, CD8 epitope-containing secondary structure elements in *yellow*; secondary structure elements lacking sequence conservation or conserved but not containing any CD8 epitope are shown in *blue* and *orange*, respectively. CD8 epitope amino acids side-chains and their contacts with adjacent protomers (shown in *grey* or *azur*) are represented as *yellow* sticks and *green* dotted lines, respectively. The receptor-binding motif (RBM) is shown as a transparent green surface; remaining portion of the RBD is represented as a transparent blue surface. The starting (R454) and ending (Y473) residues of the RBM-associated CD8 epitopes are indicated; part of the S2 subunit (*grey* ribbon) of the specific protomer under examination as well as the NTD (grey) and the RBD (azur) of adjacent protomers are displayed. The region of overlap between the RBD footprint of the S309 antibody (see text for details) and the RBD-resident epitopes 339-347 (*green opaque surface*) and 328-338 (*blue opaque surface*) is also shown. PDB code (D614G spike mutant): 7KRQ. **(C)** CD8 epitopes mapping to conserved regions of the CTD1 and CTD2 domains. The specific region under examination is circled in *red* in the trimer structure of the spike shown in the *left-side* lower part. The color-code for amino acid conservation (*i.e.*, the entropy of individual residues) is the same as above and as specified in **Figure 4** legend (*blue*: no conservation, *yellow*: 'conserved', *red*: 'highly conserved', *purple*: 'hyper conserved'); relevant amino acids are represented as colored sticks and the number (shown in *black*) corresponding to the epitope starting residue is indicated. The 630-loop and the D614G mutation are indicated and are both shown in *green*. The Fusion Peptide Proximal Region (FPPR) of the adjacent protomer is represented as beige-colored atom spheres; the NTD of an adjacent protomer is also indicated (shown in *azur*). PDB code (D614G spike mutant with the RBD in the closed conformation): 7KRS. **(D)** CD8 epitopes mapping to conserve regions of the prefusion (*left*) and postfusion (*right*) conformations of the spike S2 subunit. The specific region under examination is circled in *red* in the spike trimer structure shown in the *left-side* lower part; the prefusion S2 is shown both in a ribbon and in a molecular surface representation, while only a ribbon representation is used for the postfusion S2. The color code for sequence conservation (or lack thereof) is the same as described above for panel **(A)** Relevant amino acids are represented as colored sticks and the numbers corresponding to the starting or terminal amino acid positions of the epitopes are indicated in *black*. The positions of hinge AA residues 986 and 987 (shown in *green*), of the A899 residue that is part of the top-scoring CD8 epitope 898-906, and of the six-helix bundles 6HB-1 and 6HB-2 (postfusion conformation on the *right-side*) are also indicated. The hyper- and highly conserved regions associated to the CH and the C-terminal helix of HR1 (*upper part*) and the highly conserved region associated to the N-terminal helix of HR-1 (*lower part*) are circled. PDB codes for the prefusion and postfusion spike conformations are 6ZXN and 6XRA, respectively.

closely mimic spike antigen presentation to CD8 T cells during natural infection. Thus, CD8 T cell activation is expected to play a key and arguably more durable role also in antiviral protection induced by last-generation vaccines.

The identification of CD8 epitopes mapping on spike regions which are not prone to variation provides an additional, highly stringent criterion that may enable to select potent and potentially VOC-resistant epitopes. CD8 epitopes mapping on low entropy spike segments (listed in **Figure 3**) represent promising candidates for a CD8-potentiated and broadly protective vaccine prototype. As highlighted by the present analysis, epitope sorting can be comprehensively achieved based on a combination of different criteria including: i) epitope sequence position within highly- or hyper- conserved

TABLE 2 | CD8 T cell epitopes overlapping conserved, structurally and/or functionally crucial spike elements.

Spike regions	Specific conserved AA sequences[1]	Structural/functional role[2]	Overlapping CD8 Epitopes[3]
NTD	34-48	NTD-RBD interface (84)	35-44 36-43 41-49
RBD	331-345	Partial overlap with neutralizing Ab binding site (86, 87)	328-338 339-347
RBD	456-474	RBM flank and RBM-NTD interface (84)	454-462 458-466 462-472 464-472 464-473
CTD1	584-588	RBD-S2 FPPR relay (10, 84, 89)	583-592
CTD2	589-591 / 592-602	S1-S2 crosstalk; modulation of RBD up/down transition (10, 84, 89)	588-597
S2	748-768	Postfusion six helix-bundle (6HB-1) (10)	747-756
S2	900-909	Mutationally stabilized HexaPro spike derivative (92)	898-906
S2	910-921 / 922-928	Postfusion six-helix bundle (6HB-2) (10)	917-927
S2	987-1005	Central helix (CH) acting as a pivot point for the postfusion transition (10)	989-996 989-997 996-1004 1000-1007 1000-1008
S2	1051-1062	Connector β-sheet (10)	1051-1062 1052-1060 1052-1062 1056-1063

[1]*The amino acid position borders and the degree of sequence conservation (same color code as in* ***Figure 3*** *and* ***Table 1****) of each element are indicated.*
[2]*References to original articles where the specific role of each element or its overlap with the binding site of broadly protective neutralizing antibodies were delineated are reported in square brackets.*
[3]*The amino acid positions delimiting individual or multiples CD8 epitopes are indicated (see* ***Figure 3*** *for specific epitope features).*

spike SARS-CoV-2 regions, ii) HLA-class I allele frequency and affinity, iii) immunodominance (**Figure 3** and **Table 1**) and iv) predicted structural/functional invariance (**Table 2**). The innermost S2 central helix region, which harbors a number of CD8 epitopes (**Figures 3**, **5D** and **Table 2**), is an almost invariable, hyper-conserved portion of the spike protein that is essential to drive the prefusion to postfusion conformational transition. Within this region is located the AA 1000-1008 epitope which displays both highly significant prediction scores and immunodominance properties. Similar features are shared by another promising epitope (AA 1052-1062) which is located in the conserved, S2 connector β-sheet (**Figures 3**, **5D** and **Table 2**). While S2-located epitopes may exhibit cross-reactivity with other sarbecoviruses, CD8 epitopes mapping to the RBD, which is involved in ACE2 receptor recognition and is thus subjected to a high evolutionary pressure, are likely to be SARS-CoV-2 specific. Despite an overall high mutability, however, several CD8 epitopes are associated to conserved RBD segments (**Table 1** and **Figures 3**, **5B**). In particular, five epitopes (AA 454-473) are specifically located in the RBM subsegment and two additional epitopes map to the RBD flank (AA 328-347), a region that is targeted by neutralizing antibodies of high potential therapeutic interest (86–88).

In conclusion, it is likely that a subset of SARS-CoV-2 mutations can actually influence some CD8-mediated responses. The remaining unaffected responses, however, especially those stimulated by highly conserved epitopes, should largely compensate for this loss. Even without direct experimental data, these observations strongly support the notion that present vaccines will likely maintain a significant protection capacity also against VoCs. In other words, memory CD8 T cell responses are strongly expected to be capable of slowing-down the spread of infection and to prevent evolution to severe forms of disease, even under conditions in which protection mediated by neutralizing antibodies is significantly diminished or even lost. This also suggests that enrichment of presently available SARS-CoV-2 vaccines with highly conserved and degenerate CD8 T cell epitopes, such as the ones we have prioritized in this work, may represent a valuable strategy for amplifying CD8 T cell induction, thereby increasing vaccine robustness and long-term efficacy.

Considering that the spike protein is by far the most prevalent, if not the only target of current vaccines, we restricted our analysis to this particular target. It is known, however, that additional SARS-CoV-2 proteins are strongly targeted by CD8+ T-cell responses. In particular, the N protein has been reported to account for more than 35% of the overall CD8-mediated responses to other coronaviruses, 50% of which are induced by the spike protein (35). In human SARS-Cov-2 infection, the scenario is quite different, and the number of CD8 epitopes described so far within the N protein is about one third of those identified within the spike protein (41 N *vs* 168 S), but

the S is about 3 times longer than the N protein (56, 57, 61, 67). In addition, N is less variable than the S protein and only 7 VoC/VoI mutations (within the variants analyzed in our study) have emerged so far within N compared to 34 mutations in the case of the S protein (https://cov-lineages.org/index.html). Finally, available studies point to a hierarchy of CD8 T cell immunodominance, with a prevalent reactivity against S (accounting for approximately 26% of all the identified CD8 T cell epitopes) associated with lower but still frequent recognition of other structural and non-structural proteins, including nsp3 (20%), nsp12 (9%) as well as, N (7%), M (6%) nsp4 (5%), ORF3a (5%), nsp6 (3%) and ORF8 (1%) (78). Thus, available genetic vaccines should benefit even more substantially from the inclusion of immunodominant and possibly degenerate CD8 epitopes located outside of the spike protein that are particularly relevant to the overall potency of naturally-induced antiviral protective responses and that, obviously, cannot be stimulated by immunization with a spike-only vaccine.

AUTHOR CONTRIBUTIONS

CB, DC, and AB: design and writing of the manuscript. MR, AV, and CT: contribution to figure drawing, analysis and interpretation of data, statistical analysis. VB and PF: discussion of the concepts to be introduced in the text, contribution to the selection of the references to quote; SO and CF: critical revision of text and figures. All authors contributed to the article and approved the submitted version.

FUNDING

This work was supported by private donations to the Unit of Infectious Diseases and Hepatology (CB, MR, AV, CT, VB, PF, and CF) of the Azienda Ospedaliero-Universitaria of Parma and by a grant from the University of Parma (DC, AB, and SO) supporting research activities in the field of Covid-19 infection.

REFERENCES

1. Masters PS. The Molecular Biology of Coronaviruses. *Adv Virus Res* (2006) 66:193–292. doi: 10.1016/S0065-3527(06)66005-3
2. V'kovski P, Kratzel A, Steiner S, Stalder H, Thiel V. Coronavirus Biology and Replication: Implications for SARS-CoV-2. *Nat Rev Microbiol* (2021) 19:155–70. doi: 10.1038/s41579-020-00468-6
3. Brant AC, Tian W, Majerciak V, Yang W, Zheng Z-M. SARS-CoV-2: From its Discovery to Genome Structure, Transcription, and Replication. *Cell Biosci* (2021) 11:136. doi: 10.1186/s13578-021-00643-z
4. Harrison AG, Lin T, Wang P. Mechanisms of SARS-CoV-2 Transmission and Pathogenesis. *Trends Immunol* (2020) 41:1100–15. doi: 10.1016/j.it.2020.10.004
5. Arya R, Kumari S, Pandey B, Mistry H, Bihani SC, Das A, et al. Structural Insights Into SARS-CoV-2 Proteins. *J Mol Biol* (2021) 433:166725. doi: 10.1016/j.jmb.2020.11.024
6. Walls AC, Park YJ, Tortorici MA, Wall A, McGuire AT, Veesler D. Structure, Function, and Antigenicity of the SARS-CoV-2 Spike Glycoprotein. *Cell* (2020) 181:281–92.e6. doi: 10.1016/j.cell.2020.02.058
7. Wrapp D, Wang N, Corbett KS, Goldsmith JA, Hsieh CL, Abiona O, et al. Cryo-EM Structure of the 2019-Ncov Spike in the Prefusion Conformation. *Science* (2020) 367:1260–3. doi: 10.1101/2020.02.11.944462
8. Ke Z, Oton J, Qu K, Cortese M, Zila V, McKeane L, et al. Structures and Distributions of SARS-CoV-2 Spike Proteins on Intact Virions. *Nature* (2020) 588:498–502. doi: 10.1038/s41586-020-2665-2
9. Turoňová B, Sikora M, Schürmann C, Hagen WJH, Welsch S, Blanc FEC, et al. *In Situ* Structural Analysis of SARS-CoV-2 Spike Reveals Flexibility Mediated by Three Hinges. *Science* (2020) 370:203–8. doi: 10.1126/science.abd5223
10. Cai Y, Zhang J, Xiao T, Peng H, Sterling SM, Walsh RM, et al. Distinct Conformational States of SARS-CoV-2 Spike Protein. *Science* (2020) 369:1586–92. doi: 10.1126/science.abd4251
11. Hu B, Guo H, Zhou P, Shi ZL. Characteristics of SARS-CoV-2 and COVID-19. *Nat Rev Microbiol* (2021) 19:141–54. doi: 10.1038/s41579-020-00459-7
12. Wang MY, Zhao R, Gao LJ, Gao XF, Wang DP, Cao JM. SARS-CoV-2: Structure, Biology, and Structure-Based Therapeutics Development. *Front Cell Infect Microbiol* (2020) 10:587269. doi: 10.3389/fcimb.2020.587269
13. Nielsen SCA, Yang F, Jackson KJL, Hoh RA, Röltgen K, Jean GH, et al. Human B Cell Clonal Expansion and Convergent Antibody Responses to SARS-CoV-2. *Cell Host Microbe* (2020) 28:516–25.e5. doi: 10.1016/j.chom.2020.09.002
14. Mast FD, Fridy PC, Ketaren NE, Wang J, Jacobs EY, Olivier JP, et al. Nanobody Repertoires for Exposing Vulnerabilities of SARS-CoV-2. (2021). doi: 10.1101/2021.04.08.438911
15. Koenig PA, Das H, Liu H, Kümmerer BM, Gohr FN, Jenster LM, et al. Structure-Guided Multivalent Nanobodies Block SARS-CoV-2 Infection and Suppress Mutational Escape. *Science* (2021) 371(6530):eabe6230. doi: 10.1126/science.abe6230
16. McCarthy KR, Rennick LJ, Nambulli S, Robinson-McCarthy LR, Bain WG, Haidar G, et al. Recurrent Deletions in the SARS-CoV-2 Spike Glycoprotein Drive Antibody Escape. *Science* (2021) 371:1139–42. doi: 10.1126/science.abf6950
17. Verkhivker GM, Di Paola L. Integrated Biophysical Modeling of the SARS-CoV-2 Spike Protein Binding and Allosteric Interactions With Antibodies. *J Phys Chem B* (2021) 125:4596–619. doi: 10.1021/acs.jpcb.1c00395
18. Gobeil SM-C, Janowska K, McDowell S, Mansouri K, Parks R, Stalls V, et al. Effect of Natural Mutations of SARS-CoV-2 on Spike Structure, Conformation, and Antigenicity. *Science* (2021) 373:eabi6226. doi: 10.1126/science.abi6226
19. Martínez-Flores D, Zepeda-Cervantes J, Cruz-Reséndiz A, Aguirre-Sampieri S, Sampieri A, Vaca L. SARS-CoV-2 Vaccines Based on the Spike Glycoprotein and Implications of New Viral Variants. *Front Immunol* (2021) 12:701501. doi: 10.3389/fimmu.2021.701501
20. Naranbhai V, Garcia-Beltran WF, Mairena CB, Thierauf JC, Chang CC, Kirkpatrick G, et al. Immunogenicity of mRNA-1273, BNT162b2 and Ad26.COV2.S COVID-19 Vaccines. (2021). doi: 10.1101/2021.07.18.21260732
21. Tada T, Zhou H, Samanovic MI, Dcosta BM, Cornelius A, Mulligan MJ, et al. Comparison of Neutralizing Antibody Titers Elicited by mRNA and Adenoviral Vector Vaccine Against SARS-CoV-2 Variants. *Prepr Serv Biol* (2021). doi: 10.1101/2021.07.19.452771
22. Lopez Bernal J, Andrews N, Gower C, Gallagher E, Simmons R, Thelwall S, et al. Effectiveness of Covid-19 Vaccines Against the B.1.617.2 (Delta) Variant. *N Engl J Med* (2021) 385(7):585-94. doi: 10.1056/NEJMoa2108891
23. Nasreen S, Chung H, He S, Brown KA, Gubbay JB, Buchan SA, et al. Effectiveness of COVID-19 Vaccines Against Variants of Concern in Ontario, Canada. (2021). doi: 10.1101/2021.06.28.21259420
24. Abu-Raddad LJ, Chemaitelly H, Butt AA. Effectiveness of the BNT162b2 Covid-19 Vaccine Against the B.1.1.7 and B.1.351 Variants. *N Engl J Med* (2021) 385:187–9. doi: 10.1056/NEJMc2104974
25. Sheikh A, McMenamin J, Taylor B, Robertson C. SARS-CoV-2 Delta VOC in Scotland: Demographics, Risk of Hospital Admission, and Vaccine Effectiveness. *Lancet* (2021) 397:2461–2. doi: 10.1016/S0140-6736(21)01358-1
26. Wang Z, Muecksch F, Schaefer-Babajew D, Finkin S, Viant C, Gaebler C, et al. Naturally Enhanced Neutralizing Breadth Against SARS-CoV-2 One Year After Infection. *Nature* (2021) 595:426–31. doi: 10.1038/S41586-021-03696-9
27. Turner JS, O'Halloran JA, Kalaidina E, Kim W, Schmitz AJ, Zhou JQ, et al. SARS-CoV-2 mRNA Vaccines Induce Persistent Human Germinal Centre Responses. *Nature* (2021) 596:109–13. doi: 10.1038/s41586-021-03738-2
28. Moriyama S, Adachi Y, Sato T, Tonouchi K, Sun L, Fukushi S, et al. Temporal Maturation of Neutralizing Antibodies in COVID-19 Convalescent

Individuals Improves Potency and Breadth to Circulating SARS-CoV-2 Variants. *Immunity* (2021) 54(8):1841–52.E4. doi: 10.1016/j.immuni.2021.06.015
29. Muecksch F, Weisblum Y, Barnes CO, Schmidt F, Schaefer-Babajew D, Wang Z, et al. Affinity Maturation of SARS-CoV-2 Neutralizing Antibodies Confers Potency, Breadth, and Resilience to Viral Escape Mutations. *Immunity* (2021) 54(8):1853–68.e7. doi: 10.1016/j.immuni.2021.07.008
30. Golstein P, Griffiths GM. An Early History of T Cell-Mediated Cytotoxicity. *Nat Rev Immunol* (2018) 18:527–35. doi: 10.1038/s41577-018-0009-3
31. Hashimoto M, Im SJ, Araki K, Ahmed R. Cytokine-Mediated Regulation of CD8 T-Cell Responses During Acute and Chronic Viral Infection. *Cold Spring Harb Perspect Biol* (2019) 11:1–18. doi: 10.1101/cshperspect.a028464
32. Guidotti LG, Ishikawa T, Hobbs MV, Matzke B, Schreiber R, Chisari FV. Intracellular Inactivation of the Hepatitis B Virus by Cytotoxic T Lymphocytes Lymphocytic Choriomeningitis Virus (LCMV), the Proto-Typic Noncytopathic Virus That Requires CTL for Clear. *Immunity* (1996) 4:25–36. doi: 10.1016/s1074-7613(00)80295-2
33. Zeng C, Evans JP, King T, Zheng Y-M, Oltz EM, Whelan SPJ, et al. SARS-CoV-2 Spreads Through Cell-To-Cell Transmission. (2021). doi: 10.1101/2021.06.01.446579
34. Jackson L, Rodel H, Hwa S, Cele S, Ganga Y, Bernstein M, et al. SARS-CoV-2 Cell-to-Cell Spread Occurs Rapidly and is Insensitive to Antibody Neutralization. (2021), 1–20. doi: 10.1101/2021.06.01.446516
35. Grifoni A, Weiskopf D, Ramirez SI, Mateus J, Dan JM, Moderbacher CR, et al. Targets of T Cell Responses to SARS-CoV-2 Coronavirus in Humans With COVID-19 Disease and Unexposed Individuals. *Cell* (2020) 181:1489–501.e15. doi: 10.1016/j.cell.2020.05.015
36. Le Bert N, Tan AT, Kunasegaran K, Tham CYL, Hafezi M, Chia A, et al. SARS-CoV-2-Specific T Cell Immunity in Cases of COVID-19 and SARS, and Uninfected Controls. *Nature* (2020) 584:457–62. doi: 10.1038/s41586-020-2550-z
37. Sette A, Crotty S. Adaptive Immunity to SARS-CoV-2 and COVID-19. *Cell* (2021) 184:861–80. doi: 10.1016/j.cell.2021.01.007
38. Cohen KW, Linderman SL, Moodie Z, Czartoski J, Lai L, Mantus G, et al. Longitudinal Analysis Shows Durable and Broad Immune Memory After SARS-CoV-2 Infection With Persisting Antibody Responses and Memory B and T Cells. *Cell Rep Med* (2021) 2:100354. doi: 10.1016/j.xcrm.2021.100354
39. Geers D, Immunol S, Geers D, Shamier MC, Bogers S, Hartog GD, et al. SARS-CoV-2 Variants of Concern Partially Escape Humoral But Not T-Cell Responses in COVID-19 Convalescent Donors and Vaccinees. *Sci Immunol* (2021) 1750:1–22. doi: 10.1126/sciimmunol.abj1750
40. Skelly DT, Harding Sir William AC, Gilbert-Jaramillo Sir William J, Knight Sir William ML, Longet S, Brown A, et al. Two Doses of SARS-CoV-2 Vaccination Induce More Robust Immune Responses to Emerging SARS-CoV-2 Variants of Concern Than Does Natural Infection. *Res Sq* (2021) 12:1–28. doi: 10.21203/rs.3.rs-226857/v2
41. Tarke A, Sidney J, Methot N, Zhang Y, Dan JM, Goodwin B, et al. Negligible Impact of SARS-CoV-2 Variants on the Total CD4+ and CD8+ T Cell Reactivity in Infected or Vaccinated Individuals. *Cell Rep Med* (2021) 2 (7):100355. doi: 10.1016/j.xcrm.2021.100355
42. Painter MM, Mathew D, Goel RR, Apostolidis SA, Pattekar A, Kuthuru O, et al. Rapid Induction of Antigen-Specific CD4+ T Cells Guides Coordinated Humoral and Cellular Immune Responses to SARS-CoV-2 mRNA Vaccination. *bioRxiv* (2021) 1–26. doi: 10.1101/2021.04.21.440862
43. Kalimuddin S, Tham CYL, Qui M, de Alwis R, Sim JXY, Lim JME, et al. Early T Cell and Binding Antibody Responses Are Associated With COVID-19 RNA Vaccine Efficacy Onset. *Medicine* (2021) 2(6):1–7. doi: 10.1016/j.medj.2021.04.003
44. Tegally H, Wilkinson E, Giovanetti M, Iranzadeh A, Fonseca V, Giandhari J, et al. Detection of a SARS-CoV-2 Variant of Concern in South Africa. *Nature* (2021) 592:438–43. doi: 10.1038/s41586-021-03402-9
45. OE A, Simons LM, Adewumi OM, Fowotade ECO AA, Adeniji DTJ JA, Taiwo BO, et al. Coincident Rapid Expansion of Two SARS-CoV-2 Lineages With Enhanced Infectivity in Nigeria. *medRxiv* (2021). doi: 10.1101/2021.04.09.21255206
46. Ranjan R, Sharma A, Mahendra, Verma K, Verma MK. Characterization of the Second Wave of COVID-19 in India. (2021). doi: 10.1101/2021.04.17.21255665
47. Cherian S, Potdar V, Jadhav S, Yadav P, Gupta N, Das M, et al. Convergent Evolution of SARS-CoV-2 Spike Mutations, L452R, E484Q and P681R, in the Second Wave of COVID-19 in Maharashtra, India. *bioRxiv* (2021). doi: 10.1101/2021.04.22.440932
48. Zhang W, Govindavari JP, Davis BD, Chen SS, Kim JT, Song J, et al. Analysis of Genomic Characteristics and Transmission Routes of Patients With Confirmed SARS-CoV-2 in Southern California During the Early Stage of the US COVID-19 Pandemic. *JAMA Netw Open* (2020) 3:1–13. doi: 10.1001/jamanetworkopen.2020.24191
49. Kirby T. New Variant of SARS-CoV-2 in UK Causes Surge of COVID-19. *Lancet Respir Med* (2021) 9:e20–1. doi: 10.1016/S2213-2600(21)00005-9
50. Thompson CN, Hughes S, Ngai S, Baumgartner J, Wang JC, McGibbon E, et al. Rapid Emergence and Epidemiologic Characteristics of the SARS-CoV-2 B.1.526 Variant — New York City, New York, January 1–April 5, 2021. *MMWR* (2021) 70:712–6. doi: 10.15585/mmwr.mm7019e1
51. Davies NG, Abbott S, Barnard RC, Jarvis CI, Kucharski AJ, Munday JD, et al. Estimated Transmissibility and Impact of SARS-CoV-2 Lineage B.1.1.7 in England. *Science* (2021) 372:eabg3055. doi: 10.1126/science.abg3055
52. Frampton D, Rampling T, Cross A, Bailey H, Heaney J, Byott M, et al. Genomic Characteristics and Clinical Effect of the Emergent SARS-CoV-2 B.1.1.7 Lineage in London, UK: A Whole-Genome Sequencing and Hospital-Based Cohort Study. *Lancet Infect Dis* (2021) 3099:1–11. doi: 10.1016/S1473-3099(21)00170-5
53. Funk T, Pharris A, Spiteri G, Bundle N, Melidou A, Carr M, et al. Characteristics of SARS-CoV-2 Variants of Concern B.1.1.7, B.1.351 or P.1: Data From Seven EU/EEA Countries, Weeks 38/2020 to 10/2021. *Eurosurveillance* (2021) 26:1–10. doi: 10.2807/1560-7917.ES.2021.26.16.2100348
54. Annavajhala1 MK, Mohri H, Wang P, Zucker JE, Sheng Z, Gomez-Simmonds1 A, et al. A Novel and Expanding SARS-CoV-2 Variant, B.1.526, Identified in New York. *medRxiv* (2021). doi: 10.1101/2021.02.23.21252259
55. Ramundo MS, De Jesus JG, Andrade PS, Coletti TM. Genomics and Epidemiology of the P.1 SARS-CoV-2 Lineage in Manaus, Brazil. *Science* (2021) 372:815–21. doi: 10.1126/science.abh2644
56. Tarke A, Sidney J, Kidd CK, Dan JM, Ramirez SI, Yu ED, et al. Comprehensive Analysis of T Cell Immunodominance and Immunoprevalence of SARS-CoV-2 Epitopes in COVID-19 Cases. *Cell Rep Med* (2021) 2:100204. doi: 10.1016/j.xcrm.2021.100204
57. Schulien I, Kemming J, Oberhardt V, Wild K, Seidel LM, Killmer S, et al. Characterization of Pre-Existing and Induced SARS-CoV-2-Specific CD8+ T Cells. *Nat Med* (2021) 27:78–85. doi: 10.1038/s41591-020-01143-2
58. Prakash S, Srivastava R, Coulon P-G, Dhanushkodi NR, Chentoufi AA, Tifrea DF, et al. Genome-Wide B Cell, CD4 $^{+}$, and CD8 $^{+}$ T Cell Epitopes That Are Highly Conserved Between Human and Animal Coronaviruses, Identified From SARS-CoV-2 as Targets for Preemptive Pan-Coronavirus Vaccines. *J Immunol* (2021) 206(11):2566–82. doi: 10.4049/jimmunol.2001438
59. Habel JR, Nguyen THO, van de Sandt CE, Juno JA, Chaurasia P, Wragg K, et al. Suboptimal SARS-CoV-2–Specific CD8+ T Cell Response Associated With the Prominent HLA-A*02:01 Phenotype. *Proc Natl Acad Sci USA* (2020) 117:24384–91. doi: 10.1073/pnas.2015486117
60. Qiu C, Xiao C, Wang Z, Chen X, Gao L, Deng J, et al. CD8+ T Cell Epitope Variations Suggest a Potential Antigen Presentation Deficiency for Spike Protein of SARS-CoV-2. *bioRxiv* (2021). doi: 10.1101/2021.01.22.427863
61. Kared H, Redd AD, Bloch EM, Bonny TS, Sumatoh H, Kairi F, et al. SARS-CoV-2–Specific CD8+ T Cell Responses in Convalescent COVID-19 Individuals. *J Clin Invest* (2021) 131(5):e145476. doi: 10.1172/JCI145476
62. Shomuradova AS, Vagida MS, Sheetikov SA, Zornikova KV, Kiryukhin D, Titov A, et al. SARS-CoV-2 Epitopes Are Recognized by a Public and Diverse Repertoire of Human T Cell Receptors. *Immunity* (2020) 53:1245–57.e5. doi: 10.1016/j.immuni.2020.11.004
63. Quadeer AA, Ahmed SF, McKay MR. Landscape of Epitopes Targeted by T Cells in 852 Convalescent COVID-19 Patients: Meta-Analysis, Immunoprevalence and Web Platform. *Cell Rep Med* (2021) 100312. doi: 10.1016/j.xcrm.2021.100312
64. Schreibing F, Hannani M, Ticconi F, Fewings E, James S, Begemann M, et al. Dissecting CD8 + T Cell Pathology of Severe SARS-CoV-2 Infection by Single-Cell Epitope Mapping. *bioRxiv* (2021) 1–35. doi: 10.1101/2021.03.03.432690
65. Nielsen SS, Vibholm LK, Monrad I, Olesen R, Frattari GS, Pahus MH, et al. SARS-CoV-2 Elicits Robust Adaptive Immune Responses Regardless of

Disease Severity. *EBioMedicine* (2021) 68:103410. doi: 10.1016/j.ebiom.2021.103410
66. Agerer B, Koblischke M, Gudipati V, Montaño-Gutierrez LF, Smyth M, Popa A, et al. SARS-CoV-2 Mutations in MHC-I-Restricted Epitopes Evade CD8+ T Cell Responses. *Sci Immunol* (2021) 6:17–22. doi: 10.1126/SCIIMMUNOL.ABG6461
67. Ferretti AP, Kula T, Wang Y, Nguyen DMV, Weinheimer A, Dunlap GS, et al. Unbiased Screens Show CD8+ T Cells of COVID-19 Patients Recognize Shared Epitopes in SARS-CoV-2 That Largely Reside Outside the Spike Protein. *Immunity* (2020) 53:1095–107.e3. doi: 10.1016/j.immuni.2020.10.006
68. Gangaev A, Ketelaars SLC, Isaeva OI, Patiwael S, Dopler A, Hoefakker K, et al. Identification and Characterization of a SARS-CoV-2 Specific CD8+ T Cell Response With Immunodominant Features. *Nat Commun* (2021) 12:(1):2593. doi: 10.1038/s41467-021-22811-y
69. Nguyen THO, Rowntree LC, Petersen J, Chua BY, Hensen L, Kedzierski L, et al. CD8+ T Cells Specific for an Immunodominant SARS-CoV-2 Nucleocapsid Epitope Display High Naïve Precursor Frequency and T Cell Receptor Promiscuity. *Immunity* (2021) 54(5):1066–82. doi: 10.1016/j.immuni.2021.04.009
70. Peng Y, Mentzer AJ, Liu G, Yao X, Yin Z, Dong D, et al. Broad and Strong Memory CD4+ and CD8+ T Cells Induced by SARS-CoV-2 in UK Convalescent Individuals Following COVID-19. *Nat Immunol* (2020) 21:1336–45. doi: 10.1038/s41590-020-0782-6
71. Rha MS, Jeong HW, Ko JH, Choi SJ, Seo IH, Lee JS, et al. PD-1-Expressing SARS-CoV-2-Specific CD8+ T Cells Are Not Exhausted, But Functional in Patients With COVID-19. *Immunity* (2021) 54:44–52.e3. doi: 10.1016/j.immuni.2020.12.002
72. Chen Z, Ruan P, Wang L, Nie X, Ma X, Tan Y. T and B Cell Epitope Analysis of SARS-CoV-2 S Protein Based on Immunoinformatics and Experimental Research. *J Cell Mol Med* (2021) 25:1274–89. doi: 10.1111/jcmm.16200
73. Nelde A, Bilich T, Heitmann JS, Maringer Y, Salih HR, Roerden M, et al. SARS-CoV-2-Derived Peptides Define Heterologous and COVID-19-Induced T Cell Recognition. *Nat Immunol* (2021) 22:74–85. doi: 10.1038/s41590-020-00808-x
74. Poran A, Harjanto D, Malloy M, Arieta CM, Rothenberg DA, Lenkala D, et al. Sequence-Based Prediction of SARS-CoV-2 Vaccine Targets Using a Mass Spectrometry-Based Bioinformatics Predictor Identifies Immunogenic T Cell Epitopes. *Genome Med* (2020) 12:70. doi: 10.1186/s13073-020-00767-w
75. Stewart JJ, Lee CY, Ibrahim S, Watts P, Shlomchik M, Weigert M. Litwin S. A Shannon Entropy Analysis of Immunoglobulin and T Cell Receptor. *Mol Immunol* (1997) 34:1067–82. doi: 10.1016/S0161-5890(97)00130-2
76. Lempp FA, Soriaga L, Montiel-Ruiz M, Benigni F, Noack J, Park Y-J, et al. Membrane Lectins Enhance SARS-CoV-2 Infection and Influence the Neutralizing Activity of Different Classes of Antibodies. *bioRxiv* (2021). doi: 10.1101/2021.04.03.438258
77. Cantuti-Castelvetri L, Ojha R, Pedro LD, Djannatian M, Franz J, Kuivanen S, et al. Neuropilin-1 Facilitates SARS-CoV-2 Cell Entry and Infectivity. *Science* (2020) 370:856–60. doi: 10.1126/science.abd2985
78. Grifoni A, Sidney J, Vita R, Peters B, Crotty S, Weiskopf D, et al. SARS-CoV-2 Human T Cell Epitopes: Adaptive Immune Response Against COVID-19. *Cell Host Microbe* (2021) 29:1076–92. doi: 10.1016/j.chom.2021.05.010
79. Andreatta M, Nielsen M. Gapped Sequence Alignment Using Artificial Neural Networks: Application to the MHC Class I System. *Bioinformatics* (2016) 32:511–7. doi: 10.1093/bioinformatics/btv639
80. Ewer KJ, Barrett JR, Belij-Rammerstorfer S, Sharpe H, Makinson R, Morter R, et al. T Cell and Antibody Responses Induced by a Single Dose of ChAdOx1 Ncov-19 (AZD1222) Vaccine in a Phase 1/2 Clinical Trial. *Nat Med* (2021) 27:270–8. doi: 10.1038/s41591-020-01194-5
81. Tauzin A, Nayrac M, Benlarbi M, Gong SY, Gasser R, Beaudoin-Bussières G, et al. A Single Dose of the SARS-CoV-2 Vaccine BNT162b2 Elicits Fc-Mediated Antibody Effector Functions and T Cell Responses. *Cell Host Microbe* (2021) 29:1137–50.e6. doi: 10.1016/j.chom.2021.06.001
82. Sahin U, Muik A, Vogler I, Derhovanessian E, Kranz LM, Vormehr M, et al. BNT162b2 Vaccine Induces Neutralizing Antibodies and Poly-Specific T Cells in Humans. *Nature* (2021) 595:572–7. doi: 10.1038/s41586-021-03653-6
83. Tan AT, Lim JME, Le Bert N, Kunasegaran K, Chia A, Qui MDC, et al. Rapid Determination of the Wide Dynamic Range of SARS-CoV-2 Spike T Cell Responses in Whole Blood of Vaccinated and Naturally Infected. *bioRxiv* (2021) 2021:06. doi: 10.1101/2021.06.29.450293
84. Zhang J, Cai Y, Xiao T, Lu J, Peng H, Sterling SM, et al. Structural Impact on SARS-CoV-2 Spike Protein by D614G Substitution. *Science* (2021) 530: eabf2303. doi: 10.1126/science.abf2303
85. Hanke L, Vidakovics Perez L, Sheward DJ, Das H, Schulte T, Moliner-Morro A, et al. An Alpaca Nanobody Neutralizes SARS-CoV-2 by Blocking Receptor Interaction. *Nat Commun* (2020) 11:1–9. doi: 10.1038/s41467-020-18174-5
86. Barnes CO, Jette CA, Abernathy ME, Dam KMA, Esswein SR, Gristick HB, et al. SARS-CoV-2 Neutralizing Antibody Structures Inform Therapeutic Strategies. *Nature* (2020) 588:682–7. doi: 10.1038/s41586-020-2852-1
87. Pinto D, Park YJ, Beltramello M, Walls AC, Tortorici MA, Bianchi S, et al. Cross-Neutralization of SARS-CoV-2 by a Human Monoclonal SARS-CoV Antibody. *Nature* (2020) 583:290–5. doi: 10.1038/s41586-020-2349-y
88. Cathcart AL, Havenar-Daughton C, Lempp FA, Ma D, Schmid MA, Agostini ML, et al. The Dual Function Monoclonal Antibodies VIR-7831 and VIR-7832 Demonstrate Potent *In Vitro* and *In Vivo* Activity Against SARS-CoV-2. *bioRxiv* (2021). doi: 10.1101/2021.03.09.434607
89. Zhou T, Tsybovsky Y, Gorman J, Rapp M, Cerutti G, Chuang GY, et al. Cryo-EM Structures of SARS-CoV-2 Spike Without and With ACE2 Reveal a pH-Dependent Switch to Mediate Endosomal Positioning of Receptor-Binding Domains. *Cell Host Microbe* (2020) 28:867–79.e5. doi: 10.1016/j.chom.2020.11.004
90. Pallesen J, Wang N, Corbett KS, Wrapp D, Kirchdoerfer RN, Turner HL, et al. Immunogenicity and Structures of a Rationally Designed Prefusion MERS-CoV Spike Antigen. *Proc Natl Acad Sci USA* (2017) 114:E7348–57. doi: 10.1073/pnas.1707304114
91. Kirchdoerfer RN, Wang N, Pallesen J, Wrapp D, Turner HL, Cottrell CA, et al. Stabilized Coronavirus Spikes are Resistant to Conformational Changes Induced by Receptor Recognition or Proteolysis. *Sci Rep* (2018) 8:1–11. doi: 10.1038/s41598-018-34171-7
92. Hsieh C, Goldsmith JA, Schaub JM, Divenere AM, Kuo H, Javanmardi K, et al. Structure-Based Design of Prefusion-Stabilized SARS-CoV-2 Spikes. *Science* (2020) 369:1501–5. doi: 10.1126/science.abd0826

Conflict of Interest: CF: Grant: Gilead, Abbvie. Consultant: Gilead, Abbvie, Vir Biotechnology Inc, Arrowhead, Transgene, BMS.

The remaining authors declare that the research was conducted in the absence of any commercial or financial relationships that could be construed as a potential conflict of interest.

Publisher's Note: All claims expressed in this article are solely those of the authors and do not necessarily represent those of their affiliated organizations, or those of the publisher, the editors and the reviewers. Any product that may be evaluated in this article, or claim that may be made by its manufacturer, is not guaranteed or endorsed by the publisher.

Copyright © 2021 Boni, Cavazzini, Bolchi, Rossi, Vecchi, Tiezzi, Barili, Fisicaro, Ferrari and Ottonello. This is an open-access article distributed under the terms of the Creative Commons Attribution License (CC BY). The use, distribution or reproduction in other forums is permitted, provided the original author(s) and the copyright owner(s) are credited and that the original publication in this journal is cited, in accordance with accepted academic practice. No use, distribution or reproduction is permitted which does not comply with these terms.

frontiers in Immunology

ORIGINAL RESEARCH
published: 02 December 2021
doi: 10.3389/fimmu.2021.789735

Regulatory T Cells as Predictors of Clinical Course in Hospitalised COVID-19 Patients

Sara Caldrer[1], Cristina Mazzi[2], Milena Bernardi[1], Marco Prato[1], Niccolò Ronzoni[1], Paola Rodari[1], Andrea Angheben[1], Chiara Piubelli[1] and Natalia Tiberti[1]**

[1] Department of Infectious – Tropical Diseases and Microbiology, Istituto di Ricovero e Cura a Carattere Scientifico (IRCCS) Sacro Cuore - Don Calabria Hospital, Verona, Italy, [2] Centre for Clinical Research, Istituto di Ricovero e Cura a Carattere Scientifico (IRCCS) Sacro Cuore - Don Calabria Hospital, Verona, Italy

Background: The host immune response has a prominent role in the progression and outcome of SARS-CoV-2 infection. Lymphopenia has been described as an important feature of SARS-CoV-2 infection and has been associated with severe disease manifestation. Lymphocyte dysregulation and hyper-inflammation have been shown to be associated with a more severe clinical course; however, a T cell subpopulation whose dysfunction correlate with disease progression has yet to be identify.

Methods: We performed an immuno-phenotypic analysis of T cell sub-populations in peripheral blood from patients affected by different severity of COVID-19 (n=60) and undergoing a different clinical evolution. Clinical severity was established based on a modified WHO score considering both ventilation support and respiratory capacity (PaO2/FiO2 ratio). The ability of circulating cells at baseline to predict the probability of clinical aggravation was explored through multivariate regression analyses.

Results: The immuno-phenotypic analysis performed by multi-colour flow cytometry confirmed that patients suffering from severe COVID-19 harboured significantly reduced circulating T cell subsets, especially for $CD4^+$ T, Th1, and regulatory T cells. Peripheral T cells also correlated with parameters associated with disease severity, i.e., PaO2/FiO2 ratio and inflammation markers. $CD4^+$ T cell subsets showed an important significant association with clinical evolution, with patients presenting markedly decreased regulatory T cells at baseline having a significantly higher risk of aggravation. Importantly, the combination of gender and regulatory T cells allowed distinguishing between improved and worsened patients with an area under the ROC curve (AUC) of 82%.

Conclusions: The present study demonstrates the association between $CD4^+$ T cell dysregulation and COVID-19 severity and progression. Our results support the importance of analysing baseline regulatory T cell levels, since they were revealed able to predict the clinical worsening during hospitalization. Regulatory T cells assessment soon after hospital admission could thus allow a better clinical stratification and patient management.

Keywords: COVID-19, immunophenotype, T cell subtypes, regulatory T cells, disease severity

OPEN ACCESS

Edited by:
Laura Maggi,
Università degli Studi di Firenze, Italy

Reviewed by:
Chaofeng Han,
Second Military Medical University, China
Grace Mulcahy,
University College Dublin, Ireland

****Correspondence:***
Sara Caldrer
sara.caldrer@sacrocuore.it
Natalia Tiberti
natalia.tiberti@sacrocuore.it

Specialty section:
This article was submitted to T Cell Biology, a section of the journal Frontiers in Immunology

Received: *05 October 2021*
Accepted: *15 November 2021*
Published: *02 December 2021*

Citation:
Caldrer S, Mazzi C, Bernardi M, Prato M, Ronzoni N, Rodari P, Angheben A, Piubelli C and Tiberti N (2021) Regulatory T Cells as Predictors of Clinical Course in Hospitalised COVID-19 Patients. Front. Immunol. 12:789735. doi: 10.3389/fimmu.2021.789735

INTRODUCTION

The worldwide emergency of COVID-19 pandemic has led the scientific community to study in depth the host immune response during this acute viral illness since the broad spectrum of disease severity has suggested an important, although unclear, role of post-infection immunity. In this context, the key role of the T-cell mediated immunity has emerged and the SARS-CoV-2 specific T cell response has progressively been delineated (1, 2). Several studies have already reported that some COVID-19 patients present an impaired T cell response (3) and that severe cases are characterised by dysfunctional cellular and humoral immunity (4, 5). Lymphopenia has thus become a hallmark of COVID-19 severe disease (6, 7). Such alterations have also been shown to affect cell differentiation and increased activated T cells have been reported in severe COVID-19 (8–10). Indeed, in severe subjects, the $CD4^+$ T cell response showed a functional impairment associated with an increased expression of exhaustion markers, while a predominant activation of $CD8^+$ T cells was observed in mild patients (11). The putative association of Th1/Th2 $CD4^+$ cells with disease progression has also been investigated (12, 13), but conflicting results have been reported (14). A relation between systemic hyper-inflammation and COVID-19 severity or progression has also been described. Increased circulating levels of IL-6, IL-8 and TNF-α as well as a diminished production of type I IFN by peripheral blood immune cells at admission were in fact reported as independent predictors of disease outcome and proposed as biomarkers to guide treatment choice (15–18). A more in-depth understanding of the functional role of cell-mediated immunity in COVID-19 pathogenesis through T cell evaluation during the acute phase might be found crucial to help in patients' management and to prevent severe disease. Indeed, numerous efforts are currently ongoing to decipher the contribution of memory T cells to the adaptive response to SARS-CoV-2 (19) and to develop effective vaccines and disease control measures.

Here we performed a retrospective study to investigate the immune dysregulation associated with COVID-19 severity and clinical course. Specifically, we assessed circulating T cell subsets and systemic cytokines during the acute phase of the infection in 60 hospitalised subjects. In addition to the commonly studied $CD4^+$ and $CD8^+$ T cells, we also targeted $CD4^+$ sub-populations including Th1, Th2, Th17 and regulatory T cells (Tregs). Correlation and regression analyses were performed to establish the potential of specific immunological features for the prediction of COVID-19 clinical aggravation during hospitalisation.

METHODS

Study Population and Sample Collection

Patients diagnosed with COVID-19 and admitted to the COVID-19 ward of the IRCCS Sacro Cuore Don Calabria Hospital between March and April 2020 were consecutively included. Demography, clinical characteristics and laboratory findings upon admission were retrieved from electronic medical records (**Tables 1**, **2**). Patients were classified into three categories of severity based on a modified WHO score (20) to take into account both the type of ventilation administered and the lung function expressed through the Horowitz index (PaO_2/FiO_2 ratio - arterial oxygen partial pressure to inspired oxygen fraction). Patients were thus classified as follows: mild (score 4), if no oxygen therapy was administered or PaO_2/FiO_2 ≥300; moderate (score 5), if oxygen supplied by mask or nasal prongs, or PaO_2/FiO_2 between 150–299; severe (score≥6), if oxygen administered by NIV, high flow or intubation, or PaO_2/FiO_2 <150.

All patients signed written informed consent. The study was conducted according to the guidelines of the Declaration of Helsinki and approved by the Ethical Committee of Verona and Rovigo provinces under protocol no. 63471/2020.

Whole blood and serum samples used for experimental analyses were collected upon admission and stored at -80°C until further use.

SARS-CoV-2 Molecular and Serological Tests

COVID-19 diagnosis was performed by reverse-transcriptase real time PCR (RT-qPCR) on nasopharyngeal swab according to WHO guidelines (available at https://www.who.int/publications/i/item/diagnostic-testing-for-sars-cov-2) and applying the CDC 2019-nCoV rRT-PCR Diagnostic Panel assay and protocol (available at https://www.fda.gov/media/134922/download) (21). IgG anti-SARS-CoV2 nucleocapsid protein (IgG-N) and IgM anti-SARS-CoV2 spike protein (IgM-S), were measured in patients' serum using a chemiluminescent microparticle immunoassays (CMIA) (Abbott, Ireland) following manufacturer's instructions. Results were expressed as assay index, i.e. sample relative light unit (RLU)/calibrator RLU. The assay was considered positive for indices >1.4 or ≥1 for IgG-N and IgM-S, respectively.

Flow Cytometry Analyses

Flow cytometry analyses were performed on whole blood samples collected in EDTA, aliquoted and stored at -80°C in 10% DMSO (v/v). The list and concentration of mouse anti-human monoclonal antibodies employed (BD Biosciences, San Jose, CA, USA) are reported in **Table S1**. Samples were prepared as recommended elsewhere (22). Briefly, three test tubes containing different combinations of fluorescence-labelled antibodies were used for each patient. One hundred and twenty (120) µL of whole blood were added to each panel-tube, vortexed and incubated at room temperature for 20 minutes in the dark. Erythrocytes were lysed and sample fixed with 1X FACS Lysing solution (BD Bioscience) for 10 minutes in the dark. Samples were washed twice with PBS + 0.5% BSA (w/v) and cell pellet was finally suspended in 200 µL of PBS + 0.5% BSA. Data acquisition was performed using a CytoFlex flow cytometer (Beckman Coulter, Brea, CA, USA) with the CytExpert software v2.3 (Beckman Coulter). The stopping rule was set at 100000 events in the $CD45^+$ gate or, when this criterion could not be met due to severe leukopenia, the entire sample was

TABLE 1 | Baseline demographic and clinical characteristics of COVID-19 patients.

	Mild (n = 23)	Moderate (n = 28)	Severe (n = 9)	p-value[a]	Post-test p-value[b]
Gender (F), n (%)	12 (42.9%)	13 (46.4%)	1 (11.1%)	ns	
Age (years), median [range]	68 [20-94]	77 [43 - 93]	84 [65 - 98]	0.0215	Mi vs Mo.: 0.042 Mi vs S: 0.023
Delay between blood collection and symptom onset (days), median [range]	5.5 [1 - 32]	7 [2 - 26]	8 [1 - 17]	ns	
Fever (yes), n (%)	11 (47.8%)	10 (35.7%)	4 (44.4%)	ns	
PaO2/FiO2 ratio, median [IQR][c]	332.5 [314 - 357]	241 [223 - 275]	83 [75 - 108]	0.0001	Mi vs Mo: <0.001 Mo vs S: 0.012 Mi vs S: <0.001
Oxygen supply, n (%)				0.004	
None	9 (39.1%)	3 (10.7%)	0		
Low flow	14 (60.9%)	25 (89.3%)	7 (77.8%)		
NIV	0	0	1 (11.1%)		
Intubation	0	0	1 (11.1%)		
Presence of comorbidities (yes), n (%)	11 (47.8%)	25 (89.3%)	8 (88.9%)	0.003	
Type of co-morbidities, n (%)					
Diabetes	3 (13%)	8 (28.6%)	2 (22.2%)		
Cardiovascular diseases	9 (39.1%)	13 (46.4%)	6 (66.7%)		
Hypertension	5 (21.7%)	11 (39.3%)	2 (22.2%)		
Neoplasm	1 (4.3%)	1 (3.6%)	2 (22.2%)		
Respiratory diseases	3 (13%)	5 (17.9%)	3 (33.3%)		
Neurodegenerative diseases	0	1 (3.6%)	0		
Hormonal and metabolic disorders	1 (4.3%)	5 (17.9%)	0		
Obesity	1 (4.3%)	1 (3.6%)	0		
Other chronic diseases	2 (8.7%)	3 (10.7%)	0		
Ongoing treatment[d] (yes), n (%)	16 (69.6%)	18 (64.3%)	6 (66.7%)	ns	
Type of treatment[e], n (%)					
None	7 (30.4%)	10 (35.7%)	3 (33.3%)		
Hydroxychloroquine	7 (30.4%)	9 (32.1%)	1 (11.1%)		
Hydroxychloroquine + Tocilizumab	1 (4.3%)	0	0		
Hydroxychloroquine + antiviral	6 (26.1%)	9 (32.1%)	5 (55.6%)		
Hydroxychloroquine + antiviral + corticosteroids	1 (4.3%)	0	0		
Hydroxychloroquine + corticosteroids	1 (4.3%)	0	0		
Clinical course (worsened), n (%)	7 (30.4%)	8 (28.6%)	8 (88.9%)	0.005	
Outcome (death), n (%)	2 (8.7%)	3 (10.7%)	5 (55.6%)	0.008	

[a]Kruskal-Wallis test for comparison between continuous variables; Chi-squared or Fisher's exact test for categorical variables.
[b]Dunn post-test with Bonferroni correction. Mi, mild; Mo, Moderate; S, Severe.
[c]Missing data for 1 mild patient and 1 moderate patient.
[d]Ongoing treatment at the time of blood collection.
[e]Type of ongoing treatment at the time of blood collection. Antivirals included: darunavir/cobicistat, lopinavir/ritonavir.
IQR, interquartile range; Mild, modified WHO score = 4; Moderate, modified WHO score = 5; Severe, modified WHO score≥6.
ns, non significant.

acquired. The number of cells/μL was determined by the instrument based on the volume of sample consumed. The selection of surface markers and the gating strategy employed are reported in **Figure S1**. Data were analysed with the Kaluza software v2.1 (all from Beckman Coulter, Brea, CA, USA).

Systemic Cytokine Concentration

The serum concentration of IFN-α, IFN-γ, IL-2, IL-4, IL-5, IL-6, IL-9, IL-10, IL-12p70, IL-17A, TNF-α, GM-CSF was measured using the MACSPlex Cytokine 12 kit (Miltenyi Biotec). Samples were prepared as recommended by the manufacturer. Briefly, samples were centrifuged at 10000*g* for 5 minutes at 4°C to remove large debris and the supernatant was then diluted 1:4 with sample buffer provided within the kit. Data were acquired on a CytoFlex flow cytometer (Beckman Coulter) at a 20 μL/min flow rate. Acquisition stopping rule was set at 4000 events in the bead gate or 180μl of acquired sample. Exported data were analysed with Flowlogic software (Inivai Technologies) and the median intensity in APC was used to extrapolate cytokine concentrations. To all samples having concentration values out of range (OOR), an arbitrary value corresponding to half of the lowest measured concentration was assigned.

Statistical Analyses

Statistical analyses were performed using STATA software v14.0 (StataCorp LP, TX, USA) or SAS EG v7.1 (SAS Institute Inc., NC, USA), and plots generated with GraphPad Prism v8.3.0 (GraphPad Software, CA, USA). Non-parametric tests were applied according to data distribution. Differences in cell or cytokine concentration were assessed using the Mann-Whitney *U* test or the Kruskal-Wallis test followed by Dunn's post-test and Bonferroni correction for multiple comparisons. The Spearman coefficient was used to evaluate correlations. Significance level was set at p-value <0.05 and all tests were two-tailed. A linear regression model was used to investigate the effect of disease severity on T cell subsets and cytokines, after log transformation of

TABLE 2 | Principal laboratory findings at baseline.

	Mild (n = 23)	Moderate (n = 28)	Severe (n = 9)	p-value[a]	Post-test p-value[b]
WBC (10^9/L), median [IQR]	6.1 [4.5 - 7.2]	5.65 [3.95 - 8.25]	9.7 [9 - 11]	0.013	Mo vs. S: 0.008 Mi vs. S: 0.011
Neutrophil (10^9/L), median [IQR]	3.7 [2.52 - 5.2]	4.1 [2.35 - 6.5]	9.1 [7.8 - 10.1]	0.001	Mo vs. S: 0.002 Mi vs. S: <0.001
Neutrophil %, median [IQR]	66.6 [51.2 - 75.1]	74.9 [64.3 - 79.95]	89.5 [87.1 - 91.6]	<0.001	Mo vs. S: <0.001 Mi vs. S: <0.001
Lymphocytes (10^9/L), median [IQR]	1.3 [1 - 1.8]	0.95 [0.8 - 1.35]	0.5 [0.4 - 0.6]	<0.001	Mo vs. S: 0.01 Mi vs. S: <0.001
Lymphocytes %, median [IQR]	22.6 [17.6 - 32.3]	15.35 [11.4 - 26.45]	5.2 [3.9 - 6.5]	<0.001	Mo vs. S: <0.001 Mi vs. S: <0.001
Monocytes (10^9/L), median [IQR]	0.5 [0.3 - 0.7]	0.5 [0.3 - 0.75]	0.4 [0.2 - 0.6]	ns	
Monocytes %, median [IQR]	8.7 [5.8 - 10.1]	8.5 [6.95 - 10.95]	3.5 [3.3 - 4]	<0.001	Mo vs. S: <0.001 Mi vs. S: <0.001
CRP (mg/L), median [IQR]	47.2 [26.15 - 74.52]	92.9 [21.65 - 145.5]	124.3 [109.6 - 132]	0.015	Mi vs. S: 0.008
Ferritin (microg/L), median [IQR]	275.1 [87.6 - 757.5]	398.5 [183 - 722.8]	1110 [100 - 1486]	ns	
IL-6 (pg/ml), median [IQR]	17.36 [8.96 - 37.84]	26.24 [8.64 - 67.48]	67.12 [31.24 - 99.66]	0.048	Mi vs. S: 0.023
Creatinine (µmol/L), median [IQR]	74 [67 - 117]	74.5 [64 - 90.5]	108 [106 - 119]	0.012	Mo vs. S: 0.005 Mi vs. S: 0.023
D-Dimer (µg/L), median [IQR][c]	835 [487 - 1530]	1038 [496.5 - 2357]	2482 [1241 - 5400]	ns	
ACE (U/L)[d]	26.8 [19.7 - 31.5]	25.2 [5.3 - 39.1]	17.6 [17.7 - 25.6]	ns	
RT-qPCR Ct, median [IQR][e]	25 [21 - 32]	25 [23 - 31]	24 [19 - 30]	ns	
IgM-S (positive), n (%)[f]	12 (52.2%)	15 (53.6%)	7 (77.8%)	ns	
IgG-N (positive), n (%)[f]	9 (39.1%)	16 (57.1%)	7 (77.8%)	ns	

[a]*Kruskal-Wallis test for comparison between continuous variables.*
[b]*Dunn post-test with Bonferroni correction, Mi, mild; Mo, Moderate; S, Severe.*
[c]*Missing data for 1 mild patient.*
[d]*Missing data for 2 mild patients.*
[e]*Missing data for 2 mild patients and 2 moderate patients.*
[f]*Missing data for 4 mild patients, 3 moderate patients and 1 severe patient.*
IQR, interquartile range; Mild, modified WHO score = 4; Moderate, modified WHO score = 5; Severe, modified WHO score≥6
ns, non significant.

variables. Significant univariable models were then adjusted for the effects of covariates of interest in multivariable linear regression models. The ability of circulating cells and cytokines to predict the probability of clinical aggravation was explored using Firth logistic regression. Significant regressors (p-value from univariable analyses <0.2) were dichotomized using Receiver Operating Characteristic (ROC) curve cut-off analysis and included in multivariable Firth logistic regression models. Cut-offs were defined maximizing the sum of sensitivity and specificity (Youden's J statistic) (**Table S6**). Areas Under the Curve (AUC) were compared by the DeLong test. Goodness-of-fit measures were estimated for these models.

RESULTS

Population Characteristics

The demographic and clinical characteristics of COVID-19 patients classified as mild, moderate or severe are reported in **Table 1**. No differences in gender frequencies were observed across the three groups, while a small, although significant, difference in patients' age was observed, with severe and moderate patients being older than mild patients. Considering clinical information, the frequency of subjects presenting with fever was comparable between the three groups. Comorbidities were significantly more frequent among patients suffering from severe or moderate COVID-19 (89% for both groups) compared to the mild form (48%), with cardiovascular diseases being the most common co-morbidity. The number of patients receiving treatment was the same across the three groups and the majority of them were receiving either hydroxychloroquine or a combination of hydroxychloroquine and antivirals, as a reflection of standard of care at the time of the study. The frequency of subjects worsening during hospitalisation or having a fatal outcome was significantly higher among severe patients (89% and 56%, respectively) compared to the other groups.

The principal laboratory findings obtained on blood samples collected at the same time as those tested here are reported in **Table 2**. In agreement with already reported data, disease severity was associated with a general leucocytosis and lymphopenia (23). Severe patients presented a raised concentration of inflammatory markers, i.e., C-reactive protein (CRP) and IL-6, while other markers proposed to be related with SARS-CoV-2 infection severity, including ferritin, D-dimer and angiotensin-converting enzyme were not. Blood creatinine was also higher in severe disease compared to milder forms. No differences in the viral load, expressed as RT-qPCR Ct value, were observed between the three groups. The frequency of patients with positive IgM-S and IgG-N antibodies did not differ across the three groups.

Lymphocyte Subset Frequencies Are Associated With COVID-19 Severity

The gating strategy adopted to determine the frequency of leucocytes and lymphocyte subsets is reported in **Figure S1**.

A marked reduction in the absolute number of total lymphocytes and T cell subsets ($CD4^+$, $CD8^+$ T, Th1, Th17 and Treg) was recorded in severe COVID-19 patients compared to mild or moderate subjects, while the number of granulocytes was significantly increased in severe patients (**Figure 1** and **Table S2**).

A multivariate linear regression analysis confirmed the significant association between disease severity and the amount of the different lymphocytes, independently of the effect of age, gender, presence of fever or comorbidities, and ongoing treatment, considered as potential effect modifiers (**Table 3**). In addition, patients' gender showed a significant association with $CD4^+$ T cells, while the presence of fever and comorbidities were associated with Th1 variability.

Lymphocyte Subset Counts Correlate With Inflammation Markers and Lung Function but Not With Anti-SARS-CoV-2 Antibodies

A correlation matrix was computed to assess whether lymphocyte immuno-phenotype shows a linear relation with clinical and biochemical parameters, independently of disease severity (**Figure 2A**). The Horowitz index showed a significant correlation ($p<0.01$) with total lymphocytes and $CD3^+$ T cells (moderate positive correlation), as well as with $CD4^+$ and $CD8^+$ T cells, Th1, Th17 and Treg (weak positive correlation), indicating a relation between a reduced lung function and reduced circulating cells of the T compartment. Significant negative correlations were observed between inflammatory markers (CRP, ferritin and IL-6) and the majority of the cell subsets analysed (**Figure 2A**). In particular, the most relevant correlations having a Spearman r coefficient < -0.6 were observed for CRP and $CD4^+$ T cells, Th1, Th17 or Treg (**Figure 2B**). Finally, total lymphocytes, T cells, $CD4^+$, Th1, Th17 and Tregs showed a significant relation with RT-qPCR Ct values, pointing out that higher viral loads are accompanied by a lower absolute count of T cell subsets (**Figure 2A**). Considering anti-SARS-CoV-2 antibodies, the absolute number of the different cell types analysed did not differ between patients with negative or positive serology, neither for IgM-S nor for IgG-N antibodies (**Table S3A**). Moreover, in patients with positive serology, the cell count did not correlate with IgM-S or IgG-N indices (**Table S3B**).

The Cytokine Systemic Concentration Is Not Affected by Disease Severity

The systemic levels of selected cytokines were measured in serum samples collected on the same day as blood samples used for the immuno-phenotype analysis. IL-2 and IL-9 were excluded from further analyses as more than 90% of the measured samples had OOR values. The systemic concentration of all measured cytokines did not vary according to COVID-19 severity (**Table S2**) however, when evaluated at the individual level, it was possible to identify within each severity group, clusters of patients displaying raised levels of all or most of the assessed cytokines (**Figure S2**). Among the measured cytokines, only a few correlated significantly with the number of circulating lymphocyte populations, although the strength of the

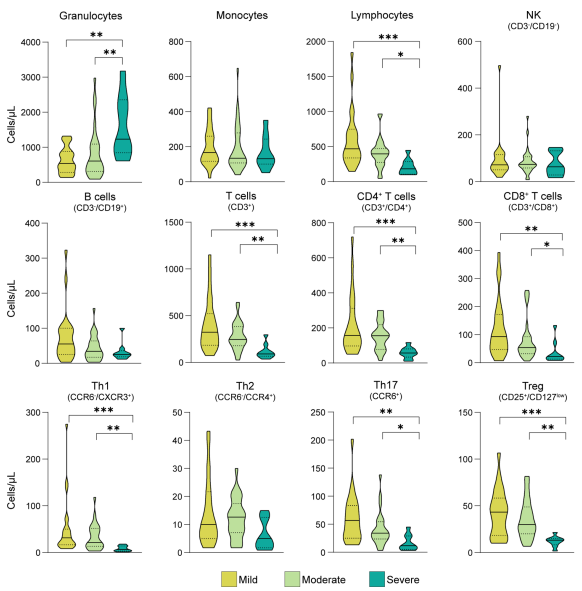


FIGURE 1 | Immunophenotypic analysis in COVID-19 patients classified according to the severity of the disease. Distribution of the absolute number of cells (expressed as cells/µl of blood) across the three groups of COVID-19 patients suffering from different disease severity, i.e. mild or score 4 (n = 23), moderate or score 5 (n = 28), severe or score ≥6 (n = 9), established according to a modified WHO classification (20). Statistical significance, set at p-value <0.05, was assessed using the Kruskal-Wallis test followed by the Dunn's post-test and Bonferroni correction for multiple comparisons. *p < 0.05; **p < 0.01; ***p < 0.001.

TABLE 3 | Multivariable linear regression analysis.

	Intercept	[95% Confidence Interval]		p-value	Adjusted R^2
Granulocytes					
Age	0.003	-0.005	0.011	0.474	0.09
Gender	0.044	-0.157	0.244	0.665	
Fever	0.062	-0.139	0.263	0.538	
Comorbidities	-0.129	-0.403	0.145	0.349	
Treatment[a]	-0.048	-0.261	0.165	0.653	
Severity					
Mild	-0.458	-0.769	-0.147	**0.005**	
Moderate	-0.386	-0.669	-0.104	**0.008**	
Lymphocytes					
Age	0.000	-0.006	0.006	0.985	0.27
Gender	0.143	-0.004	0.290	0.057	
Fever	-0.060	-0.207	0.088	0.420	
Comorbidities	-0.089	-0.290	0.111	0.376	
Treatment[a]	-0.104	-0.260	0.051	0.185	
Severity					
Mild	0.347	0.119	0.574	**0.004**	
Moderate	0.220	0.013	0.427	**0.038**	
T cells ($CD3^+$)					
Age	0.002	-0.005	0.008	0.597	0.30
Gender	0.159	-0.002	0.321	0.053	
Fever	-0.062	-0.224	0.100	0.447	
Comorbidities	-0.100	-0.321	0.121	0.368	
Treatment[a]	-0.079	-0.250	0.093	0.360	
Severity					
Mild	0.458	0.207	0.708	**0.001**	
Moderate	0.336	0.108	0.563	**0.005**	
$CD4^+$ T cells					
Age	0.001	-0.006	0.008	0.785	0.36
Gender	0.213	0.050	0.377	**0.011**	
Fever	-0.079	-0.243	0.084	0.334	
Comorbidities	-0.185	-0.408	0.037	0.101	
Treatment[a]	-0.074	-0.247	0.099	0.396	
Severity					
Mild	0.401	0.148	0.654	**0.002**	
Moderate	0.360	0.130	0.589	**0.003**	
$CD8^+$ T cells					
Age	0.003	-0.006	0.012	0.471	0.20
Gender	0.147	-0.072	0.367	0.183	
Fever	-0.063	-0.283	0.157	0.570	
Comorbidities	-0.005	-0.305	0.294	0.973	
Treatment[a]	-0.144	-0.377	0.088	0.218	
Severity					
Mild	0.560	0.221	0.900	**0.002**	
Moderate	0.347	0.038	0.655	**0.029**	
Th1 ($CCR6^-$/$CXCR3^+$)					
Age	0.004	-0.004	0.013	0.309	0.46
Gender	0.273	0.073	0.473	**0.008**	
Fever	-0.242	-0.446	-0.038	**0.021**	
Comorbidities	-0.355	-0.635	-0.075	**0.014**	
Treatment[a]	-0.008	-0.220	0.203	0.937	
Severity					
Mild	0.505	0.202	0.808	**0.002**	
Moderate	0.391	0.107	0.676	**0.008**	
Th17 ($CCR6^+$)					
Age	-0.001	-0.009	0.007	0.802	0.29
Gender	0.091	-0.106	0.288	0.357	
Fever	-0.125	-0.326	0.076	0.216	
Comorbidities	-0.199	-0.475	0.077	0.154	
Treatment[a]	-0.070	-0.278	0.139	0.505	
Severity					
Mild	0.487	0.189	0.786	**0.002**	
Moderate	0.378	0.098	0.659	**0.009**	
Treg ($CD25^+$/$CD127^{low}$)					
Age	0.003	-0.004	0.009	0.449	0.33
Gender	0.137	-0.024	0.298	0.093	
Fever	-0.087	-0.248	0.074	0.281	
Comorbidities	-0.211	-0.430	0.008	0.059	
Treatment[a]	-0.020	-0.190	0.150	0.815	
Severity					
Mild	0.421	0.173	0.670	**0.001**	
Moderate	0.426	0.200	0.653	**<0.001**	

Reference categories for categorical variables: Gender = male; Fever = no; Comorbidities = no, Treatment = no, Score = 6.

Significant p-values are reported in bold.

[a]*Treatment administered before blood collection.*

Only cell populations significant in the univariable analysis were assessed in the multivariable model.

n = 56 for Th1 and Th17.

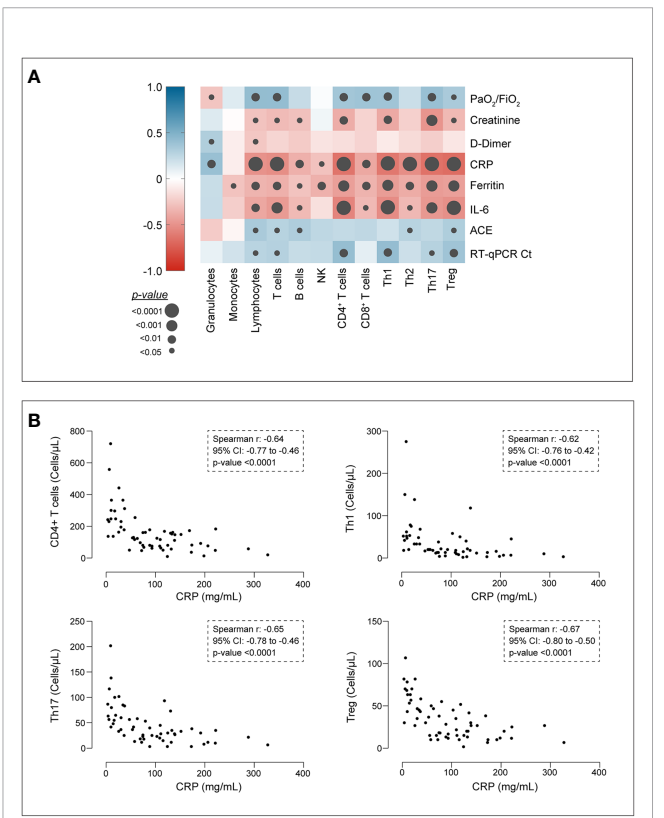


FIGURE 2 | Correlation analysis. **(A)** Correlation matrix assessing the linear correlation between cell types and relevant clinical and biochemical parameters. Colour scale indicates the Spearman ρ coefficient; grey dots indicate the significance level. Cells are expressed as cells/µL of blood. PaO_2/FiO_2, Horowitz index; creatinine, µmol/L; D-dimer, µg/L; CRP, C-reactive protein, mg/L; ferritin, µg/L; IL-6, interleukin-6 measured at the time of complete blood count, pg/mL (chemiluminescence immunoassay); ACE, angiotensin converting enzyme (U/L); RT-qPCR Ct, number of cycles. **(B)** Detailed scatter plots of correlations displaying Spearman r coefficient > |0.6|.

TABLE 4 | Multivariable logistic regression analysis for the prediction of a clinical aggravation during hospitalisation.

Parameter	Odds ratio Estimates				Likelihood Ratio test			Hosmer-Lemeshow goodness of fit		
	Reference	Odds Ratio	95% CI	p-value	$\chi2$	DF	p-value	$\chi2$	DF	p-value
$CD4^+$ T cells	≤ 136.7	6.471	1.513 - 27.673	0.012	21.756	5	<0.001	4.858	8	0.773
Gender	Female	0.234	0.055 - 0.989	0.048						
Age		1.042	0.984 - 1.104	0.157						
Comorbidity	No	1.822	0.272 - 12.217	0.537						
Treatment	No	1.939	0.410 - 9.160	0.403						
Th1 ($CCR6^-/CXCR3^+$)	≤ 18.34	7.863	1.653 - 37.396	0.010	24.204	5	<0.001	3.834	7	0.799
Gender	Female	0.156	0.031 - 0.774	0.023						
Age		1.060	0.992 - 1.132	0.085						
Comorbidity	No	3.512	0.401 - 30.799	0.257						
Treatment	No	1.776	0.369 - 8.556	0.474						
Th2 ($CCR6^-/CCR4^+$)	≤ 5	4.352	1.059 - 17.893	0.042	20.720	5	<0.001	3.237	7	0.862
Gender	Female	0.105	0.023 - 0.479	0.004						
Age		1.047	0.986 - 1.112	0.135						
Comorbidity	No	1.696	0.257 - 11.191	0.583						
Treatment	No	1.838	0.395 - 8.558	0.438						
Treg ($CD25^+/CD127^{low}$)	≤ 30	6.807	1.571 - 29.495	0.010	22.357	5	<0.001	4.606	8	0.799
Gender	Female	0.141	0.032 - 0.618	0.009						
Age		1.053	0.991 - 1.119	0.096						
Comorbidity	No	2.419	0.370 - 15.819	0.357						
Treatment	No	1.826	0.397 - 8.409	0.440						
PaO2/FiO2	≤ 186	16.678	1.925 - 144.477	0.011	24.222	5	<0.001	10.308	8	0.244
Gender	Female	0.110	0.023 - 0.529	0.006						
Age		1.032	0.974 - 1.093	0.285						
Comorbidity	No	2.064	0.308 - 13.848	0.456						
Treatment	No	1.404	0.276 - 7.138	0.683						

Treatment administered during hospitalisation included: hydroxychloroquine; corticosteroids; hydroxychloroquine + antivirals; hydroxychloroquine + corticosteroids; hydroxychloroquine + immunological treatment; hydroxychloroquine + antivirals + corticosteroids; hydroxychloroquine + antivirals + immunological treatment; hydroxychloroquine + antivirals + immunological treatment + corticosteroids.

correlation was overall weak (**Table S4**). Only IL-6 and $CD4^+$ T cells showed a moderate negative correlation (Spearman rho = -0.54, p-value <0.0001).

Patients With Decreased Specific T Cell Subsets at Baseline Have Increased Risk of Worsening During Hospitalisation

To evaluate the potential association between our experimental data and patients' clinical course, our cohort was re-classified according to the progression of patients' status as improved or worsened compared to the clinical conditions established on the day of sample collection. Clinical aggravation was determined as an increased requirement of oxygen compared to baseline or death during hospitalisation. On this base, we included 37 patients with an improved clinical course and 23 whose conditions worsened. Amongst the latter, 43.5% ultimately died from COVID-19.

Total lymphocytes, B and T cells and T subsets (except for $CD8^+$ T cells), were significantly reduced in worsening patients; $CD4^+$ T cells and Th1 cells showed the strongest differences between the two groups ($p \leq 0.0006$) (**Figure 3A** and **Table S5**). Additionally, worsening patients displayed significantly higher systemic concentrations of IFN-α (p value=0.0175) (**Figure 3B** and **Table S5**). Among the clinical and biochemical parameters already proposed as associated with disease severity, only the viral load, blood creatinine and PaO_2/FiO_2 ratio were able to differentiate between the two groups (**Figure 3C** and **Table S5**).

The multivariable logistic regression analysis revealed that subjects harbouring decreased $CD4^+$, Th1, Th2 and Tregs have a significantly increased risk of worsening during the hospitalisation, after adjusting for gender, presence of comorbidity and the administration of treatment during hospitalisation (**Table 4**). In particular, patients with baseline $CD4^+$ T cells ≤ 136.7 cells/μL have 6.5 times the odds of progression compared to subjects with higher count. Similarly, Th1 count ≤ 18.34 cells/μL, Th2 count ≤ 5 cells/μL and Treg ≤ 30 cells/μL are associated with increased risk of 7.9, 4.4 and 6.8 times, respectively. Similarly, patients with baseline PaO2/FiO2 ratio ≤186 have significantly higher odds of worsening. The multivariable analysis also confirmed a significantly higher risk for men to undergo clinical aggravation compared to women. The combination of gender and Tregs through a ROC curve selection analysis significantly improved the discriminatory ability of gender, with AUC increased from 0.75 to 0.82 (p=0.044) (**Figure 4**).

DISCUSSION

Lymphopenia is a main feature of COVID-19 infection, affecting $CD4^+$ and $CD8^+$ T cells as well as B lymphocytes, and is more pronounced in severely ill patients (23–28). Several studies are suggesting an association between an impaired, over-activated or inappropriate T-cell response with disease severity or progression (11). In our cohort of hospitalised COVID-19 patients we showed an independent association between $CD4^+$ T cell subset frequency

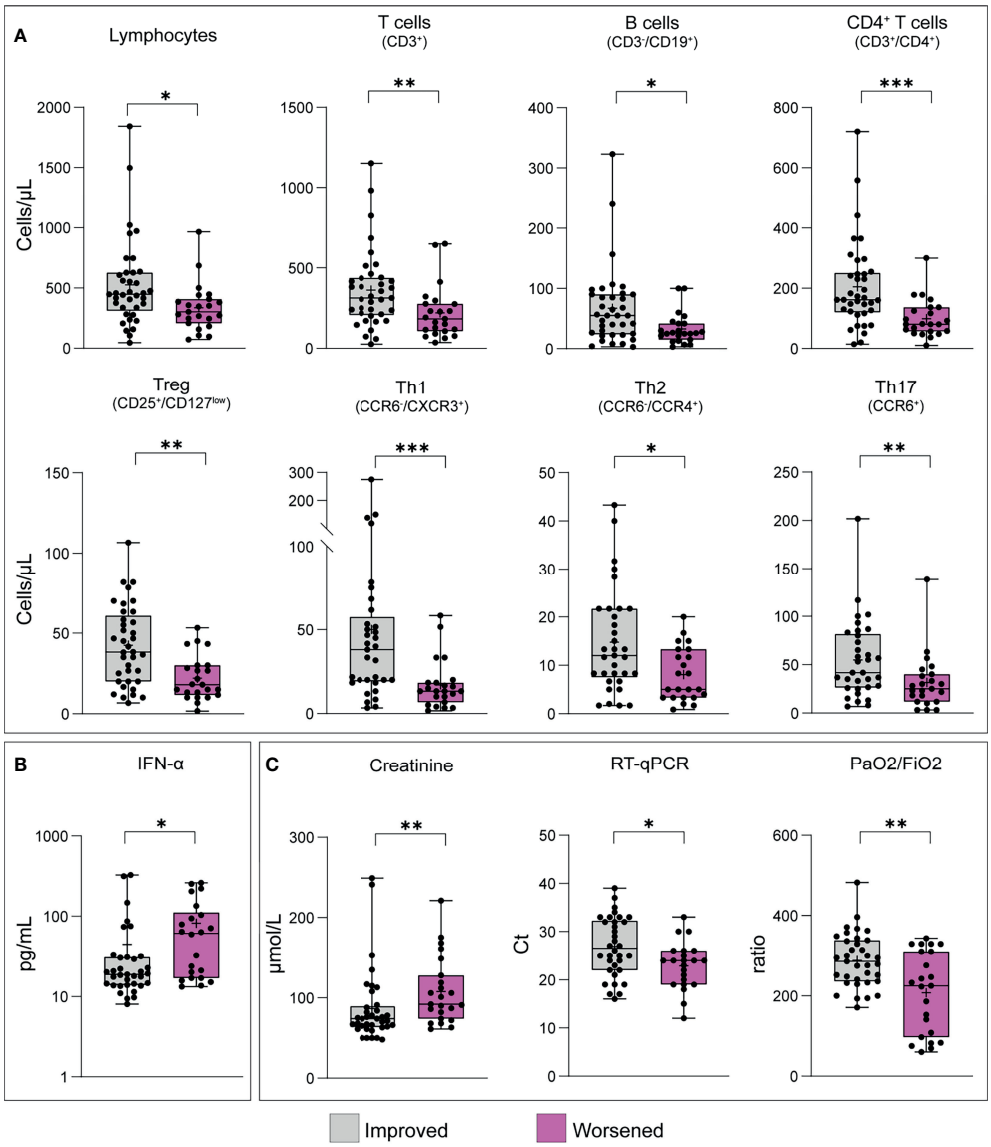
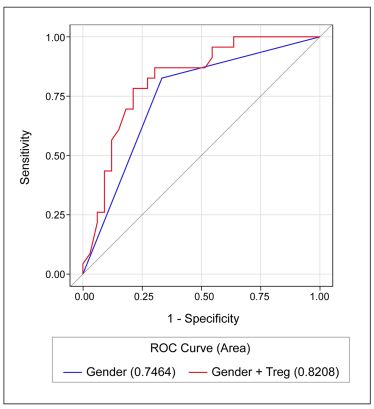


FIGURE 3 | T cell frequencies, cytokine concentrations and laboratory findings in patients classified according to the clinical course during hospitalisation. Patients were classified as improved (n = 37) or worsened (n = 23) as reported in the methods section. **(A)** T cell and T cell subset frequencies; **(B)** cytokine concentration; **(C)** laboratory findings. Only results statistically significant are reported. Statistical significance, set at p-value <0.05, was assessed using the Mann-Whitney U test. *p < 0.05; **p < 0.01; ***p < 0.001. Whiskers represent minimum and maximum values, dots represent individual observations, the + on each box indicates the mean.

and disease severity, with reduced $CD4^+$ T cells, Th1 and Tregs showing the strongest relation with a severe clinical presentation.

Recent studies reported that SARS-CoV-2 elicits a strong and broad T cell response, both $CD4^+$- and $CD8^+$-mediated with, in some cases, the development of a memory phenotype, which might lead to a long-term immunity (29). However, different scenarios in the immune response to the virus have been reported and proposed to be responsible for the wide spectrum of clinical presentation of COVID-19 (30). This was also observed in our cohort, in which patients suffering from different severity of COVID-19 displayed different levels of circulating $CD4^+$ T cell subsets. Systemic lymphopenia, which in our population seems to affect primarily $CD4^+$ T cells, could be the consequence of cell infiltration and sequestration in the lung (10). Nonetheless, it cannot be excluded that diminished circulating lymphocytes might be associated with an impaired immune response in more severe patients, potentially associated with the presence of comorbidities. Although this latter variable did not influence cell population variability in our multivariate analysis, we could not assess the effect of specific categories of comorbidities but only their cumulative effect due to the limited sample size.

We also observed a significant association between decreased circulating $CD4^+$ T cells and their subsets, but not $CD8^+$ T cells, and an aggravation of patients' clinical conditions during



			ROC Contrast		
ROC model	AUC	95% CI	Estimate	95% CI	p-value
Gender	0.7464	0.633 - 0.860	0.044	0.002 - 0.147	0.044
Gender + Tregs	0.8208	0.709 - 0.924			

FIGURE 4 | ROC curve selection analysis. ROC analysis for the discrimination of improved and worsened clinical course during hospitalisation. The best individual discriminator (i.e., gender) and the best combination (i.e., gender + Tregs) are reported. AUC, Area Under the ROC Curve; 95% CI, 95% CI confidence interval.

hospitalisation. We demonstrated that patients harbouring decreased $CD4^+$, Th1, Th2 and Tregs at baseline have a significantly higher risk of clinical deterioration, independently of their gender, age, the presence of comorbidities and treatment administration. Older age and male gender have already been highlighted as important risk factors for more severe disease and clinical course (31). This association was confirmed in our population since patients' gender was the best predictor of clinical course, when variables were considered individually (data not shown). However, the combination of gender with the number of Tregs circulating at baseline significantly improved the ability to predict clinical worsening, indicating that Treg enumeration could help in patients' stratification according to their risk of aggravation. Compared to other cell types, Tregs have been less investigated in COVID-19, although they appear to be involved in disease progression due to their participation to innate and adaptive immune responses. In particular, in the early stage of infection they were shown to downregulate T cell-mediated immune responses, while in late stage severe COVID-19 patients they reduced the hyper-inflammation through cytokine modulation (32). In our population, reduced circulating Tregs showed a strong association with both disease severity and progression, potentially as a results of an increased recruitment to the infection site, thus lung tissues, to control the local inflammation and tissue damage. Nonetheless, we cannot exclude that this Treg reduction is associated with a functional dysregulation, as already suggested by functional analyses on bronchoalveolar lavage fluid (33).

In our study we did not observe increased circulating cytokines associated with disease severity nor with the clinical course, with the exception of IFNα that raised in worsening patients. Although the cytokine storm has been reported by many as a hallmark of COVID-19 severity and critical illness (34), our results suggest that a more complex picture might accompany disease evolution in our cohort. Systemic hyper-inflammation appears to be primarily associated with COVID-19 infection *per se* rather than with disease severity. Indeed, the majority of the studies have highlighted raised inflammatory biomarkers in infected subjects compared to healthy controls, but only few have shown differences associated with disease severity (35).

The results of our study confirm that an immune signature is associated with a more severe clinical presentation and an aggravation during hospitalisation, partly in agreement with previous observations on different patterns of immune responses elicited in hospitalised patients that might benefit from a different medical intervention based on their immune signature (3).

Our study has some limitations. The inclusion of asymptomatic subjects, in addition to our hospitalised patients, could have contributed in better determining the immunophenotype associated with COVID-19 infection, independently of disease severity. Such studies are however already available in the literature and it is important to recall that during the first COVID-19 wave in Italy asymptomatic individuals were only rarely detected. The availability of additional samples taken during hospitalisation as well as at discharge could have helped in defining a more precise picture of T cell kinetics, and particularly Treg, during the infection. Nonetheless, the comprehensive characterisation of our cohort at baseline, thanks to complete and homogeneous clinical records, has allowed achieving an in depth data analysis with the evaluation of important confounding factors including comorbidities and treatment.

In our study we did not investigate the lymphocyte activation state. Even though we could not draw any conclusions regarding the functional state of the cells of interest, we highlighted the important role of less represented whole cell populations, particularly Tregs, as potential stratification markers easily measurable in small amount of blood. In this scenario, it should be mentioned that several clinical trials evaluating strategies to improve T cell response as a therapeutic intervention for COVID-19 are currently ongoing, including T cell adoptive transfer (NCT04457726, NCT04762186, https://clinicaltrials.gov/). The potential use of T cells as diagnostic tools is also under evaluation (NCT04874818). In conclusion, we have confirmed the extensive immune-dysregulation associated with COVID-19 severity and shown the association between decreased T cell subtypes, especially of T helper lineage, and an exacerbation of patients' clinical conditions during hospitalization. Based on their ability to predict clinical worsening, here we extend the potential utility of $CD4^+$ T cells measurement, especially of Tregs, for patients' stratification based on the risk of clinical deterioration early after hospital admission.

DATA AVAILABILITY STATEMENT

The datasets presented in this study can be found in online repositories. The names of the repository/repositories and

accession number(s) can be found below: Zenodo repository at https://doi.org/10.5281/zenodo.5511828.

ETHICS STATEMENT

The studies involving human participants were reviewed and approved by Ethical Committee of Verona and Rovigo provinces under protocol no. 63471/2020. The patients/participants provided their written informed consent to participate in this study.

AUTHOR CONTRIBUTIONS

CP and NT conceived the study. SC and NT designed the study. SC, MB, and MP performed the experiments. NR, AA, and PR managed sample and clinical data collection. CM and NT performed statistical analyses. SC and NT wrote the manuscript. All authors reviewed and edited the manuscript and approved the final version.

FUNDING

This work was supported by the Italian Ministry of Health "Fondi Ricerca Corrente – L1P6" to IRCCS Sacro Cuore Don Calabria Hospital and by the Italian Ministry of Health - COVID-2020-12371675.

ACKNOWLEDGMENTS

The authors wish to thank the medical and nursing staff who assisted the patients for their support in sample collection. The authors also thank Monica Degani, Eleonora Rizzi and Stefano Tais for technical support.

SUPPLEMENTARY MATERIAL

The Supplementary Material for this article can be found online at: https://www.frontiersin.org/articles/10.3389/fimmu.2021.789735/full#supplementary-material

REFERENCES

1. Grifoni A, Weiskopf D, Ramirez SI, Mateus J, Dan JM, Moderbacher CR, et al. Targets of T Cell Responses to SARS-CoV-2 Coronavirus in Humans With COVID-19 Disease and Unexposed Individuals. *Cell* (2020) 181:1489. doi: 10.1016/j.cell.2020.05.015
2. Tarke A, Sidney J, Kidd CK, Dan JM, Ramirez SI, Yu ED, et al. Comprehensive Analysis of T Cell Immunodominance and Immunoprevalence of SARS-CoV-2 Epitopes in COVID-19 Cases. *Cell Rep Med* (2021) 2:100204. doi: 10.1016/j.xcrm.2021.100204
3. Mathew D, Giles JR, Baxter AE, Oldridge DA, Greenplate AR, Wu JE, et al. Deep Immune Profiling of COVID-19 Patients Reveals Distinct Immunotypes With Therapeutic Implications. *Science* (2020) 369:eabc8511. doi: 10.1126/science.abc8511
4. Rydyznski Moderbacher C, Ramirez SI, Dan JM, Grifoni A, Hastie KM, Weiskopf D, et al. Antigen-Specific Adaptive Immunity to SARS-CoV-2 in Acute COVID-19 and Associations With Age and Disease Severity. *Cell* (2020) 183:996. doi: 10.1016/j.cell.2020.09.038
5. Weiskopf D, Schmitz KS, Raadsen MP, Grifoni A, Okba NMA, Endeman H, et al. Phenotype and Kinetics of SARS-CoV-2-Specific T Cells in COVID-19 Patients With Acute Respiratory Distress Syndrome. *Sci Immunol* (2020) 5:eabd2071. doi: 10.1126/sciimmunol.abd2071
6. Giamarellos-Bourboulis EJ, Netea MG, Rovina N, Akinosoglou K, Antoniadou A, Antonakos N, et al. Complex Immune Dysregulation in COVID-19 Patients With Severe Respiratory Failure. *Cell Host Microbe* (2020) 27:992. doi: 10.1016/j.chom.2020.04.009
7. Song JW, Zhang C, Fan X, Meng FP, Xu Z, Xia P, et al. Immunological and Inflammatory Profiles in Mild and Severe Cases of COVID-19. *Nat Commun* (2020) 11:3410. doi: 10.1038/s41467-020-17240-2
8. De Biasi S, Meschiari M, Gibellini L, Bellinazzi C, Borella R, Fidanza L, et al. Marked T Cell Activation, Senescence, Exhaustion and Skewing Towards TH17 in Patients With COVID-19 Pneumonia. *Nat Commun* (2020) 11:3434. doi: 10.1038/s41467-020-17292-4
9. Zenarruzabeitia O, Astarloa-Pando G, Terren I, Orrantia A, Perez-Garay R, Seijas-Betolaza I, et al. T Cell Activation, Highly Armed Cytotoxic Cells and a Shift in Monocytes CD300 Receptors Expression Is Characteristic of Patients With Severe COVID-19. *Front Immunol* (2021) 12:655934. doi: 10.3389/fimmu.2021.655934
10. Kuri-Cervantes L, Pampena MB, Meng W, Rosenfeld AM, Ittner CAG, Weisman AR, et al. Comprehensive Mapping of Immune Perturbations Associated With Severe COVID-19. *Sci Immunol* (2020) 5:eabdn7114. doi: 10.1126/sciimmunol.abd7114
11. Chen Z, John Wherry E. T Cell Responses in Patients With COVID-19. *Nat Rev Immunol* (2020) 20:529. doi: 10.1038/s41577-020-0402-6
12. Neidleman J, Luo X, Frouard J, Xie G, Gill G, Stein ES, et al. SARS-CoV-2-Specific T Cells Exhibit Phenotypic Features of Helper Function, Lack of Terminal Differentiation, and High Proliferation Potential. *Cell Rep Med* (2020) 1:100081. doi: 10.1016/j.xcrm.2020.100081
13. Roncati L, Nasillo V, Lusenti B, Riva G. Signals of Th2 Immune Response From COVID-19 Patients Requiring Intensive Care. *Ann Hematol* (2020) 99:1419. doi: 10.1007/s00277-020-04066-7
14. Sattler A, Angermair S, Stockmann H, Heim KM, Khadzhynov D, Treskatsch S, et al. SARS-CoV-2-Specific T Cell Responses and Correlations With COVID-19 Patient Predisposition. *J Clin Invest* (2020) 130:6477. doi: 10.1172/JCI140965
15. Del Valle DM, Kim-Schulze S, Huang HH, Beckmann ND, Nirenberg S, Wang B, et al. An Inflammatory Cytokine Signature Predicts COVID-19 Severity and Survival. *Nat Med* (2020) 26:1636. doi: 10.1038/s41591-020-1051-9
16. Herold T, Jurinovic V, Arnreich C, Lipworth BJ, Hellmuth JC, von Bergwelt-Baildon M, et al. Elevated Levels of IL-6 and CRP Predict the Need for Mechanical Ventilation in COVID-19. *J Allergy Clin Immunol* (2020) 146:128. doi: 10.1016/j.jaci.2020.05.008
17. Yang Y, Shen C, Li J, Yuan J, Wei J, Huang F, et al. Plasma IP-10 and MCP-3 Levels Are Highly Associated With Disease Severity and Predict the Progression of COVID-19. *J Allergy Clin Immunol* (2020) 146:119. doi: 10.1016/j.jaci.2020.04.027
18. Hadjadj J, Yatim N, Barnabei L, Corneau A, Boussier J, Smith N, et al. Impaired Type I Interferon Activity and Inflammatory Responses in Severe COVID-19 Patients. *Science* (2020) 369:718. doi: 10.1126/science.abc6027
19. Jung JH, Rha M-S, Sa M, Choi HK, Jeon JH, Seok H, et al. SARS-CoV-2-Specific T Cell Memory Is Sustained in COVID-19 Convalescent Patients for 10 Months With Successful Development of Stem Cell-Like Memory T Cells. *Nat Commun* (2021) 12:4043. doi: 10.1038/s41467-021-24377-1
20. Covid-infection WHOWGotCCMo. A Minimal Common Outcome Measure Set for COVID-19 Clinical Research. *Lancet Infect Dis* (2020) 20:e192. doi: 10.1016/S1473-3099(20)30483-7
21. Marcolungo L, Beltrami C, Degli Esposti C, Lopatriello G, Piubelli C, Mori A, et al. ACoRE: Accurate SARS-CoV-2 Genome Reconstruction for the Characterization of Intra-Host and Inter-Host Viral Diversity in Clinical Samples and for the Evaluation of Re-Infections. *Genomics* (2021) 113:1628. doi: 10.1016/j.ygeno.2021.04.008

22. Kalina T, Flores-Montero J, van der Velden VH, Martin-Ayuso M, Bottcher S, Ritgen M, et al. EuroFlow Standardization of Flow Cytometer Instrument Settings and Immunophenotyping Protocols. *Leukemia* (2012) 26:1986. doi: 10.1038/leu.2012.122
23. Chen G, Wu D, Guo W, Cao Y, Huang D, Wang H, et al. Clinical and Immunological Features of Severe and Moderate Coronavirus Disease 2019. *J Clin Invest* (2020) 130:2620. doi: 10.1172/JCI137244
24. Liu R, Wang Y, Li J, Han H, Xia Z, Liu F, et al. Decreased T Cell Populations Contribute to the Increased Severity of COVID-19. *Clinica Chimica Acta; Int J Clin Chem* (2020) 508:110. doi: 10.1016/j.cca.2020.05.019
25. Jiang M, Guo Y, Luo Q, Huang Z, Zhao R, Liu S, et al. T-Cell Subset Counts in Peripheral Blood Can Be Used as Discriminatory Biomarkers for Diagnosis and Severity Prediction of Coronavirus Disease 2019. *J Infect Dis* (2020) 222:198. doi: 10.1093/infdis/jiaa252
26. Qin C, Zhou L, Hu Z, Zhang S, Yang S, Tao Y, et al. Dysregulation of Immune Response in Patients With Coronavirus 2019 (COVID-19) in Wuhan, China. *Clin Infect Diseases: an Off Publ Infect Dis Soc Am* (2020) 71:762. doi: 10.1093/cid/ciaa248
27. Huang W, Berube J, McNamara M, Saksena S, Hartman M, Arshad T, et al. Lymphocyte Subset Counts in COVID-19 Patients: A Meta-Analysis. *Cytometry Part A: J Int Soc Analytical Cytol* (2020) 97:772. doi: 10.1002/cyto.a.24172
28. Liu Z, Long W, Tu M, Chen S, Huang Y, Wang S, et al. Lymphocyte Subset (CD4+, CD8+) Counts Reflect the Severity of Infection and Predict the Clinical Outcomes in Patients With COVID-19. *J Infect* (2020) 81:318. doi: 10.1016/j.jinf.2020.03.054
29. Toor SM, Saleh R, Sasidharan Nair V, Taha RZ, Elkord E. T-Cell Responses and Therapies Against SARS-CoV-2 Infection. *Immunology* (2021) 162:30. doi: 10.1111/imm.13262
30. Garcia LF. Immune Response, Inflammation, and the Clinical Spectrum of COVID-19. *Front Immunol* (2020) 11:1441. doi: 10.3389/fimmu.2020.01441
31. Gao YD, Ding M, Dong X, Zhang JJ, Kursat Azkur A, Azkur D, et al. Risk Factors for Severe and Critically Ill COVID-19 Patients: A Review. *Allergy* (2021) 76:428. doi: 10.1111/all.14657
32. Vardhana SA, Wolchok JD. The Many Faces of the Anti-COVID Immune Response. *J Exp Med* (2020) 217:e20200678. doi: 10.1084/jem.20200678
33. Kalfaoglu B, Almeida-Santos J, Tye CA, Satou Y, Ono M. T-Cell Hyperactivation and Paralysis in Severe COVID-19 Infection Revealed by Single-Cell Analysis. *Front Immunol* (2020) 11:589380. doi: 10.3389/fimmu.2020.589380
34. Fajgenbaum DC, June CH. Cytokine Storm. *New Engl J Med* (2020) 383:2255. doi: 10.1056/NEJMra2026131
35. Ghazavi A, Ganji A, Keshavarzian N, Rabiemajd S, Mosayebi G. Cytokine Profile and Disease Severity in Patients With COVID-19. *Cytokine* (2021) 137:155323. doi: 10.1016/j.cyto.2020.155323

Conflict of Interest: The authors declare that the research was conducted in the absence of any commercial or financial relationships that could be construed as a potential conflict of interest.

Publisher's Note: All claims expressed in this article are solely those of the authors and do not necessarily represent those of their affiliated organizations, or those of the publisher, the editors and the reviewers. Any product that may be evaluated in this article, or claim that may be made by its manufacturer, is not guaranteed or endorsed by the publisher.

Copyright © 2021 Caldrer, Mazzi, Bernardi, Prato, Ronzoni, Rodari, Angheben, Piubelli and Tiberti. This is an open-access article distributed under the terms of the Creative Commons Attribution License (CC BY). The use, distribution or reproduction in other forums is permitted, provided the original author(s) and the copyright owner(s) are credited and that the original publication in this journal is cited, in accordance with accepted academic practice. No use, distribution or reproduction is permitted which does not comply with these terms.

frontiers in Immunology

ORIGINAL RESEARCH
published: 06 January 2022
doi: 10.3389/fimmu.2021.774491

Comprehensive Analysis of CD4$^+$ T Cell Response Cross-Reactive to SARS-CoV-2 Antigens at the Single Allele Level of HLA Class II

You-Seok Hyun[1,2†], *Yong-Hun Lee*[1,2], *Hyeong-A Jo*[1,2], *In-Cheol Baek*[3], *Sun-Mi Kim*[3], *Hyun-Jung Sohn*[3†] *and Tai-Gyu Kim*[1,2,3*]

[1] Department of Microbiology, College of Medicine, The Catholic University of Korea, Seoul, South Korea, [2] Department of Biomedicine and Health Sciences, College of Medicine, The Catholic University of Korea, Seoul, South Korea, [3] Catholic Hematopoietic Stem Cell Bank, College of Medicine, The Catholic University of Korea, Seoul, South Korea

OPEN ACCESS

Edited by:
Alessio Mazzoni,
University of Florence, Italy

Reviewed by:
Jun Siong Low,
Institute for Research in Biomedicine (IRB), Switzerland
Susanna Dunachie,
University of Oxford, United Kingdom

***Correspondence:**
Tai-Gyu Kim
kimtg@catholic.ac.kr

†Present address:
You-Seok Hyun and Hyun-Jung Sohn, Translational and Clinical Division, ViGenCell Inc., Seoul, South Korea

Specialty section:
This article was submitted to T Cell Biology, a section of the journal Frontiers in Immunology

Received: *12 September 2021*
Accepted: *09 December 2021*
Published: *06 January 2022*

Citation:
Hyun Y-S, Lee Y-H, Jo H-A, Baek I-C, Kim S-M, Sohn H-J and Kim T-G (2022) Comprehensive Analysis of CD4$^+$ T Cell Response Cross-Reactive to SARS-CoV-2 Antigens at the Single Allele Level of HLA Class II. Front. Immunol. 12:774491. doi: 10.3389/fimmu.2021.774491

Common human coronaviruses have been circulating undiagnosed worldwide. These common human coronaviruses share partial sequence homology with severe acute respiratory syndrome coronavirus 2 (SARS-CoV-2); therefore, T cells specific to human coronaviruses are also cross-reactive with SARS-CoV-2 antigens. Herein, we defined CD4$^+$ T cell responses that were cross-reactive with SARS-CoV-2 antigens in blood collected in 2016–2018 from healthy donors at the single allele level using artificial antigen-presenting cells (aAPC) expressing a single HLA class II allotype. We assessed the allotype-restricted responses in the 42 individuals using the aAPCs matched 22 HLA-DR alleles, 19 HLA-DQ alleles, and 13 HLA-DP alleles. The response restricted by the HLA-DR locus showed the highest magnitude, and that by HLA-DP locus was higher than that by HLA-DQ locus. Since two alleles of HLA-DR, -DQ, and -DP loci are expressed co-dominantly in an individual, six different HLA class II allotypes can be used to the cross-reactive T cell response. Of the 16 individuals who showed a dominant T cell response, five, one, and ten showed a dominant response by a single allotype of HLA-DR, -DQ, and -DP, respectively. The single allotype-restricted T cells responded to only one antigen in the five individuals and all the spike, membrane, and nucleocapsid proteins in the six individuals. In individuals heterozygous for the HLA-DPA and HLA-DPB loci, four combinations of HLA-DP can be expressed, but only one combination showed a dominant response. These findings demonstrate that cross-reactive T cells to SARS-CoV-2 respond with single-allotype dominance.

Keywords: CD4$^+$ T cells, cross-reactive T cells, SARS-CoV-2, MHC class II alleles, HLA-DR, HLA-DQ, HLA-DP, immunodominance

INTRODUCTION

Severe acute respiratory syndrome coronavirus 2 (SARS-CoV-2) infection causes coronavirus disease 2019 (COVID-19). SARS-CoV-2 is clustered with SARS-CoVs of the genus *Betacoronavirus* belonging to the family Coronaviridae (1). SARS-CoV-2 consists of a lipid bilayer containing spike proteins and RNA genome bound by nucleocapsid proteins and condensed by membrane proteins (2, 3).

The spike protein binds to human angiotensin-converting enzyme 2 (hACE2), and SARS-CoV-2 enters hACE2 expressing cells *via* endocytosis (4). If a neutralizing antibody is generated to block the receptor-binding domain (RBD) of the spike protein, then the SARS-CoV-2 infection can be prevented (5).

SARS-CoV-2-specific adaptive immunity limits COVID-19 disease severity by coordinating SARS-CoV-2-specific $CD4^+$ and $CD8^+$ T cells (6). An mRNA or adenovirus-vector encoding spike protein has been developed and is used to vaccinate individuals who have been mainly unexposed to SARS-CoV-2. These vaccines induce virus-neutralizing antibody, spike protein-specific $CD8^+$ T cell, and $CD4^+$ T cell responses, boosting the humoral and cellular responses (7, 8). HLA-DR, -DQ, and -DP loci are human leukocyte antigen (HLA) class II loci, which are the MHC class II genes in humans and are recognized by $CD4^+$ T cells. The loci of HLA genes are highly polymorphic, with the polymorphic residues primarily in the peptide binding grooves (9). The peptide repertoire presented by the HLA allotypes varies so that some HLA alleles are associated with the susceptibility of the given pathogens (10–12).

For influenza-specific $CD4^+$ T cell response, T cells cross-recognize multiple strains by targeting highly conserved viral proteins, mainly internal proteins constrained by functional limitations of viral fitness (13). New SARS-CoV-2 variants have emerged, some of which harbor mutations in the spike protein and RBD. The neutralizing antibody titer, induced by vaccination or SARS-CoV-2 infection, was lower in the variants than in the wild type (14). However, there were no differences in the $CD4^+$ T cell response to the variants and wild type, and the sequences of SARS-CoV-2 T cell epitopes were not affected by the mutations found in the variants (15–17).

Among the family Coronaviridae, there are four common human coronaviruses (HCoV-299E, HCoV-NL63, HCoV-OC34, and HCoV-HKU1s) that cause mild upper respiratory illness and have been circulating undiagnosed worldwide (18). These HCoVs share partial sequence homology with SARS-CoV-2; therefore, T cells specific to the HCoVs cross-reactively responded to SARS-CoV-2 (19, 20). The cross-reactive T cells enhanced vaccine antibody responses and were suggested to be associated with milder symptoms, and T cells were indispensable for protection against SARS-CoV-2 infection in rhesus macaques (21–23). In the present study, we assessed $CD4^+$ T cell responses that are cross-reactive with SARS-CoV-2 antigens in blood collected in 2016–2018 from healthy donors at a single allele level using artificial antigen-presenting cells (aAPCs) expressing a single HLA class II allele.

MATERIALS AND METHODS

Human Blood Samples

This study was approved by the Institutional Review Board of the Catholic University of Korea (MC21SASI0009). All healthy donors provided written informed consent prior to participation in this study. The participants are ranged from 26.9 ± 5.0 years of age and composed of 4 females and 38 males. Peripheral blood mononuclear cell (PBMC) samples were obtained from 350 ml of leukapheresis products of the donors. PBMCs were further purified from the leukapheresis product by density gradient centrifugation using Ficoll–Hypaque (GE Healthcare). $CD4^+$ T cells were isolated using magnetic microbeads (AutoMacs Pro separator; Miltenyi Biotec), and the purity of the $CD4^+$ T cells was confirmed with flow cytometry (97% ± 2%). Suspended $CD4^+$ T cells in fetal bovine serum (Gibco) containing 10% dimethyl sulfoxide (Mylan) and 50% RPMI 1640 medium (Lonza) were cryopreserved in liquid nitrogen until incubation with aAPCs for ELISPOT assay.

The genomic DNA was isolated from the red blood cells and granulocytes (Tiangen Biotech Corporation). The HLA was then genotyped using polymerase chain reaction sequencing-based typing and next-generation sequencing (**Table 1**) (NCBI BioProject Accession: PRJNA721949) (MiSeqDx, Illumina), as previously described (24, 25). The resolution of the HLA types was converted to 4-digits from 6-digits to analyze the HLA molecules at the protein level.

Generation of aAPCs Expressing Single HLA Class II Allotype

For cloning, cDNAs were isolated from the lymphoblastoid cell lines typed each HLA allele (740902.50; Macherey Nagel, RT300M; Enzynomics). Unlike DRB1, there was polymorphism near the start and stop codon on DQA1, DQB1, DPA1, and DPB1 loci; therefore, each DQ and DP allele was amplified using a primer containing a short consensus sequence at the coding region and the sequence at 5′UTR or 3′UTR with mixed bases (**Table S1**). HLA class II alleles were then cloned into the pCDH lentivector (#CD523A-1; System Biosciences) using In-Fusion Cloning (EZ015TL; Enzynomics).

As previously described (26), 5×10^6 293TN producer cells (System Biosciences) were transfected (Lipofectamine 2000; Invitrogen) with 1.3 pmol psPAX2 (RRID: Addgene_12260), 0.72 pmol pMD.2G (RRID: Addgene_12259), and 1.64 pmol single HLA class II allele-encoding pCDH, and the supernatant was harvested after 2 days. The K562-based aAPCs, which do not express HLA molecules, were transduced with lentiviruses encoding an alpha and a beta chain at a multiplicity of infection (MOI) of 20. The transduced aAPCs were purified by fluorescence-activated cell sorting (FACSAria Fusion, BD Biosciences). For the sorting, the following monoclonal antibodies were used (**Table S2**): HLA-DR (clone G46-6; RRID: AB_1727527), HLA-DQ (clone Tü169; RRID: AB_2738963, Tü39; RRID: AB_395940), and HLA-DP (clone B7/21). The aAPCs were not stained with those antibodies when transduced with only an alpha chain or a beta chain. The aAPCs were then cultured in RPMI 1640 supplemented with 2 mM L-glutamine, 100 U/ml penicillin–streptomycin–amphotericin B mixture (Lonza), and 10% fetal bovine serum (Gibco). We confirmed HLA class II expression using flow cytometry (FACSCanto, BD Biosciences) before cryopreservation of the aAPCs.

Measurement of Single HLA Class II Allotype-Restricted $CD4^+$ T Cell Response by *Ex Vivo* IFN-γ ELISPOT Assay

The single HLA class II allotype-expressing aAPCs were thawed in complete media and seeded at 5×10^4 cells per a well in a 96-

TABLE 1 | Genotypes of HLA class II in 42 healthy donors.

Donor	Age	Sex	DRB1*	DRB1*	DQA1*/DQB1*	DQA1*/DQB1*	DPA1*/DPB1*	DPA1*/DPB1*
HD01	24	M	13:02	15:01	02:01/02:02	03:01/03:02	02:01/13:01	02:02/05:01
HD02	32	M	01:01	15:01	01:01/05:01	01:02/06:02	01:03/02:02	02:02/02:02
HD03	33	M	04:10	08:03	03:03/04:02	06:01/03:01	02:01/14:01	
HD04	24	M	08:03	14:05	01:03/06:01	01:04/05:03	02:02/05:01	
HD05	27	M	01:01	09:01	01:01/05:01	03:02/03:03	01:03/04:02	02:02/05:01
HD06	21	M	04:05	04:06	03:01/03:02	03:03/04:01	01:03/04:02	02:02/05:01
HD07	26	M	04:06	09:01	03:01/03:02	03:02/03:03	02:02/05:01	
HD08	19	M	08:02	14:54	01:04/05:02	03:01/03:02	01:03/04:02	02:02/05:01
HD09	30	M	04:06	08:03	03:01/03:02	06:01/03:01	01:03/02:01	02:02/05:01
HD10	31	M	04:03	13:02	03:01/03:02	01:02/06:04	02:02/05:01	01:03/04:01
HD11	25	M	01:01	14:05	01:01/05:03	01:01/05:01	01:03/02:01	
HD12	32	M	01:01	15:02	01:01/05:01	01:03/06:01	01:03/04:02	01:03/03:01
HD13	27	M	07:01	12:01	02:01/02:02		01:03/04:02	02:01/17:01
HD14	30	M	04:05	07:01	02:01/02:02	03:03/04:01	01:03/02:01	02:02/05:01
HD15	31	M	12:01		03:01/03:02	01:01/05:01	02:02/05:01	02:01/09:01
HD16	28	M	12:02	15:01	01:02/06:02	06:01/03:01	02:02/05:01	
HD17	24	M	04:06	15:01	01:02/06:02	03:01/03:02	01:03/02:01	02:02/03:01
HD18	26	M	04:06	14:05	01:01/05:03	03:01/03:02	01:03/02:01	02:02/05:01
HD19	26	M	04:05	14:05	01:04/05:03	03:03/04:01	02:02/05:01	
HD20	22	M	08:02	14:06	03:01/03:02	05:03/03:01	02:01/13:01	02:02/05:01
HD21	32	M	07:01	09:01	02:01/02:02		01:03/05:01	02:01/13:01
HD22	24	M	08:03	12:01	01:03/06:01		01:03/03:01	01:03/04:01
HD23	26	F	12:01	15:01	01:02/06:02		01:03/02:01	
HD24	28	M	08:03	15:01	01:02/06:02	01:03/06:01	01:03/04:02	02:02/05:01
HD25	45	M	13:02	16:02	01:02/06:09	01:02/05:02	01:03/02:02	02:02/05:01
HD26	23	M	04:06	09:01	03:01/03:02	03:02/03:03	02:01/14:01	02:02/05:01
HD27	33	M	04:04	09:01	03:02/03:03		01:03/04:02	02:02/05:01
HD28	24	M	08:03		01:03/06:01		01:03/04:02	02:02/05:01
HD29	25	M	04:05		03:03/04:01		01:03/04:02	
HD30	23	M	04:06	14:05	01:04/05:03	03:01/03:02	02:02/03:01	02:02/05:01
HD31	28	M	04:03	12:01	03:01/03:02	05:05/03:01	01:03/02:01	
HD32	27	M	04:06	14:54	01:04/05:03	03:01/03:02	02:01/13:01	02:02/05:01
HD33	25	M	01:01	08:03	01:01/05:01	01:03/06:01	01:03/02:01	02:02/05:01
HD34	26	M	04:04	08:03	03:01/03:02	01:03/06:01	02:02/02:02	02:01/09:01
HD35	20	F	01:01	08:03	01:01/05:01	01:03/06:01	01:03/04:02	02:02/05:01
HD36	31	M	03:01	10:01	05:01/02:01		01:03/04:01	02:01/09:01
HD37	22	M	07:01	15:01	02:01/02:02	05:05/03:01	02:02/05:01	02:01/17:01
HD38	24	F	01:01	13:02	01:01/05:01	01:02/06:04	02:02/05:01	
HD39	20	M	07:01	14:05	01:04/05:03	02:01/02:02	01:03/02:02	02:02/05:01
HD40	30	M	13:02	15:01	01:02/06:02	01:02/06:09	02:02/03:01	02:02/05:01
HD41	36	M	07:01	14:54	01:04/05:02	02:01/02:02	01:03/02:01	02:01/17:01
HD42	19	F	04:01	14:54	01:04/05:02	03:03/03:01	01:03/02:01	01:03/04:02

well cell culture plate. The aAPCs were resuspended in serum-free media and pulsed with 60 nM of each peptide pool (JPT Peptide Technologies) for 2 h at 37°C in 5% CO_2. The antigen-loaded aAPCs were washed three times with serum-free media. The peptide-pulsing and washing were performed using centrifugation and a microplate washer (405LSR; BioTek) in a 96-well cell culture plate. The 5×10^5 $CD4^+$ T cells were incubated with 5×10^4 aAPCs in an ELISPOT plate for 20 h at 37°C in 5% CO_2 (551849; BD Biosciences). The 4×10^6 to 7×10^6 and 1.8×10^7 to 2.1×10^7 $CD4^+$ T cells per donor were used for measuring SARS-CoV-2 cross-reactive $CD4^+$ T cell response by an allotype and to a SARS-CoV-2 antigen, respectively. The 5×10^6 $CD4^+$ T cells per donor were used for measuring the response by a combination of HLA-DP heterodimer. The spot forming cells (SFC) were counted using an AID ELISPOT Reader System (AID Diagnostika GmbH). The magnitude of an allotype-restricted $CD4^+$ T cell response to antigens was calculated as [(response to aAPCs expressing HLA pulsed with peptide pools) − (response to aAPCs expressing HLA)] − [(response to aAPCs pulsed with peptide pools) − (response to aAPCs)], as previously described (26, 27). The ELISPOT results were presented as SFC per million $CD4^+$ T cells.

Data Processing and Statistical Analysis

The Google Spreadsheets were used for calculating the magnitude of response by a given allotype, sorting the order of highest response, and filtering the magnitude of response by a locus and an allele. The data were visualized in Microsoft Excel, GraphPad Prism 7, and FlowJo v10 (BD). Statistical analyses were performed by GraphPad Prism 7 software. Statistical significance was determined by one-way analysis of variance [ANOVA], Pearson's correlation analysis, Welch's t-test (with a two-tailed test of significance). Values of $P < 0.05$ were considered significant. The data are expressed as means ± standard deviation or standard

error of the mean, and the sample sizes are presented in the figures.

RESULTS

SARS-CoV-2 Cross-Reactive CD4$^+$ T Cell Responses According to HLA Class II Loci and Alleles

The peptide binding grooves of HLA class I are only in the alpha chain, whereas the alpha and beta chains of HLA class II form heterodimers, presenting the epitope by a matching pair of an allotype (28). HLA-DRB1, -DQA1, -DQB1, -DPA1, and -DPB1 alleles were genotyped in 42 donors to assess the CD4$^+$ T cell responses in an allotype-specific manner (**Table 1**). The DRA locus encoding the alpha chain of HLA-DR is almost monomorphic; however, the DQA and DPA loci encoding the alpha chain of HLA-DQ and -DP are polymorphic. We further estimated the most likely haplotype for HLA-DQ and DP within individuals based on haplotype frequency. We established single HLA-DR, -DQ, and -DP allotype-expressing aAPCs of a haplotypic pair in 42 donors in addition to those previously established (**Figure S1**) (26).

CD4$^+$ T cells were stimulated with an allotype-matched aAPCs pulsed with a mixture of peptide pools of the spike, nucleocapsid, and membrane proteins. CD4+ T cells were co-cultured with unpulsed allotype-matched aAPCs and aAPCs untransduced HLA as a control. SARS-CoV-2 cross-reactive CD4$^+$ T cell responses by an allotype were measured using the IFN-γ ELISPOT assay and calculated as described in *Materials and Methods*, data shown in **Table S3**. The response of isolated CD4$^+$ T cells to aAPCs, which were untransduced with the HLA-specific lentivirus, was 1.5 ± 2.9 SFCs. The response to peptide pools- pulsed aAPCs was 1.7 ± 2.9 SFCs.

The magnitude of response by a locus was calculated by summing the responses of two alleles in each HLA-DR, -DQ, and -DP locus within an individual to understand which HLA class II locus was preferentially used in the response. Similar to the CMV pp65-specific CD4$^+$ T cell response (26), the magnitude of response by the HLA-DR locus was significantly higher than that by the HLA-DQ locus (**Figure 1A**, one-way ANOVA, p = 0.0359). The magnitude of response of the HLA-DP locus was significantly higher than that of the HLA-DQ locus (**Figure 1A**, one-way ANOVA, p = 0.0002). We classified the magnitude of response into stepwise responses with more than 100, 50, or 10 SARS-CoV-2-specific cells per 5×10^5 CD4$^+$ T cells: strong, moderate, and positive response, respectively. For the HLA-DR locus, 9.5% of the donors showed a strong response and no donors showed a moderate response (**Figure 1A**). For the HLA-DQ locus, no donors showed a strong response, and 2.4% showed a moderate response. For the HLA-DP locus, 2.4% of the donors showed a strong response, and 26.2% showed a moderate response. When the response of the HLA class II was calculated by summing the responses of the HLA-DR, -DQ, and -DP loci within an individual, the magnitude of SARS-CoV-2 cross-reactive CD4$^+$ T cell response was $53/5 \times 10^5$, which was lower than that of the CMV pp65-specific CD4$^+$ T cell responses ($267/5 \times 10^5$).

Next, we analyzed the response of each allotype to determine which allele on each locus was preferentially used. Among the 22 HLA-DR alleles, donors with DRB109:01, DRB104:06, and DRB115:01 showed strong responses (**Figure 1B**). Among the 19 HLA-DQ alleles, DQA1*03:01/DQB1*03:02 showed moderate response (**Figure 1C**). Among the 13 HLA-DP alleles, DPA1*01:03/DPB1*04:02 showed a strong response; DPA1*02:02/DPB1*05:01 and DPA1*02:01/DPB1*17:01 showed a moderate response (**Figure 1D**). In the CMV pp65-specific T cell response, the frequency of the HLA alleles correlated with the proportion of responses (26). However, in the SARS-CoV-2 cross-reactive CD4$^+$ T cell response, the proportion of positive responses of each allele was not significantly correlated with the allele frequency of HLA-DR, -DQ, and -DP (**Figure 1E**).

Allele Dominance in SARS-CoV-2 Cross-Reactive CD4$^+$ T Cell Response by an HLA Class II Within Individuals

A heterozygous individual expresses six HLA class II allotypes co-dominantly. To identify the number of allotypes used for the response, we analyzed the SARS-CoV-2 cross-reactive T cells by two allotypes of HLA-DR, -DQ, and -DP loci within individuals. Defining strong and moderate responses as dominant T cell responses, in 16/42 cases (38.1%), unexposed individuals showed a dominant T cell response restricted by one HLA allotype (**Figure 2A**). The remaining 26/42 individuals did not show a dominant T cell response by an HLA allotype. We classified the dominance of HLA allotypes 1–4 in the order of the dominant response in an individual to compare the magnitude of response without an arbitrary threshold (**Figures 2B, C**). The highest response by one allotype was significantly higher than the second, third, and fourth highest responses by the other allotypes within individuals (one-way ANOVA, p <0.0001). The probability of responding first, second, third, and fourth highest within individuals varied even among those alleles that showed a dominant T cell response (**Figure 2D**).

Antigen Immunodominance in SARS-CoV-2 Antigen-Specific CD4$^+$ T Cell Responses Within Individuals

A few epitopes account for most of the T cell responses to SARS-CoV-2 in a population (29). To determine whether epitopes of the dominant T cells by an allele were distributed in several proteins or one protein, CD4$^+$ T cells were stimulated individually by each SARS-CoV-2 peptide pool-loaded aAPCs. Of the 11 donors with dominant T cell responses, five responded primarily to one antigen with an HLA allele (**Figure 3A**). Of the 11 donors with dominant T cell responses, six responded similarly to each antigen with an HLA allele (**Figure 3B**). In the sum of dominant T cell responses by the allele of each individual, the highest response to one protein was significantly higher than the second and third highest responses to the other protein (**Figure 3C**, one-way ANOVA, p = 0.0314 for 1st vs. 2nd, p = 0.0204 for 1st vs. 3rd).

Next, we analyzed predicted half-maximal inhibitory concentration of the cross-reactive SARS-CoV-2 epitopes identified in the other study and aligned with these alleles (19) (**Figure 4**). The alleles that responded primarily to one antigen showed a higher affinity to the cross-reactive epitopes than the

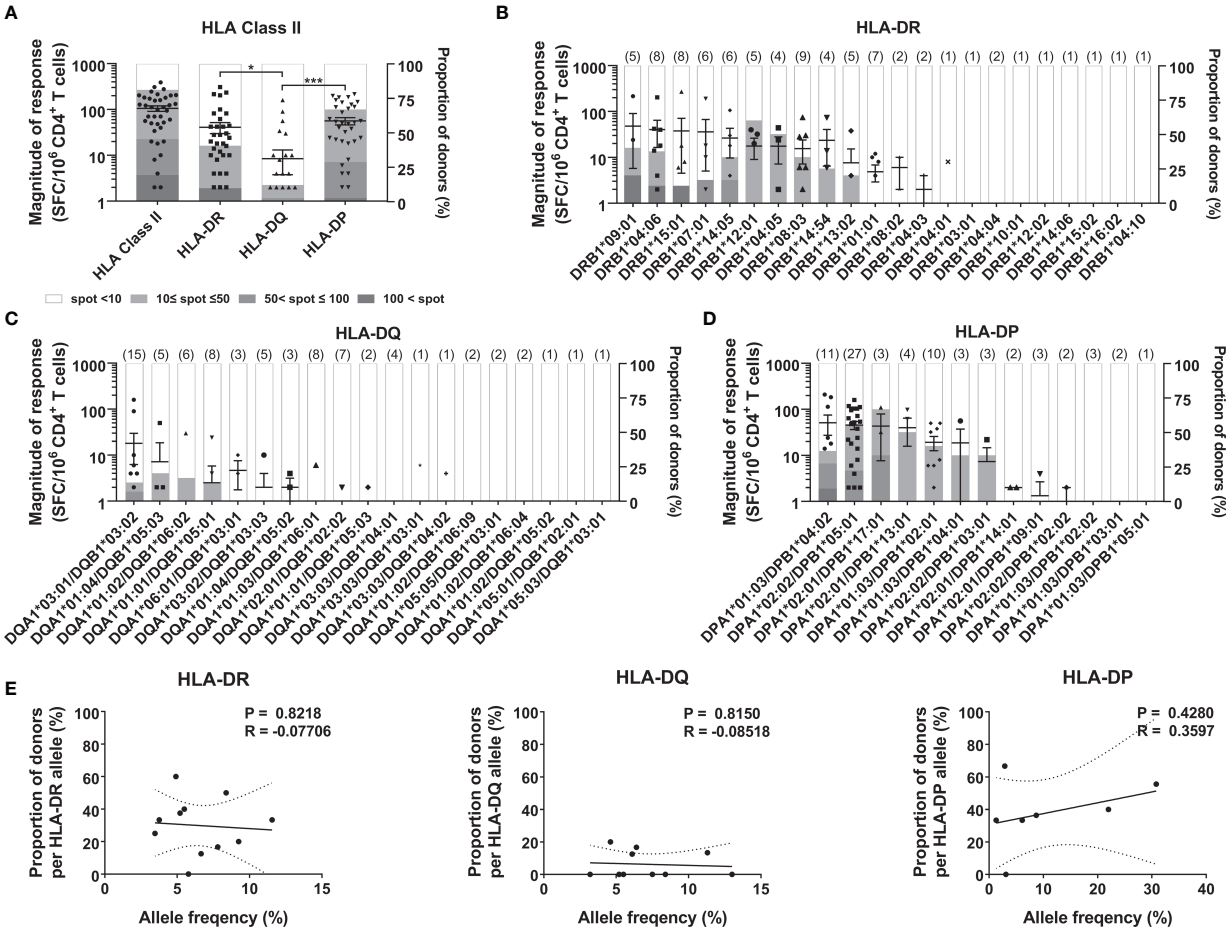
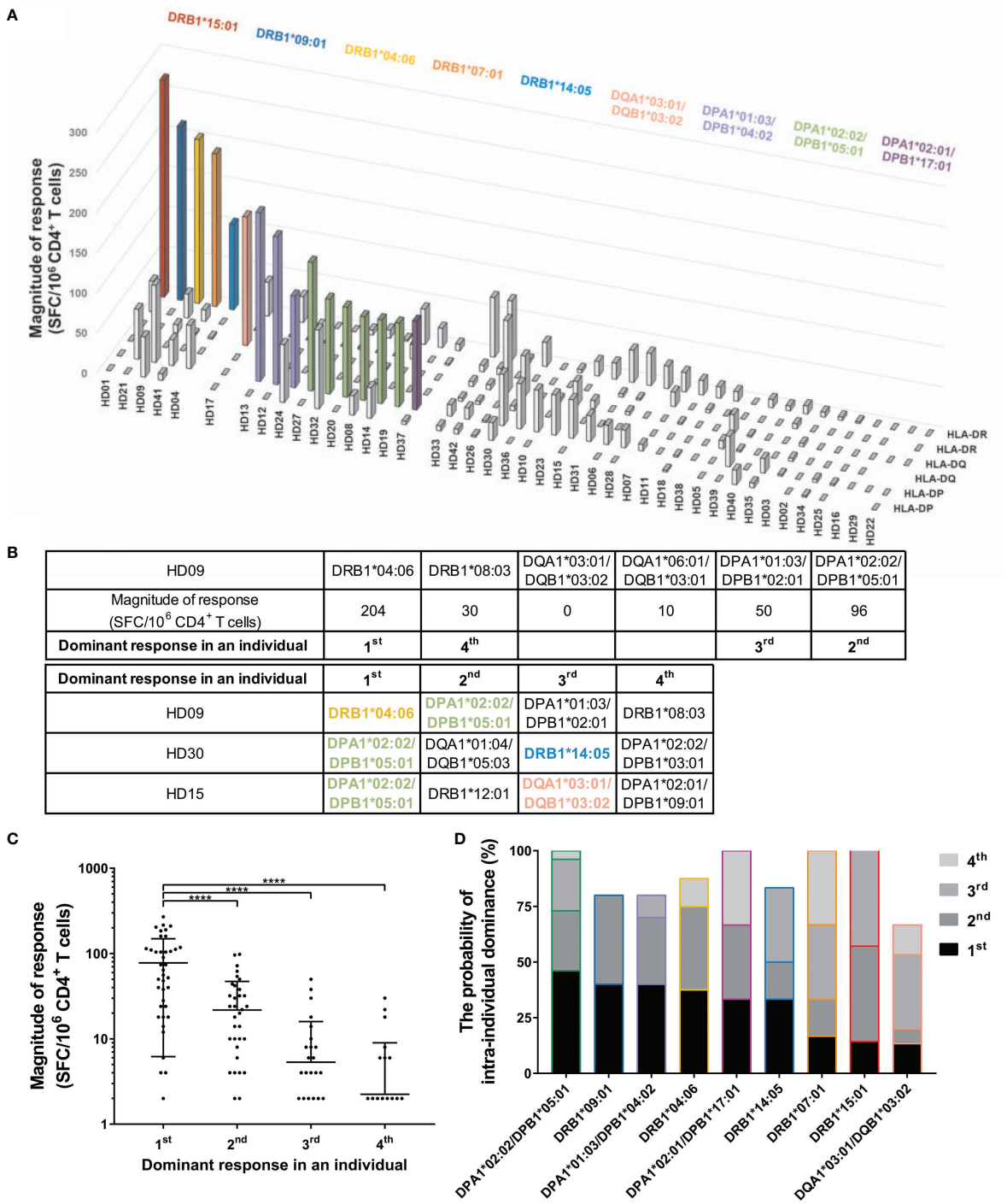


FIGURE 1 | $CD4^+$ T cell responses to SARS-CoV-2 antigens according to HLA class II loci and alleles. $CD4^+$ T cells were stimulated with an allotype-matched aAPCs pulsed with a mixture of peptide pools of spike, nucleocapsid, and membrane protein. The responses by HLA-DR, -DQ, and -DP loci **(A)**, and HLA-DR alleles **(B)**, HLA-DQ alleles **(C)**, and HLA-DP alleles **(D)** in 42 donors were compared. Each dot presents the magnitude of response by a locus or an allele in an individual. Error bars indicate the mean ± standard error of the mean (SEM), and the number of donors with the allele are shown in parentheses. The stacked bar graph presents a proportion of the classified response in donors out of the donors with the allele. Statistical analysis was performed using a one-way ANOVA. *P < 0.05, ***P < 0.001. **(E)** Correlation of allele frequency with the proportion of positive response by HLA-DR, -DQ, and -DP alleles that are in at least three individuals. Statistical analysis was performed using Pearson's correlation analysis. A line of best fit (solid lines) and the 95% confidence bands (dotted lines) were analyzed using linear regression analysis.

alleles that responded similarly to each antigen (**Figure S2A**, p <0.0001). The SARS-CoV-2 epitope recognized in unexposed donors was reported to have high homology to common cold coronaviruses (19). The epitope similarity with common cold coronaviruses (OC43, HKU1, NL63, and 229E) was aligned additionally to the binding affinity of these alleles. The conservancy correlated with higher binding in the DRB1*04:06 and DPA1*01:03/DPB1*04:02 alleles, and the other alleles did not correlate significantly (p = 0.0107 for DRB1*04:06, p = 0.0478 for DPA1*01:03/DPB1*04:02). The cross-reactive epitope discovered in the previous study was mainly a spike protein among spike, nucleocapsid and membrane protein. Considering that the DRB1*04:06 and DPA1*01:03/DPB1*04:02 responded to a spike protein, it is speculated that some alleles respond primarily to one antigen in the case of the high binding affinity or high sequence homology. In total, SARS-CoV-2 cross-reactive-dominant T cells targeted preferentially one protein by one HLA allele within an individual, although there was a deviation in the individual alleles.

SARS-CoV-2-Specific $CD4^+$ T Cell Responses by Combinations of HLA-DP Heterodimer

The HLA-DPA locus, encoding the alpha chain of HLA-DP, is polymorphic, and the common HLA-DPA alleles are DPA1*01:03, DPA1*02:02, and DPA1*02:01. DPA1*01:03 accounts for approximately half the HLA-DPA frequency; therefore, most studies did not determine the alpha chain in the peptide binding specificity of HLA-DP. However, in individuals whose HLA-DPA and HLA-DPB are double heterozygous, four combinations of the HLA-DP heterodimers



B

HD09	DRB1*04:06	DRB1*08:03	DQA1*03:01/ DQB1*03:02	DQA1*06:01/ DQB1*03:01	DPA1*01:03/ DPB1*02:01	DPA1*02:02/ DPB1*05:01
Magnitude of response (SFC/10^6 $CD4^+$ T cells)	204	30	0	10	50	96
Dominant response in an individual	**1st**	**4th**			**3rd**	**2nd**

Dominant response in an individual	**1st**	**2nd**	**3rd**	**4th**
HD09	DRB1*04:06	DPA1*02:02/ DPB1*05:01	DPA1*01:03/ DPB1*02:01	DRB1*08:03
HD30	DPA1*02:02/ DPB1*05:01	DQA1*01:04/ DQB1*05:03	DRB1*14:05	DPA1*02:02/ DPB1*03:01
HD15	DPA1*02:02/ DPB1*05:01	DRB1*12:01	DQA1*03:01/ DQB1*03:02	DPA1*02:01/ DPB1*09:01

FIGURE 2 | $CD4^+$ T cell responses restricted by single HLA class II allotype within individuals. $CD4^+$ T cells were stimulated with an allotype-matched aAPCs pulsed with a mixture of peptide pools of spike, nucleocapsid, and membrane protein. **(A)** $CD4^+$ T cell responses (vertical) by two allotypes of HLA-DR, -DQ, and -DP loci (depth) in each individual (horizontal). The magnitude of response above 50 SFCs/5 × 10^5 are colored and the alleles corresponding to the response are shown in the same color. **(B)** A schematic diagram of the analysis of dominant response in individuals. **(C)** The order of highest response by an allotype within an individual is presented as the dominant response in an individual. Each dot represents a response by an allotype. Data are shown as mean ± standard deviation (SD) of the order-specific response. Statistical analysis was performed using one-way ANOVA. ****$P < 0.0001$. **(D)** The probability of intra-individual dominance presents (the number of donors with the corresponding order from the responses by the allotype)/(the number of donors with the allotype). The donors who did not respond by any allotype were excepted. The order and color of the allele follow **(B)** and **(A)**, respectively.

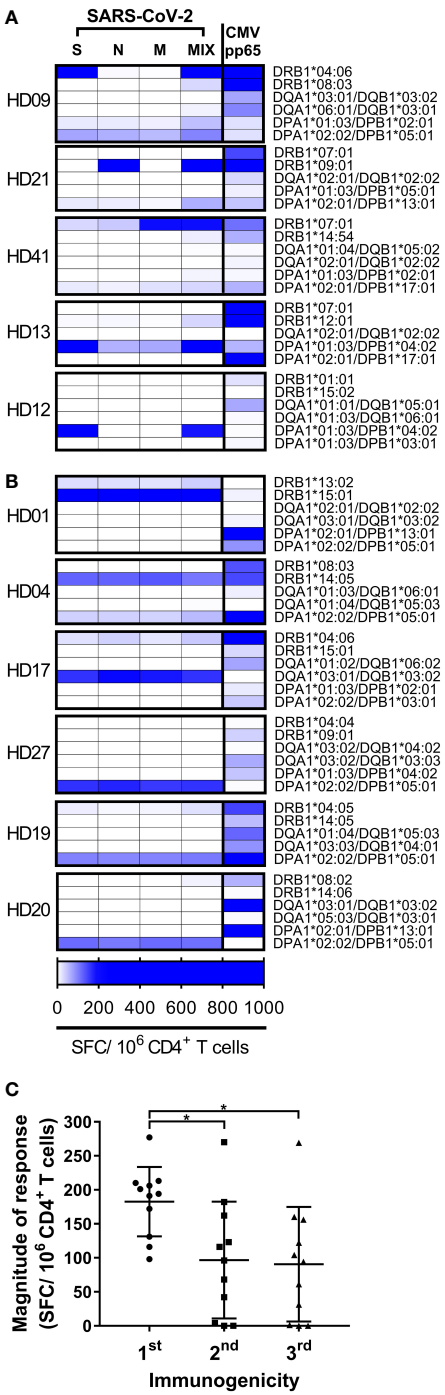


FIGURE 3 | $CD4^+$ T cell responses by each HLA class II allotype to each SARS-CoV-2 antigen in each individual. **(A, B)** $CD4^+$ T cell responses by an allotype were measured individually with spike (S), nucleocapsid (N), membrane (M), or CMV pp65, and with a mixture (MIX) of peptide pools of S, N, and M protein. High responses are highlighted at the blue end of the spectrum. **(C)** The order of immunogenicity indicates the order of highest response to S, N, or M among the responses by an allele that showed the strong response in an individual. Each dot represents a response by an allotype to a peptide pool of a protein. Data are shown as mean ± SD. Statistical analysis was performed using one-way ANOVA. *P < 0.05.

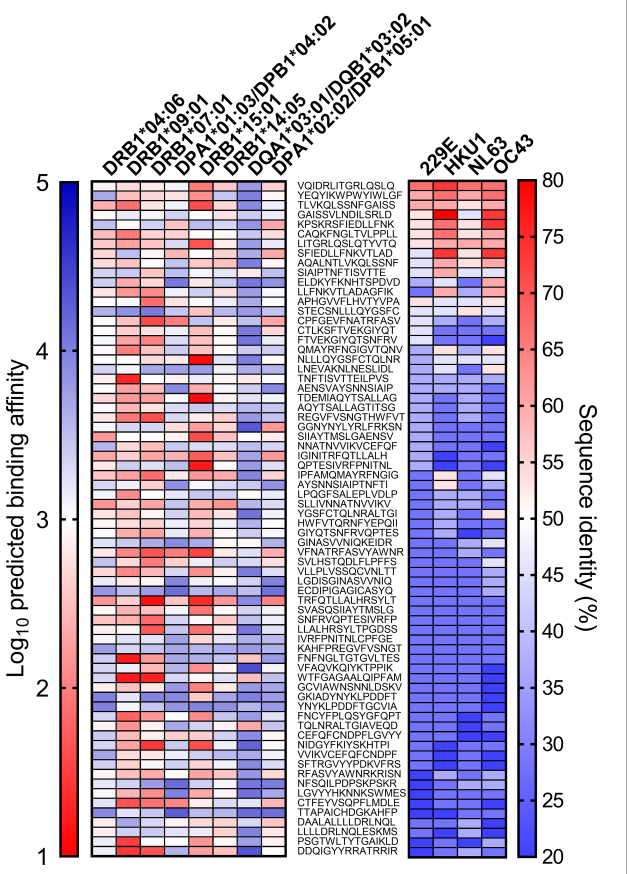


FIGURE 4 | Predicted binding affinity and homology of cross-reactive SARS-CoV-2 epitope. The SARS-CoV-2 epitope sequence that was reported previously (middle) and predicted binding affinity to the allele in **Figures 3** (left). The prediction of binding affinity (IC50) was performed with NetMHCII using the Immune Epitope Database and Analysis Resource (IEDB). Lower binding affinity presented as the red end of the spectrum indicates stronger predicted binding affinity. The sequence similarity of common cold viruses (229E, HKU1, NL63, OC43) to SARS-CoV-2 was expressed as sequence identity (%) and inferred with the epitope conservancy analysis tool (right).

are possible to be expressed and form heterodimers with different alpha chains (**Figure 5A**). To investigate the T cell response patterns for the four HLA-DP combinations, we measured the SARS-CoV-2-specific $CD4^+$ T cell responses in 19 double heterozygous individuals (**Figure 5C** and **Table 2**). Three individuals showed dominant T cell responses with two combinations, and seven individuals showed dominant T cell responses with one combination. The remaining nine individuals did not show a dominant T cell response by an HLA-DP combination. The magnitude of responses by the four combinations of HLA-DP was then compared without an arbitrary threshold, as analyzed in **Figures 2B, C**. The highest response by one combination was significantly higher than that of the second, third, and fourth highest responses by the other combinations within individuals (**Figure 5B**, one-way ANOVA, $p = 0.0001$ for 1st vs. 2nd, $p < 0.0001$ for 1st vs. 3rd and 1st vs. 4th).

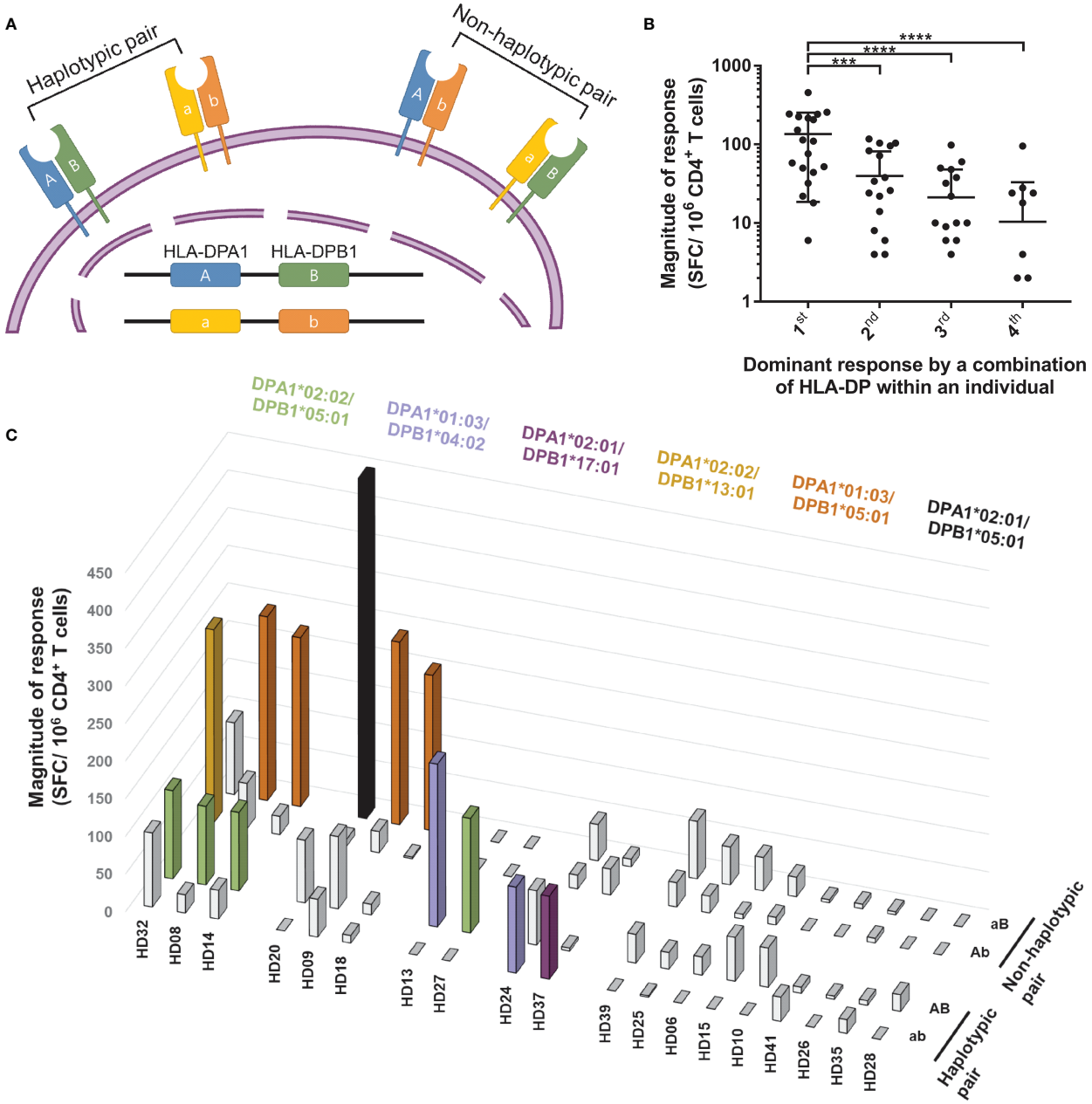


FIGURE 5 | CD4+ T cell responses restricted by HLA-DP heterodimer within individuals. CD4+ T cells were stimulated with a heterodimer-matched aAPCs pulsed with a mixture of peptide pools of spike, nucleocapsid, and membrane protein. **(A)** Schematic diagram showing two HLA-DP heterodimers encoded by the same allele on DPA and DPB loci (haplotypic pair), the other two HLA-DP heterodimers are encoded by different allele on DPA and DPB loci (non-haplotypic pair). **(B)** Dominant response by a combination of HLA-DP within an individual presents the order of highest response by an HLA-DP heterodimer within an individual. Each dot represents a response by an HLA-DP heterodimer. Data are shown as mean ± SD of 19 individuals. Statistical analysis was performed using one-way ANOVA. ***P <0.001, ****P <0.0001. **(C)** CD4+ T cell responses (vertical) by four HLA-DP combinations (depth) in each double heterozygous individual (horizontal). The magnitude of response above 50 SFCs/5 × 10^5 are colored and the alleles are presented with the same color.

Next, we divided the four combinations into a non-haplotypic pair, which was not maternal and paternal haplotypes, and a haplotypic pair, and analyzed the T cell responses (**Table 2**). We assessed the allotype-specific response at each locus, assuming T cells would respond with the HLA haplotype (**Figure 2**). However, to cytomegalovirus pp65, the dominant T cell responses were restricted by the haplotypic and non-haplotypic pairs (**Figure S3**). For SARS-CoV-2, the dominant T cell responses were by one haplotypic pair and non-haplotypic pair in individuals who showed dominant T cell responses by two combinations

TABLE 2 | Four HLA-DP combinations in 19 double heterozygous individuals.

Donor	Haplotypic pair		Non-haplotypic pair	
	ab DPA1*/DPB1*	AB DPA1*/DPB1*	Ab DPA1*/DPB1*	aB DPA1*/DPB1*
HD32	02:01/13:01	02:02/05:01	02:02/13:01	02:01/05:01
HD08	01:03/04:02	02:02/05:01	02:02/04:02	01:03/05:01
HD14	01:03/02:01	02:02/05:01	02:02/02:01	01:03/05:01
HD20	02:01/13:01	02:02/05:01	02:02/13:01	02:01/05:01
HD09	01:03/02:01	02:02/05:01	02:02/02:01	01:03/05:01
HD18	01:03/02:01	02:02/05:01	02:02/02:01	01:03/05:01
HD13	02:01/17:01	01:03/04:02	01:03/17:01	02:01/04:02
HD27	01:03/04:02	02:02/05:01	02:02/04:02	01:03/05:01
HD24	01:03/04:02	02:02/05:01	02:02/04:02	01:03/05:01
HD37	02:01/17:01	02:02/05:01	02:02/17:01	02:01/05:01
HD39	01:03/02:02	02:02/05:01	02:02/02:02	01:03/05:01
HD25	01:03/02:02	02:02/05:01	02:02/02:02	01:03/05:01
HD06	01:03/04:02	02:02/05:01	02:02/04:02	01:03/05:01
HD15	02:01/09:01	02:02/05:01	02:02/09:01	02:01/05:01
HD10	01:03/04:01	02:02/05:01	02:02/04:01	01:03/05:01
HD41	02:01/17:01	01:03/02:01	01:03/17:01	02:01/02:01
HD26	02:01/14:01	02:02/05:01	02:02/14:01	02:01/05:01
HD35	01:03/04:02	02:02/05:01	02:02/04:02	01:03/05:01
HD28	01:03/04:02	02:02/05:01	02:02/04:02	01:03/05:01

(**Figure 5C**). In individuals who showed dominant T cell responses with one combination, three responded with the non-haplotypic pair, and four responded with the haplotypic pair. Overall, antigen-specific T cells responded with an allotype of haplotypic pair and an allotype of non-haplotypic pair.

DISCUSSION

For SARS-CoV-2, the proportion of strong response by HLA-DR was higher than that by HLA-DQ and -DP (**Figure 1A**). Cytomegalovirus pp65-specific T cell response by HLA-DR was also higher than HLA-DQ and –DP (26). For SARS-CoV-2, the number of epitopes presented by HLA-DR was more than that by HLA-DQ or -DP in convalescent COVID-19 donors (29). The membrane expression of HLA-DR was higher than that of HLA-DQ and -DP in peripheral blood mononuclear cells and aAPCs transduced with a single allele at the same MOI (26, 30), suggesting that HLA-DR-restricted T cells are highly for selection against pathogens. Unlike the response to cytomegalovirus pp65, the SARS-CoV-2-specific T cell response restricted by HLA-DP was significantly higher than that by HLA-DQ, and the magnitude of the response was similar to that by HLA-DR (**Figure 1**). A conserved immunodominant region in the spike protein was restricted by HLA-DR and -DP (31), supporting the high magnitude of response by HLA-DP (**Figures 1A, B, D**).

At the population level, immunodominant epitopes for SARS-CoV-2 are presumed to be promiscuous and capable of binding multiple HLA allelic variants, similar to epitopes for *Mycobacterium tuberculosis* and Dengue virus (32–34). At the individual level, pre-existing SARS-CoV-2-specific T cells responded dominantly to one allotype (**Figures 2A, B**). Moreover, one allotype-restricted T cell responded mainly to one antigen among spike, membrane, and nucleocapsid proteins in 5/11 individuals (**Figure 3A**). The T cell response to pp65 of cytomegalovirus, which has infected most of the world's population, also showed the allele dominance within an individual (26, 27). In CMV-specific T cell responses, diverse high-affinity clones were stimulated at early time points after infection; however, at late time points, a few low-affinity clones predominated (35, 36). The allele dominance in SARS-CoV-2 cross-reactive $CD4^+$ T cells might be the survival of T cells by competing for affinity with viral peptides and HLA allotypes under infection by viruses with sequence homology.

DRB1*07:01 restricted the dominant response in HD41 (**Figure 3A**). In HD21, DRB1*09:01 restricted the dominant response and in HD13, DPA1*01:03/DPB1*04:02 restricted the dominant response and DRB1*07:01 restricted no T cell response although HD21 and HD13 expressed DRB1*07:01. In total, there was a hierarchy among the alleles that caused the dominant T cell response (**Figure 2C**). According to the expression quantitative trait locus analysis from the peripheral blood, different HLA-DR alleles biased the usage of TCR V gene encoding CDR1 and CDR2 (37). In 6/11 individuals, the responses to three different antigens were restricted by an identical HLA allele (**Figure 3B**). In tuberculosis-susceptible mice with the H2-Aj allele, the CDR3α and CDR3β repertoires were more convergent than the H2-Ab allele; therefore, different alleles shape different CDR3 landscapes (38). It is speculated that the TCR repertoire was shaped differently by the combination of the alleles in three loci, and the allele-restricted T cell was more divergent than the other allele-restricted T cell in an individual.

An allele-restricted T cell mainly responded to the spike protein in most individuals (**Figure 3A**). However, there was a dominant T cell response to the nucleocapsid or membrane proteins in an individual. COVID-19 patients with memory T cells specific for the common cold coronavirus developed mild

symptoms (21). In addition, individuals who already had spike protein-specific cross-reactive $CD4^+$ T cells showed high functional avidities throughout the initiation of the T cell response after SARS-CoV-2 infection (39). The BNT162b2 COVID-19 spike mRNA vaccine boosted the pre-existing SARS-CoV-2 spike cross-reactive T cells. Moreover, an adenovirus-based COVID-19 vaccine encoding both spike and nucleocapsid proteins elicited Th1 dominant responses after a single prime injection (40). A vaccine encoding all the spike, nucleocapsid, and membrane protein might re-activate pre-existing cross-reactive T cells and evoke secondary-like immune responses in more individuals than the only spike-encoding vaccine.

At the population level, the HLA haplotype frequency distribution could be affected by the infection of a pathogen (41, 42). For cytomegalovirus pp65, the frequency of the HLA alleles showed a correlation with the proportion of donors having a T cell response (26). However, for SARS-CoV-2, HLA-DR, -DQ, and -DP allele frequency showed no significant correlation with T cell responses (**Figure 1E**). The frequency of HLA alleles was not correlated with T cell responses because it is a cross-reactive T cell response to the newly emerged SARS-CoV-2, not common cold coronaviruses-specific T cell responses to common cold coronaviruses. In addition, in HLA-DP double heterozygous individuals, the cross-reactive T cells responded by non-haplotypic pairs, which are not associated with HLA-DP haplotype frequency (**Figure 5**). This result supports the heterozygote advantage of HLA (9, 43).

In response to SARS-CoV-2 by HLA-DP, even if the beta chains were identical, $CD4^+$ T cells responded to a specific alpha chain-combination (**Figure 5C**). An epitope of bacterial toxin PE38 restricted by specific HLA-DPB did not induce T cell responses in some individuals with HLA-DPB (44). Moreover, mycobacterial peptide-specific T cells were only stimulated by HLA-DPA-matched lymphoblastoid cell lines (45). Therefore, the peptides presented by HLA-DP were determined not only by the beta chains but also by the alpha chains, and T cells were restricted by one combination of HLA-DP to the given peptides.

Although the isolated $CD4^+$ T cells cocultured with aAPCs without HLA or antigens did not activate, the magnetic beads used to isolate $CD4^+$ T cells can lead to non-specific activation. There is also potential for the up to 3% non-pure cells remaining to act as antigen-presenting cells in this experiment. Limitations of this study include the male predominance (male 90%; female 10%) and the young age group (median age 26).

The cross-reactive SARS-CoV-2-specific $CD8^+$ T cell response should be investigated in an allotype-specific manner to understand whether the HLA class I allele-restricted response is akin to the HLA class II allele-restricted response. This study is not powered to substantiate single-allotype-dominant response in SARS-CoV-2 infection. We plan a chronological study following SARS-CoV-2 infection and vaccination to probe whether the single-allotype dominance is a general phenomenon in T cell response to viral infection. Allotype-dependency of $CD4^+$ responses to common cold coronaviruses should also be investigated how that differs from the cross-reactive responses to SARS-CoV-2. The alleles that showed a dominant response in **Figure 3** were analyzed with their predicted binding affinity and conservancy of the epitopes in **Figure 4**. However, the magnitude of response by these alleles or proportion of positive response did not correlate with binding affinity or the number of predicted binding epitopes (**Figures S2B–E**). The cross-reactive epitopes and their HLA restriction should be defined in further study.

In summary, pre-existing cross-reactive $CD4^+$ T cell response to SARS-CoV-2 was high for some HLA class II allotypes and loci. The pre-existing SARS-CoV-2-specific T cells were restricted by one allotype among HLA-DR, -DQ, and -DP allotypes within an individual, and the T cells responded greatly to one SARS-CoV-2 antigen among the spike, membrane, and nucleocapsid proteins. One combination among the four HLA-DP combinations restricted the dominant T cell response, and non-haplotypic pairs also restricted this response in HLA-DP double heterozygous individuals. These results shed light on allele dominance in cross-reactive T cell responses to SARS-CoV-2, which have implications for understanding different responses to the COVID-19 vaccine and the clinical course of COVID-19.

DATA AVAILABILITY STATEMENT

The datasets presented in this study can be found in online repositories. The names of the repository/repositories and accession number(s) can be found below: https://www.ncbi.nlm.nih.gov/bioproject/PRJNA721949/.

ETHICS STATEMENT

The studies involving human participants were reviewed and approved by the Institutional Review Board of the Catholic University of Korea (MC21SASI0009). The patients/participants provided their written informed consent to participate in this study.

AUTHOR CONTRIBUTIONS

Y-SH and T-GK conceived and designed the experiments. I-CB typed the HLA. Y-SH, Y-HL, S-MK, H-AJ, and H-JS contributed to sample preparation. Y-SH carried out the experiments. Y-SH and T-GK analyzed data and wrote the manuscript. T-GK supervised the project. All authors contributed to the article and approved the submitted version.

FUNDING

This study was supported by a grant of the Korea Health Technology R&D Project through the Korea Health Industry Development Institute (KHIDI), funded by the Ministry of Health & Welfare, Republic of Korea (HI14C3417).

ACKNOWLEDGMENTS

We thank the Catholic Hematopoietic Stem Cell Bank, College of Medicine, The Catholic University of Korea, Seoul, Republic of Korea, for typing HLA.

SUPPLEMENTARY MATERIAL

The Supplementary Material for this article can be found online at: https://www.frontiersin.org/articles/10.3389/fimmu.2021.774491/full#supplementary-material

REFERENCES

1. Gorbalenya AE, Baker SC, Baric RS, de Groot RJ, Drosten C, Gulyaeva AA, et al. The Species Severe Acute Respiratory Syndrome-Related Coronavirus: Classifying 2019-NCoV and Naming It SARS-CoV-2. *Nat Microbiol* (2020) 5 (4):536–44. doi: 10.1038/s41564-020-0695-z
2. Cubuk J, Alston JJ, Incicco JJ, Singh S, Stuchell-Brereton MD, Ward MD, et al. The SARS-CoV-2 Nucleocapsid Protein Is Dynamic, Disordered, and Phase Separates With RNA. *Nat Commun* (2021) 12(1):1936. doi: 10.1038/s41467-021-21953-3
3. Lu S, Ye Q, Singh D, Cao Y, Diedrich JK, Yates JR, et al. The SARS-CoV-2 Nucleocapsid Phosphoprotein Forms Mutually Exclusive Condensates With RNA and the Membrane-Associated M Protein. *Nat Commun* (2021) 12 (1):502. doi: 10.1038/s41467-020-20768-y
4. Ou X, Liu Y, Lei X, Li P, Mi D, Ren L, et al. Characterization of Spike Glycoprotein of SARS-CoV-2 on Virus Entry and Its Immune Cross-Reactivity With SARS-CoV. *Nat Commun* (2020) 11(1):1620. doi: 10.1038/s41467-020-15562-9
5. Khoury DS, Cromer D, Reynaldi A, Schlub TE, Wheatley AK, Juno JA, et al. Neutralizing Antibody Levels Are Highly Predictive of Immune Protection From Symptomatic SARS-CoV-2 Infection. *Nat Med* (2021) 27:1205–11. doi: 10.1038/s41591-021-01377-8
6. Rydyznski Moderbacher C, Ramirez SI, Dan JM, Grifoni A, Hastie KM, Weiskopf D, et al. Antigen-Specific Adaptive Immunity to SARS-CoV-2 in Acute COVID-19 and Associations With Age and Disease Severity. *Cell* (2020) 183(4):996–1012.e19. doi: 10.1016/j.cell.2020.09.038
7. Li J, Hui A, Zhang X, Yang Y, Tang R, Ye H, et al. Safety and Immunogenicity of the SARS-CoV-2 BNT162b1 mRNA Vaccine in Younger and Older Chinese Adults: A Randomized, Placebo-Controlled, Double-Blind Phase 1 Study. *Nat Med* (2021) 27:1062–70. doi: 10.1038/s41591-021-01330-9
8. Painter MM, Mathew D, Goel RR, Apostolidis SA, Pattekar A, Kuthuru O, et al. Rapid Induction of Antigen-Specific CD4+ T Cells Guides Coordinated Humoral and Cellular Immune Responses to SARS-CoV-2 mRNA Vaccination. *bioRxiv* (2021) 54(9):2133–42.e3. doi: 10.1016/j.immuni.2021.08.001
9. Hughes AL, Nei M. Nucleotide Substitution at Major Histocompatibility Complex Class II Loci: Evidence for Overdominant Selection. *Proc Natl Acad Sci* (1989) 86(3):958–62. doi: 10.1073/pnas.86.3.958
10. Rappazzo CG, Huisman BD, Birnbaum ME. Repertoire-Scale Determination of Class II MHC Peptide Binding *via* Yeast Display Improves Antigen Prediction. *Nat Commun* (2020) 11(1):4414. doi: 10.1038/s41467-020-18204-2
11. Tan Anthony T, Loggi E, Boni C, Chia A, Gehring Adam J, Sastry Konduru SR, et al. Host Ethnicity and Virus Genotype Shape the Hepatitis B Virus-Specific T-Cell Repertoire. *J Virol* (2008) 82(22):10986–97. doi: 10.1128/JVI.01124-08
12. Ranasinghe S, Cutler S, Davis I, Lu R, Soghoian DZ, Qi Y, et al. Association of HLA-DRB1–Restricted CD4+ T Cell Responses With HIV Immune Control. *Nat Med* (2013) 19(7):930–3. doi: 10.1038/nm.3229
13. Clemens EB, Van de Sandt C, Wong SS, Wakim LM, Valkenburg SA. Harnessing the Power of T Cells: The Promising Hope for a Universal Influenza Vaccine. *Vaccines* (2018) 6(2):18. doi: 10.3390/vaccines6020018
14. Chen RE, Zhang X, Case JB, Winkler ES, Liu Y, VanBlargan LA, et al. Resistance of SARS-CoV-2 Variants to Neutralization by Monoclonal and Serum-Derived Polyclonal Antibodies. *Nat Med* (2021) 27(4):717–26. doi: 10.1038/s41591-021-01294-w
15. Geers D, Shamier MC, Bogers S, den Hartog G, Gommers L, Nieuwkoop NN, et al. SARS-CoV-2 Variants of Concern Partially Escape Humoral But Not T-Cell Responses in COVID-19 Convalescent Donors and Vaccinees. *Sci Immunol* (2021) 6(59):eabj1750. doi: 10.1126/sciimmunol.abj1750
16. Skelly DT, Harding AC, Gilbert-Jaramillo J, Knight ML, Longet S, Brown A, et al. Two Doses of SARS-CoV-2 Vaccination Induce Robust Immune Responses to Emerging SARS-CoV-2 Variants of Concern. *Nat Commun* (2021) 12(1):5061. doi: 10.1038/s41467-021-25167-5
17. Tarke A, Sidney J, Methot N, Yu ED, Zhang Y, Dan JM, et al. Impact of SARS-CoV-2 Variants on the Total CD4+ and CD8+ T Cell Reactivity in Infected or Vaccinated Individuals. *Cell Rep Med* (2021) 2(7):100355. doi: 10.1016/j.xcrm.2021.100355
18. Liu DX, Liang JQ, Fung TS. Human Coronavirus-229e, -OC43, -NL63, and -HKU1 (Coronaviridae). *Encyclopedia Virol* (2021), 428–40. doi: 10.1016/B978-0-12-809633-8.21501-X
19. Mateus J, Grifoni A, Tarke A, Sidney J, Ramirez SI, Dan JM, et al. Selective and Cross-Reactive SARS-CoV-2 T Cell Epitopes in Unexposed Humans. *Science* (2020) 370(6512):89–94. doi: 10.1126/science.abd3871
20. Grifoni A, Sidney J, Zhang Y, Scheuermann RH, Peters B. Sette a. A Sequence Homology and Bioinformatic Approach can Predict Candidate Targets for Immune Responses to SARS-CoV-2. *Cell Host Microbe* (2020) 27(4):671–80.e2. doi: 10.1016/j.chom.2020.03.002
21. Mallajosyula V, Ganjavi C, Chakraborty S, McSween AM, Pavlovitch-Bedzyk AJ, Wilhelmy J, et al. CD8+ T Cells Specific for Conserved Coronavirus Epitopes Correlate With Milder Disease in COVID-19 Patients. *Sci Immunol* (2021) 6(61):eabg5669. doi: 10.1126/sciimmunol.abg5669
22. McMahan K, Yu J, Mercado NB, Loos C, Tostanoski LH, Chandrashekar A, et al. Correlates of Protection Against SARS-CoV-2 in Rhesus Macaques. *Nature* (2021) 590(7847):630–4. doi: 10.1038/s41586-020-03041-6
23. Mateus J, Dan JM, Zhang Z, Moderbacher CR, Lammers M, Goodwin B, et al. Low-Dose mRNA-1273 COVID-19 Vaccine Generates Durable Memory Enhanced by Cross-Reactive T Cells. *Science* (2021) 374(6566):eabj9853. doi: 10.1126/science.abj9853
24. Baek I-C, Choi E-J, Shin D-H, Kim H-J, Choi H, Kim T-G. Distributions of HLA-A, -B, and -DRB1 Alleles Typed by Amplicon-Based Next Generation Sequencing in Korean Volunteer Donors for Unrelated Hematopoietic Stem Cell Transplantation. *HLA* (2021) 97(2):112–26. doi: 10.1111/tan.14134
25. Baek I-C, Choi E-J, Shin D-H, Kim H-J, Choi H, Kim T-G. Allele and Haplotype Frequencies of Human Leukocyte Antigen-A, -B, -C, -DRB1, -DRB3/4/5, -DQA1, -DQB1, -DPA1, and -DPB1 by Next Generation Sequencing-Based Typing in Koreans in South Korea. *PLoS One* (2021) 16 (6):e0253619. doi: 10.1371/journal.pone.0253619
26. Hyun Y-S, Jo H-A, Lee Y-H, Kim S-M, Baek I-C, Sohn H-J, et al. Comprehensive Analysis of CD4+ T Cell Responses to CMV Pp65 Antigen Restricted by Single HLA-DR, -DQ, and -DP Allotype Within an Individual. *Front Immunol* (2021) 11:602014(3715). doi: 10.3389/fimmu.2020.602014
27. Hyun S-J, Sohn H-J, Lee H-J, Lee S-D, Kim S, Sohn D-H, et al. Comprehensive Analysis of Cytomegalovirus Pp65 Antigen-Specific CD8+ T Cell Responses According to Human Leukocyte Antigen Class I Allotypes and Intraindividual Dominance. *Front Immunol* (2017) 8:1591. doi: 10.3389/fimmu.2017.01591
28. Karp DR, Teletski CL, Jaraquemada D, Maloy WL, Coligan JE, Long EO. Structural Requirements for Pairing of Alpha and Beta Chains in HLA-DR and HLA-DP Molecules. *J Exp Med* (1990) 171(3):615–28. doi: 10.1084/jem.171.3.615
29. Tarke A, Sidney J, Kidd CK, Dan JM, Ramirez SI, Yu ED, et al. Comprehensive Analysis of T Cell Immunodominance and Immunoprevalence of SARS-CoV-2 Epitopes in COVID-19 Cases. *Cell Rep Med* (2021) 2(2):100204. doi: 10.1016/j.xcrm.2021.100204
30. Grifoni A, Moore E, Voic H, Sidney J, Phillips E, Jadi R, et al. Characterization of Magnitude and Antigen Specificity of HLA-DP, DQ, and DRB3/4/5 Restricted DENV-Specific CD4+ T Cell Responses. *Front Immunol* (2019) 10:1568. doi: 10.3389/fimmu.2019.01568
31. Low JS, Vaqueirinho D, Mele F, Foglierini M, Jerak J, Perotti M, et al. Clonal Analysis of Immunodominance and Cross-Reactivity of the CD4 T Cell

Response to SARS-CoV-2. *Science* (2021) 372(6548):1336–41. doi: 10.1126/science.abg8985
32. Lindestam Arlehamn CS, McKinney DM, Carpenter C, Paul S, Rozot V, Makgotlho E, et al. A Quantitative Analysis of Complexity of Human Pathogen-Specific CD4 T Cell Responses in Healthy M. Tuberculosis Infected South Africans. *PLoS Pathog* (2016) 12(7):e1005760. doi: 10.1371/journal.ppat.1005760
33. Nascimento EJ, Mailliard RB, Khan AM, Sidney J, Sette A, Guzman N, et al. Identification of Conserved and HLA Promiscuous DENV3 T-Cell Epitopes. *PLoS Negl Trop Dis* (2013) 7(10):e2497. doi: 10.1371/journal.pntd.0002497
34. Tian Y, Grifoni A, Sette A, Weiskopf D. Human T Cell Response to Dengue Virus Infection. *Front Immunol* (2019) 10:2125(2125). doi: 10.3389/fimmu.2019.02125
35. Schober K, Voit F, Grassmann S, Müller TR, Eggert J, Jarosch S, et al. Reverse TCR Repertoire Evolution Toward Dominant Low-Affinity Clones During Chronic CMV Infection. *Nat Immunol* (2020) 21(4):434–41. doi: 10.1038/s41590-020-0628-2
36. Day EK, Carmichael AJ, ten Berge IJ, Waller EC, Sissons JG, Wills MR. Rapid CD8+ T Cell Repertoire Focusing and Selection of High-Affinity Clones Into Memory Following Primary Infection With a Persistent Human Virus: Human Cytomegalovirus. *J Immunol* (2007) 179(5):3203–13. doi: 10.4049/jimmunol.179.5.3203
37. Sharon E, Sibener LV, Battle A, Fraser HB, Garcia KC, Pritchard JK. Genetic Variation in MHC Proteins Is Associated With T Cell Receptor Expression Biases. *Nat Genet* (2016) 48(9):995–1002. doi: 10.1038/ng.3625
38. Logunova NN, Kriukova VV, Shelyakin PV, Egorov ES, Pereverzeva A, Bozhanova NG, et al. MHC-II Alleles Shape the CDR3 Repertoires of Conventional and Regulatory Naïve CD4+ T Cells. *Proc Natl Acad Sci* (2020) 117(24):13659–69. doi: 10.1073/pnas.2003170117
39. Loyal L, Braun J, Henze L, Kruse B, Dingeldey M, Reimer U, et al. Cross-Reactive CD4+ T Cells Enhance SARS-CoV-2 Immune Responses Upon Infection and Vaccination. *medRxiv* (2021) 2021:4.01.21252379. doi: 10.1101/2021.04.01.21252379
40. Sieling P, King T, Wong R, Nguyen A, Wnuk K, Gabitzsch E, et al. Single Prime Had5 Spike (s) + Nucleocapsid (N) Dual Antigen Vaccination of Healthy Volunteers Induces a Ten-Fold Increase in Mean s- and N- T-Cell Responses Equivalent to T-Cell Responses From Patients Previously Infected With SARS-CoV-2. *medRxiv* (2021) 2021:4.05.21254940. doi: 10.1101/2021.04.05.21254940
41. Prugnolle F, Manica A, Charpentier M, Guégan JF, Guernier V, Balloux F. Pathogen-Driven Selection and Worldwide HLA Class I Diversity. *Curr Biol* (2005) 15(11):1022–7. doi: 10.1016/j.cub.2005.04.050
42. Manczinger M, Boross G, Kemény L, Müller V, Lenz TL, Papp B, et al. Pathogen Diversity Drives the Evolution of Generalist MHC-II Alleles in Human Populations. *PLoS Biol* (2019) 17(1):e3000131. doi: 10.1371/journal.pbio.3000131
43. Penn DJ, Damjanovich K, Potts WK. MHC Heterozygosity Confers a Selective Advantage Against Multiple-Strain Infections. *Proc Natl Acad Sci USA* (2002) 99(17):11260–4. doi: 10.1073/pnas.162006499
44. Mazor R, Addissie S, Jang Y, Tai C-H, Rose J, Hakim F, et al. Role of HLA-DP in the Presentation of Epitopes From the Truncated Bacterial PE38 Immunotoxin. *AAPS J* (2017) 19(1):117–29. doi: 10.1208/s12248-016-9986-y
45. Gaston JH, Goodall JC, Young JL, Young SP. Effect of Polymorphism of the HLA-DPA1 Chain on Presentation of Antigenic Peptides. *Hum Immunol* (1997) 54(1):40–7. doi: 10.1016/s0198-8859(97)00003-7

Conflict of Interest: The authors declare that the research was conducted in the absence of any commercial or financial relationships that could be construed as a potential conflict of interest.

Publisher's Note: All claims expressed in this article are solely those of the authors and do not necessarily represent those of their affiliated organizations, or those of the publisher, the editors and the reviewers. Any product that may be evaluated in this article, or claim that may be made by its manufacturer, is not guaranteed or endorsed by the publisher.

Copyright © 2022 Hyun, Lee, Jo, Baek, Kim, Sohn and Kim. This is an open-access article distributed under the terms of the Creative Commons Attribution License (CC BY). The use, distribution or reproduction in other forums is permitted, provided the original author(s) and the copyright owner(s) are credited and that the original publication in this journal is cited, in accordance with accepted academic practice. No use, distribution or reproduction is permitted which does not comply with these terms.

frontiers in Immunology

ORIGINAL RESEARCH
published: 26 January 2022
doi: 10.3389/fimmu.2022.801431

SARS-CoV-2 Spike-Specific CD4+ T Cell Response Is Conserved Against Variants of Concern, Including Omicron

Alessio Mazzoni[1], Anna Vanni[1], Michele Spinicci[1,2], Manuela Capone[1], Giulia Lamacchia[1], Lorenzo Salvati[1], Marco Coppi[1], Alberto Antonelli[1], Alberto Carnasciali[1], Parham Farahvachi[1], Nicla Giovacchini[1], Noemi Aiezza[1], Francesca Malentacchi[3], Lorenzo Zammarchi[1,2], Francesco Liotta[1,4,5], Gian Maria Rossolini[1,3], Alessandro Bartoloni[1,2], Lorenzo Cosmi[1,4], Laura Maggi[1†] and Francesco Annunziato[1,5†]*

[1] Department of Experimental and Clinical Medicine, University of Florence, Florence, Italy, [2] Infectious and Tropical Disease Unit, Careggi University Hospital, Florence, Italy, [3] Microbiology and Virology Unit, Careggi University Hospital, Florence, Italy, [4] Immunology and Cell Therapy Unit, Careggi University Hospital, Florence, Italy, [5] Flow Cytometry Diagnostic Center and Immunotherapy, Careggi University Hospital, Florence, Italy

Although accumulating data have investigated the effect of SARS-CoV-2 mutations on antibody neutralizing activity, less is known about T cell immunity. In this work, we found that the ancestral (Wuhan strain) Spike protein can efficaciously reactivate CD4+ T cell memory in subjects with previous Alpha variant infection. This finding has practical implications, as in many countries only one vaccine dose is currently administered to individuals with previous COVID-19, independently of which SARS-CoV-2 variant was responsible of the infection. We also found that only a minority of Spike-specific CD4+ T cells targets regions mutated in Alpha, Beta and Delta variants, both after natural infection and vaccination. Finally, we found that the vast majority of Spike-specific CD4+ T cell memory response induced by natural infection or mRNA vaccination is conserved also against Omicron variant. This is of importance, as this newly emerged strain is responsible for a sudden rise in COVID-19 cases worldwide due to its increased transmissibility and ability to evade antibody neutralization. Collectively, these observations suggest that most of the memory CD4+ T cell response is conserved against SARS-CoV-2 variants of concern, providing an efficacious line of defense that can protect from the development of severe forms of COVID-19.

Keywords: SARS-CoV-2, CD4, T cells, variants of concern (VOCs), cellular immunity, vaccination, natural infection

OPEN ACCESS

Edited by:
Francesco Dieli, University of Palermo, Italy

Reviewed by:
Marco Pio La Manna, University of Palermo, Italy
Alba Grifoni, La Jolla Institute for Immunology (LJI), United States

***Correspondence:**
Francesco Annunziato
francesco.annunziato@unifi.it

†*These authors share last authorship*

Specialty section:
This article was submitted to T Cell Biology, a section of the journal Frontiers in Immunology

Received: *25 October 2021*
Accepted: *10 January 2022*
Published: *26 January 2022*

Citation:
Mazzoni A, Vanni A, Spinicci M, Capone M, Lamacchia G, Salvati L, Coppi M, Antonelli A, Carnasciali A, Farahvachi P, Giovacchini N, Aiezza N, Malentacchi F, Zammarchi L, Liotta F, Rossolini GM, Bartoloni A, Cosmi L, Maggi L and Annunziato F (2022) SARS-CoV-2 Spike-Specific CD4+ T Cell Response Is Conserved Against Variants of Concern, Including Omicron. Front. Immunol. 13:801431. doi: 10.3389/fimmu.2022.801431

INTRODUCTION

Immunological memory is achieved by either natural infection or vaccination and can guarantee long lasting protection from moderate to severe COVID-19, in case of SARS-CoV-2 encounter. For this reason, mass vaccination strategies are currently underway to speed up the process of immunization against SARS-CoV-2. However, the exponential propagation of SARS-CoV-2

worldwide has led to the emergence of viral variants with increased transmission capability. Between the end of 2020 and the beginning of 2021, several SARS-CoV-2 variants arose, rapidly spreading worldwide and replacing the original Wuhan strain. The B.1.1.7 (Alpha) variant emerged in the UK in September 2020, showed an increased transmissibility and substituted rapidly the ancestral strain in Europe and the US (1, 2). The B.1.351 (Beta) variant instead was originally described in South Africa in May 2020 (1, 3). The WHO classified these strains as variants of concern (VOC) on December 18, 2020. The B.1.617.2 (Delta) variant which was originally detected in India, was classified as VOC on May 18, 2021, and became rapidly the leading strain worldwide (1). Nowadays, the majority of COVID-19 cases are due to the Omicron variant, which arose in South Africa and was declared by the WHO as VOC on November 26, 2021 (4). The emergence of viral variants with increased transmissibility has been associated to increased numbers of COVID-19 cases (5). Amino acid mutations in viral proteins may mine the capacity of SARS-CoV-2 specific antibodies and T cells to recognize mutated proteins, thus potentially overcoming the immunological memory-mediated protection. Particular attention is given to mutations in the Spike protein, since it is crucial in the virus infection process and it is targeted by currently approved vaccines. Accumulating evidences have shown a relatively small impact of Alpha variant on the antibody neutralization capacity, while Beta variant is associated to a significant loss of neutralizing activity. These observations were obtained both on sera from recovered individuals and from vaccinated subjects (6). Convalescent and vaccinated sera showed reduced neutralizing antibody titers also against Delta (7). Recent evidences are now demonstrating that the antibody neutralization capacity is significantly reduced against Omicron both in previously SARS-CoV-2 infected and vaccinated subjects (8), although a third, booster, vaccine administration seems to partially restore the neutralizing capability (9). Indeed, Omicron is heavily mutated in the receptor binding domain of the Spike protein, thus explaining its increased immune evasion potential (10). As far as T cell recognition is concerned, there are few information regarding the effect of viral mutations. At a clinical level, BNT162b2 and mRNA-1273 mRNA vaccines (from Pfizer/Biontech and Moderna, respectively) and the viral vector based ChAdOx1 (AstraZeneca) vaccine retain high efficacy against Alpha variant (11), while a significant loss has been demonstrated for ChAdOx1 against Beta variant (12). In this manuscript, we investigated the capability of circulating CD4+ T cells derived from subjects who recovered from SARS-CoV-2 infection or who were vaccinated with BNT162b2, mRNA-1273 or ChAdOx1, to respond to SARS-CoV-2 variants of concern including the recently emerged Omicron.

RESULTS

To evaluate the frequency of circulating CD4+ T cells specific for Spike, we stimulated *in vitro* peripheral blood mononuclear cells (PBMC) with peptide pools spanning the entire ancestral (Wuhan strain) Spike sequence. Reactive CD4+ T cells were identified based on surface CD154 expression and production of at least one among IFN-γ, TNF-α and IL-2 cytokines (13, 14). Tested PBMC had been collected from subjects who had recovered from ancestral SARS-CoV-2 infection (before October 2020) or from subjects with laboratory confirmed SARS-CoV-2 Alpha variant infection. As shown in **Figures 1A, B**, we detected comparable frequencies of ancestral (Wuhan strain) Spike-reactive CD4+ T cells in subjects with history of ancestral- or Alpha-variant infection. This finding suggests that mutations occurring in Alpha variant do not affect the global CD4+ T cell capacity to recognize the ancestral Spike protein. To gain a better insight on the effect of SARS-CoV-2 mutations on CD4+ T cell response, we stimulated PBMC from subjects with previous ancestral SARS-CoV-2 infection also with peptide pools selectively spanning regions of the ancestral Spike protein that are mutated in the Alpha, Beta or Delta variant (Alpha, Beta or Delta reference pools). As shown in **Figure 1C**, frequencies of CD4+ T cells specific for Alpha, Beta or Delta reference pools were significantly lower than those specific for the entire ancestral Spike protein. This observation suggests that a minor fraction of the entire Spike-specific CD4+ T cell population is involved in the recognition of regions mutated in Alpha, Beta and Delta variants. Indeed, they represented 11%, 7% and 10% of total CD4+ T cell response to Spike, respectively. Then, we tested if the recognition of Alpha, Beta or Delta reference pools by CD4+ T cells is affected by mutations occurring in the respective variants. To test this, PBMC from subjects with previous ancestral SARS-CoV-2 infection were stimulated with Alpha, Beta or Delta reference pools and with the corresponding mutated pools. As shown in **Figures 1C, D**, mutations occurring in Alpha variant mildly affected CD4+ T cell response. On the contrary, mutations occurring in Beta and Delta variants did not significantly reduce CD4+ T cell recognition (**Figure 1C**).

Collectively, these data show that the majority of Spike-specific CD4+ T cell response is directed to non-mutated regions and, in any case, it is similar in Wuhan strain and Alpha variant infection.

Since currently approved vaccines elicit cellular and humoral immunity against ancestral Spike protein, we decided to test whether vaccine-induced CD4+ T cell response is affected by mutations occurring in SARS-CoV-2 variants. We enrolled subjects without prior SARS-CoV-2 infection (defined by absence of compatible symptoms and absence of serum anti-Nucleoprotein IgG), immunized with double dose of either mRNA or viral-vector vaccines. As shown in **Figures 2A, B**, mRNA vaccination elicited significantly higher levels of total Spike-specific CD4+ T cells. As already observed in the context of natural infection, also the frequencies of mRNA- or viral vector-induced CD4+ T cells specific for Alpha or Beta reference pools were significantly lower than those specific for the entire ancestral Spike protein (**Figures 2C, D, F**). When assessing the impact of Alpha and Beta variants on recognition by specific CD4+ T cells, we found a mild impact of Alpha variant on mRNA-induced CD4+ T cell response with no differences in the other contexts (**Figures 2C, D, F**). We also had the possibility to test the impact of Delta variant on vaccine-induced CD4+ T cell response in a cohort of mRNA-vaccinated subjects. Similarly to

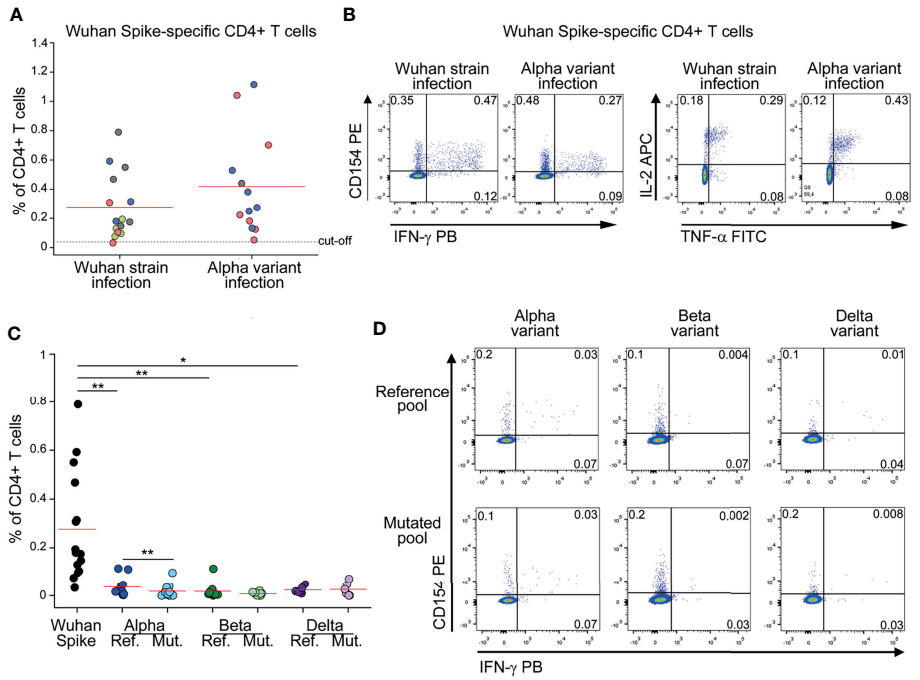


FIGURE 1 | CD4+ T cell response to Spike in subjects with previous SARS-CoV-2 infection is minimally affected by mutations occurring in Alpha, Beta and Delta variants **(A)** Frequency of CD4+ T cells specific for Wuhan Spike protein in Wuhan strain- (15) or Alpha variant- (13) infected subjects. Mild COVID-19 patients are depicted in green, moderate in red, severe in blue, critical in gray. Representative FACS plots from one subject of each group are depicted in **(B)**. **(C)** Frequency of CD4+ T cells specific for Wuhan Spike, Alpha variant reference or mutated pool, Beta variant reference or mutated pool, Delta variant reference or mutated pool in subjects with previous Wuhan strain SARS-CoV-2 infection. Representative FACS plots showing CD4+ T cells reactive to Alpha, Beta and Delta reference and mutated pools from three distinct patients are depicted in **(D)**. Data in **(A, C)** are subtracted of background, unstimulated condition. Red lines in **(A, C)** represent mean values. Dashed line in **(A)** represents cut-off value. *p < 0.05; **p < 0.01, calculated with Wilcoxon-Signed Rank test.

what observed for Alpha and Beta variants, stimulation with the entire ancestral Spike protein elicited a significantly higher frequency of reactive CD4+ T cells than the Delta reference pool (**Figure 2E**). However, no differences were detected when comparing the frequencies of CD4+ T cells specific for Delta reference or mutated pools (**Figure 2E**). Collectively, these data suggest that vaccine-induced CD4+ T cell response is minimally affected by mutations occurring in Alpha, Beta and Delta variants.

Following the rapid diffusion of the Omicron variant worldwide, we extended our study to investigate if CD4+ T cell memory response to Spike is affected by mutations present in this viral strain. We stimulated PBMC from subjects who had recovered from ancestral SARS-CoV-2 infection with a peptide pool covering the entire Spike protein, or with reference or mutated peptide pools specific for Omicron variant (**Figures 3A, B**). As previously shown for other variants, CD4+ T cell response against total Spike was significantly higher than Omicron reference pool (**Figure 3A**). Indeed, Omicron reference pool accounted for, on average, 24% of the total response against ancestral Spike. We also observed that mutations present in Omicron affect CD4+ T cell immunity, as we observed a significantly reduced response to the mutated pool when compared to the reference pool (**Figure 3A**). In particular, we found that the mutated pool elicited a 40% lower response when compared to the reference pool. Despite this loss, combining all these information our data suggest that roughly 90% of CD4+ T cell response against Omicron should be preserved with respect to ancestral Spike. We performed the same analysis also on mRNA-vaccinated subjects (**Figures 3C, D**). In this case, we had the possibility to test these subjects one month after dose 2 and dose 3 injections. CD4+ T cell response against total Spike was significantly higher than Omicron reference pool, both after dose 2 and 3 (**Figure 3C**). Omicron reference pool represented 20% and 30% of total CD4+ T cell response against Spike after dose 2 and 3, respectively. When we assessed the impact of Omicron-specific mutations, we observed that the mutated pool elicited a significantly lower response than the reference pool. In particular, we observed a 65% and 61% lower response after dose 2 and 3, respectively. Combining these data, we expect that following dose 2 and 3 of mRNA vaccination, 87% and 82% of total CD4+ T cell response to Spike should be retained against Omicron, respectively.

DISCUSSION

Our results are in harmony with published data showing that mutations occurring in common SARS-CoV-2 variants have a

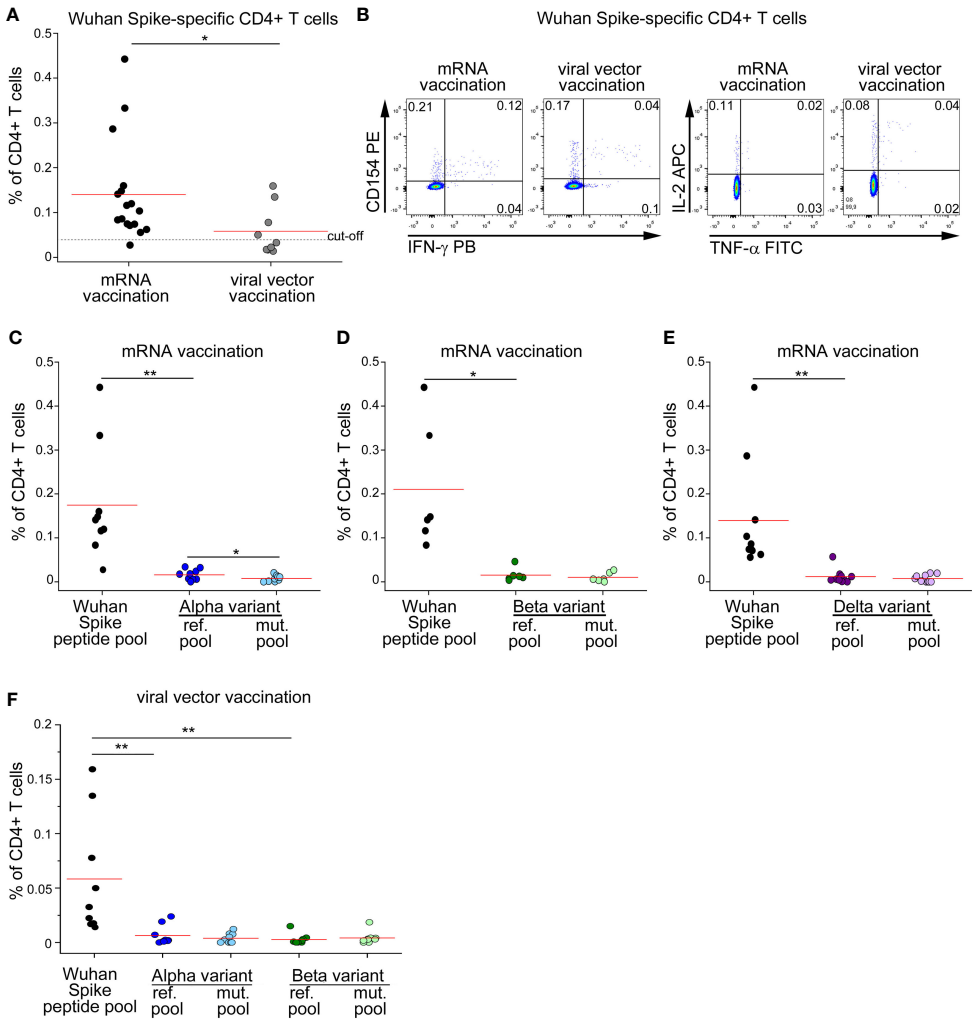


FIGURE 2 | CD4+ T cell response to Spike in vaccinated subjects is minimally affected by mutations occurring in Alpha, Beta and Delta variants. **(A)** Frequency of CD4+ T cells specific for Wuhan Spike protein in mRNA- (17) or viral vector- (9) vaccinated subjects. Representative FACS plot are depicted in **(B)**. Frequency of CD4+ T cells specific for Wuhan Spike, Alpha variant reference or mutated pool **(C)**, Beta variant reference or mutated pool **(D)**, Delta variant reference or mutated pool **(E)** in 9, 6 and 10 mRNA-vaccinated subjects, respectively. **(F)** Frequency of CD4+ T cells specific for Wuhan Spike, Alpha variant reference or mutated pool, Beta variant reference or mutated pool in 9 subjects with viral vector vaccination. Data in **(A, C–F)** are subtracted of background, unstimulated condition. Red lines in **(A, C–F)** represent mean values. Dashed line in **(A)** represents cut-off value. *$p < 0.05$; **$p < 0.01$, calculated with Mann-Whitney test **(A)** or Wilcoxon-Signed Rank test **(C–F)**.

negligible impact on T cell reactivity (15–17). Notably, these studies were performed stimulating PBMNC with full-length ancestral- or mutated-Spike. Here, we provided the complementary observation that ancestral- or Alpha variant-infection elicit comparable CD4+ T cell responses to ancestral Spike. Notably, this information was obtained from a cohort of COVID-19 patients with a wide range in terms of symptomatology, similar between ancestral- and Alpha variant-infection. This is of importance, as previous studies have shown that disease severity directly correlates to anti-SARS-CoV-2 immunity (13, 14, 18). Our observation that Alpha, Beta and Delta reference pools elicit a CD4+ T cell response significantly lower than total Spike protein provides a biological explanation for the conserved CD4+ T cell response, suggesting that the majority of CD4+ T cells target regions non-mutated in Alpha, Beta and Delta variants. This finding is supported also by a recent publication showing that the overall contribution of T cells targeting mutated regions to the total Spike-specific T cell response is on average 14% for the Alpha variant and 10% for the Beta variant (19). Moreover, despite a mild difference for Alpha variant, we observed substantially comparable responses to reference and mutated pools, suggesting that CD4+ T cells induced by ancestral infection or vaccination cross-react to Alpha, Beta and Delta variants. However, additional studies are needed to fully elucidate this concept. Notably, another research group reported a conserved response for Alpha variant (20). The recent emergence of Omicron variant is worrisome, as this variant exhibits increased

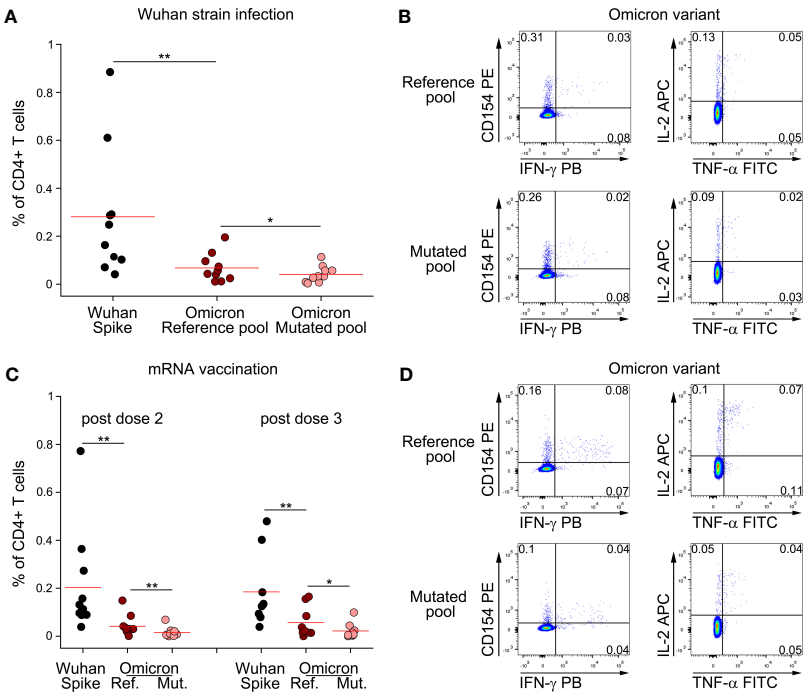


FIGURE 3 | Omicron variant does not significantly impair CD4+ T cell memory response to Spike following natural infection and mRNA vaccination. **(A)** Frequency of CD4+ T cells specific for Wuhan Spike, Omicron variant reference or mutated pool in 10 subjects with previous Wuhan strain SARS-CoV-2 infection. Representative FACS plot are depicted in **(B)**. **(C)** Frequency of CD4+ T cells specific for Wuhan Spike, Omicron variant reference or mutated pool in mRNA-vaccinated subjects enrolled after dose 2 (n=11) or dose 3 (n=9) administration. Representative FACS plot are depicted in **(D)**. Data in **(A, C)** are subtracted of background, unstimulated condition. Red lines in **(A, C)** represent mean value. *p < 0.05; **p < 0.01, calculated Wilcoxon-Signed Rank test.

transmissibility than Delta and a significant number of mutations in Spike, mainly in the receptor-binding domain. This variant has rapidly become the leading SARS-CoV-2 strain worldwide, with a rapid increase in COVID-19 cases also in highly vaccinated countries (1). Indeed, accumulating data are now showing that the neutralizing capability of convalescent or vaccinees' sera is significantly reduced against Omicron (8). Regarding T cell immunity, we found that Omicron can significantly blunt the CD4+ T cell response to the regions of Spike targeted by mutations. However, when considering the overall response to Spike, we found that the majority of the response is conserved. Our observations are in agreement with works from other groups recently released as pre-print publications, which suggest minimal escape of T cell immunity by Omicron (21–26). Although it may not be sufficient alone to guarantee protection from infection, a conserved CD4+ T cell immunity against common SARS-CoV-2 VOCs may be fundamental to reduce disease severity, as demonstrated by the importance of a rapid T cell response in preventing severe COVID-19 (27). Notably, our data show that CD4+ T cell response is conserved to variants of concern both in recovered-COVID-19 subjects as well as in vaccinated individuals. Although our cohort included only 25 individuals, we observed that mRNA vaccines elicited significantly higher CD4+ T cell response to Spike than viral vector vaccines. This is in agreement with a previous study which showed that the frequency of CD69+IFN-γ+ CD4+ T cells reactive to Spike is significantly higher following two mRNA vaccine injections than after two viral vector administrations (28). However, despite a significantly different total response to Spike, we found that in both cases the majority of CD4+ T cell response to Spike is preserved also against variants of concern.

We and others have previously demonstrated that following the first mRNA vaccine injection, Spike-specific CD4+ T cells rapidly increase in the circulation of previously infected subjects, with no additional effect following the second dose administration (29, 30). The demonstration that Spike-specific CD4+ T cells from subjects with previous Alpha variant infection recognize also the ancestral protein, suggests that vaccination may rapidly reactivate immunological memory to Spike protein also in these individuals. This is of importance, as in many countries only one vaccine dose is currently administered to individuals with previous COVID-19, regardless of which SARS-CoV-2 variant was responsible of the infection.

In conclusion, our data show that CD4+ T cell memory response to Spike is relatively conserved in the context of Alpha, Beta and Delta SARS-CoV-2 variants. Omicron variant is currently responsible for the vast majority of infections worldwide, due to significant growth advantage and potential immune escape compared to Delta variant (31). Thus, additional information on memory T cell responses to this variant are urgently needed. Our findings obtained following natural

infection and in the context of mRNA vaccination suggest that the global CD4+ T cell response is retained also against Omicron. For this reason, vaccination strategies should be implemented to rapidly achieve high immunization levels worldwide, thus conferring protection against moderate-severe COVID-19 caused by SARS-CoV-2 VOCs.

MATERIALS AND METHODS

Subjects

PBMC from 31 moderate COVID-19 patients (18 infected by the original SARS-CoV-2 Wuhan strain and 13 by the Alpha variant) were collected one month following hospital discharge. Alpha-infected subjects were enrolled between April and May 2021. Alpha infection was defined based on presence of N501Y e DEL69/70 mutation, assessed by Allplex SARS-CoV-2 Variants I Assay (Seegene). Main demographic and clinical characteristics are summarized in **Supplementary Table S1**. PBMC from 17 mRNA- and 9 viral-vector-vaccinated subjects were collected one month following the second vaccine dose administration. M: F ratio was 0.54 in the first cohort and 0.5 in the second cohort. Median age (IQR) was 45 (33-58) years for mRNA-vaccinated individuals, and 47 (30-53) years for viral-vector vaccinated subjects. Main demographic and clinical characteristics are summarized in **Supplementary Table S2**. PBMNC from 10 SARS-CoV-2 Wuhan-strain infected subjects were obtained one month after hospital discharge and tested for CD4+ T cell reactivity against Omicron variant. Main demographic and clinical characteristics are summarized in **Supplementary Table S3**. PBMC from 11 mRNA-vaccinated subjects were collected one month after the second and one month after the third dose administration and tested for CD4+ T cell reactivity against Omicron variant. Main demographic and clinical characteristics are summarized in **Supplementary Table S4**.

All the enrolled individuals were of Caucasian origin. PBMC were obtained following density gradient centrifugation of blood samples using Lymphoprep (Axis Shield Poc As™) and were frozen in FCS plus 10% DMSO and stored in liquid nitrogen.

Evaluation of SARS-CoV-2-Spike-Reactive T Cells

Identification of Spike specific CD4+ T cells was performed as previously described (9, 10). Briefly, 1.5 million thawed PBMNCs were cultured in complete RPMI plus 5% human AB serum in 96 well flat bottom plates in presence of medium alone (background, negative control) or of a pool of Spike SARS-CoV-2 peptide pools (Prot_S1, Prot_S+ and Prot_S to achieve a complete sequence coverage of the Spike protein) at 0.6 μM/peptide, (Miltenyi Biotech). Alternatively, cells were stimulated with peptide pools selectively spanning mutated regions in Alpha, Beta, Delta or Omicron variants and harboring the specific mutations (Alpha, Beta, Delta or Omicron mutated pool, Miltenyi Biotech). As a control, the same peptide pools but with the original (Wuhan strain) sequence were used (reference pool, Miltenyi Biotech). After 2 hours of incubation at 37°C, 5% CO2, Brefeldin A (5 μg/mL) was added, followed by additional 4 hours incubation. Finally, cells were fixed and stained using fluorochrome-conjugated antibodies listed in **Supplementary Table S5**. Samples were acquired on a BD LSR II flow cytometer (BD Biosciences). Cut-off values for CD4+ T cell response to total spike were calculated as mean+2SD from a population of 15 SARS-CoV-2 unexposed, unvaccinated subjects. Gating strategy for the identification of antigen-specific CD4+ T cells is reported in **Supplementary Figure 1**.

Statistics

Unpaired Mann-Whitney test was used to compare ancestral- versus Alpha variant-SARS-CoV-2 previously infected subjects, as well as mRNA versus viral vector-vaccines. Wilcoxon-Signed Rank test was used to compare the different response to total Spike, reference and mutated pools within each study group. In all cases, p values ≤0.05 were considered significant.

DATA AVAILABILITY STATEMENT

The original contributions presented in the study are included in the article/**Supplementary Material**. Further inquiries can be directed to the corresponding authors.

ETHICS STATEMENT

The studies involving human participants were reviewed and approved by Careggi University Hospital Ethical Committee. The patients/participants provided their written informed consent to participate in this study.

AUTHOR CONTRIBUTIONS

AM, AV, MCa, GL, LS, MCo, AA, NG, NA, FM, LM, AC, and PF performed the experiments. MS and LZ enrolled patients. FL, GMR AB, LC, LM, and FA supervised research. AM and FA wrote the manuscript. All authors contributed to manuscript revision, read, and approved the submitted version.

FUNDING

This study was supported by funds to the Department of Experimental and Clinical Medicine, University of Florence, derived from Ministero dell'Istruzione, dell'Università e della Ricerca (Italy) (Project Excellence Departments 2018-2022); by University of Florence, project RICTD2122; by Tuscany Region, project TagSARS-CoV-2; by Ministero della Salute, project COVID-2020-12371849.

ACKNOWLEDGMENTS

We thank all the subjects who participated to the study. The authors thank Miltenyi Biotech for gently providing Omicron reference and mutated pools.

SUPPLEMENTARY MATERIAL

The Supplementary Material for this article can be found online at: https://www.frontiersin.org/articles/10.3389/fimmu.2022.801431/full#supplementary-material

REFERENCES

1. World Health Organization (WHO). *Tracking SARS-CoV-2 Variants* . Available at: https://www.who.int/en/activities/tracking-SARS-CoV-2-variants (Accessed on January 7, 2021).
2. Volz E, Mishra S, Chand M, Barrett JC, Johnson R, Geidelberg L, et al. Assessing Transmissibility of SARS-CoV-2 Lineage B.1.1.7 in England. *Nature* (2021) 593(7858):266–9. doi: 10.1038/s41586-021-03470-x
3. Tegally H, Wilkinson E, Giovanetti M, Iranzadeh A, Fonseca V, Giandhari J, et al. Detection of a SARS-CoV-2 Variant of Concern in South Africa. *Nature* (2021) 592(7854):438–43. doi: 10.1038/s41586-021-03402-9
4. World Health Organization (WHO). *Classification of Omicron (B.1.1.529): SARS-CoV-2 Variant of Concern* . Available at: https://www.who.int/news/item/26-11-2021-classification-of-omicron-(b.1.1.529)-sars-cov-2-variant-of-concern (Accessed on January 7th, 2021).
5. *WHO COVID-19 Dashboard* . Available at: https://covid19.who.int (Accessed on January 7, 2021).
6. Bates TA, Leier HC, Lyski ZL, McBride SK, Coulter FJ, Weinstein JB, et al. Neutralization of SARS-CoV-2 Variants by Convalescent and BNT162b2 Vaccinated Serum. *Nat Commun* (2021) 12(1):5135. doi: 10.1038/s41467-021-25479-6
7. Planas D, Veyer D, Baidaliuk A, Staropoli I, Guivel-Benhassine F, Rajah MM, et al. Reduced Sensitivity of SARS-CoV-2 Variant Delta to Antibody Neutralization. *Nature* (2021) 596(7871):276–80. doi: 10.1038/s41586-021-03777-9
8. Schmidt F, Muecksch F, Weisblum Y, Silva JD, Bednarski E, Cho A, et al. Plasma Neutralization Properties of the SARS-CoV-2 Omicron Variant. *N Engl J Med* (2021). doi: 10.1056/NEJMc2119641
9. Nemet I, Kliker L, Lustig Y, Zuckerman N, Erster O, Cohen C, et al. Third BNT162b2 Vaccination Neutralization of SARS-CoV-2 Omicron Infection. *N Engl J Med* (2021). doi: 10.1056/NEJMc2119358
10. *Centers for Disease Control and Prevention. Science Brief: Omicron (B.1.1.529) Variant* (2021). Available at: https://www.cdc.gov/coronavirus/2019-ncov/science/science-briefs/scientific-brief-omicron-variant.html (Accessed on January 7, 2021).
11. Emary KRW, Golubchik T, Aley PK, Ariani CV, Angus B, Bibi S, et al. Efficacy of ChAdOx1 Ncov-19 (AZD1222) Vaccine Against SARS-CoV-2 Variant of Concern 202012/01 (B.1.1.7): An Exploratory Analysis of a Randomised Controlled Trial. *Lancet* (2021) 397(10282):1351–62. doi: 10.1016/S0140-6736(21)00628-0
12. Madhi SA, Baillie V, Cutland CL, Voysey M, Koen AL, Fairlie L, et al. Efficacy of the ChAdOx1 Ncov-19 Covid-19 Vaccine Against the B.1.351 Variant. *N Engl J Med* (2021) 384(20):1885–98. doi: 10.1056/NEJMoa2102214
13. Mazzoni A, Maggi L, Capone M, Spinicci M, Salvati L, Colao MG, et al. Cell-Mediated and Humoral Adaptive Immune Responses to SARS-CoV-2 are Lower in Asymptomatic Than Symptomatic COVID-19 Patients. *Eur J Immunol* (2020) 50(12):2013–24. doi: 10.1002/eji.202048915
14. Mazzoni A, Maggi L, Capone M, Vanni A, Spinicci M, Salvati L, et al. Heterogeneous Magnitude of Immunological Memory to SARS-CoV-2 in Recovered Individuals. *Clin Transl Immunol* (2021) 10(5):e1281. doi: 10.1002/cti2.1281
15. Tarke A, Sidney J, Methot N, Yu ED, Zhang Y, Dan JM, et al. Impact of SARS-CoV-2 Variants on the Total CD4+ and CD8+ T Cell Reactivity in Infected or Vaccinated Individuals. *Cell Rep Med* (2021) 2(7):100355. doi: 10.1016/j.xcrm.2021.100355
16. Jordan SC, Shin BH, Gadsden TM, Chu M, Petrosyan A, Le CN, et al. T Cell Immune Responses to SARS-CoV-2 and Variants of Concern (Alpha and Delta) in Infected and Vaccinated Individuals. *Cell Mol Immunol* (2021) 18 (11):2554–6. doi: 10.1038/s41423-021-00767-9
17. Neidleman J, Luo X, McGregor M, Xie G, Murray V, Greene WC, et al. mRNA Vaccine-Induced T Cells Respond Identically to SARS-CoV-2 Variants of Concern But Differ in Longevity and Homing Properties Depending on Prior Infection Status. *Elife* (2021) 10. doi: 10.7554/eLife.72619
18. Sekine T, Perez-Potti A, Rivera-Ballesteros O, Strålin K, Gorin JB, Olsson A, et al. Robust T Cell Immunity in Convalescent Individuals With Asymptomatic or Mild COVID-19. *Cell* (2020) 183(1):158–168.e14. doi: 10.1016/j.cell.2020.08.017
19. Skelly DT, Harding AC, Gilbert-Jaramillo J, Knight ML, Longet S, Brown A, et al. Two Doses of SARS-CoV-2 Vaccination Induce Robust Immune Responses to Emerging SARS-CoV-2 Variants of Concern. *Nat Commun* (2021) 12(1):5061. doi: 10.1038/s41467-021-25167-5
20. Geers D, Shamier MC, Bogers S, den Hartog G, Gommers L, Nieuwkoop NN, et al. SARS-CoV-2 Variants of Concern Partially Escape Humoral But Not T-Cell Responses in COVID-19 Convalescent Donors and Vaccinees. *Sci Immunol* (2021) 6(59). doi: 10.1126/sciimmunol.abj1750
21. Tarke A, Coelho CH, Zhang Z, Dan JM, Yu ED, Methot N, et al. SARS-CoV-2 Vaccination Induces Immunological Memory Able to Cross-Recognize Variants From Alpha to Omicron. *BioRxiv [Preprint]* (2021). doi: 10.1101/2021.12.28.474333
22. Keeton R, Tincho MB, Ngomti A, Baguma R, Benede N, Suzuki A, et al. SARS-CoV-2 Spike T Cell Responses Induced Upon Vaccination or Infection Remain Robust Against Omicron. *MedRxiv [Preprint]* (2021). doi: 10.1101/2021.12.26.21268380
23. GeurtsvanKessel CH, Geers D, Schmitz KS, Mykytyn AZ, Mart M, Lamers MM, et al. Divergent SARS CoV-2 Omicron-Specific T- and B-Cell Responses in COVID-19 Vaccine Recipients. *MedRxiv [Preprint]* (2021). doi: 10.1101/2021.12.27.21268416
24. De Marco L, D'Orso S, Pirronello M, Verdiani A, Termine A, Fabrizio C, et al. Preserved T Cell Reactivity to the SARS-CoV-2 Omicron Variant Indicates Continued Protection in Vaccinated Individuals. *BioRxiv [Preprint]* (2021). doi: 10.1101/2021.12.30.474453
25. Liu J, Chandrashekar A, Sellers D, Barrett J, Lifton M, McMahan K, et al. Vaccines Elicit Highly Cross-Reactive Cellular Immunity to the SARS-CoV-2 Omicron Variant. *MedRxiv [Preprint]* (2022). doi: 10.1101/2022.01.02.22268634
26. Gao Y, Cai C, Grifoni A, Müller TR, Niessl J, Olofsson A, et al. Ancestral SARS-CoV-2-Specific T Cells Crossrecognize Omicron (B.1.1.529). *Res Square [Preprint]* (2022). doi: 10.21203/rs.3.rs-1217466/v1
27. Tan AT, Linster M, Tan CW, Le Bert N, Ni Chia W, Kunasegaran K, et al. Early Induction of Functional SARS-CoV-2-Specific T Cells Associates With Rapid Viral Clearance and Mild Disease in COVID-19 Patients. *Cell Rep* (2021) 34(6):108728. doi: 10.1016/j.celrep.2021.108728
28. Schmidt T, Klemis V, Schub D, Mihm J, Hielscher F, Marx S, et al. Immunogenicity and Reactogenicity of Heterologous ChAdOx1 Ncov-19/mRNA Vaccination. *Nat Med* (2021) 27(9):1530–5. doi: 10.1038/s41591-021-01464-w
29. Mazzoni A, Di Lauria N, Maggi L, Salvati L, Vanni A, Capone M, et al. First-Dose mRNA Vaccination is Sufficient to Reactivate Immunological Memory to SARS-CoV-2 in Subjects Who Have Recovered From COVID-19. *J Clin Invest* (2021) 131(12):e149150. doi: 10.1172/JCI149150
30. Painter MM, Mathew D, Goel RR, Apostolidis SA, Pattekar A, Kuthuru O, et al. Rapid Induction of Antigen-Specific CD4+ T Cells is Associated With Coordinated Humoral and Cellular Immunity to SARS-CoV-2 mRNA Vaccination. *Immunity* (2021), S1074–7613(21)00308-3. doi: 10.1016/j.immuni.2021.08.001
31. European Centre for Disease Prevention and Control. *Assessment of the Further Emergence of the SARS-CoV-2 Omicron VOC in the Context of the Ongoing Delta VOC Transmission in the EU/EEA, 18th Update* (2021). Available at: https://www.ecdc.europa.eu/en/publications-data/covid-19-

assessment-further-emergence-omicron-18th-risk-assessment (Accessed on January 7, 2021).

Conflict of Interest: The authors declare that the research was conducted in the absence of any commercial or financial relationships that could be construed as a potential conflict of interest.

Publisher's Note: All claims expressed in this article are solely those of the authors and do not necessarily represent those of their affiliated organizations, or those of the publisher, the editors and the reviewers. Any product that may be evaluated in this article, or claim that may be made by its manufacturer, is not guaranteed or endorsed by the publisher.

Copyright © 2022 Mazzoni, Vanni, Spinicci, Capone, Lamacchia, Salvati, Coppi, Antonelli, Carnasciali, Farahvachi, Giovacchini, Aiezza, Malentacchi, Zammarchi, Liotta, Rossolini, Bartoloni, Cosmi, Maggi and Annunziato. This is an open-access article distributed under the terms of the Creative Commons Attribution License (CC BY). The use, distribution or reproduction in other forums is permitted, provided the original author(s) and the copyright owner(s) are credited and that the original publication in this journal is cited, in accordance with accepted academic practice. No use, distribution or reproduction is permitted which does not comply with these terms.

frontiers in Immunology

ORIGINAL RESEARCH
published: 27 January 2022
doi: 10.3389/fimmu.2022.821595

Heterologous Immunity Between SARS-CoV-2 and Pathogenic Bacteria

*Peter J. Eggenhuizen[1], Boaz H. Ng[1], Janet Chang[1], Rachel M.Y. Cheong[1], Anusha Yellapragada[1], Wey Y. Wong[1], Yi Tian Ting[1], Julie A. Monk[1], Poh-Yi Gan[1,2], Stephen R. Holdsworth[1,2] and Joshua D. Ooi[1]**

[1] Centre for Inflammatory Diseases, Department of Medicine, Monash Medical Centre, School of Clinical Sciences, Monash University, Clayton, VIC, Australia, [2] Department of Immunology, Monash Health, Monash Medical Centre, Clayton, VIC, Australia

OPEN ACCESS

Edited by:
Laura Maggi, Università degli Studi di Firenze, Italy

Reviewed by:
Carmen Fernández, Stockholm University, Sweden
Daniela Latorre, ETH Zürich, Switzerland

***Correspondence:**
Joshua D. Ooi
joshua.ooi@monash.edu

Specialty section:
This article was submitted to T Cell Biology, a section of the journal Frontiers in Immunology

Received: *24 November 2021*
Accepted: *11 January 2022*
Published: *27 January 2022*

Citation:
Eggenhuizen PJ, Ng BH, Chang J, Cheong RMY, Yellapragada A, Wong WY, Ting YT, Monk JA, Gan P-Y, Holdsworth SR and Ooi JD (2022) Heterologous Immunity Between SARS-CoV-2 and Pathogenic Bacteria. Front. Immunol. 13:821595. doi: 10.3389/fimmu.2022.821595

Heterologous immunity, when the memory T cell response elicited by one pathogen recognizes another pathogen, has been offered as a contributing factor for the high variability in coronavirus disease 2019 (COVID-19) severity outcomes. Here we demonstrate that sensitization with bacterial peptides can induce heterologous immunity to severe acute respiratory syndrome coronavirus 2 (SARS-CoV-2) derived peptides and that vaccination with the SARS-CoV-2 spike protein can induce heterologous immunity to bacterial peptides. Using *in silico* prediction methods, we identified 6 bacterial peptides with sequence homology to either the spike protein or non-structural protein 3 (NSP3) of SARS-CoV-2. Notwithstanding the effects of bystander activation, *in vitro* co-cultures showed that all individuals tested (n=18) developed heterologous immunity to SARS-CoV-2 peptides when sensitized with the identified bacterial peptides. T cell recall responses measured included cytokine production (IFN-γ, TNF, IL-2), activation (CD69) and proliferation (CellTrace). As an extension of the principle of heterologous immunity between bacterial pathogens and COVID-19, we tracked donor responses before and after SARS-CoV-2 vaccination and measured the cross-reactive T cell responses to bacterial peptides with similar sequence homology to the spike protein. We found that SARS-CoV-2 vaccination could induce heterologous immunity to bacterial peptides. These findings provide a mechanism for heterologous T cell immunity between common bacterial pathogens and SARS-CoV-2, which may explain the high variance in COVID-19 outcomes from asymptomatic to severe. We also demonstrate proof-of-concept that SARS-CoV-2 vaccination can induce heterologous immunity to pathogenic bacteria derived peptides.

Keywords: COVID-19, pathogenic bacteria, heterologous immunity, SARS-CoV-2 vaccine, cross-reactivity, memory T cell

INTRODUCTION

Heterologous immunity is when a memory T cell response elicited by one pathogen recognizes another pathogen. Heterologous immunity arising from epitope homology between severe acute respiratory syndrome coronavirus 2 (SARS-CoV-2) and other human coronaviruses has been identified as a mode of cross-protection from coronavirus disease 2019 (COVID-19) (1) (2). Additionally, individuals unexposed to SARS-CoV-2 have been shown to possess SARS-CoV-2-specific T cells (3–8). Heterologous immunity between other bacteria, such as *Mycobacterium bovis*, the bacteria contained in Bacille Calmette-Guérin vaccine (BCG), and SARS-CoV-2 has been shown as a mechanism of heterologous T cell cross-reactive immunity (9). Therefore, heterologous immunity is offered as one explanation for the variable outcomes of COVID-19 severity. However, the mechanism of heterologous immunity between SARS-CoV-2 and pathogenic bacteria has not been characterised.

Common bacterial pathogens encountered by humans throughout life produce symptoms ranging from mild to severe depending on the bacterium involved, the site of infection and the ability of the individual to mount a successful immune response to the infection. T cell involvement in clearing bacterial pathogens seeds memory T cells, which exhibit heightened functional responses upon re-infection yet can wane over time (10). These antigen-specific T cells may be able to cross-react with unrelated pathogens sharing regions of amino acid sequence homology that can act as a mimic in T cell recognition of peptide- major histocompatibility complex (MHC) in a phenomenon termed heterologous immunity (1). Re-infection with a different pathogen sharing homology regions therefore has the potential to activate these T cells and provide a level of heterologous immunity (11).

T cells forming part of an orchestrated immune response are crucial to combatting COVID-19 as COVID-19 convalescent individuals have been shown to exhibit SARS-CoV-2 specific T cell memory, whereas T cell imbalance and dysfunction is linked to severe manifestations of COVID-19 (12, 13).

In this study, we assessed *via* an *in vitro* mechanism whether pathogenic bacterial-peptide-primed T cells exhibit cross-reactivity with SARS-CoV-2-peptide or protein homologues. We extended this mechanism using direct *ex-vivo* human blood samples to assess whether SARS-CoV-2 vaccination seeds memory T cells with the capacity to cross-react with these bacterial epitopes.

MATERIALS AND METHODS

Blood Samples

Whole blood was collected from healthy donors unexposed to SARS-CoV-2 (n = 18; age: 21 to 42 years; sex: 50% [9/18] male, 50% female [9/18]). Donors were confirmed to be unexposed to SARS-CoV-2, i.e. did not display symptoms of COVID infection, did not have a prior COVID-19 infection, and were seronegative for IgG/M SARS-CoV-2 by SARS-CoV-2 Colloidal Gold Immunochromatography Assay (MyBioSource). Six of the 18 healthy donors were subsequently vaccinated either with AstraZeneca ChAdOx1-S (n = 1) or COMIRNATY BNT162b2 (mRNA) vaccine (n = 5). SARS-CoV-2 spike seroconversion was verified by IgG/M SARS-CoV-2 Colloidal Gold Immunochromatography Assay in all 6 donors and whole blood was collected for pre- and post-vaccination analyses.

Ethics

The project was performed according to the Declaration of Helsinki and was approved by Monash University Human Research Ethics Committee (project ID 25834). All donors provided written informed consent.

Immune Cell Isolation

Human peripheral blood mononuclear cells (PBMCs) were isolated from fresh whole blood by Lymphoprep density gradient medium in SepMate tubes (Stemcell) and cell number was enumerated by 0.4% (v/v) trypan blue (Sigma) on a haemocytometer. PBMCs were used for CD14+ CD16- monocyte isolation using EasySep Human Monocyte Isolation Kit (Stemcell). Freshly isolated monocytes were then differentiated into mature or immature dendritic cells (DCs) using ImmunoCult DC Culture Kit according to the manufacturer's instructions (Stemcell). Thawed PBMCs were treated with 100μg/mL DNAse I solution (Stemcell) for 15 minutes at room temperature before downstream use. CD3+ T cells were isolated from PBMCs using EasySep Human T Cell Isolation Kit (Stemcell).

Human Leukocyte Antigen Typing

High resolution (n=7) and low resolution (n=3) human leukocyte antigen (HLA) typing of class I and II alleles was performed by the Australian Red Cross Victorian Transplantation and Immunogenetics Service by next-generation sequencing (**Table S2**). To assess whether HLA typing was necessary, 8 donors were not HLA typed.

Peptide Selection and Alignment

The SARS-CoV-2 proteome (sequence ID NC_045512.2) was interrogated for sequence homology to bacteria (taxid:2) using the National Center for Biotechnology Information (NCBI) Protein BLAST search (https://blast.ncbi.nlm.nih.gov/Blast.cgi). Results were filtered to include only bacteria reported to be pathogenic to humans based on a literature search and then filtering to include homology sequences of at least 15 amino acids in length, sufficiently long enough for recognition by T cells. The 6 homologous 15mers showing highest homology between SARS-CoV-2 and pathogenic bacteria were then selected for analysis. Specifically, protein sequences from SARS-CoV-2 non-structural protein 3 (NSP3, YP_009725299.1) and SARS-CoV-2 spike glycoprotein (YP_009724390.1) with homologous bacterial protein sequences to *K. pneumoniae* O-acetyl-ADP-ribose deacetylase (PLK93285.1), *E. coli* and *C. freundii* O-acetyl-ADP-ribose deacetylase (WP_016149912.1), *K. pneumoniae* serine acetyltransferase (STW66654.1), *S.* Enteritidis AraC family transcriptional regulator (EBV2373563.1), *E. faecalis* AAA family ATPase (WP_025192929.1), *S. aureus* AAA family ATPase (MVH71995.1), *K. grimontii* AAA family ATPase (WP_155004179.1), *C. difficile* putative phosphatase (VTR10613.1), *Clostridium* spp. macro domain containing protein (WP_039218766.1) and human CLIP

(NP_001020330.1) were sourced from NCBI Protein Database (https://www.ncbi.nlm.nih.gov/protein/). SARS-CoV-2 and bacterial peptide homologues were aligned to reveal amino acid similarity and identity using EMBOSS Needle Pairwise Sequence Alignment using the BLOSUM62 matrix (14). EMBOSS Needle Pairwise Alignment was also used to align the bacterial 15mer sequences to known human coronaviruses using sequences from the NCBI Protein Database, namely SARS-CoV-2 ORF1ab (QHD43415.1), Severe Acute Respiratory Syndrome Coronavirus 1 (SARS-CoV) ORF1ab (NP_828849.7), Middle East Respiratory Syndrome Coronavirus (MERS) ORF1ab (YP_009047202.1), OC43 ORF1ab (YP_009555238.1), HKU1 ORF1ab (YP_173236.1), NL63 ORF1ab (YP_003766.2), 229E ORF1ab (NP_073549.1), SARS-CoV-2 spike (YP_009724390.1), SARS-CoV spike (YP_009825051.1), MERS spike (YP_009047204.1), OC43 spike (YP_009555241.1), HKU1 spike (YP_173238.1), NL63 spike (YP_003767.1) and 229E spike (NP_073551.1). SARS-CoV-2 variant analysis was performed on data obtained from Pangolin (https://cov-lineages.org/) and Centers of Disease Control and Prevention SARS-CoV-2 Variant Classifications and Definitions (https://www.cdc.gov/coronavirus/2019-ncov/variants/variant-info.html) using data available up to 1 January 2022.

Peptide and Protein

Peptides were synthesised as 15mers with an N-terminus free amine (H-) and a free acid group at the C-terminus (-OH) (Mimotopes). Peptide purity was determined as ≥90% by reversed-phase high-performance liquid chromatography. Peptide sequences used in this study are listed in **Figure 1** and control peptide $CLIP_{103-117}$ (PVSKMRMATPLLMQA). Peptides were reconstituted in 5% dimethyl sulfoxide (DMSO, Sigma) in sterile water (v/v). The final concentration of peptides used *in vitro* was 10µg/mL and 0.005% DMSO (v/v). SARS-CoV-2 recombinant proteins NSP3 and spike glycoprotein were purchased from MyBioSource. Proteins were >90% pure as determined by sodium dodecyl sulphate–polyacrylamide gel electrophoresis (SDS-PAGE) quantitative densitometry by Coomassie Blue staining. Proteins were reconstituted in sterile H_2O and used *in vitro* at 10µg/mL.

Peptide-HLA Binding Affinity

HLA allele global coverage of HLA-typed donors was calculated using Immune Epitope Database Analysis Resource – Population Coverage (15). NetMHCpan 4.1 was used across each bacterial homology region broken into 9mers overlapping by 1 amino acid for peptide- major histocompatibility complex (MHC) class I binding affinity. NetMHCIIpan 4.0 was used across each

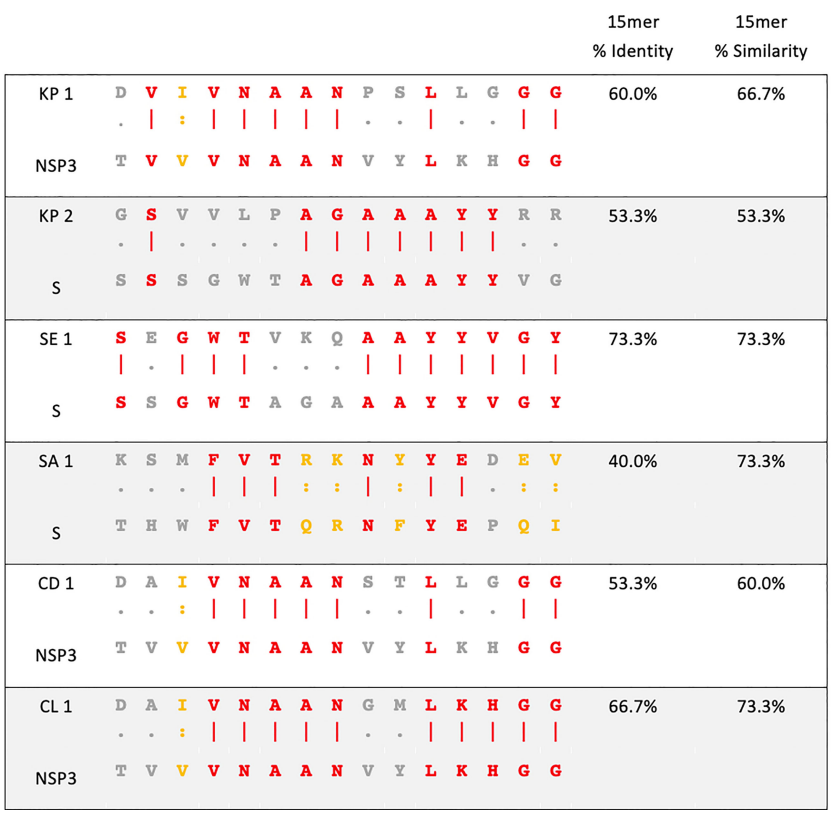


FIGURE 1 | Sequence homology between pathogenic bacteria and SARS-CoV-2. Amino acid sequence alignment of pathogenic bacteria (top) and SARS-CoV-2 (bottom) used in this study. KP- *Klebsiella pneumoniae*, SE- *Salmonella* Enteritidis, SA- *Staphylococcus aureus*, CD- *Clostridioides difficile*, CL- *Clostridium* spp., NSP3- non-structural protein 3 of SARS-CoV-2, S- spike glycoprotein of SARS-CoV-2. Red amino acid- identity. Yellow amino acid- similarity. Grey amino acid- no identity or similarity.

bacterial homology region broken into 15mers overlapping by 1 amino acid for peptide-MHC class II binding affinity (16). HLA alleles were chosen to reflect a globally representative collection of alleles as well as including the alleles of HLA-typed donors used in this study (17, 18).

Intracellular Cytokine Staining Co-Culture

Intracellular cytokine staining (ICS) *in vitro* co-culture was established for assessing T cell cross reactivity, as reported previously (19, 20). Briefly, a completely autologous co-culture of 10^5 freshly isolated human CD3+ T cells, 10^4 human immature DCs pulsed with 10μg/mL of bacterial peptide (**Figure 1**) or control peptide (PVSKMRMATPLLMQA) was established in 96 well round bottom plates (100uL/well). Positive assay control received anti-human CD2, anti-human CD3, and anti-human CD28 coated MACS iBeads (Miltenyi). Negative assay control received no peptide. Five days later, the co-culture was supplemented with 40IU/mL recombinant human IL-2 (Stemcell) and re-incubated for 2 more days before resting the culture by washing twice with PBS and re-incubation in media without peptide. After 2 days resting with no IL-2 and no peptide, 10^4 immature DCs pulsed with one of the SARS-CoV-2-peptides, recombinant SARS-CoV-2 spike protein, NSP3 protein or control peptide (PVSKMRMATPLLMQA) and 1μg/mL anti-human CD28 (clone CD28.2, eBioscience) were added. 1X protein transport inhibitor cocktail (eBioscience) was added. Positive assay control received anti-human CD2, anti-human CD3, and anti-human CD28 coated MACS iBeads (Miltenyi). Negative assay control received no peptide. Culture was incubated for 6 hours after which cells were harvested for flow cytometry analysis by ICS.

HLA blocking to verify the cross-reactive T cell responses arise from T cell interaction with peptide-MHC. HLA blocking for CD4+ T cells was achieved by mouse anti-human HLA DR/DP/DQ antibody (clone TU39, eBioscience). In instances where HLA typed individuals were *in silico* predicted to bind to only one MHC class II allele (e.g. only HLA-DP, and not -DR or -DQ), we blocked with an antibody specific for only that HLA molecule (e.g. mouse anti-human HLA-DP, clone B7/21, Abcam). HLA blocking on CD8+ T cells was achieved by mouse anti-human HLA-A/B/C antibody (clone W6/32, eBioscience). Isotype controls used were mouse IgG2a kappa (clone eBM2a, eBioscience) and mouse IgG3 (clone B10, eBioscience). Samples received 10μg/mL of individual blocking antibody to the immature DCs for 1 hour at 37°C in a 5% CO_2 incubator before pulsing with SARS-CoV-2 peptide followed by the ICS culture and staining protocol.

Direct *ex vivo* pre- and post-vaccinated ICS cultures were established as above ICS protocol with CD3+ T cells, immature DCs and bacterial peptide except the co-culture was incubated for only 2 hours after addition of peptide, after which protein transport inhibitor was added for 6 hours followed by ICS by flow cytometry.

Intracellular Cytokine Staining Flow Cytometry

Cells were harvested and initially stained with Live/Dead Fixable Near Infra-Red Dead Cell Stain Kit (Invitrogen). Surface marker staining was performed with anti-human CD3 Brilliant Violet 510 (clone OKT3, Biolegend), anti-human CD4 allophycocyanin (APC, clone OKT4, eBioscience), anti-human CD8 Alexa Fluor 488 (clone HIT8a, Biolegend) and anti-human CD69 Brilliant UV 395 (clone FN50, BD) followed by fixation and permeabilisation using Transcription Factor Staining Buffer Set (eBioscience). Intracellular marker staining was performed with anti-human interferon-γ (IFN-γ) Phycoerythrin-Cyanine7 (PE Cy7, clone 4S.B3, eBioscience), anti-human tumour necrosis factor (TNF) Brilliant Violet 421 (clone Mab11, Biolegend), anti-human IL-2 Brilliant Blue 700 (clone MQ1-17H12, BD) and anti-human perforin Phycoerythrin (PE, clone B-D48, Biolegend). In some samples, to assess T memory phenotypes, anti-human CD45RA Brilliant Violet 786 (clone HI100, BD) was added and CD69-BUV395 was replaced with CCR7-BUV395 (clone 3D12, BD) and Perforin-PE was replaced with CD69-PE (clone FN50, BD). Then, CD45RA vs. CCR7 quadrant gating of Tcm, Tem, TEMRA, T naïve and T memory subsets was performed. Single color controls were prepared using UltraComp eBeads (Invitrogen) for single colour control antibodies and ArC amine reactive compensation bead kit (Invitrogen) for Live/Dead single colour control. After staining, cells were resuspended in PBS and acquired on an LSR-Fortessa X20 flow cytometer (BD) using BD FACSDiva software version 8.0.1. Samples were analysed in FlowJo 10.6.2. Fluorescence minus one (FMO) controls were used to determine positive gating and gating strategy is found in **Figure S3A**. Positive and negative controls indicated successful assay conditions. Positive control stimulation with anti-human CD2, anti-human CD3, and anti-human CD28 coated MACS iBeads indicated CD8+ T cells showed mean % positive of 70.85%, 7.89%, 4.24%, 51.99% and 61.2% for parameters IFN-γ+, TNF+ IL2+, CD69+ and perforin+, respectively. Positive control CD4+ T cells showed a mean % positive of 54.87%, 16.16%, 8.53% and 48.87% for parameters IFN-γ+, TNF+, IL-2+ and CD69+, respectively. Negative control stimulation with no peptide values are shown in **Figures 2** and **3**. Responder individuals showed positive staining after subtraction of the primary SARS-CoV-2 response control (control-peptide-primed, SARS-CoV-2-peptide restimulated). Non-responder individuals showed no positive staining after subtraction of the primary SARS-CoV-2 response control (**Figure S2**). For quantitative and statistical analysis (**Figures 2** and **3**), the responders were selected and had the restimulation background control (bacterial-peptide primed and irrelevant peptide restimulated) subtracted from the corresponding bacterial-peptide primed, SARS-CoV-2 test sample and the primary SARS-CoV-2 response control to remove any assay-related background responses.

Proliferation Co-Culture

Proliferation co-culture was established using previously reported dual stain proliferation assay. Briefly, a completely autologous co-culture was set up with 10^5 CD3+ T cells stained with Cell Trace Yellow (CTY, Invitrogen) and co-cultured with 10^4 mature DCs pulsed with 10μg/mL bacterial peptide (**Figure 1**) or control peptide (PVSKMRMATPLLMQA) in 96 well round-bottom plate (Corning) at 100μL/well. After 7

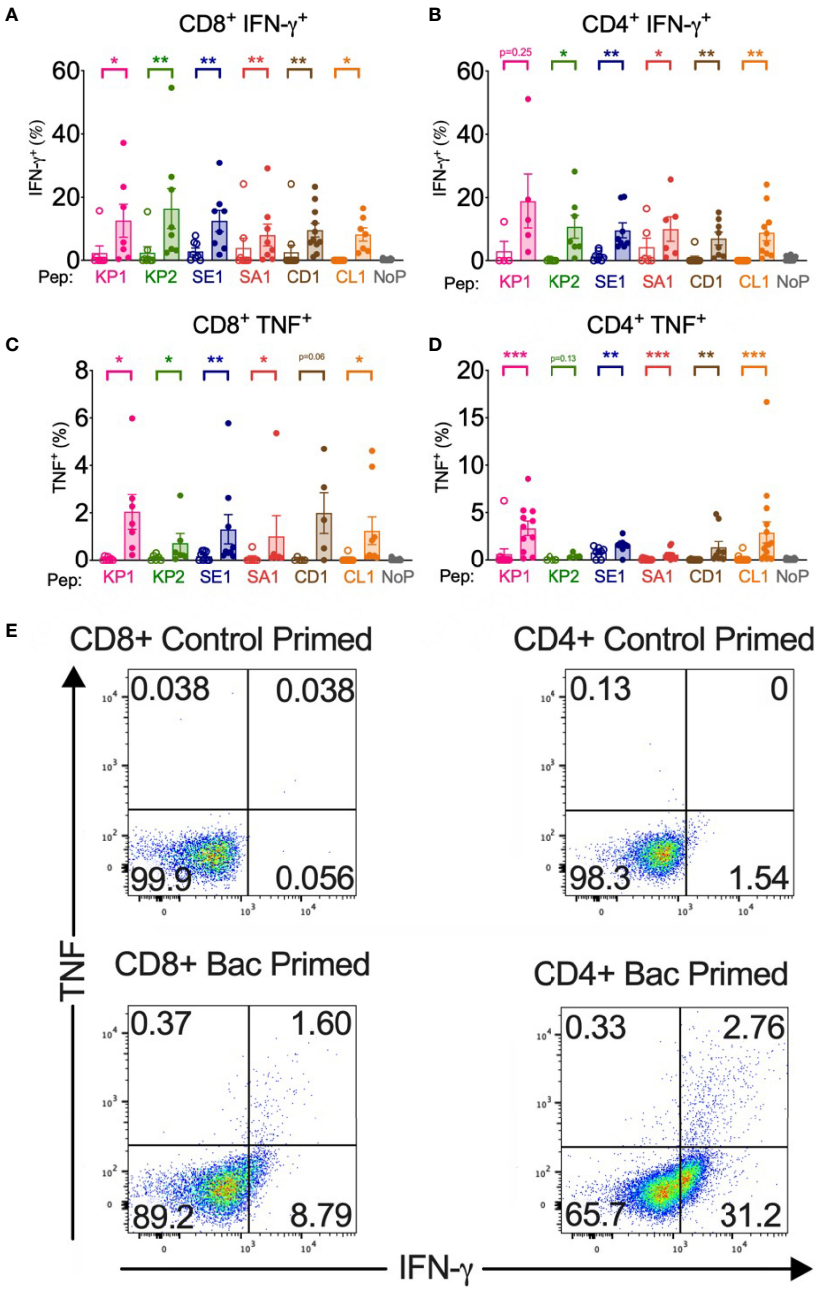


FIGURE 2 | Bacterial peptide priming enhances SARS-CoV-2 T cell cytokine expression in responders. Pathogenic bacterial peptide **(bac)** primed T cells restimulated with SARS-CoV-2-peptide measured by flow cytometry with background control values subtracted. Unshaded bars- Control primed (irrelevant peptide, PVSKMRMATPLLMQA), then restimulated with SARS-CoV-2 homologous peptide. Shaded bars– bac primed (KP1, KP2, SE1, SA1, CD1 or CL1) then SARS-CoV-2-peptide homologue restimulated. NoP – no peptide negative control. **(A)** CD8+ IFN-γ+ responses (n=7-12), **(B)** $CD4^+IFN\text{-}\gamma^+$ responses (n=5-10), **(C)** $CD8^+TNF^+$ responses (n=5-9), **(D)** $CD4^+TNF^+$ responses (n=4-15), **(E)** Representative TNF (y-axis) and IFN-γ (x-axis) dot plots of a responder donor with their corresponding SARS-CoV-2 primary response control. $^*P < 0.05$, $^{**}P < 0.01$, $^{***}P < 0.001$ by Wilcoxon-matched-pairs-signed-rank test, comparing magnitude of response to SARS-CoV-2 peptides with or without bacterial peptide priming.

days incubation at 37°C and 5% CO_2, cells were rested by washing 2X with PBS and re-incubation in media without peptide for 2 days. 2 days later, the culture was stained with Cell Trace Violet (CTV, Invitrogen). Then 10^4 SARS-CoV-2 peptide-pulsed mature DCs (or control pulsed) were added to the culture before incubation for 7 more days when they were harvested for flow cytometry analysis. At no stage was IL-2 added to the culture. Positive assay control received anti-human

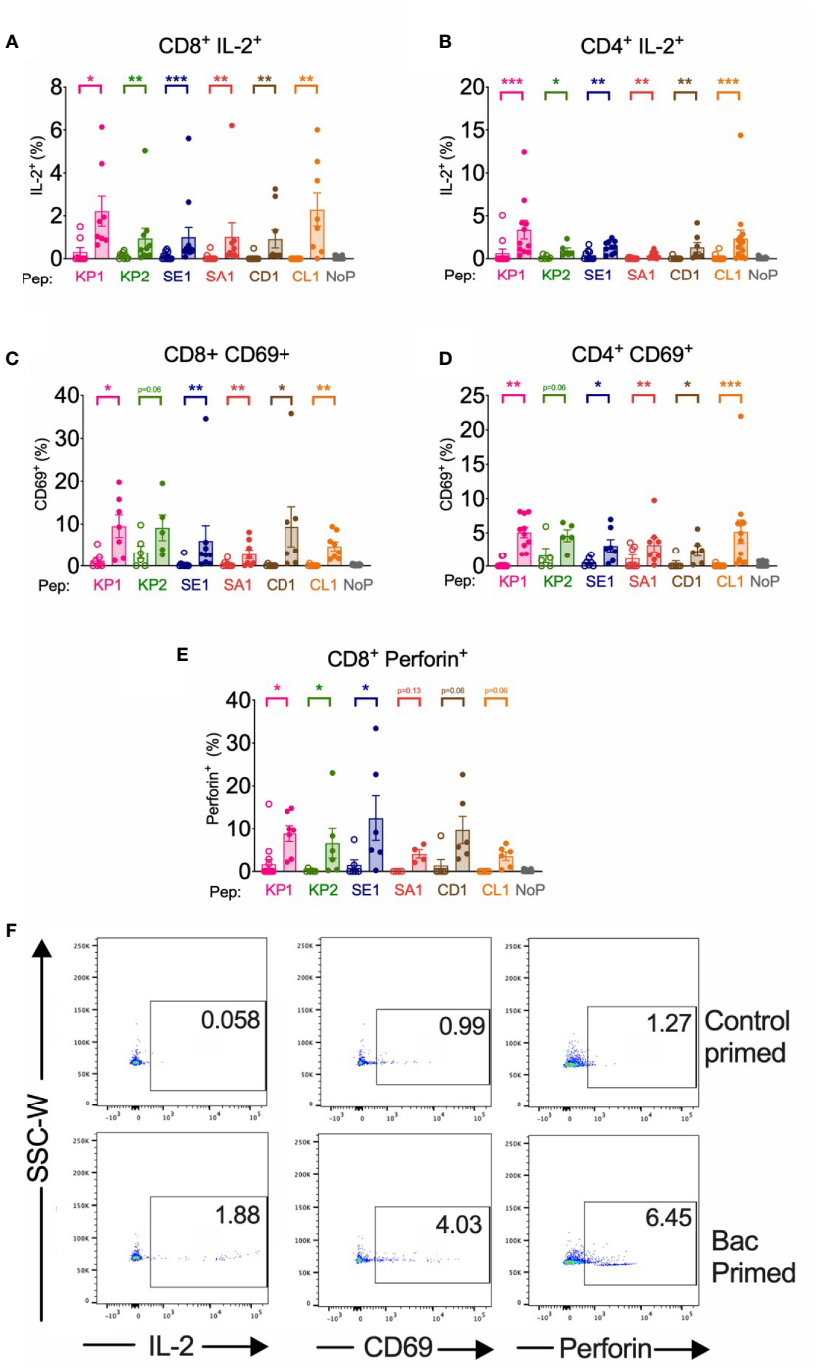


FIGURE 3 | | Bacterial peptide priming enhances IL-2, CD69 and Perforin T cell responses against SARS-CoV-2 in responders. Pathogenic bacterial-peptide (KP1, KP2, SE1, SA1, CD1 or CL1) primed (shaded bars) or control primed with irrelevant peptide (unshaded bars) $CD3^+$ T cells were restimulated with SARS-CoV-2-peptide-homologue-pulsed DCs for 6 hours and analysed by flow cytometry with background control values subtracted. NoP – no peptide negative control. $^*P < 0.05$, $^{**}P < 0.01$, $^{***}P < 0.001$ by Wilcoxon matched-pairs signed rank test. **(A)** $CD8^+$ IL-2^+ responses (n=8-12). **(B)** $CD4^+$ IL-2^+ responses (n=6-14). **(C)** $CD8^+$ $CD69^+$ responses (n=5-9). **(D)** $CD4^+$ $CD69^+$ responses (n=5-12). **(E)** $CD8^+$ $Perforin^+$ responses (n=4-15). **(F)** Representative donor T cell IL-2, CD69 and perforin dot plots of responder control-primed (top) and bacterial peptide (bac)-primed (bottom).

CD2,anti-human CD3, and anti-human CD28 coated MACS iBeads (Miltenyi) at the priming and restimulation steps. Negative assay control received no peptide at the priming and restimulation steps.

Pre- and post-vaccination proliferation assay was established as above with CD3+ T cells, mature DCs and bacterial peptides SA1, SE1 or KP2 (**Figure 1**). The T cells were stained initially with CTV only and cultured for 7 days after which CTVlo cells were analysed by flow cytometry and presented as raw data in Figure 6E.

Proliferation Flow Cytometry

Cells were harvested and initially stained with Live/Dead Fixable Near Infra-Red Dead Cell Stain Kit (Invitrogen). Surface marker staining was performed with anti-human CD3 PerCP (clone SK7, Biolegend), anti-human CD4 APC (clone OKT4, eBioscience), and anti-human CD8 Alexa Fluor 488 (clone HIT8a, Biolegend). Controls and gating and responder/non-responders were set up as for the ICS flow cytometry with the addition of Cell Trace Yellow and Violet single colour control using cultured cells. CTY vs. CTV gating was based on the point at which the first cell division took place visible by fluorescence dye dilution. CTY staining T cells before bacterial peptide stimulation, then staining with CTV pre SARS-CoV-2 peptide restimulation enabled us to determine if T cells primed with pathogenic bacterial peptides show enhanced T cell proliferation when restimulated with the SARS-CoV-2 homologous peptide by delineating the T cells which proliferated in priming only, in both priming and restimulation or not at all. Pre- and post-vaccinated proliferation assay was measured by CTV mean fluorescence intensity and presented as raw data (**Figure S6**). Gating strategy for proliferation assays is found in **Figure S3B**. Quantitative and statistical analysis was performed on the proportion of T cells in the $CTY^{lo}CTV^{lo}$ gate, being the T cells that underwent proliferation upon both priming and restimulation (**Figures 4A, B**). For such analysis, the responders were selected and had the restimulation background control (bacterial-peptide primed and irrelevant peptide restimulated) subtracted from the corresponding bacterial-peptide primed, SARS-CoV-2 test sample and the primary SARS-CoV-2 response control to remove any assay-related background stimulation.

Activation-Induced Marker Assay

Activation-induced marker (AIM) assay was established according to previously published protocols (21, 22). Briefly, 500,000 PBMCs were seeded in 96 well U bottom plates (Corning) in 100uL RPMI 1640 (Gibco) supplemented with 10% autologous serum for 3 hours at 37°C, after which 0.5µg/mL of anti-human CD40 (clone HB14, Miltenyi) was added for 15 minutes at 37°C. 10µg/mL of bacterial peptide was then added and incubated for 20 hours at 37°C, after which cells were harvested for flow cytometry.

Activation-Induced Marker Flow Cytometry

AIM markers for the detection of antigen-specific T cells were selected based on previously reported methods (21–23). Cells were harvested and initially stained with Live/Dead Fixable Aqua Dead Cell Stain Kit (Invitrogen). Surface marker staining was performed with anti-human CD3 PerCP (clone SK7, Biolegend), anti-human CD4 APC (clone OKT4, eBioscience), and anti-human CD8 Alexa Fluor 488 (clone HIT8a, Biolegend), anti-human CD69 PE (clone FN50, BD), anti-human CD45RA Brilliant Violet 711 (clone HI100, BD), anti-human CCR7 BUV395 (clone 3D12, BD), anti-human CD137 (4-1BB) Brilliant Violet 421 (clone 4B4-1, BD), anti-human CD134 (OX40) PE Cy7 (clone ACT-35, eBioscience) and anti-human CD154 (CD40L) APC Cy7 (clone TRAP1, BD). Control samples and sample acquisition were prepared as per ICS flow cytometry. AIM assay gating strategy was established (**Figure S3C**). Memory T cells were selected based on expression patterns of CD45RA and CCR7. Co-expression of CD45RA+ and CCR7+ allowed exclusion of the naïve T cell subset, leaving the T memory cells comprising subsets Tem, Tcm and TEMRA, for AIM analysis. On CD4+ T memory cells, AIM+ T cell responses were identified by co-expression of CD134 and CD137 or CD69 and CD154. On CD8+ T memory cells, AIM + T cell responses were identified by co-expression of CD69 and CD137 or CD69 and CD154.

Statistics

Flow cytometry data was processed in R Studio ver.1.3.959 and Graph Pad Prism 7 (Graphpad Software Inc.). A Shapiro-Wilk test to determine normality was performed before a two-tailed, Wilcoxon-matched-pairs-signed-rank test to compare responses of the bacterial primed T cell responders with control-primed responders and between pre- and post-vaccinated samples.

RESULTS

SARS-CoV-2 Protein Homology With Pathogenic Bacteria

BLAST to Determine Regions of Homology

BLAST identified protein sequence homology regions between SARS-CoV-2 spike glycoprotein and NSP3 and pathogenic bacteria protein sequences. The bacterial sequences are present in common bacterial pathogens as well as commensal bacteria known to have the capacity to cause infections. Namely, these bacteria are *Klebsiella pneumoniae, K. grimontii, Escherichia coli, Salmonella* Enteritidis, *Enterococcus faecalis, Staphylococcus aureus, Citrobacter freundii, Clostridioides difficile*, formerly known as *Clostridium difficile, Clostridium haemolyticum* and *Clostridium novyi.*

Six Potential 15mer Peptide Pair Homologues Identified

The homology between pathogenic bacteria and SARS-CoV-2 15mer peptide sequences was 40% to 73.3% identity and 53.3% to 73.3% similarity (**Figure 1**). When the homology regions are processed as 9mers, a sufficient length for MHCI presentation to CD8+ T cells, they exhibited up to 100% similarity and 77.7% identity (**Table S1**).

Pathogenic Bacteria Homology With SARS-CoV-2 Variants of Concern and Other Coronaviruses

Pango lineage analysis of the current SARS-CoV-2 variants of concern B.1.1.7 (Alpha), B.1.351 (Beta), P.1 (Gamma), B.1.617.2

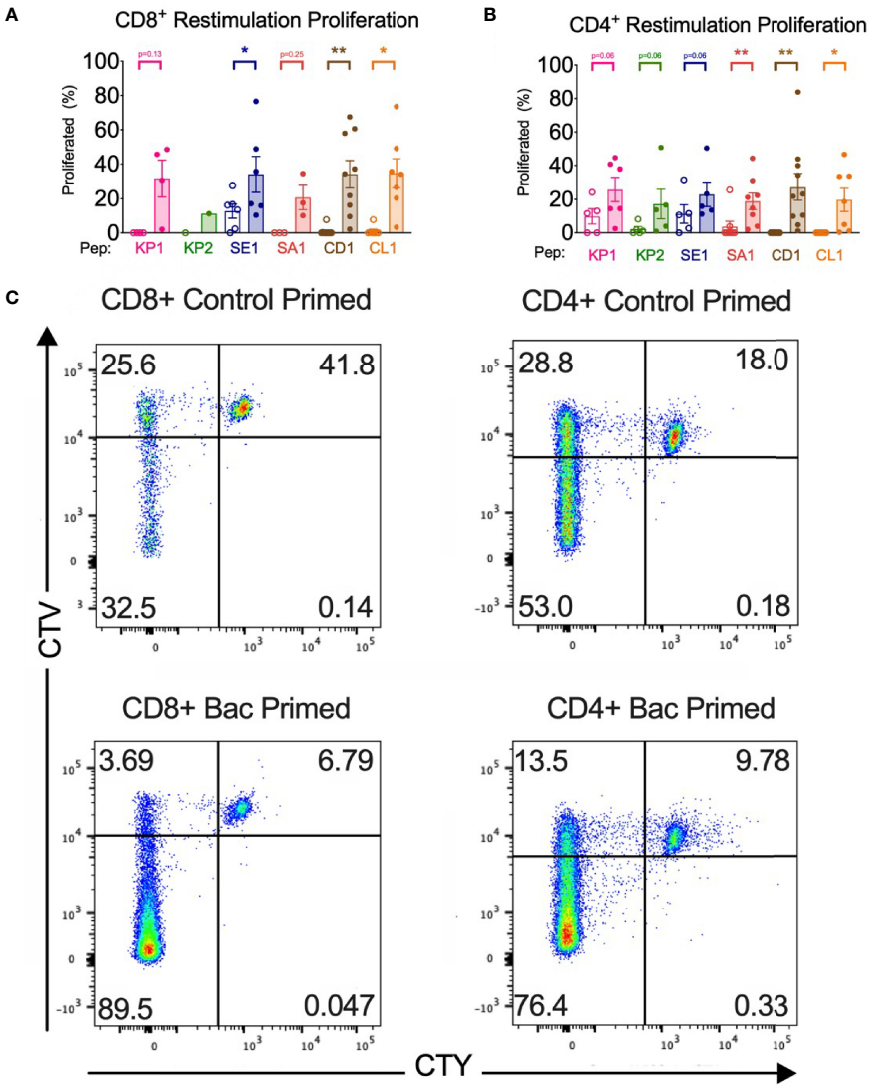


FIGURE 4 | Bacterial peptide priming increases T cell proliferation in responders. **(A)** CD8+ proliferation from restimulation is enhanced by pathogenic bacterial peptide priming (*n*=1-10). **(B)** CD4+ proliferation from restimulation is enhanced by bacterial peptide priming (*n*=5-10). Unshaded bars- Control-primed (irrelevant peptide, PVSKMRMATPLLMQA), then SARS-CoV-2-peptide restimulated. Shaded bars- bacterial peptide primed then SARS-CoV-2-peptide homologue restimulated. $^{*}P < 0.05$, $^{**}P < 0.01$ by Wilcoxon-matched-pairs-signed rank test, comparing the magnitude of response to SARS-CoV-2 peptides with or without bacterial peptide priming after subtraction of the background control. **(C)** Representative CellTrace Yellow (CTY) vs. CellTrace Violet (CTV) dot plots of CD8+ and CD4+ cultured cells. Top right quadrant gate ($CTY^{hi}CTV^{hi}$ cells) did not proliferate upon priming or restimulation. Top left quadrant gate ($CTY^{lo}CTV^{hi}$ cells) proliferated upon priming but not with restimulation. Bottom left quadrant gate ($CTY^{lo}CTV^{lo}$ cells) proliferated upon both priming and restimulation.

(Delta) and BA.1 (Omicron) and other variants of interest B.1.525 (Eta), B.1.526 (Iota), B.1.617.1 and A.23.1 showed no defining amino acid differences to the proteome reference sequence (ID NC_045512.2) at the epitopes overlapping with the regions of homology (**Table S4**). However, some sequences of variant B.1.617.2 (Delta variant) possess a S:W258L mutation (24). This affects the homology of KP2 and SE1 peptide pairs with the KP2 increasing in amino acid identity from 53.3% to 60% and SE1 decreasing in amino acid identity from 73.3% to 66.6%. Sequence alignment of pathogenic bacteria 15mers to other human coronaviruses like the more serious but less common SARS-CoV and MERS-CoV and the more common but less serious OC43, HKU1, NL63 and 229E revealed the 15mers shared some but never complete homology between the pathogenic bacteria 15mer, SARS-CoV-2 15mer and other coronaviruses (**Table S4**). Pathogenic bacteria sequences sharing homology with spike glycoprotein (KP2, SE1 and SA1) all shared more homology with SARS-CoV-2 than any of the other coronaviruses. Whereas pathogenic bacteria sequences sharing homology with NSP3 (KP1, CD1 and CL1) shared either more or less homology with other coronaviruses than SARS-CoV-2, depending on the coronavirus being aligned.

Bacterial Epitopes Have Broad MHCI and MHCII Binding Capacity

The *in silico* binding affinity of bacterial-derived epitopes to bind HLA alleles showed broad MHC class I and II binding capacity across a globally representative dataset. In addition, the HLA-typed donors represented a global MHC class I and II coverage of >97% and similar patterns of broad MHC class I and II binding affinity were observed (**Figures S1A, B**).

Based on both strong binding and high homology, 6 different 15mer peptide pairs from various bacteria were chosen for subsequent *in vitro* analysis (**Figure 1**).

T cells Primed With Bacterial Peptides Have Enhanced Immune Responses to SARS-CoV-2-Peptide Homologues

Summary analysis of CD4+ and CD8+ T cells with the parameters IFN-γ, IL-2, TNF, perforin, CD69 and proliferation assay showed all individuals (n =18) exhibited a positive response in at least one parameter across all 6 tested peptide pairs when primed with bacterial peptide and restimulated with SARS-CoV-2 peptide homologue (**Figure S2**).

Increased Cytokine Responses in CD4+ and CD8+ T Cells

15mer Homologues

CD8+ cytotoxic T cells showed significantly increased TNF, IFN-γ, and IL-2 production in at least 5 of the 6 peptide homologue pairs when pathogenic bacterial peptide primed compared with T cells primed with control peptide (**Figures 2**, **3**). Compared with control primed, TNF mean fold expression significantly increased in CD8+ T cells, except in CD1 (p= 0.06), ranging from 5.9-fold (KP2) to 65.6-fold (CD1) when bacterial peptide primed and SARS-CoV-2 restimulated. IFN-γ mean fold increase in expression from CD8+ T cells significantly increased in all peptide pairs and ranged from 4.1-fold (SA1) to 13.9-fold (KP2). CD8+ T cell IL-2 expression showed a significant mean fold increase from 5.7-fold (KP2) to 16.1-fold (CD1).

CD4+ helper T cells also showed a similar pattern of significantly increased TNF, IFN-γ and IL-2 expression in at least 5 of the 6 peptide homologue pairs (**Figures 2**, **3**). Responder individual CD4+ T cell responses showed IFN-γ significantly increased across 5 of the 6 peptide pairs, ranging from 5.7-fold (SA1) to 15.8-fold (KP1). 5 of the 6 peptide pairs showed a mean fold increase in TNF in CD4+ T cells ranging from 1-fold (SE1) to 132-fold (CD1). IL-2 expression in CD4+ T cells exhibited a significant mean fold increase in all 6 peptide pairs from 2.2-fold (SE1) to 17.9-fold (CL1).

Spike and NSP3 Protein

Recombinant NSP3 protein restimulation after bacterial peptide priming exhibited strong T cell cytotoxicity and thus no data could be generated for KP1, CD1 or CL1. Compared with control-primed and spike protein restimulated, bacterial peptide primed and spike glycoprotein restimulated T cells exhibited increased cytokine responses (**Figure S4**). TNF and IFN-γ responses were significantly increased with KP2 and SA1 primed CD4+ T cells but not SE1 primed CD4+ T cells (IFN-γ+ p = 0.06). IFN-γ responses were significantly increased with KP2 and SA1 primed CD8+ T cells whereas SE1 primed cells did not reach statistical significance (p=0.06). TNF responses were significant only with SE1 primed CD8+ T cells.

Blocking HLA Abolishes Cytokine Responses

As expected, blocking with isotype control antibody showed a positive T cell TNF and IFN-γ response, similar to no antibody treatment. HLA blocking of both MHCI- and MHCII-restricted T cell responses abolished this cytokine response indicating the cross-reactive T cell responses arise from peptide-MHC binding to the T cell receptor (TCR) on the T cell (**Figure S5**).

Potential Anti-Viral Response in CD8+ Cells

We found that in CD8+ T cells primed with pathogenic bacterial-derived peptides KP1, KP2 and SE1 had a significantly increased perforin expression upon SARS-CoV-2 restimulation when compared with control primed cells, whereas SA1, CD1 and CL1 failed to reach significance (p=0.1250, 0.06 and 0.06, respectively) (**Figures 3E, F**). The cross-reactive expression of perforin in responder individuals showed a fold-increase ranging from 4.3-fold (KP1) to 39.3-fold (KP2).

Early Activation in CD4+ and CD8+ T Cells

We found that compared with a SARS-CoV-2 primary immune response, the bacterial peptide primed T cells increased early activation marker CD69 surface expression across 5 of the 6 peptide pairs in both CD4+ and CD8+ T cells (**Figure 3**). CD69 expression exhibited a mean fold increase ranging from 1.8-fold (KP2) to 112-fold (CD1) in CD8+ cytotoxic T cells and from 1.8-fold (SA1) to 97.4-fold (CL1) in CD4+ T helper cells.

Enhanced Proliferation in CD4+ and CD8+ T Cells

All donor samples primed with bacterial peptide then SARS-CoV-2 peptide restimulated developed enhanced T cell proliferation in 5 of the 6 peptide homologue pairs (**Figure S2**). The magnitude of the enhanced proliferative response was quantified in the responders and compared with the proliferative response when control primed and SARS-CoV-2 restimulated with the background control subtracted. In 3 of the 6 tested peptide homologue pairs and across CD4+ and CD8+ T cells, a significant increase in T cell proliferation was observed when bacterial peptide primed and SARS-CoV-2 restimulated compared with control peptide primed and SARS-CoV-2 restimulated (**Figure 4**). T cell proliferation was enhanced in CD4+ cells with a mean fold increase of between 1.02-fold (SE1) and 6.63-fold (KP2) and in CD8+ T cells between 1.67-fold (SE1) and 41.6-fold (CD1). To quantify the initial proportion of T cells proliferating in response to the primary bacterial peptide stimulation, the proportion of CTV^{lo} T cells showed a mean $CD8^+$ T cell proliferation of 33.1% to 59.3% across the 6 bacterial peptides and 3.8% for no peptide. $CD4^+$ T cells showed a mean cell proliferation of 71.9% to 83.5% across the six bacterial peptides and 9.7% for no peptide (**Figure S6**).

An equal number of males (n=9) and females (n=9) were analysed in this study and no significant sex-specific differences were found in the parameters measured.

T Cells Exposed to SARS-CoV-2 Vaccination Have Enhanced Immune Responses to Bacterial-Peptide Homologues

Increased Cytokine Responses in CD4+ and CD8+ T Cells

Direct *ex vivo* cytokine responses of bacterial-peptide-stimulated CD4+ and CD8+ T cells obtained before SARS-CoV-2 vaccination exhibited lower IFN-γ; TNF and IL-2 expression than T cells obtained from the same individuals (n=6) at least 2 weeks after their second SARS-CoV-2 vaccination (**Figure 5**). Compared with pre-SARS-CoV-2 vaccinated samples, IFN-γ+ expression increased by 46.8%, 77.6% and 41.9% in CD8+ cytotoxic T cells stimulated with SA1, SE1 and KP2 peptides, respectively, from post-SARS-CoV-2 vaccinated samples. CD8+ TNF+ expression increased by 58.8%, 65.1% and 67.3% for SA1, SE1 and KP2 peptide stimulation, respectively. Mean CD8+ IL-2+ expression increased by 58.7%, 45.6% and 61.2% for SA1-, SE1- and KP2-pulsed DC stimulation, respectively. On CD4+ T cells, IFN-γ+ showed a mean increase of 43.6%, 48.9% and 38.6% for peptides SA1, SE1 and KP2, respectively. Mean CD4+ TNF+ expression increased from pre- to post-vaccinated donors by 32.0%, 58.6% and 66.2% for SA1, SE1 and KP2, respectively. CD4+ IL-2+ expression increased by 59.4%, 43.8% and 65.8% for SA1, SE1 and KP2 pulsed DC stimulation, respectively. Overall, across the 18 parameters tested, 12 reached statistical significance and each of the 3 peptides showed statistical significance in 4 of the 6 parameters tested. Direct *ex vivo* cytokine responses of SARS-CoV-2-peptide stimulated T cells before and after SARS-CoV-2 vaccination showed post-SARS-CoV-2 vaccination responses were demonstrably higher than before vaccination (**Figure S8**).There was a significant difference between the before and after SARS-CoV-2 vaccination samples across the 3 tested SARS-CoV-2 peptide homologues in the parameters CD4+ IFN-γ+; CD4+ TNF+ and CD8+ TNF+ but not in CD8+ IFN-γ+ (p=0.06). Compared with the SARS-CoV-2-peptide-stimulated, post-vaccination samples, the bacterial-peptide-stimulated, post-vaccination samples exhibited similar yet slightly lower IFN-γ responses ranging from a 0.010 to 0.23 fold decrease in mean IFN-γ expression across both CD4+ and CD8+ T cells. TNF responses showed a greater decrease with bacterial peptide stimulated post-vaccination samples exhibiting a mean fold decease ranging from 0.20 to 0.61 across CD4+ and CD8 + T cells for the 3 peptide pairs tested.

IFN-γ+ or TNF+ T Cells Predominantly Memory T Cells

We found that most IFN-γ+ or TNF+ T cells isolated from post-vaccinated samples were of a memory phenotype, being T effector memory (Tem), T central memory (Tcm) or T effector memory re-expressing CD45RA (TEMRA) (**Figure S7**). Of the CD4+ IFN-γ+ *ex-vivo* T cells, 81.14%, 81.22% and 83.06% were of memory phenotype for SA1, SE1, KP2 stimulated, respectively. The CD69+ population of CD4+ cells compared with total CD4+ cells also exhibited an increase in memory cell populations Tem and Tcm and a decrease in naïve T cells.

Enhanced Proliferation in CD4+ and CD8+ T Cells

We found that both CD4+ and CD8+ T cells underwent increased T cell proliferation in response to the 3 peptide homologues SA1, SE1 and KP2 in the post-vaccinated samples compared with the donor-matched pre-vaccinated sample as indicated by a dilution of proliferation dye as the cells undergo clonal expansion (**Figures 6E, F**). For CD4+ T cells, the mean fold decrease in CTV proliferation dye was -88.8%, -98.8% and -89.5% for SA1, SE1 and KP2, respectively. For CD8+ cytotoxic T cells, the mean decrease in CTV proliferation dye was -63.6%, -61.8% and -70.3% for SA1, SE1 and KP2, respectively. These results were significant in all 3 peptides for both CD4+ and CD8+ T cells.

Increased Antigen-Specific CD4+ and CD8+ T Memory Cells

After subtraction of the irrelevant peptide (PVSKMRMATPLLMQA) background stimulation control, we observed that when memory T cells were stimulated with the bacterial homologue peptides SA1, SE1 and KP2, the proportion of AIM+ cells increased in the post-SARS-CoV-2 vaccinated samples compared with pre-vaccinated (**Figures 6A–D**). AIM+ CD69+ CD154+ CD8+ memory T cells showed a mean increase of 79.4%, 87.1% and 88.9% for SA1, SE1 and KP2 peptide stimulation, respectively. Alternate AIM+ markers on CD8+ memory T cells by CD137+ CD69+ showed a mean increase of 76.7%, 96.7% and 91.1% for SA1, SE1 and KP2 peptide stimulation, respectively. AIM+ CD4+ memory T cells by CD134+ and CD137+ co-expression exhibited a mean increase of 79.6%, 91.3% and 90.9% % for SA1, SE1 and KP2 peptide stimulation, respectively. Alternate CD4 + AIM markers CD154+ and CD69+ on memory T cells exhibited a mean increase of 75.3%, 91.7% and 95.6% % for SA1, SE1 and KP2 peptide stimulation, respectively.

DISCUSSION

Heterologous immunity between SARS-CoV-2 and pathogenic bacteria may offer a mechanistic explanation for the diverse and unpredictable nature of COVID-19 disease severity. Six pathogenic bacteria derived epitopes sharing homology with SARS-CoV-2 spike or NSP3 protein have been shown to bind a broad set of HLA alleles and induce T cell cross reactivity in CD4+ and CD8+ T cells *in vitro*. Furthermore, *ex vivo* responses of memory T cells post-SARS-CoV-2 vaccination exhibited enhanced immune responses to bacterial-peptide homologues.

SARS-CoV-2 Protein Homology With Pathogenic Bacteria

T cell-dependent heterologous immunity can arise *via* TCR-independent or TCR-dependent pathways. TCR-independent heterologous immunity results from non-specific, virus-induced activation of cytokines, such as IL-18 and IL-12, that occurs through bystander activation and without TCR involvement (25, 26). The cytokines produced during the second infection stimulate the memory T cells from the first infection. TCR-dependent heterologous immunity results from direct cross-reactivity between unrelated pathogens, whereby an initial infection or immunisation produces memory T cells that cross-react with antigens from a second, different infection (11). Memory T cells can persist for years yet wane over time meaning

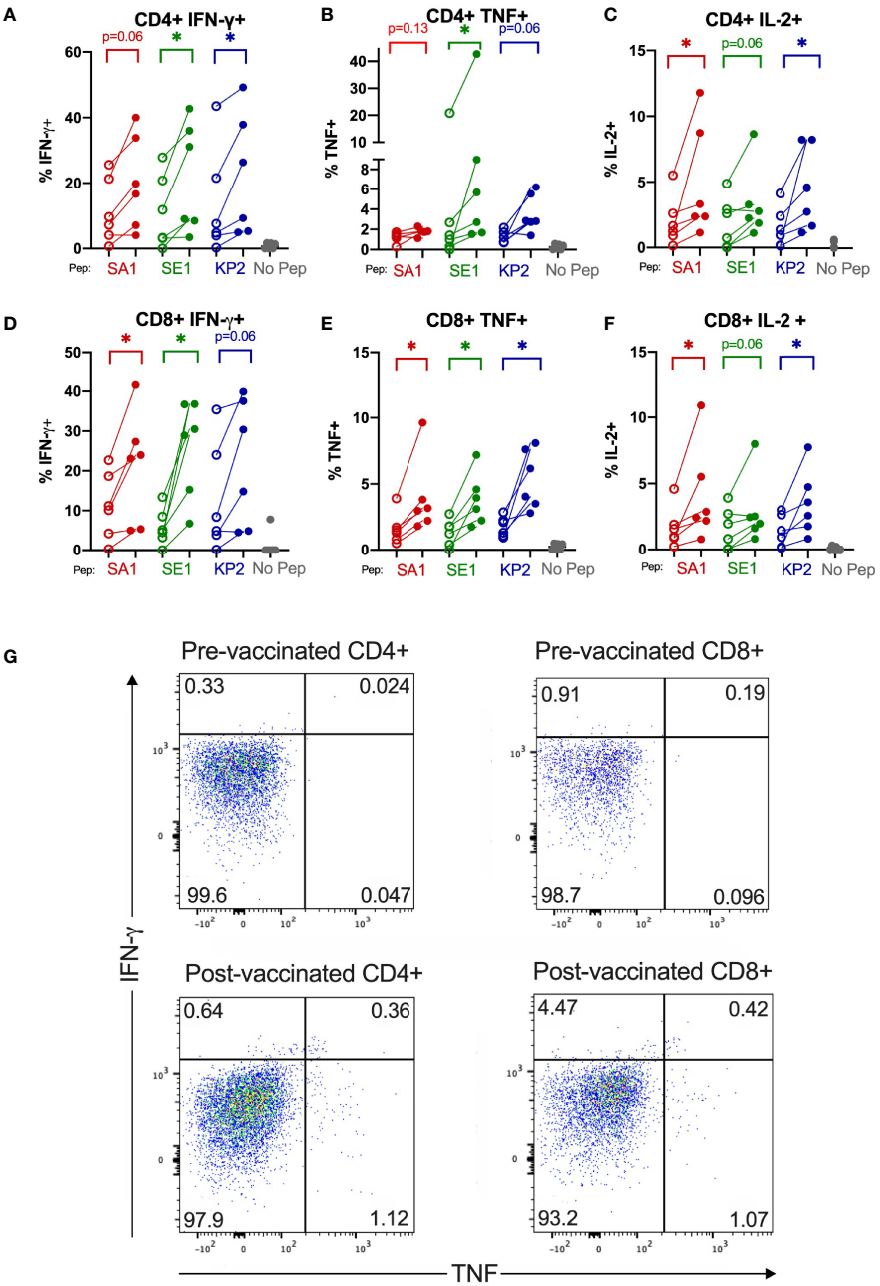


FIGURE 5 | SARS-CoV-2 vaccination enhances T cell cytokine reactivity to pathogenic bacterial homologues. Direct *ex-vivo* T cell responses of donors (n=6) pre-SARS-CoV-2 vaccination (unshaded dots) and post-SARS-CoV-2 vaccination (shaded dots) to pathogenic bacterial peptides sharing homology with SARS-CoV-2 spike (SA1, SE1 and KP2) measured by intracellular cytokine staining. No Pep – no peptide negative control. *$P < 0.05$ by Wilcoxon matched-pairs signed rank test. **(A)** $CD4^+IFN\text{-}\gamma^+$ responses (n= 6). **(B)** $CD4^+TNF^+$ responses (n= 5-6). **(C)** $CD4^+IL\text{-}2^+$ responses (n= 6). **(D)** $CD8^+IFN\text{-}\gamma^+$ responses (n= 6). **(E)** $CD8^+TNF^+$ responses (n= 6). **(F)** $CD8^+IL\text{-}2^+$ responses (n= 6). **(G)** Representative donor T cell TNF (x-axis) and IFN-γ (y-axis) dot plots of pre-vaccinated $CD4^+$ and $CD8^+$ (top) and post-vaccinated CD4+ and CD8+ (bottom) responses to bacterial peptide SE1.

prior exposure from past infections may impact the response to current infections. The phenomenon of TCR-dependent heterologous immunity is the mechanism we explored for cross-reactive responses between pathogenic bacteria and SARS-CoV-2.

In this study, we identified 6 epitopes found in a variety of pathogenic bacteria that share significant homology with spike glycoprotein or NSP3 of SARS-CoV-2 (**Figure 1**). These epitopes were assessed as 15mers, which are of appropriate length to be presented by MHC class II to CD4+ T cells. The 15mers consist

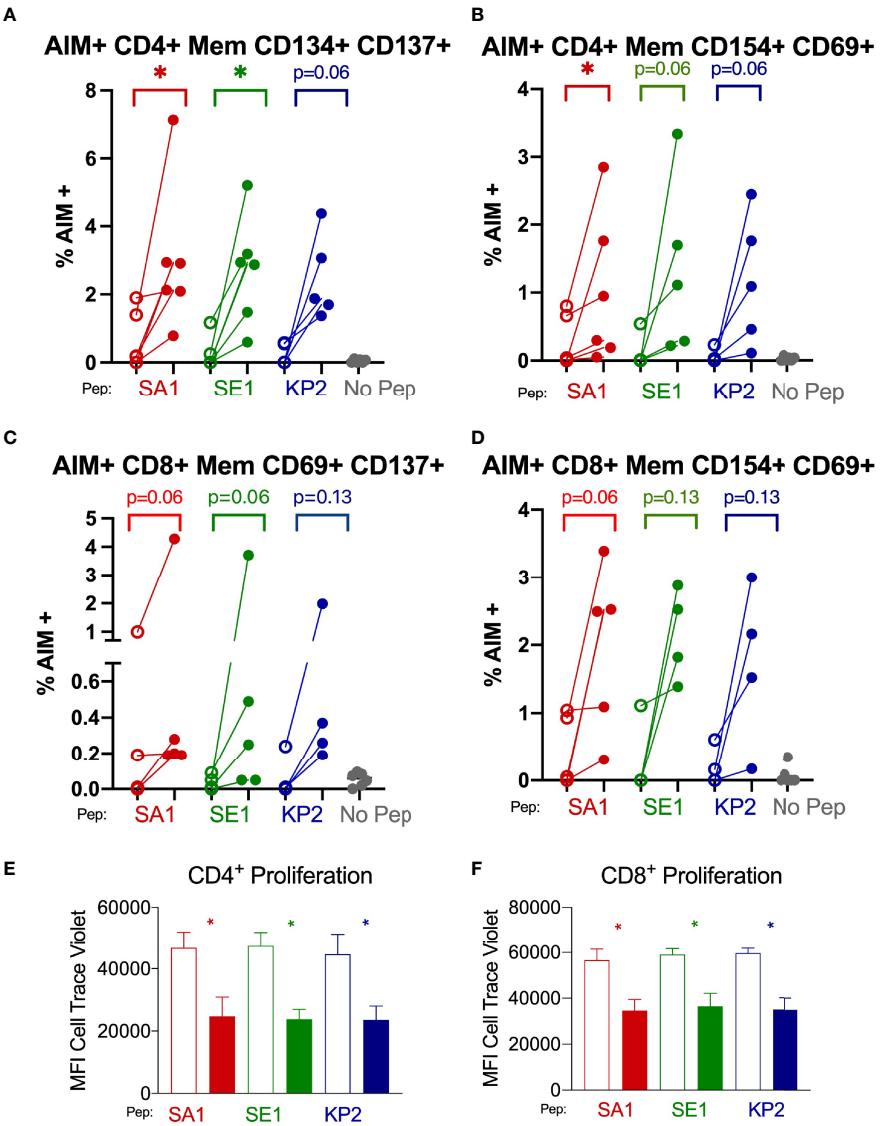


FIGURE 6 | SARS-CoV-2 vaccination enhances T memory cell reactivity to pathogenic bacterial homologues by AIM and proliferation markers Direct *ex-vivo* T memory (Mem) cell responses of donors (n=6) pre-SARS-CoV-2 vaccination (unshaded dots) and post-SARS-CoV-2 vaccination (shaded dots) to pathogenic bacterial peptides sharing homology with SARS-CoV-2 spike (SA1, SE1 and KP2) measured by activation-induced markers (AIM) signifying antigen-specific responses **(A–D)**. 7-day proliferation assay of donors (n=6) pre-vaccination (unshaded bars) and post-vaccination (shaded bars) **(E, F)**. No Pep – no peptide negative control. MFI – mean fluorescence intensity. *P < 0.05 by Wilcoxon matched-pairs signed rank test. **(A)** AIM$^+$ CD4$^+$ T memory cell responses measured by co-expression of CD134 and CD137 (n= 5-6). **(B)** AIM$^+$ CD4$^+$ T memory responses measured by co-expression of CD154 and CD69 (n= 5-6). **(C)** AIM$^+$ CD8$^+$ T memory cell responses measured by co-expression of CD69 and CD137 (n= 4-5). **(D)** AIM$^+$ CD8$^+$ T memory cell responses measured by co-expression of CD154 and CD69 (n= 4-5). **(E)** CD4$^+$ T cell proliferation in response to bacterial peptide homologues pre-and post SARS-CoV-2 vaccination (n= 6). **(F)** CD8$^+$ T cell proliferation in response to bacterial peptide homologues pre-and post SARS-CoV-2 vaccination (n= 6).

of seven 9mers overlapping by one amino acid (**Table S1**), which, through antigen presentation by dendritic cells (DCs), are able to be presented to CD8+ T cells by MHC class I.

The pathogenic bacteria that share homology with SARS-CoV-2 are *K. pneumoniae, K. grimontii, E. coli, S.* Enteritidis, *E. faecalis, S. aureus, C. freundii, C. difficile, C. haemolyticum* and *C. novyi*. They can cause infections ranging from common to rare and previous research has demonstrated T cell involvement in combatting the infections (27–46). They also have the potential to respond *via* heterologous mechanisms to cross-reactive epitopes and some of these bacteria have been isolated from the lower airways of COVID-19 patients (**Table S3**).

Recently, Sulaiman and colleagues studied the microbial signatures in the anatomically relevant lower airways of patients with severe COVID-19 requiring mechanical ventilation (47). Risk analysis from 589 respiratory cultures

taken during hospitalization showed that bacterial culture positivity for *S. aureus, E.coli* and *K. pneumoniae* was associated with increased odds of survival in individuals who survived severe COVID-19 compared with those who died from COVID-19. This resulted in odds ratios of <1 suggesting severe COVID-19 patients who are positive for these bacteria are at less risk of death than those who do not carry the bacteria in their lung. The same study also analysed the microbiome of 142 bronchoalveolar lavage samples and found no statistically significant association between clinical outcomes and culture positivity, however there was a trend towards an increased rate of positive respiratory cultures for *S. aureus*, and *K. pneumoniae* in the survival groups. RNAseq analysis of the bronchoalveolar lavage samples showed a higher differential abundance of *C. difficile* in severe COVID-19 survivors compared with deceased, whereas *S. aureus* in such analysis remained unchanged. The presence of these pathogenic bacteria in severe COVID-19 survivors compared with those who died is interesting because typically bacterial co-infection in other viral respiratory pandemics, such as 1918 and 2009 H1N1 influenza, led to poor prognosis (48, 49). Furthermore, the increased bacterial burden and presence of gut-associated bacteria in the lung also typically leads to poor prognosis in acute respiratory distress syndrome (50, 51). Therefore, the cross-reactive T cell epitopes we have identified may offer a mechanistic explanation for heterogeneous outcomes of COVID-19 disease severity and mortality, particularly in the case of *S.aureus, E.coli, K.pneumoniae* and *C.difficile* co-infection.

The identified bacteria share epitopes with a significant degree of homology to NSP3 or spike glycoprotein of SARS-CoV-2 (**Figure 1**). NSP3 is a papain-like protease that regulates SARS-CoV-2 viral spread and shares homology with O-acetyl-ADP-ribose deacetylase$_{17\text{-}31}$ from bacteria in the family Enterococcaceae, namely *K. pneumoniae, C. freundii* and *E.coli* (KP1) (52). NSP3 also shares homology with putative phosphatase$_{17\text{-}31}$ of *C.difficile* (CD1) and macro domain-containing protein$_{22\text{-}36}$ of *Clostridium* spp. such as *C.novyi* and *C.haemolyticum* (CL1). A recent study showed the NSP3 protein was the 4th most immunodominant SARS-CoV-2 protein for CD4+ T cells and the second most immumodominant protein for CD8+ T cells while spike protein was the most immunodominant SARS-CoV-2 protein for both CD4+ and CD8+ T cells (22).

The spike glycoprotein of SARS-CoV-2 is responsible for catalysing the fusion between viral and target cell membranes to initiate infection and is the key component of SARS-CoV-2 vaccines as well as a target of other therapeutics for COVID-19 (53). The spike protein shares homology with serine acetyltransferase$_{69\text{-}83}$ from *K.pneumoniae* (KP2), AraC family transcriptional regulator$_{279\text{-}293}$ from *S.*Enteritidis (SE1) and AAA family ATPase$_{80\text{-}94}$ from multiple species of family Enterobacteriaceae such as *S.aureus, E.faecalis and K.grimontii* (SA1). These regions of homology overlap with already characterised immunodominant T cell epitopes of SARS-CoV-2 spike (S) protein, namely S$_{258\text{-}266}$, S$_{261\text{-}269}$ and S$_{1101\text{-}1114}$ as MHC class I restricted and S$_{1101\text{-}1115}$ as the class II restricted immunodominant epitope (22). The immunodominant nature of these epitopes highlights their significance in SARS-CoV-2 immunity and their potential role in T cell cross-reactivity with homologous pathogenic bacterial epitopes.

Cross reactivity between other human coronaviruses and SARS-CoV-2 has been characterized and offered as an explanation for the variance of responses to COVID-19 (2). Cross reactivity of the epitopes in this study and other coronaviruses may be relevant in the bacterial epitopes sharing homology with NSP3 because there is shared homology among some coronaviruses for the aligned KP1, CD1 and CL1 sequences, sometimes more so than SARS-CoV-2 (**Table S4**). The cross-reactive potential of the bacterial epitopes KP2, SE1 and SA1 to other coronavirus spike proteins may be of less relevance because all other coronaviruses analysed share less homology to the bacterial sequence than the SARS-CoV-2 sequence. Cross-reactive responses between the bacterial sequences and other coronaviruses may be possible but was not explored in this study.

The emergence of SARS-CoV-2 variants has the potential to impact heterologous immunity to the identified epitopes if the mutations arise at those epitopes. Mutations could arise which either increase or decrease homology and thus impact the extent of a cross-reactive T cell response. To date, no defining SNP within the major variants of concern or variants of interest has impacted the homology regions except for lineage B.1.617.2 (Delta variant) which, in a subset of sequences, contain a S: W258L mutation impacting the homology of the KP2 and SE1 peptide pairs. Since the S:W258L is not a defining SNP of the delta variant, its significance is notable but likely not widespread.

For a T cell to respond to an antigen homologue, the immunogenic homologue must be able to bind with sufficient affinity to cognate MHC class I or II. HLA binding in the context of COVID-19 has been related to disease severity as patients with mild COVID-19 presented MHCI molecules with a higher theoretical affinity than COVID-19 infected individuals with moderate or severe disease (18). Here, we show by *in silico* binding prediction analysis that pathogenic bacteria-derived peptides that share homologous sequences with SARS-CoV-2-derived peptides exhibit broad and high MHC class I and II binding affinity, which permits antigen presentation across a globally representative pool of HLA alleles (**Figures S1A, B**). These high-homology and high-binding peptides were then selected for *in vitro* co-culture analysis (**Figure 1**).

T Cells Primed With Bacterial Peptides Have Enhanced Immune Responses to SARS-CoV-2-Peptide Homologues

Cross-reactive T cell responses were measured by TNF, IFN-γ, IL-2 and perforin expression by ICS, early T cell activation marker CD69 and a two-stain proliferation assay to delineate between a primary and secondary proliferative response. The enhanced cross-reactive responses in T cells primed with bacterial peptide, then SARS-CoV-2 restimulated compared with control primed and SARS-CoV-2 restimulated (**Figure 2**) confirms the high-homology and high and broad peptide-MHC

binding affinity predictions from the *in silico* analysis (**Figures 1**, **S1A, B**). Furthermore, we show the cross-reactive peptide homologues are immunogenic as they are able to elicit broad Th1-like responses in CD4+ T cells and robust CD8+ cytotoxic responses when SARS-CoV-2 peptide or protein restimulated.

IL-2, TNF and IFN-γ cytokine responses were significantly increased in at least 5 of the 6 peptide homologue pairs in both CD4+ and CD8+ T cells (**Figures 2**, **3**). The control primed samples were not all equal to zero, which may be explained by bystander effects. IL-2, TNF and IFN-γ cytokine responses were replicated when using recombinant SARS-CoV-2 spike glycoprotein (**Figure S4**) instead of spike-derived peptide signifying the antigen-specificity of the response stems from the epitope within the 15mer of the spike glycoprotein of SARS-CoV-2, a protein which has been shown to elicit dominant T cell immune responses in COVID-19 infected individuals (22). Furthermore, these data suggest the ability of DCs to process the spike protein and present the cross-reactive epitopes of KP2, SE1 and SA1 to elicit cross-reactive T cell responses in both CD4+ and CD8+ T cells. The use of whole recombinant NSP3 protein as the antigen led to significant T cell cytotoxicity meaning cross-reactive responses using NSP3 protein could not be assessed yet T cells remained viable with NSP3 peptide. NSP3, is a papain-like protease, which is necessary for the generation of the SARS-CoV-2 replicase complex that promotes viral spread and it may be the proteolytic activity of this protein impacting T cell viability *in vitro* (54, 55). NSP3 is also known to elicit immune modulating effects by blocking transcription factors NF-κB and interferon responsive factor 3 (IRF3), which has previously been reported to affect interferons and the innate immune response to SARS-CoV and SARS-CoV-2 infection (52, 56). The immunomodulatory effects of NSP3 may also impact T cell viability in this assay.

Overall, cytokine expression patterns between individuals and peptide pairs varied, which is reflected in the complex pattern of T cell cytokine expression and phenotypes that pathogenic bacteria and SARS-CoV-2 are known to produce (10, 57). This observation is similar to previously reported COVID-19 T cell responses (57) (2).

Cytokine expression was abrogated when HLA-blocking was performed indicating the mechanism behind the T cell responses arises from TCR-dependent heterologous immunity (**Figure S5**).

In cytotoxic T cells, the target cell lysis protein, perforin, significantly increased in the bacterial peptide-primed group compared with control peptide primed across 3 homologue pairs (**Figure 3E**). The increase in perforin expression suggests cross-reactive CD8+ T cells have a heightened capacity to effect an antiviral response by target cell lysis.

Both CD8+ and CD4+ T cell activation and subsequent proliferation were measured by early activation marker CD69 surface expression and proliferation dye dilution by flow cytometry. In at least 5 of the 6 peptide homologue pairs assessed, bacterial peptide sensitised T cells developed significantly enhanced activation and proliferation upon SARS-CoV-2 restimulation (**Figures 3**, **4**). An increase in T cell activation permits clonal expansion of the cross-reactive T cells and enhancement of their effector functions which is necessary to mount an effective SARS-CoV-2 immune response. Indeed, the heightened T cell activation responses likely resulted in heightened proliferative responses shown by proliferation assay where it was seen that 3 of the 6 peptide pairs showed a significant increase in $CTY^{lo}CTV^{lo}$ proliferation when bacterial peptide-primed and SARS-CoV-2 restimulated compared with control (**Figures 4A, B**). Proliferation responses compared between control primed and bacterial peptide-primed showed T cells were able to proliferate even in the control samples, which could be explained by TCR-independent effects such as bystander activation (**Figure 4C**). However, compared to control primed, the samples which underwent bacterial peptide priming proliferated more ($CTY^{lo}CTV^{lo}$).The proliferation assay with two proliferation dyes was set up to differentiate T cells proliferating in response to 1) bacterial peptide priming and not SARS-CoV-2 restimulation ($CTY^{lo}CTV^{hi}$), 2) both bacterial peptide priming and SARS-CoV-2 restimulation ($CTY^{lo}CTV^{lo}$), 3) not bacterial peptide priming but SARS-CoV-2 restimulation ($CTY^{hi}CTV^{lo}$) or 4) neither to bacterial peptide priming nor SARS-CoV-2 restimulation ($CTY^{hi}CTV^{hi}$) (**Figure 4C**). The proliferation assay showed most T cells in response to bacterial peptide priming had proliferated suggesting a proportion of them were clonally expanded, bacterial-peptide specific T cells with the rest proliferating by TCR-independent effects such as bystander activation (**Figure S6**).

In vitro assays were established with CD3+ T cells and dendritic cells as opposed to PBMCs to minimise the immunomodulatory effects other immune cells may have on the DC-T cell interaction and generate a greater resolution of the TCR-dependent responses. Due to the nature of the assay setup, not all T cells are expected to be specific for the bacterial peptide after priming as some T cells would be present after priming whose TCR cannot recognise the bacterial peptide. Upon restimulation, bystander activation has the potential to activate such non-specific T cells and contribute to the cross-reactive response. Furthermore, given there is a degree of sequence homology between the bacterial epitopes, SARS-CoV-2 epitopes and other coronavirus epitopes (Tab. S4), it is possible that some of the responses are heightened by pre-existing memory T cells to other coronaviruses or the bacterial infections. Given the samples were negative for SARS-CoV-2 spike antibodies and donors reported no previous infection with SARS-CoV-2, pre-existing SARS-CoV-2 memory T cells in the *in vitro* assays are not present.

Overall, pre-exposure to the 6 identified epitopes from pathogenic bacteria produce T cells which are able to cross-react with their corresponding SARS-CoV-2 homologous epitope. In the context of human disease, these bacterial pathogens may seed T cell memory which has the capacity to generate heightened T cell responses upon SARS-CoV-2 infection. To date, there have not been studies pairing historical infection with the aforementioned bacterial pathogens and COVID-19 severity. Such studies would be of benefit in elucidating the extent to which such cross-reactive T cells play in COVID-19 severity outcomes.

T Cells Exposed to SARS-CoV-2 Vaccination Have Enhanced Immune Responses to Bacterial-Peptide Homologues

Cytokine responses tracked between individuals before and after SARS-CoV-2 vaccination showed a significant upregulation of proinflammatory cytokines IFN-γ; TNF and IL-2 across both CD4+ and CD8+ T cells. This indicates SARS-CoV-2 vaccination, encoding spike protein, is able to seed T cell memory which has the capacity to cross-react with SA1, SE1 and KP2 epitopes of bacterial origin. Although responses were generally low in pre-vaccinated samples, there was a variation between individuals in the degree of their pre-vaccinated T cell response to the bacterial epitopes, which may be due to T cell memory seeded from prior exposure to the bacterial pathogens. SARS-CoV-2 peptide cytokine responses tracked between individuals were demonstrably higher post-vaccination (**Figure S8**), which indicates successful vaccination seeding the SARS-CoV-2 spike protein T cell memory against the particular epitopes, namely $S_{245\text{-}268}$, $S_{255\text{-}269}$ and $S_{1110\text{-}1114}$ and supports their previously reported immunodominance (22). Cytokine responses compared between post-vaccinated samples stimulated with bacterial or SARS-CoV-2 peptides showed the SARS-CoV-2 peptide stimulated samples were slightly higher than the bacterial peptide stimulated sample. This can be explained by the incomplete homology between bacterial and SARS-CoV-2 epitopes yet highlights that most of the T cells specific for the spike protein were able to cross-react with the bacterial peptide homologue.

The T cells responding to the bacterial epitopes were approximately 80% T memory phenotype (**Figure S7A**). Such a skewing of a memory response as opposed to a primary T cell response from the naïve T cell subset, and the significant increase in cytokine responses post-vaccination suggest the antigen-specific cells arose from prior exposure to the antigen homologue, most likely from SARS-CoV-2 vaccination.

T cell proliferation responses also correlated with the cytokine responses such that there was a significant increase in CD4+ and CD8+ T cell proliferation present in the post-vaccinated samples compared with pre-vaccinated when presented with the bacterial homologue peptides SA1, SE1 and KP2. This is due to the memory T cells generated by SARS-CoV-2 vaccination cross reacting with the bacterial epitopes, due to shared homology, and in turn activating the T cells to undergo clonal expansion. Such cross-reactive proliferative responses may have a role in combatting such bacterial infections in individuals who received SARS-CoV-2 vaccine. However, the presence and extent of any such protection remains to be determined.

Activation-induced marker (AIM) assays allow for the identification of TCR-dependent, antigen-specific T cell responses by analysis of the co-expression of T cell activation markers. It has been shown that bystander activation has little impact on the co-expression of such markers (21). AIM+ T cells have been used to characterise immunodominant T cell epitopes to SARS-CoV-2 and these immunodominant spike epitopes overlap with the homologous sequences in SA1, SE1 and KP2 (22). Our results indicate SA1-, SE1- and KP2-specific T memory cells were increased post-SARS-CoV-2 vaccination. The proposed mechanism for this increase is the homology shared between these bacterial epitopes and the immunodominant T cell epitopes from the spike protein. A subset of the memory T cells created in response to SARS-CoV-2 vaccination have the capacity, through their TCR, to recognise the pathogenic bacterial homologue sequences found in SA1, SE1 and KP2.

Three separate methods of tracking cross-reactive T cell responses pre- and post-SARS-CoV-2 vaccination were explored, namely ICS, proliferation assay and AIM assay and all 3 assays indicated that SARS-CoV-2 vaccination enhances the cross-reactive T cell repertoire to the bacterial epitopes found in SA1, SE1 and KP2. By having such T cell memory against not only SARS-CoV-2 but additionally, through cross reactive TCRs, *K. pneumoniae, S. enteritidis, E. faecalis, S. aureus* and *K. grimontii*, the SARS-CoV-2 vaccine has the potential to confer added T cell mediated immunity to these bacterial pathogens yet this requires further clinical correlations. The mechanism of such peptide homologues acting as cross-reactive B cell epitopes may also exist and warrants further investigation.

Limitations of the Study

It is important to consider these homologous epitopes comprise a small subset of the total number of epitopes possible from these pathogens and accordingly the extent of any cross-reactive effects against such pathogens remains to be determined. Delineation of the critical amino acids contributing to the observed cross-reactivity would assist in further characterising the epitopes. Assays to remove bystander effects would also assist in better resolving the cross-reactive immune responses. Further studies are needed to identify and characterise whether cross-reactivity results in any cross-protection or increased disease risk, particularly assessing disease severity outcomes in patients with such bacterial infections or COVID-19.

CONCLUSION

We have identified 6 epitopes originating from pathogenic bacteria that share homology with SARS-CoV-2 spike protein (3 epitopes) or NSP3 protein (3 epitopes). Collectively, the high *in silico* binding affinity of these bacterial epitopes across a globally representative set of HLA alleles, their ability to cross-react *in vitro* with SARS-CoV-2 homologous epitopes and finally the *ex vivo* increase in frequency and responsiveness of cross-reactive T cells to the spike protein homologues after SARS-CoV-2 vaccination, all indicate the 6 epitopes constitute immunodominant epitopes capable of cross-reacting between pathogenic bacteria and SARS-CoV-2 infection or vaccination. The significance of these findings could work both ways. Prior exposure to these bacterial pathogens may seed T cell memory and provide a degree of heterologous immunity during SARS-CoV-2 infection or vaccination. Conversely, SARS-CoV-2 infection or vaccination may seed T cell memory that produces a degree of heterologous immunity against bacterial pathogens. Further insight into such a

mechanism may assist in unravelling the unpredictable heterogeneity of SARS-CoV-2 clinical manifestations.

DATA AVAILABILITY STATEMENT

The original contributions presented in the study are included in the article/**Supplementary Material**. Further inquiries can be directed to the corresponding author.

ETHICS STATEMENT

The studies involving human participants were reviewed and approved by Monash University Human Research Ethics Committee (project ID 25834). The patients/participants provided their written informed consent to participate in this study.

AUTHOR CONTRIBUTIONS

PE designed the project, performed the experiments, analysed data and wrote the manuscript. BN, AY, and JC performed the experiments, analysed data and provided intellectual input. WW analysed data. RC analysed the data, wrote the manuscript and provided intellectual input, JM, YT, PG, and SH analysed data and provided intellectual input. JO designed the project, analysed data and wrote the manuscript. All authors contributed to the article and approved the submitted version.

FUNDING

The project was funded by Monash Health Foundation COVID-19 Research Fund Grant.

ACKNOWLEDGMENTS

We thank donors for their blood donations. We thank Anita Cummins, Kathleen Elford, Susan Morton and Ai-Li Yeo for phlebotomy and Seiya Fukada and Ashleigh Fell for technical assistance.

SUPPLEMENTARY MATERIAL

The Supplementary Material for this article can be found online at: https://www.frontiersin.org/articles/10.3389/fimmu.2022.821595/full#supplementary-material

REFERENCES

1. Welsh RM, Selin LK. No One is Naive: The Significance of Heterologous T-Cell Immunity. *Nat Rev Immunol* (2002) 2(6):417–26. doi: 10.1038/nri820
2. Le Bert N, Tan AT, Kunasegaran K, Tham CYL, Hafezi M, Chia A, et al. SARS-CoV-2-Specific T Cell Immunity in Cases of COVID-19 and SARS, and Uninfected Controls. *Nature* (2020) 584(7821):457–62. doi: 10.1038/s41586-020-2550-z
3. Grifoni A, Weiskopf D, Ramirez SI, Mateus J, Dan JM, Moderbacher CR, et al. Targets of T Cell Responses to SARS-CoV-2 Coronavirus in Humans With COVID-19 Disease and Unexposed Individuals. *Cell* (2020) 181(7):1489–501 e15. doi: 10.1016/j.cell.2020.05.015
4. Salkowska A, Karwaciak I, Karas K, Dastych J, Ratajewski M. SARS-CoV-2 Proteins Induce IFNG in Th1 Lymphocytes Generated From CD4+ Cells From Healthy, Unexposed Polish Donors. *Vaccines (Basel)* (2020) 8(4):673–83. doi: 10.3390/vaccines8040673
5. Braun J, Loyal L, Frentsch M, Wendisch D, Georg P, Kurth F, et al. SARS-CoV-2-Reactive T Cells in Healthy Donors and Patients With COVID-19. *Nature* (2020) 587(7833):270–4. doi: 10.1038/s41586-020-2598-9
6. Mateus J, Grifoni A, Tarke A, Sidney J, Ramirez SI, Dan JM, et al. Selective and Cross-Reactive SARS-CoV-2 T Cell Epitopes in Unexposed Humans. *Science* (2020) 370(6512):89–94. doi: 10.1126/science.abd3871
7. Nelde A, Bilich T, Heitmann JS, Maringer Y, Salih HR, Roerden M, et al. SARS-CoV-2-Derived Peptides Define Heterologous and COVID-19-Induced T Cell Recognition. *Nat Immunol* (2021) 22(1):74–85. doi: 10.1038/s41590-020-00808-x
8. Loyal L, Braun J, Henze L, Kruse B, Dingeldey M, Reimer U, et al. Cross-Reactive CD4(+) T Cells Enhance SARS-CoV-2 Immune Responses Upon Infection and Vaccination. *Science* (2021) 374:eabh1823–34. doi: 10.1101/2021.04.01.21252379
9. Eggenhuizen PJ, Ng BH, Chang J, Fell AL, Cheong RMY, Wong WY, et al. BCG Vaccine Derived Peptides Induce SARS-CoV-2 T Cell Cross-Reactivity. *Front Immunol* (2021) 12:692729. doi: 10.3389/fimmu.2021.692729
10. Shepherd FR, McLaren JE. T Cell Immunity to Bacterial Pathogens: Mechanisms of Immune Control and Bacterial Evasion. *Int J Mol Sci* (2020) 21(17):6144–76. doi: 10.3390/ijms21176144
11. Kim SK, Cornberg M, Wang XZ, Chen HD, Selin LK, Welsh RM. Private Specificities of CD8 T Cell Responses Control Patterns of Heterologous Immunity. *J Exp Med* (2005) 201(4):523–33. doi: 10.1084/jem.20041337
12. Laing AG, Lorenc A, Del Molino Del Barrio I, Das A, Fish M, Monin L, et al. A Dynamic COVID-19 Immune Signature Includes Associations With Poor Prognosis. *Nat Med* (2020) 26(10):1623–35. doi: 10.1038/s41591-020-1038-6
13. Peng Y, Mentzer AJ, Liu G, Yao X, Yin Z, Dong D, et al. Broad and Strong Memory CD4(+) and CD8(+) T Cells Induced by SARS-CoV-2 in UK Convalescent Individuals Following COVID-19. *Nat Immunol* (2020) 21(11):1336–45. doi: 10.1038/s41590-020-0782-6
14. Madeira F, Park YM, Lee J, Buso N, Gur T, Madhusoodanan N, et al. The EMBL-EBI Search and Sequence Analysis Tools APIs in 2019. *Nucleic Acids Res* (2019) 47(W1):W636–W41. doi: 10.1093/nar/gkz268
15. Weiskopf D, Angelo MA, de Azeredo EL, Sidney J, Greenbaum JA, Fernando AN, et al. Comprehensive Analysis of Dengue Virus-Specific Responses Supports an HLA-Linked Protective Role for CD8+ T Cells. *Proc Natl Acad Sci USA* (2013) 110(22):E2046–53. doi: 10.1073/pnas.1305227110
16. Reynisson B, Alvarez B, Paul S, Peters B, Nielsen M. NetMHCpan-4.1 and NetMHCIIpan-4.0: Improved Predictions of MHC Antigen Presentation by Concurrent Motif Deconvolution and Integration of MS MHC Eluted Ligand Data. *Nucleic Acids Res* (2020) 48(W1):W449–W54. doi: 10.1093/nar/gkaa379
17. Greenbaum J, Sidney J, Chung J, Brander C, Peters B, Sette A. Functional Classification of Class II Human Leukocyte Antigen (HLA) Molecules Reveals Seven Different Supertypes and a Surprising Degree of Repertoire Sharing Across Supertypes. *Immunogenetics* (2011) 63(6):325–35. doi: 10.1007/s00251-011-0513-0
18. Iturrieta-Zuazo I, Rita CG, Garcia-Soidan A, de Malet Pintos-Fonseca A, Alonso-Alarcon N, Pariente-Rodriguez R, et al. Possible Role of HLA Class-I Genotype in SARS-CoV-2 Infection and Progression: A Pilot Study in a Cohort of Covid-19 Spanish Patients. *Clin Immunol* (2020) 219:108572. doi: 10.1016/j.clim.2020.108572
19. Balz K, Trassl L, Hartel V, Nelson PP, Skevaki C. Virus-Induced T Cell-Mediated Heterologous Immunity and Vaccine Development. *Front Immunol* (2020) 11:513. doi: 10.3389/fimmu.2020.00513
20. Wedemeyer H, Mizukoshi E, Davis AR, Bennink JR, Rehermann B. Cross-Reactivity Between Hepatitis C Virus and Influenza A Virus Determinant-

Specific Cytotoxic T Cells. *J Virol* (2001) 75(23):11392–400. doi: 10.1128/JVI.75.23.11392-11400.2001
21. Reiss S, Baxter AE, Cirelli KM, Dan JM, Morou A, Daigneault A, et al. Comparative Analysis of Activation Induced Marker (AIM) Assays for Sensitive Identification of Antigen-Specific CD4 T Cells. *PloS One* (2017) 12 (10):e0186998. doi: 10.1371/journal.pone.0186998
22. Tarke A, Sidney J, Kidd CK, Dan JM, Ramirez SI, Yu ED, et al. Comprehensive Analysis of T Cell Immunodominance and Immunoprevalence of SARS-CoV-2 Epitopes in COVID-19 Cases. *Cell Rep Med* (2021) 2(2):100204. doi: 10.1016/j.xcrm.2021.100204
23. Dan JM, Lindestam Arlehamn CS, Weiskopf D, da Silva Antunes R, Havenar-Daughton C, Reiss SM, et al. A Cytokine-Independent Approach To Identify Antigen-Specific Human Germinal Center T Follicular Helper Cells and Rare Antigen-Specific CD4+ T Cells in Blood. *J Immunol* (2016) 197(3):983–93. doi: 10.4049/jimmunol.1600318
24. O'Toole A, Scher E, Underwood A, Jackson B, Hill V, McCrone JT, et al. Assignment of Epidemiological Lineages in an Emerging Pandemic Using the Pangolin Tool. *Virus Evol* (2021) 7(2):veab064. doi: 10.1093/ve/veab064
25. Raue HP, Brien JD, Hammarlund E, Slifka MK. Activation of Virus-Specific CD8+ T Cells by Lipopolysaccharide-Induced IL-12 and IL-18. *J Immunol* (2004) 173(11):6873–81. doi: 10.4049/jimmunol.173.11.6873
26. Gilbertson B, Germano S, Steele P, Turner S, Fazekas de St Groth B, Cheers C. Bystander Activation of CD8+ T Lymphocytes During Experimental Mycobacterial Infection. *Infect Immun* (2004) 72(12):6884–91. doi: 10.1128/IAI.72.12.6884-6891.2004
27. Bengoechea JA, Sa Pessoa J. Klebsiella Pneumoniae Infection Biology: Living to Counteract Host Defences. *FEMS Microbiol Rev* (2019) 43(2):123–44. doi: 10.1093/femsre/fuy043
28. Hu Y, Liu C, Shen Z, Zhou H, Cao J, Chen S, et al. Prevalence, Risk Factors and Molecular Epidemiology of Carbapenem-Resistant Klebsiella Pneumoniae in Patients From Zhejiang, China, 2008-2018. *Emerging Microbes Infect* (2020) 9(1):1771–9. doi: 10.1080/22221751.2020.1799721
29. Abbas AK, Trotta E D, Marson A, Bluestone JA. Revisiting IL-2: Biology and Therapeutic Prospects. *Sci Immunol* (2018) 3(25):eaat1482–90. doi: 10.1126/sciimmunol.aat1482
30. Percival SL, Williams DW. Chapter Six - Escherichia Coli. In: SL Percival, MV Yates, DW Williams, RM Chalmers, NF Gray, editors. *Microbiology of Waterborne Diseases, 2nd ed.* London: Academic Press (2014). p. 89–117.
31. Khalil IA, Troeger C, Blacker BF, Rao PC, Brown A, Atherly DE, et al. Morbidity and Mortality Due to Shigella and Enterotoxigenic Escherichia Coli Diarrhoea: The Global Burden of Disease Study 1990-2016. *Lancet Infect Dis* (2018) 18(11):1229–40. doi: 10.1016/S1473-3099(18)30475-4
32. Ravindran R, McSorley SJ. Tracking the Dynamics of T-Cell Activation in Response to Salmonella Infection. *Immunology* (2005) 114(4):450–8. doi: 10.1111/j.1365-2567.2005.02140.x
33. Agudelo Higuita NI, Huycke MM. Enterococcal Disease, Epidemiology, and Implications for Treatment. In: MS Gilmore, DB Clewell, Y Ike, N Shankar, editors. *Enterococci: From Commensals to Leading Causes of Drug Resistant Infection*. Boston: Massachusetts Eye and Ear Infirmary (2014).
34. Kline KA, Lewis AL. Gram-Positive Uropathogens, Polymicrobial Urinary Tract Infection, and the Emerging Microbiota of the Urinary Tract. *Microbiol Spectr* (2016) 4(2):459–502. doi: 10.1128/microbiolspec.UTI-0012-2012
35. Kao PHN, Kline KA. Dr. Jekyll and Mr. Hide: How Enterococcus Faecalis Subverts the Host Immune Response to Cause Infection. *J Mol Biol* (2019) 431 (16):2932–45. doi: 10.1016/j.jmb.2019.05.030
36. Tong SYC, Davis JS, Eichenberger E, Holland TL, Fowler VG Jr Staphylococcus Aureus Infections: Epidemiology, Pathophysiology, Clinical Manifestations, and Management. *Clin Microbiol Rev* (2015) 28(3):603–61. doi: 10.1128/CMR.00134-14
37. Hassoun A, Linden PK, Friedman B. Incidence, Prevalence, and Management of MRSA Bacteremia Across Patient Populations-a Review of Recent Developments in MRSA Management and Treatment. *Crit Care (Lond Engl)* (2017) 21(1):211–. doi: 10.1186/s13054-017-1801-3
38. Bröker BM, Mrochen D, Péton V. The T Cell Response to Staphylococcus Aureus. *Pathog (Basel Switzerland)* (2016) 5(1):31. doi: 10.3390/pathogens5010031
39. Lee R, Choi SM, Jo SJ, Lee J, Cho SY, Kim SH, et al. Clinical Characteristics and Antimicrobial Susceptibility Trends in Citrobacter Bacteremia: An 11-Year Single-Center Experience. *Infect Chemother* (2019) 51(1):1–9. doi: 10.3947/ic.2019.51.1.1
40. Liu L-H, Wang N-Y, Wu AY-J, Lin C-C, Lee C-M, Liu C-P. Citrobacter Freundii Bacteremia: Risk Factors of Mortality and Prevalence of Resistance Genes. *J Microbiol Immunol Infect* (2018) 51(4):565–72. doi: 10.1016/j.jmii.2016.08.016
41. Passet V, Brisse S. Description of Klebsiella Grimontii Sp. Nov. *Int J Syst Evol Microbiol* (2018) 68(1):377–81. doi: 10.1099/ijsem.0.002517
42. Johnston PF, Gerding DN, Knight KL. Protection From Clostridium Difficile Infection in CD4 T Cell- and Polymeric Immunoglobulin Receptor-Deficient Mice. *Infect Immun* (2014) 82(2):522–31. doi: 10.1128/IAI.01273-13
43. Yacyshyn MB, Reddy TN, Plageman LR, Wu J, Hollar AR, Yacyshyn BR. Clostridium Difficile Recurrence is Characterized by Pro-Inflammatory Peripheral Blood Mononuclear Cell (PBMC) Phenotype. *J Med Microbiol* (2014) 63(10):1260–73. doi: 10.1099/jmm.0.075382-0
44. Lagneaux AS, Hénard S, Diancourt L, Stein E, Perez P, Mathieu P, et al. Clostridium Haemolyticum Infection: A Cause of Hemolytic Anemia in a Patient With Bone Marrow Necrosis. *Microorganisms* (2021) 9(8):1568. doi: 10.3390/microorganisms9081568
45. Aronoff DM, Kazanjian PH. Historical and Contemporary Features of Infections Due to Clostridium Novyi. *Anaerobe* (2018) 50:80–4. doi: 10.1016/j.anaerobe.2017.12.012
46. Pasternack MS, Swartz MN. 96 - Myositis and Myonecrosis. In: JE Bennett, R Dolin, MJ Blaser, editors. *Mandell, Douglas, and Bennett's Principles and Practice of Infectious Diseases, Eighth Edition*. Philadelphia: W.B. Saunders (2015). p. 1216–25.e2.
47. Sulaiman I, Chung M, Angel L, Tsay JJ, Wu BG, Yeung ST, et al. Microbial Signatures in the Lower Airways of Mechanically Ventilated COVID-19 Patients Associated With Poor Clinical Outcome. *Nat Microbiol* (2021) 6 (10):1245–58. doi: 10.1038/s41564-021-00961-5
48. Morens DM, Fauci AS. The 1918 Influenza Pandemic: Insights for the 21st Century. *J Infect Dis* (2007) 195(7):1018–28. doi: 10.1086/511989
49. Shieh WJ, Blau DM, Denison AM, Deleon-Carnes M, Adem P, Bhatnagar J, et al. 2009 Pandemic Influenza A (H1N1): Pathology and Pathogenesis of 100 Fatal Cases in the United States. *Am J Pathol* (2010) 177(1):166–75.
50. Dickson RP, Schultz MJ, van der Poll T, Schouten LR, Falkowski NR, Luth JE, et al. Lung Microbiota Predict Clinical Outcomes in Critically Ill Patients. *Am J Respir Crit Care Med* (2020) 201(5):555–63. doi: 10.1164/rccm.201907-1487OC
51. Dickson RP, Singer BH, Newstead MW, Falkowski NR, Erb-Downward JR, Standiford TJ, et al. Enrichment of the Lung Microbiome With Gut Bacteria in Sepsis and the Acute Respiratory Distress Syndrome. *Nat Microbiol* (2016) 1 (10):16113. doi: 10.1038/nmicrobiol.2016.113
52. Shin D, Mukherjee R, Grewe D, Bojkova D, Baek K, Bhattacharya A, et al. Papain-Like Protease Regulates SARS-CoV-2 Viral Spread and Innate Immunity. *Nature* (2020) 587(7835):657–62. doi: 10.1038/s41586-020-2601-5
53. Cai Y, Zhang J, Xiao T, Peng H, Sterling SM, Walsh RM Jr, et al. Distinct Conformational States of SARS-CoV-2 Spike Protein. *Science* (2020) 369 (6511):1586–92. doi: 10.1126/science.abd4251
54. Harcourt BH, Jukneliene D, Kanjanahaluethai A, Bechill J, Severson KM, Smith CM, et al. Identification of Severe Acute Respiratory Syndrome Coronavirus Replicase Products and Characterization of Papain-Like Protease Activity. *J Virol* (2004) 78(24):13600–12. doi: 10.1128/JVI.78.24.13600-13612.2004
55. Lim KP, Ng LF, Liu DX. Identification of a Novel Cleavage Activity of the First Papain-Like Proteinase Domain Encoded by Open Reading Frame 1a of the Coronavirus Avian Infectious Bronchitis Virus and Characterization of the Cleavage Products. *J Virol* (2000) 74(4):1674–85. doi: 10.1128/JVI.74.4.1674-1685.2000
56. Frieman M, Ratia K, Johnston RE, Mesecar AD, Baric RS. Severe Acute Respiratory Syndrome Coronavirus Papain-Like Protease Ubiquitin-Like Domain and Catalytic Domain Regulate Antagonism of IRF3 and NF-kappaB Signaling. *J Virol* (2009) 83(13):6689–705. doi: 10.1128/JVI.02220-08
57. Altmann DM, Boyton RJ. SARS-CoV-2 T Cell Immunity: Specificity, Function, Durability, and Role in Protection. *Sci Immunol* (2020) 5(49): eabd6160–5. doi: 10.1126/sciimmunol.abd6160

Conflict of Interest: The authors declare that the research was conducted in the absence of any commercial or financial relationships that could be construed as a potential conflict of interest.

Publisher's Note: All claims expressed in this article are solely those of the authors and do not necessarily represent those of their affiliated organizations, or those of

the publisher, the editors and the reviewers. Any product that may be evaluated in this article, or claim that may be made by its manufacturer, is not guaranteed or endorsed by the publisher.

Copyright © 2022 Eggenhuizen, Ng, Chang, Cheong, Yellapragada, Wong, Ting, Monk, Gan, Holdsworth and Ooi. This is an open-access article distributed under the terms of the Creative Commons Attribution License (CC BY). The use, distribution or reproduction in other forums is permitted, provided the original author(s) and the copyright owner(s) are credited and that the original publication in this journal is cited, in accordance with accepted academic practice. No use, distribution or reproduction is permitted which does not comply with these terms.

frontiers in Immunology

ORIGINAL RESEARCH
published: 27 January 2022
doi: 10.3389/fimmu.2021.769442

T-Cell Repertoire Characteristics of Asymptomatic and Re-Detectable Positive COVID-19 Patients

Yizhe Li[1†], Jian Hu[2†], Yongsi Wang[3†], Dongdong Liu[2†], Yaling Shi[4], Jiaqi Zhang[1,2], Yuntao Liu[5], Dongzi Lin[6], Jing Lin[7], Wei Hu[1], Haolan He[8], Wei Wang[6], Wentao Fan[3], Linlin Li[3], Dawei Wang[9], Kejian Wang[10,11*] and Jianhua Xu[1*]*

[1] Department of Laboratory Medicine, Shunde Hospital of Guangzhou University of Chinese Medicine, Foshan, China, [2] Department of Laboratory Medicine, The Second Affiliated Hospital of Guangzhou University of Chinese Medicine, Guangzhou, China, [3] Department of Translational Medicine Research Institute, Guangzhou Huayin Medical Laboratory Center Ltd., Guangzhou, China, [4] Department of Laboratory Medicine, Guangzhou Eighth People's Hospital, Guangzhou Medical University, Guangzhou, China, [5] Emergency Department, The Second Affiliated Hospital of Guangzhou University of Chinese Medicine, Guangzhou, China, [6] Department of Laboratory Medicine, The Fourth People's Hospital of Foshan, Foshan, China, [7] Department of Clinical Laboratory, The First People's Hospital of Foshan, Foshan, China, [8] Department of Infectious Diseases, Guangzhou Eighth People's Hospital, Guangzhou Medical University, Guangzhou, China, [9] Department of Pulmonary and Critical Care Medicine, Shunde Hospital of Guangzhou University of Chinese Medicine, Foshan, China, [10] The Third Affiliated Hospital of Shandong First Medical University (Affiliated Hospital of Shandong Academy of Medical Sciences), Jinan, China, [11] Innovative Institute of Chinese Medicine and Pharmacy, Shandong University of Traditional Chinese Medicine, Jinan, China

OPEN ACCESS

Edited by:
Alessio Mazzoni, University of Florence, Italy

Reviewed by:
Roberta Amoriello, University of Florence, Italy
Pieter Meysman, University of Antwerp, Belgium

***Correspondence:**
Jianhua Xu
jhxu1976@gzucm.edu.cn
Kejian Wang
kejian-wang@foxmail.com
Dawei Wang
david@gzucm.edu.cn

†These authors have contributed equally to this work

Specialty section:
This article was submitted to T Cell Biology, a section of the journal Frontiers in Immunology

Received: *02 September 2021*
Accepted: *24 December 2021*
Published: *27 January 2022*

Citation:
Li Y, Hu J, Wang Y, Liu D, Shi Y, Zhang J, Liu Y, Lin D, Lin J, Hu W, He H, Wang W, Fan W, Li L, Wang D, Wang K and Xu J (2022) T-Cell Repertoire Characteristics of Asymptomatic and Re-Detectable Positive COVID-19 Patients. Front. Immunol. 12:769442. doi: 10.3389/fimmu.2021.769442

The prevention of the COVID-19 pandemic is highly complicated by the prevalence of asymptomatic and recurrent infection. Many previous immunological studies have focused on symptomatic and convalescent patients, while the immune responses in asymptomatic patients and re-detectable positive cases remain unclear. Here we comprehensively analyzed the peripheral T-cell receptor (TCR) repertoire of 54 COVID-19 patients in different courses, including asymptomatic, symptomatic, convalescent, and re-detectable positive cases. We identified a set of V–J gene combinations characterizing the upward immune responses through asymptomatic and symptomatic courses. Furthermore, some of these V–J combinations could be awakened in the re-detectable positive cases, which may help predict the risk of recurrent infection. Therefore, TCR repertoire examination has the potential to strengthen the clinical surveillance and the immunotherapy development for COVID-19.

Keywords: COVID-19, T-cell receptor, asymptomatic patient, re-detectable positive case, immune repertoire sequencing

INTRODUCTION

As a highly infectious virus, the severe acute respiratory syndrome coronavirus 2 (SARS-CoV-2) caused the pandemic of coronavirus disease 2019 (COVID-19) (1, 2). The clinical manifestations of infected patients ranged from asymptomatic condition to severe symptoms (3). Moreover, among the COVID-19 convalescent patients, some tested positive again after discharge (i.e., re-detectable positive) (4).

The global efforts to end COVID-19 are complicated by the prevalence of asymptomatic and recurrent infection. Many previous immunological studies have focused on symptomatic and convalescent patients (5–12), while the immune responses in asymptomatic patients and re-detectable positive cases remain unclear (13, 14). Unlike symptomatic patients who can be effectively identified by clinical features, asymptomatic carriers may inadvertently transmit virus to close contacts and reshape the dynamics of infection in population (15, 16). Although most re-detectable positive cases have minor symptoms and hardly disease progression upon readmission, their potential infectivity and immunological characterization remain undefined (17, 18). We performed a comprehensive analysis of the transcriptomic profiles of PBMCs from COVID-19 patients in our previous studies (19). However, the pathogenesis is not fully understood at present.

The antiviral adaptive immunity is greatly dependent on the activation of T-cells, which can selectively eliminate virus-infected host cells (20). The specificity toward viral antigens is determined by the structure of the T-cell receptor (TCR) repertoire (21). Based on the advances in sequencing technologies, the biased TCR repertoire in various infectious diseases has been revealed (22–24). Kuri-Cervantes et al. demonstrated the different trajectories of the immunologic state in moderate, severe, and recovered COVID-19 patients (25). Wauters et al. provided deep-immune trajectories of mild to critical COVID-19 by analyzing bronchoalveolar lavage samples (26). Thus, an in-depth study on the TCR characteristics in different courses of COVID-19 is critically needed (27–31).

Here we analyzed the peripheral TCR repertoire of 54 COVID-19 patients in different courses (including asymptomatic, symptomatic, convalescent, and re-detectable positive cases) along with 16 healthy donors. In particular, our results presented the unique immunological features of asymptomatic patients and re-detectable positive cases, which could provide help for clinical management and therapy development.

RESULTS

Demographic and Clinical Characteristics

A total of 54 patients with laboratory-confirmed COVID-19 disease were enrolled, including 11 asymptomatic (ASY), 19 symptomatic (SYM), 14 convalescent (CON), and 10 re-detectable positive (RDP) cases. Moreover, 16 healthy donors (HD) were recruited as the control group. As shown in **Table 1**, no significant difference in age or sex was identified between the HD group and any of the patient groups (as measured by the two-tailed Mann–Whitney U-test or Fisher's exact test). Except for one patient with preexisting chronic pharyngitis, most ASY cases had no obvious clinical symptoms during the whole disease course. All HD subjects and most ASY patients had no underlying comorbidity, while some of the SYM, CON, and RDP patients were diagnosed with hypertension, hyperlipidemia, diabetes mellitus, cardiovascular disease, chronic liver disease, or chronic kidney disease (32). The routine laboratory test results (**Supplementary Table 1**) showed that the lymphocyte levels in the SYM and CON groups were significantly lower than that in the HD group (two-tailed Mann–Whitney U-test $p < 0.05$). However, such difference was not observed in the ASY or RDP group.

Since HLA molecules play a crucial role in shaping the TCR repertoire (33), we also sought to determine whether the frequency of a certain HLA allele was imbalanced across groups. By performing Fisher's exact test following a previously published procedure (22), we confirmed that none of the HLA alleles showed significant difference (**Figure 1** and **Supplementary Table 2**), which consolidated our following findings in the TCR repertoire.

Patients in Different Courses Have Heterogeneous TCR Characteristics

On average, 10.6 million clean reads were obtained from each sample in sequencing (ranging from 6.2 to 13.2 million, see *Methods*). No significant difference was found between groups in number of reads, clonotypes, or V–J genes (**Figures 2A–C**). No significant difference in clonal diversity (as measured by D50 index and Shannon entropy) was detected between any two groups (**Figures 2D, E**), suggesting that COVID-19 might not necessarily induce a widespread change in TCR repertoire diversity. Also, we analyzed the differential expression of amino acid clonotypes in patients and healthy donors (**Figure 3**). The clonotype AAPVFVLGLQAVSTDTQY was significantly decreased in both SYM and ASY groups. Moreover, the clonotype EGAGLLQYPPLSKLF showed a significantly lower expression in both CON and RDP groups.

In the context of V–J gene usage, the similarity between subjects was measured by the Spearman's correlation (i.e., stronger positive correlation indicates higher similarity) following a previously published procedure (34). Taking HD as a reference, the highest discrepancy was found between SYM and HD. On the other hand, ASY showed significantly higher similarity to HD (**Figure 4A**), suggesting that asymptomatic patients may be subject to less changes in cellular immunology.

Furthermore, taking RDP as a reference, ASY showed the highest similarity as compared to other patient groups (**Figure 4B**). This finding is consistent with the fact that most RDP patients, just as ASY ones, exhibited no obvious clinical symptoms.

Dynamics of Gene Usage in Different Courses of COVID-19

We further analyzed the dynamics of specific V–J gene expression to identify potential key factors associated with different courses of COVID-19. Using the expression level in HD as a baseline, we identified 73 V–J pairings that exhibited not only alteration in ASY, but even more drastic changes in SYM (Cuzick's test for monotonic trend $p < 0.05$, **Figure 5A** and **Supplementary Table 3**) (35). Of note, a significant portion (30.1%, hypergeometric test $p = 1.08 \times 10^{-13}$) of the monotonic V–J pairings also showed differential usage in RDP course (RDP

TABLE 1 | Baseline characteristics of study subjects.

	Healthy (n =16)	Asymptomatic (n = 11)	Symptomatic (n = 19)	Convalescent (n = 14)	Re-detectable positive (n = 10)
Severity of the first diagnosis (n, %)					
Asymptomatic	0	11 (100%)	0	2 (14.29%)	1(10%)
Mild	0	0	2 (10.53%)	2 (14.29%)	1 (10%)
Moderate	0	0	16 (84.21%)	4 (28.57%)	8 (80%)
Severe	0	0	1 (5.26%)	6 (42.86%)	0
Age (years, median and IQR)	34.50 (27.25–44.25)	33.00 (21.00–44.00)	32.00 (23.00–48.00)	46.50 (23.50–65.75)	30.50 (24.25–59.75)
Male (n, %)	9 (56.25%)	4 (36.36%)	12 (63.16%)	10 (71.43%)	4 (40%)
Female (n, %)	7 (43.75%)	7 (63.64%)	7 (36.84%)	4 (28.57%)	6 (60%)
Comorbidities (n, %)					
Hypertension	0	0	2 (10.53%)	1 (7.14%)	2 (20%)
Hyperlipidemia	0	1 (9.09%)	2 (10.53%)	0	0
Diabetes	0	0	1 (5.26%)	1 (7.14%)	1 (10%)
Cardiovascular disease	0	0	0	1 (7.14%)	0
Chronic liver disease	0	0	2 (10.53%)	1 (7.14%)	1 (10%)
Chronic kidney disease	0	0	0	1 (7.14%)	0
Signs and symptoms (n, %)					
Cough	0	0	13 (68.42%)	4 (28.57%)	1 (10%)
Expectoration	0	0	11 (57.89%)	4 (28.57%)	1 (10%)
Rhinorrhoea	0	0	2 (10.53%)	0	0
Headache	0	0	6 (31.58%)	0	0
Fatigue	0	0	7 (36.84%)	0	0
Sore throat	0	0	3 (15.79%)	0	1 (10%)
Diarrhea	0	0	0	1 (7.14%)	0
Chest tightness	0	0	3 (15.79%)	2 (14.29%)	0
Myalgia	0	0	3 (15.79%)	1 (7.14%)	0
Chills	0	0	4 (21.05%)	1 (7.14%)	1 (10%)
Shortness of breath	0	0	1 (5.26%)	1 (7.14%)	0
Nausea and vomiting	0	0	4 (21.05%)	0	0
Dry throat	0	1 (9.09%)	3 (15.79%)	0	1 (10%)
Gastrointestinal reaction	0	0	1 (5.26%)	0	1 (10%)
Palpitation	0	0	0	0	1 (10%)
Abdominal distension, nausea and retching	0	0	2 (10.53%)	0	0
Poor stomach intake	0	0	1 (5.26%)	0	1 (10%)
Erythra	0	0	1 (5.26%)	0	0
Rhinobyon	0	0	0	0	0

vs. HD, Mann–Whitney U test $p < 0.05$, **Figure 5B** and **Supplementary Table 4**). The dynamics of these feature V–J pairings indicated that a certain immunological memory for SARS-CoV-2 could be awakened upon recurrent infection.

DISCUSSION

Asymptomatic and recurrent infection further increased the difficulty of COVID-19 prevention. Here we presented an immunological landscape of COVID-19 patients in different courses by performing TCR repertoire sequencing. In particular, while a series of prior studies focused on the immunological profiles of moderate, severe, or recovered patients, our results provided insights into the characteristics of ASY and RDP patients.

Despite numerous recent studies on COVID-19 patients, our analysis adds understanding of the immune responses to SARS-CoV-2 in several aspects. First of all, it has been repeatedly reported that symptomatic patients exhibit more severe clinical manifestations than asymptomatic ones (13, 36–38). In agreement with such observation, we found that the usage of certain V and J gene segments exhibited a monotonic trend through HD, ASY, and SYM groups, indicating potential upward immune responses from asymptomatic to symptomatic course. The V–J combinations showing monotonic changes can help narrow down the search scope of TCR specific to SARS-CoV-2 antigens, which may facilitate the development of highly targeted immunotherapies, such as engineered T-cells for infusion (39, 40).

Next, the risk factors of recurrent infection are not yet well defined (14), which urges development of useful biomarkers to enhance clinical surveillance. We found that a proportion of V–J combinations evoked by asymptomatic and symptomatic infection also changed in re-detectable positive cases. Such observation indicated the possibility of examining immune repertoire as a stringent criterion of complete recovery and an early predictor of high-risk individuals prone to recurrent infection.

Several limitations of our study should be taken into consideration. Firstly, four COVID-19 courses were characterized by blood samples collected from different individuals, rather than sequential samples from the same set of patients. Therefore, additional longitudinal studies are needed to calibrate the immunological trajectories of COVID-19. Secondly, we enrolled a limited number of patients, which makes it difficult to account for

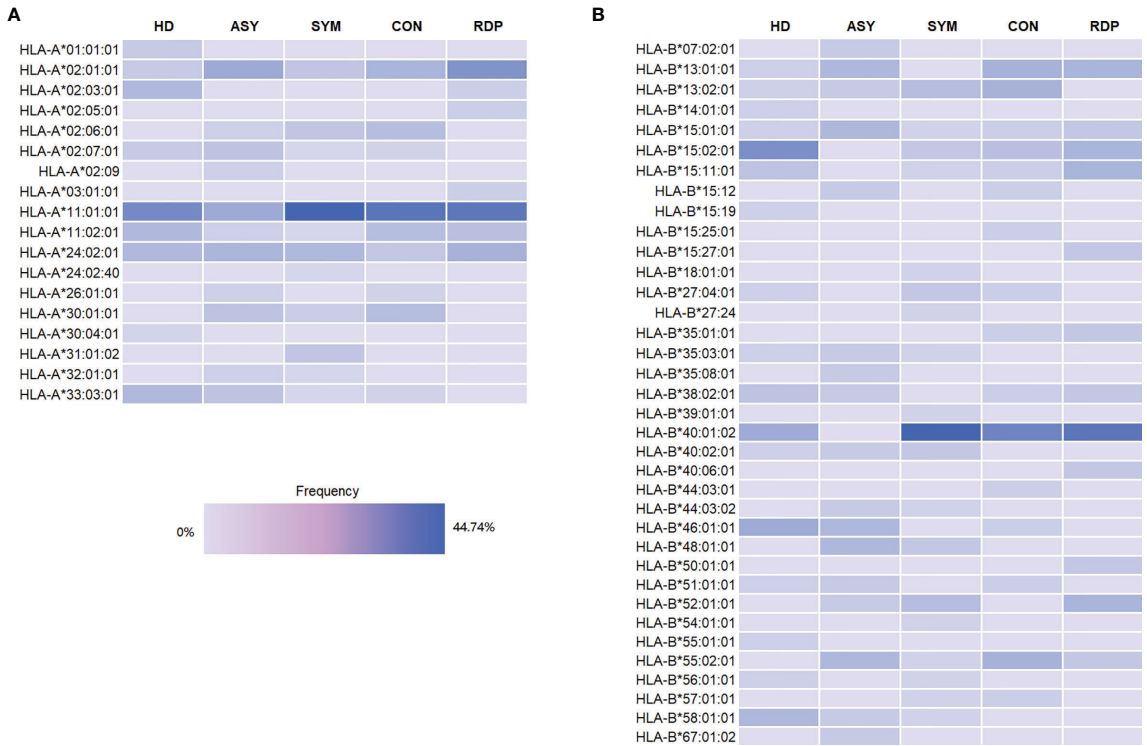


FIGURE 1 | Frequency of HLA-A **(A)** and HLA-A **(B)** alleles in different groups.

factors (e.g., diverse therapies and certain comorbidities) that may have divergent immunomodulatory effects. Subsequent efforts will optimally require larger patient cohorts to control for variations in treatment protocol and prevalence of comorbidities.

Altogether, this study provided novel insights into the TCR profiles of COVID-19 patients in different courses. A better understanding of the adaptive immunity in COVID-19 could strengthen clinical surveillance and immunotherapy development. Further large cohort studies on immune repertoire (41, 42) would be required to extend our findings.

METHODS

Patients

This study was approved by the ethics committees of the above four participant hospitals. Written informed consent was obtained from all participants enrolled in this study. Between March and May in 2020, a total of 54 patients with laboratory-confirmed COVID-19 disease were enrolled at the Guangzhou Eighth People's Hospital, the Shunde Hospital of Guangzhou University of Chinese Medicine, the Fourth People's Hospital of Foshan, and the First People's Hospital of Foshan, China. The COVID-19 patients were classified into four groups: asymptomatic group, symptomatic group, convalescent group, and re-detectable positive group.

According to the Protocol for Prevention and Control of COVID-19 (Edition 6) of National Health Commission of China (43), the asymptomatic group were those who had a positive COVID-19 RT-PCR test or specific serum IgM antibodies, diagnosed as COVID-19, but without self-perception or clinically recognizable symptoms during the whole disease course. The symptomatic group had evident clinical symptoms and were diagnosed as COVID-19 according to the Diagnosis and Treatment Protocol for Novel Coronavirus Pneumonia (Version 7) of National Health Commission of China (44). In the convalescent group, patients were those with body temperature that returned to normal for more than 3 days, respiratory symptoms significantly improved, inflammation on pulmonary obviously absorbed, and nucleic acid tests of respiratory tract samples proved negative for two consecutive times (sampling interval being at least 24 h). The re-detectable positive group was defined as patients with re-positive results of SARS-CoV-2 nucleic acid during the follow-up period after discharge from the hospital. The time between the re-positive results of the PCR test and the discharge time from the hospital ranged from 2 weeks to 1 month. Besides, 16 health donors were all enrolled at Shunde Hospital of Guangzhou University of Chinese Medicine, China, who tested negative for SARS-CoV-2 and exhibited no respiratory symptoms. Patient demographics and clinical manifestations were retrospectively reviewed. All patients had routine laboratory investigations, including complete blood count, liver function tests, blood gases analysis, and coagulation tests.

According to the Diagnosis and Treatment Protocol for Novel Coronavirus Pneumonia (Version 7) of China, the severity of

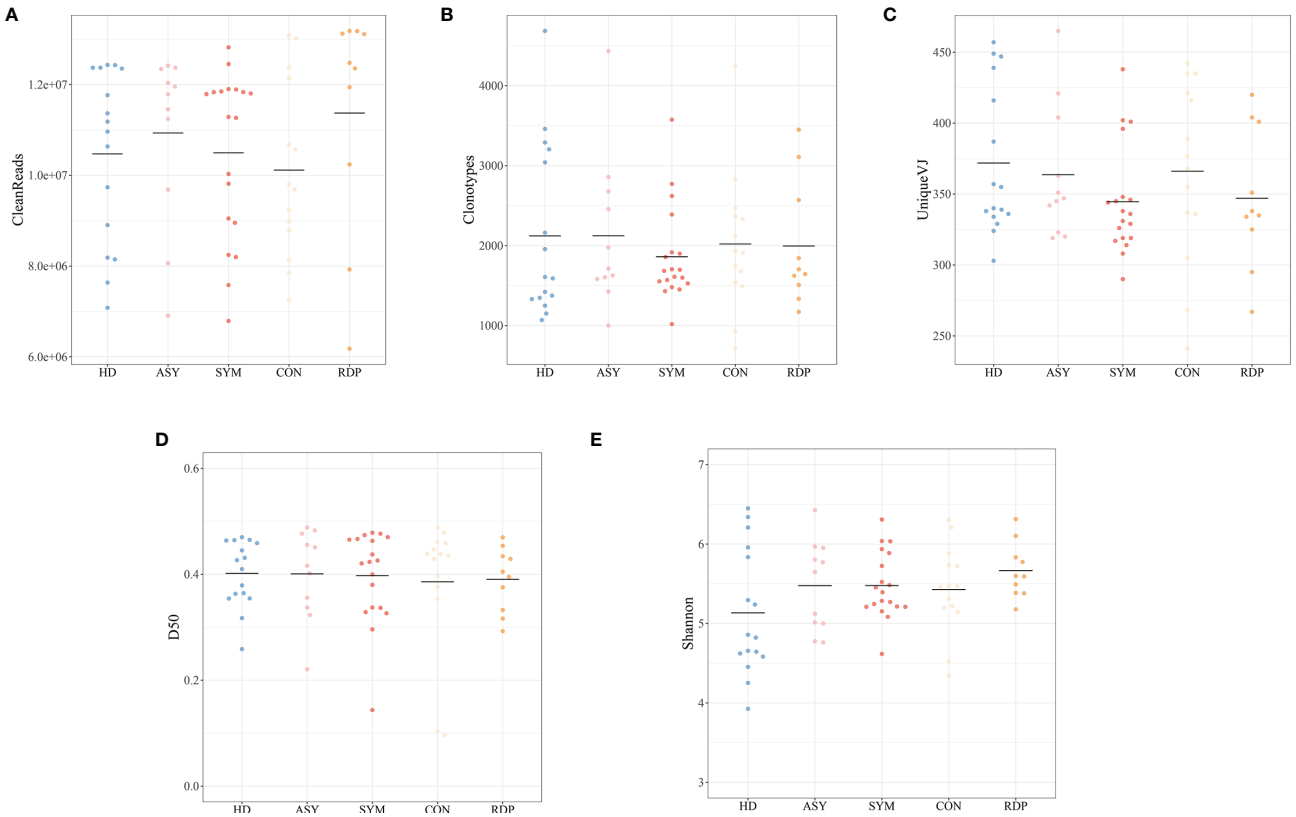


FIGURE 2 | Analysis of data quality and overall clonal diversity among different groups. **(A)** The number of clean reads. **(B)** The number of clonotypes. **(C)** The number of unique VJ pairs. **(D)** Distribution of D50 index. **(E)** Distribution of Shannon entropy.

disease was as follows: (1) mild cases displayed clinical symptoms with no imaging manifestations of pneumonia; (2) moderate cases were characterized by fever and respiratory symptoms with radiological manifestations of pneumonia; (3) severe cases must meet one of the following criteria: respiratory distress (≥30 breaths/min), oxygen saturation ≤ 93% at rest, or arterial partial pressure of oxygen (PaO2)/fraction of inspired oxygen (FiO2) ≤ 300 mmHg (l mmHg = 0.133 kPa).

RNA Extraction and cDNA Synthesis

Peripheral venous blood was collected and placed into the vacutainer tube. The time points of sample collection are shown in **Supplementary Table 5**. Peripheral blood mononuclear cells (PBMCs) are isolated from 2~4 ml human peripheral blood by Ficoll-Paque density gradient. Total RNA was isolated from PBMCs using TRIzol reagent (Invitrogen, Carlsbad, California, USA) according to the manufacturer's instruction (miRNeasy Mini Kit, Qiagen, Germany). The RNA quality inspection adopts Agilent 2100, and the quality control standard is RIN > 7.0, 28S/18S ≥ 1.0.

TCR cDNA libraries for high-throughput sequencing were prepared by 5′ rapid amplification of cDNA ends (RACE) using the SMARTScribe™ Reverse Transcriptase (Clontech, Mountain View, California, USA) as previously described (45, 46). Briefly, 0.6 μg of total RNA was mixed with the primer BC1R (**Supplementary Table 6**), which is specific for human TCRβ cDNA synthesis. To denature RNA and anneal the priming oligonucleotides, RNA was incubated at 70°C for 2 min and then at 42°C for 3 min. Switch_oligo and SMARTScribe reverse transcriptases were added for 25 μl template switching and the cDNA synthesis reaction, which was performed at 42°C for 60 min. 5U uracil DNA glycosylase (UDG) was added for digestion at 37°C for 40 min, and the product was purified with MinElute PCR Purification Kit (Qiagen, Germany).

TCR Library Preparation

Two-round PCR was performed for TCR library preparation. For the first round of PCR amplification, 45 μl of cDNA from the synthesis reaction was mixed with primers and Q5® High-Fidelity 2X Master Mix (NEB, USA). The PCR program began with an initial denaturation at 95°C for 1.5 min, followed by 18 cycles of denaturation at 95°C for 10 s, annealing of primer to DNA at 60°C for 20 s, and extension at 72°C for 40 s, and ended with an extension at 72°C for 4 min. For the second round of PCR amplification, the product from the first round of PCR was purified by QIAquick PCR Purification Kit (Qiagen, Germany), and 10 μl of the purified product was used in each 25-μl PCR reaction. The reaction was performed for 14 cycles using the

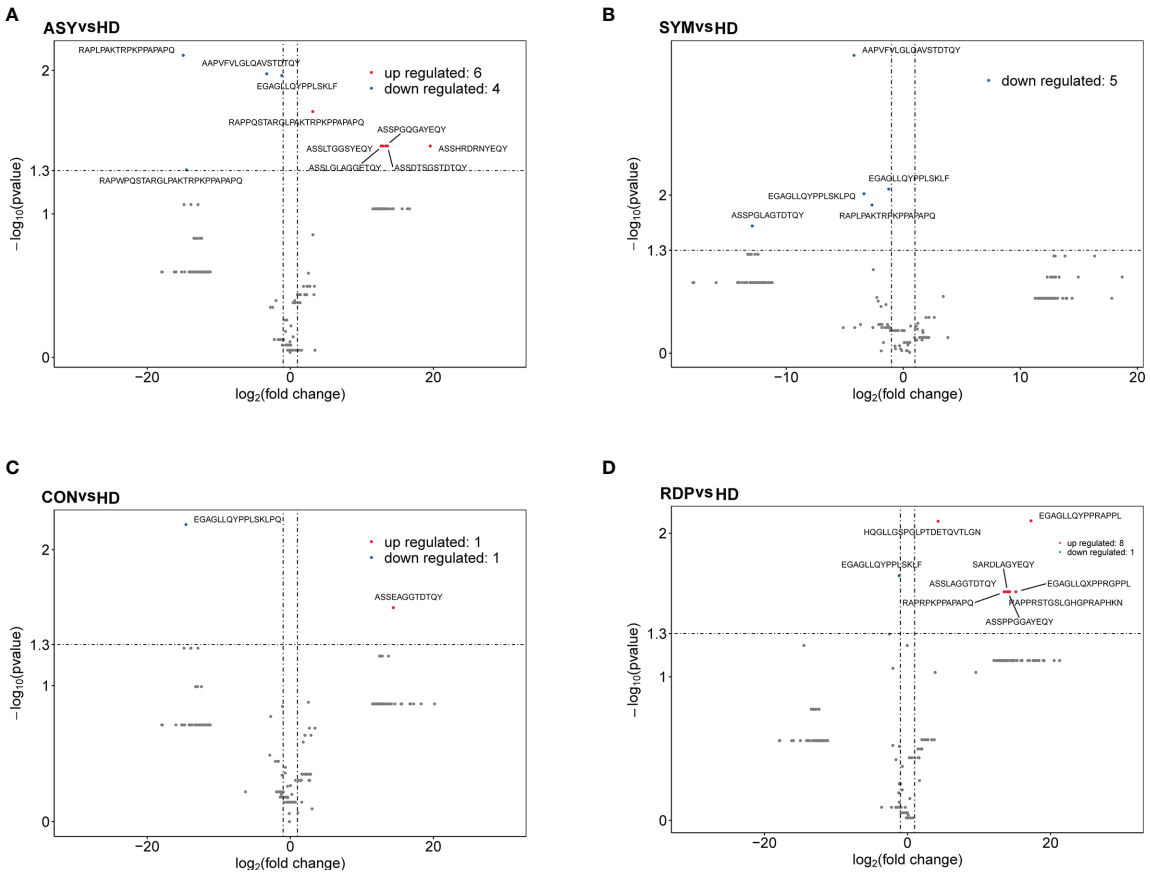


FIGURE 3 | Volcano plots showing differential expression (i.e., |log2(FC)| > 1, p < 0.05) of amino acid clonotypes between patients and healthy donors. **(A)** ASY vs. HD. **(B)** SYM vs. HD. **(C)** CON vs. HD. **(D)** RDP vs. HD.

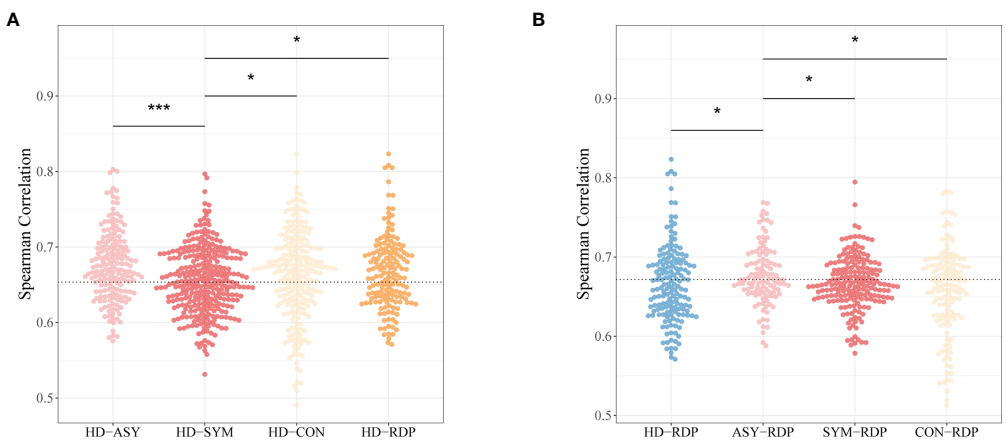


FIGURE 4 | Spearman's correlation coefficients of V–J combination profiles between different groups. **(A)** The HD-ASY similarity is significantly higher than that of HD-SYM. **(B)** ASY showed the highest similarity to RDP among all groups. Statistical significance of the difference between groups is denoted as * for P < 0.05, *** for P < 0.001.

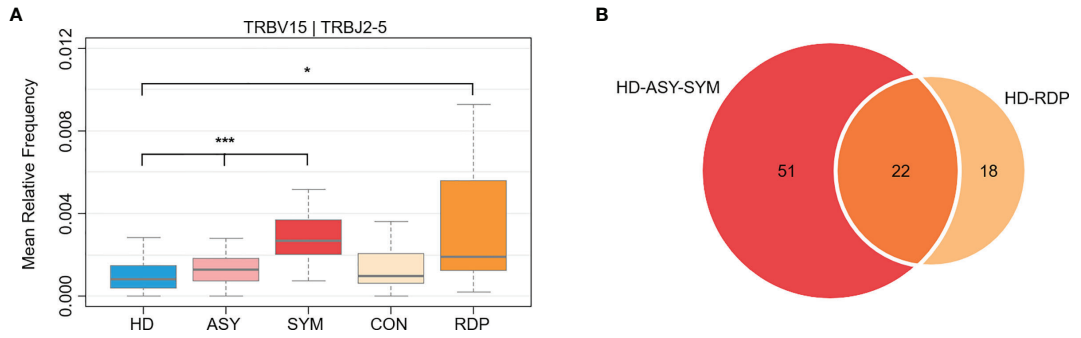


FIGURE 5 | Differential V–J gene usage between different groups. **(A)** An exemplary V–J combination showing a monotonic increase through HD, ASY, and SYM courses, as well as a significant elevation in RDP group. **(B)** Among the monotonic V–J combinations, many were also differentially expressed in RDP cases. Statistical significance of the difference between groups is denoted as * for $P < 0.05$, *** for $P < 0.001$.

first-round PCR temperature regimen. PCR products were purified using the QIAquick PCR Purification Kit (Qiagen, Germany). Illumina adaptors were ligated using NEBNext® Ultra™ II DNA Library Prep Kit for Illumina® (New England Biolabs, USA) according to the manufacturer's protocol and sequencing in the Illumina NovaSeq 6000 platform with the PE150 mode. The parameters of sequencing quality were shown in (**Supplementary Table 7**).

Data Processing and Analysis

The original data obtained from high-throughput sequencing were converted to raw sequence reads by base calling, and the results were stored in FASTQ format. Low-quality reads and reads without primers were discarded. PCR and sequencing errors were corrected by unique molecular identifiers (UMIs). The reads with same UMI were one clone. Only duplicate reads with different UMIs will be kept in downstream processing. A clonotype was defined by the CDR3 amino acid sequence for further analysis (the same UMI reads must be more than two). TCRβ V, D, and J genes and clonotype were defined according to IMGT59 and IgBLAST; TCRβ VDJ combination was defined by MiXCR. We performed mRNA-Seq profiling on 70 samples. Reads were mapped to the IPD-IMGT/HLA database and HLA-HD determining HLA alleles using mRNA-seq results (47).

Statistical Analysis

Categorical variables were described as count (%), and a two-group comparison was performed using Fisher's exact test. Continuous variables were expressed as median and interquartile range (IQR) values and compared by the Mann–Whitney U test between groups. The Spearman correlation coefficient was calculated to assess the association between two vectors of quantitative variables. The significance of monotonic trend across multiple groups was assessed by Cuzick's test (35). The significance of overlap between two gene sets was assessed by hypergeometric test (the "dhyper" function of R software). All statistical analyses were performed using R software (version 4.0.2). A two-sided p-value lower than 0.05 was considered as statistically significant.

DATA AVAILABILITY STATEMENT

The raw data supporting the conclusions of this article will be made available by the authors, without undue reservation.

ETHICS STATEMENT

This study was approved by the ethics committees of the above four participant hospitals. Written informed consent was obtained from all participants enrolled in this study.

AUTHOR CONTRIBUTIONS

JX, KW, and DW conceived and supervised the project. YS, DL, JL, and WH provided COVID-19 blood samples and clinical information. YuL, JH, DL, YW, and JZ performed the experiments and conducted the sample preparation. KW, YiL. JH, YW, YuL, and WF performed the data analysis. HH, WW, and LL coordinated the projects. YiL, JH, and KW wrote the manuscript. All authors contributed to the article and approved the submitted version.

FUNDING

This study was funded by the Science and Technology Innovation Project of Foshan Municipality (2020001000431), National Key Research and Development Project (2020YFA0708001), and Guangdong Provincial Science and Technology Project (2020A1414010363).

SUPPLEMENTARY MATERIAL

The Supplementary Material for this article can be found online at: https://www.frontiersin.org/articles/10.3389/fimmu.2021.769442/full#supplementary-material

REFERENCES

1. Wu Z, McGoogan JM. Characteristics of and Important Lessons From the Coronavirus Disease 2019 (COVID-19) Outbreak in China: Summary of a Report of 72 314 Cases From the Chinese Center for Disease Control and Prevention. *JAMA* (2020) 323(13):1239–42. doi: 10.1001/jama.2020.2648
2. Guan W-j, Liang W-h, Zhao Y, Liang H-r, Chen Z-s, Li Y-m, et al. Comorbidity and Its Impact on 1590 Patients With COVID-19 in China: A Nationwide Analysis. *Eur Respir J* (2020) 55(5):2000547. doi: 10.1183/13993003.00547-2020
3. Wang D, Hu B, Hu C, Zhu F, Liu X, Zhang J, et al. Clinical Characteristics of 138 Hospitalized Patients With 2019 Novel Coronavirus-Infected Pneumonia in Wuhan, China. *JAMA* (2020) 323(11):1061–9. doi: 10.1001/jama.2020.1585
4. Lan L, Xu D, Ye G, Xia C, Wang S, Li Y, et al. Positive RT-PCR Test Results in Patients Recovered From COVID-19. *JAMA* (2020) 323(15):1502–3. doi: 10.1001/jama.2020.2783
5. Lucas C, Wong P, Klein J, Castro TBR, Silva J, Sundaram M, et al. Longitudinal Analyses Reveal Immunological Misfiring in Severe COVID-19. *Nature* (2020) 584(7821):463–9. doi: 10.1038/s41586-020-2588-y
6. Mathew D, Giles JR, Baxter AE, Oldridge DA, Greenplate AR, Wu JE, et al. Deep Immune Profiling of COVID-19 Patients Reveals Distinct Immunotypes With Therapeutic Implications. *Science* (2020) 369(6508):eabc8511. doi: 10.1126/science.abc8511
7. Zhang JY, Wang XM, Xing X, Xu Z, Zhang C, Song JW, et al. Single-Cell Landscape of Immunological Responses in Patients With COVID-19. *Nat Immunol* (2020) 21(9):1107–18. doi: 10.1038/s41590-020-0762-x
8. Giamarellos-Bourboulis EJ, Netea MG, Rovina N, Akinosoglou K, Antoniadou A, Antonakos N, et al. Complex Immune Dysregulation in COVID-19 Patients With Severe Respiratory Failure. *Cell Host Microbe* (2020) 27(6):992–1000.e3. doi: 10.1016/j.chom.2020.04.009
9. Song JW, Zhang C, Fan X, Meng FP, Xu Z, Xia P, et al. Immunological and Inflammatory Profiles in Mild and Severe Cases of COVID-19. *Nat Commun* (2020) 11(1):3410. doi: 10.1038/s41467-020-17240-2
10. Wilk AJ, Rustagi A, Zhao NQ, Roque J, Martínez-Colón GJ, McKechnie JL, et al. A Single-Cell Atlas of the Peripheral Immune Response in Patients With Severe COVID-19. *Nat Med* (2020) 26(7):1070–6. doi: 10.1038/s41591-020-0944-y
11. Qin C, Zhou L, Hu Z, Zhang S, Yang S, Tao Y, et al. Dysregulation of Immune Response in Patients With Coronavirus 2019 (COVID-19) in Wuhan, China. *Clin Infect Dis* (2020) 71(15):762–8. doi: 10.1093/cid/ciaa248
12. Wen W, Su W, Tang H, Le W, Zhang X, Zheng Y, et al. Immune Cell Profiling of COVID-19 Patients in the Recovery Stage by Single-Cell Sequencing. *Cell Discov* (2020) 6:31. doi: 10.1038/s41421-020-0168-9
13. Long Q-X, Tang X-J, Shi Q-L, Li Q, Deng H-J, Yuan J, et al. Clinical and Immunological Assessment of Asymptomatic SARS-CoV-2 Infections. *Nat Med* (2020) 26(8):1200–4. doi: 10.1038/s41591-020-0965-6
14. An J, Liao X, Xiao T, Qian S, Yuan J, Ye H, et al. Clinical Characteristics of the Recovered COVID-19 Patients With Re-Detectable Positive RNA Test. *medRxiv* (2020) 8(17):1084. doi: 10.1101/2020.03.26.20044222
15. Rothe C, Schunk M, Sothmann P, Bretzel G, Froeschl G, Wallrauch C, et al. Transmission of 2019-Ncov Infection From an Asymptomatic Contact in Germany. *N Engl J Med* (2020) 382(10):970–1. doi: 10.1056/NEJMc2001468
16. Bai Y, Yao L, Wei T, Tian F, Jin D-Y, Chen L, et al. Presumed Asymptomatic Carrier Transmission of COVID-19. *JAMA* (2020) 323(14):1406–7. doi: 10.1001/jama.2020.2565
17. Zhu H, Fu L, Jin Y, Shao J, Zhang S, Zheng N, et al. Clinical Features of COVID-19 Convalescent Patients With Re-Positive Nucleic Acid Detection. *J Clin Lab Anal* (2020) 34(7):e23392. doi: 10.1002/jcla.23392
18. Gao Z, Xu Y, Guo Y, Xu D, Zhang L, Wang X, et al. A Systematic Review of Re-Detectable Positive Virus Nucleic Acid Among COVID-19 Patients in Recovery Phase. *Infect Genet Evol: J Mol Epidemiol Evol Genet Infect Dis* (2020) 85:104494. doi: 10.1016/j.meegid.2020.104494
19. Zhang J, Lin D, Li K, Ding X, Li L, Liu Y, et al. Transcriptome Analysis of Peripheral Blood Mononuclear Cells Reveals Distinct Immune Response in Asymptomatic and Re-Detectable Positive COVID-19 Patients. *Front Immunol* (2021) 12:716075. doi: 10.3389/fimmu.2021.716075
20. Ranasinghe S, Lamothe PA, Soghoian DZ, Kazer SW, Cole MB, Shalek AK, et al. Antiviral CD8(+) T Cells Restricted by Human Leukocyte Antigen Class II Exist During Natural HIV Infection and Exhibit Clonal Expansion. *Immunity* (2016) 45(4):917–30. doi: 10.1016/j.immuni.2016.09.015
21. Song I, Gil A, Mishra R, Ghersi D, Selin LK, Stern LJ. Broad TCR Repertoire and Diverse Structural Solutions for Recognition of an Immunodominant CD8(+) T Cell Epitope. *Nat Struct Mol Biol* (2017) 24(4):395–406. doi: 10.1038/nsmb.3383
22. Emerson RO, DeWitt WS, Vignali M, Gravley J, Hu JK, Osborne EJ, et al. Immunosequencing Identifies Signatures of Cytomegalovirus Exposure History and HLA-Mediated Effects on the T Cell Repertoire. *Nat Genet* (2017) 49(5):659–65. doi: 10.1038/ng.3822
23. Soon CF, Behrendt P, Todt D, Manns MP, Wedemeyer H, Sällberg Chen M, et al. Defining Virus-Specific CD8+ TCR Repertoires for Therapeutic Regeneration of T Cells Against Chronic Hepatitis E. *J Hepatol* (2019) 71(4):673–84. doi: 10.1016/j.jhep.2019.06.005
24. Wendel BS, del Alcazar D, He C, Del Río-Estrada PM, Aiamkitsumrit B, Ablanedo-Terrazas Y, et al. The Receptor Repertoire and Functional Profile of Follicular T Cells in HIV-Infected Lymph Nodes. *Sci Immunol* (2018) 3(22):eaan8884. doi: 10.1126/sciimmunol.aan8884
25. Kuri-Cervantes L, Pampena MB, Meng W, Rosenfeld AM, Betts MR. Comprehensive Mapping of Immune Perturbations Associated With Severe COVID-19. *Sci Immunol* (2020) 5(49):eabd7114. doi: 10.1126/sciimmunol.abd7114
26. Wauters E, Van Mol P, Garg AD, Jansen S, Van Herck Y, Vanderbeke L, et al. Discriminating Mild From Critical COVID-19 by Innate and Adaptive Immune Single-Cell Profiling of Bronchoalveolar Lavages. *Cell Res* (2021) 31(3):272–90. doi: 10.1038/s41422-020-00455-9
27. Schultheiß C, Paschold L, Simnica D, Mohme M, Willscher E, von Wenserski L, et al. Next-Generation Sequencing of T and B Cell Receptor Repertoires From COVID-19 Patients Showed Signatures Associated With Severity of Disease. *Immunity* (2020) 53(2):442–55. doi: 10.1016/j.immuni.2020.06.024
28. Galson JD, Schaetzle S, Bashford-Rogers RJM, Raybould MIJ, Kovaltsuk A, Kilpatrick GJ, et al. Deep Sequencing of B Cell Receptor Repertoires From COVID-19 Patients Reveals Strong Convergent Immune Signatures. *Front Immunol* (2020) 11:605170. doi: 10.3389/fimmu.2020.605170
29. Niu X, Li S, Li P, Pan W, Wang Q, Feng Y, et al. Longitudinal Analysis of T and B Cell Receptor Repertoire Transcripts Reveal Dynamic Immune Response in COVID-19 Patients. *Front Immunol* (2020) 11:582010. doi: 10.3389/fimmu.2020.582010
30. Zhou Y, Zhang J, Wang D, Wang D, Guan W, Qin J, et al. Profiling of the Immune Repertoire in COVID-19 Patients With Mild, Severe, Convalescent, or Retesting-Positive Status. *J Autoimmun* (2021) 118:102596. doi: 10.1016/j.jaut.2021.102596
31. Woodruff MC, Ramonell RP, Nguyen DC, Cashman KS, Saini AS, Haddad NS, et al. Extrafollicular B Cell Responses Correlate With Neutralizing Antibodies and Morbidity in COVID-19. *Nat Immunol* (2020) 21(12):1506–16. doi: 10.1038/s41590-020-00814-z
32. Xiong F, Tang H, Liu L, Tu C, Tian JB, Lei CT, et al. Clinical Characteristics of and Medical Interventions for COVID-19 in Hemodialysis Patients in Wuhan, China. *J Am Soc Nephrol* (2020) 31(7):1387–97. doi: 10.1681/asn.2020030354
33. Goldrath AW, Bevan MJ. Selecting and Maintaining a Diverse T-Cell Repertoire. *Nature* (1999) 402(6759):255–62. doi: 10.1038/46218
34. Liu X, Zhang W, Zhao M, Fu L, Liu L, Wu J, et al. T Cell Receptor β Repertoires as Novel Diagnostic Markers for Systemic Lupus Erythematosus and Rheumatoid Arthritis. *Ann Rheum Dis* (2019) 78(8):1070–. doi: 10.1136/annrheumdis-2019-215442
35. Cuzick JA. Wilcoxon-Type Test for Trend. *Stat Med* (1985) 4(1):87–90. doi: 10.1002/sim.4780040112
36. Lee Y-H, Hong CM, Kim DH, Lee TH, Lee J. Clinical Course of Asymptomatic and Mildly Symptomatic Patients With Coronavirus Disease Admitted to Community Treatment Centers, South Korea. *Emerg Infect Dis* (2020) 26(10):2346–52. doi: 10.3201/eid2610.201620
37. Lee S, Kim T, Lee E, Lee C, Kim H, Rhee H, et al. Clinical Course and Molecular Viral Shedding Among Asymptomatic and Symptomatic Patients With SARS-CoV-2 Infection in a Community Treatment Center in the Republic of Korea. *JAMA Intern Med* (2020) 180(11):1447–52. doi: 10.1001/jamainternmed.2020.3862
38. Pan Y, Yu X, Du X, Li Q, Li X, Qin T, et al. Epidemiological and Clinical Characteristics of 26 Asymptomatic Severe Acute Respiratory Syndrome Coronavirus 2 Carriers. *J Infect Dis* (2020) 221(12):1940–7. doi: 10.1093/infdis/jiaa205

39. Oh H-LJ, Chia A, Chang CXL, Leong HN, Ling KL, Grotenbreg GM, et al. Engineering T Cells Specific for a Dominant Severe Acute Respiratory Syndrome Coronavirus CD8 T Cell Epitope. *J Virol* (2011) 85(20):10464–71. doi: 10.1128/JVI.05039-11
40. Le Bert N, Tan AT, Kunasegaran K, Tham CYL, Hafezi M, Chia A, et al. SARS-CoV-2-Specific T Cell Immunity in Cases of COVID-19 and SARS, and Uninfected Controls. *Nature* (2020) 584(7821):457–62. doi: 10.1038/s41586-020-2550-z
41. Snyder TM, Gittelman RM, Klinger M, May DH, Osborne EJ, Taniguchi R, et al. Magnitude and Dynamics of the T-Cell Response to SARS-CoV-2 Infection at Both Individual and Population Levels. *medRxiv* (2020), 2020.07.31.20165647. doi: 10.1101/2020.07.31.20165647
42. Nolan S, Vignali M, Klinger M, Dines JN, Kaplan IM, Svejnoha E, et al. A Large-Scale Database of T-Cell Receptor Beta (Tcrβ) Sequences and Binding Associations From Natural and Synthetic Exposure to SARS-CoV-2. *Res Square* (2020) rs.3.rs-51964. doi: 10.21203/rs.3.rs-51964/v1
43. National Health Commission of the People's Republic of China. Protocol on Prevention and Control of Novel Coronavirus Pneumonia (Edition 6). (2020).
44. National Health Commission of the People's Republic of China. Diagnosis and Treatment Protocol for Novel Coronavirus Pneumonia (Trial Version 7). (2020).
45. Mamedov IZ, Britanova OV, Zvyagin IV, Turchaninova MA, Bolotin DA, Putintseva EV, et al. Preparing Unbiased T-Cell Receptor and Antibody cDNA Libraries for the Deep Next Generation Sequencing Profiling. *Front Immunol* (2013) 4:456. doi: 10.3389/fimmu.2013.00456
46. Chen Y, Xu Y, Zhao M, Liu Y, Gong M, Xie C, et al. High-Throughput T Cell Receptor Sequencing Reveals Distinct Repertoires Between Tumor and Adjacent non-Tumor Tissues in HBV-Associated HCC. *Oncoimmunology* (2016) 5(10):e1219010. doi: 10.1080/2162402x.2016.1219010
47. Kawaguchi S, Higasa K, Shimizu M, Yamada R, Matsuda F. HLA-HD: An Accurate HLA Typing Algorithm for Next-Generation Sequencing Data. *Hum Mutat* (2017) 38(7):788–97. doi: 10.1002/humu.23230

Conflict of Interest: Authors YW, WF and LL were employed by company Guangzhou Huayin Medical Laboratory Center Ltd.

The remaining authors declare that the research was conducted in the absence of any commercial or financial relationships that could be construed as a potential conflict of interest.

Publisher's Note: All claims expressed in this article are solely those of the authors and do not necessarily represent those of their affiliated organizations, or those of the publisher, the editors and the reviewers. Any product that may be evaluated in this article, or claim that may be made by its manufacturer, is not guaranteed or endorsed by the publisher.

Copyright © 2022 Li, Hu, Wang, Liu, Shi, Zhang, Liu, Lin, Lin, Hu, He, Wang, Fan, Li, Wang, Wang and Xu. This is an open-access article distributed under the terms of the Creative Commons Attribution License (CC BY). The use, distribution or reproduction in other forums is permitted, provided the original author(s) and the copyright owner(s) are credited and that the original publication in this journal is cited, in accordance with accepted academic practice. No use, distribution or reproduction is permitted which does not comply with these terms.

frontiers in Immunology

ORIGINAL RESEARCH
published: 07 February 2022
doi: 10.3389/fimmu.2022.817876

Children and Adults With Mild COVID-19: Dynamics of the Memory T Cell Response up to 10 Months

Patricia Kaaijk[1], Verónica Olivo Pimentel[1], Maarten E. Emmelot[1], Martien C. M. Poelen[1], Alper Cevirgel[1], Rutger M. Schepp[1], Gerco den Hartog[1], Daphne F.M. Reukers[1], Lisa Beckers[1], Josine van Beek[1], Cécile A. C. M. van Els[1,2], Adam Meijer[1], Nynke Y. Rots[1] and Jelle de Wit[1]*

[1] Centre for Infectious Disease Control, National Institute for Public Health and the Environment (RIVM), Bilthoven, Netherlands, [2] Faculty of Veterinary Medicine, Utrecht University, Utrecht, Netherlands

OPEN ACCESS

Edited by:
Pia Kvistborg, The Netherlands Cancer Institute (NKI), Netherlands

Reviewed by:
Graham J. Britton, Icahn School of Medicine at Mount Sinai, United States
Helena Nunes-Cabaço, Universidade de Lisboa, Portugal

***Correspondence:**
Patricia Kaaijk
patricia.kaaijk@rivm.nl

Specialty section:
This article was submitted to T Cell Biology, a section of the journal Frontiers in Immunology

Received: *18 November 2021*
Accepted: *18 January 2022*
Published: *07 February 2022*

Citation:
Kaaijk P, Olivo Pimentel V, Emmelot ME, Poelen MCM, Cevirgel A, Schepp RM, den Hartog G, Reukers DFM, Beckers L, van Beek J, van Els CACM, Meijer A, Rots NY and de Wit J (2022) Children and Adults With Mild COVID-19: Dynamics of the Memory T Cell Response up to 10 Months. Front. Immunol. 13:817876. doi: 10.3389/fimmu.2022.817876

Background: Severe acute respiratory syndrome coronavirus-2 (SARS-CoV-2) has led to considerable morbidity/mortality worldwide, but most infections, especially among children, have a mild course. However, it remains largely unknown whether infected children develop cellular immune memory.

Methods: To determine whether a memory T cell response is being developed, we performed a longitudinal assessment of the SARS-CoV-2-specific T cell response by IFN-γ ELISPOT and activation marker analyses of peripheral blood samples from unvaccinated children and adults with mild-to-moderate COVID-19.

Results: Upon stimulation of PBMCs with heat-inactivated SARS-CoV-2 or overlapping peptides of spike (S-SARS-CoV-2) and nucleocapsid proteins, we found S-SARS-CoV-2-specific IFN-γ T cell responses in infected children (83%) and adults (100%) that were absent in unexposed controls. Frequencies of SARS-CoV-2-specific T cells were higher in infected adults, especially several cases with moderate symptoms, compared to infected children. The S-SARS-CoV-2 IFN-γ T cell response correlated with S1-SARS-CoV-2-specific serum antibody concentrations. Predominantly, effector memory $CD4^+$ T cells of a Th1 phenotype were activated upon exposure to SARS-CoV-2 antigens. Frequencies of SARS-CoV-2-specific T cells were significantly reduced at 10 months after symptom onset, while S1-SARS-CoV-2-specific IgG concentrations were still detectable in 90% of all children and adults.

Conclusions: Our data indicate that an antigen-specific T cell and antibody response is developed after mild SARS-CoV-2 infection in children and adults. It remains to be elucidated to what extent this SARS-CoV-2-specific response can contribute to an effective recall response after reinfection.

Keywords: SARS-CoV-2, COVID-19, mild symptoms, children, T cell immunity, adaptive immunity, antibody response, cytokines

INTRODUCTION

Tremendous research efforts have advanced our understanding of immunity to SARS-CoV-2. Most data on the immune response to SARS-CoV-2 was obtained from severe COVID-19 cases (1–4). However, the vast majority of infected individuals experience mild symptoms that do not require hospitalization (5–8). The question remains whether individuals, including children, with an asymptomatic or mild SARS-CoV-2 infection, develop immune memory, which may protect against subsequent SARS-CoV-2 infections. Persons with mild or asymptomatic infections often develop an antibody response, although not all cases do (8). It has been shown that SARS-CoV-2-induced antibody levels are waning over time (6, 9–11). On the other hand, T cell immunity is predicted to persist longer; after SARS-CoV infection in 2003, it was shown that T cell responses can persist for up to 17 years (12). Some studies investigated the T cell immunity induced after SARS-CoV-2 infection in mild symptomatic adult cases (6, 8, 13–16), showing weaker T cell responses in mild than in moderate or severe COVID-19 cases. $CD4^+$ T cell responses against SARS-CoV-2 were more prominent than the $CD8^+$ T cell response in adults with mild-to-moderate infection (8, 15, 16), while qualitatively impaired $CD4^+$ T cell responses have been reported for critically ill patients (15).

Nevertheless, it remains unclear whether SARS-CoV-2 infection in children, usually showing a mild course, induces substantial T cell immunity. Only a few reports describe the immune responses in children with mild disease or asymptomatic infection, although in these studies T cells specifically reactive to SARS-CoV-2 were not investigated (17–20). Recently, a study was published investigating SARS-CoV-2 specific T cell responses in children (21). Induction of a sustainable T cell response is needed to provide immune memory for long-term protection against reinfections by facilitating an efficient and quick response upon re-exposure. Therefore, knowledge on the induction of memory T cell immunity after a mild course of SARS-CoV-2 infection in children and adults is useful for the consideration of the community mitigation measures needed to protect against COVID-19 and limit the spread of the virus.

In the present study, we examined the frequency and the phenotypic/functional characteristics of SARS-CoV-2-reactive T cells in infected children and adults with mild to moderate symptoms up to 10 months after symptom onset. In addition, T cell responses correlated with SARS-CoV-2-specific serum IgM, IgG, and IgA antibody concentrations.

MATERIAL AND METHODS

Clinical Studies

In this prospective cohort study, described previously (22), households were enrolled in which one adult (index case) tested PCR positive for SARS-CoV-2 between March-May, 2020. Blood samples were collected longitudinally from members of these households; from children (n=24) and adults (n=27) with PCR-confirmed SARS-CoV-2 infection (for details see **Table 1**). Disease severity was classified as follows: asymptomatic (absence of symptoms), mild (presence of at least one symptom such as cough, fever, loss of smell or taste, etc.; but an absence of symptoms indicative of lower airways infection), moderate (presence of shortness of breath with or without any other symptom, including hospitalized cases). In this cohort, none of the hospitalized patients were admitted to an intensive care unit, and therefore not considered severe cases. Three children remained asymptomatic during the study but

TABLE 1 | Demographic and clinical characteristics of adults (with mild versus moderate symptoms) and children with PCR confirmed SARS-CoV-2 infection and demographic data of unexposed participants.

Characteristics	Infected adults total n = 27	Infected adults mild n = 13	Infected adults moderate n = 14	Unexposed adults n = 12	Infected children n = 24	Unexposed children n = 13
Median age (range) – years	44 (18 – 87)	45 (23 – 87)	44 (18 – 54)	38 (20 – 51)	12 (2 – 16)	12 (2 – 16)
Sex – number (%)					11 (45.8)	5 (38.5)
Male	14 (51.9)	8 (61.5)	6 (42.9)	6 (50.0)	13 (54.2)	8 (61.5)
Female	13 (48.1)	5 (38.5)	8 (57.1)	6 (50.0)		
Sign and symptoms – number (%)						
Any sign or symptom	27 (100.0)	13 (100.0)	14 (100.0)	N/A	21 (87.5)	N/A
Fever	14 (51.9)	6 (46.2)	8 (57.1)		6 (25.0)	
Cough	20 (74.1)	7 (53.8)	13 (92.9)		11 (45.8)	
Chills	15 (55.6)	6 (46.2)	9 (64.3)		2 (8.3)	
Sore throat	14 (51.9)	7 (53.8)	7 (50.0)		3 (12.5)	
Runny nose	18 (66.7)	9 (69.2)	9 (64.3)		15 (62.5)	
Phlegm	12 (44.4)	5 (38.5)	7 (50.0)		2 (8.3)	
Headache	20 (74.1)	10 (76.9)	10 (71.4)		7 (29.2)	
Myalgia	20 (74.1)	9 (69.2)	11 (78.6)		1 (4.2)	
Fatigue	24 (88.9)	10 (76.9)	14 (100.0)		6 (25.0)	
Shortness of breath	12 (44.4)	0 (0.0)	12 (85.7)*		2 (8.3)	
Loss of taste or smell	11 (40.7)	3 (23.1)	8 (57.1)		3 (12.5)	
Diarrhea	11 (40.7)	6 (46.2)	5 (35.7)		2 (8.3)	

All moderate cases reported shortness of breath with the exception of two hospitalized cases.
n, number of subjects in specific group; N/A, not applicable.

tested PCR positive. Additionally, blood samples from age-matched unexposed children (n=13) and adults (n=12) were collected from two other cohort studies before the COVID-19 pandemic (respectively, 2018-2019 and 2009-2011). None of the study subjects were vaccinated against SARS-CoV-2.

The protocol for the SARS-CoV-2-related study, based on the WHO First Few Hundred (FFX) protocol, was approved by the Medical-Ethical Review Committee (MERC) of University Medical Center Utrecht (Netherlands Trial Register (https://www.trialregister.nl/): NL9850, MERC Reference number: NL13529.041.06). Protocols for the cohort studies with unexposed children (Immfact, NTR: NL9775, MERC Reference number: NL4679.094.13) and adults (NVI-255, NTR: NL1952, MERC Reference number: NL29241.000.09) (23) were approved by Medical-Ethical Review Committees of the Netherlands. Written informed consent was received from all participants and/or from parents/guardians of minor participants (<16 years old). All trial-related activities were conducted according to Good Clinical Practice, including the provisions of the Declaration of Helsinki.

Peripheral Blood Mononuclear Cells and Serum Isolation

Peripheral blood mononuclear cells (PBMCs) were isolated from heparinized blood by centrifugation on a Ficoll-Hypaque gradient (Pharmacia Biotech) and cryopreserved at -135°C until use. Serum was separated from the blood by clotting and centrifugation and stored at -80°C until analysis.

Ex Vivo Immune Profiling

Flow cytometry using Trucount tubes (BD Biosciences) was performed on fresh blood. Cells were stained for anti-human CD27 (O323), CD45 (HI30) and CD45RO (UCHL1) (all Biolegend) and CD3 (SK7), CD4 (SK3), CD8 (RPA-T8), CD38 (HIT2), and HLA-DR (G46-6) (all BD Bioscience), to analyze $CD4^+$ and $CD8^+$ T cells expressing CD38 and/or HLA-DR as markers for activated T cells.

Defrosted PBMCs from SARS-CoV-2 infected children (n=24) and adults (n=27), as well as from unexposed healthy children (n=13) and adults (n=12), were used for deep immune profiling by multicolor flow cytometry. (BD FACSymphony™). Cells were stained for anti-human CD3 (OKT3), CD14 (HCD14), CD28 (CD28.2), CD56 (5.1H11), CD57 (HNK-1), CD95 (DX2) and CCR7 (G043H7) (all Biolegend) and CD4 (RPA-T4), CD8 (RPA-T8), CD19 (SJ25C1), CD27 (L128), CD45RO (UCHL1) (all BD Bioscience) and eFluor 780 fixable viability stain (65-0865-14, ThermoFisher). For this purpose, major lymphocyte populations were discriminated by analyzing the CD3 expression to identify T cells, and identifying $CD4^+$, $CD8^+$, $CD4^+/CD8^+$ and $CD4^-/CD8^-$ T cells within the $CD3^+$ T cells, analyzing CD19 expression to detect B cells, CD56 expression for NK cells and CD14 expression to identify cells of the myelomonocyte lineage. Memory $CD4^+$ and $CD8^+$ T cell subsets were further discriminated based on CD45RO and CCR7 staining (true naïve T cells (T_N), $CD45RO^-$, $CD27^+$, $CCR7^+$, $CD95^-$; central memory T cells (T_{CM}), $CD45RO^+$, $CD27^+$; effector memory T cells (T_{EM}), $CD45RO^+$, $CD27^-$; terminally differentiated effector memory T cells re-expressing CD45RA (T_{EMRA}), $CD45RO^-$, $CD27^-$, $CD28^-$, $CD57^+$).

Flow cytometry data analysis was performed using FlowJo software, version 10 (TreeStar).

Generation of Heat-Inactivated Virus Stocks of SARS-CoV-2

SARS-CoV-2 isolate, hCoV-19/Netherlands/Zuid_Holland_0133R/2020, was obtained from a Dutch patient. Virus was grown on VERO-E6 cells in DMEM medium (Gibco; Thermo Fisher Scientific) supplemented with 1x penicillin-streptomycin-glutamine (Gibco) and 2% FBS for approximately 48 hours under BSL-3 conditions. At >90% cytopathic effect (CPE), the suspension was collected and spun down (4000 × g, 10 min) to remove cell debris. Virus stocks were aliquoted and stored at −80°C until use. The 50% tissue culture infective dose ($TCID_{50}$), $7.63.10^7$ $TCID_{50}$/ml, was determined by the Reed and Muench method. Heat-inactivation was performed by incubating the virus at 60°C for 2 hours, after which the inactivated virus stocks were stored at −80°C until use.

Interferon Gamma ELISPOT

Multiscreen filtration ELISPOT plates (Millipore, Merck) were prewetted with 35% ethanol for ≤1 minute and washed with sterile water and PBS. Plates were coated with 5 µg/mL anti-human IFN-γ antibodies (1-D1K, Mabtech) overnight (4°C), then washed with PBS. PBMCs were incubated with heat-inactivated SARS-CoV-2 (MOI-3), or 15-mers overlapping peptides (11 amino acids overlap) covering whole spike protein of SARS-CoV-2 (S-SARS-CoV-2), whole nucleocapsid protein (N-SARS-CoV-2), or S-HCoV-OC43 (0.1 µM/peptide, all JPT), seeded on ELISPOT plates (2.10^5 cells/well), and incubated for 20 hours, 37°C, 5% CO2 in 100 µl AIM-V (Lonza) with 2% human serum (Sigma). DMSO and PHA (Sigma) were negative and positive controls, respectively. Subsequently, plates were washed and incubated for 1 hour with 1 µg/mL anti-human IFN-γ detection biotinylated-antibody (7-B6-1, Mabtech) in PBS-0.05% casein (Sigma). Plates were washed and incubated with Streptavidin-poly-HRP (Sanquin) in PBS-0.05% casein for 1 hour. After washing, plates were developed with TMB substrate (Mabtech). Spots were analyzed with CTL software. The number of spots from negative controls was subtracted from total spot numbers induced by antigen-specific stimulation; more than 5 spots, after background subtraction, were considered positive.

Immunophenotyping and Expression of Activation Markers After *In Vitro* Stimulation

Activated T cells were determined by harvesting cells from the IFN-γ ELISPOT plates and subsequently flow cytometric analysis was performed using activation markers. Cells were stained for anti-human CD3 (SK7), CD4 (SK3), CD8 (RPA-T8), CD45RO (UCHL1), CD25 (2A3), CD56 (NCAM16.2), CD69 (FN50), OX40 (L106)and fixable viability stain 780 (BD Bioscience) and CCR7 (G043H7) (Biolegend). After fixation and

permeabilization, using FoxP3/Transcription Factor Staining Buffer Set (eBioscience, Thermo Fisher Scientific, Waltham, Mass) cells were stained intracellularly for anti-human, CD137 (4-1BB) and CD154 (BD Bioscience). Data were acquired on a FACS Symphony analyzer (BD) and analyzed using FlowJo (V10, Tree Star, Ashland, Ore).

Antibody Assays

IgM, IgG, and IgA concentrations against SARS-CoV-2 monomeric spike-S1 (40591-V08H; Sino Biological) were determined in serum using a fluorescent bead-based multiplex immunoassay (MIA) as published previously (24), with previously determined cut-off values for seroprevalence of 1.20, 1.04, and 0.50 AU/mL for respectively SARS-CoV-2 monomeric spike-S1-specific IgM, IgG and IgA concentrations (10).

Cytokine Release Assay

Cell-free culture supernatants were harvested from the IFN-γ ELISPOT plates and analyzed using a bead-based multiplex immunoassay (MIA) quantitating levels of IL-2, IL-4, IL-5, IL-6, IL-9, IL-10, TNF, IL-13, IL-17A, IL-17F, IL-22 (LEGENDplex; BioLegend) according to the manufacturer's instructions and using FACSCanto (BD). For analysis, the online cloud-based program, The LEGENDplex™ Data Analysis Software Suite, was used. The minimum detection threshold (MDT) for each cytokine as calculated by the manufacturer was: 1.4 pg/ml for IL-2, 0.9 pg/ml for IL-4, 1.3 pg/ml for IL-5, 1.1 pg/ml for IL-6, 1.5 pg/ml for IL-9, 0.9 pg/ml for IL-10, 0.9 pg/ml for TNF, 1.4 pg/ml for IL-13, 2.0 pg/ml for IL-17A, 1.0 pg/ml for IL-17F, and 1.5 pg/ml for IL-22. Background signal for IL-6 and TNF from unstimulated controls was as high as stimulated samples, therefore these cytokines were excluded from analysis.

Statistics

Statistical analyses were performed using GraphPad Prism version 9.1.0. For unpaired comparisons, Mann-Whitney U test (two groups) or Kruskal-Wallis rank-sum test with Dunn's *post hoc* test (≥3 groups) were used. Paired data were compared using the Wilcoxon signed-rank test (two groups) or the Friedman test with Dunn's multiple comparison test (≥3 groups). Median values for paired comparisons were calculated from subjects with complete data for all time points. Correlation coefficients (r_s) were determined with Spearman's rank correlation. Non-parametric tests were used since data were mostly non-normally distributed according to the Shapiro-Wilk test. P values <0.05 were considered significant.

RESULTS

Study Subjects

SARS-CoV-2 specific T cell responses were assessed from SARS-CoV-2-infected children and adults, and for comparison from unexposed children and adults. None of the study subjects were vaccinated against SARS-CoV-2. Demographic and clinical characteristics are presented in **Table 1**. Blood samples from 24 children and 27 adults (13 with mild symptoms and 14 with moderate symptoms, including two hospitalized cases) with PCR-confirmed SARS-CoV-2 infection were collected. The median time point of the first sample (T1) was for children 8 days [5.0-16 days] and for adults 12.5 days [interquartile range (IQR) 11-14 days] post-symptom onset. Additional blood samples were taken 10-14 days after T1 (referred to as 'T2') and only for adults also at 4-6 weeks after T1 (referred to as 'T3').

Ex Vivo Determination of Activated T Cells Over Time After SARS-CoV-2 Infection in Children and Adults

No significant differences in major immune cell types were found over time after infection neither in children nor adults, i.e. frequencies of total T cells, B cells, monocytes, or NK cells were comparable between infected groups and healthy age-matched unexposed groups (**Supplementary Figure 1**). In infected adults, slightly higher frequencies of $CD4^+$ T_{EM} (T_{EM}; $CD45RO^+$, $CD27^-$) cell subsets were found at T3 compared to T1 (4.7% vs 3.5%; P= 0.0061), but there was no significant difference in the frequency of the T_{EM} subset of these time points and the uninfected controls (3.6%). Frequencies of $CD8^+$ T_{EM} cells of infected adults were slightly higher at T2 compared to T1 (4.2% vs 3.8%; P= 0.041). No differences in memory T cell subsets were found between mild and moderate COVID-19 adults cases nor in children over time after infection.

The *ex vivo* expression of CD38 and HLA-DR on T cells was determined as a measure for antigen-specific activation after SARS-CoV-2 infection. In children, no changes in CD38/HLA-DR co-expression on $CD4^+$ T cells were found between different time points after infection (**Supplementary Figure 2A**, upper panel). In SARS-CoV-2-infected adults, a transiently higher percentage of cells expressing CD38/HLA-DR was observed within the $CD4^+$ T central memory (T_{CM}; $CD45RO^+$, $CD27^+$) subset (1.1% at T1) that declined over time after infection (to 0.55% at T2, and to 0.37% at T3) and within the $CD4^+$ terminally differentiated effector memory re-expressing CD45RA (T_{EMRA}; $CD45RO^-$, $CD27^-$, $CD28^-$, $CD57^+$) cell subset (0.58% at T1) that declined to 0.0% at both T2 and T3 (**Supplementary Figure 2B**, upper panel). In both children and adults, a higher frequency of $CD8^+$/$CD38^+$/HLA-DR^+ T cells within the T_{CM}/T_{EM}/T naïve (T_N; $CD45RO^-$, $CD27^+$, $CCR7^+$, $CD95^-$) subsets were observed at T1 [4.1%/4.9%/0.33% (children) and 5.5%/3.1%/1.0% (adults)] that declined in time after infection (to 2.7%/2.1%/0.17% (children) and 2.7%/1.7%/0.30% (adults) at T2 and to 2.2%/0.81%/0.23% (adults) at T3 (**Supplementary Figures 2A, B**, lower panels).

SARS-CoV-2 Specific IFN-γ^+ T Cell Response

IFN-γ^+-producing cells were detected by ELISPOT upon stimulation with overlapping peptides covering spike protein (S) of SARS-CoV-2 (S-SARS-CoV-2) in 83% (20/24) of infected children and in 100% (27/27) of infected adults, whereas IFN γ^+ responses were found in 0% (0/6) and 8.3% (1/12) of the unexposed children and adults, respectively. Frequencies of

SARS-CoV-2-specific IFN-γ^+ T cells were lower in infected children than in infected adults (**Figures 1A–C**); the median spot forming units (SFU)/2.10^5 PBMCs for infected children versus infected adults was 18 versus 62 (P=0.0021) at T1 upon stimulation with S-SARS-CoV-2. On average, a 2-fold higher frequency of SARS-CoV-2-specific IFN-γ^+ T cells was found in adults with moderate symptoms compared to mild symptomatic adults for the three time points. For all antigenic stimuli used (i.e. S-SARS-CoV-2, overlapping peptides covering nucleocapsid protein (N) of SARS-CoV-2 (N-SARS-CoV-2), or inactivatedwhole SARS-CoV-2), the moderately ill adults had significantly higher frequencies of IFN-γ-producing T cells compared tochildren at T1. The mild symptomatic adults also generally showed higher frequencies of SARS-CoV-2-specific IFN-γ^+ Tcells than infected children, although not statistically significant for inactivated whole SARS-CoV-2 (**Figures 1A–C**).

The pre-existing T cell response against S-HCoV-OC43 of infected children was very low, although S-HCoV-OC43-specific T cell frequency was slightly higher at T2 compared to the agematched unexposed control group (9.0 versus 1.0 SFU/2.105 PBMCs; P=0.037) (**Figure 1D**, left panel). In infected adults, no difference in numbers of S-HCoV-OC43-specific T cells was found between SARS-CoV-2-infected and unexposed adults (**Figure 1D**, right panel). In both SARS-CoV-2-infected children and adults, the frequency of IFN-γ^+ T cells was 4 to 60-fold lower after stimulation with S-HCoV-OC43 (**Figure 1D**) compared to stimulation with any of the SARS-CoV-2 antigens (**Figures 1A–C**). No significant difference in frequency of SHCoV-OC43-reactive T cells was observed between unexposed adults and unexposed children or between mild and moderate COVID-19 cases.

Activation of Effector Memory CD4$^+$ T Cells Upon SARS-CoV-2-Specific Stimulation

PBMCs were harvested from the IFN-γ ELISPOT plates to determine whether mainly CD4+ or CD8+ T cell populations became activated upon SARS-CoV-2-specific stimulation. For this purpose, the expression of the following activation markers were analyzed by flow cytometry: CD25, CD137, CD154, CD69, OX40 (25–30). Especially the CD25 (IL-2Rα) and CD137 (4-1BB) co-expression on T cells of infected subjects increased significantly upon the various SARS-CoV-2 antigenic stimulations compared to mock stimulation (**Supplementary Figure 3**). Although analysis of CD137/CD25 co-expression is generally not used by default, in the present study we used this to identify SARS-CoV-2 antigen-specific T cells.

Primarily CD4$^+$ T cells and not CD8$^+$ T cells expressed CD25/CD137 activation markers upon SARS-CoV-2 antigenic stimulation, in infected subjects (**Figure 2** and **Supplementary Figure 4**). Compared to the unexposed age-matched groups, higher frequencies of activated CD4$^+$ T cells were observed in both infected children and infected adults after stimulation with any of the three SARS-CoV-2 antigen preparations at T1. Frequencies of SARS-CoV-2-specific activated CD4$^+$ T cells were significantly lower in infected children than in adults (upon S-SARS-CoV-2-specific stimulation, 0.04% CD25$^+$/CD137$^+$ T cells of total CD4$^+$ T cells for infected children versus 0.21% for infected adults at T1; P=0.0034). Frequencies of SARS-CoV-2-specific activated CD4$^+$ T cells, irrespective of used SARS-CoV-2 antigen, were comparable between adults with moderate COVID-19 illness and mildly symptomatic adults. The observed SARS-CoV-2-specific activated CD4$^+$ T cells were mainly effector memory (CD45RO$^+$/CCR7$^-$) (TEM) (**Figure 2D**).

Correlations Between SARS-CoV-2-Specific IFN-γ^+ T Cell Responses and CD4$^+$ T Cell Response

In children,moderate correlations were observed between IFN-γ^+ T cell frequency and activated (CD137$^+$ CD25$^+$) CD4$^+$ T cells after stimulation with N-SARS-CoV-2 (r_s=0.64; P=0.004) at T2, and at T1 after stimulation with inactivated SARS-CoV-2 (r_s=0.51; P=0.012) (**Figure 3A**). In adults, IFN-γ^+ T cell frequency and activated (CD137$^+$ CD25$^+$) CD4$^+$ T cells correlated after stimulation with both S-SARS-CoV-2 and N-SARS-CoV-2 at all three time points after infection (rs ranging between 0.51-0.72) and after stimulation with inactivated SARS-CoV-2 at T1 and T2 (respectively, r_s=0.70 and r_s=0.53) (**Figure 3B**).

SARS-CoV-2-Specific Release of Cytokines

Upon stimulation with S-SARS-CoV-2, PBMCs from SARS-CoV-2-infected children secreted more IL-2 than unexposed children, albeit at very low amounts (3.7 versus 0.1 pg/ml; P=0.030). Similar trends were observed in SARS-CoV-2-infected adults compared to unexposed adults, for both IL-2 (18.0 versus 0.1 pg/ml; P=0.0003). S-SARS-CoV-2-specific IL-2 secretion was higher in infected adults compared to infected children (P=0.015). However, IL-2secretion was only significantly higher in adults with moderate COVID-19 (51.8 versus 3.7 pg/ml; P=0.023) and not in adults with mild symptoms compared to infected children (**Figure 4**). Other cytokines were only secreted at very low levels and not significantly.

Correlations Between SARS-CoV-2-Specific IFN-γ^+ T Cell Frequency and Antibody Response

Serum antibody concentrations against the SARS-CoV-2 spike S1 protein (S1-SARS-CoV-2) above the previously established cutoff level (10) at any of the two sampling time points were found in 83.3% (IgM), 79.2% (IgG), and 75.0% (IgA) of the infected children. From the four children without detectable S-SARS-CoV-2-specific T cell responses, two did have S1-SARS-CoV-2-specific IgM, IgG, and IgA antibodies; the other two did not. In adults, 100%, 96.3%, and 88.9% were seropositive for respectively, IgM, IgG, and IgA antibodies to S1-SARS-CoV-2 at any of the three sampling time points. Interestingly, in children good correlations were observed between S-SARS-CoV-2 IFN-γ^+ T cell frequency and S1-SARS-CoV-2-specific serum IgM, IgG and IgA concentrations, though this was only observed at T1 [for IgM, R_s=0.73 (P<0.0001); IgG, r_s=0.74 (P<0.0001); IgA, r_s=0.68 (P=0.0004)] (**Figure 5A**). In adults, frequency of S-SARS-CoV-2-specific T cells was also correlated with S1-SARS-CoV-2-specific

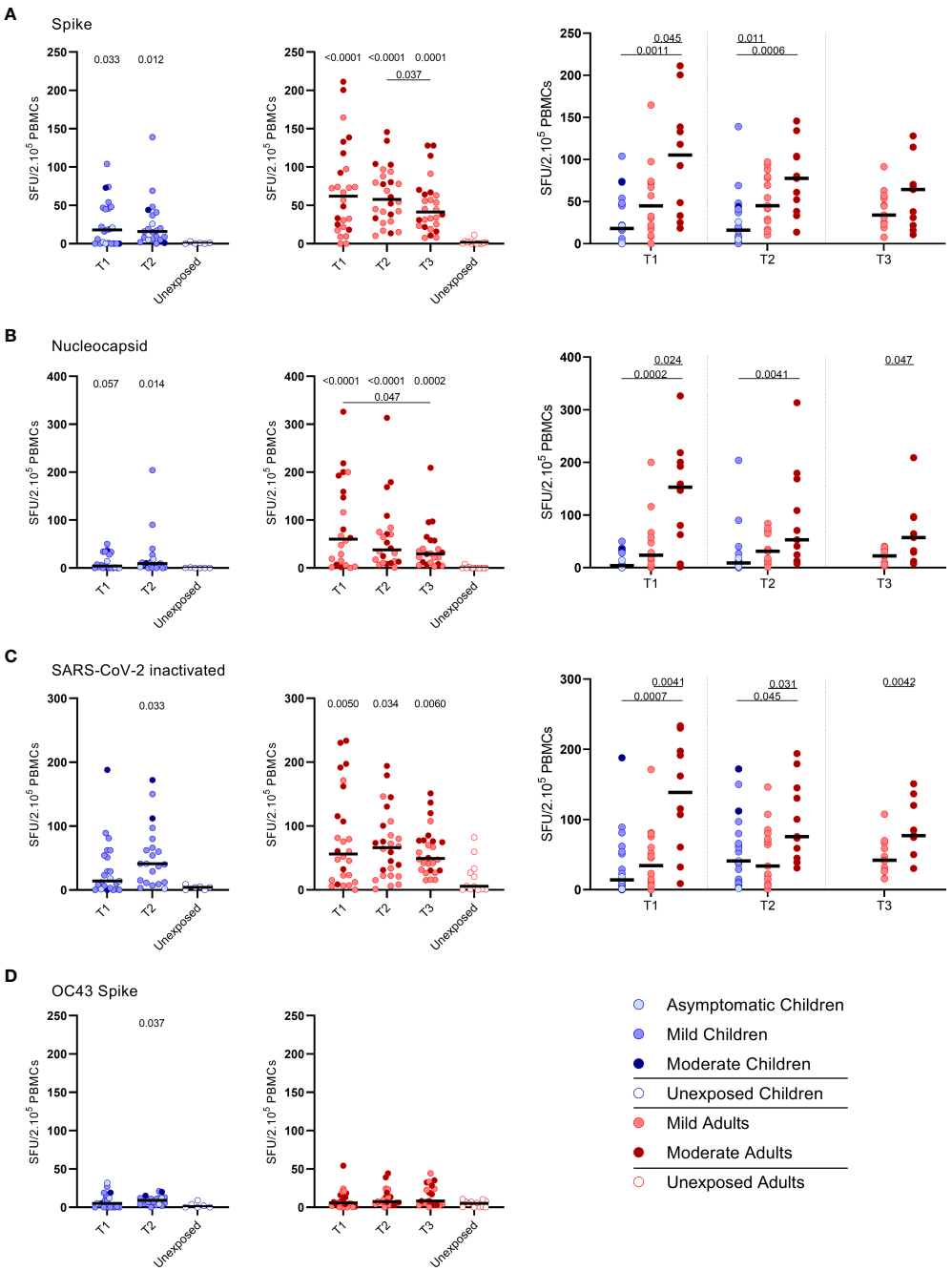


FIGURE 1 | SARS-CoV-2-specific IFN-γ$^+$ T cell response in infected children and infected adults (mild and moderate cases) versus unexposed healthy controls over time after infection. Dot plots summarizing the frequencies of IFN-γ-producing cells responding to SARS-CoV-2 and HCoV-OC43 antigens for **(A–D)** children (left panel, blue), adults (middle panel, red), and children versus mild and moderate adult cases separately (right panel), over time after infection, and compared to unexposed adults/children (ELISPOT assay). Frequencies of IFN-γ-producing cells responding to **(A)** set of overlapping peptides of SARS-CoV-2 spike protein, **(B)** set of overlapping peptides of SARS-CoV-2 nucleocapsid protein, **(C)** inactivated SARS-CoV-2, and **(D)** set of overlapping peptides of HCoV-OC43 spike protein. Each dot represents one subject. Bars indicate the median of spot-forming units per 200,000 PBMCs. SFU, spot-forming unit. **(A–D)** P values related to comparisons with the unexposed controls are listed at the top of the graph, above the corresponding group for comparison. For unpaired comparisons, Mann-Whitney U test (two-group comparisons) (mild adults versus moderate adults) or Kruskal-Wallis rank-sum test with Dunn's *post hoc* test for multiple comparisons were used (children versus mild adults versus moderate adults; unexposed versus infected children or adults at T1 versus T2 versus T3). Differences between paired data were compared using the Wilcoxon signed-rank test (for comparison of two paired groups) (infected children at T1 versus T2) or the Friedman test with Dunn's multiple comparison tests (infected adults at T1 versus T2 versus T3). Statistically significant comparisons are indicated, with P values < 0.05 considered significant. T1, first timepoint of sampling for adults median 12.5 days and children median 8 days post-symptom onset; T2, 10-14 days after T1; T3, 4-6 weeks after T1.

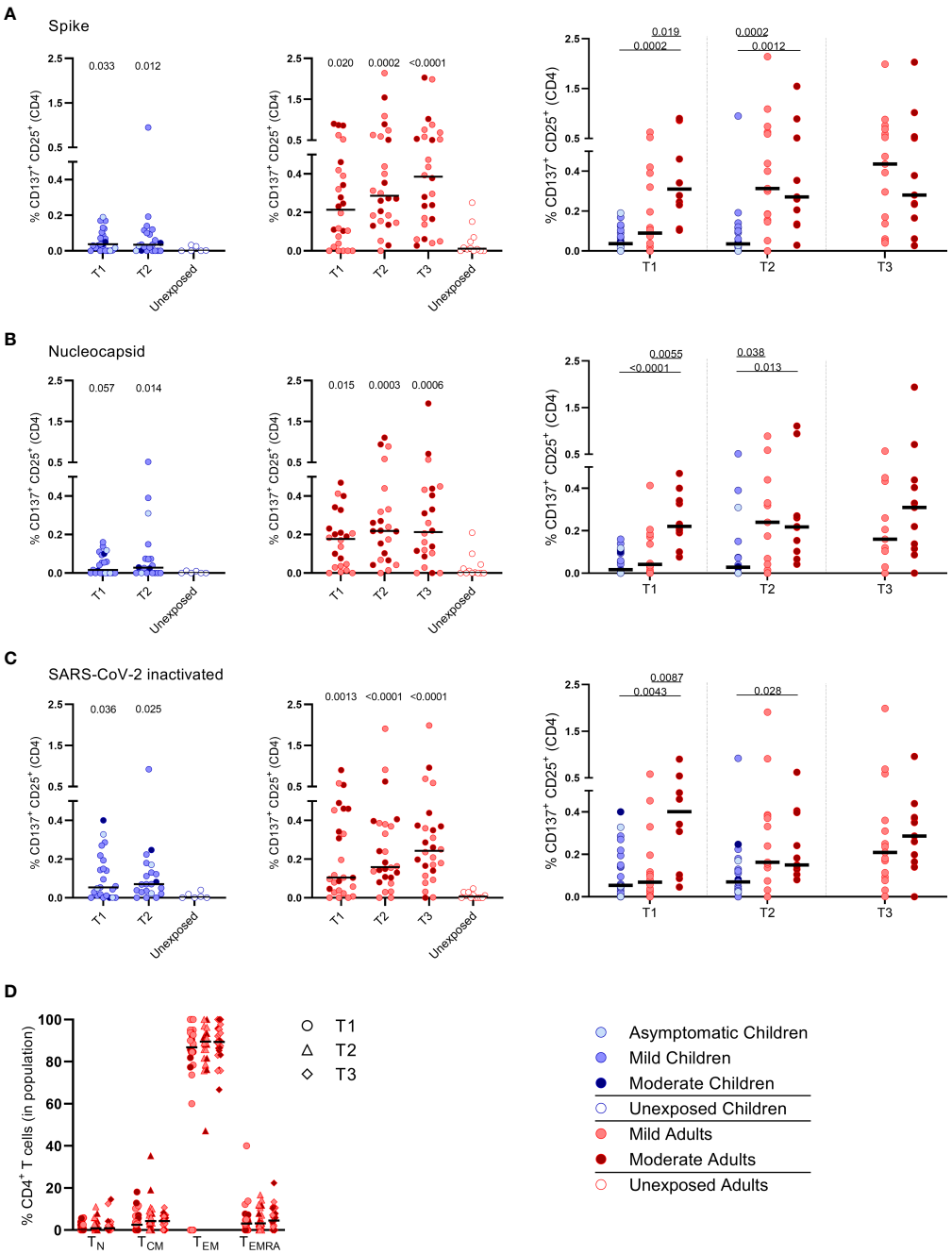


FIGURE 2 | Frequencies of activated CD4$^+$ T cells of infected children and infected adults (mild and moderate cases) versus unexposed healthy controls over time after infection. Dot plots summarizing the percentages of CD25$^+$/CD137$^+$ activated CD4$^+$ T cells responding to SARS-CoV-2 antigens for **(A–D)** children (left panel, blue), adults (middle panel, red), and children versus mild and moderate adult cases separately (right panel). Percentages of CD25$^+$/CD137$^+$ activated CD4$^+$ T cells responding to **(A)** set of overlapping peptides of SARS-CoV-2 spike protein, **(B)** set of overlapping peptides of SARS-CoV-2 nucleocapsid, **(C)** inactivated SARS-CoV-2. **(D)** Immunophenotyping at the single-cell level showing the different memory subsets within the SARS-CoV-2-specific activated CD4$^+$ T cells from infected adults. Each dot represents one subject. Bars indicate the median percentage of total CD4$^+$ T cells. **(A–C)** P values related to comparisons with the unexposed controls are listed at the top of the graph, above the corresponding group for comparison. For unpaired comparisons, Mann-Whitney U test (two-group comparisons) (mild adults versus moderate adults) or Kruskal-Wallis rank-sum test with Dunn's *post hoc* test for multiple comparisons were used (children versus mild adults versus moderate adults; unexposed versus infected children or adults at T1 versus T2 versus T3). Differences between paired data were compared using the Wilcoxon signed-rank test (for comparison of two paired groups) (infected children at T1 versus T2) or the Friedman test with Dunn's multiple comparison tests (infected adults at T1 versus T2 versus T3). Statistically significant comparisons are indicated, with P values < 0.05 considered significant. T1, first timepoint of sampling for adults median 12.5 days and children median 8 days post-symptom onset; T2, 10-14 days after T1; T3, 4-6 weeks after T1.

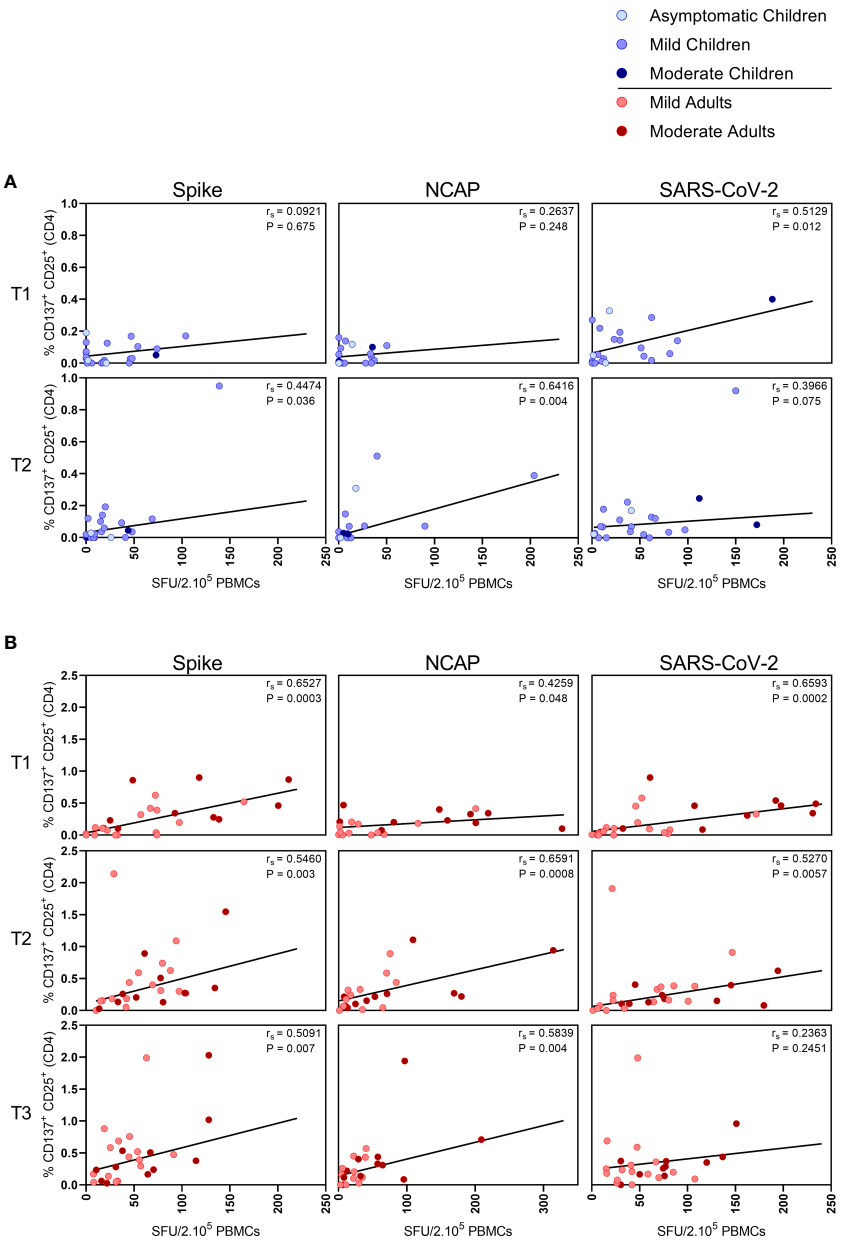


FIGURE 3 | Correlation between IFN-γ+ T cell frequency and activated CD4+ T cells. Spearman correlation between frequency of IFN-γ+ responder cells and percentages of CD25+/CD137+ activated CD4+ T cells of **(A)** children and **(B)** adults responding to a set of overlapping peptides of SARS-CoV-2 spike protein (left panel), or a set of overlapping peptides of SARS-CoV-2 nucleocapsid protein (middle panel) or inactivated SARS-CoV-2 (right panel) at different time points after infection. Each dot represents one subject. Correlation coefficients (r_s) were determined with Spearman's rank correlation. P values < 0.05 were considered significant. T1, first timepoint of sampling for adults median 12.5 days and children median 8 days post-symptom onset; T2, 10-14 days after T1; T3, 4-6 weeks after T1.

serum IgM concentrations at T2 and T3 [respectively, r_s=0.42 (P=0.03) and r_s=0.50 (P=0.01)], with S1-SARS-CoV-2-specific serum IgG concentrations at T3 [r_s=0.47 (P=0.01)], and with S1-SARS-CoV-2-specific serum IgA concentrations at T3 (r_s=0.45 (P=0.02)) (**Figure 5B**).

The median S1-SARS-CoV-2-specific serum IgG concentrations (**Figure 5C**) for infected children increased >100-fold in time after infection, from 0.21 AU/ml at T1 to 25 AU/ml at T2, while a 7-fold increase was observed for infected adults from T1 (median IgG concentration of 3.9 AU/ml) to T2 (26 AU/ml)), and an 8-fold increase from T1 to T3 (31 AU/ml) (**Figure 5C**, upper panel). Nevertheless, S1-SARS-CoV-2-specific serum IgG concentrations of infected adults experiencing moderate COVID-19 were clearly higher than levels of infected children or adults with mild symptoms at all time points after infection (**Figure 5C**, lower panel).

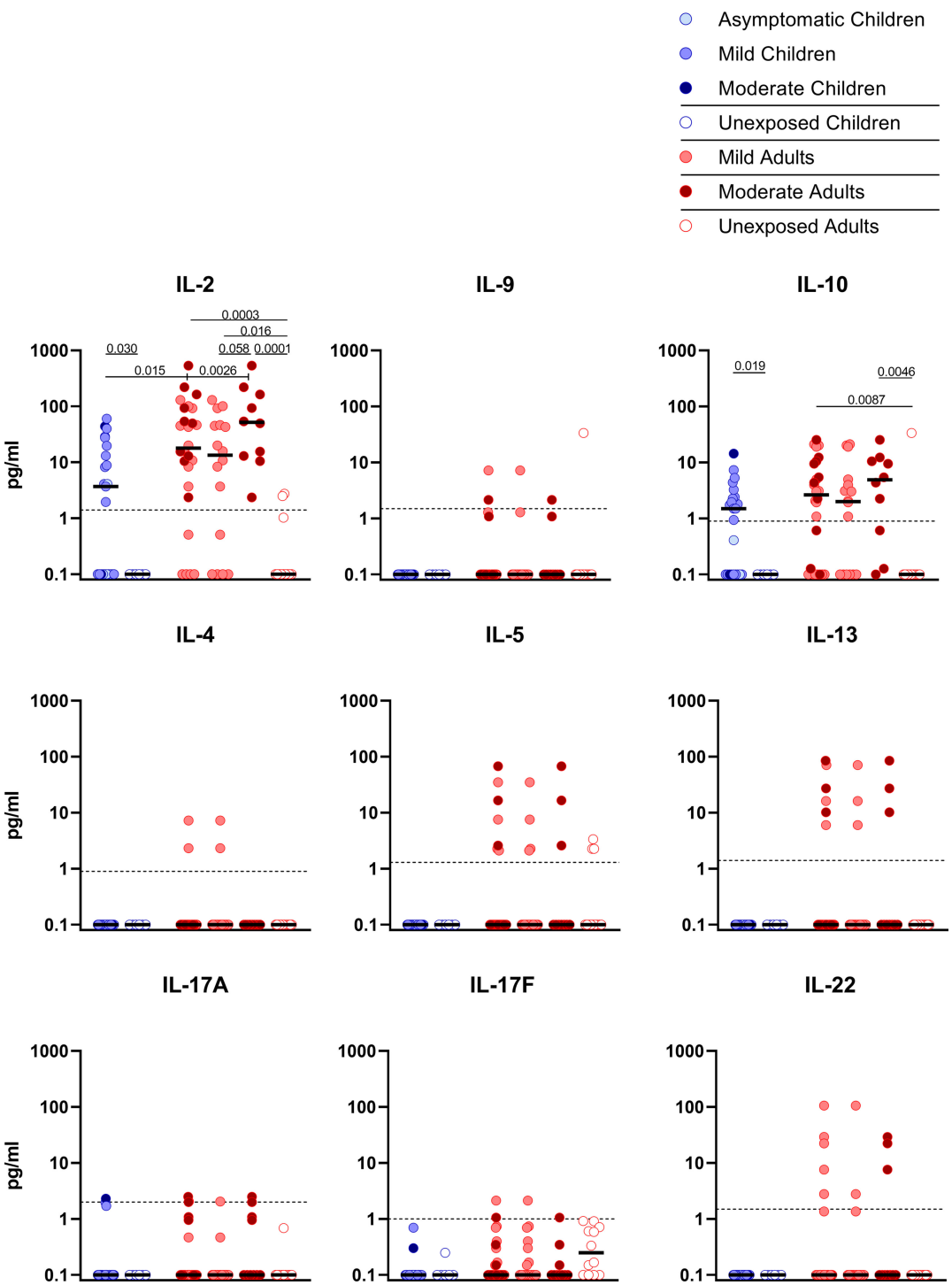


FIGURE 4 | Cytokine release in infected children and mild versus moderate symptomatic adults over time after infection. Cell-free culture supernatants were harvested from IFN-γ ELISPOT plates and the release of the following cytokines was measured in T1 samples: IL-2, IL-4, IL-5, IL-9, IL-10, IL-13, IL-17A, IL-17F, IL-22. Dot plots show the concentration of cytokines (pg/ml) after stimulation of PBMCs with a set of overlapping peptides of SARS-CoV-2 spike protein. Infected children and unexposed children versus infected adults with mild or moderate disease and unexposed adults are depicted. Minimum detection threshold (MDT) concentrations for each cytokine, as calculated by the manufacturer and mentioned in the Material and Methods section, are indicated with horizontal dotted lines. Each dot represents one subject. Bars indicate the median cytokine concentration (pg/ml). For two-group comparisons (infected children versus unexposed children), Mann-Whitney U test was used. Kruskal-Wallis rank-sum test with Dunn's *post hoc* test for multiple comparisons was used (all adults versus mild adults versus moderate adults versus unexposed adults; all adults versus mild adults versus moderate adults versus infected children). P-values ≤ 0.05 are presented.

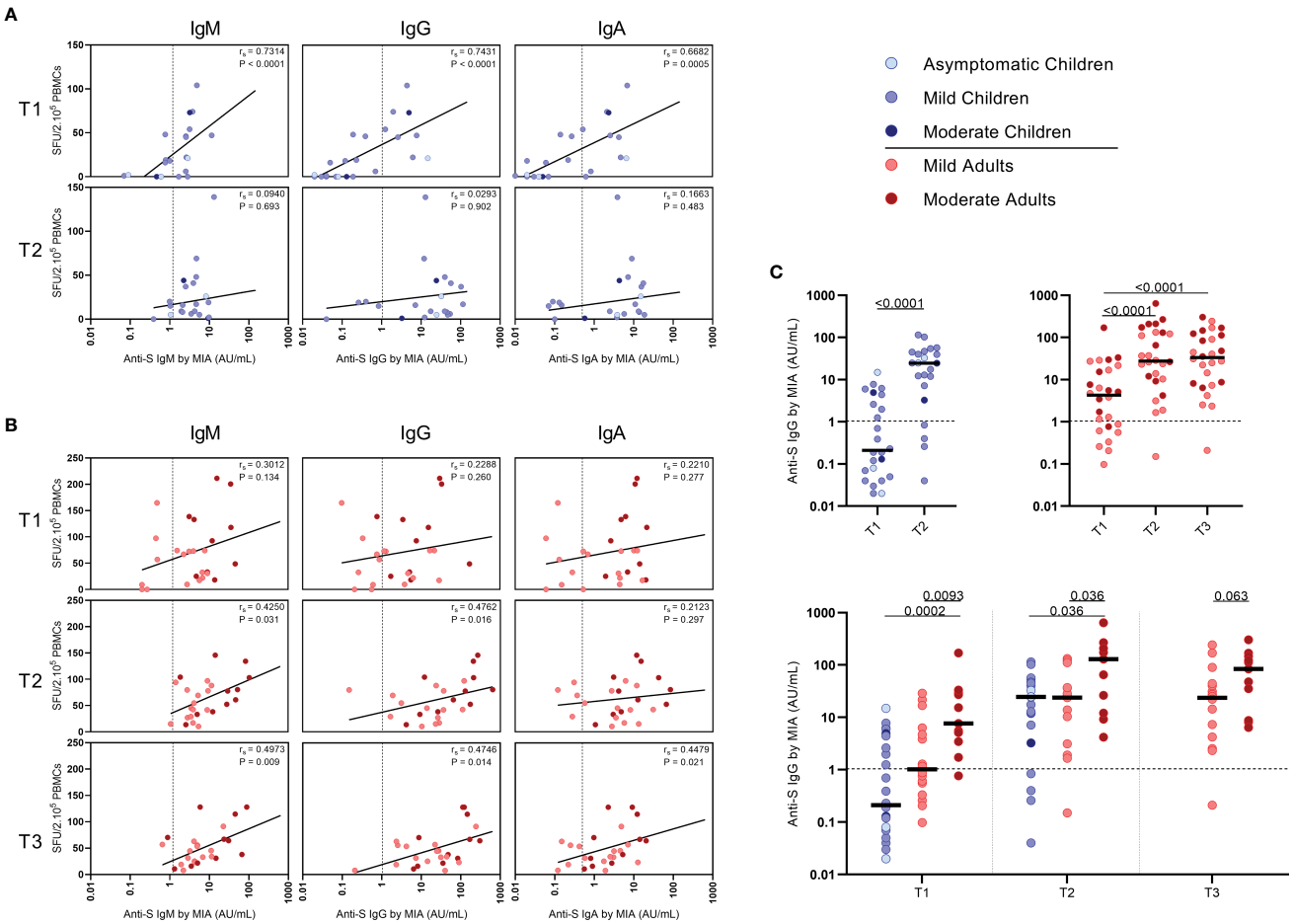


FIGURE 5 | Correlation between frequencies of SARS-CoV-2-specific IFN-γ^+ T cells and antibody concentrations to S1-SARS-CoV-2. Spearman correlation between frequency of SARS-CoV-2-specific IFN-γ^+ responder cells and concentrations of spike-S1 IgM, IgG, or IgA serum antibodies measured by multiplex immunoassay (MIA) at different time points after infection in **(A)** children and **(B)** adults. Concentrations of spike-S1 IgG serum antibodies at the various time points after SARS-CoV-2 infection in the whole group of children and adults (**C**, upper panel) and in the whole group of children versus the mild and moderate adult cases (**C**, lower panel). Cut-off values for seroprevalence are indicated with vertical or horizontal dotted lines. Each dot represents one subject. Correlation coefficients (r_s) were determined with Spearman's rank correlation. P values < 0.05 were considered significant. Differences in IgG concentrations for paired data were compared using the Wilcoxon signed-rank test (for comparison of two paired groups) (infected children at T1 versus T2) or the Friedman test with Dunn's multiple comparison tests (infected adults at T1 versus T2 versus T3). For unpaired comparisons, Mann-Whitney U test (two-group comparisons) (mild adults versus moderate adults) or Kruskal-Wallis rank-sum test with Dunn's *post hoc* test for multiple comparisons were used (children versus mild adults versus moderate adults; at T1 versus T2 versus T3). Statistically significant comparisons are indicated, with P values < 0.05 considered significant. T1, first timepoint of sampling for adults median 12.5 days and children median 8 days post-symptom onset; T2, 10-14 days after T1; T3, 4-6 weeks after T1.

SARS-CoV-2-Specific IFN-γ^+ T Cell Frequency and Antibody Response at 10 Months After Infection

To study the long-term SARS-CoV-2-specific immune response, we collected follow-up blood samples at 10 months ± 13 days after symptoms onset (referred to as 'T4') from 18 children and 21 adults. Vaccinated persons (adults: n=3) at the time of T4 sampling were excluded from analysis. In children, the median age was 12 years (5-16 years) and 56% were female at T4 sampling. The median age of adults was 44 years (18-87 years), 48% were female, and 48% were mild cases at T4 sampling.

S-SARS-CoV-2-specific IFN-γ^+ responses higher than 5 SFU/ 2.10^5 PBMCswere still found in 44% (8/18) of the infected children and 81% (17/21) of the infected adults at 10 months after symptom onset. In children, frequencies of S-SARS-CoV-2-specific IFN-g$^+$ T cells underwent a 4-fold decline at 10 months (T4) compared to frequencies at 3 weeks (T2, P=0.027) after infection, and were no longer significantly different from unexposed children (**Figure 6A**, left panel). Also in adults, IFN-γ^+ S-SARS-CoV-2-specific T cell frequencieswere 6 to 7-fold lower at 10 months compared to earlier time points after infection. In contrast to children, frequencies of SSARS-CoV-2-specific IFN-γ^+ T cells at T4 were still significantly higher in infected adults compared to unexposed adults (9.2 versus

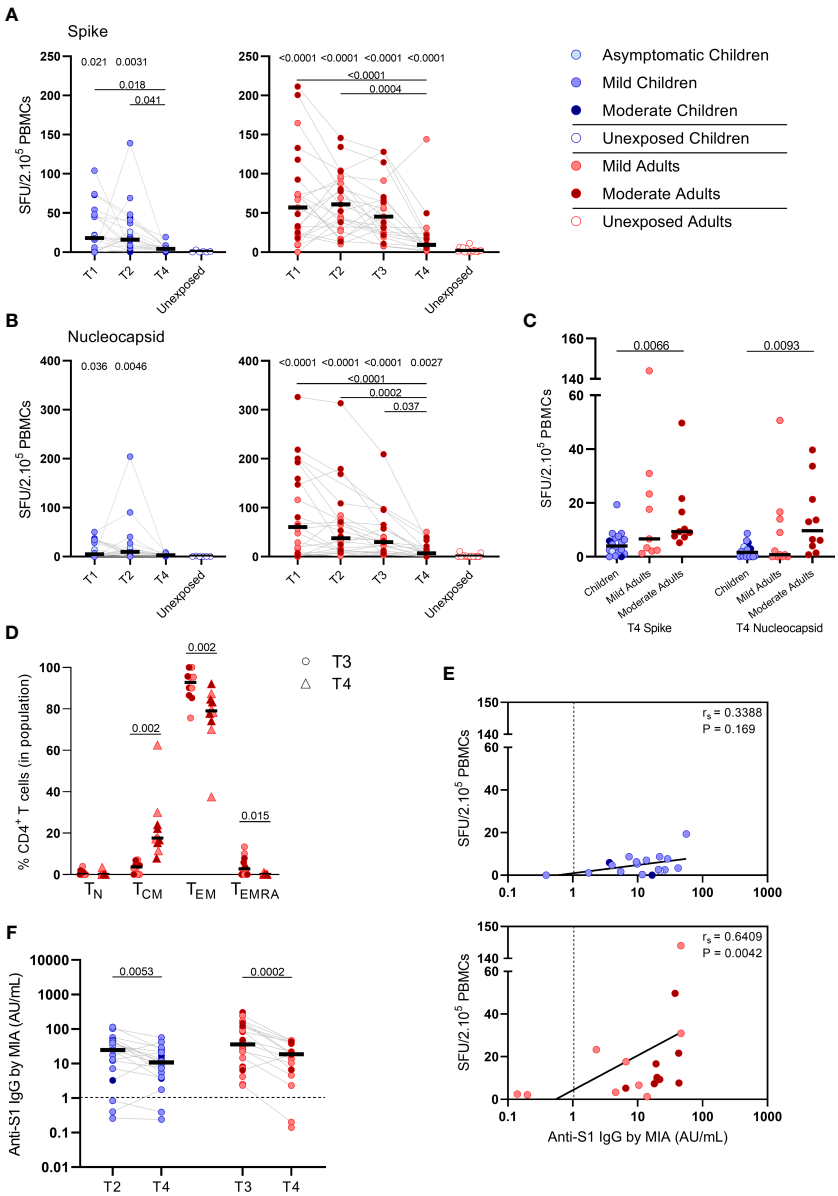


FIGURE 6 | SARS-CoV-2-specific immune response up to 10 months after infection. Dot plots summarizing the frequencies of IFN-γ-producing cells by ELISPOT assay responding to **(A)** a set of overlapping peptides of SARS-CoV-2 spike protein and **(B)** a set of overlapping peptides of SARS-CoV-2 nucleocapsid protein in children (left panel, blue) and adults (right panel, red), at different time points after infection, and compared to unexposed children/adults. **(C)** Dot plots showing the frequencies of IFN-γ-producing cells responding to SARS-CoV-2 spike and nucleocapsid proteins, at 10 months after symptom onset (T4) comparison of groups of children versus total, mild, and moderate adult cases separately. **(D)** Immunophenotyping at the single-cell level comparing the frequencies of different memory subsets from T3 versus T4 within the SARS-CoV-2-specific activated $CD4^+$ T cells from infected adults. **(E)** Spearman correlation between frequency of IFN-γ^+ responder cells and concentrations of anti-spike-S1 IgG serum antibodies measured by multiplex immunoassay (MIA) at T4 in children (upper panel, blue) and adults (lower panel, red). **(F)** Dot plots comparing the concentrations of anti-spike-S1 IgG serum antibodies at T2 or T3 versus T4 in children and adults. Each dot represents one subject. Bars indicate the median. SFU, spot-forming unit. **(A, B)** P values related to comparisons with the unexposed controls are listed at the top of the graph, above the corresponding group for comparison. For unpaired comparisons, Mann-Whitney U test (two-group comparisons) (mild adults versus moderate adults, infected children or adults at T4 versus unexposed children or adults) or Kruskal-Wallis rank-sum test with Dunn's *post hoc* test for multiple comparisons were used (children versus total adults versus mild adults versus moderate adults; unexposed versus infected children or adults at T1 versus T2 versus T3). Differences between paired data were compared using the Wilcoxon signed-rank test (for comparison of two paired groups) (memory T cell subsets at T3 versus T4; concentrations of anti-spike-S1 IgG serum antibodies at T2 or T3 versus T4) or the Friedman test with Dunn's multiple comparison tests (infected children or adults at T1 versus T2 versus T3 versus T4). Statistically significant comparisons are indicated, with P values < 0.05 considered significant. Cut-off values for seroprevalence are indicated with vertical dotted lines in **(E, F)**. Correlation coefficients (r_s) were determined with Spearman's rank correlation. Statistically significant comparisons are indicated. P values < 0.05 were considered significant. T1, first timepoint of sampling for adults median 12.5 days and children median 8 days post-symptom onset; T2, 10-14 days after T1; T3, 4-6 weeks after T1; T4, 10 months ± 13 days after symptom onset.

1.7 SFU/2.10^5 PBMCs; P=0.0003) (**Figure 6A**, right panel). IFN-γ$^+$ N-SARS-CoV-2-specific T cell frequencies also declined at 10 months upon infection in adults compared to earlier time points (7.7 SFU/2.10^5 PBMCs at T4 vs 62 (P<0.0001), 47.0 (P=0.0008), and 31.1 (P=0.039) SFU/per 2.10^5 PBMCs at T1, T2, and T3, respectively), but remained significantly higher compared to unexposed adults (0.05 SFU/2.10^5 PBMCs) (**Figure 6B**, right panel). Frequencies of IFN-γ$^+$ N-SARS-CoV-2-specific T cells were low in children and no changes over time were observed (**Figure 6B**, left panel). Similar to earlier time points, S-SARS-CoV-2-specific responses were 2.3-fold higher in adults compared to children at 10 months after infection (9.2 versus 4.0 SFU/2.10^5 SFU/PBMCs). These differences were mainly caused by slightly higher responses from adults experiencing moderate symptoms (P=0.0021) (**Figure 6C**). Albeit not significant, a trend of higher frequencies of S-SARS-CoV-2-specific IFN-γ+ T cells in infected adults with moderate symptoms persisted at 10 months compared to mild disease (**Figure 6C**). In line with results from earlier time points, the SARS-CoV-2-specific activated cells at 10 months were mainly of the effector memory (CD45RO$^+$/CCR7$^-$) (TEM) subset. Interestingly, however, a 4.7-fold increase of centralmemory T cell frequencies (CD45RO$^+$/CCR7$^+$) (T_{CM}) was found 10 months after symptom onset (from 3.7% at T3 to 17.6% at T4; P=0.002) (**Figure 6D**).

Only in adults, the frequency of S-SARS-CoV-2-specific IFNγ-producing T cells was still correlated with S1-SARS-CoV-2-specific serum IgG concentrations at 10 months after symptom onset [r_s=0.64 (P=0.004)] (**Figure 6E**). S1-SARS-CoV-2-specific IgG serum antibody concentrations significantly decreased at 10 months compared to earlier time points in both children and adults [median IgG concentrations of 10.8 AU/mL at T4 versus 24.6 AU/mL at T2 (P=0.0053) in children, and 18.7 AU/mL at T4 versus 35.8 AU/mL T3 versus in adults (P=0.0002)]. Despite this decline, 90% (18/20) of infected children and 89% (16/18) of infected adults remained S1-SARS-CoV-2-IgG seropositive 10 months after infection. No differences were observed in anti-S1-SARS-CoV-2 serum IgG concentrations at 10 months between children and adults (**Figure 6F**).

DISCUSSION

Most infections with SARS-CoV-2, especially among children, have a mild course. But, do children, despite experiencing mild infection, develop memory T cell immunity? Here, we describe the kinetics, function, and phenotype of SARS-CoV-2-specific T cells of infected children in comparison with adults experiencing mild to moderate COVID-19 symptoms. Only limited studies have been reported investigating the immune responses in children with mild/asymptomatic SARS-CoV-2 infection (17-21). The strength of our study is that we evaluated the recall T cell response upon SARS-CoV-2 specific stimulation, and compared it to unexposed children and adults.

First, we analyzed immune cell populations over time after infection. Frequencies of total T cells, B cells, monocytes, or NK cellswere comparable between healthy age-matched control groups and infected groups. However, in infected adults, slightly higher frequencies of CD4$^+$ T_{EM} and CD8$^+$ T_{EM} cell subsets were found at later time points after infection. This small increase in TEM cell subsets may be caused by an increase of circulating SARS-CoV-2-specificCD4$^+$ T_{EM} and CD8$^+$ T_{EM} cells in response to SARS-CoV-2 infection. In line with this, in infected adults also transiently higher frequencies of CD4$^+$ T_{CM} and T_{EMRA} cells expressing CD38/HLA-DR were observed early after infection,and inbothinfectedchildren and infected adults, transiently higher frequencies of CD8$^+$ T cells expressing CD38/HLA-DR were observed within the T_{CM}/T_{EM}/T_N cell subsets at the earlier time points after infection. This indicatesthat antigen-specific activation of T cells was triggered in adults as well as in children by SARS-CoV-2 infection. T cell activation, especially robust CD38$^+$/HLA-DR$^+$CD8$^+$T cell responses, has been identified as a hallmark of acute COVID-19 (2, 4, 8).

We found higher frequencies of SARS-CoV-2-specific IFN-Γ$^+$ T cells in all infected groups compared to the unexposed control groups upon any of the three antigenic stimulations that included heat-inactivated SARS-CoV-2, and overlapping peptides of SARS-CoV-2 spike protein (S-SARS-CoV-2), and nucleocapsid protein (N-SARS-CoV-2). Ingeneral, frequencies of IFN-γ$^+$-T cells reactive against SARS-CoV-2 antigens were lower in infected children, who generally had mild/asymptomatic infection, compared to infected adults. The lower SARS-CoV-2-specific T cell response observed in children suggests that other compartments of the immune system, such as the innate immune response, contribute to faster clearing of the infection, as demonstrated by others (31–33). The higher T cell responses in infected adults could largely be explained by higher T cell responses found in severalmoderate cases, although adultswith mild complaints also tended to have slightly higher responses than infected children. This is in agreement with findings from other studies showing higher frequencies of SARS-CoV-2-specific T cells in severe patients compared to mildly symptomatic patients (8, 15). In contrast, critically ill patients have been reported to exhibit qualitatively impaired S-SARS-CoV-2-specific CD4$^+$ T cell responses, indicating that a good $CD4_+$ T cell response may protect against serious disease (15). In agreement with our IFN-γ ELISPOT data, significantly lower frequencies of SARS-CoV-2-specific activated CD25$^+$ CD137$^+$ CD4$^+$ T cells were observed in infected children compared to infected adults. Recently, Cohenet al. also described that acute and memory CD4$^+$ T cells in SARS-CoV-2-infected children were significantly lower than in adults, while polyfunctional cytokine production byT cells was comparable (21). Furthermore, in accordance with Cohen et al. (21), we found that the SARS-CoV-2 activated T cells mainly belonged to the CD4$^+$ effector memory subset (T_{EM}: CD45RO$^+$/CCR7$^-$) in our experimental setting. Data on the SARS-CoV-2-specific IFN-γ$^+$ T cell response and CD4$^+$ T cell activation correlated, suggesting that IFN-γ was produced by antigen-specific CD4$^+$ T cells. Apart from IFN-γ, SARS-CoV-2-specific T cells produced IL-2, suggestive for a Th1 phenotype of the CD4$^+$ T_{EM}.

It has been demonstrated that SARS-CoV-2-specific T cell responses can be retained 6-8 months following infection

regardless of disease severity (8, 16, 34). Although, other studies showed a clear decline of the T cell response over a 6-8 month period in asymptomatic as well as symptomatic COVID-19 patients (35, 36). In our study, at 10 months after symptom onset, the frequencies of SARS-CoV-2-specific IFN-γ^+ T cells were significantly reduced in adults and were nearly undetectable in children. Whether this is a result of waning immunity or migration of memory SARS-CoV-2-specific T cells to peripheral tissues remains to be investigated. Interestingly, the memory phenotype of the activated SARS-CoV-2-specific $CD4^+$ T cells in adults showed a shift from mainly T_{EM} to a more T_{CM} phenotype at 10 months after infection; T_{CM} subset increased from 3.7% to 17.6% of the antigen-specific $CD4^+$ T cells. This T_{CM} subset may persist for longer after infection.

In contrast to the observed SARS-CoV-2-specific $CD4^+$ T cell response, we found very low frequencies of activated ($CD25^+$/$CD137^+$) $CD8^+$ T cells upon SARS-CoV-2-specific stimulation. An explanation for this may be that $CD8^+$ T cells have migrated to the local sites of infection to attack virus-infected cells or might be a result of the antigenic stimulation used in our study. Smaller peptides (9 to 10-mers instead of 15-mers) or live SARS-CoV-2 may be more suitable to measure $CD8^+$ T cell responses. Sekine et al. also observed proportionately larger SARS-CoV-2-specific $CD4^+$ T cell responses than $CD8^+$ T cell responses to different sets of overlapping peptides in the convalescent phase of both mild and severe COVID-19 cases, although in that study also IFN-γ^+ $CD8^+$ T cell responses were detected (8).

We found positive correlations between SARS-CoV-2-specific IFN-γ^+ T cell frequency and serum-IgG, -IgM, and -IgA antibody concentrations to S1-SARS-CoV-2 in both children and adults. Although, it should be taken into account that the antibody concentrations of considerable numbers of children were below the threshold for seropositivity (10). Other studies have also shown positive correlations between S-SARS-CoV-2-specific IgG antibodies and T cell responses (6, 37, 38).

Pre-existing cross-reactive T cell immunity generated by common cold human coronaviruses (HCoV) has been suggested to affect clinical outcomes of SARS-CoV-2 infection. T cell lines from unexposed healthy donors specific for S-HCoV-229E and -OC43 were cross-reactive to S-SARS-CoV-2 (39). Based on these findings, the authors suggested that children may have higher HCoV prevalence due to more frequent social contacts, explaining their lower risk for severe COVID-19 (39). In the present study, we did, however, not find a significant difference in the low frequencies of S-HCoV-OC43-reactive IFNγ^+ T cells between unexposed children and unexposed adults. In another study with mild COVID-19 adult patients, also low T cell frequencies recognizing S-HCoV-229E/S-HCoV-OC43 peptide pools were found (15). It cannot be excluded that preexisting cross-reactive immunity to other conserved parts of SARS-CoV-2 played a role, or that pre-existing immunity to other HCoV played a role. We, however, found no evidence that pre-existing S-HCoV-OC43-reactive T cells boosted upon SARS-CoV-2 infection could explain the mild course of infection.

Limited data is available on the immune response to SARS-CoV-2 in children. Here, we show that infected children do develop a SARS-CoV-2-specific T cell response. However, frequencies of SARS-CoV-2 reactive T cells were lower in infected children who almost all had mild/asymptomatic infection compared to infected adults with mild to moderate COVID-19. Predominantly $CD4^+$ T cells, and not $CD8^+$ T cells, were activated upon stimulation with SARS-CoV-2 antigens. Nevertheless, frequencies of SARS-CoV-2-specific T cells circulating in the blood were significantly reduced at 10 months after infection, although migration of memory SARS-CoV-2-specific T cells to peripheral tissues may have taken place. Importantly, our data indicate that an antigen-specific T cell and antibody response is developed after experiencing mild SARS-CoV-2 infection. It remains to be elucidated to what extent this SARS-CoV-2-specific response can contribute to an effective recall response after reinfection.

DATA AVAILABILITY STATEMENT

Datasets are available on request: The raw data supporting the conclusions of this article will be made available by the authors upon request, with consideration of the participants' privacy rights.

ETHICS STATEMENT

The studies involving human participants were reviewed and approved by Medical-Ethical Review Committee (MERC) of University Medical Center Utrecht (Netherlands Trial Register (https://www.trialregister.nl/): NL9850, MERC Reference number: NL13529.041.06). Protocols for the cohort studies with unexposed children (Immfact, NTR: NL9775, MERC Reference number: NL4679.094.13) and adults (NVI-255, NTR: NL1952, MERC Reference number: NL29241.000.09) were approved by Medical-Ethical Review Committees of the Netherlands. Written informed consent to participate in this study was provided by all participants and/or from parents/guardians of minor participants (<16 years old).

AUTHOR CONTRIBUTIONS

DR, NR, JB, and LB designed and conducted the clinical study. AM conducted and analyzed data of the PCR testing. JW, PK, ME, MP, AC, and CE designed, conducted, and acquired data of T cell immunity testing. GH and RS designed, conducted, and acquired data of antibody testing. VP and PK statistically analyzed data. VP and ME made figures. PK wrote the first draft of the manuscript and all authors contributed to the final version of the paper. All authors contributed to the article and approved the submitted version.

FUNDING

This work was supported by the Dutch Ministry of Health, Welfare, and Sport.

ACKNOWLEDGMENTS

We are grateful to the members of the Dutch FFX-COVID-19 research group of the Centre for Infectious Disease Control, National Institute for Public Health and the Environment, the Netherlands, that includes Arianne van Gageldonk-Lafeber, Wim van der Hoek, Susan van den Hof, Chantal Reusken and Inge Roof for their contribution to the design and the conduct of the SARS-CoV-2-related clinical study. We thank the Public Health Service Utrecht for assistance in the recruitment of households. We thank Anneke Westerhof, Anne-Marie van den Brandt, Anoek Backx, Bas van der Veer, Elma Smeets -Roelofs, Elsa Porter, Elske Bijvank, Fion Brouwer, Francoise van Heiningen, Gabriel Goderski, Gert-Jan Godeke, Harry van Dijken, Helma Lith, Hinke ten Hulscher, Ilse Akkerman, Ilse Schinkel, Jeroen Hoeboer, Johan Reimerink, Jolanda Kool, Josien Lanfermeijer, Joyce Greeber, Kim Freriks, Kina Helm, Lidian Izeboud, Lisa Wijsman, Liza Tymchenko, Martijn Vos, Margriet Bisschoff, Marieke Hoogerwerf, Marit de Lange, Marit Middeldorp, Marjan Bogaard, Marjan Kuijer, Nening Nanlohy, Olga de Bruin, Rob van Binnendijk, Rogier Bodewes, Ronald Jacobi, Ruben Wiegmans, Sakinie Misiedjan, Saskia de Goede, Sharon van den Brink, Sophie van Tol, Teun Guichelaar, Titia Kortbeek, and Yolanda van Weert for support during the stages of this study, household visits, processing samples and laboratory analyses.

SUPPLEMENTARY MATERIAL

The Supplementary Material for this article can be found online at: https://www.frontiersin.org/articles/10.3389/fimmu.2022.817876/full#supplementary-material

REFERENCES

1. Lucas C, Wong P, Klein J, Castro TBR, Silva J, Sundaram M, et al. Longitudinal Analyses Reveal Immunological Misfiring in Severe COVID-19. *Nature* (2020) 584(7821):463–9. doi: 10.1038/s41586-020-2588-y
2. Mathew D, Giles JR, Baxter AE, Oldridge DA, Greenplate AR, Wu JE, et al. Deep Immune Profiling of COVID-19 Patients Reveals Distinct Immunotypes With Therapeutic Implications. *Science* (2020) 369(6508): eabc8511. doi: 10.1126/science.abc8511
3. Giamarellos-Bourboulis EJ, Netea MG, Rovina N, Akinosoglou K, Antoniadou A, Antonakos N, et al. Complex Immune Dysregulation in COVID-19 Patients With Severe Respiratory Failure. *Cell Host Microbe* (2020) 27(6):992–1000.e3. doi: 10.1016/j.chom.2020.04.009
4. Kuri-Cervantes L, Pampena MB, Meng W, Rosenfeld AM, Ittner CAG, Weisman AR, et al. Comprehensive Mapping of Immune Perturbations Associated With Severe COVID-19. *Sci Immunol* (2020) 5(49):1–15. doi: 10.1126/sciimmunol.abd7114
5. Wu Z, McGoogan JM. Characteristics of and Important Lessons From the Coronavirus Disease 2019 (COVID-19) Outbreak in China: Summary of a Report of 72314 Cases From the Chinese Center for Disease Control and Prevention. *JAMA* (2020) 323(13):1239–42. doi: 10.1001/jama.2020.2648
6. Reynolds CJ, Swadling L, Gibbons JM, Pade C, Jensen MP, Diniz MO, et al. Discordant Neutralizing Antibody and T Cell Responses in Asymptomatic and Mild SARS-CoV-2 Infection. *Sci Immunol* (2020) 5(54):eabf3698. doi: 10.1126/sciimmunol.abf3698
7. Rodda LB, Netland J, Shehata L, Pruner KB, Morawski PA, Thouvenel CD, et al. Functional SARS-CoV-2-Specific Immune Memory Persists After Mild COVID-19. *Cell* (2021) 184(1):169–83.e17. doi: 10.1016/j.cell.2020.11.029
8. Sekine T, Perez-Potti A, Rivera-Ballesteros O, Stralin K, Gorin JB, Olsson A, et al. Robust T Cell Immunity in Convalescent Individuals With Asymptomatic or Mild COVID-19. *Cell* (2020) 183(1):158–68.e14. doi: 10.1016/j.cell.2020.08.017
9. Cox RJ, Brokstad KA. Not Just Antibodies: B Cells and T Cells Mediate Immunity to COVID-19. *Nat Rev Immunol* (2020) 20(10):581–2. doi: 10.1038/s41577-020-00436-4
10. den Hartog G, Vos ERA, van den Hoogen LL, van Boven M, Schepp RM, Smits G, et al. Persistence of Antibodies to SARS-CoV-2 in Relation to Symptoms in a Nationwide Prospective Study. *Clin Infect Dis* (2021) 73(12). doi: 10.1093/cid/ciab172
11. Seow J, Graham C, Merrick B, Acors S, Pickering S, Steel KJA, et al. Longitudinal Observation and Decline of Neutralizing Antibody Responses in the Three Months Following SARS-CoV-2 Infection in Humans. *Nat Microbiol* (2020) 5(12):1598–607. doi: 10.1038/s41564-020-00813-8
12. Le Bert N, Tan AT, Kunasegaran K, Tham CYL, Hafezi M, Chia A, et al. SARS-CoV-2-Specific T Cell Immunity in Cases of COVID-19 and SARS, and Uninfected Controls. *Nature* (2020) 584(7821):457–62. doi: 10.1038/s41586-020-2550-z
13. Altmann DM, Boyton RJ. SARS-CoV-2 T Cell Immunity: Specificity, Function, Durability, and Role in Protection. *Sci Immunol* (2020) 5(49):1–5. doi: 10.1126/sciimmunol.abd6160
14. Gallais F, Velay A, Nazon C, Wendling MJ, Partisani M, Sibilia J, et al. Intrafamilial Exposure to SARS-CoV-2 Associated With Cellular Immune Response Without Seroconversion, France. *Emerg Infect Dis* (2021) 27(1):113–21. doi: 10.3201/eid2701.203611
15. Oja AE, Saris A, Ghandour CA, Kragten NAM, Hogema BM, Nossent EJ, et al. Divergent SARS-CoV-2-Specific T- and B-Cell Responses in Severe But Not Mild COVID-19 Patients. *Eur J Immunol* (2020) 50(12):1998–2012. doi: 10.1002/eji.202048908
16. Zuo J, Dowell AC, Pearce H, Verma K, Long HM, Begum J, et al. Robust SARS-CoV-2-Specific T Cell Immunity is Maintained at 6 Months Following Primary Infection. *Nat Immunol* (2021) 22(5):620–6. doi: 10.1038/s41590-021-00902-8
17. Jia R, Wang X, Liu P, Liang X, Ge Y, Tian H, et al. Mild Cytokine Elevation, Moderate CD4(+) T Cell Response and Abundant Antibody Production in Children With COVID-19. *Virol Sin* (2020) 35(6):734–43. doi: 10.1007/s12250-020-00265-8
18. Moratto D, Giacomelli M, Chiarini M, Savare L, Saccani B, Motta M, et al. Immune Response in Children With COVID-19 is Characterized by Lower Levels of T-Cell Activation Than Infected Adults. *Eur J Immunol* (2020) 50(9):1412–4. doi: 10.1002/eji.202048724
19. Tosif S, Neeland MR, Sutton P, Licciardi PV, Sarkar S, Selva KJ, et al. Immune Responses to SARS-CoV-2 in Three Children of Parents With Symptomatic COVID-19. *Nat Commun* (2020) 11(1):5703. doi: 10.1038/s41467-020-19545-8
20. Petrara MR, Bonfante F, Costenaro P, Cantarutti A, Carmona F, Ruffoni E, et al. Asymptomatic and Mild SARS-CoV-2 Infections Elicit Lower Immune Activation and Higher Specific Neutralizing Antibodies in Children Than in Adults. *Front Immunol* (2021) 12:741796. doi: 10.3389/fimmu.2021.741796
21. Cohen CA, Li APY, Hachim A, Hui DSC, Kwan MYW, Tsang OTY, et al. SARS-CoV-2 Specific T Cell Responses are Lower in Children and Increase With Age and Time After Infection. *Nat Commun* (2021) 12(1):4678. doi: 10.1038/s41467-021-24938-4
22. Reukers DFM, van Boven M, Meijer A, Rots N, Reusken C, Roof I, et al. High Infection Secondary Attack Rates of SARS-CoV-2 in Dutch Households Revealed by Dense Sampling. *Clin Infect Dis* (2021) 74(1). doi: 10.1101/2021.01.26.21250512
23. Rosendahl Huber SK, Hendriks M, Jacobi RHJ, van de Kassteele J, Mandersloot-Oskam JC, van Boxtel RAJ, et al. Immunogenicity of Influenza Vaccines: Evidence for Differential Effect of Secondary Vaccination on Humoral and Cellular Immunity. *Front Immunol* (2018) 9:3103. doi: 10.3389/fimmu.2018.03103
24. den Hartog G, Schepp RM, Kuijer M, GeurtsvanKessel C, van Beek J, Rots N, et al. SARS-CoV-2-Specific Antibody Detection for Seroepidemiology: A

Multiplex Analysis Approach Accounting for Accurate Seroprevalence. *J Infect Dis* (2020) 222(9):1452–61. doi: 10.1093/infdis/jiaa479
25. Chattopadhyay PK, Yu J, Roederer M. A Live-Cell Assay to Detect Antigen-Specific CD4+ T Cells With Diverse Cytokine Profiles. *Nat Med* (2005) 11 (10):1113–7. doi: 10.1038/nm1293
26. Redmond WL, Ruby CE, Weinberg AD. The Role of OX40-Mediated Co-Stimulation in T-Cell Activation and Survival. *Crit Rev Immunol* (2009) 29 (3):187–201. doi: 10.1615/CritRevImmunol.v29.i3.10
27. Dan JM, Lindestam Arlehamn CS, Weiskopf D, da Silva Antunes R, Havenar-Daughton C, Reiss SM, et al. A Cytokine-Independent Approach To Identify Antigen-Specific Human Germinal Center T Follicular Helper Cells and Rare Antigen-Specific CD4+ T Cells in Blood. *J Immunol* (2016) 197(3):983–93. doi: 10.4049/jimmunol.1600318
28. Reiss S, Baxter AE, Cirelli KM, Dan JM, Morou A, Daigneault A, et al. Comparative Analysis of Activation Induced Marker (AIM) Assays for Sensitive Identification of Antigen-Specific CD4 T Cells. *PloS One* (2017) 12 (10):e0186998. doi: 10.1371/journal.pone.0186998
29. Wolfl M, Kuball J, Ho WY, Nguyen H, Manley TJ, Bleakley M, et al. Activation-Induced Expression of CD137 Permits Detection, Isolation, and Expansion of the Full Repertoire of CD8+ T Cells Responding to Antigen Without Requiring Knowledge of Epitope Specificities. *Blood* (2007) 110 (1):201–10. doi: 10.1182/blood-2006-11-056168
30. Betts MR, Brenchley JM, Price DA, De Rosa SC, Douek DC, Roederer M, et al. Sensitive and Viable Identification of Antigen-Specific CD8+ T Cells by a Flow Cytometric Assay for Degranulation. *J Immunol Methods* (2003) 281(1-2):65–78. doi: 10.1016/S0022-1759(03)00265-5
31. Pierce CA, Sy S, Galen B, Goldstein DY, Orner E, Keller MJ, et al. Natural Mucosal Barriers and COVID-19 in Children. *JCI Insight* (2021) 6(9):1–10. doi: 10.1172/jci.insight.148694
32. Neeland MR, Bannister S, Clifford V, Dohle K, Mulholland K, Sutton P, et al. Innate Cell Profiles During the Acute and Convalescent Phase of SARS-CoV-2 Infection in Children. *Nat Commun* (2021) 12(1):1084. doi: 10.1038/s41467-021-21414-x
33. Loske J, Rohmel J, Lukassen S, Stricker S, Magalhaes VG, Liebig J, et al. Pre-Activated Antiviral Innate Immunity in the Upper Airways Controls Early SARS-CoV-2 Infection in Children. *Nat Biotechnol* (2021). doi: 10.1038/s41587-021-01037-9
34. Sherina N, Piralla A, Du L, Wan H, Kumagai-Braesch M, Andrell J, et al. Persistence of SARS-CoV-2-Specific B and T Cell Responses in Convalescent COVID-19 Patients 6-8 Months After the Infection. *Med (N Y)* (2021) 2 (3):281–95.e4. doi: 10.1016/j.medj.2021.02.001
35. Dan JM, Mateus J, Kato Y, Hastie KM, Yu ED, Faliti CE, et al. Immunological Memory to SARS-CoV-2 Assessed for Up to 8 Months After Infection. *Science* (2021) 371(6529). doi: 10.1126/science.abf4063
36. Le Bert N, Clapham HE, Tan AT, Chia WN, Tham CYL, Lim JM, et al. Highly Functional Virus-Specific Cellular Immune Response in Asymptomatic SARS-CoV-2 Infection. *J Exp Med* (2021) 218(5):1–13. doi: 10.1084/jem.20202617
37. Weiskopf D, Schmitz KS, Raadsen MP, Grifoni A, Okba NMA, Endeman H, et al. Phenotype and Kinetics of SARS-CoV-2-Specific T Cells in COVID-19 Patients With Acute Respiratory Distress Syndrome. *Sci Immunol* (2020) 5 (48). doi: 10.1126/sciimmunol.abd2071
38. Grifoni A, Weiskopf D, Ramirez SI, Mateus J, Dan JM, Moderbacher CR, et al. Targets of T Cell Responses to SARS-CoV-2 Coronavirus in Humans With COVID-19 Disease and Unexposed Individuals. *Cell* (2020) 181(7):1489–501 e15. doi: 10.1016/j.cell.2020.05.015
39. Braun J, Loyal L, Frentsch M, Wendisch D, Georg P, Kurth F, et al. SARS-CoV-2-Reactive T Cells in Healthy Donors and Patients With COVID-19. *Nature* (2020) 587(7833):270–4. doi: 10.1038/s41586-020-2598-9

Conflict of Interest: The authors declare that the research was conducted in the absence of any commercial or financial relationships that could be construed as a potential conflict of interest.

Publisher's Note: All claims expressed in this article are solely those of the authors and do not necessarily represent those of their affiliated organizations, or those of the publisher, the editors and the reviewers. Any product that may be evaluated in this article, or claim that may be made by its manufacturer, is not guaranteed or endorsed by the publisher.

Copyright © 2022 Kaaijk, Olivo Pimentel, Emmelot, Poelen, Cevirgel, Schepp, den Hartog, Reukers, Beckers, van Beek, van Els, Meijer, Rots and de Wit. This is an open-access article distributed under the terms of the Creative Commons Attribution License (CC BY). The use, distribution or reproduction in other forums is permitted, provided the original author(s) and the copyright owner(s) are credited and that the original publication in this journal is cited, in accordance with accepted academic practice. No use, distribution or reproduction is permitted which does not comply with these terms.

frontiers | Frontiers in Immunology

CORRECTION
published: 29 April 2022
doi: 10.3389/fimmu.2022.893720

Corrigendum: Children and Adults With Mild COVID-19: Dynamics of the Memory T Cell Response Up to 10 Months

Patricia Kaaijk[1], Verónica Olivo Pimentel[1], Maarten E. Emmelot[1], Martien C. M. Poelen[1], Alper Cevirgel[1], Rutger M. Schepp[1], Gerco den Hartog[1], Daphne F. M. Reukers[1], Lisa Beckers[1], Josine van Beek[1], Cécile A. C. M. van Els[1,2], Adam Meijer[1], Nynke Y. Rots[1] and Jelle de Wit[1]*

[1] Centre for Infectious Disease Control, National Institute for Public Health and the Environment (RIVM), Bilthoven, Netherlands, [2] Faculty of Veterinary Medicine, Utrecht University, Utrecht, Netherlands

OPEN ACCESS

Edited and reviewed by:
Pia Kvistborg,
The Netherlands Cancer Institute (NKI), Netherlands

***Correspondence:**
Patricia Kaaijk
patricia.kaaijk@rivm.nl

Specialty section:
This article was submitted to T Cell Biology, a section of the journal Frontiers in Immunology

Received: 10 March 2022
Accepted: 23 March 2022
Published: 29 April 2022

Citation:
Kaaijk P, Olivo Pimentel V, Emmelot ME, Poelen MCM, Cevirgel A, Schepp RM, den Hartog G, Reukers DFM, Beckers L, van Beek J, van Els CACM, Meijer A, Rots NY and de Wit J (2022) Corrigendum: Children and Adults With Mild COVID-19: Dynamics of the Memory T Cell Response Up to 10 Months. Front. Immunol. 13:893720. doi: 10.3389/fimmu.2022.893720

Keywords: SARS-CoV-2, COVID-19, mild symptoms, children, T cell immunity, adaptive immunity, antibody response, cytokines

A Corrigendum on

Children and Adults With Mild COVID-19: Dynamics of the Memory T Cell Response Up to 10 Months

By Kaaijk P, Olivo Pimentel V, Emmelot ME, Poelen MCM, Cevirgel A, Schepp RM, den Hartog G, Reukers DFM, Beckers L, van Beek J, van Els CACM, Meijer A, Rots NY and de Wit J (2022) Front. Immunol. 13:817876. doi: 10.3389/fimmu.2022.817876

An author name was incorrectly written as **Martien Poelen**. It should be written as **Martien C. M. Poelen**.

The authors apologize for this error and state that this does not change the scientific conclusions of the article in any way. The original article has been updated.

The authors discovered an error in data export, resulting in minor data discrepancies and in the misclassification of three subjects (three subjects were actually moderate cases but were classified before corrections as mild cases).

Reanalysis of all data presented in the manuscript based on the corrected classification/data did not change the original major findings.

The corrected text for the **Abstract**, **Results** and **Discussion** sections appear below, as well as the corrected **Table 1**, **Figures 1**–**6** and **Supplementary Figures 2**, **4**.

Background: Severe acute respiratory syndrome coronavirus-2 (SARS-CoV-2) has led to considerable morbidity/mortality worldwide, but most infections, especially among children, have a mild course. However, it remains largely unknown whether infected children develop cellular immune memory.

Methods: To determine whether a memory T cell response is being developed, we performed a longitudinal assessment of the SARS-CoV-2-specific T cell response by IFN-γ ELISPOT and activation marker analyses of peripheral blood samples from unvaccinated children and adults with mild-to-moderate COVID-19.

Results: Upon stimulation of PBMCs with heat-inactivated SARS-CoV-2 or overlapping peptides of spike (S-SARS-CoV-2) and nucleocapsid proteins, we found S-SARS-CoV-2-specific IFN-γ T cell responses in infected children (83%) and adults (100%) that were absent in unexposed controls. Frequencies of SARS-CoV-2-specific T cells were higher in infected adults, especially several cases with moderate symptoms, compared to infected children. The S-SARS-CoV-2 IFN-γ T cell response correlated with S1-SARS-CoV-2-specific serum antibody concentrations. Predominantly, effector memory $CD4^+$ T cells of a Th1 phenotype were activated upon exposure to SARS-CoV-2 antigens. Frequencies of SARS-CoV-2-specific T cells were significantly reduced at 10 months after symptom onset, while S1-SARS-CoV-2-specific IgG concentrations were still detectable in 90% of all children and adults.

Conclusions: Our data indicate that an antigen-specific T cell and antibody response is developed after mild SARS-CoV-2 infection in children and adults. It remains to be elucidated to what extent this SARS-CoV-2-specific response can contribute to an effective recall response after reinfection.

RESULTS

Study Subjects

SARS-CoV-2 specific T cell responses were assessed from SARS-CoV-2-infected children and adults, and for comparison from unexposed children and adults. None of the study subjects were vaccinated against SARS-CoV-2. Demographic and clinical characteristics are presented in **Table 1**. Blood samples from 24 children and 27 adults (13 with mild symptoms and 14 with moderate symptoms, including two hospitalized cases) with PCR-confirmed SARS-CoV-2 infection were collected. The median time point of the first sample (T1) was for children 8 days [5.0-16 days] and for adults 12.5 days [interquartile range (IQR) 11-14 days] post-symptom onset. Additional blood samples were taken 10-14 days after T1 (referred to as 'T2') and only for adults also at 4-6 weeks after T1 (referred to as 'T3').

Ex Vivo Determination of Activated T Cells Over Time After SARS-CoV-2 Infection in Children and Adults

No significant differences in major immune cell types were found over time after infection neither in children nor adults, i.e. frequencies of total T cells, B cells, monocytes, or NK cells were comparable between infected groups and healthy age-matched unexposed groups (**Supplementary Figure 1**). In infected adults, slightly higher frequencies of $CD4^+$ T_{EM} (T_{EM}; $CD45RO^+$, $CD27^-$) cell subsets were found at T3 compared to T1 (4.7% vs 3.5%; P= 0.0061), but there was no significant difference in the frequency of the T_{EM} subset of these time points and the uninfected controls (3.6%). Frequencies of $CD8^+$ T_{EM} cells of infected adults were slightly higher at T2 compared to T1 (4.2% vs 3.8%; P= 0.041). No differences in memory T cell subsets were found between mild and moderate COVID-19 adults cases nor in children over time after infection.

The *ex vivo* expression of CD38 and HLA-DR on T cells was determined as a measure for antigen-specific activation after SARS-CoV-2 infection. In children, no changes in CD38/HLA-DR co-expression on $CD4^+$ T cells were found between different time points after infection (**Supplementary Figure 2A**, upper panel). In SARS-CoV-2-infected adults, a transiently higher percentage of cells expressing CD38/HLA-DR was observed within the $CD4^+$ T central memory (T_{CM}; $CD45RO^+$, $CD27^+$) subset (1.1% at T1) that declined over time after infection (to 0.55% at T2, and to 0.37% at T3) and within the $CD4^+$ terminally differentiated effector memory re-expressing CD45RA (T_{EMRA}; $CD45RO^-$, $CD27^-$, $CD28^-$, $CD57^+$) cell subset (0.58% at T1) that declined to 0.0% at both T2 and T3 (**Supplementary Figure 2B**, upper panel). In both children and adults, a higher frequency of $CD8^+$/$CD38^+$/$HLA\text{-}DR^+$ T cells within the T_{CM}/T_{EM}/T naïve (T_N; $CD45RO^-$, $CD27^+$, $CCR7^+$, $CD95^-$) subsets were observed at T1 [4.1%/4.9%/0.33% (children) and 5.5%/3.1%/1.0% (adults)] that declined in time after infection (to 2.7%/2.1%/0.17% (children) and 2.7%/1.7%/0.30% (adults) at T2 and to 2.2%/0.81%/0.23% (adults) at T3 (**Supplementary Figures 2A, B**, lower panels).

SARS-CoV-2 Specific IFN-γ^+ T Cell Response

IFN-γ^+-producing cells were detected by ELISPOT upon stimulation with overlapping peptides covering spike protein (S) of SARS-CoV-2 (S-SARS-CoV-2) in 83% (20/24) of infected children and in 100% (27/27) of infected adults, whereas IFN γ^+ responses were found in 0% (0/6) and 8.3% (1/12) of the unexposed children and adults, respectively. Frequencies of SARS-CoV-2-specific IFN-γ^+ T cells were lower in infected children than in infected adults (**Figures 1A–C**); the median spot forming units (SFU)/2.10^5 PBMCs for infected children

versus infected adults was 18 versus 62 (P=0.0021) at T1 upon stimulation with S-SARS-CoV-2. On average, a 2-fold higher frequency of SARS-CoV-2-specific IFN-γ$^+$ T cells was found in adults with moderate symptoms compared to mild symptomatic adults for the three time points. For all antigenic stimuli used (i.e. S-SARS-CoV-2, overlapping peptides covering nucleocapsid protein (N) of SARS-CoV-2 (N-SARS-CoV-2), or inactivated whole SARS-CoV-2), the moderately ill adults had significantly higher frequencies of IFN-γ-producing T cells compared to children at T1. The mild symptomatic adults also generally showed higher frequencies of SARS-CoV-2-specific IFN-γ$^+$ T cells than infected children, although not statistically significant for inactivated whole SARS-CoV-2 (**Figures 1A–C**).

The pre-existing T cell response against S-HCoV-OC43 of infected children was very low, although S-HCoV-OC43-specific T cell frequency was slightly higher at T2 compared to the age-matched unexposed control group (9.0 versus 1.0 SFU/2.10^5 PBMCs; P=0.037) (**Figure 1D**, left panel). In infected adults, no difference in numbers of S-HCoV-OC43-specific T cells was found between SARS-CoV-2-infected and unexposed adults (**Figure 1D**, right panel). In both SARS-CoV-2-infected children and adults, the frequency of IFN-γ$^+$ T cells was 4 to 60-fold lower after stimulation with S-HCoV-OC43 (**Figure 1D**) compared to stimulation with any of the SARS-CoV-2 antigens (**Figures 1A–C**). No significant difference in frequency of S-HCoV-OC43-reactive T cells was observed between unexposed adults and unexposed children or between mild and moderate COVID-19 cases.

Activation of Effector Memory CD4$^+$ T Cells Upon SARS-CoV-2-Specific Stimulation

PBMCs were harvested from the IFN-γ ELISPOT plates to determine whether mainly CD4+ or CD8+ T cell populations became activated upon SARS-CoV-2-specific stimulation. For this purpose, the expression of the following activation markers were analyzed by flow cytometry: CD25, CD137, CD154, CD69, OX40 (25-30). Especially the CD25 (IL-2Rα) and CD137 (4-1BB) co-expression on T cells of infected subjects increased significantly upon the various SARS-CoV-2 antigenic stimulations compared to mock stimulation (**Supplementary Figure 3**). Although analysis of CD137/CD25 co-expression is generally not used by default, in the present study we used this to identify SARS-CoV-2 antigen-specific T cells.

Primarily CD4$^+$ T cells and not CD8$^+$ T cells expressed CD25/CD137 activation markers upon SARS-CoV-2 antigenic stimulation, in infected subjects (**Figure 2** and **Supplementary Figure 4**). Compared to the unexposed age-matched groups, higher frequencies of activated CD4$^+$ T cells were observed in both infected children and infected adults after stimulation with any of the three SARS-CoV-2 antigen preparations at T1. Frequencies of SARS-CoV-2-specific activated CD4$^+$ T cells were significantly lower in infected children than in adults (upon S-SARS-CoV-2-specific stimulation, 0.04% CD25$^+$/CD137$^+$ T cells of total CD4$^+$ T cells for infected children versus 0.21% for infected adults at T1; P=0.0034). Frequencies of SARS-CoV-2-specific activated CD4$^+$ T cells, irrespective of used SARS-CoV-2 antigen, were comparable between adults with moderate COVID-19 illness and mildly symptomatic adults. The observed SARS-CoV-2-specific activated CD4$^+$ T cells were mainly effector memory (CD45RO$^+$/CCR7$^-$) (T_{EM}) (**Figure 2D**).

Correlations Between SARS-CoV-2-Specific IFN-γ$^+$ T Cell Responses and CD4$^+$ T Cell Response

In children, moderate correlations were observed between IFN- γ$^+$ T cell frequency and activated (CD137$^+$ CD25$^+$) CD4$^+$ T cells after stimulation with N-SARS-CoV-2 (r_s=0.64; P=0.004) at T2, and at T1 after stimulation with inactivated SARS-CoV-2 (r_s=0.51; P=0.012) (**Figure 3A**). In adults, IFN-γ$^+$ T cell frequency and activated (CD137$^+$ CD25$^+$) CD4$^+$ T cells correlated after stimulation with both S-SARS-CoV-2 and N-SARS-CoV-2 at all three time points after infection (r_s ranging between 0.51-0.72) and after stimulation with inactivated SARS-CoV-2 at T1 and T2 (respectively, r_s=0.70 and r_s=0.53) (**Figure 3B**).

SARS-CoV-2-Specific Release of Cytokines

Upon stimulation with S-SARS-CoV-2, PBMCs from SARS-CoV-2-infected children secreted more IL-2 than unexposed children, albeit at very low amounts (3.7 versus 0.1 pg/ml; P=0.030). Similar trends were observed in SARS-CoV-2-infected adults compared to unexposed adults, for both IL-2 (18.0 versus 0.1 pg/ml; P=0.0003). S-SARS-CoV-2-specific IL-2 secretion was higher in infected adults compared to infected children (P=0.015). However, IL-2 secretion was only significantly higher in adults with moderate COVID-19 (51.8 versus 3.7 pg/ml; P=0.023) and not in adults with mild symptoms compared to infected children (**Figure 4**). Other cytokines were only secreted at very low levels and not significantly.

Correlations Between SARS-CoV-2-Specific IFN-γ$^+$ T Cell Frequency and Antibody Response

Serum antibody concentrations against the SARS-CoV-2 spike S1 protein (S1-SARS-CoV-2) above the previously established cutoff level (10) at any of the two sampling time points were found in 83.3% (IgM), 79.2% (IgG), and 75.0% (IgA) of the infected children. From the four children without detectable S-SARS-CoV-2-specific T cell responses, two did have S1-SARS-CoV-2-specific IgM, IgG, and IgA antibodies; the other two did not. In adults, 100%, 96.3%, and 88.9% were seropositive for respectively, IgM, IgG, and IgA antibodies to S1-SARS-CoV-2 at any of the three sampling time points. Interestingly, in children good correlations were observed between S-SARS-CoV-2 IFN-γ$^+$ T cell frequency and S1-SARS-CoV-2-specific serum IgM, IgG and IgA concentrations, though this was only observed at T1 [for IgM, R_s=0.73 (P<0.0001); IgG, r_s=0.74 (P<0.0001); IgA, r_s=0.68 (P=0.0004)] (**Figure 5A**). In adults, frequency of S-SARS-CoV-2-specific T cells was also correlated with S1-SARS-CoV-2-

specific serum IgM concentrations at T2 and T3 [respectively, r_s=0.42 (P=0.03) and r_s=0.50 (P=0.01)], with S1-SARS-CoV-2-specific serum IgG concentrations at T3 [r_s=0.47 (P=0.01)], and with S1-SARS-CoV-2-specific serum IgA concentrations at T3 (r_s=0.45 (P=0.02)) (**Figure 5B**).

The median S1-SARS-CoV-2-specific serum IgG concentrations (**Figure 5C**) for infected children increased >100-fold in time after infection, from 0.21 AU/ml at T1 to 25 AU/ml at T2, while a 7-fold increase was observed for infected adults from T1 (median IgG concentration of 3.9 AU/ml) to T2 (26 AU/ml)), and an 8-fold increase from T1 to T3 (31 AU/ml) (**Figure 5C**, upper panel). Nevertheless, S1-SARS-CoV-2-specific serum IgG concentrations of infected adults experiencing moderate COVID-19 were clearly higher than levels of infected children or adults with mild symptoms at all time points after infection (**Figure 5C**, lower panel).

SARS-CoV-2-Specific IFN-γ$^+$ T Cell Frequency and Antibody Response at 10 Months After Infection

To study the long-term SARS-CoV-2-specific immune response, we collected follow-up blood samples at 10 months ± 13 days after symptoms onset (referred to as 'T4') from 18 children and 21 adults. Vaccinated persons (adults: n=3) at the time of T4 sampling were excluded from analysis. In children, the median age was 12 years (5-16 years) and 56% were female at T4 sampling. The median age of adults was 44 years (18-87 years), 48% were female, and 48% were mild cases at T4 sampling.

S-SARS-CoV-2-specific IFN-γ$^+$ responses higher than 5 SFU/2.10^5 PBMCs were still found in 44% (8/18) of the infected children and 81% (17/21) of the infected adults at 10 months after symptom onset. In children, frequencies of S-SARS-CoV-2-specific IFN-γ$^+$ T cells underwent a 4-fold decline at 10 months (T4) compared to frequencies at 3 weeks (T2, P=0.027) after infection, and were no longer significantly different from unexposed children (**Figure 6A**, left panel). Also in adults, IFN-γ$^+$ S-SARS-CoV-2-specific T cell frequencies were 6 to 7-fold lower at 10 months compared to earlier time points after infection. In contrast to children, frequencies of S-SARS-CoV-2-specific IFN-γ$^+$ T cells at T4 were still significantly higher in infected adults compared to unexposed adults (9.2 versus 1.7 SFU/2.10^5 PBMCs; P=0.0003) (**Figure 6A**, right panel). IFN-γ$^+$ N-SARS-CoV-2-specific T cell frequencies also declined at 10 months upon infection in adults compared to earlier time points (7.7 SFU/2.10^5 PBMCs at T4 vs 62 (P<0.0001), 47.0 (P=0.0008), and 31.1 (P=0.039) SFU/per 2.10^5 PBMCs at T1, T2, and T3, respectively), but remained significantly higher compared to unexposed adults (0.05 SFU/2.10^5 PBMCs) (**Figure 6B**, right panel). Frequencies of IFN-γ$^+$ N-SARS-CoV-2-specific T cells were low in children and no changes over time were observed (**Figure 6B**, left panel). Similar to earlier time points, S-SARS-CoV-2-specific responses were 2.3-fold higher in adults compared to children at 10 months after infection (9.2 versus 4.0 SFU/2.10^5 SFU/PBMCs). These differences were mainly caused by slightly higher responses from adults experiencing moderate symptoms (P=0.0021) (**Figure 6C**). Albeit not significant, a trend of higher frequencies of S-SARS-CoV-2-specific IFN-γ$^+$ T cells in infected adults with moderate symptoms persisted at 10 months compared to mild disease (**Figure 6C**). In line with results from earlier time points, the SARS-CoV-2-specific activated cells at 10 months were mainly of the effector memory (CD45RO$^+$/CCR7$^-$) (T_{EM}) subset. Interestingly, however, a 4.7-fold increase of central memory T cell frequencies (CD45RO$^+$/CCR7$^+$) (T_{CM}) was found 10 months after symptom onset (from 3.7% at T3 to 17.6% at T4; P=0.002) (**Figure 6D**).

Only in adults, the frequency of S-SARS-CoV-2-specific IFN-γ-producing T cells was still correlated with S1-SARS-CoV-2-specific serum IgG concentrations at 10 months after symptom onset [r_s=0.64 (P=0.004)] (**Figure 6E**). S1-SARS-CoV-2-specific IgG serum antibody concentrations significantly decreased at 10 months compared to earlier time points in both children and adults [median IgG concentrations of 10.8 AU/mL at T4 versus 24.6 AU/mL at T2 (P=0.0053) in children, and 18.7 AU/mL at T4 versus 35.8 AU/mL T3 versus in adults (P=0.0002)]. Despite this decline, 90% (18/20) of infected children and 89% (16/18) of infected adults remained S1-SARS-CoV-2-IgG seropositive 10 months after infection. No differences were observed in anti-S1-SARS-CoV-2 serum IgG concentrations at 10 months between children and adults (**Figure 6F**).

DISCUSSION

Most infections with SARS-CoV-2, especially among children, have a mild course. But, do children, despite experiencing mild infection, develop memory T cell immunity? Here, we describe the kinetics, function, and phenotype of SARS-CoV-2-specific T cells of infected children in comparison with adults experiencing mild to moderate COVID-19 symptoms. Only limited studies have been reported investigating the immune responses in children with mild/asymptomatic SARS-CoV-2 infection (17-21). The strength of our study is that we evaluated the recall T cell response upon SARS-CoV-2 specific stimulation, and compared it to unexposed children and adults.

First, we analyzed immune cell populations over time after infection. Frequencies of total T cells, B cells, monocytes, or NK cells were comparable between healthy age-matched control groups and infected groups. However, in infected adults, slightly higher frequencies of CD4$^+$ T_{EM} and CD8$^+$ T_{EM} cell subsets were found at later time points after infection. This small increase in T_{EM} cell subsets may be caused by an increase of circulating SARS-CoV-2-specific CD4$^+$ T_{EM} and CD8$^+$ T_{EM} cells in response to SARS-CoV-2 infection. In line with this, in infected adults also transiently higher frequencies of CD4$^+$ T_{CM} and T_{EMRA} cells expressing CD38/HLA-DR were observed early after infection, and in both infected children and infected adults, transiently higher frequencies of CD8$^+$ T cells expressing CD38/HLA-DR were observed within the T_{CM}/T_{EM}/T_N cell subsets at the earlier time points after infection. This indicates that antigen-specific activation of T cells was triggered in adults as well as in children by SARS-CoV-2 infection. T cell activation, especially

robust $CD38^+$/HLA-DR^+ $CD8^+$ T cell responses, has been identified as a hallmark of acute COVID-19 (2, 4, 8).

We found higher frequencies of SARS-CoV-2-specific IFN-γ^+ T cells in all infected groups compared to the unexposed control groups upon any of the three antigenic stimulations that included heat-inactivated SARS-CoV-2, and overlapping peptides of SARS-CoV-2 spike protein (S-SARS-CoV-2), and nucleocapsid protein (N-SARS-CoV-2). In general, frequencies of IFN-γ^+-T cells reactive against SARS-CoV-2 antigens were lower in infected children, who generally had mild/asymptomatic infection, compared to infected adults. The lower SARS-CoV-2-specific T cell response observed in children suggests that other compartments of the immune system, such as the innate immune response, contribute to faster clearing of the infection, as demonstrated by others (31-33). The higher T cell responses in infected adults could largely be explained by higher T cell responses found in several moderate cases, although adults with mild complaints also tended to have slightly higher responses than infected children. This is in agreement with findings from other studies showing higher frequencies of SARS-CoV-2-specific T cells in severe patients compared to mildly symptomatic patients (8, 15). In contrast, critically ill patients have been reported to exhibit qualitatively impaired S-SARS-CoV-2-specific $CD4^+$ T cell responses, indicating that a good $CD4^+$ T cell response may protect against serious disease (15). In agreement with our IFN-γ ELISPOT data, significantly lower frequencies of SARS-CoV-2-specific activated $CD25^+$ $CD137^+$ $CD4^+$ T cells were observed in infected children compared to infected adults. Recently, Cohen et al. also described that acute and memory $CD4^+$ T cells in SARS-CoV-2-infected children were significantly lower than in adults, while polyfunctional cytokine production by T cells was comparable (21). Furthermore, in accordance with Cohen et al. (21), we found that the SARS-CoV-2 activated T cells mainly belonged to the $CD4^+$ effector memory subset (T_{EM}: $CD45RO^+$/$CCR7^-$) in our experimental setting. Data on the SARS-CoV-2-specific IFN-γ^+ T cell response and $CD4^+$ T cell activation correlated, suggesting that IFN-γ was produced by antigen-specific $CD4^+$ T cells. Apart from IFN-γ, SARS-CoV-2-specific T cells produced IL-2, suggestive for a Th1 phenotype of the $CD4^+$ T_{EM}.

It has been demonstrated that SARS-CoV-2-specific T cell responses can be retained 6-8 months following infection regardless of disease severity (8, 16, 34). Although, other studies showed a clear decline of the T cell response over a 6-8 month period in asymptomatic as well as symptomatic COVID-19 patients (35, 36). In our study, at 10 months after symptom onset, the frequencies of SARS-CoV-2-specific IFN-γ^+ T cells were significantly reduced in adults and were nearly undetectable in children. Whether this is a result of waning immunity or migration of memory SARS-CoV-2-specific T cells to peripheral tissues remains to be investigated. Interestingly, the memory phenotype of the activated SARS-CoV-2-specific $CD4^+$ T cells in adults showed a shift from mainly T_{EM} to a more T_{CM} phenotype at 10 months after infection; T_{CM} subset increased from 3.7% to 17.6% of the antigen-specific $CD4^+$ T cells. This T_{CM} subset may persist for longer after infection.

n contrast to the observed SARS-CoV-2-specific $CD4^+$ T cell response, we found very low frequencies of activated ($CD25^+$/$CD137^+$) $CD8^+$ T cells upon SARS-CoV-2-specific stimulation. An explanation for this may be that $CD8^+$ T cells have migrated to the local sites of infection to attack virus-infected cells or might be a result of the antigenic stimulation used in our study. Smaller peptides (9 to 10-mers instead of 15-mers) or live SARS-CoV-2 may be more suitable to measure $CD8^+$ T cell responses. Sekine et al. also observed proportionately larger SARS-CoV-2-specific $CD4^+$ T cell responses than $CD8^+$ T cell responses to different sets of overlapping peptides in the convalescent phase of both mild and severe COVID-19 cases, although in that study also IFN-γ^+ $CD8^+$ T cell responses were detected (8).

We found positive correlations between SARS-CoV-2-specific IFN-γ^+ T cell frequency and serum-IgG, -IgM, and -IgA antibody concentrations to S1-SARS-CoV-2 in both children and adults. Although, it should be taken into account that the antibody concentrations of considerable numbers of children were below the threshold for seropositivity (10). Other studies have also shown positive correlations between S-SARS-CoV-2-specific IgG antibodies and T cell responses (6, 37, 38).

Pre-existing cross-reactive T cell immunity generated by common cold human coronaviruses (HCoV) has been suggested to affect clinical outcomes of SARS-CoV-2 infection. T cell lines from unexposed healthy donors specific for S-HCoV-229E and -OC43 were cross-reactive to S-SARS-CoV-2 (39). Based on these findings, the authors suggested that children may have higher HCoV prevalence due to more frequent social contacts, explaining their lower risk for severe COVID-19 (39). In the present study, we did, however, not find a significant difference in the low frequencies of S-HCoV-OC43-reactive IFN-γ^+ T cells between unexposed children and unexposed adults. In another study with mild COVID-19 adult patients, also low T cell frequencies recognizing S-HCoV-229E/S-HCoV-OC43 peptide pools were found (15). It cannot be excluded that pre-existing cross-reactive immunity to other conserved parts of SARS-CoV-2 played a role, or that pre-existing immunity to other HCoV played a role. We, however, found no evidence that pre-existing S-HCoV-OC43-reactive T cells boosted upon SARS-CoV-2 infection could explain the mild course of infection.

Limited data is available on the immune response to SARS-CoV-2 in children. Here, we show that infected children do develop a SARS-CoV-2-specific T cell response. However, frequencies of SARS-CoV-2 reactive T cells were lower in infected children who almost all had mild/asymptomatic infection compared to infected adults with mild to moderate COVID-19. Predominantly $CD4^+$ T cells, and not $CD8^+$ T cells, were activated upon stimulation with SARS-CoV-2 antigens. Nevertheless, frequencies of SARS-CoV-2-specific T cells circulating in the blood were significantly reduced at 10 months after infection, although migration of memory SARS-CoV-2-specific T cells to peripheral tissues may have taken place. Importantly, our data indicate that an antigen-specific T cell and antibody response is developed after experiencing mild SARS-CoV-2 infection. It remains to be elucidated to what extent this

SARS-CoV-2-specific response can contribute to an effective recall response after reinfection.

The authors apologize for these errors and state that this does not change the scientific conclusions of the article in any way. The original article has been updated.

SUPPLEMENTARY MATERIAL

The Supplementary Material for this article can be found online at: https://www.frontiersin.org/articles/10.3389/fimmu.2022.893720/full#supplementary-material

Publisher's Note: All claims expressed in this article are solely those of the authors and do not necessarily represent those of their affiliated organizations, or those of the publisher, the editors and the reviewers. Any product that may be evaluated in this article, or claim that may be made by its manufacturer, is not guaranteed or endorsed by the publisher.

Copyright © 2022 Kaaijk, Olivo Pimentel, Emmelot, Poelen, Cevirgel, Schepp, den Hartog, Reukers, Beckers, van Beek, van Els, Meijer, Rots and de Wit. This is an open-access article distributed under the terms of the Creative Commons Attribution License (CC BY). The use, distribution or reproduction in other forums is permitted, provided the original author(s) and the copyright owner(s) are credited and that the original publication in this journal is cited, in accordance with accepted academic practice. No use, distribution or reproduction is permitted which does not comply with these terms.

TABLE 1 | Demographic and clinical characteristics of adults (with mild versus moderate symptoms) and children with PCR confirmed SARS-CoV-2 infection and demographic data of unexposed participants.

Characteristics	Infected adults total n = 27	Infected adults mild n = 13	Infected adults moderate n = 14	Unexposed adults n = 12	Infected children n = 24	Unexposed children n = 13
Median age (range) – years	44 (18 – 87)	45 (23 – 87)	44 (18 – 54)	38 (20 – 51)	12 (2 – 16)	12 (2 – 16)
Sex – number (%)					11 (45.8)	5 (38.5)
Male	14 (51.9)	8 (61.5)	6 (42.9)	6 (50.0)	13 (54.2)	8 (61.5)
Female	13 (48.1)	5 (38.5)	8 (57.1)	6 (50.0)		
Sign and symptoms – number (%)						
Any sign or symptom	27 (100.0)	13 (100.0)	14 (100.0)	N/A	21 (87.5)	N/A
Fever	14 (51.9)	6 (46.2)	8 (57.1)		6 (25.0)	
Cough	20 (74.1)	7 (53.8)	13 (92.9)		11 (45.8)	
Chills	15 (55.6)	6 (46.2)	9 (64.3)		2 (8.3)	
Sore throat	14 (51.9)	7 (53.8)	7 (50.0)		3 (12.5)	
Runny nose	18 (66.7)	9 (69.2)	9 (64.3)		15 (62.5)	
Phlegm	12 (44.4)	5 (38.5)	7 (50.0)		2 (8.3)	
Headache	20 (74.1)	10 (76.9)	10 (71.4)		7 (29.2)	
Myalgia	20 (74.1)	9 (69.2)	11 (78.6)		1 (4.2)	
Fatigue	24 (88.9)	10 (76.9)	14 (100.0)		6 (25.0)	
Shortness of breath	12 (44.4)	0 (0.0)	12 (85.7)*		2 (8.3)	
Loss of taste or smell	11 (40.7)	3 (23.1)	8 (57.1)		3 (12.5)	
Diarrhea	11 (40.7)	6 (46.2)	5 (35.7)		2 (8.3)	

**All moderate cases reported shortness of breath with the exception of two hospitalized cases.*

n, number of subjects in specific group; N/A, not applicable.

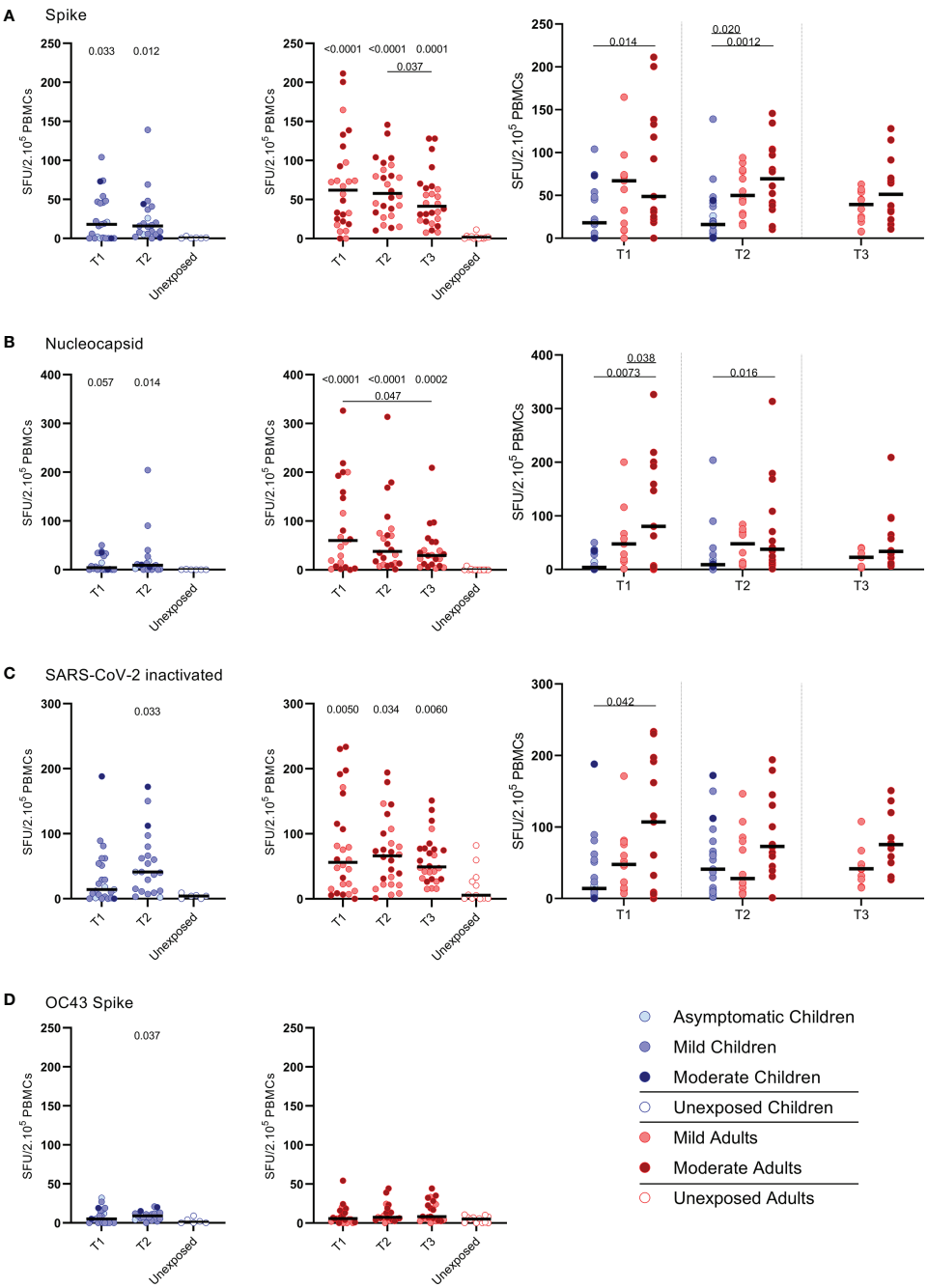


FIGURE 1 | SARS-CoV-2-specific IFN-ɣ+ T cell response in infected children and infected adults (mild and moderate cases) versus unexposed healthy controls over time after infection. Dot plots summarizing the frequencies of IFN-γ-producing cells responding to SARS-CoV-2 and HCoV-OC43 antigens for **(A–D)** children (left panel, blue), adults (middle panel, red), and children versus mild and moderate adult cases separately (right panel), over time after infection, and compared to unexposed adults/children (ELISPOT assay). Frequencies of IFN-γ-producing cells responding to **(A)** set of overlapping peptides of SARS-CoV-2 spike protein, **(B)** set of overlapping peptides of SARS-CoV-2 nucleocapsid protein, **(C)** inactivated SARS-CoV-2, and **(D)** set of overlapping peptides of HCoV-OC43 spike protein. Each dot represents one subject. Bars indicate the median of spot-forming units per 200,000 PBMCs. SFU, spot-forming unit. **(A–D)** P values related to comparisons with the unexposed controls are listed at the top of the graph, above the corresponding group for comparison. For unpaired comparisons, Mann-Whitney U test (two-group comparisons) (mild adults versus moderate adults) or Kruskal-Wallis rank-sum test with Dunn's post hoc test for multiple comparisons were used (children versus mild adults versus moderate adults; unexposed versus infected children or adults at T1 versus T2 versus T3). Differences between paired data were compared using the Wilcoxon signed-rank test (for comparison of two paired groups) (infected children at T1 versus T2) or the Friedman test with Dunn's multiple comparison tests (infected adults at T1 versus T2 versus T3). Statistically significant comparisons are indicated, with P values < 0.05 considered significant. T1, first timepoint of sampling for adults median 12.5 days and children median 8 days post-symptom onset; T2, 10-14 days after T1; T3, 4-6 weeks after T1.

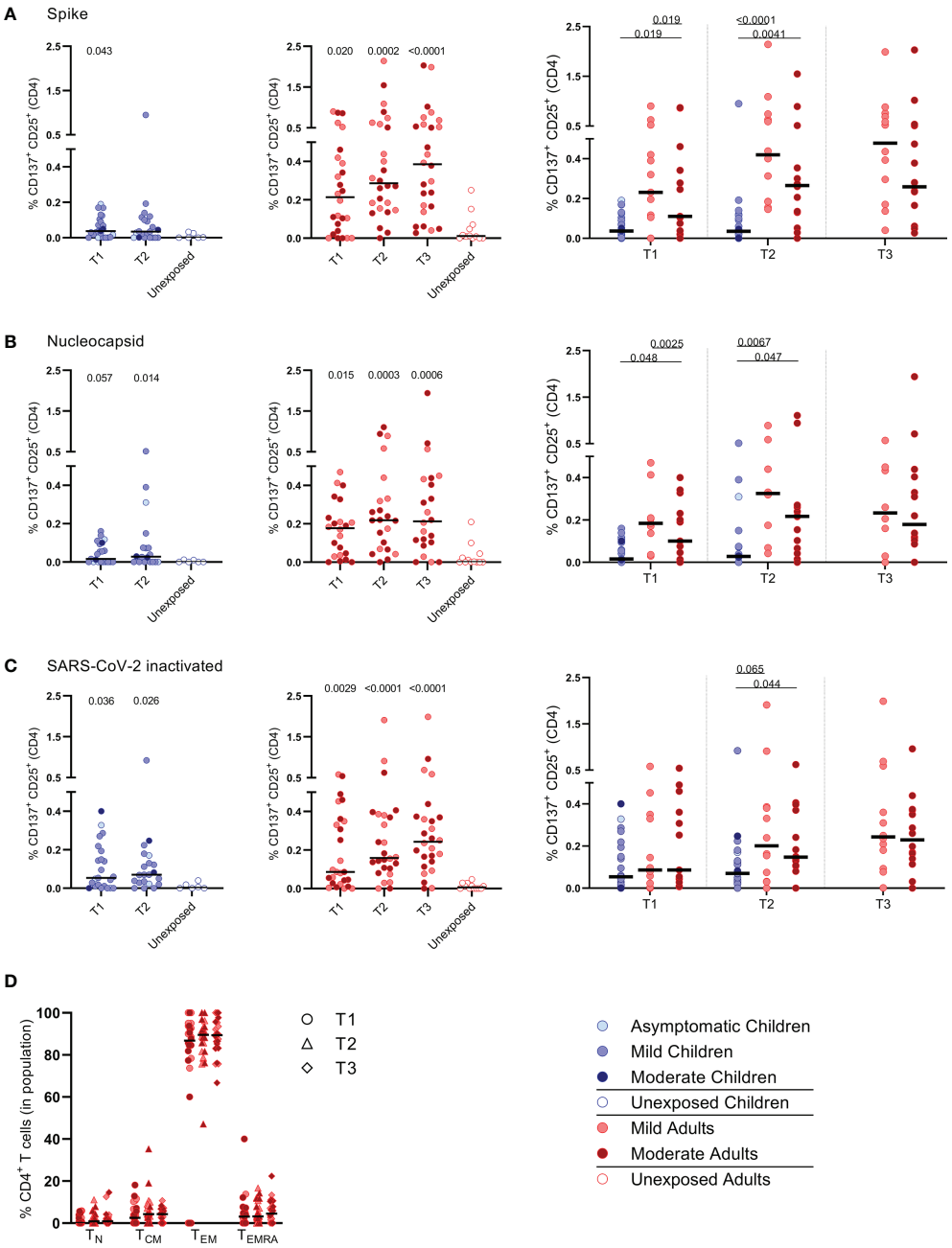


FIGURE 2 | Frequencies of activated CD4+ T cells of infected children and infected adults (mild and moderate cases) versus unexposed healthy controls over time after infection. Dot plots summarizing the percentages of CD25+/CD137+ activated CD4+ T cells responding to SARS-CoV-2 antigens for **(A–D)** children (left panel, blue), adults (middle panel, red), and children versus mild and moderate adult cases separately (right panel). Percentages of CD25+/CD137+ activated CD4+ T cells responding to **(A)** set of overlapping peptides of SARS-CoV-2 spike protein, **(B)** set of overlapping peptides of SARS-CoV-2 nucleocapsid, **(C)** inactivated SARS-CoV-2. **(D)** Immunophenotyping at the single-cell level showing the different memory subsets within the SARS-CoV-2-specific activated CD4+ T cells from infected adults. Each dot represents one subject. Bars indicate the median percentage of total CD4+ T cells. **(A–C)** P values related to comparisons with the unexposed controls are listed at the top of the graph, above the corresponding group for comparison. For unpaired comparisons, Mann-Whitney U test (two-group comparisons) (mild adults versus moderate adults) or Kruskal-Wallis rank-sum test with Dunn's post hoc test for multiple comparisons were used (children versus mild adults versus moderate adults; unexposed versus infected children or adults at T1 versus T2 versus T3). Differences between paired data were compared using the Wilcoxon signed-rank test (for comparison of two paired groups) (infected children at T1 versus T2) or the Friedman test with Dunn's multiple comparison tests (infected adults at T1 versus T2 versus T3). Statistically significant comparisons are indicated, with P values < 0.05 considered significant. T1, first timepoint of sampling for adults median 12.5 days and children median 8 days post-symptom onset; T2, 10-14 days after T1; T3, 4-6 weeks after T1.

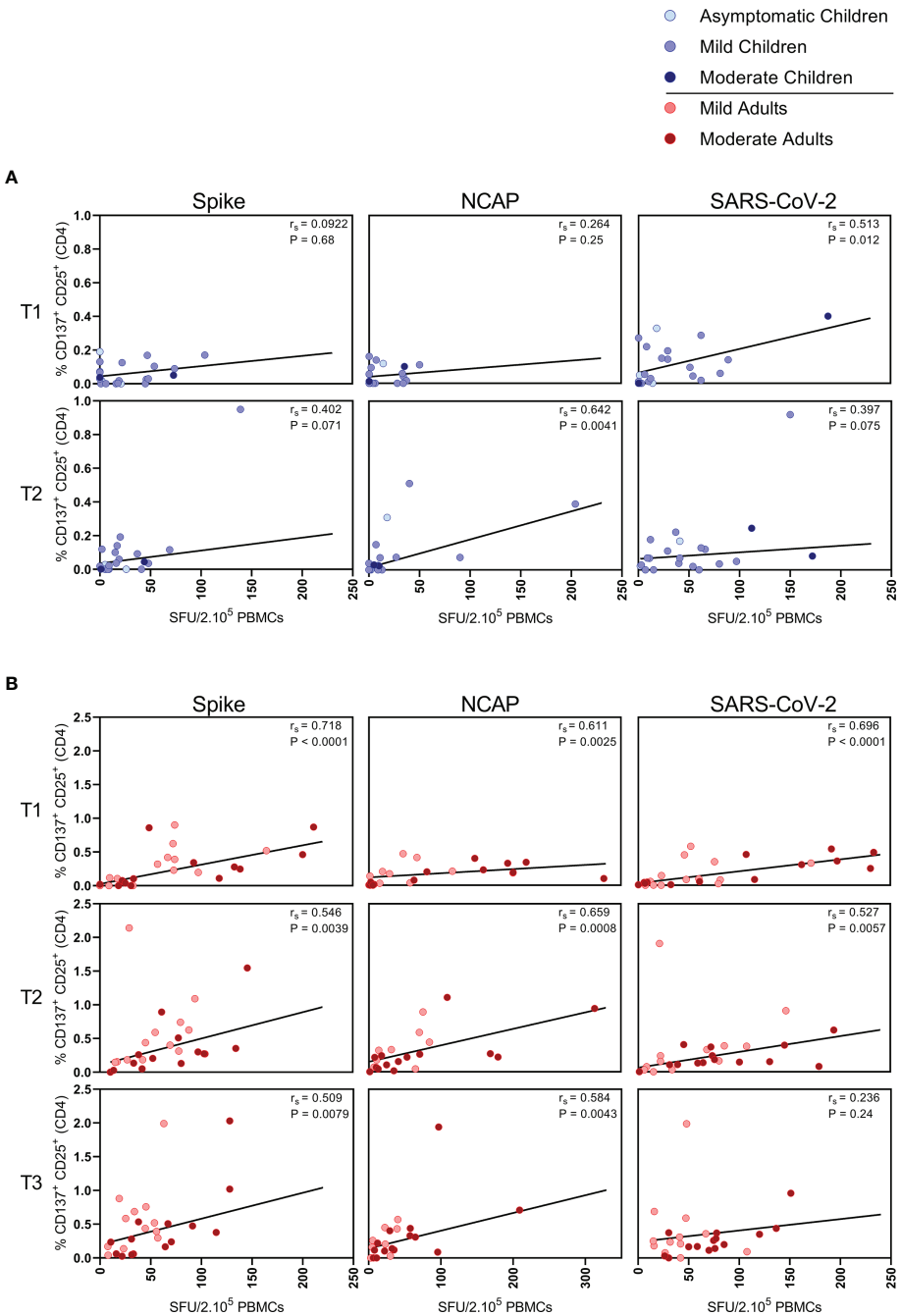


FIGURE 3 | Correlation between IFN-γ+ T cell frequency and activated CD4+ T cells. Spearman correlation between frequency of IFN-γ+ responder cells and percentages of CD25+/CD137+ activated CD4+ T cells of **(A)** children and **(B)** adults responding to a set of overlapping peptides of SARS-CoV-2 spike protein (left panel), or a set of overlapping peptides of SARS-CoV-2 nucleocapsid protein (middle panel) or inactivated SARS-CoV-2 (right panel) at different time points after infection. Each dot represents one subject. Correlation coefficients (rs) were determined with Spearman's rank correlation. P values < 0.05 were considered significant. T1, first timepoint of sampling for adults median 12.5 days and children median 8 days post-symptom onset; T2, 10-14 days after T1; T3, 4-6 weeks after T1.

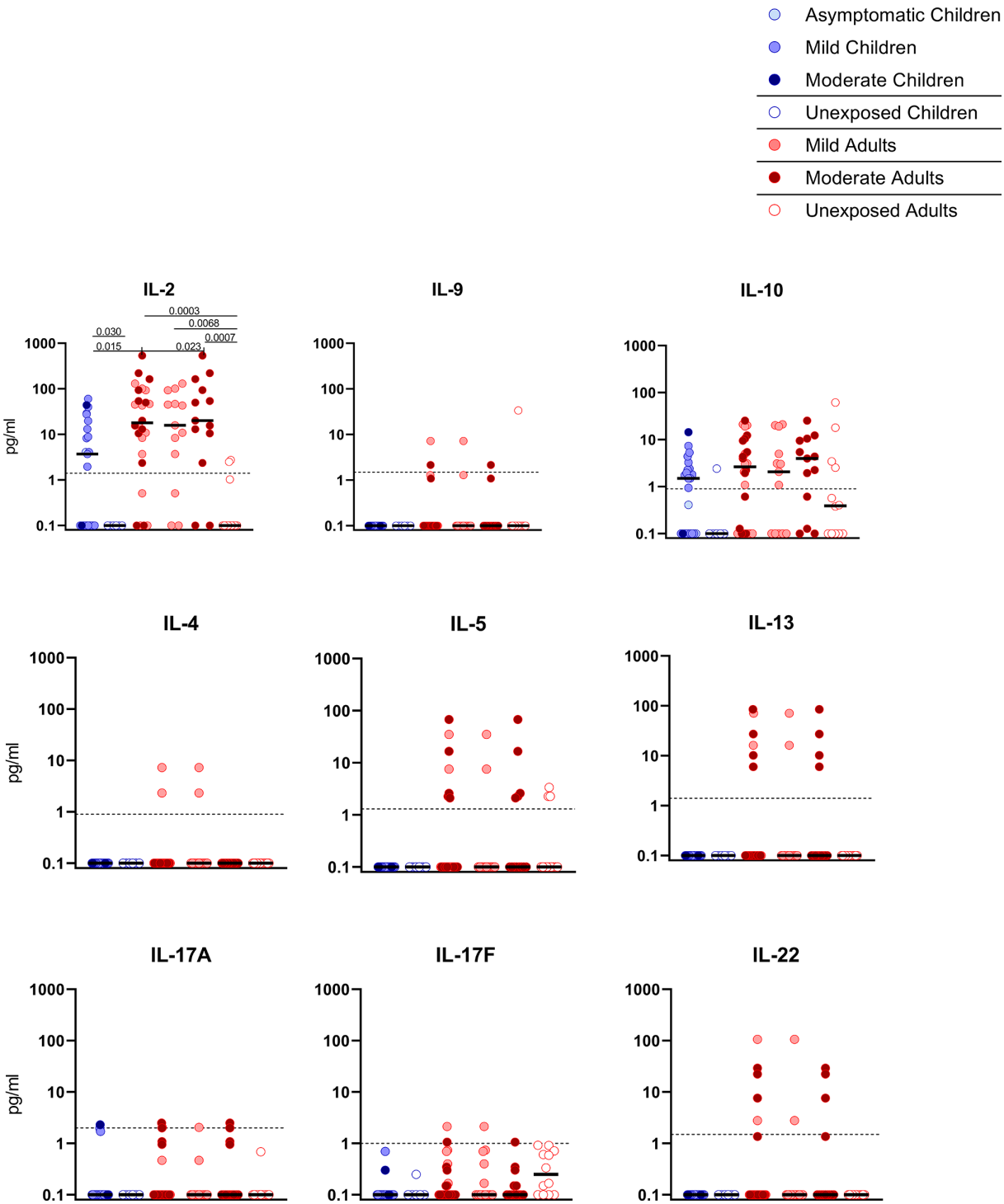


FIGURE 4 | Cytokine release in infected children and mild versus moderate symptomatic adults over time after infection. Cell-free culture supernatants were harvested from IFN-γ ELISPOT plates and the release of the following cytokines was measured in T1 samples: IL-2, IL-4, IL-5, IL-9, IL-10, IL-13, IL-17A, IL-17F, IL-22. Dot plots show the concentration of cytokines (pg/ml) after stimulation of PBMCs with a set of overlapping peptides of SARS-CoV-2 spike protein. Infected children and unexposed children versus infected adults with mild or moderate disease and unexposed adults are depicted. Minimum detection threshold (MDT) concentrations for each cytokine, as calculated by the manufacturer and mentioned in the Material and Methods section, are indicated with horizontal dotted lines. Each dot represents one subject. Bars indicate the median cytokine concentration (pg/ml). For two-group comparisons (infected children versus unexposed children), Mann-Whitney U test was used. Kruskal-Wallis rank-sum test with Dunn's post hoc test for multiple comparisons was used (all adults versus mild adults versus moderate adults versus unexposed adults; all adults versus mild adults versus moderate adults versus infected children). P-values ≤ 0.05 are presented.

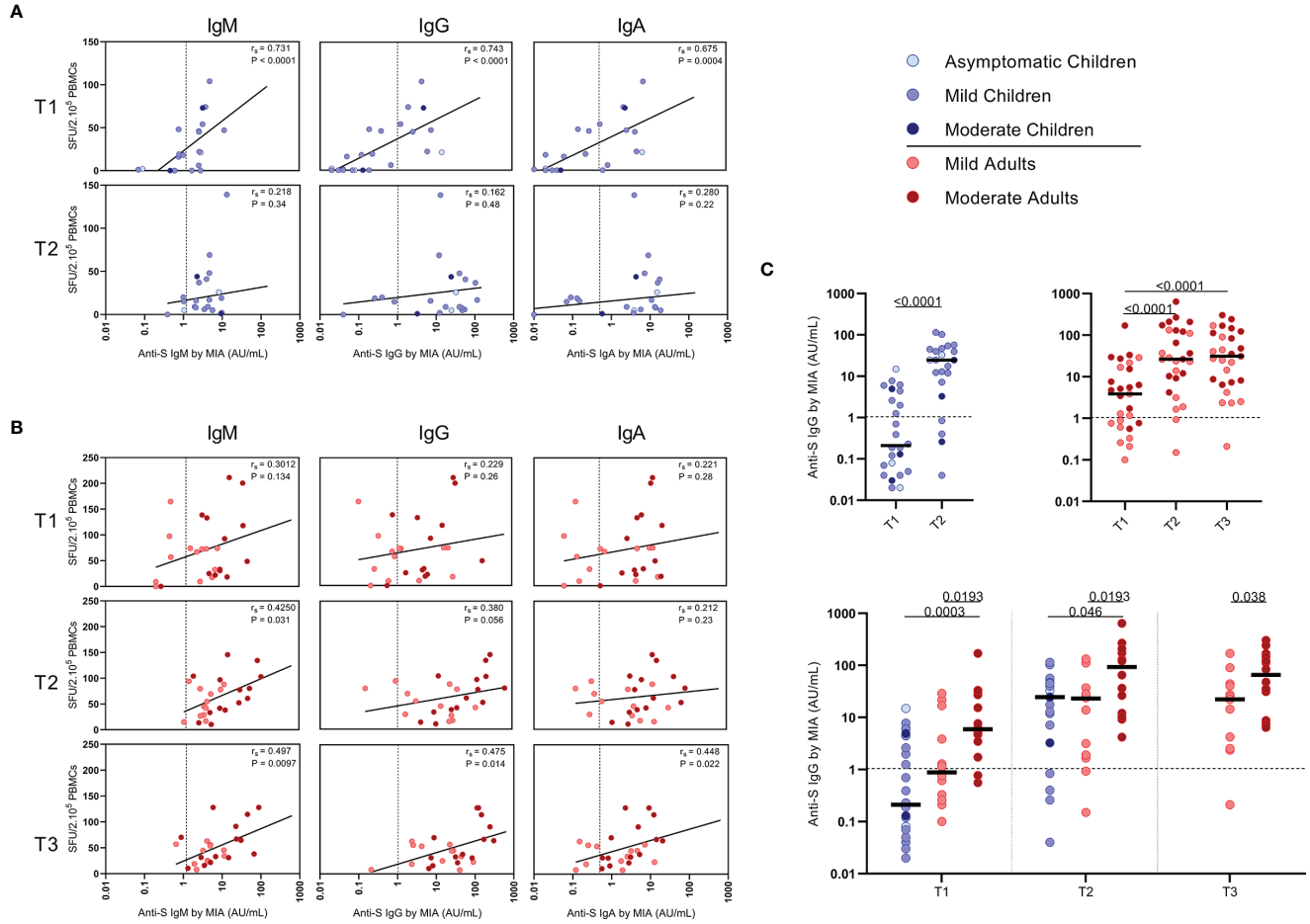


FIGURE 5 | Correlation between frequencies of SARS-CoV-2-specific IFN-γ+ T cells and antibody concentrations to S1-SARS-CoV-2. Spearman correlation between frequency of SARS-CoV-2-specific IFN-γ+ responder cells and concentrations of spike-S1 IgM, IgG, or IgA serum antibodies measured by multiplex immunoassay (MIA) at different time points after infection in **(A)** children and **(B)** adults. Concentrations of spike-S1 IgG serum antibodies at the various time points after SARS-CoV-2 infection in the whole group of children and adults (**C**, upper panel) and in the whole group of children versus the mild and moderate adult cases (**C**, lower panel). Cut-off values for seroprevalence are indicated with vertical or horizontal dotted lines. Each dot represents one subject. Correlation coefficients (rs) were determined with Spearman's rank correlation. P values < 0.05 were considered significant. Differences in IgG concentrations for paired data were compared using the Wilcoxon signed-rank test (for comparison of two paired groups) (infected children at T1 versus T2) or the Friedman test with Dunn's multiple comparison tests (infected adults at T1 versus T2 versus T3). For unpaired comparisons, Mann-Whitney U test (two-group comparisons) (mild adults versus moderate adults) or Kruskal-Wallis rank-sum test with Dunn's post hoc test for multiple comparisons were used (children versus mild adults versus moderate adults; at T1 versus T2 versus T3). Statistically significant comparisons are indicated, with P values < 0.05 considered significant. T1, first timepoint of sampling for adults median 12.5 days and children median 8 days post-symptom onset; T2, 10-14 days after T1; T3, 4-6 weeks after T1.

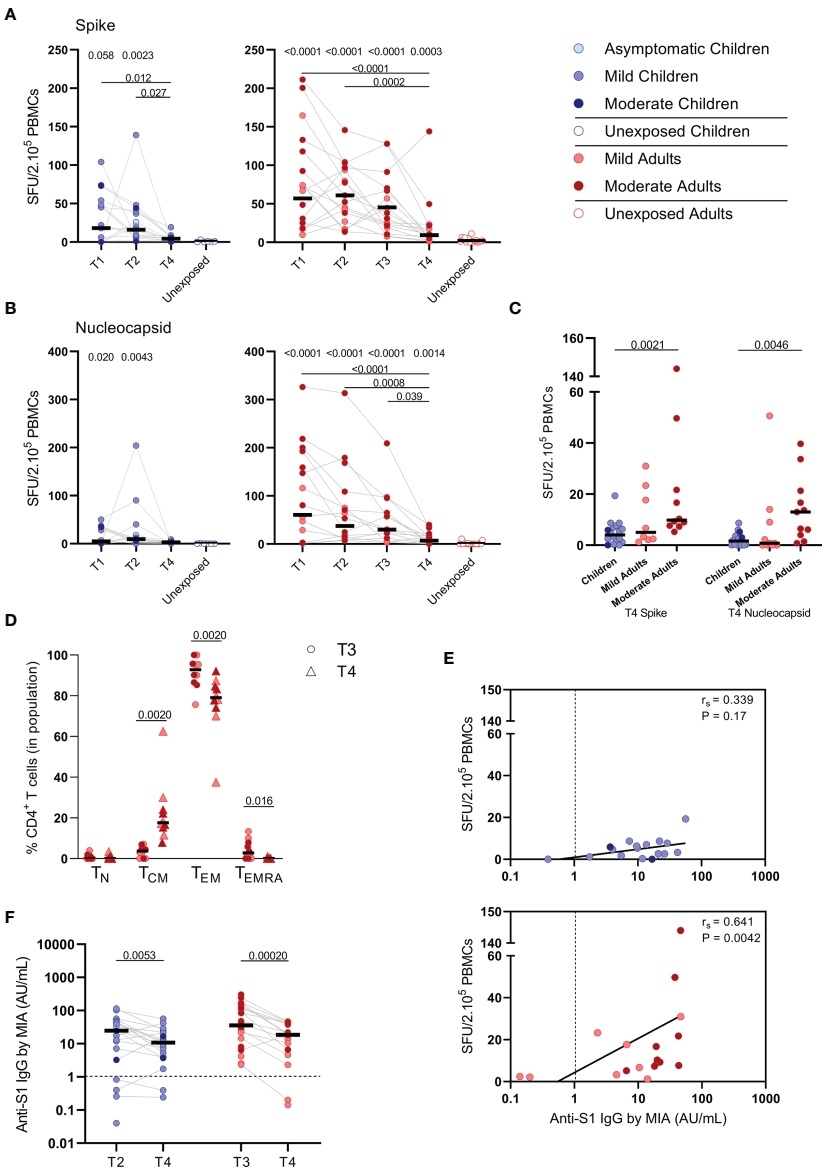


FIGURE 6 | SARS-CoV-2-specific immune response up to 10 months after infection. Dot plots summarizing the frequencies of IFN-γ-producing cells by ELISPOT assay responding to **(A)** a set of overlapping peptides of SARS-CoV-2 spike protein and **(B)** a set of overlapping peptides of SARS-CoV-2 nucleocapsid protein in children (left panel, blue) and adults (right panel, red), at different time points after infection, and compared to unexposed children/adults. **(C)** Dot plots showing the frequencies of IFN-γ-producing cells responding to SARS-CoV-2 spike and nucleocapsid proteins, at 10 months after symptom onset (T4) comparison of groups of children versus total, mild, and moderate adult cases separately. **(D)** Immunophenotyping at the single-cell level comparing the frequencies of different memory subsets from T3 versus T4 within the SARS-CoV-2-specific activated CD4+ T cells from infected adults. **(E)** Spearman correlation between frequency of IFN-γ+ responder cells and concentrations of anti-spike-S1 IgG serum antibodies measured by multiplex immunoassay (MIA) at T4 in children (upper panel, blue) and adults (lower panel, red). **(F)** Dot plots comparing the concentrations of anti-spike-S1 IgG serum antibodies at T2 or T3 versus T4 in children and adults. Each dot represents one subject. Bars indicate the median. SFU, spot-forming unit. **(A, B)** P values related to comparisons with the unexposed controls are listed at the top of the graph, above the corresponding group for comparison. For unpaired comparisons, Mann-Whitney U test (two-group comparisons) (mild adults versus moderate adults, infected children or adults at T4 versus unexposed children or adults) or Kruskal-Wallis rank-sum test with Dunn's post hoc test for multiple comparisons were used (children versus total adults versus mild adults versus moderate adults; unexposed versus infected children or adults at T1 versus T2 versus T3). Differences between paired data were compared using the Wilcoxon signed-rank test (for comparison of two paired groups) (memory T cell subsets at T3 versus T4; concentrations of anti-spike-S1 IgG serum antibodies at T2 or T3 versus T4) or the Friedman test with Dunn's multiple comparison tests (infected children or adults at T1 versus T2 versus T3 versus T4). Statistically significant comparisons are indicated, with P values < 0.05 considered significant. Cut-off values for seroprevalence are indicated with vertical dotted lines in **(E, F)**. Correlation coefficients (rs) were determined with Spearman's rank correlation. Statistically significant comparisons are indicated. P values < 0.05 were considered significant. T1, first timepoint of sampling for adults median 12.5 days and children median 8 days post-symptom onset; T2, 10-14 days after T1; T3, 4-6 weeks after T1; T4, 10 months ± 13 days after symptom onset.

frontiers in Immunology

ORIGINAL RESEARCH
published: 10 March 2022
doi: 10.3389/fimmu.2022.836495

Long Lasting Cellular Immune Response Induced by mRNA Vaccination: Implication for Prevention Strategies

Laura Vitiello[1], Lucia Gatta[2], Sara Ilari[3*], Stefano Bonassi[4,5], Mario Cristina[6], Filippo Ciatti[7], Massimo Fini[2], Stefania Proietti[4], Patrizia Russo[4,5], Carlo Tomino[2] and Dolores Limongi[5,8]*

[1] Laboratory of Flow Cytometry, IRCCS San Raffaele Roma, Rome, Italy, [2] Scientific Direction, IRCCS San Raffaele Roma, Rome, Italy, [3] Department of Health Science, Institute of Research for Food Safety and Health (IRC-FSH), University "Magna Graecia" of Catanzaro, Catanzaro, Italy, [4] Clinical and Molecular Epidemiology, IRCCS San Raffaele Roma, Rome, Italy, [5] Department of Human Sciences and Quality of Life Promotion, San Raffaele University, Rome, Italy, [6] MEBIC, IRCCS San Raffaele Roma, Rome, Italy, [7] Laboratory of Clinical Pathology, IRCCS San Raffaele Roma, Rome, Italy, [8] Laboratory of Chronic and Neurodegenerative Diseases, IRCCS San Raffaele Roma, Rome, Italy

OPEN ACCESS

Edited by:
Pia Kvistborg,
The Netherlands Cancer Institute (NKI), Netherlands

Reviewed by:
Alfred Hyoungju Kim,
Washington University School of Medicine in St. Louis, United States
Elena Ciaglia,
University of Salerno, Italy

***Correspondence:**
Sara Ilari
sara.ilari@sanraffaele.it
Laura Vitiello
laura.vitiello@sanraffaele.it

Specialty section:
This article was submitted to T Cell Biology, a section of the journal Frontiers in Immunology

Received: 15 December 2021
Accepted: 18 February 2022
Published: 10 March 2022

Citation:
Vitiello L, Gatta L, Ilari S, Bonassi S, Cristina M, Ciatti F, Fini M, Proietti S, Russo P, Tomino C and Limongi D (2022) Long Lasting Cellular Immune Response Induced by mRNA Vaccination: Implication for Prevention Strategies. Front. Immunol. 13:836495. doi: 10.3389/fimmu.2022.836495

As the COVID19 pandemic continues to spread and vaccinations are administered throughout the world at different rates and with different strategies, understanding the multiple aspects of the immune response to vaccinations is required to define more efficient vaccination strategies. To date, the duration of protection induced by COVID19 vaccines is still matter of debate. To assess whether 2-doses vaccination with BNT162b2 mRNA COVID-19 vaccine was sufficient to induce a persistent specific cellular immune response, we evaluated the presence of SARS-COV2 Spike-specific B and T lymphocytes in 28 healthcare workers 1 and 7 months after completing the vaccination cycle. The results showed that at 7 months after second dose a population of Spike-specific B lymphocytes was still present in 86% of the immunized subjects, with a higher frequency when compared to not-immunized controls (0.38% ± 0.07 vs 0.13% ± 0.03, $p<0.001$). Similarly, specific CD4+ and CD8+ T lymphocytes, able to respond *in vitro* to stimulation with Spike derived peptides, were found at 7 months. These results confirm that vaccination with BNT162b2 is able to induce a specific immune response, potentially long lasting, and could be helpful in defining future vaccination strategies.

Keywords: SARS-CoV2, mRNA vaccination, T lymphocytes activation, B lymphocytes, COVID-19

INTRODUCTION

As of December 3, 2021, more that 260 million cases of COVID-19 have been diagnosed, with more than 5 million deaths worldwide (1). Italy was the first European country to face the pandemic (2), and at the time of writing this manuscript, has counted more than 5 million confirmed cases and 134003 deaths (1). The introduction of mass vaccination changed the scenario (3), dramatically reducing the infection spread, and allowing governments to reduce or even dismiss restrictions that

characterized the pre-vaccine management of the pandemic. To date, nearly 8 billion vaccine doses have been administered (1). However, the duration of protection induced by vaccination is still matter of debate. Data from patients infected in 2002 with SARS-COV indicates that post-infection T cell memory could last up to 11year (4), while the level of circulating antibodies rapidly decline below the detection limits (5). As regards SARS-COV-2 infection, evidence shows that neutralizing antibody titers against the SARS-CoV-2 spike protein persisted for at least 5 months after infection (6). Vaccination with mRNA that encodes a SARS-CoV-2 full-length spike protein induces seroconversion in the first month after the second dose, with neutralizing anti RBD (Receptor Binding Domain) IgG traceable up to 6 months (7). A decrease in spike-specific antibodies can be observed from the second month after vaccination (7) with lower concentration observed in males and older individuals (8). Decreased antibody levels, together with the insurgence of re-infections (9) - an event that suggest a waning of the immune response - prompted public discussion about vaccination strategies and the necessity of additional doses. However, immune response to viral infections rely also on the activation of a specific cellular response. Preliminary reports described the generation of a specific T- and B- cellular memory lasting up to 8 months after SARS-CoV2 infection (10). Here, we monitored the levels of anti-RBD IgG in a cohort of 432 Health Care Workers (HCW) at IRCCS San Raffaele Roma up to 7 months after completion of the vaccination cycle. In a subgroup of 28 subjects we investigated the persistence of Spike-specific T and B lymphocytes after 1- and 7-months post vaccination with the BNT162b2 mRNA vaccine. When we started the study (March 2021), little or no evidence was available on the persistence of cellular immune response after mRNA vaccination. So, the aim of our project was to evaluate whether cellular immune response to vaccination would be persistent in time.

MATERIALS AND METHOD

Study Participants

The study was approved by the Ethic Committee of IRCCS San Raffaele Roma (POST-VAX RP 21/07). The protocol has been registered on clinicaltrial.gov (NCT05102669). The study cohort for the detection of serum IgG was composed by 432 healthcare workers (250 females 57.8% of total; mean age 50, range 27-67; males 42.2% of the cohort n=182, mean age 51, range 31-72). For the analysis of specific cellular immune response, 28 vaccinated HCW and 25 not immunized subjects were enrolled. The group of immunized subjects was composed by 16 females and 12 males (mean age 48 years, range 26-77; female mean age 48 years, range 26-63; males mean age 47 years, range 27-77). The controls group of not immunized individuals was composed by 15 females (mean age 40 years, range 30-51) and 10 males (mean age 37 years, range 26-50). Mean age for control group was 39 years (range 26-51). All the subjects declared that they never tested positive for COVID19. The absence of asymptomatic infection was confirmed by the weekly nasal swabs and rapid antigenic planned by the hospital surveillance program for all workers (Tomino, C., et al. SARS-CoV-2 epidemiological surveillance of healthcare professionals working in an inpatient rehabilitation facility. submitted).

Evaluation of Anti SARS-CoV-2 Antibodies

To evaluate total anti-SARS-CoV-2 antibodies, serum samples were collected from immunized subjects at months 1, 4 and 7 after completion of vaccination cycle. Anti-SARS-CoV-2 IgG ELISA was performed using SARS-CoV-2 IgG II Quant Reagent Kit (Abbott, Illinnois, USA). The measurement was performed by chemiluminescent microparticle immunoassay (CMIA) on a ARCHITECT analyzer (Abbott).

Cell Isolation and Stimulation

For cellular immunity analysis, venous blood was obtained 1 and 7 months after the second dose for vaccinated subjects, while samples from control subjects were obtained once. All the subjects declared that they never tested positive for COVID19. Peripheral blood mononuclear cells (PBMCs) were isolated from whole blood by density gradient centrifugation according to manufacturer's instructions (Pan Biotech). PBMC were washed and resuspended in freezing medium (FBS 10% DMSO) than stored at -80°C until the day of the assay. On the day before the assay, cells were thawed, resuspended in RPMI 1640 medium (Thermofisher) supplemented with 5% autologous serum, 100 U/ml penicillin (Thermofisher), 0.1 mg/ml streptomycin (Thermofisher). 1 ml of cell suspension (5x106cells/ml) was plated in 24-well plates and incubated at 37°C and 5%CO_2 overnight.

Detection of Spike-Responding T Cells

On the day of stimulation PBMCs were harvested and counted. Cells were washed and resuspended in culture medium at a density of 1×10^7 viable cells per mL. In brief, 100 µl of cell suspensions was seeded in flat-bottom 96-well plates and stimulated for 6 hours with or without PepTivator SARSCoV-2 protein S, S1 and S+ peptide pools (1 µg/ml each, Miltenyi Biotec, PepTivator SARS-CoV-2 Prot_S 130-126-700, cat # PepTivator SARS-CoV-2 Prot_S1, cat #130-127-041, and PepTivator SARS-CoV-2 Prot_S+, cat # 130-127-311). The PepTivator SARS-CoV-2 Prot_S contains the sequence domains aa 304-338, 421-475, 492-519, 683-707, 741-770, 785-802, and 885 – 1273 (sequence end); the PepTivator SARS-CoV-2 Prot_S1 contains the aa sequence 1–692 of the surface glycoprotein and Prot_S+ covers parts of the C-terminal S2 domain (aa 689–895)2 µL of CytoStim (Miltenyi Biotech), was used as positive control in a different well. After 2 hours of incubation, Brefeldin A (5µg/ml) was added to each well. After 4 hours, cells were collected for flow cytometry.

Cells were fixed and permeabilized then stained with CD3 Antibody, anti-human, APC,REAfinity™ (clone REA613, isotype: recombinant human IgG1); CD4 Antibody, anti-human, Vio®Bright B515, REAfinity (clone REA623, isotype: recombinant human IgG1) CD8 Antibody, anti-human, VioGreen™, REAfinity (clone REA734, isotype: recombinant human IgG1); IFN-γ Antibody, anti-human, PE, REAfinity (clone REA600, isotype: human IgG1); TNF-α Antibody, anti-human, PE-Vio®770, REAfinity (clone REA656, isotype: human

IgG1); CD14 Antibody, anti-human, VioBlue®, REAfinity (clone REA599, isotype: human IgG1); CD20 Antibody, anti-human, VioBlue®, REAfinity (clone REA780, isotype: human IgG1); CD154 Antibody, anti-human, APCVio ® 770, REAfinity (clone REA238, isotype: human IgG1) according to manufacturer instructions (Miltenyi Biotech SARS-CoV-2 Prot_S+ T Cell Analysis Kit (PBMC) human. Stained PBMC samples were acquired and analysed on FACS LSRFortessa (BD Biosciences), using FACSDiva software, v 8.0.2.

Detection of Antigen-Specific B Cells

To detect SARS-CoV-2 specific B cells, isolated PBMC were incubated with recombinant biotinylated SARS-CoV-2 RBD (0,1μg). Cell were washed then incubated with streptavidin PE (BD) for 15'. After incubation cells were washed than stained with anti-CD45 BUV395, anti CD19 APC, anti CD27 APC-R700, anti IgD BV421 (all from BD Biosciences). Stained PBMC samples were acquired and analysed on FACS LSRFortessa (BD Biosciences), using FACSDiva software, v 8.0.2.

Statistics

Sample size was predetermined using statistical methods. The experiments were not randomized and the investigators were not blinded to allocation during experiments and outcome assessment. Qualitative variables were presented as frequencies and percentages, quantitative variables were expressed as mean values and standard error (SE). Non-parametric statistical tests were used in case of non-normality: the normality of continuous variables was calculated by Kolmogorov-Smirnov test. Mann-Whitney U-test was used to compare the differences between not-immunized and immunized; while Wilcoxon signed-rank test was used to compare the differences between paired comparisons in the immunized between T1 and T7. Association between categorical variables was assessed by Chi-Square Test.

Differences in IgG in the subsets were analyzed with Friedman test and Dunn's multiple comparison test; while the differences among IgG values in the main study were analyzed by repeated-measurement two-way ANOVA and Bonferroni's multiple comparison test. A two-sided $p < 0.05$ was considered statistically significant. All analysis data were analyzed using SPSS Statistics (Version 27) and GraphPad Prism (version 8.0).

RESULTS

We enrolled 432 HCW operating at IRCCS San Raffaele Roma to evaluate the long-term efficacy of anti-COVID-19 vaccination, by measuring serum specific antibody levels. The majority of subjects were females (n=250, 57.8% of total; mean age 50, range 27-67), while males accounted for the 42.2% of the cohort (n=182, mean age 51, range 31-72). All the subject that received the vaccine had no previous history of COVID-19. We measured anti SARS-COV2 IgG levels at month 1, 4 and 7 after vaccination. As shown in **Figure 1A**, a dramatic decrease in IgG serum concentration was observed between one and four months after second dose administration (from 15.124,7AU/ml ± 636,5 to 3.260,2AU/ml ± 378,2, 78% reduction, p<0.001). An additional 67.9% decrease was observed between 4 and 7 months (3.260,2AU/ml ± 378,2 to 1.046,6AU/ml ± 248,7 p<0.001), determining an overall 93.1% reduction after 7 months from vaccination. In our cohort of vaccinated individuals, we registered 7 cases of SARS-COV2 infections, which accounts for the 1,6% of total immunized population, indicating a high efficacy of the vaccine in preventing COVID-19 in 7 months follow up. To assess the induction of a spike-specific cellular immunity, we performed flow cytometric analysis of peripheral blood B and T lymphocyte population in a subgroup of 28 vaccinated volunteers at 1 and 7 months after vaccination. These latter results were compared with a control group of 25 subjects who were not yet vaccinated.

Consistently with the general population, also in the subgroup of 28 volunteers, we observed a progressive decline in RBD-specific IgG serum concentration, with a 83.8% reduction at month 4 (12086.45AU/ml ± 1752.44 at month 1 versus 1959.81 AU/ml ± 226.52 at month 4, p=0.014) and a less pronounced decrease, i.e., 45.2% measured at month 7 (month 4: 1959.81AU/ml ± 226.52, month 7: 709.76AU/ml ± 94.68, p=0.014), for a total of 94.1% decrease after vaccination (**Figure 1B**). We analyzed the presence of RBD specific B lymphocytes by incubating cells with a biotynilated RBD, followed by staining with PE-streptavidin. **Figure 1C** shows that a population of spike specific B lymphocytes can be found up to 7 months after vaccination. Gating strategy for RBD-specific B cells identification is reported in **Figure S1**. Spike specific B cells were found to be 0.50% ± 0.13 and 0.38% ± 0.07 of total CD19+ B lymphocytes at month 1 and month 7, respectively, compared with 0.13% ± 0.03 observed in not-immunized individuals (p<0.001). Interestingly, though a decrease in the percentage of RBD-specific B lymphocytes can be observed at 7 months, this difference with the observed value at 1 month is not significant (p=0.732) but the percentage of RBD-specific B lymphocytes in immunized subjects is still higher when compared to not-vaccinated controls (p<0.001), thus suggesting that vaccination is capable to induce a long-lasting defense system ready to respond to a subsequent re-encounter with the antigen. Of note, even if in some subjects we couldn't identify Spike-specific B lymphocytes, in the majority of samples (20 out of 23, 86%) we observed the presence of RBD-binding B cells. Comparison between the decrease in humoral immunity vs the decrease specific B cellular immunity demonstrate a slower decrease in cellular response (**Figure 1D**).

We next analyzed the presence of Spike specific T lymphocytes by stimulating *in vitro* PBMC with a pool of peptides derived from Spike, and assessed T cells activation by flow cytometry. To stimulate cells we used peptides derived from the Spike protein of the "wild type" Wuhan variant of the virus. The production of INFγ and TNFα from CD8+ T cells and the production of TNFα, IFNα and the upregulation of CD154 (CD40L) on CD4+ T cells were considered indicative of antigen specific T cell activation. After paired background subtraction from parallel unstimulated cultures, we found that, both at 1 month and 7 months after vaccination, spike-derived peptides induced a specific T cell response, both in CD4+ and in CD8+ T lymphocytes. Gating strategy is depicted in the **Figure S2**. **Figure 2** shows the percentages of Spike-specific

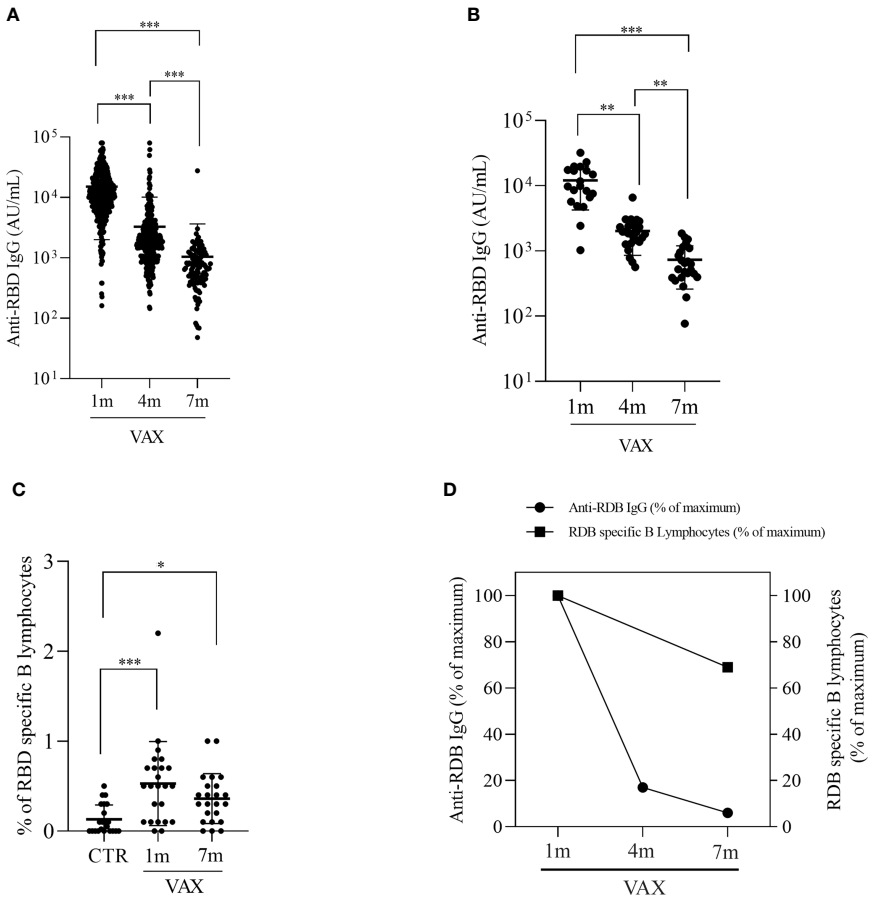


FIGURE 1 | Analysis of anti RBD specific IgG levels and RBD specific B lymphocytes in immunized subjects. **(A)** Concentration of anti-RBD IgG at 1, 4 and 7 months post second dose vaccination in the HCW cohort. Data were were analyzed by repeated-measurement two-way ANOVA and Bonferroni's multiple comparison test. A two-sided $p < 0.05$ was considered statistically significant. **(B)** Concentrationof anti-RBD IgG at 1-, 4- and 7- months post vaccination in the subgroup of subjects that were analyzed also for cellular populations. Differences were analyzed with Friedman test and Dunn's multiple comparison test. **(C)** comparision of circulating RBD specific B lymphocytes in not immunized controls (CTR) and in vaccinated subjects at 1 and 7 months, measured by flow cytometry. **(D)** comparision between the decline in anti-RBD IgG levels and in RBD specific B lymphocytes. Results are expressed as percentage of initial measured levels. *$p < 0.05$ **$p < 0.01$. ***$p < 0.001$.

CD4 T cells observed in not-immunized subjects (CTR) and in vaccinated individuals at 1 and 7 months. We observed in immunized subjects a higher percentage of Spike-specific CD4 T lymphocytes both at 1 and 7 months, compared to not-vaccinated controls, in all the analyzed populations: INFγ+ CD4+ T cells (0.21 ± 0.05 and 0.28 ± 0.04 versus 0.04 ± 0.02, p<0.05, **Figure 2A**); TNFα+ CD4+ T cells (0.20 ± 0.03 and 0.35 ± 0.05 versus 0.04 ± 0.02, p<0.001, **Figure 2B**); INFγ+ TNFα+ CD4+ T cells (0.08 ± 0.02 and 0.25 ± 0.04 versus 0.02 ± 0.01, p<0.05, **Figure 2C**); and CD154+ TNFα+ CD4 T cells (0.62 ± 0.17 and 0.88 ± 0.10 versus 0.20 ± 0.05, p<0.05, **Figure 2D**). The same analysis was conducted on Spike-specific cytokines producing CD8+ T cells. Accordingly, we found that immunized subjects showed higher percentage of cytokine producing CD8+ T lymphocytes after stimulation with Spike derived peptides, both at 1 month and 7 months after vaccination, when compared to not immunized subjects. The observed percentages of cytokines producing cells in vaccinated versus not immunized workers are shown in **Figure 3**, in particular: INFγ+ CD8+ T (0.21 ± 0.05 at month 1 and 0.37 ± 0.06 at month 7 versus 0.03 ± 0.01 in the controls, p<0.001, **Figure 3A**); TNFα+ CD8+ T (0.25 ± 0.07 at month 1 and 0.48 ± 0.07 at month 7 versus 0.05 ± 0.01 in the controls, p<0.01, **Figure 3B**); and INFγ+ TNFα+ CD8+ T (0.08 ± 0.01 at month 1 and 0.33 ± 0.06 at month 7 versus 0.02 ± 0.01 in the controls, p<0.05, **Figure 3C**). A specific T cell response to spike stimulation was observed in 83% and 79% of subjects at 7 months for CD4+ and CD8+ lymphocytes, respectively.

DISCUSSION

Vaccine efficacy and persistence of protection in time are a matter of debate both in the scientific community and in the general public. Here, we report the results observed 7 months

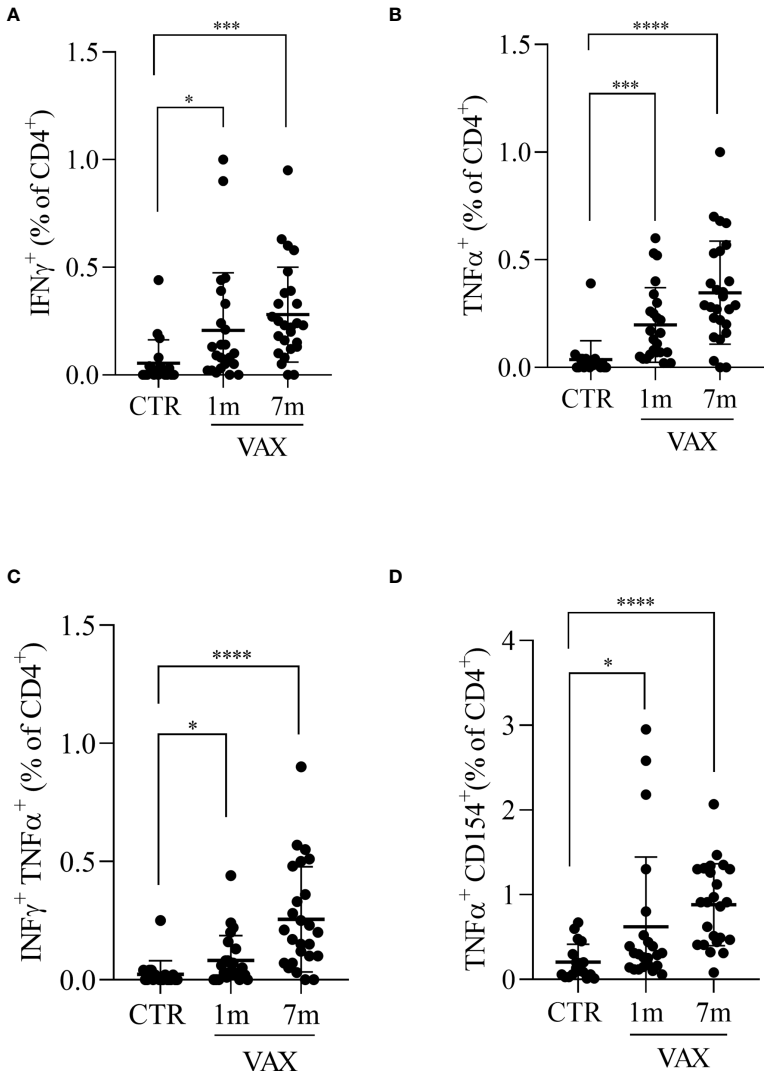


FIGURE 2 | Analysis of CD4 + T lymphocytes response to Spike derived peptides. Total PBMCs were stimulated *in vitro* with a pool of peptide derived from Spike (Wuhan variant). After 6 hours incubation in the presence of brefeldin A during the last 4 hours, PBMCs were stained and analyzed by flow cytometry for the production of INFγ **(A)**, TNFα **(B)**, for the simultaneous production of INFγ and TNFα **(C)**, or for the production of TNFα in CD154+ CD4+ T lymphocytes **(D)**. Cells from immunized subjects, analyzed at 1 and 7 months after vaccination cycle completion, were compared with cells from not-vaccinated controls (CTR). Data were analyzed using Mann-Whitney U-test *p<0.05; ***p< 0.001; ****p<0.0001.

after completion of vaccination cycle with the BNT162b2 mRNA vaccine in a cohort of health care workers. We first evaluate the serum concentration of anti-RBD specific IG, and found a dramatic decrease in time. However, decrease of specific antibody levels in serum is a common and expected feature of vaccination (11), and should not rise concern as long as the vaccination is able to induce the expansion of B lymphocytes populations specific to the antigen of interest, such as plasma cells that reside in secondary lymphoid tissues and secrete circulating antibodies and memory B cells that enhance protection by secreting antibodies in a paracrine way after pathogen entry (12). Previous reports indicate that vaccination with BNT162b2 vaccine induces the expansion of a population of spike-specific memory B lymphocytes that were still detectable after 3 months post second dose (13). Our results show that 7 months after primary vaccination a population of RBD-binding B lymphocytes, potentially able to steadily secrete specific anti-spike antibodies, can be found in immunized subjects.

Along with B lymphocytes, T lymphocytes are essential players in the protection against viral infection mainly by killing virus-infected host cells (14) and by providing help to B cells in differentiating into memory B cells and in producing antibodies (15). T lymphocytes play a key role in the host defense against SARS-COV2, as T lymphopenia has been correlated to poor prognosis (16). Thus, we have investigated whether *in vitro* stimulation of PBMCs from vaccinated individuals with a pool of

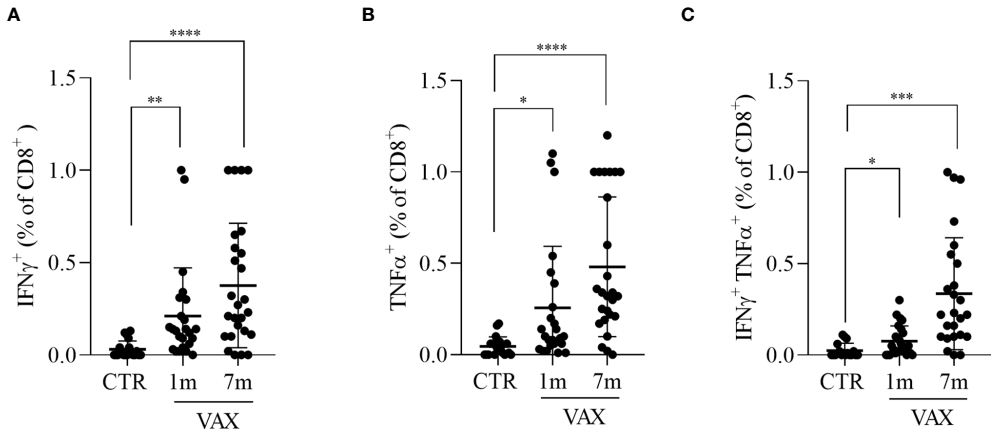


FIGURE 3 | Analysis of CD8+ T lymphocytes response to Spike derived peptides. Total PBMCs were stimulated *in vitro* with a pool of peptide derived from Spike (Wuhan variant). After 6 hours incubation in the presence of brefeldin A during the last 4 hours, PBMCs were stained and analyzed by flow cytometry for the production of INFγ **(A)**, TNFα **(B)**, or for the simultaneous production of INFγ and TNFα **(C)** in CD8+ T cells. Cells from immunized subjects, analyzed at 1 and 7 months after vaccination cycle completion, were compared with cells from not-vaccinated controls (CTR). Data were analyzed using Mann-Whitney U-test *p<0.05; **p<0.01; ***p< 0.001; ****p<0.0001.

peptides derived from the Spike protein resulted in activation of specific CD4+ and CD8+ T lymphocytes, as it was described in COVID-19 patients (17). Our results indicate that mRNA vaccination induces a robust response from cytokines-producing T lymphocytes, that lasts up to 7 months, in keeping with previous results (18, 19) as it is observed also in individuals recovered from SARS-COV2 infection (20, 21). In our *in vitro* experiments, we observed that both CD4+ and CD8+ T lymphocytes were capable to produce IFNg, with small difference between the two subsets. Previous results showed a greater difference in the amount of IFNg produced by CD4+ and CD8+ T cells (22, 23). This apparent discrepancy can be explained considering the different assays used (flow cytometry identification of IFNγ positive cells versus ELISA or ELISPOT assays), but also the subjects included in the studies (immunized subjects or infected patients). We cannot exclude that a quantitative assay such as ELISA performed on our samples could have highlighted the same differences described from other groups. We observed a contraction of the humoral immune response that was evident 4 months after completion of vaccination cycle. However, this contraction is expected after vaccination (9) and it is also observed in follow up studies of COVID-19 recovered patients (24–26), but since no vaccination from Jenner's first observations to now has been so deeply in the spotlight of media and of public opinion, this gave rise to concerns on the duration and the efficacy of the protection induced by anti-SARS-COV2 vaccination. Our data could slightly put the worries in perspective. Analysis of the immune response to SARS-COV2 infection in patients showed that the severity of the illness was strongly correlated to a decrease in the absolute numbers of T lymphocytes (27), together with a decrease in NK cells numbers (28). Moreover, patients with impaired humoral immunity but conserved T cell populations respond efficiently to SARS-COV2 infection. In addition, in patients who experienced severe COVID-19 T lymphocytes subpopulation were shown to be impaired, with a reduction in the percentages of effector memory CD4+ T helper cells (29), a decrease in the percentage of IFNγ producing cells (30) and in Th17 cells (29) together with an expansion of Th2 lymphocytes (29). Our data shows that mRNA vaccination can induce the expansion of populations of Spike-specific B and T lymphocytes population that persist in time and, in some individuals, appears to be increased at 7 months after vaccination compared to values observed at 1 month. Although we have not analyzed the expression of memory markers, we could assume that the spike specific T lymphocytes producing lymphocytes that we observed, possibly are memory or effect memory cells, given the short stimulation time, as memory cells display a faster production of cytokines, comparing to naïve T cells (31). This would be in keeping with results from Guerrera et al. (19) that observed the prevalence of central memory (CM) and effector memory (EM) subsets in Spike-specific CD4+ T cells and of CM, EM and terminally differentiated (EMRA) subsets in CD8+ T. Specific cellular immunity, mediated by T and B lymphocytes, can steadily respond and restrict viral infection, even in subjects with very low concentration of neutralizing antibodies (32, 33), thus preventing or reducing symptoms of COVID-19, and possibly reducing spreading of virus to others (34, 35).

Our work has strengths and limits. One of the limits is the low number of subjects included in the study on cellular response to Spike, a number that was chosen after calculation of the sample size needed to achieve statistical significance, on the basis of studies performed in COVID patients (17). Another limit is the use of total anti-RBD IgG, instead of neutralizing antibodies, as an indicator of humoral response. Although we are aware that the measurement of neutralizing antibodies gives a better indication of the real effectiveness in blocking the viral infection, we chose to compare the Spike-specific circulating B

lymphocytes with the levels of total IgG as this is what diagnostic laboratories measure when people check for their immune status. Moreover, while we analyze the expression of Th1 cytokines (IFNγ and TNFα), we did not investigate whether mRNA vaccination against SARS COV2 is able to induce also a population of Th2 lymphocytes. While there are several reports, direct or indirect (30, 36), of an induction of Th2 lymphocytes in COVID 19 patients, that is associated with a more severe disease and a poorer prognosis, to our knowledge there are no reports that analyzed the presence of Th2 cells induction by mRNA vaccination. The strength of this work is to have analyzed both B and T lymphocytes populations, in order to achieve a broader description of the adaptive immune response.

Our data, together with results from other groups (13, 19) sustain the evidence that immunization induced by mRNA vaccination is efficient and long lasting, even if the decrease in antibody levels fuels the fear of losing protection in time. The emergence of various variants of concern prompted new discussions on the efficacy of currently available vaccines. At the moment, the Delta and the Omicron variants represent the most prevalent variants. Recent evidences, however, demonstrated that T cell response induced by mRNA vaccination is able to recognize both Omicron and Delta, with an efficacy comparable or only slightly reduced compared to the response elicited by the wild type (Whuan) variant (37, 38). In the light of these data, we can assume that the prolonged response that we and others observed in immunized subject is potentially capable to control the infection also from delta and Omicron variants. It is true that some categories of individuals may have a worse response to vaccination (immunocompromised subjects, elderly people) and also in our cohort we could not observe the presence of RBD –specific B lymphocytes in 14% of subjects and lack of T cell specific response in 17% (for CD4+ subset) and 21% (for CD8+ lymphocytes) of vaccinated individuals, however the majority of vaccinated subjects in our observation showed the presence of specific T and B cells population that potentially can protect from SARS-COV2 infection. The presence of non-responding individuals should be kept in mind when considering to reduce containment measures. However, our data show that vaccine is highly effective in inducing a specific cellular response that lasts in months. In light of these results, the need for subsequent booster doses of vaccine could be reconsidered, and priority should be given to those who still didn't receive even a single dose of vaccine, or to specific fragile populations. To date, there aren't studies demonstrating a reduced effect of vaccination against severe disease in healthy subjects (39, 40); furthermore, spreading the message that booster doses should be given broadly, and not to selected categories of subjects for which there is a demonstrated need for a subsequent dose, could further reduce confidence in vaccines in those who are already skeptical about their efficacy (41). The currently available vaccines are safe, efficient in preventing the diseases and save lives: priority should be given to those who still haven't received the primary vaccination and to fragile or highly exposed to risk population, keeping in mind that we are all connected and none of us could be out of risk until we all will be protected. Booster doses would ensure additional protection to already immunized subjects, thus strengthening the individual, but since our aim is to ensure global protection to the whole population we should give priority to primary vaccination.

DATA AVAILABILITY STATEMENT

The raw data supporting the conclusions of this article will be made available by the authors, without undue reservation.

ETHICS STATEMENT

The studies involving human participants were reviewed and approved by Ethic Committee of IRCCS San Raffaele Roma. The patients/participants provided their written informed consent to participate in this study.

AUTHOR CONTRIBUTIONS

Designing research studies, LV, DL, CT, and MF. Conducting experiments, LV. Acquiring data, LV, FC, and MC. Analyzing data, LV, LG, SI, SP, and SB. Writing the manuscript, LV, SI, SB, and PR. All authors contributed to the article and approved the submitted version.

FUNDING

The work was supported by Italian Ministry of Health ("Ricerca Corrente") to IRCCS San Raffaele Roma.

SUPPLEMENTARY MATERIAL

The Supplementary Material for this article can be found online at: https://www.frontiersin.org/articles/10.3389/fimmu.2022.836495/full#supplementary-material

REFERENCES

1. WHO. World Health Organization, in: *WHO Coronavirus Disease (COVID-19) Dashboard* (2021). Available at: https://covid19.who.int/ (Accessed December 3, 2021).
2. Onder G, Rezza G, Brusaferro S. Case-Fatality Rate and Characteristics of Patients Dying in Relation to COVID-19 in Italy. *JAMA* (2020) 323(18):1775–6. doi: 10.1001/jama.2020.4683
3. Haas EJ, Angulo FJ, McLaughlin JM, Anis E, Singer SR, Khan F, et al. Impact and Effectiveness of mRNA BNT162b2 Vaccine Against SARS-CoV-2 Infections and COVID-19 Cases, Hospitalisations, and Deaths Following a Nationwide Vaccination Campaign in Israel: An Observational Study Using National Surveillance Data. *Lancet* (2021) 397(10287):1819–29. doi: 10.1016/S0140-6736(21)00947-8
4. Ng OW, Chia A, Tan AT, Jadi RS, Leong HN, Bertoletti A, et al. Memory T Cell Responses Targeting the SARS Coronavirus Persist Up to 11 Years Post-Infection. *Vaccine* (2016) 34(17):2008–14. doi: 10.1016/j.vaccine.2016.02.063
5. Cao WC, Liu W, Zhang PH, Zhang F, Richardus JH. Disappearance of Antibodies to SARS-Associated Coronavirus After Recovery. *N Engl J Med* (2007) 357(11):1162–3. doi: 10.1056/NEJMc070348

6. Wajnberg A, Amanat F, Firpo A, Altman DR, Bailey MJ, Mansour M, et al. Robust Neutralizing Antibodies to SARS-CoV-2 Infection Persist for Months. *Science* (2020) 370(6521):1227–30. doi: 10.1126/science.abd7728
7. Ponticelli D, Antonazzo IC, Caci G, Vitale A, Ragione GD, Romano ML, et al. Dynamics of Antibody Response to BNT162b2 mRNA COVID-19 Vaccine After 6 Months. *J Travel Med* (2021) 2(8):taab173. doi: 10.1093/jtm/taab173
8. Tsatsakis A, Vakonaki E, Tzatzarakis M, Flamourakis M, Nikolouzakis TK, Poulas K, et al. Immune Response (IgG) Following Full Inoculation With BNT162b2 COVID19 mRNA Among Healthcare Professionals. *Int J Mol Med* (2021) 48(5):200. doi: 10.3892/ijmm.2021.5033
9. Sotoodeh Ghorbani S, Taherpour N, Bayat S, Ghajari H, Mohseni P, Hashemi Nazari SS. Epidemiologic Characteristics of Cases With Reinfection, Recurrence, and Hospital Readmission Due to COVID-19: A Systematic Review and Meta-Analysis. *J Med Virol* (2022) 94(1):44–53. doi: 10.1002/jmv.27281
10. Dan JM, Mateus J, Kato Y, Hastie KM, Yu ED, Faliti CE, et al. Immunological Memory to SARS-CoV-2 Assessed for Up to 8 Months After Infection. *Science* (2021) 371(6529):eabf4063. doi: 10.1126/science.abf4063
11. Pollard AJ. Bijker EM. A Guide to Vaccinology: From Basic Principles to New Developments. *Nat Rev Immunol* (2021) 21(2):83–100. doi: 10.1038/s41577-020-00479-7
12. Yoshida T, Mei H, Dorner T, Hiepe F, Radbruch A, Fillatreau S, et al. Memory B and Memory Plasma Cells. *Immunol Rev* (2010) 237(1):117–39. doi: 10.1111/j.1600-065X.2010.00938.x
13. Piano Mortari E, Russo C, Vinci MR, Terreri S, Fernandez Salinas A, Piccioni L, et al. Highly Specific Memory B Cells Generation After the 2nd Dose of BNT162b2 Vaccine Compensate for the Decline of Serum Antibodies and Absence of Mucosal IgA. *Cells* (2021) 10(10):2541. doi: 10.3390/cells10102541
14. Koszinowski UH, Reddehase MJ, Jonjic S. The Role of CD4 and CD8 T Cells in Viral Infections. *Curr Opin Immunol* (1991) 3(4):471–5. doi: 10.1016/0952-7915(91)90005-l
15. Aranburu A, Piano Mortari E, Baban A, Giorda E, Cascioli S, Marcellini V, et al. Human B-Cell Memory is Shaped by Age- and Tissue-Specific T-Independent and GC-Dependent Events. *Eur J Immunol* (2017) 47(2):327–44. doi: 10.1002/eji.201646642
16. Shrotri M, van Schalkwyk MCI, Post N, Eddy D, Huntley C, Leeman D, et al. T Cell Response to SARS-CoV-2 Infection in Humans: A Systematic Review. *PloS One* (2021) 16(1):e0245532. doi: 10.1371/journal.pone.0245532
17. Braun J, Loyal L, Frentsch M, Wendisch D, Georg P, Kurth F, et al. SARS-CoV-2-Reactive T Cells in Healthy Donors and Patients With COVID-19. *Nature* (2020) 587(7833):270–4. doi: 10.1038/s41586-020-2598-9
18. Goel RR, Painter MM, Apostolidis SA, Mathew D, Meng W, Rosenfeld AM, et al. mRNA Vaccines Induce Durable Immune Memory to SARS-CoV-2 and Variants of Concern. *Science* (2021) 374(6572):eabm0829. doi: 10.1126/science.abm0829
19. Guerrera G, Picozza M, D'Orso S, Placido R, Pirronello M, Verdiani A, et al. BNT162b2 Vaccination Induces Durable SARS-CoV-2 Specific T Cells With a Stem Cell Memory Phenotype. *Sci Immunol* (2021) 6(66):eabl5344. doi: 10.1126/sciimmunol.abl5344
20. Kang CK, Kim M, Lee S, Kim G, Choe PG, Park WB, et al. Longitudinal Analysis of Human Memory T-Cell Response According to the Severity of Illness Up to 8 Months After Severe Acute Respiratory Syndrome Coronavirus 2 Infection. *J Infect Dis* (2021) 224(1):39–48. doi: 10.1093/infdis/jiab159
21. Rodda LB, Netland J, Shehata L, Pruner KB, Morawski PA, Thouvenel C, et al. Functional SARS-CoV-2-Specific Immune Memory Persists After Mild COVID-19. *Res Sq* (2020) 184(1):169–83.e17. doi: 10.21203/rs.3.rs-57112/v1
22. Mele D, Calastri A, Maiorano E, Cerino A, Sachs M, Oliviero B, et al. High Frequencies of Functional Virus-Specific CD4(+) T Cells in SARS-CoV-2 Subjects With Olfactory and Taste Disorders. *Front Immunol* (2021) 12:748881. doi: 10.3389/fimmu.2021.748881
23. Le Bert N, Clapham HE, Tan AT, Chia WN, Tham CYL, Lim JM, et al. Highly Functional Virus-Specific Cellular Immune Response in Asymptomatic SARS-CoV-2 Infection. *J Exp Med* (2021) 218(5):e20202617. doi: 10.1084/jem.20202617
24. Le Bert N, Chia WN, Wan WY, Teo AKJ, Chong SZ, Tan N, et al. Widely Heterogeneous Humoral and Cellular Immunity After Mild SARS-CoV-2 Infection in a Homogeneous Population of Healthy Young Men. *Emerg Microbes Infect* (2021) 10(1):2141–50. doi: 10.1080/22221751.2021.1999777
25. Schiffner J, Backhaus I, Rimmele J, Schulz S, Mohlenkamp T, Klemens JM, et al. Long-Term Course of Humoral and Cellular Immune Responses in Outpatients After SARS-CoV-2 Infection. *Front Public Health* (2021) 9:732787. doi: 10.3389/fpubh.2021.732787
26. Gluck V, Grobecker S, Kostler J, Tydykov L, Bertok M, Weidlich T, et al. Immunity After COVID-19 and Vaccination: Follow-Up Study Over 1 Year Among Medical Personnel. *Infection* (2021) 1–8. doi: 10.1007/s15010-021-01703-9
27. Diao B, Wang C, Tan Y, Chen X, Liu Y, Ning L, et al. Reduction and Functional Exhaustion of T Cells in Patients With Coronavirus Disease 2019 (COVID-19). *Front Immunol* (2020) 11:827. doi: 10.3389/fimmu.2020.00827
28. Giamarellos-Bourboulis EJ, Netea MG, Rovina N, Akinosoglou K, Antoniadou A, Antonakos N, et al. Complex Immune Dysregulation in COVID-19 Patients With Severe Respiratory Failure. *Cell Host Microbe* (2020) 27(6):992–1000 e3. doi: 10.1016/j.chom.2020.04.009
29. Golovkin A, Kalinina O, Bezrukikh V, Aquino A, Zaikova E, Karonova T, et al. Imbalanced Immune Response of T-Cell and B-Cell Subsets in Patients With Moderate and Severe COVID-19. *Viruses* (2021) 13(10):1966. doi: 10.3390/v13101966
30. Chen G, Wu D, Guo W, Cao Y, Huang D, Wang H, et al. Clinical and Immunological Features of Severe and Moderate Coronavirus Disease 2019. *J Clin Invest* (2020) 130(5):2620–9. doi: 10.1172/JCI137244
31. Kloosterboer FM, van Luxemburg-Heijs SA, Willemze R, Falkenburg JH. Similar Potential to Become Activated and Proliferate But Differential Kinetics and Profiles of Cytokine Production of Umbilical Cord Blood T Cells and Adult Blood Naive and Memory T Cells. *Hum Immunol* (2006) 67(11):874–83. doi: 10.1016/j.humimm.2006.02.040
32. Hughes R, Whitley L, Fitovski K, Schneble HM, Muros E, Sauter A, et al. COVID-19 in Ocrelizumab-Treated People With Multiple Sclerosis. *Mult Scler Relat Disord* (2021) 49:102725. doi: 10.1016/j.msard.2020.102725
33. Montero-Escribano P, Matias-Guiu J, Gomez-Iglesias P, Porta-Etessam J, Pytel V, Matias-Guiu JA. Anti-CD20 and COVID-19 in Multiple Sclerosis and Related Disorders: A Case Series of 60 Patients From Madrid, Spain. *Mult Scler Relat Disord* (2020) 42:102185. doi: 10.1016/j.msard.2020.102185
34. Shamier MCTA, Bogers S, de Wilde J, IJpelaar J, van der Kleij WA, de Jager H, et al. Virological Characteristics of SARS-CoV-2 Vaccine Breakthrough Infections in Health Care Workers [Preprint]. (2021). doi: 10.1101/2021.08.20.21262158
35. Ke R, Martinez PP, Smith RL, Gibson LL, Achenbach CJ, McFall S, et al. Longitudinal Analysis of SARS-CoV-2 Vaccine Breakthrough Infections Reveal Limited Infectious Virus Shedding and Restricted Tissue Distribution. *medRxiv* (2021). doi: 10.1101/2021.08.30.21262701
36. Roncati L, Nasillo V, Lusenti B, Riva G. Signals of Th2 Immune Response From COVID-19 Patients Requiring Intensive Care. *Ann Hematol* (2020) 99(6):1419–20. doi: 10.1007/s00277-020-04066-7
37. Woldemeskel BA, Garliss CC, Blankson JN. mRNA Vaccine-Elicited SARS-CoV-2-Specific T Cells Persist at 6 Months and Recognize the Delta Variant. *Clin Infect Dis* (2021) ciab915 doi: 10.1093/cid/ciab915
38. Gao Y, Cai C, Grifoni A, Muller TR, Niessl J, Olofsson A, et al. Ancestral SARS-CoV-2-Specific T Cells Cross-Recognize the Omicron Variant. *Nat Med* (2022). doi: 10.1038/s41591-022-01700-x
39. Connolly CM, Teles M, Frey S, Boyarsky BJ, Alejo JL, Werbel WA, et al. Booster-Dose SARS-CoV-2 Vaccination in Patients With Autoimmune Disease: A Case Series. *Ann Rheum Dis* (2021) 81(2):291–93. doi: 10.1136/annrheumdis-2021-221206
40. The Lancet R. COVID-19: Is the Rush to Boost Backed by Science? *Lancet Rheumatol* (2021) 3(11):e737. doi: 10.1016/S2665-9913(21)00330-1
41. Krause PR, Fleming TR, Peto R, Longini IM, Figueroa JP, Sterne JAC, et al. Considerations in Boosting COVID-19 Vaccine Immune Responses. *Lancet* (2021) 398(10308):1377–80. doi: 10.1016/S0140-6736(21)02046-8

Conflict of Interest: The authors declare that the research was conducted in the absence of any commercial or financial relationships that could be construed as a potential conflict of interest.

Publisher's Note: All claims expressed in this article are solely those of the authors and do not necessarily represent those of their affiliated organizations, or those of the publisher, the editors and the reviewers. Any product that may be evaluated in

this article, or claim that may be made by its manufacturer, is not guaranteed or endorsed by the publisher.

Copyright © 2022 Vitiello, Gatta, Ilari, Bonassi, Cristina, Ciatti, Fini, Proietti, Russo, Tomino and Limongi. This is an open-access article distributed under the terms of the Creative Commons Attribution License (CC BY). The use, distribution or reproduction in other forums is permitted, provided the original author(s) and the copyright owner(s) are credited and that the original publication in this journal is cited, in accordance with accepted academic practice. No use, distribution or reproduction is permitted which does not comply with these terms.

frontiers in Immunology

ORIGINAL RESEARCH
published: 31 March 2022
doi: 10.3389/fimmu.2022.846248

Humoral and Cellular Immunogenicity and Safety of Five Different SARS-CoV-2 Vaccines in Patients With Autoimmune Rheumatic and Musculoskeletal Diseases in Remission or With Low Disease Activity and in Healthy Controls: A Single Center Study

Gábor J. Szebeni[1,2,3†‡], Nikolett Gémes[1,4†], Dániel Honfi[5], Enikő Szabó[1], Patrícia Neuperger[1,4], József Á. Balog[1,4], Lajos I. Nagy[6], Zoltán Szekanecz[7], László G. Puskás[1,6], Gergely Toldi[8] and Attila Balog[5*‡]*

[1] Biological Research Centre, Laboratory of Functional Genomics, Szeged, Hungary, [2] Department of Physiology, Anatomy and Neuroscience, Faculty of Science and Informatics, University of Szeged, Szeged, Hungary, [3] CS-Smartlab Devices, Kozarmisleny, Hungary, [4] Doctoral School in Biology, Faculty of Science and Informatics, University of Szeged, Szeged, Hungary, [5] Department of Rheumatology and Immunology, Faculty of Medicine, Albert Szent-Gyorgyi Health Centre, University of Szeged, Szeged, Hungary, [6] Avidin Ltd., Szeged, Hungary, [7] Division of Rheumatology, Faculty of Medicine, University of Debrecen, Debrecen, Hungary, [8] Liggins Institute, University of Auckland, Auckland, New Zealand

Background: Vaccine-induced immunity is essential for controlling the COVID-19 pandemic. Data on humoral and cellular immunogenicity and safety of different SARS-CoV-2 vaccines in patients with autoimmune rheumatic and musculoskeletal diseases (RMDs) are limited.

Methods: A single center observational study evaluated the immunogenicity and safety of the two-dose regimen of the BBIBP-CorV inactivated, Gam-COVID-Vac and AZD1222 adenovirus-based, and BNT162b2 and mRNA-1273 mRNA-based vaccines in patients with RMDs (n = 89) compared with healthy controls (n = 74). Neutralizing anti-RBD (receptor binding domain) specific antibodies and SARS-CoV-2 specific T-cell response were measured one and four months after the second vaccine dose in parallel with vaccination efficacy and safety.

Results: Disease-specific comparison showed that antibody response at four months was higher in spondylarthropathies compared to rheumatoid arthritis and autoimmune RMDs. Risk factors for reduced immunogenicity included longer disease duration, positive immunoserological profile and anti-CD20 therapy of patients. The rate of positive anti-RBD antibody response for healthy controls versus patients after 4 months post

OPEN ACCESS

Edited by:
Laura Maggi, Università degli Studi di Firenze, Italy

Reviewed by:
Javier Carbone, Gregorio Marañón Hospital, Spain
Ferenc Uher, Central Hospital of Southern Pest, Hungary

***Correspondence:**
Gábor J. Szebeni
szebeni.gabor@brc.hu
Attila Balog
balog.attila@med.u-szeged.hu

†These authors have contributed equally to this work and share first authorship

‡These authors share senior authorship

Specialty section:
This article was submitted to T Cell Biology, a section of the journal Frontiers in Immunology

Received: *30 December 2021*
Accepted: *04 March 2022*
Published: *31 March 2022*

Citation:
Szebeni GJ, Gémes N, Honfi D, Szabó E, Neuperger P, Balog JÁ, Nagy LI, Szekanecz Z, Puskás LG, Toldi G and Balog A (2022) Humoral and Cellular Immunogenicity and Safety of Five Different SARS-CoV-2 Vaccines in Patients With Autoimmune Rheumatic and Musculoskeletal Diseases in Remission or With Low Disease Activity and in Healthy Controls: A Single Center Study. Front. Immunol. 13:846248. doi: 10.3389/fimmu.2022.846248

vaccination was 69% vs. 55% for the inactivated viral vaccine BBIBP-CorV, 97% vs. 53% for the pooled data of adenovirus vector-based vaccines Gam-COVID-Vac and AZD1222, or 100% vs. 81% for the pooled data of mRNA vaccines BNT162b2 and mRNA-1273, respectively. Patients who received the Gam-COVID-Vac or mRNA-1273 vaccines had a higher proportion of TNF-α producing CD4+ T-cells upon SARS-CoV-2 antigen stimulation compared to the inactivated viral vaccine.

Conclusion: All five investigated vaccines were immunogenic in the majority of patients and healthy controls with variable antibody and T-cell response and an acceptable safety profile.

Keywords: SARS-CoV-2 vaccination, rheumatic and musculoskeletal diseases, anti-RBD neutralizing antibodies, CD4+ T-cell response, CD8+ T-cell response

INTRODUCTION

Efficient control of the COVID-19 pandemic has become a crucial public health and economic priority worldwide. Vaccination against the SARS-CoV-2 virus has proven to be a cornerstone of preventative strategies. The BBIBP-CorV inactivated viral, Gam-COVID-Vac and AZD1222 adenovirus-based, and BNT162b2 and mRNA-1273 mRNA-based vaccines have demonstrated a high efficacy rate with an acceptable safety profile (1–5).

Patients with autoimmune rheumatic and musculoskeletal diseases (RMDs) are at increased risk of infections, including vaccine-preventable infectious diseases (6). While vaccinations are essential in their management, the drugs used to treat RMDs may reduce responses to vaccines. Available data regarding the effect of disease modifying anti-rheumatic drugs (DMARDs) on vaccine immunogenicity, and vaccination recommendations for RMD patients were summarized recently (7). An active disease with ongoing inflammatory response is known to be associated with a higher risk of infections and reduced response to vaccination (8, 9). However, the effect of vaccination in patients with low disease activity and stable immune suppressive therapy is less described. In particular, the effect of disease duration on the immunogenicity of SARS-CoV-2 vaccines has only been partially investigated. Another question of interest is whether patients receiving biological disease modifying anti-rheumatic drug (bDMARD) therapy, and specifically those on B-cell inhibitors, show a reduced response to SARS-CoV-2 vaccination (10, 11).

Prioritized vaccination of patients with autoimmune and inflammatory RMDs to reduce COVID-19 risk was proposed by the American College of Rheumatology (ACR) (12), and a considerable amount of data on the efficacy and safety of mRNA-based vaccination in immunosuppressed patients is available (11). However, data on adenovirus-based and inactivated SARS-CoV-2 vaccines in patients with autoimmune and inflammatory RMDs are limited (13, 14).

Therefore, we aimed to perform a prospective observational study to evaluate the humoral and cellular immunogenicity, efficacy, and safety of the BBIBP-CorV inactivated viral, Gam-COVID-Vac and AZD1222 adenovirus-based, and BNT162b2 and mRNA-1273 mRNA-based vaccines in patients with autoimmune and inflammatory RMDs compared with healthy controls.

MATERIALS AND METHODS

Ethics Statement

The study involving human participants was reviewed and approved by the Human Investigation Review Board of the University of Szeged under the Project Identification Code 96/2021-SZTE-KREB. The patients/participants provided their written informed consent to participate in this study. Healthy controls were staff members of the Biological Research Centre of Szeged, Hungary or the University of Szeged, Hungary. Subjects were informed about the study by a physician and acute SARS-CoV-2 infection was ruled out by qPCR. Laboratory studies and interpretations were performed on coded samples lacking personal and diagnostic identifiers. The study was adhered to the tenets of the most recent revision of the Declaration of Helsinki.

Study Design

This prospective observational study was conducted at the Department of Rheumatology and Immunology of Albert Szent-Györgyi Medical School, University of Szeged, Hungary between May 2021 and September 2021. The primary end point was the humoral and cellular immunogenicity of the BBIBP-CorV inactivated viral, Gam-COVID-Vac and AZD1222 adenovirus-based, and BNT162b2 and mRNA-1273 mRNA-based vaccines in adult patients with autoimmune and inflammatory RMDs compared with healthy controls measured at one and four months following the second vaccine dose. Secondary end points included:

1. Effect of immunosuppressive treatment on the production of anti-RBD neutralizing antibodies and SARS-CoV-2 specific T-cell response in RMD patients.
2. Comparison of the production of anti-RBD neutralizing antibodies and SARS-CoV-2 specific T-cell response based on the type of vaccination.

Study Population

Characteristics of the study participants (89 patients with autoimmune and inflammatory RMDs and 74 healthy controls) and the type of SARS-CoV-2 vaccination they received are summarized in **Table 1**. All participants received two doses of the relevant vaccine in line with recommendations of the respective manufacturer (BBIBP-CorV—Beijing Institute, China; Gam-COVID-Vac—Gamaleya Research Institute, Russia; AZD1222—AstraZeneca, UK; BNT162b2—Pfizer-BioNTech, USA; and mRNA-1273—Moderna, USA). Second shots were administered 4 weeks after the first dose for all types of the investigated vaccines. Adult patients were enrolled during regular visits at the Department of Rheumatology and Immunology (University of Szeged, Hungary) based on the following inclusion criteria: rheumatoid arthritis (RA)—ACR/European League Against Rheumatism (EULAR) 2010 classification criteria (15); psoriatic arthritis (PsA)—Classification Criteria for PsA (16); axial spondyloarthritis (axSpA)—Assessment of SpondyloArthritis International Society classification criteria (17); systemic lupus erythematosus (SLE)—ACR 1997 (18) or Systemic Lupus Erythematosus International Collaborating Clinics 2012 criteria (19); systemic vasculitis, namely, large vessel vasculitis (LVV), antineutrophil cytoplasmic antibody-associated vasculitis (AAV), granulomatosis with polyangiitis (GPA) and eosinophilic GPA—Chapel Hill Consensus Conference definitions (20); Sjögren syndrome (SS) ACR/EULAR 2016 criteria (21); systemic sclerosis (SSc)—ACR/EULAR 2013 criteria (22); idiopathic inflammatory myopathy (IIM)—ACR/EULAR 2017 classification criteria (23); Behcet's disease—International Criteria for Behcet's Disease (ICBD) (24). All patients were either in remission or had a low disease activity. All patients were on stable medication for at least the last eight weeks before enrolment. A stable dose of glucocorticoid (GC) ≤4 mg per day was permitted. The medication of the patients is summarized in **Table 2**. Patients were instructed to continue all medications during the vaccination period, except for rituximab treatment which was delayed after the vaccination. Exclusion criteria for all groups were previous COVID-19 infection, pregnancy and history of past vaccination allergy. Additional exclusion criteria for controls were history of RMDs and immunosuppressive treatment.

TABLE 1 | Demographic characteristics and the type of SARS-CoV-2 vaccination of patients with autoimmune and inflammatory RMDs and healthy controls.

	Age, years	Female	Disease duration, years	BBIBP-CorV	Gam-Covid-Vac	AZD1222	BNT162b2	mRNA-1273
Controls, n = 74	43 ± 12.5	46 (62%)	–	18 (24%)	16 (22%)	14 (19%)	16 (22%)	10 (13%)
All patients with aiRMDs, n = 89	59 ± 14	64 (72%)	11 ± 8.4	11 (12%)	8 (9%)	20 (22%)	34 (39%)	16 (18%)
RA, n = 41	62 ± 10.1	33 (83%)	12 ± 9.1	6 (15%)	5 (12%)	8 (19%)	20 (49%)	2 (5%)
PsA, n = 7	50 ± 6.6	4 (57%)	9 ± 6.6	0	1 (14%)	1 (14%)	2 (29%)	3 (43%)
AxSpa, n = 12	48 ±14.1	1 (8%)	13 ± 10.2	2 (17%)	0	1 (8%)	4 (33%)	5 (42%)
SLE n = 11	52 ±14.1	1 (9%)	13 ± 9.4	0	1 (9%)	3 (27%)	4 (37%)	3 (27%)
SS n = 4	62 ± 12	4 (100%)	9 ± 3.9	1 (25%)	0	2 (50%)	1 (25%)	0
IIM n= 1	75	1 (100%)	6	0	0	0	1 (100%)	0
SSc n = 1	73	1 (100%)	3	0	0	0	1 (100%)	0
LVV, n = 5	70 ± 6.3	4 (80%)	4 ± 3.3	1 (20%)	0	0	2 (40%)	2 (40%)
AAV, n = 6	69 ± 11	4 (67%)	8 ± 2.9	0	1 (17%)	1 (17%)	3 (50%)	1 (17%)
Other vasculitis, n = 1	54	1 (100%)	13	0	0	1 (100%)	0	0

Data are presented as mean ± SD or n (%). AAV, antineutrophil cytoplasmic antibody (ANCA)-associated vasculitis; aiRMD, autoimmune and inflammatory rheumatic and musculoskeletal disease; AxSpA, axial spondyloarthritis; IIM, idiopathic inflammatory myositis; LVV, large vessel vasculitis; PsA, psoriatic arthritis; RA, rheumatoid arthritis; SLE, systemic lupus erythematosus, SS, Sjögren syndrome; SSc, systemic sclerosis.

TABLE 2 | Therapies used in patients with autoimmune and inflammatory RMDs.

	GC	cDMARD	bDMARD	Anti-CD20	BLySi	JAKi
All patients with aiRMDs, n = 89	16 (18%)	43 (48%)	35 (39%)	8 (9%)	2 (2%)	1 (1%)
RA, n = 41	3 (7%)	17 (41%)	18 (44%)	4 (10%)	0	1 (2%)
PsA, n = 7	0	2 (29%)	5 (71%)	0	0	0
AxSpa, n = 12	0	1 (8%)	11 (92%)	0	0	0
SLE n = 11	4 (36%)	9 (8%)	0	0	2 (18%)	0
SS n = 4	1 (25%)	4 (100%)	0	0	0	0
IIM n= 1	1 (100%)	1 (100%)	0	1 (100%)	0	0
SSc n = 1	0	0	0	1 (100%)	0	0
LVV, n = 5	3 (60%)	3 (60%)	1 (20%)	0	0	0
AAV, n = 6	3 (50%)	5 (83%)	0	2 (33%)	0	0
Other vasculitis, n = 1	1 (100%)	1 (100%)	0	0	0	0

Data are presented as n (%). AAV, antineutrophil cytoplasmic antibody (ANCA)-associated vasculitis; aiRMD, autoimmune and inflammatory rheumatic and musculoskeletal disease; AxSpA, axial spondyloarthritis; IIM, idiopathic inflammatory myositis; LVV, large vessel vasculitis; PsA, psoriatic arthritis; RA, rheumatoid arthritis; SLE, systemic lupus erythematosus, SS, Sjögren syndrome; SSc, systemic sclerosis; GC, glucocorticoids; cDMARD, conventional DMARD, namely, methotrexate, leflunomide, azathioprine, chloroquine, hidroxychloroquin; bDMARD, biological DMARD, namely, tumor necrosis factor alpha inhibitors (12 patients with RA and 8 patients with AxSpa and 2 patients with PsA), interleukin 17 inhibitors (3 patients with AxSpa and 3 patients PsA), interleukin 6 inhibitors (6 patients with RA and 1 patients with LVV); LySi, BLyS-specific inhibitor, belimumab; JAKi, janus kinase inhibitor.

Measurement of Neutralizing Anti-RBD Specific Antibodies

Peripheral venous blood was taken into serum separator tubes (BD Vacutainer, Becton Dickinson, Sunnyvale, CA, USA). Sera were separated by centrifugation at 1,000*g* for 15 min. Quantitative measurement of neutralizing anti-RDB specific IgG-type antibody titers was performed with the Siemens Advia Centaur XPT system using the Siemens Healthineers SARS-CoV-2 IgG assay (sCOVG) (Siemens Healthineers, Munich, Germany). This is a fully automated two−step sandwich immunoassay using indirect chemiluminescent technology. Briefly, sera were incubated with the Solid Phase Reagent containing a preformed complex of streptavidin-coated microparticles and biotinylated SARS-CoV-2 recombinant antigens (S1 RBD, Wuhan strain) capturing SARS-CoV-2 specific antibodies in the specimen. The antibody–antigen complex was washed, and Lite Reagent was added consisting of an acridinium-ester-labeled anti-human IgG mouse monoclonal antibody. The entire complex was washed, and the signal was generated in the presence of Lite Reagent bound to the Solid Phase *via* the anti-SARS-CoV-2 IgG: SARS-CoV-2 antigen complex. When a direct relationship exists between the amount of SARS-CoV-2 IgG antibody present in the sample, the amount of relative light units (RLUs) is detected by the system. A reactive or non-reactive result was determined by the sCOVG Index Value established with the calibrators. The analytical measurement interval was 0.50–150.00 Index (U/ml). Non-reactive: <1.0 Index; the sample was considered negative for SARS-CoV-2 antibodies. Reactive: ≥1.0 Index; the sample was considered positive for SARS-CoV-2 antibodies. Measured Index Values were converted into WHO 20/136 approved international units of 1,000 Binding Antibody Unit per milliliter (BAU/ml) using the following equation: (sCOVG Index) ∗ 21.8 = 1 BAU/ml, where the diagnostic cut-off value was 21.8 BAU/ml) (25).

Measurement of SARS-CoV-2 Specific T-Cell Response

Peripheral venous blood was taken into Lithium Heparin treated tubes (BD Vacutainer, Becton Dickinson, Sunnyvale, CA, USA). Peripheral blood mononuclear cells (PBMCs) were isolated by Ficoll density gradient centrifugation using Leucosep tubes (Greiner Bio-One, Kremsmünster, Austria). Cells were pelleted by centrifugation at 800*g* for 20 min. The ring of PBMCs was harvested by pipetting and diluted with 15 ml PBS, then centrifuged at 350*g* for 5 min. The supernatant (S/N) was removed. If necessary, red blood cells were lysed by 2 ml ACK solution (prepared in our laboratory: 0.15 M NaH_4Cl, 10 mM $KHCO_3$, 0.1 mM Na_2EDTA, pH7.4, Merck, USA) at room temperature (RT) for 2 min. Cells were washed with 15 ml PBS and centrifuged at 350*g* for 5 min. Cells were resuspended in 320 µl complete RPMI-1640 cell culture media (Lonza, Switzerland) containing 10% FCS (Euroclone, Italy), 100 U/ml penicillin sodium salt and 100 µg/ml streptomycin sulfate salt (Merck, USA). PBMCs were divided into 3 wells for the following samples (1): untreated, (2) S-M-N Peptivator (Miltenyi Biotec, Germany) stimulated, (3) polyclonal activator stimulated (Cytostim, Miltenyi Biotec, Germany) in 100 µl/well on a 96-well plate (Corning, USA).

The SARS-CoV-2-specific T-cell response was measured using the SARS-CoV-2 T-Cell Analysis Kit for human PBMCs according to the instructions of the manufacturer (Miltenyi Biotec, Germany) with the following peptide pools: Peptivator SARS-CoV-2 Prot_M 6 nmol/peptide, Peptivator SARS-CoV-2 Prot_N 6 nmol/peptide, Peptivator SARS-CoV-2 Prot_S 6nmol/peptide. Peptide pools were dissolved in 200–200 µl sterile water/10% DMSO. Then 2-2 µl of S, M, and N peptide pools were added to the S-M-N stimulated wells, while 2 µl CytoStim was added to the polyclonal activator stimulated wells. After incubation at 37° C, 5% CO2 for 2h, Brefeldin-A was added to all wells at 2 µg/ml final concentration. Cells were incubated at 37°C, 5% CO2 for 16 h. Next day 100 µl cold (4°C) PEB buffer (0.5% BSA, 2 mM EDTA in PBS) was added to the wells. Cells were resuspended and pipetted into 12 × 75 mm FACS tubes (VWR International, USA) and diluted with 500 µl PEB buffer. Cells were centrifuged at 500*g* for 5 min, the S/N was removed. The Viobility 405/452 Fixable Dye was dissolved in 100 µl DMSO, then the working concentration of 100× dilution was prepared in PBS. Cells were resuspended in 100 µl Viobility Fixable Dye and incubated at RT for 10 min. Cells were washed with 500 µl PBS, centrifuged at 500*g* for 5 min. The S/N was removed, cells were resuspended in 100 µl PEB buffer. Approximately 100 µl Inside Fix solution was added to each sample and incubated at RT for 20 min. Cells were washed with 500 µl PBS, centrifuged at 500*g* for 5 min. The S/N was removed, then 100 µl Inside Perm was added to each sample. Cells were resuspended, incubated for 3 min at RT, diluted with 600 µl PBS, then centrifuged at 500*g* for 5 min. The S/N was removed then the antibody cocktail was added to the cells in 100 µl Inside Perm. The antibody cocktail consisted of 100× dilutions of anti-CD3 APC (clone REA613), anti-CD4 VioBright B515 (clone REA623), anti-CD8 VioGreen (clone REA734), anti-IFN-γ PE (clone 45-15), anti-TNF-α PE-Vio770 (clone cA2), anti-CD14 VioBlue (clone TÜK4), antiCD20 VioBlue (clone LT20), and anti-CD154 (CD40L) APC-Vio770. Cells were incubated at RT for 30 min. Cells were washed with 500 µl PBS, centrifuged at 500*g* for 5 min. Cells were resuspended in 400 µl PEB and minimum 1×10^5 $CD3^+$ cells were acquired on Cytoflex S fluorescence activated cell sorter (FACS) (Beckman Coulter, USA). Manual gating was used to determine $CD4^+$ or $CD8^+$ T-cells within live $CD14^-$ $CD20^-$ $CD3^+$ lymphocytes in CytExpert (Beckman Coulter) (**Supplementary Figure 1A**). Reactive cells were gated as $CD4^+TNF\text{-}\alpha^+$, $CD4^+IFN\gamma^+$, $CD4^+CD40L^+$, $CD8^+TNF\text{-}\alpha^+$ and $CD8^+IFN\gamma^+$ upon S-M-N or polyclonal stimuli (**Supplementary Figure 1B**). Cell numbers in the reporting gates were normalized to parental $CD4^+$ or $CD8^+$ cells (reactive cell number/parental cell number × 10^6), then background was normalized *via* subtraction of untreated from the stimulated. Finally, reactive cell numbers are shown in relation to 10^6 $CD4^+$ or $CD8^+$ T-cells, the diagnostic cut-off value was 400 reactive cells of 10^6 parental population.

Statistical Analysis

Data are expressed as median [interquartile range]. Comparisons were made using Kruskal–Wallis, Mann–Whitney and Wilcoxon

signed rank tests, as data were non-normally distributed according to the Kolmogorov–Smirnov test. p-values less than 0.05 were considered significant. Statistics were calculated using the GraphPad Prism 8 software (GraphPad, San Diego, CA, USA).

RESULTS

Clinical Characteristics

There was no significant flare or relapse among patients with autoimmune and inflammatory RMDs during the observation period following vaccination. No alteration or adjustment of DMARD therapy or the dosage of GC following vaccination was necessary in any of the patients. None of the participants were diagnosed with COVID-19 infection. The safety profile of vaccines amongst healthy controls and patients is presented in **Supplementary Tables 1** and **2**, respectively.

Humoral Immunogenicity of the Investigated Vaccines

The antibody response was compared between RA, spondylarthropathies (axSpA and PsA) and autoimmune RMDs (SSc, SLE, SS, IIM, LVV, AAV, and Behcet disease) at one- and four-months post vaccination. The antibody level was higher at four months in spondylarthropathies compared to RA and autoimmune RMDs (**Figure 1A**, p = 0.0048). Following this, we compared patient subgroups based on disease duration (<10 years versus ≥10 years) and immune serological (autoantibody) profile. The anti-RBP antibody response was higher at one month compared to four months post vaccination in patients who were diagnosed <10 years ago (**Figure 1B**, p = 0.0158), whereas it was comparable in patients diagnosed ≥10 years ago. The antibody response was lower at four months compared to one month in seropositive patients (**Figure 1C**, p = 0.0036), whereas it was comparable in seronegative patients. We also compared patients receiving conventional DMARDs to those on biological DMARD therapy. Within the subgroup of patients on bDMARD therapy, those on B-cell inhibitory treatment showed lower antibody levels both at one- and four-months post vaccination compared to those receiving other biologicals (**Figure 1D**, p = 0.0074 and p = 0.0055, respectively).

Next, we compared healthy controls and patients based on the vaccines they received. In healthy controls, vaccination with BNT162b2 or mRNA-1273 vaccines produced a higher antibody level at one month post vaccination in comparison to the other vaccines (**Figure 2A**, p <0.0001). Antibody levels decreased by 4 months compared to one month post vaccination in those who received the BNT162b2 vaccine (**Figure 2A**, p = 0.0106). However, antibody levels at four months were still higher in individuals vaccinated with Gam-COVID-Vac, BNT162b2 or mRNA-1273 vaccines compared to those who received the BBIBP-CorV vaccine (**Figure 2A**, p <0.0001). In patients, vaccination with BNT162b2 or mRNA-1273 vaccines produced a higher antibody level at one month post vaccination in comparison to the BBIBP-CorV vaccine (**Figure 2B**, p = 0.0122). Antibody levels at four months were higher in patients vaccinated with the mRNA-1273 vaccine compared to those who received BBIBP-CorV or AZD1222 vaccines (**Figure 2B**, p = 0.0107). Antibody levels decreased by

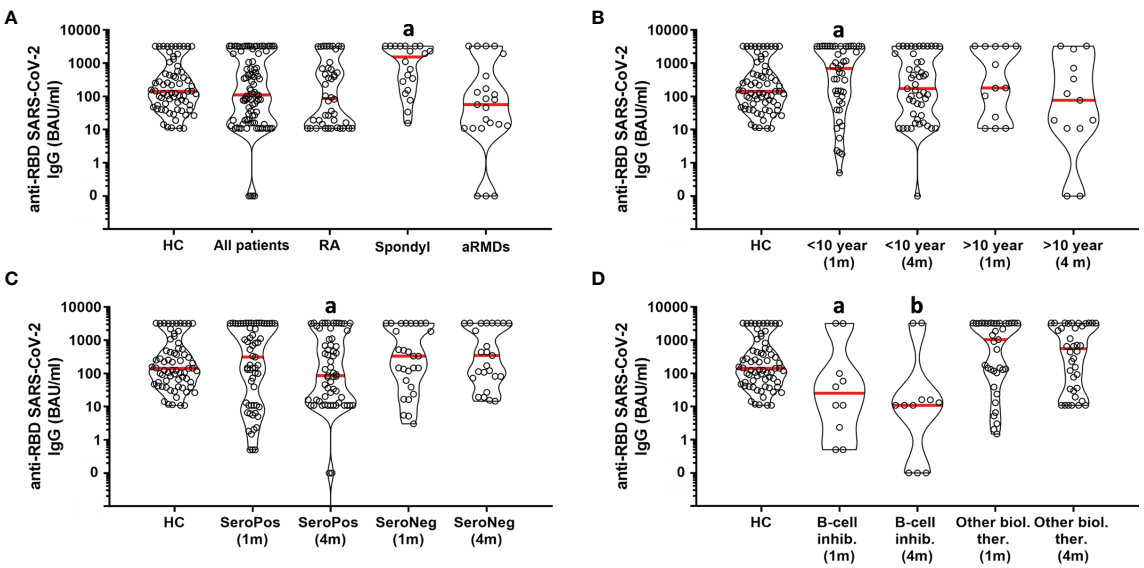


FIGURE 1 | Influence of clinical parameters on SARS-CoV-2 neutralizing antibody levels in RMD patients. HC, healthy controls; RA, rheumatoid arthritis; Spondyl, spondylarthropathies; aRMDs, autoimmune rheumatic and musculoskeletal diseaases. **(A)** a vs. HC, All patients, RA, aRMDs (p = 0.0048). **(B)** a vs. HC, <10 year (4 m), >10 year (1 m), >10 year (4 m) (p = 0.0158). **(C)** a vs. SeroPos (1 m), SeroNeg (1 m), SeroNeg (4 m) (p = 0.0036). **(D)** a vs. Other biol. ther. (1 m) (p = 0.0074), b vs. Other biol. ther. (4 m) (p = 0.0055).

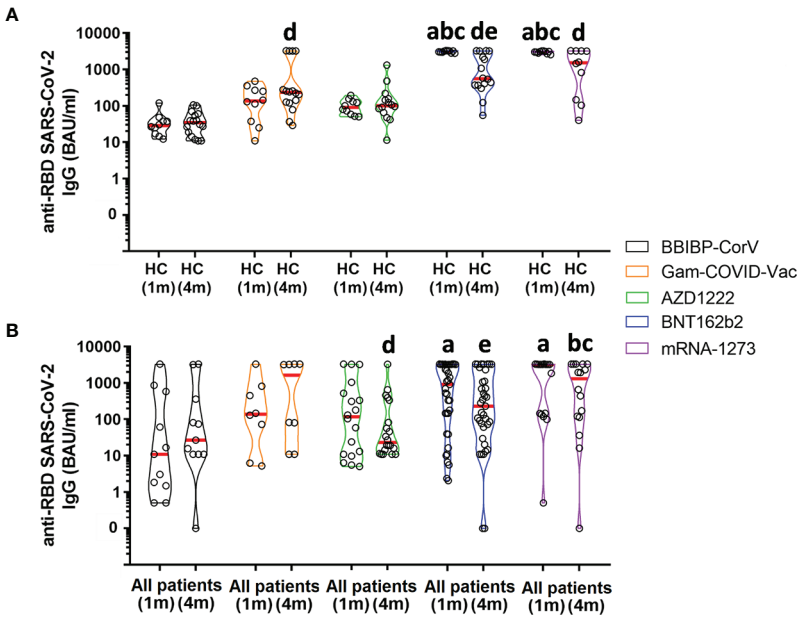


FIGURE 2 | SARS-CoV-2 neutralizing antibody levels in healthy controls and RMD patients receiving different types of vaccines. HC, healthy controls. **(A)** a vs. BBIBP-CorV (1 m) (p <0.0001), b vs. Gam-COVID-Vac (1 m) (p <0.0001), c vs. AZD1222 (1 m) (p <0.0001), d vs. BBIBP-CorV (4 m) (p = 0.0106), e vs. BNT162b2 (1 m) (p <0.0001). **(B)** a vs. BBIBP-CorV (1 m) (p = 0.0122), b vs. BBIBP-CorV (4 m) (p = 0.0107), c vs. AZD1222 (4 m) (p = 0.0107), d vs. AZD1222 (1 m) (p = 0.0179), e vs. BNT162b2 (1 m) (p = 0.0298).

4 months compared to one month post vaccination in those who received AZD1222 (**Figure 2B**, p = 0.0179) or BNT162b2 vaccines (**Figure 2B**, p = 0.0298).

Data of AZD1222 and Gam-COVID-Vac adenovirus vector-based vaccines or BNT162b2 and mRNA-1273 mRNA vaccines were pooled to calculate the rate of individuals with a positive anti-RBD antibody response to the same type of vaccine at 4 months post vaccination. The satisfactory response rate for healthy controls versus patients with autoimmune and inflammatory RMDs was 69% vs. 55% for the inactivated viral vaccine (BBIBP-CorV), 97% vs. 53% for the adenovirus vector-based vaccines (Gam-COVID-Vac and AZD1222), and 100% vs. 81% for the mRNA vaccines (BNT162b2 and mRNA-1273), respectively.

Cellular Immunogenicity of the Investigated Vaccines

No difference was detected in the studied cellular parameters when RA, spondylarthropathies and autoimmune RMDs were compared. Similarly, no difference was noted based on disease duration or biological therapy received. The proportion of TNF-α producing CD4 cells was higher in seronegative compared to seropositive patients upon stimulation with S/M/N-peptides (411 [188–670] vs 176 [0–466] cells/10^6 reactive CD4 cell, p = 0.0112), whereas there was no difference upon polyclonal stimulation.

There was no statistically significant difference in the prevalence of reactive TNF-α- (**Figures 3A, B**) or IFN-γ-producing $CD8^+$ T cells (**Figures 3C, D**) upon S/M/N or polyclonal stimulation between healthy controls or patients receiving different vaccine types. The proportion of $CD8^+$ TNF-α^+ responders amongst healthy controls versus patients 4 months post vaccination were 23% vs. 20% for BBIBP-CorV, 23% vs. 25% for pooled cases of Gam-COVID-Vac and AZD1222, and 15% vs 32% for pooled cases of BNT162b2 and mRNA-1273 vaccinated individuals. The percentage of $CD8^+$ IFNγ^+ responders among healthy controls versus patients 4 months post vaccination were 8% vs 20% for BBIBP-CorV, 23% vs 32% for pooled cases of Gam-COVID-Vac and AZD1222, and 15% vs 32% for pooled cases of BNT162b2 and mRNA-1273 vaccinated individuals.

Patients who were vaccinated with the BBIBP-CorV vaccine had a lower proportion of TNF-α-producing $CD4^+$ cells upon stimulation with S/M/N-peptides compared to those who received the Gam-COVID-Vac or mRNA-1273 vaccines (**Figure 4A**, p = 0.0316), whereas there was no difference upon polyclonal stimulation (**Figure 4B**). Patients, who received the inactivated virus vaccine or vector vaccines showed a tendency for lower proportions of $CD4^+$ IFNγ^+ T-cells compared to healthy controls upon stimulation with S/M/N-peptides (**Figure 4C**). On the other hand, patients who received the BBIBP-CorV vaccine had a higher proportion of IFNγ-producing $CD4^+$ cells upon polyclonal stimulation compared to those vaccinated with the Gam-COVID-Vac or AZD1222 vaccines (**Figure 4D**, p = 0.0047). Healthy controls who were vaccinated with the BNT162b2 vaccine had a lower proportion of $CD40L^+$ $CD4^+$ cells upon stimulation with S/M/N-peptides compared to those who received the BBIBP-CorV

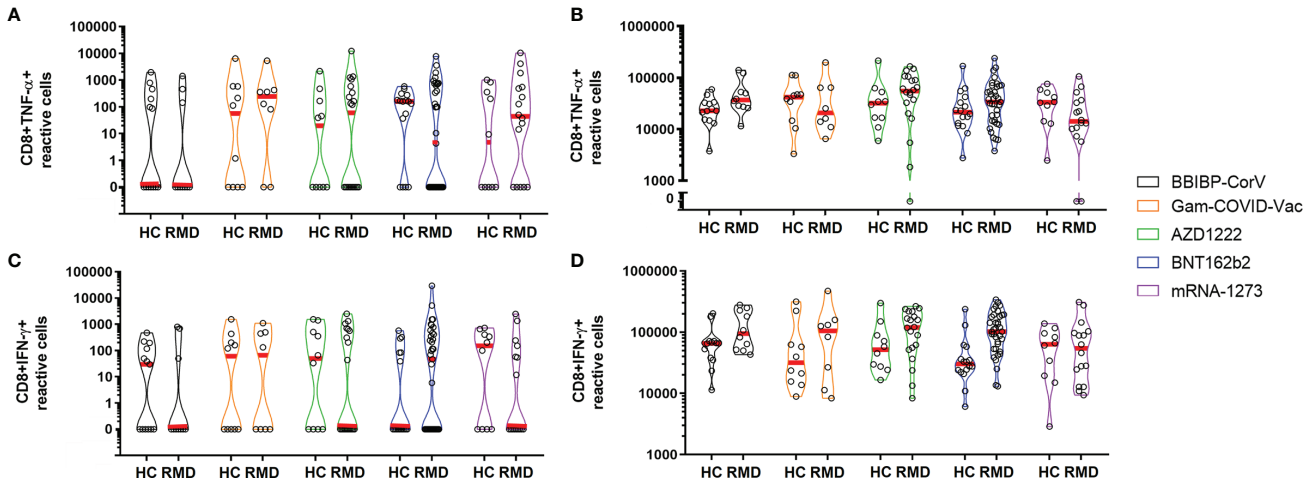


FIGURE 3 | $CD8^+$ T-cell responses in healthy controls and RMD patients receiving different types of vaccines upon S/M/N peptide **(A, C)** or polyclonal **(B, D)** stimulation. HC, healthy controls; RMD, rheumatic and musculoskeletal disease. No statistically significant difference was detected.

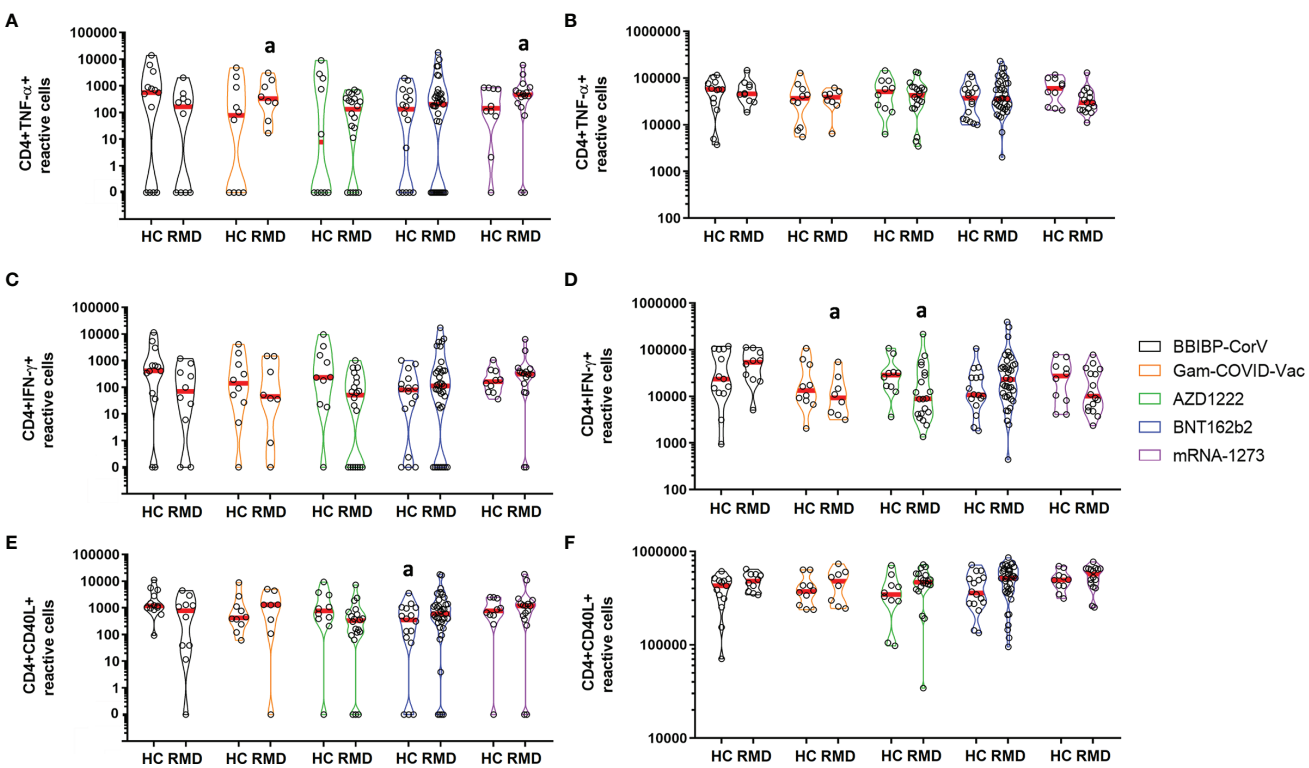


FIGURE 4 | $CD4^+$ T-cell responses in healthy controls and RMD patients receiving different types of vaccines upon S/M/N peptide **(A, C, E)** or polyclonal **(B, D, F)** stimulation. HC, healthy controls; RMD, rheumatic and musculoskeletal disease. **(A)** a vs. BBIBP-CorV (RMD) (p = 0.0316). **(D)** a vs. BBIBP-CorV (RMD) (p = 0.0047). **(E)** a vs. BNT162b2 (RMD) (p = 0.011).

vaccine (**Figure 4E**, p = 0.011), whereas there was no difference upon polyclonal stimulation (**Figure 4F**).

The proportion of $CD4^+$ TNF-α^+ responders amongst healthy controls versus patients 4 months post vaccination were 62% vs 20% for BBIBP-CorV, 36% vs 25% for pooled cases of Gam-COVID-Vac and AZD1222, and 31% vs 42% for pooled cases of BNT162b2 and mRNA-1273 vaccinated individuals. The proportion of $CD4^+$ IFNγ^+ responders among

healthy controls versus patients 4 months post vaccination were 62% vs 20% for BBIBP-CorV, 36% vs 18% for pooled cases of Gam-COVID-Vac and AZD1222, and 23% vs 28% for pooled cases of BNT162b2 and mRNA-1273 vaccinated individuals. The percentage of $CD4^+$ $CD40L^+$ responders amongst healthy controls versus patients 4 months post vaccination were 92% vs 60% for BBIBP-CorV, 68% vs 54% for pooled cases of Gam-COVID-Vac and AZD1222, and 62% vs 70% for pooled cases of BNT162b2 and mRNA-1273 vaccinated individuals.

DISCUSSION

Our study provides detailed information regarding the impact of autoimmune and inflammatory RMDs, disease duration, the immune profile of the patients and various immunosuppressive treatments on vaccine-induced immunogenicity against SARS-CoV-2. We report the results of the first single center prospective study conducted during the COVID-19 pandemic to investigate the complex short and medium-term immune response to a large variety of SARS-CoV-2 vaccines in autoimmune and inflammatory RMDs patients. We demonstrated that all five investigated vaccines were immunogenic in the majority of patients and healthy controls with variable antibody and T-cell response and an acceptable safety profile (**Supplementary Tables 1, 2**). These findings support the results of recent studies where considerable immunogenicity was induced by anti-SARS-CoV-2 mRNA vaccines (26).

SARS-CoV-2 vaccination of RMD patients, however, raises several questions, including how disease activity and immune-suppressive therapy may influence their response. Immunosuppressive drugs may reduce immunogenicity of vaccines, but the protective benefit is generally favorable. The current approach to COVID-19 vaccination of RMD patients is based on data extrapolated from studies on other vaccines, and SARS-CoV-2 vaccination data are scarce. Reduced immunogenicity to anti-SARS-CoV-2 mRNA vaccine by GC therapy was also reported (11, 26). However, there are limitations to drawing a clear conclusion including the low dosage of GC and its combination with other cDMARDs and bDMARDs. Our results confirmed that long term stable low dosage of GC therapy, cDMARDs and most of the bDMARDs have no significant effect on the production of anti-RBD binding antibodies in autoimmune and inflammatory RMDs patients with low disease activity or in remission. The Siemens Advia Centaur sCOVG assay was used in our laboratory to detect the SARS-CoV-2 specific anti-RBD binding antibodies. Irsara et al. showed good correlation ($r = 0.84$) of Centaur results with virus neutralization titers and concluded that quantitative sCOVG SARS-CoV-2 S1-RBD IgG levels could be used as a surrogate for virus neutralization capacity (27). On the other hand, patients on B-cell inhibitory treatment showed lower antibody responses both at one- and four-months post vaccination compared to those receiving other immune suppressive treatment. The timing of B-cell depleting therapy appears to be a crucial question in terms of vaccination. In case of RMD patients in remission or with a low disease activity, delaying B-cell depleting therapy could potentially prevent the impaired immunogenicity to COVID-19 vaccination. Our results are in line with literature data, that specific antibody production following vaccination may be compromised in patients with B-cell depleting therapy (28).

The risk of impaired immunogenicity based on disease duration in RMD patients with low disease activity has not been documented. The initial antibody response, measured at one month, is higher in patients with shorter disease duration. On the contrary, a longer disease duration even with low disease activity or remission is associated with impaired antibody response, which may be associated with a longer cumulative exposure to immune suppressive therapy. Several studies suggested dynamic changes of the immune phenotype of patients over time in spite of low disease activity or remission (29). Our results suggest that all patients with a long disease duration (over 10 years) require increased attention irrespective of disease activity based on the potential higher risk of reduced immunogenicity. Furthermore, since the antibody response at four months was higher in spondylarthropathies compared to RA and autoimmune RMDs, a disease specific vaccination strategy of RMD patients should also be considered.

It is tempting to speculate whether there is an additional risk of reduced immunogenicity in autoimmune and inflammatory RMDs patients with a higher disease activity. Further studies are needed in this group the patient belongs to. The question of booster vaccine doses of at risk patient groups is extremely important. Recent data confirmed that a homologous additional BNT162b2 vaccine dose and temporary discontinuation of DMARD therapy results in a significant anti-S1 response in the majority of patients with RA who had an impaired anti-S1 response to the standard two-dose vaccination regimen (30). Studies with larger patient cohorts will help determine whether and how often booster vaccination is necessary to optimize the vaccine-induced humoral and cellular immune response in specific patient groups with autoimmune and inflammatory RMDs.

Patients with a positive immune-serological profile, namely, antinuclear antibody, anti-mutated citrullinated vimentin, rheumatoid factor, or anti-neutrophil cytoplasmic antibody show a more rapid decline in anti-RBD neutralizing antibodies by four months post vaccination than patients with a negative immune-serological profile. Both B-cells and T-cells have important roles in the pathogenesis of autoimmune and inflammatory RMDs. However, the proportion of different T-cell subtypes and the amount of autoantibody producing B-cells is variable. Recent studies suggest that RA leads to higher inflammatory activity in seronegative compared with seropositive patients at the time of diagnosis, and the treatment response was lower in seronegative compared with seropositive patients. The highest disease burden of all phenotypes was also found among RA autoantibody-negative patients, at baseline and after 2 years (31). Different therapeutic response was described for new immunomodulatory therapies based on ANA-positivity. This observation possibly relates to the important role of ANAs in cytokine production and tissue inflammation and damage. Several patients with a positive ANA test result were found to have a higher risk of infections. ANA testing

was also used as an initial screen in patients with non-specific clinical symptoms, such as fever, joint pain, myalgias, fatigue, rash, or anemia, and the likelihood of an ANA-positive result due to infection was higher (32). The study of Simon et al. measured SARS-CoV-2 specific antibody levels and reported a more heterogeneous composition of patients with immune mediated inflammatory disease (IMID): spondyloarthritis (SpA/psoriatic arthritis) (32.1%), rheumatoid arthritis (RA) (29.8%), inflammatory bowel disease (9.5%), psoriasis (9.5%) and systemic IMIDs (33). Kempis et al. reported a focused study on 53 RA patients versus 20 healthy controls followed by mRNA-based vaccines (9 subjects got mRNA-1273, the rest got BNT162b2) measuring also anti-SARS-CoV-2 specific antibodies (34). Mrak et al. showed that 39% of Rituximab treated IMID patients showed seroconversion followed by mRNA-based vaccination (28). To the best of our knowledge, this is the first study which confirms the role of the immune-serological profile, both cellular and humoral immunity of autoimmune and inflammatory RMDs patients testing 5 different SARS-CoV-2 specific vaccines.

The BBIBP-CorV vaccine appears to produce the lowest, while BNT162b2 and mRNA-1273 vaccines the highest antibody response in both healthy individuals and patients both at one- and four months post immunization. Therefore, using an mRNA-based vaccine in patients receiving B-cell inhibitory therapy is of key importance in view of our finding that these patients showed lower antibody responses both at one and four months in comparison to those receiving other biologicals. Patients vaccinated with the BBIBP-CorV vaccine seem to produce a lower level of humoral response, but a higher cellular response is seen compared to other vaccines upon SARS-CoV-2-specific S/M/N-peptide stimulation. This is in line with the more complex antigenic composition of the inactivated vaccine. The rate of responders was in line with literature data regarding healthy controls (35). Our current results demonstrated lower proportions of autoimmune and inflammatory RMD patients above the diagnostic cut-off value for neutralizing antibody production in comparison to healthy controls, mainly in the cases of inactivated and adenovirus vector-based vaccines. However, T-cell response rates were comparable in autoimmune and inflammatory RMDs patients and controls.

In summary, we confirmed novel clinical risk factors of impaired immunogenicity in autoimmune and inflammatory RMDs patients, and we described the variation of their humoral and cellular immune response to five different SARS-CoV-2 vaccines. This knowledge can influence clinical decision making and inform strategies for vaccination in order to reduce and prevent the occurrence of COVID-19 infections among these patients. Our data draws attention to the importance of booster SARS-CoV-2 vaccines among autoimmune and inflammatory RMDs patients with specific clinical risk factors, namely, disease duration and immune serological profile, and those with RA or autoimmune RMDs. The variable humoral and cellular immune response between the different vaccines might help optimize the timing and dosage of booster vaccination. The differences in humoral and cellular immunogenicity in autoimmune and inflammatory RMDs patients compared to controls may necessitate the implementation of alterations in their vaccination strategy. It may be advantageous to recommend mRNA-based vaccines for patients with RMD, or at least that mRNA-based vaccines are used for booster doses. Overall, there was no hospitalization or death due to COVID-19 in the medical history of the studied RMDs or healthy controls.

DATA AVAILABILITY STATEMENT

The raw data supporting the conclusions of this article will be made available by the authors, without undue reservation.

ETHICS STATEMENT

The studies involving human participants were reviewed and approved by the Human Investigation Review Board of the University of Szeged. The patients/participants provided their written informed consent to participate in this study.

AUTHOR CONTRIBUTIONS

GJS and AB conceived of and designed the study, participated in data collection and analysis. GT and AB supervised clinical data management. AB organized and supervised the vaccination protocol. NG, ES, PN, and JB performed experiments measuring SARS-CoV-2 specific T-cell responses. LIN performed the measurement of SARS-CoV-2 specific neutralizing anti-RBD specific antibodies. DH and AB collected epidemiological and clinical data and assisted with the identification of SARS-CoV-2 infection and follow-up of patients. GJS, GT and AB analyzed the data. GJS and GT prepared the figures. GJS and LGP were responsible for laboratories. GJS verified the data and had access to raw data. GJS, GT, and AB wrote the manuscript, and GJS, ZS, GT, and AB revised the manuscript. GJS and AB had final responsibility for the decision to submit for publication. All authors helped to edit the manuscript. All authors listed have made a substantial, direct, and intellectual contribution to the work and approved it for publication.

FUNDING

This study was supported by the grant 2020-1.1.6-JÖVŐ-2021-00003 from the National Research, Development, and Innovation Office (NKFIH), Hungary. This manuscript was prepared with the professional support of the doctoral student scholarship program of the Ministry of Innovation and Technology, financed by the National Research, Development, and Innovation Fund for JB (KDP-17-4/PALY-2021, 1000464).

SUPPLEMENTARY MATERIAL

The Supplementary Material for this article can be found online at: https://www.frontiersin.org/articles/10.3389/fimmu.2022.846248/full#supplementary-material

REFERENCES

1. Polack FP, Thomas SJ, Kitchin N, Absalon J, Gurtman A, Lockhart S, et al. Safety and Efficacy of the BNT162b2 mRNA Covid-19 Vaccine. *N Engl J Med* (2020) 383(27):2603–15. doi: 10.1056/NEJMoa2034577
2. Baden LR, El Sahly HM, Essink B, Kotloff K, Frey S, Novak R, et al. Efficacy and Safety of the mRNA-1273 SARS-CoV-2 Vaccine. *N Engl J Med* (2021) 384 (5):403–16. doi: 10.1056/NEJMoa2035389
3. Voysey M, Clemens SAC, Madhi SA, Weckx LY, Folegatti PM, Aley PK, et al. Safety and Efficacy of the ChAdOx1 Ncov-19 Vaccine (AZD1222) Against SARS-CoV-2: An Interim Analysis of Four Randomised Controlled Trials in Brazil, South Africa, and the UK. *Lancet* (2021) 397(10269):99–111. doi: 10.1016/S0140-6736(20)32661-1
4. Logunov DY, Dolzhikova IV, Shcheblyakov DV, Tukhvatulin AI, Zubkova OV, Dzharullaeva AS, et al. Safety and Efficacy of an Rad26 and Rad5 Vector-Based Heterologous Prime-Boost COVID-19 Vaccine: An Interim Analysis of a Randomised Controlled Phase 3 Trial in Russia. *Lancet* (2021) 397 (10275):671–81. doi: 10.1016/S0140-6736(21)00234-8
5. Xia S, Zhang Y, Wang Y, Wang H, Yang Y, Gao GF, et al. Safety and Immunogenicity of an Inactivated SARS-CoV-2 Vaccine, BBIBP-CorV: A Randomised, Double-Blind, Placebo-Controlled, Phase 1/2 Trial. *Lancet Infect Dis* (2021) 21(1):39–51. doi: 10.1016/S1473-3099(20)30831-8
6. Furer V, Rondaan C, Heijstek M, van Assen S, Bijl M, Agmon-Levin N, et al. Incidence and Prevalence of Vaccine Preventable Infections in Adult Patients With Autoimmune Inflammatory Rheumatic Diseases (AIIRD): A Systemic Literature Review Informing the 2019 Update of the EULAR Recommendations for Vaccination in Adult Patients With AIIRD. *RMD Open* (2019) 5(2):e001041. doi: 10.1136/rmdopen-2019-001041
7. Friedman MA, Curtis JR, Winthrop KL. Impact of Disease-Modifying Antirheumatic Drugs on Vaccine Immunogenicity in Patients With Inflammatory Rheumatic and Musculoskeletal Diseases. *Ann Rheum Dis* (2021) 80(10):1255–65. doi: 10.1136/annrheumdis-2021-221244
8. Gluck T, Muller-Ladner U. Vaccination in Patients With Chronic Rheumatic or Autoimmune Diseases. *Clin Infect Dis* (2008) 46(9):1459–65. doi: 10.1086/587063
9. Crowson CS, Hoganson DD, Fitz-Gibbon PD, Matteson EL. Development and Validation of a Risk Score for Serious Infection in Patients With Rheumatoid Arthritis. *Arthritis Rheum* (2012) 64(9):2847–55. doi: 10.1002/art.34530
10. Deepak P, Kim W, Paley MA, Yang M, Carvidi AB, El-Qunni AA, et al. Glucocorticoids and B Cell Depleting Agents Substantially Impair Immunogenicity of mRNA Vaccines to SARS-CoV-2. *medRxiv* (2021). doi: 10.1101/2021.04.05.21254656
11. Furer V, Eviatar T, Zisman D, Peleg H, Paran D, Levartovsky D, et al. Immunogenicity and Safety of the BNT162b2 mRNA COVID-19 Vaccine in Adult Patients With Autoimmune Inflammatory Rheumatic Diseases and in the General Population: A Multicentre Study. *Ann Rheum Dis* (2021) 80 (10):1330–8. doi: 10.1136/annrheumdis-2021-220647
12. Curtis JR, Johnson SR, Anthony DD, Arasaratnam RJ, Baden LR, Bass AR, et al. American College of Rheumatology Guidance for COVID-19 Vaccination in Patients With Rheumatic and Musculoskeletal Diseases: Version 2. *Arthritis Rheumatol* (2021) 73(8):e30–45. doi: 10.1002/art.41877
13. Baimukhamedov C, Makhmudov S, Botabekova A. Seropositive Rheumatoid Arthritis After Vaccination Against SARS-CoV-2 Infection. *Int J Rheum Dis* (2021) 24(11):1440–1. doi: 10.1111/1756-185X.14220
14. Cherian S, Paul A, Ahmed S, Alias B, Manoj M, Santhosh AK, et al. Safety of the ChAdOx1 Ncov-19 and the BBV152 Vaccines in 724 Patients With Rheumatic Diseases: A Post-Vaccination Cross-Sectional Survey. *Rheumatol Int* (2021) 41(8):1441–5. doi: 10.1007/s00296-021-04917-0
15. Aletaha D, Neogi T, Silman AJ, Funovits J, Felson DT, Bingham CO3rd, et al. 2010 Rheumatoid Arthritis Classification Criteria: An American College of Rheumatology/European League Against Rheumatism Collaborative Initiative. *Arthritis Rheum* (2010) 62(9):2569–81. doi: 10.1002/art.27584
16. Taylor W, Gladman D, Helliwell P, Marchesoni A, Mease P, Mielants H, et al. Classification Criteria for Psoriatic Arthritis: Development of New Criteria From a Large International Study. *Arthritis Rheum* (2006) 54(8):2665–73. doi: 10.1002/art.21972
17. Rudwaleit M, van der Heijde D, Landewe R, Listing J, Akkoc N, Brandt J, et al. The Development of Assessment of SpondyloArthritis International Society Classification Criteria for Axial Spondyloarthritis (Part II): Validation and Final Selection. *Ann Rheum Dis* (2009) 68(6):777–83. doi: 10.1136/ard.2009.108233
18. Hochberg MC. Updating the American College of Rheumatology Revised Criteria for the Classification of Systemic Lupus Erythematosus. *Arthritis Rheum* (1997) 40(9):1725. doi: 10.1002/art.1780400928
19. Petri M, Orbai AM, Alarcon GS, Gordon C, Merrill JT, Fortin PR, et al. Derivation and Validation of the Systemic Lupus International Collaborating Clinics Classification Criteria for Systemic Lupus Erythematosus. *Arthritis Rheum* (2012) 64(8):2677–86. doi: 10.1002/art.34473
20. Jennette JC, Falk RJ, Bacon PA, Basu N, Cid MC, Ferrario F, et al. 2012 Revised International Chapel Hill Consensus Conference Nomenclature of Vasculitides. *Arthritis Rheum* (2013) 65(1):1–11. doi: 10.1002/art.37715
21. Shiboski CH, Shiboski SC, Seror R, Criswell LA, Labetoulle M, Lietman TM, et al. 2016 American College of Rheumatology/European League Against Rheumatism Classification Criteria for Primary Sjogren's Syndrome: A Consensus and Data-Driven Methodology Involving Three International Patient Cohorts. *Arthritis Rheumatol* (2017) 69(1):35–45. doi: 10.1002/art.39859
22. van den Hoogen F, Khanna D, Fransen J, Johnson SR, Baron M, Tyndall A, et al. 2013 Classification Criteria for Systemic Sclerosis: An American College of Rheumatology/European League Against Rheumatism Collaborative Initiative. *Ann Rheum Dis* (2013) 72(11):1747–55. doi: 10.1136/annrheumdis-2013-204424
23. Lundberg IE, Tjarnlund A, Bottai M, Werth VP, Pilkington C, Visser M, et al. 2017 European League Against Rheumatism/American College of Rheumatology Classification Criteria for Adult and Juvenile Idiopathic Inflammatory Myopathies and Their Major Subgroups. *Ann Rheum Dis* (2017) 76(12):1955–64. doi: 10.1136/annrheumdis-2017-211468
24. International Team for the Revision of the International Criteria for Behcet's D. The International Criteria for Behcet's Disease (ICBD): A Collaborative Study of 27 Countries on the Sensitivity and Specificity of the New Criteria. *J Eur Acad Dermatol Venereol* (2014) 28(3):338–47. doi: 10.1111/jdv.12107
25. Saiag E, Goldshmidt H, Sprecher E, Ben-Ami R, Bomze D. Immunogenicity of a BNT162b2 Vaccine Booster in Health-Care Workers. *Lancet Microbe* (2021) 2(12):e650. doi: 10.1016/S2666-5247(21)00272-X
26. Geisen UM, Berner DK, Tran F, Sumbul M, Vullriede L, Ciripoi M, et al. Immunogenicity and Safety of Anti-SARS-CoV-2 mRNA Vaccines in Patients With Chronic Inflammatory Conditions and Immunosuppressive Therapy in a Monocentric Cohort. *Ann Rheum Dis* (2021) 80(10):1306–11. doi: 10.1136/annrheumdis-2021-220272
27. Irsara C, Egger AE, Prokop W, Nairz M, Loacker L, Sahanic S, et al. Clinical Validation of the Siemens Quantitative SARS-CoV-2 Spike IgG Assay (sCOVG) Reveals Improved Sensitivity and a Good Correlation With Virus Neutralization Titers. *Clin Chem Lab Med* (2021) 59(8):1453–62. doi: 10.1515/cclm-2021-0214
28. Mrak D, Tobudic S, Koblischke M, Graninger M, Radner H, Sieghart D, et al. SARS-CoV-2 Vaccination in Rituximab-Treated Patients: B Cells Promote Humoral Immune Responses in the Presence of T-Cell-Mediated Immunity. *Ann Rheum Dis* (2021) 80(10):1345–50. doi: 10.1136/annrheumdis-2021-220781
29. Dulic S, Vasarhelyi Z, Sava F, Berta L, Szalay B, Toldi G, et al. T-Cell Subsets in Rheumatoid Arthritis Patients on Long-Term Anti-TNF or IL-6 Receptor Blocker Therapy. *Mediators Inflamm* (2017) 2017:6894374. doi: 10.1155/2017/6894374
30. Schmiedeberg K, Vuilleumier N, Pagano S, Albrich WC, Ludewig B, Kempis JV, et al. Efficacy and Tolerability of a Third Dose of an mRNA Anti-SARS-CoV-2 Vaccine in Patients With Rheumatoid Arthritis With Absent or Minimal Serological Response to Two Previous Doses. *Lancet Rheumatol* (2021) 4(1):e11–3. doi: 10.1016/S2665-9913(21)00328-3
31. Luurssen-Masurel N, Weel A, Hazes JMW, de Jong PHPtREACH group investigators. The Impact of Different (Rheumatoid) Arthritis Phenotypes on Patients' Lives. *Rheumatol (Oxf)* (2021) 60(8):3716–26. doi: 10.1093/rheumatology/keaa845
32. Im JH, Chung MH, Park YK, Kwon HY, Baek JH, Lee SY, et al. Antinuclear Antibodies in Infectious Diseases. *Infect Dis (Lond)* (2020) 52(3):177–85. doi: 10.1080/23744235.2019.1690676

33. Simon D, Tascilar K, Fagni F, Kronke G, Kleyer A, Meder C, et al. SARS-CoV-2 Vaccination Responses in Untreated, Conventionally Treated and Anticytokine-Treated Patients With Immune-Mediated Inflammatory Diseases. *Ann Rheum Dis* (2021) 80(10):1312–6. doi: 10.1136/annrheumdis-2021-220461
34. Rubbert-Roth A, Vuilleumier N, Ludewig B, Schmiedeberg K, Haller C, von Kempis J. Anti-SARS-CoV-2 mRNA Vaccine in Patients With Rheumatoid Arthritis. *Lancet Rheumatol* (2021) 3(7):e470–2. doi: 10.1016/S2665-9913(21)00186-7
35. Thieme CJ, Anft M, Paniskaki K, Blazquez-Navarro A, Doevelaar A, Seibert FS, et al. Robust T Cell Response Toward Spike, Membrane, and Nucleocapsid SARS-CoV-2 Proteins Is Not Associated With Recovery in Critical COVID-19 Patients. *Cell Rep Med* (2020) 1(6):100092. doi: 10.1016/j.xcrm.2020.100092

Conflict of Interest: Author GS was employed by the company Cs-Smartlab Devices Ltd. Authors LN and LP were employed by the company Avidin Ltd.

The remaining authors declare that the research was conducted in the absence of any commercial or financial relationships that could be construed as a potential conflict of interest.

Publisher's Note: All claims expressed in this article are solely those of the authors and do not necessarily represent those of their affiliated organizations, or those of the publisher, the editors and the reviewers. Any product that may be evaluated in this article, or claim that may be made by its manufacturer, is not guaranteed or endorsed by the publisher.

Copyright © 2022 Szebeni, Gémes, Honfi, Szabó, Neuperger, Balog, Nagy, Szekanecz, Puskás, Toldi and Balog. This is an open-access article distributed under the terms of the Creative Commons Attribution License (CC BY). The use, distribution or reproduction in other forums is permitted, provided the original author(s) and the copyright owner(s) are credited and that the original publication in this journal is cited, in accordance with accepted academic practice. No use, distribution or reproduction is permitted which does not comply with these terms.

frontiers | Frontiers in Immunology

REVIEW
published: 01 April 2022
doi: 10.3389/fimmu.2022.864298

CD8$^+$ T Cells in SARS-CoV-2 Induced Disease and Cancer—Clinical Perspectives

Keywan Mortezaee[1*] *and Jamal Majidpoor*[2]

[1] Department of Anatomy, School of Medicine, Kurdistan University of Medical Sciences, Sanandaj, Iran, [2] Department of Anatomy, Faculty of Medicine, Infectious Diseases Research Center, Gonabad University of Medical Sciences, Gonabad, Iran

Dysregulated innate and adaptive immunity is a sign of SARS-CoV-2-induced disease and cancer. CD8$^+$ T cells are important cells of the immune system. The cells belong to the adaptive immunity and take a front-line defense against viral infections and cancer. Extreme CD8$^+$ T-cell activities in the lung of patients with a SARS-CoV-2-induced disease and within the tumor microenvironment (TME) will change their functionality into exhausted state and undergo apoptosis. Such diminished immunity will put cancer cases at a high-risk group for SARS-CoV-2-induced disease, rendering viral sepsis and a more severe condition which will finally cause a higher rate of mortality. Recovering responses from CD8$^+$ T cells is a purpose of vaccination against SARS-CoV-2. The aim of this review is to discuss the CD8$^+$ T cellular state in SARS-CoV-2-induced disease and in cancer and to present some strategies for recovering the functionality of these critical cells.

Keywords: CD8$^+$ T cell, SARS-CoV-2, cancer, exhaustion, memory T cell, immune checkpoint inhibitor (ICI), hypoxia, programmed death 1 receptor (PD-1)

OPEN ACCESS

Edited by:
Laura Maggi,
Università degli Studi di Firenze, Italy

Reviewed by:
Laura Vitiello,
IRCCS San Raffaele Roma, Italy
Ciputra Hartana,
Ragon Institute, United States

***Correspondence:**
Keywan Mortezaee
keywan987@yahoo.com;
mortezaee.k@muk.ac.ir

Specialty section:
This article was submitted to T Cell Biology, a section of the journal Frontiers in Immunology

Received: *28 January 2022*
Accepted: *07 March 2022*
Published: *01 April 2022*

Citation:
Mortezaee K and Majidpoor J (2022) CD8$^+$ T Cells in SARS-CoV-2 Induced Disease and Cancer—Clinical Perspectives. Front. Immunol. 13:864298. doi: 10.3389/fimmu.2022.864298

HIGHLIGHTS

- CD8$^+$ T cells are infrequent in severe SARS-CoV-2-induced diseases.
- Vaccination against SARS-CoV-2 induces CD8$^+$ T-cell responses.
- Vascular abnormality-related CD8$^+$ T-cell dysfunction is potentiated in SARS-CoV-2 cancer cases.
- Stem-like and bystander CD8$^+$ T cells strengthen defense against SARS-CoV-2 and cancer.
- Immunological competence is higher in antiviral vs. antitumoral CD8$^+$ T cells.
- Aging, obesity, hypoxia, and chronic inflammation account for dysfunctional CD8$^+$ T cells.
- ICI is safe in cancer patients who are affected by SARS-CoV-2.

INTRODUCTION

Severe acute respiratory syndrome coronavirus 2 (SARS-CoV-2)-induced diseases are a major concern for global public health in the current years. There are three (1) or four (2) clinical stages for SARS-CoV-2-induced diseases. The four-stage disease includes asymptomatic, mild-to-moderate, severe-to-critical, and chronic-fibrotic states (2). Cancer patients are at a high-risk group (3) in which SARS-CoV-2 is more aggressive in patients with active cancer (4, 5), and the rate of mortality is high in such cases (6). Lung cancer patients affected from SARS-CoV-2 represent more severe

conditions. The need for hospitalization is reported in over half of such cases, and death occurs in about a quarter of patients (7). This is mostly due to the immunosuppressive cellular state in the immune ecosystem of cancer (3).

Responses from adaptive immunity emerged in about the first 7 to 10 days of SARS-CoV-2 infection (8). $CD8^+$ T cells are the critical cells of adaptive immunity (9). The cells are known as active responders to viral antigens (10). The cells take central roles for controlling viral infection (9) and directly participate in viral clearance (11). $CD8^+$ T cells are also considered as the front-line defense against cancer (12) and form a backbone for successful cancer immunotherapy. The irreversible dysfunctional state in $CD8^+$ T cells and the scarcity of antigens in antigen presentation machinery are all responsible for the lack of response from solid tumors to immunotherapy (13). Low infiltration or retarded functionality of $CD8^+$ T cells will define immune escape and cold immunity (12), such as for tumors like prostatic, pancreatic, breast, ovarian, and colon cancers (14, 15). $CD8^+$ T cells overexpressing co-inhibitory receptors on their surface display deviated activation and functionality (16). In adoptive cell therapy (ACT) of cancer, the functionality and specificity of $CD8^+$ T cells are enhanced using genetically modified receptors, so-called chimeric antigen receptors. Revitalization of dysfunctional $CD8^+$ T cells is also the current focus in cancer immune checkpoint inhibitor (ICI) therapy (13).

$CD8^+$ T cells evolve in different processes from life to death including clonal expansion, memory T-cell generation, and exhaustion. Long-lived effector T cells when exposed to a certain antigen undergo a resting state through forming memory cells. Such memory T cells when exposed to the same pathogen will recover their effector activity and render faster responses, thereby providing sustained immunity (17). Patients with asymptomatic or mild SARS-CoV-2-induced disease show strong virus-specific and sustained responses from $CD8^+$ T cells (18). SARS-CoV-2-specific $CD8^+$ T cells in mild cases show a higher production of interferon (IFN)-γ compared with severe/critical cases (19). By contrast, patients with moderate or severe symptomatic disease represent minimal induction of $CD8^+$ T cells (18). The fraction of $CD8^+$ T cells is also reduced in patients with a severe (compared with mild) disease (9, 20). These are indicative of the negative impact of SARS-CoV-2-induced diseases on $CD8^+$ T-cell fraction and functionality. This review aims at discussing the $CD8^+$ T cellular state in SARS-CoV-2-induced diseases and in cancer, focusing on interrelated events and introducing potential management strategies.

LYMPHOPENIA AND HYPERINFLAMMATION IN SARS-COV-2-INDUCED DISEASES AND THE ACTIVITY OF $CD8^+$ T CELLS

Lymphopenia or lymphocytopenia is a common characteristic of severe SARS-CoV-2-induced diseases (21, 22). As reported by Wang and colleagues, 69.5% (237/344) of patients in the intensive care unit (ICU) showed lymphocytopenia, which was prominent in non-survivors (23). Lymphopenia occurs due to acute viral infections, which increases the risk of infection-associated hospitalization and mortality. Consistent reduction of T cells is found in peripheral blood of cases with a SARS-CoV-2-induced disease (24). Besides $CD8^+$ T cells (9), patients with a severe disease display considerable reduction in the number of $CD4^+$ T, NK, and NKT cells. Such reduced presentation is more predominant for $CD8^+$ T cells compared with that for $CD4^+$ T cells in which the $CD4^+/CD8^+$ T cell ratio is considerably higher in severe (vs. mild) cases (25). Reduction of the lymphocyte count in peripheral blood is presumably indicative of higher inflammatory infiltration into the lung area (24). Patients with a critical disease who have a lymphocyte count lower than 5% following disease onset need intensive care therapy, whereas in cases with a moderate disease variation of such parameter after disease onset is very scare (4). The cell count and characterization of different subpopulations of T cells are evaluated in patients with a SARS-CoV-2-induced disease. A lower absolute number of both $CD4^+$ and $CD8^+$ T cells in such cases were found (26). The respective counts of $CD4^+$ and $CD8^+$ T cells negatively associated with patients' survival are 400 and 300 cells per μL, which were restored after disease resolution (27). Lower rates of proliferation of terminally differentiated T cells in patients with SARS-CoV-2 infection compared with that for healthy subjects were also attested (26). A point here is that patients with active SARS-CoV-2 show a lower absolute number of $CD8^+$ T cells. The existing cells are in the hyperactive state (28) and are more prone to turn into an exhaustive state. A low fraction of $CD8^+$ T cells is attributed to the development of acute respiratory distress syndrome (ARDS) in patients with active SARS-CoV-2 (29). Lung overload with such hyperactive cells results in the release of high concentrations of chemokines and cytokines, which is a common event in patients with a severe disease (22). This is indicative of the importance of the adequate number of $CD8^+$ T cells for providing protection against the virus in which even in the presence of functional $CD8^+$ T cells such patients will show a progress in the disease toward ARDS.

Hyperinflammation is a common symptom and a cause of lymphopenia in patients with a SARS-CoV-2-induced disease (24). Hyperinflammation is potentially destructive to host cells. Cytokine surge within the body causes multiorgan injury (22). Patients with a severe disease show a significant increase in the serum levels of IL-6, IL-10, and TNF-α (25). Here, the number of T cells is inversely correlated with serum concentrations of IL-6, IL-10, and TNF-α. The fraction of these inflammatory cytokines was reduced after disease resolution (27). Cases with active SARS-CoV-2 infection show signs of immune activity within the respiratory system (30). It seems that a higher inflammatory infiltration toward the lungs is partially responsible for a decrease in the number of lymphocytes within peripheral blood (24). Here, a moderate disease is correlated with a high T-cell fraction, whereas severe cases show a high fraction of inflammatory monocytes as well as neutrophils (30). Single immune cell landscape was recently characterized in bronchoalveolar lavage fluid of patients displaying varying degrees of SARS-CoV-2-induced disease. Liao and colleagues in this study attested the

abundant presence of pro-inflammatory monocyte-derived macrophages in the lavage fluid of cases with a severe disease, while highly clonally expanded $CD8^+$ T cells were more observable in the cases with a moderate disease. The amplification index for $CD8^+$ T cells for moderate cases was >5 cells compared to the severe/critical cases. In fact, lung macrophages in severe cases may be responsible for local inflammation through promoting the recruitment of inflammatory monocytes and neutrophils, which is mediated *via* CCR1 and CXCR2. By contrast, macrophages in moderate cases produce chemokines for more attraction of T cells, which is mediated through engagement of CXCR3 and CXCR6 (31). Therefore, the significantly higher neutrophil count (vs. lymphocyte count) in severe vs. moderate cases of SARS-CoV-2-induced disease could be asserted, as illustrated elsewhere (9), rendering a high neutrophil-to-lymphocyte ratio (NLR) in such cases (32). The predictive value of NLR in a more severe disease is a focus of a recent systematic review in the area (33). NLR is a marker of systemic inflammation (30) and a reliable and easily measurable parameter in patients with a SARS-CoV-2-induced disease, the measurement of which will help early diagnosis and timely management of this devastating disease (33, 34). Aberrant neutrophil responses occur as a result of exacerbated inflammation, tissue hypoxia, and uncontained viral replication (35). Hypoxia promotes a vicious cycling of neutrophil reactivity in injured lung tissue. In patients with a severe SARS-CoV-2-induced disease, reduced saturation of O_2 within the blood may cause hypoxia-inducible factor (HIF)-1α activation and excessive neutrophil function in such cases. Neutrophils produce LCN2, HGF, and RETN that their evaluation within plasma is considered as a predictive marker of a critical disease and mortality. A point to consider here is that neutrophil changes are attributed not only to its counts but also to its altered phenotypical states in which patients with a severe (vs. mild) disease show a high fraction of pre-mature or immature cells (36). This is indicative of the impact of SARS-CoV-2 in triggering emergency granulopoiesis and the pre-mature mobilization of bone marrow-derived neutrophil precursors (37). Precise delineation of different subsets of neutrophils can, thus, be considered as a marker of severe SARS-CoV-2 induced disease (38).

Key Notes

Lymphopenia is a marker of more severe SARS-CoV-2-induced diseases. Extreme T-cell activity within the lungs causes hyperinflammation. NLR measurement is of prognostic value in patients with active SARS-CoV-2.

$CD8^+$ T CELLS IN CANCER

Signaling pathways and biological mechanisms rendered by $CD8^+$ T cells undergo changes in a progressive cancer (39). Reactivation of these cells is important therapeutically even in patients with advanced cancers. Patients with head and neck squamous cell carcinoma (HNSCC), for instance, show higher overall survival (OS) when the fraction of $CD8^+$ T cells is increased at recurrence (39).

Tumoral Infiltration of $CD8^+$ T Cells

Efficacy of immunotherapy relies partly on $CD8^+$ T-cell trafficking into the tumor area (40). Infiltration of $CD8^+$ T cells is low in advanced cold cancers, which is a reason for low or no immunotherapy response from such type of cancer (12). Colorectal cancer (CRC), for instance, shows lower $CD8^+$ T-cell density in advanced vs. early stages (40). In patients with advanced pancreatic cancer, low infiltration of $CD8^+$ T cells and high expression of programmed death ligand-1 (PD-L1) are associated with high number of cancer stem cells (CSCs), which show immunosuppressive effects (41). In addition, presence of $CD8^+$ T cells is also considered as a prognostic marker in breast cancer (42), which is associated with reduced risk of death from the disease (43). By contrast, T-cell infiltration is higher in hot cancers, thereby representing better response to ICI therapy (40). The fraction of cytotoxic T cells (CTLs) is different in three categories of tumor patients. Based on outcomes of a quite recent study, patients in the "inflamed" group represented intraepithelial CTLs of >500 cells/mm^2, whereas cases in the "immune desert" group had a stromal CTL fraction of ≤50 cells/mm^2. Patients who are not included in this cutoff range were placed in the category of the "immune excluded" group, showing a quite low number of intraepithelial CTLs (44).

Key Note

Patients with diverse immune landscapes display different fractions of $CD8^+$ T cells.

Cross Talks Between $CD8^+$ T and Other Cells of the Tumor Microenvironment

Cancer-associated fibroblasts (CAFs) are the dominant cells of the tumor microenvironment (TME) that take multifaceted roles for promoting tumor aggression and metastasis (45). CAFs suppress the intra-tumoral migration of $CD8^+$ T cells (46) and exclude their contact with cancer cells. This is mediated through release of C–X–C chemokine ligand 12 (CXCL12), as well as promoting extracellular matrix (ECM) stiffness (45). High activity of CAFs within the edge or invasive front of cancer and their exposure to the hypoxic conditions in this tumor region is a reason for the cold immunity of this area. $CD8^+$ T cells are immunologically ignored in the edge area. The cells are induced by macrophage type 1 (M1) cells to recruit into the core area of tumor, rendering higher sensitivity of this tumor region to therapy (47). M1 cells are called classically activated cells. The cells represent a pro-inflammatory signature and have antitumor activities (48). $CD8^+$ T cells possibly have a negative cross talk with myeloid-derived suppressor cells (MDSCs) in which a fall in the number of MDSCs infers a rise in the fraction of $CD8^+$ T cells (49).

$CD8^+$ T cells, dendritic cells (DCs), and natural killer (NK) cells form a net of functional circuity. The activity of NK cells is induced by $CD8^+$ T cells. Such functional circuity will lead to a

co-operative activity, maximizing effector functions of these critical cells against cancer (50). $CD8^+$ T cells form CTLs upon exposure to the antigen-presenting cells (APCs), such as DCs. CTLs recognize major histocompatibility complex-1 (MHC-1)-bounded antigens expressed on target cells (17). Naïve $CD8^+$ T cells will become activated when they are under exposure to the mature DCs (51) (**Figure 1**).

Key Note

Co-operative activity within the NK/DC/$CD8^+$ T-cell axis is effective for retarding immunological ignorance.

Inverse Cross Talking Between $CD8^+$ T Cells With Regulatory T Cells in SARS-CoV-2-Induced Disease and Cancer

Regulatory T cells (Tregs) are the key components of adaptive immunity; their activity is attributed to the maintenance of tolerance to self-antigens, thereby prohibiting autoimmune diseases (52). In the context of cancer, Treg depletion increases $CD8^+$ T-cell responses, which is mediated partly *via* recovering the functionality of exhausted $CD8^+$ T cells (53). Tregs prevent cytokine storm and reduction of tissue damage (24). Excessive inflammation is a hallmark of SARS-CoV-2-induced diseases, and Tregs are for restraining ample inflammatory events (54). To support this idea, high Treg number is detected in patients with milder symptoms from SARS-CoV-2-induced diseases (2). Patients with severe disease experience a low number of Tregs (32). A question here is whether Treg-depleting strategies are applicable for cancer patients with a severe SARS-CoV-2-induced disease. T cells show higher responses to self-antigens when the number of $FOXP3^+$ Tregs is reduced. This will lead to the development of autoimmune-like responses from T cells to self-antigens, a result of which is the depletion of immunological resources (55). Thus, Tregs act as a double-edged sword through suppressing excessive inflammation, while possibly lowering host defense to act against SARS-CoV-2-related infection (28). In fact, Tregs are possibly attributed to the reduction of antiviral defense in patients with the early-stage SARS-CoV-2-induced disease, while they ameliorate inflammation-induced organ damage in cases with the late-stage disease (28). Assessment of baseline Treg levels after hospital admission for SARS-CoV-2-induced diseases is important due to predicting clinical worsening of the disease. Based on the outcomes of a study, patients harboring reduced baseline levels of Th1, Th2, and Tregs are more prone to display signs of clinical deterioration (56).

The Treg compartment displays unique changes in patients with a severe SARS-CoV-2-induced disease (57). Such cases show divergent deviations and perturbations in Treg phenotypes (54).

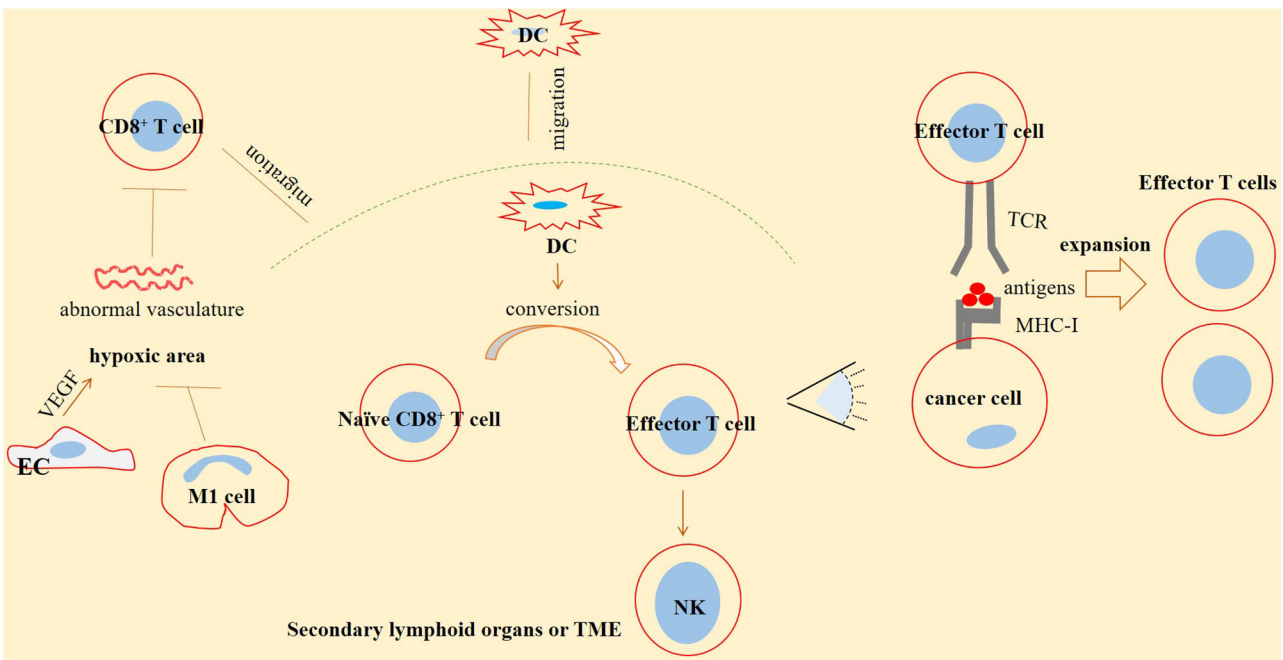


FIGURE 1 | $CD8^+$ T-cell infiltration and effector function against cancer. $CD8^+$ T cells are infiltrated into the tumor microenvironment (TME) and secondary lymphoid organs. Here, $CD8^+$ T cells are converted into effector T cells under exposure to dendritic cells (DCs) migrated toward the area and form a functional circuity with DCs and natural killer (NK) cells. A normal vasculature is an inducer of $CD8^+$ T-cell migration toward the tumor area. Generally, tumor vasculature is abnormal in solid cancers, especially in advanced stages, which is a reason for higher immune escape and resistance. High vascular endothelial growth factor (VEGF) release from endothelial cells (ECs) is a key promoter of such abnormality. High VEGF is linked with hypoxia and a leaky vasculature. Macrophage type 1 (M1) cells are antitumor cells of TME that are acting for strengthening immune effector function through promoting vascular normality. T-cell receptors (TCRs) expressed on infiltrated $CD8^+$ T cells are able to detect antigens bounded to the major histocompatibility complex-1 (MHC-1), expressed on the surface of tumor cells, a result of which is the expansion of effector T cells able to act against cancer.

Based on outcomes of one study, the fraction of Tregs is reduced in hospitalized patients, whereas cytotoxic T helper and follicular helper T cells show an increased fraction (58). Galván-Peña and colleagues reported that patients with a severe disease had a distinct transcriptomic profiling, delineated by increased intracellular level of the transcription factor FOXP3, which is associated with poor outcomes. Such an increase in the FOXP3 expression was in coincidence with a rise in the percentage of Tregs in most of the patients (but not all). Interestingly, in patients with a rise in FOXP3 and Tregs there was a reduction in the expression of the transcription factor CD45RA, which is a marker of naïve Tregs. However, Tbet, which controls preferentially responses from Th1 cells, was overrepresented on Tregs in patients with a severe disease. It seems that blood Tregs from patients with a SARS-CoV-2-induced disease turned into the cells resembling that of tumor-infiltrating Tregs (54). The level of naïve Tregs is increased significantly postinfection. Due to the dual activity of Tregs in suppression of immune responses and promotion of tissue repair, an expansion in the level of naïve Tregs can be an effort for restoring equilibrium in the Treg pool upon facing both tissue injury and inflammation (59). Treg depletion is a possible strategy for enhancing CD8+ T-cell functionality in cancer patients, but as is mentioned above, it may strengthen viral persistence when such cases also have SARS-CoV-2-related infection (**Figure 2**).

Key Note

Treg depletion may strengthen viral persistence in cancer patients with active SARS-CoV-2. Divergent deviations of Tregs exist

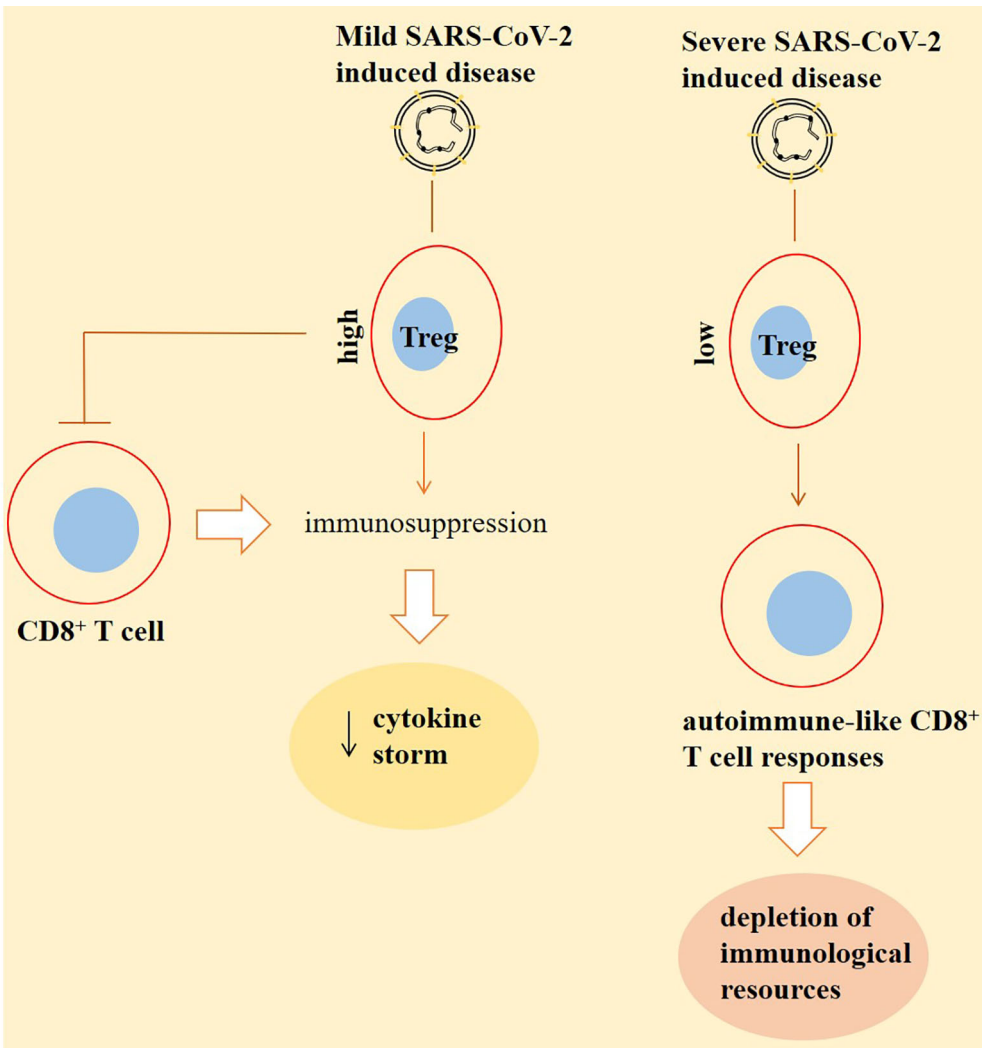


FIGURE 2 | Inverse cross talking between CD8+ T cells with regulatory T cells (Tregs) in patients with a SARS-CoV-2-induced disease. Tregs are high in patients with a mild disease. This will result in immunosuppression partly by suppressing the activity of CD8+ T cells. Such immunosuppression further reduces the extent of cytokine storm, thereby lessening the severity of the condition. By contrast, the number of Tregs is low in severe cases. This will cause responses from CD8+ T cells to self-antigens, and the cells are representing autoimmune-like states, which results in the depletion of immunological resources to combat against the virus. The outcome of this autoimmunity is higher viral persistence and a more severe condition.

among patients with a severe SARS-CoV-2-induced disease, which is seemingly resembling of Tregs in cancer patients.

CD8+ T-CELL EXPRESSION PROFILE IN SARS-COV-2-INDUCED DISEASE AND CANCER

NK group 2 member A (NKG2A) is a receptor that belongs to the lectin family and forms a heterodimer with its co-receptor CD94 (also called KLRD1). CD94/NKG2A sends inhibitory signals (60), and its enhanced expression is seen on exhausted NK and CD8+ T cells in patients with a SARS-CoV-2-induced disease. The concomitant reduced expression of CD94/NKG2A occurs in convalescent individuals (4). The expression of NKG2A on CD8+ T cells is high in patients with an acute severe/critical disease (61), delineating the activity of this inhibitory receptor in promoting the severity of condition in patients with a SARS-CoV-2-induced disease. CD94/NKG2A surface co-expression is reported in about 50% of CD8+ T cells, and its selective expression is linked with poor clinical outcomes in HNSCC patients. In fact, the induction of NKG2A on CD8+ T cells infiltrated into the tumor area is a mechanism of immunosuppression in patients with cancer. Blockade of this inhibitory receptor can improve the efficacy of vaccination therapy against cancer, represented by delayed tumor recurrence after therapy (62). By contrast, natural killer group 2, member D (NKG2D, also called CD314), is an activating receptor of the lectin family. NKG2D is expressed on the surface of NK and CD8+ T cells and acts as a killer of infected or cancer cells (63). The constitutive expression of NKG2D on human CD8+ T cells (64) is linked positively with their functional memory features (65). The activity of NKG2D on CD8+ T cells needs the parallel activation of the T-cell receptor (TCR). This is different from the active NKG2D on NK cells in which the killing responses to NKG2D are unleashed without a need for concurrent TCR activity (64). The expression of CD107a is a marker of cellular activation that is linked with cytotoxic degranulation (66). CD8+ T cells from patients with a SARS-CoV-2-induced disease also overexpress CD69 and T-cell immunoglobulin mucin-3 (TIM-3) (67). CD69 is a marker of T-cell activation, and TIM-3 is the checkpoint and co-inhibitory molecule (**Figure 3**).

Interleukin 33 (IL-33) increases CD8+ T-cell functionality (68) and is contributed to its proliferation and infiltration of CD8+ T cells, thereby acting as a suppressor of tumor growth (69). The soluble suppressor of tumorigenicity 2 (sST2, also called IL-1RL1) is a receptor that binds with IL-33 and is contributed to the local limitation of off-target IL-33 activity and thereby prohibits inadequate inflammatory responses (68). sST2 is considered as a prognostic biomarker in SARS-CoV-2-induced diseases (70). There is a high serum level of sST2 and a negative correlation between serum sST2 with CD8+ T cell count in patients with an active SARS-CoV-2 infection (71). Analysis of bronchoalveolar lavage fluid in patients with mild-to-severe SARS-CoV-2-induced diseases shows a population of cells with the activity of IL-33 production and an increase in their fraction upon disease progression (72). The activity of IL-33 contributed to tissue remodeling, homeostasis, and repair during acute SARS-CoV-2 infection, mediated partly *via* increasing the number of CD8+ T cells. By contrast, during chronic SARS-CoV-2 infection, the regulatory impact of sST2 over IL-33 activity is overwhelmed, thereby causing an over-release of IL-33 and persistent inflammatory response from CD8+ T cells, which finally causes tissue damage (68). During severe infection with SARS-CoV-2, tight interactions between active immune cells with the airway epithelium will cause epithelial damage, a result of which is high IL-33 release. Over-release of IL-33 impairs antiviral activity of CD8+ T cells and initiates inflammatory responses within the lungs. A consequence of such dampened antiviral immunity is hyperinflammation, delayed viral clearance, and more severe infections (73) (**Figure 1**).

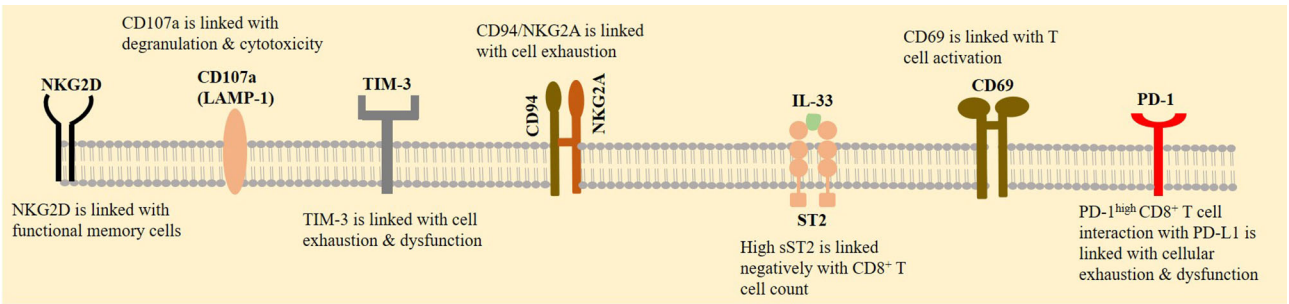


FIGURE 3 | CD8+ T-cell expression profile. A rise in the expression of natural killer group 2, member A (NKG2A) is contributed to the exhaustion of CD8+ T cells in patients with a SARS-CoV-2-induced disease, whereas natural killer group 2, member D (NKG2D) is contributed to the functional memory T cells. CD8+ T-cell activation is also promoted by overexpression of CD69. CD107a is another marker of cellular activation. By contrast, T-cell immunoglobulin mucin-3 (TIM-3) and programmed death 1 receptor (PD-1) are checkpoints that their increased expression on CD8+ T cells is indicative of their impaired functionality. Interleukin 33 (IL-33) activity enhances CD8+ T-cell functionality, proliferation, and infiltration. Soluble suppressor of tumorigenicity 2 (sST2) is a receptor that binds with IL-33 and is contributed to the local limitation of off-target IL-33 activity.

Key Note

High expressions of NKG2A and NKG2D are representative of the respective CD8+ T-cell exhaustion and functional memory features. IL-33 is a tumor suppressor, but its upregulation in lung epithelial cells is contributed to the hyperinflammation in patients with severe SARS-CoV-2.

CD8+ T CELLULAR STATES IN SARS-COV-2-INDUCED DISEASE AND CANCER

CD8+ Memory and Effector T Cells

Successful immunotherapy relies on recovering antigen-specific effector memory T cells within the TME (74). Memory CD8+ T cells are important for promoting sustained immunity against cancer (75). Central memory, effector memory, resident memory, and stem-like memory cells are different subsets in this category. Resident memory T cells are placed in local tissue areas and contribute to the immediate response to secondary infection, whereas central memory and effector memory T cells circulate within blood, and their target organs are secondary lymphoid tissues (76).

Memory T cells are considered as a hallmark of antiviral immunity (77). The cells are presented in convalescent individuals from SARS-CoV-2-induced diseases (78) and are generated as a response to vaccination, infection, or after viral reexposure (8). Memory T cells are important for quick responses against infection, and their presence is a reason for the low severe condition experienced by patients upon viral reentry (21, 79). During recovery from SARS-CoV-2-induced diseases, dysfunctional T cells are converted into functional CD8+ memory T cells (61). Bert and colleagues evaluated T-cell responses in patients that recovered from SARS, the disease related to the SARS-CoV infection. They noticed the presence of memory T cells reactive to the SARS-CoV N protein 17 years after the SARS outbreak in 2003 (80). The dynamic transition between effector and memory T cells is also reported in SARS-CoV-2-specific CD8+ T cells (81). Such CD8+ memory T cells will reach a peak at about 2 weeks after infection with this virus. The cells are also detectable even after 100 days (8), and their response against SARS-CoV-2 is maintained for 10 months. The cells are able to form stem-like memory cells (82), but their fraction is reduced over time (8) (**Figures 4**, **5**).

Key Note

CD8+ memory T cells provide protection against viral reentry, but their fraction is reduced over time.

Stem-Like CD8+ T Cells

T-cell memory in cancer and cancer immunotherapy relies on the formation of antigen-specific stem-like progenitor cells (83). Stem-like T cells are T-cell factor (TCF)-1^{high} memory cells that represent higher proliferative capacity and produce a larger number of effector cells, as compared with other T-cell memory subsets (76). Stem-like memory T cells are multi-potent and have self-renewal potential (84). The activity of stem-like CD8+ T cells contributes to the complete regression of tumor and tumor-infiltrating lymphocyte (TIL) persistence in patients receiving ACT (85). Two subtypes of stem-like progenitor memory of CD8+ T cells are identified: progenitor cells committed to functional lineage that lack the T-cell immunoreceptor with Ig and ITIM (TIGIT) and programmed death 1 receptor (PD-1), and those committed to dysfunctional lineages that express PD-1 and TIGIT and represent exhausted-like T cells (83). Functional stem-like CD8+ T cells are negative for CD39 and CD69 (85) but highly express CD28 and TCF1 and

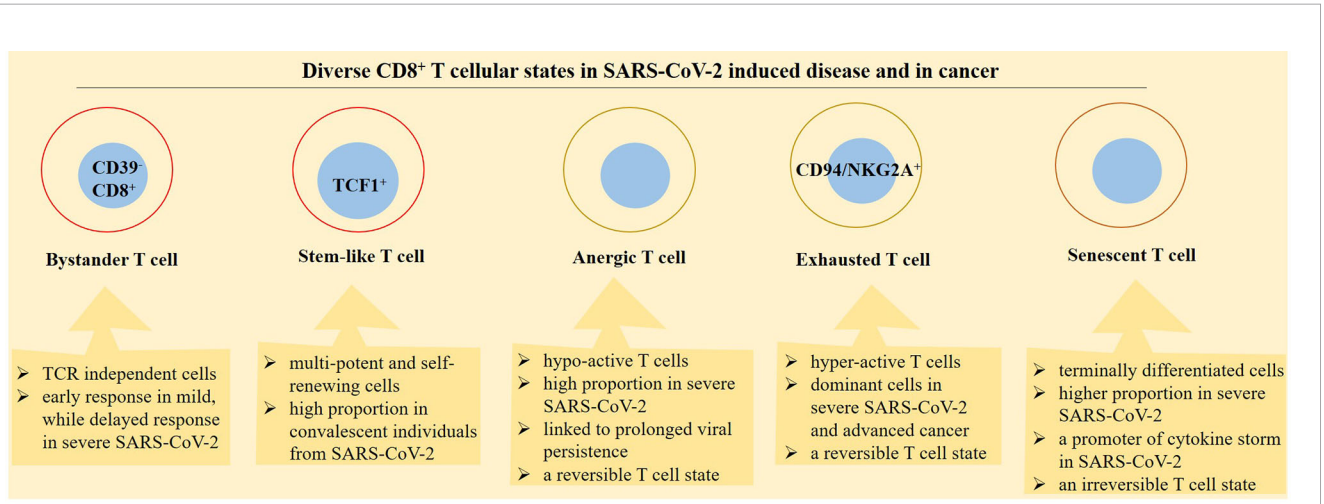


FIGURE 4 | Diverse functional profile of different CD8+ T-cell states in patients with a SARS-CoV-2-induced disease and cancer. Bystander, stem-like, anergic, exhausted, and senescence are diverse cellular states in relation with CD8+ T cells. The activity of bystander cells is independent on T-cell receptors (TCRs). Stem-like CD8+ T cells are placed in designated immune niches and act for formation of effector T cells. Anergic T cells are hypo-reactive, whereas exhausted T cells are hyperreactive but both cellular states are reversible. Senescence is a term used for terminally differentiated T cells and is considered as an irreversible T-cell state.

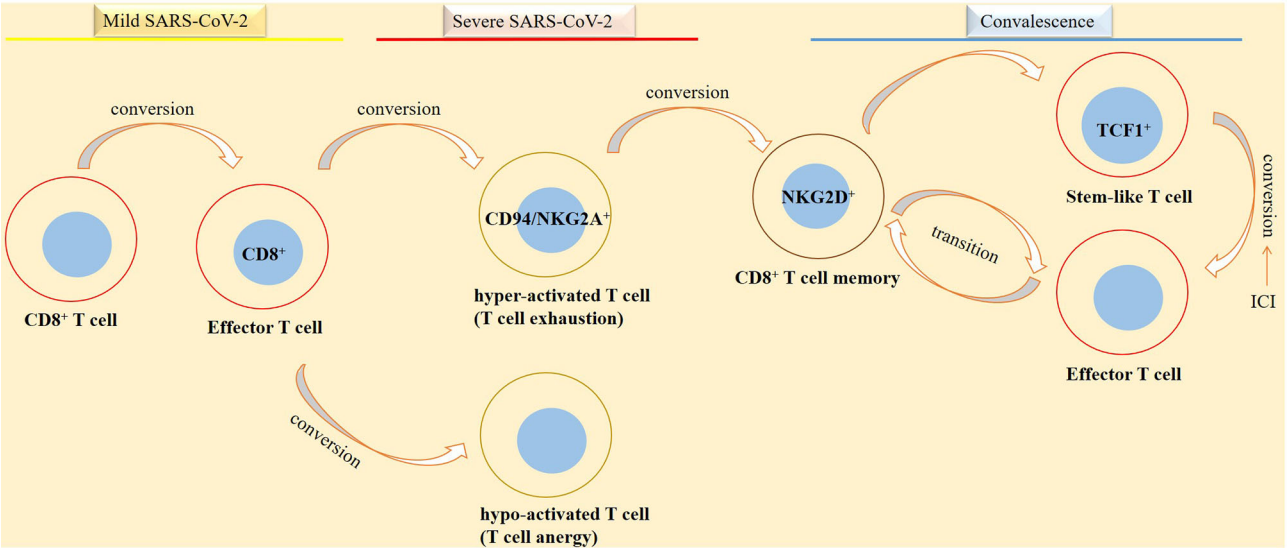


FIGURE 5 | Phases of SARS-CoV-2 induced disease in relation with $CD8^+$ T-cell activity. $CD8^+$ T cells take diverse functionality in different phases of SARS-CoV-2 induced disease. In patients with a mild disease $CD8^+$ T cells are converted into functional effector cells for taking action against the virus. By contrast, in patients with a severe disease, $CD8^+$ T cells are converted into either a hyperactive or a hypo-active phenotype, designated by the respective exhaustive and anergic cellular state with both representing T-cell dysfunctionality against the virus. In convalescent individuals from a SARS-CoV-2-induced disease, there is a different story. In such cases, stem-like and effector cells are formed in order for promoting action against viral reentry or reducing the hazard effect of the virus on tissues or organs.

are characterized as $TIM\text{-}3^-CD28^+TCF1^+$ cells (86). Such cells are dependent on TCF1 for recalling their self-renewal potential (87). $TCF1^+PD\text{-}1^+CD8^+$ T cells share features of central memory T cells but do not represent an effector signature (88). In fact, progenitor T cells with $TCF1^+PD\text{-}1^+$ signature are referred to as memory-like cells, whereas cells with a $TCF1^-PD\text{-}1^+$ expression profile are referred to as exhausted cells (87). The identity of the memory $CD8^+$ T-cell pool is important from the therapeutic standpoint. Is this send a message to use ICI therapy for reinstating functional stem-like cells in immune niches? Stem-like $TCF1^+PD\text{-}1^+CD8^+$ T cells are able to form differentiated T cells ($TCF1^-PD\text{-}1^+CD8^+$) as a response to ICI, and their contribution is vital for controlling cancer upon ICI treatment. Therefore, a proliferative response in $CD8^+$ T-cell progeny is occurring in patients receiving ICI (89).

Generally, T cells will lose their effector function and promote terminally differentiated exhausted phenotype when they are under exposure to chronic infections or are encountered to the immunosuppressive milieu of TME (88, 90, 91). $TCF1^+PD\text{-}1^+CD8^+$ T cells contribute to sustained immunity in patients with chronic viral infection (88), such as SARS-CoV-2-induced disease (84). Stem-like $CD8^+$ memory T cells exist in convalescent SARS-CoV-2 individuals, and their presence is possibly indicative of long-term protection against the virus (79). Based on findings from a study, stem-like memory T cells are successfully generated in convalescent individuals, which reached a peak at about 120 days post-symptom onset (84). This is indicative of the importance of these cells in patient recovery from SARS-CoV-2-induced diseases (**Figures 4**, **5**).

Key Note

The activity of stem-like $CD8^+$ T cells is contributed to the complete regression of tumor and long-term protection against SARS-CoV-2.

Hyper/Hypo Active and Senescent T Cells

Hyperactivation or exhaustion is a dominate immune response in severe SARS-CoV-2-induced diseases (67). Exhaustion is a term used for progressive weakness in cytokine generation and cytotoxicity. $CD8^+$ T cells are turned into an exhausted state upon chronic exposure with cancer antigens, viral infection, or in the context of autoimmune disease. The activity of these cells in chronic inflammatory conditions is inefficient, and they are not able to clear the infection (90). Thus, exhausted T cells are epigenetically distinct from memory and effector T cells through displaying defective functionality. Exhaustion is, in fact, a differentiation process that eventually causes cell death (17). $CD8^+$ T cells sustain the state of exhaustion even after resolution of viral infection. Such exhausted cells show lower clonal expansion and lower encoding for molecules related to the cytotoxicity but higher rates of genes responsive to type 1 interferon (92). Kusnadi and colleagues in a study evaluated the nature of virus-reactive $CD8^+$ T cells in single-cell transcriptomes of patients with a SARS-CoV-2-induced disease. Exhausted SARS-CoV-2-reactive cells showed higher frequency and represented lower inflammatory and cytotoxicity features in patients with a mild disease. By contrast, in patients with a severe disease SARS-CoV-2-reactive cells in the dominant non-exhausted subtype showed a feature of $CD8^+$ T-cell memory cells, represented by enrichment with transcripts related to

the antiapoptotic, pro-survival, and co-stimulation. Such cells displayed different characteristics with that for cells reactive to influenza, which is indicative of diverse functional features and transcriptome profiling for $CD8^+$ T cells upon exposure to the various types of viruses (93). $PD\text{-}1^-CTLA\text{-}4^-TIGIT^-$ $CD8^+$ T cells is a non-exhausted subset that shows reduced frequency in severe diseases. Inhibition of PD-1, CTLA-4, and TIGIT is an effective way for maintaining the antiviral activity of $CD8^+$ T cells (94).

Anergy is a state of impaired or hypo-reactivity (95) that is occurring in cells under suboptimal stimulation (96). T-cell anergy occurs in tumors (96) and is referred to both $CD4^+$ and $CD8^+$ T cells (97). Anergy is different from exhaustion and senescence. Anergy occurs during T-cell priming, whereas T-cell exhaustion occurs in cells with prior effector function but becomes silenced gradually due to the continuous presentation of antigens. Senescence is a state of growth arrest in a cell undertaking extensive proliferation due to repeated stimulation (98). Senescent T cells are terminally differentiated and represent telomerase shortening and irreversible (or stable) cell-cycle arrest (96). Thus, although both senescent and exhaustive T cells are under continuous stimulation, the latter cell type can retain its functionality under exposure to appropriate stimuli (99, 100). Exhausted T cells display elevated inhibitory checkpoints, such as PD-1 and TIM-3, which do not occur in senescent T cells. A distinct phenotype is seen in senescent cells in which the cells show downregulation of co-stimulatory molecules including CD27 and CD28 but highly express markers like CD57 (101, 102).

T cells may turn into anergic state upon exposure to an immunosuppressive TME (97). Tumor-specific T cells show dysfunction due to exposure to several inhibitory signals from the complex TME (96). TME is represented by insufficient nutrient provision for immune cells. $CD8^+$ T cells take an optimal function when they are under exposure to a normal high-glucose content, whereas the cells upon exposure to a hypoglycemic milieu will transit into energy and finally undergo apoptosis (103). DC immaturity, weak co-stimulation, and/or the activity of inhibitory signals are factors related to the insufficient or suboptimal presentation of tumor antigens on T cells (97). The immunosuppressive TME presents high number and activity of Tregs. Tregs prime DCs to induce anergy in conventional T cells. This is mediated in a CTLA-4-dependent manner in which the constitutive expression of this checkpoint on Tregs results in trans-endocytosis of B7 ligands on DCs. This is followed by degradation of such ligands, which interferes with the CD28 co-stimulatory capacity of DCs (104). Thus, immature DCs in TME are not able to provide optimal T-cell activation due to lacking ligands for engaging with CD28 (105).

T-cell anergy is also considered as a hallmark of SARS-CoV-2-induced disease and is correlated with severity of the condition (95). Results of a study showed more pronounced hyporeactive T cells in hospitalized patients with a SARS-CoV-2-induced disease, and such severe hyporeactive T cells are correlated with prolonged viral persistence. SARS-CoV-2-mediated T cell hypoactivity is independent on the activity of immunosuppressive drugs administered to such patients. Such hyporeactive cells were generated due to extrinsic T-cell factors and were due to plasma components, and they were partially recovered by IL-2 (106). Hopefully, anergic T cells can be reversed after recovery from critically ill SARS-CoV-2 induced diseases.

Exposure to IL-2 partially recovered hyporeactive T cells induced by SARS-CoV-2 (95, 106) and cancer. PD-1 promotes anergy in $CD8^+$ T cells through hampering the autocrine production of IL-2 from the cells. IL-2 re-complementation, by contrast, recovers the activity of anergic T cells irrespective of PD-1 expression on the cells (107). IL-2 inhibits anergic T cells through induction of JAK and mTOR and mediates its effects through suppressing the expression of genes related to anergy induction including Cbl-b and Ikaros (108). There are also transcription factors, such as nuclear factor of activated T cells (NFAT) and Egr2/3 related to the clonal T-cell anergy (109). NFAT is an important regulator of T-cell activation; its activity is related to the induction of a hyporesponsive cellular state (exhaustion or anergy) in both $CD4^+$ and $CD8^+$ T cells (110). Egr2 induces Ndrg1, which is kept at high levels in anergic T cells at resting state. Ndrg1 is, thus, a factor related to the clonal T cell anergy where its degradation is induced by IL-2 treatment (109).

T-cell senescence occurs in patients with chronic viral infections, autoimmune disorders, and cancer (101, 111). Malignant tumors induce T-cell senescence in order to evade from immune surveillance (101). Senescent T cells are also contributed to the pathogenesis of SARS-CoV-2-induced diseases (112). Severe infection with SARS-CoV-2 mimics a senescence immune state. The proportion of senescent $CD8^+$ T cells is higher in patients with severe (vs. mild) disease. Such senescent cells are not able to produce cytotoxic molecules. Instead, they are equipped with senescence-associated secretory phenotype (SASP). SASP is a term used for a broad spectrum of molecules secreted by senescent cells, which might be a promoter of cytokine storm in patients with severe SARS-CoV-2 induced disease (111). Immunosenescence augments susceptibility to SARS-CoV-2 and blunts the efficacy of vaccination. Senescent immune cells are higher in aged individuals, which is related to the retarded immunity to vaccination therapy among elderly populations (113). Younger cases with chronic viral infection also show senescent $CD8^+$ T cells (102) (**Figure 5**).

Key Note

T-cell exhaustion, anergy, and senescence are occurring in severe SARS-CoV-2-induced diseases and cancer.

Bystander $CD8^+$ T Cells

Bystander T cells are not pathogen specific, but they are able to impact the course of immune responses (114). The cells are $CD39^-$ $CD8^+$ (115), and their activation is independent on TCR signaling, rather than occurring in the context of autoimmune diseases, infection, and cancer. Such TCR-independent T-cell activation is seen mainly in $CD8^+$ T cells (65). The quality of T cells infiltrated into different types of human cancers have recently been described. Bystander $CD8^+$ T cells show high fractions in patients with non-melanoma cancers, such as ovarian and renal cancers (116). Bystander-activated $CD8^+$ T cells release cytokines, such as IFN-γ that support immune defenses against infection. Cytokine release from activated bystander cells occurs even when the cells are not stimulated by antigens. Thus, due to not being specific, the cytolytic

activity of these cells may cause host tissue damage (114, 117). For instance, in non-small cell lung cancer (NSCLC) patients under treatment with immunotherapy, a high fraction of bystander cells within the lungs can impair immune responses and enhance the rate of toxicities (118). Early responses from bystander $CD8^+$ T cells are seen in cases with mild or asymptomatic SARS-CoV-2-induced disease. Such cases show no signs of systemic inflammation. This is comparable with delayed bystander $CD8^+$ T-cell responses and vigorous systemic inflammation in patients with severe disease (119).

Key Note

Early response from bystander $CD8^+$ T cells is protective against SARS-CoV-2-induced diseases, while their high fractions impair immune responses in cancer patients.

ANTIVIRAL VS. ANTITUMOR $CD8^+$ T CELLS

Antiviral $CD8^+$ T cells often represent higher polyclonality, frequency, and functionality compared with antitumor $CD8^+$ T cells. Suggested reasons for such higher immunological competence in antiviral $CD8^+$ T cells are as follows: (1) antiviral $CD8^+$ T cells are generated as a response to highly immunogenic viral antigens (120), and (2) antitumor $CD8^+$ T cells represent diminished activity due to being under exposure to the immunosuppressive TME (120, 121). To explain the latter, solid cancers develop a microenvironment that includes complex signaling along with several cells. Both antitumor and pro-tumor cells existed in this ecosystem, but a tumor with a progressive stage and the number of antitumor cells far exceed that for pro-tumor cells. This occurs due to higher infiltration of pro-tumor cells or even from altered functionality of antitumor cells. The heterogeneity among cells within the TME along with complex conditions including nutrient deprivation, hypoxia, chronic inflammation, and altered redox systems all indicate constant and more pronounced impact over antitumor cells of the immune system, $CD8^+$ T cells in particular. Thus, it is fair to assert that the quality of $CD8^+$ T cells in an aggressive tumor that is developed toward metastasis is far diminished or may be taken by a terminally exhausted state, which may not be recovered after therapy.

Key Note

Immunological competence is higher in antiviral $CD8^+$ T cells compared with antitumoral $CD8^+$ T cells.

$CD8^+$ T CELLS IN CONVALESCENT INDIVIDUALS FROM SARS-COV-2-INDUCED DISEASES

Rapid and robust responses from $CD8^+$ T cells along with responses from Th1 cells efficiently curtail viral replication and viral-related antigen production (18). Specific $CD8^+$ T-cell responses are identified in post-symptomatic individuals who had a persistent SARS-CoV-2-induced disease (based on PCR data) and that the persisted disease was not contagious in such individuals (24). Based on one study, $CD8^+$ T cells are detected in 70% of convalescent cases (122), and in another work SARS-CoV-2-specific $CD8^+$ T cells are detected in 87% of convalescent patients. This is comparable with the 53% rate of SARS-CoV-2-specific $CD8^+$ T cells in the acute phase of the disease (123). T cells display active cytotoxic phenotype during the acute phase of the disease (79). The cells are IFN-γ positive in majority of samples from patients with an acute disease or in convalescent individuals (123). $CD8^+$ T cells from convalescent individuals have broad activities through targeting the whole viral proteome and both structural and non-structural epitopes (81). SARS-CoV-2-specific $CD8^+$ T cells are detectable for 5 months after convalescence from the severe/critical disease (61). However, transfusion of convalescent plasma from recovered individuals is not effective for recovering $CD8^+$ T-cell effector function in patients with a severe disease in which the fraction of active $CD8^+$ T cells is reduced at 28 days' post-transfusion (124).

Key Notes

Reduction of active $CD8^+$ T cells shortly after convalescent plasma transfusion from patients with severe SARS-CoV-2 induced disease is indicative of the weakness of this approach for proving protection on other individuals.

$CD8^+$ T-CELL RESPONSES IN DIFFERENT TYPES OF VACCINATION AGAINST SARS-COV-2

$CD8^+$ T-cell responses are elicited by several vaccines against SARS-CoV-2 (125). BBV152 (also called Covaxin) is an inactivated SARS-CoV-2 vaccine formulated by a collaborative work between Bharat Biotech and the Indian Council of Medical Research. Administration of BBV152 to healthy adults enhanced $CD8^+$ T-cell responses (126). Responses from these cells are expected to facilitate patient recovery and possibly prevent severe diseases. In regard with the Ad26.COV2.S vaccine developed by Johnson & Johnson company, $CD8^+$ T-cell responses were seen in the respective 51% and 64% of cases receiving low and high doses of vaccination and that the rate was considerably lower in older individuals. Response from $CD8^+$ T cells to the mRNA vaccine developed by Pfizer-BioNTech was 76% (127). The AZD1222 (AstraZeneca) vaccine is developed based on the S protein-encoded replication-deficient chimpanzee adenoviral vector (ChAdOx1) (128). Responses from $CD4^+$ Th1 and $CD8^+$ T cells were characterized after AZD1222 vaccination. Two doses of AZD1222 showed considerable responses from both cell types in all adult age groups (18–85 years old). In addition, both cell types showed a high rate of poly-functionality, which is representative of the strengthening of the power of the immune system to act against SARS-CoV-2 spike protein (129).

BNT162b2 is a nanoparticle-formulated RNA vaccine developed by Pfizer and encodes the full-length spike protein of SARS-CoV-2. Based on outcomes of one study, the efficacy of

BNT162b2 for preventing SARS-CoV-2 was 95% (130). BNT162b2 vaccination showed S-specific $CD8^+$ T-cell expansion in most participants. A high fraction of $CD8^+$ T cells was able to produce IFN-γ and that the cells had effector-memory phenotype. In addition to this, Th1 $CD4^+$ T cells also showed expansion in most of the participants. These are indicative of the BNT162b2-mediated combined cellular and humoral responses from the immune system for providing protection against SARS-CoV-2-induced diseases (131). In a study, T-cell responses were measured in healthcare workers previously infected with SARS-CoV-2 and received one dose of BNT162b2 vaccination and in individuals without prior infection with such virus but receiving one or two doses of the vaccine. Results showed higher T-cell responses against spike proteins in previously infected cases than infection-naïve individuals. T-cell responses in previously infected cases receiving one dose of vaccine were equivalent with those for infection-naïve individuals receiving two vaccine doses (132). This has also been approved by another study in which prior SARS-CoV-2 infection resulted in more responses from B and T cells to the vaccination with BNT162b2 and that the high antibody concentration in individuals with previous exposure to the virus and receiving one dose of vaccine was comparable with cases receiving two doses of vaccine. This is indicative of the adequate protection evolved by the one-dose vaccine for boosting immunity against the severe disease in recipients with prior exposure to SARS-CoV-2 (133). From what is discussed above, it could be asserted that T cells provide a level of immunity in cases with prior exposure to SARS-CoV-2, and their contribution is seemingly important for reducing the possibility of progressive disease in cases with second exposure to the virus. In fact, the activity of T cells will strengthen the efficacy of vaccination therapy against the virus. Outcomes of a study on gynecologic malignancies showed that cancer patients recovered from SARS-CoV-2 infection may also be protected from reinfection by such virus quite similar to that in non-cancer SARS-CoV-2 cases (134). This presumably indicates that T cells recalled for providing protection against SARS-CoV-2 are specific to that virus and being different from what acted against cancer. However, this is not indicative of insufficiency of cancer-specific $CD8^+$ T cells on SARS-CoV-2. Potentiating the fraction and activity of such cells in cancer patients can also be effective to provide protection against SARS-CoV-2, as discussed further.

Key Note

SARS-CoV-2 vaccines act for recovering $CD8^+$ T-cell responses.

$CD8^+$ T CELLS AND CHECKPOINTS IN CANCER PATIENTS WITH SARS-COV-2

Immune checkpoints are referred to as molecules that act as gatekeepers in immune responses and are considered as immune regulators. Checkpoints used for ICI therapy are TIM-3, cytotoxic T lymphocyte associated antigen-4 (CTLA-4), and PD-L1 (99, 100). In addition, TIGIT is a novel checkpoint receptor identified on the surface of $CD8^+$ T cells, and its expression is related to the T-cell exhaustion and immune escape in patients with bladder cancer (135).

Generally, the expression of TIM-3 and PD-1 on T cells is indicative of their impaired functionality (136). TIM-3 is overexpressed on $CD8^+$ T cells in patients with SARS-CoV-2-induced disease (67), and its level is higher in cases with severe (vs. mild) disease, while it will become normalized in convalescent individuals (137). A higher number of functional (not exhausted) $PD\text{-}1^+$ $CD8^+$ T cells are also reported in patients with SARS-CoV-2 (138). IFN-γ-producing $PD\text{-}1^+$ $CD8^+$ T cells are active during the acute phase of viral infection (139). A point here is that PD-1 expression on the surface of $CD8^+$ T cells is "transient" during the acute phase of viral infection in which upon viral clearance this receptor shows a downregulated expression profile (90). This is comparable with the "sustained" PD-1 expression on $CD8^+$ T cells in patients with chronic infection or in cancer cases, rendering T-cell exhaustion or dysfunction (90, 140). PD(L)-1 is considered as a biomarker of poor prognosis only when PD-1 is overexpressed on antitumor immune cells, and simultaneously PD-L1 is highly expressed in the TME. This is important from a therapeutic standpoint in which a high expression of PD-1 on antitumor immune cells in a $PD\text{-}L1^{low}$ tumor area is considered as a suppressor of tumor, whereas the cells placed in the $PD\text{-}L1^{high}$ environment will lose their antitumor activity or may even take tumor-promoting function (99).

ICI seems to act at the cross-road between SARS-CoV-2-induced disease and cancer (141). ICI can be used for modifying the immune system in cancer patients with active SARS-CoV-2 (3). Cancer patients treated with PD(L)-1 blockade during the pre-infectious phase of SARS-CoV-2 are more resistant to the attack from the virus (142), and during the early phase of SARS-CoV-2 infection such therapy can contribute to the viral clearance (141). PD(L)-1 inhibitor therapy can thus provide a timeline therapeutic schedule for cancer patients (143), and restoring (or reactivation) of T-cell functionality mediated by such therapy can possibly be a winning step for beating SARS-CoV-2 infection (144). A recent study investigated the effects of chemo- or immunotherapy on the immune state in patients with gynecological malignancies who also had SARS-CoV-2 infection. Outcomes showed that in patients receiving chemotherapy no considerable changes occurred in the fraction and activity of B and T cells, but they mainly had neutropenia. By contrast, patients receiving PD-1 inhibitor therapy showed a massive rise in the cytotoxic scores for NK and T cells and that this therapy facilitated T-cell expansion in such cases (134). This is indicative of higher efficacy of immunotherapy over chemotherapy in cancer patients with active SARS-CoV-2.

A possible challenge for the use of ICI in cancer patients who also have active SARS-CoV-2 is a possible risk of experiencing cytokine release syndrome, which is a key contributor to the SARS-CoV-2-related mortality (3) and mediated *via* the impact of ICI in boosting T-cell migration toward the site(s) of infections (141). However, outcomes of a recent report attested

augmented T-cell immunity in melanoma patients with SARS-CoV-2-induced disease treated with ICI and that such cases did not show exacerbation of inflammation (145). Pneumonitis occurring in patients with active SARS-CoV-2 is also presented in cases receiving ICI, which is seemingly indicative of a synergy in the manifestation of symptoms in such patients. However, pneumonitis is seen in 0.3% to 2% of patients receiving ICI, so it is not considered as a high-risk indicator for SARS-CoV-2 cases (3). Outcomes of a study by Luo and colleagues showed a safety profile for PD-1 inhibitor therapy in lung cancer patients who are also affected by SARS-CoV-2 (7). Results of a recent preliminary study also showed no rise in the rate of SARS-CoV-2-related mortality in melanoma patients receiving ICI therapy compared to the targeted therapy or treatment-naïve patients (146). These outcomes are indicative of the safety of PD(L)-1 inhibitor therapy in cancer patients with active SARS-CoV-2. A limited number of works in this area will ask for more future studies and gathering of more information in regard with the precise impact of ICI therapy in patients with SARS-CoV-2-induced disease.

Key Note

PD(L)-1 blockade is presumably safe in cancer patients with SARS-CoV-2, and its application is beneficial for reducing the risk of attack from the virus.

FACTORS INFLUENCING CD8+ T-CELL ACTIVITY IN SARS-COV-2-INDUCED DISEASE AND CANCER

The Impact of Aging and Obesity

Most cancers are evolved in patients with ages over 60, the age range estimated to dominate more than 20% of the world's society by year 2050, which is alarming as an economic burden related to healthcare provision (147). Outcomes of a recent systematic review showed more pronounced survival benefits related to the PD(L)-1 blockade among cancer patients aged <75 compared with cases ≥75 (148). The efficacy of the SARS-CoV-2 vaccination is also noticeably diminished with age, which is due presumably to a decline in responses from innate and adaptive immunity as a result of aging (149). $CD8^+$ T cells are less frequent in aged HNSCC patients, and a high expression of PD-1 on peripheral T cells is reported in such population (150). Studies showed that $CD8^+$ T cells are less frequent in SARS-CoV-2 patients aged >45 compared with cases with ages <45 (24), and that the cells are not detectable in patients over 80 (28). Besides, the basal pro-inflammatory state is higher in older individuals. These along with the diminished capability for mounting appropriate immune responses are reasons for the higher severity of condition in aged SARS-CoV-2 patients (151). Aging also causes higher accumulation of senescent immune cells (152), which is a reason for higher baseline inflammation in such populations (113) and their more vulnerability to SARS-CoV-2-induced diseases (152).

Obesity is an established risk factor of cancer development, which represents a global rise and poses a high cost over public health (153). Obesity is among preexisting conditions that cause patients to be prone to a more severe SARS-CoV-2 disease (154). A possibility of experiencing a severe disease is twice in obese individuals compared with normal-weight SARS-CoV-2 patients (155). Obesity alters the balance between innate and adaptive immunity. It links with a state of low-grade chronic inflammation (154). Chronic inflammation related to obesity alters immune functionality. The number of dysfunctional $CD8^+$ T cells is increased with obesity (156). T-cell exhaustion is induced by cellular interactions occurring within adipose tissue (157). Generally, diets interfering with metabolic pathways are linked positively to the increased risk of carcinogenesis (158). $CD8^+$ T cells show alterations in metabolic fitness in obese individuals. Such altered metabolic activity influences differentiation and effector activity of $CD8^+$ T cells and their transition into memory cells (159). Impaired activity of $CD8^+$ T cells also occurs in obese patients with SARS-CoV-2-induced disease, which is indicative of a more severe condition in such cases (156). A mechanism by which obesity contributes to the increased risk of tumorigenesis is by promoting constant upregulation of PD-1 on $CD8^+$ T cells and their further dysfunction (160). Transition from $PD\text{-}1^-$non-exhausted $CD8^+$ T cells into $PD\text{-}1^+$-exhausted $CD8^+$ T cells is reported in breast cancer mice receiving high-fat diet (161). Taken together, it could be asserted that aging and obesity are key risk factors of cancer development, and aged or obese patients experience more severe disease upon exposure to SARS-CoV-2 due partly to the attenuated $CD8^+$ T-cell activity (**Figure 6**).

Key Note

$CD8^+$ T cells are less frequent with aging, and their activity is diminished in obese individuals.

Chronic Inflammation and Hypoxia

Chronic inflammation is a major risk factor of cancer. Conditions like chronic inflammation and autoimmunity account for about 15%–20% of all types of cancers. An organ with long-lasting inflammation is more prone to tumor development (162). Examples are numerous in this context, such as chronic obstructive pulmonary disease (COPD) (163), inflammatory bowel disease (IBD) (164), cirrhosis (165, 166), and chronic pancreatitis (167), which are the basis for the development of lung cancer, colorectal cancer, hepatocellular carcinoma (HCC), and pancreatic cancer. In regard to HCC, inflammatory-related events can cause chronic liver fibrosis and further chronic damages in this organ (168). A possible reason for an increase in the risk of tumorigenesis is the interrelation between chronic inflammation and chronic oxidative stress (17, 169) and the resulting impaired immune functionality and further tissue dysfunction (170). This is indicative of the virtue of using antioxidants, such as melatonin for modifying inflammatory and oxidative events in favor of immune activation against chronic injuries and cancer (171).

Chronic inflammation causes abnormal cytokine production (172), and patients with chronic inflammatory-related diseases are more prone to the SARS-CoV-2 infection. Diabetes, for instance, is a chronic inflammatory disease that affects cellular

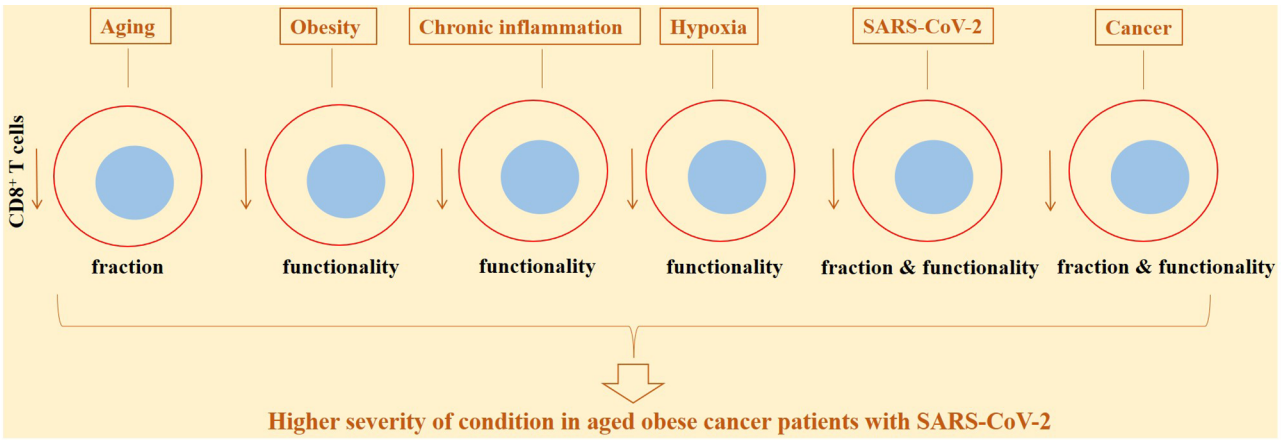


FIGURE 6 | $CD8^+$ T-cell diverse functionality and fraction in response to different conditions, in cancer patients and in cases with active SARS-CoV-2. The activity and fraction of $CD8^+$ T cells are influenced from several conditions. Aging, obesity, chronic inflammation, and hypoxia are among the most important contributors in this context, rendering lower responses to anticancer therapies or reducing the efficacy of vaccination against SARS-CoV-2.

proliferation, differentiation, and function of innate and adaptive immunity (173). $CD8^+$ T cells undergo exhaustion in the chronic inflammatory setting. $CD8^+$ T cells served to trigger potent responses against viral infections for resolving infection. However, chronic infection is established when viruses are able to overcome this control. In fact, $CD8^+$ T-cell exhaustion occurring in such conditions is a result of their constant responses to the long-lasting viral replication and the resulting continuous antigen stimulation (174). Chronic antigen stimulation drives $CD8^+$ T-cell exhaustion, which further reduces their secretory cytokines. Finally, the cells undergo progressive loss of functionality (175) and apoptosis (174).

Hypoxia is another factor that is linked with tumorigenesis, tumor progression, and SARS-CoV-2 pathogenesis. Hypoxic areas are common in patients with solid tumors, which is due partly to the abnormal tumor vessels (176, 177). Hypoxia is induced by SARS-CoV-2 (178). It occurs as a response to severe respiratory dysfunction, which causes a discrepancy between uptake and consumption of O_2 (179). HIFs are by-products of hypoxia that are stimulated within inflammatory tissues. There is a positive link between acute systemic hypoxia with mortality from severe SARS-CoV-2-induced diseases. SARS-CoV-2 promotes cytokine storm, particularly in the lung environment. HIF-1α functions as an inflammatory stimulant, mediated through provoking the transition of preexisting cytokine storm into a fulminant condition (178). Low O_2 reduces antiviral responses from $CD8^+$ T cells (180). Hypoxia reduces T-cell effector function through increasing the expression of co-inhibitors on $CD8^+$ T cells (176). Hypoxic tumors generally show a lower fraction of $CD8^+$ T cells. $CD8^+$ T cells either avoid hypoxic regions or show reduced ability to expand in such areas (181, 182). Hypoxic tensions mainly influence antigen-experienced $CD8^+$ T cells, namely, memory and effector cells (not naïve $CD8^+$ T cells) (182). Exposure of exhaustive $CD8^+$ T cells to hypoxic conditions will promote a terminal exhaustive state in such cells that are unable to recover their effector function after ICI therapy (183). Hypoxia induces the generation of reactive oxygen species (ROS) in T cells of patients with progressive (severe/critical) SARS-CoV-2-induced diseases, as compared with cases that recovered from critical diseases. High ROS accumulation and defective T-cell mitochondria are associated with severe SARS-CoV-2 diseases (184) (**Figure 6**).

Key Note

Areas of chronic inflammation and hypoxia favor more dysfunctional $CD8^+$ T cells in patients with SARS-CoV-2 induced diseases and cancer.

Aberrant Angiogenesis and Abnormal Vasculature

SARS-CoV-2 in relation to hypoxia promotes vascular abnormality (a leaky architecture) (185). A leaky vasculature is also a common feature of cold cancers. The vascular endothelial growth factor (VEGF, also called VEGF-A) is a cytokine that vitally contributes to angiogenesis (186). The rate of VEGF expression is considerably higher in patients with SARS-CoV-2-induced disease compared with healthy individuals (187). High activity of VEGF promotes vascular permeability (186). Administration of the VEGF inhibitor bevacizumab in patients with severe SARS-CoV-2-induced disease significantly improved the PaO_2/FiO_2 ratio and O_2 status (188). SARS-CoV-2 uses angiotensin-converting enzyme 2 (ACE2) as a receptor to attach the cellular membrane and enter the intracellular milieu. ACE2 is suppressed by SARS-CoV-2 upon cellular entry, and the activity of VEGF is inhibited by ACE2. The outcome of these inter-inhibitory effects is the high VEGF activity and acute lung injury (187).

Abnormal vasculature leads tumors toward metastasis. Metastasis is a main cause of cancer-related death, which

accounts for over 90% of deaths from cancer (189). Abnormal tumor vasculature hampers effective infiltration of $CD8^+$ T cells into the tumor area. Normalization of tumor vessels by strategies, such as M1 polarization (121), causes more infiltration of $CD8^+$ T cells, thereby hampering immune escape and tumor metastasis (190). FASL expressed in tumor endothelial cells (ECs) is a barrier for $CD8^+$ T-cell infiltration into the tumor area (186).

The expression of VEGF is upregulated in hypoxic conditions, and its upregulation reduces immune effector function. VEGF impedes DC maturation, thus causing $CD8^+$ T-cell inactivation. VEGF induces PD-1 expression on $CD8^+$ T cells and PD-L1 upregulation in the microenvironment of tumors like glioblastoma, thereby causing $CD8^+$ T-cell exhaustion (191). VEGF-D is another cytokine in the VEGF family. VEGF-D contributes to the formation of lymphatic vessels (186). Upregulation of VEFG-D contributes to severe SARS-CoV-2-induced diseases (192). High VEGF-D expression is negatively related to the survival of patients with metastatic CRC (193). There is no direct evidence for the possible relation between VEGF-D with $CD8^+$ T-cell activity in SARS-CoV-2 cancer patients, which requires focus in future studies.

Key Note

High VEGF activity is presumably related to the $CD8^+$ T-cell dysfunction in patients with a SARS-CoV-2-induced disease and cancer.

Boosting $CD8^+$ T-Cell Activity Against SARS-CoV-2-Induced Disease and Cancer

$CD8^+$ T cells are without a doubt one of the most important cells of the immune system to act against SARS-CoV-2-induced disease and cancer, so their fraction and function are affected by a number of strategies for suppressing tumor development or vaccines against SARS-CoV-2. Evaluation of the fraction and functionality of these critical cells within circulation can, thus, be of prognostic, diagnostic, and therapeutic importance. The aim of new immunotherapeutic strategies is to target co-inhibitory receptors on T cells or improve their tumor recognition abilities and responses against tumor-specific antigens. In fact, responses to immunotherapy are evolved when T cells are directed more toward tumor neoantigens. Peptide-based vaccines are examples in this context. Short peptides directly bind to the HLA-I molecules and act as mounting MHC-I-restricted antigen-specific responses from $CD8^+$ T cells. Long synthetic peptides must be presented by APCs to represent a T-cell response. Long peptide vaccination usually causes higher immunity compared with short peptides and induces responses from both $CD4^+$ T-helper and $CD8^+$ cytotoxic T cells when they are conjugated with effective adjuvant (194). T-cell expansion and strengthening of their antitumor reactivity are achieved after systemic administration of tumor-associated antigens (TAAs). Such approach is effective in patients receiving adoptive T-cell transfer (ACT) (195). The efficacy of antitumor T cells in patients receiving T-cell therapy can also be improved through improving T-cell stemness (196). $CD8^+$ T cells in the TME are under exposure to hypoxic conditions, which poses a strong negative impact on their effector function. Thus, a suggested strategy is to modify HIF expression, HIF-2α in particular, in such cells in order to strengthen the adaptation of transferred T cells to the hypoxic conditions of such milieu (197). Outcomes of a recent study showed a positive link between breast cancer exposure to carcinogens with increased infiltration and strengthened antitumor activity of $CD8^+$ T cells. Mice upon exposure to the 12-dimethylbenz[a]anthracene (DMBA) carcinogen showed cancer cell upregulation of chemokine (C–C motif) ligand 21 (CCL21) and strengthened antigen presentation activity. CCL21 activity was associated with higher tumor mutational burden (TMB) as well as strengthened T-cell immunity. $CD8^+$ T cells were diminished after deletion of the CCL21 receptor, an outcome of which was severe liver and lung metastasis. The results of this study are indicative of the link between carcinogen exposure with stimulation of immune activating factors in cancer cells for potentiating the activity of $CD8^+$ T cells against tumor metastasis (198). Cytokine-based therapy using agonists of the TNF receptor family has shown promising antitumor effects, mediated through strengthening the activity of $CD8^+$ T cells. An example in this context is the CD137 agonist which shows antitumor activity against gastric cancer (199). Long-lasting responses from T cells can also be elicited using vaccine-based vectors. Cytomegalovirus, for instance, can be used as a vaccine vector for tumor-specific responses from $CD8^+$ T cells (200). Strategies can also be expanded through strengthening the intra-tumoral infiltration of $CD8^+$ T cells, as is known that cancer cells have developed several mechanisms to diminish homing of T cells and their access to the tumor tissue (201). Reshaping metabolic systems in $CD8^+$ T cells is important for boosting their function in the TME that is generally under consistent nutrient and O_2 deprivation. Strengthening fatty acid catabolism is a strategy to improve the antitumor capacity of $CD8^+$ TILs. Such metabolically modified T cells presumably show higher antitumor potentials in patients receiving ICI therapy, such as PD-1 inhibitor drugs (202).

Strengthening $CD8^+$ T-cell activity is not only effective for cancer but also promising against SARS-CoV-2-induced diseases. SARS-CoV-2 infection triggers cellular immune responses through CD8 overexpression and CTL hyperactivation (203). $CD8^+$ T-cell responses are reported to be stimulated using SARS-CoV-2 vaccine boosters (204), and SARS-CoV-2 mRNA vaccines cause fast and stable mobilization of such cells (205). SARS-CoV-2-specific cellular and humoral responses to the inactivated virus vaccine CoronaVac immunization have also been attested (206).

CONCLUSIONS

From what is discussed above, it can be concluded that the infiltration and activity of $CD8^+$ T cells can be used as a biomarker of response in cancer patients with SARS-CoV-2-induced diseases, and their dysfunctionality is a dominant reason for a more severe condition. Persistent infection and sustained

stimulation are factors associated with the exhaustive state in $CD8^+$ T cells (10). In addition, unpredictable responses to immunotherapy are predictable in cancer patients due to the heterogeneity in TIL composition and phenotype (115). This along with the diminished responses from T cells to SARS-CoV-2 in cancer patients is linked with the severe infection and the dismal outcomes in SARS-CoV-2-infected cases with cancer (5). The severity of the condition is also affected from the type of cancer. In patients with lung cancer, for instance, more severe SARS-CoV-2 diseases are expected in comparison with gastrointestinal and breast cancers (207). Recovering the activity of such important cells is the key in the area of cancer therapy and in relation with the development of vaccines against SARS-CoV-2 and better outcomes of vaccination. In fact, the importance of the link between T-cell responses with milder disease will highlight the potential of considering non-spike proteins in SARS-CoV-2-based vaccination therapy (208). The acceleration or amplification of antiviral T cell immunity using ICIs can be a strategy for improving the efficacy of vaccination and establishing long-lasting immunity in cancer patients with active SARS-CoV-2 infection, as what was reported for melanoma patients (145).

AUTHOR CONTRIBUTIONS

Collection and revision of information, KM. Conceptualization, KM. Writing, original draft preparation, review, and editing, JM and KM. Both authors contributed to the article and approved the submitted version.

ACKNOWLEDGMENTS

This work was supported by the ethical agreement from Kurdistan University of Medical Sciences (ethical code: IR.MUK.REC.1400.154).

REFERENCES

1. Santa Cruz A, Mendes-Frias A, Oliveira AI, Dias L, Rita Matos A, Carvalho A. IL-6 is a Biomarker for the Development of Fatal SARS-CoV-2 Pneumonia. *Front Immunol* (2021) 12:263. doi: 10.3389/fimmu.2021.613422
2. Zizzo G, Cohen PL. Imperfect Storm: Is Interleukin-33 the Achilles Heel of COVID-19? *Lancet Rheumatol* (2020) 2:e779–90. doi: 10.1016/S2665-9913(20)30340-4
3. Pezeshki PS, Rezaei N. Immune Checkpoint Inhibition in COVID-19: Risks and Benefits. *Expert Opin Biol Ther* (2021) p:1–7. doi: 10.1080/14712598.2021.1887131
4. Antonioli L, Fornai M, Pellegrini C, Blandizzi C. NKG2A and COVID-19: Another Brick in the Wall. *Cell Mol Immunol* (2020) 17(6):672–4. doi: 10.1038/s41423-020-0450-7
5. Bilich T, Roerden M, Maringer Y, Nelde A, Heitmann JS, Dubbelaar ML, et al. Preexisting and Post–COVID-19 Immune Responses to SARS-CoV-2 in Patients With Cancer. *Cancer Discov* (2021) 11(8):1982–95. doi: 10.1158/2159-8290.CD-21-0191
6. Bange EM, Han NA, Wileyto P, Kim JY, Gouma S, Robinson J, et al. CD8+ T Cells Contribute to Survival in Patients With COVID-19 and Hematologic Cancer. *Nat Med* (2021) p:1–10. doi: 10.1038/s41591-021-01386-7
7. Luo J, Rizvi H, Egger JV, Preeshagul IR, Wolchok JD, Hellmann MD. Impact of PD-1 Blockade on Severity of COVID-19 in Patients With Lung Cancers. *Cancer Discov* (2020) 10(8):1121–8. doi: 10.1158/2159-8290.CD-20-0596
8. Stephens DS, McElrath MJ. COVID-19 and the Path to Immunity. *Jama* (2020) 324(13):1279–81. doi: 10.1001/jama.2020.16656
9. Zheng M, Gao Y, Wang G, Song G, Liu S, Sun D, et al. Functional Exhaustion of Antiviral Lymphocytes in COVID-19 Patients. *Cell Mol Immunol* (2020) 17(5):533–5. doi: 10.1038/s41423-020-0402-2
10. Baral S, Antia R, Dixit NM. A Dynamical Motif Comprising the Interactions Between Antigens and CD8 T Cells may Underlie the Outcomes of Viral Infections. *Proc Natl Acad Sci* (2019) 116(35):17393–8. doi: 10.1073/pnas.1902178116
11. Lineburg KE, Grant EJ, Swaminathan S, Chatzileontiadou DSM, Szeto C, Sloane H, et al. CD8+ T Cells Specific for an Immunodominant SARS-CoV-2 Nucleocapsid Epitope Cross-React With Selective Seasonal Coronaviruses. *Immunity* (2021) 54(5):1055–1065. e5. doi: 10.1016/j.immuni.2021.04.006
12. Majidpoor J, Mortezaee K. Interleukin-2 Therapy of Cancer-Clinical Perspectives. *Int Immunopharmacol* (2021) 98:107836. doi: 10.1016/j.intimp.2021.107836
13. Raskov H, Orhan A, Christensen JP, Gögenur I. Cytotoxic CD8+ T Cells in Cancer and Cancer Immunotherapy. *Br J Cancer* (2021) 124(2):359–67. doi: 10.1038/s41416-020-01048-4
14. Mortezaee K. Enriched Cancer Stem Cells, Dense Stroma, and Cold Immunity: Interrelated Events in Pancreatic Cancer. *J Biochem Mol Toxicol* (2021) 35(4):e22708. doi: 10.1002/jbt.22708
15. Mortezaee K, Najafi M. Immune System in Cancer Radiotherapy: Resistance Mechanisms and Therapy Perspectives. *Crit Rev Oncol/Hematol* (2020) p:103180. doi: 10.1016/j.critrevonc.2020.103180
16. Dolina JS, Van Braeckel-Budimir N, Thomas GD, Salek-Ardakani S. CD8+ T Cell Exhaustion in Cancer. *Front Immunol* (2021) p:2880. doi: 10.3389/fimmu.2021.715234
17. Mortezaee K. Redox Tolerance and Metabolic Reprogramming in Solid Tumors. *Cell Biol Int* (2021) 45(2):273–86. doi: 10.1002/cbin.11506
18. Gao L, Zhou J, Yang S, Wang L, Chen X, Yang Y, et al. The Dichotomous and Incomplete Adaptive Immunity in COVID-19 Patients With Different Disease Severity. *Signal Transduct Target Ther* (2021) 6(1):1–10. doi: 10.1038/s41392-021-00525-3
19. Lafon E, Diem G, Witting C, Zaderer V, Bellmann-Weiler RM, Reindl M, et al. Potent SARS-CoV-2-Specific T Cell Immunity and Low Anaphylatoxin Levels Correlate With Mild Disease Progression in COVID-19 Patients. *Front Immunol* (2021) p:2171. doi: 10.3389/fimmu.2021.684014
20. Odak I, Barros-Martins J, Bošnjak B, Stahl K, David S, Wiesner O, et al. Reappearance of Effector T Cells is Associated With Recovery From COVID-19. *EBioMedicine* (2020) 57:102885. doi: 10.1016/j.ebiom.2020.102885
21. Ferreras C, Pascual-Miguel B, Mestre-Durán C, Navarro-Zapata A, Clares-Villa L, Martín-Cortázar C, et al. SARS-CoV-2-Specific Memory T Lymphocytes From COVID-19 Convalescent Donors: Identification, Biobanking, and Large-Scale Production for Adoptive Cell Therapy. *Front Cell Dev Biol* (2021) 9:293. doi: 10.3389/fcell.2021.620730
22. Majidpoor J, Mortezaee K. Interleukin-6 in SARS-CoV-2 Induced Disease: Interactions and Therapeutic Applications. *Biomed Pharmacother* (2021) p:112419. doi: 10.1016/j.biopha.2021.112419
23. Wang Y, Lu X, Li Y, Chen H, Chen T, Su N, et al. Clinical Course and Outcomes of 344 Intensive Care Patients With COVID-19. *Am J Respir Crit Care Med* (2020) 201(11):1430–4. doi: 10.1164/rccm.202003-0736LE
24. Gao M, Liu Y, Guo M, Wang Q, Wang Y, Fan J, et al. Regulatory CD4+ and CD8+ T Cells are Negatively Correlated With CD4+/CD8+ T Cell Ratios in Patients Acutely Infected With SARS-CoV-2. *J Leukocyte Biol* (2021) 109(1):91–7. doi: 10.1002/JLB.5COVA0720-421RR
25. Li M, Guo W, Dong Y, Wang X, Dai D, Liu X, et al. Elevated Exhaustion Levels of NK and CD8+ T Cells as Indicators for Progression and Prognosis of COVID-19 Disease. *Front Immunol* (2020) p:2681. doi: 10.3389/fimmu.2020.580237
26. De Biasi S, Meschiari M, Gibellini L, Bellinazzi C, Borella R, Fidanza L, et al. Marked T Cell Activation, Senescence, Exhaustion and Skewing Towards

TH17 in Patients With COVID-19 Pneumonia. *Nat Commun* (2020) 11 (1):1–17. doi: 10.1038/s41467-020-17292-4
27. Diao B, Wang C, Tan Y, Chen X, Liu Y, Ning L, et al. Reduction and Functional Exhaustion of T Cells in Patients With Coronavirus Disease 2019 (COVID-19). *Front Immunol* (2020) p:827. doi: 10.3389/fimmu.2020.00827
28. Wang Y, Zheng J, Sahidul Islam Md, Yang Y, Hu Y, Chen X. The Role of CD4+ FoxP3+ Regulatory T Cells in the Immunopathogenesis of COVID-19: Implications for Treatment. *Int J Biol Sci* (2021) 17(6):1507. doi: 10.7150/ijbs.59534
29. Anft M, Paniskaki K, Blazquez-Navarro A, Doevelaar A, Seibert FS, Hölzer B, et al. COVID-19-Induced ARDS Is Associated With Decreased Frequency of Activated Memory/Effector T Cells Expressing CD11a++. *Mol Ther* (2020) 28(12):2691–702. doi: 10.1016/j.ymthe.2020.10.001
30. Maucourant C, Filipovic I, Ponzetta A, Aleman S, Cornillet M, Hertwig L, et al. Natural Killer Cell Immunotypes Related to COVID-19 Disease Severity. *Sci Immunol* (2020) 5(50):eabd6832. doi: 10.1126/sciimmunol.abd6832
31. Liao M, Liu Y, Yuan J, Wen Y, Xu G, Zhao Z, et al. Single-Cell Landscape of Bronchoalveolar Immune Cells in Patients With COVID-19. *Nat Med* (2020) 26(6):842–4. doi: 10.1038/s41591-020-0901-9
32. QinC Z. Dysregulation of Immune Response in Patients With COVID-19 in Wuhan, China. *Clin Infect Dis* (2020) 71:762–8. doi: 10.2139/ssrn.3541136
33. Li X, Liu C, Mao Z, Xiao M, Wang L, Qi S, et al. Predictive Values of Neutrophil-to-Lymphocyte Ratio on Disease Severity and Mortality in COVID-19 Patients: A Systematic Review and Meta-Analysis. *Crit Care* (2020) 24(1):1–10. doi: 10.1186/s13054-020-03374-8
34. Jimeno S, Ventura PS, Castellano JM, García-Adasme SI, Miranda M, Touza P, et al. Prognostic Implications of Neutrophil-Lymphocyte Ratio in COVID-19. *Eur J Clin Invest* (2021) 51(1):e13404. doi: 10.1111/eci.13404
35. Dennison D, Al Khabori M, Al Mamari S, Aurelio A, Al Hinai H, Al Maamari K, et al. Circulating Activated Neutrophils in COVID-19: An Independent Predictor for Mechanical Ventilation and Death. *Int J Infect Dis* (2021) 106:155–9. doi: 10.1016/j.ijid.2021.03.066
36. Reusch N, De Domenico E, Bonaguro L, Schulte-Schrepping J, Baßler K, Schultze JL, et al. Neutrophils in COVID-19. *Front Immunol* (2021) 12:952. doi: 10.3389/fimmu.2021.652470
37. Hazeldine J, Lord JM. Neutrophils and COVID-19: Active Participants and Rational Therapeutic Targets. *Front Immunol* (2021) 12:2097. doi: 10.3389/fimmu.2021.680134
38. Ackermann M, Anders H-J, Bilyy R, Bowlin GR, Daniel C, De Lorenzo R, et al. Patients With COVID-19: In the Dark-NETs of Neutrophils. *Cell Death Different* (2021) 28(11):3125–39. doi: 10.1038/s41418-021-00805-z
39. So YK, Byeon S-J, Ku BM, Ko YH, Ahn MJ, Son YI, et al. An Increase of CD8 + T Cell Infiltration Following Recurrence is a Good Prognosticator in HNSCC. *Sci Rep* (2020) 10(1):1–9. doi: 10.1038/s41598-020-77036-8
40. Wang D, Yu W, Lian J, Wu Q, Liu S, Yang L, et al. Th17 Cells Inhibit CD8+ T Cell Migration by Systematically Downregulating CXCR3 Expression via IL-17a/STAT3 in Advanced-Stage Colorectal Cancer Patients. *J Hematol Oncol* (2020) 13:1–15. doi: 10.1186/s13045-020-00897-z
41. Hou Y-C, Chao Y-J, Hsieh M-H, Tung H-L, Wang H-C, Shan Y-S. Low CD8 + T Cell Infiltration and High PD-L1 Expression are Associated With Level of CD44+/CD133+ Cancer Stem Cells and Predict an Unfavorable Prognosis in Pancreatic Cancer. *Cancers* (2019) 11(4):541. doi: 10.3390/cancers11040541
42. Jin YW, Hu P. Tumor-Infiltrating CD8 T Cells Predict Clinical Breast Cancer Outcomes in Young Women. *Cancers* (2020) 12(5):1076. doi: 10.3390/cancers12051076
43. Ali H, Provenzano E, Dawson SJ, Blows FM, Liu B, Shah M, et al. Association Between CD8+ T-Cell Infiltration and Breast Cancer Survival in 12 439 Patients. *Ann Oncol* (2014) 25(8):1536–43. doi: 10.1093/annonc/mdu191
44. Echarti A, Hecht M, Büttner-Herold M, Haderlein M, Hartmann A, Fietkau R, et al. CD8+ and Regulatory T Cells Differentiate Tumor Immune Phenotypes and Predict Survival in Locally Advanced Head and Neck Cancer. *Cancers* (2019) 11(9):1398. doi: 10.3390/cancers11091398
45. Najafi M, Mortezaee K, Majidpoor J. Stromal Reprogramming: A Target for Tumor Therapy. *Life Sci* (2019) 239:117049. doi: 10.1016/j.lfs.2019.117049
46. Farhood B, Najafi M, Mortezaee K. Cancer-Associated Fibroblasts: Secretions, Interactions, and Therapy. *J Cell Biochem* (2019) 120(3):2791–800. doi: 10.1002/jcb.27703
47. Mortezaee K. Hypoxia Induces Core-to-Edge Transition of Progressive Tumoral Cells: A Critical Review on Differential Yet Corroborative Roles for HIF-1α and HIF-2α. *Life Sci* (2020) 242:117145. doi: 10.1016/j.lfs.2019.117145
48. Farhood B, Najafi M, Salehi E, Goradel NH, Nashtaei MS, Khanlarkhani N, et al. Disruption of the Redox Balance With Either Oxidative or Anti-Oxidative Overloading as a Promising Target for Cancer Therapy. *J Cell Biochem* (2019) 120(1):71–6. doi: 10.1002/jcb.27594
49. Mortezaee K. Myeloid-Derived Suppressor Cells in Cancer Immunotherapy-Clinical Perspectives. *Life Sci* (2021) p:119627. doi: 10.1016/j.lfs.2021.119627
50. Uzhachenko RV, Shanker A. CD8+ T Lymphocyte and NK Cell Network: Circuitry in the Cytotoxic Domain of Immunity. *Front Immunol* (2019) 10:1906. doi: 10.3389/fimmu.2019.01906
51. Menares E, Gálvez-Cancino F, Cáceres-Morgado P, Ghorani E, López E, Díaz X, et al. Tissue-Resident Memory CD8+ T Cells Amplify Anti-Tumor Immunity by Triggering Antigen Spreading Through Dendritic Cells. *Nat Commun* (2019) 10(1):1–12. doi: 10.1038/s41467-019-12319-x
52. Han S, Toker A, Liu ZQ, Ohashi PS. Turning the Tide Against Regulatory T Cells. *Front Oncol* (2019) 9:279. doi: 10.3389/fonc.2019.00279
53. Li C, Jiang P, Wei S, Xu X, Wang J. Regulatory T Cells in Tumor Microenvironment: New Mechanisms, Potential Therapeutic Strategies and Future Prospects. *Mol Cancer* (2020) 19(1):1–23. doi: 10.1186/s12943-020-01234-1
54. Galván-Peña S, Leon J, Chowdhary K, Michelson DA, Vijaykumar B, Yang L, et al. Profound Treg Perturbations Correlate With COVID-19 Severity. *Proc Natl Acad Sci* (2021) 118(37):e2111315118. doi: 10.1073/pnas.2111315118
55. Kalfaoglu B, Almeida-Santos J, Tye CA, Satou Y, Ono M. T-Cell Dysregulation in COVID-19. *Biochem Biophys Res Commun* (2021) 538:204–10. doi: 10.1016/j.bbrc.2020.10.079
56. Caldrer S, Mazzi C, Bernardi M, Prato M, Ronzoni N, Rodari P, et al. Regulatory T Cells as Predictors of Clinical Course in Hospitalised COVID-19 Patients. *Front Immunol* (2021) 12:789735–5. doi: 10.3389/fimmu.2021.789735
57. Vick SC, Frutoso M, Mair F, Konecny AJ, Greene E, Wolf CR, et al. A Differential Regulatory T Cell Signature Distinguishes the Immune Landscape of COVID-19 Hospitalized Patients From Those Hospitalized With Other Respiratory Viral Infections. *MedRxiv* (2021) 7. doi: 10.1126/sciadv.abj0274
58. Meckiff BJ, Ramírez-Suástegui C, Fajardo V, Chee SJ, Kusnadi A, Simon H, et al. Imbalance of Regulatory and Cytotoxic SARS-CoV-2-Reactive CD4+ T Cells in COVID-19. *Cell* (2020) 183(5):40–1353.e16. doi: 10.1016/j.cell.2020.10.001
59. Ryan FJ, Hope CM, Masavuli MG, Lynn MA, Mekonnen ZA, Lip Yeow AE, et al. Long-Term Perturbation of the Peripheral Immune System Months After SARS-CoV-2 Infection. *BMC Med* (2022) 20(1):1–23. doi: 10.1186/s12916-021-02228-6
60. Haanen JB, Cerundolo V. NKG2A, a New Kid on the Immune Checkpoint Block. *Cell* (2018) 175(7):1720–2. doi: 10.1016/j.cell.2018.11.048
61. Gangaev A, Ketelaars S LC, Isaeva OI, Patiwael S, Dopler A, Hoefakker K, et al. Identification and Characterization of a SARS-CoV-2 Specific CD8+ T Cell Response With Immunodominant Features. *Nat Commun* (2021) 12 (1):1–14. doi: 10.1038/s41467-021-22811-y
62. van Montfoort N, Borst L, Korrer MJ, Sluijter M, Marijt KA, Santegoets SJ, et al. NKG2A Blockade Potentiates CD8 T Cell Immunity Induced by Cancer Vaccines. *Cell* (2018) 175(7):1744–55.e15. doi: 10.1016/j.cell.2018.10.028
63. Lonez C, Verma B, Hendlisz A, Aftimos P, Awada A, Van Den Neste E, et al. Study Protocol for THINK: A Multinational Open-Label Phase I Study to Assess the Safety and Clinical Activity of Multiple Administrations of NKR-2 in Patients With Different Metastatic Tumour Types. *BMJ Open* (2017) 7 (11):e017075. doi: 10.1136/bmjopen-2017-017075
64. Prajapati K, Perez C, Plaza Rojas LB, Burke B, Guevara-Patino JA. Functions of NKG2D in CD8+ T Cells: An Opportunity for Immunotherapy. *Cell Mol Immunol* (2018) 15(5):470–9. doi: 10.1038/cmi.2017.161
65. Whiteside SK, Perez C, Plaza Rojas LB, Burke B, Guevara-Patino JA. Bystander T Cells: A Balancing Act of Friends and Foes. *Trends Immunol* (2018) 39(12):1021–35. doi: 10.1016/j.it.2018.10.003

66. Lorenzo-Herrero S, Sordo-Bahamonde C, Gonzalez S, López-Soto A. CD107a Degranulation Assay to Evaluate Immune Cell Antitumor Activity. In: *Cancer Immunosurveillance*. New York: Springer (2018). p. 119–30. doi: 10.1007/978-1-4939-8885-3_7
67. Varchetta S, Mele D, Oliviero B, Mantovani S, Ludovisi S, Cerino A, et al. Unique Immunological Profile in Patients With COVID-19. *Cell Mol Immunol* (2021) 18(3):604–12. doi: 10.1038/s41423-020-00557-9
68. Mehraj V, Ponte R, Routy J-P. The Dynamic Role of the IL-33/ST2 Axis in Chronic Viral-Infections: Alarming and Adjuvanting the Immune Response. *EBioMedicine* (2016) 9:37–44. doi: 10.1016/j.ebiom.2016.06.047
69. Dreis C, Ottenlinger FM, Putyrski M, Ernst A, Huhn M, Schmidt KG, et al. Tissue Cytokine IL-33 Modulates the Cytotoxic CD8 T Lymphocyte Activity During Nutrient Deprivation by Regulation of Lineage-Specific Differentiation Programs. *Front Immunol* (2019) 10:1698. doi: 10.3389/fimmu.2019.01698
70. Ragusa R, Basta G, Del Turco S, Caselli C. A Possible Role for ST2 as Prognostic Biomarker for COVID-19. *Vasc Pharmacol* (2021) p:106857. doi: 10.1016/j.vph.2021.106857
71. Zeng Z, Hong X-Y, Li Y, Chen W, Ye G, Li Y, et al. Serum-Soluble ST2 as a Novel Biomarker Reflecting Inflammatory Status and Illness Severity in Patients With COVID-19. *Biomarkers Med* (2020) 14(17):1619–29. doi: 10.2217/bmm-2020-0410
72. Stanczak MA, Sanin DE, Apostolova P, Nerz G, Lampaki D, Hofmann M, et al. IL-33 Expression in Response to SARS-CoV-2 Correlates With Seropositivity in COVID-19 Convalescent Individuals. *Nat Commun* (2021) 12(1):1–9. doi: 10.1038/s41467-021-22449-w
73. Liang Y, Ge Y, Sun J. IL-33 in COVID-19: Friend or Foe? *Cell Mol Immunol* (2021) 18(6):1602–4. doi: 10.1038/s41423-021-00685-w
74. Principe N, Kidman J, Goh S, Tilsed CM, Fisher SA, Fear VS. Tumor Infiltrating Effector Memory Antigen-Specific CD8+ T Cells Predict Response to Immune Checkpoint Therapy. *Front Immunol* (2020) 11:2907. doi: 10.3389/fimmu.2020.584423
75. Han J, Khatwani N, Searles TG, Turk MJ, Angeles CV. Memory CD8+ T Cell Responses to Cancer. *Semin Immunol* (2020) 49:101435. doi: 10.1016/j.smim.2020.101435.
76. Ando M, Ito M, Srirat T, Kondo T, Yoshimura A. Memory T Cell, Exhaustion, and Tumor Immunity. *Immunol Med* (2020) 43(1):1–9. doi: 10.1080/25785826.2019.1698261
77. Rodda LB, Netland J, Shehata L, Pruner KB, Morawski PA, Thouvenel CD, et al. Functional SARS-CoV-2-Specific Immune Memory Persists After Mild COVID-19. *Cell* (2021) 184(1):169–83.e17. doi: 10.1016/j.cell.2020.11.029
78. Zhang F, Gan R, Zhen Z, Hu X, Li X, Zhou F, et al. Adaptive Immune Responses to SARS-CoV-2 Infection in Severe Versus Mild Individuals. *Signal Transduct Target Ther* (2020) 5(1):1–11. doi: 10.1038/s41392-020-00263-y
79. Sekine T, Perez-Potti A, Rivera-Ballesteros O, Strålin K, Gorin J-B, Olsson A, et al. Robust T Cell Immunity in Convalescent Individuals With Asymptomatic or Mild COVID-19. *Cell* (2020) 183(1):158–68.e14. doi: 10.1016/j.cell.2020.08.017
80. Le Bert N, Tan A T, Kunasegaran K YL, Tham C, Hafezi M, Chia A, et al. SARS-CoV-2-Specific T Cell Immunity in Cases of COVID-19 and SARS, and Uninfected Controls. *Nature* (2020) 584(7821):457–62. doi: 10.1038/s41586-020-2550-z
81. Kared H, Redd AD, Bloch EM, Bonny TS, Sumatoh H, Kairi F, et al. SARS-CoV-2–Specific CD8+ T Cell Responses in Convalescent COVID-19 Individuals. *J Clin Invest* (2021) 131(5):e145476. doi: 10.1172/JCI145476
82. Jung JH, Rha M-S, Sa M, Choi HK, Jeon JH, Seok H, et al. SARS-CoV-2-Specific T Cell Memory is Sustained in COVID-19 Convalescent Patients for 10 Months With Successful Development of Stem Cell-Like Memory T Cells. *Nat Commun* (2021) 12(1):1–12. doi: 10.1038/s41467-021-24377-1
83. Galletti G, De Simone G MC, Mazza E, Puccio S, Mezzanotte C, Bi TM, et al. Two Subsets of Stem-Like CD8+ Memory T Cell Progenitors With Distinct Fate Commitments in Humans. *Nat Immunol* (2020) 21(12):1552–62. doi: 10.1038/s41590-020-0791-5
84. Jung JH, Rha MS, Sa M, Choi HK, Jeon JH, Seok H, et al. SARS-CoV-2-Specific T Cell Memory is Sustained in COVID-19 Convalescents for 8 Months With Successful Development of Stem Cell-Like Memory T Cells. *medRxiv* (2021) 12:4043. doi: 10.1101/2021.03.04.21252658
85. Krishna S, Lowery FJ, Copeland AR, Bahadiroglu E, Mukherjee R, Jia L, et al. Stem-Like CD8 T Cells Mediate Response of Adoptive Cell Immunotherapy Against Human Cancer. *Science* (2020) 370(6522):1328–34. doi: 10.1126/science.abb9847
86. Harjes U. The Source Within– Intratumoural Stem-Like T Cells Give Rise to Differentiated T Cells. *Nat Rev Cancer* (2020) 20(3):140–0. doi: 10.1038/s41568-020-0239-0
87. Held W, Siddiqui I, Schaeuble K, Speiser DE, et al. Intratumoral CD8+ T Cells With Stem Cell–Like Properties: Implications for Cancer Immunotherapy. *Sci Trans Med* (2019) 11(515):eaay6863. doi: 10.1126/scitranslmed.aay6863
88. Utzschneider DT, Charmoy M, Chennupati V, Pousse L, Ferreira DP, Calderon-Copete S. T Cell Factor 1-Expressing Memory-Like CD8+ T Cells Sustain the Immune Response to Chronic Viral Infections. *Immunity* (2016) 45(2):415–27. doi: 10.1016/j.immuni.2016.07.021
89. Siddiqui I, Schaeuble K, Chennupati V, Fuertes Marraco SA, Calderon-Copete S, Ferreira DP, et al. Intratumoral Tcf1+ PD-1+ CD8+ T Cells With Stem-Like Properties Promote Tumor Control in Response to Vaccination and Checkpoint Blockade Immunotherapy. *Immunity* (2019) 50(1):195–211. e10. doi: 10.1016/j.immuni.2018.12.021
90. Collier JL, Weiss SA, Pauken KE, Sen DR, Sharpe AH. Not-So-Opposite Ends of the Spectrum: CD8+ T Cell Dysfunction Across Chronic Infection, Cancer and Autoimmunity. *Nat Immunol* (2021) p:1–11. doi: 10.1038/s41590-021-00949-7
91. Im SJ, Hashimoto M, Gerner MY, Lee J, Kissick HT, Burger MC, et al. Defining CD8+ T Cells That Provide the Proliferative Burst After PD-1 Therapy. *Nature* (2016) 537(7620):417–21. doi: 10.1038/nature19330
92. Kusnadi A, Ramírez-Suástegui C, Fajardo V, Chee SJ, Meckiff BJ, Simon H, et al. Severely Ill COVID-19 Patients Display Impaired Exhaustion Features in SARS-CoV-2-Reactive CD8+ T Cells. *Sci Immunol* (2021) 6(55):eabe4782. doi: 10.1126/sciimmunol.abe4782
93. Kusnadi A, Ramírez-Suástegui C, Fajardo V, Chee SJ, Meckiff BJ, Simon H, et al. Severely Ill Patients With COVID-19 Display Impaired Exhaustion Features in SARS-CoV-2–Reactive CD8+ T Cells. *Sci Immunol* (2021) 6(55):eabe4782. doi: 10.1126/sciimmunol.abe4782
94. Zheng H-Y, Zhang M, Yang C-X, Zhang N, Wang X-C, Yang X-P, et al. Elevated Exhaustion Levels and Reduced Functional Diversity of T Cells in Peripheral Blood may Predict Severe Progression in COVID-19 Patients. *Cell Mol Immunol* (2020) 17(5):541–3. doi: 10.1038/s41423-020-0401-3
95. Renner K, Müller C, Tiefenböck C, Salewski JN, Winter F, Buchtler S, et al. T Cell Anergy in COVID-19 Reflects Virus Persistence and Poor Outcomes. *medRxiv* (2020) 2020.09.21.20198671. doi: 10.21203/rs.3.rs-76318/v1
96. Xia A, Zhang Y, Xu J, Yin T, Lu X-J. T Cell Dysfunction in Cancer Immunity and Immunotherapy. *Front Immunol* (2019) 10:1719. doi: 10.3389/fimmu.2019.01719
97. Abe BT, Macian F. Uncovering the Mechanisms That Regulate Tumor-Induced T-Cell Anergy. *Oncoimmunology* (2013) 2(2):e22679. doi: 10.4161/onci.22679
98. Catakovic K, Klieser E, Neureiter D, Geisberger R. T Cell Exhaustion: From Pathophysiological Basics to Tumor Immunotherapy. *Cell Commun Signal* (2017) 15(1):1–16. doi: 10.1186/s12964-016-0160-z
99. Majidpoor J, Mortezaee K. The Efficacy of PD-1/PD-L1 Blockade in Cold Cancers and Future Perspectives. *Clin Immunol* (2021) p:108707. doi: 10.1016/j.clim.2021.108707
100. Mortezaee K. Immune Escape: A Critical Hallmark in Solid Tumors. *Life Sci* (2020) p:118110. doi: 10.1016/j.lfs.2020.118110
101. Zhang J, He T, Xue L, Guo H. Senescent T Cells: A Potential Biomarker and Target for Cancer Therapy. *EBioMedicine* (2021) 68:103409. doi: 10.1016/j.ebiom.2021.103409
102. Liu X, Hoft DF, Peng G. Senescent T Cells Within Suppressive Tumor Microenvironments: Emerging Target for Tumor Immunotherapy. *J Clin Invest* (2020) 130(3):1073–83. doi: 10.1172/JCI133679
103. Maimela NR, Liu S, Zhang Y. Fates of CD8+ T Cells in Tumor Microenvironment. *Comput Struct Biotechnol J* (2019) 17:1–13. doi: 10.1016/j.csbj.2018.11.004
104. Waldman AD, Fritz JM, Lenardo MJ. A Guide to Cancer Immunotherapy: From T Cell Basic Science to Clinical Practice. *Nat Rev Immunol* (2020) 20(11):651–68. doi: 10.1038/s41577-020-0306-5

105. Lanitis E, Dangaj D, Irving M, Coukos G. Mechanisms Regulating T-Cell Infiltration and Activity in Solid Tumors. *Ann Oncol* (2017) 28:xii18–32. doi: 10.1093/annonc/mdx238
106. Renner K, Schwittay T, Chaabane S, Gottschling J, Müller C, Tiefenböck C, et al. Severe T Cell Hyporeactivity in Ventilated COVID-19 Patients Correlates With Prolonged Virus Persistence and Poor Outcomes. *Nat Commun* (2021) 12(1):1–11. doi: 10.1038/s41467-021-23334-2
107. Chikuma S, Terawaki S, Hayashi T, Nabeshima R, Yoshida T, Shibayama S, et al. PD-1-Mediated Suppression of IL-2 Production Induces CD8+ T Cell Anergy In Vivo. *J Immunol* (2009) 182(11):6682–9. doi: 10.4049/jimmunol.0900080
108. Duré M, Macian F. IL-2 Signaling Prevents T Cell Anergy by Inhibiting the Expression of Anergy-Inducing Genes. *Mol Immunol* (2009) 46(5):999–1006. doi: 10.1016/j.molimm.2008.09.029
109. Oh YM, Park HB, Shin JH, Lee JE, Park HY, Kho DH, et al. Ndrg1 is a T-Cell Clonal Anergy Factor Negatively Regulated by CD28 Costimulation and Interleukin-2. *Nat Commun* (2015) 6(1):1–14. doi: 10.1038/ncomms9698
110. Zhang Z, Liu S, Zhang B, Qiao L, Zhang Y, Zhang Y. T Cell Dysfunction and Exhaustion in Cancer. *Front Cell Dev Biol* (2020) 8:17. doi: 10.3389/fcell.2020.00017
111. Omarjee L, Janin A, Perrot F, Laviolle B, Meilhac O, Mahe G. Targeting T-Cell Senescence and Cytokine Storm With Rapamycin to Prevent Severe Progression in COVID-19. *Clin Immunol* (2020) 216:108464. doi: 10.1016/j.clim.2020.108464
112. Nehme J, Borghesan M, Mackedenski S, Bird TG, Demaria M. Cellular Senescence as a Potential Mediator of COVID-19 Severity in the Elderly. *Aging Cell* (2020) 19(10):e13237. doi: 10.1111/acel.13237
113. Cox LS, Bellantuono I, Lord JM, Sapey E, Mannick JB, Partridge L, et al. Tackling Immunosenescence to Improve COVID-19 Outcomes and Vaccine Response in Older Adults. *Lancet Healthy Longevity* (2020) 1(2):e55–7. doi: 10.1016/S2666-7568(20)30011-8
114. Kim T-S, Shin E-C. The Activation of Bystander CD8+ T Cells and Their Roles in Viral Infection. *Exp Mol Med* (2019) 51(12):1–9. doi: 10.1038/s12276-019-0316-1
115. Simoni Y, Becht E, Fehlings M, Loh CY, Koo S-L, Weng Teng KW, et al. Bystander CD8+ T Cells are Abundant and Phenotypically Distinct in Human Tumour Infiltrates. *Nature* (2018) 557(7706):575–9. doi: 10.1038/s41586-018-0130-2
116. Gokuldass A, Draghi A, Papp K, Borch TH, Nielsen M, Wulff Westergaard MC, et al. Qualitative Analysis of Tumor-Infiltrating Lymphocytes Across Human Tumor Types Reveals a Higher Proportion of Bystander CD8+ T Cells in Non-Melanoma Cancers Compared to Melanoma. *Cancers* (2020) 12(11):3344. doi: 10.3390/cancers12113344
117. Lee H-G, Cho M-Z, Choi J-M. Bystander CD4+ T Cells: Crossroads Between Innate and Adaptive Immunity. *Exp Mol Med* (2020) 52(8):1255–63. doi: 10.1038/s12276-020-00486-7
118. Reuben A, Zhang J, Gittelman R, Chiou S, Li J, Fujimoto J, et al. MA11. 09 Increased Frequency of Bystander T Cells in the Lungs Is Associated With Recurrence in Localized Non-Small Cell Lung Cancer. *J Thorac Oncol* (2019) 14(10):S293. doi: 10.1016/j.jtho.2019.08.589
119. Bergamaschi L, Mescia F, Turner L, Hanson AL, Kotagiri P, Dunmore BJ, et al. Longitudinal Analysis Reveals That Delayed Bystander CD8+ T Cell Activation and Early Immune Pathology Distinguish Severe COVID-19 From Mild Disease. *Immunity* (2021) 54(6):1257–1275. e8. doi: 10.1016/j.immuni.2021.05.010
120. Gujar S, Pol JG, Kim Y, Kroemer G. Repurposing CD8+ T Cell Immunity Against SARS-CoV-2 for Cancer Immunotherapy: A Positive Aspect of the COVID-19 Pandemic? *Oncoimmunology* (2020) 9(1):1794424. doi: 10.1080/2162402X.2020.1794424
121. Mortezaee K. Normalization in Tumor Ecosystem: Opportunities and Challenges. *Cell Biol Int* (2021) 45:2017–30. doi: 10.1002/cbin.11655
122. Grifoni A, Weiskopf D, Ramirez SI, Mateus J, Dan JM, Moderbacher CR, et al. Targets of T Cell Responses to SARS-CoV-2 Coronavirus in Humans With COVID-19 Disease and Unexposed Individuals. *Cell* (2020) 181(7):1489–501.e15. doi: 10.1016/j.cell.2020.05.015
123. Moderbacher CR, Ramirez SI, Dan JM, Grifoni A, Hastie KM, Weiskopf D, et al. Antigen-Specific Adaptive Immunity to SARS-CoV-2 in Acute COVID-19 and Associations With Age and Disease Severity. *Cell* (2020) 183(4):996–1012.e19. doi: 10.1016/j.cell.2020.09.038
124. Acosta-Ampudia Y, Monsalve DM, Rojas M, Rodríguez Y, Gallo JE, Carlos Salazar-Uribe JC, et al. COVID-19 Convalescent Plasma Composition and Immunological Effects in Severe Patients. *J Autoimmun* (2021) 118:102598. doi: 10.1016/j.jaut.2021.102598
125. Tarke A, Sidney J, Methot N, Yu ED, Zhang Y, Dan JM, et al. Impact of SARS-CoV-2 Variants on the Total CD4+ and CD8+ T Cell Reactivity in Infected or Vaccinated Individuals. *Cell Rep Med* (2021) p:100355. doi: 10.1016/j.xcrm.2021.100355
126. Ella R, Vadrevu KM, Jogdand H, Prasad S, Reddy S, Sarangi V, et al. Safety and Immunogenicity of an Inactivated SARS-CoV-2 Vaccine, BBV152: A Double-Blind, Randomised, Phase 1 Trial. *Lancet Infect Dis* (2021) 21(5):637–46. doi: 10.1016/S1473-3099(20)30942-7
127. Brüssow H. COVID-19: Vaccine's Progress. *Microb Biotechnol* (2021) 14:1246–57. doi: 10.1111/1751-7915.13818
128. Koch T, Mellinghoff SC, Shamsrizi P, Addo MM, Dahlke C. Correlates of Vaccine-Induced Protection Against SARS-CoV-2. *Vaccines* (2021) 9(3):238. doi: 10.3390/vaccines9030238
129. Swanson PA, Padilla M, Hoyland W, McGlinchey K, Fields PA, Bibi S, et al. T-Cell Mediated Immunity After AZD1222 Vaccination: A Polyfunctional Spike-Specific Th1 Response With a Diverse TCR Repertoire. *MedRxiv* (2021) 13:eabj7211 . doi: 10.1101/2021.06.17.21259027
130. Polack FP, Thomas SJ, Kitchin N, Absalon J, Gurtman A, Lockhart S, et al. Safety and Efficacy of the BNT162b2 mRNA Covid-19 Vaccine. *N Engl J Med* (2020) 385:1761–73. doi: 10.1056/NEJMoa2034577
131. Sahin U, Muik A, Vogler I, Derhovanessian E, Kranz LM, Vormehr M, et al. BNT162b2 Induces SARS-CoV-2-Neutralising Antibodies and T Cells in Humans. *MedRxiv* (2020) 2020.12.09.20245175. doi: 10.1101/2020.12.09.20245175.
132. Angyal A, Longet S, Moore SC, Payne RP, Harding A, Tipton T, et al. T-Cell and Antibody Responses to First BNT162b2 Vaccine Dose in Previously SARS-CoV-2-Infected and Infection-Naive UK Healthcare Workers: A Multicentre, Prospective, Observational Cohort Study. *Lancet Microbe* (2022) 3(1):e21–31. doi: 10.1016/S2666-5247(21)00275-5.
133. Zollner A, Watschinger C, Rössler A, Farcet MR, Penner A, Böhm V, et al. B and T Cell Response to SARS-CoV-2 Vaccination in Health Care Professionals With and Without Previous COVID-19. *EBioMedicine* (2021) 70:103539. doi: 10.1016/j.ebiom.2021.103539
134. Qin T, Guo E, Lu F, Fu Y, Liu S, Xiao R, et al. Impact of Chemotherapy and Immunotherapy on the Composition and Function of Immune Cells in COVID-19 Convalescent With Gynecological Tumors. *Aging (Albany NY)* (2021) 13(23):24943. doi: 10.18632/aging.203739
135. Liu Z, Zhou Q, Wang Z, Zhang H, Zeng H, Huang Q, et al. Intratumoral TIGIT+ CD8+ T-Cell Infiltration Determines Poor Prognosis and Immune Evasion in Patients With Muscle-Invasive Bladder Cancer. *J Immunother Cancer* (2020) 8(2):e000978. doi: 10.1136/jitc-2020-000978
136. Bonifacius A, Tischer-Zimmermann S, Dragon AC, Gussarow D, Vogel A, Krettek U, et al. COVID-19 Immune Signatures Reveal Stable Antiviral T Cell Function Despite Declining Humoral Responses. *Immunity* (2021) 54(2):340–354. e6. doi: 10.1016/j.immuni.2021.01.008
137. Herrmann M, Schulte S, Wildner NH, Wittner M, Brehm TT, Ramharter M, et al. Analysis of Co-Inhibitory Receptor Expression in COVID-19 Infection Compared to Acute Plasmodium Falciparum Malaria: lAG-3 and TIM-3 Correlate With T Cell Activation and Course of Disease. *Front Immunol* (2020) 11:1870. doi: 10.3389/fimmu.2020.01870
138. Rha M-S, Jeong HW, Ko JH, Seong Choi J, Seo IH, Lee JS, et al. PD-1-Expressing SARS-CoV-2-Specific CD8+ T Cells are Not Exhausted, But Functional in Patients With COVID-19. *Immunity* (2021) 54(1):44–52. e3. doi: 10.1016/j.immuni.2020.12.002
139. Westmeier J, Paniskaki K, Karaköse Z, Werner T, Sutter K, Dolff S, et al. Impaired Cytotoxic CD8+ T Cell Response in Elderly COVID-19 Patients. *MBio* (2020) 11(5):e02243–20. doi: 10.1128/mBio.02243-20
140. Kang CK, Han G-C, Kim M, Kim G, Shin HM, Song K-H, et al. Aberrant Hyperactivation of Cytotoxic T-Cell as a Potential Determinant of COVID-19 Severity. *Int J Infect Dis* (2020) 97:313–21. doi: 10.1016/j.ijid.2020.05.106
141. Maio M, Hamid O, Larkin J, Covre A, Altomonte M, Calabrò L, et al. Immune Checkpoint Inhibitors for Cancer Therapy in the COVID-19 Era.

Clin Cancer Res (2020) 26(16):4201–5. doi: 10.1158/1078-0432.CCR-20-1657
142. Gatto L, Franceschi E, Di Nunno V, Brandes AA. Potential Protective and Therapeutic Role of Immune Checkpoint Inhibitors Against Viral Infections and COVID-19. 2020. *Future Med* (2020) 12:1111–4. doi: 10.2217/imt-2020-0109
143. Vivarelli S, Falzone L, Grillo CM, Scandurra G, Torino F, Libra M. Cancer Management During COVID-19 Pandemic: Is Immune Checkpoint Inhibitors-Based Immunotherapy Harmful or Beneficial? *Cancers* (2020) 12(8):2237. doi: 10.3390/cancers12082237
144. Vivarelli S, Falzone L, Torino F, Scandurra G, Russo G, Bordonaro R, et al. Immune-Checkpoint Inhibitors From Cancer to COVID−19: A Promising Avenue for the Treatment of Patients With COVID−19. *Int J Oncol* (2021) 58(2):145–57. doi: 10.3892/ijo.2020.5159
145. Yatim N, Boussier J, Tetu P, Smith N, Bruel T, Charbit B, et al. Immune Checkpoint Inhibitors Increase T Cell Immunity During SARS-CoV-2 Infection. *Sci Adv* (2021) 7(34):eabg4081. doi: 10.1126/sciadv.abg4081
146. Gonzalez-Cao M, Basa MA, Puertolas T, Muñoz E, Manzano JL, Carrera C, et al. Cancer Immunotherapy Does Not Increase the Risk of Death by COVID-19 in Melanoma Patients. *MedRxiv* (2020) 2020.05.19.20106971. doi: 10.1101/2020.05.19.20106971
147. Fane M, Weeraratna AT. How the Ageing Microenvironment Influences Tumour Progression. *Nat Rev Cancer* (2020) 20(2):89–106. doi: 10.1038/s41568-019-0222-9
148. Huang X-Z, Gao P, Song Y-X, Sun J-X, Chen X-W, Zhao J-H, et al. Efficacy of Immune Checkpoint Inhibitors and Age in Cancer Patients. *Immunotherapy* (2020) 12(8):587–603. doi: 10.2217/imt-2019-0124
149. Koff WC, Williams MA. Covid-19 and Immunity in Aging Populations—a New Research Agenda. *N Engl J Med* (2020) 383(9):804–5. doi: 10.1056/NEJMp2006761
150. Jeske SS, Schuler PJ, Doescher J, Theodoraki MN, Laban S, Brunner C, et al. Age-Related Changes in T Lymphocytes of Patients With Head and Neck Squamous Cell Carcinoma. *Immun Ageing* (2020) 17(1):1–11. doi: 10.1186/s12979-020-0174-7
151. de Candia P, Prattichizzo F, Garavelli S, Matarese G. T Cells: Warriors of SARS-CoV-2 Infection. *Trends Immunol* (2020) 42:18–30. doi: 10.1016/j.it.2020.11.002
152. Nicoli F, Solis-Soto MT, Paudel D, Marconi P, Gavioli R, Appay V, et al. Age-Related Decline of De Novo T Cell Responsiveness as a Cause of COVID-19 Severity. *Geroscience* (2020) 42(4):1015–9. doi: 10.1007/s11357-020-00217-w
153. Goto H, Shimono Y, Funakoshi Y, Imamura Y, Toyoda M, Kiyota N, et al. Adipose-Derived Stem Cells Enhance Human Breast Cancer Growth and Cancer Stem Cell-Like Properties Through Adipsin. *Oncogene* (2019) 38 (6):767–79. doi: 10.1038/s41388-018-0477-8
154. Pérez-Galarza J, Prócel C, Cañadas C, Aguirre D, Pibaque R, Bedón R, et al. Immune Response to SARS-CoV-2 Infection in Obesity and T2D: Literature Review. *Vaccines* (2021) 9(2):102. doi: 10.3390/vaccines9020102
155. Richter FC, Alrubayyi A, Crespo ATOxford-Cardiff COVID-19 Literature Consortium, , Hulin-Curtis S. Impact of Obesity and SARS-CoV-2 Infection: Implications for Host Defence-a Living Review. *Oxford Open Immunol* (2021) 2(1):iqab001. doi: 10.1093/oxfimm/iqab001
156. Andrade FB, Gualberto A, Rezende C, Percegoni N, Gameiro J, Hottz ED. The Weight of Obesity in Immunity From Influenza to COVID-19. *Front Cell Infect Microbiol* (2021) 11:170. doi: 10.3389/fcimb.2021.638852
157. Porsche CE, Delproposto JB, Geletka L, O'Rourke R, Lumeng CN. Obesity Results in Adipose Tissue T Cell Exhaustion. *JCI Insight* (2021) 6(8):e139793. doi: 10.1172/jci.insight.139793
158. Clarke MF. Clinical and Therapeutic Implications of Cancer Stem Cells. *N Engl J Med* (2019) 380(23):2237–45. doi: 10.1056/NEJMra1804280
159. Turbitt WJ, Rosean CB, Weber KS, Norian LA. Obesity and CD8 T Cell Metabolism: Implications for Anti-Tumor Immunity and Cancer Immunotherapy Outcomes. *Immunol Rev* (2020) 295(1):203–19. doi: 10.1111/imr.12849
160. Baracho GV, Song H-W, Taylor I, Mortimer S, Widmann S, Tyznik AJ. Assessing CD8+ Cytotoxic T-Cell Dysfunction in Obesity and its Implications in Anti-PD-1 Blockade Therapy. *Am Assoc Immnol* (2020) 204:no. 1 Supplement 86.27.
161. Kado T, Nawaz A, Takikawa A, Usui I, Tobe K. Linkage of CD8+ T Cell Exhaustion With High-Fat Diet-Induced Tumourigenesis. *Sci Rep* (2019) 9 (1):1–8. doi: 10.1038/s41598-019-48678-0
162. Mortezaee K, Majidpoor J. Key Promoters of Tumor Hallmarks. *Int J Clin Oncol* (2021) p:1–14. doi: 10.1007/s10147-021-02074-9
163. Altorki NK, Markowitz GJ, Gao D, Port JL, Saxena A, Stiles B, et al. The Lung Microenvironment: An Important Regulator of Tumour Growth and Metastasis. *Nat Rev Cancer* (2019) 19(1):9–31. doi: 10.1038/s41568-018-0081-9
164. Mollinedo F. Neutrophil Degranulation, Plasticity, and Cancer Metastasis. *Trends Immunol* (2019) 40(3):228–42. doi: 10.1016/j.it.2019.01.006
165. Craig AJ, Von Felden J, Garcia-Lezana T, Sarcognato S, Villanueva A. Tumour Evolution in Hepatocellular Carcinoma. *Nat Rev Gastroenterol Hepatol* (2020) 17(3):139–52. doi: 10.1038/s41575-019-0229-4
166. Mortezaee K, Sabbaghziarani F, Omidi A, Dehpour AR, Omidi N, Ghasemi S, et al. Therapeutic Value of Melatonin Post-Treatment on CCl4-Induced Fibrotic Rat Liver. *Can J Physiol Pharmacol* (2016) 94(2):119–30. doi: 10.1139/cjpp-2015-0266
167. Korpela T, Udd M, Mustonen H, Ristimäki A, Haglund C, Seppänen H, et al. Association Between Chronic Pancreatitis and Pancreatic Cancer: A 10-Year Retrospective Study of Endoscopically Treated and Surgical Patients. *Int J Cancer* (2020) 147(5):1450–60. doi: 10.1002/ijc.32971
168. Mortezaee K. Nicotinamide Adenine Dinucleotide Phosphate (NADPH) Oxidase (NOX) and Liver Fibrosis: A Review. *Cell Biochem Funct* (2018) 36 (6):292–302. doi: 10.1002/cbf.3351
169. Mortezaee K, Goradel NH, Amini P, Shabeeb D, Musa AE, Najafi M, et al. NADPH Oxidase as a Target for Modulation of Radiation Response; Implications to Carcinogenesis and Radiotherapy. *Curr Mol Pharmacol* (2019) 12(1):50–60. doi: 10.2174/1874467211666181010154709
170. Chernyak B, Popova EN, Prikhodko AS, Grebenchikov OA, Zinovkina LA, Zinovkin RA. COVID-19 and Oxidative Stress. *Biochem (Moscow)* (2020) 85 (12):1543–53. doi: 10.1134/S0006297920120068
171. Mortezaee K. Human Hepatocellular Carcinoma: Protection by Melatonin. *J Cell Physiol* (2018) 233(10):6486–508. doi: 10.1002/jcp.26586
172. Chiappetta S, Sharma AM, Bottino V, Stier C. COVID-19 and the Role of Chronic Inflammation in Patients With Obesity. *Int J Obes* (2020) 44 (8):1790–2. doi: 10.1038/s41366-020-0597-4
173. Rahmani-Kukia N, Abbasi A. Physiological and Immunological Causes of the Susceptibility of Chronic Inflammatory Patients to COVID-19 Infection: Focus on Diabetes. *Front Endocrinol* (2021) 12:84. doi: 10.3389/fendo.2021.576412
174. Elsaesser HJ, Mohtashami M, Osokine I, Snell LM, Cunningham CR, Boukhaled GM, et al. Chronic Virus Infection Drives CD8 T Cell-Mediated Thymic Destruction and Impaired Negative Selection. *Proc Natl Acad Sci* (2020) 117(10):5420–9. doi: 10.1073/pnas.1913776117
175. Schäfer S, Zernecke A. CD8+ T Cells in Atherosclerosis. *Cells* (2021) 10 (1):37. doi: 10.3390/cells10010037
176. Zhang Y, Ertl HC. Starved and Asphyxiated: How can CD8+ T Cells Within a Tumor Microenvironment Prevent Tumor Progression. *Front Immunol* (2016) 7:32. doi: 10.3389/fimmu.2016.00032
177. Mortezaee K, Majidpoor J. The Impact of Hypoxia on Immune State in Cancer. *Life Sci* (2021) 286:120057. doi: 10.1016/j.lfs.2021.120057
178. AbdelMassih A, Yacoub E, Husseiny RJ, Kamel A, Hozaien R, El Shershaby M, et al. Hypoxia-Inducible Factor (HIF): The Link Between Obesity and COVID-19. *Obes Med* (2020) p:100317. doi: 10.1016/j.obmed.2020.100317
179. Ferraro E, Germanò M, Mollace R, Mollace V, Malara N. HIF-1, the Warburg Effect, and Macrophage/Microglia Polarization Potential Role in COVID-19 Pathogenesis. *Oxid Med Cell Longevity* (2021) 2021:8841911. doi: 10.1155/2021/8841911
180. Saragovi A, Abramovich I, Omar I, Arbib E, Toker O, Gottlieb E, et al. Systemic Hypoxia Inhibits T Cell Response by Limiting Mitobiogenesis via Matrix Substrate-Level Phosphorylation Arrest. *Elife* (2020) 9:e56612. doi: 10.7554/eLife.56612
181. Mayer A, Haist M, Loquai C, Grabbe S, Rapp M, Roth W, et al. Role of Hypoxia and the Adenosine System in Immune Evasion and Prognosis of Patients With Brain Metastases of Melanoma: A Multiplex Whole Slide Immunofluorescence Study. *Cancers* (2020) 12(12):3753. doi: 10.3390/cancers12123753

182. Vuillefroy de Silly R, Dietrich P-Y, Walker PR. Hypoxia and Antitumor CD8 + T Cells: An Incompatible Alliance? *Oncoimmunology* (2016) 5(12): e1232236. doi: 10.1080/2162402X.2016.1232236
183. Mortezaee K, Majidpoor J. (Im) Maturity in Tumor Ecosystem. *Front Oncol* (2022) 11:813897. doi: 10.3389/fonc.2021.813897
184. Siska PJ, Decking S-M, Babl N, Matos C, Bruss C, Singer K, et al. Metabolic Imbalance of T Cells in COVID-19 is Hallmarked by Basigin and Mitigated by Dexamethasone. *J Clin Invest* (2021) 131(22):e148225. doi: 10.1172/JCI148225
185. Cai M, Chen X, Shan J, Yang R, Guo Q, Bi X, et al. Intermittent Hypoxic Preconditioning: A Potential New Powerful Strategy for COVID-19 Rehabilitation. *Front Pharmacol* (2021) 12. doi: 10.3389/fphar.2021.643619
186. Majidpoor J, Mortezaee K. Angiogenesis as a Hallmark of Solid Tumors-Clinical Perspectives. *Cell Oncol* (2021) p:1–23. doi: 10.1007/s13402-021-00602-3
187. Turkia M. COVID-19, Vascular Endothelial Growth Factor (VEGF) and Iodide. In: *Vascular Endothelial Growth Factor (VEGF) and Iodide* (2020). doi: 10.2139/ssrn.3604987
188. Pang J, Xu F, Aondio G, Li Y, Fumagalli A, Lu M, et al. Efficacy and Tolerability of Bevacizumab in Patients With Severe Covid-19. *Nat Commun* (2021) 12(1):1–10. doi: 10.1038/s41467-021-21085-8
189. Mortezaee K. Organ Tropism in Solid Tumor Metastasis: An Updated Review. *Future Oncol* (2021) 17(15):1943–61. doi: 10.2217/fon-2020-1103
190. Majidpoor J, Mortezaee K. Steps in Metastasis: An Updated Review. *Med Oncol* (2021) 38(1):1–17. doi: 10.1007/s12032-020-01447-w
191. Tamura R, Tanaka T, Akasaki Y, Murayama Y, Yoshida K, Sasaki H. The Role of Vascular Endothelial Growth Factor in the Hypoxic and Immunosuppressive Tumor Microenvironment: Perspectives for Therapeutic Implications. *Med Oncol* (2020) 37(1):1–14. doi: 10.1007/s12032-019-1329-2
192. Kong Y, Han J, Wu X, Zeng H, Liu J, Zhang H. VEGF-D: A Novel Biomarker for Detection of COVID-19 Progression. *Crit Care* (2020) 24(1):1–4. doi: 10.1186/s13054-020-03079-y
193. Izawa N, Shitara K, Masuishi T, Denda T, Yamazaki K, Moriwaki T, et al. Vascular Endothelial Growth Factor (VEGF)-D and Clinical Outcomes in Metastatic Colorectal Cancer (mCRC) Patients (Pts) Treated With Second-Line FOLFIRI Plus Bevacizumab (Bev): A Biomarker Study of the WJOG 6210G Trial. *Am Soc Clin Oncol* (2020) 38:226. doi: 10.1200/JCO.2020.38.4_suppl.226
194. Lee N-R, Ban J, Lee N-J, Yi C-M, Choi J-Y, Kim H, et al. Activation of RIG-I-Mediated Antiviral Signaling Triggers Autophagy Through the MAVS-TRAF6-Beclin-1 Signaling Axis. *Front Immunol* (2018) 9:2096. doi: 10.1101/340323
195. Jæhger DE, Hübbe ML, Kræmer MK, Clergeaud G, Olsen AV, Stavnsbjerg C, et al. Enhancing Adoptive CD8 T Cell Therapy by Systemic Delivery of Tumor Associated Antigens. *Sci Rep* (2021) 11(1):1–19. doi: 10.1038/s41598-021-99347-0
196. Kishton RJ, Vodnala SK, Vizcardo R, Restifo NP. Next Generation Immunotherapy: Enhancing Stemness of Polyclonal T Cells to Improve Anti-Tumor Activity. *Curr Opin Immunol* (2022) 74:39–45. doi: 10.1016/j.coi.2021.10.001
197. Chen J. Hif1α or HIF2α: Enhancing CD8+ T-Cell Fitness for Antitumor Immunity. *Cancer Immunol Res* (2021) 9(4):364–4. doi: 10.1158/2326-6066.CIR-21-0114
198. Li K, Li T, Feng Z, Huang M, Wei L, Yan Z, et al. CD8+ T Cell Immunity Blocks the Metastasis of Carcinogen-Exposed Breast Cancer. *Sci Adv* (2021) 7(25):eabd8936. doi: 10.1126/sciadv.abd8936
199. Hu B-S, Tang T, Jia J-L, Xie B-C, Wu T-L, Sheng Y-Y, et al. CD137 Agonist Induces Gastric Cancer Cell Apoptosis by Enhancing the Functions of CD8+ T Cells via NF-κb Signaling. *Cancer Cell Int* (2020) 20(1):1–14. doi: 10.1186/s12935-020-01605-0
200. Beyranvand Nejad E, Ratts RB, Panagioti E, Meyer C, Oduro JD, Cicin-Sain L, et al. Demarcated Thresholds of Tumor-Specific CD8 T Cells Elicited by MCMV-Based Vaccine Vectors Provide Robust Correlates of Protection. *J Immunother Cancer* (2019) 7(1):1–17. doi: 10.1186/s40425-019-0500-9
201. Zhang J, Endres S, Kobold S. Enhancing Tumor T Cell Infiltration to Enable Cancer Immunotherapy. *Immunotherapy* (2019) 11(3):201–13. doi: 10.2217/imt-2018-0111
202. Zhang Y, Kurupati R, Liu L, Zhou XY, Zhang G, Hudaihed A, et al. Enhancing CD8+ T Cell Fatty Acid Catabolism Within a Metabolically Challenging Tumor Microenvironment Increases the Efficacy of Melanoma Immunotherapy. *Cancer Cell* (2017) 32(3):377–391.e9. doi: 10.1016/j.ccell.2017.08.004
203. Ganji A, Farahani I, Khansarinejad B, Ghazavi A, Mosayebi G. Increased Expression of CD8 Marker on T-Cells in COVID-19 Patients. *Blood Cells Molecules Dis* (2020) 83:102437. doi: 10.1016/j.bcmd.2020.102437
204. Nguyen AT, Szeto C, Chatzileontiadou DSM, Marcus Tong ZW, Dewar-Oldis MJ, Cooper L, et al. COVID-19 Vaccine Booster Induces a Strong CD8 + T Cell Response Against Omicron Variant Epitopes in HLA-A* 02: 01+ Individuals. *bioRxiv* (2022) 2022.01.12.473243. doi: 10.1101/2022.01.12.473243
205. Oberhardt V, Luxenburger H, Kemming J, Schulien I, Ciminski K, Giese S, et al. Rapid and Stable Mobilization of CD8+ T Cells by SARS-CoV-2 mRNA Vaccine. *Nature* (2021) 597(7875):268–73. doi: 10.1038/s41586-021-03841-4
206. Chen Y, Yin S, Tong X, Tao Y, Ni J, Pan J, et al. Dynamic SARS-CoV-2-Specific B-Cell and T-Cell Responses Following Immunization With an Inactivated COVID-19 Vaccine. *Clin Microbiol Infect* (2021) 28:410–8. doi: 10.1016/j.cmi.2021.10.006
207. Salomé B, Horowitz A. Impaired Cd4 T-Cell Response to sARs-coV-2: Rationale for PD-1 Blockade in Patients With Cancer and cOVID-19? *Cancer Discov* (2021) 11(8):1877–8. doi: 10.1158/2159-8290.CD-21-0613
208. Peng Y, Mentzer AJ, Liu G, Yao X, Yin Z, Dong D, et al. Broad and Strong Memory CD4+ and CD8+ T Cells Induced by SARS-CoV-2 in UK Convalescent Individuals Following COVID-19. *Nat Immunol* (2020) 21 (11):1336–45. doi: 10.1038/s41590-020-0782-6

Conflict of Interest: The authors declare that the research was conducted in the absence of any commercial or financial relationships that could be construed as a potential conflict of interest.

Publisher's Note: All claims expressed in this article are solely those of the authors and do not necessarily represent those of their affiliated organizations, or those of the publisher, the editors and the reviewers. Any product that may be evaluated in this article, or claim that may be made by its manufacturer, is not guaranteed or endorsed by the publisher.

Copyright © 2022 Mortezaee and Majidpoor. This is an open-access article distributed under the terms of the Creative Commons Attribution License (CC BY). The use, distribution or reproduction in other forums is permitted, provided the original author(s) and the copyright owner(s) are credited and that the original publication in this journal is cited, in accordance with accepted academic practice. No use, distribution or reproduction is permitted which does not comply with these terms.

frontiers | Frontiers in Immunology

ORIGINAL RESEARCH
published: 27 April 2022
doi: 10.3389/fimmu.2022.891524

In Silico Analysis Predicts a Limited Impact of SARS-CoV-2 Variants on CD8 T Cell Recognition

Olga I. Isaeva[1,2,3†], *Steven L. C. Ketelaars*[1†] *and Pia Kvistborg*[1*]

[1] Department of Molecular Oncology and Immunology, Netherlands Cancer Institute, Amsterdam, Netherlands, [2] Department of Tumor Biology and Immunology, Netherlands Cancer Institute, Amsterdam, Netherlands, [3] Oncode Institute, Utrecht, Netherlands

Since the start of the COVID-19 pandemic, mutations have led to the emergence of new SARS-CoV-2 variants, and some of these have become prominent or dominant variants of concern. This natural course of development can have an impact on how protective the previously naturally or vaccine induced immunity is. Therefore, it is crucial to understand whether and how variant specific mutations influence host immunity. To address this, we have investigated how mutations in the recent SARS-CoV-2 variants of interest and concern influence epitope sequence similarity, predicted binding affinity to HLA, and immunogenicity of previously reported SARS-CoV-2 CD8 T cell epitopes. Our data suggests that the vast majority of SARS-CoV-2 CD8 T cell recognized epitopes are not altered by variant specific mutations. Interestingly, for the CD8 T cell epitopes that are altered due to variant specific mutations, our analyses show there is a high degree of sequence similarity between mutated and reference SARS-CoV-2 CD8 T cell epitopes. However, mutated epitopes, primarily derived from the spike protein, in SARS-CoV-2 variants Delta, AY.4.2 and Mu display reduced predicted binding affinity to their restriction element. These findings indicate that the recent SARS-CoV-2 variants of interest and concern have limited ability to escape memory CD8 T cell responses raised by vaccination or prior infection with SARS-CoV-2 early in the pandemic. The overall low impact of the mutations on CD8 T cell cross-recognition is in accordance with the notion that mutations in SARS-CoV-2 are primarily the result of receptor binding affinity and antibody selection pressures exerted on the spike protein, unrelated to T cell immunity.

Keywords: SARS-CoV-2, CD8 T cell epitopes, SARS-CoV-2 variants, CD8 T cells, bioinformatics & computational biology

OPEN ACCESS

Edited by:
Varun Sasidharan Nair, Helmholtz Association of German Research Centers (HZ), Germany

Reviewed by:
Daniel Smrz, Charles University, Czechia
Alison Tarke, La Jolla Institute for Immunology (LJI), United States

***Correspondence:**
Pia Kvistborg
p.kvistborg@nki.nl

†These authors have contributed equally to this work, share first authorship and are listed in an alphabetical order

Specialty section:
This article was submitted to T Cell Biology, a section of the journal Frontiers in Immunology

Received: *07 March 2022*
Accepted: *28 March 2022*
Published: *27 April 2022*

Citation:
Isaeva OI, Ketelaars SLC and Kvistborg P (2022) In Silico Analysis Predicts a Limited Impact of SARS-CoV-2 Variants on CD8 T Cell Recognition. Front. Immunol. 13:891524. doi: 10.3389/fimmu.2022.891524

INTRODUCTION

The COVID-19 pandemic caused by SARS-CoV-2 is having a global catastrophic impact on public health and social economy (1, 2). SARS-CoV-2 was first identified in humans in late 2019 in Wuhan, China, and the outbreak was designated as a pandemic by the WHO on March 11th, 2020 (3, 4). The early variant of SARS-CoV-2 (also known as lineage B or Wuhan-Hu-1; UniProt: UP000464024; Genome accession: MN908947) is hereafter referred to as 'reference SARS-CoV-2'.

SARS-CoV-2 is a single-stranded RNA virus characterized by an inherently high mutation rate, short replication time and high virion yield (5–8). As the virus spreads, this leads to a high genetic diversity and allows the virus to evolve rapidly as a result of natural selection pressures, including those originating from the host immune system. Mutations accumulate over time and result in amino acid changes that decrease the antigenicity of immune targeted proteins. This gradual change in antigenicity of viral proteins, driven by selective immune pressure, is known as antigenic drift (9). Antigenic drift allows viruses to continuously evade host immunity, facilitating recurrent viral outbreaks. In acute infectious disease, antigenic drift is primarily driven by antibody responses leading to selection of escape mutants (9). In accordance with this, many of the amino acid changes in SARS-CoV-2 variants are located in the spike protein, the main target of neutralizing antibodies (10). These antibodies form the only immune mechanism that is able to provide sterilizing immunity, preventing host cells from being infected. The rate of evolution of the SARS-CoV-2 spike protein is much higher than that of similar proteins in other known viruses that cause acute infectious disease in humans. For example, its rate of evolution is approximately 10-fold higher than the evolution rate of the influenza A hemagglutinin and neuraminidase proteins (9). In addition, a large number of amino acid changes have accumulated in SARS-CoV-2 proteins that are not known antibody targets (11). These amino acid changes may have inferred a fitness advantage to the virus unrelated to antibody immunity, as antigenic drift is primarily driven by antibody responses in acute viral infections (6, 9, 12, 13).

Even though T cells are unlikely to be a main source to antigenic drift there is ample evidence for the importance of these cells in protection against severe and critical COVID-19 and re-infections: 1) Depletion of CD8 T cells led to impaired clearance of SARS-CoV-2 in a COVID-19 mouse model (14) and breakthrough infections in a rhesus macaque model upon rechallenge; 2) Lower baseline peripheral blood CD8 T cell counts have been shown to correlate with decreased patient survival (15, 16); and 3) CD8 T cells have also been shown to impact COVID-19 disease severity: high percentages of HLA-DR+CD38hi CD8+ T cells in peripheral blood of COVID-19 patients were demonstrated to correlate with disease severity (17), and early bystander CD8 T cell activation combined with absence of systemic inflammation was shown to predict asymptomatic or mild disease (18). Combined, these observations suggest that CD8 T cell immunity is important for protection against reinfection and severe COVID-19 disease (19).

As a direct consequence of antigenic drift, several SARS-CoV-2 variants defined by amino acid changes that directly impact virus transmissibility, pathogenicity, infectivity and/or antigenicity have emerged (20). The most prominent SARS-CoV-2 variants in Europe were designated as variants of concern (VOC) (Alpha, B.1.1.7; Beta, B.1.351; Gamma, P.1; Delta, B.1.617.2; Omicron, B.1.1.529) and variants of interest (VOI) (Lambda, C.37; Mu, B.1.621; "Delta Plus", AY.4.2) according to the European Centre for Disease Prevention and Control (ECDC) designation (21). All VOC and VOI except AY.4.2 were also designated as VOC or VOI by the World Health Organization at the moment of this investigation (20). SARS-CoV-2 variant Alpha was the dominant variant in circulation starting in late 2020 and was subsequently replaced by SARS-CoV-2 variant Delta which accounted for 90% of the infections worldwide by August 2021. In November 2021, SARS-CoV-2 variant Omicron was first detected. It was responsible for at least 92% of global SARS-CoV-2 infections by February 2022 [**Figure 1A** (22)]. There is accumulating evidence that recent SARS-CoV-2 variants including Beta, Delta and Omicron are less efficiently neutralized by vaccine recipients' sera (23, 24). In terms of T cell immunity, there is experimental data by other groups showing that T cell responses induced by reference SARS-CoV-2 generally cross-recognize SARS-CoV-2 variants Alpha, Beta, Gamma, Delta and Omicron (25–29). However, these papers do not include systematic data regarding the effect of SARS-CoV-2 variant-specific amino acid changes on the properties of previously recognized CD8 T cell epitopes.

In this work, we investigate the potential consequences of variant specific mutations on the SARS-CoV-2 specific CD8 T cell responses raised by either natural infection or vaccination based on in silico analysis. In particular, we explore changes in predicted binding affinity of the epitopes to their HLA restriction elements, predicted immunogenicity and likelihood of CD8 T cell receptor cross-recognition of epitopes between the reference SARS-CoV-2 strain and SARS-CoV-2 variants of interest and concern (**Figure 1B**). We perform these analyses pan-proteome to identify the degree of protection after a natural infection. Furthermore, the vaccines currently approved by WHO are limited to the spike protein (30). Therefore, we have also conducted the analyses focused on CD8 T cell recognized epitopes derived from the spike protein only to determine the degree of the vaccine-mediated protection.

MATERIALS AND METHODS

Identification of Dominant Non-Synonymous Mutations in SARS-CoV-2 Variants

The list of SARS-CoV-2 variants of interest and variants of concern has been compiled according to the WHO and ECDC designations as of December 10, 2021. For each of the variants, a list of mutations present in 75% of the GISAID sequences for the corresponding PANGO lineage was compiled *via* the outbreak.info API. The lists of mutations per lineage can be found in **Supplementary Table 1** (31, 32).

Parsing of CD8 T Cell Recognized SARS-CoV-2 Epitopes Using IEDB

The table of T cell assay results was downloaded from the IEDB website on December 8, 2021 (33, 34). The table was filtered to include only linear SARS-CoV-2 epitopes in humans, presented in context of the MHC class I. Only epitopes from patients with infectious disease were included. Only positive assays with negative adoptive flag field were included. The tables of variant

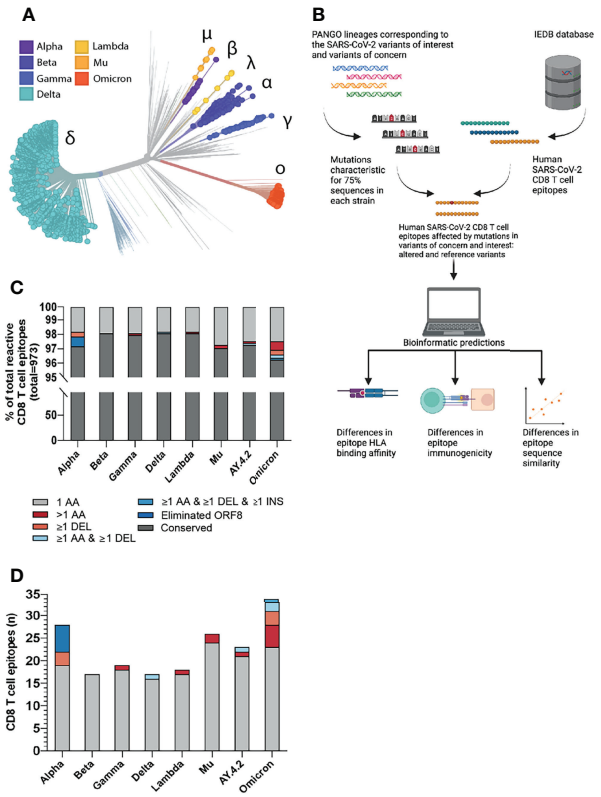


FIGURE 1 | Overview of the investigated SARS-CoV-2 CD8 T cell reactive epitopes. **(A)** Phylogenetic tree where isolates originating from variants of concern (VOCs) Alpha, Beta, Gamma, Delta and Omicron are highlighted, as well as variants of interest (VOIs) Lambda and Mu. AY.4.2 is a subvariant of Delta and overlaps with the Delta branch. The length of the branches reflects the time of emergence. Visualization generated using the Nextstrain platform (22). **(B)** Depiction of the project workflow. Created with Biorender. **(C)** Stacked bar graph indicating the percentages of CD8 T cell recognized epitopes per variant that are conserved or harbor the indicated types of mutations. **(D)** Numbers of CD8 T cell recognized epitopes per variant that harbor the indicated types of mutations.

mutations and SARS-CoV-2 CD8 T cell recognized epitopes were subsequently intersected. CD8 T cell recognized epitopes that were deduced from reactive overlapping peptide pools were filtered from the list. Epitopes with published HLA restriction elements were manually curated. The final list of epitopes and corresponding HLA alleles is shown in the **Supplementary Tables 2**, **3**.

Epitope Analysis

The normalized epitope similarity score between the altered and reference SARS-CoV-2 CD8 T cell recognized epitope was calculated as described by Frankild et al. (35). This method does not allow the calculation of the similarity score between two sequences of differing lengths. For this reason, we have set the sequence similarity score of CD8 T cell recognized epitopes harboring deletions and/or insertions to 0. IEDB's epitope cluster analysis tool was additionally used on each reference and altered epitope to determine if the epitope pairs share a sequence identity of 80%, 80-90% or more than 90% (36). The parameters used were: minimum sequence identity threshold: 80%, 90%. Minimum/Maximum peptide length: NA. Clustering method: fully interconnected clusters (cliques).

IEDB's T cell class I pMHC immunogenicity prediction tool was used to compare the immunogenicity of the altered and reference SARS-CoV-2 CD8 T cell recognized epitopes (37). The default setting was used, masking the 1st, 2nd and C-terminus amino acids of the epitopes in the analysis.

For all parsed reference SARS-CoV-2 CD8 T cell recognized epitopes with experimentally validated HLA restriction information, the predicted binding affinity to the given HLA was calculated for both the reference and altered epitope using NetMHCpan-4.1 (38). The predicted binding affinity is expressed as the half-maximal inhibitory concentration IC50 nM. For each paired reference and altered epitope, the fold change in predicted binding affinity as a result of the mutation(s) was calculated. A 2-fold change in predicted binding affinity was defined as a decrease in predicted binding affinity, a fold change below 0.5 as an increase in predicted binding affinity and a fold change between 0.5 and 2 was conservatively defined as neutral. CD8 T cell recognized epitopes overlapping with a deletion and/or insertion and not predicted to bind to the HLA as a result of the mutation were defined as decreased in predicted binding affinity.

Statistical Analysis

For all analyzed SARS-CoV-2 CD8 T cell recognized reference and altered epitope pairs, differences in predicted immunogenicity and predicted binding affinity were assessed using a two-tailed

Wilcoxon matched-pairs signed rank test. The increase in fractions of CD8 T cell recognized epitopes with decreased binding affinity and/or an epitope sequence similarity <85% was also assessed using a two-tailed Wilcoxon matched-pairs signed rank test. Comparisons in log2 fold change predicted binding affinity and/or epitope sequence similarity between spike and non-spike protein-derived mutated CD8 T cell recognized epitopes were assessed using a two-tailed Mann–Whitney *U* test. Differences were considered significant if $P < 0.05$. Statistical analysis was performed with GraphPad Prism [version: 8.4.2, for Windows, GraphPad Software, San Diego, California USA (39)].

RESULTS

A Minor Fraction of SARS-CoV-2 Derived CD8 T Cell Recognized Epitopes Are Mutated in Variants of Concern and Interest

We focused our analysis on the current SARS-CoV-2 variants of concern (VOC) (Alpha, B.1.1.7; Beta, B.1.351; Gamma, P.1; Delta, B.1.617.2; Omicron, B.1.1.529) and variants of interest (VOI) (Lambda, C.37; Mu, B.1.621; "Delta Plus", AY.4.2). First, we identified the non-synonymous amino acid substitutions, insertions and deletions that were present in at least 75% of total virus isolates for each variant in the GISAID database (per December 6th, 2021 (31, 40);, as compared to the reference SARS-CoV-2 variant (**Supplementary Table 1**). Next, we parsed all 973 unique experimentally validated CD8 T cell recognized reference SARS-CoV-2 derived epitopes identified in patients with COVID-19, per December 8th 2021, from the Immune Epitope Database (IEDB) (34, 41) and aligned these with the sequences spanning the identified non-synonymous mutations in the investigated SARS-CoV-2 variants (**Figure 1B**). Specifically, all SARS-CoV-2 CD8 T cell epitopes detected in patients with COVID-19 were included. Epitopes deduced from peptide pools, in which the exact reactive peptide is not validated, were filtered out. In addition, studies conducted in the adoptive transfer setting were filtered out. Subsequently, we proceeded with the bioinformatic analysis of differences in HLA binding affinity, immunogenicity and sequence similarity between altered and reference epitopes (**Figure 1B**).

The vast majority of the 973 included CD8 T cell recognized epitopes was found to be conserved across the different variants (median: 97.8%, range: 96.5-98.3%): we identified a total of 93 unique epitopes that harbored one or more mutations (**Figure 1C**). Specifically, between 17 and 34 unique epitopes per variant (median: 21) overlap with one or more amino acid substitutions, deletions and/or insertions (**Figure 1D** and **Supplementary Tables 2, 3**). Six CD8 T cell recognized epitopes were considered eliminated in SARS-CoV-2 variant Alpha as they were located downstream of a stop-codon mutation (ORF8 Q27*); three additional epitopes contain a deletion (SΔ69/70 or Δ144/144). In SARS-CoV-2 variant Beta, the identified CD8 T cell recognized epitopes only contain single amino acid substitutions. Altered CD8 T cell recognized epitopes in the more recent Gamma, Delta, Lambda, Mu and AY.4.2 SARS-CoV-2 variants do not harbor single deletions but harbor other types of mutations, for example, epitopes with mutations consisting of more than one amino acid substitution (Gamma, Lambda, Mu and AY.4.2; n = 1, 1, 2 and 1, respectively) or an epitope with a deletion (SΔ157-158) together with an amino acid substitution (Delta and AY.4.2). The recently emerged SARS-CoV-2 Omicron variant harbors the largest number of CD8 T cell recognized epitopes that overlap with non-synonymous mutations (n=34). These mutations result in epitopes with single (n=23), double (n=2) and triple (n=3) amino acid substitutions; single deletions (n=3); a combined amino acid substitution and deletion (n=2), and even a combined substitution, deletion and insertion (n=1) (**Figure 1D** and **Supplementary Tables 2, 3**).

To be able to investigate the potential consequences of the variant specific mutations on T cell recognition, we made a list of all variant specific CD8 T cell epitopes based on the variant specific mutations. For the analyses investigating the likelihood of T cell receptor cross-recognition and epitope immunogenicity of the altered epitopes, we included the 93 unique CD8 T cell recognized epitopes with variant specific mutations. For the prediction of HLA binding affinity, we limited the analysis to the 74 of the 93 epitopes for which HLA restriction elements had been experimentally determined by the scientific community (**Supplementary Tables 2, 3**). In total, these epitopes bind 27 HLA alleles, with between 1 and 14 epitopes per allele (median: 3, **Figure S1A**).

Properties of Altered Epitopes Are Highly Conserved Between Variants and Reference SARS-CoV-2 CD8 T Cell Recognized Epitopes

Amino acid changes in SARS-CoV-2-derived CD8 T cell epitopes can reduce the sequence similarity to the reference epitope. The more distinct the biochemical properties of an amino acid substitution are compared to the reference amino acid, the greater the dissimilarity. This could lead to reduced or abrogated activation of memory CD8 T cells reacting to the altered epitope. The epitope sequence similarity of the altered epitope to the reference epitope can therefore be used as an *in silico* proxy for likelihood of T cell receptor cross-recognition.

To test the epitope sequence similarity between the variant-specific and matched reference epitopes, we conducted two analyses: 1) We compared the sequence similarity between the reference and the altered epitopes using a previously published method (35). Importantly, this method incorporates the biochemical properties of amino acid substitutes to score the epitope sequence similarity, which is crucial in epitope cross-recognition by CD8 T cell receptors. Experimental data demonstrate that CD8 T cell receptor recognition drops to 50% if peptide similarity drops below 85% (42). We found that the vast majority (median: 90%, range: 65-100%) of the reference and the matched variant specific CD8 T cell epitopes share over 85% sequence similarity (**Figures 2A** and **S2A**). 2) In addition, we measured the degree of sequence similarity between the pairs

of epitopes using the IEDB clustering tool which performs a local alignment (36). In contrast to the first method, the IEDB clustering tool allows comparison of epitopes of differing lengths (e.g. due to insertions/deletions). Data from our previous experiments in the tumor setting suggests that a sequence similarity above 80% could serve as an indicator of potential TCR cross-reactivity (43, 44). The majority (median: 93%, range: 73-100%) of reference SARS-CoV-2 epitopes and variant derived epitopes share at least 80% similarity (**Figure S2B**). Taken together, these *in silico* analyses suggest that the ability of memory CD8 T cells, induced by natural infection with the reference virus, to respond to the included variants is not significantly impaired.

The likelihood that a certain peptide is immunogenic can be predicted based on the presence and, importantly, positioning of amino acids with certain biochemical properties (37). To investigate whether a SARS-CoV-2 CD8 T cell recognized epitope is predicted to be more or less immunogenic as a result of an amino acid change, we applied the IEDB T cell class I pMHC immunogenicity prediction tool to the set of reference SARS-CoV-2 CD8 T cell recognized epitopes and variant derived epitopes. This tool uses a large set of known peptide immunogenicity values to computationally predict whether CD8 T cell epitopes are immunogenic (i.e., likelihood for T cell recognition) or not (37). Surprisingly, the epitopes derived from the Omicron and Lambda variants were predicted to be significantly more and less immunogenic, respectively (Omicron: p=0.0042, (Lambda: p=0.03; **Figure 2B**). For all included SARS-CoV-2 variants, a large fraction of mutated epitopes was predicted to be either more immunogenic (median: 47%, range: 11-57%) or unchanged in immunogenicity (median: 28%, range: 19-44%). Between 6% and 44% (median: 24%) of variant specific CD8 T cell recognized epitopes were predicted to be less immunogenic as a result of the mutation (**Figure S3A**). Taken together, these analyses indicate that there is a high degree of sequence similarity between altered and reference epitopes in all analyzed SARS-CoV-2 variants, which is likely to result in a high degree of CD8 T cell cross-reactivity between these epitopes.

A Minor Fraction of Mutated Epitopes From Delta and AY.4.2 Exhibit Reduced Predicted Binding Affinity to MHC Class I

Amino acid changes in CD8 T cell recognized epitopes may result in altered binding affinity to the corresponding HLA

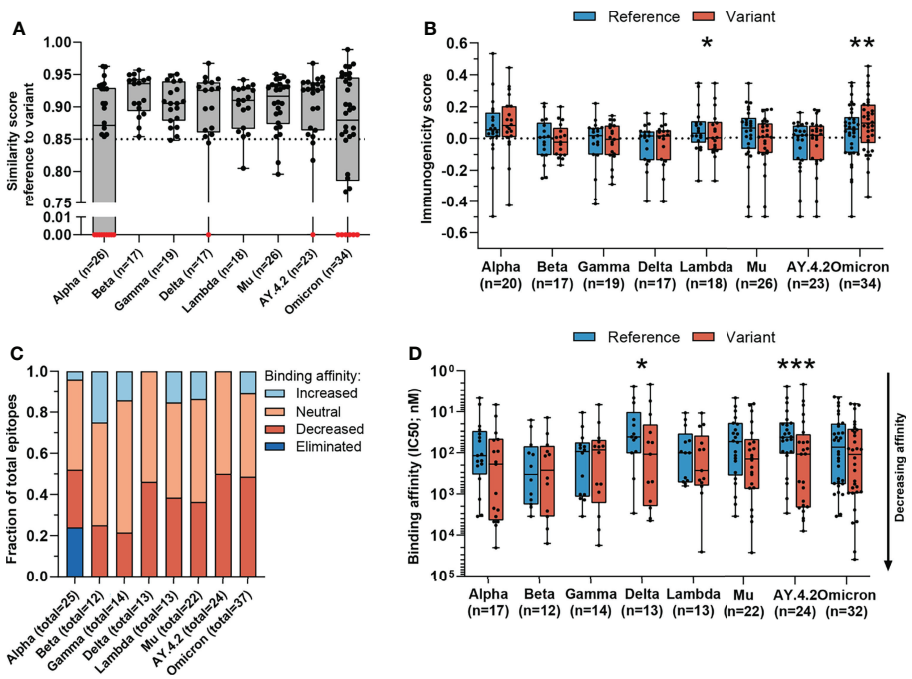


FIGURE 2 | Sequence similarity and predicted binding affinity of mutated CD8 T cell recognized epitopes. **(A)** Sequence similarity scores between the reference SARS-CoV-2 CD8 T cell recognized epitopes and the altered epitopes. Sequence similarity of epitopes in red is set to zero as a result of one or more deletions/insertions in the epitope sequence (Alpha, n = 3; Delta, n = 2; AY.4.2, n = 2; Omicron, n = 13) or due to the ORF8 Q27* stop codon mutation (Alpha, n = 6). **(B)** Box plot indicating the predicted immunogenicity of the reference SARS-CoV-2 CD8 T cell recognized epitopes and the altered epitopes according to the IEDB T cell class I pMHC immunogenicity prediction tool. **(C)** Fractions of total altered CD8 T cell recognized epitopes where the predicted binding affinity of the epitope to the corresponding HLA restriction element was increased (≤0.5-fold change in IC50), remained neutral (0.5< fold change in IC50 <2) or was decreased (≥2-fold change in IC50) as a result of the mutation. Epitopes were considered eliminated as a result of the ORF8 Q27* stop codon mutation (Alpha variant). **(D)** Box plot indicating the predicted binding affinity IC50 (nM) of the reference and altered CD8 T cell recognized epitope to the corresponding HLA restriction element. Box plots indicate the median (line), 25th and 75th percentile (box), min and max (whiskers), and all data points (single circles). Statistical significance was tested with a two-tailed Wilcoxon matched-pairs signed rank test. Variation in numbers of epitopes in the analyses are due to inclusion of epitopes binding one or more HLA restriction elements. *P < 0.05, **P < 0.01, ***P < 0.001. n indicates the number of epitopes analyzed per group.

restriction elements. This may result in altered presentation of the epitope on the surface of SARS-CoV-2 infected cells, making the infected cells less visible to T cell recognition. To estimate the changes in binding affinity of the altered epitopes, we used the 74 unique SARS-CoV-2 CD8 T cell recognized epitopes with previously experimentally validated HLA restriction elements. We used the NetMHCpan-4.1 tool to predict the binding affinity of each reference and variant specific CD8 T cell epitope to the matched HLA restriction element (38). In this analysis, epitopes that can bind to more than one HLA allele were included for each of the HLA allele they bind to.

For each included SARS-CoV-2 variant, we observed decreased binding affinity, defined as a ≥2-fold change in IC50 value for a subset of the variant specific epitopes (median 37% of epitopes, range: 21%-50%) (**Figure 2C**). Between 41% and 64% (median: 50%) of variant specific epitopes retained their predicted binding affinity (neutral; 0.5< fold change in IC50 <2), and for between 0% and 25% (median: 12%) of altered epitopes an increased binding affinity was predicted (≤0.5-fold change in IC50 value). Following a comparison of the difference in predicted binding affinity of the paired reference SARS-CoV-2 CD8 T cell recognized epitopes and mutated epitopes, the small set of epitopes of the Delta variant and its subvariant AY.4.2 were predicted to have a significantly reduced binding affinity to the HLA as a result of their mutations (Delta: p=0.01, AY.4.2: p=0.0002; **Figure 2D**). Importantly, despite these statistically significant differences, these results are derived from a highly limited number of epitopes (12 and 18 altered epitopes derived from Delta and AY.4.2, respectively, out of a total of 973 CD8 T cell recognized epitopes per variant).

A Larger Fraction of Spike Derived CD8 T Cell Epitopes Are Affected by Variant Specific Mutations Compared to Pan Proteome Derived Epitopes

To date, it is estimated that since the start of the pandemic there have been more than 400 million COVID-19 cases (45). This translates to approximately 5% of the world population, however, many cases were never included in the official statistics. In contrast, it is estimated that over half of the world population (62.6% on February 25, 2022) has received at least one dose of a COVID-19 vaccine based on the reference SARS-CoV-2 sequence of the spike protein (46). Of all the proteins encoded by SARS-CoV-2, the spike protein is subject to the highest rate of evolution (10). As a consequence, spike protein-derived CD8 T cell recognized epitopes are inherently the least conserved T cell epitopes of the SARS-CoV-2 proteome. Therefore, individuals that have not been infected but have only received the vaccine may have a lower level of protective CD8 T cell immunity as their T cell immunity is limited to epitopes from the spike protein.

We performed our analysis on spike protein-derived epitopes only. The SARS-CoV-2 spike protein encodes 263 previously identified CD8 T cell recognized epitopes. The majority of these 263 CD8 T cell recognized epitopes is conserved across the variants included in our analysis (median: 95.1%, range: 92.0-96.6%) corresponding to between 9 and 21 (median: 13) epitopes per variant which have alterations in the amino acid sequence (**Figures 3A**, **S1C**, **Supplementary Tables 2, 3**). The majority (median 84%, range: 52-100%) of these mutated variant specific epitopes share at least 85% similarity with the corresponding references epitopes (**Figures 3B** and **S2C**) based on the IEDB epitope clustering tool (median 89%, range: 71-100%; **Figure S2D**).

Interestingly, the mutated spike protein-derived epitopes from the Alpha, AY.4.2 and Omicron variants are predicted to be significantly more immunogenic compared to reference (Alpha: p=0.0034, AY.4.2: p=0.031, Omicron: p=0.0065; **Figure 3C**). A large fraction of mutated epitopes was predicted to be either more immunogenic (median: 63%, range: 22-79%) or unchanged in immunogenicity (median: 20%, range: 11-31%). Between 6% and 67% (median: 15%) of variant specific CD8 T cell recognized epitopes were predicted to be less immunogenic as a result of the mutation (**Figure S3B**). Furthermore, for each included SARS-CoV-2 variant, decreased binding affinity is predicted (≥2-fold change in IC50 value; **Figure 3D**) for a subset of the altered epitopes (median 48% of epitopes, range: 22%-75%). Between 25% and 59% (median: 44%) of altered epitopes retained their predicted binding affinity (neutral; 0.5< fold change in IC50 <2), and between 0% and 25% (median: 6%) of altered epitopes had an increased predicted binding affinity (≤0.5-fold change in IC50 value). Spike protein-derived CD8 T cell recognized epitopes of the Delta, Mu and AY.4.2 variants were predicted to have a significantly reduced binding affinity to the HLA as a result of their mutations (Delta: p=0.016, Mu: p=0.017, AY.4.2: p=0.0002; **Figure 3E**). Importantly, despite these statistically significant differences, these results are derived from only 8 to 14 (median: 12) unique CD8 T cell recognized epitopes that are mutated per variant, out of a total of 263 unique epitopes per variant.

Next, we tested whether variant-specific mutations may have a more profound effect on spike protein-derived CD8 T cell recognized epitopes compared to non-spike. We performed the analysis on non-spike protein-derived epitopes and compared these to the results above. As expected, a smaller fraction of CD8 T cell recognized epitopes in the SARS-CoV-2 spike protein were found to be conserved compared to those in non-spike proteins (median: 95.1%, range: 92.0-96.6%; versus median: 98.9%, range: 98.0-99.2%; **Figures S1C, D**). All epitopes overlapping with multi-amino acid substitutions, deletions and/or insertions except one were located in the SARS-CoV-2 spike protein (**Figures S1F, G**). Such multi-amino acid changes are expected to lead to a lower sequence similarity between altered and reference epitopes. In line with this, there was a significantly lower sequence similarity between mutated and reference CD8 T cell recognized epitopes in the spike protein, compared to the single-amino acid mutations in non-spike proteins (in variants Delta, p=0.043; AY.4.2, p=0.047; Omicron, p=0.028; **Figure 4A**).

Across the investigated SARS-CoV-2 variants, the fraction of CD8 T cell recognized epitopes with low (<85%) sequence similarity to reference epitopes was significantly higher in spike versus non-spike protein-derived epitopes (p=0.016, **Figure 4B**).

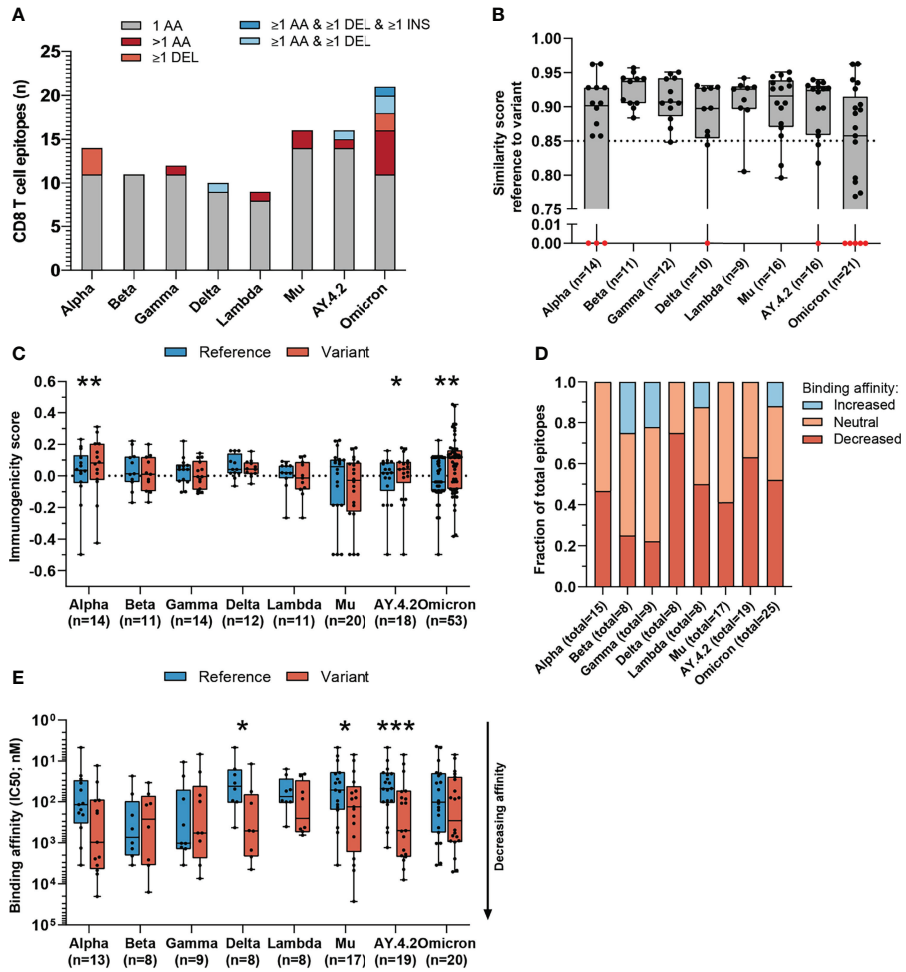


FIGURE 3 | Sequence similarity and predicted binding affinity of mutated CD8 T cell recognized epitopes derived from the spike protein. **(A)** Numbers of spike protein-derived CD8 T cell recognized epitopes per variant that harbor the indicated categories of mutations. **(B)** Sequence similarity scores between the spike protein-derived reference SARS-CoV-2 CD8 T cell recognized epitopes and the matched variant epitopes. Sequence similarity of epitopes in red is set to zero as a result of one or more deletions/insertions in the epitope sequence (Alpha, n = 3; Delta, n = 2; AY.4.2, n = 2; Omicron, n = 12) **(C)** Box plot indicating the predicted immunogenicity of the spike protein-derived reference SARS-CoV-2 CD8 T cell recognized epitopes and the altered epitopes according to the IEDB T cell class I pMHC immunogenicity prediction tool. **(D)** Fractions of total altered spike protein-derived CD8 T cell recognized epitopes where the predicted binding affinity of the epitope to the corresponding HLA restriction element was increased (≤0.5-fold change in IC50), remained neutral (0.5< fold change in IC50 <2) or was decreased (≥2-fold change in IC50) as a result of the mutation. **(E)** Box plot indicating the predicted binding affinity IC50 (nM) of the reference and altered spike protein-derived CD8 T cell recognized epitope to the corresponding HLA restriction element. Box plots indicate the median (line), 25th and 75th percentile (box), min and max (whiskers), and all data points (single circles). Statistical significance was tested with a two-tailed Wilcoxon matched-pairs signed rank test. Variation in numbers of epitopes in the analyses are due to inclusion of epitopes binding one or more HLA restriction elements. AA, amino acid; DEL, deletion; INS, insertion. *P < 0.05, **P < 0.01, ***P < 0.001. n indicates the number of epitopes analyzed per group.

Additionally, mutations in the spike protein of the Delta, Mu and AY.4.2 variants were more detrimental to predicted HLA binding affinity compared to non-spike protein mutations (Delta: p=0.019, Mu: p=0.025, AY.4.2: p=0.030; **Figure 4C**). In accordance with this, the fraction of CD8 T cell recognized epitopes with decreased predicted binding affinity was significantly higher in spike versus non-spike protein-derived epitopes across the variants (p=0.016, **Figure 4D**). However, despite these statistically significant differences, these results are derived from a limited number of unique mutated CD8 T cell recognized epitopes per variant.

The overrepresentation of altered CD8 T cell recognized epitopes with multiple amino acid changes, insertions and deletions in the spike protein is clearly pronounced. Accordingly, these epitopes are more profoundly affected in terms of epitope sequence similarity, predicted binding affinity and immunogenicity compared to non-spike protein derived epitopes. These results may be unrelated to T cell immunity and may be explained for example by the high rate of evolution of the spike protein due to natural selection pressure by antibody responses. In line with this, a substantial part (median: 65%, range: 36-75%) of the unique spike protein-derived CD8 T cell

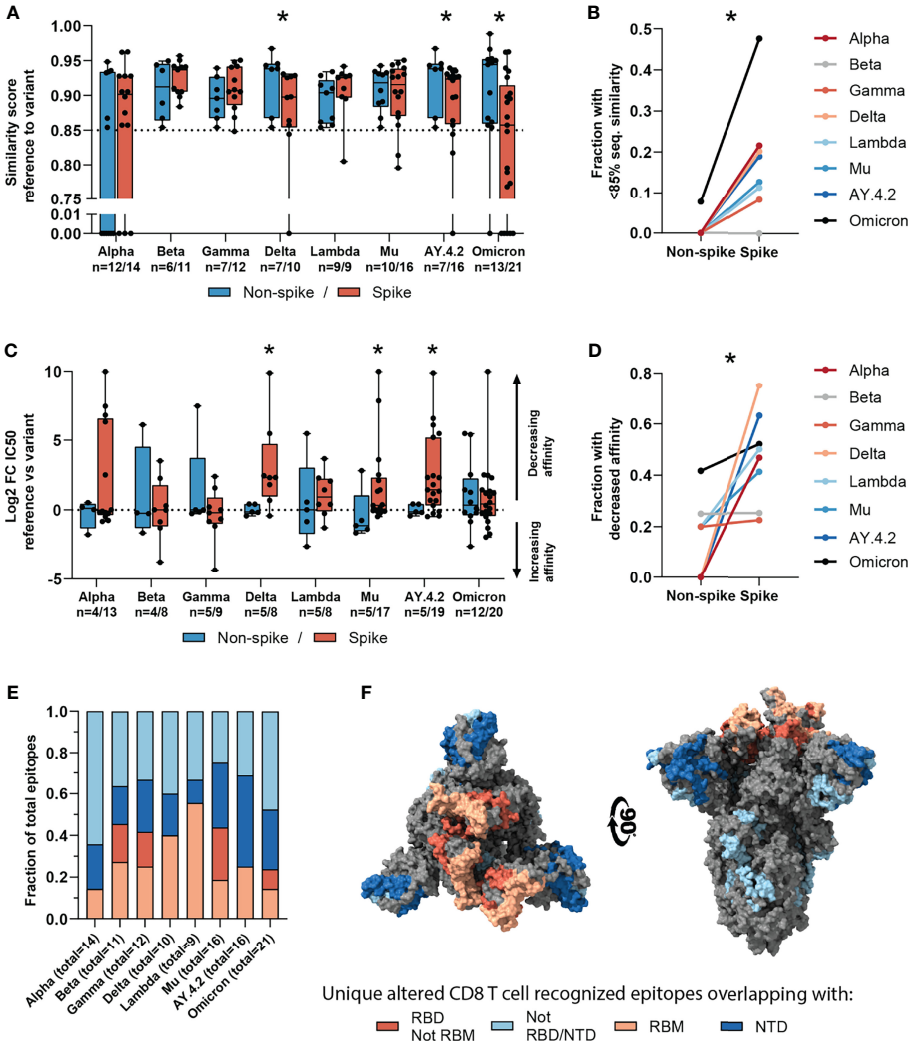


FIGURE 4 | Sequence similarity and predicted binding affinity of spike- versus non-spike-derived mutated CD8 T cell recognized epitopes. **(A)** Box plot comparing the sequence similarity of the altered spike and non-spike protein-derived CD8 T cell recognized epitopes, to the reference epitopes. Sequence similarity of indicated epitopes is set to zero as a result of one or more deletions/insertions in the epitope sequence (Alpha, n = 6/3; Delta, n = 0/2; AY.4.2, n = 0/2; Omicron, n = 1/12). **(B)** Fraction of spike versus non-spike protein-derived epitopes where the sequence similarity of the epitope to the reference epitope dropped below 85% as a result of the mutation. **(C)** Box plot comparing the log2 fold change in predicting binding affinity of spike and non-spike protein-derived CD8 T cell recognized epitopes to the corresponding HLA restriction element, as a result of the mutation. **(D)** Fraction of spike versus non-spike protein-derived CD8 T cell recognized epitopes where the predicted binding affinity of the epitope to the corresponding HLA restriction element was decreased (≥2-fold change in IC50) as a result of the mutation. **(E)** Fractions of unique spike protein-derived CD8 T cell recognized epitopes overlapping with a mutation located in the N-terminal domain (NTD), receptor-binding domain (RBD), receptor-binding motif (RBM) or a mutation located outside of these domains. **(F)** SARS-CoV-2 spike trimer in the open conformation with one erect RBD. Colors represent unique altered CD8 T cell recognized epitopes overlapping with the indicated domains. Image produced with ChimeraX using PDB accession: 6ZGG. Box plots indicate the median (line), 25th and 75th percentile (box), min and max (whiskers), and all data points (single circles). Statistical significance was tested with a two-tailed Mann–Whitney *U* test **(A, C)** or with a two-tailed Wilcoxon matched-pairs signed rank test **(B, D)**. Variation in numbers of epitopes in the analyses are due to inclusion of epitopes binding one or more HLA restriction elements. *P < 0.05. n indicates the number of epitopes analyzed per group.

recognized epitopes that overlap mutations were located in key domains that are associated with cell attachment and are antibody targets (N-terminal domain, NTD; receptor-binding domain, RBD; receptor-binding motif, RBM; **Figure 4E**). Moreover, they are primarily present on the surface of the spike protein, making them accessible to host antibodies (**Figure 4F**).

DISCUSSION

After the initial SARS-CoV-2 outbreak, SARS-CoV-2 variants Alpha, Delta and Omicron have replaced the previous variant as the globally dominant SARS-CoV-2 variant (31, 32). This is the result of accumulated mutations resulting in amino acid changes that have allowed these variants to evade immunity in the general

population. This notion is supported by for example data showing that serum from vaccine-recipients is less effective at neutralizing SARS-CoV-2 variants Delta and Omicron (23, 24). The mutations do not appear to prevent general cross-recognition of SARS-CoV-2 variants by T cells induced by reference SARS-CoV-2 (25–29). However, systematic data regarding the effect of SARS-CoV-2 variant-specific amino acid changes on the properties of the previously recognized CD8 T cell epitopes has been lacking.

Our analyses revealed that the vast majority of both the spike (median: 95.1%, range: 92.0-96.6%) and pan-proteome (median: 98.9%, range: 98.0-99.2%) derived CD8 T cell recognized epitopes were conserved in the investigated SARS-CoV-2 variants. In accordance with the experimental data described above, this suggests that memory T cell responses are not likely to be diminished upon re-infection by a different SARS-CoV-2 variant, or upon infection by one of the SARS-CoV-2 variants after vaccination. In addition, for the minority of presented CD8 T cell recognized epitopes that is altered by mutations, the high degree of sequence similarity to the reference epitopes will likely also not prevent cross-recognition by memory CD8 T cells.

The finding that CD8 T cell epitopes from SARS-CoV-2 were generally conserved is in accordance with the concept of antigenic drift. Antigenic drift driven by selective pressure from T cells is largely irrelevant in acute viral infections such as SARS-CoV-2 due to the huge polymorphism of HLA loci in a population and the diverse antigen repertoire these complexes present to T cells (9). Antigenic drift is likely to have a stochastic influence on T cell epitopes - a 'bystander effect'. Our observations are in line with this notion. First, for the minority of CD8 T cell recognized epitopes that overlap with mutations, epitope sequences are generally conserved in terms of sequence similarity to the reference sequence. Second, the majority (median: 55.6%, range: 46.2-78.6%) of these CD8 T cell recognized epitopes are predicted to possess unchanged or even increased binding affinity to the HLA allele as a result of the mutation. Third, the mutations in the CD8 T cell recognized epitopes in SARS-CoV-2 variants AY.4.2 and Omicron are predicted to result in more immunogenic, rather than less immunogenic T cell epitopes. Fourth, many of the observed changes in predicted binding affinity and sequence similarity of mutated CD8 T cell recognized epitopes in comparison to the reference epitopes, are indeed driven by mutations in the spike protein. Finally, the majority (median: 65%, range: 36-75%) of spike protein-derived CD8 T cell recognized epitopes that overlap with a mutation are located in key domains that are frequently recognized by antibody responses and/or are involved in cell attachment (10). Therefore, on the basis of our analysis and as expected, there is no indication of T cell based selective pressure on SARS-CoV-2 leading to alteration of the CD8 T cell recognized epitopes.

As SARS-CoV-2 derived T cell epitopes are not subject to substantial antigenic drift, T cells are likely to remain consistent in their recognition of infected cells. However, the stochastic influence by the mutations focused on the spike protein affects the ability of spike protein-derived T cell epitopes to be presented to the immune system or to be recognized by previously induced T cell responses. This is most pronounced for the SARS-CoV-2 variants Delta, AY.4.2 and Omicron, which are also most efficient at escaping humoral immunity as a result of numerous mutations in the spike protein. These variants also have the largest, albeit overall minor, negative effect on epitope presentation relative to the other SARS-CoV-2 variants. By only targeting the spike protein, the vaccine induced immunity is limited to SARS-CoV-2 T cell epitopes which are most prone to a 'bystander' effect as a result of the high mutation rate of the spike protein. Even though the currently approved vaccines only include the spike protein, our data suggest that T cell immunity can protect against severe COVID-19. However, it does seem like a logical approach to develop next generation vaccines incorporating other parts of the SARS-CoV-2 proteome which can lead to a broader T cell response providing protection should the spike protein undergo further changes over time.

DATA AVAILABILITY STATEMENT

The original contributions presented in the study are included in the article/**Supplementary Material**. Further inquiries can be directed to the corresponding author.

AUTHOR CONTRIBUTIONS

OI and SK performed the experiments, analyzed the data and wrote the manuscript. PK obtained the funding and supervised the study. All authors contributed to the article and approved the submitted version.

FUNDING

The project was funded with the Netherlands Cancer Institute Kvistborg group start-up funding.

SUPPLEMENTARY MATERIAL

The Supplementary Material for this article can be found online at: https://www.frontiersin.org/articles/10.3389/fimmu.2022.891524/full#supplementary-material

REFERENCES

1. Lam ME. United by the Global COVID-19 Pandemic: Divided by Our Values and Viral Identities. *Humanities Soc Sci Commun* (2021) 8:1–6. doi: 10.1057/s41599-020-00679-5
2. Lambert H, Gupte J, Fletcher H, Hammond L, Lowe N, Pelling M, et al. COVID-19 as a Global Challenge: Towards an Inclusive and Sustainable Future. *Lancet Planet Health* (2020) 4:e312–4. doi: 10.1016/S2542-5196(20)30168-6
3. Roberts DL, Rossman JS, Jarić I. Dating First Cases of COVID-19. *PloS Pathog* (2021) 17:e1009620. doi: 10.1371/journal.ppat.1009620

4. Worobey M. Dissecting the Early COVID-19 Cases in Wuhan. *Science* (2021) 374:1202–4. doi: 10.1126/science.abm4454
5. Amicone M, Borges V, Alves MJ, Isidro J, Zé-Zé L, Duarte S, et al. Mutation Rate of SARS-CoV-2 and Emergence of Mutators During Experimental Evolution. *bioRxiv* (2021) 2021. doi: 10.1101/2021.05.19.444774
6. Domingo E, Holland JJ. and Fitness for Survival. *Annu Rev Microbiol* (1997) 51:151–78. doi: 10.1146/annurev.micro.51.1.151
7. Sanjuán R, Domingo-Calap P. Mechanisms of Viral Mutation. *Cell Mol Life Sci* (2016) 73:4433–48. doi: 10.1007/s00018-016-2299-6
8. Duffy S, Shackelton LA, Holmes EC. Rates of Evolutionary Change in Viruses: Patterns and Determinants. *Nat Rev Genet* (2008) 9:267–76. doi: 10.1038/nrg2323
9. Yewdell JW. Antigenic Drift: Understanding COVID-19. *Immunity* (2021) 54:2681–7. doi: 10.1016/j.immuni.2021.11.016
10. Harvey WT, Carabelli AM, Jackson B, Gupta RK, Thomson EC, Harrison EM, et al. SARS-CoV-2 Variants, Spike Mutations and Immune Escape. *Nat Rev Microbiol* (2021) 19:409–24. doi: 10.1038/s41579-021-00573-0
11. Martin DP, Weaver S, Tegally H, San JE, Shank SD, Wilkinson E, et al. The Emergence and Ongoing Convergent Evolution of the SARS-CoV-2 N501Y Lineages. *Cell* (2021) 184:5189–200.e7. doi: 10.1016/j.cell.2021.09.003
12. Huang K-YA, Rijal P, Schimanski L, Powell TJ, Lin T-Y, McCauley JW, et al. Focused Antibody Response to Influenza Linked to Antigenic Drift. *J Clin Invest* (2015) 125:2631–45. doi: 10.1172/JCI81104
13. Das SR, Hensley SE, Ince WL, Brooke CB, Subba A, Delboy MG, et al. Defining Influenza A Virus Hemagglutinin Antigenic Drift by Sequential Monoclonal Antibody Selection. *Cell Host Microbe* (2013) 13:314–23. doi: 10.1016/j.chom.2013.02.008
14. Sun J, Zhuang Z, Zheng J, Li K, Wong RL-Y, Liu D, et al. Generation of a Broadly Useful Model for COVID-19 Pathogenesis, Vaccination, and Treatment. *Cell* (2020) 182:734–43.e5. doi: 10.1016/j.cell.2020.06.010
15. Luo M, Liu J, Jiang W, Yue S, Liu H, Wei S. IL-6 and CD8+ T Cell Counts Combined Are an Early Predictor of in-Hospital Mortality of Patients With COVID-19. *JCI Insight* (2020) 5(13):e139024. doi: 10.1172/jci.insight.139024
16. Liu Q, Fang X, Tokuno S, Chung U, Chen X, Dai X, et al. Prediction of the Clinical Outcome of COVID-19 Patients Using T Lymphocyte Subsets With 340 Cases From Wuhan, China: A Retrospective Cohort Study and a Web Visualization Tool. *Medrxiv* (2020). doi: 10.2139/ssrn.3557995
17. Du J, Wei L, Li G, Hua M, Sun Y, Wang D, et al. Persistent High Percentage of HLA-DRCD38 CD8 T Cells Associated With Immune Disorder and Disease Severity of COVID-19. *Front Immunol* (2021) 12:735125. doi: 10.3389/fimmu.2021.735125
18. Bergamaschi L, Mescia F, Turner L, Hanson AL, Kotagiri P, Dunmore BJ, et al. Longitudinal Analysis Reveals That Delayed Bystander CD8+ T Cell Activation and Early Immune Pathology Distinguish Severe COVID-19 From Mild Disease. *Immunity* (2021) 54:1257–75.e8. doi: 10.1016/j.immuni.2021.05.010
19. McMahan K, Yu J, Mercado NB, Loos C, Tostanoski LH, Chandrashekar A, et al. Correlates of Protection Against SARS-CoV-2 in Rhesus Macaques. *Nature* (2020) 590:630–4. doi: 10.1038/s41586-020-03041-6
20. *Tracking SARS-CoV-2 Variants*. Available at: https://www.who.int/activities/tracking-SARS-CoV-2-variants (Accessed March 2, 2022).
21. SARS-CoV-2 Variants of Concern as of 24 February 2022, in: *European Centre for Disease Prevention and Control*. Available at: https://www.ecdc.europa.eu/en/covid-19/variants-concern (Accessed March 2, 2022).
22. Hadfield J, Megill C, Bell SM, Huddleston J, Potter B, Callender C, et al. Nextstrain: Real-Time Tracking of Pathogen Evolution. *Bioinformatics* (2018) 34:4121–3. doi: 10.1093/bioinformatics/bty407
23. Davis C, Logan N, Tyson G, Orton R, Harvey WT, Perkins JS, et al. Reduced Neutralisation of the Delta (B.1.617.2) SARS-CoV-2 Variant of Concern Following Vaccination. *PloS Pathog* (2021) 17:e1010022. doi: 10.1371/journal.ppat.1010022
24. Planas D, Saunders N, Maes P, Guivel-Benhassine F, Planchais C, Buchrieser J, et al. Considerable Escape of SARS-CoV-2 Omicron to Antibody Neutralization. *Nature* (2022) 602:671–5. doi: 10.1038/s41586-021-04389-z
25. Jordan SC, Shin B-H, Gadsden T-AM, Chu M, Petrosyan A, Le CN, et al. T Cell Immune Responses to SARS-CoV-2 and Variants of Concern (Alpha and Delta) in Infected and Vaccinated Individuals. *Cell Mol Immunol* (2021) 18:2554–6. doi: 10.1038/s41423-021-00767-9
26. Tarke A, Sidney J, Methot N, Yu ED, Zhang Y, Dan JM, et al. Impact of SARS-CoV-2 Variants on the Total CD4 and CD8 T Cell Reactivity in Infected or Vaccinated Individuals. *Cell Rep Med* (2021) 2:100355. doi: 10.1016/j.xcrm.2021.100355
27. Melo-González F, Soto JA, González LA, Fernández J, Duarte LF, Schultz BM, et al. Recognition of Variants of Concern by Antibodies and T Cells Induced by a SARS-CoV-2 Inactivated Vaccine. *Front Immunol* (2021) 10:747830. doi: 10.3389/fimmu.2021.747830
28. Thiruvengadam R, Awasthi A, Medigeshi G, Bhattacharya S, Mani S, Sivasubbu S, et al. Effectiveness of ChAdOx1 Ncov-19 Vaccine Against SARS-CoV-2 Infection During the Delta (B.1.617.2) Variant Surge in India: A Test-Negative, Case-Control Study and a Mechanistic Study of Post-Vaccination Immune Responses. *Lancet Infect Dis* (2021) 22(4):473–82. doi: 10.1016/S1473-3099(21)00680-0
29. Keeton R, Tincho MB, Ngomti A, Baguma R, Benede N, Suzuki A, et al. T Cell Responses to SARS-CoV-2 Spike Cross-Recognize Omicron. *Nature* (2022) 603:488–92. doi: 10.1038/s41586-022-04460-3
30. Martínez-Flores D, Zepeda-Cervantes J, Cruz-Reséndiz A, Aguirre-Sampieri S, Sampieri A, Vaca L. SARS-CoV-2 Vaccines Based on the Spike Glycoprotein and Implications of New Viral Variants. *Front Immunol* (2021) 12:701501. doi: 10.3389/fimmu.2021.701501
31. Elbe S, Buckland-Merrett G. Data, Disease and Diplomacy: GISAID's Innovative Contribution to Global Health. *Global Challenges* (2017) 1:33–46. doi: 10.1002/gch2.1018
32. *Outbreak.Info*. Available at: https://outbreak.info/ (Accessed March 2, 2022).
33. IEDB.org. *Free Epitope Database and Prediction Resource*. Available at: http://www.iedb.org (Accessed March 2, 2022).
34. Vita R, Mahajan S, Overton JA, Dhanda SK, Martini S, Cantrell JR, et al. The Immune Epitope Database (IEDB): 2018 Update. *Nucleic Acids Res* (2019) 47:D339–43. doi: 10.1093/nar/gky1006
35. Frankild S, de Boer RJ, Lund O, Nielsen M, Kesmir C. Amino Acid Similarity Accounts for T Cell Cross-Reactivity and for "Holes" in the T Cell Repertoire. *PloS One* (2008) 3:e1831. doi: 10.1371/journal.pone.0001831
36. Dhanda SK, Vaughan K, Schulten V, Grifoni A, Weiskopf D, Sidney J, et al. Development of a Novel Clustering Tool for Linear Peptide Sequences. *Immunology* (2018) 155:331–45. doi: 10.1111/imm.12984
37. Calis JJA, Maybeno M, Greenbaum JA, Weiskopf D, De Silva AD, Sette A, et al. Properties of MHC Class I Presented Peptides That Enhance Immunogenicity. *PloS Comput Biol* (2013) 9:e1003266. doi: 10.1371/journal.pcbi.1003266
38. Reynisson B, Alvarez B, Paul S, Peters B, Nielsen M. NetMHCpan-4.1 and NetMHCIIpan-4.0: Improved Predictions of MHC Antigen Presentation by Concurrent Motif Deconvolution and Integration of MS MHC Eluted Ligand Data. *Nucleic Acids Res* (2020) 48:W449–54. doi: 10.1093/nar/gkaa379
39. *Home - GraphPad*. Available at: www.graphpad.com (Accessed March 2, 2022).
40. Shu Y, McCauley J. GISAID: Global Initiative on Sharing All Influenza Data - From Vision to Reality. *Euro Surveill* (2017) 22(13):30494. doi: 10.2807/1560-7917.ES.2017.22.13.30494
41. IEDB.org. *Free Epitope Database and Prediction Resource*. Available at: http://www.iedb.org.
42. Lee JK, Stewart-Jones G, Dong T, Harlos K, Di Gleria K, Dorrell L, et al. T Cell Cross-Reactivity and Conformational Changes During TCR Engagement. *J Exp Med* (2004) 200:1455–66. doi: 10.1084/jem.20041251
43. Kvistborg P, Philips D, Kelderman S, Hageman L, Ottensmeier C, Joseph-Pietras D, et al. Anti-CTLA-4 Therapy Broadens the Melanoma-Reactive CD8+ T Cell Response. *Sci Transl Med* (2014) 6:254ra128. doi: 10.1126/scitranslmed.3008918
44. Gangaev A, Ketelaars SLC, Isaeva OI, Patiwael S, Dopler A, Hoefakker K, et al. Identification and Characterization of a SARS-CoV-2 Specific CD8+ T Cell Response With Immunodominant Features. *Nat Commun* (2021) 12:1–14. doi: 10.1038/s41467-021-22811-y
45. COVID-19 Situation Update Worldwide, as of Week 7, Updated 24 February 2022 in: *European Centre for Disease Prevention and Control*. Available at: https://www.ecdc.europa.eu/en/geographical-distribution-2019-ncov-cases (Accessed March 2, 2022).
46. Ritchie H, Mathieu E, Rodés-Guirao L, Appel C, Giattino C, Ortiz-Ospina E, et al. Coronavirus Pandemic (COVID-19). In: *Our World in Data*. (2020).

Available at: https://ourworldindata.org/coronavirus (Accessed March 2, 2022).

Conflict of Interest: The authors declare that the research was conducted in the absence of any commercial or financial relationships that could be construed as a potential conflict of interest.

Publisher's Note: All claims expressed in this article are solely those of the authors and do not necessarily represent those of their affiliated organizations, or those of the publisher, the editors and the reviewers. Any product that may be evaluated in this article, or claim that may be made by its manufacturer, is not guaranteed or endorsed by the publisher.

Copyright © 2022 Isaeva, Ketelaars and Kvistborg. This is an open-access article distributed under the terms of the Creative Commons Attribution License (CC BY). The use, distribution or reproduction in other forums is permitted, provided the original author(s) and the copyright owner(s) are credited and that the original publication in this journal is cited, in accordance with accepted academic practice. No use, distribution or reproduction is permitted which does not comply with these terms.

frontiers | Frontiers in Immunology

ORIGINAL RESEARCH
published: 10 June 2022
doi: 10.3389/fimmu.2022.886431

Remodeling of T Cell Dynamics During Long COVID Is Dependent on Severity of SARS-CoV-2 Infection

Milena Wiech[1†], Piotr Chroscicki[1†], Julian Swatler[1‡], Dawid Stepnik[1‡], Sara De Biasi[2], Michal Hampel[3], Marta Brewinska-Olchowik[1], Anna Maliszewska[3], Katarzyna Sklinda[4], Marek Durlik[3,5], Waldemar Wierzba[6,7], Andrea Cossarizza[2,8] and Katarzyna Piwocka[1]*

[1] Laboratory of Cytometry, Nencki Institute of Experimental Biology, Polish Academy of Sciences, Warsaw, Poland, [2] Department of Medical and Surgical Sciences for Children and Adults, University of Modena and Reggio Emilia School of Medicine, Modena, Italy, [3] Department of Gastroenterological Surgery and Transplantology, Central Clinical Hospital of the Ministry of Interior, Warsaw, Poland, [4] Department of Radiology, Centre of Postgraduate Medical Education, Warsaw, Poland, [5] Departament of Gastroenterological Surgery and Transplantology, Centre of Postgraduate Medical Education, Warsaw, Poland, [6] Central Clinical Hospital of the Ministry of Interior, Warsaw, Poland, [7] University of Humanities and Economics, Lodz, Poland, [8] National Institute for Cardiovascular Research, Bologna, Italy

OPEN ACCESS

Edited by:
Veronika Zarnitsyna, Emory University, United States

Reviewed by:
Benjamin Bonnet, Centre Hospitalier Universitaire de Clermont-Ferrand, France
Joy Phillips, San Diego State University, United States

***Correspondence:**
Katarzyna Piwocka
k.piwocka@nencki.edu.pl

[†]These authors have contributed equally to this work

[‡]These authors have contributed equally to this work

Specialty section:
This article was submitted to T Cell Biology, a section of the journal Frontiers in Immunology

Received: *28 February 2022*
Accepted: *22 April 2022*
Published: *10 June 2022*

Citation:
Wiech M, Chroscicki P, Swatler J, Stepnik D, De Biasi S, Hampel M, Brewinska-Olchowik M, Maliszewska A, Sklinda K, Durlik M, Wierzba W, Cossarizza A and Piwocka K (2022) Remodeling of T Cell Dynamics During Long COVID Is Dependent on Severity of SARS-CoV-2 Infection. Front. Immunol. 13:886431. doi: 10.3389/fimmu.2022.886431

Several COVID-19 convalescents suffer from the post-acute COVID-syndrome (PACS)/long COVID, with symptoms that include fatigue, dyspnea, pulmonary fibrosis, cognitive dysfunctions or even stroke. Given the scale of the worldwide infections, the long-term recovery and the integrative health-care in the nearest future, it is critical to understand the cellular and molecular mechanisms as well as possible predictors of the longitudinal post-COVID-19 responses in convalescent individuals. The immune system and T cell alterations are proposed as drivers of post-acute COVID syndrome. However, despite the number of studies on COVID-19, many of them addressed only the severe convalescents or the short-term responses. Here, we performed longitudinal studies of mild, moderate and severe COVID-19-convalescent patients, at two time points (3 and 6 months from the infection), to assess the dynamics of T cells immune landscape, integrated with patients-reported symptoms. We show that alterations among T cell subsets exhibit different, severity- and time-dependent dynamics, that in severe convalescents result in a polarization towards an exhausted/senescent state of CD4+ and CD8+ T cells and perturbances in CD4+ Tregs. In particular, CD8+ T cells exhibit a high proportion of CD57+ terminal effector cells, together with significant decrease of naïve cell population, augmented granzyme B and IFN-γ production and unresolved inflammation 6 months after infection. Mild convalescents showed increased naïve, and decreased central memory and effector memory CD4+ Treg subsets. Patients from all severity groups can be predisposed to the long COVID symptoms, and fatigue and cognitive dysfunctions are not necessarily related to exhausted/senescent state and T cell dysfunctions, as well as unresolved inflammation that was found only in severe convalescents. In conclusion, the post-COVID-19 functional remodeling of T cells could be seen as a two-step process, leading to distinct convalescent immune states at 6 months after infection. Our data imply that attenuation of the functional polarization

together with blocking granzyme B and IFN-γ in CD8+ cells might influence post-COVID alterations in severe convalescents. However, either the search for long COVID predictors or any treatment to prevent PACS and further complications is mandatory in all patients with SARS-CoV-2 infection, and not only in those suffering from severe COVID-19.

Keywords: COVID-19, long COVID, post-acute COVID-syndrome (PACS), convalescents, immune system, T cell exhaustion/senescence, inflammation resolution, full spectral cytometry

INTRODUCTION

COVID-19 disease, caused by severe acute respiratory syndrome coronavirus 2 (SARS-CoV-2), has emerged at the end of 2019 and has become an ongoing pandemic, as officially declared by the WHO in March 2020 (1–3). Although SARS-Cov-2 infection and the course of COVID-19 illness is mild in a large proportion of infected individuals (4), a number of patients develop severe symptoms that can result in a fatal event (5–9). To date, there have been over 499 million globally reported cases and over 6,1 mln COVID-19–related deaths (Johns Hopkins Coronavirus Resource Center. Johns Hopkins website. https://coronavirus.jhu.edu/; updated 11th April 2022).

Number of studies have already indicated that several individuals convalescent from COVID-19 suffer from the post-acute COVID-syndrome (PACS), also referred to as "long COVID", that is characterized, among others, by long-lasting symptoms, such as fatigue, dyspnea, pulmonary fibrosis, stroke, and other cerebrovascular events, as well as cognitive and neurological dysfunctions (2, 10). This significantly affects both the quality of life and everyday activities, and is also relevant in terms of future medical treatments. Although the majority of long-term studies have concentrated on patients experiencing a severe form of COVID-19, recent data show that different types of PACS-related symptoms can be found not only in them, but also in mild and even asymptomatic cases, although in such cases, the immune landscape and possible mechanisms are far less clear (11–15). However, despite the number of studies on COVID-19, little is known about the mechanisms, nor about molecular and cellular changes in these long-term effects, as well as about the presence of possible predictors. Nevertheless, changes in the peripheral immune system, which persist long after the infection is cleared, might have potential implications for understanding symptoms and identify predictors associated with long COVID (14, 16–18). Therefore, given the scale of the worldwide infections, the long-term recovery and the integrative health-care in the future perspective, it is critical to understand molecular and cellular mechanisms of immune responses in convalescent individuals of different severity of the disease.

The immune system immediately responds to infection with SARS-CoV-2 (19), and several perturbations in individuals with severe infection have been described in detail since the earliest moments of the pandemic (20–24). Systemic inflammation and markedly high levels of proinflammatory cytokines in plasma, named "cytokine storm", are characteristic for COVID-19 severe patients and are recognized as clinical predictors of disease outcome and mortality (25, 26). Therefore coordinated resolution of inflammation is necessary for successful recovery from acute infection, as persistent inflammatory state can lead to dysregulated immune responses (27–29).

Most severe COVID-19 convalescents have a low number of monocytes, helper T cells, memory B cells and proliferating lymphocytes over time (30, 31). Several reports showed that COVID-19 convalescence may be long and characterized by dysregulation of adaptive immunity, regarding specific CD4+ and CD8+ T cells, that express exhaustion markers for months after symptom onset (14, 32). Those alterations are associated with diminished immune activation and proinflammatory signaling (including IFN-γ, TNF-α, IL-2, IL-6) (26, 27). Finally, plasma level of inflammatory proteins, including IFN-γ, IL-6, and TNF-α, which is elevated during acute infection (26, 33), resolves over time in patients who fully recover after severe COVID-19, but remains elevated in patients with ineffective resolution of inflammation, leading to progression into persistent chronic inflammation (31). However, long-lasting studies of the immune landscape upon COVID-19 recovery are still not complete and crucial questions remain about the long-term immune responses due to COVID-19 of different severity. One of the open questions concerns the role of the severity of the infection in causing alterations in functionality and activity of immune cells in convalescent patients, and in other post-COVID-19 long-lasting symptoms.

Here, we describe our longitudinal studies of convalescent patients who had experienced a mild, moderate or severe COVID-19, who were interrogated at two time-points (up to 3 and 6 months from the diagnosis), to assess the dynamics of immune changes of post-COVID-19. Using classical and spectral cytometry, followed by unsupervised analysis, we report an in-depth characterization of phenotypic and functional remodeling of different T cell subsets during recovery from COVID-19. Long-lasting immune changes are then interpreted taking into account T cell polyfunctionality and the levels of plasmatic inflammatory markers.

Finally, we discuss whether the observed changes are related to the development of PACS symptoms, depending on the severity of the disease. The immune spectrum and T cell polyfunctionality undergo significant dynamics during COVID-19 recovery, which result in the very different landscapes and distinct convalescent immune states at 3 or 6 months after the infection. We also describe how several immune changes and PACS symptoms are severity-dependent, being more frequent in severe convalescents, but also appearing in individuals who recovered from mild and moderate COVID-19.

METHODS

Ethics Statement

The study protocol was approved by the ethics committee of the Central Clinical Hospital of the Internal Affairs and Administration Ministry in Warsaw (Decision No 151/2020) with informed consent of enrolled individuals. The study was performed in accordance with the latest version of the Declaration of Helsinki and the guidelines for good clinical practice.

Stratification of COVID-19 Patients

A total of 59 male COVID-19 recovered patients between 27-64 years of age were included in the study and divided into three age-matched groups according to the severity of disease measured by the size of lung lesions confirmed by computed tomography scan and the type of applied oxygen therapy. All patients were hospitalized over the period of 25th June - 3rd November 2020 or 13th March – 23rd April 2021 at the Central Clinical Hospital of the Ministry of Interior and Administration in Warsaw. In all cases, the SARS-CoV-2 infection was confirmed by positive RT-PCR test and indicated a day of diagnosis (genotyping of viral variant was not performed; however at that time the alpha variant was dominant in Poland while the first cases of delta variant have been identified in June 2021). Patients with severe COVID-19 symptoms were selected based on the coverage of lung parenchyma with ground-glass opacities (GGO) at the range of 20 – 83% and treatment by active or passive high-flow oxygen supply (>15 l/min). Patients with moderate COVID-19 symptoms had GGO occupying 5 – 19% of lung parenchyma and were treated with low-flow oxygen supply (≤15 l/min). Patients with mild COVID-19 symptoms had GGO below 5% of lung parenchyma and received low-flow or no oxygen supply during hospitalization. Dexamethasone was applied during hospitalization to 19 of severe (out of 22), 13 of moderate (out of 21) and 6 of mild (out of 16) patients, following the clinical recommendations, and any immunomodulatory drug has not been applied. The age-matched group of 13 men without medical history of any coronavirus infections and no IgG antibodies against SARS-CoV-2 S1/S2 in the peripheral blood served as a reference group (healthy). Patients were interrogated at two time-points: time-point I up to 3 months and time-point II up to 6 months from the diagnosis. None of the analyzed convalescents or healthy controls underwent anti-COVID-19 vaccine before blood donation, none of the convalescents included in the studies was re-infected with SARS-CoV-2 till the follow-up interview. The detailed information is present in **Supplementary Table 1**.

Blood Collection and Isolation of Mononuclear Cells

30 mL of peripheral blood was collected from each patient in vacuettes containing ethylenediamine-tetraacetic acid. Blood was immediately processed. Plasma was collected after centrifugation of whole blood at 150 rcf for 15 minutes at RT. Collected supernatant (*i.e.* plasma) has been transferred to a clean 15 mL conical tube and centrifuged at 2120 rcf for 15 minutes at + 4°C to deplete platelets and residual cells. Following centrifugation, plasma was aliquoted and stored at - 80°C until use. Isolation of peripheral blood mononuclear cells (PBMC) was performed using ficoll-hypaque (Lymphoprep, Stem Cell) according to standard procedures (34). PBMC were then stored in cryovials at the concentration of 4–10x10^6/mL in liquid nitrogen in fetal bovine serum supplemented with 10% dimethyl sulfoxide. To avoid and minimize the so-called "batch effect" and variability due to processing across long timespan and to increase data quality and reproducibility, 12 (for cytokine staining) or 24 (for phenotyping) samples were thawed simultaneously, stained using one master antibodies cocktail and acquired with the same instrument settings. Measurements were taken from individual patients; in the case of plasma, each measurement was performed in duplicate and only the mean was considered and shown.

Quantification of Cytokine and Antibody Levels in Blood Plasma

The plasma levels of 13 molecular species was quantified using a BioLegend platform (LEGENDplex™ HU Essential Immune Response Panel (13-plex), BioLegend) for the simultaneous detection of the following molecules: IL-4, IL-2, CXCL10 (IP-10), IL-1β, TNF-α, CCL2 (MCP-1), IL-17A, IL-6, IL-10, IFN-γ, IL-12p70, CXCL8 (IL-8), TGF-β1, according to the manufacturer's instruction. The level of IgG and IgM antibodies against SARS-CoV-2 was measured using quantitative chemiluminescence immunoassay according to the manufacturer's instruction (DiaSorin).

T Cell Immunophenotype by Polychromatic Full Spectrum Flow Cytometry

Thawed PBMCs were washed with RPMI 1640 supplemented with 10% fetal bovine serum and 1% each of l-glutamine, sodium pyruvate, nonessential amino acids, antibiotics, 0.1 M HEPES, 55 μM β-mercaptoethanol and 0.02 mg/ml DNAse. After the second washing step using PBS, PBMCs were counted and stained with viability dye Live/Dead Blue (Thermo Fisher Scientific) and a panel of 24 fluorescent mAbs for surface staining: CD45-Krome Orange, CD3-APC-AF750, CD4-cFluor 584, CD8-BV510, CD127-APC-R700, CD25-BV421, CD45RA-BUV395, CCR7-BV785, CD27-PECy7, CD28-BUV737, CD38-APCFire810, CD57-Pacific Blue, HLA-DR-BUV805, CD95-PECy5, PD1-BV650, CCR6-BV711, CCR4-BB700, CD161-PerCP, CD73-BUV496, ICOS-BUV563, BTLA-BUV661, CCR8-PE-Dazzle 594, CD39-PECy5.5, TIGIT-BV605. Cells were washed twice with PBS, and fixed/permeabilized with eBioscience Foxp3 Transcription Factor Staining Buffer Set (Thermo Fisher Scientific). Then cells were stained with additional mAbs for intracellular staining: Foxp3-APC, Helios-FITC, RORγt-PE. Along with side and forward scatter signals, signals were obtained from all the fluorochrome-labeled mAbs. A minimum of 1,000,000 cells per sample were acquired on an Cytek Aurora flow cytometer (Cytek Biosciences). For optimal unmixing of results, for less abundant and dim markers reference controls have been prepared with the use of UltraComp eBeads

Compensation Beads (Thermo Fisher Scientific) - CD25-BV421, PD1-BV650, CCR6-BV711, CCR4-BB700, CD161-PerCP, CD73-BUV496, ICOS-BUV563, BTLA-BUV661, CCR8-PE-Dazzle 594, CD39-PECy5.5, TIGIT-BV605, Foxp3-APC, Helios-FITC, RORgt-PE. In case of abundant surface markers, the single staining has been done on cells (PBMCs) - CD45-Krome Orange, CD3-APC-AF750, CD4-cFluor584, CD8-BV510, CD127-APC-R700, CD45RA-BUV395, CD27-PECy7, CD28-BUV737, CD38-APCFire810, CD57-Pacific Blue, HLA-DR-BUV805, CD95-PECy5. All antibodies used are presented in **Supplementary Table 3**. Analysis of cellular phenotypes was performed using FlowJo software (Becton Dickinson).

In Vitro Stimulation and Intracellular Staining of Cytokines and Foxp3 Using Full Spectrum Cytometry

For functional assays on cytokine production by T cells, thawed isolated PBMCs were cultured overnight in RPMI 1640 supplemented with 10% fetal bovine serum and 1% each of L-glutamine, sodium pyruvate, nonessential amino acids, antibiotics, 0,1 M HEPES, 55 μM β-mercaptoethanol. After the resting step, cells were counted and stimulated for 16 h at 37°C in a 5% CO2 atmosphere with anti-CD3/CD28 (1 μg/mL) in the U-bottom 96-well plate containing complete culture medium. For each sample, at least $2x10^6$ ($2 - 4 x10^6$) cells were left unstimulated as negative control, and at least 2 million (2 - 4 mln) cells were stimulated. All samples were incubated with a protein transport inhibitor containing brefeldin A (GolgiPlug, BD), monensin (GolgiStop, BD) and previously titrated concentration of CD107a-AF488. After stimulation, cells were stained with eFluor 455UV fixable viability dye (Thermo Fisher Scientific) and surface mAbs recognizing CD4-AF700, and CD8-APC-Cy7 (BioLegend). Cells were washed with PBS, and fixed and permeabilized with the eBioscience Foxp3/Transcription Factor Staining Buffer Set (Thermo Fisher Scientific) for detection of intracellular/nuclear antigens. Cells were next stained with previously titrated mAbs recognizing CD3-BUV496 (Becton Dickinson), Foxp3 PE (Thermo Fisher Scientific), TGF-β BV421 (Becton Dickinson), IL-17-PE-Cy7, TNF-α-BV605, IFN-γ-BV510, IL-2-APC, or granzymeB-PerCP-Cy5.5 (Biolegend). All antibodies used are presented in **Supplementary Table 3**. Then, a minimum of 700,000 cells per sample were acquired on the Cytek Aurora cytometer (Cytek Bioscience). Spectral unmixing has been done using UltraComp eBeads Compensation Beads (Thermo Fisher Scientific) stained separately with each individual antibody. Samples were analyzed using SpectroFlo (Cytek Bioscience) software by standard gating to eliminate aggregates and dead cells, and to identify CD3+ T cells divided into CD4+ T cells and CD8+ T cells. Additionally among CD4+ cells, regulatory T cells (Tregs) have been distinguished on the basis of Foxp3 transcription factor expression. In each group of cells the levels of above mentioned cytokines have been measured and analyzed. Manual analysis of populations producing individual cytokines was performed using SpectroFlo software and GraphPad Prism for statistics and visualization. Statistics has been done using one-way ANOVA test (* $p \leq 0,05$; ** $p \leq 0,01$; *** $p \leq 0,001$), data are shown as Mean ± SD.

Representation of High-Parameter Flow Cytometry (Phenotypes)

Compensated and cleaned by FlowAI Flow Cytometry Standard (FCS) 3.0 files were imported into FlowJo software version 10 (Becton Dickinson, San Josè, CA) and preprocessed by removing damaged cells and doublets. Then were selected live, undamaged CD45+CD3+CD4+ subpopulation (CD4+ T cell subset), CD45+CD3+CD8+ (CD8+ T cell subset) and CD45+CD3+CD4+CD25+CD127- (Treg cell subset). Collected subsets were normalized using cytoNorm and gaussNorm methods. All subsets were downsampled (35 000 cells per sample for CD4+ and CD8+ T cell subset and 3 000 cells for Treg subset). All downsampled cells were exported for further analysis in R using Bioconductor libraries CATALYST (version 1.16.2) and diffcyt (version 1.12.0). The data were transformed using arcsine cofactor to make distributions more symmetric and to map them to the comparable range of expression. Outliers samples were filtered out. The cell population identification was performed through unsupervised clustering using the FlowSOM (version 2.0.0) algorithm (K= 20 for CD4+ T and CD8+ T and 6 for Treg cells subset). 2D visual representation was performed applying Uniform Manifold Approximation and Projection (UMAP) on 1000 cells per sample. Then, clusters with similar distribution were merged. Statistical analysis was performed using generalized linear mixed models (GLMM) applying as FDR cutoff = 0.05.

Representation of High-Parameter Flow Cytometry (Cytokines)

Compensated and cleaned by FlowAI Flow Cytometry Standard (FCS) 3.0 files were imported into FlowJo software version 10 (Becton Dickinson, San Josè, CA) and preprocessed by removing damaged cells and doublets. Then were selected live, undamaged CD3+CD4+ subpopulation (CD4+ T cell subset), CD3+CD8+ (CD8+ T cell subset) and CD3+CD4+FoxP3+ (Treg cell subset). All subsets were downsampled (40 000 cells per sample for CD4+ and CD8+ T cell subset and 3 400 cells for Treg subset). All downsampled cells were exported for further analysis in R using Bioconductor libraries CATALYST (version 1.16.2) and diffcyt (version 1.12.0). The data were transformed using arcsine cofactor to make distributions more symmetric and to map them to the comparable range of expression. Outliers samples were filtered out. The cell population identification was performed through unsupervised clustering using the FlowSOM (version 2.0.0) algorithm (K= 30). 2D visual representation was performed applying Uniform Manifold Approximation and Projection (UMAP) on 1000 cells per sample. Then, clusters with similar distribution were merged. Statistical analysis was performed using generalized linear mixed models (GLMM) applying as FDR cutoff = 0.05.

Statistical Analysis

Statistical analyses were performed using Prism 6.0 (GraphPad Software Inc, la Jolla, USA). Quantitative variabilities were compared using a two-sided Mann-Whitney test, non-parametric T-test, or one-way ANOVA test, as indicated. For unsupervised analysis, the statistical analysis of grouped data

(with non-normal distribution) was performed using generalized linear mixed models (GLMM) applying FDR cutoff = 0.05. Data are presented as individual values, means and standard errors of the mean. * p<0,05; ** p<0,01; *** p<0,001; **** p<0,0001.

RESULTS

Characteristics of the Study Participants

We have enrolled a total of 59 patients (all male) at the age of 27-64, who have recovered from COVID-19 disease. All patients were diagnosed with SARS-CoV-2 infection based on a positive RT-PCR test from a nasopharyngeal swab specimen. If necessary, lung pneumonia was evaluated by a CT scan. Depending on the disease course of COVID-19, no oxygen supply or the therapy including low-flow oxygen supply (≤15 l/min; 51 patients) or high-flow oxygen supply (>15 l/min; 4 patients) was applied. **Supplementary Table 1** shows detailed individual clinical characteristics of all patients. 36 patients had COVID-19 comorbidities, among which hypertension (18 patients), smoking (10 patients) and obesity (9 patients) were the most common (all identified comorbidities are shown in **Supplementary Table 2**). For the presented study, patients were stratified based on the size of ground glass opacities (GGO, measured as percentage of lung parenchyma by CT) and type of the oxygen supply received. Patients were divided into 3 COVID-19 severity groups: mild (GGO ≤ 5, low-flow or without oxygen supply; n=16) moderate (GGO>5 and ≤20, low-flow oxygen supply; n=21) and severe (GGO≥21 or high-flow oxygen supply; n=22) (**Table 1** and **Supplementary Table 1**). Following COVID-19 recovery, peripheral blood was collected at two time regimes: up to 3 months (time-point I) and up to 6 months (time-point II) after the diagnosis, to investigate short- and long-lasting responses of the adaptive immune system in COVID-19 convalescents. None of the patients was either vaccinated against COVID-19 or re-infected with SARS-CoV-2 virus till the follow-up interview. This was followed by analysis of the most common post-COVID-19 syndrome symptoms, such as fatigue, dyspnea and cognitive dysfunctions, to check whether any of these symptoms might correlate with the observed immunological changes. The experimental pipeline of the study is presented on **Figure 1A**. The group of 13 age- and

TABLE 1 | Patients stratification into the COVID-19 severity groups: Healthy, Mild, Moderate and Severe.

COVID-19 severity group	Cumulative				Time-point I		Time-point II	
					14-90 days since diagnosis		91-180 days since diagnosis	
	n	Age	CT lung scan GGO [%]	Type of oxygen therapy	n	Age	n	Age
HEALTHY	13	47 (29-59)	NA	NA	NA	NA	NA	NA
MILD	16	45 (35-59)	2 (0-5)	-/low-flow passive	15	46 (35-59)	13	41 (35-53)
MODERATE	21	44 (27-63)	12 (6-20)	low-flow passive	20	44,5 (30-63)	12	43,5 (27-63)
SEVERE	22	46 (33-64)	34,5 (16-83)	passive/active	20	46 (33-64)	11	52 (36-64)

NA, not applicable.

All patients were hospitalized over the period of 25th June - 3rd November 2020 or 13th March – 23rd April 2021 at the Central Clinical Hospital of the Ministry of Interior and Administration in Warsaw. Selection is based on the size of ground glass opacities (GGO) measured as percentage of lung parenchyma by CT lung scan and type of the oxygen therapy: low-flow or without oxygen supply (mild), low-flow passive oxygen supply (moderate) and high-flow oxygen supply/active oxygen supply (severe). Age is shown as median with range in years. Cumulative data of all patients included into studies as well as data for patients analysed in each time-point (I and II) are shown.

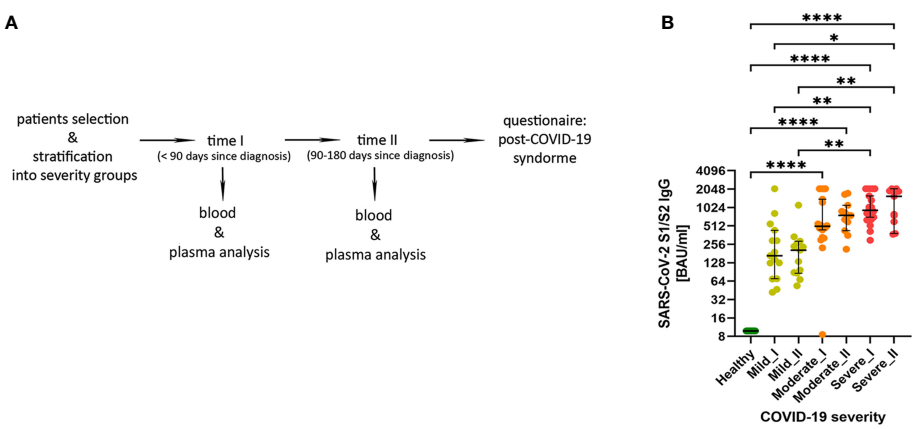


FIGURE 1 | **(A)** The experimental pipeline. **(B)** IgG antibodies against SARS-Cov-2 S1/S2 antigens in COVID-19 convalescent individuals. Type of severity (mild, moderate and severe) as well as time-points (I or II) are indicated. Data shown in the log2 scale represent individual values, median +/- 95% CI (confidence interval). Statistics analysis by non-parametric T-test, *p ≤0,05; **p ≤ 0,01; ***p≤ 0,001; ****p≤ 0,0001.

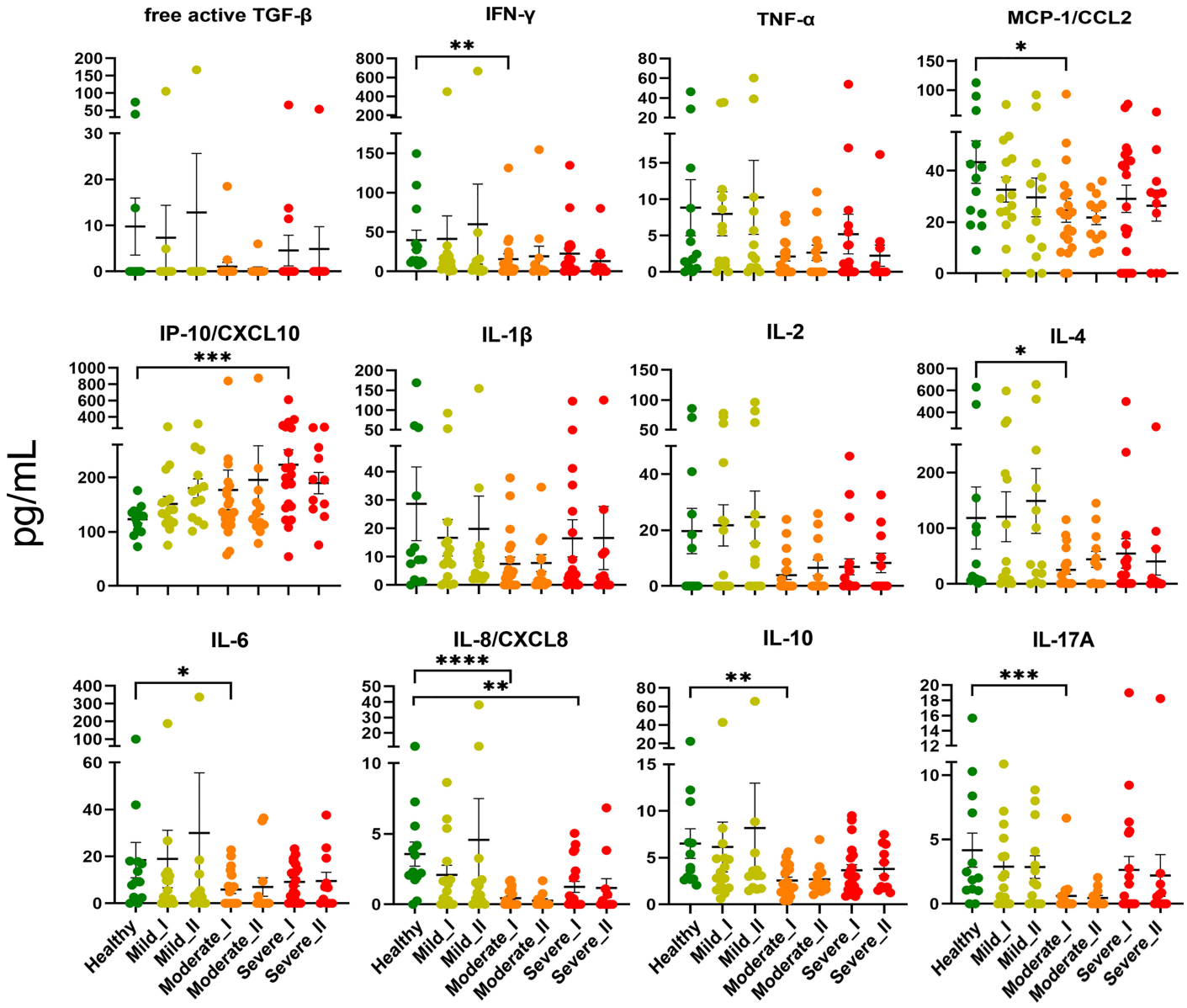


FIGURE 2 | Plasma level of cytokines and chemokines from COVID-19 convalescents and controls. Quantification of cytokines and other mediators in plasma obtained from COVID-19 convalescents after severe (time-point I, n=20, time-point II, n=11), moderate (time-point I, n=20, time-point II, n=12) and mild disease (time-point I, n = 15, time-point II, n=13) at two time points after disease confirmation and from healthy controls (n = 13). Data represent individual values, mean (centre bar) ± SD (upper and lower bars). Statistical analysis by one-way ANOVA test, *p ≤ 0,05; **p ≤ 0,01; ***p ≤ 0,001; ****p ≤ 0,0001.

sex-matched individuals, without documented SARS-CoV-2 infection and no detectable IgG antibodies against SARS-CoV-2 S1/S2 in plasma, served as a healthy reference control group.

Using plasma from convalescent patients and healthy donors, we examined the presence and temporal changes of the IgG antibodies fraction towards SARS-Cov-2 S1/S2 antigens. We have observed an increase in median IgG antibody levels that correlated with COVID-19 severity stages, with significant changes in moderate and severe post-COVID-19 patients (as compared to healthy and mild individuals). This was visible already at time-point I and further pronounced at the longer recovery time-point II (**Figure 1B**), also confirming the rationale behind our criteria for patients' stratification.

Cytokine Levels in Convalescent Patients' Plasma

First, to assess whether the cytokine storm (one of the hallmarks of COVID-19 disease (25, 26) is still present in convalescent patients, we measured levels of 13 cytokines, chemokines and other immune mediators in plasma of convalescent patients and healthy controls (**Figure 2**). The cytokine storm has already been attenuated following recovery from COVID-19, as levels of TNF-α, free active TGF-β, IFN-γ, IL-1β, IL-2, IL-4, IL-6, IL-8, IL-10, IL-12p70, IL-17 and MCP-1/CCL2 during convalescence were not higher compared to healthy volunteers. However, the opposite effect, namely decreased levels of IL-4, IL-6, IL-8, IL-10 and IL-17, were observed in convalescent patients after moderate/severe COVID-19, compared to mild convalescents and healthy controls. Among all analyzed factors, chemokine IP-10/CXCL10, a marker of suppressed immune function and regulator of neutrophils function, was maintained at a higher level at time-point I in individuals convalescent from severe disease.

Characterization and Dynamic Changes in CD4+ T Cell Subsets

To assess immune system remodeling and T cell subset dynamic changes upon recovery from COVID-19 of different severity, we studied CD4+ T cells, regulatory T cells (Tregs) and CD8+ T cells in convalescent patients at time-points I and II, as well as in healthy donors, using 28 parameter full spectrum flow cytometry. Immune cell populations were first categorized into 2 major T cell lineages, based on identification of T lymphocytes as viable CD45+ CD3+ cells, and CD4 and CD8 markers (the full gating strategy is present on **Supplementary Figure 1**). Each cell type was further divided into subsets, based on functional marker expression, including activation and maturation status. Therefore, expression of markers to identify different subsets of naïve (CCR7+ CD45RA+ CD28+ CD27+), T stem cell memory cells (TSCM; CCR7+ CD45RA+ CD28+ CD27+ CD95+), central memory (CM; CCR7+ CD45RA- CD28+ CD27+), effector memory (EM; CCR7- CD45RA- CD28+/- CD27+/-), terminal effector (TE; CCR7- CD45RA+ CD28+/- CD27+/-), together with additional activation (CD38, HLA-DR, ICOS) and exhaustion/senescence (CD57, CD95, PD-1) or dysfunction (CD39) markers and finally differentiation subsets within Treg cells (identified as CD25hi CD127lo) have been assessed. Composition of basal markers for each functional subset are presented in **Table 2**. The general gating strategy is shown on **Supplementary Figure 1**. Unsupervised analysis was performed to investigate all potential changes at once and to visualize the complex responses (described in detail in Materials and Methods). The same approach was used to study CD4+, Treg and CD8+ T cells, and specific markers used for unsupervised analysis of each population are presented on **Figures 3B**, **4B**, **5B**, respectively.

For CD4+ cells, we generated 14 metaclusters, that represent different CD4+ T cell functional types, based on differential expression of activation, differentiation and exhaustion markers (all markers are presented on **Figure 3B**). The dimensionality reduction method UMAP was used to distinguish and visualize populations (**Figure 3A** and **Supplementary Figures 2–4**), which have been identified using FlowSOM metaclustering and which characteristics are presented as a heatmap (**Figure 3B**). Clusters were compared between healthy donors and all severity groups of COVID-19 convalescent patients (mild, moderate, severe) at time-points I and II by differential analysis (**Figures 3C, D**).

We found that the naïve CD4+ T cells, even though the most abundant, were similar between all groups and times (**Figures 3B, C**). Central memory (CM) T cells clusters were highly represented (**Figure 3B**) and significantly changed among CD4+ cells, although two different schemes of responses were observed (**Figure 3D**). We noticed that the frequency of CM cells expressing CCR4 increased dependently on the severity at time-point I and further increased at time-point II, exhibiting significant expansion in severe individuals (**Figure 3D**), whereas activated CM population expressing CD38 and ICOS, even if significantly increased after moderate and severe COVID-19 at 3 months after COVID-19 (time-point I), strongly decreased at longer recovery till 6 months after COVID-19 (time-point II) in all groups (**Figure 3D**). Pools of activated effector memory (EM) cells generally increased at time-point II in a severity-dependent manner. These included activated EM cells with solely expression of HLA-DR, which showed high abundance in severe convalescents at time-point II, and EM cells co-expressing CD28, CD39 and CD95, together with HLA-DR (**Figure 3D**). Cluster of the effector memory cells expressing exhaustion marker PD-1 showed a similar increasing trend

TABLE 2 | T cell phenotypes distinguished during manual and unsupervised analyses of CD4+ and CD8+ cells.

Cell population	Phenotype – specific marker composition
Naïve	CCR7+ CD45RA+ CD28+ CD27+
TSCM – T stem cell memory	CCR7+ CD45RA+ CD28+ CD27+ CD95+
CM – central memory	CCR7+ CD45RA- CD28+ CD27+
EM – effector memory	CCR7- CD45RA- CD28+/- CD27+/-
TE – terminal effector	CCR7- CD45RA+ CD28+/- CD27+/-
Activated	CD38+ HLA-DR+
Exhausted	CD57+ PD-1+
Treg	CD25+ CD127low
Non suppressive/unstable Treg	Foxp3low CD45RA-

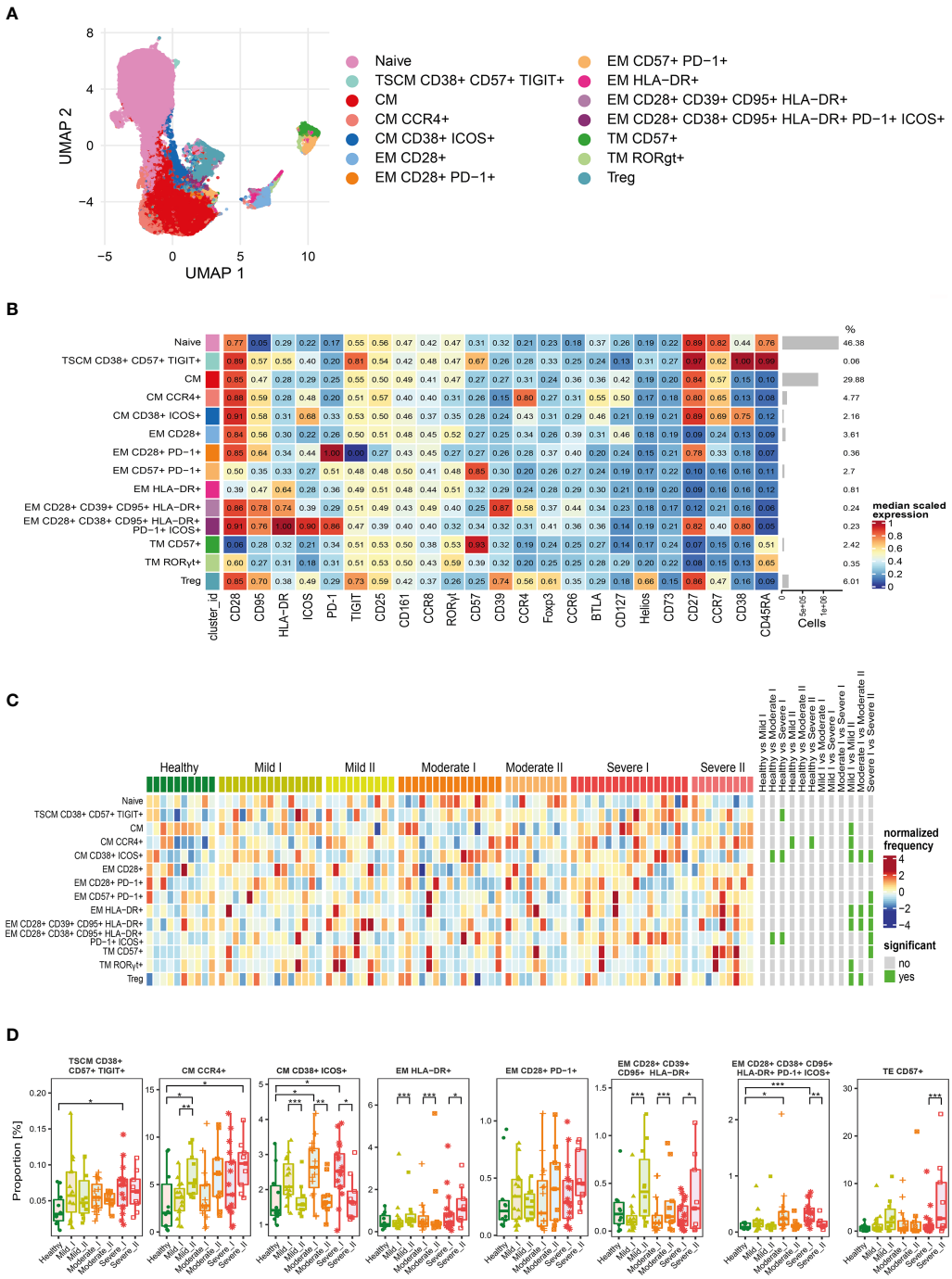


FIGURE 3 | Unsupervised analysis of CD4+ T cells and their characterization. **(A)** Uniform Manifold Approximation and Projection (UMAP) UMAP representation of CD4+ T cell landscape. **(B)** Heat map representing different clusters identified by FlowSOM, with relative identity and percentages in healthy controls and convalescent patients. The color in the heat map represents the median of the arcsinh, 0–1 transformed marker expression calculated over cells from all the samples, varying from blue for lower expression to red for higher expression. Each cluster has a unique color assigned (bar on the left). Barplots along the rows (clusters) and values on the right indicate the relative sizes of clusters. **(C)** Differential analysis of all severity groups of COVID-19 convalescent patients (mild, moderate, severe), as well as healthy donors at the time points I and II. The heat represents arcsine-square-root transformed cell frequencies that were subsequently normalized per cluster (rows) to mean zero and standard deviation of one. The color of the heat varies from dark blue indicating relative under-representation to red indicating relative over-representation. Bars at the right indicate significantly differentially abundant clusters (green). **(D)** Differential proportion of selected clusters presented as % of CD4+ cells. *p ≤ 0,05; **p ≤ 0,01; ***p ≤ 0,001

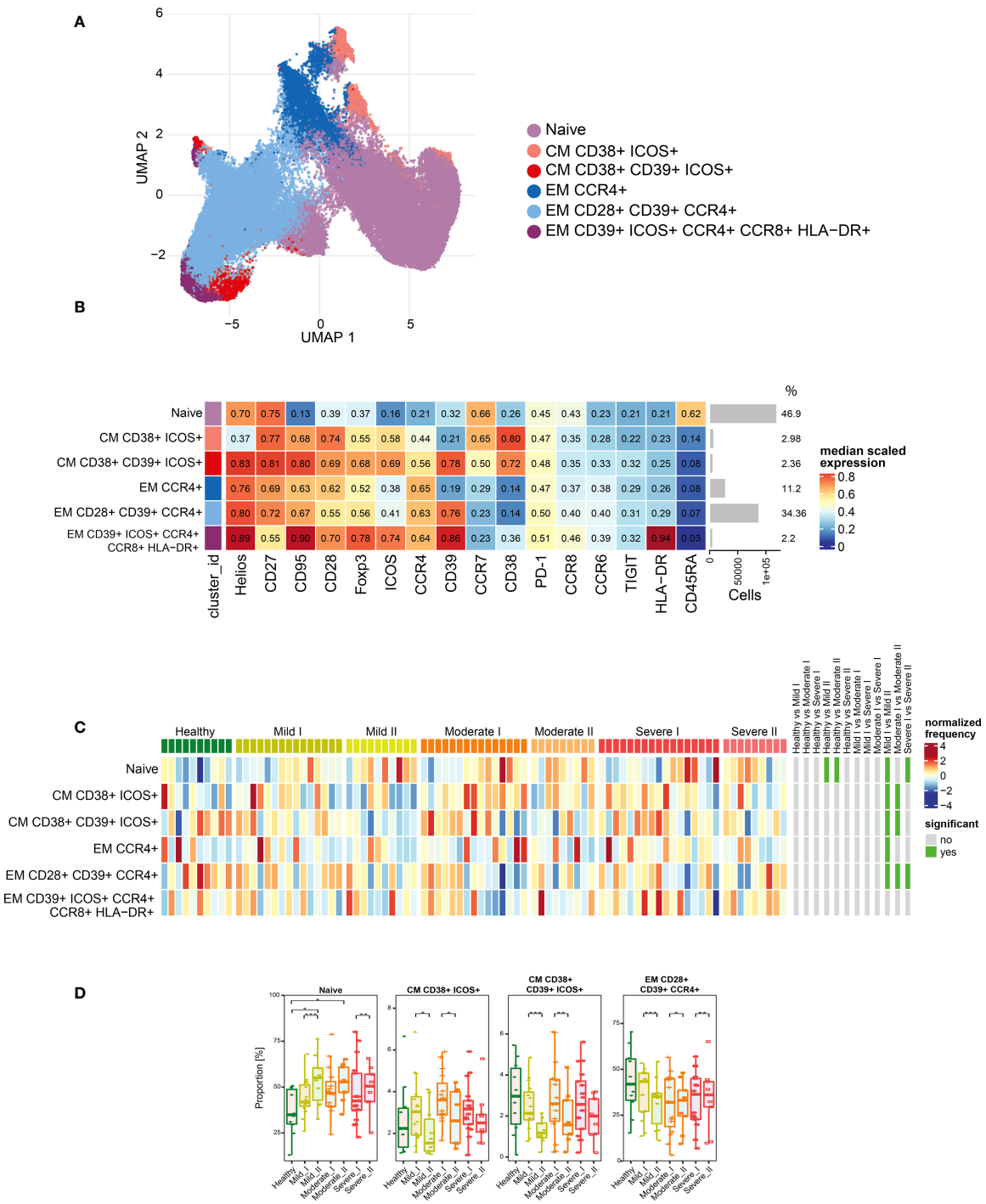


FIGURE 4 | Unsupervised analysis of Treg cells and their characterization. **(A)** Uniform Manifold Approximation and Projection (UMAP) UMAP representation of Treg cell landscape. **(B)** Heat map representing different clusters identified by FlowSOM, with relative identity and percentages in healthy controls and convalescent patients. The color in the heat map represents the median of the arcsinh, 0–1 transformed marker expression calculated over cells from all the samples, varying from blue for lower expression to red for higher expression. Each cluster has a unique color assigned (bar on the left). Barplots along the rows (clusters) and values on the right indicate the relative sizes of clusters. **(C)** Differential analysis of all severity groups of COVID-19 convalescent patients (mild, moderate, severe), as well as healthy donors at the time points I and II. The heat represents arcsine-square-root transformed cell frequencies that were subsequently normalized per cluster (rows) to mean zero and standard deviation of one. The color of the heat varies from dark blue indicating relative under-representation to red indicating relative over-representation. Bars at the right indicate significantly differentially abundant clusters (green). **(D)** Differential proportion of selected clusters presented as % of Treg cells. *p ≤ 0,05; **p ≤ 0,01; ***p ≤ 0,001.

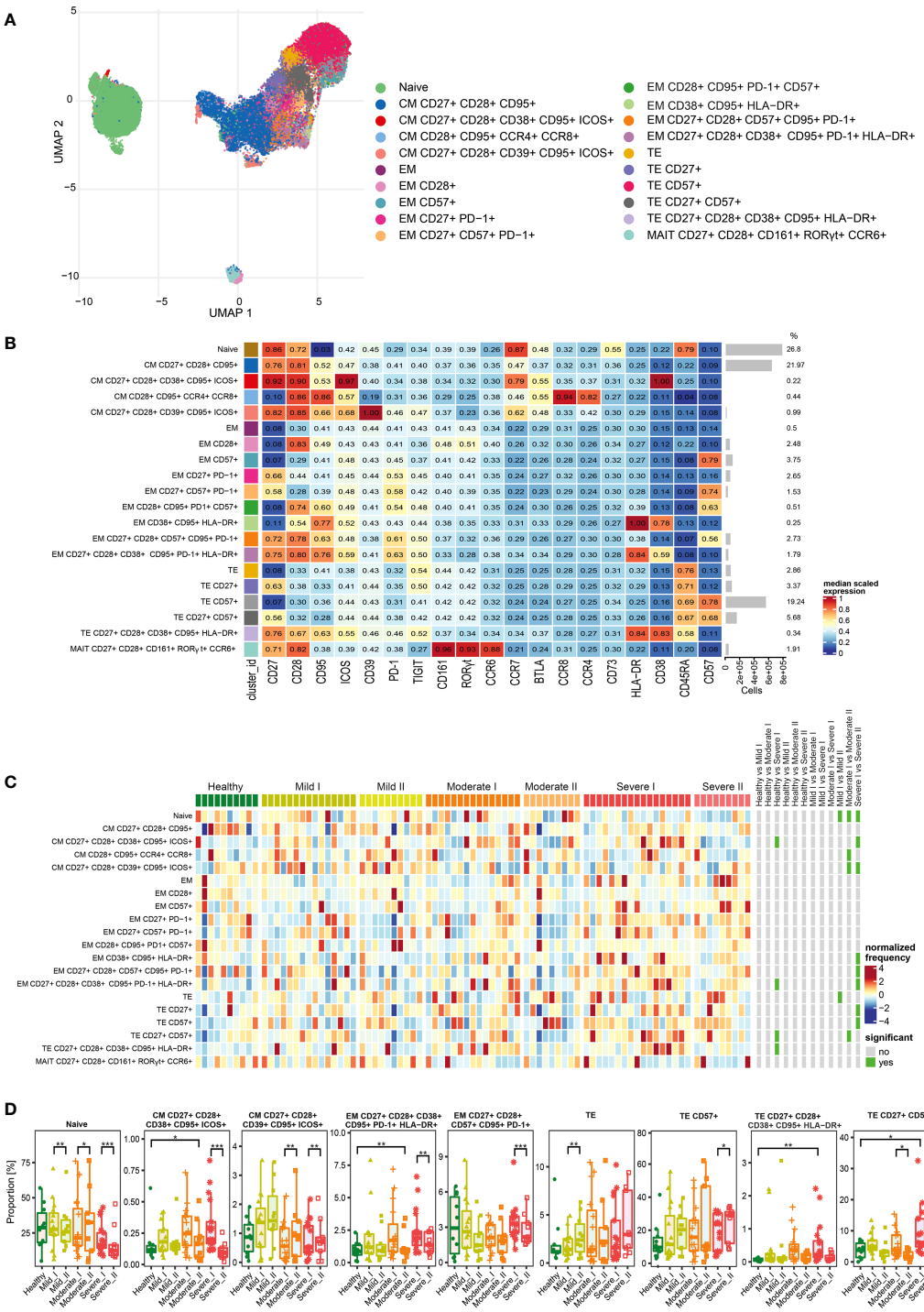


FIGURE 5 | Unsupervised analysis of CD8+ T cells and their characterization. **(A)** Uniform Manifold Approximation and Projection (UMAP) UMAP representation of CD8+ T cell landscape. **(B)** Heat map representing different clusters identified by FlowSOM, with relative identity and percentages in healthy controls and convalescent patients. The color in the heat map represents the median of the arcsinh, 0–1 transformed marker expression calculated over cells from all the samples, varying from blue for lower expression to red for higher expression. Each cluster has a unique color assigned (bar on the left). Barplots along the rows (clusters) and values on the right indicate the relative sizes of clusters. **(C)** Differential analysis of all severity groups of COVID-19 convalescent patients (mild, moderate, severe), as well as healthy donors at the time points I and II. The heat represents arcsine-square-root transformed cell frequencies that were subsequently normalized per cluster (rows) to mean zero and standard deviation of one. The color of the heat varies from dark blue indicating relative under-representation to red indicating relative over-representation. Bars at the right indicate significantly differentially abundant clusters (green). **(D)** Differential proportion of selected clusters presented as % of CD8+ cells. *p ≤ 0,05; ** p ≤ 0,01; *** p ≤ 0,001

(**Figure 3D**). Moreover, also the terminal effector memory cells (TE) that express CD57, marker associated with exhaustion/senescence, significantly increased in severe convalescents at longer recovery time-point II (**Figure 3D**). On the other hand, EM cells expressing CD38, CD95, HLA-DR, PD-1 and ICOS showed the dynamics similar to CM cells expressing CD38 and ICOS, namely increase at time-point I followed by significant drop at time-point II (**Figure 3D**). We have also found a very small population of CD4+ T stem cell memory cells (TSCM) with expression of CD38, CD57, and TIGIT, that increased at time I in severe convalescent patients, though this was not further observed after longer recovery at time II (**Figure 3D**). Altogether these data indicate that the long-term recovery of severe convalescents leads to decrease in number of activated central memory CD4+ cells, increase in population of CCR4+ CM cells which indirectly support immunosuppressive activity of Treg cells, accompanied by skewed polarization of CD4+ T cells towards the exhaustion/senescent state.

As our panel contained CD25, CD127 and transcription factors Foxp3 and Helios, we were able to identify a population of regulatory T cells. Then, following analysis of functional markers by FlowSOM metaclustering (all markers are presented on **Figure 4B**), we identified and visualized 6 subsets of Treg cells (**Figures 4A, B** and **Supplementary Figures 2, 5, 6**). Among Treg cells, we observed an increase in the most abundant subset of naïve cells at both time-points of recovery (**Figures 4B–D**). This was accompanied by a significant decrease in CD38 and ICOS-expressing CM Treg cells at time-point II (**Figures 4C, D**), similarly to the changes described above in CD4+ cells (**Figure 3D**). However, in Treg cells such an effect was especially visible during recovery in mild and moderate convalescents, as compared to the severe group (**Figure 4D**). Effector Tregs that express CD28, CD39 and CCR4, established a highly represented subset (**Figures 4B–D**). They showed time-dependent significant decrease in mild convalescents or increase observed in moderate and severe (**Figure 4D**). Altogether, these data suggest either a block in Treg maturation, or an increase in influx of naïve Treg cells, correlating with reduced population of potentially immunosuppressive Tregs in mild and moderate, but not in severe convalescents upon long-term recovery.

Characterization and Dynamic Changes in CD8+ T Cell Subsets

After analysis of functional markers in CD8+ T cells subset (all markers are shown on **Figure 5B**), followed by FlowSOM meta-clustering, we have identified 20 functional clusters, visualized by UMAP (**Figure 5A** and **Supplementary Figures 2, 7, 8**) and presented as a heat map (**Figure 5B**). Then, as described above, differential analysis has been performed to compare all severity groups and the analyzed time-points.

The naïve population was also the most abundant among CD8+ cells (**Figures 5B–D**). However, we noticed the time-dependent decrease of naïve cells number, especially visible in severe convalescents (**Figure 5D**). Central memory cells were also highly represented among CD8+ population (**Figure 5B**). Among those, central memory cells expressing CD27, CD28, CD39, CD95 and ICOS showed increased frequencies especially in mild convalescents, and decrease in moderate and severe. On the other hand, CM cells expressing CD38, CD95 and ICOS showed reduced frequencies visible at time-point II, coming back to the baseline level of healthy donors (**Figures 5C, D**). Identified clusters of effector memory (EM) cells were either not frequent or not significantly changed (**Figure 5D**). The dynamics towards increased senescence/exhaustion was clearly visible among terminal effector cells of severe convalescents at time-point II. The frequency of TE CD8+ cells expressing CD57 has generally increased among convalescent patients and represented around 40% of all CD8+ cells at time-point II (**Figures 5B–D**). Identified terminal effector CD8+ cells expressing activation markers HLA-DR and CD38 (CD27+ CD28+ CD38+ CD95+ HLA-DR+) constituted a small population increased at time-point I in the severe group, although it reversed to the level of healthy donors at the second time-point (**Figure 5D**). In general, at time-point II we noticed largely reduced populations of CM, EM and TE CD8+ cells expressing CD27 and CD28 markers (**Figure 5D**), indicating attenuation of CD8+ T cells activation, expansion and differentiation from memory into effector CD8+ T cells (35). Finally, we identified a cluster of mucosal associated invariant T (MAIT) cells, however the frequencies did not differ either between severity types or time-points (**Figures 5B, C**).

Altogether we found that the long-term post-COVID-19 recovery leads to the time-dependent decrease of naïve and central memory populations of CD8+ T cells, accompanied by significant increase in terminal effector subsets expressing the exhaustion/senescence markers, observed in severe convalescents. This could suggest that CD8+ cells exhibit strong polarization towards an exhausted state visible in severe post-COVID-19 patients upon long-term recovery.

Ex Vivo Production of Cytokines

Next, we have studied production of seven different functional molecules in CD4+, Treg and CD8+ T cells, including IFN-γ, IL-17, IL-2, TNF-α, TGF-β and granzyme-B, along with expression of degranulation marker CD107a (LAMP-1). First, the classical approach, based on two-dimensional cell type identification by manual sequential gating, has been performed. In each group of identified cells (CD4+, CD4+Tregs, CD8+), the levels of above-mentioned cytokines have been measured using the full spectrum Cytek Aurora cytometer. The full gating strategy is presented on **Supplementary Figure 9**.

The total production of each cytokine is summarized in **Supplementary Figure 10**. We found that CD4+ cells from severe convalescent patients had significantly higher capacity to produce TNF-α, IL-2 and CD107a at time-point I, compared to healthy controls and mild/moderate COVID-19 convalescents (**Supplementary Figure 10A**). Increased production of these cytokines was also observed for Foxp3+ Treg cells (**Supplementary Figure 10B**). Importantly, Tregs from severe convalescents also showed increased production of IL-17, IL-2+IL1-7 and IFN-γ at time-point I. This was observed neither for mild or moderate patients nor for healthy donors. However, at time-point II, we noticed a significant decrease in the production of all

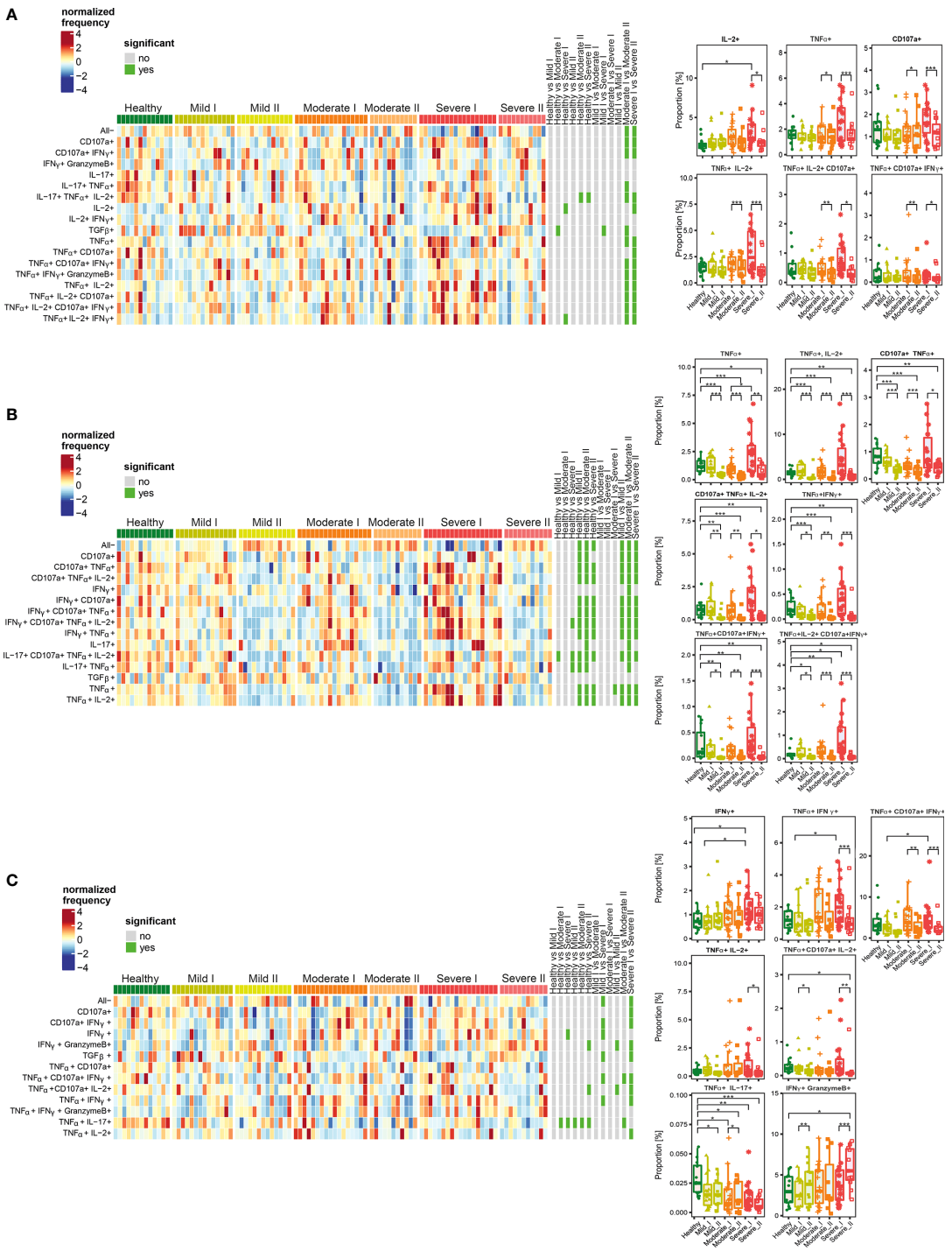


FIGURE 6 | Unsupervised analysis of cytokine production by CD4+ **(A)**, Treg **(B)** and CD8+ **(C)** cells from convalescent patients after mild, moderate and severe COVID-19 as well as healthy donors analyzed at time I and time II. Upper panels - Heatmaps showing cell clusters identified by FlowSOM with differential analysis of all severity groups of COVID-19 convalescent patients (mild, moderate, severe) as well as healthy controls at the time points I and II. The heat represents arcsine-square-root transformed cell frequencies that were subsequently normalized per cluster (rows) to mean of zero and standard deviation of one. The color of the heat varies from dark blue indicating relative under-representation to red indicating relative over-representation. Bars at the right indicate signi ficant differentially abundant clusters (green). The population without any activity (negative for all markers) has been marked as “All-”. Lower panels – differential proportion of selected clusters presented as % of analyzed cells. *p ≤ 0,05; **p ≤ 0,01; ***p ≤ 0,001.

above mentioned cytokines, in both CD4+ and Treg cells, especially in severe convalescent patients (**Supplementary Figures 10A, B**). CD8+ T cells did not exhibit significantly higher production of most of the analyzed cytokines. Only in severe convalescents at time-point II, we observed slight decrease in production of CD107a and visible, though not statistically significant, increased production of Granzyme B (**Supplementary Figure 10C**).

We then investigated CD4+, Treg and CD8+ T cells polyfunctionality by analyzing simultaneous production of TNF-α, CD107a, IFN-γ, IL-2, IL-17, granzyme-B and TGF-β by mild, moderate and severe COVID-19 convalescent patients at recovery time-point I and time-point II, as well as by healthy donors (**Figure 6**). Polyfunctional studies, considering several cytokines produced simultaneously by T cells, have enabled deeper deciphering of T cell functions during COVID-19 convalescence. Based on the use of seven functional markers for FlowSOM metaclustering, we could discriminate up to 22 different populations of CD8+, CD4+ and Treg cells able to produce one or more molecules simultaneously, in different combinations. Next, the differential analysis together with statistical analysis has been performed for each cluster and shown on a heatmap (**Figures 6A–C**, upper panels), as well as graphs showing differential proportions (presented for selected clusters) (**Figures 6A–C**, lower panels).

Among CD4+ T cells, we identified clusters of cells characterized by higher simultaneous production of different combinations of IL-2, TNF-α, CD107a and IFN-γ, at the recovery time-point I in severe convalescent patients, compared to moderate and mild post-COVID19, as well as healthy individuals (**Figure 6A**). The observed upregulation in simultaneous production of those cytokines in identified polyfunctional clusters persisted up to 3 months after recovery (time-point I), and was followed by significant decrease at time-point II, especially in severe patients (**Figure 6A**).

Functional clusters identified among Treg cells showed high proportion of cells with simultaneous production of different combinations of TNF-α, IL-2, CD107a, and IFN-γ (which have been found before in the entire population of CD4+ cells) at time-point I in severe post-COVID-19 patients (**Figure 6B**). However, similarly to CD4+ cells, later during recovery at time-point II, the amount of cells among almost all identified clusters significantly decreased and dropped even below the level found in healthy donors. Interestingly, such a significant drop in cytokines production was visible not only in severe post-COVID patients, but also in moderate and mild, even though previous increase observed at time I was not as strong as in severe cases.

Among CD8+ T cells (**Figure 6C**), the responses and polyfunctionality changes were not as strong as in CD4+ and Treg cells. We identified clusters characterized by higher proportion of IFN-γ-, TNF-α- and CD107a-producing cells in severe convalescents at time-point I. As in other T cell populations, such increased production of cytokines at time-point I was followed by decrease at time-point II. Additionally, a strong, severity- and time-dependent decrease in production of TNF-α together with IL-17 was observed. Specifically for CD8+ cells, a population showing simultaneous production of IFN-γ together with Granzyme B was identified. Production of these cytokines increased dependent on disease severity and time, showing significant increase in severe convalescents at time-point II, compared to healthy individuals. Such an effect was predominant in severe patients at time II.

Altogether, these data show that CD4+, Tregs, as well as CD8+ cells from severe convalescent individuals, at time-point I presented functional types which predominantly produced proinflammatory TNF-α, IL-2, IFN-γ and CD107a at high levels. Longer recovery (time-point II) led to strong decrease of most of the analyzed factors, not only in severe, but also in moderate patients. This has often exhibited levels lower than in healthy donors. Finally, the increased proportion of CD8+ cells producing Granzyme B together with IFN-γ was specifically characteristic for severe post-COVID-19 patients at time II, indicating unresolved inflammation. Such a trend was also found in CD4+ cells, although without statistical significance.

Post-Acute COVID-19 Syndrome in Convalescent Patients After Mild, Moderate and Severe COVID-19

The appearance of post-acute COVID-19 syndrome (PACS, signs and symptoms beyond 12 weeks), also called "long COVID", has often been observed, significantly decreasing the quality of patients' life (16). These symptoms include tiredness, fatigue (extreme tiredness), shortness of breath and dyspnea but also a broad range of cognitive symptoms such as difficulties in concentration and memory ("brain fog"), sleep problems, depression and others (36, 37). Importantly, it seems that they appear not only in convalescents recovering from severe COVID-19, but also in those who suffered from moderate, mild and even asymptomatic forms of disease. Even if the appearance of long COVID is already broadly recognized, the molecular mechanisms leading to those long-term effects are still not clear. Nevertheless, the long-lasting immune system-related factors, T cell exhaustion and neuroinflammation are proposed

TABLE 3 | Appearance of post- acute COVID-19 syndrome (PACS, signs and symptoms beyond 12 weeks) in post-COVID-19 patients from all severity groups.

COVID-19 severity group	Cognitive dysfunction	Fatigue	Dyspnea
MILD (n=13)	30,7% (4/13)	38,4% (5/13)	15% (2/13)
MODERATE (n=17)	70,5% (12/17)	47,1% (8/17)	17,6% (3/17)
SEVERE (n=16)	43,7% (7/16)	50,5% (8/16)	50,0% (8/16)

Data have been collected during an interview made by a clinician.

as very probable drivers (38). Therefore we have assessed the common symptoms of the prolonged PACS in the convalescent patients, depending on the disease severity. The data have been collected at the 1-year follow-up interview made by a clinician, in which patients have been asked about presence of cognitive symptoms/brain fog, fatigue and dyspnea/shortness of breath, all lasting over 3 months.

Supplementary Table 4 shows that long COVID, independently on the type of PACS symptoms, was found in 81% (13/16) of severe, 70% (12/17) of moderate and 61% (8/13) of mild convalescents, therefore indicating that PACS is severity-independent. Moreover we observed that different types of symptoms showed different distributions and co-existence.

Looking closer into the PACS symptoms we found that dyspnea or fatigue lasting over 3 months, presented the most prevalent PACS symptoms observed in 50% of patients after severe COVID-19, accompanied by cognitive PACS symptoms found in 43,7% of cases (**Table 3**). In the majority of severe convalescents, co-existence of at least two symptoms was observed (**Supplementary Table 4**). In moderate or mild convalescents, dyspnea was present in a much lower number of cases and represented 17,6% or 15%, respectively. Interestingly, prolonged cognitive impairment was predominant and reported by 70% of moderate convalescent patients, accompanied with fatigue reported by 47% and dyspnea appearing only in 17,6% (**Table 3**). Such cognitive impairment reported by moderate convalescents often co-existed with fatigue but not dyspnea symptoms. Moreover, fatigue never existed without additional cognitive dysfunction (**Supplementary Table 4**). Finally, a significant number of mild convalescents still indicated PACS, which has been represented by fatigue (38% of cases) and cognitive dysfunctions (30% of cases), but not dyspnea (only 15% of cases) (**Table 3**). The clear co-existence of any symptoms was not observed in the mild group, however the presence of cognitive dysfunctions together with fatigue was still visible in 2 out of 8 mild cases with PACS (**Supplementary Table 4**). In none of the patients, stroke or heart attack appeared after COVID-19.

Altogether we found that among the PACS symptoms, fatigue and cognitive dysfunctions were highly represented in all groups, including mild post-COVID-19 patients, often co-existed, and had no significant relationship with the severity of the disease. On the other hand, dyspnea dominated in convalescents recovering from severe forms of the disease. Its presence was much lower in moderate or mild post-COVID-19. Interestingly, prolonged cognitive dysfunctions were predominant in patients after moderate COVID-19, and significantly present not only in severe, but also in patients recovering from mild COVID-19.

DISCUSSION

Persistent symptoms of post-acute COVID-syndrome - PACS (named also "long COVID"), representing incomplete recovery from COVID-19, lead to continued health-related problems, reported by over 30% of all convalescents (regardless of the severity of the initial infection) (2, 10, 39, 40). As they can lead to significant complications, such health conditions represent an emerging medical and global problem in the nearest future (10). Therefore, studies which analyze convalescent subjects months after the disease of different severity are crucial to address and develop an integrative healthcare approach.

Most investigations describe PACS about 1-3 month after recovery, or just report severe convalescents, and scanty data exist that compare changes in T cell subsets from convalescent individuals who had experienced mild, moderate or severe COVID-19. Here we show several immune parameters collected at two time-points, i.e., up to 3 and 6 months after mild, moderate or severe infection, and provide information about the persistence of PACS. We have found that recovery from severe COVID-19 leads to functional shift after the first 3 months post-infection, resulting in polarization towards an exhausted/senescent state of CD4+ and CD8+ T cells and perturbations in CD4+ Treg subsets, clearly visible at 6 months after COVID-19. In terms of functionality, these changes are accompanied by attenuation of the unstable Th1/Th17-like Treg phenotype and proinflammatory polarization of CD4+ (which was still observed at 3 months after primary infection). CD8+ cells which were particularly polarized towards the terminal effector state, simultaneously increased proportion of Granzyme B and IFN-γ-producing cells, indicating prolonged cytotoxic capabilities and unresolved pro-inflammatory traits.

On the other hand, mild convalescents do not show polarization of T cells towards the exhausted/senescent state but are characterized by increased population of naïve Tregs, concurrently with decrease in CM and EM Tregs. Furthermore, we have discovered that several post-acute COVID symptoms, such as fatigue and cognitive dysfunction are severity-independent and are not necessarily related to exhausted/senescent state and dysfunctions of CD4+, CD8+ and Treg cells found in severe convalescents.

Immune dysregulation has been associated with post-acute COVID-19 recovery (41). Several previous reports showed that T cell activation/exhaustion remain elevated following SARS-CoV-2 infection (14, 32, 33) as well as in severe convalescents (42). Particularly, T cell exhaustion seems to play a significant role in post-COVID-19, as blockade of the PD-1/PD-L1 axis led to restoration of T cell function and reversal of the observed post-acute COVID-19 immune abnormalities (43). Consistently with this, we also identified increased presence of exhausted (PD-1-expressing) and senescent (CD57-expressing) EM and TE CD4+ and CD8+ T cells in severe convalescents. Such phenotyping remodeling has been noticed during COVID-19 infection (33), nevertheless, we showed that significant skewing towards the exhausted/senescent phenotype is observed after the first 3 months of recovery in severe patients.

We identified CD8+ T cells as particularly polarized towards the exhausted/senescent state in severe, but not mild and moderate convalescents after 6 months-long recovery. The frequency of terminal effector CD8+ T cells expressing CD57, finally achieved about 40% of all CD8+ T cells. Different subsets of CD8+ cells additionally exhibited a decrease of CD27 and

CD28 expression, characteristic for attenuation of T cell activation and expansion as well as age-associated decline of immune function (44, 45). Therefore, prevalence of subsets with increased CD57 expression, together with decreased expression of CD27 and CD28, indicates expansion of CD8+ T cells polarized towards a dysfunctional terminally differentiated state, lacking full effector capability. Such population can play a significant role in various diseases or conditions, associated with chronic immune activation such as, among others, HIV infection, cancer, intracellular infections, chronic pulmonary diseases and autoimmune diseases, as well as has a great influence on age-related changes in the immune system (46, 47). This was observed together with a strong decrease in naïve CD8+ T cell numbers. Our data are in agreement with reports in which elevated exhaustion of CD8+ cells has been proposed as an indicator for progression and prognosis of COVID-19 disease (48), as well as lower frequency of naïve CD8+T cells has been identified in the short-term post-COVID-19 studies (49). Therefore, such a highly represented dysfunctional exhausted/senescent CD8+ population might be involved in the post-COVID pathogenesis but also will provide the suppressive tumor-promoting microenvironment (41). Altogether this indicates that convalescents recovering from severe COVID-19 might face the long-lasting dysfunctions in T cell responses, that result in potentially weaker immunity to other infections, cancer and other diseases, which can significantly affect health or medical treatment of patients.

The number of Tregs is significantly reduced in COVID-19 patients and perturbances in Treg activity correlate with COVID-19 severity, risk of respiratory failure and higher mortality (50, 51). We saw that different subsets of Treg show different dynamics between the short (until 3 months) and the long-term (until 6 months) post-COVID-19 responses. This included a decreased population of ICOS-expressing CM Treg cells, which was most abundant in mild convalescents at the second time-point. ICOS is highly expressed by activated CD4+ and Treg cells, and improves the survival, proliferation, also favouring the suppressive function of Treg cells (52). Our observations are in accordance with cytometric and transcriptomic analyses, which revealed a distinct Treg signature in severe patients, resembling immunosuppressive and tumor infiltrating features and correlating with poor prognosis (50). Simultaneously, long-term data revealed significant increase in Treg naïve subset in mild and moderate, but not severe, convalescents. Overall, these results could indicate a lower suppressive functions and either a block in maturation, or an increased influx of naïve Treg cells into the circulation in convalescents, especially at longer time after mild or moderate COVID-19. Moreover, at the first time-point Tregs from severe convalescents produce more IL-2, IL-2 plus IL-17 and IFN-γ, suggesting the presence of polarization into unstable Th1/Th17-like states. These data imply improper function of Treg cells during COVID-19 recovery, possibly affecting incomplete resolution of inflammation.

Concerning T cell polyfunctionality, CD4+, Treg, as well as CD8+ T cells from moderate and severe convalescents presented functional types which simultaneously produced high levels of Th1 and Th17 cytokines, (as revealed by intracellular staining showing different combinations of TNF-α, IL-2, CD107a and IFN-γ), until 3 months of recovery. This is consistent with other studies which indicated proinflammatory Th1/Th17 state of T cells after severe COVID-19 (26, 33, 53). These data suggest impaired/slowed resolution of inflammation, which is otherwise crucial to prevent the progression from non-resolving acute inflammation to persistent chronic inflammation (54). An effective resolution of inflammation is crucial for severe convalescents. We found that longer recovery (3-6 months) leads to strong inhibition of simultaneous production of those cytokines, and additionally TNF-α plus IL-17, often below the level observed in healthy controls. Our finding is supported by other studies, which showed decreased levels of Th1-polarized CD4+ cells during recovery from COVID-19 (55).

Severe post-COVID-19 patients exhibited an increased proportion of CD8+ cells producing Granzyme B together with IFN-γ upon long recovery, suggesting the persistence of a strong cytotoxic T cell responses. This is consistent with data showing prolonged enhancement of Granzyme B production by cytotoxic T lymphocytes in post-recovery patients (56). Also, IFN-γ produced by CD8+ T cells, which remained persistently high at 8 months after infection, has been recently considered a long COVID predictor (57). This could imply that $CD8^{+}CD57^{+}$ T cells exhibiting enhanced cytotoxic potencies, and impaired proliferative capability, are recruited to the peripheral blood and the unresolved chronic inflammatory state is maintained in severe convalescents long after recovery from COVID-19. These observations might provide future opportunities for prevention and treatment. Blocking/inhibition of Granzyme B production is currently investigated in different therapies, including autoimmune diseases (58, 59). Also, development of pro-resolution strategies and implementation of so-called "resolution pharmacology" was proposed (60) to prevent the prolonged chronic inflammatory state, leading to a plethora of diseases (54). Such therapeutic modalities might be also an opportunity for severe COVID-19 convalescent individuals to prevent the post-acute COVID syndrome and further possible complications.

We found that long-COVID-19 effects, such as fatigue and/or cognitive dysfunction, appear significantly in all convalescents, often showing co-existence. The incidence of the post-COVID syndrome is commonly estimated at 10-35%, while for previously hospitalized patients it may reach 85% (61). Thus, the role of different variants of SARS-CoV-2 remains to be elucidated.

Pathogenesis of PACS is complex, and dysregulated T cell functions have been proposed as one of its drivers (62, 63). Even with limitations of our studies, such as relatively basic clinical review of PACS symptoms and relatively low number of cases in each group (about 20-25), together with a broad range of age (without dividing into age-related groups) of only male patients, our data suggest that PACS symptoms are present also in mild/moderate convalescents and are not exclusively related to exhaustion/senescence of CD4+ and CD8+ T cells, or to a

defective resolution of inflammatory phenomena. Such observation is still preliminary, based on the limited number of cases and addresses only T cells subsets, however indicates that different mechanisms, which might depend or not on COVID-19 severity, can be involved in different types of PACS symptoms. Similar conclusions have been driven by the recently released comprehensive sc-RNASeq studies of patients until 6 months post-infection (17). Authors showed that even mild convalescents might have long-lasting changes in the transcriptome of blood cells. Our observation is also consistent with deep multi-omic studies reporting that patients with mild and severe/acute COVID-19 exhibited similar PACS symptoms, and different immune endotypes correlated with different PACS symptoms (18). This suggests that different repertoire of immune cells might be responsible for different manifestations of post-COVID symptoms. However, those studies have focused on a shorter period after severe COVID-19 infection, whereas our data showed that there is a further significant remodeling of the immune response at longer post-COVID time (at 3-6 months).

We can conclude that dysregulated immunity of CD4+, CD8+ and Treg cells is, to an extent, maintained for the first 3 months post COVID-19, followed by a functional switch partially visible at 3-6 month. The magnitude of observed phenomena is different for severe and mild/moderate patients. This manifests itself as long-lasting attenuation of T cell activation and expansion, and skewing towards an exhausted/senescent state, particularly in CD8+ T cells. Together with prolonged unresolved inflammation, it might result in dysfunctions in T cell responses causing a potentially weaker immunity. These severe immune dysfunctions specifically co-existed together with the pulmonary complications/dyspnea, however this was not found for PACS symptoms such as fatigue and cognitive dysfunction, which were present not only in severe, but also in a substantial percentage of mild and moderate convalescents. On the other hand, the long-term responses in mild or moderate COVID-19 convalescents result in lower polarization towards exhausted/senescent state, attenuation of the immunosuppressive subsets, associated with increased amount of circulating naïve Treg cells. Therefore this data, even if performed on a limited number of cases, indicate that some PACS problems, such as fatigue and cognitive dysfunction are rather severity-independent. We propose that they are probably not related to the polarization of T cells towards exhaustion/senescence state, which has been found by us predominantly in severe convalescents, however this needs further deeper studies.

Finally, whilst it is a growing area of medicine and research, we chose not to study individuals who received recently developed anti-COVID-19 vaccines. We assume that this would make investigation of the mechanisms more complex, possibly leading to potentially skewed interpretation and conclusions. Moreover, with a big probability all analyzed patients were infected with the alpha variant of SARS-CoV-2 virus, as identification of the first cases of delta variant in Poland began in June 2021, so after we have finalized our studies. Future deep, long-lasting studies of COVID-19 of all severity stages, together with selected age-related and male/female groups are needed to better understand the nature of association of the long-term defects in the immune system with prolonged responses that include metabolic changes of immune cells, as well as emerging neurological manifestations. Such studies will potentially uncover the relation of dysregulated immunity, acute or chronic immune responses and different PACS symptoms. In any case, either the search for long COVID predictors or any treatment to prevent the post-COVID syndrome and further possible complications is mandatory in all patients with SARS-CoV-2 infection, and not only in those suffering from severe/acute COVID-19.

DATA AVAILABILITY STATEMENT

The original contributions presented in the study are included in the article/**Supplementary Material**. Further inquiries can be directed to the corresponding author.

ETHICS STATEMENT

The studies involving human participants were reviewed and approved by ethics committee of the Central Clinical Hospital of the Internal Affairs and Administration Ministry in Warsaw (Decision No 151/2020) with informed consent of enrolled individuals. The study was performed in accordance with the latest version of the Declaration of Helsinki and the guidelines for good clinical practice. The patients/participants provided their written informed consent to participate in this study.

AUTHOR CONTRIBUTIONS

MW, MB-O, and PC performed experiments; MW, PC, DS, and JS performed data analyses; PC and KP coordinated cooperation with clinics; MH, AM, MD, and WW coordinated and performed patients identification and clinical analysis; MH, AM, and PC organized and coordinated convalescents blood donation and questionnaire; KS performed CT lung analysis; MW, PC, JS, and KP conceptualized experiments; KP conceptualized and supervised the project; MW, PC, DS, and KP prepared figures and tables; MW, PC, JS, DS, and KP prepared draft of the manuscript; AC, SDB, JS, MW, and PC were involved in data discussion and interpretation; MW, PC, DS, JS, MH, SDB, AC, and KP prepared and reviewed final version of the manuscript; All authors have read and agreed to the published version of the manuscript.

FUNDING

This work has been funded by grant from Foundation for Polish Science TEAM-TECH Core Facility Plus/2017–2/2 (POIR.04.04.00-00-23C2/17-00) co-financed by the European

Union under the European Regional Development Fund to KP. JS was supported by EMBO Scientific Exchange Grant (Short-Term Fellowship) STF-8905.

ACKNOWLEDGMENTS

We would like to acknowledge all COVID19-convalescents who participated in these studies. Olivier Jaen (Cytek Biosciences) is acknowledged for his support and technical suggestions in multicolor panel development using CYTEK Aurora.

SUPPLEMENTARY MATERIAL

The Supplementary Material for this article can be found online at: https://www.frontiersin.org/articles/10.3389/fimmu.2022.886431/full#supplementary-material

REFERENCES

1. Zhu N, Zhang D, Wang W, Li X, Yang B, Song J, et al. A Novel Coronavirus From Patients With Pneumonia in China, 2019. *N Engl J Med* (2020) 382 (8):727–33. doi: 10.1056/NEJMoa2001017
2. Huang C, Huang L, Wang Y, Li X, Ren L, Gu X, et al. 6-Month Consequences of COVID-19 in Patients Discharged From Hospital: A Cohort Study. *Lancet Lond Engl* (2021) 397(10270):220–32. doi: 10.1016/S0140-6736(20)32656-8
3. Marshall M. The Four Most Urgent Questions About Long COVID. *Nature* (2021) 594(7862):168–70. doi: 10.1038/d41586-021-01511-z
4. Wang W, Xu Y, Gao R, Lu R, Han K, Wu G, et al. Detection of SARS-CoV-2 in Different Types of Clinical Specimens. *JAMA* (2020) 323(18):1843–4. doi: 10.1001/jama.2020.3786
5. Chen G, Wu D, Guo W, Cao Y, Huang D, Wang H, et al. Clinical and Immunological Features of Severe and Moderate Coronavirus Disease 2019. *J Clin Invest* (2020) 130(5):2620–9. doi: 10.1172/JCI137244
6. Chua RL, Lukassen S, Trump S, Hennig BP, Wendisch D, Pott F, et al. COVID-19 Severity Correlates With Airway Epithelium–Immune Cell Interactions Identified by Single-Cell Analysis. *Nat Biotechnol* (2020) 38 (8):970–9. doi: 10.1038/s41587-020-0602-4
7. Li Q, Guan X, Wu P, Wang X, Zhou L, Tong Y, et al. Early Transmission Dynamics in Wuhan, China, of Novel Coronavirus-Infected Pneumonia. *N Engl J Med* (2020) 382(13):1199–207. doi: 10.1056/NEJMoa2001316
8. Wu Z, McGoogan JM. Characteristics of and Important Lessons From the Coronavirus Disease 2019 (COVID-19) Outbreak in China: Summary of a Report of 72 314 Cases From the Chinese Center for Disease Control and Prevention. *JAMA* (2020) 323(13):1239. doi: 10.1001/jama.2020.2648
9. Cohen KW, Linderman SL, Moodie Z, Czartoski J, Lai L, Mantus G, et al. Longitudinal Analysis Shows Durable and Broad Immune Memory After SARS-CoV-2 Infection With Persisting Antibody Responses and Memory B and T Cells. *Cell Rep Med* (2021) 2(7):100354. doi: 10.1016/j.xcrm.2021.100354
10. Roth A, Chan PS, Jonas W. Addressing the Long COVID Crisis: Integrative Health and Long COVID. *Glob Adv Health Med* (2021) 10:216495612110565. doi: 10.1177/21649561211056597
11. Sekine T, Perez-Potti A, Rivera-Ballesteros O, Strålin K, Gorin J-B, Olsson A, et al. Robust T Cell Immunity in Convalescent Individuals With Asymptomatic or Mild COVID-19. *Cell* (2020) 183(1):158–68.e14. doi: 10.1016/j.cell.2020.08.017
12. Malkova A, Kudryavtsev I, Starshinova A, Kudlay D, Zinchenko Y, Glushkova A, et al. Post COVID-19 Syndrome in Patients With Asymptomatic/Mild Form. *Pathog Basel Switz* (2021) 10(11):1408. doi: 10.3390/pathogens10111408
13. Sudre CH, Murray B, Varsavsky T, Graham MS, Penfold RS, Bowyer RC, et al. Attributes and Predictors of Long COVID. *Nat Med* (2021) 27(4):626–31. doi: 10.1038/s41591-021-01292-y
14. Files JK, Boppana S, Perez MD, Sarkar S, Lowman KE, Qin K, et al. Sustained Cellular Immune Dysregulation in Individuals Recovering From SARS-CoV-2 Infection. *J Clin Invest* (2021) 131(1):140491. doi: 10.1172/JCI140491
15. García-Abellán J, Padilla S, Fernández-González M, García JA, Agulló V, Andreo M, et al. Antibody Response to SARS-CoV-2 Is Associated With Long-Term Clinical Outcome in Patients With COVID-19: A Longitudinal Study. *J Clin Immunol* (2021) 41(7):1490–501. doi: 10.1007/s10875-021-01083-7
16. Peluso MJ, Deitchman AN, Torres L, Iyer NS, Munter SE, Nixon CC, et al. Long-Term SARS-CoV-2-Specific Immune and Inflammatory Responses in Individuals Recovering From COVID-19 With and Without Post-Acute Symptoms. *Cell Rep* (2021) 36(6):109518. doi: 10.1016/j.celrep.2021.109518
17. Ryan FJ, Hope CM, Masavuli MG, Lynn MA, Mekonnen ZA, Yeow AEL, et al. Long-Term Perturbation of the Peripheral Immune System Months After SARS-CoV-2 Infection. *BMC Med* (2022) 20(1):26. doi: 10.1186/s12916-021-02228-6
18. Su Y, Yuan D, Chen DG, Ng RH, Wang K, Choi J, et al. Multiple Early Factors Anticipate Post-Acute COVID-19 Sequelae. *Cell* (2022) 185(5):881–95.e20. doi: 10.1016/j.cell.2022.01.014
19. Zhao J, Sun L, Zhao Y, Feng D, Cheng J, Zhang G. Coronavirus Endoribonuclease Ensures Efficient Viral Replication and Prevents Protein Kinase R Activation. *J Virol* (2020) 95(7):e02103–20. doi: 10.1128/JVI.02103-20
20. De Biasi S, Lo Tartaro D, Meschiari M, Gibellini L, Bellinazzi C, Borella R, et al. Expansion of Plasmablasts and Loss of Memory B Cells in Peripheral Blood From COVID-19 Patients With Pneumonia. *Eur J Immunol* (2020) 50 (9):1283–94. doi: 10.1002/eji.202048838
21. Gibellini L, De Biasi S, Paolini A, Borella R, Boraldi F, Mattioli M, et al. Altered Bioenergetics and Mitochondrial Dysfunction of Monocytes in Patients With COVID-19 Pneumonia. *EMBO Mol Med* (2020) 12(12): e13001. doi: 10.15252/emmm.202013001
22. Bernardes JP, Mishra N, Tran F, Bahmer T, Best L, Blase JI, et al. Longitudinal Multi-Omics Analyses Identify Responses of Megakaryocytes, Erythroid Cells, and Plasmablasts as Hallmarks of Severe COVID-19. *Immunity* (2020) 53 (6):1296–1314.e9. doi: 10.1016/j.immuni.2020.11.017
23. Sosa-Hernández VA, Torres-Ruíz J, Cervantes-Díaz R, Romero-Ramírez S, Páez-Franco JC, Meza-Sánchez DE, et al. B Cell Subsets as Severity-Associated Signatures in COVID-19 Patients. *Front Immunol* (2020) 11:611004. doi: 10.3389/fimmu.2020.611004
24. Kwiecień I, Rutkowska E, Kłos K, Więsik-Szewczyk E, Jahnz-Różyk K, Rzepecki P, et al. Maturation of T and B Lymphocytes in the Assessment of the Immune Status in COVID-19 Patients. *Cells* (2020) 9(12):E2615. doi: 10.3390/cells9122615
25. Huber S, Massri M, Grasse M, Fleischer V, Kellnerová S, Harpf V, et al. Systemic Inflammation and Complement Activation Parameters Predict Clinical Outcome of Severe SARS-CoV-2 Infections. *Viruses* (2021) 13 (12):2376. doi: 10.3390/v13122376
26. De Biasi S, Tartaro DL, Gibellini L, Paolini A, Quong A, Petes C, et al. Endogenous Control of Inflammation Characterizes Pregnant Women With Asymptomatic or Paucisymptomatic SARS-CoV-2 Infection. *Nat Commun* (2021) 12(1):4677. doi: 10.21203/rs.3.rs-263619/v1
27. Carvalho T, Krammer F, Iwasaki A. The First 12 Months of COVID-19: A Timeline of Immunological Insights. *Nat Rev Immunol* (2021) 21(4):245–56. doi: 10.1038/s41577-021-00522-1
28. Schultze JL, Aschenbrenner AC. COVID-19 and the Human Innate Immune System. *Cell* (2021) 184(7):1671–92. doi: 10.1016/j.cell.2021.02.029
29. Sette A, Crotty S. Adaptive Immunity to SARS-CoV-2 and COVID-19. *Cell* (2021) 184(4):861–80. doi: 10.1016/j.cell.2021.01.007
30. Lau AWY, Turner VM, Bourne K, Hermes JR, Chan TD, Brink R. BAFFR Controls Early Memory B Cell Responses But Is Dispensable for Germinal Center Function. *J Exp Med* (2021) 218(2):e20191167. doi: 10.1084/jem.20191167
31. Talla A, Vasaikar SV, Lemos MP, Moodie Z, Lee Pebworth M-P, Henderson KE, et al. Longitudinal Immune Dynamics of Mild COVID-19 Define Signatures of Recovery and Persistence. *bioRxiv* [Preprint] (2021) 05 (26):442666. doi: 10.1101/2021.05.26.442666

32. Gangaev A, Ketelaars SLC, Isaeva OI, Patiwael S, Dopler A, Hoefakker K, et al. Identification and Characterization of a SARS-CoV-2 Specific CD8+ T Cell Response With Immunodominant Features. *Nat Commun* (2021) 12(1):2593. doi: 10.1038/s41467-021-22811-y
33. De Biasi S, Meschiari M, Gibellini L, Bellinazzi C, Borella R, Fidanza L, et al. Marked T Cell Activation, Senescence, Exhaustion and Skewing Towards TH17 in Patients With COVID-19 Pneumonia. *Nat Commun* (2020) 11 (1):3434. doi: 10.21203/rs.3.rs-23957/v1
34. Cossarizza A, Chang H, Radbruch A, Abrignani S, Addo R, Akdis M, et al. Guidelines for the Use of Flow Cytometry and Cell Sorting in Immunological Studies (Third Edition). *Eur J Immunol* (2021) 51(12):2708–3145. doi: 10.1002/eji.202170126
35. Tomiyama H, Matsuda T, Takiguchi M. Differentiation of Human CD8 $^{+}$ T Cells From a Memory to Memory/Effector Phenotype. *J Immunol* (2002) 168 (11):5538–50. doi: 10.4049/jimmunol.168.11.5538
36. Balcom EF, Nath A, Power C. Acute and Chronic Neurological Disorders in COVID-19: Potential Mechanisms of Disease. *Brain J Neurol* (2021) 144 (12):3576–88. doi: 10.1093/brain/awab302
37. Ellul MA, Benjamin L, Singh B, Lant S, Michael BD, Easton A, et al. Neurological Associations of COVID-19. *Lancet Neurol* (2020) 19(9):767–83. doi: 10.1016/S1474-4422(20)30221-0
38. Fernández-Castañeda A, Lu P, Geraghty AC, Song E, Lee M-H, Wood J, et al. Mild Respiratory SARS-CoV-2 Infection Can Cause Multi-Lineage Cellular Dysregulation and Myelin Loss in the Brain. *BioRxiv Prepr Serv Biol* (2022) 2022:01.07.475453. doi: 10.1101/2022.01.07.475453
39. Carfì A, Bernabei R, Landi F. Gemelli Against COVID-19 Post-Acute Care Study Group. Persistent Symptoms in Patients After Acute COVID-19. *JAMA* (2020) 324(6):603–5. doi: doi: 10.1001/jama.2020.12603
40. Harapan BN, Yoo HJ. Neurological Symptoms, Manifestations, and Complications Associated With Severe Acute Respiratory Syndrome Coronavirus 2 (SARS-CoV-2) and Coronavirus Disease 19 (COVID-19). *J Neurol* (2021) 268(9):3059–71. doi: 10.1007/s00415-021-10406-y
41. Proal AD, VanElzakker MB. Long COVID or Post-Acute Sequelae of COVID-19 (PASC): An Overview of Biological Factors That May Contribute to Persistent Symptoms. *Front Microbiol* (2021) 12:698169. doi: 10.3389/fmicb.2021.698169
42. Kratzer B, Trapin D, Ettel P, Körmöczi U, Rottal A, Tuppy F, et al. Immunological Imprint of COVID-19 on Human Peripheral Blood Leukocyte Populations. *Allergy* (2021) 76(3):751–65. doi: 10.1111/all.14647
43. Loretelli C, Abdelsalam A, D'Addio F, Ben Nasr M, Assi E, Usuelli V, et al. PD-1 Blockade Counteracts Post-COVID-19 Immune Abnormalities and Stimulates the Anti-SARS-CoV-2 Immune Response. *JCI Insight* (2021) 6 (24):e146701. doi: 10.1172/jci.insight.146701
44. Weng N-P, Akbar AN, Goronzy J. CD28(-) T Cells: Their Role in the Age-Associated Decline of Immune Function. *Trends Immunol* (2009) 30(7):306–12. doi: 10.1016/j.it.2009.03.013
45. Pinti M, Appay V, Campisi J, Frasca D, Fülöp T, Sauce D, et al. Aging of the Immune System: Focus on Inflammation and Vaccination. *Eur J Immunol* (2016) 46(10):2286–301. doi: 10.1002/eji.201546178
46. Strioga M, Pasukoniene V, Characiejus D. CD8+ CD28- and CD8+ CD57+ T Cells and Their Role in Health and Disease. *Immunology* (2011) 134(1):17–32. doi: 10.1111/j.1365-2567.2011.03470.x
47. Agrati C, De Biasi S, Fidanza L, Gibellini L, Nasi M, Pinti M, et al. The Importance of Advanced Cytometry in Defining New Immune Cell Types and Functions Relevant for the Immunopathogenesis of HIV Infection. *AIDS Lond Engl* (2020) 34(15):2169–85. doi: 10.1097/QAD.0000000000002675
48. Li M, Guo W, Dong Y, Wang X, Dai D, Liu X, et al. Elevated Exhaustion Levels of NK and CD8+ T Cells as Indicators for Progression and Prognosis of COVID-19 Disease. *Front Immunol* (2020) 11:580237. doi: 10.3389/fimmu.2020.580237
49. Gong F, Dai Y, Zheng T, Cheng L, Zhao D, Wang H, et al. Peripheral CD4+ T Cell Subsets and Antibody Response in COVID-19 Convalescent Individuals. *J Clin Invest* (2020) 130(12):6588–99. doi: 10.1172/JCI141054
50. Galván-Peña S, Leon J, Chowdhary K, Michelson DA, Vijaykumar B, Yang L, et al. Profound Treg Perturbations Correlate With COVID-19 Severity. *Proc Natl Acad Sci USA* (2021) 118(37):e2111315118.
51. Wang H, Wang Z, Cao W, Wu Q, Yuan Y, Zhang X. Regulatory T Cells in COVID-19. *Aging Dis* (2021) 12(7):1545. doi: 10.14336/AD.2021.0709
52. Chen Q, Mo L, Cai X, Wei L, Xie Z, Li H, et al. ICOS Signal Facilitates Foxp3 Transcription to Favor Suppressive Function of Regulatory T Cells. *Int J Med Sci* (2018) 15(7):666–73. doi: 10.7150/ijms.23940
53. Martonik D, Parfieniuk-Kowerda A, Rogalska M, Flisiak R. The Role of Th17 Response in COVID-19. *Cells* (2021) 10(6):1550. doi: 10.3390/cells10061550
54. Sugimoto MA, Sousa LP, Pinho V, Perretti M, Teixeira MM. Resolution of Inflammation: What Controls Its Onset? *Front Immunol* (2016) 7:160. doi: 10.3389/fimmu.2016.00160
55. García-González P, Tempio F, Fuentes C, Merino C, Vargas L, Simon V, et al. Dysregulated Immune Responses in COVID-19 Patients Correlating With Disease Severity and Invasive Oxygen Requirements. *Front Immunol* (2021) 12:769059. doi: 10.3389/fimmu.2021.769059
56. Mitsuyama Y, Yamakawa K, Kayano K, Maruyama M, Wada T, Fujimi S. Prolonged Enhancement of Cytotoxic T Lymphocytes in the Post-Recovery State of Severe COVID-19. *J Intensive Care* (2021) 9(1):76. doi: 10.1186/s40560-021-00591-3
57. Phetsouphanh C, Darley DR, Wilson DB, Howe A, Munier CML, Patel SK, et al. Immunological Dysfunction Persists for 8 Months Following Initial Mild-to-Moderate SARS-CoV-2 Infection. *Nat Immunol* (2022) 23(2):210–6. doi: 10.1038/s41590-021-01113-x
58. Novais FO, Nguyen BT, Scott P. Granzyme B Inhibition by Tofacitinib Blocks the Pathology Induced by CD8 T Cells in Cutaneous Leishmaniasis. *J Invest Dermatol* (2021) 141(3):575–85. doi: 10.1016/j.jid.2020.07.011
59. Hiroyasu S, Zeglinski MR, Zhao H, Pawluk MA, Turner CT, Kasprick A, et al. Granzyme B Inhibition Reduces Disease Severity in Autoimmune Blistering Diseases. *Nat Commun* (2021) 12(1):302. doi: 10.1038/s41467-020-20604-3
60. Perretti M, Leroy X, Bland EJ, Montero-Melendez T. Resolution Pharmacology: Opportunities for Therapeutic Innovation in Inflammation. *Trends Pharmacol Sci* (2015) 36(11):737–55. doi: 10.1016/j.tips.2015.07.007
61. Pavli A, Theodoridou M, Maltezou HC. Post-COVID Syndrome: Incidence, Clinical Spectrum, and Challenges for Primary Healthcare Professionals. *Arch Med Res* (2021) 52(6):575–81. doi: 10.1016/j.arcmed.2021.03.010
62. Maltezou HC, Pavli A, Tsakris A. Post-COVID Syndrome: An Insight on Its Pathogenesis. *Vaccines* (2021) 9(5):497. doi: 10.3390/vaccines9050497
63. Siemińska I, Węglarczyk K, Surmiak M, Kurowska-Baran D, Sanak M, Siedlar M, et al. Mild and Asymptomatic COVID-19 Convalescents Present Long-Term Endotype of Immunosuppression Associated With Neutrophil Subsets Possessing Regulatory Functions. *Front Immunol* (2021) 12:748097. doi: 10.3389/fimmu.2021.748097

Conflict of Interest: The authors declare that the research was conducted in the absence of any commercial or financial relationships that could be construed as a potential conflict of interest.

Publisher's Note: All claims expressed in this article are solely those of the authors and do not necessarily represent those of their affiliated organizations, or those of the publisher, the editors and the reviewers. Any product that may be evaluated in this article, or claim that may be made by its manufacturer, is not guaranteed or endorsed by the publisher.

Copyright © 2022 Wiech, Chroscicki, Swatler, Stepnik, De Biasi, Hampel, Brewinska-Olchowik, Maliszewska, Sklinda, Durlik, Wierzba, Cossarizza and Piwocka. This is an open-access article distributed under the terms of the Creative Commons Attribution License (CC BY). The use, distribution or reproduction in other forums is permitted, provided the original author(s) and the copyright owner(s) are credited and that the original publication in this journal is cited, in accordance with accepted academic practice. No use, distribution or reproduction is permitted which does not comply with these terms.

frontiers | Frontiers in Immunology

TYPE Original Research
PUBLISHED 04 October 2022
DOI 10.3389/fimmu.2022.1004656

Check for updates

OPEN ACCESS

EDITED BY
Sara De Biasi,
University of Modena and Reggio Emilia, Italy

REVIEWED BY
Giovanna Borsellino,
Santa Lucia Foundation (IRCCS), Italy
Florian Mair,
ETH Zürich, Switzerland
Geng Meng,
China Agricultural University, China

*CORRESPONDENCE
Jun Dong
dong@drfz.de

†These authors share last authorship

SPECIALTY SECTION
This article was submitted to T Cell Biology, a section of the journal Frontiers in Immunology

RECEIVED 27 July 2022
ACCEPTED 20 September 2022
PUBLISHED 04 October 2022

CITATION
Li J, Reinke S, Shen Y, Schollmeyer L, Liu Y-C, Wang Z, Hardt S, Hipfl C, Hoffmann U, Frischbutter S, Chang H-D, Alexander T, Perka C, Radbruch H, Qin Z, Radbruch A and Dong J (2022) A ubiquitous bone marrow reservoir of preexisting SARS-CoV-2-reactive memory CD4$^+$ T lymphocytes in unexposed individuals. *Front. Immunol.* 13:1004656. doi: 10.3389/fimmu.2022.1004656

COPYRIGHT
© 2022 Li, Reinke, Shen, Schollmeyer, Liu, Wang, Hardt, Hipfl, Hoffmann, Frischbutter, Chang, Alexander, Perka, Radbruch, Qin, Radbruch and Dong. This is an open-access article distributed under the terms of the Creative Commons Attribution License (CC BY). The use, distribution or reproduction in other forums is permitted, provided the original author(s) and the copyright owner(s) are credited and that the original publication in this journal is cited, in accordance with accepted academic practice. No use, distribution or reproduction is permitted which does not comply with these terms.

A ubiquitous bone marrow reservoir of preexisting SARS-CoV-2-reactive memory CD4$^+$ T lymphocytes in unexposed individuals

Jinchan Li[1], Simon Reinke[2], Yu Shen[1], Lena Schollmeyer[1], Yuk-Chien Liu[1], Zixu Wang[1], Sebastian Hardt[3], Christian Hipfl[3], Ute Hoffmann[1,4], Stefan Frischbutter[5,6], Hyun-Dong Chang[4], Tobias Alexander[7], Carsten Perka[3], Helena Radbruch[8], Zhihai Qin[9], Andreas Radbruch[1†] and Jun Dong[1*†]

[1]Cell Biology, Deutsches Rheuma-Forschungszentrum Berlin (DRFZ), Institute of the Leibniz Association, Berlin, Germany, [2]Berlin Brandenburg Center for Regenerative Therapies (BCRT), Charité - Universitätsmedizin Berlin, Corporate Member of Freie Universität Berlin, Humboldt-Universität zu Berlin, and Berlin Institute of Health, Berlin, Germany, [3]Center for Musculoskeletal Surgery, Charité - Universitätsmedizin Berlin, Corporate Member of Freie Universität Berlin, Humboldt-Universität zu Berlin, and Berlin Institute of Health, Berlin, Germany, [4]Schwiete-Laboratory for Microbiota and Inflammation, Deutsches Rheuma-Forschungszentrum Berlin (DRFZ), Institute of the Leibniz Association, Berlin, Germany, [5]Institute of Allergology, Charité - Universitätsmedizin Berlin, corporate member of Freie Universität Berlin, Humboldt-Universität zu Berlin, and Berlin Institute of Health, Berlin, Germany, [6]Allergology and Immunology, Fraunhofer Institute for Translational Medicine and Pharmacology (ITMP), Berlin, Germany, [7]Department of Rheumatology and Clinical Immunology, Charité - Universitätsmedizin Berlin, Corporate Member of Freie Universität Berlin, Humboldt-Universität zu Berlin, and Berlin Institute of Health, Berlin, Germany, [8]Institute of Neuropathology, Charité - Universitätsmedizin Berlin, Corporate Member of Freie Universität Berlin, Humboldt-Universität zu Berlin, and Berlin Institute of Health, Berlin, Germany, [9]Medical Research Center, The First Affiliated Hospital of Zhengzhou University, Zhengzhou, China

Circulating, blood-borne SARS-CoV-2-reactive memory T cells in persons so far unexposed to SARS-CoV-2 or the vaccines have been described in 20-100% of the adult population. They are credited with determining the efficacy of the immune response in COVID-19. Here, we demonstrate the presence of preexisting memory CD4$^+$ T cells reacting to peptides of the spike, membrane, or nucleocapsid proteins of SARS-CoV-2 in the bone marrow of all 17 persons investigated that had previously not been exposed to SARS-CoV-2 or one of the vaccines targeting it, with only 15 of these persons also having such cells detectable circulating in the blood. The preexisting SARS-CoV-2-reactive memory CD4$^+$ T cells of the bone marrow are abundant and polyfunctional, with the phenotype of central memory T cells. They are tissue-resident, at least in those persons who do not have such cells in the blood, and about 30% of them express CD69. Bone marrow resident SARS-CoV-2-reactive memory CD4$^+$ memory T cells are also abundant in vaccinated persons analyzed 10-168 days after 1°-4° vaccination. Apart from securing the bone marrow, preexisting cross-reactive memory CD4$^+$ T cells may play an

important role in shaping the systemic immune response to SARS-CoV-2 and the vaccines, and contribute essentially to the rapid establishment of long-lasting immunity provided by memory plasma cells, already upon primary infection.

KEYWORDS

SARS-CoV-2, cross-reactive, memory CD4+ T lymphocytes, human bone marrow, peripheral blood, polyfunctional, tissue-resident memory T cells (Trm)

Introduction

Human severe acute respiratory syndrome coronavirus 2 (SARS-CoV-2) causes the coronavirus disease 2019 (COVID-19), which poses a substantial threat to public health. The individual human response against the SARS-CoV-2 varies dramatically, from asymptomatic to severe disease characterized by pneumonia and acute respiratory distress syndrome (ARDS) often resulting in death. Presently, it is unclear why only a few of the infected develop severe COVID-19, and most are protected from it.

One reason may be preexisting cross-reactive immunological memory to SARS-CoV-2. Recent studies have revealed preexisting, cross-reactive T cell immunity to SARS-CoV-2 in unexposed healthy donors and asymptomatic COVID-19 patients. We and others have shown that SARS-CoV-2-reactive T cells could be detected in the peripheral blood (1–7) of more than 20% of healthy individuals who had previously not been exposed to SARS-CoV-2 or a vaccine mimicking it (2–11). A correlation of T cell reactivity towards SARS-CoV-2 spike (S) protein and human common cold corona viruses (HCoVs) (3, 9, 12, 13), suggestive of cross-reactivity, was only observed in unexposed healthy donors but not in COVID-19 convalescents (6, 12). These circulating, preexisting cross-reactive $CD4^+$ T cells from unexposed healthy donors had pro-inflammatory Th1 and Tfh-like anti-viral potential (1, 13). Such cells likely contribute to fast and efficient immune responses against SARS-CoV-2 (2–4, 6, 12, 14, 15), and their presence correlates with protection of naïve individuals against SARS-CoV-2 infection in COVID-19 contacts (4).

Circulating memory T cells reactive to a particular antigen are easy to identify, but little is known about their persistence (16) and their contribution to long-term memory. Their exclusive contribution to systemic and tissue-specific immunity is challenged by the increasing realization of the relevance of tissue-resident memory T cells (Trm) (17–19). $CD69^+$ Trm have been described (19–22), as well as $CD69^-$ Trm (22). In particular, $CD4^+$ Trm of the lung mediating local immunity to respiratory viruses (23, 24) and presumably also to SARS-CoV2 (25) have been reported.

We have previously shown that bone marrow provides dedicated niches for the long-term maintenance of immune memory cells (26). Trm of human bone marrow maintain long-term memory to systemic antigens, in particular viruses like measles, mumps, and rubella, even when their circulating counterparts are no longer detectable (19). Following a systemic challenge, bone marrow Trm are rapidly mobilized and then contribute essentially to the secondary immune response (27). Here, we compare preexisting, SARS-CoV-2 cross-reactive memory $CD4^+$ T lymphocytes of bone marrow and blood of 17 individuals. Bone marrow of all individuals did contain preexisting, persistent, polyfunctional SARS-CoV-2-reactive memory $CD4^+$ T lymphocytes, in numbers largely exceeding those circulating in their blood. At frequencies of above 10^{-4} among memory $CD4^+$ T cells, these Trm qualify a significant pillar of preexisting immunity to SARS-CoV-2.

Materials and methods

Study subjects

This study was conducted in accordance with the approval from the local ethics committee (Ethikkommission der Charité-Univerisitätsmedizin Berlin; EA1/005/21) and informed consent obtained according to the Declaration of Helsinki. Thirty-one paired bone marrow biopsy (BM) and peripheral blood (PB) samples were collected from anonymous systemically healthy individuals (13 male and 18 female; age ± SEM = 66.52 ± 2.65) undergoing hip replacement surgery at the Charité – Universitätsmedizin Berlin from September 2020 to May 2022. The study cohort consisted of 17 SARS-CoV-2 and the vaccines unexposed donors and 14 vaccinated donors. Samples from donors 1-17 and donors 18-31 were collected before and after the COVID-19 vaccination campaign in Germany (Dec. 2020), respectively. Donors 18-31 had been vaccinated either with or without booster vaccination (since Oct 2021). Donors 1-22 were also validated for levels of SRARS-CoV-2 S- (spike) or N- (nucleocapsid) protein specific antibody titres in plasma isolated from PB samples.

Sample collection and preparation

BM and PB samples were subject to preparation in less than 4 hours as described previously (19, 28). Briefly, peripheral blood mononuclear cells (PBMCs) were isolated from 5-15 mL blood samples (diluted with room temperature PBS buffer at a 1:1 ratio) by density gradient centrifugation using Ficoll-Paque Plus (Cytiva). Bone marrow mononuclear cells (BMMCs) were filtered through a 70 μM cell strainer prior to density gradient centrifugation using Ficoll-Paque Plus. The resulting plasma layers from PB samples were collected as plasma samples and stored at -80°C until further use. Cell number was determined using a MACSQuant (Miltenyi Biotech).

Determination of spike- and nucleocapsid-protein specific antibodies by enzyme-linked immunosorbent assay

To evaluate the levels of IgG antibodies specific to spike S1 and nucleocapsid proteins of SARS-CoV-2 in plasma samples, respective human IgG ELISA Kits from Biolegend were used according to the manufacturer's instructions. In short, plasma samples were tested at serial dilutions of 1:500, 1:1000, 1:2000, 1:4000 and 1:8000, each with two technical replicates. Absorbance was read immediately by Spectramax Plus 384 Microplate Reader at 450 nm. Data were analyzed using the Graphpad Prism 9.1.0.

Flow cytometry analysis

Staining, data acquisition, and analysis were carried out as described previously (19, 28). Briefly, eight- to twelve- colour flow cytometry analysis was performed for the analysis of cell count, phenotype, and cytokine profile using a MACSQuant Analyzer 10 flow cytometer (Miltenyi Biotec) and LSRFortessa flow cytometer (BD Biosciences). The following anti-human antibodies were used to stain cells in four different panels: 1). propidium iodide (PI), or DAPI; 2). CD3 BV785, CD19 BV510, CD14 PO, CD4 PE-Cy5, CD8 PE, CD45RO BV650, CD154 BV421, IFN-γ PE-Cy7, IL-2 FITC, TNF-α Allophycocyanin, and fixable Live/Dead PO; 3). CD3 BV785, CD4 PE-Cy5, CD14 PO, CD19 BV510, Live/Dead PO, CD45RA BV605, CCR7 A488, CD154 PE, IL-2 APC-Cy7, TNF-α Allophycocyanin, and IFN-γ PE-Cy7; and 4). CD3 BV785, CD4 PE-Cy5, Live/Dead PO, CD14 PO, CD19 BV510, CD45RO BV650, CD154 PE, IL-2 APC-Cy7, TNF-α Allophycocyanin, IFN-γ PE-Cy7, and CFSE. Stained cells were acquired using FACSDiva (BD Biosciences) software and data were analyzed with FlowJo (BD Biosciences).

Identification of *ex vivo* antigen-reactive memory $CD4^+$ T lymphocytes

BMMCs and PBMCs were cultured separately in RPMI 1640 Supplementaled with 1% GlutaMAX, 100 U/mL penicillin, 100 μg/mL streptomycin, and 5% (vol/vol) human AB serum. According to cell count, cells were seeded in an appropriate culture plate at a cell density of $1\text{-}2 \times 10^7$ cells/mL. Anti-CD28 (1 μg/mL), CMV (38 μg/mL), tetanus toxoid (TT; 1 lethal factor [Lf]/mL), or a mixture of three peptide pools – the spike-, membrane-, and nucleocapsid-protein of SARS-Cov-2 (0.6 nmol of each peptide/mL) were used to stimulate cells. Stimulation with CD28 alone and in combination with Staphylococcus enterotoxin B (SEB; 1μg/ml) were used as negative and positive controls, respectively. For each condition, at least $5\text{-}10 \times 10^6$ cells were stimulated for a total of 12 h at 37° and 5% CO_2, with brefeldin A (1 μg/mL) added to the mixture for the last 10 h. Stimulated cells were first stained for surface antigens followed by fixation with 2% paraformaldehyde and permeabilizing solution 2 according to the manufacture's instruction. Antigen-reactive memory $CD4^+$ T cells were identified as Live/Dead$^-$CD19$^-$CD14$^-$CD3$^+$CD8$^-$ CD4$^+$CD45RO$^+$ (/CD45RA$^-$CCR7$^{+/-}$) CD154$^+$cytokine$^+$. About 2×10^6 lymphocytes were analyzed for each condition.

Alternatively, $CD69^+$ BMMCs were isolated using the CD69 MicroBead Kit according to the manufacturer recommendations. Magnetically separated (flow-through) $CD69^-$ BMMCs were labelled with carboxyfluorescein succinimidyl ester (CFSE) at the final concentration of 1 μM. The CFSE labelled $CD69^-$ BMMCs were then mixed with the $CD69^+$ BMMCs and co-cultured for antigenic stimulation under conditions as described above. Antigen-reactive memory $CD4^+$ T cells from $CD69^-$ and $CD69^+$ subsets of BMMCs were identified as Live/Dead$^-$CD19$^-$ CD14$^-$CD3$^+$CD8$^-$CD4$^+$CD45RO$^+$CFSE$^{+/-}$ CD154$^+$cytokine$^+$.

Statistics

Statistical analyses were performed with Graphpad Prism software (version 9.1.0). For analysis of paired blood and bone marrow samples, Wilcoxon matched-pairs signed rank test was used. For analysis of unpaired samples, Mann–Whitney U test

was used. A p-value < 0.05 was considered statistically significant; *p<0.05, **p<0.01, ***p<0.001, and ****p<0.0001.

Results

Bone marrow hosts SARS-CoV-2 reactive memory CD4$^+$ T cells in both unexposed and vaccinated donors

Paired bone marrow and blood samples (Figure 1A) were obtained from 31 individuals (aged 35 to 87 years) that had not been infected with SARS-CoV-2. Of those, 17 unexposed (donors 1-17) were examined prior to and 14 vaccinated (donors 18-31) after 1° (donors 18-20), or 10-168 days after 3° (donors 21-28 and 30, 31) or 4° (donor 29) vaccination, respectively (Table 1). While the former were seronegative for S (Figure 1B) and N (Figure 1C) proteins of SARS-CoV-2, the latter were positive for S and negative for N.

To identify SARS-CoV-2-reactive memory CD4$^+$ T cells (31), we determined the frequencies of memory CD4$^+$ T cells reacting to a mixture of peptides of the S, M, and N proteins of SARS-CoV-2 in both bone marrow and blood of each individuals (Figure 1A). For this, bone marrow and blood mononuclear cells were stimulated with the S/M/N peptides and anti-CD28 for 12 h, and reactive CD4$^+$ T cells were identified according to the expression of the activation-induced marker CD154 (32, 33), and one or more of the cytokines IFN-γ, IL-2, and TNF-α, as assessed by intracellular immunofluorescence (Figure 1D). Frequencies of cells reacting to stimulation with "anti-CD28 alone", i.e. the background control, were subtracted from the frequencies of cells reacting to "anti-CD28 plus antigen". The superantigen SEB, and alternatively CMV-pp65 or tetanus toxoid (TT) were included as controls for stimulation (Supplemental Figures 1A, B and data not shown).

CD154$^+$cytokine$^+$ cells reacting to SARS-CoV-2 were detectable in the blood of 15 donors and in bone marrow of all 17 immunologically naïve donors, at median frequencies significantly higher in bone marrow than in blood, 0.256% (IQR, 0.055%-0.516%) *vs* 0.071% (IQR, 0.018%-0-091%) (p<0.01) (Supplemental Figure 1B). Interestingly, in two of the unexposed donors, SARS-CoV-2-reactive memory CD4$^+$ T cells were only detectable in bone marrow but not in blood (Supplemental Figure 1B; highlighted), at the detection limit of 10^{-4} among memory CD4$^+$ T cells. In vaccinated donors, frequencies of SARS-CoV-2 reactive CD4$^+$CD154$^+$cytokine$^+$ T cells were higher in bone marrow than in blood in 5 of 14 donors (Supplemental Figure 1B).

Based on the frequencies of gated populations and the reasonable estimate that the number of T cells in the bone marrow is 25 × 10^9, compared to 7 × 10^9 in the blood (29, 30), human bone marrow of unexposed individuals thus hosts in average (median) sixteen (IQR, 9-13) times more SARS-CoV-2-reactive memory CD4$^+$ T cells than blood (p<0.0001) (Figure 1E), roughly 1.4 × 10^7 cells. Compared to this, only about three times more SARS-CoV-2-reactive memory CD4$^+$ T cells were found in bone marrow than in blood in 7 of 14 vaccinated donors analyzed (Figure 1E). Three vaccinated donors did not show a dominant SARS-CoV-2-reactive memory CD4$^+$ T cell pool of the bone marrow (Figure 1E).

Bone marrow SARS-CoV-2 reactive memory CD4$^+$ T cells are polyfunctional

We next compared the functional imprinting of SARS-CoV-2-reactive memory CD4$^+$ T cells from bone marrow and blood. Both frequencies (Supplemental Figure 1C) and absolute numbers (Figure 1F) of SARS-CoV-2-reactive memory CD4$^+$ T cells expressing IFN-γ, TNF-α or IL-2 were significantly higher for bone marrow as compared to blood of unexposed donors. For example, IL-2-producers were detected at median frequencies of 0.207% (IQR, 0.025%-0.276%) for bone marrow versus 0.062% (IQR, 0.004%-0.086%) for blood (Supplemental Figure 1C). Median absolute cell numbers were 1.1 ×10^7 for bone marrow versus 8.2 × 10^5 for blood (Figure 1F). In the 14 vaccinated donors analyzed, absolute numbers (Figure 1F) of SARS-CoV-2-reactive memory T cells expressing each of these three cytokines from bone marrow were significantly higher in the bone marrow than in blood, although not in terms of frequencies in most donors (Supplemental Figure 1C).

When comparing cells expressing only one of the cytokines analyzed, or two or even all three, all were significantly more abundant among bone marrow cells than those of blood from unexposed donors, except for T cells producing only TNF-α (Figure 1G). In terms of frequencies, the cells coexpressing two or three of the cytokines were significantly higher among bone marrow cells than those of blood (Supplemental Figure 1D). For vaccinated donors, IFN-γ$^+$ single-, IFN-γ$^+$TNF-α$^+$ double-, IL-2$^+$TNF-α$^+$ double-, and triple-producers were significantly more abundant among bone marrow memory T cells than among memory T cells of the blood (Figure 1G). In terms of frequencies, only IFN-γ$^+$ single-producers were significant more frequent among bone marrow cells than those of blood (Supplemental Figure 1D).

With considerable individual variation (Figure 1H), polyfunctional SARS-CoV-2 reactive memory T cells, i.e. those imprinted to reexpress two or three of the cytokines IL-2, IFN-γ, and TNF-α, were significantly more abundant among bone marrow cells than among blood cells, both in naïve (2.8 × 10^6 [IQR, 0.6-4.2 × 10^6] *vs* 1.1 × 10^5 [IQR, 0.4-3.1 × 10^5]) and vaccinated donors (4.9 × 10^6 [IQR, 2.2-21 × 10^6] *vs* 1.9 × 10^6 [IQR, 1.0-5.5 × 10^6]) (Figure 1I). The demonstration of those cells even in donors 4 and 7, who did not have detectable numbers of such cells circulating in the blood, implies that those cells are CD4$^+$ Trm of bone marrow.

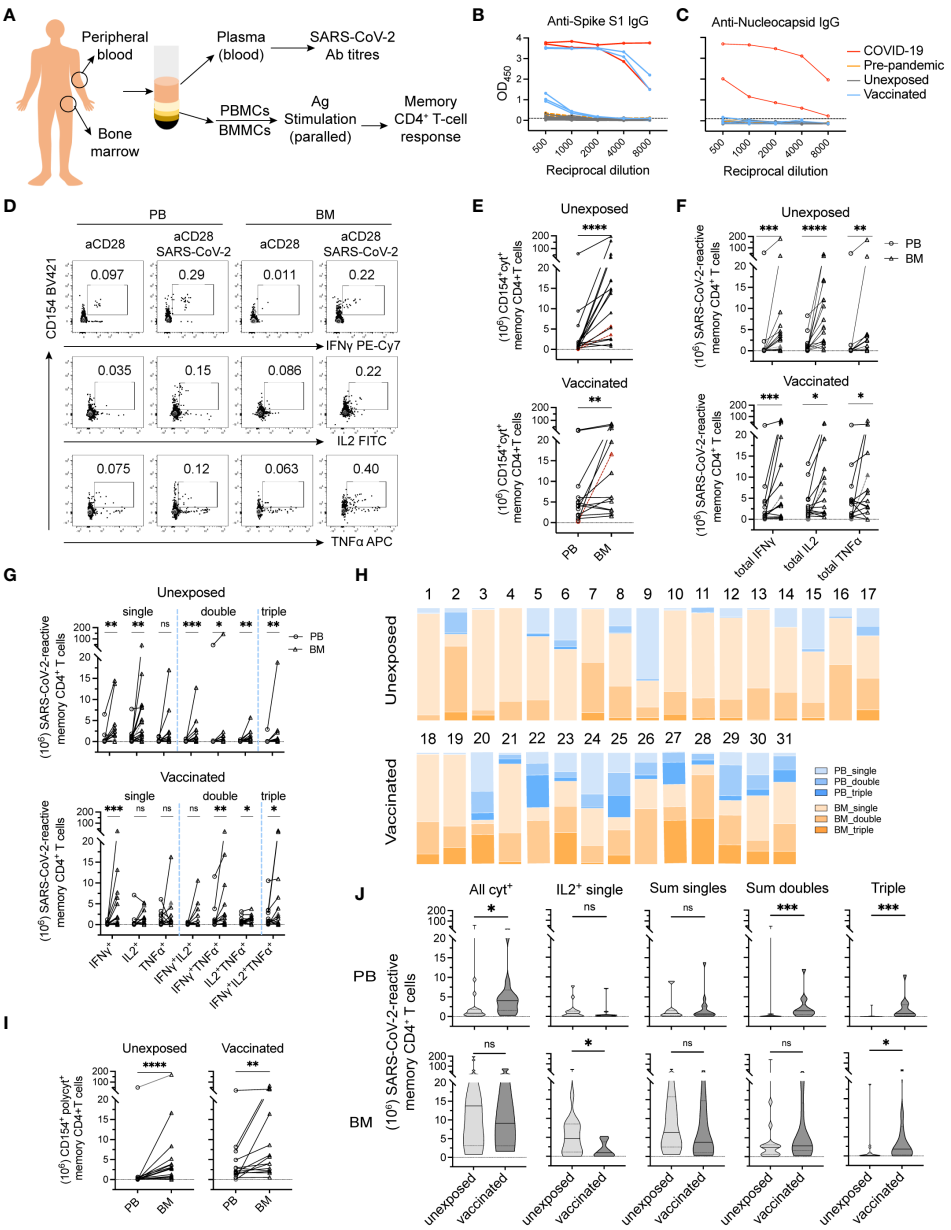


FIGURE 1
Bone marrow hosts polyfunctional memory CD4$^+$ T cells against SARS-CoV-2 in both unexposed and vaccinated adult donors. **(A)** Flowchart of experimental setup. Mononuclear cells isolated from paired peripheral blood (PB) and bone marrow biopsy (BM) samples were collected from adult donors. Plasma from PB samples were collected for measuring IgG titers specific for SARS-CoV-2 Spike and Nucleocapsid proteins. PBMCs and BMMCs were stimulated with S/M/N peptides mix of SARS-CoV-2 and analyzed for antigen-reactive memory CD4$^+$ T cell responses. (**B** + **C**) Levels of antibodies to SARS-CoV-2 S **(B)** and N **(C)** proteins were measured using serial dilutions (two technical replicates of each dilution) of donor's plasma in an Enzyme-Linked Immunosorbent Assay (ELISA). Red line, positive controls (n = 2) from acute phase ICU COVID-19 patients analyzed in previous study (1); yellow lines, negative control samples collected prior to COVID-19 pandemic (Pre-pandemic; n = 2); black lines, samples from unexposed donors (Unexposed; n = 17); blue lines, samples from COVID-19 vaccinated donors (Vaccinated; n = 5). The Y-axis corresponds to the mean optical density (OD) values assessed at 450 nm as depicted reciprocal dilutions on the X-axis. **(D)** Representative plots showing SARS-CoV-2-reactive memory CD4$^+$ T cells expressing CD154 and one or more of the induced cytokine production (IL-2, TNF-α, or IFN-γ). **(E–G)** Estimated absolute numbers (29, 30) of CD154$^+$cytokine$^+$ (**E**; all cytokine producing cells), total individual CD154$^+$cytokine$^+$ **(F)** and single, double and triple cytokine-producing cells **(G)**. Symbols in red and dashed lines indicate estimated cell numbers of PB calculated according to frequencies under detection limit (10^{-4} of memory CD4$^+$ T cells). **(H)** Proportions of single, double, and triple cytokine-producing cells from **(G)** among total antigen-reactive cells **(E)** to the sum of PB and BM from donors analyzed on the individual levels. **(I)** Estimated absolute numbers of polyfunctional cells between paired blood and bone marrow samples. **(J)** Shown are estimated absolute numbers of indicated cell types in unexposed *vs* vaccinated donors. Values are presented as median (thick line) with 25th- and 75th-percentile. *p < 0.05, **p < 0.01, ***p < 0.001, ****p < 0.0001; ns, not significant.

Taken together, our results demonstrate a significant population of polyfunctional, SARS-CoV-2-reactive memory $CD4^+$ Trm in the bone marrow in all 17 naïve and 14 vaccinated individuals analyzed.

Composition of bone marrow cytokine-expressing SARS-CoV-2-reactive memory $CD4^+$ T cells in vaccinated donors

Among our vaccinees, SARS-CoV-2-reactive memory T cell responses did not shown patterns related to number of vaccinations received (data now shown). In addition, between our two subcohorts, the age and sex of naïve and vaccinated donors were comparable (Table 1). We thus could fairly compare the composition of SARS-CoV-2-reactive memory $CD4^+$ T cells from blood and bone marrow with respect to their cytokine expression upon restimulation, i.e. their functional potential. For blood, both frequencies (Supplemental Figure 1E) and absolute cell numbers (Figure 1J) of the sum of double producers and triple producers, expressing TNF-α (Supplemental Figure 1F), were significantly increased in vaccinated donors, in line with the significant increase in total numbers of SARS-CoV-2-reactive cells (Supplemental Figure 1E and Figure 1J). For bone marrow, a significant decrease in single IL-2-producers was observed, in terms of both frequencies (Supplemental Figure 1E) and cell numbers (Figure 1J). Numbers of triple producers were significantly increased in bone marrow of vaccinated donors (Figure 1J), although they were not in terms of frequencies (Supplemental Figure 1E). Overall, we detected about equal

TABLE 1 Study subjects.

Donor	Sample	Relative to COVID-19vaccination campaign	Vaccine	Vaccinationstatus	Sex	Age
1	Sep.2020	No	—	—	F	43
2	Sep.2020	No	—	—	M	35
3	Sep.2020	No	—	—	F	55
4	Sep.2020	No	—	—	M	77
5	Sep.2020	No	—	—	M	67
6	Sep.2020	No	—	—	M	66
7	Oct.2020	No	—	—	F	61
8	Oct.2020	No	—	—	F	53
9	Oct.2020	No	—	—	F	48
10	Nov.2020	No	—	—	F	57
11	Nov.2020	No	—	—	F	75
12	Nov.2020	No	—	—	M	85
13	Dec.2020	No	—	—	M	40
14	Dec.2020	No	—	—	F	80
15	Dec.2020	No	—	—	F	78
16	June 2021	No	—	—	F	80
17	Oct.2021	No	—	—	M	69
18	July 2021	Yes	unk	w/o booster	M	63
19	July 2021	Yes	unk	w/o booster	M	78
20	Oct.2021	Yes	unk	w/o booster	M	58
21	Dec.2021	Yes	Moderna	3×, 10 d	M	61
22	Dec.2021	Yes	BioNTech	3×, 6 wks	F	79
23	Jan.2022	Yes	BioNTech	3×, 9 wks	F	80
24	Feb.2022	Yes	Moderna	3×, 9 wks	M	85
25	Feb. 2022	Yes	Moderna	3×, 6 wks	F	54
26	Feb. 2022	Yes	Moderna	3×, 11 wks	M	74
27	Mar. 2022	Yes	Moderna	3×, 15 wks	F	49
28	Mar. 2022	Yes	BioNTech	3×, 17 wks	F	87
29	May 2022	Yes	BioNTech	4×, 6 wks	F	85
30	May 2022	Yes	Moderna	3×, 21 wks	F	59
31	May 2022	Yes	BioNTech	3×, 24 wks	F	81

Information about sample collection date, relative to COVID-19 vaccination campaign, injected vaccine, vaccination status, sex, and age of study subjects. —, not applicable. unk, unknown.

absolute numbers and frequencies of bone marrow SARS-CoV-2-reactive cells in naïve and vaccinated donors, with the exception of cells expressing only IL-2 (Figure 1J and Supplemental Figures 1E, F). Taken together, these results demonstrate an effect of COVID-19 vaccines on reshaping the composition of bone marrow SARS-CoV-2-reactive memory $CD4^+$ T cells, consistent with mobilization and participation of $CD4^+$ Trm of bone marrow, especially those expressing only IL-2 upon restimulation, in the vaccine-induced immune reaction.

SARS-CoV-2-reactive central memory $CD4^+$ T cells of bone marrow

We next determined whether the preexisting SARS-CoV-2-reactive $CD154^+$ memory $CD4^+$ T cells would resemble central memory T (Tcm) cells, expressing C-C chemokine receptor 7 (CCR7), with the potential to participate in secondary immune reactions in germinal centers, as opposed to $CCR7^-$ effector memory T (Tem) cells. SARS-CoV-2-reactive $CD154^+$ $CD4^+$ T cells (Supplemental Figure 2A) were stained for their expression of CCR7 and CD45RA (Figure 2A). In the two naïve and three vaccinated donors analyzed, SARS-CoV-2-reactive $CCR7^+CD45RA^-$ Tcm cells (Supplemental Figure 2B) were more frequent than $CCR7^-CD45RA^-$ Tem cells in both bone marrow and blood, ranging from 50-70% (Supplemental Figure 2C). In absolute numbers, bone marrow contained up to 1.5×10^8 SARS-CoV-2-reactive $CD154^+$ Tcm cells (Figure 2B) and up to about 0.8×10^8 Tem cells (Figure 2C). Thus, bone marrow of naïve and vaccinated donors contained a prominent population of SARS-CoV-2-reactive Tcm cells (Figure 2D).

SARS-CoV-2 reactive $CD69^+$ memory $CD4^+$ Trm of bone marrow

CD69 is discussed as a key marker of Trm (34–37), although also $CD69^-$ cells can be tissue-resident (22). We thus analyzed the CD69 phenotype of bone marrow SARS-CoV-2-reactive memory $CD4^+$ T cells. Because CD69 is upregulated upon activation, we thus isolated $CD69^+$ and $CD69^-$ cells ex vivo from bone marrow (Figure 3A) of 4 vaccinated donors by magnetic cell sorting, labelled the $CD69^-$ cells with carboxyfluorescein succinimidyl ester (CFSE) and mixed them with the unlabeled $CD69^+$ cells of the same bone marrow (Supplemental Figure 3A), and stimulated them with the S/M/N peptides. The reaction of $CD69^+$ and $CD69^-$ from bone marrow was compared to that of ($CD69^-$) memory T cells from their paired blood sample (Figure 3B). Both, $CD69^+$ and $CD69^-$ SARS-CoV-2-reactive $CD154^+$cytokine$^+$ memory $CD4^+$ T cells were readily detectable in the bone marrow (Supplemental Figure 3B), and frequencies of either compartment were even higher than that of blood cells in 2 out of the 4 analyzed donors (Supplemental Figure 3C). Different to their blood counterparts (>98% being $CD69^-$), 30% to 50% of bone marrow memory $CD4^+$ T cells of these four vaccinated

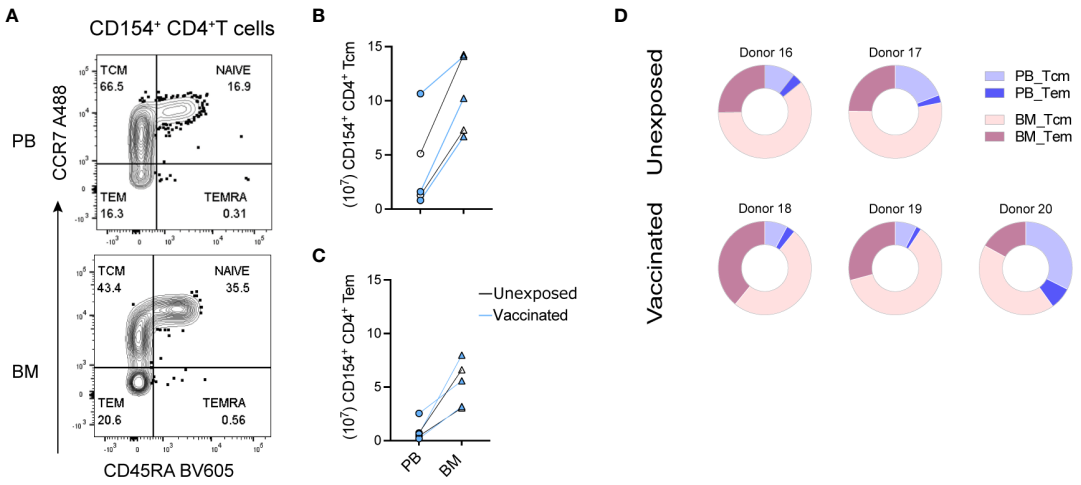


FIGURE 2
Central memory SARS-CoV-2-reactive memory $CD4^+$ T cells of bone marrow. Paired PBMCs and BMMCs from two naïve and three vaccinated donors stimulated with S/M/N of SARS-CoV-2 and analyzed for SARS-CoV-2-reactive $CD154^+$ $CD4^+$ T cells. **(A)** Representative flow cytometric plots showing their counter expressions for CD45RA and CCR7 on $CD154^+$ $CD4^+$ T cells (Supplemental Figure 2A). (**B + C**) Estimated absolute numbers of $CD45RA^-CCR7^+$ Tcm **(B)** and $CD45RA^-CCR7^-$ Tem **(C)** types of SARS-CoV-2-reactive $CD154^+$ memory $CD4^+$ T cells of PB and BM, calculated using the frequency (Supplemental Figures 2B, C) of these cells and the estimated numbers of T cells within BM and PB as described in Figure 1. Blue symbols represent data obtained from vaccinated donors. **(D)** Pie charts showing the proportion of SARS-CoV-2-reactive $CD154^+$ memory $CD4^+$ T cells in the sum of PB and BM as well as their distribution to Tcm and Tem compartments.

donors expressed CD69, and thus qualify as bona fide Trm (Supplemental Figure 3A). In terms of absolute numbers, these Trm represent 15% to 56% of the sum of blood and bone marrow SARS-CoV-2-reactive memory $CD4^+$ T cells (Figure 3C). This shows that after vaccination, a substantial number of Trm are maintained in the bone marrow. Whether and if so which $CD69^-$ cells are also tissue-resident, remains to be shown. For the preexisting SARS-CoV-2-reactive memory $CD4^+$ T cells of naïve individuals described above, the absence of such cells in the circulation of donors 4 and 7 (Figure 1H) would argue *per se*, that all their preexisting bone marrow memory T cells are tissue resident, be they $CD69^+$ or $CD69^-$.

Discussion

Memory T cells cross-reactive to SARS-CoV-2 S, M, N, and/or envelope peptides have been identified in the peripheral blood of unexposed individuals (1–8,) in 20%-100% of the adult population, depending on the method used to identify them. By their numbers, adapted functional imprinting and fast reaction, these cells have the potential to shape immune reactions to SARS-CoV-2 upon infection of naïve individuals, for the good or for the worse (2–4, 6, 12, 14, 15). Whether and if so which ones could possibly serve as a correlate of protection, is less clear (5). Since the original observation that secondary immune reactions are dependent on tissue-resident, but not on circulating lymphocytes (38), it has become increasingly clear that prominent populations of memory T cells are residing in epithelial tissues, including the lung (39, 40), and also in the bone marrow (17, 41). We have shown that in bone marrow prominent populations of $CD4^+$ and $CD8^+$ memory T lymphocytes are maintained as Trm, resting individually in niches provided by mesenchymal stromal cells (34, 42). In particular, such memory T cells maintain memory for viral pathogens infecting *via* the airways, but triggering systemic immune reactions, like measles, mumps and rubella (19). We have recently also shown that bone marrow $CD4^+$ Trm are mobilized into the blood within a day in secondary immune reactions and contribute significantly to the systemic reaction (27). Here we demonstrate that bone marrow also hosts significant numbers of memory $CD4^+$ T cells reactive to SARS-CoV-2, in particular cross-reactive memory T cells preexisting in naïve, SARS-CoV-2 neither infected nor vaccinated individuals.

In all of 17 seronegative, naïve individuals, bone marrow did host SARS-CoV-2 cross-reactive memory $CD4^+$ T cells, at absolute numbers of 10^6 to more than 10^7, numbers about the same as those of measles-, rubella-, or mumps-specific memory $CD4^+$ T cells (19). In 15 out of those 17 naïve individuals, sixteen times more SARS-CoV-2 cross-reactive memory $CD4^+$ T cells were present in bone marrow than in blood. In the remaining two naïve individuals, such cells were present only in the bone marrow but not in blood, at a limit of detection of 10^{-4}. The presence in bone marrow of all naïve individuals analyzed, of a population of memory $CD4^+$ T cells, equal in size to other memories providing long-term immunity to airborne pathogens triggering systemic immune reactions, recapitulates our previous observation for memory T cells reactive to other airborne viruses (19). SARS-CoV-2 obviously is in the same category, and, is mimicked by other antigens, presumably HCoVs, establishing a prominent preexisting population of memory $CD4^+$ T cells recognizing SARS-CoV-2 peptides in the bone marrow of naïve individuals. The elevated levels of blood SARS-CoV-2-reactive memory $CD4^+$

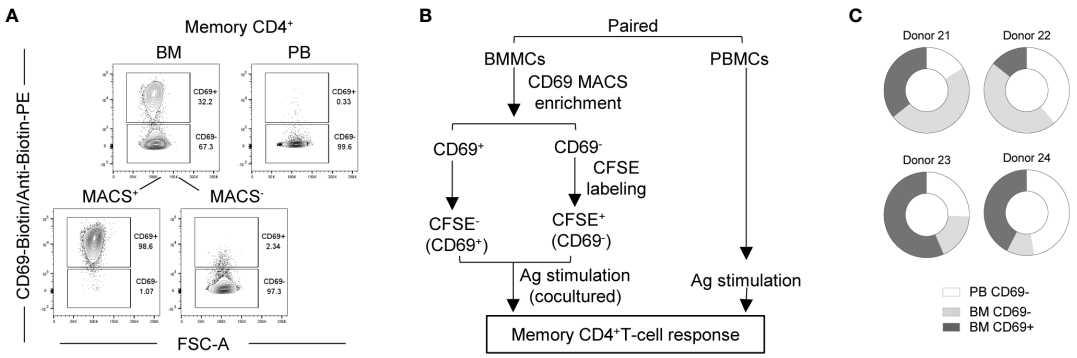


FIGURE 3
Bone marrow contains $CD69^+$ and $CD69^-$ SARS-CoV-2 reactive memory $CD4^+$ T cells. Bone marrow $CD69^+$ and $CD69^-$ cells from four vaccinated donors were analyzed for their memory $CD4^+$ T cell response to SARS-CoV-2 in comparison with that of paired blood. **(A)** Representative plots showing CD69 expression by memory $CD4^+$ T cells from a paired blood and bone marrow samples pre- and/or post-MACS. **(B)** Experimental scheme. **(C)** Estimated absolute numbers of SARS-CoV-2-reactive $CD154^+$cytokine$^+$ memory $CD4^+$ T cells using the frequency (Supplemental Figure 3C) of these cells and the estimated numbers of T cells within BM and PB of healthy young adults as described in Figure 1E.

T cells detected in vaccinated donors are in line with studies showing that higher frequencies of SARS-CoV-2-reactive $CD4^+$ T cells could be induced by infection (14) or vaccination (12) from previously unexposed donors, which thereafter show cross-reactive $CD4^+$ T cells in the peripheral blood. However, these enhanced numbers of circulating memory T cells upon vaccination are not at the expense of bone marrow memory. Numbers and composition of bone marrow memory $CD4^+$ T cells in vaccinated individuals is similar to that of naïve individuals, with the exception of a drop in IL-2 single producers.

Which antigens did prime the SARS-CoV-2-reactive memory T cells in the naïve individuals analyzed? SARS-CoV-2 related viruses, such as endemic HCoVs or SARS have been discussed (5, 7, 9, 10, 31, 43), as well as unrelated viruses, such as CMV, influenza virus, EBV, and adenoviruses. Moreover, even upon measles-mumps-rubella (MMR), or Tetanus-Diphtheria-Pertussis (Tdap) vaccination, generation of cross-reactive T cells that mitigate COVID-19 has been described (44). The present analysis does not provide clues to the original antigenic provocations establishing the SARS-CoV-2 reactive circulating and bone marrow Trm populations, except that it is clear that this cross-reactive memory is ubiquitous, polyfunctional and contains a considerable population of central memory $CD4^+$ T cells.

The SARS-CoV-2 cross-reactive memory $CD4^+$ T cells in the bone marrow of adult humans are functionally superior to their circulating counterparts, in terms of imprinting for expression of cytokines upon restimulation. Many of them then display an IFN-γ- and IL-2-imprinted, "polyfunctional" Th1 profile. This suggests that bone marrow resident, cross-reactive memory $CD4^+$ T cells would provide superior protection, when compared to their circulating counterparts (5). It has been demonstrated that the initial frequency of IL-2 secreting cross-reactive memory T cells is associated with protection of naïve individuals from infection in COVID-19 contacts (4), and SARS-CoV-2-reactive IFN-γ-secreting T cells have been associated with protection from reinfection (45). Notably, polyfunctionality of SARS-CoV-2 spike-reactive $CD4^+$ T cells correlates with low severity of COVID-19 (13). In addition to their polyfunctionality, many bone marrow resident SARS-CoV-2-reactive memory $CD4^+$ T cells are of the $CCR7^+$ Tcm type, indicating the potential of self-renewal, progression into effector cell differentiation, and also qualifying them as helper cells for follicular immune reactions (46, 47). As polyfunctional Tcm cells they resemble SARS-CoV-2 $CD4^+$ T cells 12 months post-infection (48). Together with the plethora of data reporting the SARS-CoV-2-reactive, circulating memory $CD4^+$ T cells, the present data demonstrate that there is also a preexisting potent population of bone marrow-resident memory $CD4^+$ t cells, comparable to those reactive to measles, mumps, or rubella. It becomes evident that SARS-CoV-2 did meet a human population with most adult individuals having a prominent, persistent, polyfunctional cross-reactive immunological memory T-cell population. Thus, vaccination and infection did meet "prepared" immune systems with preexisting systemic $CD4^+$ T-cell immunity. Of note, however, the ubiquitous preexisting $CD4^+$ T cell memory is not matched with an equally ubiquitous B cell memory (49). Nevertheless, an efficient germinal center reaction is established in this dialog between preexisting memory T cells and newly recruited naïve B cells (50). Since the establishment of immunological memory is considered to depend on signal from $CD4^+$ memory T cells, this might have contributed to the impressive establishment of memory plasma cells in the bone marrow of most convalescent or vaccinated individuals, after only one infection or two vaccine encounters 3 to 4 weeks apart (51). It is tempting to speculate that the preexisting T cell memory may also have contributed to the rapid, prominent and obviously protective immune responses to SARS-CoCV-2 in most infected individuals (2–4, 6, 12, 14, 15). Conversely, the few severely affected individuals may have had a no or a malfunctional preexisting $CD4^+$ T cell memory (5) (31, 52, 53).

Since access to human bone marrow is limited, the present study is limited in this aspect as well, to a small cohort of 17 naïve and 14 vaccinated individuals. Further analyses of the role of Trm in infection and vaccine responses would benefit from a non-invasive access to these Trm. We have recently shown that bone marrow Trm specific for the MMR vaccine are mobilized within a day into the blood following a secondary MMR vaccination, and contribute essentially to the secondary immune reaction (27). Notably, also cross-reactive Trm, e.g. such recognizing both TT and measles, were mobilized by MMR revaccination (27). Thus, preexisting Trm when reactivated and mobilized into the blood on their way to the secondary systemic immune reaction, can be assessed in the blood on day 1 after challenge, as compared to the circulating cells that are accessible already on day 0.

Our cohort of 17 naïve probands was too small to compare young and aged individuals, with 11 individuals analyzed aged 60 or above, to answer the question whether those bone marrow resident cross-reactive memory T cells have a different phenotype or repertoire or are missing at all in some of them, explaining the retarded reaction to vaccination in some elderly (54) and the enhanced, but still low incidence of severe COVID-19 in the elderly (5). In view of the ubiquitous presence of these cells in all our probands, the existence of experienced single and/or polyfunctional memory T cells cross-reactive and quickly reacting to SARS-CoV-2 might be a decisive advantage in successful immune reactions and moderate to mild COVID-19, also in the elderly, considering the immediate attempt of the virus to evade our immune response, by inducing expression of the immunosuppressive cytokine TGF-β (1, 55, 56).

Data availability statement

The original contributions presented in the study are included in the article/Supplementary Material. Further inquiries can be directed to the corresponding author.

Ethics statement

This study was reviewed and approved by Ethikkommission der Charité-Univerisitätsmedizin Berlin; EA1/005/21. The patients/participants provided their written informed consent to participate in this study. Written informed consent was obtained from the individual(s) for the publication of any potentially identifiable images or data included in this article.

Author Contributions

Conceptualization: JD. Methodology: JL, YS, LS, SF, JD. Investigation: JL, YS, LS, ZW. Formal Analysis: JL, YS, LS, YCL, JD. Resources: SR, SH, CH, UH, HDC, TA, CP, HR, ZQ. Interpretation: JL, YS, LS, AR, JD. Visualization: JL, JD. Funding Acquisition: JD, AR. Project Administration: JD. Supervision, JD. Writing – Original Draft, JD. Writing – Review and Editing, AR, JD. All authors contributed to the article and approved the submitted version.

Funding

Chinesisch-Deutsches Zentrum für Wissenschaftsförderung (CDZ; DFG im Ausland) grant C-0072 (JD). Deutsche Forschungsgemeinschft (DFG) Project 389687267 (JD and AR). Leibniz science Campus Chronic Inflammation (www.chronische-entzuendung.org). HDC was supported by Dr. Rolf M. Schwiete Foundation.

Acknowledgments

We are thankful to Antje Blankenstein and Johanna Penzlin for organizing patient materials, to Dr. Weijie Du for technical support, to Dr. Liqun He for his comments on data presentation, and to Drs. Alex Schefold, Petra Bacher and Chiara Romagnani for their critical comments on the manuscript/findings. We also want to thank Hilmar Frank for his expert IT solutions to figure preparation.

Conflict of interest

The authors declare that the research was conducted in the absence of any commercial or financial relationships that could be construed as a potential conflict of interest.

Publisher's note

All claims expressed in this article are solely those of the authors and do not necessarily represent those of their affiliated organizations, or those of the publisher, the editors and the reviewers. Any product that may be evaluated in this article, or claim that may be made by its manufacturer, is not guaranteed or endorsed by the publisher.

Supplementary material

The Supplementary Material for this article can be found online at: https://www.frontiersin.org/articles/10.3389/fimmu.2022.1004656/full#supplementary-material

References

1. Ferreira-Gomes M, Kruglov A, Durek P, Heinrich F, Tizian C, Heinz GA, et al. SARS-CoV-2 in severe COVID-19 induces a TGF-beta-dominated chronic immune response that does not target itself. *Nat Commun* (2021) 12(1):1961. doi: 10.1038/s41467-021-22210-3

2. Le Bert N, Tan AT, Kunasegaran K, Tham CYL, Hafezi M, Chia A, et al. SARS-CoV-2-specific T cell immunity in cases of COVID-19 and SARS, and uninfected controls. *Nature* (2020) 584(7821):457–62. doi: 10.1038/s41586-020-2550-z

3. Swadling L, Diniz MO, Schmidt NM, Amin OE, Chandran A, Shaw E, et al. Pre-existing polymerase-specific T cells expand in abortive seronegative SARS-CoV-2. *Nature* (2022) 601(7891):110–7. doi: 10.1038/s41586-021-04186-8

4. Kundu R, Narean JS, Wang L, Fenn J, Pillay T, Fernandez ND, et al. Cross-reactive memory T cells associate with protection against SARS-CoV-2 infection in COVID-19 contacts. *Nat Commun* (2022) 13(1):80. doi: 10.1038/s41467-021-27674-x

5. Bacher P, Rosati E, Esser D, Martini GR, Saggau C, Schiminsky E, et al. Low-avidity CD4(+) T cell responses to SARS-CoV-2 in unexposed individuals and humans with severe COVID-19. *Immunity* (2020) 53(6):1258–71 e5. doi: 10.1016/j.immuni.2020.11.016

6. Steiner S, Sotzny F, Bauer S, Na IK, Schmueck-Henneresse M, Corman VM, et al. HCoV- and SARS-CoV-2 cross-reactive T cells in CVID patients. *Front Immunol* (2020) 11:607918. doi: 10.3389/fimmu.2020.607918

7. Braun J, Loyal L, Frentsch M, Wendisch D, Georg P, Kurth F, et al. SARS-CoV-2-reactive T cells in healthy donors and patients with COVID-19. *Nature* (2020) 587(7833):270–4. doi: 10.1038/s41586-020-2598-9

8. Jarjour NN, Masopust D, Jameson SC. T Cell memory: Understanding COVID-19. *Immunity* (2021) 54(1):14–8. doi: 10.1016/j.immuni.2020.12.009

9. Nelde A, Bilich T, Heitmann JS, Maringer Y, Salih HR, Roerden M, et al. SARS-CoV-2-derived peptides define heterologous and COVID-19-induced T cell recognition. *Nat Immunol* (2021) 22(1):74–85. doi: 10.1038/s41590-020-00808-x

10. Low JS, Vaqueirinho D, Mele F, Foglierini M, Jerak J, Perotti M, et al. Clonal analysis of immunodominance and cross-reactivity of the CD4 T cell response to SARS-CoV-2. *Science* (2021) 372(6548):1336–41. doi: 10.1126/science.abg8985

11. Quiros-Fernandez I, Poorebrahim M, Fakhr E, Cid-Arregui A. Immunogenic T cell epitopes of SARS-CoV-2 are recognized by circulating memory and naive CD8 T cells of unexposed individuals. *EBioMedicine* (2021) 72:103610. doi: 10.1016/j.ebiom.2021.103610

12. Mateus J, Grifoni A, Tarke A, Sidney J, Ramirez SI, Dan JM, et al. Selective and cross-reactive SARS-CoV-2 T cell epitopes in unexposed humans. *Science* (2020) 370(6512):89–94. doi: 10.1126/science.abd3871

13. Sekine T, Perez-Potti A, Rivera-Ballesteros O, Strålin K, Gorin JB, Olsson A, et al. Robust T cell immunity in convalescent individuals with asymptomatic or mild COVID-19. *Cell* (2020) 183(1):158–68.e14. doi: 10.1016/j.cell.2020.08.017

14. Loyal L, Braun J, Henze L, Kruse B, Dingeldey M, Reimer U, et al. Cross-reactive CD4(+) T cells enhance SARS-CoV-2 immune responses upon infection and vaccination. *Science* (2021) 374(6564):eabh1823. doi: 10.1126/science.abh1823

15. Sagar M, Reifler K, Rossi M, Miller NS, Sinha P, White LF, et al. Recent endemic coronavirus infection is associated with less-severe COVID-19. *J Clin Invest* (2021) 131(1):e143380. doi: 10.1172/JCI143380

16. Zarnitsyna VI, Akondy RS, Ahmed H, McGuire DJ, Zarnitsyn VG, Moore M, et al. Dynamics and turnover of memory CD8 T cell responses following yellow fever vaccination. *PloS Comput Biol* (2021) 17(10):e1009468. doi: 10.1371/journal.pcbi.1009468

17. Radbruch A, McGrath MA, Siracusa F, Hoffmann U, Sercan-Alp O, Hutloff A, et al. Homeostasis and durability of T-cell memory-the resting and the restless T-cell memory. *Cold Spring Harb Perspect Biol* (2021) 13(7):331–46. doi: 10.1101/cshperspect.a038083

18. Kumar BV, Connors TJ, Farber DL. Human T cell development, localization, and function throughout life. *Immunity* (2018) 48(2):202–13. doi: 10.1016/j.immuni.2018.01.007

19. Okhrimenko A, Grun JR, Westendorf K, Fang Z, Reinke S, von Roth P, et al. Human memory T cells from the bone marrow are resting and maintain long-lasting systemic memory. *Proc Natl Acad Sci U S A* (2014) 111(25):9229–34. doi: 10.1073/pnas.1318731111

20. Farber DL, Yudanin NA, Restifo NP. Human memory T cells: generation, compartmentalization and homeostasis. *Nat Rev Immunol* (2014) 14(1):24–35. doi: 10.1038/nri3567

21. Mackay LK, Rahimpour A, Ma JZ, Collins N, Stock AT, Hafon M-L, et al. The developmental pathway for CD103+CD8+ tissue-resident memory T cells of skin. *Nat Immunol* (2013) 14(12):1294–301. doi: 10.1038/ni.2744

22. Steinert EM, Schenkel JM, Fraser KA, Beura LK, Manlove LS, Igyarto BZ, et al. Quantifying memory CD8 T cells reveals regionalization of immunosurveillance. *Cell* (2015) 161(4):737–49. doi: 10.1016/j.cell.2015.03.031

23. Teijaro JR, Turner D, Pham Q, Wherry EJ, Lefrançois L, Farber DL. Cutting edge: Tissue-retentive lung memory CD4 T cells mediate optimal protection to respiratory virus infection. *J Immunol* (2011) 187(11):5510–4. doi: 10.4049/jimmunol.1102243

24. Snyder ME, Finlayson MO, Connors TJ, Dogra P, Senda T, Bush E, et al. Generation and persistence of human tissue-resident memory T cells in lung transplantation. *Sci Immunol* (2019) 4(33):eaav5581. doi: 10.1126/sciimmunol.aav5581

25. Grau-Exposito J, Sanchez-Gaona N, Massana N, Suppi M, Astorga-Gamaza A, Perea D, et al. Peripheral and lung resident memory T cell responses against SARS-CoV-2. *Nat Commun* (2021) 12(1):3010. doi: 10.1038/s41467-021-23333-3

26. Chang HD, Radbruch A. Maintenance of quiescent immune memory in the bone marrow. *Eur J Immunol* (2021) 51(7):1592–601. doi: 10.1002/eji.202049012

27. Cendon C, Du W, Durek P, Liu YC, Alexander T, Serene L, et al. Resident memory CD4+ T lymphocytes mobilize from bone marrow to contribute to a systemic secondary immune reaction. *Eur J Immunol* (2022) 52(5):737–52. doi: 10.1002/eji.202149726

28. Cossarizza A, Chang HD, Radbruch A, Abrignani S, Addo R, Akdis M, et al. Guidelines for the use of flow cytometry and cell sorting in immunological studies (third edition). *Eur J Immunol* (2021) 51(12):2708–3145. doi: 10.1002/eji.202170126

29. Di Rosa F, Pabst R. The bone marrow: a nest for migratory memory T cells. *Trends Immunol* (2005) 26(7):360–6. doi: 10.1016/j.it.2005.04.011

30. Trepel F. Number and distribution of lymphocytes in man. *A Crit analysis. Klin Wochenschr* (1974) 52(11):511–5. doi: 10.1007/BF01468720

31. Grifoni A, Weiskopf D, Ramirez SI, Mateus J, Dan JM, Moderbacher CR, et al. Targets of T cell responses to SARS-CoV-2 coronavirus in humans with COVID-19 disease and unexposed individuals. *Cell* (2020) 181(7):1489–501.e15. doi: 10.1016/j.cell.2020.05.015

32. Frentsch M, Arbach O, Kirchhoff D, Moewes B, Worm M, Rothe M, et al. Direct access to CD4+ T cells specific for defined antigens according to CD154 expression. *Nat Med* (2005) 11(10):1118–24. doi: 10.1038/nm1292

33. Chattopadhyay PK, Yu J, Roederer M. A live-cell assay to detect antigen-specific CD4+ T cells with diverse cytokine profiles. *Nat Med* (2005) 11 (10):1113–7. doi: 10.1038/nm1293

34. Tokoyoda K, Zehentmeier S, Hegazy AN, Albrecht I, Grun JR, Lohning M, et al. Professional memory CD4+ T lymphocytes preferentially reside and rest in the bone marrow. *Immunity* (2009) 30(5):721–30. doi: 10.1016/j.immuni.2009.03.015

35. Shinoda K, Tokoyoda K, Hanazawa A, Hayashizaki K, Zehentmeier S, Hosokawa H, et al. Type II membrane protein CD69 regulates the formation of resting T-helper memory. *Proc Natl Acad Sci* (2012) 109(19):7409–14. doi: 10.1073/pnas.1118539109

36. Siracusa F, Durek P, McGrath MA, Sercan-Alp O, Rao A, Du W, et al. CD69 (+) memory T lymphocytes of the bone marrow and spleen express the signature transcripts of tissue-resident memory T lymphocytes. *Eur J Immunol* (2019) 49 (6):966–8. doi: 10.1002/eji.201847982

37. Kumar BV, Ma W, Miron M, Granot T, Guyer RS, Carpenter DJ, et al. Human tissue-resident memory T cells are defined by core transcriptional and functional signatures in lymphoid and mucosal sites. *Cell Rep* (2017) 20(12):2921–34. doi: 10.1016/j.celrep.2017.08.078

38. McGregor DD, Gowans JL. The antibody response of rats depleted of lymphocytes by chronic drainage from the thoracic duct. *J Exp Med* (1963) 117 (2):303–20. doi: 10.1084/jem.117.2.303

39. Sathaliyawala T, Kubota M, Yudanin N, Turner D, Camp P, Thome JJ, et al. Distribution and compartmentalization of human circulating and tissue-resident memory T cell subsets. *Immunity* (2013) 38(1):187–97. doi: 10.1016/j.immuni.2012.09.020

40. Jameson SC, Masopust D. Diversity in T cell memory: an embarrassment of riches. *Immunity* (2009) 31(6):859–71. doi: 10.1016/j.immuni.2009.11.007

41. Chang HD, Tokoyoda K, Radbruch A. Immunological memories of the bone marrow. *Immunol Rev* (2018) 283(1):86–98. doi: 10.1111/imr.12656

42. Sercan Alp Ö, Durlanik S, Schulz D, McGrath M, Grün JR, Bardua M, et al. Memory CD8+ T cells colocalize with IL-7+ stromal cells in bone marrow and rest in terms of proliferation and transcription. *Eur J Immunol* (2015) 45(4):975–87. doi: 10.1002/eji.201445295

43. Dykema AG, Zhang B, Woldemeskel BA, Garliss CC, Cheung LS, Choudhury D, et al. Functional characterization of CD4+ T cell receptors crossreactive for SARS-CoV-2 and endemic coronaviruses. *J Clin Invest* (2021) 131(10):e146922. doi: 10.1172/JCI146922

44. Mysore V, Cullere X, Settles ML, Ji X, Kattan MW, Desjardins M, et al. Protective heterologous T cell immunity in COVID-19 induced by the trivalent MMR and tdap vaccine antigens. *Med (N Y)* (2021) 2(9):1050–71.e7. doi: 10.1016/j.medj.2021.08.004

45. Wyllie D, Mulchandani R, Jones HE, Taylor-Phillips S, Brooks T, Charlett A, et al. SARS-CoV-2 responsive T cell numbers are associated with protection from COVID-19: A prospective cohort study in keyworkers. *medRxiv* (2020). doi: 10.1101/2020.11.02.20222778

46. Sallusto F, Lenig D, Forster R, Lipp M, Lanzavecchia A. Two subsets of memory T lymphocytes with distinct homing potentials and effector functions. *Nature* (1999) 401:708–12. doi: 10.1038/44385

47. Reinhardt RL, Khoruts A, Merica R, Zell T, Jenkins MK. Visualizing the generation of memory CD4 T cells in the whole body. *Nature* (2001) 410 (6824):101–5. doi: 10.1038/35065111

48. Lu Z, Laing ED, Pena DaMata J, Pohida K, Tso MS, Samuels EC, et al. Durability of SARS-CoV-2-Specific T-cell responses at 12 months postinfection. *J Infect Dis* (2021) 224(12):2010–9. doi: 10.1093/infdis/jiab543

49. Ng KW, Faulkner N, Cornish GH, Rosa A, Harvey R, Hussain S, et al. Preexisting and *de novo* humoral immunity to SARS-CoV-2 in humans. *Science* (2020) 370(6522):1339–43. doi: 10.1126/science.abe1107

50. Kim W, Zhou JQ, Horvath SC, Schmitz AJ, Sturtz AJ, Lei T, et al. Germinal centre-driven maturation of b cell response to mRNA vaccination. *Nature* (2022) 604(7904):141–5. doi: 10.1038/s41586-022-04527-1

51. Turner JS, Kim W, Kalaidina E, Goss CW, Rauseo AM, Schmitz AJ, et al. SARS-CoV-2 infection induces long-lived bone marrow plasma cells in humans. *Nature* (2021) 595(7867):421–5. doi: 10.1038/s41586-021-03647-4

52. Rydyznski Moderbacher C, Ramirez SI, Dan JM, Grifoni A, Hastie KM, Weiskopf D, et al. Antigen-specific adaptive immunity to SARS-CoV-2 in acute COVID-19 and associations with age and disease severity. *Cell* (2020) 183(4):996–1012.e19. doi: 10.1016/j.cell.2020.09.038

53. Peng Y, Mentzer AJ, Liu G, Yao X, Yin Z, Dong D, et al. Broad and strong memory CD4(+) and CD8(+) T cells induced by SARS-CoV-2 in UK convalescent

individuals following COVID-19. *Nat Immunol* (2020) 21(11):1336–45. doi: 10.1038/s41590-020-0782-6

54. Romero-Olmedo AJ, Schulz AR, Hochstatter S, Das Gupta D, Virta I, Hirseland H, et al. Induction of robust cellular and humoral immunity against SARS-CoV-2 after a third dose of BNT162b2 vaccine in previously unresponsive older adults. *Nat Microbiol* (2022) 7(2):195–9. doi: 10.1038/s41564-021-01046-z

55. Wang W, Chen J, Hu D, Pan P, Liang L, Wu W, et al. SARS-CoV-2 n protein induces acute kidney injury *via* Smad3-dependent G1 cell cycle arrest mechanism. *Adv Sci (Weinh)* (2022) 9(3):e2103248. doi: 10.1002/advs.202103248

56. Witkowski M, Tizian C, Ferreira-Gomes M, Niemeyer D, Jones TC, Heinrich F, et al. Untimely TGFbeta responses in COVID-19 limit antiviral functions of NK cells. *Nature* (2021) 600(7888):295–301. doi: 10.1038/s41586-021-04142-6

frontiers | Frontiers in Immunology

TYPE Original Research
PUBLISHED 12 October 2022
DOI 10.3389/fimmu.2022.1012526

Check for updates

OPEN ACCESS

EDITED BY
Laura Maggi,
Università degli Studi di Firenze,
Italy

REVIEWED BY
Per thor Straten,
Herlev Hospital, Denmark
Ritthideach Yorsaeng,
Chulalongkorn University, Thailand

*CORRESPONDENCE
Viktor Umansky
v.umansky@dkfz.de

†These authors share senior authorship

SPECIALTY SECTION
This article was submitted to
T Cell Biology,
a section of the journal
Frontiers in Immunology

RECEIVED 05 August 2022
ACCEPTED 26 September 2022
PUBLISHED 12 October 2022

CITATION
Özbay Kurt FG, Lepper A, Gerhards C, Roemer M, Lasser S, Arkhypov I, Bitsch R, Bugert P, Altevogt P, Gouttefangeas C, Neumaier M, Utikal J and Umansky V (2022) Booster dose of mRNA vaccine augments waning T cell and antibody responses against SARS-CoV-2.
Front. Immunol. 13:1012526.
doi: 10.3389/fimmu.2022.1012526

COPYRIGHT
© 2022 Özbay Kurt, Lepper, Gerhards, Roemer, Lasser, Arkhypov, Bitsch, Bugert, Altevogt, Gouttefangeas, Neumaier, Utikal and Umansky. This is an open-access article distributed under the terms of the Creative Commons Attribution License (CC BY). The use, distribution or reproduction in other forums is permitted, provided the original author(s) and the copyright owner(s) are credited and that the original publication in this journal is cited, in accordance with accepted academic practice. No use, distribution or reproduction is permitted which does not comply with these terms.

Booster dose of mRNA vaccine augments waning T cell and antibody responses against SARS-CoV-2

Feyza Gül Özbay Kurt[1,2,3,4], Alisa Lepper[1,2,3,4], Catharina Gerhards[5], Mathis Roemer[5], Samantha Lasser[1,2,3,4], Ihor Arkhypov[1,2,3,4], Rebekka Bitsch[1,2,3,4], Peter Bugert[6], Peter Altevogt[1,2,3,4], Cécile Gouttefangeas[7], Michael Neumaier[5], Jochen Utikal[1,2,3,4†] and Viktor Umansky[1,2,3,4*†]

[1]Skin Cancer Unit, German Cancer Research Center (DKFZ), Heidelberg, Germany, [2]Department of Dermatology, Venereology and Allergology, University Medical Center Mannheim, Ruprecht-Karl University of Heidelberg, Mannheim, Germany, [3]DKFZ-Hector Cancer Institute, University Medical Center Mannheim, Mannheim, Germany, [4]Mannheim Institute for Innate Immunoscience (MI3), Medical Faculty Mannheim, University of Heidelberg, Mannheim, Germany, [5]Institute for Clinical Chemistry, Medical Faculty Mannheim, University of Heidelberg, Mannheim, Germany, [6]German Red Cross Blood Service Baden-Württemberg – Hessen, Institute of Transfusion Medicine and Immunology, Medical Faculty Mannheim, Heidelberg University, Mannheim, Germany, [7]Department of Immunology, Institute for Cell Biology, University of Tübingen, Tübingen, Germany

A gradual decay in humoral and cellular immune responses over time upon SAR1S-CoV-2 vaccination may cause a lack of protective immunity. We conducted a longitudinal analysis of antibodies, T cells, and monocytes in 25 participants vaccinated with mRNA or ChAdOx1-S up to 12 weeks after the 3rd (booster) dose with mRNA vaccine. We observed a substantial increase in antibodies and CD8 T cells specific for the spike protein of SARS-CoV-2 after vaccination. Moreover, vaccination induced activated T cells expressing CD69, CD137 and producing IFN-γ and TNF-α. Virus-specific CD8 T cells showed predominantly memory phenotype. Although the level of antibodies and frequency of virus-specific T cells reduced 4-6 months after the 2nd dose, they were augmented after the 3rd dose followed by a decrease later. Importantly, T cells generated after the 3rd vaccination were also reactive against Omicron variant, indicated by a similar level of IFN-γ production after stimulation with Omicron peptides. Breakthrough infection in participants vaccinated with two doses induced more SARS-CoV-2-specific T cells than the booster vaccination. We found an upregulation of PD-L1 expression on monocytes but no accumulation of myeloid cells with MDSC-like immunosuppressive phenotype after the vaccination. Our results indicate that the 3rd vaccination fosters antibody and T cell immune response independently from vaccine type used for the first two injections. However, such immune response is attenuated over time, suggesting thereby the need for further vaccinations.

KEYWORDS

SARS-CoV-2, mRNA vaccine, vector vaccine, booster dose, T cell response, antibodies

Introduction

In December 2019, the novel beta coronavirus, severe acute respiratory syndrome coronavirus 2 (SARS-CoV-2), has emerged, infected humans, and led to coronavirus disease 2019 (COVID-19) (1). Several effective vaccines were developed and applied in various countries to fight the pandemic disease.

The structure of the SARS-CoV-2 virion is comprised of the nucleocapsid (N), membrane (M), envelope (E), and spike (S) proteins (2, 3). S protein consists of two subunits, S1 and S2. While S1 contains the receptor binding domain (RBD), which has a crucial function in the virus entry into cells through interaction with human angiotensin converting enzyme-2 (ACE2) receptor, S2 has other basic elements to mediate membrane fusion. Moreover, S protein plays a crucial role in the induction of neutralizing antibodies and T-cell responses (2, 3). Most current authorized vaccines rely on the translation of viral S messenger RNA (mRNA) to protein (4). Two main technologies were used to manufacture SARS-CoV-2 vaccines: mRNA-based vaccines and viral vector-based vaccines. RNA-based vaccines like BNT162b2 from BioNTech and mRNA-1273 from Moderna use mRNA to deliver genetic information to produce S glycoprotein antigen (5, 6). The viral vector-based vaccines such as ChAdOx1-S (ChAd) from AstraZeneca and Ad26.COV.2.S from Johnson and Johnson employs non-replicating adenovirus as a vehicle to deliver the genetic code of S antigen (7). Results from earlier clinical trials demonstrated that both vaccines could generate a significant amount of neutralizing antibodies and virus-specific T cells, leading to the protection against COVID-19 (6, 8–10).

A coordinated response between the humoral and cellular immune system is required in host defense against SARS-CoV-2 (11). Most protective antibody responses are dependent on the help of CD4 T cells (12). Induction of virus-specific CD8 T cells was shown to correlate with the viral clearance and to interact with the innate immune responses in disease control (13). Moreover, the generation of effective T cell memory is critical to promote a long-term protective immunity to SARS-CoV-2 (14). Several reports have shown that both mRNA and vector vaccines elicit virus-specific memory T cell responses (15–17). Long-term monitoring of T cell responses is important to understand the effectiveness of protection against SARS-CoV-2.

Emergence of different variants has generated concern about the effectiveness of immunity after vaccination (18, 19). In November 2021, the Omicron variant (B.1.1.529) has rapidly become a dominant strain in most countries (20). Carrying a large number of mutations in its spike protein, this variant has a stronger binding capacity to human ACE2 protein (21) and an increased transmissibility (22) than the original strain. A number of reports demonstrated that 3 doses of vaccination generate higher responses against Omicron than 2 doses (23–25). Furthermore, T cells could play a critical role in preventing severe COVID-19 caused by Omicron due to their ability to provide long-lasting immunity and recognize the virus through different sites (26).

Numerous viruses were shown to decrease the frequency of myeloid antigen presenting cells and expand myeloid-derived suppressor cells (MDSC), a heterogeneous population of myeloid cells inhibiting functions of T and NK cells (27), as an immune evasion strategy (28). It was reported that functionally active monocytic (M)-MDSC accumulated in COVID-19 patients (29). However, a detailed understanding of the alterations in myeloid cells during vaccination is lacking.

In the present study, we characterized T cell and antibody responses as well as changes in myeloid cells, starting from the baseline up to 3 months after the 3rd dose (booster) vaccination. Moreover, the level of antibodies and virus-specific T cells were measured in persons with breakthrough infections after two doses of vaccination. We found that the 3rd dose strongly enhanced both antibody and T cell responses, which decreased 6 months after the 2nd dose. Furthermore, we demonstrated the accumulation and activation of virus-specific memory CD8 T cells induced by vaccination. Importantly, after the 3rd dose, T cells showed reactivity against the Omicron variant. Hence, our findings highlight the significance of booster vaccination in strengthening waning T cell and antibody-mediated immunity.

Methods

Participant recruitment and sample collection

Participants were enrolled from February 2021 to April 2022 at the University Medical Center Mannheim, Germany (Supplementary Table 1). Written informed consents were obtained from all the participants prior to the study that was approved by the local Ethics Committee (2010-318N-MA and 2020-556N). Peripheral blood was collected at the following time points: pre-vaccination (T0), 2-3 weeks after the 1st vaccination (T1), two weeks (T2) and 12 weeks after the 2nd vaccination (T3), before the 3rd vaccination (4-6 months after the 2nd vaccination; T4), two weeks (T5) and 12 weeks after the 3rd vaccination (T6; Figure 1A). In addition, we collected data regarding local and systemic solicited adverse events after vaccination. In the grading of adverse events, we used an FDA Toxicity Grading Scale (30). For those participants who got infected with SARS-CoV-2, blood samples were collected three and twelve weeks after the disease recovery confirmed by the PCR test.

HLA typing was performed according to the standard protocol. HLA-A alleles of participants are shown in Supplementary Table 2. Heparinized blood samples were

10.3389/fimmu.2022.1012526

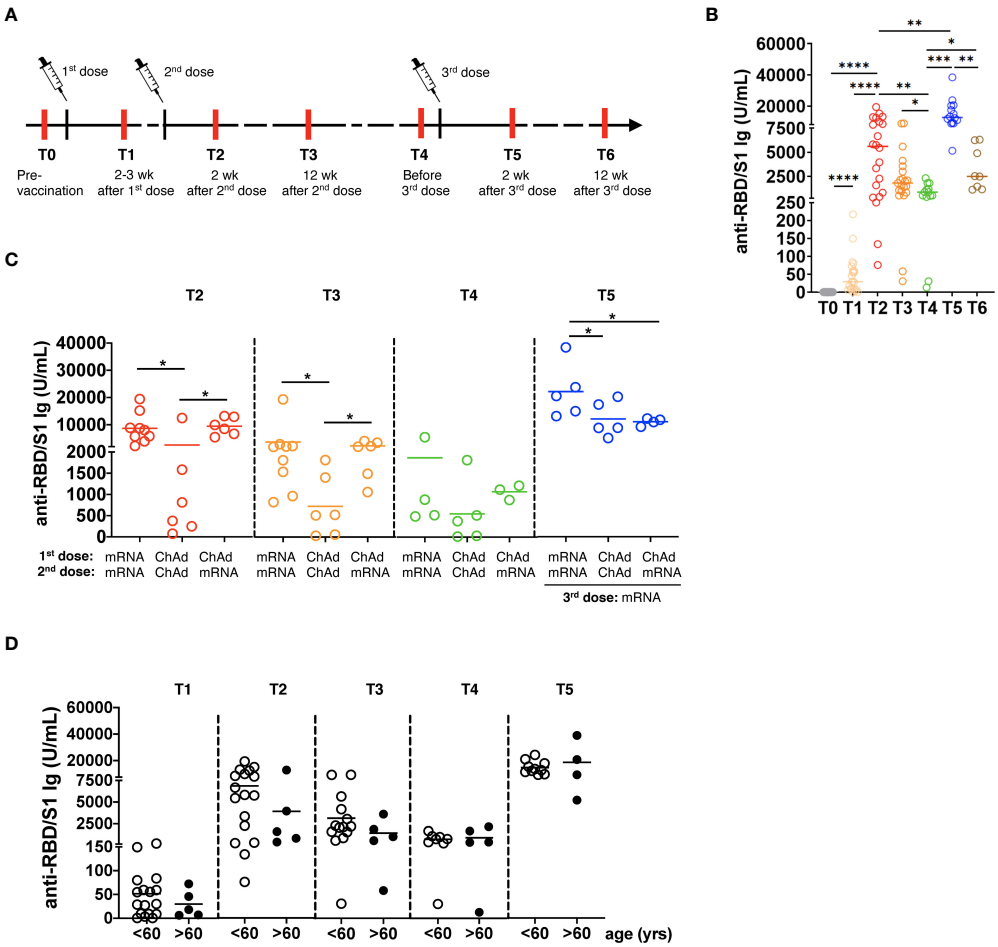


FIGURE 1
Generation of SARS-CoV-2 specific antibodies following vaccination. **(A)** The study design is presented. Red lines show the time of blood draw. **(B)** Total anti-spike RBD/S1 immunoglobulins (Ig) were measured in the serum of participants by the quantitative electrochemiluminescence immunoassay (ECLIA) and presented as U/mL (n=21). **(C)** Anti-RBD/S1 Ig levels in the serum of participants vaccinated two times with mRNA (mRNA/mRNA, n=9), two times with ChAd (ChAd/ChAd, n=6) or with ChAd/mRNA (n=6) are expressed as U/mL. **(D)** Anti-RBD/S1 Ig are measured in participants of >60 years (n=5) or <60 years (n=16) old and expressed as U/mL. wk: weeks; yrs: years; *P<0.05, **P<0.01, ***P<0.001, ****P<0.0001.

subjected to the density gradient using Biocoll (Biochrom). Peripheral blood mononuclear cells (PBMC) were isolated *via* density gradient centrifugation using Biocoll (Biochrom) and cryopreserved in X-VIVO medium (Lonza) supplemented with 30% fetal bovine serum (FBS, Pan Biotech) and 10% DMSO in liquid nitrogen. Serum samples were collected and stored at -80°C.

Anti-SARS-CoV-2 antibody detection

Analysis of total anti-spike RBD/S1 Ig was performed in serum by the quantitative electrochemiluminescence immunoassay (ECLIA) Elecsys® Anti-SARS-CoV-2 S (Roche, Germany) assay approved by FDA and CE. After internal verification according to ISO 15189, the analysis was conducted according to the manufacturer's instructions. The results were presented in U/mL and considered positive if ≥0.8 U/mL. SARS-CoV-2 anti-N Ig were detected by the qualitative Elecsys® anti-SARS-CoV-2 assay (Roche, Germany) approved by FDA and CE. Values with a cut-off index (COI) ≥ 1.0 were considered positive.

Flow cytometry

For MHC I dextramer staining, we chose two epitopes specific for each HLA-A subtype (Supplementary Table 3)

10.3389/fimmu.2022.1012526

from the SARS-CoV-2 derived epitopes with the strongest predicted affinity to MHC class I molecules defined by Immudex (Copenhagen, Denmark). PBMC ($2x10^6$) were thawed, washed, and rested in X-VIVO medium containing 10% FBS for 1.5 h followed by the staining with pooled dextramers for each HLA-A subtype according to the Immudex protocol. Dead cells were excluded using Fixable viability stain-BV510 (BD Biosciences). The monoclonal antibodies (mAbs) for extracellular markers are listed in Supplementary Table 3.

The production of ROS and NO by myeloid cells was detected using CellROX™ Deep Red reagent and DAF-FM diacetate (Thermo Fisher), respectively.

For intracellular staining of IFN-γ and TNF-α, PBMC ($2x10^6$) were rested overnight in X-VIVO medium containing 10% FBS and cells ($2x10^6$) were stimulated in X-VIVO medium containing 5% human serum with pooled 0.6 nmol (1 µg) of overlapping 15mer peptides spanning the immunodominant sequence domains of spike SARS-CoV-2 protein (PepTivator SARS-CoV-2 Prot_S, Miltenyi Biotech) or CMV pp65 peptide pool (Miltenyi Biotec) for 6 h at 37°C and 5% CO_2 in the presence of anti-CD28 monoclonal mAbs (1 µg/mL; Beckman Coulter). PBMC cultured in the medium with 2% sterile water or stimulated with phorbol myristate acetate (PMA; 50 ng/mL) and ionomycin (1µM) (Sigma Aldrich) were used as a negative control and positive control, respectively. In some experiments, cells were stimulated with a peptide pool spanning mutated regions in the BA.1 variant of Omicron variant (PepTivator SARS-CoV-2 Prot_S B.1.1.529/BA.1 Mutation pool, Miltenyi Biotec) or the same peptide pool with the original Wuhan strain sequence (PepTivator SARS-CoV-2 Prot_S B B.1.1.529/BA.1 WT Reference pool, Miltenyi Biotec) used as a control. After 2 h of incubation, GolgiStop (BD Biosciences) was added, and cells were further incubated for 4 h followed by the fixation and permeabilization with Cytofix/Cytoperm fixation/permabilization solution kit (BD Biosciences). Acquisition was performed using FACSLyric™ (BD Biosciences), and data were analyzed using FlowJo v10 software (BD Biosciences).

Statistical analysis

Statistical analysis was performed using GraphPad Prism software version 8.3.1. Data distribution was determined by Shapiro-Wilks normality test. The Wilcoxon signed-rank test was used to compare paired samples. The Wilcoxon rank-sum test (Mann–Whitney *U* test) was used to compare unpaired samples and the Kruskal–Wallis *H* test was used to test for differences between multiple study groups. A value of $p < 0.05$ was considered statistically significant.

Results

Participant characteristics

Out of 25 recruited participants, 13 received homologous vaccination with mRNA vaccines BNT162b2 (n=12) and mRNA-1273 (n=1), 6 had homologous vaccination with ChAd and 6 were vaccinated with ChAd and BNT162b2 (Supplementary Table 1). Furthermore, 14 participants received booster vaccination with BNT162b2 (n=13) and mRNA-1273 (n=1) 4-6 months after the 2nd vaccination. The amounts of BNT162b2 and mRNA-1273 used for prime doses are 30 µg and 100 µg and for the booster 30 µg and 50 µg respectively. One participant was previously infected with SARS-CoV-2 and subsequently vaccinated with two doses of BNT162b2. The rest of the participants had no SARS-CoV-2 infection prior to vaccination, which was confirmed by testing immunoglobulins (Ig) against N protein (<1.0 COI) and RBD/S1 protein (<0.8 U/ml). Prior to the first vaccination, an assessment regarding a previous infection was possible *via* the presence of anti-N- or/and anti-RBS-Ig. However, after vaccination, a vaccine breakthrough was verified at humoral level solely by the presence of anti-N-antibodies since they were unaffected by vaccination agents. During the study, 3 participants had a breakthrough SARS-CoV-2 infection defined by a positive PCR test on days 83-157 after two vaccinations with BNT162b2. All infected individuals had mild symptoms. Side effects after vaccination were classified as mild or moderate.

Restoration of diminished vaccine-induced antibody levels after the booster dose

We analyzed the concentrations of total Ig against RBD/S1 protein at different time points (Figure 1A) and found its significant elevation after the 1st and 2nd vaccination followed by a substantial decrease before the 3rd vaccination (4-6 months after the 2nd vaccination; $p< 0.01$; Figure 1B). Importantly, the levels of antibodies reached the highest values 2 weeks after the 3rd immunization dose and then significantly decreased after 12 weeks, although remaining higher than those before the 3rd vaccination.

Next, we investigated the influence of vaccine type on the level of antibody production. Homologous mRNA/mRNA vaccination induced significantly higher anti-RBD/S1 Ig production compared to homologous ChAd/ChAd vaccination (Figure 1C). Three months after vaccination, participants who received mRNA/mRNA or ChAd/mRNA vaccination showed significantly higher Ig levels than those vaccinated with homologous ChAd/ChAd. Moreover, 3 doses of mRNA

10.3389/fimmu.2022.1012526

vaccines induced a considerably stronger antibody response than two doses of ChAd followed by mRNA vaccination (Figure 1C). Interestingly, participants older than 60 years displayed a tendency for decreased values of anti-RBD/S1 Ig after 2nd dose of vaccination as compared to those below 60 (Figure 1D).

Stimulation of SARS-CoV-2-specific CD8 T cells following the booster dose

To study SARS-CoV-2 spike-specific CD8 T cells, we applied MHC I dextramers containing SARS-Cov-2 spike peptides and the HLA-A allele that was chosen according to the HLA-A typing of each participant (Supplementary Tables 2, 3). For dextramer staining, we chose only one HLA-A allele of each participant. Gating strategy for SARS-CoV-2-specific CD8 T cells is shown in Supplementary Figure 1. In 3 of 21 participants, we observed dextramer-binding SARS-CoV-2-specific CD8 T cells already at the pre-vaccination time point (T0; Figure 2A, B). The frequency of virus-specific CD8 T cells was remarkably elevated after the 1st and 2nd vaccinations. Similar to the antibody levels, the frequency of specific CD8 T cells gradually decreased 12 weeks and 4-6 months after the 2nd dose. The booster dose strongly increased the frequency of SARS-CoV-2-specific CD8 T cells followed by its reduction 3 months after the 3rd vaccination (Figure 2A, B). Investigating the effect of the vaccine type on the production of SARS-CoV-2-specific CD8 T cells, we found no significant differences in their frequencies in participants immunized with different vaccines (Figure 2C).

Next, we analyzed the activation status and memory phenotype of induced virus-specific CD8 T cells. Already 2 weeks after 2nd vaccination (T2), dextramer+ cells expressed a significantly higher level of CD69 and CD137 as compared to their control counterparts (dextramer- cells), indicating their activation (Figures 3A-C).

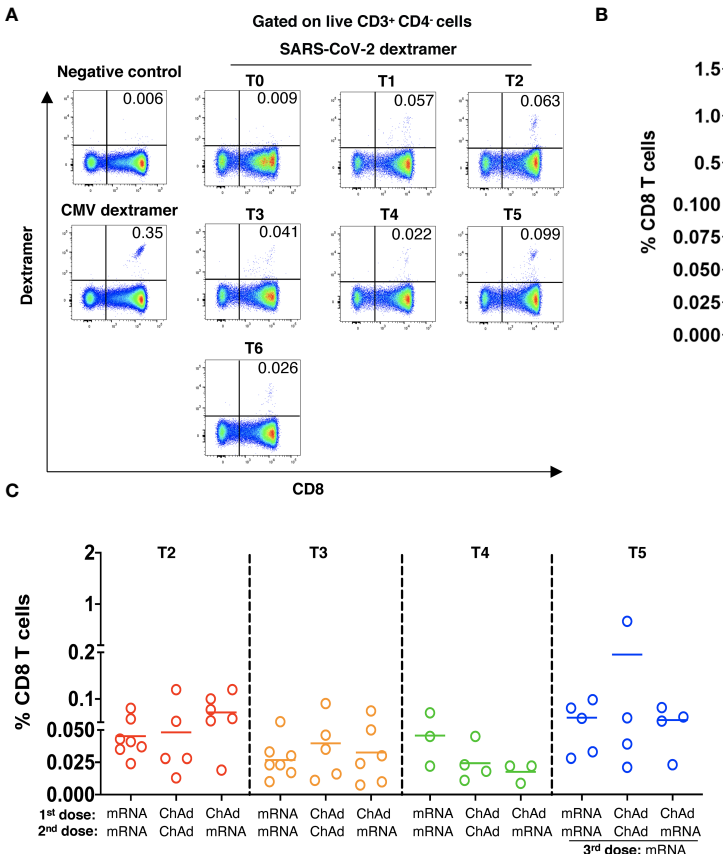


FIGURE 2
Induction of SARS-CoV-2 specific CD8 T cells after vaccination. PBMC (2x10^6) were stained with MHC I dextramers containing SARS-CoV-2 spike peptides and the HLA-A allele that was chosen according to the HLA-A typing of each participant (Supplementary Tables 2, 3) followed by flow cytometry. **(A)** Representative dot plots for SARS-CoV-2-specific CD8 T cells (dextramer$^+$CD8$^+$), for cells stained with negative control dextramers (T5), or for CMV specific CD8 T cells (positive control, T5). **(B)** Spike specific CD8 T cells in vaccinated participants are shown as the percentage of dextramer$^+$CD8$^+$ T cells within total CD8 T cells with the subtraction of positively stained cells in the negative control (n=21). **(C)** Virus specific CD8 T cells in participants vaccinated two times with mRNA (mRNA/mRNA, n=7), two times with ChAd (ChAd/ChAd, n=5) or with ChAd/mRNA (n=5) are shown as the percentage of dextramer$^+$CD8$^+$ T cells among total CD8 T cells. *P<0.05, ***P<0.001, ****P<0.0001.

10.3389/fimmu.2022.1012526

Importantly, the expression of CD69 and CD137 of spike-specific CD8 T cells stayed at the high level over the whole study. Interestingly, we did not see any significant upregulation in the frequency of $CD69^+CD137^+$ subset (data not shown).

Measuring effector memory $CD45RO^+CCR7^-$ SARS-CoV-2-specific CD8 T cells (T_{EM}), we demonstrated their increase as compared to their $dextramer^-$ counterparts after the 2nd dose of vaccination (T2) followed by a gradual decrease over time and again, a significant elevation after the 3rd dose (T5; Figures 3D, E). However, we observed no significant difference between the frequency of T_{EM} between $dextramer^+$ and $dextramer^-$ cells 3 months after the 3rd dose (T6; Figures 3D, E). Interestingly, T_{EM} was found to be a predominant T cell subset among SARS-CoV-2-specific CD8 T cells after the 2nd and 3rd vaccination doses (T2 and T5; Supplementary Figure 2). In contrast to T_{EM}, the frequency of $CD45RO^+CCR7^+$ central memory (T_{CM}) subset was significantly higher among SARS-CoV-2-specific CD8 T cells than in their control counterparts throughout the vaccination procedure (T1-T6; Figures 3D, F). The frequency of $CD45RO^-CCR7^+$ naive and stem memory cells (T_N+T_{SCM}) was significantly lower among virus-specific CD8 T cells than within their $dextramer^-$ counterparts (Figure 3G). Furthermore, the frequency of terminally differentiated memory T cells (T_{EMRA}) among SARS-CoV-2-specific CD8 T cells was higher than in $dextramer^-$ cells and remained the largest subset 12 weeks and 4-6 months after the 2nd vaccination (T3 and T4; Figure 3H and Supplementary Figure 2).

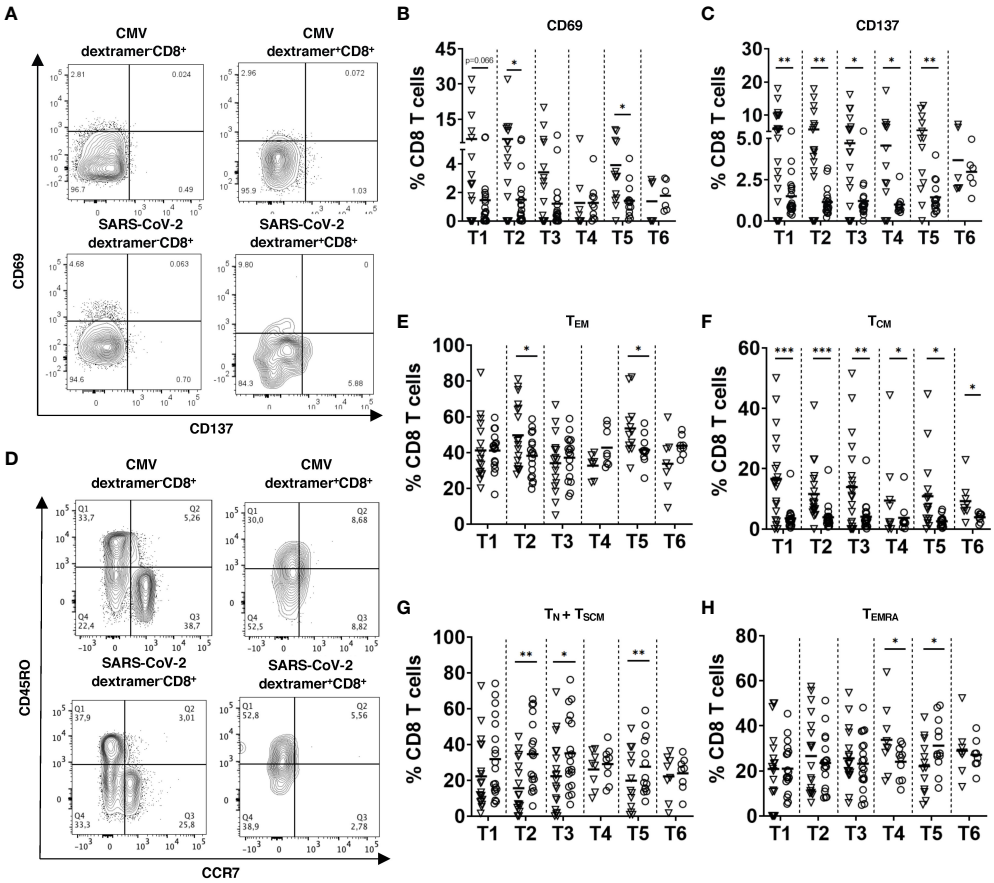


FIGURE 3
Activation status and memory phenotype of SARS-CoV-2 specific CD8 T cells. PBMC ($2x10^6$) were stained with respective SARS-CoV-2 spike or CMV MHC I dextramers and mAbs for CD3, CD4, CD8, CD69, CD137, CD45RO, and CCR7 followed by FACS analysis. **(A)** Representative dot plots for CD69 and CD137 expression on CMV or SARS-CoV-2 $dextramer^+CD8^+$ and $dextramer^-CD8^+$ T cells 2 weeks after the 3rd dose (T5). CD69 **(B)** and CD137 **(C)** expression on SARS-CoV-2 $dextramer^+CD8^+$ and $dextramer^-CD8^+$ T cells from vaccinated individuals (n=19) is presented as the frequency of $CD69^+$ or $CD137^+$ cells within the CD8 T cell subset. **(D)** Representative dot plots for CD45RO and CCR7 expression on $dextramer^+CD8^+$ and $dextramer^-CD8^+$ T cells at T5. **(E-H)** Results for $CD45RO^+CCR7^-$ effector memory (T_{EM}, E), $CD45RO^+CCR7^+$ central memory (T_{CM}, F), $CD45RO^-CCR7^+$ naive and stem cell memory (T_N + T_{SCM}, G) and $CD45RO^-CCR7^-$ terminally differentiated memory T cells (T_{EMRA}, H) from vaccinated participants (n=19) are shown as the percentage of corresponding subsets among $dextramer^+CD8^+$ or $dextramer^-CD8^+$ T cells. Data for $dextramer^+CD8^+$ and $dextramer^-CD8^+$ T cells are shown as inverted triangles and circles respectively. Data were excluded when event count <20 in $Dextramer^+$ $CD8^+$ cells. *P<0.05, **P<0.01, ***P<0.001.

Induction of functional SARS-CoV-2-specific T cells upon booster vaccination with reactivity to Omicron variant

Next, we tested if induced SARS-CoV-2-specific CD8 and CD4 T cells are functionally active based on IFN-γ and TNF-α production. For this, PBMC from 14 participants were stimulated with pooled overlapping 15mer peptides of SARS-Cov 2 Prot_S. Gating strategy for CD8 and CD4 T cells producing IFN-γ and TNF-α is shown in Supplementary Figure 3. In 6 of 14 participants, we observed the production of IFN-γ and TNF-α already at the baseline (T0; Figures 4A, B, E). In response to peptide stimulation, CD8 T cells collected 2 weeks after the 2nd dose significantly increased IFN-γ production (T2; Figure 4B). Similar to other tested immune parameters, the level of IFN-γ was reduced 4-6 months after the 2nd vaccination and was remarkably enhanced following the 3rd dose (T4 and T5 respectively; Figure 4B). Similar to IFN-γ CD8 T cells produced also significantly higher amounts of TNF-α after the 3rd dose (Figures 4D, E). Furthermore, we found that CD4 T cells could also increase the secretion of IFN-γ and TNF-α after 3rd vaccination in response to peptide stimulation, although to a lesser extent than CD8 T cells (Figure 4C, F). In addition, no significant effect of the type of vaccine was found on the capacity of CD8 T cells to increase the production of IFN-γ (Figures 4G) and TNF-α (data not shown). To assess the T cell response of vaccinated participants against the Omicron variant, we measured IFN-γ production by CD8 and CD4 T cells taken from 7 participants 2 weeks after the 3rd dose and stimulated with pooled overlapping 15mer peptides spanning the mutated region in Omicron spike protein. The reference peptide pool covering the homologous domains of the Wuhan variant was used as a control. Although we observed a tendency of decreased level of IFN-γ response against the Omicron peptides by both CD8 and CD4 T cells as compared to the reference peptides, the difference was not statistically significant (Figures 4H, I).

Infection after vaccination promotes a higher level of T cells than the booster dose

Breakthrough infections after the 2nd dose of vaccination occurred in three participants approximately 4 months after the 2nd dose. The level of anti-RBD/S1 antibodies measured around 3 weeks after the disease recovery was only slightly higher than 2 weeks after the 3rd dose of vaccination (T5) in non-infected participants (Figure 5A). On the contrary, breakthrough infections induced significantly elevated frequencies of SARS-CoV-2-specific CD8 T cells as compared to those after the 3rd dose (Figures 5B, C). However, these CD8 T cells showed no upregulation of CD69 and accumulation of cells with memory phenotype, in contrast to CD8 T cells measured after the 3rd dose (Figure 5D). In addition, we observed no differences in the frequency of IFN-γ producing CD8 T cells stimulated by breakthrough infections or the 3rd vaccination dose (Figure 5E).

In one participant infected with SARS-CoV-2 before vaccination, we found an increased level of antibodies after the 2nd dose as compared to that in uninfected participants after the 3rd dose, whereas the frequency of SARS-COV-2-specific CD8 T cells was lower at this time point (Supplementary Table 4).

Vaccination promoted upregulation of PD-L1 expression on CD14^{+}HLA-DR^{+} monocytes

Finally, we studied the alterations of circulating myeloid cells following the vaccination. After the 3rd dose (T5), the frequency of CD14^{+}HLA-DR^{+} cells was elevated as compared to the baseline (Figures 6A, B). Moreover, the frequency of CD14^{+}HLA-DR^{-} myeloid cells within PBMC showed a slight increase at this time point (Figure 6C). Interestingly, the expression of PD-L1 was significantly upregulated on CD14^{+}HLA-DR^{+} monocytes after the 2nd dose (Figures 6D, E), whereas the frequency of PD-L1^{+} CD14^{+}HLA-DR^{-} cells remained low at different time points after vaccination (Supplementary Figure 4A). In addition, we observed no statistically significant differences in the production of reactive oxygen species (ROS) and nitric oxide (NO) by both CD14^{+}HLA-DR^{+} and CD14^{+}HLA-DR^{-} myeloid cells upon the vaccination (Supplementary Figures 4B-E).

Discussion

In this study, we observed a gradual decrease in anti-RBD/S Ig concentrations in the serum of participants within 6 months after the 2nd vaccination dose that was in agreement with a previous publication, demonstrating a substantial decrease of anti-S neutralizing Ig after the 2nd dose of BNT162b2 (31). Moreover, it was reported that aged participants displayed lower antibody level and its more drastic decrease over time after vaccination (32). Here, we also observed lower and less persistent antibody levels in participants >60 years old than those in younger donors. However, these differences were not statistically significant since the antibody response was heterogeneous due to the different vaccination settings applied in this study. In addition, each dose of mRNA-1273 contains more mRNA than BNT162b2, which might explain the heterogeneity in antibody responses.

Analyzing the effect of different vaccines, we demonstrated that the injection of ChAd followed by mRNA vaccines or

10.3389/fimmu.2022.1012526

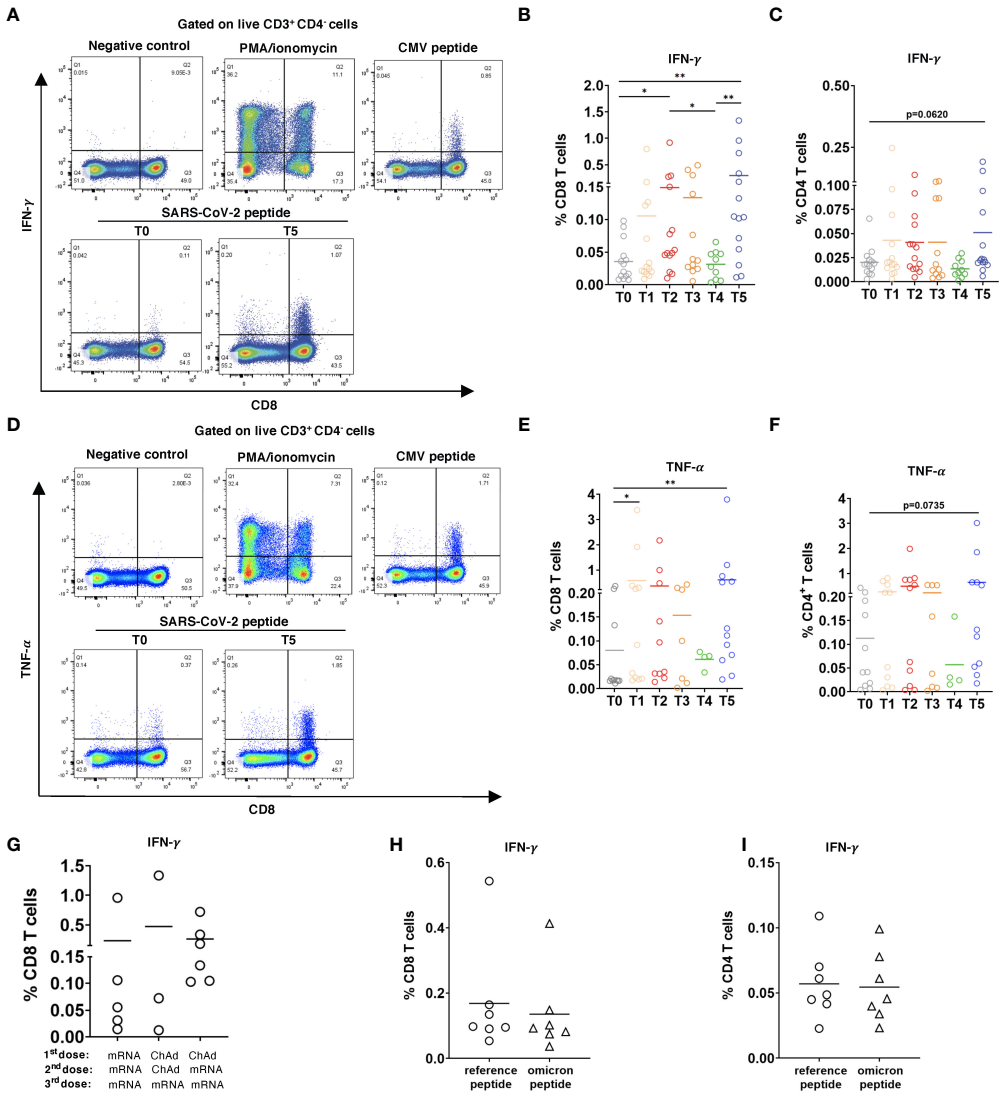


FIGURE 4
CD8 and CD4 T cell responses to SARS-CoV-2 peptides. PBMC ($2x10^6$) were stimulated with SARS-CoV-2 S overlapping peptide pool and anti-CD28 mAb for 6h. The treatment with PMA/ionomycin or CMV peptide pool were used as positive controls, whereas the incubation in medium containing 2% sterile water instead of peptides was considered as negative control. **(A)** Representative dot plots for IFN-γ. production by CD8 T cells at T0 and T5. Negative and positive controls are shown at T5. **(B)** Data are presented as the percentage of IFN-γ^+ CD8 T cells among total CD8 T cells, **(C)** as well as IFN-γ^+CD4$^+$ T cells among total CD4 T cells with the subtraction of positively stained cells in the negative control (n=14). **(D)** Representative dot plots for TNF-α production by CD8 T cells at T0 and T5. **(D-F)** Results are shown as the percentage of TNF-α^+ CD8$^+$ T cells among total CD8 T cells (n= 11, [**(E)**] and TNF-α^+CD4$^+$ T cells [n=7, **(F)**] among total CD4 T cells. **(G)** Data on IFN-γ producing CD8 T cells in participants vaccinated two times with mRNA (mRNA/mRNA, n=5), two times with ChAd (ChAd/ChAd, n=3) or with ChAd/mRNA (n=6) are presented as the frequency of IFN-γ^+CD8$^+$ T cells among total CD8 T cells. **(H, I)** PBMC were stimulated with Omicron peptide pool and reference peptide pool for 6h in the presence of anti-CD28 mAb. Frequency of IFN-γ^+CD8$^+$ T cells among total CD8 T cells [n=7, **(H)**] and IFN-γ^+CD4$^+$ T cells among total CD4 T cells [n=7, **(i)**] are shown. *P < 0.05, **P < 0.01.

homologous mRNA/mRNA setting induced a higher level of anti-RBD/S1 Ig than ChAd/ChAd immunization. These data are in accordance with that from Barros-Martins et al. (33) who reported stronger antibody responses against SARS-CoV-2 after heterologous mRNA/ChAd vaccination. Our findings showed that booster mRNA dose elevated anti-RBD/S1 Ig levels, which waned after 6 months. Other authors also observed an augmentation of humoral immune responses induced by the booster dose using BNT162b2 (34). Therefore, the administration of booster doses seems to be critically

10.3389/fimmu.2022.1012526

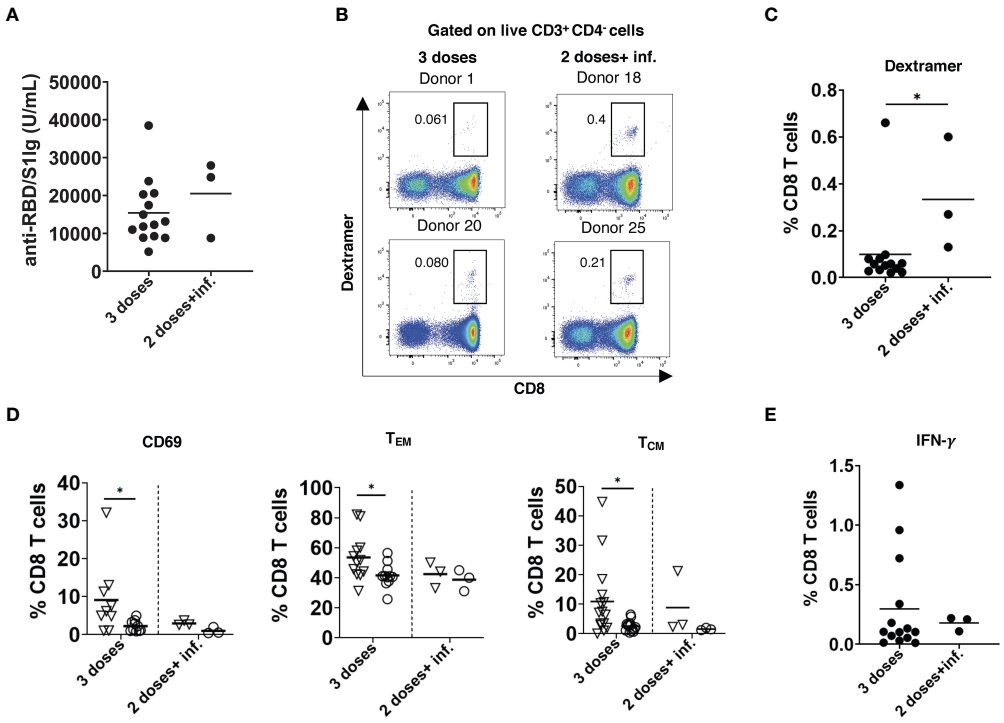


FIGURE 5
Effect of breakthrough SARS-CoV-2 infection on antibody and T cell responses in vaccinated participants. **(A)** Total RBD/S1 Ig were measured in the serum of participants infected after 2 doses of vaccination (2 doses + inf.; n=3) or after 3rd dose (n=14) and expressed as U/mL. **(B)** Representative dot plots for SARS-CoV-2 spike specific CD8 T cells (dextramer$^+$CD8$^+$) from both groups. **(C)** Spike-specific CD8$^+$ T cells infected after 2 doses of vaccination (n=3) or after 3rd dose (n=14) are shown as the percentage of dextramer$^+$CD8$^+$ T cells within total CD8 T cells. **(D)** Frequency of spike-specific CD69$^+$, T_{EM}, and T_{CM} CD8 T cells after infection (n=3) and 3rd dose of vaccination (n=14) are presented as the percentage within total CD8 T cells. Dextramer$^+$CD8$^+$ and dextramer$^-$CD8$^+$ are indicated as inverted triangles and circles, respectively. **(E)** PBMC were stimulated with SARS-CoV-2 S peptide pool and anti-CD28 mAb for 6h. Data are presented as the percentage of IFN-γ$^+$CD8$^+$ T cells among total CD8 T cells (n=3 and 14 respectively). *$P < 0.05$.

important for the generation of anti-spike SARS-CoV-2 antibodies.

In parallel to augmented antibody responses, we observed a strong induction of virus-specific CD8 T cells (measured by dextramer staining) followed by a substantial reduction 4-6 months after the 2nd dose and reaching a maximum after the 3rd vaccination that was also reported by others (35, 36). Intriguingly, in contrast to humoral responses, we detected no differences in the induction of anti-viral CD8 T cells in various vaccination settings.

It is known that long-lived memory T cells are required to protect the host from re-infection. Consistent with the recent publications (31, 37), we found that SARS-CoV-2-specific memory CD8 T cells peaked 2 weeks after the 2nd dose and remained detectable for 4-6 months. Importantly, the boost vaccination generated a robust expansion of effector and central memory CD8 T cells. Furthermore, we found that SARS-CoV-2-specific CD8 T cells had predominantly a T_{EMRA} phenotype after 4-6 months that is in accordance with another report showing that T_{EM} emerged after SARS-CoV-2 infection converted over time to T_{EMRA} phenotype (38). Additionally, virus-specific CD8 T_{EMRA} cells were found to be dominant in convalescent COVID-19 individuals (39). Since these cells represent a heterogeneous population (40), more studies are required to decipher their importance for long-lasting anti-viral immunity.

We also found that virus-specific CD8 T cells upregulate the activation markers CD69 and CD137. Although some previous papers reported that most of these cells expressed both markers (41, 42), we failed to detect any double positive SARS-CoV-2-specific CD8 T cells, indicating that different T cell subsets express CD69 or CD137. Moreover, we tested if spike-specific T cells were functionally active by measuring intracellular IFN-γ and TNF-α in CD8 and CD4 T cells upon the stimulation with pooled overlapping 15mer peptides. Functional CD8 T cell responses were markedly increased after the 2nd with a maximum after the 3rd vaccination, whereas the stimulation of cytokine production by CD4 T cells was lower. In line with this, it was previously demonstrated that the functionality of SARS-CoV-2-specific CD4 T cells induced by vaccination was reduced compared to that of

10.3389/fimmu.2022.1012526

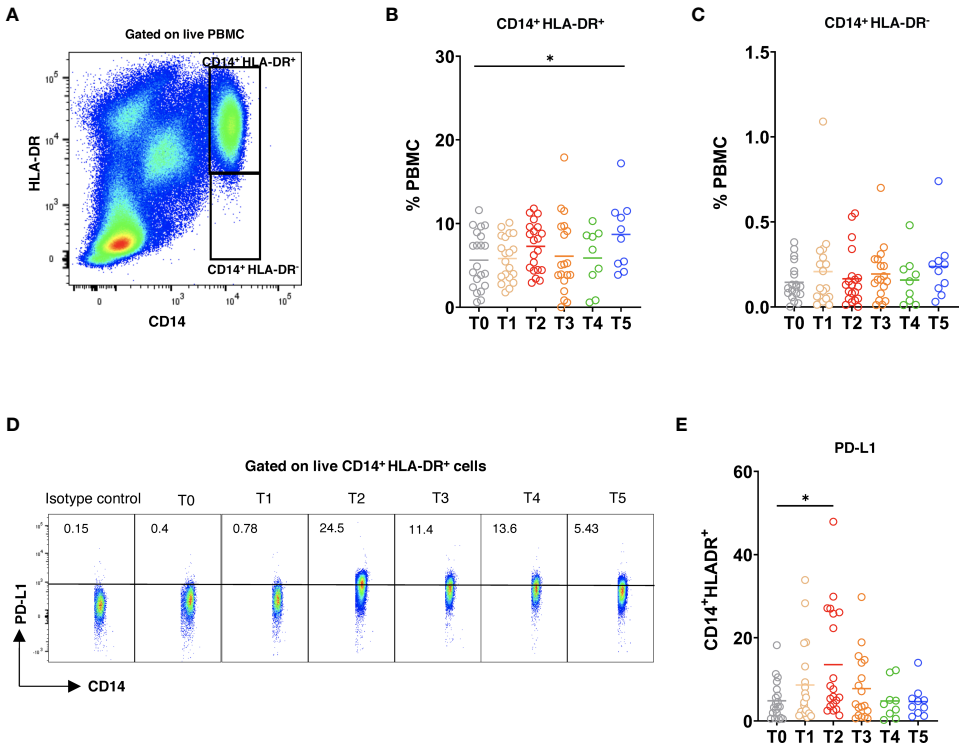


FIGURE 6
Myeloid cell phenotype after vaccination. PBMC were stained with 7AAD, CD14, HLA-DR, and PD-L1 mAbs and measured by flow cytometry. **(A)** Representative dot plots for $CD14^+HLA\text{-}DR^+$ and $CD14^+HLA\text{-}DR^-7AAD^-$ live myeloid cells. $CD14^+HLA\text{-}DR^+$ **(B)** and $CD14^+HLA\text{-}DR^-$ **(C)** cells were analyzed at different time points and are shown as the frequency of respective subset among total PBMC (n=21). **(D)** Representative dot plots for PD-L1 expression on $CD14^+HLA\text{-}DR^+$ cells. **(E)** Data are presented as the percentage of $PD\text{-}L1^+CD14^+HLA\text{-}DR^+$ cells among total $CD14^+HLA\text{-}DR^+$ cells. *$P < 0.05$.

CD8 T cells (43). Intriguingly, in contrast to humoral responses, we detected no differences in the cytokine production by CD8 T cells upon viral peptide stimulation in various vaccination settings.

In some donors, we found SARS-CoV-2-specific T cells before vaccination, although they have no detectable Ig against nucleocapsid protein, which excludes the possibility of pre-exposure to SARS-CoV-2. Similarly, previous publications described SARS-CoV-2-specific T cells in individuals without the history of COVID-19 (44–46). This might be explained by the pre-exposition of such participants to other coronaviruses that induce T cells cross-reacting to SARS-CoV-2 (47). However, the presence of pre-existing virus-specific CD8 T cells had no effect on the efficiency of functional T cell induction upon vaccination.

Decay in humoral and T cell immune response and against emerging new SARS-CoV-2 variants might lead to breakthrough infections (48). In our study, 3 participants were infected with SARS-CoV-2 approximately 5 months after the 2nd dose of mRNA vaccination. Interestingly, such breakthrough infection induced higher numbers of SARS-CoV-2-specific T cells than the booster vaccination, whereas the antibody response does not significantly differ. Since the Omicron variant has become the dominant one, leading to breakthrough infections, we investigated functional reactivity of T cells from participants receiving the 3rd vaccination dose against this variant. We found no statistically significant differences between IFN-γ production in T cells stimulated by the Omicron and reference peptides. Our findings are in agreement with the studies demonstrating a minimal escape of the Omicron variant from T cell immune response (49, 50). Although it might not be sufficient for preventing infection, an existing CD8 T cell immune response against Omicron might help to reduce disease severity.

Although some reports demonstrated dysregulation of monocytic cells in COVID-19 infection (51, 52), the dynamics of such alterations during vaccination are not clear. Our findings demonstrated that the frequency of $CD14^+HLA\text{-}DR^+$ monocytes is enhanced after the booster dose. In line with our findings, Liu et al. (53) reported that the frequency of CD14 monocytes was increased following vaccination. Moreover, it was demonstrated that different monocyte subsets were emerged during the disease progression in COVID-19 patients (54). Further studies are needed to characterize monocyte changes upon vaccination. Interestingly, we failed to observe the vaccination-induced accumulation of $CD14^+HLA\text{-}DR^-$ cells that could be considered as a counterpart of MDSC in donors.

In contrast, Falck-Jones et al. (29) and Sacchi et al. (55) reported an expansion of MDSC that inhibit T cell responses in patients with severe COVID-19. This difference could be due to a long-term virus persistence in COVID-19 patients supporting the accumulation of MDSC. The upregulation of PD-L1 expression as well as the production of ROS and NO are important strategies used by MDSC to suppress T cell responses (27). Therefore, we examined these parameters in both myeloid subsets and found that PD-L1 expression is upregulated on $CD14^{+}HLA\text{-}DR^{+}$ monocytes after the 2nd dose, which could be characterized as a protective mechanism suppressing overactivated T cells induced by vaccines.

Taken together, our data demonstrated that the 3rd (booster) dose of vaccination induced a maximum production of anti-RBD/S1 Ig and functionally active SARS-CoV-2-specific CD8 T cells, showing memory phenotype and secreting the cytokines IFN-γ and TNF-α. Importantly, we found no accumulation of myeloid cells with MDSC-like immunosuppressive phenotype following the vaccination. An observed decrease in both antibody and T cell responses 3 months after the booster dose could lead to breakthrough infections in some cases, indicating that further booster vaccinations should be implemented to achieve long-term immunity against COVID-19 caused by SARS-CoV-2.

Data availability statement

The original contributions presented in the study are included in the article/Supplementary Material. Further inquiries can be directed to the corresponding author.

Ethics statement

This study was reviewed and approved by the Ethics Committee of University Medical Center Mannheim (2010-318N-MA and 2020-556N). The participants provided their written informed consent to participate in this study.

Author contributions

VU, JU, and MN designed the study. FK, AL, SL, IA, and RB performed the experiments. FK performed the data analysis. CGe, MR measured the antibodies by ECLIA. PB contributed to the HLA typing of the donors. CGo contributed to the design and analysis of T cells by flow cytometry. FK and VU wrote the manuscript. All authors contributed to the article and approved the submitted version.

Funding

This work was supported by the German Academic Exchange Service (DAAD to FK), the German Federal Ministry of Education and Research (BMBF) – SERPENTINE project in the ERA PerMed network (01KU2017 to VU), the German Research Foundation (DFG) – project number 259332240/RTG 2099 (to JU and VU).

Acknowledgments

We thank Yvonne Nowak, Sayran Arif-Said (both Department of Dermatology, Venereology and Allergology, University Medical Center Mannheim) and Ludmila Umansky (Department of Department of Neurology, University Medical Center Mannheim) for the preparation of PBMC and serum samples, Ameli Götz and Ruth Leiblein (Institute for Clinical Chemistry, Medical Faculty Mannheim, University of Heidelberg) for help with the antibody detection and Frank Stötzer (Institute of Transfusion Medicine and Immunology, Heidelberg University) for HLA typing of the donors and Immudex (Copenhagen, Denmark) for providing MHC I Dextramer® reagents. We thank all donors for their participation.

Conflict of interest

The authors declare that the research was conducted in the absence of any commercial or financial relationships that could be construed as a potential conflict of interest.

Publisher's note

All claims expressed in this article are solely those of the authors and do not necessarily represent those of their affiliated organizations, or those of the publisher, the editors and the reviewers. Any product that may be evaluated in this article, or claim that may be made by its manufacturer, is not guaranteed or endorsed by the publisher.

Supplementary material

The Supplementary Material for this article can be found online at: https://www.frontiersin.org/articles/10.3389/fimmu.2022.1012526/full#supplementary-material

References

1. Hu B, Guo H, Zhou P, Shi ZL. Characteristics of SARS-CoV-2 and COVID-19. *Nat Rev Microbiol* (2021) 19(3):141–54. doi: 10.1038/s41579-020-00459-7

2. Mariano G, Farthing RJ, Lale-Farjat SLM, Bergeron JRC. Structural characterization of SARS-CoV-2: Where we are, and where we need to be. *Front Mol Biosci* (2020) 7:605236. doi: 10.3389/fmolb.2020.605236

3. Ke Z, Oton J, Qu K, Cortese M, Zila V, McKeane L, et al. Structures and distributions of SARS-CoV-2 spike proteins on intact virions. *Nature* (2020) 588 (7838):498–502. doi: 10.1038/s41586-020-2665-2

4. Jeyanathan M, Afkhami S, Smaill F, Miller MS, Lichty BD, Xing Z. Immunological considerations for COVID-19 vaccine strategies. *Nat Rev Immunol* (2020) 20(10):615–32. doi: 10.1038/s41577-020-00434-6

5. Corbett KS, Edwards DK, Leist SR, Abiona OM, Boyoglu-Barnum S, Gillespie RA, et al. SARS-CoV-2 mRNA vaccine design enabled by prototype pathogen preparedness. *Nature* (2020) 586(7830):567–71. doi: 10.1038/s41586-020-2622-0

6. Baden LR, El Sahly HM, Essink B, Kotloff K, Frey S, Novak R, et al. Efficacy and safety of the mRNA-1273 SARS-CoV-2 vaccine. *N Engl J Med* (2021) 384 (5):403–16. doi: 10.1056/NEJMoa2035389

7. Zhao J, Zhao S, Ou J, Zhang J, Lan W, Guan W, et al. COVID-19: Coronavirus vaccine development updates. *Front Immunol* (2020) 11:602256. doi: 10.3389/fimmu.2020.602256

8. Sahin U, Muik A, Derhovanessian E, Vogler I, Kranz LM, Vormehr M, et al. COVID-19 vaccine BNT162b1 elicits human antibody and TH1 T cell responses. *Nature* (2020) 586(7830):594–9. doi: 10.1038/s41586-020-2814-7

9. Folegatti PM, Ewer KJ, Aley PK, Angus B, Becker S, Belij-Rammerstorfer S, et al. Safety and immunogenicity of the ChAdOx1 nCoV-19 vaccine against SARS-CoV-2: a preliminary report of a phase 1/2, single-blind, randomised controlled trial. *Lancet* (2020) 396(10249):467–78. doi: 10.1016/S0140-6736(20)31604-4

10. Wheeler SE, Shurin GV, Yost M, Anderson A, Pinto L, Wells A, et al. Differential antibody response to mRNA COVID-19 vaccines in healthy subjects. *Microbiol Spectr* (2021) 9(1):e0034121. doi: 10.1128/Spectrum.00341-21

11. Shah VK, Firmal P, Alam A, Ganguly D, Chattopadhyay S. Overview of immune response during SARS-CoV-2 infection: Lessons from the past. *Front Immunol* (2020) 11:1949. doi: 10.3389/fimmu.2020.01949

12. Swain SL, McKinstry KK, Strutt TM. Expanding roles for CD4(+) T cells in immunity to viruses. *Nat Rev Immunol* (2012) 12(2):136–48. doi: 10.1038/nri3152

13. Tan AT, Linster M, Tan CW, Le Bert N, Chia WN, Kunasegaran K, et al. Early induction of functional SARS-CoV-2-specific T cells associates with rapid viral clearance and mild disease in COVID-19 patients. *Cell Rep* (2021) 34 (6):108728. doi: 10.1016/j.celrep.2021.108728

14. Sette A, Crotty S. Adaptive immunity to SARS-CoV-2 and COVID-19. *Cell* (2021) 184(4):861–80. doi: 10.1016/j.cell.2021.01.007

15. Ewer KJ, Barrett JR, Belij-Rammerstorfer S, Sharpe H, Makinson R, Morter R, et al. T Cell and antibody responses induced by a single dose of ChAdOx1 nCoV-19 (AZD1222) vaccine in a phase 1/2 clinical trial. *Nat Med* (2021) 27 (2):270–8. doi: 10.1038/s41591-020-01194-5

16. Guerrera G, Picozza M, D'Orso S, Placido R, Pirronello M, Verdiani A, et al. BNT162b2 vaccination induces durable SARS-CoV-2-specific T cells with a stem cell memory phenotype. *Sci Immunol* (2021) 6(66):eabl5344. doi: 10.1126/sciimmunol.abl5344

17. Sadoff J, Le Gars M, Shukarev G, Heerwegh D, Truyers C, de Groot AM, et al. Interim results of a phase 1-2a trial of Ad26.COV2.S covid-19 vaccine. *N Engl J Med* (2021) 384(19):1824–35. doi: 10.1056/NEJMoa2034201

18. Tegally H, Wilkinson E, Lessells RJ, Giandhari J, Pillay S, Msomi N, et al. Sixteen novel lineages of SARS-CoV-2 in south Africa. *Nat Med* (2021) 27(3):440–6. doi: 10.1038/s41591-021-01255-3

19. Voloch CM, da Silva Francisco RJr., de Almeida LGP, Cardoso CC, Brustolini OJ, Gerber AL, et al. Genomic characterization of a novel SARS-CoV-2 lineage from Rio de Janeiro, Brazil. *J Virol* (2021) 95(10):e00119-21. doi: 10.1128/JVI.00119-21

20. Karim SSA, Karim QA. Omicron SARS-CoV-2 variant: a new chapter in the COVID-19 pandemic. *Lancet* (2021) 398(10317):2126–8. doi: 10.1016/S0140-6736(21)02758-6

21. Lupala CS, Ye Y, Chen H, Su XD, Liu H. Mutations on RBD of SARS-CoV-2 omicron variant result in stronger binding to human ACE2 receptor. *Biochem Biophys Res Commun* (2022) 590:34–41. doi: 10.1016/j.bbrc.2021.12.079

22. Greaney AJ, Loes AN, Crawford KHD, Starr TN, Malone KD, Chu HY, et al. Comprehensive mapping of mutations in the SARS-CoV-2 receptor-binding domain that affect recognition by polyclonal human plasma antibodies. *Cell Host Microbe* (2021) 29(3):463–76 e6. doi: 10.1016/j.chom.2021.02.003

23. Accorsi EK, Britton A, Fleming-Dutra KE, Smith ZR, Shang N, Derado G, et al. Association between 3 doses of mRNA COVID-19 vaccine and symptomatic infection caused by the SARS-CoV-2 omicron and delta variants. *JAMA* (2022) 327 (7):639–51. doi: 10.1001/jama.2022.0470

24. Wu M, Wall EC, Carr EJ, Harvey R, Townsley H, Mears HV, et al. Three-dose vaccination elicits neutralising antibodies against omicron. *Lancet* (2022) 399 (10326):715–7. doi: 10.1016/S0140-6736(22)00092-7

25. Yoon SK, Hegmann KT, Thiese MS, Burgess JL, Ellingson K, Lutrick K, et al. Protection with a third dose of mRNA vaccine against SARS-CoV-2 variants in frontline workers. *N Engl J Med* (2022) 386(19):1855–7. doi: 10.1056/NEJMc2201821

26. Moss P. The T cell immune response against SARS-CoV-2. *Nat Immunol* (2022) 23(2):186–93. doi: 10.1038/s41590-021-01122-w

27. Veglia F, Sanseviero E, Gabrilovich DI. Myeloid-derived suppressor cells in the era of increasing myeloid cell diversity. *Nat Rev Immunol* (2021) 21(8):485–98. doi: 10.1038/s41577-020-00490-y

28. Koushki K, Salemi M, Miri SM, Arjeini Y, Keshavarz M, Ghaemi A. Role of myeloid-derived suppressor cells in viral respiratory infections; hints for discovering therapeutic targets for COVID-19. *BioMed Pharmacother* (2021) 144:112346. doi: 10.1016/j.biopha.2021.112346

29. Falck-Jones S, Vangeti S, Yu M, Falck-Jones R, Cagigi A, Badolati I, et al. Functional monocytic myeloid-derived suppressor cells increase in blood but not airways and predict COVID-19 severity. *J Clin Invest* (2021) 131(6):e144734. doi: 10.1172/JCI144734

30. US Food and Drug Administration. *Toxicity grading scale for healthy adult and adolescent volunteers enrolled in preventive vaccine clinical trials* (2007). Available at: https://www.fda.gov/regulatory-information/search-fda-guidance-documents/toxicity-grading-scale-healthy-adult-and-adolescent-volunteers-enrolled-preventive-vaccine-clinical.

31. Levin EG, Lustig Y, Cohen C, Fluss R, Indenbaum V, Amit S, et al. Waning immune humoral response to BNT162b2 covid-19 vaccine over 6 months. *N Engl J Med* (2021) 385(24):e84. doi: 10.1056/NEJMoa2114583

32. Faro-Viana J, Bergman ML, Goncalves LA, Duarte N, Coutinho TP, Borges PC, et al. Population homogeneity for the antibody response to COVID-19 BNT162b2/Comirnaty vaccine is only reached after the second dose across all adult age ranges. *Nat Commun* (2022) 13(1):140. doi: 10.1038/s41467-021-27761-z

33. Barros-Martins J, Hammerschmidt SI, Cossmann A, Odak I, Stankov MV, Morillas Ramos G, et al. Immune responses against SARS-CoV-2 variants after heterologous and homologous ChAdOx1 nCoV-19/BNT162b2 vaccination. *Nat Med* (2021) 27(9):1525–9. doi: 10.1038/s41591-021-01449-9

34. Busà R, Sorrentino MC, Russelli G, Amico G, Miceli V, Miele M, et al. Specific anti-SARS-CoV-2 humoral and cellular immune responses after booster dose of BNT162b2 pfizer-BioNTech mRNA-based vaccine: Integrated study of adaptive immune system components. *Front Immunol* (2022) 13:856657(856657). doi: 10.3389/fimmu.2022.856657

35. Barda N, Dagan N, Cohen C, Hernan MA, Lipsitch M, Kohane IS, et al. Effectiveness of a third dose of the BNT162b2 mRNA COVID-19 vaccine for preventing severe outcomes in Israel: an observational study. *Lancet* (2021) 398 (10316):2093–100. doi: 10.1016/S0140-6736(21)02249-2

36. Chu L, Vrbicky K, Montefiori D, Huang W, Nestorova B, Chang Y, et al. Immune response to SARS-CoV-2 after a booster of mRNA-1273: an open-label phase 2 trial. *Nat Med* (2022). 28(5):1042–9. doi: 10.1038/s41591-022-01739-w

37. Perez-Alos L, Armenteros JJA, Madsen JR, Hansen CB, Jarlhelt I, Hamm SR, et al. Modeling of waning immunity after SARS-CoV-2 vaccination and influencing factors. *Nat Commun* (2022) 13(1):1614. doi: 10.1038/s41467-022-29225-4

38. Adamo S, Michler J, Zurbuchen Y, Cervia C, Taeschler P, Raeber ME, et al. Signature of long-lived memory CD8(+) T cells in acute SARS-CoV-2 infection. *Nature* (2022) 602(7895):148–55. doi: 10.1038/s41586-021-04280-x

39. Neidleman J, Luo X, Frouard J, Xie G, Gill G, Stein ES, et al. SARS-CoV-2-Specific T cells exhibit phenotypic features of helper function, lack of terminal differentiation, and high proliferation potential. *Cell Rep Med* (2020) 1(6):100081. doi: 10.1016/j.xcrm.2020.100081

40. Martin MD, Badovinac VP. Defining memory CD8 T cell. *Front Immunol* (2018) 9:2692. doi: 10.3389/fimmu.2018.02692

41. Tan AT, Lim JM, Le Bert N, Kunasegaran K, Chia A, Qui MD, et al. Rapid measurement of SARS-CoV-2 spike T cells in whole blood from vaccinated and naturally infected individuals. *J Clin Invest* (2021) 131(17):e152379. doi: 10.1172/JCI152379

42. Jung JH, Rha MS, Sa M, Choi HK, Jeon JH, Seok H, et al. SARS-CoV-2-specific T cell memory is sustained in COVID-19 convalescent patients for 10

months with successful development of stem cell-like memory T cells. *Nat Commun* (2021) 12(1):4043. doi: 10.1038/s41467-021-24377-1

43. Oberhardt V, Luxenburger H, Kemming J, Schulien I, Ciminski K, Giese S, et al. Rapid and stable mobilization of CD8(+) T cells by SARS-CoV-2 mRNA vaccine. *Nature* (2021) 597(7875):268–73. doi: 10.1038/s41586-021-03841-4

44. Echeverria G, Guevara A, Coloma J, Ruiz AM, Vasquez MM, Tejera E, et al. Pre-existing T-cell immunity to SARS-CoV-2 in unexposed healthy controls in Ecuador, as detected with a COVID-19 interferon-gamma release assay. *Int J Infect Dis* (2021) 105:21–5. doi: 10.1016/j.ijid.2021.02.034

45. Swadling L, Diniz MO, Schmidt NM, Amin OE, Chandran A, Shaw E, et al. Pre-existing polymerase-specific T cells expand in abortive seronegative SARS-CoV-2. *Nature* (2022) 601(7891):110–7. doi: 10.1038/s41586-021-04186-8

46. Braun J, Loyal L, Frentsch M, Wendisch D, Georg P, Kurth F, et al. SARS-CoV-2-reactive T cells in healthy donors and patients with COVID-19. *Nature* (2020) 587(7833):270–4. doi: 10.1038/s41586-020-2598-9

47. Le Bert N, Tan AT, Kunasegaran K, Tham CYL, Hafezi M, Chia A, et al. SARS-CoV-2-specific T cell immunity in cases of COVID-19 and SARS, and uninfected controls. *Nature* (2020) 584(7821):457–62. doi: 10.1038/s41586-020-2550-z

48. Kuhlmann C, Mayer CK, Claassen M, Maponga T, Burgers WA, Keeton R, et al. Breakthrough infections with SARS-CoV-2 omicron despite mRNA vaccine booster dose. *Lancet* (2022) 399(10325):625–6. doi: 10.1016/S0140-6736(22)00090-3

49. GeurtsvanKessel CH, Geers D, Schmitz KS, Mykytyn AZ, Lamers MM, Bogers S, et al. Divergent SARS-CoV-2 omicron-reactive T and b cell responses in COVID-19 vaccine recipients. *Sci Immunol* (2022) 7(69):eabo2202. doi: 10.1126/sciimmunol.abo2202

50. Naranbhai V, Nathan A, Kaseke C, Berrios C, Khatri A, Choi S, et al. T Cell reactivity to the SARS-CoV-2 omicron variant is preserved in most but not all individuals. *Cell* (2022) 185(7):1259. doi: 10.1016/j.cell.2022.03.022

51. Bonnet B, Cosme J, Dupuis C, Coupez E, Adda M, Calvet L, et al. Severe COVID-19 is characterized by the co-occurrence of moderate cytokine inflammation and severe monocyte dysregulation. *EBioMedicine* (2021) 73:103622. doi: 10.1016/j.ebiom.2021.103622

52. Schulte-Schrepping J, Reusch N, Paclik D, Bassler K, Schlickeiser S, Zhang B, et al. Severe COVID-19 is marked by a dysregulated myeloid cell compartment. *Cell* (2020) 182(6):1419–40 e23. doi: 10.1016/j.cell.2020.08.001

53. Liu J, Wang J, Xu J, Xia H, Wang Y, Zhang C, et al. Comprehensive investigations revealed consistent pathophysiological alterations after vaccination with COVID-19 vaccines. *Cell Discovery* (2021) 7(1):99. doi: 10.1038/s41421-021-00329-3

54. Chevrier S, Zurbuchen Y, Cervia C, Adamo S, Raeber ME, de Souza N, et al. A distinct innate immune signature marks progression from mild to severe COVID-19. *Cell Rep Med* (2021) 2(1):100166. doi: 10.1016/j.xcrm.2020.100166

55. Sacchi A, Grassi G, Bordoni V, Lorenzini P, Cimini E, Casetti R, et al. Early expansion of myeloid-derived suppressor cells inhibits SARS-CoV-2 specific T-cell response and may predict fatal COVID-19 outcome. *Cell Death Dis* (2020) 11 (10):921. doi: 10.1038/s41419-020-03125-1

frontiers | Frontiers in Immunology

TYPE Original Research
PUBLISHED 16 December 2022
DOI 10.3389/fimmu.2022.1066176

Check for updates

OPEN ACCESS

EDITED BY
Alessio Mazzoni,
University of Florence, Italy

REVIEWED BY
Francesco Nicoli,
University of Ferrara, Italy
Patrick Maschmeyer,
Charité Universitätsmedizin Berlin, Germany

*CORRESPONDENCE
Rafael Kramann
rkramann@gmx.net

†These authors have contributed equally to this work and share first authorship

‡These authors have contributed equally to this work and share last authorship

SPECIALTY SECTION
This article was submitted to T Cell Biology, a section of the journal Frontiers in Immunology

RECEIVED 10 October 2022
ACCEPTED 14 November 2022
PUBLISHED 16 December 2022

CITATION
Schreibing F, Hannani MT, Kim H, Nagai JS, Ticconi F, Fewings E, Bleckwehl T, Begemann M, Torow N, Kuppe C, Kurth I, Kranz J, Frank D, Anslinger TM, Ziegler P, Kraus T, Enczmann J, Balz V, Windhofer F, Balfanz P, Kurts C, Marx G, Marx N, Dreher M, Schneider RK, Saez-Rodriguez J, Costa I, Hayat S and Kramann R (2022) Dissecting CD8+ T cell pathology of severe SARS-CoV-2 infection by single-cell immunoprofiling.
Front. Immunol. 13:1066176.
doi: 10.3389/fimmu.2022.1066176

Dissecting CD8+ T cell pathology of severe SARS-CoV-2 infection by single-cell immunoprofiling

Felix Schreibing[1,2†], Monica T. Hannani[1,3†], Hyojin Kim[1], James S. Nagai[4,5], Fabio Ticconi[4,5], Eleanor Fewings[3], Tore Bleckwehl[1], Matthias Begemann[6], Natalia Torow[7], Christoph Kuppe[1,2], Ingo Kurth[6], Jennifer Kranz[1,8,9], Dario Frank[10], Teresa M. Anslinger[1,2], Patrick Ziegler[11], Thomas Kraus[11], Jürgen Enczmann[12], Vera Balz[12], Frank Windhofer[12], Paul Balfanz[13], Christian Kurts[14], Gernot Marx[15], Nikolaus Marx[13], Michael Dreher[16], Rebekka K. Schneider[17,18], Julio Saez-Rodriguez[3,5], Ivan Costa[4,5‡], Sikander Hayat[1‡] and Rafael Kramann[1,2,19*‡]

[1]Institute of Experimental Medicine and Systems Biology, Medical Faculty, RWTH Aachen University, Aachen, Germany, [2]Department of Renal and Hypertensive Disorders, Rheumatological and Immunological Diseases (Medical Clinic II), Medical Faculty, RWTH Aachen University, Aachen, Germany, [3]Institute for Computational Biomedicine, Heidelberg University, Faculty of Medicine, Heidelberg University Hospital, Heidelberg, Germany, [4]Institute for Computational Genomics, Medical Faculty, RWTH Aachen University, Aachen, Germany, [5]Joint Research Center for Computational Biomedicine, RWTH Aachen University Hospital, Aachen, Germany, [6]Institute of Human Genetics, Medical Faculty, RWTH Aachen University, Aachen, Germany, [7]Institute of Medical Microbiology, Medical Faculty, RWTH Aachen University, Aachen, Germany, [8]Department of Urology and Pediatric Urology, RWTH Aachen University, Aachen, Germany, [9]Department of Urology and Kidney Transplantation, Martin Luther University (Saale), Halle, Germany, [10]Department of Medicine, St Antonius Hospital, Eschweiler, Germany, [11]Institute for Occupational, Social and Environmental Medicine, Medical Faculty, RWTH Aachen University, Aachen, Germany, [12]Institute for Transplantation Diagnostics and Cell Therapeutics, Medical Faculty, University Hospital Düsseldorf, Düsseldorf, Germany, [13]Department of Cardiology, Angiology and Intensive Care Medicine, Medical Faculty, RWTH Aachen University, Aachen, Germany, [14]Institute of Molecular Medicine and Experimental Immunology, Medical Faculty, University of Bonn, Bonn, Germany, [15]Department of Intensive and Intermediate Care, Medical Faculty, RWTH Aachen University, Aachen, Germany, [16]Department of Pneumology and Intensive Care Medicine, Medical Faculty, RWTH Aachen University, Aachen, Germany, [17]Institute of Cell and Tumor Biology, Medical Faculty, RWTH Aachen University, Aachen, Germany, [18]Department of Developmental Biology, Erasmus Medical Center, Rotterdam, Netherlands, [19]Department of Internal Medicine, Erasmus Medical Center (MC), Rotterdam, Netherlands

Introduction: SARS-CoV-2 infection results in varying disease severity, ranging from asymptomatic infection to severe illness. A detailed understanding of the immune response to SARS-CoV-2 is critical to unravel the causative factors underlying differences in disease severity and to develop optimal vaccines against new SARS-CoV-2 variants.

Methods: We combined single-cell RNA and T cell receptor sequencing with CITE-seq antibodies to characterize the $CD8^+$ T cell response to SARS-CoV-2 infection at high resolution and compared responses between mild and severe COVID-19.

Results: We observed increased $CD8^+$ T cell exhaustion in severe SARS-CoV-2 infection and identified a population of NK-like, terminally differentiated $CD8^+$ effector T cells characterized by expression of *FCGR3A* (encoding CD16). Further characterization of NK-like $CD8^+$ T cells revealed heterogeneity among $CD16^+$ NK-like $CD8^+$ T cells and profound differences in cytotoxicity, exhaustion, and NK-like differentiation between mild and severe disease conditions.

Discussion: We propose a model in which differences in the surrounding inflammatory milieu lead to crucial differences in NK-like differentiation of $CD8^+$ effector T cells, ultimately resulting in the appearance of NK-like $CD8^+$ T cell populations of different functionality and pathogenicity. Our in-depth characterization of the $CD8^+$ T cell-mediated response to SARS-CoV-2 infection provides a basis for further investigation of the importance of NK-like $CD8^+$ T cells in COVID-19 severity.

KEYWORDS

SARS-CoV-2, scRNA-seq, scTCR-seq, immunoprofiling, $CD8^+$ T cells, FCGR3A, CD16, NK-like T cell

Introduction

More than two years into the pandemic, severe acute respiratory syndrome coronavirus type 2 (SARS-CoV-2) still poses significant challenges to the healthcare system, the economy, and the public. According to the WHO Coronavirus Dashboard there have been more than 590 million confirmed cases and more than 6.4 million deaths due to COVID-19 so far (August 2022) (1). Although some pharmacological therapeutic options are available today (2), the molecular mechanisms that drive the progression to a severe disease condition remain largely unknown, making vaccination an important instrument to prevent the occurrence of a life-threatening scenario. However, despite vaccine efficacy, particularly in preventing severe COVID-19 (3, 4), breakthrough infections occur repeatedly (5) and can result in severe disease (6–8) as well as serious long-term health consequences (9). Thus, a detailed understanding of the cellular and molecular mechanisms that determine the severity of SARS-CoV-2 infection is crucial to help developing targeted therapies and to improve vaccination strategies.

Much attention has been paid to the SARS-CoV-2-specific antibody response in the public debate, however, several studies point to a critical role of T cells (10), particularly $CD8^+$ T cells, in controlling SARS-CoV-2 infection (11, 12). Impairments of the T cell compartment have been suggested to be involved in the pathogenesis of severe COVID-19. For instance, $CD8^+$ T cell counts have been found to be substantially reduced in severe and fatal COVID-19 compared with mild cases (13). Additionally, hyperactivated $CD8^+$ T cell states have been associated with COVID-19 lethality and severity (14–16) and $CD8^+$ T cell exhaustion has been identified as a characteristic of severe SARS-CoV-2 infection (16).

Single-cell RNA-sequencing (scRNA-seq) techniques offer the opportunity to investigate cellular heterogeneity, to uncover cell type-specific gene expression and to dissect cell type-specific differences between disease conditions. Various studies have used scRNA-seq to investigate the innate and adaptive immune response in COVID-19 (17–24). Additionally, within recent years, scRNA-seq has led to the discovery of large phenotypic diversity within the $CD8^+$ T cell compartment (25, 26).

In this study, we perform scRNA-seq combined with single-cell T cell receptor sequencing (scTCR-seq) and surface protein profiling using cellular indexing of transcriptomes and epitopes by sequencing (CITE-seq) (27) of $CD8^+$ T cells in mild and severe COVID-19 and healthy controls. We observe large functional and phenotypic heterogeneity within the $CD8^+$ T cell compartment and identify increased $CD8^+$ T cell exhaustion

in individuals with severe SARS-CoV-2 infection. By performing trajectory inference, we identify a terminally differentiated $CD16^+$ $CD8^+$ effector cell population with an NK-like phenotype that might be relevant in viral control. Deeper profiling of these NK-like T cells reveals heterogeneity within this population and substantial phenotypic differences between mild and severe disease. Thus, our study provides insights into a poorly described $CD8^+$ T cell population that might be important for the antiviral response against SARS-CoV-2. Moreover, aberrant differentiation of this subpopulation might be crucially involved in the pathogenesis of severe SARS-CoV-2 infections.

Materials and methods

Study design

With this study we wanted to dissect the differences in $CD8^+$ T cell responses between individuals with mild and severe SARS-CoV-2 infection at a single-cell resolution. We performed scRNA and TCR-seq to identify differences in gene expression characteristics and clonal expansion between $CD8^+$ T cells from the different disease conditions. Additionally, we used CITE-seq antibodies to identify functional subgroups of $CD8^+$ T cells and to perform a surface-protein profiling.

Patient recruitment and clinical data

Laboratory-confirmed COVID-19 patients were recruited from the University Hospital of the RWTH Aachen University and from the Sankt Antonius Hospital Eschweiler from May to September 2020. All patients provided informed consent and the study was performed in accordance with the Declaration of Helsinki. For patients who were not able to give consent themselves, their legal representative agreed to their participation in the study. The study protocol was reviewed and approved by the Ethical Board of the RWTH Aachen University Hospital (vote: EK 078/20). Initially, 12 COVID-19 patients (6 with mild COVID-19 and 6 with severe COVID-19) and 3 healthy volunteers were included in the study. After initial processing of the single-cell data, we observed an extremely high proportion of effector cells in one healthy control sample. In addition, the respective healthy volunteer reported an unclear infection in early January 2020, approximately four months before the start of the study. Since we could not rule out that the patient had been infected with SARS-CoV-2, we excluded this sample in order to avoid a bias. Thus, the final analyses were carried out on samples from 6 individuals with mild COVID-19, 6 samples with severe COVID-19 and 2 control samples. Patients were pseudonymized and clinical as well as epidemiological data were obtained from the electronic hospital information system "CGM Medico". Clinical data is provided in Table S2.

Group allocation

Based on the clinical course, patients were divided into two major groups: severe or mild SARS-CoV-2 infection. Patients with asymptomatic infection and symptomatic patients who did not require mechanical ventilation were allocated to the group of mild infection. Symptomatic patients who required mechanical ventilation were allocated to the group of severe SARS-CoV-2 infection. Group allocation for each patient is shown in Table S2.

Sample collection and PBMC isolation

10-30 ml of blood per patient were collected in either 9 ml S-Monovettes, K3 EDTA 92x16 mm, or in 5.5 ml S-Monovettes, 75x15 mm, provided by Sarstedt (Nümbrecht, Germany). The samples were stored at 4°C for a maximum of 7 hours until further processing. Peripheral blood mononuclear cells (PBMCs) were isolated by Ficoll gradient centrifugation. The isolated PBMCs were resuspended in 10% DMSO in FCS and immediately frozen gradually. The frozen PBMC samples were stored at -152°C. In addition, serum samples were frozen for each patient. After thawing, the PBMCs were immediately diluted with 10 ml 5% FCS in PBS and centrifuged at 500 rcf for 5 minutes. The supernatant was removed and the PBMCs were resuspended in 5 ml 5% FCS in PBS and filtered through a 20 µm pluriStrainer® provided by pluriSelect (Leipzig, Germany) to obtain a single-cell solution.

SARS-CoV-2 antibody testing

To exclude healthy controls with a previous SARS-CoV-2 infection, we tested the subjects for SARS-CoV-2-specific IgG antibodies by performing the Euroimmun anti-SARS-CoV-2 ELISA (IgG) (EUROIMMUN, Lübeck, Germany) (Table S2). An IgG ratio of > 2.5 was considered a positive test, a ratio between 0.8 and 2.5 was considered an intermediate result and a ratio < 0.8 was considered a negative test (28).

Single-cell immune profiling of $CD8^+$ T cells

PBMC samples were thawed as described above. After the PBMCs were passed through a strainer, a second centrifugation was performed. The supernatant was removed and cells were diluted in 100 µl 5% FCS in PBS. 5 µl Human TruStain FcX (BioLegend) was added and incubated for 10 minutes at 4°C.

The panel of 15 TotalSeq-C antibodies (BioLegend) was pooled, using 0.5 µg of each antibody (Table S1). Samples were incubated with MHC class I Dextramer reagents provided by Immudex (Copenhagen, Denmark) for 10 minutes at 4°C, followed by a 30 minute incubation with the TotalSeq-C antibody pool and 5 µl of a PE/Cyanine7 anti-human CD8 antibody (BioLegend) at 4°C. Cells were washed two times using 3 ml 5% FCS in PBS and rediluted in 2 ml 5% FCS in PBS. For the detection of dead cells, DAPI was added at a final concentration of 0.5 µg/ml. Cells were sorted into 1% BSA in PBS on a Sony Cell Sorter by gating on two populations; a PE^+ population (MHC I Dextramer reagent-positive) to enrich for SARS-CoV-2-specific T cells and a $CD8^+$ PE^- fraction (Figure S1A). If the number of PE^+ cells did not exceed 10,000 cells, a maximum of 3,000 $CD8^+$ PE^- cells were added prior to single-cell partitioning and barcoding *via* Chromium Controller (10x Genomics). For each sample, three libraries were prepared; a 5′ gene expression library (GEX), a T cell receptor enriched library (VDJ), and a surface protein library containing the TotalSeq-C barcodes (ADT). After fluorometric quantification, the libraries were pooled in a 5:1:1 ratio for the GEX library, the VDJ enriched library and the ADT library, respectively. The pooled libraries were again quantified using a Quantus™ Fluorometer (Promega, Madison, Wisconsin, USA) and sequenced on a NextSeq 500 platform (Illumina, San Diego, CA, USA) with 2x 150 cycles.

Single-cell RNA seq data processing

Raw scRNA-seq FASTQ files were aligned to the human GRCh38 genome with *Cell Ranger* (4.0.0) with default settings (10x Genomics). For every patient, the paired GEX and ADT libraries were processed together with the *count* function and the VDJ enriched library was processed separately with the *vdj* method. Downstream analysis was conducted with *Seurat* (4.0) (29) in *R* version 4.0.3. Cells with < 200 or > 3,000 detected genes and more than 10% mitochondrial read content were filtered out (Figures S1H–J are referred to for scRNA quality control metrics per sample). The GEX and ADT assays were log and centered log ratio (CLR) normalized, respectively, and were subsequently scaled with default settings.

Clustering and cell annotation

In order to cluster and characterize cell subtypes, the samples were integrated based on the GEX libraries for a first round of clustering. For each sample, the top 2,000 most variable genes were obtained using the *FindVariableFeatures* function in Seurat *version 4.0* and dimensional reduction was performed on the variable features with a principal component analysis (PCA). To account for batch-effects, the samples were integrated using the *harmony* algorithm version 0.1.0 (30) with default setting, 'sample' as the batch variable, and the data was embedded in a Uniform Manifold Approximation and Projection (UMAP) using 30 principal components. A nearest neighbor graph was built with 30 principal components using *FindNeighbors* and unsupervised clustering was performed using a Louvain algorithm with *FindClusters* and a resolution of 1. In order to determine cluster-specific markers, a Wilcoxon rank sum test was performed with *FindMarkers* using min.pct = 0.25. Only genes with a false discovery rate (FDR) < 5% were considered. High-level cell annotation of the clusters was performed on the integrated data followed by filtering of non-T cells and clusters consisting mainly of low-quality cells. A second round of clustering was performed as described above using a resolution of 0.5. Low-level annotation of the resulting clusters was based on a combination of GEX and ADT marker expression. One healthy sample was removed from the study as the volunteer informed us of an unknown infection in early January 2020 and exhibited high levels of differentiated effector T cells. Cell-cycle analysis was performed on the clusters using *CellCycleScoring* (Figure S1G) and mitochondrial gene content was computed per disease condition (Figure S1J). After the final round of annotation and after determining the average cell proportions per condition, we removed all cells that were annotated as MAIT cells, γδ T cells and atypical NKT cells to achieve a dataset of only $CD8^+$ T cells. Cells that expressed either TRAV1-2, TRAJ33 or both, which are T cell receptor genes characteristic of MAIT cells, were also excluded from the analysis. Lastly, T cells with missing TCR-seq information (Figure S1F) were removed, resulting in a final dataset of 25,506 cells for all downstream analysis.

Differential gene expression and gene set enrichment analysis

The final dataset consists of control (n = 2,086 cells), mild (n = 12,251 cells), and severe disease conditions (n = 11,169 cells). For functional characterization of the differences between the disease conditions, differential gene expression analysis was performed with *FindMarkers* using min.pct = 0.25 and FDR < 5%. When contrasting conditions, only cell types with counts > 20 in both groups were considered for the analysis. A pre-ranked gene set enrichment analysis was performed with the *fgsea* package (31). The gene sets C2, C5 (subcategory BP), C7, C8 and H were used for the analysis and were downloaded with the *msigdbr* package. Selected gene sets with an FDR < 5% were visualized as bar plots. A full list of significantly differentially expressed genes in each $CD8^+$ T cell population and corresponding gene sets is provided in Table S4. Differentially expressed genes between disease conditions in $CD16^+$ $CD8^+$ T_{EMRA} subpopulations and associated gene sets for each test are listed in Tables S6, S7, respectively.

Subclustering of CD8$^+$ NK-like T_{EMRA} cells

For subclustering, CD8$^+$ NK-like T_{EMRA} cells were subsetted using the *subset* function in *Seurat*. The subset was normalized, variable features were identified and the data was scaled following the standard *Seurat* workflow. Dimensional reduction was performed and the subset was re-integrated with the *harmony* algorithm version 0.1.0 using 'patient' as the batch variable. A shared nearest neighbor graph was built with 20 principal components using *FindNeighbors* and unsupervised clustering was performed on the re-integrated data using a Louvain-based algorithm with *FindClusters* and a resolution of 1. Marker genes were identified with *FindMarkers* using min.pct = 0.5 and FDR < 5%.

Calculation of functional scores

Gene sets for the calculation of exhaustion and cytotoxicity scores were adopted from Baryawno et al. (32). For the estimation of an NK-like phenotype (NK cell signature score), we used a gene set derived from the cell type signature gene set 'HAY_BONE_MARROW_NK_CELLS' (33). For the calculation of an apoptosis score we used the 'REACTOME_APOPTOSIS' gene set, obtained from MSigDB. A score value for each gene set was calculated for each cell using the *AddModuleScore* function in *Seurat* and score values were plotted as violin plots using the *VlnPlot* function in *Seurat*. For the comparison of functional scores within CD16$^+$ CD8$^+$ T_{EMRA}-1 cells between the mild and the severe disease condition, CD8$^+$ NK-like T_{EMRA}-1 cells were subsetted using the *subset* function in *Seurat*. Violin plots were created using the *geom_violin* function combined with the *geom_boxplot* function in the *ggplot2* package (3.3.6) and significance tests were performed using Wilcoxon test within the *stat_compare_means* function in *ggpubr* (0.4.0).

Integration with reference CD8$^+$ T cell dataset and reference mapping of exhausted and NK-like populations

To computationally validate our findings in a larger dataset, we subsetted the large reference dataset from Ren et al. (34) for all CD8$^+$ T cells. We then generated two reference datasets. The first one was generated by filtering the CD8$^+$ T cells for data that was generated from frozen PBMCs using 5′-sequencing to match the conditions of our dataset. This PBMC-derived reference CD8$^+$ T cell dataset was used for investigation of exhaustion as well as for the integration with our dataset to validate the existence of an NK-like CD8$^+$ T cell population. For integration, the CD8$^+$ reference dataset was re-integrated with the *harmony* (0.1.0) algorithm using 'patient' as the batch variable and subsequently clustered using the Louvain algorithm implemented in *Seurat* (Figures S3A–C). Next, anchors were identified and the reference CD8$^+$ T cell dataset was integrated with our dataset using *Seurat* (Figures S3D–G). The proportion of cells from our dataset (query) in the integrated clusters was calculated by dividing the absolute number of cells of a certain CD8$^+$ T cell subtype in each integrated subcluster by the total count of cells of this subtype in our dataset. Results were visualized as heatmap using *pheatmap* package (1.0.12).

To isolate and subcluster NK-like CD8$^+$ T cells in the reference dataset, cell IDs of all cells that clustered together with our CD8$^+$ NK-like T_{EMRA} cells in the integrated dataset were isolated using the *WhichCells* function in *Seurat*. These cells were annotated as 'NK_like_subset' in the reference dataset based on cell ID. Further, all NK-like CD8$^+$ T cells in the reference dataset were subclustered as described above (Figures S7D–F). The same cell ID-based approach was used to identify cells in the reference dataset that mapped to exhausted CD8$^+$ T cells in our dataset.

Besides the PBMC-derived reference dataset, we also filtered the large CD8$^+$ T cell dataset for samples derived from bronchoalveolar lavage fluid (BAL). The BAL-derived CD8$^+$ T cell reference dataset was re-integrated as described above (Figures S3H–J) and used to investigate exhaustion in lung-derived CD8$^+$ T cells.

Mild and severe disease scores

To identify gene sets in NK-like CD8$^+$ T cells that are related to disease severity, we performed differential gene expression analysis between all CD8$^+$ NK-like T_{EMRA} cells from the mild and the severe condition using the *FindMarkers* function with a min.pct = 0.5 and FDR < 5%. Next, we identified genes differentially expressed between the two disease conditions, which overlapped with highly significant marker genes of our CD8$^+$ NK-like T_{EMRA} population. To optimize identification of gene sets, the p-value threshold for the selection of CD8$^+$ NK-like T_{EMRA} marker genes was adjusted multiple times. Finally, choosing only the most significant marker genes with a p-value threshold of 1e-17 yielded best results. Genes with an average $\log_2$-fold change > 0 in differential expression analysis between mild and severe COVID-19 were combined into the 'mild disease score', while genes with an average $\log_2$-fold change < 0 were combined into the 'severe disease score'.

Mild and severe disease score values were calculated for every cell in our CD8$^+$ NK-like T_{EMRA} cell subset as well as for every cell in the reference NK-like CD8$^+$ T cell subset using *AddModuleScore*. Results were grouped by condition (query and reference) and by outcome (reference) and plotted as boxplots using *geom_boxplot* in *ggplot2* package (3.3.6). Lastly score values were calculated for every cell in our whole dataset as

well as for every cell in the reference CD8$^+$ T cell dataset and score values were projected onto the UMAP using the *FeaturePlot* function in *Seurat*. To investigate cell type-specific score values, score values were plotted per cell type using the *VlnPlot* function in *Seurat* (Figures S7H, I).

Signaling pathway and transcription factor activity

Signaling pathway activities were estimated with PROGENy (35, 36) using the top 500 footprint genes per pathway. To test for significant differences between the conditions, Wilcoxon rank sum tests were performed on relevant pathways and cell types with FDR < 5%. Transcription factor activities were computed with the *viper* package (1.24.0) (37) using regulons with confidence levels A, B or C from DoRothEA (38). The changes in transcription factor activity were estimated per cell type using the condition contrasts obtained from differential gene expression analysis with *FindMarkers*. Transcription factor activities with FDR < 5% in pairwise comparisons between the conditions were visualized with *geom_tile* function in *ggplot2*. Figure S6G is referred to for all PROGENy pathway activities per condition.

Data integration for cell-cell communication analysis

To estimate cell-cell interactions between our CD8$^+$ T cell populations and non-T cell populations, our dataset was integrated with a selected subset of data from Ren et al. (34). For sample selection from the public dataset, we included 16 disease samples (mild/moderate = 4, severe/critical = 12) where matched samples from both PMBCs and bronchoalveolar lavage fluid (BAL) were available. Additionally, we included 6 healthy controls. In total, the subsetted public dataset consisted of 119,587 disease and 41,919 healthy cells (total n = 161,506) (Table S10).

Integration of our single-cell dataset with the public dataset was performed using *harmony* (0.1.0). Briefly, different samples were used as the batch variable to account for batch-effects between the two datasets. Network neighborhood algorithm, followed by the Louvian clustering approach implemented in *Seurat* (4.1.1), was used to identify cell-clusters in the integrated dataset. The final integrated dataset consisted of a total of 187,012 cells from 36 samples.

Cell-cell communication

To predict cell-cell interactions, *LIANA* (0.1.6) (39) was used per disease condition with the *statistical_analysis* method. Cell types with counts > 20 per condition were included in the analysis and the log-normalized and scaled counts were used as input. Ligand-receptor interactions with p-value < 0.05 were considered for the downstream analyses.

CrossTalkeR (40) was used to compute changes in ligand-receptor interactions between the conditions. Briefly, *CrossTalkeR* constructs representations of the ligand-receptor networks for each condition, where the edges of the network are weighted by the number of interactions and the sum of weights of the interaction-pairs obtained by *LIANA*. Differential cell-cell interaction networks were constructed by subtracting the condition state network from the control states.

For the characterization of differences in interactions with CD8$^+$ NK-like T_{EMRA} cells between the conditions, differential cell-cell interactions that were predicted by *CrossTalkeR* were filtered for CD8$^+$ NK-like T_{EMRA} cells as *receptor* cluster, while all non-CD8$^+$ T cells were considered as *ligand* cluster (except for megakaryocytes). Differential absolute LR-Scores were plotted as dot plots for selected interactions that have been shown to be relevant in NK cell development and function.

To focus on differences in selected interactions between mild and severe SARS-CoV-2 infection, all CD8$^+$ T cell populations were regarded as *receptor* cluster, while the same cell types as before were regarded as *ligand* clusters. Boxplots displaying the LR-Scores for each predicted interaction, grouped by condition, were plotted using the *geom_boxplot* function in *ggplot2*. Wilcoxon-test was used to compare for statistical differences between the mild and the severe condition using the *stat_compare_means* function in *ggpubr*.

Trajectory inference and pseudotemporal differential gene expression

In order to estimate CD8$^+$ T cell differentiation, trajectory inference was performed with *Slingshot* (2.2.1) (41). In addition to the previously removed MAIT, γδ, NKT cell populations, CD8$^+$ CD73$^+$ T_{reg} populations were also excluded from the pseudotime analysis in order to only include T cell subpopulations likely to originate from the CD8$^+$ naïve T cells. The final dataset for trajectory analyses consisted of 24,716 cells. *Slingshot* was run on the UMAP embedding of the remaining clusters and the CD8$^+$ naïve T cell population was manually designated as the root of all inferred trajectories. Two trajectories were determined by the pseudotime analysis; the short-lived effector cell (SLEC) lineage and exhaustion (EX) lineage. In order to test for significant differences between the distribution of the mild and the severe disease conditions across pseudotime, a Kolmogorov-Smirnov test was performed for each lineage.

For temporal differential gene expression analysis between the two trajectories, *tradeSeq* (1.8.0) was used (42). A negative binomial generalized additive model (NB-GAM) was built on the 10,000

most variable genes and pseudotimes for the mild and severe conditions using the *fitGAM* function. In order to study differences in temporal gene expression between the conditions, a condition-specific smoother was computed per lineage. 6 knots were used for the NB-GAM (Figure S4A is referred to for a visualization of the knots projected onto the integrated UMAP). Differential gene expression between the progenitor and differentiated cell populations was performed with *startVsEndTest* using l2fc = $\log_2(2)$. The significant genes from the test were modeled with *predictSmooth* using nPoints = 50 and visualized with *pheatmap*. The expression of significant genes across pseudotime was visualized with *plotSmoothers*. To characterize potential early drivers of differentiation towards the two trajectories, *earlyDETest* was used at the bifurcation point (between knots 2 and 3) with l2fc = $\log_2(1.5)$. Differential gene expression between the end stages of the lineages was performed with *diffEndTest* using l2fc = $\log_2(2)$. Temporal differential expression between the mild and severe conditions for each lineage was computed with *conditionTest* using l2fc = $\log_2(2)$, global = TRUE, and pairwise = TRUE. For all tests performed with *tradeSeq*, only genes with FDR < 5% were considered. For each test performed with *tradeSeq*, all genes were ranked based on the estimated Wald statistic and a gene set enrichment analysis was performed as previously described. Table S5 is referred to for a full list of significantly differentially expressed genes for each test.

T cell receptor clonality analysis

In order to study T cell receptor (TCR) clonality in the scRNA data, TCR clonotypes were assigned based on the VDJ library using the *cellranger vdj* function. For the analysis, only MHC class I restricted T cell subtypes were considered. For clonality analysis in the $CD8^+$ reference dataset, the data frame containing TCR-seq data was loaded into *R*. The reference dataset was filtered for cells for which TCR-seq data were available in the data frame and vice versa. Finally, TCR-seq data was added to the dataset using the *AddMetaData* function implemented in *Seurat*. The clonotypes were grouped based on the level of expansion and designated as; single ($n = 1$), small ($1 < n \leq 5$), medium ($5 < n \leq 20$), large ($20 < n \leq 100$), or hyperexpanded ($n > 100$). The relative abundance of the clonotype size groups was computed for the conditions and cell types and visualized as bar charts. Figures S5A, D, E are referred to for the TCR clonotype size distribution for each cell type per condition in our dataset, the PBMC-derived, and the BAL-derived $CD8^+$ reference datasets, respectively.

In order to estimate changes in TCR diversity between the disease conditions during $CD8^+$ T cell differentiation, the Shannon diversity index was calculated over pseudotime for the SLEC and EX trajectories. Cells in the two trajectories were grouped into 8 different sets by ascending order of pseudotime. For each bin, the TCR chains were extracted along with the condition (mild or severe) and chain (TRA or TRB) level information. TCR sequences were rearranged into the 'TCR_V_CDR3_TCR_J' format for TRA and TRB chains, and subsequently these sequences were combined into a format 'TRA_V_CDR3A_TRA_J_TRB_V_CDR3B_TRB_J' to calculate the Shannon index based on the total TCR sequence information. Shannon entropy was then applied on the occurrence of several TCR chains by using the *vegan* package (2.6.2) (43).

To investigate overlap in TCR repertoires between the three conditions, TCR sequences were first rearranged into the 'TCR_V_CDR3_TCR_J' format. Overlap between the conditions was calculated and visualized separately for TCR alpha and beta chain with the *ggvenn* function in the *ggvenn* package (0.1.9).

To quantify clonotype similarity between $CD16^+$ $CD8^+$ T_{EMRA} subpopulations (Figure S6C), the Morisita index was calculated. To this end, TCR sequences were again rearranged into the 'TCR_V_CDR3_TCR_J' format and the absolute count of each TCR sequence per $CD16^+$ $CD8^+$ T_{EMRA} subtype was calculated. Morisita index was calculated using the *repOverlap* function implemented in *immunarch* package (0.7.0) with.*method* = *'morisita'* and.*col* = *'v+aa+j'*. Overlap was visualized using the *vis* function implemented in *immunarch*.

Calculation of CDR3 abundance

To calculate the frequency of TRA and TRB CDR3 usage, TCR sequences were rearranged into the 'TCR_V_CDR3_TCR_J' format. The absolute count of each unique TCR sequence was calculated for each condition and for T cell receptor alpha and beta chains separately and divided by the total count of TCR sequences in the respective condition. The top 15 CDR3 sequences were visualized as bar charts.

Analysis of flow cytometry data

To investigate the expression of surface protein receptors associated with $CD8^+$ T cell exhaustion and to confirm the existence of $CD16^+$ $CD8^+$ T_{EMRA} subsets identified in the scRNA-seq dataset, we analyzed data from a publicly available flow cytometry dataset containing the same disease conditions as our dataset (44).

Flow cytometry data were processed using *FlowJo* version 10.8.1, and the output was subsequently analyzed and visualized in *R*.

Statistical analysis

Statistical analyses were performed using *R* version 4.0.3 and *GraphPad Prism* version 9. Unless stated otherwise, significance

was estimated with Wilcoxon rank sum tests. *p*-values were adjusted for multiple testing with the Benjamini-Hochberg method with FDR < 5%. Throughout the paper, significance was depicted as: **** = p-value ≤ 0.0001, *** = p-value ≤ 0.001, ** = p-value ≤ 0.01, * = p-value < 0.05.

Results

A population of exhausted CD8$^+$ T cells is exclusive for severe COVID-19

To investigate CD8$^+$ T cell heterogeneity in SARS-CoV-2 infection, we first performed single-cell immunoprofiling of CD8$^+$ T cells (5´ sequencing, 10x Genomics) by combining scRNA-seq with TCR-seq and single-cell proteomics (CITE-seq antibodies, Table S1). To this end, CD8$^+$ T cells were isolated from patients (Table S2) with mild COVID-19 (n = 6), severe COVID-19 (n = 6), and healthy controls (n = 3) and enriched for SARS-CoV-2-specific CD8$^+$ T cells by FACS sorting using MHC I Dextramer reagents (Figures 1A, S1A). Of note, during the analysis, we detected a high proportion of a specific effector cell population in a healthy control who informed us of an unclear infection in early January 2020, approximately four months before the start of the study, and we therefore excluded this sample from the study (healthy controls, n = 2).

Unsupervised clustering and subsetting for CD8$^+$ T cells captured 30,623 cells and 13 distinct clusters (Figures 1B, S1B–J). Functional annotation of T cell subclusters was based on RNA and protein expression of CD45RA, CCR7 (45) and specific T cell effector markers (Figure 1C and Table S3) (46). We identified 10 functional subpopulations of CD8$^+$ T cells as well as three small populations that were annotated as atypical NKT cells (NKT), mucosal-associated invariant T cells (MAIT) and γδ T cells (Figures 1B–D, S1B, C). Since we aimed at investigating CD8$^+$ αβ T cells, these three subpopulations were excluded from all further analysis. T cells expressing one or both of the T cell receptor genes characteristic of MAIT cells, TRAV1-2 and TRAJ33, were also excluded. Additionally, since we aimed to analyze clonal expansion, T cells with missing TCR-seq information (Figure S1F) were removed, leaving us with a final dataset of 25,506 cells for all downstream analyses.

Two clusters strongly expressed natural killer (NK) cell markers *KLRC2* and *NCR3*, and were therefore annotated as NK-like CD8$^+$ early effector T cells (NK T_{eff}) and NK-like CD8$^+$ effector memory T cells re-expressing CD45RA (NK T_{EMRA}). To validate our functional annotation, we investigated the expression of established markers *KLRG1* and *IL7R* (47, 48) in each cluster (Figure 1E). In accordance with our annotation, terminally differentiated effector populations (CD8$^+$ T_{EMRA} and CD8$^+$ NK T_{EMRA}) displayed high expression of *KLRG1* and low *IL7R* expression, while naïve (CD8$^+$ T_N) and central memory T cells (CD8$^+$ T_{CM}) expressed high levels of *IL7R* and low levels of *KLRG1* (Figure 1E). CD8$^+$ NK T_{eff} cells and CD8$^+$ effector memory T cells 1 (T_{EM1}) expressed both *KLRG1* and high levels of *IL7R* and therefore may represent populations of memory precursor effector cells (MPEC) (47, 48).

To identify differences in CD8$^+$ T cell populations between mild and severe COVID-19, we performed differential gene expression analysis between cells from mild and severe SARS-CoV-2 infection, followed by gene set enrichment analysis (GSEA) (Figure 1F and Table S4). GSEA revealed the enrichment of gene sets associated with T cell effector differentiation and T cell activation in severe COVID-19, whereas genes related to CD8$^+$ T cell memory differentiation were enriched in mild COVID-19, indicating that CD8$^+$ T cell fate is strongly directed toward a highly activated effector phenotype in severe SARS-CoV-2 infection (Figure 1F and Table S4). Furthermore, we observed enrichment of genes associated with the term 'GSE26495_PD1HIGH_VS_PD1LOW_CD8_TCELL_DN' in CD8$^+$ T_{EMRA} cells in mild COVID-19. PD-1 is an inhibitory receptor that has been associated with T cell exhaustion, suggesting that CD8$^+$ T_{EMRA} cells in mild SARS-CoV-2 infection, compared to severe infection, resemble cells with low PD-1 expression and thus exhibit a less exhausted phenotype (Figure 1F). Interestingly, we detected a small population of exhausted CD8$^+$ T cells (T_{EX}) characterized by expression of *TIGIT*, *CTLA4*, *CD279* (PD-1) and *HAVCR2* (Tim-3) that was exclusive to the severe COVID-19 group (Figures 1B, G), a finding which has been reported by others before (49, 50).

Validation of CD8$^+$ T cell exhaustion in COVID-19

Exhausted T cells display a strong impairment of effector functions (51) and are typically seen in chronic infections or tumors, where chronic antigenic stimulation induces exhaustion (52). To investigate the functional relevance of exhaustion in our dataset, we calculated cytotoxicity and exhaustion scores previously described (32, 53) (Figures 2A, S2A, B). Exhaustion appeared to increase almost linearly with increasing cytotoxicity, resulting in high cytotoxicity and exhaustion scores in particular effector cell populations (Figure S2A). T_{EX} cells exhibited extremely high exhaustion scores with presumably moderate cytotoxicity (Figures 2A, S2A), suggesting a disturbed balance between the expression of inhibitory receptors and the cytotoxic functions of CD8$^+$ T cells. Comparison of exhaustion scores between the CD8$^+$ T cell populations revealed highest exhaustion scores in T_{EX} cells (Figures 2B, S2C). Comparison of exhaustion scores of all CD8$^+$ T cells between conditions revealed significantly higher exhaustion scores in severe SARS-CoV-2 infection compared to mild disease or healthy controls (Figure 2C).

To further investigate CD8$^+$ T cell exhaustion, we first analyzed a publicly available flow cytometry dataset (Figures 2D, S2D) generated by the COMBAT consortium (44). Analysis of PD-1 and TIM3 expression, two markers of

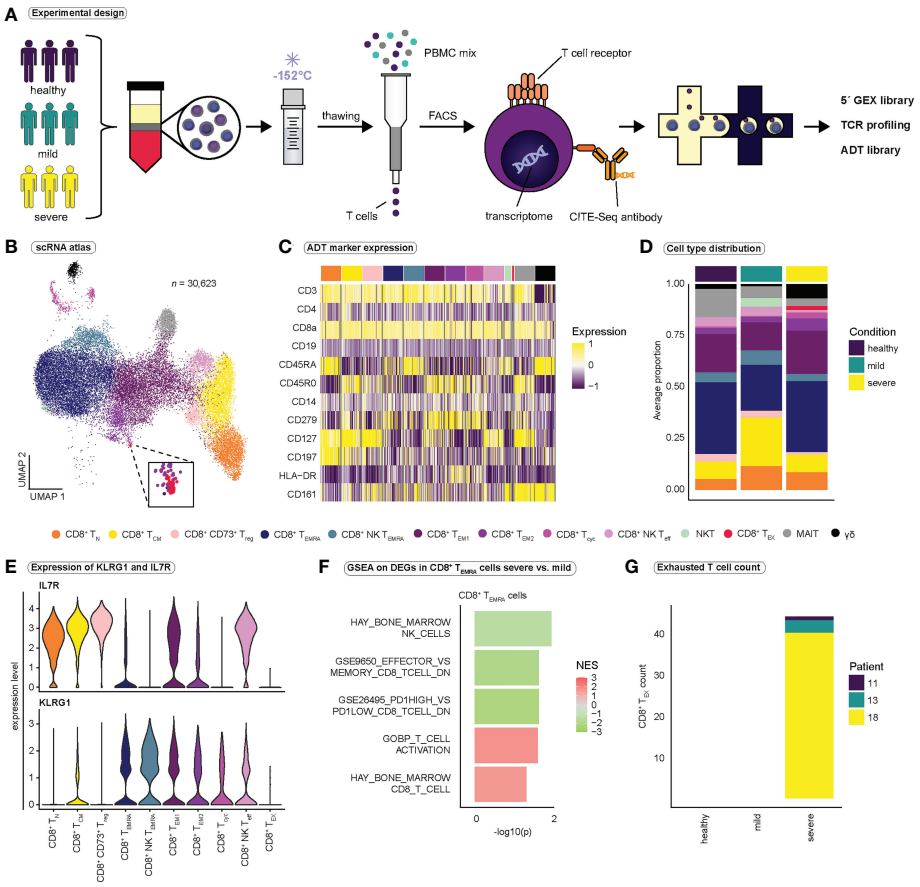


FIGURE 1
Study design and identification of functional subsets of CD8$^+$ T cells. **(A)** Schematic overview of the study design. PBMCs were isolated from healthy volunteers, patients with mild, and patients with severe COVID-19. PBMCs were gradually frozen and stored at -152°C until further processing. After thawing, T cells were isolated using magnetic activated cell sorting. CD8$^+$ T cells were obtained by FACS, and CD8$^+$ T cells were then subjected to the 10x pipeline. **(B)** Integrated UMAP projection of all 13 CD8$^+$ T cell subpopulations (*n* = 30,623) **(C)** Scaled expression of antibody-derived tag (ADT) markers (CITE-seq) per CD8$^+$ T cell subpopulation. **(D)** Average proportion of CD8$^+$ T cell subsets for the healthy (*n* = 2), mild (*n* = 6), and severe (*n* = 6) condition. Cell type proportions per patient are reported in Figure S1C. **(E)** Expression of *KLRG1* and *IL7R* per CD8$^+$ T cell population. **(F)** Selected gene sets enriched in CD8$^+$ T_{EMRA} cells when comparing severe to mild COVID-19 (for a full list of gene sets see Table S4) **(G)** Number of exhausted CD8$^+$ T cells per condition and patient. FACS, fluorescence activated cell sorting; TCR, T cell receptor; GEX, gene expression; ADT, antibody-derived tag; CD8$^+$ T_N, CD8$^+$ naïve T cells; CD8$^+$ T_{CM}, CD8$^+$ central memory cells; CD8$^+$ CD73$^+$ Treg, CD8$^+$ CD73$^+$ regulatory T cells; CD8$^+$ T_{EMRA}, CD8$^+$ terminally differentiated effector memory cells re-expressing CD45RA; CD8$^+$ NK T_{EMRA}, CD8$^+$ NK-like terminally differentiated effector memory cells re-expressing CD45RA; CD8$^+$ T_{EM1}, CD8$^+$ effector memory cells 1; CD8$^+$ T_{EM2}, CD8$^+$ effector memory cells 2; CD8$^+$ T_{cyc}, CD8$^+$ cycling effector cells; CD8$^+$ NK T_{eff}, CD8$^+$ NK-like early effector T cells; NKT, atypical NKT cells; CD8$^+$ T_{EX}, CD8$^+$ exhausted T cells; MAIT, Mucosal associated invariant T cells; γδ, γδ T cells; GSEA, gene set enrichment analysis.

T cell exhaustion, revealed significantly higher frequencies of double-positive cells (PD-1$^+$TIM3$^+$) in COVID-19 compared to healthy controls, although no significant difference was observed between mild and severe infection (Figure 2D).

Since the size of our single-cell dataset was limited, we wanted to investigate exhaustion in a large public dataset by Ren et al. (34). Therefore, after filtering the reference dataset for 5´-sequencing samples and samples derived from frozen PBMCs to match our samples, we extracted all CD8$^+$ T cells, resulting in a reference dataset of 114,209 CD8$^+$ T cells. However, by investigating exhaustion scores in the reference dataset, we were unable to clearly identify a CD8$^+$ T cell population characterized by extremely high exhaustion scores (Figure S2E). In addition, comparison of exhaustion scores of all CD8$^+$ T cells between conditions revealed lower exhaustion scores in severely/critically ill patients compared to mild/moderate illness or controls (Figure 2E). Interestingly, when comparing exhaustion scores in all CD8$^+$ T cells between outcome groups, patients who succumbed to COVID-19 displayed the highest exhaustion scores (Figure 2F).

To uncover exhausted T cells in the reference dataset, we integrated the reference dataset with our CD8$^+$ T cell dataset. Most of our T_{EX} cells mapped onto one distinct subcluster (cluster CD8$^+$_T_4) in the integrated dataset (Figure 2G).

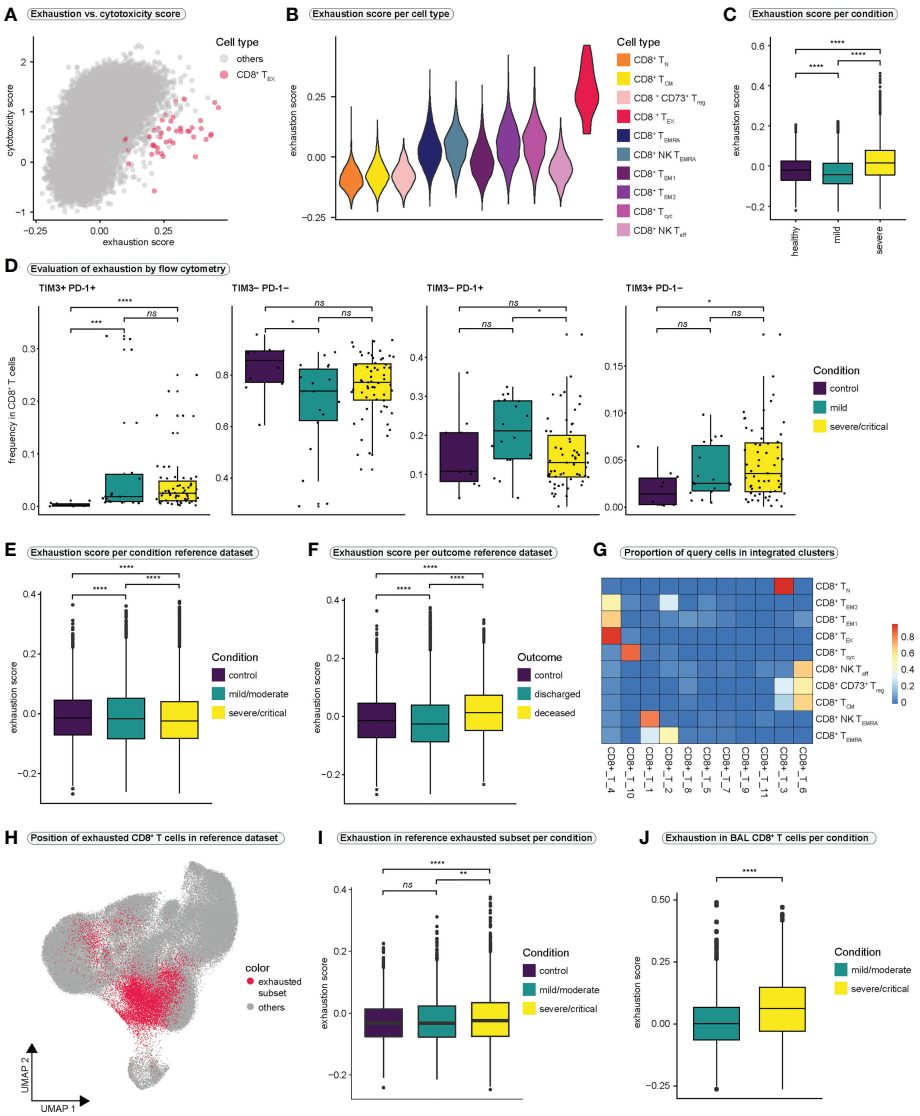


FIGURE 2
$CD8^+$ T cell exhaustion in COVID-19 **(A)** Relationship between T cell exhaustion and cytotoxicity. Each $CD8^+$ T cell is placed in the coordinate system according to its individual exhaustion and cytotoxicity score value. To highlight the position of $CD8^+$ exhausted T cells, all other $CD8^+$ T cell populations are colored in gray. A version of this plot with cell type-specific and condition-specific colors is available in Figure S2A, S2B, respectively. **(B)** Violin plot of exhaustion scores per cell type. **(C)** Exhaustion scores in all $CD8^+$ T cells per condition. (Kruskal-Wallis test: $H\ (2) = 2407$, $p < 0.0001$; healthy vs. mild: $p < 0.0001$; healthy vs. severe: $p < 0.0001$, mild vs. severe: $p < 0.0001$) **(D)** Frequencies of cells expressing different combinations of the exhaustion markers PD-1 and TIM3 in all $CD8^+$ T cells as examined by flow cytometry. ($TIM3^+PD\text{-}1^+$: Kruskal-Wallis test: $H(2) = 21.59$, $p < 0.0001$; control vs. mild: $p = 0.0002$; control vs. severe/critical: $p < 0.0001$, mild vs. severe/critical: $p = 0.8933$; $TIM3^-PD\text{-}1^-$: Kruskal-Wallis test: $H(2) = 6.314$, $p = 0.0426$; control vs. mild: $p = 0.036$; control vs. severe/critical: $p = 0.1046$, mild vs. severe/critical: $p = 0.1689$; $TIM3^-PD\text{-}1^+$: Kruskal-Wallis test: $H(2) = 6.07$, $p = 0.0481$; control vs. mild: $p = 0.1303$; control vs. severe/critical: $p = 0.9359$, mild vs. severe/critical: $p = 0.0484$, $TIM3^+PD\text{-}1^-$: Kruskal-Wallis test: $H(2) = 6.287$, $p = 0.0431$; control vs. mild: $p = 0.1369$; control vs. severe/critical: $p = 0.0377$, mild vs. severe/critical: $p = 0.4863$) **(E)** Exhaustion score in all $CD8^+$ T cells in the reference dataset per condition. (Kruskal-Wallis test: $H(2) = 149.7$, $p < 0.0001$; control vs. mild: $p < 0.0001$; control vs. severe/critical: $p < 0.0001$, mild vs. severe/critical: $p < 0.0001$) **(F)** Exhaustion score in all $CD8^+$ T cells in the reference dataset per outcome. (Kruskal-Wallis test: $H(2) = 1328$, $p < 0.0001$; control vs. discharged: $p < 0.0001$; control vs. deceased: $p < 0.0001$, discharged vs. deceased: $p < 0.0001$) **(G)** Heatmap displaying the proportions of query cell types that mapped to each cluster in the integrated dataset. High values indicate that most cells of a query cluster were assigned to a distinct cluster in the reference dataset. **(H)** Projection of cells that mapped to exhausted $CD8^+$ T cells from the query dataset onto the UMAP of the reference dataset. **(I)** Exhaustion scores per condition in cells from the reference dataset that mapped to exhausted $CD8^+$ T cells in the query dataset. (Kruskal-Wallis test: $H(2) = 31.24$, $p < 0.0001$; control vs. mild/moderate: $p = 0.1054$; control vs. severe/critical: $p < 0.0001$, mild/moderate vs. severe/critical: $p = 0.0011$) **(J)** Exhaustion scores per condition in $CD8^+$ T cells from bronchoalveolar lavage fluid. (Kolmogorov-Smirnov test: $D = 0.2422$, $p < 0.0001$) BAL, bronchoalveolar lavage. **** = p-value ± 0.0001, *** = p-value ± 0.001, ** = p-value ± 0.01, * = p-value < 0.05, ns = not significant.

Projecting all cells from this subcluster back to the UMAP of the CD8$^+$ T cell reference dataset revealed that the exhausted T cells were distributed across the UMAP space of the reference dataset, rather than forming a distinct cluster (Figure 2H). This explained why we were unable to identify a distinct cluster with a high exhaustion score in the reference dataset. Thus, we focused on the newly identified subset of exhausted T cells in the reference dataset and compared exhaustion scores within these cells between conditions. We observed significantly higher exhaustion scores in the exhausted subset in severe/critical COVID-19 as compared to mild/moderate disease and healthy controls (Figure 2I). Similarly, patients who died due to COVID-19 revealed highest exhaustion scores in their exhausted subset (Figure S2F).

Lastly, we asked whether exhaustion is more pronounced in CD8$^+$ T cells that are close to the site of infection. To this end, we generated a second CD8$^+$ T cell reference dataset by filtering all CD8$^+$ T cells from the Ren dataset (34) for cells derived from bronchoalveolar lavage (BAL) fluid. Also in this dataset we did not identify a cluster characterized by excessively high exhaustion scores (Figure S2G). However, when comparing the exhaustion scores of all BAL-derived CD8$^+$ T cells between the conditions and the outcomes of SARS-CoV-2 infection, the group of severely infected individuals and the group that succumbed to COVID-19 clearly displayed higher exhaustion scores than the group with mild infection or the group that recovered from SARS-CoV-2 infection, respectively (Figures 2J and S2H). Since the differences in exhaustion scores between the conditions were more pronounced in BAL-derived CD8$^+$ T cells, it is conceivable that CD8$^+$ T cells that are close to the site of infection undergo more severe exhaustion, an effect that seems to be pronounced in severe and critical SARS-CoV-2 infection. For an overview over the reference and the integrated datasets, we refer to Figures S3A-J.

SARS-CoV-2 infection drives terminal effector differentiation towards an NK-like phenotype

To investigate CD8$^+$ T cell differentiation we predicted pseudotime trajectories using Slingshot (41). As input for inference of differentiation trajectories by Slingshot, we manually defined the cluster of CD8$^+$ naïve T cells as the root of all differentiation trajectories. Slingshot predicted two differentiation pathways (Figures 3A, S4A), both originating in naïve CD8$^+$ T cells and passing through the effector memory stage. Trajectory 1 continued toward the T_{EMRA} and the NK T_{EMRA} stages and was termed 'short lived effector cell lineage' (SLEC). Trajectory 2 ended in close proximity to the exhausted CD8$^+$ T cell population; we therefore termed this lineage 'exhaustion lineage' (EX) (Figure 3A). Investigation of pseudotime-dependent cell densities revealed highest cell densities in early stages of pseudotime in mild COVID-19 for both lineages, whereas there appeared to be a significant shift in cell densities toward the late stages of differentiation in severe COVID-19 (Figure 3B). Surprisingly, cells from healthy controls showed a similar distribution of cell densities as cells from severely infected patients. Because Figure 3B displays only the number of cells at a given differentiation stage, and bias may occur in single-cell experiments regarding the ratio of different cell populations to each other, comparisons of absolute frequencies in single-cell datasets should be evaluated with caution. In our case, it is conceivable that the distribution in healthy controls is partly due to the smaller number of cells in this group.

To verify our lineage assignments and to compare trajectories between mild and severe disease conditions, we performed trajectory-based differential expression analysis for sequencing data (tradeSeq) (42) (Table S5). tradeSeq revealed a significant downregulation of *IL7R* (Figure S4B) and a significant upregulation of *KLRG1* (Figures 3C, D) along the SLEC lineage, suggestive of effector differentiation, while significant upregulation of *CTLA4* along the EX lineage mainly in the severe condition (Figure S4B), supported the concept of an 'exhaustion lineage'. Comparison between the disease conditions indicated significantly stronger expression of certain NK cell receptors (*CD160*, *KLRC2*, *KLRC3*, *KLRF1*, *KIR3DL2*, *NCR1*, *NCR3*) along the SLEC lineage in mild COVID-19 compared to severe COVID-19 (Figures 3D, S4C, D). These results suggest that NK cell receptors are expressed during effector differentiation in SARS-CoV-2 infections and that in severe COVID-19 the expression profile of these receptors differs from the one in mild COVID-19. Since CD8$^+$ NK T_{EMRA} cells represent a final state of the SLEC lineage (Figure 3A), and this population is particularly characterized by the expression of NK cell receptors, we concluded that the observed differences could be the result of differences in the differentiation of CD8$^+$ NK T_{EMRA} cells in severe SARS-CoV-2 infection. To deeply characterize this population, we examined the genes differentially expressed in CD8$^+$ NK T_{EMRA} cells as compared to all other CD8$^+$ T cell populations (Figure 3E and Table S3). Strikingly, CD8$^+$ NK T_{EMRA} cells displayed strong upregulation of *FCGR3A* (CD16), *KLRF1* and certain killer cell immunoglobulin-like receptors (KIRs), strong downregulation of *IL7R* (Figure 3E), and expression of *IKZF2*. CD16$^+$ CD8$^+$ T cell populations have been previously observed in different chronic viral infections (54, 55). Naluyima et al. have described a population of terminally differentiated CD16$^+$ CD8$^+$ T cells characterized by the expression of KIRs, KLRF1, IKZF2 as well as low expression levels of IL7R that were able to mediate antibody-dependent cellular cytotoxicity (ADCC) (54). These cells strongly resembled our CD8$^+$ NK T_{EMRA} population and we verified low IL7R (CD127) expression at a surface protein level using our CITE-seq data (Figure S4E). In summary, SARS-CoV-2 infection seems to induce a

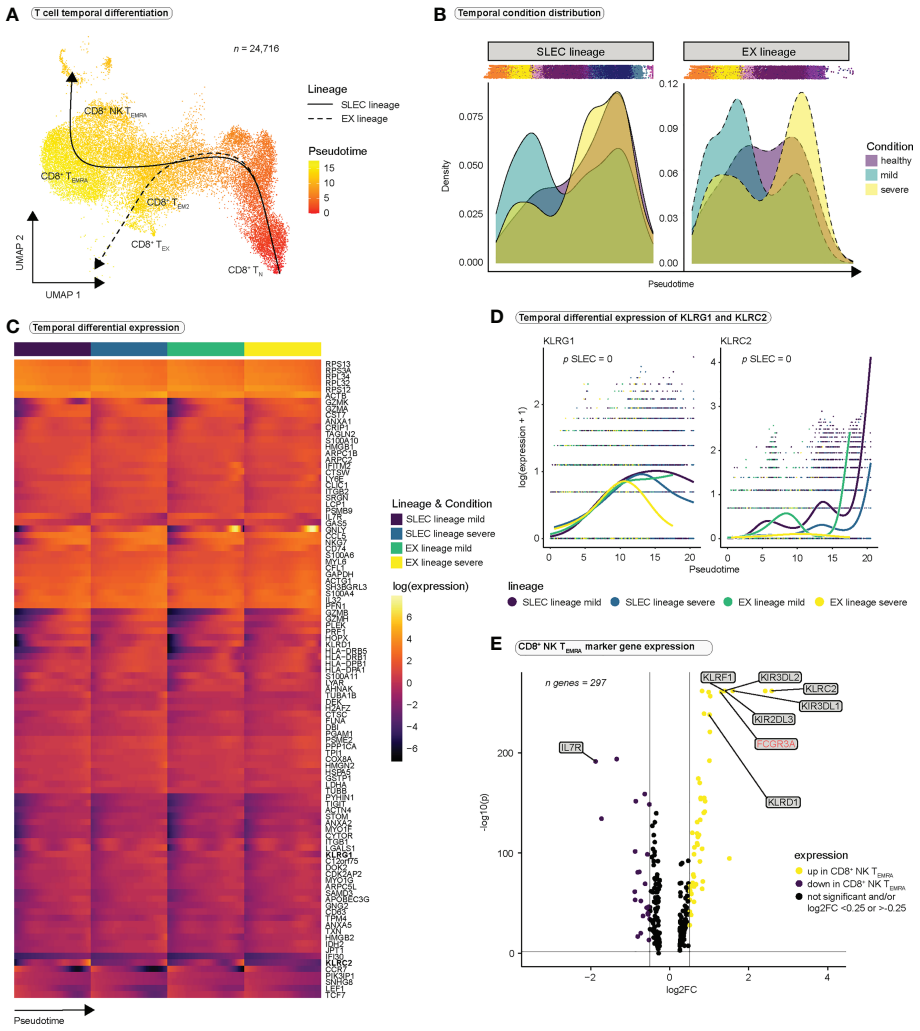


FIGURE 3
$CD8^+$ T cells differentiate towards an NK-like phenotype during SARS-CoV-2 infection. **(A)** Pseudotimes and estimated trajectories projected onto the integrated UMAP of cell types likely originating in naïve $CD8^+$ T cells (n = 24,716). For trajectory inference with Slingshot, naïve $CD8^+$ T cells were manually chosen as the origin of differentiation. **(B)** Temporal distribution of cell densities for all three conditions across pseudotime. Shifts in distribution between the mild and the severe condition for the short-lived effector cells (SLEC) and exhaustion (EX) lineage were tested with the Kolmogorov-Smirnov method (EX: D = 0.40237, p < 2.2e-16, SLEC: D = 0.31004, p < 2.2e-16). **(C)** Heatmap depicts differentially expressed genes between the progenitor and differentiated cell populations across pseudotime (start vs. end testing). **(D)** Smoothed expression of *KLRG1* and *KLRC2* across pseudotime with the y-axis on natural logarithmic scale. p-values report the result of differential expression analysis between progenitor and differentiated cell states across pseudotime (start vs. end testing). An extended panel of genes and their UMAP projections are reported in Figure S4. **(E)** Volcano plot of genes differentially expressed in $CD8^+$ NK-like T_{EMRA} cells.

population of terminally differentiated $CD16^+$ $CD8^+$ effector T cells, which are observed in other chronic viral infections and appear to differ between the disease conditions.

T cell receptor diversity in mild and severe COVID-19

Next, we asked whether there are differences in clonal expansion of $CD8^+$ T cells between the COVID-19 disease conditions. Superimposing TCR clonality on our UMAP indicated an increase in clonal expansion along the differentiation trajectories (Figure 4A), consistent with clonal expansion and differentiation after antigen encounter. As expected, effector cell populations ($CD8^+$ T_{EM1}, $CD8^+$ T_{EM2}, $CD8^+$ T_{cyc}, $CD8^+$ T_{EMRA}, $CD8^+$ NK T_{EMRA}) displayed highest relative abundance of hyperexpanded clones and hyperexpansion appeared to be more pronounced in severe COVID-19 (Figures 4B, S5A). Only $CD8^+$ NK T_{EMRA} cells appeared to be more expanded in mild than in severe COVID-

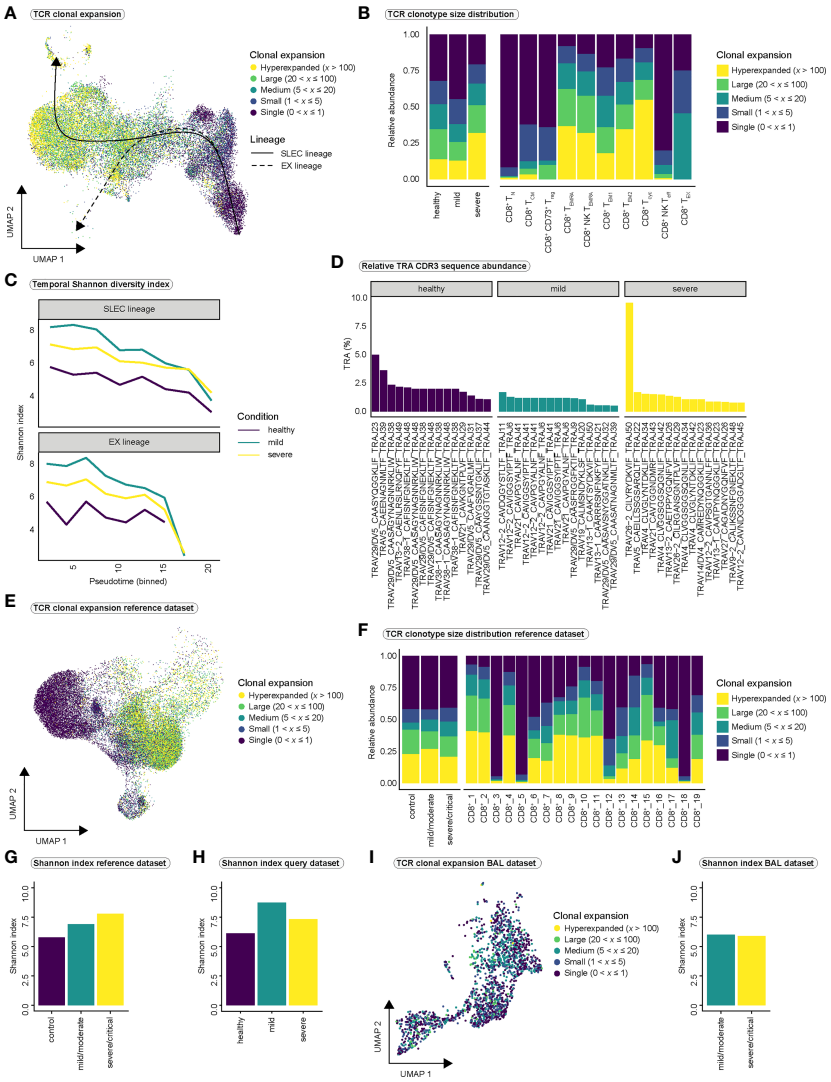


FIGURE 4
Clonal expansion and TCR diversity in COVID-19. **(A)** T cell receptor clonal expansion projected onto the integrated UMAP of cell types. **(B)** Distribution of clonal expansion within the conditions (left) and within the CD8$^+$ T cell populations (right), displayed as relative abundance of clonotype expansion groupings (Figure S5A is referred to for abundance per cell type within each condition). **(C)** Shannon diversity index as a measure of clonal diversity across pseudotime for the three conditions among SLEC and EX lineages. Shannon index was calculated on the whole TCR sequences, including TRA and TRB chains. **(D)** Relative proportion of CDR3 sequences of the 15 most abundant clones to the total number of CDR3 sequences per condition for the TRA chain (Figure S5C is referred to for the relative proportion of CDR3 sequences for the TRB chain). **(E)** TCR clonal expansion projected onto the UMAP of the PBMC-derived CD8$^+$ reference dataset. **(F)** Distribution of clonal expansion within the conditions (left) and within the CD8$^+$ T cell populations (right), displayed as relative abundance of clonotype expansion groupings for the PBMC-derived reference dataset. (Figure S5D is referred to for abundance per cell type within each condition of the reference dataset). **(G)** Shannon diversity index per condition for the PBMC-derived reference dataset and **(H)** for our query dataset. **(I)** TCR clonal expansion projected onto the UMAP of the BAL-derived CD8$^+$ reference dataset. **(J)** Shannon diversity index per condition for the BAL-derived reference dataset. TCR, T cell receptor; SLEC, short-lived effector cell; EX, exhaustion; TRA, T cell receptor alpha chain; TRB, T cell receptor beta chain; CDR3, Complementarity determining region 3; BAL, bronchoalveolar lavage.

19 (Figure S5A). Because strong expansion of individual clones can affect TCR diversity, we calculated the Shannon diversity index as a measure of TCR repertoire diversity over pseudotime using the whole TCR sequence and observed a decrease in diversity for all three conditions (Figure 4C). However, at most time points, the TCR repertoire appeared to be more diverse in mild SARS-CoV2 infection than in severe infection in both lineages (Figure 4C). Analysis of TCR overlap for both the T cell receptor alpha (TRA) and T cell receptor beta (TRB) chains revealed no significant differences in overlap between the two disease states and the diseased and healthy states (Figure S5B). Next, we calculated the relative contribution of the CDR3

sequences of the top 15 clonotypes to the overall CDR3 pool in the respective conditions for the TRA chain (Figure 4D) and the TRB chain (Figure S5C). Even though we observed one clone that was highly hyperexpanded and occupied a larger portion of the TCR space than all other clones in severe COVID-19, we did not observe major differences between mild and severe disease (Figures 5D, S5C). The Shannon diversity index and analysis of CDR3 abundance both indicated lowest TCR diversity in healthy controls.

We validated our findings in the large PBMC-derived $CD8^+$ T cell reference dataset (Figures 4E–H) but observed only minor differences in the distribution of clonotype sizes between conditions (Figures 4F, S5D). As in our dataset, control $CD8^+$ T cells displayed the lowest TCR diversity as measured by Shannon index in the reference dataset (Figure 4G–H). However, in contrast to our data (Figures 4C, H), mildly infected individuals did not show the highest TCR diversity (Figures 4G–H). In summary, we observe highly expanded $CD8^+$ effector T cell populations in SARS-CoV-2 infection. However, our results do not suggest major differences in T cell expansion or T cell receptor diversity between mild and severe COVID-19. TCR diversity seems to increase in response to SARS-CoV-2 infection as indicated by the higher Shannon index in mild and severe COVID-19 compared to healthy controls. It is conceivable that more T cells are released into the blood during the course of infection to diversify the TCR repertoire and to thus induce an immune response against a maximum number of viral antigens. This may explain the observed differences in Shannon index between healthy controls and disease conditions.

Finally, we investigated clonal expansion in the BAL-derived $CD8^+$ reference dataset (Figures 4I, J, S5E). This analysis confirmed our previous observation that no major differences in overall TCR diversity exist between mild and severe SARS-CoV-2 infection (Figure 4J). However, we observed a difference in clonal expansion between mild and severe infection in a cell type we termed BAL_$CD8^+$_7. While this cell type exhibited the lowest expansion in severe COVID-19, it showed strong clonal expansion in mild COVID-19 (Figure S5E). Interestingly, BAL_$CD8^+$_7 cells were mainly characterized by the expression of *FCGR3A* and *KLRF1* (Figure S5F), suggesting that this population resembles our $CD8^+$ NK-like T_{EMRA} cells. Since we also observed stronger expansion of this cell type in mild than in severe SARS-CoV-2 infection in our dataset (Figure S5A), the findings of the BAL dataset confirmed our previous findings.

Subtypes of NK cell-like $CD8^+$ T cells in SARS-CoV-2 infection

Trajectory analysis suggested a $CD16^+$ $CD8^+$ T cell population (previously termed $CD8^+$ NK T_{EMRA} cells) as a final state of $CD8^+$ terminal effector differentiation that seemed to differ in phenotypic characteristics between mild and severe COVID-19. Recently, Georg et al. discovered highly activated and highly cytotoxic $CD16^+$ T cells among the $CD4^+$ and $CD8^+$ T cell compartments which were more abundant in severe COVID-19 as compared to mild disease or healthy controls and had the ability to elicit antibody-dependent cellular cytotoxicity (ADCC) (56). Because of the potential relevance of these $CD16^+$ $CD8^+$ T cells for both, effective antiviral response as well as immunopathology, we focused our analysis on $CD8^+$ NK T_{EMRA} cells.

To investigate cellular heterogeneity among $CD16^+$ $CD8^+$ T cells, we subclustered our $CD8^+$ NK T_{EMRA} population, resolving six subclusters (Figure 5A), which we termed $CD16^+$ $CD8^+$ T_{EMRA} cells-1 to 6. All subpopulations were present in every condition (Figure 5B) and in most patients (Figure S6A). However, the $CD16^+$ $CD8^+$ T_{EMRA}-1 cluster accounted for the largest subpopulation and appeared to be more abundant in mild disease and healthy controls, whereas the $CD16^+$ $CD8^+$ T_{EMRA}-6 cluster was more abundant in severe disease (Figure 5B). Analysis of clonal expansion revealed stronger clonal expansion in $CD16^+$ $CD8^+$ T_{EMRA} cells in mild disease, while the lowest proportion of hyperexpanded clones was observed in subcluster 6 cells (Figure S6B). To quantify overlap in TCR repertoires between the $CD16^+$ $CD8^+$ T_{EMRA} subsets, we calculated the Morisita index (Figure S6C). While there appeared to be large overlap in TCR repertoire between subsets 1-5, $CD16^+$ $CD8^+$ T_{EMRA}-6 cells displayed lowest levels of overlap with other subclusters (Figure S6C). The strong similarity in TCR repertoires of subsets 1-5 may indicate that these subpopulations are derived from each other in a continuous differentiation process, whereas subset 6 cells may arise as a result of an alternative differentiation process. Differential gene expression analysis between the 6 subclusters (Table S6) revealed high expression of *BTG1* in $CD16^+$ $CD8^+$ T_{EMRA}-1 cells (Figure 5C), a gene that has been shown to be involved in the maintenance of a quiescent state in T cells (57). In contrast, $CD16^+$ $CD8^+$ T_{EMRA}-6 cells differentially expressed MHC class II genes *HLA-DRA* and *HLA-DQB1* (Figure 5C), which are known to be upregulated by activated T cells (58, 59), indicating a high activation state of subset 6 cells, similar to the populations described by Georg et al. (56). We further investigated expression of specific genes related to NK cell function and observed strong expression of *KLRF1* and *FCGR3A* in $CD16^+$ $CD8^+$ T_{EMRA}-2 to 5 cells (Figure S6D), indicating that these cells strongly resembled the population described by Naluyima et al. in HIV infection (54). Despite their effector phenotype, $CD16^+$ $CD8^+$ T_{EMRA}-1 cells exhibited expression of *IL7R* (Figure S6D), which may indicate a more naïve phenotype, compared to the other subpopulations, or the potential to develop into memory T cells (48, 60). Surface expression of IL7R (CD127) on subcluster 1 cells and surface expression of HLA-DR on subcluster 6 cells were validated using our CITE-seq data (Figure 5D). Interestingly, we further observed expression of CD161, another NK cell receptor on subcluster 2-5 cells (Figure S6E).

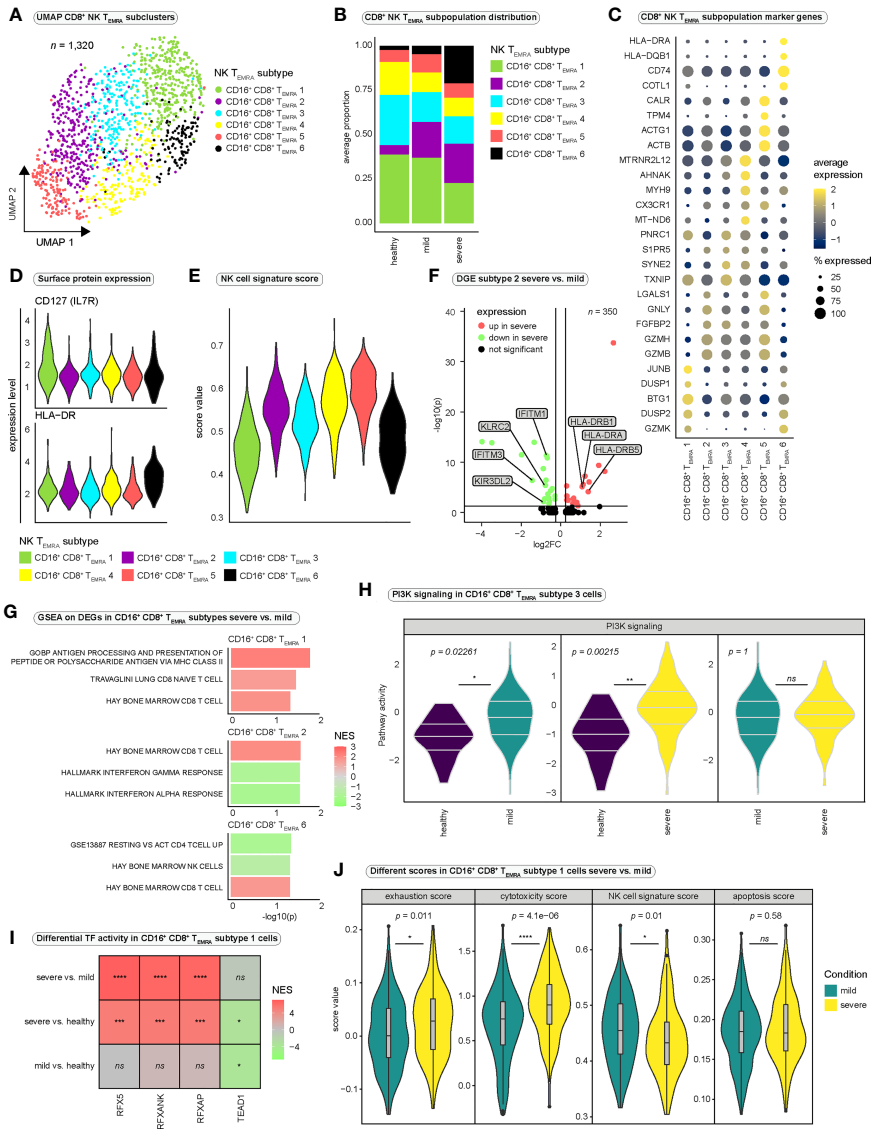


FIGURE 5
Heterogeneity among CD8$^+$ NK-like terminally differentiated effector memory T cells re-expressing CD45RA. **(A)** Integrated UMAP projection of subclustered CD8$^+$ NK-like T_{EMRA} cells (CD16$^+$ CD8$^+$ T_{EMRA} cells) (*n* = 1,320). **(B)** Average proportion of CD16$^+$ CD8$^+$ T_{EMRA} subsets for the three conditions. Cell type proportions per patient are reported in Figure S6A. **(C)** Average expression of marker genes differentially expressed in the six CD16$^+$ CD8$^+$ T_{EMRA} subsets. **(D)** Surface expression (CITE-seq) of IL7R and HLA-DR per CD16$^+$ CD8$^+$ T_{EMRA} subtype. **(E)** NK cell signature scores of the six CD16$^+$ CD8$^+$ T_{EMRA} subsets. **(F)** Differentially expressed genes in CD16$^+$ CD8$^+$ T_{EMRA}-2 cells between the severe and the mild disease condition. **(G)** Selected significantly enriched gene sets for genes differentially expressed in the indicated CD16$^+$ CD8$^+$ T_{EMRA} subtypes between mild and severe disease groups. Positive normalized enrichment scores (NES) indicate enrichment in the severe disease condition. **(H)** PI3K pathway activity in CD16$^+$ CD8$^+$ T_{EMRA}-3 cells estimated with PROGENy. Significance was tested using Wilcoxon rank sum test. All PROGENy pathways are reported in Figure S6G. **(I)** Differential transcription factor activity (DoRothEA) estimated with *msviper* in CD16$^+$ CD8$^+$ T_{EMRA}-1 cells between the severe and the mild condition. Positive NES values indicate increased activity in severe SARS-CoV-2 infection. **(J)** Different functional scores applied to CD16$^+$ CD8$^+$ T_{EMRA}-1 cells and compared between severe and mild COVID-19 (Wilcoxon rank sum test). DGE, differential gene expression; log2FC, log2 fold change; GSEA, gene set enrichment analysis; NES, normalized enrichment score; PI3K, Phosphoinositide 3-kinase; TF, transcription factor.

To quantify and compare functional characteristics of the different subpopulations, we calculated functional scores for every cell and compared it between the subsets (Figures 5E, S6F). Interestingly, CD16$^+$ CD8$^+$ T_{EMRA}-1 and -6 cells displayed the lowest NK cell signature score, suggesting differences in NK-like differentiation between the subpopulations (Figure 5E). Regarding the expression of genes involved in T cell quiescence and homeostasis, it is conceivable that subcluster 1

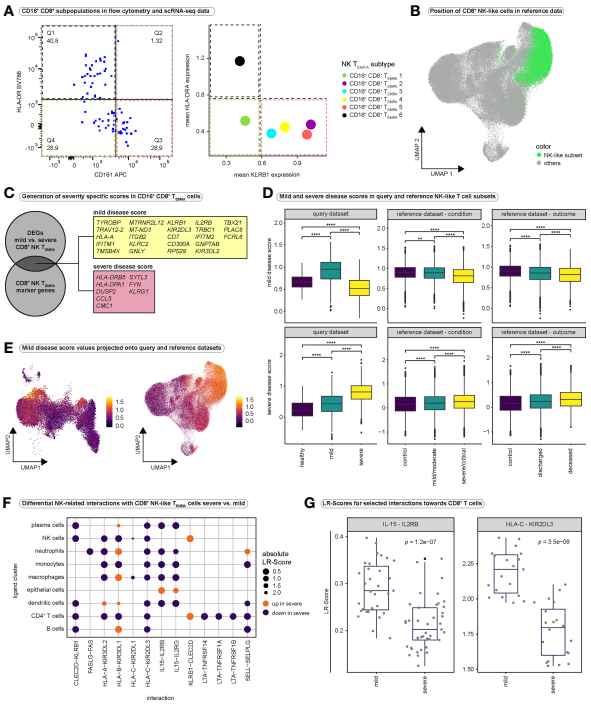


FIGURE 6
Validation of CD16$^+$ CD8$^+$ T_{EMRA} cells and cell-cell interaction analysis. **(A)** Validation of the existence of CD16$^+$ CD8$^+$ T_{EMRA} subsets, identified in scRNA-seq data. The expression of HLA-DR (highly expressed in CD16$^+$ CD8$^+$ T_{EMRA}-6 cells) and CD161 (highly expressed by CD16$^+$ CD8$^+$ subsets 2 to 5) was investigated in single, live CD16$^+$ CD8$^+$ T cells in a flow cytometry dataset (left panel). As a comparison, the mean expression of the corresponding genes (*HLA-DRA* as an example of an HLA-DR gene, as well as *KLRB1* encoding CD161) in the CD16$^+$ CD8$^+$ subpopulations is shown (right panel). **(B)** UMAP embedding of the CD8$^+$ T cell reference dataset (n = 114,209). Cells that mapped together with the CD8$^+$ NK-like T_{EMRA} cells from our query dataset after integration are highlighted in green. **(C)** Schematic illustrating the generation of mild and severe disease scores. Differential gene expression analysis was performed between mild and severe disease groups for all CD16$^+$ CD8$^+$ T_{EMRA} cells. Differentially expressed genes that overlapped with highly significant marker genes of CD16$^+$ CD8$^+$ T_{EMRA} cells (CD8$^+$ NK-like T_{EMRA} cells) were identified. Genes that were differentially upregulated in cells from mild disease (average log2-fold change > 0.25) were combined into the mild disease score, whereas genes that were differentially downregulated in cells from mild disease (average log2-fold change < 0.25) were combined into the severe disease score. **(D)** Comparison of mild (top) and severe (bottom) disease scores in NK-like CD8$^+$ T cell subsets between conditions in our query dataset (left), between conditions in the PBMC-derived reference dataset (middle) and between outcome groups in the PBMC-derived reference dataset (right). Kruskal-Wallis test was used for significance testing. (query mild disease score: Kruskal-Wallis test: $H(2) = 462.6$, $p < 0.0001$; healthy vs. mild: $p < 0.0001$; healthy vs. severe: $p < 0.0001$, mild vs. severe: $p < 0.0001$; query severe disease score: Kruskal-Wallis test: $H(2) = 330.5$, $p < 0.0001$; healthy vs. mild: $p < 0.0001$; healthy vs. severe: $p < 0.0001$, mild vs. severe: $p < 0.0001$; reference mild disease score condition: Kruskal-Wallis test: $H(2) = 778.6$, $p < 0.0001$; control vs. mild/moderate: $p = 0.0046$; control vs. severe/critical: $p < 0.0001$, mild/moderate vs. severe/critical: $p < 0.0001$; reference severe disease score condition: Kruskal-Wallis test: $H(2) = 246.2$, $p < 0.0001$; control vs. mild/moderate: $p < 0.0001$; control vs. severe/critical: $p < 0.0001$, mild/moderate vs. severe/critical: $p < 0.0001$; reference mild disease score outcome: Kruskal-Wallis test: $H(2) = 258.2$, $p < 0.0001$; control vs. deceased: $p = < 0.0001$; control vs. discharged: $p < 0.0001$, deceased vs. discharged: $p < 0.0001$; reference severe disease score outcome: Kruskal-Wallis test: $H(2) = 203.9$, $p < 0.0001$; control vs. deceased: $p = < 0.0001$; control vs. discharged: $p < 0.0001$, deceased vs. discharged: $p < 0.0001$) **(E)** Mild disease score values projected onto the UMAP embeddings of our query CD8$^+$ T cell dataset (left) and the reference CD8$^+$ T cell dataset (right). Projections for severe disease score values are depicted in Figure S7G. **(F)** Differential ligand-receptor interactions between severe and mild COVID-19. To assess interactions between CD8$^+$ T cells and non-T cells our dataset was integrated with the whole reference dataset and interactions were predicted using *LIANA*. Differential interactions were then calculated using *CrossTalkeR* for selected interactions, relevant in NK cell development and function. A group of ligand clusters was selected and NK-like CD8$^+$ T_{EMRA} cells were regarded as receptor cluster. The size of the dots indicates the absolute value of the differential LR-Score. The color indicates the direction of the change in ligand-receptor interactions; orange indicates increased interactions in severe COVID-19, purple indicates decreased interactions in severe COVID-19. **(G)** Boxplots displaying differences in LR-Scores for selected interactions between severe and mild COVID-19. All CD8$^+$ T cell populations were regarded as receptor population and all other populations (except megakaryocytes) were regarded as ligand population for this purpose. DEGs, differentially expressed genes; LR-Score = ligand-receptor score.

cells represent a CD16$^+$ CD8$^+$ progenitor population from which, controlled by the influences of the prevailing milieu, the various other subpopulations emerge, acquiring further NK-like characteristics during differentiation.

We next performed differential gene expression analysis between the conditions for every CD16$^+$ CD8$^+$ T_{EMRA} subcluster (Figure 5F and Table S6). Despite that only a limited number of differentially expressed genes proved significant due to

the small sample size, the differential expression of MHC class II genes in severe SARS-CoV-2 infection in different subpopulations (Figure 5F and Table S6) supported the suggestion of a strong activation state of NK-like CD8$^+$ T cells in severe COVID-19. Differential expression of NK cell receptor genes, such as *KLRC2* and *KIR3DL2* in CD16$^+$ CD8$^+$ T_{EMRA}-2 cells in mild COVID-19 compared with severe COVID-19 further strengthened the hypothesis of profound differences in NK-like differentiation between disease conditions.

Performing GSEA on the differentially expressed genes revealed the enrichment of the gene ontology (GO-) term "GOBP Antigen Processing And Presentation Of Peptide Or Polysaccharide Antigen *Via* MHC Class II" in subcluster 1 in severe disease (Figure 5G and Table S7), which is consistent with the differential expression of MHC class II genes (Table S6). Strikingly, while various CD8$^+$ T cell signature genes were enriched in different CD16$^+$ CD8$^+$ T_{EMRA} subtypes in severe SARS-CoV-2 infection, cells in subcluster 6 were negatively enriched in genes associated with "Hay Bone Marrow NK cells" (Figure 5G and Table S7). Thus, we concluded that compared to CD16$^+$ CD8$^+$ T_{EMRA} cells from patients with mild SARS-CoV-2 infection, cells from severely affected individuals are impaired in their NK-like differentiation and are rather characterized by CD8$^+$ T cell-like traits, than by NK-like characteristics (Figure 5G).

We then inferred pathway activity in CD16$^+$ CD8$^+$ T_{EMRA} cells and observed significantly stronger PI3K signaling in CD16$^+$ CD8$^+$ T_{EMRA}-3 cells in the diseased conditions when compared to healthy controls (Figures 5H, S6G). Several NK cell receptors mediate their signals *via* the PI3K pathway (61, 62) and especially ADCC, a key function of NK cells, which is triggered upon CD16 ligation is mediated *via* the PI3K pathway (63). Thus, increased PI3K activity could indicate increased ligation of Fcγ-receptor-IIIa and a relevance for ADCC in the immune response to COVID-19. Inference of transcription factor activity predicted significantly stronger activity of the Regulatory Factor X (RFX) transcription factor family in severe COVID-19 when compared to mild disease in all 6 NK-like subtypes (Figures 5I, S6H, I; Table S8). Since these transcription factors are involved in the regulation of MHC class II genes (64), higher activity is in accordance with differential expression of MHC class II genes and the enrichment in GO-terms related to antigen processing *via* MHC class II in severe SARS-CoV-2 infection.

To further dissect functional differences between mild and severe SARS-CoV-2 infection, we focused on CD16$^+$ CD8$^+$ T_{EMRA}-1 cells, which we suspected to be the earliest of the six subpopulations in terms of NK-like differentiation. We assigned different functional scores to all CD16$^+$ CD8$^+$ T_{EMRA}-1 cells and compared them between mild and severe disease. While there were no significant differences in apoptosis (apoptosis score), CD16$^+$ CD8$^+$ T_{EMRA}-1 cells were significantly more exhausted and cytotoxic in severe COVID-19 (Figure 5J). Furthermore, a significantly higher NK cell signature score in mild COVID-19 (Figure 5J) further supported the hypothesis of impaired NK-like differentiation in severe SARS-CoV-2 infection, which appeared to be present already at the early stage of CD16$^+$ CD8$^+$ T_{EMRA}-1 cells.

In summary we observed several subsets of CD16$^+$ CD8$^+$ T_{EMRA} cells in SARS-CoV-2 infection, which rather represent a continuum in NK-like differentiation than distinct cellular subpopulations. Four subsets strongly expressed *KLRF1* and *FCGR3A*, displayed surface expression of CD161 and resembled a population of CD16$^+$ CD8$^+$ T cells that has previously been described in other viral infections (54, 55). Another subset with the lowest amount of hyperexpanded clones, the lowest overlap in TCR repertoire with other subsets, and surface expression of HLA-DR, indicating high activation status, was more abundant in severe COVID-19. A larger subset of CD16$^+$ CD8$^+$ T cells that displayed surface expression of IL7R and a lower NK cell signature than the previously mentioned subsets was present in all three conditions. However, cells in this subset differed strongly between mild and severe disease. Investigation of NK cell characteristics revealed profound differences between mild and severe COVID-19 and suggested impaired NK-like differentiation in severe COVID-19. It is conceivable that CD16$^+$ CD8$^+$ T_{EMRA}-1 cells represent the initial population from which, depending on the cytokine milieu and the stimulation of specific surface receptors, the different CD16$^+$ subpopulations develop.

CD16$^+$ CD8$^+$ NK-like derived gene sets are related to severity and outcome of SARS-CoV-2 infection

Since our CD16$^+$ CD8$^+$ T cell subset only consisted of 1,320 cells, we aimed at verifying the existence of an NK-like CD8$^+$ T cell population by flow cytometry as well as in the CD8$^+$ reference dataset (34).

To this end, we again used the public flow cytometry dataset (44) (Figure S7A). CD16$^+$ CD8$^+$ T_{EMRA} subsets were combined into three groups, based on the expression of HLA-DR and CD161. CD16$^+$ CD8$^+$ T_{EMRA}-1 cells only displayed low expression of *HLA-DRA* and *KLRB1* (encoding CD161) in the scRNA-seq data (CD161$^-$ HLA-DR$^-$), whereas subsets 2-5 expressed high levels of *KLRB1* (CD161$^+$ HLA-DR$^-$), and CD16$^+$ CD8$^+$ T_{EMRA}-6 cells displayed high expression of *HLA-DRA* (CD161$^-$ HLA-DR$^+$) (Figure 6A). Flow cytometry identified all three subsets of CD16$^+$ CD8$^+$ T cells (Figure 6A). Even though CD161$^-$ HLA-DR$^+$ (CD16$^+$ CD8$^+$ T_{EMRA}-6 cells) were least frequent in both datasets, flow cytometry did not show higher frequencies of this population in severely and critically ill patients (Figure S7B). Additionally, while in flow cytometry data CD161$^-$ HLA-DR$^-$ cells (CD16$^+$ CD8$^+$ T_{EMRA}-1 cells) accounted for the majority of CD16$^+$ CD8$^+$ T cells, in scRNA-seq data

subsets 2-5 ($CD161^+$ $HLA\text{-}DR^-$) made up the largest proportion of $CD16^+$ $CD8^+$ T cells (Figure S7B).

Next, we aimed at identifying $CD16^+$ $CD8^+$ T cells in the large PBMC-derived $CD8^+$ reference dataset. Most of our $CD8^+$ NK-like T_{EMRA} cells mapped onto one distinct subcluster (cluster $CD8^+$_T_1) in the integrated dataset (Figure 2G). Projecting all cells from this subcluster to the UMAP of the $CD8^+$ T cell reference dataset revealed that the NK-like $CD8^+$ T cell population represented a distinct region in the UMAP space of the reference dataset (Figure 6B). We verified expression of *FCGR3A* in these reference NK-like $CD8^+$ T cells and observed strong expression of *FCGR3A* (Figure S7C).

Next, we investigated whether genes that characterize $CD16^+$ $CD8^+$ T_{EMRA} cells have a relevance for disease severity. We therefore performed differential gene expression analysis between $CD16^+$ $CD8^+$ T_{EMRA} cells from mild and severe COVID-19 (Table S9). Among the differentially expressed genes, we identified several genes that overlapped with highly significant marker genes of our $CD8^+$ NK-like T_{EMRA} population (Table S3). We combined marker genes that were differentially upregulated in mild COVID-19 into a 'mild disease score' and marker genes differentially upregulated in severe disease into a 'severe disease score'(Figure 6C). Indeed, patients with mild COVID-19 displayed significantly higher "mild disease score" values, while severely affected patients displayed highest "severe disease score" values in their $CD8^+$ NK-like T cells (Figure 6D). To independently validate our scores, we subsetted all cells from the reference dataset that mapped together with our $CD8^+$ NK-like T_{EMRA} cells in the integrated dataset (Figures S7D–F) and calculated score values for these reference cells. Also in the reference data, control subjects and patients with mild/moderate SARS-CoV2 infection displayed significantly higher "mild disease score" values and patients with severe infection displayed highest "severe disease score" values (Figure 6D). Strikingly, patients that succumbed to COVID-19 displayed lowest mild disease score, and highest severe disease score values as compared to patients who survived and healthy controls (Figure 6D). However, it is important to note, that due to the nature of single-cell experiments and the comparison of thousands of cells, even minor changes can yield significant p-values.

Mapping these disease scores back to our whole dataset as well as the whole $CD8^+$ reference dataset revealed high specificity of the mild disease score to $CD8^+$ NK-like cells, while the severe disease score did not show specificity to a certain population (Figures 6E, S7G–I). In summary, our molecular signature that was specific to $CD16^+$ $CD8^+$ T cells was significantly elevated in $CD16^+$ $CD8^+$ T cells from individuals with mild COVID-19, while the molecular signature that was elevated in patients with severe SARS-CoV-2 infection did not show the same specificity for $CD16^+$ $CD8^+$ T cells. Thus, we conclude that a proper and specific NK-like differentiation of $CD8^+$ effector T cells might be protective against severe COVID-19, while a dysfunctional NK-like differentiation with nonspecific changes such as hyperactivation in NK-like $CD8^+$ T cells might be a mechanism involved in the pathogenesis of severe COVID-19.

Differential cell-cell interactions could drive differences in NK-like $CD8^+$ T cell differentiation

To investigate factors that could drive NK-like differentiation of $CD8^+$ T cells, we integrated our dataset with selected samples (Table S10) from the same publicly available single-cell dataset as described above (34) and performed cell-cell interaction analysis. We first focused our analysis on NK cell-related interactions between non-$CD8^+$ populations and NK-like T_{EMRA} cells (Figures 6F, S8A, B) and investigated differences in these interactions between mild and severe SARS-CoV-2 infection (Figure 6F). Differential interaction analysis (Table S11) revealed differences in various interactions that have been related to NK cell development (65). Particularly, interactions between ligands on non-$CD8^+$ populations and KIRs on NK-like T_{EMRA} cells seemed to be more abundant in mild COVID-19 (Figures 6F, S8A, C). Moreover, we observed increased *IL15* interactions in mild disease (Figure 6F). IL15 has been shown to be a highly relevant cytokine in the development of NK cells (66–68). Next, we compared predicted ligand-receptor (LR) scores for selected interactions, this time considering all $CD8^+$ T cell populations as receptor populations (Figure 6G, S8C). Interestingly, LR-Scores for *IL15-IL2RB* interactions were significantly higher in mild COVID-19 compared to severe COVID-19 (Figure 6G). Moreover, LR-Scores for various interactions between MHC-I molecules and NK cell receptors were significantly higher in mild SARS-CoV-2 infection (Figures 6G, S8C). KIR2DL1, KIR2DL3, KIR3DL1 and KIR3DL2 (Figures 6G, S8C) are inhibitory NK cell receptors and enhanced interactions *via* these receptors on $CD8^+$ T cells could indicate a more balanced functional regulation of $CD8^+$ T cells in mild COVID-19. In contrast, we observed significantly increased LR-Scores for various CC chemokine-interactions in severe COVID-19 compared to mild COVID-19 (Figure S8C). In summary, IL15 could be involved in the acquisition of an NK-like phenotype during $CD8^+$ effector differentiation in SARS-CoV-2 infection. Differences in NK cell-related interactions as well as differences in cytokine milieu could drive the observed differences in $CD16^+$ $CD8^+$ T_{EMRA} cells between mild and severe disease.

Discussion

In this study we explored cellular heterogeneity within the $CD8^+$ T cell compartment in SARS-CoV-2 infection and investigated differences between mild and severe COVID-19.

We observed large heterogeneity among $CD8^+$ T cells, representing different functional subsets. A subpopulation of exhausted $CD8^+$ T cells was observed in severe COVID-19 in our scRNA-seq dataset. However, whereas flow cytometry indicated increased exhaustion in COVID-19, we did not observe significant differences between mild and severe infection. Targeted analysis of exhausted T cells in a large reference dataset ultimately revealed significantly higher exhaustion scores in patients with severe SARS-CoV-2 infection, as well as in patients who died due to COVID-19. These differences were even more pronounced in lung-derived $CD8^+$ T cells, suggesting that the location of $CD8^+$ T cells is relevant for the occurrence of $CD8^+$ T cell exhaustion in COVID-19. Our findings are in line with previous reports about an increase in exhaustion characteristics in $CD8^+$ T cells in severe SARS-CoV-2 infection (50, 69, 70). Trajectory-analysis indicated two differentiation pathways, one corresponding to short-lived effector cell differentiation and one corresponding to T cell exhaustion. Upregulation of NK cell-related genes along the SLEC lineage pointed us to a subset of terminally differentiated $CD8^+$ effector T cells that were characterized by the expression of *FCGR3A* (encoding CD16), *IKZF2* (encoding the transcription factor Helios) and *KLRF1* (encoding the NK cell receptor NKp80). Deeper investigation of this NK-like $CD8^+$ T_{EMRA} population revealed various $CD16^+$ $CD8^+$ T cell subsets.

A first subset ($CD16^+$ $CD8^+$ T_{EMRA}-1) was present in all three conditions and was characterized by moderate expression of *FCGR3A*, surface expression of IL7R as well as a relatively low NK-like phenotype. Besides this first $CD16^+$ $CD8^+$ T_{EMRA} population, four strongly clonally expanded subsets ($CD16^+$ $CD8^+$ T_{EMRA}-2 to -5), characterized by high expression of *FCGR3A*, *KLRF1* and surface expression of CD161 were observed in all conditions, whereas a highly activated and less expanded subset ($CD16^+$ $CD8^+$ T_{EMRA}-6) was enriched in severe cases of COVID-19.

Differential gene expression analysis suggested substantial differences in activation status and expression of NK cell receptors in $CD16^+$ $CD8^+$ T_{EMRA} cells between mild and severe disease and applying functional scores to $CD16^+$ $CD8^+$ T_{EMRA}-1 cells revealed higher cytotoxicity, a higher exhaustion signature as well as decreased NK cell signature scores in severe SARS-CoV-2 infection as compared to mild.

We confirmed the existence of different $CD16^+$ $CD8^+$ T cell subsets by flow cytometry, although the relative proportions of the different subsets in all $CD16^+$ $CD8^+$ T cells differed between flow cytometry and scRNA-seq. These differences could be explained by two crucial points. First, there is a discrepancy between gene expression and protein expression, such that a high abundance of mRNA of a gene does not translate 1:1 into a high expression of the corresponding protein. Because the $CD16^+$ $CD8^+$ subpopulations in the scRNA-seq dataset are defined by their transcriptome, whereas in flow cytometry they are defined at the protein level, this may lead to shifts in the frequency distribution of the subpopulations. Second, however, scRNA-seq is much better suited to characterize subtle differences between cell populations, whereas the discrimination of subtypes in flow cytometry was based on two markers only.

$CD16^+$ $CD8^+$ T cell subsets have been observed in various conditions. In chronic, untreated HIV infection a $CD16^+$ $CD8^+$ population with high expression of NKp80 and Helios transcription factor has been described (54). Previously, Björkström et al. had detected a similar, and clonally expanded subpopulation in chronic hepatitis C virus (HCV) infection (55). Both papers reported the ability of $CD16^+$ $CD8^+$ T cells to mediate ADCC or at least effector functions in response to engagement of CD16 (54, 55). These populations strongly resembled our $CD16^+$ $CD8^+$ T_{EMRA}-2 to -5 populations, suggesting a potential relevance for ADCC in the antiviral response to SARS-CoV-2 infection. Moreover, $CD16^+$ $CD8^+$ T_{EMRA}-2 to -5 cells displayed strong surface expression of CD161. CD161 is an NK cell receptor that has been suggested to mark long-lived antigen-specific T cells within the $CD4^+$ compartment (71). Additionally, $CD161^+$ T cells have been reported to respond to IL-12 and IL-18 in a TCR-independent manner (72). We therefore hypothesize that properly differentiated 'bona fide' $CD16^+$ $CD8^+$ T cells also contribute to antiviral defense by TCR-independent mechanisms through their NK-like differentiation. Of particular interest is the fact that ADCC can also be mediated by non-neutralizing antibodies, which may have particular relevance for the design of future vaccines (73, 74).

On the other hand, a highly activated population of $CD16^+$ $CD8^+$ T_{EMRA} cells has recently been described in severe COVID-19 and the authors suggested a role for these cells in immunopathology of severe infection by ADCC-mediated endothelial damage (56). The existence of pathogenic T cell populations has already been suggested by others in COVID-19 (14) and other diseases (75, 76). Interestingly, the highly activated phenotype and the specificity to the severe disease condition reported by Georg et al. resembled the $CD16^+$ $CD8^+$ T_{EMRA} subset 6 in our dataset. We therefore hypothesize that $CD16^+$ $CD8^+$ T cells are not inherently pathological in nature. We propose a model in which terminally differentiated $CD16^+$ $CD8^+$ T cells develop in the context of SARS-CoV-2 infection as part of effector differentiation, but in which differences in further differentiation of these cells eventually occur depending on the surrounding cytokine milieu, as well as stimulation of specific surface receptors. Adequate differentiation conditions the emergence of the 'bona fide' $IZKF2^+$ $KLRF1^+$ $CD16^+$ $CD8^+$ T cells, which may contribute to the clearance of the virus through ADCC and thus protect against severe courses. Defective NK-like differentiation could lead to the emergence of the highly activated and potentially pathogenic $CD16^+$ $CD8^+$ subtypes. It is conceivable that these dysfunctional subpopulations contribute to disease progression as suggested by Georg et al. (56). This is

supported by the observation that a gene set, differentially expressed in NK-like CD8$^+$ T_{EMRA} cells in mild COVID-19 when compared to severe disease, is highly specific to NK-like CD8$^+$ T_{EMRA} cells, whereas a gene set differentially expressed in NK-like CD8$^+$ T_{EMRA} cells in severe disease does not show high specificity to this population. Thus, high expression of NK-like CD8$^+$ T_{EMRA}-specific genes is related to mild disease while unspecific changes in CD16$^+$ CD8$^+$ T cells, especially high activation state, seems to be related to severe disease.

Indeed, a recent single-cell analysis identified CD16$^+$ CD8$^+$ T cells in smokers and non-smokers (77). When compared to non-smokers, CD16$^+$ CD8$^+$ T cells in smokers displayed elevated *TOX* expression, a transcription factor involved in T cell exhaustion (78), indicating a dysfunctional state of these cells (77). Further, expression of certain cytotoxic effector molecules as well as certain MHC class II genes was elevated in CD16$^+$ CD8$^+$ T cells from smokers (77). These results clearly illustrate that under certain circumstances, CD16$^+$ CD8$^+$ T cells can acquire dysfunctional phenotypes. Interestingly, Georg et al. showed that C3a is able to induce differentiation of CD16$^+$ CD8$^+$ T cells (56). To gain further insights into factors that might drive the differentiation of CD16$^+$ CD8$^+$ T cells, we performed cell-cell interaction analysis. When comparing predicted interactions with CD8$^+$ T cells between mild and severe SARS-CoV-2 infection, we observed stronger interactions with KIR receptors (KIR3DL2, KIR2DL1, KIR2DL3) in CD16$^+$ CD8$^+$ T_{EMRA} cells derived from mildly affected individuals. It is known that inhibitory KIRs counteract activating signals downstream of the TCR (79). Additionally, in transgenic mice, ligation of KIR2DL3 by its cognate MHC class I ligand has been shown to reduce activation-induced cell death, thereby promoting survival of a subset of CD8$^+$ memory cells (80). These findings may partially explain the differences in activation status between CD16$^+$ CD8$^+$ T_{EMRA} cells in mild and severe disease. Furthermore, filtering our cell-cell interaction data for mechanisms involved in NK-cell differentiation revealed increased IL-15 signaling towards CD8$^+$ T cells in mild COVID-19 (Figure 6G). Previous studies have demonstrated the ability of IL-15 to induce an NK-like phenotype in CD8$^+$ T cells (81, 82), suggesting differences in IL-15 signaling between mild and severe SARS-CoV-2 infection as a potential mechanism that drives differences in the generation of different CD8$^+$ NK-like T cell phenotypes.

Nonetheless, our study has some limitations. A main limitation of our study is the small number of healthy controls, which limits the interpretation of comparisons with the healthy control group. To overcome this limitation, we validated our main observations and key points in a large reference dataset. Another limitation is the heterogeneity of diseased patients with respect to the duration of infection at the time point of sampling, a limitation that is also present in the reference dataset and that must be taken into account when interpreting the results. Finally, when interpreting statistical comparisons in single-cell datasets, it must be considered that due to the comparison of thousands of single cells, even smaller changes can cause statistical significance.

In summary, by investigating CD8$^+$ T cells in SARS-CoV-2 infection at high resolution, we observed different subsets of NK-like CD16$^+$ CD8$^+$ T_{EMRA} cells, a population that only few reports have observed before. We deeply characterized these cells and suggest a role for CD16$^+$ CD8$^+$ T cells in the immune response against SARS-CoV-2 by mediating ADCC. By inferring cell-cell interactions, we identify factors that could be involved in the differentiation of CD16$^+$ CD8$^+$ T cells. We suggest that differences in the cytokine milieu in severe as compared to mild SARS-CoV-2 infection result in disturbances of this NK-like differentiation process, potentially leading to the generation of dysfunctional or even pathogenic CD16$^+$ CD8$^+$ T cell subsets that are characterized by high activation status and low NK-like phenotype, whereas properly differentiated NK-like T_{EMRA} cells that acquire NK cell specific characteristics confer protection against the virus. Although we validated our results in a flow cytometry and in a large scRNA-seq dataset, future studies will have to validate our findings in larger cohorts to dissect the factors that drive NK-like differentiation of CD8$^+$ T cells as well as their role in health and disease. However, the ability to elicit ADCC represents another mechanism for combating the virus and could also represent a crucial role for non-neutralizing antibodies in viral defense, which would also affect future vaccine designs.

Data availability statement

A list of CITE-seq antibodies used in this study is provided in Table S1. Code used for data analysis is available at https://github.com/KramannLab/Covid_immunoprofiling. Raw sequencing data are available at the European Nucleotide Archive (ENA) at: https://www.ebi.ac.uk/ena/browser/view/PRJEB57300. Pre-processed data including R objects are available at Zenodo: 10.5281/zenodo.7129229

Ethics statement

The studies involving human participants were reviewed and approved by Ethical Board of the RWTH Aachen University Hospital. The patients/participants provided their written informed consent to participate in this study.

Author contributions

Conceptualization: FS, CKup, SH, RK. Data Curation: FS, MH, HK, SH. Formal Analysis: FS, MH, HK, TB, FT, EF, JN, TA,

SH. Funding Acquisition: EF, IC, RK. Investigation: FS, MH, MB, NT, PZ, VB, FW. Methodology: FS, MH, HK, CKup, SH, RK. Project Administration: FS, SH, RK. Resources: IK, JK, DF, TK, JE, PB, CKur, GM, NM, MD, RS, JS-R, IC, SH, RK. Software: FS, MH, HK, TB, FT, EF, JN, JS-R, IC, SH. Supervision: IC, SH, RK. Validation: FS, MH. Visualization: FS, MH, HK, TB, JN, SH. Writing – Original Draft Preparation: FS, MH. Writing – Review & Editing: HK, TB, FT, EF, JN, MB, NT, Ckup, IK, JK, DF, TA, PZ, TK, JE, VB, FW, PB, Ckur, GM, NM, MD, RS, JS-R, IC, SH, RK. All authors contributed to the article and approved the submitted version.

Funding

German Research Foundation grant DFG: KR 4073/11-1 (RK). German Research Foundation grant SFBTRR219, Project ID 322900939 (RK). German Research Foundation grant CRU344, P1 (RK). European Research Council grant ERC-StG 677448 (RK). State of North Rhine-Westphalia grant Return to NRW (RK). BMBF grant NUM-COVID19, Organo-Strat 01KX2021 (RK). CRU5011 (RK). ERC-CoG 101043403 (RK). German Research Foundation grant CRU 344, Z (IC). BMBF grant eMed Consortia Fibromap (RK, RS, IC). Bioinformatics DATa ENvironment (BioDATEN) project (EF).

Acknowledgments

We thank the COVID Aachen Study (COVAS) for contributing patient specimens to the study and the Genomics Facility of the Interdisciplinary Center for Clinical Research (IZKF) Aachen for sequencing experiments. Special thanks go to Jasmin Hübner and Stephan Klinkenberg for their extraordinary help in sequencing the samples.

Conflict of interest

Author JS-R declares funding from GSK and Sanofi and consultant fees from Travere Therapeutics, Owkin and Astex Pharmaceuticals unrelated to this study. Author SH has funding from Novo Nordisk. Author RK has grants from Travere Therapeutics, Galapagos, Chugai, and Novo Nordisk and is a consultant or received honoraria from Bayer, Pfizer, Novo Nordisk, Lilly-Pharma and Gruenenthal.

The remaining authors declare that the research was conducted in the absence of any commercial or financial relationships that could be construed as a potential conflict of interest.

Publisher's note

All claims expressed in this article are solely those of the authors and do not necessarily represent those of their affiliated organizations, or those of the publisher, the editors and the reviewers. Any product that may be evaluated in this article, or claim that may be made by its manufacturer, is not guaranteed or endorsed by the publisher.

Supplementary material

The Supplementary Material for this article can be found online at: https://www.frontiersin.org/articles/10.3389/fimmu.2022.1066176/full#supplementary-material

SUPPLEMENTARY TABLE 3
Marker genes differentially expressed in each $CD8^+$ T cell subtype.

SUPPLEMENTARY TABLE 4
Results of differential gene expression analysis and gene set enrichment analysis on genes differentially expressed in $CD8^+$ T cell populations between mild and severe COVID-19

SUPPLEMENTARY TABLE 5
tradeSeq results.

SUPPLEMENTARY TABLE 6
Marker genes differentially expressed in $CD16^+$ $CD8^+$ T cell subtypes and differential gene expression analysis results in $CD16^+$ $CD8^+$ T cell subtypes between the conditions.

SUPPLEMENTARY TABLE 7
Results of gene set enrichment analysis on genes differentially expressed in $CD16^+$ $CD8^+$ T cell subtypes between the conditions.

SUPPLEMENTARY TABLE 8
Results of differential transcription factor activity in $CD16^+$ $CD8^+$ T cell subtypes between the conditions.

SUPPLEMENTARY TABLE 9
Differential gene expression analysis results between mild and severe SARS-CoV-2 infection in $CD8^+$ NK-like T_{EMRA} cells.

SUPPLEMENTARY TABLE 11
Cell-cell interactions analysis results.

References

1. WHO. *Coronavirus (COVID-19) dashboard*. Available at: https://covid19.who.int/ (Accessed August 23, 2022).

2. Sanyaolu A, Okorie C, Marinkovic A, Prakash S, Williams M, Haider N, et al. Current advancements and future prospects of COVID-19 vaccines and therapeutics: a narrative review. *Ther Adv Vaccines Immunother* (2022) 10:25151355221097559. doi: 10.1177/25151355221097559

3. Baden LR, El Sahly HM, Essink B, Kotloff K, Frey S, Novak R, et al. Efficacy and safety of the mRNA-1273 SARS-CoV-2 vaccine. *N Engl J Med* (2021) 384:403–16. doi: 10.1056/NEJMoa2035389

4. Polack FP, Thomas SJ, Kitchin N, Absalon J, Gurtman A, Lockhart S, et al. Safety and efficacy of the BNT162b2 mRNA covid-19 vaccine. *N Engl J Med* (2020) 383:2603–15. doi: 10.1056/NEJMoa2034577

5. Kuhlmann C, Mayer CK, Claassen M, Maponga T, Burgers WA, Keeton R, et al. Breakthrough infections with SARS-CoV-2 omicron despite mRNA vaccine booster dose. *Lancet* (2022) 399:625–6. doi: 10.1016/S0140-6736(22)00090-3

6. Shastri J, Parikh S, Aggarwal V, Agrawal S, Chatterjee N, Shah R, et al. Severe SARS-CoV-2 breakthrough reinfection with delta variant after recovery from breakthrough infection by alpha variant in a fully vaccinated health worker. *Front Med* (2021) 8:737007. doi: 10.3389/fmed.2021.737007

7. Wang SY, Juthani PV, Borges KA, Shallow MK, Gupta A, Price C, et al. Severe breakthrough COVID-19 cases in the SARS-CoV-2 delta (B.1.617.2) variant era. *Lancet Microbe* (2022) 3:e4–5. doi: 10.1016/S2666-5247(21)00306-2

8. Juthani PV, Gupta A, Borges KA, Price CC, Lee AI, Won CH, et al. Hospitalisation among vaccine breakthrough COVID-19 infections. *Lancet Infect Dis* (2021) 21:1485–6. doi: 10.1016/S1473-3099(21)00558-2

9. Al-Aly Z, Bowe B, Xie Y. Long COVID after breakthrough SARS-CoV-2 infection. *Nat Med* (2022) 28:1461–7. doi: 10.1038/s41591-022-01840-0

10. Kingstad-Bakke B, Lee W, Chandrasekar SS, Gasper DJ, Salas-Quinchucua C, Cleven T, et al. Vaccine-induced systemic and mucosal T cell immunity to SARS-CoV-2 viral variants. *Proc Natl Acad Sci USA* (2022) 119:e2118312119. doi: 10.1073/pnas.2118312119

11. You M, Chen L, Zhang D, Zhao P, Chen Z, Qin E-Q, et al. Single-cell epigenomic landscape of peripheral immune cells reveals establishment of trained immunity in individuals convalescing from COVID-19. *Nat Cell Biol* (2021) 23:620–30. doi: 10.1038/s41556-021-00690-1

12. Adamo S, Michler J, Zurbuchen Y, Cervia C, Taeschler P, Raeber ME, et al. Signature of long-lived memory CD8+ T cells in acute SARS-CoV-2 infection. *Nature* (2021) 602:148–55. doi: 10.1038/s41586-021-04280-x

13. Hasan MZ, Islam S, Matsumoto K, Kawai T. Meta-analysis of single-cell RNA-seq data reveals phenotypic switching of immune cells in severe COVID-19 patients. *Comput Biol Med* (2021) 137:104792. doi: 10.1016/j.compbiomed.2021.104792

14. Kuchroo M, Huang J, Wong P, Grenier J-C, Shung D, Tong A, et al. Multiscale PHATE identifies multimodal signatures of COVID-19. *Nat Biotechnol* (2022) 40:681–91. doi: 10.1038/s41587-021-01186-x

15. Kang CK, Han G-C, Kim M, Kim G, Shin HM, Song K-H, et al. Aberrant hyperactivation of cytotoxic T-cell as a potential determinant of COVID-19 severity. *Int J Infect Dis* (2020) 97:313–21. doi: 10.1016/j.ijid.2020.05.106

16. Zheng H-Y, Zhang M, Yang C-X, Zhang N, Wang X-C, Yang X-P, et al. Elevated exhaustion levels and reduced functional diversity of T cells in peripheral blood may predict severe progression in COVID-19 patients. *Cell Mol Immunol* (2020) 17:541–3. doi: 10.1038/s41423-020-0401-3

17. Wilk AJ, Rustagi A, Zhao NQ, Roque J, Martínez-Colón GJ, McKechnie JL, et al. A single-cell atlas of the peripheral immune response in patients with severe COVID-19. *Nat Med* (2020) 26:1070–6. doi: 10.1038/s41591-020-0944-y

18. Wen W, Su W, Tang H, Le W, Zhang X, Zheng Y, et al. Immune cell profiling of COVID-19 patients in the recovery stage by single-cell sequencing. *Cell Discovery* (2020) 6:31. doi: 10.1038/s41421-020-0168-9

19. Liao M, Liu Y, Yuan J, Wen Y, Xu G, Zhao J, et al. Single-cell landscape of bronchoalveolar immune cells in patients with COVID-19. *Nat Med* (2020) 26:842–4. doi: 10.1038/s41591-020-0901-9

20. Cao Y, Su B, Guo X, Sun W, Deng Y, Bao L, et al. Potent neutralizing antibodies against SARS-CoV-2 identified by high-throughput single-cell sequencing of convalescent patients' b cells. *Cell* (2020) 182:73–84.e16. doi: 10.1016/j.cell.2020.05.025

21. Yao C, Bora SA, Parimon T, Zaman T, Friedman OA, Palatinus JA, et al. Cell-Type-Specific immune dysregulation in severely ill COVID-19 patients. *Cell Rep* (2021) 34:108590. doi: 10.1016/j.celrep.2020.108590

22. Li S, Wu B, Ling Y, Guo M, Qin B , Ren X, et al. Epigenetic landscapes of single-cell chromatin accessibility and transcriptomic immune profiles of T cells in COVID-19 patients. *Front Immunol* (2021) 12:625881. doi: 10.3389/fimmu.2021.625881

23. Wauters E, Van Mol P, Garg AD, Jansen S, Van Herck Y, Vanderbeke L, et al. Discriminating mild from critical COVID-19 by innate and adaptive immune single-cell profiling of bronchoalveolar lavages. *Cell Res* (2021) 31:272–90. doi: 10.1038/s41422-020-00455-9

24. Unterman A, Sumida TS, Nouri N, Yan X, Zhao AY, Gasque V, et al. Single-cell multi-omics reveals dyssynchrony of the innate and adaptive immune system in progressive COVID-19. *Nat Commun* (2022) 13:440. doi: 10.1038/s41467-021-27716-4

25. Szabo PA, Levitin HM, Miron M, Snyder ME, Senda T, Yuan J, et al. Single-cell transcriptomics of human T cells reveals tissue and activation signatures in health and disease. *Nat Commun* (2019) 10:4706. doi: 10.1038/s41467-019-12464-3

26. Andreatta M, Corria-Osorio J, Müller S, Cubas R, Coukos G, Carmona SJ. Interpretation of T cell states from single-cell transcriptomics data using reference atlases. *Nat Commun* (2021) 12:2965. doi: 10.1038/s41467-021-23324-4

27. Stoeckius M, Hafemeister C, Stephenson W, Houck-Loomis B, Chattopadhyay PK, Swerdlow H, et al. Simultaneous epitope and transcriptome measurement in single cells. *Nat Methods* (2017) 14:865–8. doi: 10.1038/nmeth.4380

28. Meyer B, Torriani G, Yerly S, Mazza L, Calame A, Arm-Vernez I, et al. Validation of a commercially available SARS-CoV-2 serological immunoassay. *Clin Microbiol Infect* (2020) 26:1386. doi: 10.1016/j.cmi.2020.06.024

29. Hao Y, Hao S, Andersen-Nissen E, Mauck WM, Zheng S, Butler A, et al. Integrated analysis of multimodal single-cell data. *Cold Spring Harbor Lab* (2020). 184(13):3573–87.e29. doi: 10.1101/2020.10.12.335331

30. Korsunsky I, Millard N, Fan J, Slowikowski K, Zhang F, Wei K, et al. Fast, sensitive and accurate integration of single-cell data with harmony. *Nat Methods* (2019) 16:1289–96. doi: 10.1038/s41592-019-0619-0

31. Korotkevich G, Sukhov V, Budin N, Shpak B, Artyomov MN, Sergushichev A. Fast gene set enrichment analysis. *bioRxiv* (2019). doi: 10.1101/060012

32. Baryawno N, Kfoury Y, Severe N, Mei S, Gustafsson K, Hirz T, et al. Human prostate cancer bone metastases have an actionable immunosuppressive microenvironment. *bioRxiv* (2020). doi: 10.1101/2020.03.19.998658

33. Hay SB, Ferchen K, ChEtal K, Grimes HL, Salomonis N. The human cell atlas bone marrow single-cell interactive web portal. *Exp Hematol* (2018) 68:51–61. doi: 10.1016/j.exphem.2018.09.004

34. Ren X, Wen W, Fan X, Hou W, Su B, Cai P, et al. COVID-19 immune features revealed by a large-scale single-cell transcriptome atlas. *Cell* (2021) 184:5838. doi: 10.1016/j.cell.2021.10.023

35. Schubert M, Klinger B, Klünemann M, Sieber A, Uhlitz F, Sauer S, et al. Perturbation-response genes reveal signaling footprints in cancer gene expression. *Nat Commun* (2018) 9:20. doi: 10.1038/s41467-017-02391-6

36. Holland CH, Tanevski J, Perales-Patón J, Gleixner J, Kumar MP, Mereu E, et al. Robustness and applicability of transcription factor and pathway analysis tools on single-cell RNA-seq data. *Genome Biol* (2020) 21:36. doi: 10.1186/s13059-020-1949-z

37. Alvarez MJ, Shen Y, Giorgi FM, Lachmann A, Ding BB, Ye BH, et al. Functional characterization of somatic mutations in cancer using network-based inference of protein activity. *Nat Genet* (2016) 48:838–47. doi: 10.1038/ng.3593

38. Garcia-Alonso L, Holland CH, Ibrahim MM, Turei D, Saez-Rodriguez J. Benchmark and integration of resources for the estimation of human transcription factor activities. *Genome Res* (2019) 29:1363–75. doi: 10.1101/gr.240663.118

39. Dimitrov D, Türei D, Garrido-Rodriguez M, Burmedi PL, Nagai JS, Boys C, et al. Comparison of methods and resources for cell-cell communication inference from single-cell RNA-seq data. *Nat Commun* (2022) 13:1–13. doi: 10.1038/s41467-022-30755-0

40. Nagai JS, Leimkühler NB, Schneider RK, Costa IG. CrossTalkeR: Analysis and visualisation of ligand receptor networks. *Cold Spring Harbor Lab* (2021) 37 (22):4263–5. doi: 10.1101/2021.01.20.427390

41. Street K, Risso D, Fletcher RB, Das D, Ngai J, Yosef N, et al. Slingshot: cell lineage and pseudotime inference for single-cell transcriptomics. *BMC Genomics* (2018) 19:477. doi: 10.1186/s12864-018-4772-0

42. Van den Berge K, Roux de Bézieux H, Street K, Saelens W, Cannoodt R, Saeys Y, et al. Trajectory-based differential expression analysis for single-cell sequencing data. *Nat Commun* (2020) 11:1201. doi: 10.1038/s41467-020-14766-3

43. Website. Oksanen J, Simpson G, Blanchet F, Kindt R, Legendre P, Minchin P, et al. *_vegan: Community ecology package_* (2022). Available at: https://CRAN.R-project.org/package=vegan.

44. Consortium Co-19 MBAt (COMBAT), DJ A, Ai Z, Ainsworth M, Allan C, Allcock A. A blood atlas of COVID-19 defines hallmarks of disease severity and specificity. *Cell* (2022) 185(5):916–38.e58. doi: 10.1016/j.cell.2022.01.012

45. Sallusto F, Lenig D, Förster R, Lipp M, Lanzavecchia A. Two subsets of memory T lymphocytes with distinct homing potentials and effector functions. *Nature* (1999) 401:708–12. doi: 10.1038/44385

46. van Aalderen MC, van den Biggelaar M, Remmerswaal EBM, van Alphen FPJ, Meijer AB, Ten Berge IJM, et al. Label-free analysis of CD8 T cell subset proteomes supports a progressive differentiation model of human-Virus-Specific T cells. *Cell Rep* (2017) 19:1068–79. doi: 10.1016/j.celrep.2017.04.014

47. Joshi NS, Cui W, Chandele A, Lee HK, Urso DR, Hagman J, et al. Inflammation directs memory precursor and short-lived effector CD8(+) T cell fates *via* the graded expression of T-bet transcription factor. *Immunity* (2007) 27:281–95. doi: 10.1016/j.immuni.2007.07.010

48. Kaech SM, Tan JT, Wherry EJ, Konieczny BT, Surh CD, Ahmed R. Selective expression of the interleukin 7 receptor identifies effector CD8 T cells that give rise to long-lived memory cells. *Nat Immunol* (2003) 4:1191–8. doi: 10.1038/ni1009

49. Zheng M, Gao Y, Wang G, Song G, Liu S, Sun D, et al. Functional exhaustion of antiviral lymphocytes in COVID-19 patients. *Cell Mol Immunol* (2020) 17:533–5. doi: 10.1038/s41423-020-0402-2

50. Hadjadj J, Yatim N, Barnabei L, Corneau A, Boussier J, Smith N, et al. Impaired type I interferon activity and inflammatory responses in severe COVID-19 patients. *Science* (2020) 369:718–24. doi: 10.1126/science.abc6027

51. Zajac AJ, Blattman JN, Murali-Krishna K, Sourdive DJ, Suresh M, Altman JD, et al. Viral immune evasion due to persistence of activated T cells without effector function. *J Exp Med* (1998) 188:2205–13. doi: 10.1084/jem.188.12.2205

52. Wherry EJ. T Cell exhaustion. *Nat Immunol* (2011) 12:492–9. doi: 10.1038/ni.2035

53. Li H, van der Leun AM, Yofe I, Lubling Y, Gelbard-Solodkin D, van Akkooi ACJ, et al. Dysfunctional CD8 T cells form a proliferative, dynamically regulated compartment within human melanoma. *Cell* (2019) 176:775–789.e18. doi: 10.1016/j.cell.2018.11.043

54. Naluyima P, Lal KG, Costanzo MC, Kijak GH, Gonzalez VD, Blom K, et al. Terminal effector CD8 T cells defined by an IKZF2+IL-7R– transcriptional signature express FcγRIIIA, expand in HIV infection, and mediate potent HIV-specific antibody-dependent cellular cytotoxicity. *J Immunol* (2019) 203:2210–21. doi: 10.4049/jimmunol.1900422

55. Björkström NK, Gonzalez VD, Malmberg K-J, Falconer K, Alaeus A, Nowak G, et al. Elevated numbers of FcγRIIIA+ (CD16+) effector CD8 T cells with NK cell-like function in chronic hepatitis c virus infection. *J Immunol* (2008) 181:4219–28. doi: 10.4049/jimmunol.181.6.4219

56. Georg P, Astaburuaga-García R, Bonaguro L, Brumhard S, Michalick L, Lippert LJ, et al. Complement activation induces excessive T cell cytotoxicity in severe COVID-19. *Cell* (2021) 185(3):493–512.e25. doi: 10.1016/j.cell.2021.12.040

57. Hwang SS, Lim J, Yu Z, Kong P, Sefik E, Xu H, et al. mRNA destabilization by BTG1 and BTG2 maintains T cell quiescence. *Science* (2020) 367:1255–60. doi: 10.1126/science.aax0194

58. Holling TM, Schooten E, van Den Elsen PJ. Function and regulation of MHC class II molecules in T-lymphocytes: Of mice and men. *Hum Immunol* (2004) 65:282–90. doi: 10.1016/j.humimm.2004.01.005

59. Holling TM, van der Stoep N, Quinten E, van den Elsen PJ. Activated human T cells accomplish MHC class II expression through T cell-specific occupation of class II transactivator promoter III. *J Immunol* (2002) 168:763–70. doi: 10.4049/jimmunol.168.2.763

60. Schluns KS, Kieper WC, Jameson SC, Lefrançois L. Interleukin-7 mediates the homeostasis of naïve and memory CD8 T cells. *vivo. Nat Immunol* (2000) 1:426–32. doi: 10.1038/80868

61. Marti F, Xu CW, Selvakumar A, Brent R, Dupont B, King PD. LCK-phosphorylated human killer cell-inhibitory receptors recruit and activate phosphatidylinositol 3-kinase. *Proc Natl Acad Sci USA* (1998) 95:11810–5. doi: 10.1073/pnas.95.20.11810

62. Eissmann P, Beauchamp L, Wooters J, Tilton JC, Long EO, Watzl C. Molecular basis for positive and negative signaling by the natural killer cell receptor 2B4 (CD244). *Blood* (2005) 105:4722–9. doi: 10.1182/blood-2004-09-3796

63. Kanakaraj P, Duckworth B, Azzoni L, Kamoun M, Cantley LC, Perussia B. Phosphatidylinositol-3 kinase activation induced upon fc gamma RIIIA-ligand interaction. *J Exp Med* (1994) 179:551–8. doi: 10.1084/jem.179.2.551

64. Garvie CW, Boss JM. Assembly of the RFX complex on the MHCII promoter: Role of RFXAP and RFXB in relieving autoinhibition of RFX5. *Biochim Biophys Acta* (2008) 1779:797–804. doi: 10.1016/j.bbagrm.2008.07.012

65. Colucci F, Caligiuri MA, Di Santo JP. What does it take to make a natural killer? *Nat Rev Immunol* (2003) 3:413–25. doi: 10.1038/nri1088

66. Gilmour KC, Fujii H, Cranston T, Davies EG, Kinnon C, Gaspar HB. Defective expression of the interleukin-2/interleukin-15 receptor beta subunit leads to a natural killer cell-deficient form of severe combined immunodeficiency. *Blood* (2001) 98:877–9. doi: 10.1182/blood.V98.3.877

67. Kennedy MK, Glaccum M, Brown SN, Butz EA, Viney JL, Embers M, et al. Reversible defects in natural killer and memory CD8 T cell lineages in interleukin 15-deficient mice. *J Exp Med* (2000) 191:771–80. doi: 10.1084/jem.191.5.771

68. Fehniger TA, Suzuki K, Ponnappan A, VanDeusen JB, Cooper MA, Florea SM, et al. Fatal leukemia in interleukin 15 transgenic mice follows early expansions in natural killer and memory phenotype CD8+ T cells. *J Exp Med* (2001) 193:219–31. doi: 10.1084/jem.193.2.219

69. Song J-W, Zhang C, Fan X, Meng F-P, Xu Z, Xia P, et al. Immunological and inflammatory profiles in mild and severe cases of COVID-19. *Nat Commun* (2020) 11:3410. doi: 10.1038/s41467-020-17240-2

70. Zhang J-Y, Wang X-M, Xing X, Xu Z, Zhang C, Song J-W, et al. Single-cell landscape of immunological responses in patients with COVID-19. *Nat Immunol* (2020) 21:1107–18. doi: 10.1038/s41590-020-0762-x

71. Alsuliman A, Muftuoglu M, Khoder A, Ahn Y-O, Basar R, Verneris MR, et al. A subset of virus-specific CD161 T cells selectively express the multidrug transporter MDR1 and are resistant to chemotherapy in AML. *Blood* (2017) 129:740–58. doi: 10.1182/blood-2016-05-713347

72. Fergusson JR, Smith KE, Fleming VM, Rajoriya N, Newell EW, Simmons R, et al. CD161 defines a transcriptional and functional phenotype across distinct human T cell lineages. *Cell Rep* (2014) 9:1075–88. doi: 10.1016/j.celrep.2014.09.045

73. Terajima M, Co MDT, Cruz J, Ennis FA. High antibody-dependent cellular cytotoxicity antibody titers to H5N1 and H7N9 avian influenza a viruses in healthy US adults and older children. *J Infect Dis* (2015) 212:1052–60. doi: 10.1093/infdis/jiv181

74. Padilla-Quirarte HO, Lopez-Guerrero DV, Gutierrez-Xicotencatl L, Esquivel-Guadarrama F. Protective antibodies against influenza proteins. *Front Immunol* (2019) 0:1677. doi: 10.3389/fimmu.2019.01677

75. Annibali V, Ristori G, Angelini DF, Serafini B, Mechelli R, Cannoni S, et al. CD161(high)CD8+T cells bear pathogenetic potential in multiple sclerosis. *Brain* (2011) 134:542–54. doi: 10.1093/brain/awq354

76. Kleinschek MA, Boniface K, Sadekova S, Grein J, Murphy EE, Turner SP, et al. Circulating and gut-resident human Th17 cells express CD161 and promote intestinal inflammation. *J Exp Med* (2009) 206:525–34. doi: 10.1084/jem.20081712

77. Martos SN, Campbell MR, Lozoya OA, Wang X, Bennett BD, Thompson IJB, et al. Single-cell analyses identify dysfunctional CD16 CD8 T cells in smokers. *Cell Rep Med* (2020) 1(4):100054. doi: 10.1016/j.xcrm.2020.100054

78. Khan O, Giles JR, McDonald S, Manne S, Ngiow SF, Patel KP, et al. TOX transcriptionally and epigenetically programs CD8 T cell exhaustion. *Nature* (2019) 571:211–8. doi: 10.1038/s41586-019-1325-x

79. Phillips JH, Gumperz JE, Parham P, Lanier LL. Superantigen-dependent, cell-mediated cytotoxicity inhibited by MHC class I receptors on T lymphocytes. *Science* (1995) 268:403–5. doi: 10.1126/science.7716542

80. Ugolini S, Arpin C, Anfossi N, Walzer T, Cambiaggi A, Förster R, et al. Involvement of inhibitory NKRs in the survival of a subset of memory-phenotype CD8+ T cells. *Nat Immunol* (2001) 2:430–5. doi: 10.1038/87740

81. Correia MP, Cardoso EM, Pereira CF, Neves R, Uhrberg M, Arosa FA. Hepatocytes and IL-15: A favorable microenvironment for T cell survival and CD8 + T cell differentiation. *J Immunol* (2009) 182:6149–59. doi: 10.4049/jimmunol.0802470

82. Correia MP, Costa AV, Uhrberg M, Cardoso EM, Arosa FA. IL-15 induces CD8+ T cells to acquire functional NK receptors capable of modulating cytotoxicity and cytokine secretion. *Immunobiology* (2011) 216:604–12. doi: 10.1016/j.imbio.2010.09.012

COPYRIGHT

© 2022 Schreibing, Hannani, Kim, Nagai, Ticconi, Fewings, Bleckwehl, Begemann, Torow, Kuppe, Kurth, Kranz, Frank, Anslinger, Ziegler, Kraus, Enczmann, Balz, Windhofer, Balfanz, Kurts, Marx, Marx, Dreher, Schneider, Saez-Rodriguez, Costa, Hayat and Kramann. This is an open-access article distributed under the terms of the Creative Commons Attribution License (CC BY). The use, distribution or reproduction in other forums is permitted, provided the original author(s) and the copyright owner(s) are credited and that the original publication in this journal is cited, in accordance with accepted academic practice. No use, distribution or reproduction is permitted which does not comply with these terms.

frontiers | Frontiers in Immunology

TYPE Original Research
PUBLISHED 04 January 2023
DOI 10.3389/fimmu.2022.1001430

Check for updates

OPEN ACCESS

EDITED BY
Sara De Biasi,
University of Modena and Reggio Emilia, Italy

REVIEWED BY
Neeraj Kumar,
Northwestern University, United States
Abdul Rasheed Baloch,
University of Karachi, Pakistan
Suneel Kateriya,
Jawaharlal Nehru University, India

*CORRESPONDENCE
Muhammad Shehzad Khan
mskhan5-c@my.cityu.edu.hk
Yong Liu
liuyong@fynu.edu.cn

†These authors have contributed equally to this work

SPECIALTY SECTION
This article was submitted to T Cell Biology, a section of the journal Frontiers in Immunology

RECEIVED 23 July 2022
ACCEPTED 28 November 2022
PUBLISHED 04 January 2023

CITATION
Khan MS, Khan IM, Ahmad SU, Rahman I, Khan MZ, Khan MSZ, Abbas Z, Noreen S and Liu Y (2023) Immunoinformatics design of B and T-cell epitope-based SARS-CoV-2 peptide vaccination.
Front. Immunol. 13:1001430.
doi: 10.3389/fimmu.2022.1001430

COPYRIGHT
© 2023 Khan, Khan, Ahmad, Rahman, Khan, Khan, Abbas, Noreen and Liu. This is an open-access article distributed under the terms of the Creative Commons Attribution License (CC BY). The use, distribution or reproduction in other forums is permitted, provided the original author(s) and the copyright owner(s) are credited and that the original publication in this journal is cited, in accordance with accepted academic practice. No use, distribution or reproduction is permitted which does not comply with these terms.

Immunoinformatics design of B and T-cell epitope-based SARS-CoV-2 peptide vaccination

Muhammad Shehzad Khan[1,2*†], Ibrar Muhammad Khan[1†], Syed Umair Ahmad[3], Ishrat Rahman[4], Muhammad Zahoor Khan[5,6], Muhammad Shah Zeb Khan[7,8], Zain Abbas[9], Shumaila Noreen[10] and Yong Liu[1*]

[1]Anhui Province Key Laboratory of Embryo Development and Reproduction Regulation, Anhui Province Key Laboratory of Environmental Hormone and Reproduction, School of Biological and Food Engineering, Fuyang Normal University, Fuyang, China, [2]Department of Physics, College of Science, City University of Hong Kong, Kowloon, Hong Kong SAR, China, [3]Department of Bioinformatics Hazara University Mansehra, Mansehra, Pakistan, [4]Department of Basic Dental Sciences, College of Dentistry, Princess Nourah Bint Abdulrahman University, Riyadh, Saudi Arabia, [5]Department of Animal Breeding and Genetics, Faculty of Veterinary and Animal Sciences, University of Agriculture, Dera Ismail Khan, Pakistan, [6]State Key Laboratory of Animal Nutrition, Beijing Engineering Technology Research Center of Raw Milk Quality and Safety Control, College of Animal Science and Technology, China Agricultural University, Beijing, China, [7]Department of Biotechnology, University of Science and Technology of Bannu, Bannu, Pakistan, [8]School of Biomedical Science and Biomedical Engineering, Southeast University, Nanjing, China, [9]Department of Life Sciences, University of Management and Technology, Lahore, Pakistan, [10]Department of Zoology, Hazara University, Mansehra, Pakistan

SARS-COV-2 is a virulent respiratory virus, first identified in China (Wuhan) at the end of 2019. Scientists and researchers are trying to find any possible solution to this deadly viral disease. Different drug source agents have been identified, including western medicine, natural products, and traditional Chinese medicine. They have the potential to counteract COVID-19. This virus immediately affects the liver and causes a decrease in oxygen levels. In this study, multiple vacciome approaches were employed for designing a multi-epitope subunit vaccine for battling against SARS-COV-2. Vaccine designing, immunogenicity, allergenic, and physico-chemical assessment were performed by using the vacciome approach. The vaccine design is likely to be antigenic and produce potent interactions with ACE2 and NSP3 receptors. The developed vaccine has also been given to in-silico cloning models and immune response predictions. A total number of 12 CTL and 12 HTL antigenic epitopes were predicted from three selected covid-19 virulent proteins (spike protein, nucleocapsid protein, and membrane proteins, respectively) based on C-terminal cleavage and MHC binding scores. These predicted epitopes were amalgamated by AYY and GPGPG linkers, and a β-

defensins adjuvant was inserted into the N-terminus of this vaccine. This analysis shows that the recommended vaccine can produce immune responses against SARS-COV-2. Designing and developing of the mentioned vaccine will require further experimental validation.

KEYWORDS

SARS-CoV-2, COVID-19, vaccine designing, vacciome, docking

Introduction

The SARS-CoV-2 virus (formerly 2019-nCoV) broke out in Wuhan, China, in December 2019 and circulated rapidly around the world, mainly in China, Italy, Germany, Japan, the USA, Iran, Pakistan, UAE, India, South Korea, and Russia. According to WHO, On 19 September 2022, 612,236,677 confirmed cases of coronavirus 2019 (COVID-19), and 6,514,397 deaths were reported. Scientists are struggling to find a solution to treat this deadly disease. To date more than 30 agents has been identified, including natural products, western medicine, and traditional Chinese medicine, which may be effective against COVID-19 (1).

Coronaviruses are positive-stranded RNA viruses that consist of a large genome among all viral RNAs, ranging from 27 to 32 kb. Similarly, it places inside a helical capsid made of nucleocapsid (N) protein and surrounded by an envelope. The three structural proteins are referred to as membrane protein (M), envelope protein (E), and spike protein (S). Proteins M and E are involved in the viral organization, while S-proteins invade viral cells in host cells. Some coronaviruses also contain proteins associated with the envelope of haemagglutinin esterase protein (HE). Of all the synthetic proteins, the spike forms the great speculation from the viral segment that made coronaviruses look like crowns (hence its name; corona in Latin means crown) (2).

Concerning health threats from coronaviruses, are permanent and long-lasting. Understanding the behavior of coronaviruses and controlling their spread, have vital effects on global health and economic stability (3). Coronaviruses are a member of the family Coronaviridae in the order of Nidovirales (4). However, they can divide into four categories: Alpha - coronavirus, Beta-coronavirus, Gamma-coronavirus, and Delta-coronavirus. Alpha-and beta-coronaviruses infect mammals, gamma-coronaviruses infect bird species, and delta infects both mammals and birds. Coronaviruses are classified in the order Nidovirales within the family Coronaviridae and the subfamily Coronavirinae. In the beginning, the classification of members of this subfamily was determined by their serological connections, but now it is determined by meeting a certain amount of sequence identity in a few replicase areas. This new taxonomic revision is a stark contrast to the older method (the pp1ab polyprotein and the ORF1ab gene). In accordance with these criteria, the family Coronavirinae is subdivided into four genera, namely alpha-, beta-, gamma-, and deltacoronavirus. This new split supersedes the old classification of antigenic groups 1, 2, 3, and 4. The complete species list that was proposed by the International Committee on the *Taxonomy of Viruses (ICTV)*, which also included the genus that was found in birds. Alpha- and beta CoVs infect both humans and domestic animals, whereas gamma- and delta CoVs are primarily linked with avian hosts, even though they have been found in marine mammal species and in several Asian predators. Coronaviruses, also known as CoVs, are members of a broad family of viruses that are enclosed and have a genome consisting of a single strand of RNA. These viruses are always present in mammals and birds and pose a threat to humans as well as other animals, including livestock. The *Coronaviruses (CoVs)* that are carried by avian species are classified into the genera gamma- and delta coronaviruses respectively. The avian coronavirus is the most well-known member of the gamma-CoV family. Avian coronavirus is the technical term for the infectious bronchitis viruses (IBVs) that can be found in chickens and other domestic birds such as turkeys, guinea hens, and quails. These IBVs can also infect humans. IBVs have also been discovered in wild birds that were reported to be in good health, which suggests that wild birds could act as the vector between domestic and wild birds. In addition, other coronaviruses besides IBVs have been identified in wild birds, which suggests that these creatures play a significant role in the epidemiology of other *gamma CoVs and delta CoVs*. Representative alpha-coronaviruses include human coronavirus NL63 (HCoV-NL63), porcine transmissible gastroenteritis coronavirus (TGEV), PEDV and porcine Coronavirus (PRCV). Representative beta-coronaviruses include SARS-CoV, MERS-CoV, bat coronavirus HKU4, mouse hepatitis coronavirus (MHV), bovine coronavirus (BCoV) and human coronavirus OC43. Gamma representing delta - coronaviruses include bronchitis coronavirus (IBV) and porcine delta-coronavirus (PdCV) (5).

Additionally, the spike is a critical factor for viral load and tissue tropism and is the deep inducer of immune responses (6).

Therefore, it appears that the link between SARS-CoV and respiratory epithelia plays a vital role in the genes of SARS. Cellular receptors are linked to other coronaviruses associated with human disease. Recently, angiotensin-converting enzyme 2 (ACE2) has been identified as the receptor for both SARS-CoV (7) and NSP3.The multi-domain non-structural protein 3 (Nsp3), which has an average molecular mass of about 200 kD, is the largest protein that the coronavirus (CoV) genome can encode. Nsp3 is an essential part of the replication/transcription complex. It is made up of several domains, whose organization differs amongst CoV genera due to domain duplication or absence. The ubiquitin-like domain 1 (Ubl1), the Glu-rich acidic domain (also known as the "hypervariable region"), a macrodomain (also known as the "X domain"), the papain-like protease 2 (PL2pro), and the Nsp3 ectodomain (3Ecto) are the eight Nsp3 domains that are present in all known CoVs. Additionally, the TM1 and TM2 transmembrane domains are present in all CoVs. Nuclear magnetic resonance (NMR) spectroscopy and/or X-ray crystallography have both been used to examine the three-dimensional structures of domains in the N-terminal two thirds of Nsp3 since the outbreaks of the Middle East Respiratory Syndrome coronavirus (MERS-CoV) in 2012 and the severe acute respiratory syndrome coronavirus (SARS-CoV) in 2003.

The rate of RNA virus mutations aids in viral adaptability by striking a balance between genomic variety and the integrity of genetic information. The biological characterisation of viral mutations can offer priceless insights for analysing immune evasion, pathogenesis, and viral treatment resistance related pathways. Studies on viral mutations are also important for developing novel vaccines, antiviral medications, and diagnostic tests. The viral enzymes that replicate the nucleic acids are responsible for the viral genome's mutagenesis process, which is regulated by post-replicative nucleic acid repair and/or proofreading capabilities with little to none. Host enzymes, spontaneous nucleic acid damage brought on by physical and chemical mutagens, recombination events, and specific genetic components are other processes that cause mutations. Other variables, such as those that affect the template sequence and structure involved in viral replication, can influence the rate of mutation. Multi-domain proteins called RNA-dependent RNA polymerases (RdRps) can catalyse the creation of phosphodiester linkages between ribonucleotides in the presence of a divalent metal ion. With certain exceptions, such as the Nidovirales order (to which the Coronavirus genus belongs), which stands out for having the biggest RNA genomes, RNA polymerase lacks proofreading capabilities in most viruses. Coronavirus nsp3-RdRp plays a vital role in replication Non-structural proteins (nsps), which are created as byproducts of the cleavage of viral polyproteins to promote virus replication and transcription, control the sophisticated machinery used by nidoviruses to synthesize RNA (8). ACE2 is a membrane-bound aminopeptidase expressed in vascular endothelial, renal, and cardiovascular tissue and epithelia of the small intestine and testicles (9). The extracellular region ACE2 component, which includes first-helix and lysine 353 and adjacent remnants of the N-terminus of alpha-helix (sheet-5) interacts closely with the SARS-CoV S glycoprotein receptor binding compound (10). Similarly, SARS-CoV nsp3 is a major protein of 1922 (11) amino acids, thought to have at least seven domains: (1) N-terminal Glu-rich acidic (AD) domain; (2) X domain (XD) with poly binding (ADP-ribose) and SUD domain (SARS-CoV Unique Domain, entries not found in any other coronavirus to date) directly related to oligo (G) - strands (7, 12) a papain-like protease (PLP2), recently shown to show the function of removing ubiquitin (8, 13); an unknown domain that may extend the papain-like protease domain, called PLnc's Papain-Like noncanonical domain (9); transmembrane domain (14) corresponding to the N-terminal of the Y-domain; and (10) the remainder of the Y domain, the abbreviation "Y domain" will be used for this part of this study. The transmembrane domains that distribute most of the nsp3, nsp4 and nsp6 are considered compact/compact (RTC) compact devices. Current advances in the field of vacciome (15–17) and the availability of various epitope drug design tools have greatly enhanced research into the development of potential vaccine candidates (18–22).

Epitope-based vaccine design is one of the reliable, accurate, and fast way to design vaccines against toxic viruses. Therefore, this study aimed to sign up a multi-epitope subunit vaccine against SARS-CoV-2. Here, we used three antigenic proteins (spike protein, nucleocapsid protein, and membrane protein) from SARS-CoV-2 to design B and T-cell epitopes in them. Similarly, HTL epitope prediction was performed, and a final vaccine composed of multiple epitopes was developed. In addition, we used a molecular entry method followed by a strong thermodynamics print, an *in-silico* expression profile, and an agent-based modeling device to ensure the stability, speech, and response of antibodies irritated by the last vaccine.

Material and methods

Virulence protein collection

Proteins are vital for the development of vaccines; therefore, we have selected three toxic proteins against Covid-19, including spike protein, nucleocapsid protein, and membrane protein, according to their role in covid-19 respiratory diseases. The workflow of this scientific study is shown in Figure 1.

Predictions of CTL (MHC-I binding) epitope

Cytotoxic T-lymphocytes consist of CD8 and a subset of T cells that respond to the killing of cells charged by infra cellular

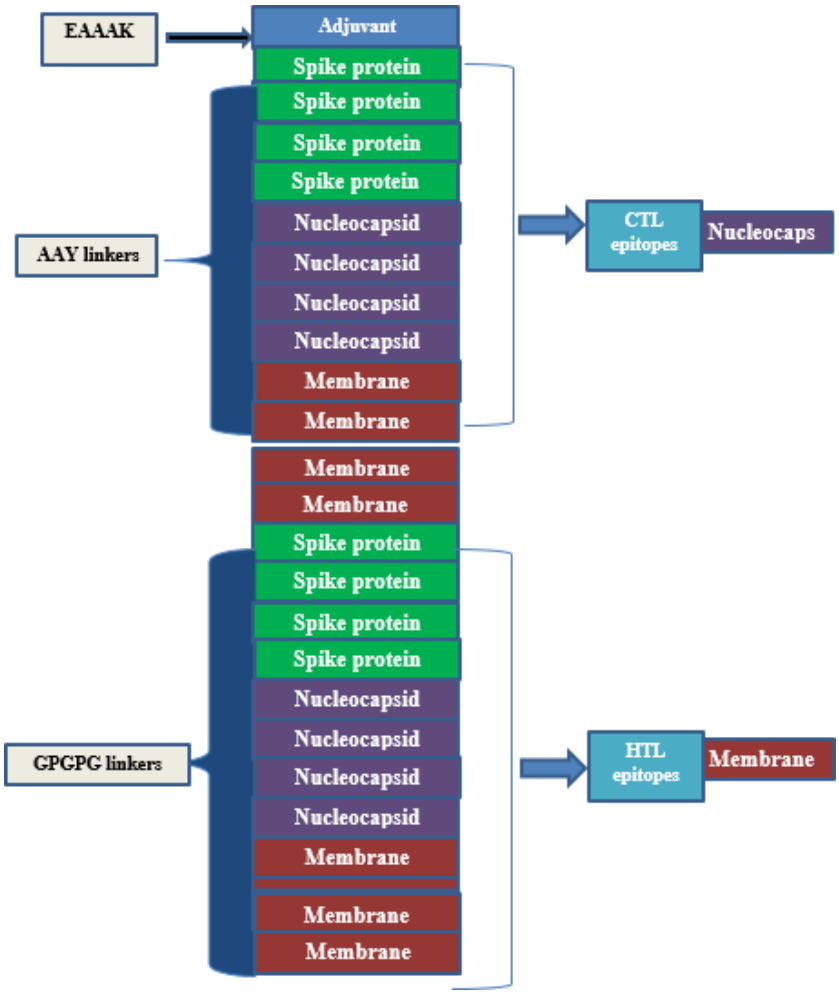


FIGURE 1
Schematic diagram to construct vaccine against SARS-COV-2.

TABLE 1 Helper-T-Lymphocytes epitopes are given in the table along with their scores predicted by IEDB MHC class II serve.

Alleles	Start	End	Peptide sequence	Method	Percentile rank
HLA-DRB1*01:01	513	527	LSFELLHAPATVCGP	Consensus (comb.lib./smm/nn)	0.03
HLA-DRB1*01:01	512	526	VLSFELLHAPATVCG	Consensus (comb.lib./smm/nn)	0.03
HLA-DRB1*01:01	511	525	VVLSFELLHAPATVC	Consensus (comb.lib./smm/nn)	0.03
HLA-DRB1*01:01	514	528	SFELLHAPATVCGPK	Consensus (comb.lib./smm/nn)	0.09
HLA-DRB4*01:01	218	232	TALALLLLDRLNQLE	Consensus (comb.lib./smm/nn)	0.66
HLA-DRB5*01:01	84	98	QIGYYRRATRRVRGG	Consensus (comb.lib./smm/nn)	0.67
HLA-DRB4*01:01	217	231	ETALALLLLDRLNQL	Consensus (comb.lib./smm/nn)	0.76
HLA-DRB5*01:01	83	97	DQIGYYRRATRRVRG	Consensus (smm/nn/sturniolo)	0.77
HLA-DRB1*01:01	144	158	IRGHLRMAGHSLGRC	Consensus (comb.lib./smm/nn)	0.19
HLA-DRB1*01:01	143	157	IIRGHLRMAGHSLGR	Consensus (comb.lib./smm/nn)	0.27
HLA-DRB1*01:01	145	159	RGHLRMAGHSLGRCD	Consensus (comb.lib./smm/nn)	0.31
HLA-DRB4*01:01	42	56	NRFLYIIKLVFLWLL	Consensus (comb.lib./smm/nn)	0.39

fungus infections, viruses, bacteria, or protozoan. Similarly, CTL epitopes (MHC-I) are predicted in three negative covid-19 proteins (Spike protein, nucleocapsid protein, and membrane protein) by the online tool NetCTL1.2 (http://www.cbs.dtu.dk/services/NetCTL/) (23). Based on C-terminal cleavage values, transport-related proteins, and MHC binding points- I, this server predicts 9-mer protein epitopes. Then neural implantation system was followed by a C terminal cleavage server and binding peptides in MHC-I. The weight matrix obtained optimal mobility efficiency. Epitopes predicted at 0.75 (by default parameters) and reduced> E.

Prediction of HTL (MHC-II binding) epitopes

Helper cells (T-lymphocyte) are the critical player in both humoral and cell-mediated immune responses. Therefore, HTL receptor-specific epitopes were possibly an essential part of the prophylactic and immunotherapeutic vaccine. In this study, for the selected three virulent proteins of covid-19, including Spike protein, nucleocapsid protein, and membrane protein, the MHC-II binding-epitopes (HTL) were predicted using a web tool IEDB MHC-II (http://tools.iedb.org/mhcii/). In this sense, we used MHC alleles, including HLA-DRB1*01:01, HLA-DRB3*01:01, HLA-DRB4*01:01, and HLA-DRB5*01:01 and IEBD recommended 2.22 predicted method to detect 15-mer length epitopes. This server defines the affinity of peptides towards the MHC-II based on the lower percentile ranked in Table 1.

Prediction of B-cell epitopes

B-cells are a chief player in the defense system of epitopes associated with the B-cell receptor, which plays a key role in developing antibody vaccines following antibody production. Therefore, to predict specific B-cell epitopes, the ABCPREDS (http://crdd.osdd.net/raghava/abcpred/) server has been used (24). ABCPRED is primarily responsible for protecting the immune system, which, in turn, provides long-term immunity. To predict B-cell linear epitopes, ABCPRED used a neural implant network based on a repetitive neural network (machine-based process) using patterns of limited length to predict 20-mer B-cell epitopes. Dissolved B cell epitopes are predicted by web server Ellipro (http://tools.iedb.org/ellipro/). The ElliPro suite uses fossil fusion algorithm and Thornton technology to predict B cells (conformational epitopes). This server mainly uses Jsmol to generate 3D links for server-predicted epitopes (25). Similarly, available data are available and confirm the immunodeficiency of a sub-unit vaccine designed.

Composition of multi-epitope subunit vaccine

A synthetic vaccine of 386 amino acid residues was eventually developed with 12 HTL and 12 CTL epitopes, based on its high binding and non-allergenic properties naturally. To create a multi-epitope-subunit vaccine, the EAAAK connector was bound as an adjuvant with intra-CTL and Intra-HTL epitopes compiled by AAY and GPGPG linker, respectively. Eventually, vaccine formulation was achieved with adjuvant, linker, CTL, and HTL epitopes from N-terminal to C-terminal, respectively. These links are vital for two reasons; links effectively block the formation of neo-epitopes (junctional epitopes) and improve epitope presentation. The linkers such as AAY, EAAAK, and GPGPG are utilized rather frequently in the process of developing vaccines. Linkers being utilized so that the epitopes could be combined, and an adjuvant being incorporated into the procedure so that the immune response of the host could be stimulated. The VaxiJen 2.0 web server was used once more to do additional research into the antigenicity and allergenicity of the construct.

Allergies to antigenicity treatment

Allergies and overuse of the immune system are experienced in the past, usually harmless substances that can cause skin rashes, rashes, inflammation of the mucous membranes, and sneezing. Allergies to these predictable components of the vaccine were determined using the online tool AllerTOP (https://www.ddg-pharmfac.net/AllerTOP/), and it found that the vaccine protein is anti-inflammatory and safe for human use. The vaccine prescribed to the person in charge should have a great immune system that can trigger a high immune response, leading to the formation of memory cells against pathogenic epitopes. To determine the immunodeficiency of a synthetic vaccine, two online servers including Vaxijen2.0 (http://www.ddg-pharmfac.net/vaxijen/VaxiJen/VaxiJen.html) (26) and AntigenPro (http://scratch.proteomics.ics.uci.edu/) were used by entering a build-up tree sequence as a query.

Physiochemical properties

The antibodies of the predicted vaccine were determined with the ProtParam server (https://web.expasy.org/protparam/) and tested with seven parameters. This server determines the composition of accurate amino acids, an indicator of instability, aliphatic points, *in vivo* half-life, molecular weight, *in vitro* half-life, Grand Average of Hydropathicity (GRAVY), and pI theory (27).

Secondary structure modeling

The secondary structure was predicted according to the vaccine sequence by the 'PSIPRED' web server (http://bioinf.cs.ucl.ac.uk/psipred/). In addition, this tool can be used for internal networks (feed-forward) to process Position Specific Scoring Matrix (PSSM) predictive properties for secondary properties using the PSIPRED (28).

3D structure assumptions, refinement, and validation

In the 3D architecture prediction of vaccine formulation, the freely available web server Robetta (https://robetta.bakerlab.org/) has been used (29). This server is constantly updated with CAMEO and a visualization of the UCSF camera tool used. With the analysis of the predicted model, the Galaxy Refine online tool (http://galaxy.seoklab.org/) for continuous development (30). Similarly, the server uses the CASP10 command to upgrade the 3D query status. Alternatively, the side chains of proteins also rebuild through the CASP10 process followed by reloading. and using 3D architecture simulation for continuous relaxation. Possibly, the refinement of the Galaxy was used for the continuous development of 3D editors in terms of world-class and structural quality (30). For power reduction and structural adjustment, UCSC camera software was used. To validate the structure and test, ensure that 3D is used to analyze the coherence of the atomic (3D) model in its amino acid sequence (31), which is incorrect to test the arrangement of different atoms in the protein model and rampage tools used.

Codon efficacy and *in-silico* expression vaccine

The reverse translation and optimization of the *Java Codon Adaptation Tool (*Jcat**)** have been used, to obtain a high-level expression in *E. coli*. Jcat calculates CAI scores and GC content in question in order to achieve the highest quote. In the Prokaryotic ribosome, the termination and autonomy of the binding sites are selected. Similarly, the Ndel and Xhol limitation sites are set to follow the translated sequence. Finally, the prepared vaccine was combined with pET-32a + MEV plasmid with a snap-gene software package.

Molecular docking of vaccine with ACE2 and NSP3

Chemical insertion is a calculation method, which can predict the desired shape of the ligand molecule in the receptor molecule in its complex form. It also calculates the binding bond between the two molecules (ligand and receptor) in the terms of goal-scoring activities. Vaccine molecules made ACE2 and NSP3 proteins, directly affected by covid-19 was docked *via* the Cluspro online server (https://cluspro.org/login.php) (32).

Molecular dynamics simulation

The Desmond program of Schrödinger software 2021-2 (Schrödinger, LLC, New York, NY, USA) (33) with the OPLS4 (Optimized Potentials for Liquid Simulation) (34) force field was used for MD simulation to analyze protein conformational changes. A simulated triclinic periodic boundary box with a 10 extension in each direction was used to solve the GluN2B protein structures, and an explicit solvation model (Monte-Carlo equilibrated SPC) was used for each system. Lennard-Jones interactions (cut-off = 10) and the SHAKE algorithm governed covalent bond mobility (35). 0.15 M Na+Cl was added to neutralize the system during solvation. At 300 K and 1 bar pressure, the NPT ensemble class reduced the energy of protein models until a gradient threshold of 25 kcal/mol was reached. Each system had a single MD run, and all simulated trajectories were re-covered in 20 ps. The Particle Mesh Ewald (PME) method was utilized to compute long-range coulombic interactions, and the RESPA integrator (36) was used to govern all covalent bonds associated with hydrogen atoms, with an inner time step of 2 fs. For short-range electrostatic interactions, 9.0 was chosen; for long-range van der Waals (VDW), uniform density was employed. At 300 K and 1 atmosphere, a Nosé–Hoover thermostat (37) with a 12-ps relaxation time was used. The Martyna–Tobias–Klein barostat approach (38) with a 12 ps relaxation length was used. The molecular simulation was performed at 1 atm pressure and 300 **K** temperature for a 100 ns NPT production run under the OPLS4 force field.Two post molecular dynamics simulation analysis i.e., RMSD and RMSF was performed for all the system.

Imitation of MD simulation

The dynamics of a molecule were performed using Desmond. Desmond is a software developed at D.E. Shaw research, which analyzes the fastest mimicry of cells of biological processes in normal computer clusters. Ten cut cutoff radius of non-bond interaction is considered. Transmission analysis of ten nanoseconds trajectories was performed with PTRAJ52 and CPPTRAJ. Two statistical parameters are calculated RMSD and RMSF for all systems (Figure 2).

Results

Covid-19 protein sequence collection

In 2019, a new infectious illness caused by a coronavirus has emerged and is rapidly spreading over the globe. Severe acute respiratory syndrome coronavirus 2 is a new coronavirus that causes this condition (SARS-CoV-2). The S1 and S2 subunits make up the SARS-CoV-2 spike (S) protein, which is essential

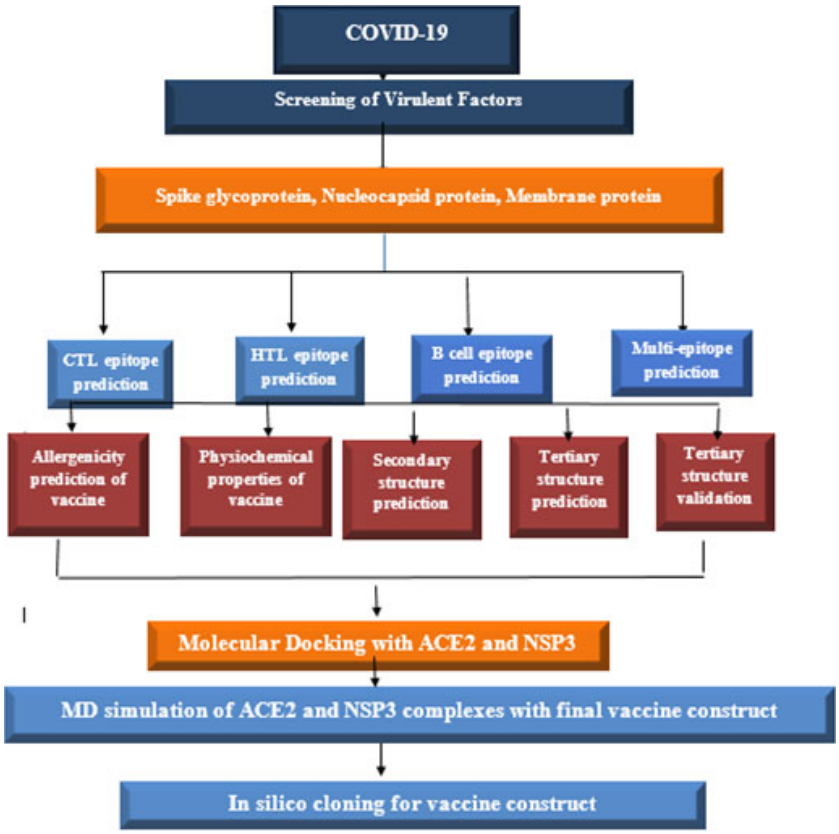


FIGURE 2
The structural arrangement of the final vaccine candidate constructed from CTL and HTL epitopes using different linkers.

for receptor identification and cell membrane fusion. By generating a six-helical bundle *via* the two-heptad repeat domain, the S2 subunit enables viral cell membrane fusion, whereas the S1 subunit has a receptor-binding domain that identifies and attaches to the host receptor angiotensin-converting enzyme 2. The sequence of covid-19 protein spike proteins is composed of 1273 amino acids weighing 141,178 (Da), while the nucleocapsid protein contains 422 amino acids counting 46,025 (Da) and membrane protein containing 221 amino acids mass 25,061 (Da) retrieved from UniProt (https://www.uniprot.org/) database.

Antigenicity of toxic proteins Covid-19

It is possible to have access to the antigenicity of a variety of covid-19 proteins by logging onto the web server Vaxijen2.0 (http://www.ddg-pharmfac.net/vaxijen/VaxiJen/VaxiJen.html). This server is located at: http://www.ddg-pharmfac.net/vaxijen/VaxiJen/VaxiJen.html. According to the research, these proteins are the ones that are responsible for carrying the antigen characteristics in a school that is continuously formed by a spike feeder, Nucleocapsid, and protein membranes (0.47, 0.48, and 0.59, respectively). In a similar fashion, the points for antigenicity potential reflect the anti-genic status of the selected sequence (proteins) that were used in the creation of a sub-unit vaccination. This was done to create a more effective vaccination.

Prediction of CTL and HTT epitopes

Epitope prediction algorithms, with extensive allelic coverage, have recently been created, verified, and shown to be reliable techniques for predicting the binding affinities of peptides to MHC molecules. The identification of T-cell epitopes produced from the vaccine virus confirmed the efficacy and usefulness of computational in silico analysis for broadly finding CD8 + T-cell epitopes (39). 49 CTL epitopes were discovered in that ground-breaking study, and it was later shown that they accounted for 95% of the whole CD8 response to the Influenza viruses. Since then, several research have employed in silico epitope identification techniques to locate potential epitopes for inclusion in carefully crafted multivalent

vaccinations meant to guard against diseases brought on by a variety of viral and bacterial pathogens. For instance, research has demonstrated that vaccinations based on epitopes can successfully elicit immune responses that are protective against a variety of diseases, including the influenza and HIV viruses. Strong CTL responses have been seen following epitope delivery by DNA vaccines or DNA-launched nanoparticle vaccinations.

The CTL epitopes were predicted using NetCTL, which estimated 58 CTL epitopes with a length of 9mer length. In all, only 12 epitopes were selected based on different terms of the binding effects of MHC and the non-allergenic nature of these three potent proteins responsible for the design of the vaccine. HTL epitopes predicted that MHC alleles HLA-DRB1 * 01: 01, HLA-DRB3 * 01: 01, HLA-DRB4 * 01: 01, and HLA-DRB5 * 01: 01 using a web tool binding to IEBD MHC-II continuously elevated 12 HTL epitopes 15 to 15 ounces from each harmful protein in different areas based on the lowest level of percentile (Table 1).

Composition of multi-epitopes vaccine

The final vaccine is made up of 386 and 12 amino acids, which were selected because of their capacity to bind (they are CTL and HTL epitopes), the fact that they are non-allergenic, and the fact that they contain antigenic qualities. In addition to this, the amino acids were selected because of the ease with which they could be produced (Table 2). In addition to this, both the GPGPG linkage and the AAY linkage were incorporated into the process of developing the comprehensive multi-epitope vaccine. The CTL epitopes were included into the manufacturing process of the adjuvant in a manner that is analogous to the one described in the previous paragraph. This was accomplished through the utilization of the EAAAK link. GPGPG and AAYlinkers were able to successfully generate an attachment of HTL and CTL epitopes adjuvant to the N-terminus side of the anti-corrosion drug by combining their efforts. In order for this goal to be accomplished, the two linkers that were being utilized were consolidated into a single one. In addition to this, a piece of software known as BLAST was utilized in order to incorporate newly anticipated epitopes into the investigation. This was done to avoid using homologous epitopes along with different kinds of human proteins (Figure 2 and Table 2).

Predictions of B cell epitopes

B cell epitopes that have been predicted with the use of a process referred to as ABCpred, which is a complex computer

TABLE 2 CTL and HTL epitopes were used to construct the final vaccine structure based on combined score.

Sequence	Combine score	Type of epitope
WTAGAAAYY	3.11	CTL epitope
TSNQVAVLY	3.08	CTL epitope
CVADYSVLY	2.58	CTL epitope
KTSVDCTMY	2.38	CTL epitope
LSPRWYFYY	2.34	CTL epitope
GTTLPKGFY	1.68	CTL epitope
LLNKHIDAY	1.39	CTL epitope
NTASWFTAL	0.95	CTL epitope
GTDSGFAAY	3.43	CTL epitope
YSNRNRFLY	2.73	CTL epitope
VATSRTLSY	1.46	CTL epitope
WIMLLQFAY	1.16	CTL epitope
LSFELLHAPATVCGP	0.03	HTL epitope
VLSFELLHAPATVCG	0.03	HTL epitope
VVLSFELLHAPATVC	0.03	HTL epitope
SFELLHAPATVCGPK	0.09	HTL epitope
IRGHLRMAGHSLGRC	0.19	HTL epitope
IIRGHLRMAGHSLGR	0.27	HTL epitope
RGHLRMAGHSLGRCD	0.31	HTL epitope
NRFLYIIKLVFLWLL	0.39	HTL epitope
TALALLLLDRLNQLE	0.66	HTL epitope
QIGYYRRATRRVRGG	0.67	HTL epitope
ETALALLLLDRLNQL	0.76	HTL epitope
DQIGYYRRATRRVRG	0.77	HTL epitope

algorithm. The utilization of this approach allowed to produce these forecasts. This strategy was utilized throughout the course of the investigation so that we could arrive at these conclusions. Using this method, 20-mer epitopes are selected for further study depending on the number of exceptional epitope sites that can be discovered in each of the areas in which they are located. This is done to maximize the amount of information that can be gleaned from the study. This assists in reducing the number of possible candidates that need to be investigated. The National Center for Biotechnology Information (NCBI) is the organization that is responsible for the creation of this methodology. On the other hand, we utilized continuous epitopes that totaled 55 amino acids in length when combined. These are the ones that, in our opinion, stand out as being particularly remarkable. Following that, these epitopes were disassembled, and then reassembled into a three-dimensional pharmacological model with a probability of around 0.618. In a method that is somewhat like this, the epitopes are designated by the yellow zone, whereas most of the polyprotein is shown by the gray region (Figure 3).

Characterization of physiochemical properties and secondary structure prediction

The result also showed that the last vaccine is non-allergic with 0.32 points in the 0.4 automatic thresholds calculated using the Vaxigen 2.0 sever (21). Since causal microorganisms no longer need to be cultivated, the creation of vaccines in the post-genomic age frequently starts with an in-silico analysis of genome information to identify the most likely protective antigens. Despite the approach's obvious benefits, like speed and cost effectiveness, its success still depends on how well the antigen is predicted. Most methods identify antigens by sequence alignment. This is a problem for several reasons. Even while certain proteins may have comparable structures and biological characteristics, some proteins lack evident sequence similarities. A sequence's antigenicity may be encoded in a deceptive way that made it impossible to directly identify by sequence alignment. The absence of similarity to antigens of known provenance will prevent the development of truly novel antigens. We provide a new alignment-free method for antigen prediction to get over the drawbacks of alignment-dependent methods. Models for the prediction of entire protein antigenicity were developed using protein datasets. 100 recognized antigens and 100 non-antigens made up each group. Internal leave-one-out cross-validation and external validation utilizing test sets were used to evaluate the resulting models. The stability of the distinction between antigens and non-antigens was evaluated using an additional five training sets for each class of antigens. Both validations of the models showed good performance, with prediction accuracy ranging from 70% to 82.85%. The models were put into practice on a server that we've named VaxiJen2.0.

At the same time, the weight of the vaccine is as high as 40825.88, which is likely to favor the weakness of the last vaccine. Similarly, the theoretical pI is to be approximately 9.54. The average life expectancy in mammalian reticulocytes was 1hours, *in vitro*, while 30 min in yeast and 10 hours *E. coli in vivo*. With an

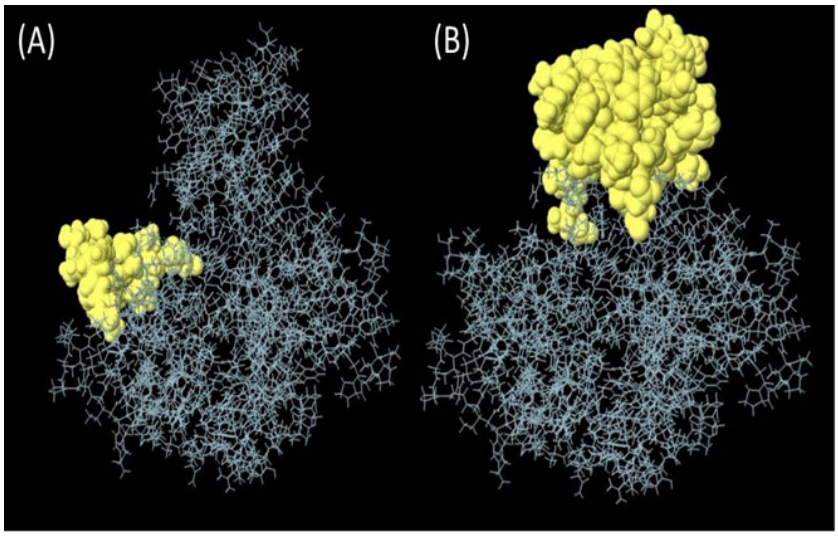


FIGURE 3
(A) Linear epitopes predicted by ABCpred and **(B)** discontinuous (conformational) epitopes predicted by ellipro visualized in jsmol, yellow part showed predicted epitope.

extinction coefficient of 7568 and an instability rating of 33.29, it's clear that this medicine is in a relatively stable state. Also, the highest value of the aliphatic index was seen (82.85), while the lowest value of the sub-unit vaccine, hydropathicity (GRAVY), was seen (0.046) and immunosuppressive medicine. The second structure for the construction of the vaccine was predicted using a cartoon PSIPRED image and a CFSSP online server for the construction of the secondary structure. The secondary prediction model consisted of 47.2% α-helix, 42.0% β-sheet, and 10.0% coils (Figure 4).

Tertiary structures prediction, refinement, and validation

Robetta's web server used an abinitio method model to generate the final multi-epitope vaccine design's three-dimensional structure. This was done to ensure that the vaccine would be effective. This structure was erected specifically for the administration of vaccinations. This server generates forecasts for the five different built-in policy versions that have the best chance of being the most successful overall. The z-score value that the UCSF camera determined to be the most accurate may be used to select the first model as the one that would be utilized to represent the data. This would ensure that the most accurate picture possible is produced. This option is available for selection. The strands, which are made up of black helixes, are represented by the color. The Green represents the coils, while blue cyan represents the strands that are made up of the black helixes (Figure 5). Similarly, the Galaxy Refine server was tracked to further improve the selected model-1, tested with GDT-HA (0.9916), RMSD (0.262), Ramachandran strategy (97.4), MolProbity (1.736)), and bad rotamers (0.7) and school conflict (12.8). Similarly, power is reduced with UCSF Chimera software and the structure was also tested to check the quality with the ERRAT web tool (Figure 6), which indicates a standard 95.24 standard. The vertical axis represents points, while the horizontal axis represents the protein residue. (Figures 6A, B). The 3D architecture validation revealed that 87.82% of the fossils had an estimated 3D-1D scale> = 0.2 (Figure 7). The Figure 5 **is** analysis of the Ramachandran Plan also showed that 97.4% of the remains were in the best region (> 90%), of all, 0.8% in the permitted area, and 0.0% in the outdoor area. The Ramachandran plot represents peptide torsional angles (phi and psi) in two dimensions. the torsion angles N(i-1),C(i),Ca (i),N(i) and C(i),N(i),C(i+1). G. N. Ramachandran et al. produced the plot by putting on the x-axis and on the y-axis in 1963. This graphic shows what torsional angle variants are possible. Each residue's torsional angle determines the placement of its planar peptide bond in reference to that of its two neighbors. Steric hindrance prevents various angle combinations and residue conformations. Ramachandran plots reveal which torsional angles are permitted in peptide structure. Right: ribonuclease H's Ramachandran plot.

Codon alteration and in silico cloning

Here, the Jcat server was used to quantify the expression of the multi-epitope *E. coli* vaccine (type K12). Satisfactory inputs used 1150 nucleotides in total. Similarly, codon production was performed, and the Codon Adaptation Index (CAI) is known as 0.94, while GC content is 59%. The clone length was 6986 kbp, and NdeI and XhoI block sites were created and integrated into the pET32a + Mev vector (Figure 7). The sequence of the target in the Clone is indicated in blue between the block areas. The targeted sequence is surrounded by 6-histidine residues on both sides, which will assist in purification purposes.

Molecular docking of vaccine complex

The conclusion of the research on molecular docking that was carried out with ClusPro resulted in the construction of a total of thirty different kinds of structures. Because the binding energies of those 10 dock complexes were the lowest compared to the other thirty that might have been used, those ten were chosen as the best ones to use. In addition to those alternatives, we also considered several others. It was able to retrieve the dock complexes in the very best state that it would have been feasible for them to be in at the time of their retrieval. This was the very best state that it would have been possible for them to be in. They were in the absolute finest conceivable state that could have been achieved by them now. In a similar vein, protein-protein interaction complexes and the method by which they preferentially bind offer for a great engagement with the final vaccine. Even though the proteins ACE2 and NSP3 are part of these complexes, this is not an exhaustive list of the components that go into making up these complexes. This is since these complexes have limited connectivity capabilities, which means that they can only attach themselves to specific proteins. The reason for this is because these complexes have restricted connection capabilities (Figure 1).

Interaction analysis of dock complex

The complex's two-dimensional structure, which is made up of the protein and the ligand, as well as how these two elements interact with one another, are depicted in a diagram on the page. The website also includes a graphic that shows the interaction between the ligand and the protein (Figure 8). The statistical analysis's results make it clearly clear that the receptor molecule and the peptide units interact on an atomic level. The results of the investigation directly led to the conclusion that was made. This conclusion may be deduced from the investigation's findings. These conclusions were reached after considering the study's findings, which allowed us to reach the ones mentioned previously in this paragraph. The Van der Waals force, ion contacts, and hydrogen bond formation are a few examples of

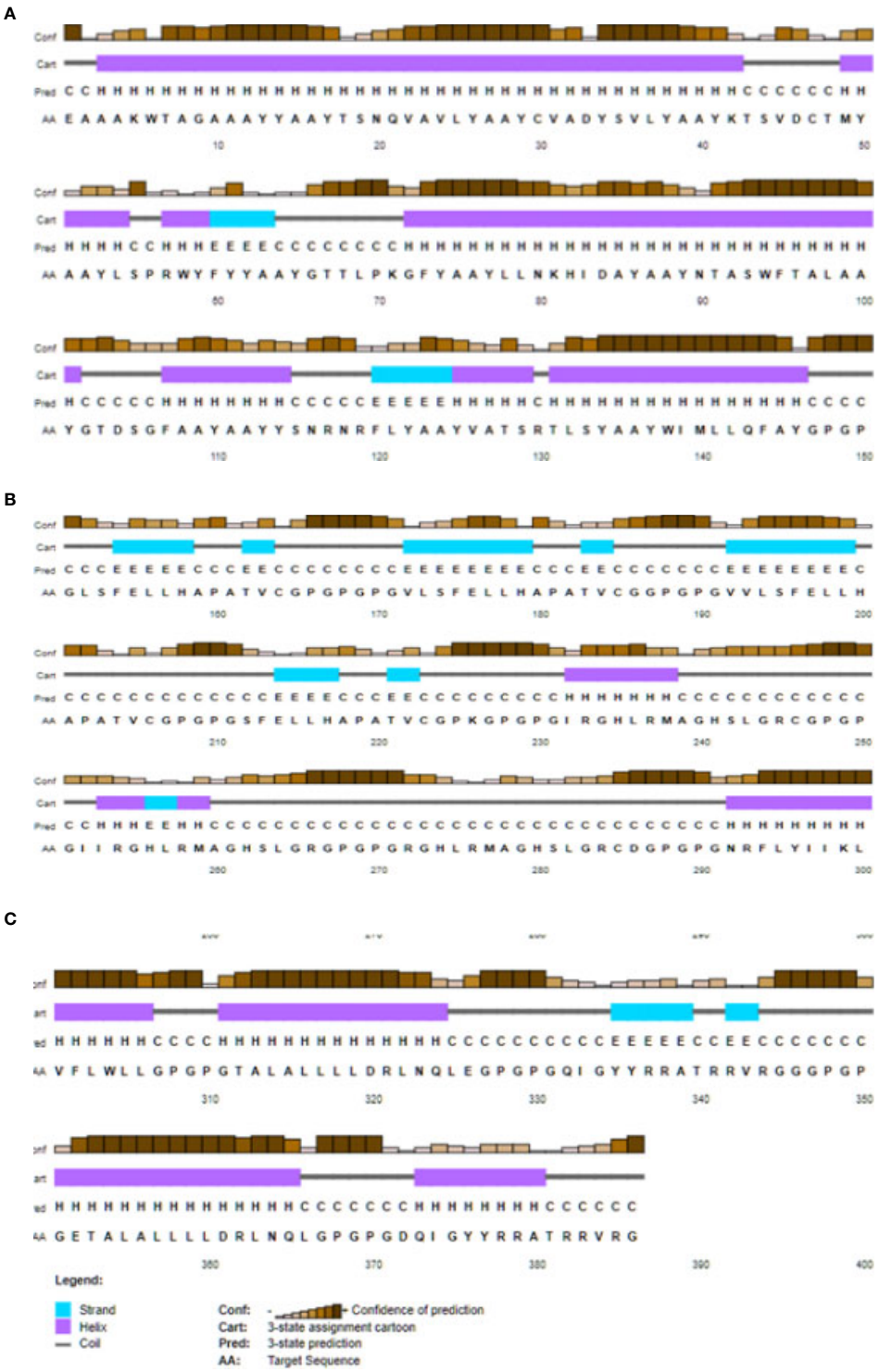


FIGURE 4
PSIPRED web tool predicted secondary structure elements Early predictions cantered on helix- or sheet-forming amino acids and free energy. 60% accurate residue (helix/sheet/coil) prediction. Multiple sequence alignment boosted accuracy to 80%; knowing amino acid distribution at a site (and in its surroundings) sharpens understanding of structural patterns there. Random coils may form in glycine-containing proteins.95% of homologous proteins have helix-favouring amino acids. Hydrophobicity may imply a -helix-compatible pattern of residue solvent accessibility. The secondary **(A)** represent the prediction model consisted of 47.2% α-helix, **(B)** 42.0% β-sheet, and **(C)** and 10.0% coils.

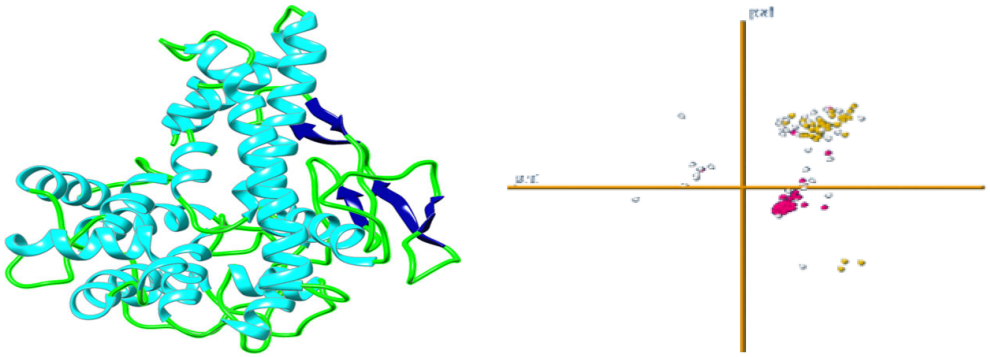


FIGURE 5
3D predicted tertiary structure of vaccine construct.

these interactions, however they can take many different forms. One sort of contact is represented by the formation of hydrogen bonds

By connecting existing atoms with dashed lines, hydrogen bonding is indicated. Hydrogen from the protein itself is used to connect the remaining atoms. In a similar way to the preceding one, an arc is also used to represent hydrophobic interactions, where an arc represents protein residues. The ligand atoms connected to these connections, on the other hand, are the focus of the light speakers' attention. Residues and receptors are both capable of developing interactions with one another. In addition to exhibiting different interactions, such as the interaction of hydrogen, ionic, and Vander Waals, residues and receptors also form π-π interactions.

Molecular dynamic simulation analysis

The "Fluctuation plot" tab oversees building a collaborative 2D structure that correctly displays the residual output seen in all MD simulations. This structure depicts the residual output in the appropriate manner. This tab can be found in the centre of the window's interface. Given that RMSF will take place later than the global position, it is reasonable to anticipate that there will be some variation in the value of this variable. A one-of-a-kind structure that is made up of a single chain is created as a result of the presence of several protein chains in a system. Monitoring the RMSD protein can offer information about the ordered structure of the protein across all of its mimics. This information can be useful in identifying potential problems.

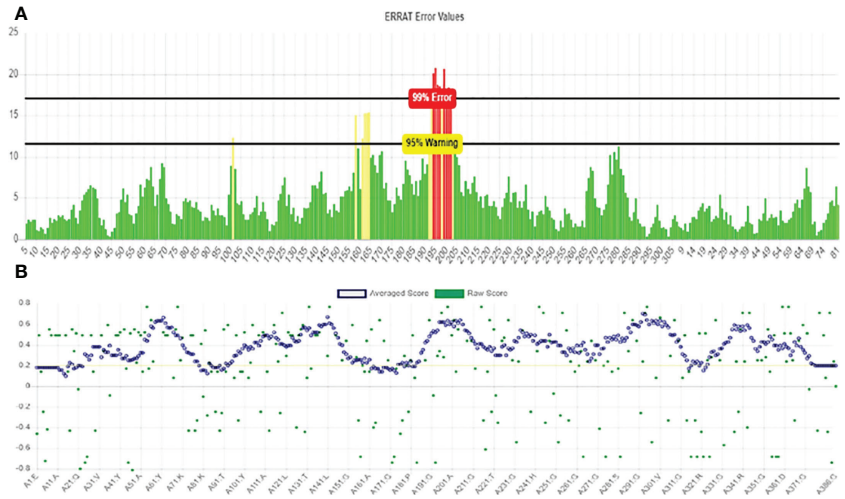


FIGURE 6
Verification of the vaccine construct model using **(A)** ERRAT plot for vaccine construct model and **(B)** Verify 3D results.

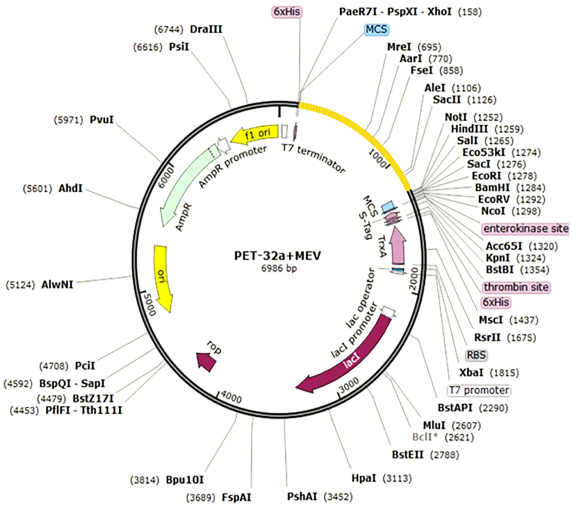


FIGURE 7
In silico cloning for adapted vaccine sequence into pET32a+MEV vector. Different epitopes of three proteins and merged it one sequence and then out sequence show this vector image. Our sequence is probably attached every clone vector.

This information may be helpful in determining the likelihood of certain problems. When it comes to relatively small proteins like those that can be found all over the world, it is not a problem at all to switch up the order of the first three locations.

A handy tool for reflecting local changes in the protein line is called the Rotated Root Factor, which is also commonly referred to as RMSF for its shorter form. It was determined that there were still some ACE2 and NSP3 receptors present

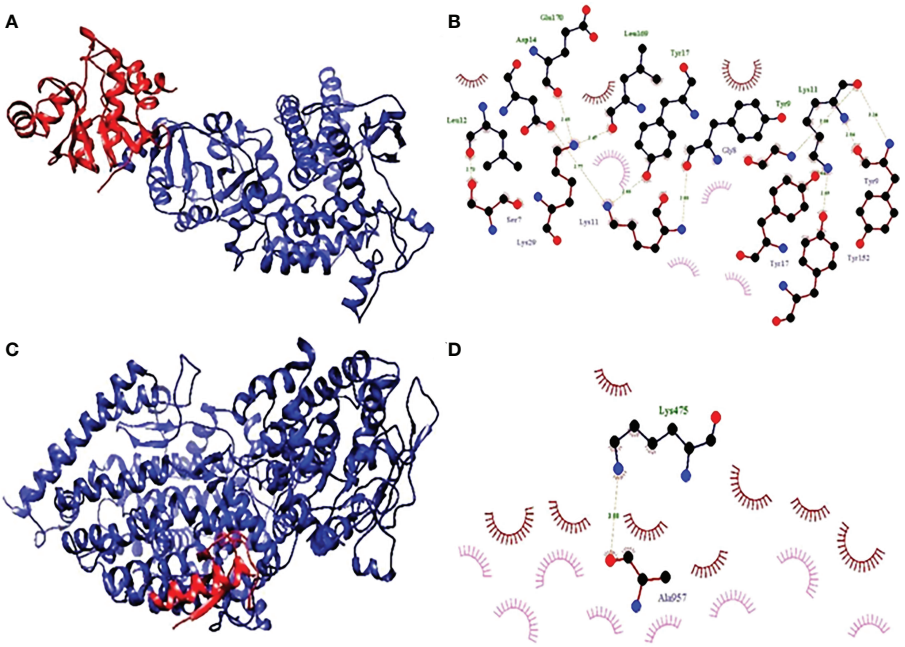


FIGURE 8
(A) Hydrophobicity and **(B)** interaction analysis of ACE3 with final vaccine construct. **(C)** Hydrophobicity and **(D)** interaction analysis of NSP3 with final vaccine construct.

because to the severity of the intermediate RMSF 2 that was discovered (Figure 9).

Discussion

The scientific field of bioinformatics makes use of a wide range of computer technology for the purposes of predicting genetic factors, measuring texts of a certain kind, protein structures, and cell-based locations. In a similar manner, diseases and cell mutations are related with the non-symptomatic features of the proteins that are impacted by the mutation. One example of how this approach might be put into practice is the prediction of a viable pharmacological formulation based on proteins that are engaged in the pathophysiological process of a certain sickness. Research that is centered on a sequential order is still yielding profitable results as of this moment in time about the examination of the possibilities for covid therapy (22). This is because there is now an abundance of data and information that can be easily accessed on the proteomes and genomes of a wide range of viruses. Because of this, vaccinations are built up entirely of peptides, and the creation of these peptides may be helped along by a broad range of bioinformatics techniques (23). However, even though the concept of a vaccination based on an epitope is already in its early phases of research for a range of infectious illnesses, it is still challenging to reach the goal of developing a SARS-COV-2 epitope vaccine.

Research that is based on sequential steps is still producing fruitful results in terms of exploring the potential applications of covid treatment at the present time. This is due to the wealth of data and information that is now readily available on the proteomes and genomes of a wide variety of viruses. The production of vaccines, which are made up entirely of peptides, is possible with the support of a wide variety of various bioinformatics techniques. Nevertheless, even though the idea of a vaccination based on an epitope is now in its early phases of research for a variety of infectious diseases, the development of a SARS-COV-2 epitope vaccine is still difficult to achieve. In the current research, an attempt is made to create an in-silico epitope vaccine for SARS-CoV2 that, ideally, will be successful in treating both illnesses at the same time. This is the goal of the research. It considers this to be a standard modification, which may be compared to the distribution of a low-volume vaccination containing *E. coli* to a select group of people. Considering this fact, we made the decision to carry out this experiment using the vaccination method to evaluate the efficacy of the vaccine protein, as well as its stability and the presence of significant amounts of *E. coli*. Specifically, we wanted to find out whether the protein could withstand the presence of *E. coli* (K12 type). By far the most frequent host strains for pDNA propagation are E. coli K-12 strains (40). To select the

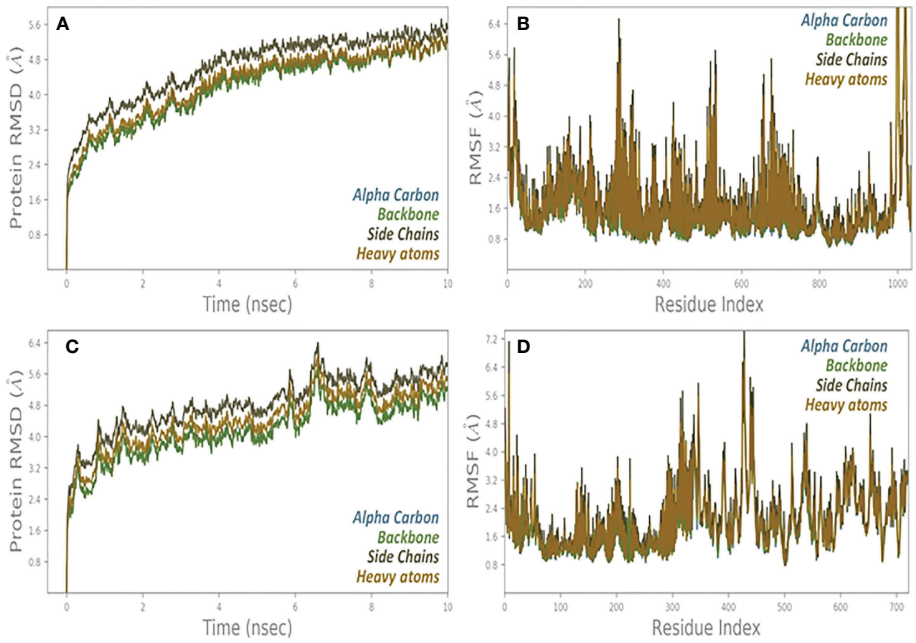


FIGURE 9
(A) RMSD and **(B)** RMSF analysis of MD simulation trajectories of vaccine complex with ACE2 receptor. **(C)** RMSD and **(D)** RMSF analysis of MD simulation trajectories of vaccine complex with NSP3 receptor.

best host strain for pDNA processing, depending on both the quality and quantity of supercoiling, the E. coli genotype is important (40).

The great majority of pDNA replications are carried out by *E. coli* K-12 strains, making them the most prevalent host strains (40). When looking for the best host strain for pDNA processing, it is critical to consider the genotype of the *E. coli* strain in question. When making this decision, you will need to consider both the level of supercoiling and its total quantity (40). In contrast, the use of complete agent-based studies examined the specific reaction when a drug sequence was introduced. The vaccine may be found to be non-allergenic, antigenic, safe, and can effectively control the coronavirus (24). By using clinical trials, it is still necessary to investigate the reliability and effectiveness of the vaccine. As such, this is mandatory to develop novel drugs in a very short time to find a way to control the possibility of progressively increasing diseases (25).

In addition, the physio-chemical properties of the vaccine were particularly evident in the use of the online prototype ProtParam, tested based on seven parameters, including half-life, aliphatic index and isoelectric point, molecular weight, instability index, *Grand Average of Hydropathicity* (GRAVY), and -coefficients of extinction. With an extinction coefficient of 7568 and an instability rating of 33.29, it's clear that this medicine is in a relatively stable state. Also, the highest value of the aliphatic index was seen (82.85), while the lowest value of the sub-unit vaccine, hydropathicity GRAVY, was seen (0.046). The estimated value of the aliphatic index represents a subunit vaccine designed for the high value of the aliphatic index, the higher the height. At the same time, the negative GRAVY value of the subunit input drug represents the status of the hydrophobic vaccine. Overall, a vaccine is designed for immunogenic, thermostable, and hydrophobic (12). The predicted higher education structure of the vaccine (Figure 5) showed that all the formed lines were in the allowed range. Therefore, showed that the available model structure represented a high-level model. This finding is a pivotal result because a high percentage of the remains were in the preferred location. Similarly, the probability points further confirmed the immunogenic findings and the validity of the proposed vaccine (26, 41).

Docking shows the binding position of the connecting molecule towards the receivers. The 3D structure of the vaccine and the receptors considered to be receptor molecules is shown in (Figure 8). The results or suspensions of the vessels showed excellent interaction of the last vaccine composed with receptor proteins. Chain protein receptors ACE2 and NSP3 showed interactions with the multi-epitope vaccine, as can be seen in (Figure 9). These statistics have shown that both the recipient chains and the vaccine chains are represented here in different colors on arrival. By the interaction between vaccine peptide residues and the amino acids ACE2 and NSP3 receptor protein. The chain's excellent binding location to the region that interacts with NSP3 and ACE2 suggests that it may be obstructing the interaction between the spike and ACE2 and blocking viral entrance into the host cells. It demonstrated a strong affinity for various SARS-CoV-2 structural and non-structural proteins (NSPs), which play a variety of roles in the life cycle of the virus. Significant binding of ACE2 with RdRp points to its function in preventing viral replication and, ultimately, virus proliferation. It demonstrated a strong affinity for various SARS-CoV-2 structural and non-structural proteins (NSPs), which play a variety of roles in the life cycle of the virus. Significant binding of ACE2 with RdRp points to its function in preventing viral replication and, ultimately, virus proliferation. The interaction that is depicted by LIGPLOT + is the interaction that is not only mediated by hydrophobic contacts but also by hydrogen bonds. This interaction takes place between two molecules. This is something that may be detected in the binding combination of active ACE2 residues and NSP3 receptors with multi-epitope immunization units that are compressed into a binding-protein packet. This is something that may be observed. Vaccines have the capacity to generate positive connections with ACE2 and NSP3 receptors, as demonstrated by the findings of this interaction analysis, which found that immunizations have this potential. The immunological response involves the participation of these receptors. This provides an explanation for why vaccinations have the potential to play a significant role in the case of covid-19. The time-dependent behavior of multi-epitope vaccines induced by ACE2 and NSP3 receptors modelled for 10-ns MD simulations to seek changes in the structures of both interacting particles adopted during simulation. The time-dependent behavior of multi-epitope vaccines induced by ACE2 and NSP3 receptors modelled for 10-ns MD simulations to seek changes in the structures of both interacting particles adopted during simulation. It was chief to understand enough changes to affect the binding of the construction on the fixed side. The epitope sequence was expressed in the body's immune system, to inform and build up immune responses. In thus study, two statistical parameters calculate for this program including RMSD and RMSF (Figure 9). RMSD measured the innate distance between the atomic nuclei of a large protein. The RMSD structure shows the RMSD protein emergence (left of the Y-axis). All independent frames align to the spinal cord of the frame, and then the RMSD is calculated based on the choice of atoms.

Conclusion

The COVID-19 epidemic is not only a health crisis, but also a global political, social, and economic crisis. The main goal of vaccine development is to develop a safe and effective vaccine that can reduce this fatal infection rate. The design of vacciome-based vaccines is relatively stable, reliable, fast, safe, expensive,

and effective. We predicted epitopes and collaborated with them to develop a multidisciplinary epitope vaccine. Our evaluation was based on an analysis of the structure of the individual receiving the vaccine and the inclusion of cells and the study of MD simulations. The structures of ACE2 and NSP3 were very stable in their natural function, with a strong concentration of cells around ten ns. Our target candidate can stimulate the immune system and immune system by providing that these B and T-cells are selected in the final vaccine formulation. By doing it all together, according to physicochemical tests and immunological analysis and formulation, this vaccine can reduce the rate of infection (SARS-COV-2).

Data availability statement

The original contributions presented in the study are included in the article/supplementary material. Further inquiries can be directed to the corresponding authors.

Author contributions

Conceptualization, MSK, IMK and SUA; methodology, IMK and ZA; software, SN and MZK; validation, YL, MSK and IMK; formal analysis, IR; investigation, YL; resources, YL; data curation, MSK; writing-original draft preparation, MSK; writing-review and editing, YL; IMK; visualization, SN; supervision, YL; project administration, YL. All authors contributed to the article and approved the submitted version.

Funding

Industry-University-Research Project of Fuyang Normal University (HX2021027000 and HX2022048000) funded this work.

Acknowledgments

Princess Nourah bint Abdulrahman University Researchers Supporting Project number (PNURSP2023R179), Princess Nourah bint Abdulrahman University, Riyadh, Saudi Arabia.

Conflict of interest

The authors declare that the research was conducted in the absence of any commercial or financial relationships that could be construed as a potential conflict of interest.

Publisher's note

All claims expressed in this article are solely those of the authors and do not necessarily represent those of their affiliated organizations, or those of the publisher, the editors and the reviewers. Any product that may be evaluated in this article, or claim that may be made by its manufacturer, is not guaranteed or endorsed by the publisher.

References

1. Chen N, Zhou M, Dong X, Qu J, Gong F, Han Y, et al. Epidemiological and clinical characteristics of 99 cases of 2019 novel coronavirus pneumonia in wuhan, China: a descriptive study. *Lancet* (2020) 395(10223):507–13. doi: 10.1016/S0140-6736(20)30211-7

2. Kumar N, Singh A, Grover S, Kumari A, Kumar Dhar P, Chandra R, et al. HHV-5 epitope: A potential vaccine candidate with high antigenicity and large coverage. *J Biomolecular Structure Dynamics* (2019) 37(8):2098–109. doi: 10.1080/07391102.2018.1477620

3. Kumar N, Sood D, Chandra R. Design and optimization of a subunit vaccine targeting COVID-19 molecular shreds using an immunoinformatics framework. *RSC Adv* (2020) 10(59):35856–72. doi: 10.1039/D0RA06849G

4. Zhao J, Falcón A, Zhou H, Netland J, Enjuanes L, Pérez Breña P, et al. Severe acute respiratory syndrome coronavirus protein 6 is required for optimal replication. *J Virol* (2009) 83(5):2368–73. doi: 10.1128/JVI.02371-08

5. Kumar N, Sood D, Sharma N, Chandra R. Multiepitope subunit vaccine to evoke immune response against acute encephalitis. *J Chem Inf Modeling* (2020) 60 (1):421–33. doi: 10.1021/acs.jcim.9b01051

6. Liang JQ, Fang S, Yuan Q, Huang M, Chen RA, Fung TS, et al. N-linked glycosylation of the membrane protein ectodomain regulates infectious bronchitis virus-induced ER stress response, apoptosis and pathogenesis. *Virology* (2019) 531:48–56. doi: 10.1016/j.virol.2019.02.017

7. Branco ACCC, Sato MN, Alberca RW. The possible dual role of the ACE2 receptor in asthma and coronavirus (SARS-CoV2) infection. *Front Cell infection Microbiol* (2020) 10:550571. doi: 10.3389/fcimb.2020.550571

8. Tan YW, Fung TS, Shen H, Huang M, Liu DX. Coronavirus infectious bronchitis virus non-structural proteins 8 and 12 form stable complex independent of the non-translated regions of viral RNA and other viral proteins. *Virology* (2018) 513:75–84. doi: 10.1016/j.virol.2017.10.004

9. Santos RA, Ferreira AJ, Simões e Silva AC. Recent advances in the angiotensin-converting enzyme 2–angiotensin (1–7)–Mas axis. *Exp Physiol* (2008) 93(5):519–27. doi: 10.1113/expphysiol.2008.042002

10. Jia HP, Look DC, Shi L, Hickey M, Pewe L, Netland J, et al. ACE2 receptor expression and severe acute respiratory syndrome coronavirus infection depend on differentiation of human airway epithelia. *J Virol* (2005) 79(23):14614–21. doi: 10.1128/JVI.79.23.14614-14621.2005

11. Imbert I, Snijder EJ, Dimitrova M, Guillemot J-C, Lécine P, Canard B. The SARS-coronavirus PLnc domain of nsp3 as a replication/transcription scaffolding protein. *Virus Res* (2008) 133(2):136–48. doi: 10.1016/j.virusres.2007.11.017

12. Ahmad SU, Kiani BH, Abrar M, Jan Z, Zafar I., Ali Y, et al. A comprehensive genomic study, mutation screening, phylogenetic and statistical analysis of SARS-CoV-2 and its variant omicron among different countries. *J Infect Public Health* (2022) 15(8):878–91. doi: 10.1016/j.jiph.2022.07.002

13. Nicholson B, Leach CA, Goldenberg SJ, Francis DM, Kodrasov MP, Tian X, et al. Characterization of ubiquitin and ubiquitin-like-protein isopeptidase activities. *Protein Sci* (2008) 17(6):1035–43. doi: 10.1110/ps.083450408

14. Kanjanahaluethai A, Chen Z, Jukneliene D, Baker SC. Membrane topology of murine coronavirus replicase nonstructural protein 3. *Virology* (2007) 361 (2):391–401. doi: 10.1016/j.virol.2006.12.009

15. Kumar N, Admane N, Kumari A, Sood D, Grover S, Prajapati VK, et al. Cytotoxic T-lymphocyte elicited vaccine against SARS-CoV-2 employing immunoinformatics framework. *Sci Rep* (2021) 11(1):7653. doi: 10.1038/s41598-021-86986-6

16. Agarwal D, Zafar I, Ahmad SU, Kumar S, Sundaray JK, Rather MA, et al. Structural, genomic information and computational analysis of emerging coronavirus (SARS-CoV-2). *Bull Natl Res Cent.* (2022) 46(1):1–16. doi: 10.1186/s42269-022-00861-6

17. Kumar N, Sood D, Chandra R. Vaccine formulation and optimization for human herpes virus-5 through an immunoinformatics framework. *ACS Pharmacol Trans Sci* (2020) 3(6):1318–29. doi: 10.1021/acsptsci.0c00139

18. Khan M, Khan S, Ali A, Akbar H, Sayaf AM, Khan A, et al. Immunoinformatics approaches to explore helicobacter pylori proteome (Virulence factors) to design b and T cell multi-epitope subunit vaccine. *Sci Rep* (2019) 9(1):1–13. doi: 10.1038/s41598-019-49354-z

19. Zafar I, Iftikhar R, Ahmad SU, Rather MA. Genome wide identification, phylogeny, and synteny analysis of sox gene family in common carp (Cyprinus carpio). *Biotechnol Rep* (2021) 30:e00607. doi: 10.1016/j.btre.2021.e00607

20. Khan S, Khan A, Rehman AU, Ahmad I, Ullah S, Khan AA, et al. Immunoinformatics and structural vaccinology driven prediction of multi-epitope vaccine against mayaro virus and validation through in-silico expression. *Infect Genet Evol* (2019) 73:390–400. doi: 10.1016/j.meegid.2019.06.006

21. Khan S, Ali SS, Zaheer I, Saleem S, Ziaullah, Zaman N, et al. Proteome-wide mapping and reverse vaccinology-based b and T cell multi-epitope subunit vaccine designing for immune response reinforcement against porphyromonas gingivalis. *J Biomolecular Structure Dynamics* (2022) 40(2):833–47. doi: 10.1080/07391102.2020.1819423

22. Gul H, Ali SS, Saleem S, Khan S, Khan J, Wadood A, et al. Subtractive proteomics and immunoinformatics approaches to explore bartonella bacilliformis proteome (virulence factors) to design b and T cell multi-epitope subunit vaccine. *Infect Genet Evol* (2020) 85:104551. doi: 10.1016/j.meegid.2020.104551

23. Larsen MV, Lundegaard C, Lamberth K, Buus S, Lund O, Nielsen M. Large-Scale validation of methods for cytotoxic T-lymphocyte epitope prediction. *BMC Bioinf* (2007) 8(1):1–12. doi: 10.1186/1471-2105-8-424

24. Saha S, Raghava GPS. Prediction of continuous b-cell epitopes in an antigen using recurrent neural network. *Proteins: Structure Function Bioinf* (2006) 65 (1):40–8. doi: 10.1002/prot.21078

25. Ponomarenko J, Bui H-H, Li W, Fusseder N, Bourne PE, Sette A, et al. ElliPro: a new structure-based tool for the prediction of antibody epitopes. *BMC Bioinf* (2008) 9(1):1–8. doi: 10.1186/1471-2105-9-514

26. Doytchinova IA, Flower DR. VaxiJen: a server for prediction of protective antigens, tumour antigens and subunit vaccines. *BMC Bioinf* (2007) 8(1):1–7. doi: 10.1186/1471-2105-8-4

27. Bashir Z, Ahmad SU, Kiani BH, Jan Z, Khan N, Khan U, et al. Immunoinformatics approaches to explore B and T cell epitope-based vaccine designing for SARS-CoV-2 Virus. *Pak J Pharm Sci* (2021) 34.

28. McGuffin LJ, Bryson K, Jones DT. The PSIPRED protein structure prediction server. *Bioinformatics* (2000) 16(4):404–5. doi: 10.1093/bioinformatics/16.4.404

29. Kim DE, Chivian D, Baker D. Protein structure prediction and analysis using the robetta server. *Nucleic Acids Res* (2004) 32(suppl_2):W526–31. doi: 10.1093/nar/gkh468

30. Heo L, Park H, Seok C. GalaxyRefine: Protein structure refinement driven by side-chain repacking. *Nucleic Acids Res* (2013) 41(W1):W384–8. doi: 10.1093/nar/gkt458

31. Eisenberg D, Lüthy R, Bowie J. VERIFY3D: assessment of protein models with three-dimensional profiles. *Methods Enzymology* (1997) 10:396–404. doi: 10.1016/S0076-6879(97)77022-8

32. Kozakov D, Hall DR, Xia B, Porter KA, Padhorny D, Yueh C, et al. The ClusPro web server for protein–protein docking. *Nat Protoc* (2017) 12(2):255–78. doi: 10.1038/nprot.2016.169

33. Rani I, Kalsi A, Kaur G, Sharma P, Gupta S, Gautam RK, et al. Modern drug discovery applications for the identification of novel candidates for COVID-19 infections. *Ann Med Surg* (2022) 104125. doi: 10.1016/j.amsu.2022.104125

34. Doherty B, Zhong X, Gathiaka S, Li B, Acevedo O. Revisiting OPLS force field parameters for ionic liquid simulations. *J Chem Theory Comput* (2017) 13 (12):6131–45. doi: 10.1021/acs.jctc.7b00520

35. Kräutler V, Van Gunsteren WF, Hünenberger PH. A fast SHAKE algorithm to solve distance constraint equations for small molecules in molecular dynamics simulations. *J Comput Chem* (2001) 22(5):501–8. doi: 10.1002/1096-987X(20010415)22:5<501::AID-JCC1021>3.0.CO;2-V

36. Tuckerman M, Berne BJ, Martyna GJ. Reversible multiple time scale molecular dynamics. *J Chem Phys* (1992) 97(3):1990–2001. doi: 10.1063/1.463137

37. Evans DJ, Holian BL. The nose–hoover thermostat. *J Chem Phys* (1985) 83 (8):4069–74. doi: 10.1063/1.449071

38. Martyna GJ, Tobias DJ, Klein ML. Constant pressure molecular dynamics algorithms. *J Chem Phys* (1994) 101(5):4177–89. doi: 10.1063/1.467468

39. Mahajan S, Kode V, Bhojak K. Immunodominant T-cell epitopes from the SARS-CoV-2 spike antigen reveal robust pre-existing T-cell immunity in unexposed individuals. *Sci Rep* (2022) 11:13164. doi: 10.1038/s41598-021-92521-4

40. Hayashi K, Morooka N, Yamamoto Y, Choi S, Ohtsubo E, Baba T, et al. Highly accurate genome sequences of the Escherichia coli K-12 strains MG1655 and W3110. *Mol Syst Biol* (2006). doi: 10.1038/msb4100049

41. Ahmad SU, Khan MS, Jan Z, Khan N, Ali A, Rehman N, et al. Genome wide association study and phylogenetic analysis of novel SARS-COV-2 virus among different countries. *Pak J Pharm Sci* (2021) 34 (4).

frontiers | Frontiers in Immunology

TYPE Original Research
PUBLISHED 09 February 2023
DOI 10.3389/fimmu.2023.1123724

Check for updates

OPEN ACCESS

EDITED BY
Silvia Piconese,
Sapienza University of Rome, Italy

REVIEWED BY
Antonino Cassotta,
Institute for Research in Biomedicine (IRB), Switzerland
Kyra Zens,
University of Zurich, Switzerland

*CORRESPONDENCE
Sara De Biasi
sara.debiasi@unimore.it

†These authors share senior authorship

SPECIALTY SECTION
This article was submitted to T Cell Biology, a section of the journal Frontiers in Immunology

RECEIVED 14 December 2022
ACCEPTED 23 January 2023
PUBLISHED 09 February 2023

CITATION
Lo Tartaro D, Paolini A, Mattioli M, Swatler J, Neroni A, Borella R, Santacroce E, Di Nella A, Gozzi L, Busani S, Cuccorese M, Trenti T, Meschiari M, Guaraldi G, Girardis M, Mussini C, Piwocka K, Gibellini L, Cossarizza A and De Biasi S (2023) Detailed characterization of SARS-CoV-2-specific T and B cells after infection or heterologous vaccination. *Front. Immunol.* 14:1123724. doi: 10.3389/fimmu.2023.1123724

COPYRIGHT
© 2023 Lo Tartaro, Paolini, Mattioli, Swatler, Neroni, Borella, Santacroce, Di Nella, Gozzi, Busani, Cuccorese, Trenti, Meschiari, Guaraldi, Girardis, Mussini, Piwocka, Gibellini, Cossarizza and De Biasi. This is an open-access article distributed under the terms of the Creative Commons Attribution License (CC BY). The use, distribution or reproduction in other forums is permitted, provided the original author(s) and the copyright owner(s) are credited and that the original publication in this journal is cited, in accordance with accepted academic practice. No use, distribution or reproduction is permitted which does not comply with these terms.

Detailed characterization of SARS-CoV-2-specific T and B cells after infection or heterologous vaccination

Domenico Lo Tartaro[1], Annamaria Paolini[1], Marco Mattioli[1], Julian Swatler[1,2], Anita Neroni[1], Rebecca Borella[1], Elena Santacroce[1], Alessia Di Nella[1], Licia Gozzi[3], Stefano Busani[4,5], Michela Cuccorese[6], Tommaso Trenti[6], Marianna Meschiari[3], Giovanni Guaraldi[3,4], Massimo Girardis[4,5], Cristina Mussini[3,4], Katarzyna Piwocka[2], Lara Gibellini[1], Andrea Cossarizza[1,7†] and Sara De Biasi[1*†]

[1]Department of Medical and Surgical Sciences for Children and Adults, University of Modena and Reggio Emilia School of Medicine, Modena, Italy, [2]Laboratory of Cytometry, Nencki Institute of Experimental Biology, Warsaw, Poland, [3]Infectious Diseases Clinics, Azienda Ospedaliero-Universitaria (AOU) Policlinico di Modena, Modena, Italy, [4]Department of Surgery, Medicine, Dentistry and Morphological Sciences, University of Modena and Reggio Emilia, Modena, Italy, [5]Department of Anesthesia and Intensive Care, Azienda Ospedaliero-Universitaria (AOU) Policlinico and University of Modena and Reggio Emilia, Modena, Italy, [6]Department of Laboratory Medicine and Pathology, Diagnostic Hematology and Clinical Genomics, Azienda Unità Sanitaria Locale AUSL/AOU Policlinico, Modena, Italy, [7]National Institute for Cardiovascular Research, Bologna, Italy

The formation of a robust long-term antigen (Ag)-specific memory, both humoral and cell-mediated, is created following severe acute respiratory syndrome coronavirus 2 (SARS-CoV-2) infection or vaccination. Here, by using polychromatic flow cytometry and complex data analyses, we deeply investigated the magnitude, phenotype, and functionality of SARS-CoV-2-specific immune memory in two groups of healthy subjects after heterologous vaccination compared to a group of subjects who recovered from SARS-CoV-2 infection. We find that coronavirus disease 2019 (COVID-19) recovered patients show different long-term immunological profiles compared to those of donors who had been vaccinated with three doses. Vaccinated individuals display a skewed T helper (Th)1 Ag-specific T cell polarization and a higher percentage of Ag-specific and activated memory B cells expressing immunoglobulin (Ig)G compared to those of patients who recovered from severe COVID-19. Different polyfunctional properties characterize the two groups: recovered individuals show higher percentages of $CD4^+$ T cells producing one or two cytokines simultaneously, while the vaccinated are distinguished by highly polyfunctional populations able to release four molecules, namely, CD107a, interferon (IFN)-γ, tumor necrosis factor (TNF), and interleukin (IL)-2. These data suggest that functional and phenotypic properties of SARS-CoV-2 adaptive immunity differ in recovered COVID-19 individuals and vaccinated ones.

KEYWORDS

SARS-CoV-2, antigen-specific response, polyfunctionality, T cells, B cells, cytokine

Introduction

Memory is the main characteristic of the immune system, being at the basis of its efficacy and functionality, and indeed the activation of secondary response is the crucial strategy utilized by vaccination. Natural infection and vaccines induce the formation and subsequent expansion of antigen (Ag)-specific cells that can block pathogens as soon as they try to invade the host. The creation of a pool of long-living memory T and B cells able to respond to future *stimuli* is crucial for vaccine efficacy, as well as the plasma level of antibodies (1).

During natural infection, typically after a couple of weeks, the magnitude of the severe acute respiratory syndrome coronavirus 2 (SARS-CoV-2)-specific $CD4^+$ and $CD8^+$ memory T-cell response peaks at the maximum and is of the order of 0.5% and 0.2% of the repertoire, respectively (2). $CD4^+$ T cells display a memory profile (including a specific subset formed by stem cell memory) and are able to produce high levels of both IL-2 and T helper (Th)1 cytokines (3–5). $CD4^+$ T-cell response is greater than the $CD8^+$ counterpart (2). Robust immunity is certainly maintained by more than 6 months, but the duration of SARS-CoV-2-specific T cells could depend also on the clinical severity of the initial infection (6). Long-lived T-cell responses and efficient response to SARS-CoV-2 are characterized by a $CD45RA^+$ effector-memory phenotype and a potent activation of the interferon (IFN) transcriptomic signature whose magnitude is largely due to the genetic background of the host (7–10).

Regarding B-cell response, which is highly altered during coronavirus disease 2019 (COVID-19) (11), in the plasma of most individuals, anti-SARS-CoV-2 antibodies (Abs) persist for more than 6 months after primary infection, but some patients rapidly lose their specific Abs (6, 12, 13). However, specific memory B cells (MBCs) predominantly express immunoglobulin $(Ig)M^+$ or $IgG1^+$ and rise until 150 days after infection (14), regardless of age (15). Receptor-binding domain (RBD)-specific IgG^+ MBCs are predominantly $CD27^+$, and their number significantly correlates with circulating follicular helper T-cell numbers (14).

Vaccination against SARS-CoV-2 induces a robust specific immune response. $CD8^+$ T-cell response can be detected as early as 11 days after the first vaccination (16), and such cells can recognize immunodominant peptides from ORF1ab (17). Two-dose vaccination with BNT162b2 leads to strong generation of virus-specific $CD4^+$ T-cell responses with a Th1 profile, and it is detectable 6 months after vaccination (18–21). Spike-specific antibodies peak after 7 days, and titers and *Angiotensin-converting enzyme 2* (ACE2)/RBD binding-inhibiting activity is still observed after 6 months, despite a progressive decline over time. Concomitant to antibody reduction, spike-specific MBCs, mostly switched to IgG, increase and persist 6 months after vaccination (22). T-cell responses after vaccination are of similar magnitude to those seen after natural infection, although they seem to be more differentiated with the presence of T stem cell memory (T_{SCM}) subsets (23). An adenovirus-based vaccine generates a higher magnitude of spike-specific T cells (24, 25), while mRNA vaccines develop higher antibody titers. For this reason, heterologous vaccines have been used in clinical practice (26, 27).

As vaccination and natural infection increase across the world, there is growing interest in predicting the risk of primary infection or reinfection. Observational and limited comparison between natural and vaccine-induced immunity showed that the protection against SARS-CoV-2 infection was significantly higher in COVID-19 recovered individuals if compared to that of those vaccinated who additionally received a booster vaccine (28). Antibodies decline more rapidly following vaccination in naive individuals than those in individuals who have recovered from COVID-19, but they display the same frequencies of spike-specific B and $CD4^+$ T cells at 8 months after vaccination (29). However, besides the magnitude of the spike-specific antibody response or neutralizing titer, the percentage, phenotypic identity, and functional profile of specific cellular immune responses have not been taken into account as immune correlates of protection.

Here, by using high-parameter polychromatic flow cytometry and sophisticated data analyses, we deeply investigated the magnitude, phenotype, and functionality of SARS-CoV-2–specific immune memory in two groups of healthy subjects after heterologous vaccination compared to those of a group of subjects who recovered from SARS-CoV-2 infection.

Results

Study design

Three groups of donors were enrolled in this study. The first one was composed of nine COVID-19 recovered patients (hereafter called REC; mean age of 35.1 ± 11.1 years), with a mean of 131.1 days (range 64–165 days) from last infection during follow-up visits at the Infectious Diseases Clinics of the Azienda Ospedaliero-Universitaria Policlinico di Modena. All REC had symptoms consistent with COVID-19 and positive PCR-based testing for SARS-CoV-2 over the period of March 2020–August 2020. Within this group, four patients were classified as severe (35.3 ± 5.68 years) while five patients were moderate (35.0 ± 7.4) according to World Health Organization guidelines (30). Given that there were no differences between moderate and severe recovered individuals and their low number, they were considered as a unique group for the statistical analysis. Twenty-three vaccinated donors were enrolled in this study, and they were divided into two groups: one was composed of 11 donors with a mean of 31.1 days (range 30–35 days) after the third dose of SARS-CoV-2 vaccine (hereafter defined MIX; 27.0 ± 4.5 years); these subjects were vaccinated with three different vaccines (first dose: ChAdOx1; second dose: BNT162b2; third dose: mRNA-1273). The second group was composed of 12 donors with a mean of 33.9 days (range 26–44 days, hereafter defined RNA; 35.3 ± 11.3 years) after being vaccinated with two different RNA vaccines (first and second doses: BNT162b2; third dose: mRNA-1273). Each participant, including healthy donors, provided informed consent according to the Helsinki Declaration, and all uses of human material have been approved by the local Ethics Committee (Comitato Etico dell'Area Vasta Emilia Nord, protocol number 177/2020, 11 March 2020) and by the University Hospital Committee (Direzione Sanitaria dell'Azienda Ospedaliero Universitaria di Modena, protocol number 7531, 11 March 2020). The clinical characteristics of all participants are reported in Table 1 and in the *Methods* section.

MIX showed a skewed Th1 Ag-specific $CD4^+$ T-cell polarization compared to that of recovered ones

To investigate the percentage of Ag-specific T cells, we used T-cell receptor (TCR)-dependent activation-induced marker (AIM) assays to identify and quantify SARS-CoV-2-specific $CD4^+$ T cells (31–34). We

10.3389/fimmu.2023.1123724

TABLE 1 Demographic and clinical characteristics of COVID-19 recovered patients and vaccinated donors.

Variable	REC (n=9)	MIX (n=11)	RNA (n=12)	p-value (REC*vs*MIX)	p-value (REC*vs*RNA)	p-value (MIX*vs*RNA)
Demographic characteristics						
Age (mean years, range)[1]	35.1 (22.0-41.0)	27.0 (22.0-39.0)	35.3 (23.0-62.0)	0.0177	ns	ns
Sex (Male, %)[2]	88.9	27.3	45.5	0.0098	ns	ns
Race/Ethnicity						
White: Non-Hispanic or Latino (%)[3]	66.7	100	100	ns	ns	ns
White: Hispanic or Latino (%)[3]	11.1	0	0	/	/	/
Black (%)[3]	22.2	0	0	/	/	/
Hospitalization status						
Never hospitalized (%)	11.1	/	/	/	/	/
Hospitalized (%)	88.9	/	/	/	/	/
Days of hospitalization (mean days, range)	11.6 (4.0-17.0)	/	/	/	/	/
Sample Collection						
Sample Collection Dates	March 2020-August 2020	December 2021-January 2022	December 2021-January 2022	/	/	/
Days post symptom onset or third dose vaccine (mean days, range) [1]	131.1 (64.0-165.0)	31.8 (30.0-35.0)	33.9 (26.0-44.0)	0.0004	0.0009	ns
Disease Severity						
Moderate (%)	55.6% (5/9)	/	/	/	/	/
Severe (%)	44.4% (4/9)	/	/	/	/	/
Vaccine type						
First dose	/	ChAdOx1	BNT162b2	/	/	/
Second dose	/	BNT162b2	BNT162b2	/	/	/
Third dose	/	mRNA-1273	mRNA-1273	/	/	/
Detection of SARS-CoV-2 IgG						
IgG, Index mean value AU/mL (± SD)[1]	1,344.2 (±663.4)	12,205.4 (±9,457.4)	6,422.1 (±2,496.1)	0.0001	0.0011	ns

[1]Kruskal-Wallis test with Original FDR methods of Benjamini and Hochberg;
[2]Fisher's exact test;
[3]Chi-squared test;
ns, not significant; SD, standard deviation; AU, arbitrary unit.

stimulated peripheral blood mononuclear cells (PBMCs) from nine REC patients and 11 MIX and 12 RNA donors overnight with 15-mer peptides with 11-amino acid overlap, covering the complete sequence of Wuhan SARS-CoV-2 spike glycoprotein (see *Methods* for details).

The phenotype of Ag-specific T cells (i.e., those $CD137^+CD69^+$) within $CD4^+$ T cells, hereafter termed Ag^+CD4^+ T cells, was first analyzed by manual gating and compared with the non-Ag-specific $CD4^+$ T cell counterparts ($CD137^-CD69^-$, hereafter called Ag^-CD4^+). Ag^+CD4^+ T cells showed different cell subset distributions (in terms of the expression of differentiation markers such as CD45RA, CCR7, CD28, and CD95) and Th cell polarization (evaluated by the expression of CCR6 and CXCR3). Ag^+CD4^+ T displayed a low percentage of naive (N, $CD45RA^+CCR7^+CD28^+CD95^-$) and higher frequencies of memory compartment such as central memory (CM; $CD45RA^-CCR7^+CD28^+CD95^+$), transitional memory (TM; $CD45RA^-CCR7^-CD28^+CD95^+$), effector memory (EM; $CD45RA^-CCR7^-CD28^-CD95^+$), and T_{SCM} ($CD45RA^+CCR7^+CD28^+CD95^+$) and a similar percentage of terminally differentiated effector memory (EMRA; $CD45RA^+CCR7^-CD28^-CD95^+$) (Supplementary Figures S1A, B). Considering T-cell polarization, in comparison with Ag^-CD4^+ T cells, those Ag-specific displayed a higher percentage of Th1 ($CXCR3^+CCR6^-$), Th17 ($CXCR3^-CCR6^+$), and Th1/Th17 (CXCR3+CCR6+) and a lower percentage of Th0/Th2 ($CXCR3^-CCR6^-$) (Supplementary Figure S1C).

To gain a more detailed overview on the differentiation status and Th-polarization, we took advantage of unsupervised FlowSOM clustering. This analysis revealed a total of 19 clusters, and within these, six clusters represented SARS-CoV-2-reactive $CD4^+$ T cells expressing CD69 and CD137 (Figures 1A, B; Supplementary Figure S2).

The frequencies of the different clusters of T cells within Ag^-CD4^+ T cells were similar in the three groups of individuals as

10.3389/fimmu.2023.1123724

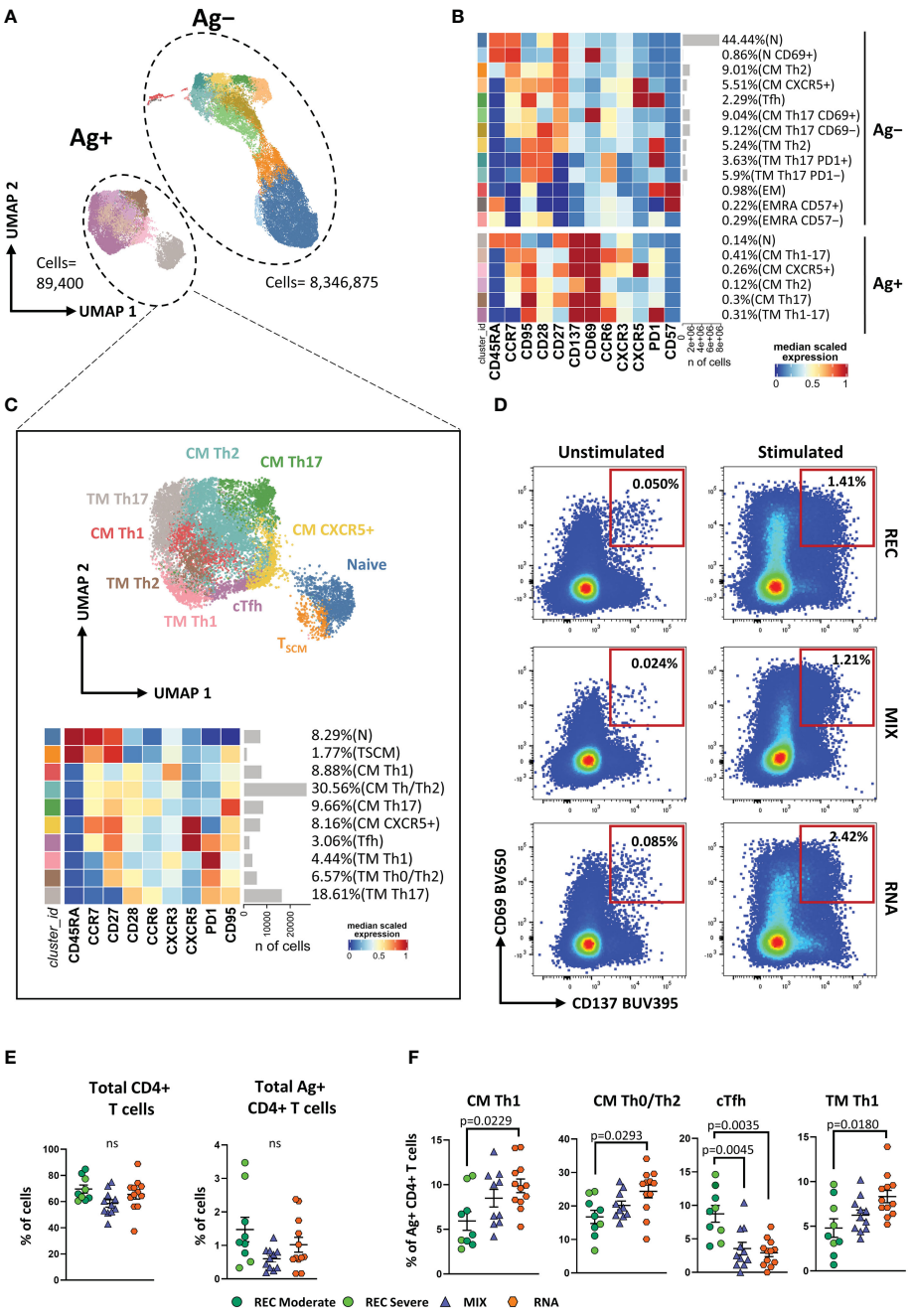


FIGURE 1
Immune phenotyping of antigen-specific CD4$^+$ T cells. **(A)** Uniform Manifold Approximation and Projection (UMAP) plot shows the 2D spatial distribution of 8,436,275 cells from nine donors who recovered from SARS-CoV-2 infection (REC, severe = 4 and moderate = 5) and 23 vaccinated donors (MIX = 11 and RNA = 12) embedded with FlowSOM clusters. Ag$^+$, antigen-specific CD4$^+$ T cells; Ag$^-$, non-antigen-specific CD4$^+$ T cells. **(B)** Heatmap of the median marker intensities of the 12 lineage markers across the 19 cell populations obtained with FlowSOM algorithm after the manual metacluster merging. The colors of cluster_id column correspond to the colors used to label the UMAP plot clusters. The color in the heatmap is referred to the median of the *arcsinh* marker expression (0–1 scaled) calculated over cells from all of the samples. Blue represents lower expression, while red represents higher expression. Light gray bar along the rows (clusters) and values in brackets indicate the relative sizes of the clusters. N, naive; T_{SCM}, T stem cell memory; CM, central memory; TM, transitional memory; EM, effector memory; EMRA, effector memory reexpressing the CD45RA; cTfh, circulating T follicular helper cells. The black bar on the right is used to group Ag$^+$ or Ag$^-$ subpopulations. **(C)** UMAP and heatmap visualization of 10 manually merged antigen-specific CD4$^+$ T-cell clusters. **(D)** Representative dot plots showing manual gating analysis of Ag-specific (CD137$^+$CD69$^+$) CD4$^+$ T cells after overnight stimulation with spike protein compared to unstimulated control [activation-induced marker assay (AIM assay)]. Numbers in the dot plots indicate the percentage of cells identified by manual gating. **(E)** Dot plots show the total percentage of antigen-specific CD4$^+$ T cells. Kruskal–Wallis test with Benjamini–Hochberg correction for multiple comparisons was used to test the differences among the three groups. **(F)** Dot plots show the cell percentage of the antigen-specific CD4$^+$ T cells. The central bar represents the mean ± SEM. Generalized linear mixed model (GLMM) test was used for the statistical analysis. Adjusted P-values are reported in the figure. ns, not significant.

shown in Supplementary Figure S3. We focused our attention on Ag^+CD4^+ T cells that were selected and reclustered. We obtained 10 clusters, representing different subpopulations of Ag^+ T cells. We found naive T cells that were defined as $CD45RA^+CCR7^+CD27^+CD95^-$, T_{SCM} as $CD45RA^+CCR7^+CD27^+CD95^+$, CM Th1 as $CCR7^+CD45RA^-CCR6^-CXCR3^+$ (CM Th1), CM Th0/Th2 as $CCR7^+CD45RA^-CCR6^-CXCR3^-$, CM Th17 as $CCR7^+CD45RA^-CCR6^+CXCR3^-$, CM $CXCR5^+$ as $CCR7^+CD45RA^-CXCR5^+PD\text{-}1^-$, circulating T follicular helper as $CCR7^+CD45RA^-CXCR5^+PD\text{-}1^+$ (cTfh), TM Th1 as $CCR7^-CD45RA^-CD28^+CXCR3^+$ (TM Th1), TM Th0/Th2 as $CCR7^-CD45RA^-CD28^+CCR6^-CXCR3^-$, and TM Th17 as $CCR7^-CD45RA^-CD28^+CCR6^+CXCR3^-$(Figure 1C).

The percentage of total $CD4^+$ and Ag^+ $CD4^+$ T cells was similar among the three groups (Figures 1D, E). Despite that, within the latter, we observed a different distribution of the populations among REC and vaccinated groups (both MIX and RNA). RNA displayed higher percentages of CM Th1, CM Th0/Th2, and TM Th1 if compared to those in REC subjects. Moreover, both MIX and RNA showed a lower percentage of cTfh cells (Figure 1F). No differences were found between Ag^+CD4^+ T-cell clusters of MIX and RNA. Similar percentages of all other clusters were present in REC, MIX, and RNA subjects (Supplementary Figure S4).

Vaccinated individuals showed a higher percentage of Tc1-like Ag-specific $CD8^+$ T cells compared to that of recovered subjects

The AIM assay was used for $CD8^+$ T-cell analysis to identify and quantify SARS-CoV-2-specific (see *Methods*). We first manually gated different subpopulations of T cells on the basis of differentiation markers and cytotoxic-polarization markers (Tc-polarization). We observed that Ag^+CD8^+ T cells, if compared to Ag^-CD8^+ T lymphocytes, displayed lower percentages of N and higher percentages of T_{SCM}, CM, and TM; similar percentages of both EM and EMRA were found (Supplementary Figures S5A, B). In terms of Tc-polarization, similar percentages of Tc1 cells were found within Ag^+ and Ag^-CD8^+ T cells. However, Ag^+CD8^+ T cells were characterized by higher percentages of both Tc17 and Tc1/Tc17 and lower percentages of Tc0/Tc2 (Supplementary Figure S5C).

As for $CD4^+$ T-cell analysis, we applied unsupervised analysis and found 21 clusters, of which six were SARS-CoV-2-reactive $CD8^+$ T cells (Figures 2A, B; Supplementary Figure S6A). Considering Ag^-CD8^+ T cells, both MIX and RNA showed increased levels of TM Tc17 $CD69^+$, TM Tc0/Tc2, and TM Th0/Th2 $PD1^+$ $CXCR5^+$ if compared to those of REC subjects. Furthermore, RNA showed a higher percentage of TM Tc1 $PD1^+$ $CXCR5^+$ compared to those of REC and MIX (Supplementary Figure S7). Ag^+CD8^+ T cells were selected and after reclustering, 11 clusters were identified. Besides naive T cells and T_{SCM}, defined as $CD45RA^+CCR7^+CD27^+CD28^+CD95^-$ and $CD45RA^+CCR7^+CD27^+CD28^+CD95^+$, respectively, we found two clusters of CM T cells defined as follows: CM Tc1 $PD\text{-}1^-$ that were $CD45RA^-CCR7^+CD28^+CXCR3^+PD\text{-}1^-$ and CM Tc1 $PD\text{-}1^+$ that were $CD45RA^-CCR7^+CD28^+CXCR3^+PD\text{-}1^+$.

Among effector Ag^+CD8^+ T cells, we found five clusters defined as TM Tc1 $PD\text{-}1^-$ ($CCR7^-CD45RA^-CD28^+CXCR3^+PD\text{-}1^-$), TM Tc1 $PD\text{-}1^+$ ($CCR7^-CD45RA^-CD28^+CXCR3^+PD\text{-}1^+$), TM Tc0/Tc2 ($CCR7^-CD45RA^-CD28^+CCR6^-CXCR3^-$), TM Tc17 ($CCR7^-CD45RA^-CD28^+CCR6^+CXCR3^-$), and EM Tc1 $CD57^+$ $PD\text{-}1^+$ ($CCR7^-CD45RA^-CD28^-CD57^+PD\text{-}1^+$). Moreover, three populations of effector memory cells reexpressing CD45RA (EMRA) were detected, i.e., EMRA Tc1 $CD57^-$ $PD\text{-}1^+$ ($CCR7^-CD45RA^+CXCR3^+CD57^-PD\text{-}1^+$), EMRA Tc1 $CD57^+$ $PD\text{-}1^+$ ($CCR7^-CD45RA^+CXCR3^+CD57^+PD\text{-}1^+$), and EMRA Tc1 $CD57^+$ $PD\text{-}1^-$ ($CCR7^-CD45RA^+CXCR3^+CD57^+PD\text{-}1^-$) (Figure 2C).

Similar percentages of total $CD8^+$ and Ag^+CD8^+ T cells were found among the three groups (Figures 2D, E). However, within the Ag^+ population, we observed increased percentages of EM Tc1 $CD57^+$ $PD\text{-}1^+$ in both vaccinated groups if compared to that in the recovered ones (Figure 2F). Furthermore, MIX and RNA showed increased levels of EMRA Tc1 $CD57^+$ $PD\text{-}1^+$ terminal effector $CD8^+$ T cells compared to that in REC. Finally, we observed that the percentage of EMRA Tc1 $CD57^+$ $PD\text{-}1^-$ terminal effector $CD8^+$ T cells was higher in MIX compared to those of both REC and RNA (Figure 2E). Similar percentages of all other subpopulations were found among REC, MIX, and RNA (Supplementary Figure S8).

Patients who recovered from COVID-19 display more polyfunctional antigen-specific $CD4^+$ T cells compared to those in vaccinated donors

Besides Th-polarization, the functional properties of Ag^+-specific T cells were investigated by measuring the percentages of cells producing IFN-γ, tumor necrosis factor (TNF), interleukin (IL)-2, IL-17, and granzyme B (GZMB), along with the expression of the degranulation marker CD107a. The percentages of cells producing cytokines were assessed following 16 h of *in vitro* stimulation with SARS-CoV-2 peptide pool covering the complete sequence of Wuhan SARS-CoV-2 spike glycoprotein. The gating strategy is reported in Supplementary Figure S9.

REC displayed a higher percentage of $CD4^+$ T cells producing TNF, IL-2, and IL-17 than that in the MIX group, but not with respect to that of the RNA group. Furthermore, a higher percentage of $CD4^+$ T cells producing IL-2 and TNF was observed in RNA compared to that in MIX subjects. Similar percentages of IFN-γ, CD107a, and GZMB were found among the three groups (Figure 3A, B).

Polyfunctional properties were investigated in $CD4^+$ and $CD8^+$ T cells by analyzing the simultaneous production of TNF, CD107a, IFN-γ, IL-2, and IL-17 using the bioinformatic Simplified Presentation of Incredibly Complex Evaluation (SPICE) tool. Among $CD4^+$ T cells, REC exhibited a different polyfunctionality profile from those who had been vaccinated (Figure 3C). In particular, REC displayed a higher percentage of $CD4^+$ T cells simultaneously producing IL-2 and TNF compared to those in MIX and RNA. The percentage of $CD4^+$ T cells producing TNF or IL-17 was higher in REC compared to those in both vaccinated groups. Moreover, RNA exhibited higher percentages of $CD4^+$ T cells simultaneously producing IL-2 and TNF or IL-2 alone compared to those in MIX. Furthermore, we found that both vaccinated groups displayed higher percentages of cells defined as "highly polyfunctional" as simultaneously producing CD107a, IFN-γ, IL-2, and TNF compared to those in REC (Figure 3D). The functional properties of $CD8^+$ T were similar between the three groups (Supplementary Figure S10).

10.3389/fimmu.2023.1123724

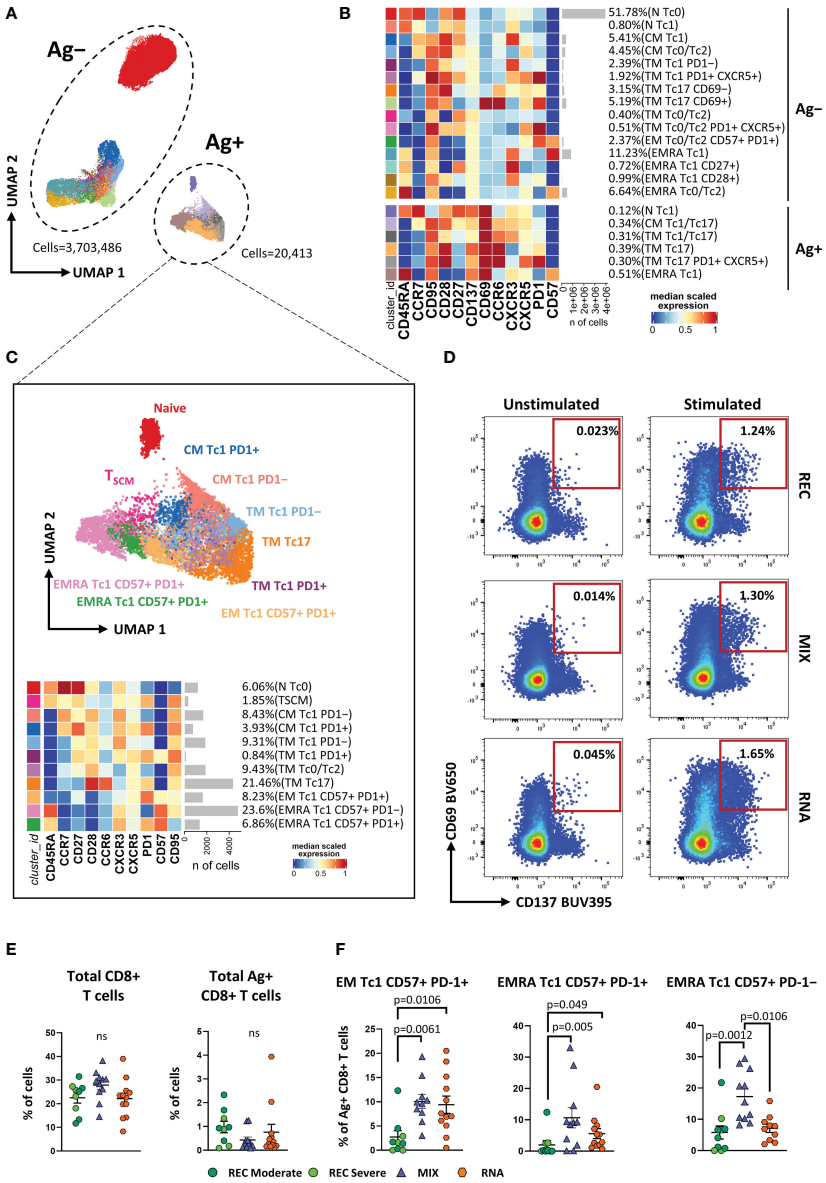


FIGURE 2
Immune phenotyping of antigen-specific CD8$^+$ T cells. **(A)** UMAP plot shows the 2D spatial distribution of 3,723,899 cells from nine donors who recovered from SARS-CoV-2 infection (REC, severe = 4 and moderate = 5) and 23 vaccinated donors (MIX = 11 and RNA = 12) embedded with FlowSOM clusters. Ag$^+$, antigen-specific CD8$^+$ T cells; Ag$^-$, non-antigen-specific CD8$^+$ T cells. **(B)** Heatmap of the median marker intensities of the 12 lineage markers across the 21 cell populations obtained with FlowSOM algorithm after the manual metacluster merging. The colors of cluster_id column correspond to the colors used to label the UMAP plot clusters. The color in the heatmap is referred to the median of the *arcsinh* marker expression (0–1 scaled) calculated over cells from all of the samples. Blue represents lower expression, while red represents higher expression. Light gray bar along the rows (clusters) and values in brackets indicate the relative sizes of the clusters. N, naive; CM, central memory; TM, transitional memory; EM, effector memory; EMRA, effector memory reexpressing the CD45RA. The black bar on the right is used to group Ag$^+$ or Ag$^-$ subpopulations. **(C)** Uniform Manifold Approximation and Projection UMAP and heatmap visualization of 11 manually merged antigen-specific CD8$^+$ T cell clusters. **(D)** Representative dot plots showing manual gating analysis of Ag-specific (CD137$^+$CD69$^+$) CD8$^+$ T cells after overnight stimulation with spike protein compared to unstimulated control [activation-induced marker assay (AIM assay)]. Numbers in the dot plots indicate the percentage of cells identified by manual gating. **(E)** Dot plots show the total percentage of antigen-specific CD8$^+$ T cells. Kruskal–Wallis test with Benjamini–Hochberg correction for multiple comparisons was used to test the differences among the three groups. **(F)** Dot plots show the relative cell percentage of the antigen-specific CD8$^+$ T-cell clusters of nine donors who recovered from SARS-CoV-2 infection (REC, severe = 4 and moderate = 5) and 23 vaccinated donors (MIX = 11 and RNA = 12). The central bar represents the mean ± SEM. Generalized linear mixed model GLMM test was used for the statistical analysis. Adjusted P-values are reported in the figure. ns, not significant.

Vaccinated donors showed a higher percentage of antigen-specific and activated memory B cells expressing IgG compared to that in REC

SARS-CoV-2 antibodies decline already as early as 21 days after infection or vaccination (6). However, long-lived MBCs constitute a durable long-term memory and provide a rapid recall response differentiating into high-affinity matured plasma cells (35). For this reason, we measured the frequencies of circulating SARS-CoV-2 spike-specific B cells (Ag$^+$ B cells) (see *Methods*).

Similar percentages of total B cells were found among the three groups (Figure 4A). However, both MIX and RNA showed a higher percentage of Ag$^+$ B cells (defined as CD45$^+$CD19$^+$decoy$^-$Spike-

10.3389/fimmu.2023.1123724

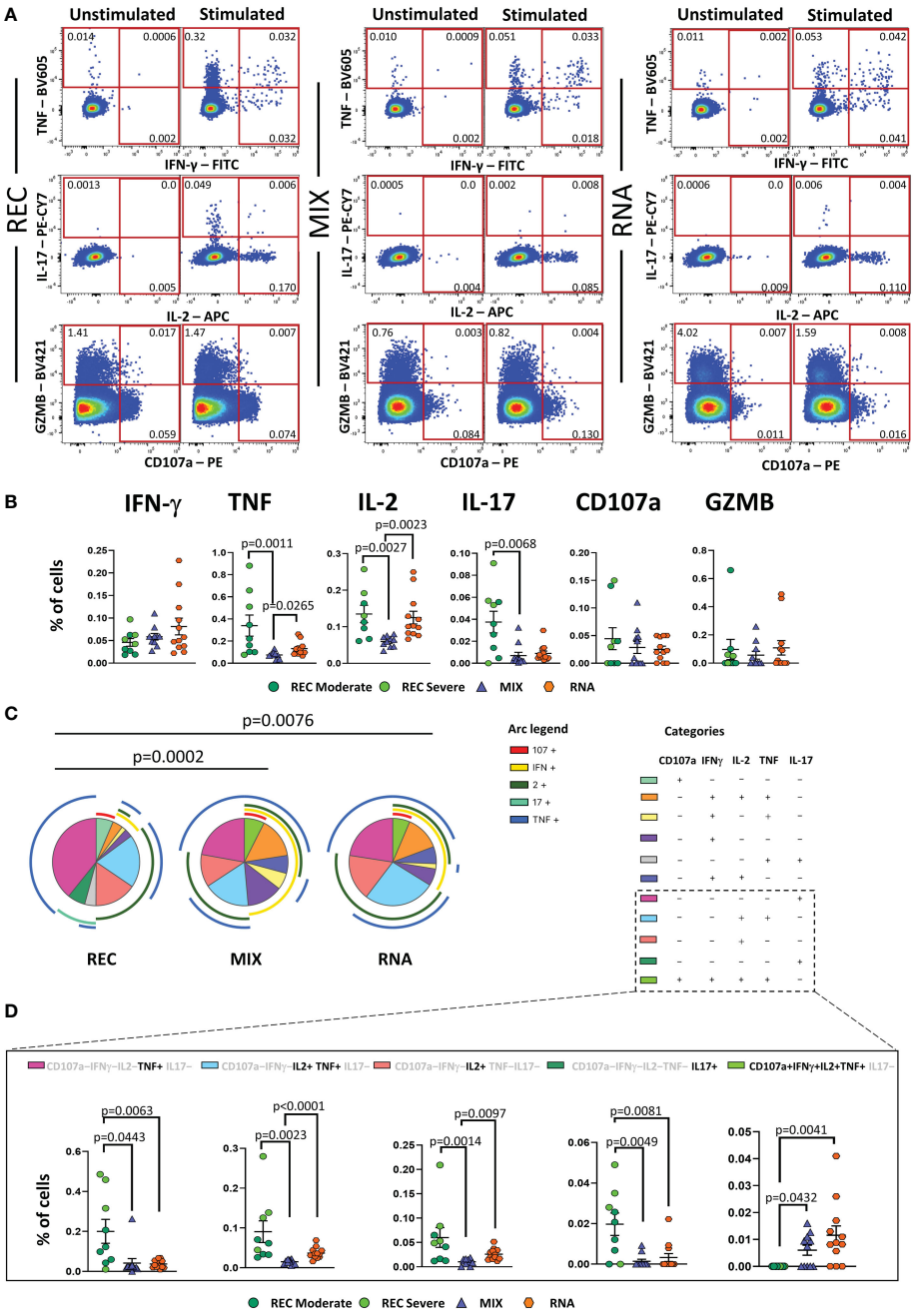


FIGURE 3
Cytokine production and polyfunctionality of antigen-specific CD4$^+$ T cells. **(A)** Representative dot plots showing manual gating analysis of intracellular cytokine production of CD4$^+$ T lymphocytes after overnight stimulation with spike protein compared to unstimulated control. Numbers in the dot plots indicate the percentage of cells identified by the gates. **(B)** Comparison between the total production of IFN-γ, TNF, IL-17, IL-2, CD107a, and GZMB by CD4$^+$ T cells after *in vitro* stimulation with 15-mer peptides, covering the complete sequence of Wuhan SARS-CoV-2 spike glycoprotein. Data represent individual values from nine healthy subjects who recovered from SARS-CoV-2 infection (REC, severe = 4 and moderate = 5) and 23 vaccinated donors (MIX= 11 and RNA = 12). Mean (center bar) ± SEM (upper and lower bars). Kruskal–Wallis test with Benjamini–Hochberg correction for multiple comparisons was used to test the differences among the three groups. **(C)** Pie charts representing the proportion of responding CD4$^+$ T cells producing different combinations of CD107a, IL-2, IL-17, IFN-γ, and TNF after *in vitro* stimulation with 15-mer peptides, covering the complete sequence of Wuhan SARS-CoV-2 spike glycoprotein. Frequencies were corrected by background subtraction as determined in non-stimulated controls using SPICE software. Pie arches represent the total production of different cytokines. **(D)** Percentage of polyfunctional population within CD4$^+$ T cells. Kruskal–Wallis test with Benjamini–Hochberg correction for multiple comparisons was used to test the differences among the three groups. Adjusted P-values are indicated in the figure.

BUV661$^+$Spike-BV650$^+$) when compared to that in REC (Figure 4B).

By applying manual gating, we observed that Ag$^+$ B cells compared to its Ag$^-$ counterpart displayed a lower percentage of naive B cells and an increased percentage of memory switched, memory unswitched and of CD27$^-$IgD$^-$ B cells (Supplementary Figure S11A). Moreover, after vaccination or SARS-CoV-2 infection, ~42%–96% of Ag$^+$ B cells were IgG$^+$. This percentage decreased to ~5%–22% in the Ag$^-$ B cells, where ~69%–90% of cells were IgD$^+$IgM$^+$ (Supplementary Figure S11B). Furthermore, the

10.3389/fimmu.2023.1123724

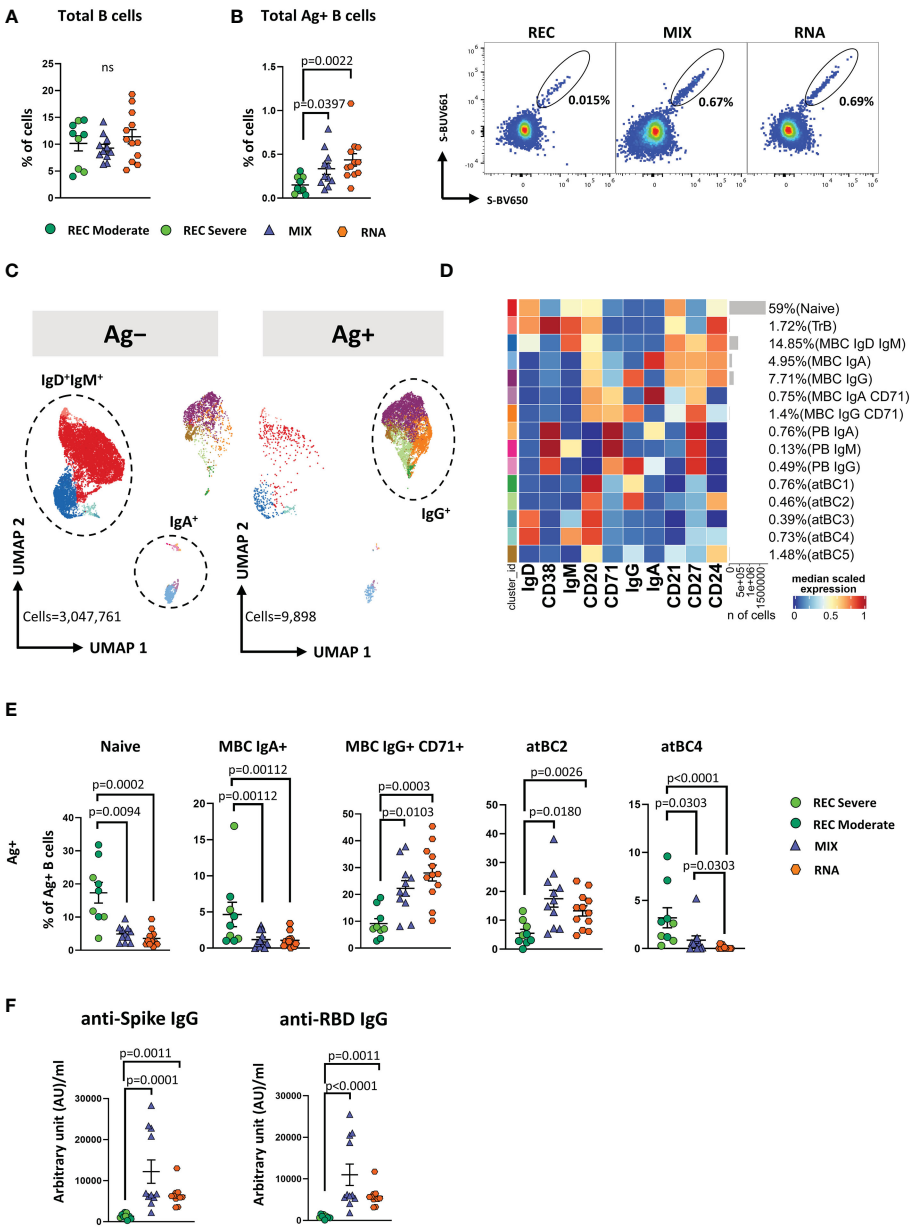


FIGURE 4
Immune phenotyping of antigen-specific CD19$^+$ B cells. **(A)** Dot plots show the total percentage of CD19$^+$ B cells. Kruskal–Wallis test with Benjamini–Hochberg correction for multiple comparisons was used to test the differences among the three groups. **(B)** Dot plots show the total percentage of antigen-specific CD19$^+$ B cells (left); representative dot plots showing manual gating analysis of Ag$^+$ B cells from REC, MIX, and RNA. Numbers in the dot plots indicate the percentage of cells identified by the gates (right). Kruskal–Wallis test with Benjamini–Hochberg correction for multiple comparisons was used to test the differences among the three groups. **(C)** UMAP plot shows the 2D spatial distribution of 3,057,659 cells from nine donors who recovered from SARS-CoV-2 infection (REC, severe = 4 and moderate = 5) and 23 vaccinated donors (MIX = 11 and RNA = 12) embedded with FlowSOM clusters. Ag$^+$, antigen-specific CD19$^+$ B cells; Ag$^-$, non-antigen-specific CD19$^+$ B cells. **(D)** Heatmap of the median marker intensities of the 10 lineage markers across the 15 cell populations obtained with FlowSOM algorithm after the manual metacluster merging. The colors of cluster_id column correspond to the colors used to label the UMAP plot clusters. The color in the heatmap is referred to the median of the *arcsinh* marker expression (0–1 scaled) calculated over cells from all of the samples. Blue represents lower expression, while red represents higher expression. Light gray bar along the rows (clusters) and values in brackets indicate the relative sizes of the clusters. N, naive; TrB, transitional B cells; MBC, memory B cell; atBC, atypical B cell. **(E)** Dot plots show the percentage of 15 Ag$^+$ B cell clusters among nine donors who recovered from SARS-CoV-2 infection (REC, severe = 4 and moderate = 5) and 23 vaccinated donors (MIX = 11 and RNA = 12). The central bar represents the mean ± SEM. GLMM test was used for the statistical analysis. Adjusted P-values are reported in the figure. **(F)** Anti-spike and anti-RBD IgG concentrations in plasma samples from REC, MIX, and RNA individuals. Kruskal–Wallis test with Benjamini–Hochberg correction for multiple comparisons was used to test the differences among the three groups. Adjusted P-values are indicated in the figure.

percentage of IgA$^+$ B cells was higher in the Ag$^-$ compartment (Supplementary Figure S11B).

To deeply characterize both Ag$^-$ and Ag$^+$ B cells, we took advantage of unsupervised clustering. The analysis revealed 15 clusters, spanning from naive to atypical B cells (atBCs; CD21$^-$CD27$^-$CD38$^-$) (36) (Figures 4C, D; Supplementary Figure S12A).

Besides naive and transitional B cells (TrB), respectively defined as naive: CD20$^+$CD21$^+$CD24$^+$CD38$^-$IgD$^+$IgM$^+$ and TrB: CD20$^+$CD21$^+$

$CD24^+CD38^+IgD^+IgM^+$, we found five clusters of MBCs defined as follows: MBC IgD^+ IgM^+ ($CD20^+CD21^+CD24^+CD27^+IgD^+IgM^+$), MBC IgA^+ ($CD20^+CD21^+CD24^+CD27^+IgA^+$), MBC IgG^+ ($CD20^+CD21^+CD24^+CD27^+IgG^+$), MBC IgA^+ $CD71^+$ ($CD20^+CD21^+CD24^+CD27^+IgA^+CD71^+$), and MBC IgG^+ $CD71^+$ ($CD20^+CD21^+CD24^+CD27^+IGA^+CD71^+$). Among plasmablasts (PBs), we found the following three clusters: PB IgA^+ as $CD27^+CD71^+CD38^{++}IgA^+$, PB IgM^+ as $CD27^+CD71^+CD38^{++}IgM^+$, and PB IgG^+ as $CD27^+CD71^+CD38^{++}IgG^+$. Together with naive, TrBs, MBCs, and PBs, we identified five clusters of atBCs, i.e., atBC1 as $CD21^-CD27^-CD20^+IgG^+$, atBC2 as $CD21^-CD27^-CD24^+CD20^+IgG^+$, atBC3 as $CD21^-CD27^-CD20^+IgD^+$, atBC4 as $CD21^-CD27^-CD20^+IgD^+IgM^+$, and atBC5 as $CD21^-CD27^-CD20^+CD24^+$.

Within Ag^- B cells, MIX and RNA showed higher levels of MBC IgD^+IgM^+ and lower levels of atBC5 compared to those in REC (Supplementary Figure S13). Within Ag^+ B cells, MIX and RNA displayed lower percentages of naive, MBC IgA^+, and atBC4 B cells if compared to those in REC, while the percentages of MBC IgG^+ $CD71^+$ and atBC2 were significantly higher (Figure 4E). Moreover, REC displayed a higher percentage of atBC4 cells if compared to those in MIX and RNA (Figure 4E). Similar percentages of all other subpopulations were found among REC, MIX, and RNA subjects (Supplementary Figure S14).

In addition, we measured IgG antibodies able to bind the spike and the RBD of the S1 subunit of the spike protein (the latter known as neutralizing antibodies). We observed that both vaccinated groups had higher levels of anti-spike and anti-RBD-binding IgG compared to those in REC subjects (Figure 4F).

Recovered patients show different immunological profiles compared to those of vaccinated donors

The principal component analysis (PCA) computed using the complete phenotype of Ag^+ B and T cells, $CD4^+$ T cell polyfunctionality, plasmatic anti-spike, and anti-RBD antibodies showed that the group of REC clusters in a different position of the two-dimensional PCA space if compared to MIX and RNA, which are almost entirely overlapping (Figure 5A, left). Immune features related to the amount of MBC IgA, $CD107a^-IFN\text{-}\gamma^-IL2^-TNF^+IL17^-$, $CD107a^-IFN\text{-}\gamma^-IL2^+TNF^+IL17^-$, $CD107a^-IFN\text{-}\gamma^-IL2^-TNF^-IL17^+$, and naive B cells (more abundant in REC subjects) were the main drivers of the clusterization of samples in two different areas (Figure 5A, right). Moreover, the picture of PCA contribution also reveals that both vaccinated groups were characterized by increased levels of MBC IgG $CD71^+$, anti-spike, and anti-RBD IgG antibodies (Figure 5A, right).

By using the same parameters used to perform the PCA, we assessed the existence of immunological correlations between the variables within the REC, MIX, and RNA groups. It is to note that in REC, but not in the MIX and RNA groups, a strong positive correlation was present among the percentages of MBC IgA $CD71^+$ and all polyfunctional $CD4^+$ T-cell subsets (Figure 5B, Supplementary Figure S15). The percentages of MBC IgD^+ IgM^+, transitional, and naive B cells inversely correlate with all polyfunctional $CD4^+$ T-cell subsets (Figure 5B, Supplementary Figure S15).

Discussion

Vaccines are designed to induce a long-term adaptive immune response that confers durable protection. In this study, as revealed by PCA, we report that COVID-19 recovered patients show different long-term immunological profiles compared to those of donors who had been vaccinated with three doses (either with adenovirus or mRNA technologies). Vaccinated individuals display a skewed Th1 Ag-specific T-cell polarization and a higher percentage of Ag-specific and activated MBCs expressing IgG compared to those of patients who recovered from severe COVID-19. Different polyfunctional properties characterize the two groups: recovered individuals show higher percentages of $CD4^+$ T cells producing one or two cytokines simultaneously, while vaccinated donors are distinguished by highly polyfunctional populations able to release four molecules such as CD107a, IFN-γ, TNF, and IL-2.

SARS-CoV-2 entry route shapes the innate immune response, as major players such as macrophages and neutrophils contribute to recruit T and B cells that should mount a local specific immune response, with the consequent production of mucosal antibodies. This means that different adaptive mechanisms are involved in the protective immunity generated by the infection or vaccination. Indeed, we found that recovered individuals are characterized by higher percentages of MBCs producing IgA if compared to those of vaccinated ones. However, systemic and mucosal IgA responses are variably induced in response to vaccination and are associated with protection against subsequent infection (37, 38).

SARS-CoV-2-specific cells wane more slowly than do antibodies [reviewed in (39)], and T cells able to exert an efficient protection are those capable of exerting many functions simultaneously. Polyfunctional T-cell responses have been documented also in HIV-1 (40), hepatitis B virus vaccine (41), and vaccinia-induced responses (42), indicating that highly functional T-cell responses are commonly found in response to other viral infections and vaccination and are effectively controlled by cellular immunity. The functional population able to produce four cytokines or more is likely of significant immunologic importance because it could directly eliminate virally infected cells (assuming that such cells express or upregulate CD107a) and suppress viral replication while maintaining itself without $CD4^+$ T-cell help through autocrine production of IL-2.

We found that vaccinated donors are characterized by MBCs IgG-switched that express CD71. Ag-specific B cells can be divided into antibody-secreting cells (or PBs) and MBCs after infection or vaccination. A particular subset of B cells, called activated B cells, is distinct from antibody-secreting cells and is committed to the MBC lineage. Activated B cells are characterized by the expression of CD71, which is the transferrin receptor and indicates higher activation status and proliferative capabilities (43). This population is also typically found in blood after infection with Ebola or influenza virus and also after vaccination (44–46).

As far as vaccination strategy is concerned, the ChAdOx1 vaccine uses a nonreplicating adenovirus as a vector to introduce into the cells of the recipient's DNA coding for the spike protein of SARS-CoV-2. BNT162b2 instead uses messenger RNA (mRNA) coding for spike, which cells take up and use to synthetize the protein. mRNA vaccines are good at inducing antibody responses, and the vector-based

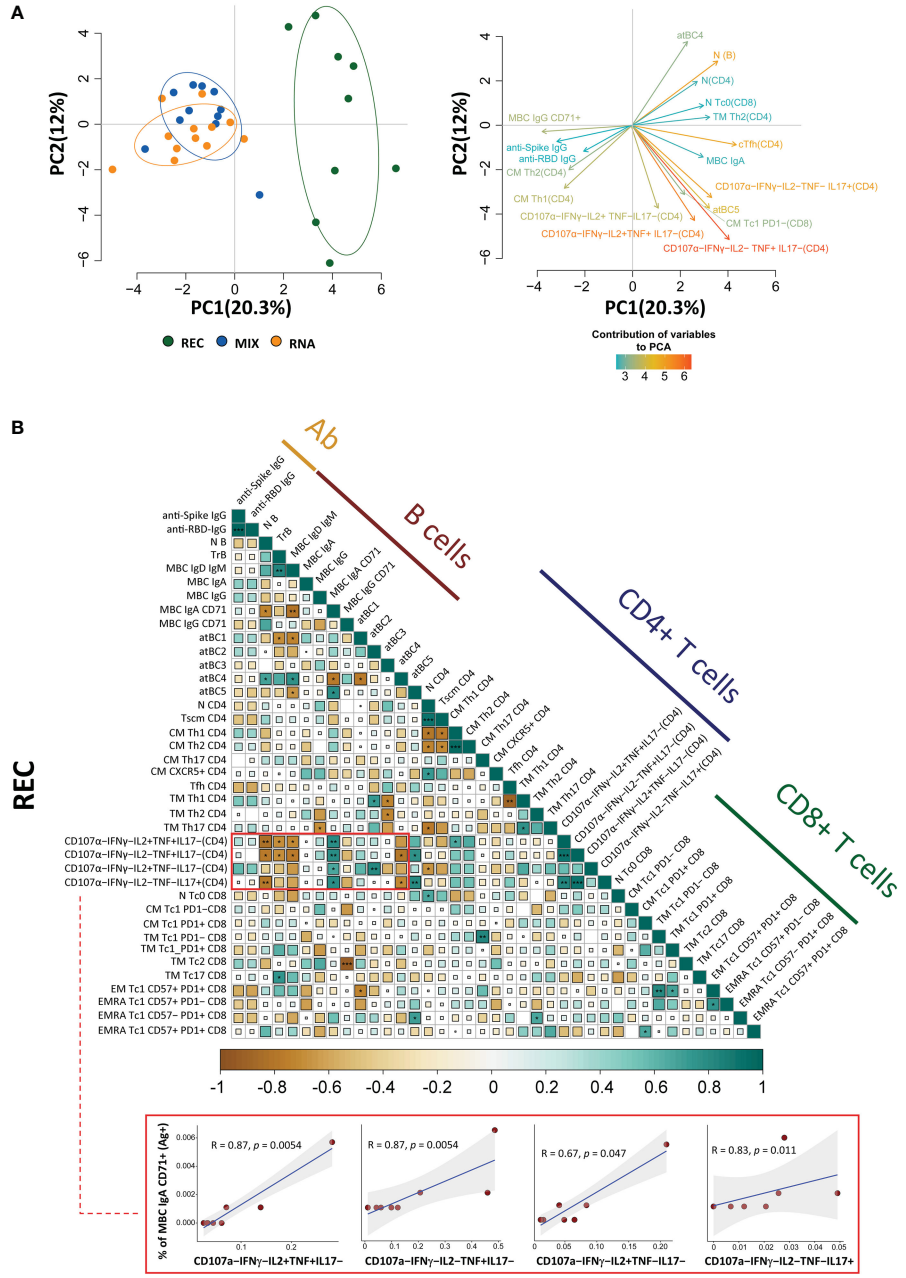


FIGURE 5
Principal component analysis and correlogram reveal that REC is different from MIX and RNA. **(A)** (Left) Principal component analysis (PCA) using the plasma level of anti-SARS-CoV-2 IgG antibodies, Ag-specific T, B-cell percentages, and the fraction of polyfunctional CD4$^+$ T cells from REC, MIX, and RNA subjects. REC, green circles (n = 9); MIX, blue circles (n = 11); RNA, orange circles (n = 12). (Right) Contribution of the different variables to PCA. The color of the arrows underlines the contribution level, while the position underlines the positive or negative contribution. Negatively correlated variables are positioned on opposite sides of the plot origin (opposed quadrants). **(B)** Correlogram of REC. Spearman R (ρ) values are shown from brown (–1.0) to green (1.0); color intensity and areas of square are proportional to correlation coefficients R. Spearman rank two-tailed P-value was indicated by *P < 0.05, **P < 0.01, and ***P < 0.001. Additional XY scatter plots that specifically show the relationship between the variables that are most correlated are displayed. Each scatter plot reports the regression line (blue), the Spearman R (ρ) value, the exact two-tailed P-value, and the 95% confidence bands (light gray).

vaccines are better at triggering T-cell responses. In a Spanish study, people who received a dose of the Pfizer-BioNTech vaccine 8 weeks after an initial AstraZeneca dose had few side effects and a robust antibody response 2 weeks after the second shot, suggesting that mixing the two types of vaccine may give the immune system multiple ways to recognize a pathogen (47). However, in our small cohort of vaccinated individuals, the immunological response was not different in the two groups of individuals who received different vaccination strategies likely because the immune response has been investigated after the third dose.

We are well aware that this study has some limitations. First of all, the number of patients studied is low, but the B- and T-cell compartments were investigated in-depth in terms of phenotype and functionality. Second, the number of days post symptom onset (for recovered individuals) or after the third dose of the vaccine (for vaccinated ones) is different. This could be relevant when interpreting

the results regarding SARS-CoV-2-specific antibodies or the percentage of Ag-specific B cells and cTfh cells in recovered patients. Third, a group of donors who developed hybrid immunity characterized by immunity developed by natural infection and vaccination.

However, our study can provide a novel characterization of the humoral and cellular immune responses upon COVID-19 vaccination or infection by including the fine phenotypic and functional analysis of Ag-specific B and T cells together with the comparison between different vaccination strategies (after the third dose of vaccination) and natural infection.

Methods

Blood collection and isolation of mononuclear cells

Up to 30 ml of blood was collected from each patient in vacuettes containing ethylenediaminetetraacetic acid (EDTA). Blood was immediately processed. Isolation of PBMCs was performed using Ficoll-Hypaque according to standard procedures (48). PBMCs were stored in liquid nitrogen in fetal bovine serum (FBS) supplemented with 10% dimethyl sulfoxide (DMSO). Plasma was stored at -80°C until use.

Activation-induced cell marker assay and T-cell phenotype

Isolated PBMCs were thawed and rested for 6 h. After resting, CD40-blocking antibody (0.5 µg/ml final concentration) (Miltenyi Biotec, Bergisch Gladbach, Germany) was added to the cultures 15 min before stimulation. PBMCs were cultured in a 96-well plate in the presence of 15-mer peptides with 11-amino acid overlap, covering the complete sequence of Wuhan SARS-CoV-2 spike glycoprotein (PepTivator SARS-CoV-2 Prot_S complete, Miltenyi Biotec, Bergisch Gladbach, Germany) together with 1 µg/ml of anti-CD28 (Miltenyi Biotec, Germany). PBMCs were stimulated for 18 h at 37°C in a 5% CO_2 atmosphere in complete culture medium (RPMI 1640 supplemented with 10% FBS and 1% each of L-glutamine, sodium pyruvate, nonessential amino acids, antibiotics, 0.1 M 4-(2-hydroxyethyl)-1-piperazineethanesulfonic acid (HEPES), and 55 µM β-mercaptoethanol) (33, 34). For each stimulated sample, an unstimulated one was prepared as a negative control. After stimulation, cells were washed with Phosphate buffer saline (PBS) and stained with PromoFluor IR-840 (Promokine, PromoCell, Heidelberg, Germany) for 20 min at room temperature (RT). Next, cells were washed with FACS buffer (PBS added with 2% FBS) and stained with the following fluorochrome-labeled monoclonal antibodies (mAbs) for 30 min at 37°C: CXCR5-BUV661, CCR6-BUV496, and CXCR3-BV785. Finally, cells were washed with FACS buffer and stained for 20 min at RT with Duraclone IM T-cell panel (Beckman Coulter, Brea, CA, USA) containing CD45-Krome Orange, CD3-APC-A750, CD4-APC, CD8-AF700, CD27-PC7, CD57-Pacific Blue, CD279 (PD1)-PC5.5, CD28-ECD, CCR7-PE, and CD45RA-FITC and added with three other fluorescent mAbs, i.e., CD69-BV650, CD137-BUV395, and CD95-BV605. Samples were acquired on a CytoFLEX LX flow cytometer (Beckman Coulter). All reagents used for T-cell phenotype are reported in Supplementary Table S1. All mAbs added to DuraClone IM T cells were previously titrated on human PBMCs and used at the concentration giving the best signal-to-noise ratio. The gating strategy used to identify $CD4^+$ and $CD8^+$ T cells is reported in Supplementary Figure S16.

Intracellular cytokine staining

Isolated PBMCs were thawed and rested for 6 h. PBMCs were then cultured in the presence of 15-mer peptides with 11-amino acid overlap, covering the complete sequence of Wuhan SARS-CoV-2 spike glycoprotein (PepTivator SARS-CoV-2 Prot_S complete, Miltenyi Biotec, Bergisch Gladbach, Germany) together with 1 µg/ml of anti-CD28 (Miltenyi Biotec, Germany). PBMCs were stimulated for 16 h at 37°C in a 5% CO_2 atmosphere in complete culture medium (RPMI 1640 supplemented with 10% FBS and 1% each of L-glutamine, sodium pyruvate, nonessential amino acids, antibiotics, 0.1 M HEPES, and 55 µM β-mercaptoethanol). For each stimulated sample, an unstimulated one was prepared as a negative control. All samples were incubated with protein transport inhibitor containing brefeldin A (Golgi Plug, Becton Dickinson) and monensin (Golgi Stop, Becton Dickinson) and previously titrated concentration of CD107a-PE (BioLegend, San Diego, CA, USA). After stimulation, cells were washed with PBS and stained with LIVE/DEAD fixable Aqua (ThermoFisher Scientific, USA) for 20 min at RT. Next, cells were washed with FACS buffer and stained with surface mAbs recognizing CD3-PE.Cy5, CD4-AF700, and CD8-APC.Cy7 (BioLegend, San Diego, CA, USA). Cells were washed with FACS buffer and fixed and permeabilized with the Cytofix/Cytoperm buffer set (Becton Dickinson Bioscience, San Jose, CA, USA) for cytokine detection. Then, cells were stained with previously titrated mAbs recognizing IL-17-PE-Cy7, TNF-BV605, IFN-γ-FITC, IL-2-APC, and GZMB BV421 (all mAbs from BioLegend). Samples were acquired on an Attune NxT acoustic cytometer (ThermoFisher Scientific, USA). Supplementary Table S1 reports mAb titers, clones, catalog numbers, and type of fluorochrome used in the panel. Gating strategy used to identify and analyze the intracellular cytokine production of $CD4^+$ and $CD8^+$ T lymphocytes is reported in Supplementary Figure S9.

Detection of SARS-CoV-2-specific B cells

Thawed PBMCs were washed twice with RPMI 1640 supplemented with 10% FBS and 1% each of L-glutamine, sodium pyruvate, nonessential amino acids, antibiotics, 0.1 M HEPES, 55 µM β-mercaptoethanol, and 0.02 mg/ml DNAse. PBMCs were washed with PBS and stained using viability marker PromoFluor IR-840 (Promokine, PromoCell, Heidelberg, Germany) for 20 min at RT in PBS. Next, cells were washed with PBS and stained for 15 min at RT with streptavidin-AF700 (decoy channel; ThermoFisher Scientific, USA) to remove false-positive SARS-CoV-2-specific B cells. After washing with FACS buffer, cells were stained with biotinylated full-length SARS-CoV-2 spike protein (R&D Systems, Minneapolis, USA) labeled with different streptavidin-fluorophore conjugates. Full-length biotinylated spike protein was mixed and incubated with streptavidin-BUV661 (Becton Dickinson) or

streptavidin-BV650 (BioLegend) at a 6:1 mass ratio for 15 min at RT. All samples were stained with both fluorescent biotinylated biotinylated spike protein for 1 h at 4°C. Then, cells were washed with FACS buffer and stained for 20 min at RT with DuraClone IM B cells (Beckman Coulter, Brea, CA, USA) containing the following lyophilized directly conjugated mAbs: anti-IgD-FITC, CD21-PE, CD19-ECD, CD27-PC7, CD24-APC, CD38-AF750, anti-IgM-PB, and CD45-KrO to which the following drop-in antibodies were added: CD71-BUV395, CD20-BV785, anti-IgG-BUV496, and anti-IgA-PerCP-Vio700. Samples were acquired on a CytoFLEX LX flow cytometer (Beckman Coulter). A minimum of 1,000,000 cells per sample were acquired. All reagents used for B-cell phenotype are reported in Supplementary Table S1. All mAbs added to DuraClone IM B cells were previously titrated on human PBMCs and used at the concentration giving the best signal-to-noise ratio. The gating strategy used to identify Ag^- and Ag^+ B cells is reported in Supplementary Figure S17.

Computational analysis of flow cytometry data

T-cell analysis

Compensated Flow Cytometry Standard (FCS) 3.0 files were imported into FlowJo software version v10.7.1 and analyzed by standard gating to remove doublets, aggregates, and dead cells. For *ex vivo* immunophenotyping of non-antigen-specific (Ag^-) and antigen-specific (Ag^+) T cells of both $CD4^+$ and $CD8^+$, we analyzed only the data of stimulated samples. For each sample, we therefore selected data from all living $CD4^+$ or $CD8^+$ T cells and imported them in R using flowCore package v2.4.0 (49) for a total of 8,436,275 $CD4^+$ T cells (of which 89,400 were SARS-CoV-2-specific) and 3,723,899 $CD8^+$ T cells (of which 20,413 were SARS-CoV-2-specific). Further analysis was performed using CATALYST v1.17.3 (50). All data obtained by flow cytometry were transformed in R using hyperbolic arcsine "*arcsinh* (x/cofactor)" applying manually defined cofactors (where x is the fluorescence-measured intensity value). Clustering and dimensional reduction were performed using FlowSOM (version 2.4.0) and Uniform Manifold Approximation and Projection (UMAP) (version 0.2.8.0) algorithms, respectively. The Ag^+ $CD4^+$ and $CD8^+$ T-cell clusters have been reanalyzed more in-depth by performing a new step of clustering using the following markers: CD45RA, CCR7, CD27, CD28, PD-1, CCR6, CXCR3, CXCR5, and CD95. Starting from 15 clusters of either $CD4^+$ T cells or $CD8^+$ T cells, reclustering gave origin to 10 clusters of $CD4^+$ T cells and 11 of $CD8^+$ T lymphocytes. The quality control (QC) of clustering for $CD4^+$ and $CD8^+$ T cells is reported in Supplementary Figures S2 and S6, respectively.

B-cell analysis

Compensated FCS 3.0 files were imported into FlowJo software version v10.7.1 and analyzed by standard gating to remove doublets, aggregates, and dead cells and identify $CD19^+$ B cells. Then, from the total $CD19^+$ B cells, we excluded decoy-positive B cells to remove false-positive SARS-CoV-2-specific B cells. For each sample, we selected the SARS-CoV-2-specific B cells as positive cells for both Spike_streptavidin-BUV661 and Spike_streptavidin-BV650 (we referred to as Ag^+ B cells). The remaining double-negative cells were non-SARS-CoV-2-specific B cells (we referred to as Ag^- B cells). Then, we exported for each sample separately both Ag^+ and Ag^- B cells and imported them in R using flowCore package v2.4.0 for a total of 3,057,659 $CD19^+$ B cells (of which 9,898 were SARS-CoV-2-specific). The unsupervised analysis was performed using CATALYST v1.17.3. All data were transformed in R using hyperbolic arcsin (*arcsinh* x/cofactor) applying manually defined cofactors (where x is the fluorescence-measured intensity value). Clustering and dimensional reduction were performed using FlowSOM and UMAP algorithms, respectively. The QC of clustering for B cells is reported in Supplementary Figure S12.

Measuring anti-SARS-CoV-2 anti-spike and anti-RBD IgG antibodies

Anti-spike antibody levels were measured by qualitative and semiquantitative chemiluminescent microparticle immunoassay (CMIA). AdviseDx SARS-CoV-2 IgG II assay (Abbott) was used to detect plasmatic IgG antibodies able to bind the RBD of the S1 subunit of the spike protein. Plasma, SARS-CoV-2 Ag-coated paramagnetic microparticles, and assay diluent are combined and incubated. The anti-spike IgG antibodies present in the sample bind to the SARS-CoV-2 Ag-coated paramagnetic microparticles. The mixture was then washed. Anti-human IgG acridinium-labeled conjugate was added and incubated to create a reaction mixture. The resulting chemiluminescent reaction was measured as a relative light unit (RLU). There is a direct relationship between the amount of IgG antibodies to SARS-CoV-2 in the sample and the RLU detected by the system optics. Results from the anti-spike AdviseDx SARS-CoV-2 IgG II assay are reported as arbitrary units per milliliter (AU/ml). As recommended, we applied a cutoff of 50 AU/ml as a positive threshold. Every measurement was performed on Abbott "Alinity I" platform. The level of anti-RBD IgG antibodies was calculated by using NAB Neutralizing Antibody kit (SGM Italia).

Principal component analysis and correlation plot

PCA was performed and visualized in R using prcomp and pca3d package. To perform PCA, we used a matrix containing the level of plasmatic anti-SARS-CoV-2 IgG antibodies, Ag-specific T, B-cell percentages, and the fraction of polyfunctional $CD4^+$ T cells (Supplementary Table S2). The total contribution of a given variable retained by PC1 and PC2 is equal to [(C1 * Eig1) + (C2 * Eig2)]/(Eig1 + Eig2), where C1 and C2 are the contributions of the variable on PC1 and PC2; Eig1 and Eig2 are the eigenvalues of PC1 and PC2.

Correlation analysis was performed on the same parameters used to run the PCA (see above) except the following features that were not used for the correlation analysis of REC donors because they were not available: PB IgA, PB, and $CD107a^+IFN\text{-}\gamma^+IL2^+TNF^+IL17^-$. Pairwise correlations between variables were calculated and visualized as a correlogram using R packages stats (version 3.6.2) and corrplot (version 0.90). Spearman's rank correlation coefficient (ρ) was indicated by color scale; significance was indicated by asterisks (* $P < 0.05$; ** $P < 0.005$; *** $P < 0.0005$).

Statistical analysis

Differential cell population abundance analysis was performed using generalized linear mixed model (GLMM) implemented within diffcyt package (51) applying FDR cutoff = 0.05; each P-value was reported in the figure. Quantitative variables were compared using Kruskal–Wallis nonparametric test corrected for multiple comparisons by controlling the false discovery rate (FDR), method

of Benjamini and Hochberg. Statistically significant adjusted P-values are represented. Statistical analysis of cytokine production was performed using GraphPad Prism version 8 (GraphPad Software Inc., La Jolla, USA). The total percentage of Ag-specific (Ag^+CD4^+ and Ag^+CD8^+) T-cell data has been calculated as background subtracted data. SPICE software (version 6, kindly provided by Dr. Mario Roederer, Vaccine Research Center, NIAID, NIH, Bethesda, MD, USA) was used to analyze flow cytometry data on T-cell polyfunctionality (52). Data from the total cytokine production are represented as individual values, means, and standard errors of the mean. Regarding polyfunctionality, data in pie charts are represented as median values, and statistical analysis was performed using the permutation test. Data in graphs are represented as individual values, means, and standard errors of the mean.

Data availability statement

The original contributions presented in the study are included in the article/Supplementary Material. Further inquiries can be directed to the corresponding author.

Ethics statement

The studies involving human participants were reviewed and approved by Each participant, including healthy donors, provided informed consent according to Helsinki Declaration, and all uses of human material have been approved by the local Ethical Committee (Comitato Etico dell'Area Vasta Emilia Nord, protocol number 177/2020, March 11th, 2020) and by the University Hospital Committee (Direzione Sanitaria dell'Azienda Ospedaliero Universitaria di Modena, protocol number 7531, March 11th, 2020). The patients/participants provided their written informed consent to participate in this study.

Author contributions

DT, AP, AN, RB, JS, LGi, ES, AD, MC carried out experiments. DT and AP drafted the figures. DT and AN drafted and revised the tables. MMe, MMa, MG, GG, SB, CM, TT followed patients. LGo drafted and revised the clinical tables. AP performed ICS analysis. DT and KP performed bioinformatic and statistical analyses. DT, SB and AC conceived the study. SB and AC wrote the manuscript. All authors contributed to the article and approved the submitted version.

Acknowledgments

SB and LGi are Marylou Ingram Scholar of the International Society for Advancement of Cytometry (ISAC) for the period 2015–2020 and 2020–2025, respectively. Drs. Paola Paglia (ThermoFisher Scientific, Monza, Italy), Leonardo Beretta (Beckman Coulter, Milan, Italy) are acknowledged for their support in providing reagents and materials in this study, and for precious technical suggestions. JS was supported by EMBO Scientific Exchange Grant (Short-Term Fellowship) STF-8905. This study was partially supported by unrestricted donations from Glem Gas spa (San Cesario, Modena, Italy), Sanfelice 1893 Banca Popolare (San Felice sul Panaro, Modena, Italy), Rotary Club Distretto 2072 (Clubs: Modena, Modena L.A. Muratori, Carpi, Sassuolo, and Castelvetro di Modena), BPER Banca and FAR 2022 by the University of Modena and Reggio Emilia ("Features and magnitude of long- and short-term immune memory against smallpox and COVID-19"). AD has been supported by a 2021 FAR fellowship from the University of Modena and Reggio Emilia. Finally, we gratefully acknowledge the subjects who donated blood to participate in this study.

Conflict of interest

The authors declare that the research was conducted in the absence of any commercial or financial relationships that could be construed as a potential conflict of interest.

The reviewer AC declared a past co-authorship with some of the authors to the handling editor.

Publisher's note

All claims expressed in this article are solely those of the authors and do not necessarily represent those of their affiliated organizations, or those of the publisher, the editors and the reviewers. Any product that may be evaluated in this article, or claim that may be made by its manufacturer, is not guaranteed or endorsed by the publisher.

Supplementary material

The Supplementary Material for this article can be found online at: https://www.frontiersin.org/articles/10.3389/fimmu.2023.1123724/full#supplementary-material

References

1. Moss P. The T cell immune response against SARS-CoV-2. *Nat Immunol* (2022) 23 (2):186–93. doi: 10.1038/s41590-021-01122-w

2. Cohen KW, Linderman SL, Moodie Z, Czartoski J, Lai L, Mantus G, et al. Longitudinal analysis shows durable and broad immune memory after SARS-CoV-2 infection with persisting antibody responses and memory b and T cells. *Cell Rep Med* (2021) 2(7):100354. doi: 10.1016/j.xcrm.2021.100354

3. Rha MS, Jeong HW, Ko JH, Choi SJ, Seo IH, Lee JS, et al. PD-1-Expressing SARS-CoV-2-Specific CD8(+) T cells are not exhausted, but functional in patients with COVID-19. *Immunity* (2021) 54(1):44–52 e43. doi: 10.1016/j.immuni.2020.12.002

4. Jung JH, Rha MS, Sa M, Choi HK, Jeon JH, Seok H, et al. SARS-CoV-2-specific T cell memory is sustained in COVID-19 convalescent patients for 10 months with successful development of stem cell-like memory T cells. *Nat Commun* (2021) 12 (1):4043. doi: 10.1038/s41467-021-24377-1

5. Paolini A, Borella R, Neroni A, Lo Tartaro D, Mattioli M, Fidanza L, et al. Patients recovering from severe COVID-19 develop a polyfunctional antigen-

specific CD4+ T cell response. *Int J Mol Sci* (2022) 23(14):8004. doi: 10.3390/ijms23148004

6. Dan JM, Mateus J, Kato Y, Hastie KM, Yu ED, Faliti CE, et al. Immunological memory to SARS-CoV-2 assessed for up to 8 months after infection. *Science* (2021) 371 (6529):eabf4063. doi: 10.1126/science.abf4063

7. Adamo S, Michler J, Zurbuchen Y, Cervia C, Taeschler P, Raeber ME, et al. Signature of long-lived memory CD8(+) T cells in acute SARS-CoV-2 infection. *Nature* (2022) 602(7895):148–55. doi: 10.1038/s41586-021-04280-x

8. Niemi ME, Karjalainen J, Liao RG, Neale BM, Daly M, Ganna A, et al. Initiative c-HG: Mapping the human genetic architecture of COVID-19. *Nature* (2021) 600 (7889):472–7. doi: 10.1038/s41586-021-03767-x

9. Kousathanas A, Pairo-Castineira E, Rawlik K, Stuckey A, Odhams CA, Walker S, et al. Whole-genome sequencing reveals host factors underlying critical COVID-19. *Nature* (2022) 607(7917):97–103. doi: 10.1038/s41586-022-04576-6

10. Pathak GA, Karjalainen J, Stevens C, Neale BM, Daly M, Ganna A, et al. Initiative c-HG: A first update on mapping the human genetic architecture of COVID-19. *Nature* (2022) 608(7921):E1–E10. doi: 10.1038/s41586-022-04826-7

11. De Biasi S, Lo Tartaro D, Meschiari M, Gibellini L, Bellinazzi C, Borella R, et al. Expansion of plasmablasts and loss of memory b cells in peripheral blood from COVID-19 patients with pneumonia. *Eur J Immunol* (2020) 50(9):1283–94. doi: 10.1002/eji.202048838

12. Long QX, Tang XJ, Shi QL, Li Q, Deng HJ, Yuan J, et al. Clinical and immunological assessment of asymptomatic SARS-CoV-2 infections. *Nat Med* (2020) 26(8):1200–4. doi: 10.1038/s41591-020-0965-6

13. Sekine T, Perez-Potti A, Rivera-Ballesteros O, Stralin K, Gorin JB, Olsson A, et al. Robust T cell immunity in convalescent individuals with asymptomatic or mild COVID-19. *Cell* (2020) 183(1):158–168 e114. doi: 10.1016/j.cell.2020.08.017

14. Hartley GE, Edwards ESJ, Aui PM, Varese N, Stojanovic S, McMahon J, et al. Rapid generation of durable b cell memory to SARS-CoV-2 spike and nucleocapsid proteins in COVID-19 and convalescence. *Sci Immunol* (2020) 5(54):eabf8891. doi: 10.1126/sciimmunol.abf8891

15. Jeffery-Smith A, Burton AR, Lens S, Rees-Spear C, Davies J, Patel M, et al. SARS-CoV-2-specific memory b cells can persist in the elderly who have lost detectable neutralizing antibodies. *J Clin Invest* (2022) 132(2):e152042. doi: 10.1172/JCI152042

16. Oberhardt V, Luxenburger H, Kemming J, Schulien I, Ciminski K, Giese S, et al. Rapid and stable mobilization of CD8(+) T cells by SARS-CoV-2 mRNA vaccine. *Nature* (2021) 597(7875):268–73. doi: 10.1038/s41586-021-03841-4

17. Gangaev A, Ketelaars SLC, Isaeva OI, Patiwael S, Dopler A, Hoefakker K, et al. Identification and characterization of a SARS-CoV-2 specific CD8(+) T cell response with immunodominant features. *Nat Commun* (2021) 12(1):2593. doi: 10.1038/s41467-021-22811-y

18. Sahin U, Muik A, Vogler I, Derhovanessian E, Kranz LM, Vormehr M, et al. BNT162b2 vaccine induces neutralizing antibodies and poly-specific T cells in humans. *Nature* (2021) 595(7868):572–7. doi: 10.1038/s41586-021-03653-6

19. Skelly DT, Harding AC, Gilbert-Jaramillo J, Knight ML, Longet S, Brown A, et al. Two doses of SARS-CoV-2 vaccination induce robust immune responses to emerging SARS-CoV-2 variants of concern. *Nat Commun* (2021) 12(1):5061. doi: 10.1038/s41467-021-25167-5

20. Agrati C, Castilletti C, Goletti D, Sacchi A, Bordoni V, Mariotti D, et al. Persistent spike-specific T cell immunity despite antibody reduction after 3 months from SARS-CoV-2 BNT162b2-mRNA vaccine. *Sci Rep* (2022) 12(1):6687. doi: 10.1038/s41598-022-07741-z

21. Goel RR, Painter MM, Apostolidis SA, Mathew D, Meng W, Rosenfeld AM, et al. mRNA vaccines induce durable immune memory to SARS-CoV-2 and variants of concern. *Science* (2021) 374(6572):abm0829. doi: 10.1126/science.abm0829

22. Ciabattini A, Pastore G, Fiorino F, Polvere J, Lucchesi S, Pettini E, et al. Evidence of SARS-CoV-2-Specific memory b cells six months after vaccination with the BNT162b2 mRNA vaccine. *Front Immunol* (2021) 12:740708. doi: 10.3389/fimmu.2021.740708

23. Guerrera G, Picozza M, D'Orso S, Placido R, Pirronello M, Verdiani A, et al. BNT162b2 vaccination induces durable SARS-CoV-2-specific T cells with a stem cell memory phenotype. *Sci Immunol* (2021) 6(66):eabl5344. doi: 10.1126/sciimmunol.abl5344

24. Parry H, Bruton R, Stephens C, Brown K, Amirthalingam G, Otter A, et al. Differential immunogenicity of BNT162b2 or ChAdOx1 vaccines after extended-interval homologous dual vaccination in older people. *Immun Ageing* (2021) 18(1):34. doi: 10.1186/s12979-021-00246-9

25. Parry H, Bruton R, Tut G, Ali M, Stephens C, Greenwood D, et al. Immunogenicity of single vaccination with BNT162b2 or ChAdOx1 nCoV-19 at 5-6 weeks post vaccine in participants aged 80 years or older: An exploratory analysis. *Lancet Healthy Longev* (2021) 2(9):e554–60. doi: 10.1016/S2666-7568(21)00169-0

26. Stuart ASV, Shaw RH, Liu X, Greenland M, Aley PK, Andrews NJ, et al. Immunogenicity, safety, and reactogenicity of heterologous COVID-19 primary vaccination incorporating mRNA, viral-vector, and protein-adjuvant vaccines in the UK (Com-COV2): A single-blind, randomised, phase 2, non-inferiority trial. *Lancet* (2022) 399(10319):36–49. doi: 10.1016/S0140-6736(21)02718-5

27. Pozzetto B, Legros V, Djebali S, Barateau V, Guibert N, Villard M, et al. Immunogenicity and efficacy of heterologous ChAdOx1-BNT162b2 vaccination. *Nature* (2021) 600(7890):701–6. doi: 10.1038/s41586-021-04120-y

28. Goldberg Y, Mandel M, Bar-On YM, Bodenheimer O, Freedman LS, Ash N, et al. Protection and waning of natural and hybrid immunity to SARS-CoV-2. *N Engl J Med* (2022) 386(23):2201–12. doi: 10.1056/NEJMoa2118946

29. Mazzoni A, Di Lauria N, Maggi L, Salvati L, Vanni A, Capone M, et al. First-dose mRNA vaccination is sufficient to reactivate immunological memory to SARS-CoV-2 in subjects who have recovered from COVID-19. *J Clin Invest* (2021) 131(12):e149150. doi: 10.1172/JCI149150

30. Marshall JC, Murthy S, Diaz J, Adhikari NK, Angus DC, Arabi YM, et al. Characterisation WHOWGotC, management of c-i: A minimal common outcome measure set for COVID-19 clinical research. *Lancet Infect Dis* (2020) 20(8):e192–7. doi: 10.1016/S1473-3099(20)30483-7

31. Bacher P, Scheffold A. Flow-cytometric analysis of rare antigen-specific T cells. *Cytometry A* (2013) 83(8):692–701. doi: 10.1002/cyto.a.22317

32. Reiss S, Baxter AE, Cirelli KM, Dan JM, Morou A, Daigneault A, et al. Comparative analysis of activation induced marker (AIM) assays for sensitive identification of antigen-specific CD4 T cells. *PloS One* (2017) 12(10):e0186998. doi: 10.1371/journal.pone.0186998

33. Grifoni A, Weiskopf D, Ramirez SI, Mateus J, Dan JM, Moderbacher CR, et al. Targets of T cell responses to SARS-CoV-2 coronavirus in humans with COVID-19 disease and unexposed individuals. *Cell* (2020) 181(7):1489–1501 e1415. doi: 10.1016/j.cell.2020.05.015

34. De Biasi S, Paolini A, Lo Tartaro D, Gibellini L, Cossarizza A. Analysis of antigen-specific T and b cells for monitoring immune protection against SARS-CoV-2. *Curr Protoc* (2023) 3(1):e636. doi: 10.1002/cpz1.636

35. Turner JS, Kim W, Kalaidina E, Goss CW, Rauseo AM, Schmitz AJ, et al. SARS-CoV-2 infection induces long-lived bone marrow plasma cells in humans. *Nature* (2021) 595(7867):421–5. doi: 10.1038/s41586-021-03647-4

36. Sutton HJ, Aye R, Idris AH, Vistein R, Nduati E, Kai O, et al. Atypical b cells are part of an alternative lineage of b cells that participates in responses to vaccination and infection in humans. *Cell Rep* (2021) 34(6):108684. doi: 10.1016/j.celrep.2020.108684

37. Sheikh-Mohamed S, Isho B, Chao GYC, Zuo M, Cohen C, Lustig Y, et al. Systemic and mucosal IgA responses are variably induced in response to SARS-CoV-2 mRNA vaccination and are associated with protection against subsequent infection. *Mucosal Immunol* (2022) 15(5):799–808. doi: 10.1038/s41385-022-00511-0

38. Montague BT, Wipperman MF, Chio E, Crow R, Hooper AT, O'Brien MP, et al. Elevated serum IgA following vaccination against SARS-CoV-2 in a cohort of high-risk first responders. *Sci Rep* (2022) 12(1):14932. doi: 10.1038/s41598-022-19095-7

39. Sette A, Crotty S. Immunological memory to SARS-CoV-2 infection and COVID-19 vaccines. *Immunol Rev* (2022) 310(1):27–46. doi: 10.1111/imr.13089

40. Betts MR, Nason MC, West SM, De Rosa SC, Migueles SA, Abraham J, et al. HIV Nonprogressors preferentially maintain highly functional HIV-specific CD8+ T cells. *Blood* (2006) 107(12):4781–9. doi: 10.1182/blood-2005-12-4818

41. De Rosa SC, Lu FX, Yu J, Perfetto SP, Falloon J, Moser S, et al. Vaccination in humans generates broad T cell cytokine responses. *J Immunol* (2004) 173(9):5372–80. doi: 10.4049/jimmunol.173.9.5372

42. Precopio ML, Betts MR, Parrino J, Price DA, Gostick E, Ambrozak DR, et al. Immunization with vaccinia virus induces polyfunctional and phenotypically distinctive CD8(+) T cell responses. *J Exp Med* (2007) 204(6):1405–16. doi: 10.1084/jem.20062363

43. Ellebedy AH, Jackson KJ, Kissick HT, Nakaya HI, Davis CW, Roskin KM, et al. Defining antigen-specific plasmablast and memory b cell subsets in human blood after viral infection or vaccination. *Nat Immunol* (2016) 17(10):1226–34. doi: 10.1038/ni.3533

44. Wrammert J, Onlamoon N, Akondy RS, Perng GC, Polsrila K, Chandele A, et al. Rapid and massive virus-specific plasmablast responses during acute dengue virus infection in humans. *J Virol* (2012) 86(6):2911–8. doi: 10.1128/JVI.06075-11

45. Wrammert J, Miller J, Akondy R, Ahmed R. Human immune memory to yellow fever and smallpox vaccination. *J Clin Immunol* (2009) 29(2):151–7. doi: 10.1007/s10875-008-9267-3

46. Wrammert J, Ahmed R. Maintenance of serological memory. *Biol Chem* (2008) 389(5):537–9. doi: 10.1515/bc.2008.066

47. Borobia AM, Carcas AJ, Perez-Olmeda M, Castano L, Bertran MJ, Garcia-Perez J, et al. Immunogenicity and reactogenicity of BNT162b2 booster in ChAdOx1-s-primed participants (CombiVacS): A multicentre, open-label, randomised, controlled, phase 2 trial. *Lancet* (2021) 398(10295):121–30. doi: 10.1016/S0140-6736(21)01420-3

48. Cossarizza A, Chang HD, Radbruch A, Abrignani S, Addo R, Akdis M, et al. Guidelines for the use of flow cytometry and cell sorting in immunological studies (third edition). *Eur J Immunol* (2021) 51(12):2708–3145. doi: 10.1002/eji.202170126

49. Hahne F, LeMeur N, Brinkman RR, Ellis B, Haaland P, Sarkar D, et al. flowCore: A bioconductor package for high throughput flow cytometry. *BMC Bioinf* (2009) 10:106. doi: 10.1186/1471-2105-10-106

50. Nowicka M, Krieg C, Crowell HL, Weber LM, Hartmann FJ, Guglietta S, et al. CyTOF workflow: Differential discovery in high-throughput high-dimensional cytometry datasets. *F1000Res* (2017) 6:748. doi: 10.12688/f1000research.11622.3

51. Weber LM, Nowicka M, Soneson C, Robinson MD. Diffcyt: Differential discovery in high-dimensional cytometry *via* high-resolution clustering. *Commun Biol* (2019) 2:183. doi: 10.1038/s42003-019-0415-5

52. Roederer M, Nozzi JL, Nason MC. SPICE: exploration and analysis of post-cytometric complex multivariate datasets. *Cytometry A* (2011) 79(2):167–74. doi: 10.1002/cyto.a.21015

frontiers | Frontiers in Immunology

TYPE Original Research
PUBLISHED 05 May 2023
DOI 10.3389/fimmu.2023.1123807

Check for updates

OPEN ACCESS

EDITED BY
Paola Contini,
University of Genoa, Italy

REVIEWED BY
Anna Vanni,
University of Florence, Italy
Lavanya Visvabharathy,
Northwestern University, United States

*CORRESPONDENCE
Sara De Biasi
sara.debiasi@unimore.it

†These authors have contributed equally to this work

RECEIVED 14 December 2022
ACCEPTED 26 April 2023
PUBLISHED 05 May 2023

CITATION
De Biasi S, Mattioli M, Meschiari M, Lo Tartaro D, Paolini A, Borella R, Neroni A, Fidanza L, Busani S, Girardis M, Coppi F, Mattioli AV, Guaraldi G, Mussini C, Cossarizza A and Gibellini L (2023) Prognostic immune markers identifying patients with severe COVID-19 who respond to tocilizumab. *Front. Immunol.* 14:1123807. doi: 10.3389/fimmu.2023.1123807

COPYRIGHT
© 2023 De Biasi, Mattioli, Meschiari, Lo Tartaro, Paolini, Borella, Neroni, Fidanza, Busani, Girardis, Coppi, Mattioli, Guaraldi, Mussini, Cossarizza and Gibellini. This is an open-access article distributed under the terms of the Creative Commons Attribution License (CC BY). The use, distribution or reproduction in other forums is permitted, provided the original author(s) and the copyright owner(s) are credited and that the original publication in this journal is cited, in accordance with accepted academic practice. No use, distribution or reproduction is permitted which does not comply with these terms.

Prognostic immune markers identifying patients with severe COVID-19 who respond to tocilizumab

Sara De Biasi[1*], Marco Mattioli[1], Marianna Meschiari[2], Domenico Lo Tartaro[1], Annamaria Paolini[1], Rebecca Borella[1], Anita Neroni[1], Lucia Fidanza[1], Stefano Busani[3], Massimo Girardis[3], Francesca Coppi[4], Anna Vittoria Mattioli[1], Giovanni Guaraldi[2], Cristina Mussini[2], Andrea Cossarizza[1,5†] and Lara Gibellini[1†]

[1]Department of Medical and Surgical Sciences for Children and Adults, University of Modena and Reggio Emilia School of Medicine, Modena, Italy, [2]Infectious Diseases Clinics, Azienda Ospedaliera Universitaria (AOU) Policlinico and University of Modena and Reggio Emilia, Modena, Italy, [3]Department of Anesthesia and Intensive Care, Azienda Ospedaliera Universitaria (AOU) Policlinico and University of Modena and Reggio Emilia, Modena, Italy, [4]Department of Metabolic Sciences and Neurosciences, Azienda Ospedaliera Universitaria (AOU) Policlinico and University of Modena and Reggio Emilia, Modena, Italy, [5]National Institute for Cardiovascular Research, Bologna, Italy

Introduction: A growing number of evidences suggest that the combination of hyperinflammation, dysregulated T and B cell response and cytokine storm play a major role in the immunopathogenesis of severe COVID-19. IL-6 is one of the main pro-inflammatory cytokines and its levels are increased during SARS-CoV-2 infection. Several observational and randomized studies demonstrated that tocilizumab, an IL-6R blocker, improves survival in critically ill patients both in infectious disease and intensive care units. However, despite transforming the treatment options for COVID-19, IL-6R inhibition is still ineffective in a fraction of patients.

Methods: In the present study, we investigated the impact of two doses of tocilizumab in patients with severe COVID-19 who responded or not to the treatment by analyzing a panel of cytokines, chemokines and other soluble factors, along with the composition of peripheral immune cells, paying a particular attention to T and B lymphocytes.

Results: We observed that, in comparison with non-responders, those who responded to tocilizumab had different levels of several cytokines and different T and B cells proportions before starting therapy. Moreover, in these patients, tocilizumab was further able to modify the landscape of the aforementioned soluble molecules and cellular markers.

Conclusions: We found that tocilizumab has pleiotropic effects and that clinical response to this drug remain heterogenous. Our data suggest that it is possible to identify patients who will respond to treatment and that the administration of tocilizumab is able to restore the immune balance through the re-establishment of different cell populations affected by SARS-COV-2 infection, highlighting the importance of temporal examination of the pathological features from the diagnosis.

KEYWORDS

SARS-CoV-2, COVID-19, tocilizumab, cytokines, B cells, T cells

Introduction

Most SARS-CoV-2 infections are asymptomatic or pauci-symptomatic. However, a proportion of individuals develop a severe disease, characterized by a progressive respiratory failure after the onset of dyspnea and hypoxemia (1). It is well known that the combination of hyperinflammation, dysregulation in T and B cell response and cytokine storm are responsible for the development of severe and eventually fatal COVID-19 (2–4). Plasma levels of several inflammatory cytokines, such as interleukin (IL)-6, tumor necrosis factor (TNF), granulocyte-macrophage colony-stimulating factor (GM-CSF), and granulocyte colony-stimulating factor (G-CSF) are indeed increased after SARS-CoV-2 infection, in patients with the severe disease (3–6).

IL-6 is one of the main pro-inflammatory cytokines. It regulates several aspects of innate and adaptive immunity, including the differentiation of B lymphocytes, cytotoxic T cells, and macrophage/monocyte functions (7, 8). IL-6 exists both as a soluble and membrane-bound molecule, and is typically found in the blood of healthy individuals at very low concentrations (1-5 pg/mL) (9). Its levels increase during acute and/or chronic inflammation (10, 11). IL-6 binds to IL-6 receptor (IL-6R, or CD126) and glycoprotein 130 (gp130) to form a hexameric complex that transduces IL-6 signal through the Janus kinase (JAK) and signal transducer and activator of transcription (STAT) pathway (10). In the context of disease, IL-6 can have both local and systemic deleterious inflammatory effects. Indeed, the association between high IL-6 concentration (> 80 pg/mL) and respiratory failure and/or death has been confirmed in several studies and posed the rationale for the use of IL-6 blockers in the management of patients with severe COVID-19 (12, 13).

Tocilizumab is a humanized antibody that targets IL-6R and inhibits the binding of IL-6 to both soluble and membrane forms of the receptor. It interferes with IL-6 signaling and dampen inflammation. The single-cell RNA-seq analysis of peripheral blood mononuclear cells (PBMCs) isolated from two severe COVID-19 patients treated with tocilizumab, at the severe and remission disease stages, revealed that a monocyte-associated cytokine storm is present in patients at the severe stage and that tocilizumab can weaken this inflammatory response (14). Both case-control studies and randomized trials of tocilizumab in COVID-19 have demonstrated that it improves survival and reduces the chances of progressing to invasive mechanical ventilation in hospitalized COVID-19 patients with hypoxia and systemic inflammation (15, 16). Data from the REMAP-CAP and RECOVERY trials revealed that combining corticosteroids with tocilizumab yields cumulative benefits for mortality and morbidity in severe COVID-19 (15, 17). However, as already observed for other immunotherapeutic drugs in other diseases, including chronic inflammatory diseases and cancer, a proportion of patients did not derive benefits from tocilizumab treatment (18, 19).

In the present study, we aimed at identifying possible prognostic biomarkers related to the response to this drug. For this reason, we profiled the plasma levels of several cytokines, chemokines and other soluble factors in patients with severe COVID-19 who responded or not to tocilizumab, and we examined how tocilizumab impacted the composition of peripheral immune cells.

Results

Modulation of plasma cytokines and chemokines during tocilizumab treatment

The plasma profiling of 62 cytokines, chemokines and other soluble factors involved in several immune responses was first performed in 23 patients with severe COVID-19, responding or not to tocilizumab. The drug was given twice, 12 hours apart, by intravenous or subcutaneous route (see Methods for details). Plasma molecules were quantified at the baseline (T0, before the beginning of treatment), two days (T2) and seven days (T7) after the first dose of the drug. Most patients were sampled during the acute phase of the infection: 13 patients responded to therapy, whereas 10 patients did not. Demographic information, clinical data, blood parameters and arterial haemogas analysis, collected at T0, are reported in Supplementary Table 1.

Figure 1 shows plasma levels of several cytokines/chemokines and other soluble factors in responder and non-responder patients. Concerning pro-inflammatory cytokines, we found that after 2 days

10.3389/fimmu.2023.1123807

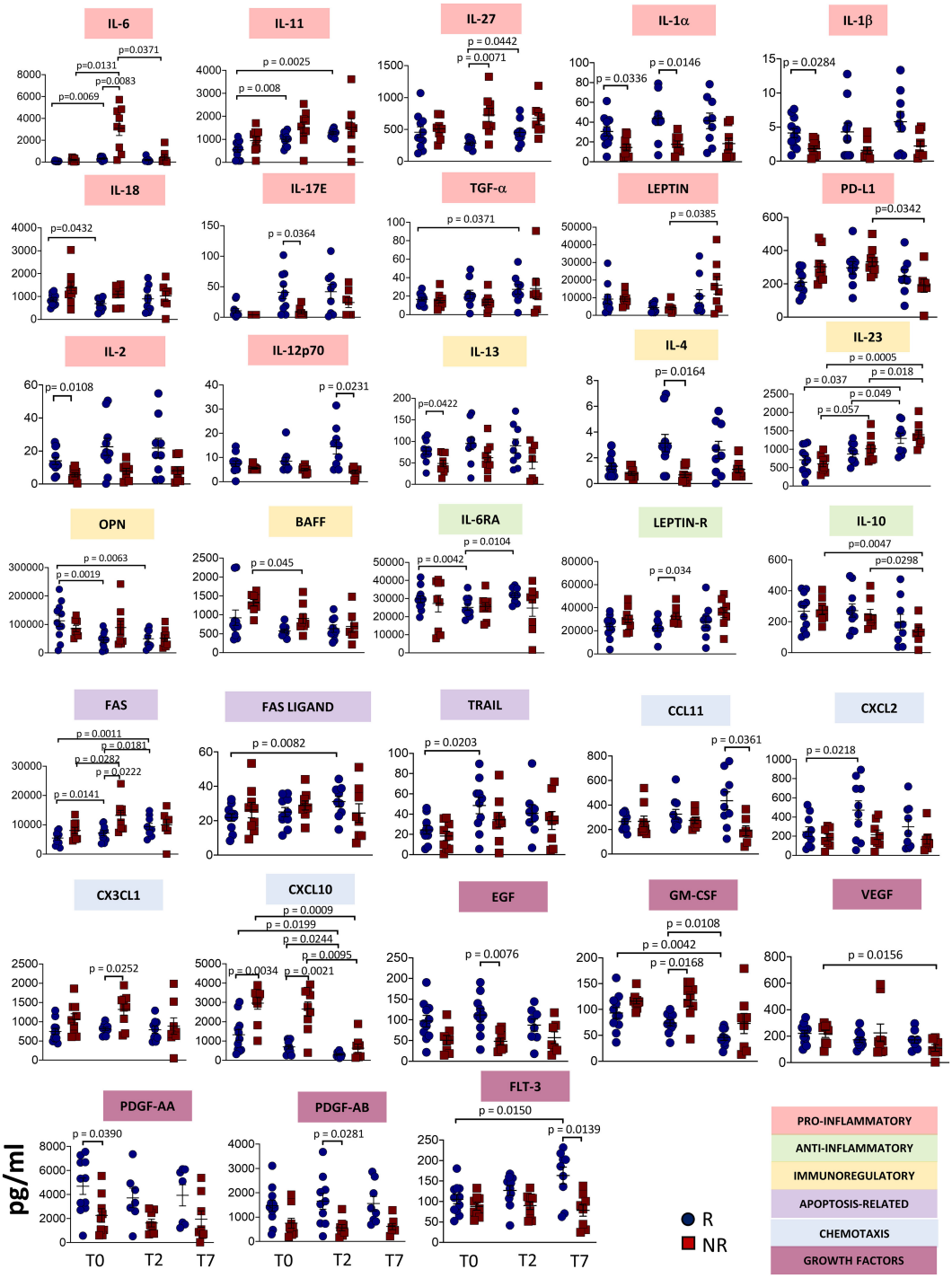


FIGURE 1
Plasmatic level of different soluble molecules in responder and non-responder patients. Quantification of cytokines and other mediators in plasma obtained from COVID-19 patients responding (R) or not (NR) to tocilizumab (n = 23). Data represent individual values, mean (centre bar) ± SEM (upper and lower bars). Statistical analysis by two-way ANOVA followed by Bonferroni correction; if not indicated, p-value is not significant.

of therapy IL-6 and IL-27 plasma concentrations strongly increased in non-responders. IL-11 levels did not differ between responders and non-responders, but increased in responders after therapy. Non-responders had lower basal levels of interleukin IL-1α, IL-1β, while in responders at T2 IL-18 decreased and IL-17E increased. Level of TGF-α increased over time in responders. Leptin level increased from T2 to T7 in non-responders, while PD-L1 decreased. IL-2 level was lower in non-responders at T0 and significant differences were observed at T7 between responders and non-responders for IL-12p70.

The concentrations of IL-6RA reached the minimum value at T2 in responders. At T2, Leptin receptor (Leptin R) was different

between responders and non-responders, with higher level in the latter. IL-10 decreased during therapy in non-responders. IL-2 and IL-13 plasma levels were lower in non-responders at T0, while IL-4 level was lower at T2. Significant differences were observed at T7 between responders and non-responders for IL-12p70. We also noted that IL-23 increased after one week of treatment in both groups of patients. Levels of optineurin (OPN) decreased during therapy in patients responding to tocilizumab. The level of B-cell activating factor (BAFF) decreased in non-responders during therapy.

Apoptosis-related molecules have been investigated. FAS levels increased during therapy in responder and non-responder patients, but higher levels have been detected in non-responders at T2. FAS ligand and TRAIL levels increased in responders, at T7 and T2, respectively.

Plasma concentrations of C-C Motif Chemokine Ligand (CCL)-11 were lower in non-responders at T7, while C-X-C motif chemokine ligand (CXCL)-2 was higher at T2 in responders. CX3CL1 was higher at T2 in non-responders. CXCL10 plasma levels decreased over time in both groups of patients, but non-responders displayed higher levels at T0. This difference was maintained at T2 and at T7.

Regarding growth factors, in responders epidermal growth factor (EGF) was higher at T2 whereas GM-CSF decreased with time. Vascular endothelial growth factor (VEGF) decreased in non-responders over time. Levels of platelet-derived growth factor (PDGF)-AA were lower at the baseline in non-responders. (PDGF)-AB was lower in non-responders at T2. Fms related receptor tyrosine kinase 3 (FLT-3 ligand, also known as CD135) decreased after seven days in non-responders, but increased in responders. All the other soluble molecules remained unchanged in responders and non-responders (Supplementary Figure 1).

Circulating plasmablasts decreased in responders after therapy

To investigate how immune responses vary in the presence of tocilizumab, we profiled B cells and T cells by using polychromatic flow cytometry. After unsupervised analysis, nine distinct cell clusters have been identified (UMAP and heatmap are reported in Figures 2A, B) on the basis of the surface protein expression (Supplementary Figure 2). Besides a population of cells negative for all the activation/differentiation markers analyzed, naïve B cells are defined as $IgM^+IgD^+CD24^+CD21^+CD38^-CD27^-$ while transitional B cells are $IgM^+IgD^+CD24^+CD21^+CD38^+CD27^-$ memory unswitched B cells are defined as $IgM^+IgD^+CD24^+CD21^+CD38^-CD27^+$ while memory switched B cells are $IgM^-IgD^-CD24^+CD21^+CD38^-CD27^+$. Memory IgM only B cells are $IgM^+IgD^-CD24^+CD21^+CD38^-CD27^+$. Plasmablasts are $IgM^{-/+}IgD^-CD24^-CD21^-CD38^+CD27^+$. Finally, exhausted B cells are those $CD21^-$ and $CD24^-$ (2).

Before therapy (T0), responders showed a higher percentage and absolute number of total B cells and a higher absolute number of memory IgM-only subpopulation compared to non-responders. After two days of therapy, plasmablasts not expressing IgM increases in non-responders compared to responder patients. Responders show an increase in both absolute number and percentage of memory switch B cell population compared to non-responders. After seven days of therapy, we observed an increase in absolute number of total B cells and naïve B cell subpopulation in both responder and non-responder patients, an increase in percentage of plasmablast IgM^+ in responder patients, a decrease in percentage of plasmablast IgM^- and an increase in absolute number of exhausted B cell and surface- subpopulation in both groups. Finally, non-responder patients display a decrease of absolute number of transitional B cells (Figure 2C).

Tocilizumab induces a redistribution in memory T cell pool

T cell compartment of patient with COVID-19 pneumonia displays marked T cell activation, senescence, exhaustion and skewing towards Th17 (3). Given that also T cells expressed CD126 and could be tuned by Tocilizumab administration, we investigated the T cells landscape of patients undergoing anti-IL6R-therapy.

Eighteen clusters of $CD4^+$ T cells were recognized after unsupervised analysis on the basis of different expression of differentiation (CD45RA, CCR7, CD25, CD95, CD27, CD28, CD57) and activation markers (HLA-DR, CD28, PD1) (Figures 3A, B; Supplementary Figure 3, 4). Naïve T cells (N) were defined as expressing CD45RA, CCR7, CD27, CD28, CD127, CD25 and lack of expression of CD95, CD38 and HLA-DR. Moreover, a population of recently activated naïve T cells has been recognized as those expressing CD38. CD38 is a multifunctional molecule, belonging to the family of ectoenzymes and it induces intracellular calcium release. The expression of CD38 identifies a hypo-proliferative $CD4^+$ T-cell subset that, following TCR stimulation, retains expression of naïve cell surface markers including CD45RA and CCR7 (20). We were able also to identify T cells stem memory (T_{SCM}) as naïve cells expressing CD95 and CD38. Central memory T cells (CM) were those expressing CCR7, CD95 and not CD45RA, then four subsets of central memory were found: one expressing CD38, one expressing PD-1, one co-expressing CD38 and PD-1 and one activated ($CD38^+HLA\text{-}DR^+$) expressing also PD-1. Three populations of transitional memory (TM) were found as they do not express CD45RA and CCR7, but they express CD28. Moreover, one population of TM is phenotypically resting, one population is expressing CD38 and PD1 and another subset is highly activated as it expresses high level of HLA-DR, CD38 and PD-1. In particular, PD-1 is expressed during the early phase of T cell activation when naïve T cells differentiate into effector cells: it is rapidly expressed after antigen stimulation of naïve T cells with a kinetics of expression similar to the expression of early activation markers (CD69 and CD25) (21, 22). Effector memory T cells (EM) are characterized by the lack of the expression of CD28, CD45RA and CCR7. Two different populations of EM have been identified: one has been identified as a population of phenotypically resting cells and the other as exhausted cells as it expresses CD57 and PD-1. A population of terminally differentiated T cells (TE) were found as effector memory

10.3389/fimmu.2023.1123807

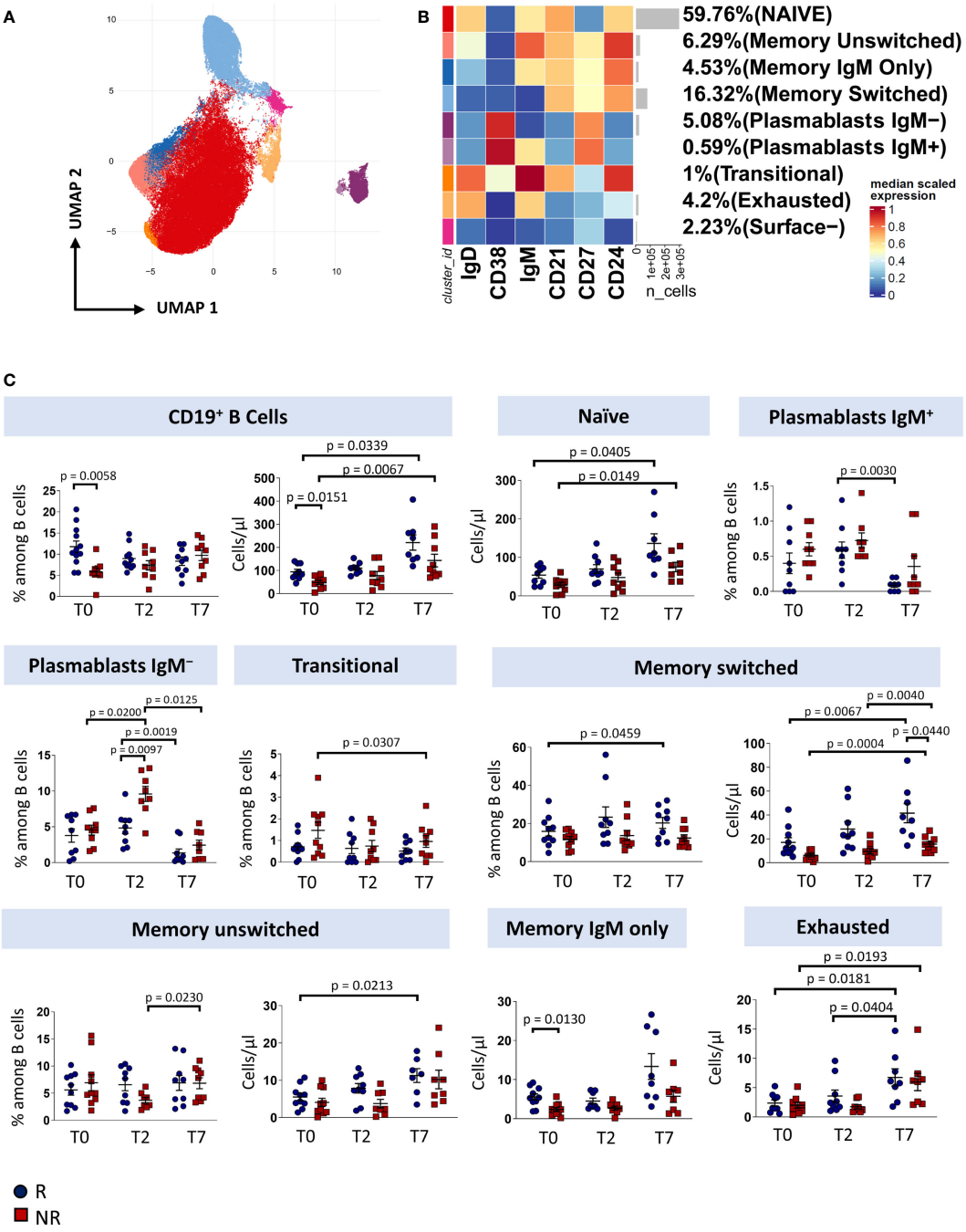


FIGURE 2
B cells landscape of COVID-19 patients treated with tocilizumab. **(A)** Uniform Manifold Approximation and Projection (UMAP) representation of the B-cell landscape. Each color is assigned according to the cluster identification palette. **(B)** Heatmap representing different B-cell clusters identified by FlowSOM, with relative identity and percentages. The colors in the heatmap represent the median of the arcsinh, 0-1 transformed marker expression calculated over cells from all the samples, varying from blue for lower expression to red for higher expression. Each cluster has a unique color assigned (bar on the left). **(C)** Statistical analysis of the different cell populations identified as in **(B)** Comparison between responders (R, blue circles) and non-responders (NR, red squares) at different treatment timepoints. The dot plots show the relative abundancies (left plot) and the absolute numbers (right plot) of populations found within B cells. Data represent individual percentage values (dots), median (center bar) and SEM (upper and lower bars). Statistical analysis by two-way ANOVA test with Bonferroni correction has been used. Exact p-value is indicated in the figure.

re-expressing CD45RA. Finally, putative T regulatory cells (T_{reg}) were defined as those expressing CD25 and not expressing CD127. Four populations were found: naïve T_{reg} expressing CD45RA and CCR7, central memory T_{reg} as those not expressing CD45RA and expressing CCR7, central memory T_{reg} expressing also CD38 and effector memory T_{reg} as those characterized by the lack of expression of both previous markers.

The percentage of $CD4^+$ T cells was influenced by therapy, as in responders it increased at T2 and decreased at T7. The absolute number increased at T2 and T7 in responders, and only from T0

10.3389/fimmu.2023.1123807

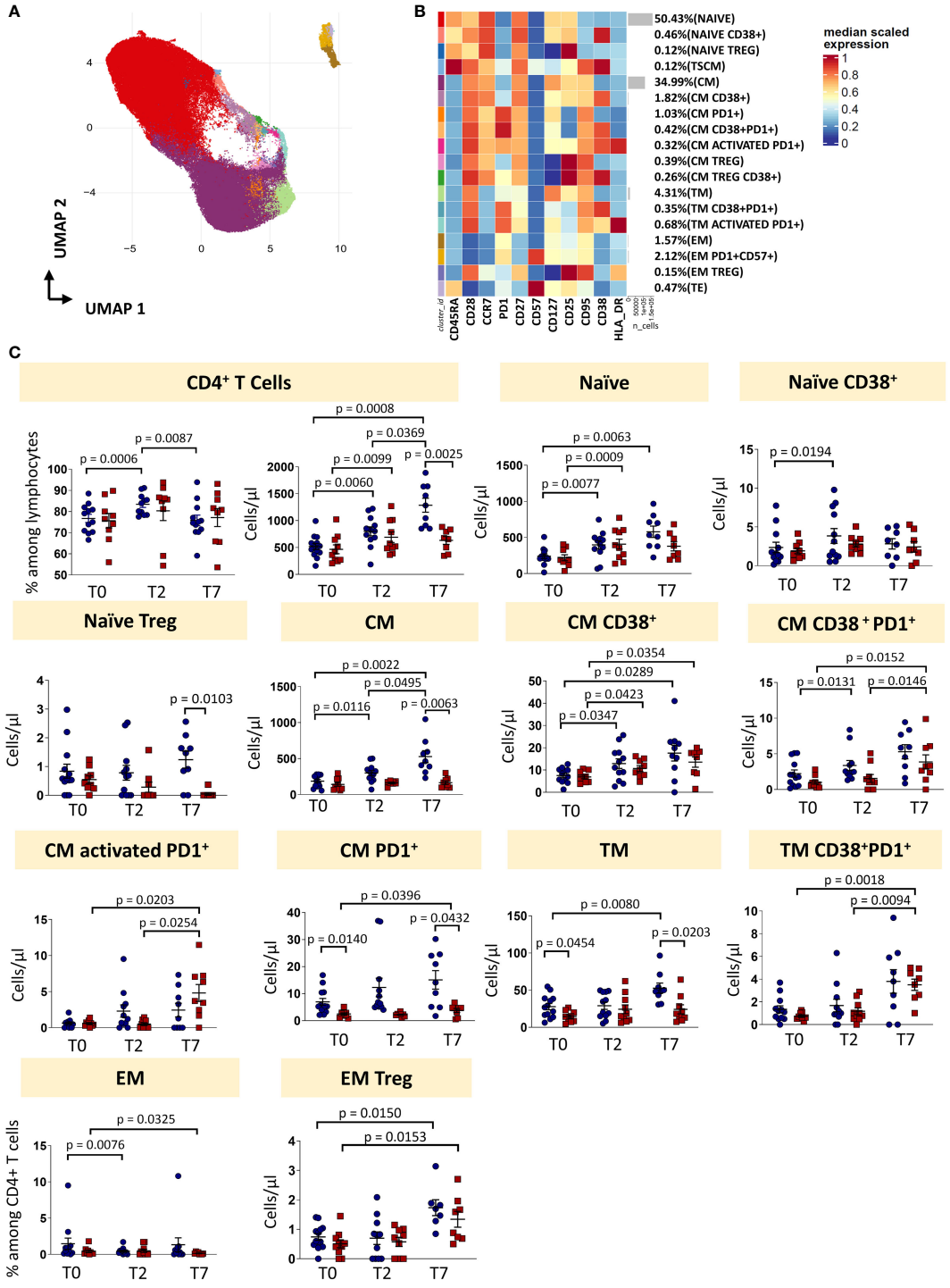


FIGURE 3
CD4 T cells landscape of COVID-19 patients treated with tocilizumab. **(A)** Uniform Manifold Approximation and Projection (UMAP) representation of the CD4 T cell landscape. Each color is assigned according to the cluster identification palette. **(B)** Heatmap representing different cell clusters identified by FlowSOM, with relative identity and percentages. The colors in the heatmap represent the median of the arcsinh, 0-1 transformed marker expression calculated over cells from all the samples, varying from blue for lower expression to red for higher expression. Each cluster has a unique color assigned (bar on the left). **(C)** Statistical analysis of the different CD4 T cells populations identified as in **(B)** Comparison between responders (R, blue circles) and non-responders (NR, red squares) at different treatment timepoints. The dot plots show the relative abundancies and/or absolute numbers of subpopulations found within CD4 T cells. Data represent individual percentage values (dots), median (center bar) and SEM (upper and lower bars). Statistical analysis by two-way ANOVA test with Bonferroni correction has been used. Exact p-value is indicated in the figure. T_{SCM}, T cells stem memory; CM, central memory; TM, transitional memory; EM, effector memory; TREG, T regulatory cells; TE, terminally differentiated T cells re-expressing CD45RA.

and T2 in non-responders. At T7, the absolute number of $CD4^+$ T cells was lower in non-responders if compared to responders. The absolute number of naïve T cells increased in responders (until T7) and non-responders (until T2). Naïve $CD38^+$ T cells increased in responders from T0 to T2, while the absolute number of naïve Treg at T7 was higher in responders *vs* non-responders. Absolute number of CM T cells increased after treatment in responders, but not in non-responders. The same trend was observed for the absolute number of CM $CD38^+$ T cells and CM $CD38^+$ T cells expressing PD-1 for responders and non-responders. The absolute number of activated CM expressing PD-1 increased in non-responders, but did not change in responders. Absolute numbers of CM T cells expressing PD-1 were higher in responders at each time points. Absolute number of TM cells was higher at T0 and T7 in responders and increased during therapy for responder patients. The absolute number of TM expressing CD38 and PD-1 increased in non-responders after therapy, but did not change in responders. The percentage of EM T cells decreased in non-responders from T0 to T7 and in responders from T0 to T2. The absolute number of EM Treg increased in both responders and non-responders after therapy (from T0 to T7).

To sum up, even if the percentage of total $CD4^+$ T is modulated by the therapy, the proportion of different $CD4^+$ T cell subpopulations remained unchanged. However, the increased of the absolute number of $CD4^+$ T cells in responders was likely responsible for all the differences found in the main subpopulations (Figure 3C, exact p-values are reported in the figures).

Regarding $CD8^+$ T cell subsets, twenty-two clusters of CD8 T cells have been identified by unsupervised analysis on the basis of different expression of differentiation (CD45RA, CCR7, CD25, CD95, CD27, CD28, CD57) and activation markers (HLA-DR, CD28, PD-1) (Figures 4A, B; Supplementary Figures 5, 6). These populations span the entire spectrum of differentiation and activation status. As for $CD8^+$ T cell subsets, naïve cells, naïve cells expressing CD38, T_{SCM}, T_{SCM} expressing CD38, CM, CM co-expressing CD38 and PD-1, TM, EM and TE were identified. Of the TM population, we found four different subsets: a subset of phenotypically resting cells, a subset of TM expressing HLA-DR, a subset of TM expressing CD38 and PD-1, a subset of activated TM also expressing PD1 and a subset of exhausted TM ($CD57^+PD1^+$). Moreover, we found four populations of EM: EM phenotypically resting, EM expressing only CD57, EM expressing CD38 and CD57, EM co-expressing CD57 and HLA-DR. Finally, seven populations of TE cells have been identified: TE phenotypically resting, TE expressing HLA-DR, TE expressing $CD38^+$, TE expressing CD57, TE activated ($CD38^+HLA\text{-}DR^+$), TE co-expressing CD57 and HLA-DR, and TE co-expressing CD38 and CD57.

The percentage of $CD8^+$ T cells decreased from T0 at T2 in both groups of patients, even if in responders the percentage increased at T7, reaching a similar level of T0. As far as the absolute number is concerned, responders were characterized by an increase of $CD8^+$ T cells at T7. Similar absolute numbers of $CD8^+$ T cells were observed in non-responders. At T7, responders were characterized by increased absolute number of naïve, naïve $CD38^+$, CM, TM and EM T cells. The absolute number of T pedix SCM $CD38^+$ was different at T0 and T2 between responders and non-responders, with higher level in responders. Non-responders had higher absolute number of CM $CD38^+PD\text{-}1^+$ and TM $CD38^+PD\text{-}1^+$, at T7. Moreover, at T7, responders showed higher levels of TM and EM if compared to non-responders. The percentages of TE decreased at T7 in non-responders and at T2 in responders. The percentage of TE $CD38^+CD57^+$ decreased at T2 in non-responders (Figure 4C, exact p values are reported in the figures).

We wondered whether the two groups of patients could be identified based on immunological and clinical parameters before therapy initiation (T0), predicting who will benefit from therapy and who will not. By using the principal component analysis (PCA), we saw that non-responders clusterize on the left side of the first dimension (PC1, representing 17% of variance), while responder patients clusterize on the right side (Figure 5A), meaning that before starting therapy they were extremely different from both immunological and clinical point of view. Besides the level of pO2/FiO2, the immunological parameters that were the main responsible for the clusterization in responders were plasma levels of IL-2, IL-13, IL-1α, the absolute number of B cells as well as the memory unswitched B subset and among $CD4^+$ T cells those TM expressing CD38 and PD1. Plasma levels of CXCL10, CXC3CL1, BAFF and the absolute number of different subpopulations of $CD8^+$ T cells such as those EM expressing CD38, CD57 and HLA-DR were the major contributors for the clusterization of non-responders along PC1 (Figure 5B). Moreover, as previously reported, age, levels of D-dimer, SOFA score and levels of creatine are the major demographic/clinical features that are mostly associated to worse disease outcome and lack of response to therapy (2–6).

Discussion

Several observational and randomized studies, including TESEO, RECOVERY and REMAP-CAP, demonstrated that tocilizumab is effective in COVID-19 patients with hypoxemia and in need of oxygen therapy and that it improves survival in critically ill patients in intensive care units (ICUs) (15–17, 23). Despite transforming the treatment options for COVID-19, IL-6R inhibition is still ineffective in a fraction of patients. Thus, to identify possible differences between patients responding or not, we deeply investigated the humoral and adaptive immune compartments of COVID-19 patients undergoing tocilizumab treatment. We found that patients who respond to therapy, are characterized by high basal level of plasmatic IL-1β, IL-1α, IL-2, IL-13 and PDGF and lower level of CXCL10, higher number of B, $CD4^+$ and $CD8^+$ T cells which increase after therapy (Figure 6).

Tocilizumab is a monoclonal antibody that blocks interleukin-6 signaling, reducing downstream effects on inflammation and the immune response, which is largely used for years by rheumatologists. Tocilizumab binds to both soluble (s)IL-6R and membrane (m)IL-6R, thus inhibiting IL-6 binding to its receptors and leading to the blockade of the IL-6 signaling without interfering with other cytokines of the IL-6 family (24). IL-6 is essential for the maturation of B cells and it acts as a T cell survival factor driving T cell expansion under inflammatory conditions, but not during normal homeostasis (25, 26). IL-6

10.3389/fimmu.2023.1123807

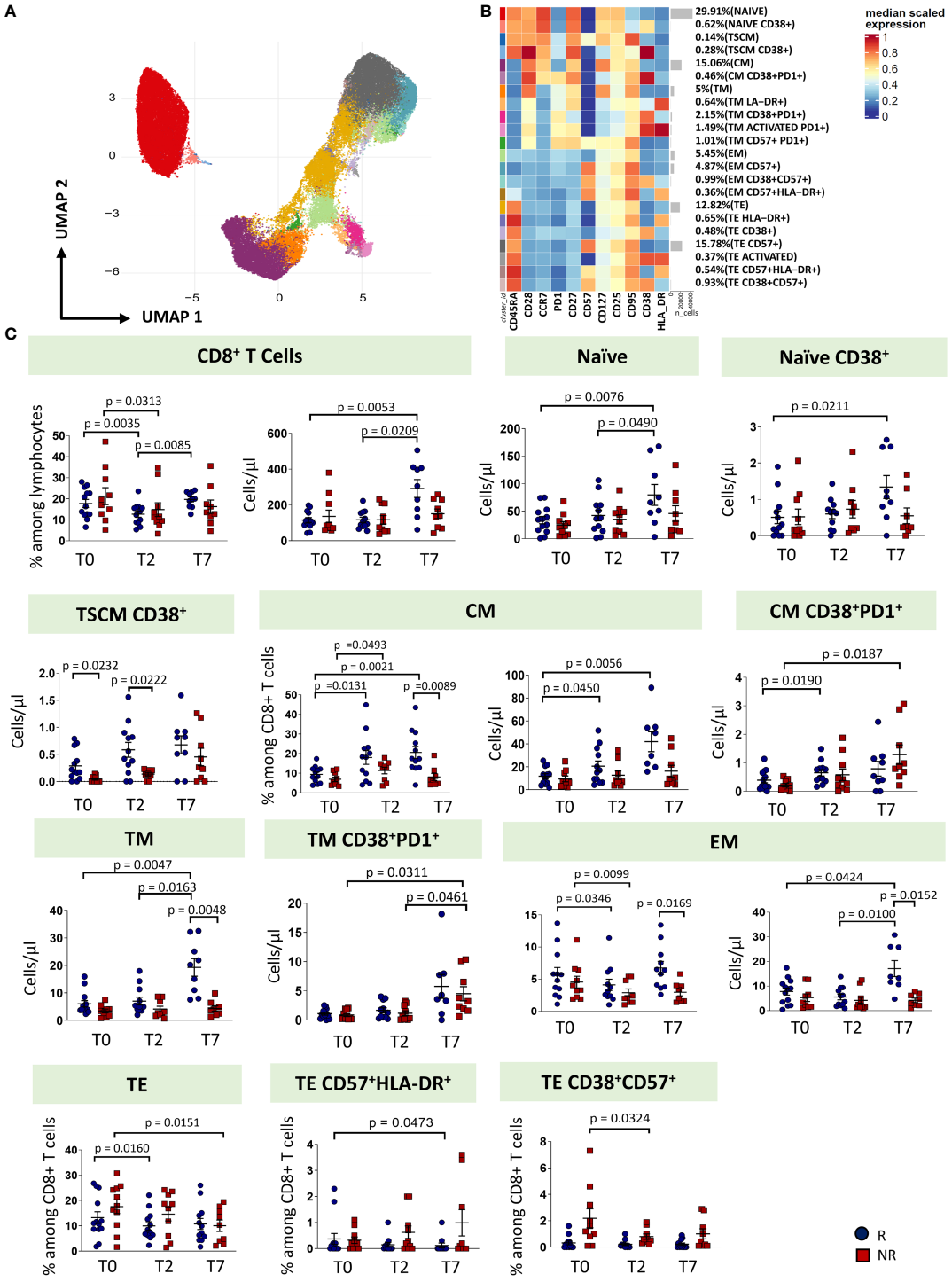


FIGURE 4
CD8 T cells landscape of COVID-19 patients treated with tocilizumab. **(A)** Uniform Manifold Approximation and Projection (UMAP) representation of the CD8 T cell landscape. Each color is assigned according to the cluster identification palette. **(B)** Heatmap representing different cell clusters identified by FlowSOM, with relative identity and percentages. The colors in the heatmap represent the median of the arcsinh, 0-1 transformed marker expression calculated over cells from all the samples, varying from blue for lower expression to red for higher expression. Each cluster has a unique color assigned (bar on the left). **(C)** Statistical analysis of the different CD8 T cells populations identified as in **(B)** Comparison between responders (R, blue circles) and non-responders (NR, red squares) at different treatment timepoints. The dot plots show the relative abundancies and/or absolute numbers of subpopulations found within CD8 T cells. Data represent individual percentage values (dots), median (center bar) and SEM (upper and lower bars). Statistical analysis by two-way ANOVA test with Bonferroni correction has been used. Exact p-value is indicated in the figure. T_{SCM}, T cells stem memory; CM, central memory; TM, transitional memory; EM, effector memory; TE, terminally differentiated T cells re-expressing CD45RA.

10.3389/fimmu.2023.1123807

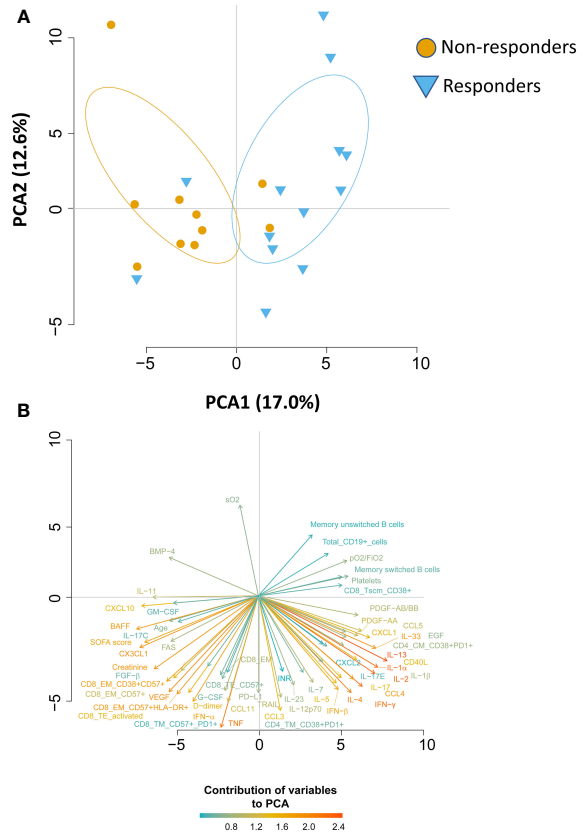


FIGURE 5
Principal Component Analysis (PCA) reveals that responder and non-responder patients are different before starting therapy. **(A)** PCA showing the distribution of responder and non-responder patients. **(B)** Plot displaying the variables as vectors, indicating the direction of each variable to the overall distribution. The strength of each variable is represented by colors: orange color represents a strong contribution, light blue color represents a milder contribution. Length and direction of the arrows indicate the weight and correlation for each parameter.

also inhibits TGF-β-induced Treg differentiation (27), and this reinforces its inflammatory aspect.

We found that, at the time of treatment initiation, COVID-19 patients who responded to tocilizumab had higher levels of several pro-inflammatory cytokines, including IL-1β, IL-1α and IFN-β. This is in agreement with a previous observation showing that the efficacy of tocilizumab is higher in COVID-19 patients with a hyperinflammatory state (28). Similarly, in patients with high IL-6, early administration of tocilizumab was associated with improvement in oxygenation, indicated as the ratio between arterial oxygen tension and fraction of inspired oxygen (29). In our cohort, IL-6 plasma levels were not different between patients responding or not to therapy at the time of treatment initiation, but in non-responders such levels increased after two days of therapy. In other conditions, including rheumatoid arthritis (RA) and Castleman disease, both serum IL-6 and sIL-6R increase in patients after administration of tocilizumab while the disease symptoms ameliorates (30). In this setting, it is likely that free serum IL-6 increases because IL-6R-mediated consumption of IL-6 is inhibited by the unavailability of tocilizumab-free IL-6R, and thus that serum IL-6 during the inhibition of its receptor by tocilizumab represents the actual endogenous production of IL-6 (30). In our cohort, IL-6 levels increased after two days of therapy in non-responders. We could hypothesize that, also in this case, plasma IL-6 levels represent the actual endogenous production of IL-6 and the true disease activity of patients when the causal factors of IL-6 overproduction are not adequately counterbalanced. Conversely, in responders, causal factors are neutralized and IL-6 level decreases by natural protein degradation.

Tocilizumab acts by inhibiting IL-6 and its autocrine activity on B cell growth, and is expected to inhibit the differentiation of B cells and the survival of plasma cells (31, 32). We found that tocilizumab affects B cell homeostasis in all COVID-19 patients, responding or not to therapy. The number of B cells, and in particular the number of naïve B cells and of memory switched B cells, increases after tocilizumab administration irrespective of response to treatment. In neuromyelitis optica spectrum disorder (NMOSD), tocilizumab treatment led to an increase in the number of naïve B cells and decreases in the number of memory B cells and antibody-secreting B cells (31). B cell phenotype and $IgD^{-}CD27^{-}$ memory B cells are also affected by tocilizumab in patients with RA (33). Concerning the response to tocilizumab, we found that responders have a higher basal number of B cells if compared to non-responders. In particular, patients with high number of memory switched and memory IgM only cells will more likely benefit from the treatment if compared to patients with lower numbers. In other settings, i.e. patients with RA who had an inadequate response to disease-modifying antirheumatic drugs and a TNF inhibitor, tocilizumab proved more effective than rituximab in B cell-poor but not in B cell-rich patients (34).

IL-6 also acts on T cells, and its inhibition has several implications both on $CD4^{+}$ or $CD8^{+}$ T cells. Responder patients have higher number of $CD4^{+}$ and $CD8^{+}$ T cells, with a particular increase of naïve and recently activated memory T cell population after therapy. In inflammation due to RA, tocilizumab contributes to induce the increase of protective Treg and to inhibit the Th17 phenotype (35–37). Six hallmarks describe the main alterations occurring in the early infection phase with SARS-CoV-2 and in the course of the disease, which predispose to severe illness. These six hallmarks, that we have observed in our previous studies, are: i) dysregulated type I IFN activity; ii) hyperinflammation; iii) lymphopenia; iv) lymphocyte impairment; v) dysregulated myeloid response; and vi) heterogeneous adaptive immunity to the virus (38). Concerning tocilizumab treatment, we found that patients responding to therapy were characterized by higher level of inflammation and higher levels of B cells and T cells if compared to those not responding, whereas non-responders were characterized by leukopenia. Moreover, patients who respond to therapy were characterized by a higher activation of the immune system (identified as the expression of recent markers of activation such as CD38 and PD1) and the increase of naïve T cells, together with the decrease of plasmablasts. Accumulating evidence is implicating immunosuppression in the development of severe COVID-19. Therefore, COVID-19 management should aim to reverse immunosuppression and prevent resultant opportunistic infections. In line with these observations, timing of tocilizumab

10.3389/fimmu.2023.1123807

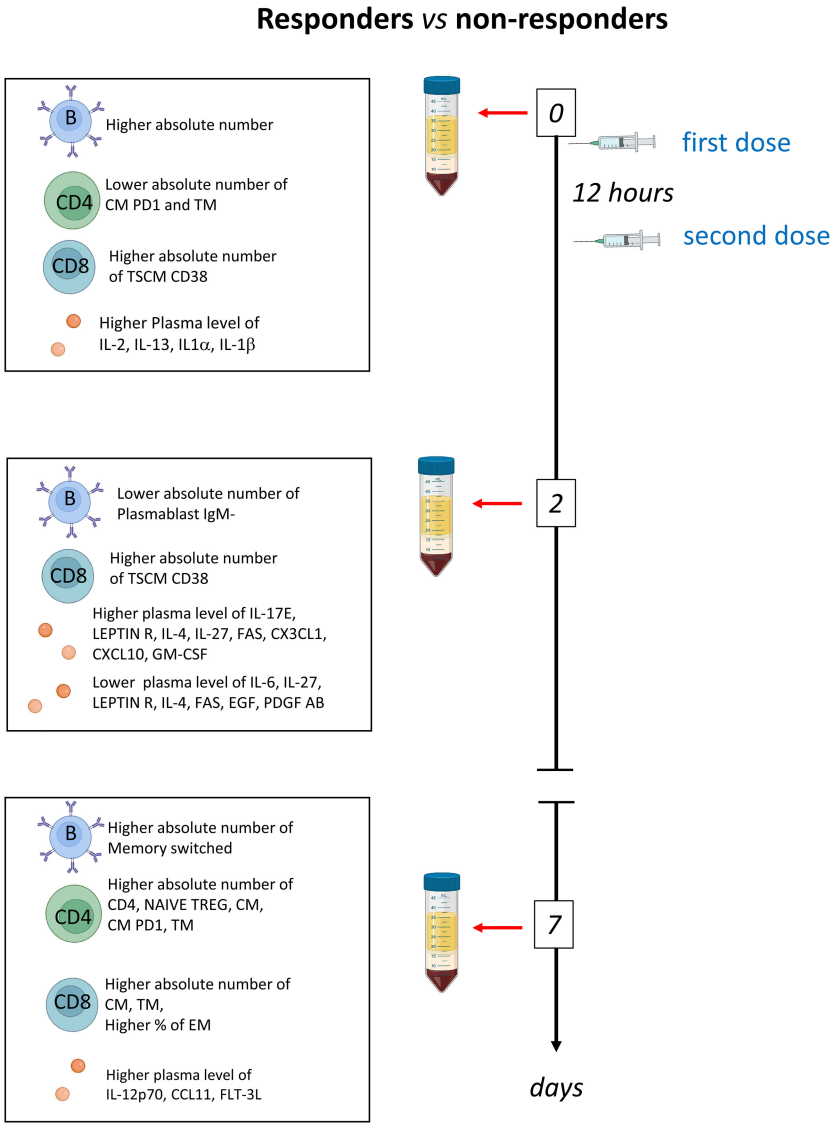


FIGURE 6
Schematic summary of the main results obtained before therapy (T0) and after two (T2) and 7 days (T7) in responder and non-responders. Tocilizumab was administered immediately after the first blood collection and 12 hours later.

administration plays a crucial role, as if patient is experiencing immunoparalysis, or, on the other hand, has poor or negligible symptoms, tocilizumab is likely unable to induce a clinically useful response.

We acknowledge that our study has some limitations. The observational nature and the limited number of patients represent a first weakness of this study. This is a single centre study, and the results may not be generalizable to the wider population. However, the longitudinal design with a close follow-up represents a remarkable strength together with the accurate assessment of cellular immune response and the comprehensive analysis of soluble factors, at different time points, before treatment and after two and seven days of treatment. To our knowledge this is the first study to date in which the immunological differences between COVID-19 patients responding or not to tocilizumab have been evaluated.

In conclusion, we found that tocilizumab has pleiotropic effects and that clinical response to this drug remain heterogenous. However, our data suggest that it is possible to identify patients who will respond to treatment and that the administration of tocilizumab is able to restore the immune balance through the re-establishment of different cell populations affected by SARS-COV-2 infection, highlighting the importance of temporal examination of the pathological features from the diagnosis.

Methods

Patients and study design

This is a case-control, longitudinal, single-center study, approved by the local Ethical Committee (Comitato Etico

dell'Area Vasta Emilia Nord, protocol number 177/2020, March 11th, 2020) and by the University Hospital Committee (Direzione Sanitaria dell'Azienda Ospedaliero-Universitaria di Modena, protocol number 7531, March 11th, 2020). Each participant provided informed consent according to Helsinki Declaration, and all uses of human material have been approved by the same Committees. A total of 23 patients with severe COVID-19 was included in the study; they were all treated with tocilizumab. Thirteen patients were responders to therapy, whereas ten patients were non-responders. All patients had severe pneumonia, defined as at least one of the following: (i) presence of a respiratory rate of 30 or more breaths per minute, (ii) peripheral blood oxygen saturation (SaO_2) of less than 93% in room air, (iii) a ratio of arterial oxygen partial pressure (PaO2) to fractional inspired oxygen (FiO_2) of less than 300 mm Hg in room air, and (iv) lung infiltrates of more than 50% within 24–48 h, according to Chinese management guidelines for COVID-19 (version 6.0) (39). All patients received standard of care treatment at the time of hospital admission according to the regional COVID-19 guidelines of Emilia Romagna. In addition to the standard of care treatment, patients also received tocilizumab treatment. Depending on the availability of specific formulation at time of treatment, twelve patients received tocilizumab by intravenous administration at 8 mg/kg bodyweight (up to a maximum of 800 mg) given twice, 12 hours apart, while eleven patients received it by subcutaneous route at a dose of 162 mg administered in two simultaneous doses, one in each thigh (i.e., 324 mg in total). This particular subcutaneous approach was used to mimic, as much as possible, the pharmacokinetic activity of the intravenous formulation in order to achieve similar levels of drug exposure. After the administration of tocilizumab, patients were divided into 2 groups based on its clinical effects: 13 did not required invasive mechanical ventilation and were classified as responder, meanwhile 10 required invasive mechanical ventilation and were classified as non-responder. Three patients of the non-responder group died between 13 and 29 days after admission. We recorded demographic data, medical history, and main laboratory findings from each patient. For details, see Supplementary Table 1. These data are referred to hospital admission, before starting therapy (T0).

Blood collection and isolation of mononuclear cells

Up to 20 mL of blood were collected from each patient in vacuettes containing ethylenediamine-tetraacetic acid (EDTA). Blood was immediately processed. Isolation of peripheral blood mononuclear cells (PBMC) was performed using ficoll-hypaque according to standard procedures. PBMC were stored in liquid nitrogen in fetal bovine serum (FBS) supplemented with 10% dimethyl sulfoxide (DMSO). Plasma was stored at -80°C until use. Measurements were taken from individual patients; in the case of plasma, each measurement was performed in duplicate and only the mean was considered and shown.

Quantification of cytokine plasma levels

The plasma levels of 62 molecular species were quantified using a Luminex platform (Human Cytokine Discovery, R&D System, Minneapolis, MN) for the simultaneous detection of the following molecules: G-CSF, PDGF-AA, EGF, PDGF-AB/BB, VEGF, GM-CSF, FGF, GRZB, IL-1A, IL-1RA, IL-2, IL-27, IL-4, IL-6, IL-10, IL-13, TNF, IL-17C, IL-11, IL-18, IL-23, IL-6RA, IL-19, IFN-α, IFN-β, IL-3, IL-5, IL-7, IL-12p70, IL-15, IL-33, TGF- β, IFN- γ, IL-1B, IL-17, IL-17E, CCL3, CCL11, CCL20, CXCCL1, CXCL2, CCL5, CCL2, CCL4, CCL19, CXCL1, CXCL10, PD-L1, FLT-3, TACI, FAS, LEPTIN R, APRIL, OPN, BAFF, LEPTIN, BMP4, CD40 LIGAND, FAS LIGAND, BMP7, BMP2, TRAIL, according to the manufacturer's instruction. Data represent the mean of two technical replicates.

Polychromatic flow cytometry

All data obtained by flow cytometric assays have been produced according to the state-of-the-art technologies, as described (40).

B cell characterization

Thawed PBMC were washed twice with RPMI 1640 supplemented with 10% fetal bovine serum and 1% each of l-glutamine, sodium pyruvate, nonessential amino acids, antibiotics, 0.1 M HEPES, 55 μM β-mercaptoethanol and 0.02 mg/ml DNAse. Thawed PBMC were stained with viability marker Promokine IR-840 (PromoCell GmbH, Heidelberg, Germany) for 20 min at room temperature in PBS. One million PBMC were washed with FACS buffer and stained with DuraClone IM B cells containing the following lyophilized directly conjugated mAbs: IgD-FITC, CD21-PE, CD19-ECD, CD27-PC7, CD24-APC, CD38-AF750, IgM-PB, CD45-KrO. Cells were washed with FACS buffer and acquired at Cytoflex LX flow cytometer (Beckman Coulter, Hialeah, FL). A minimum of 500,000 cells was acquired on a CytoFLEX LX flow cytometer (Beckman Coulter).

T cell characterization

Thawed PBMC were washed twice with RPMI 1640 supplemented with 10% fetal bovine serum and 1% each of l-glutamine, sodium pyruvate, nonessential amino acids, anti- biotics, 0.1 M HEPES, 55 μM β-mercaptoethanol and 0.02 mg/ml DNAse. Up to 1 million PBMC were stained with the Duraclone IM T cell panel (Beckman Coulter) added with another five fluorescent mAbs and a marker of cell viability. Along with side and forward scatter signals, signals were obtained from different fluorochrome-labeled mAbs, i.e., CD45 conjugated with Krome Orange, CD3 APC-A750, CD4-APC, CD8-AF700, CD27-PC7, CD57-Pacific Blue, CD279 (PD1)-PC5.5, CD28-ECD, CCR7-PE, CD45RA-FITC, HLA-DR-

BUV661, CD127-BV650, CD25-BV785, CD95-BUV395, CD38-BUV496, and PromoFluor-840 (Promokine, PromoCell, Heidelberg, Germany). A minimum of 500,000 cells per sample were acquired on a CytoFLEX LX flow cytometer (Beckman Coulter).

Representation of high parameter flow cytometry

Flow Cytometry Standard (FCS) 3.0 files were imported into FlowJo software version X (Becton Dickinson, San Joseè, CA), and analyzed by standard gating to eliminate aggregates and dead cells, and to identify $CD3^+CD4^+$ T cells, $CD3^+CD8^+$ T cells (Supplementary Figures 7) and $CD19^+$ B cells (Supplementary Figures 8). Data were exported for further analysis in R, by following a script that makes use of Bioconductor libraries and R statistical packages (CATALYST 1.10.1). The script is available at: https://github.com/HelenaLC/CATALYST). The selection of cofactor for data transformation was checked on Cytobank premium version (see: cytobank.org). Metaclustering (K=25) was performed by using FlowSOM algorithm. Dimensional reduction was performed using UMAP algorithm.

B cell UMAP graphs stratified by patient at time T0, T2 and T7 are reported in Supplementary Figures 9A–C, respectively. B cell projection of UMAP graphs stratified by patient showing the FlowSOM clusters at time T0, T2, T7 are reported in Supplementary Figures 10A–C, respectively. $CD4^+$ T cell UMAP graphs stratified by patient at time T0, T2 and T7 are reported in Supplementary Figures 11A–C, respectively. $CD4^+$ T cell projection of UMAP graphs stratified by patient showing the FlowSOM clusters at time T0, T2, T7 are reported in Supplementary Figures 12A–C, respectively. $CD8^+$ T cell UMAP graphs stratified by patient at time T0, T2 and T7 are reported in Supplementary Figures 13A–C, respectively. $CD8^+$ T cell projection of UMAP graphs stratified by patient showing the FlowSOM clusters at time T0, T2, T7 are reported in Supplementary Figures 14A–C, respectively.

Principal component analysis

We have then investigated the role of B and T cells along with several clinical and biochemical parameters. For this purpose, we used the principal component analysis (PCA), a dimension reduction method that retains the characteristics of a data set that contribute most to its variance, by keeping lower order principal components (PCs) and ignoring the others (41). PCA uses an orthogonal transformation to collapse the dataset containing correlated parameters to a smaller set of linearly uncorrelated variables known as PCs, such that each PC is a weighted combination of all the markers. We performed this analysis to test whether subject classification was possible based on the B and T cell profile, cytokines and/or clinical data. Thus, PCA was carried out on the clinical events (responder or non-responder), and a dataset comprising 137 parameters that included age, blood pH, pCO_2 (mmHg), pO_2 (mmHg), sO_2 (%), pO_2/FiO_2 ratio, ALT (U/L), total bilirubin (mg/dL), CK (U/L), creatinine (mg/dL), D-Dimer (ng/mL), Hb (g/dL), white blood cells, WBC (N/μL), red blood cells, RBC (10^6/μL), INR (ratio), LDH (U/L), CRP (mg/dL), platelets (10^9/L), respiratory rate (breaths/minute), systolic blood pressure (mmHg), heart rate (beats/minute), SOFA score, different absolute numbers of B-cell populations (naïve, memory switched, memory IgM-only, transitional, memory unswitched, plasmablasts, exhausted, surface-) and T-cell subpopulations.

Statistical analysis

High-dimensional cytometric analysis was performed by using differential discovery in high-dimensional cytometry *via* high-resolution clustering. Quantitative variables were compared using Two-way ANOVA with Bonferroni correction. Data are represented as individual values, means, and standard errors of the mean. Statistical analyses were performed using Prism 8.4.3 (GraphPad Software Inc., La Jolla, USA).

Data availability statement

The raw data supporting the conclusions of this article will be made available by the authors, without undue reservation.

Ethics statement

The studies involving human participants were reviewed and approved by Comitato Etico dell'Area Vasta Emilia Nord, protocol number 177/2020 Direzione Sanitaria dell'Azienda Ospedaliero-Universitaria di Modena, protocol number 7531. The patients/participants provided their written informed consent to participate in this study.

Author contributions

LG, SDB, MMa and DT carried out experiments and drafted the figures. AP, RB, AN, LF, MMa, DT collected and stored PBMC samples. LG, SDB drafted and revised the figures and the tables. MMe, GG, CM, SB, MG, FC, AM followed patients. SDB, LG, DT, MMa performed bioinformatic and statistical analyses. LG, SDB, CM and AC conceived the study and wrote the manuscript. All authors contributed to the article and approved the submitted version.

Funding

This study was partially supported by unrestricted donations from Glem Gas spa (San Cesario, Modena, Italy), Sanfelice 1893 Banca Popolare (San Felice sul Panaro, Modena, Italy), Rotary Club Distretto 2072 (Clubs: Modena, Modena L.A. Muratori, Carpi, Sassuolo, and Castelvetro di Modena), BPER Banca and FAR 2022 by the University of Modena and Reggio Emilia ("Features and magnitude of long- and short-term immune memory against smallpox and COVID-19").

Acknowledgments

SDB and LG are Marylou Ingram Scholar of the International Society for Advancement of Cytometry (ISAC) for the period 2015–2020 and 2020–2025, respectively. Drs. Paola Paglia (ThermoFisher Scientific, Monza, Italy), Leonardo Beretta (Beckman Coulter, Milan, Italy) are acknowledged for their support in providing reagents and materials in this study, and for precious technical suggestions. Finally, we gratefully acknowledge the subjects who donated blood to participate in this study.

Conflict of interest

The authors declare that the research was conducted in the absence of any commercial or financial relationships that could be construed as a potential conflict of interest.

Publisher's note

All claims expressed in this article are solely those of the authors and do not necessarily represent those of their affiliated organizations, or those of the publisher, the editors and the reviewers. Any product that may be evaluated in this article, or claim that may be made by its manufacturer, is not guaranteed or endorsed by the publisher.

Supplementary material

The Supplementary Material for this article can be found online at: https://www.frontiersin.org/articles/10.3389/fimmu.2023.1123807/full#supplementary-material

References

1. Verity R, Okell LC, Dorigatti I, Winskill P, Whittaker C, Imai N, et al. Estimates of the severity of coronavirus disease 2019: a model-based analysis. *Lancet Infect Dis* (2020) 20(6):669–77. doi: 10.1016/S1473-3099(20)30243-7

2. De Biasi S, Lo Tartaro D, Meschiari M, Gibellini L, Bellinazzi C, Borella R, et al. Expansion of plasmablasts and loss of memory b cells in peripheral blood from COVID-19 patients with pneumonia. *Eur J Immunol* (2020) 50(9):1283–94. doi: 10.1002/eji.202048838

3. De Biasi S, Meschiari M, Gibellini L, Bellinazzi C, Borella R, Fidanza L, et al. Marked T cell activation, senescence, exhaustion and skewing towards TH17 in patients with COVID-19 pneumonia. *Nat Commun* (2020) 11(1):3434. doi: 10.1038/s41467-020-17292-4

4. Gibellini L, De Biasi S, Paolini A, Borella R, Boraldi F, Mattioli M, et al. Altered bioenergetics and mitochondrial dysfunction of monocytes in patients with COVID-19 pneumonia. *EMBO Mol Med* (2020) 12(12):e13001. doi: 10.15252/emmm.202013001

5. Gibellini L, De Biasi S, Meschiari M, Gozzi L, Paolini A, Borella R, et al. Plasma cytokine atlas reveals the importance of TH2 polarization and interferons in predicting COVID-19 severity and survival. *Front Immunol* (2022) 13:842150. doi: 10.3389/fimmu.2022.842150

6. Lo Tartaro D, Neroni A, Paolini A, Borella R, Mattioli M, Fidanza L, et al. Molecular and cellular immune features of aged patients with severe COVID-19 pneumonia. *Commun Biol* (2022) 5(1):590. doi: 10.1038/s42003-022-03537-z

7. Kishimoto T. Interleukin-6: from basic science to medicine–40 years in immunology. *Annu Rev Immunol* (2005) 23:1–21. doi: 10.1146/annurev.immunol.23.021704.115806

8. Murakami M, Kamimura D, Hirano T. Pleiotropy and specificity: insights from the interleukin-6 family of cytokines. *Immunity* (2019) 50(4):812–31. doi: 10.1016/j.immuni.2019.03.027

9. Wolf J, Rose-John S, Garbers C. Interleukin-6 and its receptors: a highly regulated and dynamic system. *Cytokine* (2014) 70(1):11–20. doi: 10.1016/j.cyto.2014.05.024

10. Choy EH, De Benedetti F, Takeuchi T, Hashizume M, John MR, Kishimoto T. Translating IL-6 biology into effective treatments. *Nat Rev Rheumatol* (2020) 16(6):335–45. doi: 10.1038/s41584-020-0419-z

11. Rose-John S, Winthrop K, Calabrese L. The role of IL-6 in host defence against infections: immunobiology and clinical implications. *Nat Rev Rheumatol* (2017) 13(7):399–409. doi: 10.1038/nrrheum.2017.83

12. Chen LYC, Hoiland RL, Stukas S, Wellington CL, Sekhon MS. Confronting the controversy: interleukin-6 and the COVID-19 cytokine storm syndrome. *Eur Respir J* (2020) 56(4):2003006. doi: 10.1183/13993003.03006-2020

13. Chen LYC, Hoiland RL, Stukas S, Wellington CL, Sekhon MS. Assessing the importance of interleukin-6 in COVID-19. *Lancet Respir Med* (2021) 9(2):e13. doi: 10.1016/S2213-2600(20)30600-7

14. Guo C, Li B, Ma H, Wang X, Cai P, Yu Q, et al. Single-cell analysis of two severe COVID-19 patients reveals a monocyte-associated and tocilizumab-responding cytokine storm. *Nat Commun* (2020) 11(1):3924. doi: 10.1038/s41467-020-17834-w

15. Group RC. Tocilizumab in patients admitted to hospital with COVID-19 (RECOVERY): a randomised, controlled, open-label, platform trial. *Lancet* (2021) 397(10285):1637–45. doi: 10.1016/S0140-6736(21)00676-0

16. Guaraldi G, Meschiari M, Cozzi-Lepri A, Milic J, Tonelli R, Menozzi M, et al. Tocilizumab in patients with severe COVID-19: a retrospective cohort study. *Lancet Rheumatol* (2020) 2(8):e474–84. doi: 10.1016/S2665-9913(20)30173-9

17. Investigators R-C, Gordon AC, Mouncey PR, Al-Beidh F, Rowan KM, Nichol AD, et al. Interleukin-6 receptor antagonists in critically ill patients with covid-19. *N Engl J Med* (2021) 384(16):1491–502. doi: 10.1056/NEJMoa2100433

18. Borcoman E, Kanjanapan Y, Champiat S, Kato S, Servois V, Kurzrock R, et al. Novel patterns of response under immunotherapy. *Ann Oncol* (2019) 30(3):385–96. doi: 10.1093/annonc/mdz003

19. De Biasi S, Gibellini L, Lo Tartaro D, Puccio S, Rabacchi C, Mazza EMC, et al. Circulating mucosal-associated invariant T cells identify patients responding to anti-PD-1 therapy. *Nat Commun* (2021) 12(1):1669. doi: 10.1038/s41467-021-21928-4

20. Scalzo-Inguanti K, Plebanski M. CD38 identifies a hypo-proliferative IL-13-secreting CD4+ T-cell subset that does not fit into existing naive and memory phenotype paradigms. *Eur J Immunol* (2011) 41(5):1298–308. doi: 10.1002/eji.201040726

21. Jubel JM, Barbati ZR, Burger C, Wirtz DC, Schildberg FA. The role of PD-1 in acute and chronic infection. *Front Immunol* (2020) 11:487. doi: 10.3389/fimmu.2020.00487

22. Ahn E, Araki K, Hashimoto M, Li W, Riley JL, Cheung J, et al. Role of PD-1 during effector CD8 T cell differentiation. *Proc Natl Acad Sci U.S.A.* (2018) 115(18):4749–54. doi: 10.1073/pnas.1718217115

23. Abidi E, El Nekidy WS, Alefishat E, Rahman N, Petroianu GA, El-Lababidi R, et al. Tocilizumab and COVID-19: timing of administration and efficacy. *Front Pharmacol* (2022) 13:825749. doi: 10.3389/fphar.2022.825749

24. Mihara M, Kasutani K, Okazaki M, Nakamura A, Kawai S, Sugimoto M, et al. Tocilizumab inhibits signal transduction mediated by both mIL-6R and sIL-6R, but not by the receptors of other members of IL-6 cytokine family. *Int Immunopharmacol* (2005) 5(12):1731–40. doi: 10.1016/j.intimp.2005.05.010

25. Li B, Jones LL, Geiger TL. IL-6 promotes T cell proliferation and expansion under inflammatory conditions in association with low-level RORgammat expression. *J Immunol* (2018) 201(10):2934–46. doi: 10.4049/jimmunol.1800016

26. Roldan E, Brieva JA. Terminal differentiation of human bone marrow cells capable of spontaneous and high-rate immunoglobulin secretion: role of bone marrow stromal cells and interleukin 6. *Eur J Immunol* (1991) 21(11):2671–7. doi: 10.1002/eji.1830211105

27. Bettelli E, Carrier Y, Gao W, Korn T, Strom TB, Oukka M, et al. Reciprocal developmental pathways for the generation of pathogenic effector TH17 and regulatory T cells. *Nature* (2006) 441(7090):235–8. doi: 10.1038/nature04753

28. Rodriguez-Bano J, Pachon J, Carratala J, Ryan P, Jarrin I, Yllescas M, et al. Treatment with tocilizumab or corticosteroids for COVID-19 patients with hyperinflammatory state: a multicentre cohort study (SAM-COVID-19). *Clin Microbiol Infect* (2021) 27(2):244–52. doi: 10.1016/j.cmi.2020.08.010

29. Galvan-Roman JM, Rodriguez-Garcia SC, Roy-Vallejo E, Marcos-Jimenez A, Sanchez-Alonso S, Fernandez-Diaz C, et al. IL-6 serum levels predict severity and response to tocilizumab in COVID-19: an observational study. *J Allergy Clin Immunol* (2021) 147(1):72–80 e78. doi: 10.1016/j.jaci.2020.09.018

30. Nishimoto N, Terao K, Mima T, Nakahara H, Takagi N, Kakehi T. Mechanisms and pathologic significances in increase in serum interleukin-6 (IL-6) and soluble IL-6 receptor after administration of an anti-IL-6 receptor antibody, tocilizumab, in patients with rheumatoid arthritis and castleman disease. *Blood* (2008) 112(10):3959–64. doi: 10.1182/blood-2008-05-155846

31. Liu Y, Zhang H, Zhang TX, Yuan M, Du C, Zeng P, et al. Effects of tocilizumab therapy on circulating b cells and T helper cells in patients with neuromyelitis optica spectrum disorder. *Front Immunol* (2021) 12:703931. doi: 10.3389/fimmu.2021.703931

32. Snir A, Kessel A, Haj T, Rosner I, Slobodin G, Toubi E. Anti-IL-6 receptor antibody (tocilizumab): a b cell targeting therapy. *Clin Exp Rheumatol* (2011) 29 (4):697–700. doi: 10.1136/ard.2010.149005.1

33. Moura RA, Quaresma C, Vieira AR, Goncalves MJ, Polido-Pereira J, Romao VC, et al. B-cell phenotype and IgD-CD27- memory b cells are affected by TNF-inhibitors and tocilizumab treatment in rheumatoid arthritis. *PloS One* (2017) 12(9):e0182927. doi: 10.1371/journal.pone.0182927

34. Humby F, Durez P, Buch MH, Lewis MJ, Rizvi H, Rivellese F, et al. Rituximab versus tocilizumab in anti-TNF inadequate responder patients with rheumatoid arthritis (R4RA): 16-week outcomes of a stratified, biopsy-driven, multicentre, open-label, phase 4 randomised controlled trial. *Lancet* (2021) 397(10271):305–17. doi: 10.1016/S0140-6736(20)32341-2

35. Kikuchi J, Hashizume M, Kaneko Y, Yoshimoto K, Nishina N, Takeuchi T. Peripheral blood CD4(+)CD25(+)CD127(low) regulatory T cells are significantly increased by tocilizumab treatment in patients with rheumatoid arthritis: increase in regulatory T cells correlates with clinical response. *Arthritis Res Ther* (2015) 17:10. doi: 10.1186/s13075-015-0526-4

36. Pesce B, Soto L, Sabugo F, Wurmann P, Cuchacovich M, Lopez MN, et al. Effect of interleukin-6 receptor blockade on the balance between regulatory T cells and T helper type 17 cells in rheumatoid arthritis patients. *Clin Exp Immunol* (2013) 171 (3):237–42. doi: 10.1111/cei.12017

37. Samson M, Audia S, Janikashvili N, Ciudad M, Trad M, Fraszczak J, et al. Brief report: inhibition of interleukin-6 function corrects Th17/Treg cell imbalance in patients with rheumatoid arthritis. *Arthritis Rheum* (2012) 64(8):2499–503. doi: 10.1002/art.34477

38. Mazzoni A, Salvati L, Maggi L, Annunziato F, Cosmi L. Hallmarks of immune response in COVID-19: exploring dysregulation and exhaustion. *Semin Immunol* (2021) 55:101508. doi: 10.1016/j.smim.2021.101508

39. Zhou F, Yu T, Du R, Fan G, Liu Y, Liu Z, et al. Clinical course and risk factors for mortality of adult inpatients with COVID-19 in wuhan, China: a retrospective cohort study. *Lancet* (2020) 395(10229):1054–62. doi: 10.1016/S0140-6736(20)30566-3

40. Cossarizza A, Chang HD, Radbruch A, Abrignani S, Addo R, Akdis M, et al. Guidelines for the use of flow cytometry and cell sorting in immunological studies (third edition). *Eur J Immunol* (2021) 51:2708–3145. doi: 10.1002/eji.202170126

41. Borella R, De Biasi S, Paolini A, Boraldi F, Lo Tartaro D, Mattioli M, et al. Metabolic reprograming shapes neutrophil functions in severe COVID-19. *Eur J Immunol* (2022) 52(3):484–502. doi: 10.1002/eji.202149481

frontiers | Frontiers in Immunology

TYPE Original Research
PUBLISHED 06 July 2023
DOI 10.3389/fimmu.2023.1222170

Effect of antiviral and immunomodulatory treatment on a cytokine profile in patients with COVID-19

Diana Martonik[1]*, Anna Parfieniuk-Kowerda[1], Aleksandra Starosz[2], Kamil Grubczak[2], Marcin Moniuszko[2,3] and Robert Flisiak[1]

[1]Department of Infectious Diseases and Hepatology, Medical University of Bialystok, Bialystok, Poland, [2]Department of Regenerative Medicine and Immune Regulation, Medical University of Bialystok, Bialystok, Poland, [3]Department of Allergology and Internal Medicine, Medical University of Bialystok, Bialystok, Poland

Check for updates

OPEN ACCESS

EDITED BY
Alessio Mazzoni,
University of Florence, Italy

REVIEWED BY
Maria Salagianni,
Biomedical Research Foundation of the Academy of Athens (BRFAA), Greece
Fabio Seiti Yamada Yoshikawa,
Chiba University, Japan

*CORRESPONDENCE
Diana Martonik
diana.martonik@umb.edu.pl

RECEIVED 13 May 2023
ACCEPTED 20 June 2023
PUBLISHED 06 July 2023

CITATION
Martonik D, Parfieniuk-Kowerda A, Starosz A, Grubczak K, Moniuszko M and Flisiak R (2023) Effect of antiviral and immunomodulatory treatment on a cytokine profile in patients with COVID-19. *Front. Immunol.* 14:1222170. doi: 10.3389/fimmu.2023.1222170

COPYRIGHT
© 2023 Martonik, Parfieniuk-Kowerda, Starosz, Grubczak, Moniuszko and Flisiak. This is an open-access article distributed under the terms of the Creative Commons Attribution License (CC BY). The use, distribution or reproduction in other forums is permitted, provided the original author(s) and the copyright owner(s) are credited and that the original publication in this journal is cited, in accordance with accepted academic practice. No use, distribution or reproduction is permitted which does not comply with these terms.

Background: The severity of COVID-19 is associated with an elevated level of a variety of inflammatory mediators. Increasing evidence suggests that the Th17 response contributes to the severity of COVID-19 pneumonia, whereas Th22 response plays a regulatory role in SARS-CoV-2 infection. Two main types of available COVID-19 treatments are antivirals and immunomodulatory drugs; however, their effect on a cytokine profile is yet to be determined.

Methods: This study aim to analyse a cytokine profile in peripheral blood from patients with COVID-19 (n=44) undergoing antiviral or/and immunomodulatory treatment and healthy controls (n=20). Circulating CD4+ and CD8+ T cells and their intracellular expression of IL-17A and IL-22 were assessed by flow cytometry.

Results: Initial results showed an overexpression of IL-17F, IL-17A, CCL5/RANTES, GM-CSF, IL-4, IL-10, CXCL-10/IP-10 and IL-6 in COVID-19 patients compared to healthy controls. Treatment with remdesivir resulted in a significant decline in concentrations of IL-6, IL-10, IFN-alpha and CXCL10/IP-10. Immunomodulatory treatment contributed to a significant downregulation of IL-10, IFN-alpha, CXCL10/IP-10 and B7-H3 as well as upregulation of IL-22 and IL-1 beta. A combination of an antiviral and immunomodulatory treatment resulted in a significant decrease in IL-17F, IL-10, IFN-alpha, CXCL10/IP-10 and B7-H3 levels as well as an increase in IL-17A and IL-1 beta. We found significantly higher percentage of both CD4+ and CD8+ T cells producing IL-17A and CD4+ T cells producing IL-22 in patients with COVID-19.

Conclusion: Administration of antiviral or/and immunomodulatory treatment resulted in a significant downregulation of pro-inflammatory cytokine expression and an upregulation of T cell absolute counts in most cases, thus showing effectiveness of treatment in COVID-19. SARS-CoV-2 infection induced cytokine overexpression in hospitalized patients with COVID-19 as well as lymphopenia,

10.3389/fimmu.2023.1222170

particularly a decrease in CD4+ and CD8+ T cell counts. Moreover, despite the reduced counts of CD4+ and CD8+ T cells, both subsets showed overactivation and increased expression of IL-17A and IL-22, thus targeting Th17 response might alleviate inflammatory response in severe disease.

KEYWORDS

COVID-19, SARS-CoV-2, Th17 cells, CD4+ T cells, CD8+ T cells, cytokines, treatment

1 Introduction

At the end of 2019, an unprecedented epidemic of pneumonia caused by a novel beta coronavirus, termed SARS-CoV-2 afterward, emerged in Wuhan (China) (1). The rapid spread of the virus worldwide resulted in global pandemic of the subsequent disease COVID-19 announced by WHO on 11 March 2020. Most people infected with SARS-CoV-2 experience mild to moderate respiratory disease that resolves on its own. However, elderly people and those burdened with comorbidities such as chronic respiratory disease, cardiovascular disease, diabetes, and cancer are more likely to develop severe COVID-19 (2).

Cytokine release syndrome (CRS), which is an excessive response to the production of pro-inflammatory cytokines and chemokines, may be responsible for the severe course of the disease according to research. Unusually high release of cytokines triggering immunopathological reaction is described as "cytokine storm" (1, 2). Studies have shown that the severity of COVID-19 is associated with an elevated level of inflammatory mediators such as tumor necrosis factor (TNF), CXC-chemokine ligand 10 (CXCL-10), monocyte chemoattractant protein 1 (MCP-1), interleukin (IL)-2, IL-6, IL-7, and IL-10. Elevated concentration of IL-6 has been shown to strongly correlate with COVID-19 mortality (3, 4). Aberrant release of pro-inflammatory mediators leads to apoptosis of lung epithelial and endothelial cells causing damage to the microvascular and alveolar epithelial cell barrier which leads to vascular leakage, alveolar oedema, and hypoxia (5). There is evidence that both Th17 and Th22 response can play an immunomodulatory role in some diseases, including viral infections. It has been shown that in some situations Th17 and Th22 can exert opposite immune effects. Increasing evidence suggests that the Th17 response contributes to the severity of COVID-19 pneumonia, whereas Th22 response plays a regulatory role in SARS-CoV-2 infection (6, 7).

There are two main types of available COVID-19 treatments – antivirals and immunomodulatory drugs. Remdesivir, an antiviral medication, has received significant recognition for its capacity to control and regulate the viral load and has been approved for the treatment of patients with COVID-19. It is a broad-spectrum nucleoside analogue that can target variety of single-stranded RNA viruses, including coronaviruses. Its primary mechanism of action is the inhibition of RNA-dependent RNA polymerase thus leading to the suppression of SARS-CoV-2 replication in respiratory-associated epithelial cells (8, 9). Immunomodulatory agents modify the response of the immune system by activating, inhibiting, or modulating various immune system components. Tocilizumab is a recombinant humanized monoclonal antibody that binds to IL-6 receptors to exert immunosuppressive effects and attenuate IL-6 activity. It was approved for treatment of the CRS in severe COVID-19 (9, 10). Glucocorticoids (GCs) are recommended for the treatment of oxygen-requiring patients with COVID-19. GCs exhibit pharmacologic effect through classic genomic mechanisms. Some immunosuppressive effects are based on the induction of gene transcription and synthesis of NF-kB protein inhibitors, resulting in inhibition of the synthesis of downstream proteins such as IL-1 and IL-6. GCs reduce the activation, proliferation, and survival of both T cells and macrophages. The dosage and timing of administration of GCs have a significant impact on the outcome of the critically ill patients. The initiation of the immune defense mechanism is inhibited by the premature administration of GCs, which raises the viral load and ultimately has negative consequences. Therefore, GCs are mainly used to treat critically ill patients with CRS (10, 11).

In this study, we performed an evaluation of immunological features of patients with COVID-19 hospitalized in the Department of Infectious Diseases and Hepatology at the Medical University of Bialystok Clinical Hospital, who were treated with tocilizumab, glucocorticoids and/or remdesivir. We aimed to assess the effect of treatment on a cytokine and T cell profiles, including the intracellular expression of IL-17A and IL-22. We showed that administration of antiviral or/and immunomodulatory treatment resulted in a significant downregulation of pro-inflammatory cytokine expression and an upregulation of T cell absolute counts in most cases, thus showing effectiveness of treatment in COVID-19.

2 Materials and methods

2.1 Study population

The study included 44 patients with COVID-19 hospitalized in the Department of Infectious Diseases and Hepatology at the Medical University of Bialystok Clinical Hospital in January to May 2021, who were treated with tocilizumab, glucocorticoids and/or remdesivir. SARS-CoV-2 infection was confirmed with reverse transcription polymerase chain reaction (RT-PCR) in a certified diagnostic facility before hospital admission. In addition, 20

volunteers vaccinated against SARS-CoV-2 with no inflammatory or autoimmune disease were enrolled as a control group.

Vital signs included in Modified Early Warning Score (MEWS) (oxygen saturation, heart rate, blood pressure, respiratory rate, body temperature, alertness, diuresis), full blood count, coagulation parameters, acute-phase proteins, and other tests necessary for proper care in accordance with good clinical practice were measured before and during treatment. MEWS score allows to stratify patients according to their clinical condition:

1. Asymptomatic or mild type
2. Stable patients with respiratory and/or systemic symptoms
3. Clinically unstable patients with respiratory failure
4. Patient in critical condition (acute respiratory distress syndrome)

Patients with asymptomatic/mild disease and patients in whom inflammatory changes in the lungs were not confirmed by imaging studies were excluded from the study. Additional exclusion criteria were the presence of autoimmune diseases, malignancy, and current immunomodulatory treatment for diseases other than COVID-19. Management and treatment followed current national recommendations for COVID-19 (12, 13).

Remdesivir was administered to patients admitted to the hospital during first week from the onset of symptoms, dexamethasone was given to patients receiving antiviral drug, who also required oxygen therapy and tocilizumab was administered to patients with IL-6 concentration above 100 pg/mL. Treatment was classified as follows: a) antiviral therapy – remdesivir; b) immunomodulatory therapy – tocilizumab or/and dexamethasone; c) mixed therapy – combination of antiviral and immunomodulatory treatment.

Patients with oxygen saturation (SpO_2) of 90% or lower on room air who required high-flow oxygen therapy or non-invasive mechanical ventilation with bilevel positive airway pressure (BiPAP) mode to correct hypoxemia, were categorized as having severe COVID-19. Patients who did not meet the criteria for severe COVID-19 were classified as moderate. Schematic diagram of the treatment regimen is presented in Figure 1 and Supplementary Figure 1.

2.2 Sample collection and the purification of peripheral blood mononuclear cells (PBMCs)

Blood samples were collected from each participant by venipuncture in a 7,5 ml S-Monovette tube with clot activator (Sarstedt, Germany) and 4,9 ml S-Monovette tube with EDTA (Sarstedt, Germany) on hospital admission before treatment administration and on the fifth day of treatment. The collected samples were centrifuged, and serum and plasma were frozen at -80 degrees Celsius. Density gradient centrifugation with Pancoll 1.077 g/l (PAN Biotech, Germany) was used for isolation of PBMCs, then the cells were washed twice in phosphatate-buffered saline (Corning, VA, USA) and cryopreserved in fetal bovine serum (PAN Biotech, Germany) with 10% dimethyl sulfoxide (Sigma-Aldrich, MO, USA).

2.3 Immunoenzymatic assay (ELISA)

Enzyme-linked immunoabsorbent assays for the quantitative detection of human IL-17A, IL-17F, IL-22 and IL-23 (Invitrogen, Thermo Fisher Scientific, MA, USA) were performed according to the manufacturer's protocols and an absorbance level was read at 450 nm wavelength using BioTek EL800 microplate reader (Agilent Technologies, CA, USA). The level of each biomarker is expressed in pg/mL.

2.4 Multiplex assay

A 17-plex Luminex assay (R&D Systems, MN, USA) was used for quantification of serum biomarkers, including: B7-H3, CCL2,

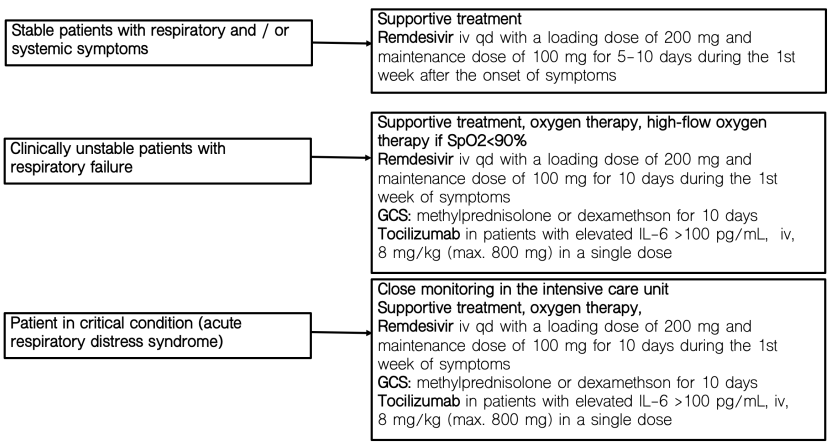


FIGURE 1
Therapeutic recommendations for COVID-19 at the time of the study.

CCL5, CXCL10, IFN-alpha, IFN-gamma, IL-1 beta, IL-4, IL-6, IL-6R, IL-10, IL-13, IL-21, IL-28B, IL-33, GM-CSF, TIM-1. Measurements were performed according to the manufacturer's instruction on a Bio-Plex 200 System (Bio-Rad Laboratories, CA, USA). The level of each biomarker is expressed in pg/mL.

2.5 Flow cytometry

Thawing of cryopreserved PBMCs and resuspension in the complete culture medium (RPMI 1640 with 10% fetal bovine serum (PAN Biotech, Germany)) was followed by counting and viability verification using 0.4% trypan blue solution (cells demonstrated viability of 95-100%). For the flow cytometric assessment of Th17 and Th22 cells, 500,000 cells were used. Intracellular detection of IL-17A and IL-22 was facilitated by 4-hour incubation at 37°C with Leukocyte Activation Cocktail with brefeldin A (BD Pharmingen; BD Bioscience, CA, USA). Initial extracellular staining with monoclonal antibodies conjugated with fluorochromes included: anti-CD4 FITC (clone RPA-T4) and anti-CD8 PE-Cy7 (clone RPA-T8) (BD Bioscience, CA, USA). Following 25 minutes of incubation at room temperature, in the dark, unbound antibodies were washed out with the phosphate-buffered saline without calcium and magnesium (PBS; Corning, VA, USA). Subsequently, cells were permeabilized by Permeabilization Buffer 2 (BD Bioscience, CA, USA) for intracellular staining using: anti-IL-17A PE (clone SCPL1362) and anti-IL-22 Alexa Fluor 647 (clone MH22B2) (BD Bioscience, CA, USA). After incubation and washing steps, cells were preserved using CellFix reagent (BD Bioscience, CA, USA) and stored at 4°C prior to data acquisition on the FACS Calibur flow cytometer (BD Bioscience, CA, USA). Flow cytometric analyses were performed using the FlowJo® software (Tree Star Inc., OR, USA).

Lymphocytes were initially distinguished on the basis of their morphology: relative size (FSC; forward scatter) and granularity (SSC; side scatter). Next, the detection of the helper (Th) CD4+ and cytotoxic (Tc) CD8+ T cell subsets was performed. Furthermore, the intracellular expression of IL-17A and IL-22 was assessed within mentioned subsets of lymphocytes. Implemented processing of the flow cytometric data allowed for determining the studied T cell populations frequencies and absolute cell numbers. The representative gating strategy, based on proper FMO and unstained controls, is presented in Figure 2.

2.6 Statistical analysis

Statistical analysis was performed with GraphPad (Prism Software, CA, USA). Comparative analysis between groups according to the distribution was carried out by t-test or Mann-Whitney U test for continuous data and chi-square for categorical data. For comparison between groups before and during the treatment, paired t-test and Wilcoxon matched pairs signed rank test were applied followed by two-stage linear step-up procedure of Benjamini, Krieger and Yekutieli. To assess the panoramic profile of

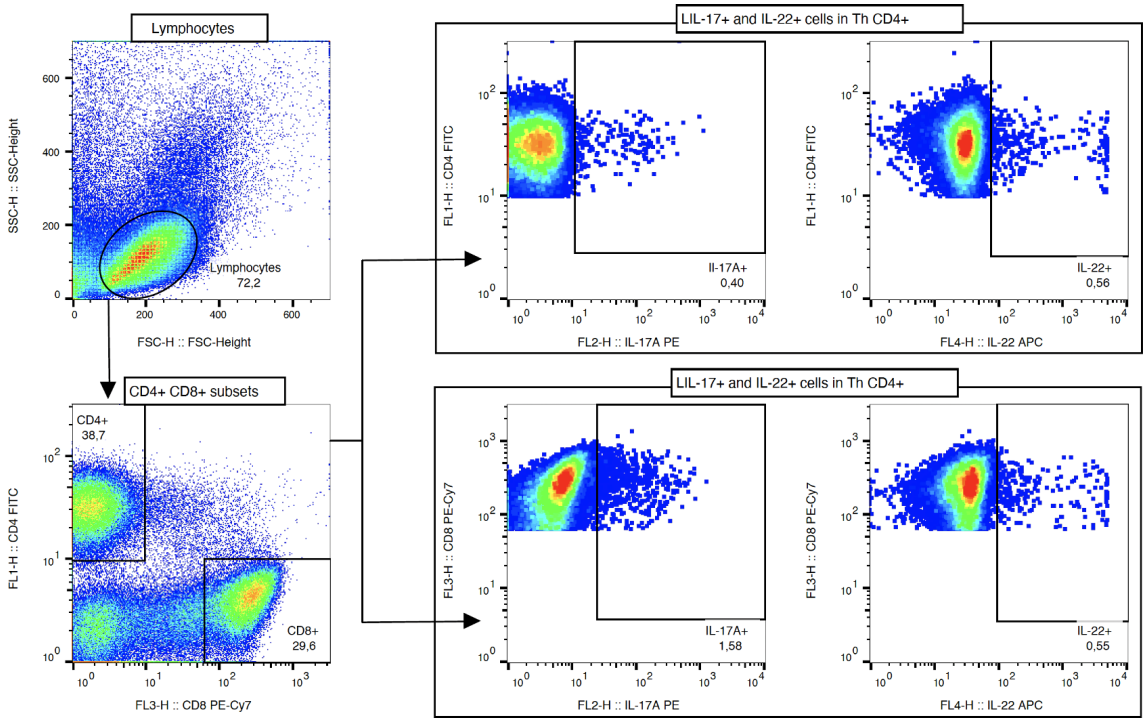


FIGURE 2
The representative gating strategy, based on proper FMO and unstained controls.

10.3389/fimmu.2023.1222170

serum biomarkers and absolute counts of immune cells in peripheral blood, data was normalized with log transformation. The correlation between analyzed parameters was assessed with Spearman correlation test. The differences were considered statistically significant if $p<0.05$.

3 Results

3.1 General characteristics

General characteristics of patients (n=44) and controls (n=20) are presented in Table 1. Among patients, majority were male (72.7%) with a median age of 63 years, whereas among controls majority were female (55.0%) with a median age of 57. Among severe COVID-19, all patients were male with a median age of 67 years (Supplementary Table 1). The most frequently occurring comorbidities both in patients and controls were hypertension (56.8% and 20.0% respectively) and dyslipidaemia (18.2% and 10.0% respectively). The median time from onset of symptoms to hospitalization was 7.0 days. On hospital admission, the median of the lung involvement in CT scan was 40.0%, whereas the median of oxygen saturation was 90.0%. Lung involvement in CT scan showed significant negative correlation with oxygen saturation (r=-0.487, p=0.002) and lymphocytes percentage (r=-0.407, p=0.010), and positive correlation with LDH level (r=0.425, p=0.011). Heatmap of Spearman's correlation of laboratory findings and general characteristics is presented in Figure 3.

3.2 Laboratory findings

On admission 65.9% of patients showed lymphocytopenia, while leukocyte counts were normal. Alanine aminotransferase, aspartate aminotransferase and D-dimer levels were significantly higher in patients than in controls (p=0.006, p<.001 and p<.001 respectively). Detailed analysis of laboratory findings in patients and controls is presented in Table 2. LDH levels were significantly higher in patients with severe COVID-19, compared to patients with moderate disease (p=0.040) (Supplementary Table 2). Lymphocytes percentage correlated negatively with CRP (r=-0.730, p<.001), fibrinogen (r=-0.555, p<.001), LDH (r=-0.473, p<.001), and D-dimers (r=-0.428, p<.001). Additionally, lymphocytes percentage showed strong positive correlation with SpO_2 (r=0.655, p<.001).

3.3 Immunological features before the treatment

Serum concentrations of IL-17F (p<.001), IL-17A (p=0.018), CCL5/RANTES (p<.001), GM-CSF (p<.001), IL-4 (p<.001), IL-10 (p<.001), CXCL10/IP-10 (p<.001) and IL-6 (p<.001) were significantly upregulated in patients, comparing to healthy controls (Figure 4A). Furthermore, IL-10 and CXCL10/IP-10 were significantly higher in patients with severe COVID-19 (p=0.018 and p=0.004 respectively) (Figure 4A). Whereas analysis of circulating immune cell subsets demonstrated significant decrease

TABLE 1 General characteristics of COVID-19 patients and control group.

Variables	Patients (n=44)	Healthy controls (n=20)	p
Age, y	63.0 (51.5-70.5)	57.0 (51.5-63.0)	0.087
Gender, male	32 (72.7%)	9 (45.0%)	0.032*
BMI, kg/m^2	29.7 (27.7-33.9)	26.0 (24.2-30.7)	0.010*
SpO_2, %	90.0 (84.5-94.0)	–	–
Time from onset, days	7.0 (5.0-9.0)	–	–
Disease severity			
Moderate, n (%) Severe, n (%)	35 (79.5%) 9 (20.5%)	- -	- -
Comorbidities			
Hypertension, n (%) Diabetes, n (%) Asthma, n (%) Dyslipidaemia, n (%)	25 (56.8%) 7 (16.0%) 3 (6.8%) 8 (18.2%)	4 (20.0%) 0 (0.0%) 1 (5.0%) 2 (10.0%)	0.010* 0.059 0.937 0.403
Symptoms			
Fever, n (%) Cough, n (%) Dyspnoea, n (%) Fatigue, n (%)	32 (72.7%) 28 (63.6%) 24 (54.6%) 23 (52.3%)	- - - -	–
Lung involvement in CT scan on admission, %	40.0 (40.0-60.0)	–	–

Data represented as number or median (IQR). BMI, body mass index; SpO_2, oxygen saturation; *, statistical significance.

10.3389/fimmu.2023.1222170

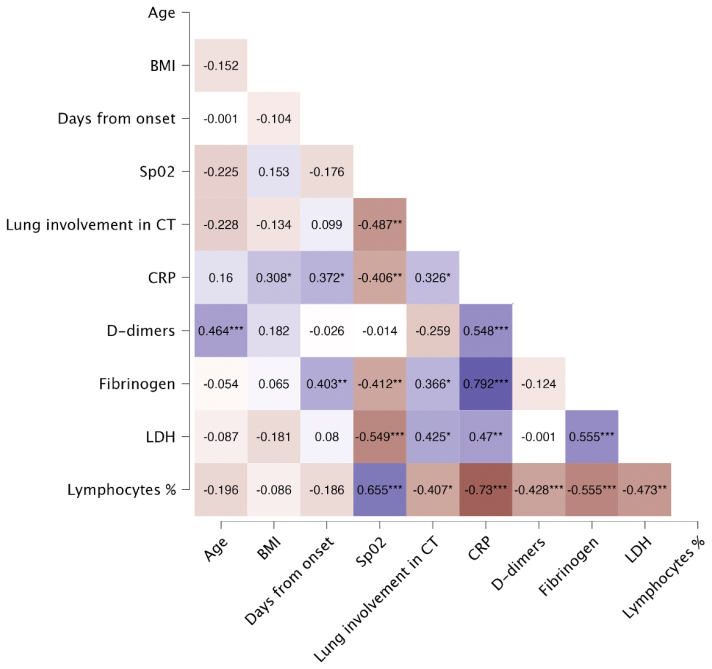


FIGURE 3
Spearman's correlation of laboratory findings and general characteristics of patients on the day of hospital admission. Heatmap demonstrates exact values of Spearman's r. BMI, body mass index; CRP, C-reactive protein; CT, computed tomography; LDH, lactate dehydrogenase; Lymphocytes %, percentage of lymphocytes; SpO_2, oxygen saturation. The levels of significance were indicated as: * = p<.05, ** = p<.01, *** = p <.001.

TABLE 2 Laboratory findings in COVID-19 patients and control group.

Variables	Normal range	Patients (n=44)	Healthy controls (n=20)	p
ALT, IU/L	<31.0	46.0 (23.0-62.0)	24.5 (20.0-30.0)	0.006*
AST, IU/L	<32.0	53.0 (44.0-74.0)	22.0 (19.0-29.0)	<.001*
CRP, mg/dL	<5.0	93.6 (58.9-132.3)	1.1 (0.6-2.4)	<.001*
PCT, ng/mL	<0.05	0.09 (0.05-0.16)	–	–
D-dimers, ng/mL	<500.0	892.0 (638.0-1439.0)	250.0 (182.0-382.0)	<.001*
Fibrinogen, mg/dL	200.0-400.0	645.0 (527.0-758.0)	–	–
LDH, U/I	135.0-214.0	476.0 (345.3-615.5)	–	–
Leukocyte count, $x10^9$/L	4.0-10.0	5.6 (4.7-8.7)	5.8 (5.0-7.3)	0.902
Neutrophil count, $x10^9$/L	1.6-7.2	4.3 (3.1-7.3)	3.1 (2.5-4.1)	0.018*
Lymphocyte count, $x10^9$/L	0.8-4.7	0.8 (0.7-1.2)	2.0 (1.6-2.5)	<.001*

(Continued)

10.3389/fimmu.2023.1222170

TABLE 2 Continued

Variables	Normal range	Patients (n=44)	Healthy controls (n=20)	p
Lymphocytes, %	18.0-48.0	12.8 (8.8-20.1)	32.4 (28.4-36.9)	<.001*
Haemoglobin, g/dL	12.0-16.0	14.8 (13.3-15.4)	14.4 (13.6-15.3)	0.848
Platelet count, x10^9/L	130.0-350.0	183.0 (139.0-261.5)	233.0 (207.0-294.0)	0.015*
INR	0.8-1.2	1.2 (1.1-1.2)	1.0 (1.0-1.1)	<.001*

Data represented as number or median (IQR). ALT, alanine aminotransferase; AST, aspartate aminotransferase; CRP, C-reactive protein; INR, international normalized ratio; LDH, lactate dehydrogenase; PCT, procalcitonin; *, statistical significance.

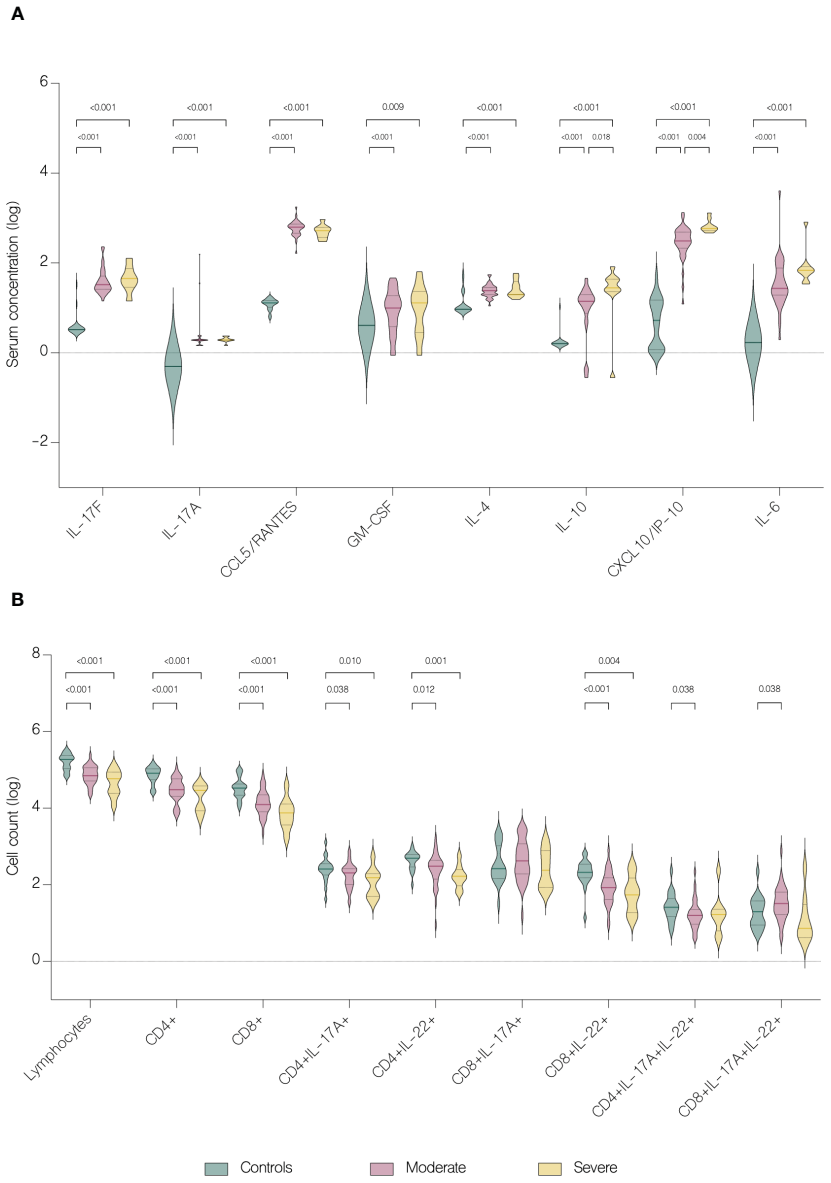


FIGURE 4
Immunological features in healthy controls and patients. Data represented as median (—) and quartiles (⋯). **(A)** Serum concentration of cytokines in healthy controls and patients with moderate and severe disease on hospital admission; **(B)** T cell counts in healthy controls and patients with moderate and severe disease on hospital admission.

10.3389/fimmu.2023.1222170

of absolute numbers of total lymphocytes, as well as both CD4+ and CD8+ T cells (Figure 4B). Nevertheless, both the percentages of CD4 + and CD8+ T cells expressing IL-17A were higher in patients with moderate (p<.001 and p<.001 respectively) and severe disease (p=0.004 and p=0.009 respectively) than in controls. In addition, patients with moderate disease had higher percentage of CD4+ T cells expressing IL-22 (p=0.006) compared to controls (Figure 5). Lung involvement in CT scan correlated positively with percentage of CD4 + T cells producing both IL-17A and IL-22 (r=0.474, p=0.005) and negatively with IFN-lambda 3 (r=-0.435, p=0.010). In contrast, SpO2 correlated positively with IFN-lambda 3 (r=0.441, p=0.007) and negatively with IL-6 (r=-0.567, p=0.007). CRP correlated positively with percentage of CD8+ producing IL-17A (r=0.531, p<.001) and percentage of CD8+ producing both IL-17A and IL-22 (r=0.431, p<.001). Moreover, CRP correlated negatively with lymphocytes count (r=-0.438, p<.001) as well as CD4+ (r=-0.467, p<.001) and CD8+ (r=-0.444, p<.001). Time from onset correlated positively with IL-23 (r=0.415, p=0.009) (Figure 6).

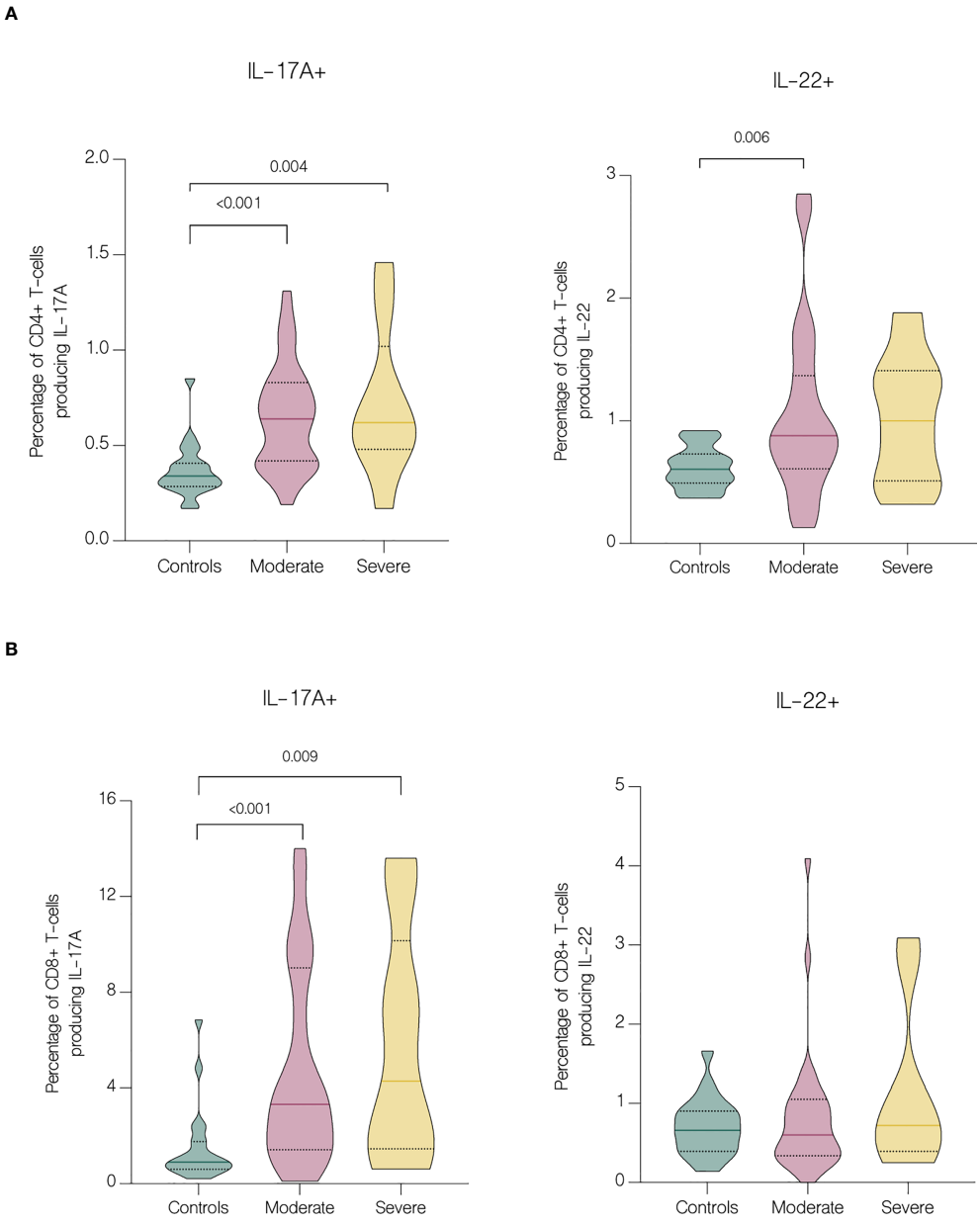


FIGURE 5
Intracellular expression of IL-17A and IL-22 by CD4+ and CD8+ T cells in controls and patients with moderate and severe disease. Data represented as median (—) and quartiles (·····). **(A)** Cytokine production by CD4+ cells in controls and patients with moderate and severe disease on hospital admission; **(B)** Cytokine production by CD8+ cells in controls and patients with moderate and severe disease on hospital admission.

10.3389/fimmu.2023.1222170

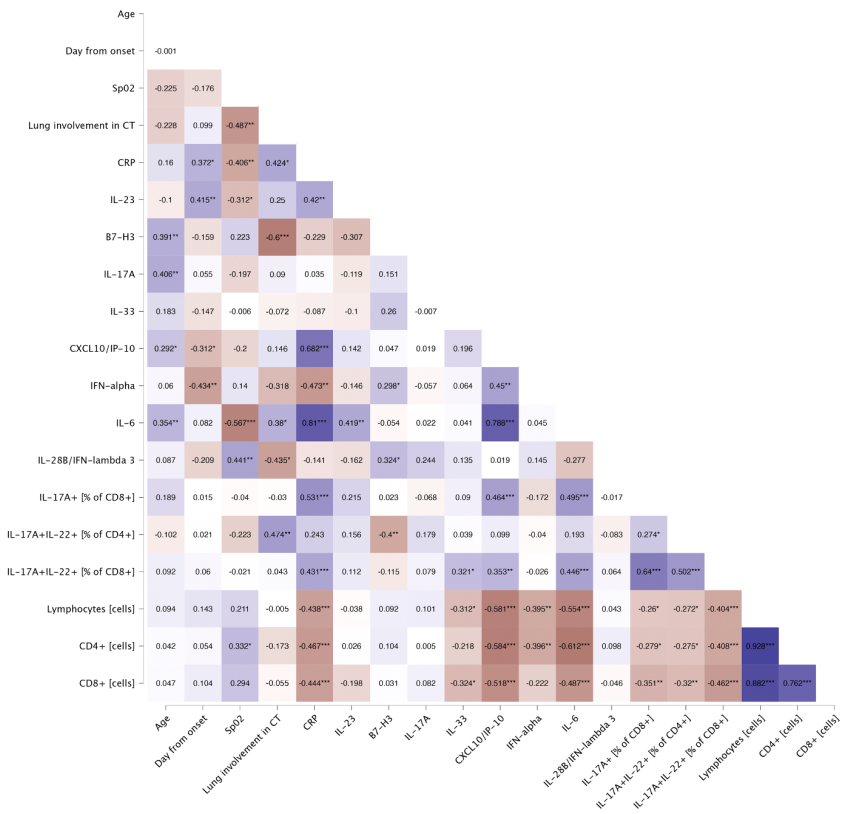


FIGURE 6
Spearman's correlation of general characteristics and immunological features of patients on the day of hospital admission. Heatmap demonstrates exact values of Spearman's r. CRP, C-reactive protein; CT, computed tomography; SpO_2, oxygen saturation. The levels of significance were indicated as: * = p<.05, ** = p<.01, *** = p <.001.

3.4 Effect of treatment on immunological features of patients

On the fifth day of treatment, the overall level of IL-17A (p<.001), IL-22 (p=0.003), IL-1 beta (p=0.026), CCL5/RANTES (p=0.036) and GM-CSF (p=0.024) significantly increased. Whereas the level of IL-17F (p=0.024), IL-10 (p<.001), IFN-gamma (p=0.011), IFN-alpha (p<.001), CXCL10/IP-10 (p<.001) and B7-H3 (<.001) significantly decreased (Figure 7A). However, compared to patients with moderate COVID-19, the overall serum levels of IL-10 (p<.001), IFN-gamma (p=0.037), CCL2/MCP-1 (p=0.008), CXCL10/IP-10 (p<.001) and IL-6 (p=0.001) were significantly upregulated in severe patients on fifth day of treatment (Figure 8).

IL-6 concentration decreased significantly with antiviral treatment (p=0.047) but increased in patients in other treatment groups, although without statistical significance (p=0.067) (Figure 9). Moreover, there was a statistically significant increase of IL-6 in patients with severe COVID-19 (p=0.016) compared to patients with moderate disease (Figure 10). Compared to other therapies, only patients with immunomodulatory treatment showed an increase of IL-22 level (p=0.031), whereas combination of immunomodulatory and antiviral treatments resulted in a significant increase of IL-17A (p=0.046) and a decrease of IL-17F (p=0.027) in these patients (Figure 9). Concentration of IL-1 beta increased significantly in both groups treated with immunomodulatory drugs (p=0.030) and a combination of immunomodulatory and antiviral drugs (p=0.030) (Figure 9). In contrast to the group with severe COVID-19, in patients with moderate disease IL-1 beta levels were significantly reduced (p=0.022) on fifth day of treatment, suggesting its contribution to worse clinical outcomes (Figure 10).

The overall number of lymphocytes, and both CD4+ and CD8+ T cell subsets significantly increased with treatment (p<.001), including CD4+ and CD8+ producing IL-17A (p=0.003 and p=0.016 respectively) (Figure 7B). However, patients with moderate disease demonstrated immune response to treatment with a significant increase in both CD4+ and CD8+ T cell counts (p<.001 and p=0.002 respectively), while in patients with severe disease there was no significant difference in any subset (p=0.126 and p=0.152 respectively) (Figure 11). There were no statistically significant differences of T cell counts between the different treatment groups, however the percentage of IL-22 producing CD4+ T cells was markedly lower in patients treated with immunomodulatory drugs (p=0.035) (Figure 12).

10.3389/fimmu.2023.1222170

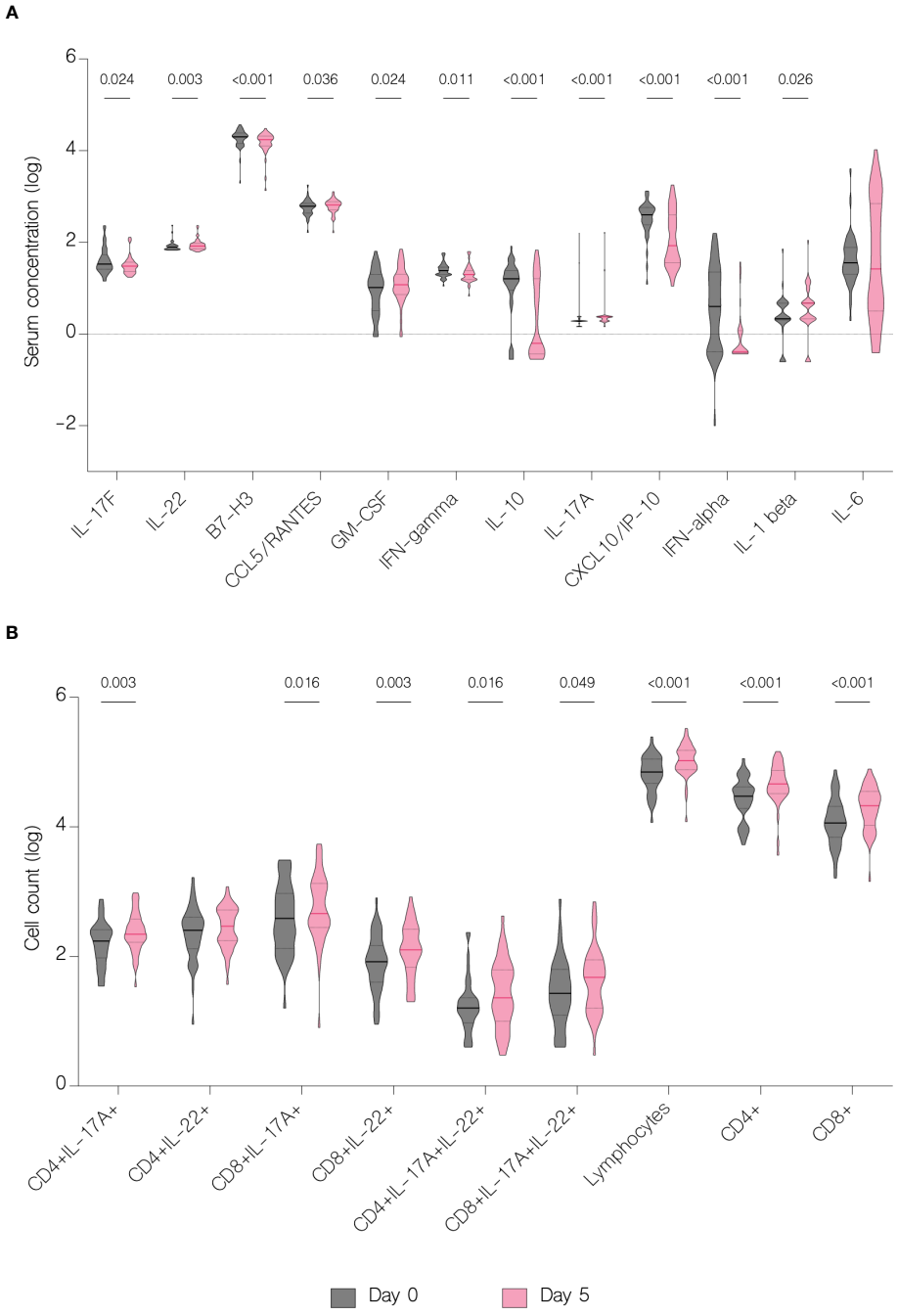


FIGURE 7
Immunological features before and during treatment. Data represented as median (—) and quartiles (⋯). **(A)** Serum concentration of cytokines before treatment administration and on the fifth day of treatment; **(B)** T cell counts before treatment administration and on the fifth day of treatment.

4 Discussion

Laboratory parameters have potential value in risk assessment and COVID-19 outcomes prediction, as early recognition of disease progression is essential for effective management and intervention. Several biomarkers were proposed as potential predictors of the COVID-19 outcome based on the hyperinflammatory state and hypercoagulability involved in pathophysiology of severe disease, such as CRP, PCT, IL-6, D-dimers and LDH (14). Many studies reported that elevated levels of ALT, AST, CRP, PCT, IL-6, D-dimers and LDH, and depressed counts of lymphocytes and platelets in patients with COVID-19 were associated with disease severity (14–19). Consistently with previous findings, in our study patients had significantly higher levels of ALT, AST, CRP and D-dimers and lower counts of lymphocytes and platelets compared to controls. In addition, patients had elevated levels of PCT, fibrinogen

10.3389/fimmu.2023.1222170

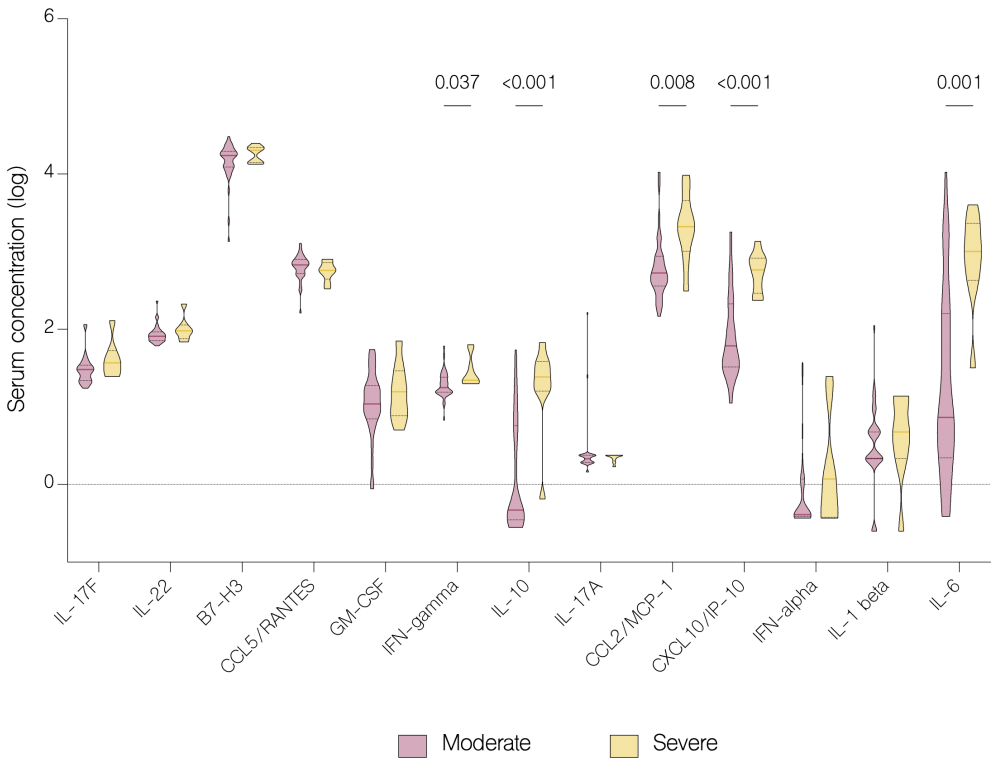


FIGURE 8
Serum concentration of cytokines in patients with moderate and severe COVID-19 on the fifth day of treatment. Data represented as median (—) and quartiles (⋯).

and LDH. Moreover, patients with severe disease had significantly higher level of LDH, while there was no statistical difference in other laboratory parameters.

Impairment of immune responses resulting in an excessive inflammation is a hallmark of COVID-19. In addition to the virus-induced direct lung injury, excessive activation of immune system in response to SARS-CoV-2 invasion triggers immune cells to release both pro- and anti-inflammatory cytokines, such as IL-1 beta, IL-6, IL-10, IL-17, TNF and CCL2/MCP-1 (20). We have demonstrated that concentrations of several cytokines, including CCL5/RANTES, GM-CSF, IL-4, IL-6, IL-10 and CXCL10/IP-10, were significantly upregulated in patients with COVID-19 versus healthy controls. Moreover, upon admission patients with severe disease had higher concentration of IL-10 and CXCL10/IP-10 than patients with moderate disease. These results are in accordance with the studies reporting an elevation of IL-1 beta, IL-6, IL-10, GM-CSF, CXCL10/IP-10, CCL2/MCP-1, CCL5/RANTES and IFN-gamma in the blood samples of COVID-19 patients (21–23). Furthermore, Huang et al. observed higher concentration of IL-10, CXCL10/IP-10 and CCL2/MCP-1 in intensive care COVID-19 patients versus non intensive care patients (21).

Several studies reported decrease in CD4+ and CD8+ T cells counts in patients with COVID-19 (23–27). Hence, it has been suggested that the counts of CD4+ and CD8+ T cells can be a diagnostic marker of COVID-19 activity and predictor of disease severity (25). Patients in our study had significantly reduced both CD4+ and CD8+ absolute counts, but without significance between moderate and severe disease. However, on fifth day of hospitalization patients with severe disease had lower lymphocytes, CD4+ and CD8+ T cells count, which may be explained by the fact that in majority of severe cases, the disease progressed during hospitalization. In contrast to the group with severe COVID-19, patients with moderate disease showed clinical response to treatment, with a significant increase in both CD4+ and CD8+ T cells count. Similar results were obtained by Wang et al. showing an increase in CD8+ T cells and B-cells in response to treatment in patients with COVID-19. Moreover, authors indicated that the decrease of these cell subsets might serve as an independent predictor of poor treatment response (26). In our study, despite the depleted absolute numbers of CD4+ and CD8+ T cells, these cells showed overactivation and increased expression of IL-17A and IL-22. We found significantly higher percentage of both CD4+ and CD8+ T cells producing IL-17A and CD4+ T cells producing IL-22 in patients with COVID-19. These results correspond to the study of De Biasi et al. that reported an increase in percentages of T cell subsets producing IL-17A (22). Similarly, Cagan et al. reported increased numbers of CD4+ and CD8+ T cells producing IL-22 and CD8+ T cells producing IL-17A (7).

The production of IL-17A, a cytokine with both protective and pathogenic role, is the hallmark of the Th17 response. IL-17A has the ability to activate a wide range of inflammatory pathways, which can cause tissue damage and illness aggravation. Several indicators pointed to the likely role of IL-17A in COVID-19 clinical outcomes prompting considerations of using this cytokine as a marker of disease severity (20, 28–30). Previous study noted significantly

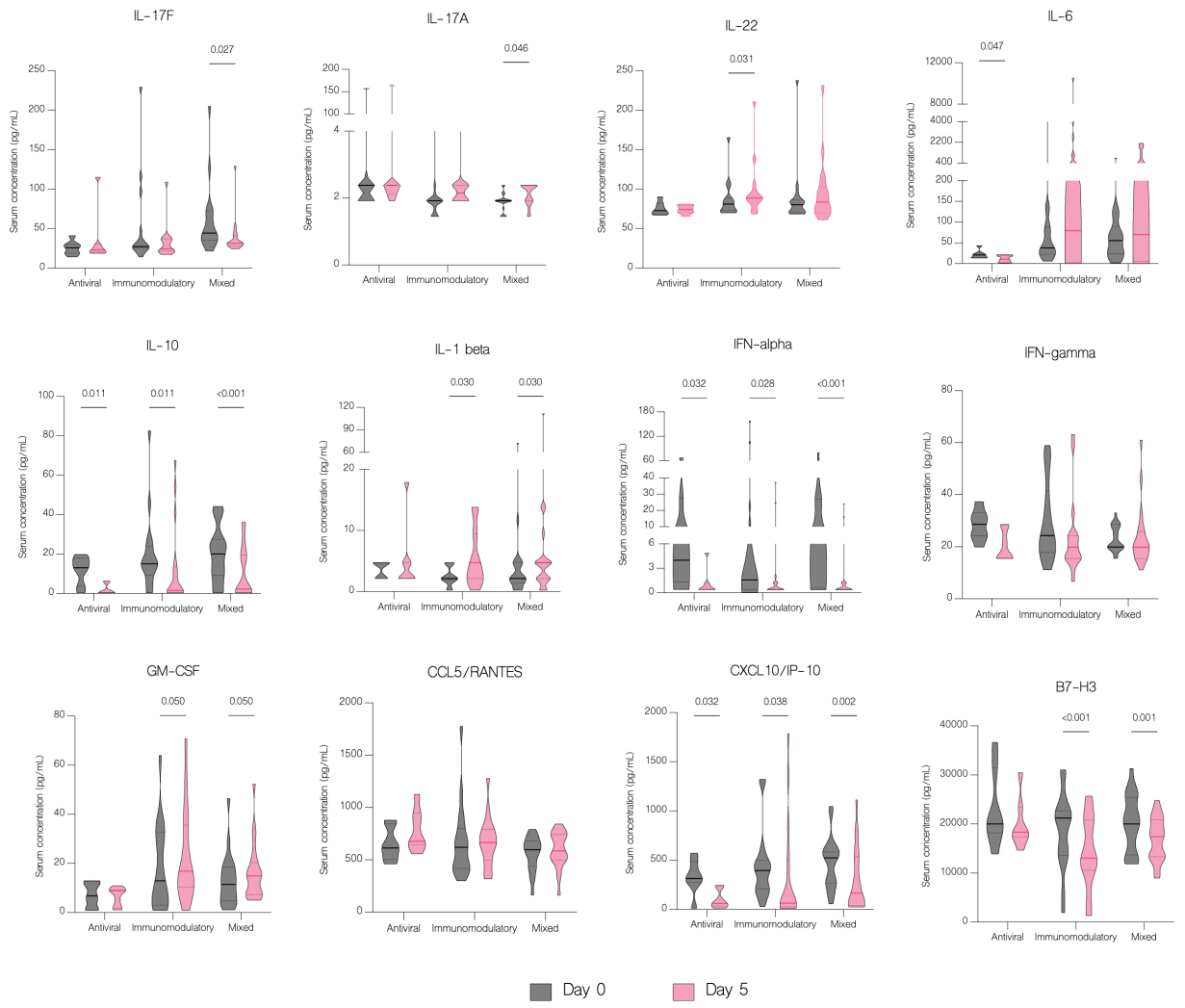


FIGURE 9
The effect of treatment on a cytokine profile in different treatment groups. Serum concentration of cytokines in different treatment groups, classified as follows: antiviral – remdesivir; immunomodulatory – tocilizumab or/and dexamethasone; mixed – combination of antiviral and immunomodulatory treatment. Data represented as median (—) and quartiles (┈┈).

upregulated IL-17A and IL-17F in patients with COVID-19 (23). Likewise, patients with COVID-19 in our study had significantly greater level of IL-17A and IL-17F than controls, but without significance between patients with moderate and severe disease. This observation is in accordance with the study of Huang et al. that reported significantly higher concentration of IL-17A in ICU patients compared to healthy controls but without significance between ICU and non-ICU care (21). Similarly, Mostafa et al. also noted upregulated levels of IL-17A in paediatric patients with COVID-19, however no association with disease outcome was found (31). In contrast, Liu et al. demonstrated significantly higher level of IL-17 in patients with severe COVID-19 compared to patients with mild disease. Moreover, IL-17 has been shown to positively correlate with Murray score, an indicator of lung injury severity (32). Another study showed an increase of IL-17 both in plasma and saliva of patients with severe COVID-19 compared to mild and asymptomatic patients. In addition, elevated levels of IL-17 were reported in nasal swabs and lung autopsies of COVID-19 patients and were associated with higher concentrations of other proinflammatory cytokines, including IL-1 beta, IL-6, IL-8, and IL-23 (33).

Another cytokine associated with Th17 response with both protective and pathogenic role is IL-22. It regulates host defense at barrier surfaces and promotes tissue regeneration yet has been linked to several diseases characterized by inflammatory tissue pathology (34). However, recent study of Das et al. reported potent immune boosting and antiviral properties of IL-22 in respiratory syncytial virus (RSV) infection and since COVID-19 have pathological characteristics like other viral respiratory infections it is reasonable to speculate that IL-22 may also limit the severity of SARS-CoV-2 infection (34, 35). We found elevated levels of IL-22 in patients on admission. In addition, concentrations of IL-22 in our patients significantly increased during hospitalization. Likewise, previous studies showed upregulated

10.3389/fimmu.2023.1222170

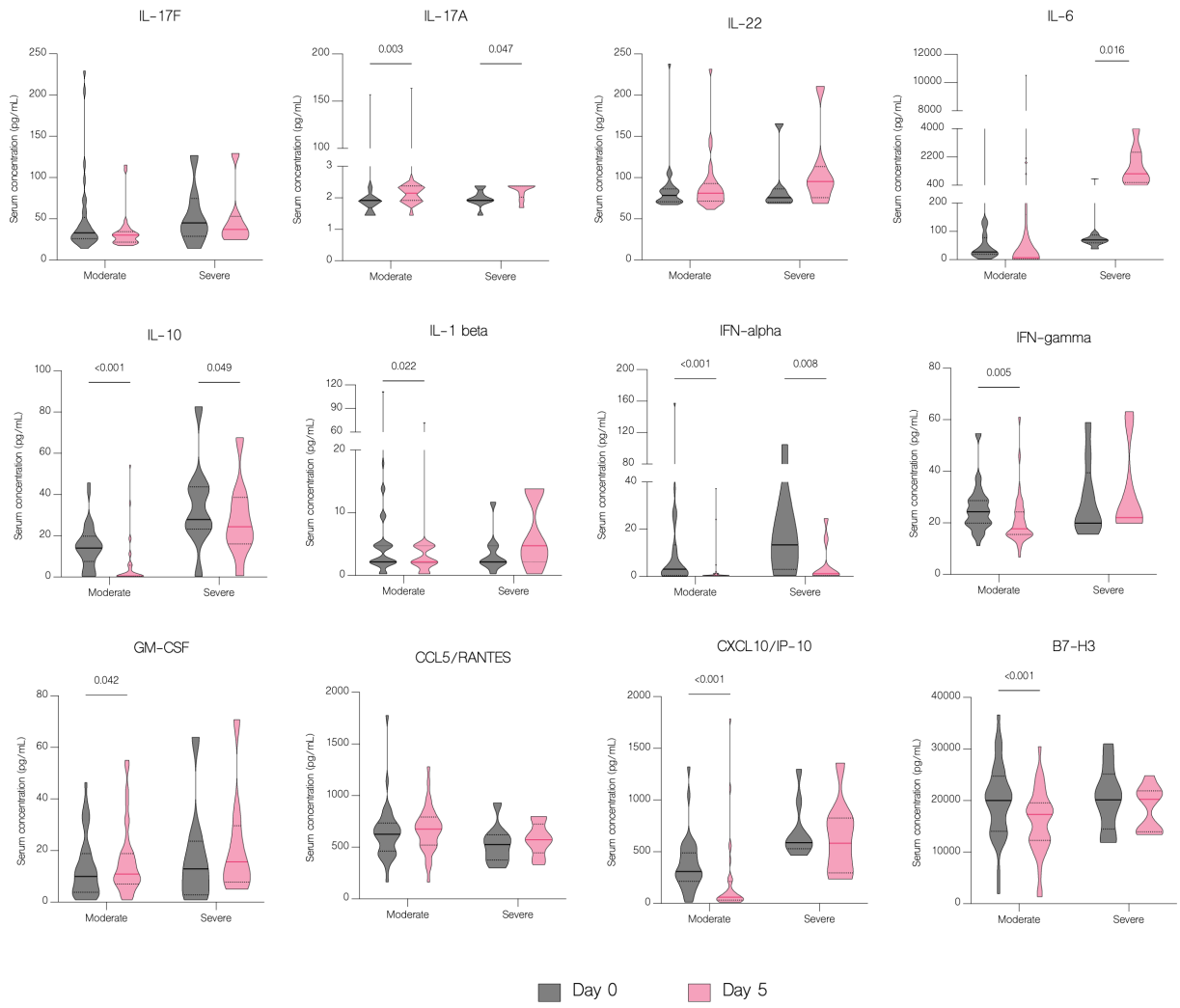


FIGURE 10
The effect of treatment on a cytokine profile by severity. Serum concentration of cytokines in patients with moderate and severe disease before treatment administration and on the fifth day of treatment. Data represented as median (—) and quartiles (⋯).

levels of IL-22 in both paediatric and adult patients with COVID-19, however no association with disease outcome or severity was found (23, 31). During inflammation, group 3 innate lymphoid cells (ILC3s) produce IL-17 and IL-22 upon stimulation with IL-1 beta and IL-23. In our study, despite no significant increase in T cell subsets in patients with severe disease there was an increase in IL-17A and IL-22 concentration which might be associated with ILC3s. In addition, it has been shown that lower abundance of ILCs in the blood was associated with longer hospitalization in individuals with COVID-19, hence there might be a correlation between decreased ILCs in the blood and severe disease (36, 37).

The number of available studies on the effect of antiviral and immunomodulatory treatment on a cytokine profile in patients with COVID-19 is scarce, hence the impact of treatment on the immune response is still unclear. In our study, treatment with remdesivir (RDV) resulted in a significant decline in concentrations of IL-6, IL-10, IFN-alpha and CXCL10/IP-10. Moreover, IFN-gamma and IL-1 beta were markedly decreased in patients treated with RDV, although without statistical significance. We were unable to find another study to which to compare our findings, however our results suggest attenuation of an excessive immune response in patients receiving antiviral treatment. Immunomodulatory treatment resulted in a significant downregulation of IL-10, IFN-alpha, CXCL10/IP-10 and B7-H3 as well as upregulation of IL-22 and IL-1 beta. The report of Ponthieux et al. showed an increase in IL-1 beta, IL-2, IL-4, IL-10, IL-12p70, IL-18 and IL-6R levels in patients with COVID-19 treated with tocilizumab achieving maximal values two to four days after drug administration. The authors of the study attributed these findings to an anti-inflammatory effect of IL-6, which was previously observed by other researchers (38, 39). However, in an experimental model of oleic acid-induced acute lung injury (ALI) both tocilizumab (TCZ) and dexamethasone (DEX) significantly reduced the expression of IL-1 beta, IL-6, IL-8, and TNF-alpha (40). Furthermore, DEX significantly reduced IL-8 levels in tracheal aspirates of mechanically ventilated children with RSV infection (41). In addition, DEX inhibited the secretion of IL-6 and CXCL8 in

10.3389/fimmu.2023.1222170

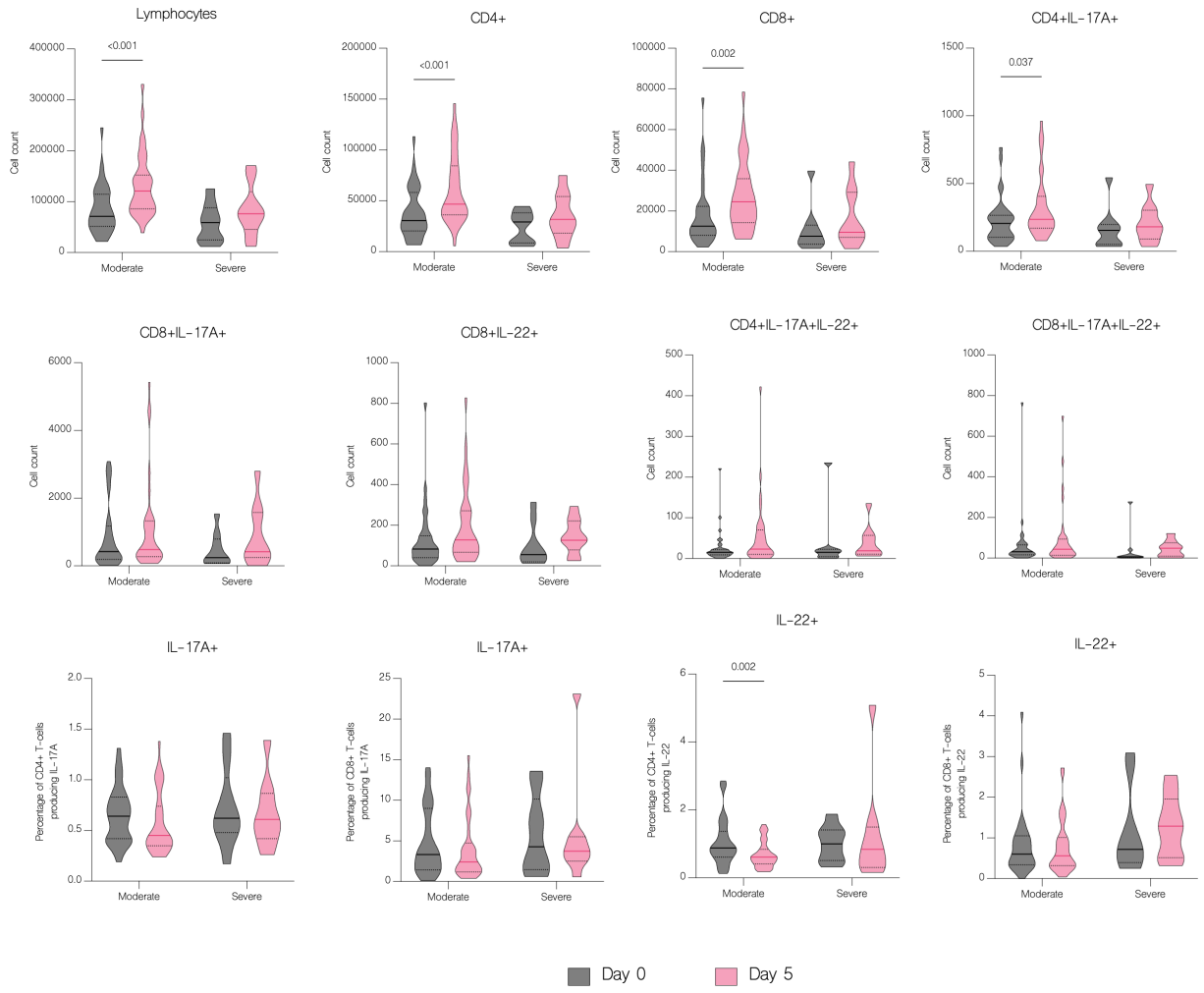


FIGURE 11
The effect of treatment on T cell counts in patients by severity. T cell counts before treatment administration and on the fifth day of treatment in patients with moderate and severe disease. Data represented as median (—) and quartiles (┈).

human lung fibroblasts (42). Another study with an oleic acid-induced ALI demonstrated that DEX inhibits the expression of IL-6, TNF-alpha and VEGF while promoting the expression of IL-10 (43). Immunomodulatory treatment inhibits the expression of proinflammatory cytokines and promotes the expression of anti-inflammatory cytokines, hence alleviating tissue damage during infections. In our study, a combination of an antiviral and immunomodulatory treatment resulted in a significant decrease in IL-17F, IL-10, IFN-alpha, CXCL10/IP-10 and B7-H3 levels as well as an increase in IL-17A and IL-1 beta. However, an upregulation of proinflammatory cytokines, such as IL-17A and IL-1 beta, might be associated with higher number of severe cases and deaths in this group, if untreated. In fact, IL-1 beta was significantly lower in patients with moderate disease and markedly higher in patients with severe disease, although without statistical significance. Lastly, patients treated with antiviral drug, immunomodulatory drug or both demonstrated clinical response to treatment with an increase in lymphocyte, CD4+ and CD8+ counts, without difference between the treatment groups.

5 Conclusions

SARS-CoV-2 infection induced cytokine overexpression in hospitalized patients with COVID-19 as well as lymphopenia, particularly a decrease in CD4+ and CD8+ T cell counts. Moreover, despite the reduced counts of CD4+ and CD8+ T cells, both subsets showed overactivation and increased expression of IL-17A and IL-22, thus targeting Th17 response might alleviate inflammatory response in severe disease.

Administration of antiviral or/and immunomodulatory treatment resulted in a significant downregulation of pro-inflammatory cytokine expression and an upregulation of T cell absolute counts in most cases, thus showing effectiveness of treatment in COVID-19.

6 Limitations of the study

This study has some limitation. Firstly, small number of participants due to not meeting the inclusion criteria, as well as prompt initiation of therapy not allowing for sampling prior to the

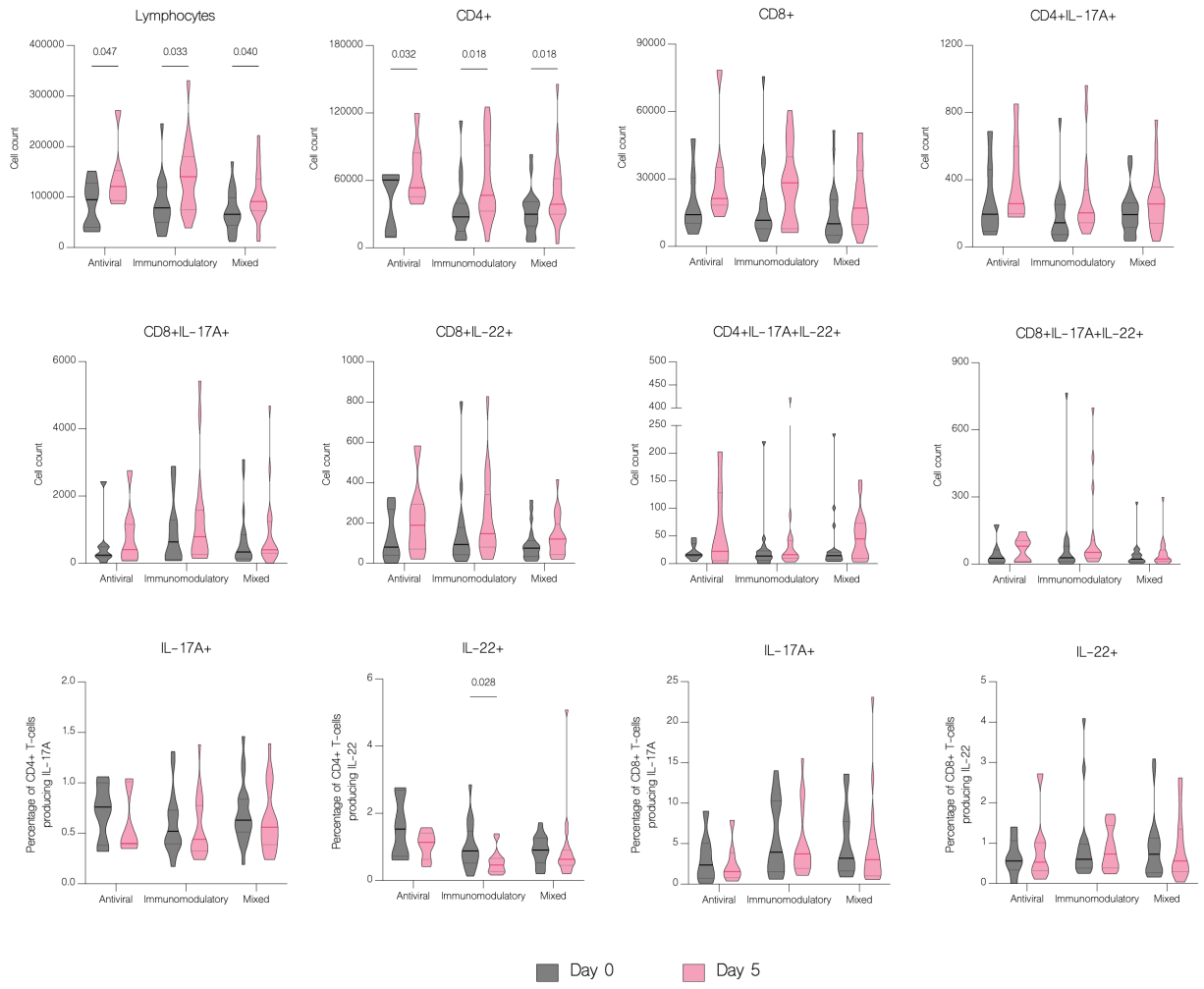


FIGURE 12
The effect of treatment on T cell counts in patients in different treatment groups. T cell counts before treatment administration and on the fifth day of treatment in different treatment groups, classified as follows: antiviral – remdesivir; immunomodulatory – tocilizumab or/and dexamethasone; mixed – combination of antiviral and immunomodulatory treatment. Data represented as median (—) and quartiles (┈).

treatment. Secondly, with the limited number of participants, it is difficult to evaluate risk factors for severity and mortality with multivariable-adjusted models. Finally, statistical results and p-values should be interpreted cautiously, as non-significant p-values do not necessarily rule out the difference between patients with moderate and severe disease.

Data availability statement

The raw data supporting the conclusions of this article will be made available by the authors, without undue reservation.

Ethics statement

The studies involving human participants were reviewed and approved by Ethical Committee at the Medical University of Bialystok - APK.002.6.2021. The patients/participants provided their written informed consent to participate in this study.

Author contributions

DM, AP-K, and KG contributed to conception and design of the study. DM, AS, and KG have performed the experiments, acquired and analyzed the data. DM, AP-K, KG, MM, and RF prepared the manuscript. All authors contributed to the article and approved the submitted version.

Funding

This research was funded with subventions of Medical University of Bialystok SUB/1/DN/21/001/1156 and SUB/1/DN/21/003/1156.

Conflict of interest

The authors declare that the research was conducted in the absence of any commercial or financial relationships that could be construed as a potential conflict of interest.

Publisher's note

All claims expressed in this article are solely those of the authors and do not necessarily represent those of their affiliated organizations, or those of the publisher, the editors and the reviewers. Any product that may be evaluated in this article, or claim that may be made by its manufacturer, is not guaranteed or endorsed by the publisher.

Supplementary material

The Supplementary Material for this article can be found online at: https://www.frontiersin.org/articles/10.3389/fimmu.2023.1222170/full#supplementary-material

References

1. Kaur S, Bansal R, Kollimuttathuillam S, Gowda AM, Singh B, Mehta D, et al. The looming storm: blood and cytokines in COVID-19. *Blood Rev* (2021) 46:100743. doi: 10.1016/j.blre.2020.100743

2. Darif D, Hammi I, Kihel A, El Idrissi Saik I, Guessous F, Akarid K. The pro-inflammatory cytokines in COVID-19 pathogenesis: what goes wrong? *Microb Pathog* (2021) 153:104799. doi: 10.1016/j.micpath.2021.104799

3. Yongzhi X. COVID-19-associated cytokine storm syndrome and diagnostic principles: an old and new issue. *Emerg Microbes Infect* (2021) 10(1):266–76. doi: 10.1080/22221751.2021.1884503

4. Hasanvand A. COVID-19 and the role of cytokines in this disease. *Inflammopharmacology* (2022) 30(3):789–98. doi: 10.1007/s10787-022-00992-2

5. Sun X, Wang T, Cai D, Hu Z, Chen J, Liao H, et al. Cytokine storm intervention in the early stages of COVID-19 pneumonia. *Cytokine Growth Factor Rev* (2020) 53:38–42. doi: 10.1016/j.cytogfr.2020.04.002

6. Gong J, Zhan H, Liang Y, He Q, Cui D. Role of Th22 cells in human viral diseases. *Front Med (Lausanne)* (2021) 8:708140. doi: 10.3389/fmed.2021.708140

7. Cagan E, Tezcan G, Simsek A, Kizmaz MA, Dombaz F, Asan A, et al. The age-dependent role of Th22, Tc22, and Tc17 cells in the severity of pneumonia in COVID-19 immunopathogenesis. *Viral Immunol* (2022) 35(4):318–27. doi: 10.1089/vim.2021.0132

8. Rehman SU, Yoo HH. COVID-19 challenges and its therapeutics. *BioMed Pharmacother* (2021) 142:112015. doi: 10.1016/j.biopha.2021.112015

9. Fernandes Q, Inchakalody VP, Merhi M, Mestiri S, Taib N, Moustafa Abo El-Ella D, et al. Emerging COVID-19 variants and their impact on SARS-CoV-2 diagnosis, therapeutics and vaccines. *Ann Med* (2022) 54(1):524–40. doi: 10.1080/07853890.2022.2031274

10. Tang Y, Liu J, Zhang D, Xu Z, Ji J, Wen C. Cytokine storm in COVID-19: the current evidence and treatment strategies. *Front Immunol* (2020) 11:1708. doi: 10.3389/fimmu.2020.01708

11. Ye Q, Wang B, Mao J. The pathogenesis and treatment of the `Cytokine storm' in COVID-19. *J Infect* (2020) 80(6):607–13. doi: 10.1016/j.jinf.2020.03.037

12. Flisiak R, Horban A, Jaroszewicz J, Kozielewicz D, Pawłowska M, Parczewski M, et al. Management of SARS-CoV-2 infection: recommendations of the polish association of epidemiologists and infectiologists as of march 31, 2020. *Pol Arch Intern Med* (2020) 130(4):352–7. doi: 10.20452/pamw.15424

13. Flisiak R, Horban A, Jaroszewicz J, Kozielewicz D, Mastalerz-Migas A, Owczuk R, et al. Management of SARS-CoV-2 infection: recommendations of the polish association of epidemiologists and infectiologists as of April 26, 2021. *Pol Arch Intern Med* (2021) 131(5):487–96. doi: 10.20452/pamw.15979

14. Hariyanto TI, Japar KV, Kwenandar F, Damay V, Siregar JI, Lugito NPH, et al. Inflammatory and hematologic markers as predictors of severe outcomes in COVID-19 infection: a systematic review and meta-analysis. *Am J Emerg Med* (2021) 41:110–9. doi: 10.1016/j.ajem.2020.12.076

15. Terpos E, Ntanasis-Stathopoulos I, Elalamy I, Kastritis E, Sergentanis TN, Politou M, et al. Hematological findings and complications of COVID-19. *Am J Hematol* (2020) 95(7):834–47. doi: 10.1002/ajh.25829

16. Malik P, Patel U, Mehta D, Patel N, Kelkar R, Akrmah M, et al. Biomarkers and outcomes of COVID-19 hospitalisations: systematic review and meta-analysis. *BMJ Evid Based Med* (2021) 26(3):107–8. doi: 10.1136/bmjebm-2020-111536

17. Battaglini D, Lopes-Pacheco M, Castro-Faria-Neto HC, Pelosi P, Rocco PRM. Laboratory biomarkers for diagnosis and prognosis in COVID-19. *Front Immunol* (2022) 13:857573. doi: 10.3389/fimmu.2022.857573

18. Topp G, Bouyea M, Cochran-Caggiano N, Ata A, Torres P, Jacob J, et al. Biomarkers predictive of extubation and survival of COVID-19 patients. *Cureus* (2021) 13(6):e15462. doi: 10.7759/cureus.15462

19. Iwamura APD, Tavares da Silva MR, Hümmelgen AL, Soeiro Pereira PV, Falcai A, Grumach AS, et al. Immunity and inflammatory biomarkers in COVID-19: a systematic review. *Rev Med Virol* (2021) 31(4):e2199. doi: 10.1002/rmv.2199

20. Martonik D, Parfieniuk-Kowerda A, Rogalska M, Flisiak R. The role of Th17 response in COVID-19. *Cells* (2021) 10(6). doi: 10.3390/cells10061550

21. Huang C, Wang Y, Li X, Ren L, Zhao J, Hu Y, et al. Clinical features of patients infected with 2019 novel coronavirus in wuhan, China. *Lancet* (2020) 395(10223):497–506. doi: 10.1016/S0140-6736(20)30183-5

22. De Biasi S, Meschiari M, Gibellini L, Bellinazzi C, Borella R, Fidanza L, et al. Marked T cell activation, senescence, exhaustion and skewing towards TH17 in patients with COVID-19 pneumonia. *Nat Commun* (2020) 11(1):3434. doi: 10.1038/s41467-020-17292-4

23. Song JW, Zhang C, Fan X, Meng FP, Xu Z, Xia P, et al. Immunological and inflammatory profiles in mild and severe cases of COVID-19. *Nat Commun* (2020) 11(1):3410. doi: 10.1038/s41467-020-17240-2

24. Liu Z, Long W, Tu M, Chen S, Huang Y, Wang S, et al. Lymphocyte subset (CD4+, CD8+) counts reflect the severity of infection and predict the clinical outcomes in patients with COVID-19. *J Infect* (2020) 81(2):318–56. doi: 10.1016/j.jinf.2020.03.054

25. Jiang M, Guo Y, Luo Q, Huang Z, Zhao R, Liu S, et al. T Cell subset counts in peripheral blood can be used as discriminatory biomarkers for diagnosis and severity prediction of coronavirus disease 2019. *J Infect Dis* (2020) 222(2):198–202. doi: 10.1093/infdis/jiaa252

26. Wang F, Nie J, Wang H, Zhao Q, Xiong Y, Deng L, et al. Characteristics of peripheral lymphocyte subset alteration in COVID-19 pneumonia. *J Infect Dis* (2020) 221(11):1762–9. doi: 10.1093/infdis/jiaa150

27. Huang L, Shi Y, Gong B, Jiang L, Zhang Z, Liu X, et al. Dynamic blood single-cell immune responses in patients with COVID-19. *Signal Transduct Target Ther* (2021) 6(1):110. doi: 10.1038/s41392-021-00526-2

28. Orlov M, Wander PL, Morrell ED, Mikacenic C, Wurfel MM. A case for targeting Th17 cells and IL-17A in SARS-CoV-2 infections. *J Immunol* (2020) 205(4):892–8. doi: 10.4049/jimmunol.2000554

29. Parackova Z, Bloomfield M, Klocperk A, Sediva A. Neutrophils mediate Th17 promotion in COVID-19 patients. *J Leukoc Biol* (2021) 109(1):73–6. doi: 10.1002/JLB.4COVCRA0820-481RRR

30. Hotez PJ, Bottazzi ME, Corry DB. The potential role of Th17 immune responses in coronavirus immunopathology and vaccine-induced immune enhancement. *Microbes Infect* (2020) 22(4-5):165–7. doi: 10.1016/j.micinf.2020.04.005

31. Ahmed Mostafa G, Mohamed Ibrahim H, Al Sayed Shehab A, Mohamed Magdy S, AboAbdoun Soliman N, Fathy El-Sherif D. Up-regulated serum levels of interleukin (IL)-17A and IL-22 in Egyptian pediatric patients with COVID-19 and MIS-c: relation to the disease outcome. *Cytokine* (2022) 154:155870. doi: 10.1016/j.cyto.2022.155870

32. Liu Y, Zhang C, Huang F, Yang Y, Wang F, Yuan J, et al. Elevated plasma levels of selective cytokines in COVID-19 patients reflect viral load and lung injury. *Natl Sci Rev* (2020) 7(6):1003–11. doi: 10.1093/nsr/nwaa037

33. Sharif-Askari FS, Sharif-Askari NS, Hafezi S, Mdkhana B, Alsayed HAH, Ansari AW, et al. Interleukin-17, a salivary biomarker for COVID-19 severity. *PloS One* (2022) 17(9):e0274841. doi: 10.1371/journal.pone.0274841

34. Fang S, Ju D, Lin Y, Chen W. The role of interleukin-22 in lung health and its therapeutic potential for COVID-19. *Front Immunol* (2022) 13:951107. doi: 10.3389/fimmu.2022.951107

35. Das S, St Croix C, Good M, Chen J, Zhao J, Hu S, et al. Interleukin-22 inhibits respiratory syncytial virus production by blocking virus-mediated subversion of cellular autophagy. *iScience* (2020) 23(7):101256. doi: 10.1016/j.isci.2020.101256

36. Hoffmann JP, Kolls JK, McCombs JE. Regulation and function of ILC3s in pulmonary infections. *Front Immunol* (2021) 12:672523. doi: 10.3389/fimmu.2021.672523

37. Silverstein NJ, Wang Y, Manickas-Hill Z, Carbone C, Dauphin A, Boribong BP, et al. Innate lymphoid cells and COVID-19 severity in SARS-CoV-2 infection. *Elife* (2022) 11. doi: 10.7554/eLife.74681

38. Ponthieux F, Dauby N, Maillart E, Fils JF, Smet J, Claus M, et al. Tocilizumab-induced unexpected increase of several inflammatory cytokines in critically ill COVID-19 patients: the anti-inflammatory side of IL-6. *Viral Immunol* (2022) 35(1):60–70. doi: 10.1089/vim.2021.0111

39. Scheller J, Chalaris A, Schmidt-Arras D, Rose-John S. The pro- and anti-inflammatory properties of the cytokine interleukin-6. *Biochim Biophys Acta* (2011) 1813(5):878–88. doi: 10.1016/j.bbamcr.2011.01.034

40. Terzi F, Demirci B, Çınar İ, Alhilal M, Erol HS. Effects of tocilizumab and dexamethasone on the downregulation of proinflammatory cytokines and upregulation of antioxidants in the lungs in oleic acid-induced ARDS. *Respir Res* (2022) 23(1):249. doi: 10.1186/s12931-022-02172-w

41. van Woensel JB, Lutter R, Biezeveld M, Dekker T, Nijhuis M, van Aalderen WM, et al. Effect of dexamethasone on tracheal viral load and interleukin-8 tracheal concentration in children with respiratory syncytial virus infection. *Pediatr Infect Dis J* (2003) 22(8):721–6. doi: 10.1097/01.inf.0000078165.62923.15

42. Higham A, Singh D. Dexamethasone and p38 MAPK inhibition of cytokine production from human lung fibroblasts. *Fundam Clin Pharmacol* (2021) 35(4):714–24. doi: 10.1111/fcp.12627

43. Qin M, Qiu Z. Changes in TNF-α, IL-6, IL-10 and VEGF in rats with ARDS and the effects of dexamethasone. *Exp Ther Med* (2019) 17(1):383–7. doi: 10.3892/etm.2018.6926

frontiers | Frontiers in Immunology

TYPE Brief Research Report
PUBLISHED 11 March 2024
DOI 10.3389/fimmu.2024.1329846

Check for updates

OPEN ACCESS

EDITED BY
Laura Maggi,
University of Florence, Italy

REVIEWED BY
Ravi Kumar Sharma,
Karolinska Institutet (KI), Sweden
Luka Cicin-Sain,
Helmholtz Association of German Research Centers (HZ), Germany

*CORRESPONDENCE
James J. Moon
jjmoon@mgh.harvard.edu

†PRESENT ADDRESS
Sara Landeras-Bueno,
Universidad Cardenal Herrera-CEU, CEU Universities, Valencia, Spain

‡These authors share first authorship

§These authors share last authorship

RECEIVED 30 October 2023
ACCEPTED 29 January 2024
PUBLISHED 11 March 2024

CITATION
Bricio-Moreno L, Barreto de Albuquerque J, Neary JM, Nguyen T, Kuhn LF, Yeung Y, Hastie KM, Landeras-Bueno S, Olmedillas E, Hariharan C, Nathan A, Getz MA, Gayton AC, Khatri A, Gaiha GD, Ollmann Saphire E, Luster AD and Moon JJ (2024) Identification of mouse CD4$^+$ T cell epitopes in SARS-CoV-2 BA.1 spike and nucleocapsid for use in peptide:MHCII tetramers.
Front. Immunol. 15:1329846.
doi: 10.3389/fimmu.2024.1329846

COPYRIGHT
© 2024 Bricio-Moreno, Barreto de Albuquerque, Neary, Nguyen, Kuhn, Yeung, Hastie, Landeras-Bueno, Olmedillas, Hariharan, Nathan, Getz, Gayton, Khatri, Gaiha, Ollmann Saphire, Luster and Moon. This is an open-access article distributed under the terms of the Creative Commons Attribution License (CC BY). The use, distribution or reproduction in other forums is permitted, provided the original author(s) and the copyright owner(s) are credited and that the original publication in this journal is cited, in accordance with accepted academic practice. No use, distribution or reproduction is permitted which does not comply with these terms.

Identification of mouse CD4$^+$ T cell epitopes in SARS-CoV-2 BA.1 spike and nucleocapsid for use in peptide:MHCII tetramers

Laura Bricio-Moreno[1,2,3‡], Juliana Barreto de Albuquerque[1,2,3‡], Jake M. Neary[1,2], Thao Nguyen[1,2], Lucy F. Kuhn[1,2], YeePui Yeung[1,2], Kathryn M. Hastie[4], Sara Landeras-Bueno[4†], Eduardo Olmedillas[4], Chitra Hariharan[4], Anusha Nathan[5,6], Matthew A. Getz[5], Alton C. Gayton[5], Ashok Khatri[3,7], Gaurav D. Gaiha[3,5,8], Erica Ollmann Saphire[4,9], Andrew D. Luster[1,2,3§] and James J. Moon[1,2,3,10*§]

[1]Center for Immunology and Inflammatory Diseases, Massachusetts General Hospital, Boston, MA, United States, [2]Division of Rheumatology, Allergy, and Immunology, Massachusetts General Hospital, Boston, MA, United States, [3]Harvard Medical School, Boston, MA, United States, [4]Center for Vaccine Innovation, La Jolla Institute for Immunology, La Jolla, CA, United States, [5]Ragon Institute of MGH, MIT, and Harvard, Cambridge, MA, United States, [6]Program in Health Sciences and Technology, Harvard Medical School and Massachusetts Institute of Technology, Boston, MA, United States, [7]Endocrine Division, MGH, Boston, MA, United States, [8]Division of Gastroenterology, MGH, Boston, MA, United States, [9]Department of Medicine, University of California San Diego, La Jolla, CA, United States, [10]Division of Pulmonary and Critical Care Medicine, MGH, Boston, MA, United States

Understanding adaptive immunity against SARS-CoV-2 is a major requisite for the development of effective vaccines and treatments for COVID-19. CD4$^+$ T cells play an integral role in this process primarily by generating antiviral cytokines and providing help to antibody-producing B cells. To empower detailed studies of SARS-CoV-2-specific CD4$^+$ T cell responses in mouse models, we comprehensively mapped I-A^b-restricted epitopes for the spike and nucleocapsid proteins of the BA.1 variant of concern via IFNγ ELISpot assay. This was followed by the generation of corresponding peptide:MHCII tetramer reagents to directly stain epitope-specific T cells. Using this rigorous validation strategy, we identified 6 immunogenic epitopes in spike and 3 in nucleocapsid, all of which are conserved in the ancestral Wuhan strain. We also validated a previously identified epitope from Wuhan that is absent in BA.1. These epitopes and tetramers will be invaluable tools for SARS-CoV-2 antigen-specific CD4$^+$ T cell studies in mice.

KEYWORDS

C57BL/6, epitope mapping, HexaPro, vFLIP, immunodominance

Introduction

Severe acute respiratory syndrome coronavirus 2 (SARS-CoV-2) is the causative pathogen of the coronavirus disease 2019 (COVID-19) pandemic that has become an epic global health crisis (1). The unprecedented effort to develop vaccines and treatments for this disease has put forth an urgency to better understand how adaptive immunity develops to the virus.

As with most other viral pathogens, effective immunity to SARS-CoV-2 involves a combination of humoral responses from B cells and antibodies as well as cellular responses from $CD4^+$ and $CD8^+$ T cells (2, 3). While the significance of virus-specific antibodies and particularly their neutralizing function in COVID-19 is unquestioned, there is growing appreciation for the parallel protective role provided by virus-specific T cells, due in part to their greater resistance to immune evasion by viral evolution and perhaps greater stability over time (4).

T cells recognize peptides processed from antigenic proteins and presented by major histocompatibility complex (MHC) proteins on the surface of antigen-presenting cells (APCs). Identification of the sequences of such peptide epitopes from SARS-CoV-2 proteins enables detailed analyses of SARS-CoV-2-specific T cell populations by informing the design of *in vitro* stimulation assays as well as the generation of peptide:MHC tetramer reagents that can directly stain SARS-CoV-2-specific T cells. Considerable progress has been made in the identification of human T cell epitopes for SARS-CoV-2 antigens, resulting in the generation and use of SARS-CoV-2-specific peptide:MHC tetramers for studies of viral epitope-specific T cell responses (5). However, there are only a few reported sequences of mouse T cell epitopes that would benefit immunological studies in mouse models (6–11).

In this report, we performed a comprehensive mapping of $CD4^+$ T cell epitopes in SARS-CoV-2 spike and nucleocapsid proteins for C57BL/6 (B6) mice, the most widely used strain for immunological studies. Overlapping peptide libraries for these proteins were screened for reactivity to T cells in immunized mice by interferon-γ (IFNγ) ELISpot assay. Peptide : MHCII tetramer reagents were then generated for candidate peptide epitopes and used to measure the expansion of T cell populations with specificity for these epitopes and compare their relative immunogenicity. In all, we identified 6 novel epitopes in spike and 3 in nucleocapsid, which will be useful for future studies of T cell responses to SARS-CoV-2 in mice.

Materials and methods

Mice

C57BL/6 mice were purchased from Jackson Laboratory and housed under specific-pathogen-free conditions at Massachusetts General Hospital. Male and female mice were immunized between 6-16 weeks of age.

Proteins

SARS-CoV-2 Wuhan-Hu-1 (D614G) or SARS-CoV-2 BA.1 spike was expressed in the "HexaPro" background (12) as previously reported (13, 14). Briefly, ExpiCHO-S cells (Thermo Fisher) were maintained and transfected according to the manufacturer's protocol. Transfected cells were harvested 7-8 days after transfection. Cultures were clarified by centrifugation and BioLock (IBA Life Sciences) added. The Twin-StrepII-Tagged-proteins were purified over a StrepTrap-HP column equilibrated with 25mM Tris pH 7.5, 200mM NaCl (TBS). After extensive washing, bound proteins were eluted in TBS buffer supplemented with 5mM d-desthiobiotin (Sigma Aldrich). Affinity-purified proteins were incubated with HRV-3C protease to remove purification tags and subsequently purified by size-exclusion-chromatography on a Superose 6 Increase column (GE Healthcare) in TBS.

Alternatively, HexaPro spike proteins were expressed in *Drosophila* S2 cells as previously described for the production of peptide:MHCII tetramers (15). Briefly, the same sequences were cloned into the pR expression vector and expressed in stably transfected S2 cells. Protein was harvested from cell culture supernatants and purified by binding to a nickel-nitrilotriacetic acid (Ni-NTA) column (Novagen) followed by elution with 1M imidazole containing 0.2% octyl β-D-glucopyranoside. After concentration through 100kD centrifugation filters (Millipore), the protein was further purified by size-exclusion chromatography on a Sephacryl 300 column (GE Healthcare) in PBS.

For memory T cell experiments, the VFLIP prefusion stabilized version of SARS-CoV-2 Wuhan spike was used instead (16). This protein was generated in ExpiCHO-S cells as described above.

Recombinant SARS-CoV-2 BA.1 nucleocapsid protein was subcloned into the pET46 vector (Novagen) with an upstream 6xHis tag and expressed in Rosetta2 pLysS *E. coli* (Novagen). Cells were lysed with an M-110P microfluidizer (Microfluidics) in 50 mM HEPES pH 7.5, 500 mM NaCl, 10% glycerol, 20 mM imidazole, 6M urea, 1 µl Benzonase Nuclease (Millipore). Recombinant protein was purified by binding to Ni-NTA beads (Qiagen) and eluted in the same buffer supplemented with 300 mM imidazole. The resulting sample was then dialyzed overnight in Snakeskin dialysis tubing with 10-kDa pore size in refolding buffer (50 mM HEPES pH 7.5, 500 mM NaCl, 10% glycerol) and further purified by size-exclusion chromatography on a Superose 200 Increase column (GE Healthcare).

Peptides

Peptide libraries for BA.1 spike and nucleocapsid (15-mers with 4aa overlap) were synthesized at a purity of at least 70% by the MGH Peptide Core (17). All others were custom ordered through Genscript.

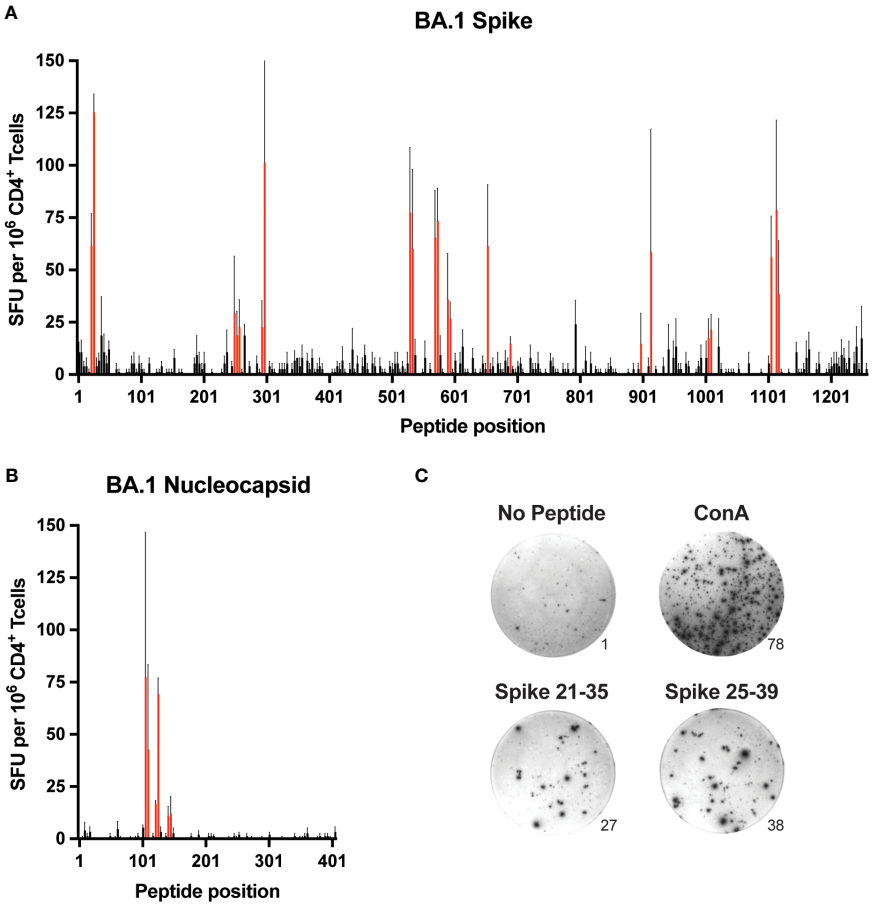


FIGURE 1
Comprehensive mapping of $CD4^+$ T cell epitopes in SARS-CoV-2 BA.1 spike and nucleocapsid proteins C57BL/6 mice were immunized subcutaneously (s.c.) with BA.1 spike or nucleocapsid proteins plus CFA as adjuvant, and 9-10 days later, $CD4^+$ T cells from secondary lymphoid organs (SLO) were assessed for IFNγ production by ELISpot following *in vitro* restimulation with peptide libraries covering the entire sequence of **(A)** spike and **(B)** nucleocapsid. Mean values ± SEM (thin black lines extending above bars) are shown for n=3 independent experiments. Red bars indicate putative epitopes that were subsequently evaluated by peptide:MHCII tetramer staining. **(C)** Representative images of ELISpot samples stimulated with PBS alone (No peptide, negative control), Concanavalin A (Con A, positive control), or overlapping peptides encompassing the S-26 epitope of spike (Spike 21-25 and Spike 25-39). Numbers at the lower right edges of images indicate the raw number of spot-forming units counted per well.

Immunizations

100 µg of recombinant protein or peptide was emulsified in a 1:1 mix of 0.9% saline and complete Freund's adjuvant (CFA) (Sigma-Aldrich) and injected subcutaneously at the back of the neck and base of the tail (50 µl each site). For memory T cell studies, a priming dose of 10 µg of spike protein was mixed with 20 µg of polyinosinic:polycytidylic acid (poly(I:C))(InvivoGen) in 50 µl of 0.9% saline and injected intramuscularly in the back leg. A boost immunization was administered intranasally under anesthesia three weeks later using the same dose of spike protein in 30 µl of 0.9% saline.

T cells and APCs for ELISpot assays

Secondary lymphoid organs (SLO) including the spleen and various skin-draining lymph nodes (e.g., brachial, axillary, inguinal, mandibular, accessory mandibular, parotid, iliac, and mesenteric) (18), were harvested from mice 9-10 days post-immunization and processed into single cell suspensions by mechanical disruption over nylon mesh. $CD4^+$ T cells were then isolated via a negative selection $CD4^+$ T cell isolation kit (Miltenyi). For APCs, splenocytes were isolated from naïve mice, subjected to red cell lysis with ACK lysis buffer (Corning) at RT for 5 min, washed, and then irradiated at 2500 rads.

ELISpot assays

IFNγ ELISpot assays were performed using a commercially available kit in accordance with its instructions (Mabtech). Briefly, 2.5 x 10^5 $CD4^+$ T cells were incubated with 2.5 x 10^5 irradiated APCs in 200 µl R10 media (RPMI 1640 + 10% FBS, pen/strep, 2-ME) in each well of a 96-well pre-coated ELISpot plate. Single peptides from the spike and nucleocapsid libraries were added to each well at a final concentration of 20 µg/ml. Positive

10.3389/fimmu.2024.1329846

TABLE 1 I-A^b-restricted $CD4^+$ T cell epitopes in SARS-CoV-2 BA.1 spike and nucleocapsid.

Epitope	Residues (BA.1)	Residues (Wuhan)	Sequence (MHC-binding core in bold)	ELISpot Response	Tetramer Response to:	
					Peptide Immunization	Protein Immunization
Spike						
S-26	26-37	26-37	PAYTNSFTRGVY	+++	+++	+++
S-254*	254-265	257-268	GWTAGAAAYYVG	+	–	ND
S-298	298-309	301-312	CTLKSFTVEKGI	+++	++	+++
S-529*	529-540	532-543	NLVKNKCVNFNF	++	–	ND
S-571	571-582	574-585	DAVRDPQTLEIL	++	+	++
S-592	592-603	595-606	VSVITPGTNTSN	+	ND	ND
S-655	655-666	658-669	NSYECDIPIGAG	++	ND	ND
S-690	690-700	693-703	IAYTMSLGAEN	+	++	+
S-899	899-910	902-913	MAYRFNGIGVTQ	+	–	ND
S-914	914-925	917-928	YENQKLIANQFN	++	–	–
S-1008	1008-1019	1011-1022	QLIRAAEIRASA	+	+	+/-
S-1104	1104-1115	1107-1118	RNFYEPQIITTD	++	+++	+++
S-1116	1116-1127	1119-1130	NTFVSGNCDVVI	++	–	–
Absent in HexaPro Spike construct:						
S-883*	883-893	886-896	WTFGAGAALQI	+	+	ND
Absent in BA.1 but present in Wuhan:						
S-63*	NA	63-74	TWFHAIHVSGTN	+++	+++	+++
Nucleocapsid						
N-107*	107-118	110-121	FYYLGTGPEAGL	++	++	++
N-125*	125-136	128-139	DGIIWVATEGAL	++	++	++
N-143	143-154	146-157	IGTRNPANNAAI	+	+++	+++
Absent in BA.1 but present in Wuhan:						
N-8	NA	8-19	NQRNAPRITFGG	+	ND	ND

Validated epitopes in bold.
Predicted MHC-binding core underlined.
*Multiple tetramers generated to test epitope.
+ = weak response.
++ = moderate response.
+++ = strong response.
ND, not determined.
NA, not applicable.

control wells were set up with 10 µg/ml Concanavalin A (ConA) (Sigma-Aldrich) and negative control wells with no stimulus. After overnight (16-18h) incubation at 37C with 5% CO_2, plates were washed and developed according to kit instructions. Dried plates were then analyzed on a Mabtech ASTOR ELISpot reader for quantification of spot-forming units (SFU), which were then expressed as SFU per 10^6 $CD4^+$ T cells after subtraction of background signal determined by the average of negative control (cells + media alone) wells. Machine settings for spot size and brightness were preserved as best possible across experiments.

Tetramers

The generation of peptide:MHCII tetramers has been described in detail (15). In brief, soluble heterodimeric I-A^b molecules covalently linked to peptide epitopes were expressed and biotinylated in stably transfected *Drosophila* S2 cells. Following immunoaffinity purification, these biotinylated peptide:MHCII complexes were titrated and tetramerized to streptavidin pre-conjugated to R-phycoerythrin (PE), allophycocyanin (APC), or R-phycoerythrin-cyanine-7 (PE-Cy7) fluorochromes (Prozyme,

10.3389/fimmu.2024.1329846

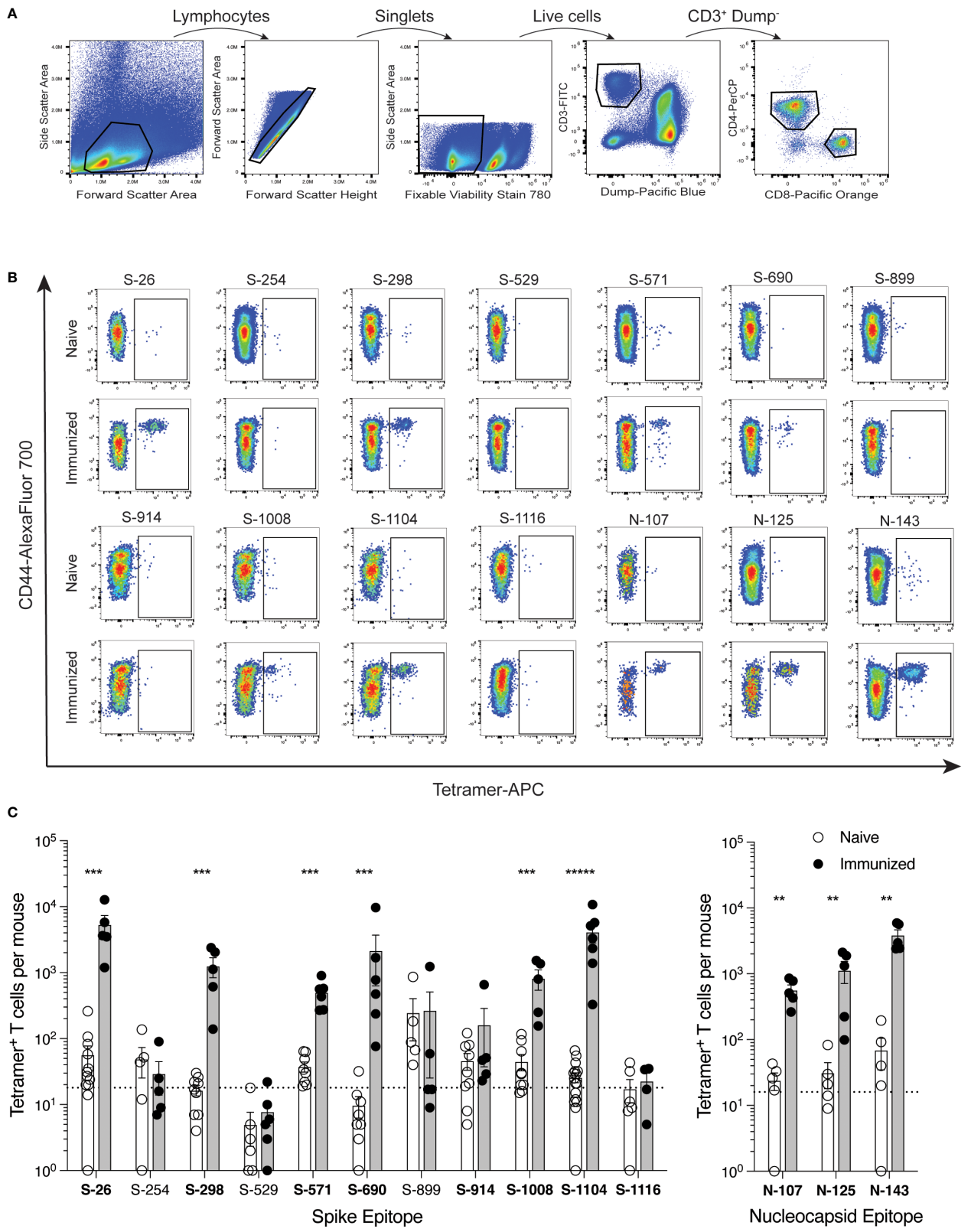


FIGURE 2
Identification of SARS-CoV-2 epitope-specific CD4$^+$ T cells by peptide:MHCII tetramers C57BL/6 mice were immunized s.c. with candidate epitope peptides plus CFA as adjuvant, and 7 days later, epitope-specific CD4$^+$ T cells from the SLO were detected by peptide:MHCII tetramer-based cell enrichment and flow cytometry. **(A)** Flow cytometry gating strategy for analysis of lymphocyte$^+$ single cell$^+$ live$^+$ dump (B220, CD11b, CD11c, F4/80)$^-$ CD3$^+$ CD4$^+$ events. **(B)** Representative flow cytometry plots of CD4$^+$ gated events illustrating tetramer staining of epitope-specific T cells from naïve and corresponding peptide-immunized mice. APC-conjugated tetramer staining is shown exclusively for comparison purposes, but all three fluorochrome versions were used to generate data. **(C)** Quantification of epitope-specific CD4$^+$ T cells from naïve and immunized mice. Mean values ± SEM are shown for n=4-16 mice per epitope across multiple independent experiments. Dotted lines represent the limit of detection as defined by the mean numbers of CD8$^+$tetramer$^+$ events per mouse. Bold font indicates epitopes subsequently evaluated in protein immunization experiments. Statistical significance was calculated via Mann-Whitney tests **(B, C)**; **p < 0.01, ***p < 0.001, *****p < 0.00001.

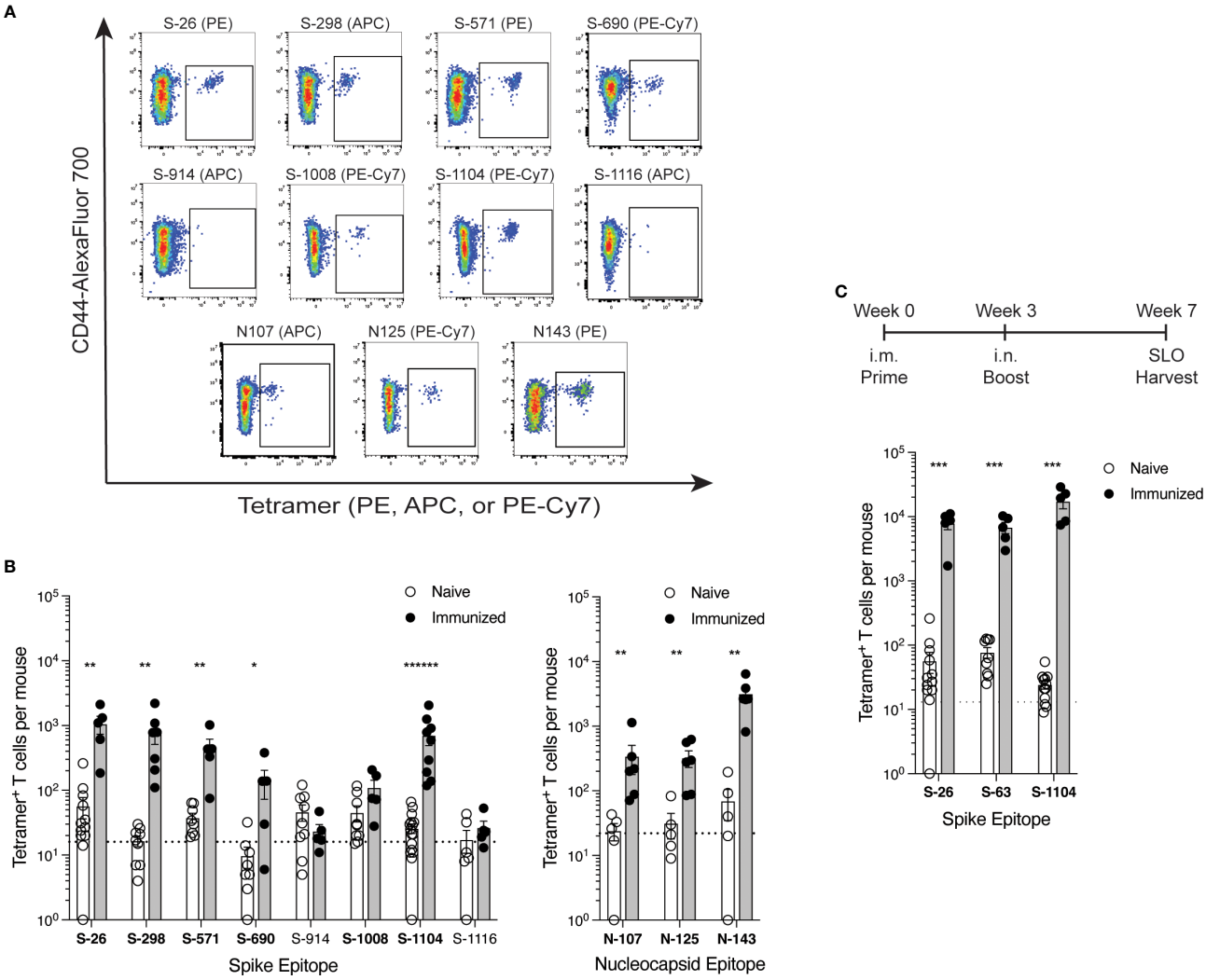


FIGURE 3
Comparison of SARS-CoV-2 epitope-specific CD4$^+$ T cell responses after protein immunization **(A, B)** C57BL/6 mice were immunized s.c. with spike or nucleocapsid protein plus CFA as adjuvant, and 7 days later, epitope-specific CD4$^+$ T cells from the SLO were detected by tetramer-based cell enrichment and flow cytometry. **(A)** Representative flow cytometry plots of CD4$^+$ gated events illustrating tetramer staining of epitope-specific T cells from protein-immunized mice. **(B)** Quantification of epitope-specific CD4$^+$ T cells from naïve and immunized mice. Naive mice data is the same as in Figure 2C. Mean values ± SEM are shown for n=5-16 mice per epitope across multiple independent experiments. Bold font indicates epitopes validated by statistically significant increases in frequency upon immunization. **(C)** C57BL/6 mice were primed intramuscularly (i.m.) with Wuhan spike protein plus poly (I:C) as adjuvant, and 3 weeks later, boosted intranasally (i.n.) with the same dose. Four weeks later, epitope-specific memory CD4$^+$ T cells from the SLO were enumerated by tetramer-based cell enrichment and flow cytometry. Naive data is the same as in Figure 2C and Supplementary Figure S2. Mean values ± SEM are shown for n=5 mice per epitope. Dotted lines represent the limit of detection as defined by the mean numbers of CD8$^+$tetramer$^+$ events per mouse. Statistical significance was calculated via Mann-Whitney tests **(B)** and **(C)**; *p < 0.05, **p < 0.01, ***p < 0.001, ******p < 0.000001.

Thermo-Fisher). All three fluorochrome versions were used in calculations of epitope-specific T cell frequencies.

Tetramer-based T cell enrichment and flow cytometry

SLO were harvested from mice 7-8 days post-immunization and processed into single cell suspensions by mechanical disruption over nylon mesh. For memory T cell studies, SLO also included lung draining mediastinal lymph nodes and were harvested 4 weeks post-boost. Tetramer-based enrichment of epitope-specific T cells from these samples was performed as described in detail (19). Flow cytometry was performed with the Aurora spectral flow cytometer (Cytek). In general, ~0.5 - 2.0 x 10^6 total enriched cells containing ~2000 - 8000 CD4$^+$ T cells were collected per sample. Data analysis was performed with FlowJo software (Treestar).

Statistical analysis

All statistical analysis was performed on Prism (GraphPad).

Results

Screening of peptide libraries by IFNγ ELISpot

To facilitate detailed studies of SARS-CoV-2-specific $CD4^+$ T cell responses in B6 mice, we performed a comprehensive screen of potential I-A^b-restricted epitopes in SARS-CoV-2 spike and nucleocapsid proteins, which have been shown to be major immunogenic targets of $CD4^+$ T cells during infection in humans (20). The sequences used in our study were from the Omicron (BA.1) variant strain due to the timing of when our studies began.

B6 mice were immunized subcutaneously with recombinant spike or nucleocapsid protein emulsified in complete Freund's adjuvant (CFA), and 7-10 days later, expanded $CD4^+$ T cells were isolated from pooled secondary lymphoid organs (SLO) consisting of spleen and skin-draining lymph nodes. To identify epitopes, the T cells were restimulated *in vitro* with individual peptides from a library of overlapping peptides (15-mer with 4 residue overlap) covering the entire sequence of each protein. Epitope-specific responses were gauged by the production of interferon γ (IFNγ) via ELISpot assay (Figure 1 and Supplementary File 1). Based on an initial arbitrary threshold signal of ~20 spot-forming units (SFU) per million $CD4^+$ T cells, a total of 13 regions representing putative epitopes were identified in spike, and 3 were identified in nucleocapsid (Table 1).

Tetramer-based validation of epitopes

To further validate these epitopes, we generated I-A^b tetramer reagents to directly stain epitope-specific $CD4^+$ T cells. Tetramers were constructed with minimal peptide sequences (10-11 residues) representing each putative epitope as inferred from the overlap between neighboring immunogenic peptides as well as the use of computational tools that predict peptide binding registers in I-A^b (21, 22) (Table 1). In some cases where minimal epitope sequences were not obvious, multiple tetramers were generated to cover the best possibilities from each immunogenic region (data not shown).

Mice were immunized with each minimal peptide, and 7 days later the expansion of $CD4^+$ T cells specific for that peptide was assessed by corresponding tetramer staining and magnetic cell enrichment (Figure 2). Six of the 13 spike epitopes (S-26, S-298, S-571, 6-690, S-1008, and S-1104) and all three of the nucleocapsid epitopes (N-107, N-125, N-143) exhibited immunogenicity based on observed increases in tetramer-positive T cell frequencies following immunization. Despite having excellent MHC-binding prediction scores, tetramers for spike epitopes S-592 and S-655 were consistently fraught with issues of high background staining and the immunogenicity of these epitopes could not be ascertained (data not shown).

Peptides were chosen for these immunizations to provide maximal levels of peptide:MHCII complex presentation that could test whether the epitope was capable of evoking a T cell response. Once epitopes were validated in this way, tetramers were then used to detect epitope-specific T cells following immunization of mice with whole spike or nucleocapsid protein (Figure 3). This additional step addressed the immunogenicity of each epitope when the efficiency by which it is processed from protein and presented by antigen-presenting cells is also considered. Eight spike epitopes and 3 nucleocapsid epitopes were chosen for testing by protein immunization based on their initial promise of immunogenicity in early peptide immunization experiments, albeit only 6 of the spike epitopes and all 3 nucleocapsid epitopes were ultimately validated by peptide immunization as described above. With the exception of S-1008, all 9 of the epitopes that were validated by peptide immunizations also elicited a reliable response by protein immunization. Responses ranged from minimal to robust, and they reflected the same general hierarchy of epitope immunodominance seen in the peptide studies.

Validation of additional epitopes

The spike protein used in our studies was the previously described HexaPro construct engineered to remain in a prefusion trimer complex due to the introduction of 6 stabilizing proline substitutions (12). To determine whether any potential epitopes were affected by these mutations, we immunized mice with peptides corresponding to native sequences at these locations and assessed T cell responses by IFNγ ELISpot (Supplementary Figure S1, Supplementary File 1). One of these peptides generated a weak response, which was supported by tetramer staining experiments showing a trend of expanded T cells in mice immunized with a minimal epitope sequence from this region (S-883, Table 1).

All of the identified SARS-CoV-2 BA.1 spike and nucleocapsid epitopes in our study are completely conserved from the ancestral Wuhan-Hu-1 strain. However, there are two previously reported epitopes in Wuhan, spike residues 62-78 and nucleocapsid residues 9-23 (10), that are mutated in BA.1 and therefore were not identified in our screen. To compare the immunogenicity of these epitopes to the new ones identified in our current study, and to find any other potential epitopes in Wuhan spike and nucleocapsid, we performed further ELISpot experiments using Wuhan spike and nucleocapsid proteins and a set of Wuhan peptides covering all the sites that are mutated in BA.1 (Supplementary Figures S2A, B, Supplementary File 1). Consistent with earlier reports, we found a very strong response to the spike 62-78 region and a very weak response to the nucleocapsid 9-23 region. We also generated a corresponding tetramer with a minimal sequence for the strong spike epitope (S-63, Table 1) and tested it in mice immunized with peptide or Wuhan spike protein (Supplementary Figures S2C, D). Responses to this epitope were very robust and superior to the responses for any of the newly identified epitopes.

Validation of epitopes in memory T cell populations

To further assess the relevance of these epitopes in T cell immunity to spike antigen, we used tetramers to detect the

frequencies of epitope-specific T cells among memory $CD4^+$ T cells generated after a 7-week prime-boost immunization scheme. Because subcutaneous immunization with CFA creates an antigen depot unsuitable for the study of memory T cells, we primed mice intramuscularly with a soluble dose of HexaPro Wuhan spike protein and poly(I:C) as adjuvant, and then three weeks later, boosted them intranasally with the same dose. At 4 weeks post-boost, we found robust frequencies of T cells specific for the newly identified S-26 and S-1104 epitopes in addition to the previously known S-63 epitope in the SLO (Figure 3C), demonstrating the contribution of these new epitopes in long term $CD4^+$ T cell responses to SARS-CoV-2 spike.

Discussion

In this study, we provide a comprehensive mapping and evaluation of mouse I-A^b-restricted $CD4^+$ T cell epitopes in spike and nucleocapsid, two of the major immunogens of the SARS-CoV-2 virus. This was done systematically by screening a library of overlapping peptides covering the entire sequences of these proteins by IFNγ ELISpot assay. This was followed up with the generation of peptide:MHCII tetramer reagents, which were used to validate candidate epitopes as well as evaluate their relative immunogenicity The result of our labor-intensive empirical approach was a more rigorous identification of epitopes than what computational approaches of epitope prediction alone can provide. However, we did use computational approaches to help narrow down minimal peptide epitope sequences during the design of tetramers.

In total, we discovered 6 immunogenic epitopes in spike (S-26, S-298, S-571, 6-690, S-1008, and S-1104) and 3 in nucleocapsid (N-107, N-125, N-143) (summarized in Table 1), which to the best of our knowledge are all novel. The weak S-1008 epitope was only reliably immunogenic in response to peptide and not protein immunization. One additional weak spike epitope (S-883) lies in a region affected by a proline substitution (A889P) used in the prefusion stabilization of the HexaPro construct (but not current vaccines in the U.S.), highlighting potential caveats of using HexaPro and other engineered versions of viral proteins for immunological studies.

We also validated a previously identified immunodominant spike epitope (S-63) that is present in the Wuhan strain but absent in the BA.1 variant that was studied in our report (10). A tetramer representing this epitope (residues 62-76) was successfully used in a previous study (23). The tetramer created in our current study differs by containing a smaller, minimal peptide sequence (residues 63-74) for this epitope, which limits potential issues that may arise from alternative stretches of amino acids occupying the MHC-binding groove (24). Our ELISpot experiments also confirmed a very weak response to the previously identified nucleocapsid epitope (residues 9-23) of Wuhan that is also absent in BA.1 (10), but we did not investigate this further with tetramers. Interestingly, the two previous studies mapping $CD4^+$ T cell epitopes in C57BL/6 mice only identified these two epitopes and not any of our novel ones (10, 11). As the S-63 epitope is considerably more immunodominant than the others in primary immune responses, this discrepancy could simply be due to differences in the sensitivity of our methods, or perhaps differences in epitope immunodominance patterns resulting from the different ways in which mice were immunized with antigen.

The frequencies of epitope-specific T cells determined by tetramer staining were in the general range of 10^1 - 10^2 cells per naive mouse, increasing variably up to as much as 3 x 10^4 cells in immunized mice, which is consistent with past observations of other epitope-specific $CD4^+$ T cell populations (25). Assuming that there are approximately 2 x 10^7 total $CD4^+$ T cells in the tissues we sampled per mouse, this translates into frequencies of 0.5 - 5 per million $CD4^+$ T cells and 1500 per million $CD4^+$ T cells in naive and immunized mice, respectively. Frequencies in protein immunized mice were more typically in the range of 10^2 - 10^3 cells (5 - 50 per million), which generally correlated with frequencies determined by ELISpot.

The most notable limitation of our study is that despite our comprehensive efforts, additional epitopes may have been missed. Several candidates identified by the ELISpot assay were not successfully validated by tetramers. It is not clear whether this was due to inaccurate prediction of minimal epitope sequences that were used in tetramer design or other technical issues related to tetramer generation. Although we screened potential epitopes masked by proline substitutions in HexaPro spike, we did not screen the truncated 63 amino acids of the C-terminus that are replaced with a Foldon domain in this construct (12). Finally, our assay relies specifically on T cell production of IFNγ, and although unlikely, it is possible that other epitopes preferentially generating other non-Th1 cell lineages were missed.

All of the newly identified epitopes are conserved between BA.1 and the ancestral Wuhan strain as well as Alpha, Gamma, Delta, BA.2, BA.5, XBB.1.5, EG.5.1, and the mouse adapted strain MA10 (26), and differences with Beta, BA.4, and BQ.1.1 are limited to just one epitope each (S-690, N-143, N-125, respectively). The S-63 epitope notwithstanding, this is not entirely surprising as there is unlikely to be immune selective pressure against mouse T cell epitopes in a human virus. However, it is noteworthy that human T cell epitopes have also been generally conserved across variants of concern, suggesting that immune evasion is driven predominantly by antibody rather than T cell recognition (17, 27). A welcome consequence of this conservation is that the epitopes described here for BA.1 can also be used for studies of Wuhan and other variant strains. It will be interesting to see if further epitope mapping for other variants will identify additional epitopes discordant with BA.1.

The identification of these I-A^b-restricted epitopes will be very useful for studies of $CD4^+$ T cell immunity in C57BL/6 mice, the most commonly used strain in immunological research and the background for most hACE2 transgenic mice used in SARS-CoV-2 infection studies (28, 29). There is an appreciable difference in immunogenicity between the two strongest epitopes (S-26, S-1104) and the rest, so we propose the use of these epitopes along with S-63, if applicable, for robust studies of antigen-specific $CD4^+$ T cells, especially if tetramers are to be used.

Data availability statement

The raw data supporting the conclusions of this article will be made available by the authors, without undue reservation.

Ethics statement

The animal study was approved by Massachusetts General Hospital IACUC. The study was conducted in accordance with the local legislation and institutional requirements.

Author contributions

LB: Conceptualization, Data curation, Formal analysis, Investigation, Methodology, Validation, Writing – review & editing. JB: Conceptualization, Data curation, Formal analysis, Investigation, Methodology, Validation, Writing – original draft, Writing – review & editing. JN: Data curation, Investigation, Methodology, Validation, Writing – review & editing. TN: Data curation, Investigation, Methodology, Validation, Writing – review & editing. LK: Investigation, Methodology, Writing – review & editing. YY: Investigation, Writing – review & editing. KH: Resources, Writing – review & editing. SL: Resources, Writing – review & editing. EO: Methodology, Resources, Writing – review & editing. CH: Resources, Writing – review & editing. AN: Resources, Writing – review & editing. MG: Resources, Writing – review & editing. AG: Resources, Writing – review & editing. AK: Resources, Writing – review & editing. GG: Funding acquisition, Resources, Writing – review & editing. EO: Funding acquisition, Project administration, Resources, Writing – review & editing. AL: Conceptualization, Formal analysis, Funding acquisition, Project administration, Resources, Supervision, Writing – review & editing. JM: Conceptualization, Data curation, Formal analysis, Funding acquisition, Investigation, Methodology, Project administration, Resources, Supervision, Validation, Writing – original draft, Writing – review & editing.

Funding

The author(s) declare financial support was received for the research, authorship, and/or publication of this article. This work was supported by the National Institutes of Health (P01 AI165072 for EOS, AL, and JM, DP2 AI154421, R01 AI176533, DP1 DA058476 for GG), the Massachusetts Consortium on Pathogen Readiness (GG and JM), Bill and Melinda Gates Foundation (GG), Burroughs Wellcome Career Award for Medical Scientists (GG), Howard Goodman Fellowship (GG), and the Massachusetts General Hospital Executive Committee on Research (AL and JM).

Acknowledgments

We thank Tianyi Bai for assistance with tetramer and protein production, Hugh Chen for help with ELISpot assays, and Daniel Shin, Ryan Nelson, Maisa Takenaka, and Stephen Elledge for helpful discussions.

Conflict of interest

GG receives research funding from Merck and Moderna.

The remaining authors declare that the research was conducted in the absence of any commercial or financial relationships that could be construed as a potential conflict of interest.

Publisher's note

All claims expressed in this article are solely those of the authors and do not necessarily represent those of their affiliated organizations, or those of the publisher, the editors and the reviewers. Any product that may be evaluated in this article, or claim that may be made by its manufacturer, is not guaranteed or endorsed by the publisher.

Supplementary material

The Supplementary Material for this article can be found online at: https://www.frontiersin.org/articles/10.3389/fimmu.2024.1329846/full#supplementary-material

References

1. ;Li J, Lai S, Gao GF, Shi W. The emergence, genomic diversity and global spread of SARS-CoV-2. *Nature*. (2021) 600(7889):408–18. doi: 10.1038/s41586-021-04188-6

2. Röltgen K, Boyd SD. Antibody and B cell responses to SARS-CoV-2 infection and vaccination: the end of the beginning. *Annu Rev Pathol*. (2023) 19:69–97. doi: 10.1146/annurev-pathmechdis-031521-042754

3. Sette A, Sidney J, Crotty S. T cell responses to SARS-CoV-2. *Annu Rev Immunol*. (2023) 41:343–73. doi: 10.1146/annurev-immunol-101721-061120

4. Petrone L, Sette A, de Vries RD, Goletti D. The importance of measuring SARS-CoV-2-specific T-cell responses in an ongoing pandemic. *Pathogens*. (2023) 12(7):862. doi: 10.3390/pathogens12070862

5. Nelson RW, Chen Y, Venezia OL, Majerus RM, Shin DS, MGH COVID-19 Collection & Processing Team, et al. SARS-CoV-2 epitope-specific $CD4^+$ memory T cell responses across COVID-19 disease severity and antibody durability. *Sci Immunol*. (2022) 7(73):eabl9464. doi: 10.1126/sciimmunol.abl9464

6. Davenport BJ, Morrison TE, Kedl RM, Klarquist J. Conserved and novel mouse CD8 T cell epitopes within SARS-CoV-2 spike receptor binding domain protein identified following subunit vaccination. *J Immunol*. (2021) 206(11):2503–7. doi: 10.4049/jimmunol.2100195

7. Joag V, Wijeyesinghe S, Stolley JM, Quarnstrom CF, Dileepan T, Soerens AG, et al. Cutting edge: mouse SARS-CoV-2 epitope reveals infection and vaccine-elicited CD8 T cell responses. *J Immunol*. (2021) 206(5):931–5. doi: 10.4049/jimmunol.2001400

8. Smith CC, Olsen KS, Gentry KM, Sambade M, Beck W, Garness J, et al. Landscape and selection of vaccine epitopes in SARS-CoV-2. *Genome Med*. (2021) 13(1):101. doi: 10.1186/s13073-021-00910-1

9. Yang J, Kim E, Lee JS, Poo H. A murine $CD8^+$ T cell epitope identified in the receptor-binding domain of the SARS-CoV-2 spike protein. *Vaccines (Basel)*. (2021) 9 (6):641. doi: 10.3390/vaccines9060641

10. Zhuang Z, Lai X, Sun J, Chen Z, Zhang Z, Dai J, et al. Mapping and role of T cell response in SARS-CoV-2-infected mice. *J Exp Med*. (2021) 218(4):e20202187. doi: 10.1084/jem.20202187

11. Wang Y, Wang B, Zhao Z, Xu J, Zhang Z, Zhang J, et al. Effects of SARS-CoV-2 omicron BA.1 spike mutations on T-cell epitopes in mice. *Viruses*. (2023) 15(3):763. doi: 10.3390/v15030763

12. Hsieh CL, Goldsmith JA, Schaub JM, DiVenere AM, Kuo HC, Javanmardi K, et al. Structure-based design of prefusion-stabilized SARS-CoV-2 spikes. *Science*. (2020) 369(6510):1501–5. doi: 10.1126/science.abd0826

13. Hastie KM, Li H, Bedinger D, Schendel SL, Dennison SM, Li K, et al. Defining variant-resistant epitopes targeted by SARS-CoV-2 antibodies: A global consortium study. *Science*. (2021) 374(6566):472–8. doi: 10.1126/science.abh2315

14. Hastie KM, Yu X, Ana-Sosa-Batiz F, Zyla DS, Harkins SS, Hariharan C, et al. Potent Omicron-neutralizing antibodies isolated from a patient vaccinated 6 months before Omicron emergence. *Cell Rep*. (2023) 42(5):112421. doi: 10.1016/j.celrep.2023.112421

15. Moon JJ, Pepper M. Generation of allergen-specific tetramers for a murine model of airway inflammation. *Methods Mol Biol*. (2018) 1799:165–81. doi: 10.1007/978-1-4939-7896-0_14

16. Olmedillas E, Mann JC, Peng W, Wang Y, Diaz Avalos R, Bedinger D, et al. Structure-based design of a highly stable, covalently-linked SARS-CoV-2 spike trimer with improved structural properties and immunogenicity. *bioRxiv*. (2021), 2021.05.06.441046. doi: 10.1101/2021.05.06.441046

17. Naranbhai V, Nathan A, Kaseke C, Berrios C, Khatri A, Choi S, et al. T cell reactivity to the SARS-CoV-2 Omicron variant is preserved in most but not all individuals. *Cell*. (2022) 185(7):1041–51. doi: 10.1016/j.cell.2022.01.029

18. Van den Broeck W, Derore A, Simoens P. Anatomy and nomenclature of murine lymph nodes: Descriptive study and nomenclatory standardization in BALB/cAnNCrl mice. *J Immunol Methods*. (2006) 312(1-2):12–9. doi: 10.1016/j.jim.2006.01.022

19. Legoux FP, Moon JJ. Peptide:MHC tetramer-based enrichment of epitope-specific T cells. *J Vis Exp*. (2012) 68):e4420. doi: 10.3791/4420

20. Grifoni A, Weiskopf D, Ramirez SI, Mateus J, Dan JM, Moderbacher CR, et al. Targets of T cell responses to SARS-CoV-2 coronavirus in humans with COVID-19 disease and unexposed individuals. *Cell*. (2020) 181(7):1489–501. doi: 10.1016/j.cell.2020.05.015

21. Lee SJ, McLachlan JB, Kurtz JR, Fan D, Winter SE, Baumler AJ, et al. Temporal expression of bacterial proteins instructs host CD4 T cell expansion and Th17 development. *PloS Pathog*. (2012) 8(1):e1002499. doi: 10.1371/journal.ppat.1002499

22. Dhanda SK, Mahajan S, Paul S, Yan Z, Kim H, Jespersen MC, et al. IEDB-AR: immune epitope database-analysis resource in 2019. *Nucleic Acids Res*. (2019) 47(W1): W502–6. doi: 10.1093/nar/gkz452

23. Mao T, Israelow B, Peña-Hernández MA, Suberi A, Zhou L, Luyten S, et al. Unadjuvanted intranasal spike vaccine elicits protective mucosal immunity against sarbecoviruses. *Science*. (2022) 378(6622):eabo2523. doi: 10.1126/science.abo2523

24. Landais E, Romagnoli PA, Corper AL, Shires J, Altman JD, Wilson IA, et al. New design of MHC class II tetramers to accommodate fundamental principles of antigen presentation. *J Immunol*. (2009) 183(12):7949–57. doi: 10.4049/jimmunol.0902493

25. Jenkins MK, Moon JJ. The role of naive T cell precursor frequency and recruitment in dictating immune response magnitude. *J Immunol*. (2012) 188 (9):4135–40. doi: 10.4049/jimmunol.1102661

26. Leist SR, Dinnon KH, Schäfer A, Tse LV, Okuda K, Hou YJ, et al. A mouse-adapted SARS-CoV-2 induces acute lung injury and mortality in standard laboratory mice. *Cell*. (2020) 183(4):1070–85. doi: 10.1016/j.cell.2020.09.050

27. Tarke A, Sidney J, Methot N, Yu ED, Zhang Y, Dan JM, et al. Impact of SARS-CoV-2 variants on the total $CD4^+$ and $CD8^+$ T cell reactivity in infected or vaccinated individuals. *Cell Rep Med*. (2021) 2(7):100355. doi: 10.1016/j.xcrm.2021.100355

28. McCray PB, Pewe L, Wohlford-Lenane C, Hickey M, Manzel L, Shi L, et al. Lethal infection of K18-hACE2 mice infected with severe acute respiratory syndrome coronavirus. *J Virol*. (2007) 81(2):813–21. doi: 10.1128/JVI.02012-06

29. Muñoz-Fontela C, Dowling WE, Funnell SGP, Gsell PS, Riveros-Balta AX, Albrecht RA, et al. Animal models for COVID-19. *Nature*. (2020) 586(7830):509–15. doi: 10.1038/s41586-020-2787-6

Frontiers in Immunology

Explores novel approaches and diagnoses to treat immune disorders.

The official journal of the International Union of Immunological Societies (IUIS) and the most cited in its field, leading the way for research across basic, translational and clinical immunology.

Discover the latest Research Topics

See more →



Frontiers

Avenue du Tribunal-Fédéral 34
1005 Lausanne, Switzerland
frontiersin.org

Contact us

+41 (0)21 510 17 00
frontiersin.org/about/contact